Composition en éléments traces de la chalcopyrite

Son potentiel comme minéral indicateur et les implications dans **l'exploration minérale**

Thèse

Enzo Caraballo

Sous la direction de :

Georges Beaudoin, directeur de recherche

Sarah Dare, codirectrice de recherche

Résumé

La chalcopyrite est un sulfure de cuivre et de fer trouvé dans une grande variété de gîtes minéraux. Sa composition en éléments traces est très variable. Parmi les facteurs les plus importants qui contrôlent sa concentration en éléments traces se trouvent la structure cristalline, les coefficients de partage (chalcopyrite-liquide, chalcopyrite-minéraux qui co-cristallisent) et la composition du magma/fluide hydrothermal, lesquels reflètent les conditions physico-chimiques de l'environnement géologique de formation. Ces caractéristiques, ainsi que ses propriétés physiques, favorisent la chalcopyrite comme un potentiel minéral indicateur pour l'exploration. Avec l'objectif de déterminer les critères géochimiques permettant son utilisation comme un minéral indicateur, des échantillons appartenant à 8 types de dépôts à l'échelle mondiale, dont 2 magmatiques (sulfures à Ni-Cu et EGP lités) et 6 hydrothermaux (porphyres, sulfures massifs volcanogènes (SMV), iron-oxide-copper-gold (IOCG), skarn, or épithermal et or orogénique), ont été analysés par microsonde électronique (EPMA) et par ablation laser et spectrométrie de masse à plasma à couplage inductif (LA-ICP-MS). La composition en éléments traces de la chalcopyrite a été examinée à l'aide de méthodes statistiques pour caractériser sa variation dans les différents types de dépôts, lesquelles combinées avec l'apprentissage automatique, a permis le développement de modèles de discrimination.

Cette étude montre que la différence la plus importante dans la composition de la chalcopyrite demeure entre les systèmes magmatiques et hydrothermaux. Le Ni détermine cette différence, enrichi dans la chalcopyrite magmatique par rapport à celle hydrothermale. Dans les systèmes magmatiques (chapitre 1), les processus ayant lieu pendant la cristallisation qui exercent une influence sur certains éléments ont été identifiés. La chalcopyrite des dépôts d'EGP lités est enrichie en Se et appauvrie en Te-Sn-Bi-In, comme une conséquence des rapports élevés magma/liquide sulfuré (facteur-R) pendant la cristallisation. La cristallisation fractionnée du liquide sulfuré dans les dépôts de sulfures à Ni-Cu impacte également sur la composition en éléments traces dans la chalcopyrite. Ainsi, la chalcopyrite formée à partir d'une solution solide intermédiaire (iss), cristallisant en dernier à partir d'un liquide résiduel riche en Cu, est enrichie en éléments incompatibles (Ag-Bi-Cd-Pb-Se-Sn-Tl), par rapport à celle formée d'une solution solide de monosulfure (mss) riche en Fe. Cela constitue la base des modèles de classification supervisée par l'analyse discriminante par les moindres carrés partiels (PLS-DA) développés dans cette étude, lesquels permettent de discriminer entre les deux types de dépôts magmatiques (sulfure à Ni-Cu vs. EGP lités) et le type de minerais.

Dans les dépôts de SMV (chapitre 2), la concentration des éléments traces dans la chalcopyrite dépend de la composition (conditionnée par la roche encaissante), la température et de la nature du fluide hydrothermal. La PLS-DA indique que la composition en éléments traces de la chalcopyrite varie en fonction du sous-type lithostratigraphique. Ainsi, la chalcopyrite des SMV du sous-type ultramafique est enrichie en Ni-Co-Te, tandis que celle des SMV dans les environnements siliciclastique-felsique a des teneurs élevées en Sb-Bi-In. Dans les

SMV en contexte mafique et siliciclastique-mafique, le Pb et Mn sont, respectivement, enrichis dans la chalcopyrite, tandis que dans celle des dépôts bimodal-felsique et mafique montrent une composition similaire. Des modèles de prédiction Random Forest (RF) ont été développés, un algorithme plus adapté et performant que la PLS-DA en raison du nombre élevé de classes (types de gîtes), afin de classifier la chalcopyrite parmi les 6 contextes lithostratigraphiques des SMV.

Quatre algorithmes d'apprentissage automatique (Artificial Neural Network (ANN), RF, K-Nearest Neigbor (KNN) et Naïve Bayes (NB)) et une méthode statistique de classification supervisée (PLS-DA) sont comparés afin de classifier la chalcopyrite parmi les 8 types de dépôts (chapitre 3), dont le RF donne une performance plus élevée. Trois modèles RF ont été développés: le premier, permettant la classification entre chalcopyrite hydrothermale et magmatique; le deuxième, pour déterminer sa provenance selon le type de dépôt magmatique (sulfures à Ni-Cu vs. EGP lités); et le troisième, lequel discrimine la chalcopyrite parmi les 6 types de dépôts hydrothermaux. Ces modèles ont été testés sur des données compilées de la littérature et sur des grains analysés de chalcopyrite récupérés de sédiments de tills et eskers de la Province de Churchill (Québec, Canada), et démontre l'utilisation de la chimique de la chalcopyrite pour déterminer sa provenance aux fins d'exploration minérale.

Une importante variation des éléments traces dans la chalcopyrite est présente dans chaque type de dépôt; néanmoins, sa composition a une signature particulière selon le contexte de formation. Cela met en évidence le fort potentiel de discrimination de la source de minéralisation, démontré par les modèles de discrimination. Cette étude démontre que la chalcopyrite peut être utilisée comme un minéral indicateur et offre l'opportunité d'appliquer ces méthodes dans les sédiments en exploration minérale.

Abstract

Chalcopyrite is a Cu-Fe sulfide found in a wide diversity of mineral deposits. Its trace element composition is highly variable. The crystal structure, the partition coefficient (chalcopyrite-liquid, chalcopyrite-co-crystallizing minerals), and the composition of magma/fluid are major factors controlling the trace element content in chalcopyrite, which reflects the physicochemical conditions of geological environment of formation. These characteristics, as well as its physical properties, make chalcopyrite a potential indicator mineral for exploration. In order to determine geochemical criteria enabling the use of chalcopyrite as an indicator mineral, samples from 8 deposit types worldwide, including 2 magmatic (Ni-Cu sulfide and Reef-type PGE) and 6 hydrothermal (porphyry, volcanogenic massif sulfides (VMS), iron oxide-copper-gold (IOCG), skarn, epithermal gold and orogenic gold), were analysed by electron probe micro-analysis (EPMA) and LA-ICP-MS (laser ablation-inductively coupled plasma-mass spectrometry). The data were investigated with univariate, bivariate and multivariate statistical methods to characterise its variation in the different deposit types, which combined with the machine learning, enabled the development of discrimination models in order to determine the provenance of chalcopyrite.

This study shows that the most important difference in trace element composition of chalcopyrite is observed between magmatic and hydrothermal systems. According to our results, Ni determines this difference, with values significatively higher in chalcopyrite formed in Ni-Cu sulfide and Reef-type PGE deposits than in hydrothermal deposits.

In magmatic systems (chapter 1), the statistical analysis allowed the recognition of the processes occurring during crystallisation that affect the concentration of certain elements. In Reef-type PGE deposits, the high values of magma/sulfide liquid ratio (R-factor) during crystallisation led to Se enrichment (a strongly chalcophile element), whereas Te, Sn, Bi and In are depleted in chalcopyrite, compared to those formed in Ni-Cu sulfide deposits. Furthermore, the variation in trace elements in chalcopyrite is influenced by fractional crystallisation of sulfide liquid in Ni-Cu sulfide deposits. Thus, chalcopyrite from intermediate solid solution (iss), which crystallised from a Cu-rich residual liquid, is enriched in incompatible elements (Ag, Bi, Cd, Pb, Se, Sn and Tl) compared to chalcopyrite from an early-forming Fe-rich monosulfide solid solution (mss). These geochemical characteristics constitute the basis of the classification models with partial least squares-discriminant analysis (PLS-DA) to determine the deposit type (Ni-Cu sulfide vs. Reef-type PGE deposits) and ore type (Cu-rich vs. Fe-rich). In hydrothermal systems, the concentration of trace elements in chalcopyrite depends on hydrothermal fluid composition, which is a function of host rock composition, temperature, and nature of the fluid source. The PLS-DA results show that, in VMS deposits (chapter 2), trace elements in chalcopyrite vary in function of VMS setting, which is determined by the host rock composition. Chalcopyrite from ultramafic-hosted VMS is rich in Ni, Co and Te, whereas chalcopyrite from siliciclastic-felsic setting VMS has high values of Sb, Bi and In. Chalcopyrite from

mafic and siliciclastic-mafic settings VMS is respectively high in Pb and Mn, whereas chalcopyrite from bimodal-mafic setting has similar trace element composition to those from bimodal-felsic subtype. Random Forest classifiers were developed and were shown to be more adapted and performance than PLS-DA because of high number of classes (deposit types), in order to classify chalcopyrite according to the 6 VMS lithostratigraphic settings.

When 4 machine learning algorithms (Artificial Neural Network (ANN), Random Forest (RF), K-Nearest Neigbor (KNN) et Naïve Bayes (NB)) and a supervised classification multivariate method (PLS-DA) are compared to classify chalcopyrite according to 8 different deposit types (chapter 3), the RF model reported the highest performance. Three RF prediction models were developed. The first discriminates between magmatic and hydrothermal deposits; the second, discriminates between magmatic deposits (Ni-Cu sulfide and Reef-type PGE) and the third, discriminates between the 6 different hydrothermal deposits. These models were tested on literature data and chalcopyrite data from grains recovered from tills and eskers in Churchill Province (Québec, Canada), and demonstrate that chalcopyrite chemistry can be used to determine its provenance for mineral exploration.

Although the trace element composition of chalcopyrite shows important variability within a deposit type, the results reveal that the chalcopyrite records a characteristic signature in its chemical composition according to the ore forming environment and highlights a strong potential to discriminate the source of mineralisation, as demonstrated by the RF models. This study demonstrates that chalcopyrite could be used as an indicator mineral and provides an opportunity to apply these methods in overburden sediments for mineral exploration.

Table des matières

Résumé ii
Abstract iv
Table des matières vi
Liste des figures ix
Liste des tableaux xi
Liste des abréviations, sigles, acronymes xii
Remerciements xiv
Avant-propos xv
Introduction 1
Contexte et problématique 1
Chalcopyrite comme un minéral indicateur 1
But et Objectifs 5
Méthodologie 6
Plan de la thèse 6
References 7
Chapitre 1 Variation of trace elements in chalcopyrite from worldwide Ni-Cu sulfide and Reef-type PGE deposits: implications for mineral exploration 13
1.1 Résumé 14
1.2 Abstract 15
1.3 Introduction 16
1.4 Methodology 18
1.4.1 Sample Selection 18
1.4.2 Analytical Methods 19
1.4.3 Statistical Methods 21
1.5 Results 26
1.5.1 Petrography 26
1.5.2 Trace Elements in Chalcopyrite 28
1.5.3 Mantle-normalized Multi-Element Patterns 29
1.5.4 Multivariate Data Analysis 34
1.5.5 Distribution of Trace Elements Between Chalcopyrite and Other Sulfides 38
1.6 Discussion 41
1.6.1 Overview of Processes that Control the Variation of Trace Elements in Chalcopyrite 41
1.6.2 Trace Element Composition of Chalcopyrite as an Exploration Tool 47

1.6.3 New Discriminant Binary Diagrams 47
1.7 Conclusions 52
1.8 Acknowledgements 52
1.9 References 54
Chapitre 2 Trace element composition of chalcopyrite from volcanogenic massive sulfide deposits: variation and implications for provenance recognition 62
2.1 Résumé 63
2.2 Abstract 63
2.3 Introduction 64
2.4 Methodology 67
2.4.1 Sample Selection 67
2.4.2 Petrography 69
2.4.3 Analytical Methods 69
2.4.4 Statistical Methods 71
2.5 Results 78
2.5.1 Petrography 78
2.5.2 Trace Element Composition of Chalcopyrite 79
2.5.3 Exploratory PLS-DA 84
2.5.4 Supervised Classification and Regression with Random Forest 93
2.6 Discussion 94
2.6.1 Trace Element Composition of Chalcopyrite as a Tool to Sulfide Assemblage Recognition 96
2.6.2 Trace Element Composition of Chalcopyrite as a Tool to VMS Setting Recognition 96
2.6.3 Predicting Lithostratigraphic Setting of VMS-SMS Deposits with Random Forest (from affinity to VMS subtype) 101
2.6.4 Effects of Metamorphism on Classifier Predictions 103
2.7 Conclusions 106
2.8 Acknowledgements 107
2.9 References 108
Chapitre 3 Trace element composition of chalcopyrite as a tool for deposit type discrimination: a machine learning approach 119
3.1 Résumé 120
3.2 Abstract 121
3.3 Introduction 121
3.4 Methodology 123
3.4.1 Trace Element Dataset of Chalcopyrite 123
3.4.2 Analytical Methods 125

3.4.3 Statistical Methods 126
3.5 Results 131
3.5.1 Trace Elements in Chalcopyrite 131
3.5.2 Classifier Performances 134
3.6 Discussion 138
3.6.1 Trace Element Composition of Chalcopyrite as a Tool to Fingerprint Deposit Types 140
3.6.2 Effect of the Proportion of Censored Values and Missing Elements on Predictions 141
3.6.3 Other Factors Potentially Affecting the Predictions 143
3.6.4 Application of RF Models to Detrital Chalcopyrite from Glacial Sediments 145
3.6.5 Metamorphism and Potential Effect on Model Predictions 148
3.7 Conclusions 148
3.8 Acknowledgements 149
3.9 References 149
Conclusion générale 161
Composition en éléments traces de la chalcopyrite comme indicateur du type de dépôt magmatique 161
Les éléments traces de la chalcopyrite comme critère de discrimination de sous-types de SMV 162
Discrimination de types de dépôts avec les éléments traces de la chalcopyrite et une approche d'apprentissage automatique 163
Limitations et recommandations 166
Bibliographie 167
Annexe A 187
Annexe B 237
Annexe C 285

Liste des figures

Fig. 1. 1 Location of selected magmatic sulfide deposits in this study. Ni-Cu sulfide deposits classification according to Naldrett (2004). Generalized geologic map of the world (Chorlton, 2007). N = number of samples. 21

Fig. 1. 2 Reflected light photographs of chalcopyrite from different ore types and sulfide textures from Ni-Cu sulfide (a-l) and Reef-type PGE deposits (m-p). 27

Fig. 1. 3 Pie charts summarizing relative modal proportions (%) of major sulfides, normalized to 100% sulfide) in the analyzed samples from (a) Ni-Cu sulfide and (b) Reef-type PGE deposits. Ccp: chalcopyrite, Cbn: cubanite, Po: pyrrhotite, Py: pyrite, Pn: pentla ndite. Detailed compositions given in Annexe A1. 28

Fig. 1. 4 Boxplots showing trace elements in chalcopyrite from Ni-Cu sulfide and Reef-type PGE deposits. n: number of analyzed grains. Q1 and Q3 denote first and third quartiles, respectively. 33

Fig. 1. 5 Multi-element diagrams of chalcopyrite from Ni-Cu sulfide deposits according to ore type and sulfide textures from zoned deposits (a-f) and unzoned deposits (g-j).. 35

Fig. 1. 6 Multi-element diagram for chalcopyrite from Reef-type PGE deposits (a) and comparison with Ni-Cu sulfide deposits (b). 36

Fig. 1. 7 Preliminary PLS-DA models for trace element composition of chalcopyrite from magmatic sulfide deposits (Ni-Cu sulfide, Reef-type PGE).. 40

Fig. 1. 8 Optimized PLS-DA models for trace element composition of chalcopyrite from magmatic sulfide deposits (Ni-Cu sulfide, Reef-type PGE). 43

Fig. 1. 9 Effect of fractionation of sulfide liquid on PLS-DA in chalcopyrite from zoned deposits. 45

Fig. 1. 10 Prediction of published data on PLS-DA models. Model by deposit type (a-b) shows a high accuracy (89.6%) in classification, whereas for c and d classification is not possible between chalcopyrite Fe-rich and unzoned and moderate between Cu-rich and the remaining (61.7%). 49

Fig. 1. 11 New discriminant binary diagrams, based on PLS-DS results from this study, that could be used as complementary tools in prediction tasks in addition to PLS-DA models. 50

Fig. 1. 12 Evaluation of performance of the Se/(Te+Bi)/Se discriminant diagram by magmatic sulfide deposit type (accuracy 91.9%). 51

Fig. 2. 1 Location of selected VMS-SMS deposits in this study. Classification according to Franklin et al. (2005) and Patten et al. (2022). Generalized geologic map of the world (Chorlton, 2007). N= number of samples. ... 69

Fig. 2. 2 Reflected light micro-photographs of chalcopyrite from VMS-SMS deposits from Cu-rich (A-C) and Zn-rich (D-F) samples.. 80

Fig. 2. 3 Boxplots showing the variation of selected trace elements (in ppm) in chalcopyrite according to the geological setting of the deposit. n: number of analyses. Q1 and Q3 indicate first and third quartiles, respectively. 82

Fig. 2. 4 Binary diagrams of elements with highest Pearson correlation coefficients showing grouping in function of the geological setting of the deposit. Chalcopyrite from ultramafic deposits is separated from the remaining classes in most diagrams, in a lesser extent mafic and siliciclastic-felsic subtypes. clr: centered-log transformation; r: Pearson correlation coefficient; p: p-value. 83

Fig. 2. 5 Binary diagrams by deposit showing differences between chalcopyrite in function of ccp/(ccp+sp) ratio and ore type. Dashed lines show approximately limits between groups. 84

Fig. 2. 6 PLS-DA on trace elements in chalcopyrite by geological setting of the deposit..... 91

Fig. 2. 7 Metamorphic grades of samples projected on PLS-DA results according to lithotectonic settings..... 92

Fig. 2. 8 The ccp/(ccp+sp) ratio of the samples projected on PLS-DA results, showing that sulfide proportions have no impact on grouping according to lithotectonic settings..... 95

Fig. 2. 9 PLS-DA on trace elements in chalcopyrite from bimodal-mafic (A, B), bimodal-felsic (C, D) and siliciclastic-felsic deposits (E, F) according to ccp/(ccp+sp) ratio. In bold-italic trimmed means of chalcopyrite-sphalerite proportion of each group delineated by the dotted lines..... 97

Fig. 2. 10 Variable importance measures of the optimal elements after recursive feature elimination for the (A) RFmodel.01 (affinity), (B) RFmodel.02-A (mafic-ultramafic-siliciclastic mafic), and (C) RFmodel.02-B (bimodal mafic-bimodal felsic). MDA: Mean Decrease in Accuracy; GINI: Gini index; MDA+GINI: total scores. 98

Fig. 2. 11 Random Forest regression model results for chalcopyrite from bimodal-mafic (A, B), bimodal-felsic (C, D) and siliciclastic-felsic (E, F) settings..... 100

Figure 3. 1 Location of selected deposits. Generalized geologic map of the world (Chorlton, 2007). N= number of samples for this study (number of samples from literature in brackets)..... 124

Figure 3. 2 Boxplots showing the variation of selected trace elements (in ppm) in chalcopyrite according to the deposit type. 132

Figure 3. 3 Binary diagrams showing data points of chalcopyrite (left) and density binary plot using centred-log-ratio (clr) values (right) for elements that best show a marked difference between chalcopyrite from magmatic and hydrothermal deposits..... 133

Figure 3. 4 Ternary diagrams of trace element composition of chalcopyrite (left) and data density ternary diagrams (right) showing the relative proportion amongst Ni-Sb-Co (A-B), Ni-Ga-In (C-D), Ni-Cd-Se (E-F). Data is centred to geometric mean (c) and standardised to the total variance (superscript)..... 135

Figure 3. 5 Multi-element diagrams, normalized to primitive mantle of chalcopyrite from magmatic deposits (A) (after Caraballo et al., 2022), hydrothermal deposits (B) and comparison of medians for both classes (C).. . 136

Figure 3. 6 Performances on training and test data of supervised classification algorithms with transformed data (Yeo-Johnson). 137

Figure 3. 7 Variable importance coefficients according to Gini index. A) RF model to discriminate between chalcopyrite from magmatic and hydrothermal deposits, and B) RF model to discriminate chalcopyrite according to magmatic deposit type, and C) RF model to discriminate chalcopyrite according to hydrothermal deposit type. 138

Figure 3. 8 Predictions of blind chalcopyrite data using RF mag-hyd model. 142

Figure 3. 9 Predictions of blind chalcopyrite data using RF mag model. 144

Figure 3. 10 Predictions of blind chalcopyrite data using RF hyd model. 145

Figure 3. 11 Application of the three RF models on data of detrital chalcopyrite grains (n=630; Duran et al., 2019) from glacial sediment and eskers overlying the Churchill Province, Canada..... 147

Liste des tableaux

Table 1. 1 Summary of studied magmatic sulfide deposits in this study (details of sulfide textures and opaque mineralogy in Annexe A1). 25

Table 1. 2 Summary of selected trace element composition (ppm) of chalcopyrite from Ni-Cu sulfide and Reef-type PGE deposits used for multivariate statistical analysis. 30

Table 2. 1 Summary of studied VMS and SMS deposits (details of sulfide textures and opaque mineralogy in Annexe B1) 72

Table 2. 2 Summary of selected trace elements (ppm) in chalcopyrite from volcanogenic massive deposits used for multivariate statistical analysis and machine learning. 87

Table 2. 3 Classification performance estimators of the Random Forest models. 93

Table 2. 4 Confusion matrix and performance estimators for RFmodel.01 on test data. 94

Table 2. 5 Confusion matrix and performance estimators for RFmodel.02-A on test data. 94

Table 2. 6 Confusion matrix and performance estimators for RFmodel.02-B on test data. 95

Table 2. 7 Results of the predictions of literature data with all elements required by the RF models. 102

Table 2. 8 Results of the predictions of literature data with missing elements using RF models. 104

Liste des abréviations, sigles, acronymes

EPMA: Electron probe microanalyzer

LA-ICP-MS: Laser ablation-inductively coupled plasma-mass spectrometry

ppm: parts-per million

SEM: Scanning electron microprobe

VMS: Volcanogenic massive sulfide

SMV: Sulfures massifs volcanogènes

IOCG: Iron Oxide Copper Gold

PGE: Platinum Group Elements

EGP: Éléments du groupe du platine

Ccp : chalcopyrite

Cbn : cubanite

Sp: sphalerite

Pn: pentlandite

Po: pyrrhotite

Mag: magnetite

RF: Random Forest

ANN: Artificial Neural Network

KNN: K-Nearest Neighbors

NB: Naive Bayes

PLS-DA: Partial least squares discriminant analysis

PCA: Principal component analysis

Si tu tombes n-fois, lève-toi n+1

Remerciements

Ce doctorat représente beaucoup plus qu'une étape professionnelle et académique pour moi, laquelle un effort titanesque, du point de vue psychologique, a été nécessaire pendant des années. Ce doctorat représente un changement de vie (pour le mieux évidement) avec des très gros sacrifices oui, mais pour le mieux. Voilà l'impact qui a eu ce projet sur moi et mon entourage, ce n'est pas juste un diplôme.

Merci Georges. Ce courriel que tu m'as envoyé l'été 2017 pour une entrevue a été le départ de ce long voyage. Merci pour ta confiance, ta patience, ton soutien et merci pour ton empathie pendant les moments difficiles. Mille merci pour ton soutien académique.

Thank you, Sarah. Thank you for your invaluable academic support, your confidence, and thank you very much for your empathy in the hardest moments. Thank you for your patience and for make me write better in English.

Merci Dominique Genna pour ton précieux soutien et ta disposition de transmettre tes connaissances pour le deuxième article. Merci Jorge Relvas, Sven Pettersen et Stephen Piercey pour vos précieux commentaires et m'aider à élever la qualité du deuxième article.

Merci Josée. Merci pour m'avoir permis d'être ton assistant d'enseignement en minéralogie appliquée pendant ces années. Merci pour ta confiance et pour l'opportunité de faire à nouveau ce que j'aime le plus, enseigner la minéralogie optique. Cela a été un véritable plaisir.

Merci à ceux qui ont, d'une façon ou autre, contribué à faire de ce voyage un peu plus 'facile' : Simon, Alexandre, Haiming, Ana, Edmond, FX, Victor, etc. Juste une petite conversation était suffisante pour se déconnecter de temps en temps.

Merci Iliana, merci ma famille, merci mes amis vénézuéliens. Il n'y a pas assez de mots de remerciement pour eux. Sin ellos no sería quien soy.

Avant-propos

Ce doctorat a eu comme résultat les articles scientifiques suivants :

Article 1: Premier auteur, intitulé *Variation of trace elements in chalcopyrite from worldwide Ni-Cu sulfide and Reef-type PGE deposits: implications for mineral exploration*: Mineralium Deposita, v. 57, p. 1293-1321. Accepté le 25 décembre 2021 et publié le 5 avril 2022, par *Enzo Caraballo, Sarah Dare, and Georges Beaudoin.* Cet article présente l'étude et comparaison de la composition en éléments traces et sa variation de la chalcopyrite provenant des dépôts de sulfure magmatiques à Ni-Cu et EGP lités, en utilisant des méthodes statistiques univariées et bivariées, ainsi que le développement d'un modèle de classification supervisée par l'analyse discriminante des moindre carrés partiels (PSL-DA). Ma contribution: 1. collecte des échantillons dans la collection de minéraux du département de géologie et génie géologique de l'Université Laval et à travers de la collaboration de plusieurs collègues au Canada et à l'international; 2. Préparation des échantillons (coupe en bloc) pour l'élaboration des lames et sections polies, 3. Analyse minéralogique des échantillons par microscopie optique et chimique des grains de chalcopyrite par microsonde électronique, microscope électronique à balayage et LA-ICP-MS; 4. Analyse des données géochimiques avec des méthodes statistiques multivariées et le développement de modèles de prédiction; et 5. Rédaction.

Article 2: Premier auteur, intitulé *Trace element composition of chalcopyrite from volcanogenic massive sulfide deposits: variation and implications for provenance recognition*, par *Enzo Caraballo, Georges Beaudoin, Sarah Dare, Dominique Genna, Sven Petersen, Jorge Relvas, Stephen Piercey*. Cet article, accepté le 5 avril 2023 dans Economic Geology, présente l'étude et la comparaison de la composition en éléments traces de la chalcopyrite entre les subtypes de dépôts de sulfure massifs volcanogènes (SMV) en utilisant PLS-DA et propose un modèle de classification Random Forest (RF). Ma contribution: 1. collecte des échantillons dans la collection de minéraux du département de géologie et génie géologique de l'Université Laval et à travers de la collaboration de plusieurs collègues au Canada et à l'international; 2. Préparation des échantillons (coupe en bloc) pour l'élaboration des lames et sections polies, 3. Analyse minéralogique des échantillons par microscopie optique et chimique des grains de chalcopyrite par microsonde électronique, microscope électronique à balayage et LA-ICP-MS; 4. Analyse des données géochimiques avec des méthodes statistiques multivariées et le développement de modèles de prédiction avec apprentissage automatique; et 5. Rédaction.

Article 3: Premier auteur, intitulé *Trace element composition of chalcopyrite as a tool for deposit type discrimination: a machine learning approach*, par *Enzo Caraballo, Georges Beaudoin, Sarah Dare, 2022*. Dans cet article (soumis le 25 mai 2023 dans Journal of Geochemical Exploration), la variation de la composition en éléments traces de la chalcopyrite, provenant de 8 types de dépôts, est étudiée avec une approche d'apprentissage automatique, et présente une comparaison de plusieurs algorithmes dans le but de déterminer

le plus adapté afin prédire le type de dépôt. Ma contribution: 1. collecte des échantillons dans la collection de minéraux du département de géologie et génie géologique de l'Université Laval et à travers de la collaboration de plusieurs collègues au Canada et à l'international; 2. Préparation des échantillons (coupe en bloc) pour l'élaboration des lames et sections polies, 3. Analyse minéralogique des échantillons par microscopie optique et chimique des grains de chalcopyrite par microsonde électronique, microscope électronique à balayage et LA-ICP-MS; 4. Analyse des données géochimiques avec des méthodes statistiques multivariées et le développement de modèles de prédiction en utilisant l'apprentissage automatique; et 5. Rédaction.

Introduction

Contexte et problématique

La chalcopyrite se forme, soit comme un constituant mineur ou majeur, dans une grande diversité de dépôt, dans des systèmes magmatiques (sulfure à Ni-Cu-EGP) et hydrothermaux (SMV, porphyre, IOCG, skarn, or épithermal, or orogénique, sulfures massifs exhalatifs-sédimentaires (SEDEX) et lits rouges). La composition en éléments traces de la chalcopyrite est très variable et reflète les conditions physico-chimiques de l'environnement géologique de formation, et parmi les facteurs qui contrôlent cette variabilité se trouvent: a) la structure cristalline, b) les coefficients de partage (entre la chalcopyrite et le liquide, et les minéraux qui co-cristallisent), c) la composition chimique du magma ou fluide hydrothermal, et d) la nature du fluide hydrothermal.

Plusieurs études sur les éléments traces dans la chalcopyrite, avec une approche métallogénique et petrogénetique, ont montré que sa composition est fortement variable, soit dans des systèmes magmatiques (Barnes et al., 2006; Barnes et al., 2008; Caraballo et al., 2022; Chen et al., 2015; Czamanske et al., 1992; Dare et al., 2014; Dare et al., 2010b; Dare et al., 2010a, 2011; Djon and Barnes, 2012; Duran et al., 2016b; Godel and Barnes, 2008; Godel et al., 2007; Holwell and McDonald, 2007; Mansur et al., 2020; Marfin et al., 2020; Piña et al., 2012a), soit dans des systèmes hydrothermaux (Agangi et al., 2018; Bajwah et al., 1987; Butler and Nesbitt, 1999; Cabri et al., 1985; Chowdhury et al., 2020; Cook et al., 2011; George et al., 2016; George et al., 2018b; Harris et al., 1984; Hawley and Nichol, 1961a; Huston et al., 1995; Kase, 1987; Martin et al., 2019; Martin et al., 2018; Maslennikov et al., 2009a; Maslennikov et al., 2009b; Moggi-Cecchi et al., 2002; Reich et al., 2013b; Reich et al., 2020; Rose, 1967; Wang et al., 2015; Wohlgemuth-Ueberwasser et al., 2015; Xie et al., 2020; Yang et al., 2022; Yano, 2012; Yuan et al., 2018; Zhao et al., 2020; Zhao et al., 2021a). Cette variabilité pourrait potentiellement être utilisée aux fins d'identification du type de dépôt pour l'exploration (Bédard et al., 2017; Caraballo et al., 2022; Duran et al., 2019a; Goulet, 2016; Mansur et al., 2021).

Bien que des études sur les éléments traces et leur variabilité en fonction du type de gîte aient été menées sur plusieurs sulfures, il n'existe pas suffisamment d'information concernant la chalcopyrite pour évaluer sa capacité en tant que discriminateur génétique des différents environnements métallogéniques. Donc, la question demeure dans le fait d'examiner la capacité de ce minéral comme un indicateur de type de dépôts à partir de sa composition chimique.

Chalcopyrite comme un minéral indicateur

Un minéral indicateur, lorsqu'il est trouvé dans les sédiments, fourni des informations de la présence d'un type de minéralisation, d'une altération hydrothermale, ou une lithologie, alors que l'étude de ses caractéristiques morphologiques, texturales et géochimiques pourrait apporter de l'information concernant le transport, distance

et nature de la minéralisation (McClenaghan, 2005). Parmi les conditions nécessaires pour considérer un minéral comme un minéral indicateur se trouvent : a) une gravité spécifique relativement élevée (G.E.>3.2) qui permet une concentration par densité, b) des caractéristiques visuelles distinctives (couleur, habitus) avec une taille minimale autour de 0.25 mm pour une récupération efficace dans des échantillons de sédiments (e.g., till, fluviatiles, sols), c) une résistance relativement élevée à la météorisation en surface (e.g., oxydation) et au transport, d) bonne capacité à héberger des éléments chimiques sensibles aux changements dans les environnements de formation (Averill, 2001; Averill, 2011b; McClenaghan, 2005). La chalcopyrite réunie toutes les caractéristiques nécessaires pour être considérée comme un minéral indicateur. Avec une gravité spécifique de 4.1-4.3, la chalcopyrite est facilement récupérable par densité, et ses propriétés visuelles permettent la reconnaître facilement par microscope optique et loupe (e.g., couleur jaune, faible clivage), en comparaison avec les autres sulfures (pyrite, pentlandite, pyrrhotite, etc.).

Les mécanismes de dissolution des sulfures ont été amplement étudiées dans le domaine de la métallurgie (extraction de métaux, hydrométallurgie) et de l'environnement (pollution par drainage acide). L'exploitation de sulfures, le traitement de minerais, et les déchets métallurgiques sont connus comme les sources de pollution industrielle les plus dangereuses pour l'environnement (Chanturiya et al., 2022). La chalcopyrite se trouve parmi les sulfures les plus résistants à la dissolution, et plusieurs hypothèses ont été proposées afin d'expliquer les mécanismes qui conduisent à une lente cinétique de lixiviation. Rimstidt et al. (1993) comparent les taux de réaction de la galène, la sphalérite, la chalcopyrite et l'arsénopyrite en présence de Fe^{3+} dans des conditions similaires à celles trouvées dans les sites de météorisation de dépôts de sulfures. La dissolution d'un minéral nécessite la suppression d'électrons des orbitales de liaison par un oxydant en solution, dans ce cas le Fe^{3+}, lequel provient de l'oxydation du Fe^{2+}, mis en solution par la dissolution de minéraux tels que la pyrite, la pyrrhotite, les silicates, les oxydes et/ou les carbonates de fer (Crundwell et al., 2021; Rimstidt et al., 1993). Dans son étude, Rimstidt et al. (1993) concluent que la chalcopyrite registre les taux de réaction les plus faibles par rapport les autres sulfures analysés.

La résistance à la dissolution de la chalcopyrite est souvent expliquée par la formation d'une couche stable sur la surface pendant sa lixiviation (passivation layer), constituée principalement par du soufre (S_0), disulfure (S_2^{2-}), polysulfure (S_n^{2-}), CuS_2, CuS, Cu_5FeS_4, jarosite, oxydes, et/ou hydroxydes, laquelle pourrait avoir un effet « protecteur » qui réduit la cinétique de la lixiviation (Chanturiya et al., 2022; Tian et al., 2021). Néanmoins, d'autres modèles de dissolution sont proposés basés sur la structure électronique des sulfures (Crundwell, 1988, 2021; Crundwell et al., 2021; O'Connor and Eksteen, 2020). Crundwell (2021) propose, basé sur la structure électronique de la bande supérieure de valence, une liste de certains sulfures organisée selon la résistance à la dissolution, dont la chalcopyrite se trouve parmi les plus résistants, à cause de sa structure de semiconducteur avec des bandes de valence non-liants (Tableau 2).

Tableau 1. Comparaison de la résistance à la dissolution et la stabilité pami les sulfures les plus communs.

Resistance[1]	Stabilité[2]	Minéral	Formule
	Très instable	Pentlandite	$(Ni,Fe)_9S_8$
	Très instable	Millérite	NiS
	Très instable	Sulfures d'EGP	
Moins résistant	Très instable	Pyrrhotite	$Fe_{1-x}S$
		Chalcocite	Cu_2S
		Covellite	CuS
		Bornite	Cu_5FeS_4
		Galène	PbS
		Arsenopyrite	FeAsS
		Sphalérite	(Zn,Fe)S
	Instable	Pyrite	FeS_2
		Marcasite	FeS_2
	Marginalement stable	Chalcopyrite	$CuFeS_2$
		Enargite	Cu_3AsS_4
Plus résistant		Molybdenite	MoS_2

[1]D'après Crundwell (2022). [2]D'après Averill (2011)

Le potentiel de la chalcopyrite comme un minéral indicateur a été mis en valeur avec l'étude de la fraction de minéraux lourds de sédiments superficiels en environnement glaciaire. Averill (2001) remarque que la chalcopyrite est un bon minéral indicateur de dépôts de sulfures massifs, tels que SMV, skarn et Ni-Cu-EGP, indiquant que ce minéral est nominalement stable dans des sédiments superficiels. Averill (2011b) indique que la chalcopyrite peut être utilisée comme un minéral indicateur, car une proportion élevée de grains survit dans de conditions glaciales à tropicales humides, ce qui place la chalcopyrite comme marginalement stable dans une échelle relative (Tableau 2). Hashmi et al. (2015a) démontrent que l'étude de la composition de sédiments de tills au Mont Polley, Colombie Britannique, peut être utilisée pour détecter la minéralisation de porphyres à Cu-Au sous la couverture de sédiments glaciaires, principalement par la présence de minéraux indicateurs comme la chalcopyrite. Plouffe et al. (2016) montre dans son étude sur la géochimie et minéralogie des tills en Colombie Britannique, que la distribution de la concentration de Cu et des grains de chalcopyrite dans les tills est dérive de l'érosion de minéralisations de porphyres à Cu. Plouffe et al. (2022) montrent des anomalies de chalcopyrite avec une extension de 30 km^2 dans les sédiments de tills associées au dépôt de porphyre à Cu-Mo de Gibraltar (Colombie-Britannique). Duran et al. (2019a) analysent la composition en éléments traces de 639 grains de chalcopyrite récupérés de sédiments de tills et eskers provenant de la Province de Churchill (Québec, Canada). Cette étude, laquelle comprend une superficie de 31 250 km^2, a révélé une présence moyenne de 1-61 grains de pyrite et chalcopyrite ± sulfarséniques dans chaque échantillon, ce qui confirme son potentiel comme minéral indicateur.

La chalcopyrite possède une structure dérivée de celle de la sphalérite, dans laquelle le Fe et le Cu occupent des interstices tétraédriques (Vaughan, 2006). Un des facteurs qui peut contrôler l'incorporation de certains

éléments traces dans la structure cristalline de la chalcopyrite est leur état d'oxydation et leur rayon ionique (Figure 1). George et al. (2018b) indiquent que cette incorporation est plus complexe dans ce minéral par rapport les autres sulfures, particulièrement la galène et la sphalérite. La température peut également contrôler l'incorporation des éléments traces dans la structure cristalline. Kojima and Sugaki (1985), dans leur étude sur les relations de phases dans le système Cu-Fe-Zn-S entre 500° et 300°C sous conditions hydrothermales, déterminent que la chalcopyrite peut dissoudre jusqu'à 0,9 % de Zn à 500°C, 0,8 % à 400°C et 0,6 % à 300°C. Cela pourrait suggérer qu'à haute température la structure subi une dilatation thermique, permettant l'incorporation d'ions plus grands.

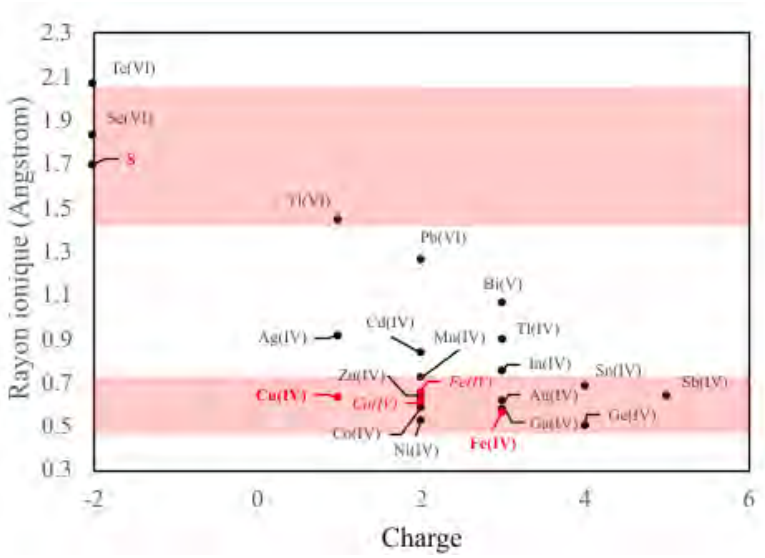

Figure 1. Rayon ionique des éléments traces trouvés fréquemment dans la chalcopyrite. Entre parenthèse le numéro de coordination. En rouge gras : Cu et Fe dans la chalcopyrite d'après Pearce et al. (2006), en rouge italique : Cu et Fe dans la chalcopyrite d'après Todd et al. (2003) et Mikhlin et al. (2005). Modifié de George et al. (2018b).

À la différence d'autres sulfures (e.g., sphalérite et galène), la chalcopyrite forme des liens essentiellement covalents (Hall and Stewart, 1973), et il n'y a pas un consensus sur l'état d'oxydation du Cu et du Fe. Todd et al. (2003) et Mikhlin et al. (2005) signalent que l'état d'oxydation dans la chalcopyrite est $Cu^{2+}Fe^{2+}S_2$. Cependant, Pearce et al. (2006) montrent, sur la base de données XPS (spectrométrie de photoémission de rayons X) et XAS (spectroscopie d'absorption de rayons X) que le Cu est principalement monovalent et le Fe trivalent ($Cu^{+}Fe^{3+}S_2$). Ces derniers auteurs indiquent que le Cu^{2+} dans les sulfures est très rare et suggèrent que la présence de pics à 931.0 eV (indiquant du Cu bivalent) dans les spectres peut être expliquée par la contamination de phases minérales avec du Cu^{2+} ($CuFeS_2$, CuS et CuO). Goh et al. (2006) concluent, à partir des analyses NEXAFS (spectroscopie de structure fine près du front d'absorption de rayons X), qu'il n'y a pas d'évidence pour représenter la chalcopyrite comme $Cu^{2+}Fe^{2+}S_2^{2-}$. Également, une discussion existe encore sur l'état d'oxydation du fer (Fe^{2+} ou Fe^{3+}). Néanmoins, la substitution des éléments traces dans la chalcopyrite semble être restreinte à des ions avec des valeurs entre 1+ et 4+. Aucune étude portant sur les états d'oxydation

du fer et du cuivre dans la chalcopyrite n'a eu une approche pratique qui considère une relation avec les conditions de formation, et en conséquence, les types de gîtes.

Plusieurs études sur la chalcopyrite en tant que minéral indicateur ont été réalisées (Bédard et al., 2017; Duran et al., 2019a; George et al., 2018b; Goulet, 2016; Mansur et al., 2021; Marfin et al., 2020), dont la majorité a développé de diagrammes discriminatoires empiriques (Duran et al., 2019a; George et al., 2018b; Goulet, 2016; Mansur et al., 2021). Celles réalisées avec une approche statistique multivariée sont rares, telle que l'analyse en composantes principales (Bédard et al., 2017) ou l'analyse de regroupement (Marfin et al., 2020). Bédard et al. (2017), à partir d'une analyse en composantes principales (ACP) sur la composition en éléments traces de la chalcopyrite, démontrent le potentiel de ce minéral pour déterminer le type de dépôt. Ils ont montré que certains éléments ont de signatures spécifiques dans les dépôts SMV (Ag, Sn, Zn et Se), Ni-Cu-EGP (Ni, Te et Pd), or orogénique et lits rouges (Au et As), porphyres et skarn (Sb, In et Se) et IOCG (Zn et Ba). Par ailleurs, Marfin et al. (2020) dans une étude réalisée au dépôt de sulfures à Ni-Cu à Oktyabrsk (Noril'sk, Russie), développent un modèle de classification de la chalcopyrite en fonction du type de minerais (massif, disséminé et veinules-disséminé), basé sur une analyse de regroupement (cluster analysis). Néanmoins, des études avec une approche d'apprentissage automatique sont absentes. Ce doctorat présente les premières études sur la composition en éléments traces de la chalcopyrite en utilisant cette approche, principalement le Random Forest.

But et Objectifs

Ce doctorat vise à évaluer la chalcopyrite comme un minéral indicateur et à développer une méthodologie permettant la discrimination des différents types de dépôts en utilisant sa composition en éléments traces. Les objectifs spécifiques sont:

1. Déterminer la composition en éléments majeurs et traces dans la chalcopyrite provenant de plusieurs dépôts représentatifs à l'échelle mondiale.
2. Caractériser les associations minérales (texture, proportions, morphologie) et examiner leur potentiel contrôle sur la composition de la chalcopyrite.
3. Caractériser la composition chimique de la chalcopyrite dans les dépôts de sulfure à Ni-Cu et EGP-lités et évaluer son potentiel comme un minéral indicateur pour discriminer entre ces deux types dépôts et sa variation en fonction de la cristallisation fractionnée (Ni-Cu), en utilisant des méthodes d'analyse statistiques multivariées (PLS-DA) combinée avec la compréhension des processus qui contrôlent la concentration des éléments traces de la chalcopyrite.
4. Étudier la variation de la composition en éléments traces de la chalcopyrite dans les dépôts de sulfures massifs volcanogènes (SMV), établir des critères compositionnels qui permettent la discrimination

parmi les 6 types de SMV en utilisant des méthodes d'analyse statistiques multivariées et développer un modèle de discrimination avec Random Forest.

5. Déterminer le modèle d'apprentissage automatique le plus adapté pour prédire la source de la chalcopyrite parmi 8 types de dépôts (Ni-Cu, EGP-lités, SMV, porphyres, skarn, IOCG, or orogénique et or épithermal) en utilisant les éléments traces.

Méthodologie

La méthodologie a consisté en 3 parties fondamentales : 1) l'analyse minéralogique et la description pétrographique des échantillons par des techniques de microscopie optique à lumière réfléchie et par microscope électronique à balayage (MEB); 2) l'analyse des éléments majeurs par microsonde électronique (EPMA) et les éléments traces par ablation laser et spectrométrie de masse à plasma à couplage inductif (LA-ICP-MS), respectivement; et 3) l'analyse de la base des données géochimiques par des méthodes d'analyses classique, univariées et bivariées, le développement de modèles prédictifs de discrimination avec le PLS-DA et Random Forest, et comparaison avec d'autres méthodes d'apprentissage automatique.

Avant l'analyse statistique des éléments traces, les variables avec plus de 40% de valeurs censurées (<limite de détection) ont été retirées de la base des données. Les valeurs censurées ont été imputées par l'algorithme log-ratio Expectation-Maximisation (lrEM) avec zComposition de R (Palarea-Albaladejo and Martín-Fernández, 2015). Les valeurs censurées des analyses de chalcopyrite de la littérature faisant partie de la base des données utilisée dans les modèles pour prédire la provenance parmi les 8 types de dépôts, ont été imputées avec l'algorithme missForest (Stekhoven and Bühlmann, 2012). Pour les analyses statistiques bivariées, l'analyse de corrélation et le PLS-DA, les données ont été transformées avec le centered log-ratio procedure (Egozcue and Pawlowsky-Glahn, 2011; Filzmoser et al., 2009; Pawlowsky-Glahn and Buccianti, 2011) afin d'éviter des fausses corrélations entre les variables. Le PLS-DA a été utilisée pour identifier des regroupements en fonction du type de dépôt et pour déterminer l'importance des variables pour la classification. Dans les contextes avec 4 classes ou plus, l'apprentissage automatique a été utilisée afin de développer des modèles de prédiction en fonction du type de dépôt, particulièrement le Random Forest. D'autres algorithmes ont été testés, tels que le ANN (Artificial Neural Network), KNN (K-Nearest Neighbors) et NB (Naïves Bayes).

Plan de la thèse

Cette thèse présente les résultats de cette recherche, laquelle est constituée par une introduction générale, trois chapitres correspondant aux articles scientifiques, une discussion et une conclusion générale.

Le chapitre 1 (Caraballo et al., 2022) décrit les résultats de l'étude de la composition en éléments traces de la chalcopyrite dans des dépôts magmatiques de sulfures à Ni-Cu et EGP lités. Ce chapitre présent une analyse

statistique exploratoire des données et une caractérisation en fonction du type de dépôt (Ni-Cu et EGP lités) et du type minerais (riche en Cu et riche en Fe). Finalement deux modèles de classification PLS-DA sont proposés comme des outils pour déterminer la provenance de la chalcopyrite selon le type de dépôt et le type de minerais.

Le chapitre 2 (Caraballo et al., 2023 in press) montre la caractérisation de la composition chimique de la chalcopyrite dans les dépôts SMV. Ce chapitre présente les résultats de l'analyse statistique univariée, bivariée et multivariée sur la base de données des éléments traces dans la chalcopyrite, avec une description de sa variabilité en fonction du soustype de SMV. Pour la première fois, une approche d'apprentissage automatique est réalisée, spécifiquement le développement des modèles de prédiction Random Forest afin de discriminer parmi les 6 soustypes de SMV (ultramafique, mafique, bimodal-mafique, bimodal-felsic, siliciclastique-mafique et siliciclastique-felsique).

Le chapitre 3 montre une analyse de la composition en éléments traces de la chalcopyrite exclusivement avec une approche d'apprentissage automatique, afin de déterminer l'algorithme le plus adapté pour déterminer la provenance parmi 8 types de dépôts (magmatiques et hydrothermaux). Une comparaison de 4 algorithmes d'apprentissage automatique (Random Forest, Artificial Neural Network, K-Nearest Neighbor et Naïve Bayes) et une méthode statistique multivariée (PLS-DA) est faite. Finalement, ce chapitre présente une application sur des grains analysés de chalcopyrite (Duran et al. 2019) récupérés de sédiments de tills et eskers de la Province de Churchill (Québec, Canada), et démontre l'utilisation de la chimique de la chalcopyrite pour déterminer la provenance de sédiments aux fins d'exploration minérale.

References

Agangi, A., Reddy, S., Plavsa, D., Vieru, C., Selvaraja, V., LaFlamme, C., Jeon, H., Martin, L., Nozaki, T., and Takaya, Y., 2018, Subsurface deposition of Cu-rich massive sulphide underneath a Palaeoproterozoic seafloor hydrothermal system—the Red Bore prospect, Western Australia: Mineralium Deposita, p. 1-18.

Averill, S. A., 2001, The application of heavy indicator mineralogy in mineral exploration with emphasis on base metal indicators in glaciated metamorphic and plutonic terrains: Geological Society, London, Special Publications, v. 185, p. 69-81.

Averill, S. A., 2011, Viable indicator minerals in surficial sediments for two major base metal deposit types: Ni-Cu-PGE and porphyry Cu: Geochemistry: Exploration, Environment, Analysis, v. 11, p. 279-291.

Bajwah, Z. U., Seccombe, P. K., and Offler, R., 1987, Trace element distribution, Co: Ni ratios and genesis of the Big Cadia iron-copper deposit, New South Wales, Australia: Mineralium Deposita, v. 22, p. 292-300.

Barnes, S.-J., Cox, R. A., and Zientek, M. L., 2006, Platinum-group element, gold, silver and base metal distribution in compositionally zoned sulfide droplets from the Medvezky Creek Mine, Noril'sk, Russia: Contributions to Mineralogy and Petrology, v. 152, p. 187-200.

Barnes, S.-J., Prichard, H. M., Cox, R. A., Fisher, P. C., and Godel, B., 2008, The location of the chalcophile and siderophile elements in platinum-group element ore deposits (a textural, microbeam and whole

rock geochemical study): Implications for the formation of the deposits: Chemical Geology, v. 248, p. 295-317.

Bédard, É., Goulet, A., Sappin, A.-A., Makvandi, S., and Beaudoin, G., 2017, Chalcopyrite as an indicator mineral to fingerprint mineral deposit types: a preliminary study: Mineral Resources to Discover-Proceedings of the 14th SGA Biennial Meeting, Québec City, Canada, 2017, p. 1115-1118.

Butler, I. B., and Nesbitt, R. W., 1999, Trace element distributions in the chalcopyrite wall of a black smoker chimney: insights from laser ablation inductively coupled plasma mass spectrometry (LA–ICP–MS): Earth and Planetary Science Letters, v. 167, p. 335-345.

Cabri, L. J., Campbell, J. L., Laflamme, J. H. G., Leigh, R. G., Maxwell, J. A., and Scott, J. D., 1985, Proton-microprobe analysis of trace elements in sulfides from some massive-sulfide deposits: The Canadian Mineralogist, v. 23, p. 133-148.

Caraballo, E., Dare, S., and Beaudoin, G., 2022, Variation of trace elements in chalcopyrite from worldwide Ni-Cu sulfide and Reef-type PGE deposits: implications for mineral exploration: Mineralium Deposita, v. 57, p. 1293-1321.

Chanturiya, V. A., Krasavtseva, E. A., and Makarov, D. V., 2022, Electrochemistry of Sulfides: Process and Environmental Aspects: Sustainability, v. 14, p. 11285.

Chen, L.-M., Song, X.-Y., Danyushevsky, L. V., Wang, Y.-S., Tian, Y.-L., and Xiao, J.-F., 2015, A laser ablation ICP-MS study of platinum-group and chalcophile elements in base metal sulfide minerals of the Jinchuan Ni–Cu sulfide deposit, NW China: Ore Geology Reviews, v. 65, p. 955-967.

Chowdhury, S., Pal, D. C., Papineau, D., and Lentz, D. R., 2020, Major and trace element and multiple sulfur isotope composition of sulfides from the Paleoproterozoic Surda copper deposit, Singhbhum shear Zone, India: Implications for the mineralization processes: Ore Geology Reviews, v. 120, p. 103396.

Cook, N. J., Ciobanu, C. L., Danyushevsky, L. V., and Gilbert, S., 2011, Minor and trace elements in bornite and associated Cu–(Fe)-sulfides: A LA-ICP-MS studyBornite mineral chemistry: Geochimica et Cosmochimica Acta, v. 75, p. 6473-6496.

Crundwell, F. K., 1988, The influence of the electronic structure of solids on the anodic dissolution and leaching of semiconducting sulphide minerals: Hydrometallurgy, v. 21, p. 155-190.

Crundwell, F. K., 2021, The impact of light on understanding the mechanism of dissolution and leaching of sphalerite (ZnS), pyrite (FeS2) and chalcopyrite (CuFeS2): Minerals Engineering, v. 161, p. 106728.

Crundwell, F. K., Bryson, L. J., van Aswegen, A., and Knights, B. D. H., 2021, Effect of chopped light on the dissolution and leaching of chalcopyrite: Minerals Engineering, v. 160, p. 106703.

Czamanske, G. K., Kunilov, V. E., Zientek, M. L., Cabri, L. J., Likhachev, A. P., Calk, L. C., and Oscarson, R. L., 1992, A proton microprobe study of magmatic sulfide ores from the Noril'sk-Talnakh District, Siberia: The Canadian Mineralogist, v. 30, p. 249-287.

Dare, S. A., Barnes, S.-J., Prichard, H. M., and Fisher, P. C., 2014, Mineralogy and geochemistry of Cu-rich ores from the McCreedy East Ni-Cu-PGE deposit (Sudbury, Canada): implications for the behavior of platinum group and chalcophile elements at the end of crystallization of a sulfide liquid: Economic Geology, v. 109, p. 343-366.

Dare, S. A. S., Barnes, S.-J., and Prichard, H. M., 2010b, The distribution of platinum group elements (PGE) and other chalcophile elements among sulfides from the Creighton Ni–Cu–PGE sulfide deposit, Sudbury, Canada, and the origin of palladium in pentlandite: Mineralium Deposita, v. 45, p. 765-793.

Dare, S. A. S., Barnes, S.-J., Prichard, H. M., and Fisher, P. C., 2010a, The timing and formation of platinum-group minerals from the Creighton Ni-Cu-platinum-group element sulfide deposit, Sudbury, Canada: Early crystallization of PGE-rich sulfarsenides: Economic Geology, v. 105, p. 1071-1096.

Dare, S. A. S., Barnes, S.-J., Prichard, H. M., and Fisher, P. C., 2011, Chalcophile and platinum-group element (PGE) concentrations in the sulfide minerals from the McCreedy East deposit, Sudbury, Canada, and the origin of PGE in pyrite: Mineralium Deposita, v. 46, p. 381-407.

Djon, M. L. N., and Barnes, S.-J., 2012, Changes in sulfides and platinum-group minerals with the degree of alteration in the Roby, Twilight, and High Grade Zones of the Lac des Iles Complex, Ontario, Canada: Mineralium Deposita, v. 47, p. 875-896.

Duran, C. J., Barnes, S.-J., and Corkery, J. T., 2016, Trace element distribution in primary sulfides and Fe–Ti oxides from the sulfide-rich pods of the Lac des Iles Pd deposits, Western Ontario, Canada: Constraints on processes controlling the composition of the ore and the use of pentlandite compositions in exploration: Journal of Geochemical Exploration, v. 166, p. 45-63.

Duran, C. J., Dubé-Loubert, H., Pagé, P., Barnes, S.-J., Roy, M., Savard, D., Cave, B. J., Arguin, J.-P., and Mansur, E. T., 2019, Applications of trace element chemistry of pyrite and chalcopyrite in glacial sediments to mineral exploration targeting: Example from the Churchill Province, northern Quebec, Canada: Journal of Geochemical Exploration, v. 196, p. 105-130.

Egozcue, J. J., and Pawlowsky-Glahn, V., 2011, Análisis composicional de datos en Ciencias Geoambientales: Boletín Geológico y Minero, v. 122, p. 439-452.

Filzmoser, P., Hron, K., and Reimann, C., 2009, Principal component analysis for compositional data with outliers: Environmetrics, v. 20, p. 621-632.

George, L. L., Cook, N. J., and Ciobanu, C. L., 2016, Partitioning of trace elements in co-crystallized sphalerite–galena–chalcopyrite hydrothermal ores: Ore Geology Reviews, v. 77, p. 97-116.

George, L. L., Cook, N. J., Crowe, B. B., and Ciobanu, C. L., 2018, Trace elements in hydrothermal chalcopyrite: Mineralogical Magazine, v. 82, p. 59-88.

Godel, B., and Barnes, S.-J., 2008, Platinum-group elements in sulfide minerals and the whole rocks of the JM Reef (Stillwater Complex): Implication for the formation of the reef: Chemical Geology, v. 248, p. 272-294.

Godel, B., Barnes, S.-J., and Maier, W. D. J. J. o. P., 2007, Platinum-group elements in sulphide minerals, platinum-group minerals, and whole-rocks of the Merensky Reef (Bushveld Complex, South Africa): implications for the formation of the reef, v. 48, p. 1569-1604.

Goh, S. W., Buckley, A. N., Lamb, R. N., Rosenberg, R. A., and Moran, D., 2006, The oxidation states of copper and iron in mineral sulfides, and the oxides formed on initial exposure of chalcopyrite and bornite to air: Geochimica et Cosmochimica Acta, v. 70, p. 2210-2228.

Goulet, A., 2016, Composition chimique de la chalcopyrite et application à l'exploration minérale, *in* Département de géologie et génie géologique, U. L., ed., p. 99.

Hall, S., and Stewart, J., 1973, The crystal structure refinement of chalcopyrite, CuFeS2: Acta Crystallographica Section B, v. 29, p. 579-585.

Harris, D. C., Cabri, L. J., and Nobiling, R., 1984, Silver-bearing chalcopyrite, a principal source of silver in the Izok Lake massive-sulfide deposit; confirmation by electron-and proton-microprobe analyses: The Canadian Mineralogist, v. 22, p. 493-498.

Hashmi, S., Ward, B., Plouffe, A., Leybourne, M., and Ferbey, T., 2015, Geochemical and mineralogical dispersal in till from the Mount Polley Cu-Au porphyry deposit, central British Columbia, Canada: Geochemistry: Exploration, Environment, Analysis, v. 15, p. 234-249.

Hawley, J., and Nichol, I., 1961, Trace elements in pyrite, pyrrhotite and chalcopyrite of different ores: Economic Geology, v. 56, p. 467-487.

Holwell, D. A., and McDonald, I., 2007, Distribution of platinum-group elements in the Platreef at Overysel, northern Bushveld Complex: a combined PGM and LA-ICP-MS study: Contributions to Mineralogy and Petrology, v. 154, p. 171-190.

Huston, D. L., Sie, S. H., Suter, G. F., Cooke, D. R., and Both, R. A., 1995, Trace elements in sulfide minerals from eastern Australian volcanic-hosted massive sulfide deposits; Part I, Proton microprobe analyses of pyrite, chalcopyrite, and sphalerite, and Part II, Selenium levels in pyrite; comparison with delta 34 S values and implications for the source of sulfur in volcanogenic hydrothermal systems: Economic Geology, v. 90, p. 1167-1196.

Kase, K., 1987, Tin-bearing chalcopyrite from the Izumo vein, Toyoha mine, Hokkaido, Japan: The Canadian Mineralogist, v. 25, p. 9-13.

Kojima, S., and Sugaki, A. J. E. G., 1985, Phase relations in the Cu-Fe-Zn-S system between 500 degrees and 300 degrees C under hydrothermal conditions, v. 80, p. 158-171.

Mansur, E. T., Barnes, S.-J., and Duran, C. J., 2021, An overview of chalcophile element contents of pyrrhotite, pentlandite, chalcopyrite, and pyrite from magmatic Ni-Cu-PGE sulfide deposits: Mineralium Deposita, p. 1-26.

Mansur, E. T., Barnes, S.-J., Duran, C. J., and Sluzhenikin, S. F., 2020, Distribution of chalcophile and platinum-group elements among pyrrhotite, pentlandite, chalcopyrite and cubanite from the Noril'sk-Talnakh ores: Implications for the formation of platinum-group minerals: Mineralium Deposita, v. 55, p. 1215-1232.

Marfin, A. E., Ivanov, A. V., Abramova, V. D., Anziferova, T. N., Radomskaya, T. A., Yakich, T. Y., and Bestemianova, K. V., 2020, A Trace Element Classification Tree for Chalcopyrite from Oktyabrsk Deposit, Norilsk–Talnakh Ore District, Russia: LA-ICPMS Study: Minerals, v. 10, p. 716.

Martin, A. J., Keith, M., McDonald, I., Haase, K. M., McFall, K. A., Klemd, R., and MacLeod, C. J., 2019, Trace element systematics and ore-forming processes in mafic VMS deposits: Evidence from the Troodos ophiolite, Cyprus: Ore Geology Reviews, v. 106, p. 205-225.

Martin, A. J., McDonald, I., MacLeod, C. J., Prichard, H. M., and McFall, K., 2018, Extreme enrichment of selenium in the Apliki Cyprus-type VMS deposit, Troodos, Cyprus: Mineralogical Magazine, v. 82, p. 697-724.

Maslennikov, V., Maslennikova, S., Large, R., and Danyushevsky, L., 2009a, Study of trace element zonation in vent chimneys from the Silurian Yaman-Kasy volcanic-hosted massive sulfide deposit (Southern Urals, Russia) using laser ablation-inductively coupled plasma mass spectrometry (LA-ICPMS): Economic Geology, v. 104, p. 1111-1141.

Maslennikov, V. V., Maslennikova, S. P., Large, R. R., and Danyushevsky, L. V., 2009b, Study of trace element zonation in vent chimneys from the Silurian Yaman-Kasy volcanic-hosted massive sulfide deposit (Southern Urals, Russia) using laser ablation-inductively coupled plasma mass spectrometry (LA-ICPMS): Economic Geology, v. 104, p. 1111-1141.

McClenaghan, M. B., 2005, Indicator mineral methods in mineral exploration: Geochemistry: Exploration, Environment, Analysis, v. 5, p. 233-245.

Mikhlin, Y., Tomashevich, Y., Tauson, V., Vyalikh, D., Molodtsov, S., and Szargan, R., 2005, A comparative X-ray absorption near-edge structure study of bornite, Cu5FeS4, and chalcopyrite, CuFeS2: Journal of Electron Spectroscopy and related phenomena, v. 142, p. 83-88.

Moggi-Cecchi, V., Cipriani, C., Rossi, P., Ceccato, D., Rudello, V., and Somacal, H., 2002, Trace element contents and distribution maps of chalcopyrite: a micro-PIXE study: PERIODICO di MINERALOGIA, v. 71, p. 101-9.

O'Connor, G. M., and Eksteen, J. J., 2020, A critical review of the passivation and semiconductor mechanisms of chalcopyrite leaching: Minerals Engineering, v. 154.

Palarea-Albaladejo, J., and Martín-Fernández, J. A., 2015, zCompositions—R package for multivariate imputation of left-censored data under a compositional approach: Chemometrics and Intelligent Laboratory Systems, v. 143, p. 85-96.

Pawlowsky-Glahn, V., and Buccianti, A., 2011, Compositional data analysis: Theory and applications, John Wiley & Sons, 378 p, 378 p.

Pearce, C. I., Pattrick, R. A. D., Vaughan, D. J., Henderson, C. M. B., and Van der Laan, G., 2006, Copper oxidation state in chalcopyrite: Mixed Cu d9 and d10 characteristics: Geochimica et Cosmochimica Acta, v. 70, p. 4635-4642.

Piña, R., Gervilla, F., Barnes, S.-J., Ortega, L., and Lunar, R., 2012, Distribution of platinum-group and chalcophile elements in the Aguablanca Ni–Cu sulfide deposit (SW Spain): evidence from a LA-ICP-MS study: Chemical Geology, v. 302, p. 61-75.

Plouffe, A., Ferbey, T., Hashmi, S., and Ward, B., 2016, Till geochemistry and mineralogy: vectoring towards Cu porphyry deposits in British Columbia, Canada: Geochemistry: Exploration, Environment, Analysis, v. 16, p. 213-232.

Plouffe, A., Kjarsgaard, I. M., Ferbey, T., Wilton, D. H. C., Petts, D. C., Percival, J. B., Kobylinski, C. H., and McNeil, R., 2022, Detecting Buried Porphyry Cu Mineralization in a Glaciated Landscape: A Case Study from the Gibraltar Cu-Mo Deposit, British Columbia, Canada: Economic Geology, v. 117, p. 777-799.

Reich, M., Palacios, C., Barra, F., and Chryssoulis, S., 2013, “Invisible” silver in chalcopyrite and bornite from the Mantos Blancos Cu deposit, northern Chile: European Journal of Mineralogy, v. 25, p. 453-460.

Reich, M., Román, N., Barra, F., and Morata, D., 2020, Silver-rich chalcopyrite from the active Cerro Pabellón geothermal system, Northern Chile: Minerals, v. 10, p. 113.

Rimstidt, J. D., Chermak, J. A., and Gagen, P. M., 1993, Rates of Reaction of Galena, Sphalerite, Chalcopyrite, and Arsenopyrite with Fe(III) in Acidic Solutions, Environmental Geochemistry of Sulfide Oxidation, 550. ACS Symposium Series, American Chemical Society, p. 2-13.

Rose, A. W., 1967, Trace elements in solflde minerals from the Central district, New Mexico and the Bingham district, Utah: Geochimica et Cosmochimica Acta, v. 31, p. 547-585.

Stekhoven, D. J., and Bühlmann, P., 2012, MissForest—non-parametric missing value imputation for mixed-type data: Bioinformatics, v. 28, p. 112-118.

Tian, Z., Li, H., Wei, Q., Qin, W., and Yang, C., 2021, Effects of redox potential on chalcopyrite leaching: An overview: Minerals Engineering, v. 172, p. 107135.

Todd, E., Sherman, D., and Purton, J., 2003, Surface oxidation of chalcopyrite (CuFeS2) under ambient atmospheric and aqueous (pH 2-10) conditions: Cu, Fe L-and O K-edge X-ray spectroscopy: Geochimica et Cosmochimica Acta, v. 67, p. 2137-2146.

Vaughan, D. J., 2006, Sulfide mineralogy and geochemistry: introduction and overview: Reviews in Mineralogy and Geochemistry, v. 61, p. 1-5.

Wang, Z., Xu, D., Zhang, Z., Zou, F., Wang, L., Yu, L., and Hu, M., 2015, Mineralogy and trace element geochemistry of the Co-and Cu-bearing sulfides from the Shilu Fe–Co–Cu ore district in Hainan Province of South China: Journal of Asian Earth Sciences, v. 113, p. 980-997.

Wohlgemuth-Ueberwasser, C. C., Viljoen, F., Petersen, S., and Vorster, C., 2015, Distribution and solubility limits of trace elements in hydrothermal black smoker sulfides: An in-situ LA-ICP-MS study: Geochimica et Cosmochimica Acta, v. 159, p. 16-41.

Xie, J., Tang, D., Qian, L., Wang, Y., and Sun, W., 2020, Geochemistry of sulfide minerals from skarn Cu (Au) deposits in the Fenghuangshan ore field, Tongling, eastern China: Insights into ore-forming process: Ore Geology Reviews, v. 122, p. 103537.

Yang, C., Beaudoin, G., Tang, J.-X., Song, Y., Wang, L.-Q., and Huang, X.-W., 2022, Cu-sulfide mineralogy, texture, and geochemistry in the Tiegelongnan porphyry-epithermal copper system, Tibet, China: Mineralium Deposita, v. 57, p. 759-779.

Yano, R. I., 2012, Trace element distribution in chalcopyrite-bearing porphyry and skarn deposits, University of Nevada, Reno.

Yuan, B., Yang, Y., Yu, H., Zhao, Y., Ding, Q., Yang, J., and Tang, X., 2018, Geochemistry of pyrite and chalcopyrite from an active black smoker in 49.6°E Southwest Indian Ridge: Marine Geophysical Research, v. 39, p. 441-461.

Zhao, X.-Y., Zhong, H., Mao, W., Bai, Z.-J., and Xue, K., 2020, Molybdenite Re-Os dating and LA-ICP-MS trace element study of sulfide minerals from the Zijinshan high-sulfidation epithermal Cu-Au deposit, Fujian Province, China: Ore Geology Reviews, v. 118, p. 103363.

Zhao, Y., Chen, S., Tian, H., Zhao, J., Tong, X., and Chen, X., 2021, Trace element and S isotope characterization of sulfides from skarn Cu ore in the Laochang Sn-Cu deposit, Gejiu district, Yunnan, China: Implications for the ore-forming process: Ore Geology Reviews, v. 134, p. 104155.

Chapitre 1 Variation of trace elements in chalcopyrite from worldwide Ni-Cu sulfide and Reef-type PGE deposits: implications for mineral exploration

Enzo Caraballo[1], Sarah Dare[2], Georges Beaudoin[1]

[1]Université Laval, QC; [2]Université du Québec à Chicoutimi, QC

1.1 Résumé

Chalcopyrite de 13 dépôts représentatifs à l'échelle mondiale de sulfures de Ni-Cu et d'EGP lités a été analysée par ablation laser et spectrométrie de masse à plasma à couplage inductif (LA-ICP-MS) afin d'évaluer son potentiel en tant que minéral indicateur pour exploration. La base des données des éléments traces a été investiguée par l'analyse discriminante par les moindres carrés partiels (PLS-DA), laquelle, combinée avec des diagrammes binaires discriminants, permet l'identification des critères géochimiques pour la discrimination du type de dépôt (sulfures de Ni-Cu vs. EGP lités) et du type de minerais (riche en Cu vs. Riche en Fe). Un premier model PLS-DA (avec le Bi, In, Se, Sn et Te) discrimine la chalcopyrite par type de dépôt; celle des dépôts d'EGP lités est enrichie en Se par rapport à la chalcopyrite des dépôts de sulfures de Ni-Cu comme un résultat de valeurs plus élevées du factor-R, alors que la chalcopyrite des dépôts de sulfures de Ni-Cu est enrichie en Te, Bi et Sb. La cristallisation des minéraux du groupe du platine (MGP) dans les dépôts d'EGP lités normalement réduit la concentration de Te, Bi et Sb dans la chalcopyrite co-existant, en augmentant les différences entre ces deux types de dépôts. Le deuxième model PLS-DA (avec le Sb, Se, Sn, Tl et Zn) discrimine par type de minerais, en montrant que la chalcopyrite des échantillons riches en Cu est enrichie en Sn, Se et Ze par rapport à la chalcopyrite des échantillons riches en Fe/non zonés, principalement à cause du fractionnement des sulfures. Des diagrammes binaires discriminants Se/(Te+Bi) vs. Se et 2Zn/(3Se+5Sn) vs. Se sont proposés afin de discriminer la chalcopyrite par type de dépôt et type de minerais, respectivement. Cette étude démontre que la composition en éléments traces de la chalcopyrite permet son emploi en tant que mineral indicateur pour l'exploration.

Mots clés : Chalcopyrite, dépôts magmatiques, LA-ICP-MS, PLS-DA, éléments traces, nickel, cuivre, EGP

1.2 Abstract

Chalcopyrite from 13 worldwide representative Ni-Cu sulfide and Reef-type PGE deposits were investigated using laser ablation-inductively coupled plasma-mass spectrometry (LA-ICP-MS) to evaluate its potential as an indicator mineral for exploration. Trace element data was investigated with PLS-DA (partial least square-discriminant analysis) which, combined with discriminant binary diagrams, allows identification of geochemical criteria for discrimination of deposit type (Ni-Cu sulfide vs. Reef-type PGE) and ore type (Cu-rich vs. Fe-rich). A first PLS-DA model (using Bi, In, Se, Sn and Te) discriminates chalcopyrite by deposit type; those from Reef-type PGE have higher Se relative to Ni-Cu sulfide deposits, as a result of higher R factors, whereas chalcopyrite from Ni-Cu sulfide deposits is higher in Te, Bi and Sb. Platinum Group Mineral (PGM) crystallization in Reef-type PGE deposits typically deplete Te, Bi and Sb in co-existing chalcopyrite, enhancing the differences between these two deposit types. The second PLS-DA model (based on Sb, Se, Sn, Tl and Zn) discriminates by ore type, showing that chalcopyrite from Cu-rich samples is enriched in Sn, Se and Zn relative to Fe-rich/unzoned samples, mainly as a result of sulfide fractionation. Complementary discriminant diagrams Se/(Te+Bi) vs. Se and 2Zn/(3Se+5Sn) vs. Se are proposed to discriminate chalcopyrite by deposit type and ore type, respectively. This study demonstrates that the trace element composition of chalcopyrite enables its use as an indicator mineral for exploration.

Keywords: Chalcopyrite, magmatic deposits, LA-ICP-MS, Partial Least Square-Discriminant Analysis, trace elements, nickel, copper, PGE

1.3 Introduction

Chalcopyrite is a common sulfide found in a large variety of mineral deposits ranging from magmatic (Ni-Cu-platinum group element (PGE) sulfide systems) to hydrothermal (porphyry, iron oxide copper-gold, volcanogenic massive sulfides, orogenic gold, epithermal gold, Cu-skarn, sedimentary exhalative sulfides and red beds) environments. Numerous studies have analyzed trace elements in sulfides, including chalcopyrite, with aim to document the distribution of chalcophile elements among the sulfides and to understand the metallogenesis and petrogenesis of magmatic sulfide deposits (Barnes et al., 2006; Barnes et al., 2008; Chen et al., 2015; Czamanske et al., 1992; Dare et al., 2014; Dare et al., 2010b; Dare et al., 2010a, 2011; Djon and Barnes, 2012; Duran et al., 2016b; Godel and Barnes, 2008; Godel et al., 2007; Holwell and McDonald, 2007; Mansur et al., 2020; Piña et al., 2012a) and hydrothermal systems (Agangi et al., 2018; Bajwah et al., 1987; Butler and Nesbitt, 1999; Cabri et al., 1985; Cook et al., 2011; George et al., 2016; George et al., 2018b; Harris et al., 1984; Hawley and Nichol, 1961a; Huston et al., 1995; Kase, 1987; Maslennikov et al., 2009a; Maslennikov et al., 2009b; Moggi-Cecchi et al., 2002; Reich et al., 2013b; Rose, 1967; Wang et al., 2015; Wohlgemuth-Ueberwasser et al., 2015). These studies show that the composition of chalcopyrite is highly variable, and that magmatic chalcopyrite can potentially be distinguished from hydrothermal chalcopyrite (Bédard et al., 2017; Duran et al., 2019b; Goulet, 2016; Mansur et al., 2021).

As the trace element content of chalcopyrite is controlled by its crystal structure, partitioning with co-crystallizing minerals, and magma/fluid composition, this variability probably reflects the geological environment in which it formed (George et al., 2016; George et al., 2018b), thus making it a potential indicator for provenance studies (Duran et al., 2019b). Furthermore, chalcopyrite has a higher stability than other sulfides (pentlandite, pyrrhotite, pyrite and PGE-sulfides) in weathering environments (Averill, 2011a; Plouffe et al., 2016) and its widespread distribution in mineral deposits makes chalcopyrite a potential indicator mineral for exploration. Its physical properties (high density, poor cleavage, moderate hardness) are favorable for recovery from glacial sediments (Averill, 2011a).

An indicator mineral provides evidence for the presence of a type of mineralization, hydrothermal alteration, or lithology in bedrock; their morphology, textures and/or geochemistry may be investigated in order to obtain information about transport and nature of mineralization (McClenaghan, 2005). Multivariate statistical analysis is useful in investigating thoroughly the chemical variation of large datasets of trace elements of indicator minerals, such as magnetite (Makvandi et al., 2016a; Makvandi et al., 2016b), scheelite (Sciuba et al., 2020), tourmaline (Sciuba et al., 2021) and gold (De Bronac de Vazelhes, 2019; Liu and Beaudoin, 2021; Liu et al., 2021). Only few studies have investigated chalcopyrite as an indicator mineral, from sediments and mineralized bedrock associated with magmatic sulfide deposits (Ni-Cu-PGE and reef-type PGE: Duran et al., 2019b; Mansur

et al., 2021), porphyry deposits (Goulet, 2016; Hashmi et al., 2015b; Lazich, 2010; Plouffe et al., 2016), and other deposit types (Bédard et al., 2017).

Magmatic sulfide deposits are classified into two types: a) Ni-Cu-(PGE) deposits, generally characterized by high sulfide contents (20-90 vol.%), high concentrations of Ni and Cu, and that typically occur at the margins (contact-style), or in the fractured footwall, of mafic-ultramafic igneous rocks (intrusive and extrusive) (Naldrett, 2004); and b) Reef-type PGE deposits, which are sulfide poor (0.5-5 vol.%) with high values of PGE occurring in stratiform mineralization within some layered mafic-ultramafic intrusions (Godel, 2015; Naldrett, 2004). The studies of Duran et al. (2016a), Duran et al. (2019b) and Mansur et al. (2021) further show that it is possible to distinguish reliably between Ni-Cu sulfide and Reef-type PGE deposits using Pd and Rh contents in pentlandite, and although they also demonstrated that chalcopyrite shows significant differences in PGE between both deposits, this topic needs to be investigated further using a full suite of trace elements.

Previous studies show that several processes control the trace element composition of base metal sulfides (BMS), including chalcopyrite, in magmatic sulfide deposits, as recently reviewed by Mansur et al. (2021). These processes are 1) crustal contamination of the mantle-derived magma, principally by S-rich sediments (e.g. black shales xenoliths; Ripley and Li, 2013; Samalens et al., 2017a), which induces sulfide-saturation and the formation of an immiscible sulfide liquid; 2) interaction between sulfide liquid and magma (R-factor), thought to be an important control on the content of strongly to highly chalcophile elements (e.g., PGE) in base metal sulfides (Barnes and Lightfoot, 2005); 3) fractional crystallization of the sulfide liquid during crystallization of a Fe-rich monosulfide solid solution (MSS) at 1180°C, and formation of Cu-rich intermediate solid solution (ISS) at 900°C from the residual Cu-rich liquid (Barnes and Lightfoot, 2005; Dare et al., 2014; Mansur et al., 2020; Naldrett, 2004). In a few cases, this process can lead to zoning (Fe-rich and Cu-rich ore bodies) on a deposit scale, such as Noril'sk and Sudbury (Dare et al., 2011; Duran et al., 2017); 4) exsolution of pyrrhotite and pentlandite (±chalcopyrite, ±pyrite ± platinum group minerals (PGM)) from MSS (<600°C), and chalcopyrite and pyrrhotite (±cubanite) from ISS (Mansur et al., 2021); 5) crystallization of platinum-group minerals (PGM) from late, residual liquid (Cafagna and Jugo, 2016; Dare et al., 2014; Duran et al., 2017; Liu and Brenan, 2015) and 6) alteration and remobilization by later hydrothermal fluids. These processes affecting the composition of BMS are not necessarily mutually exclusive and the complexity could potentially hinder its application as an exploration tool. As such, we demonstrate here that a multivariate statistical approach is successful to discriminate the type of magmatic sulfide deposit and the ore type.

Although magmatic sulfides form by similar processes in both deposit types, there are clear differences between Ni-Cu sulfide and Reef-type PGE deposits. Whereas sulfides in Reef-type PGE deposits occur typically as disseminations, within silicate or chromite rocks, at or near the base of defined cyclic horizons (Godel et al., 2006; Godel et al., 2007; Naldrett, 2004), in Ni-Cu sulfide deposits, sulfides occur as massive and semi-massive

mineralization and are principally located in conduit systems (i.e. Voisey's Bay and Eagle; Ripley and Li, 2011) and at the base of the complexes and/or at footwall fractures (i.e. Sudbury; Dare et al., 2014; Dare et al., 2010b). These differences could affect considerably the exploration strategies, e.g., in terms of geophysical surveys (Balch, 2005; Green and Peck, 2005; Naldrett, 2004; Schulz et al., 2014). Thus, discriminating deposit type using trace element composition in chalcopyrite as an indicator mineral could be an important tool to help guide exploration strategies in covered terrains.

This study is part of a larger study which aims to evaluate the full potential of chalcopyrite chemistry as an indicator mineral for mineral exploration using multivariate statistical analysis combined with an understanding of the processes that control the trace element content of chalcopyrite. In this contribution we investigate systematically the variation of 36 trace elements in chalcopyrite, measured using LA-ICP-MS, from worldwide magmatic Ni-Cu-PGE deposits, as a function of the deposit type (Ni-Cu sulfide and Reef-type PGE deposits), ore type (Fe-rich, Cu-rich) and sulfide texture (massive to disseminated) to evaluate the potential of chalcopyrite to be used as an indicator mineral for magmatic sulfide deposits. Since multivariate statistical analysis requires a consistent list of trace elements, we re-analysed well characterized samples from previous studies (Table 1.1). We analyzed trace elements commonly measured in magmatic sulfides (chalcophile elements, including platinum group elements), as well as several elements not analyzed in previous studies, such as lithophile elements (Ti and Mn) and lithophile/weakly chalcophile elements (Ga and Ge).

1.4 Methodology

1.4.1 Sample Selection

Seventy-seven chalcopyrite-bearing samples were selected from worldwide Ni-Cu-(PGE) sulfide and Reef-type PGE deposits (Fig. 1.1), the majority of which are well-characterized (whole-rock, petrography, mineral chemistry using electron probe microanalysis (EPMA) and LA-ICP-MS) in previous studies (Table 1.1). Ni-Cu sulfide samples (N=65) are from 19 different deposits, belonging to 6 types according to classification based on related magmatism (Naldrett, 2004): 1) NC-1: komatiite (N=11), 2) NC-2: flood basalt (N=14), 3) NC-3: ferropicrite (N=6), 4) NC-4: anorthosite-granite-troctolite (N=12), 5) NC-5: picrite to tholeiite (N=4) and 6) NC-6: impact melt (N=18). The samples were classified (Annexe A1) according to modal percentages of pyrrhotite (Po), pentlandite (Pn), chalcopyrite (Ccp) and cubanite (Cbn), the Ni/Cu ratio in the whole rock, and location in the deposit to define Fe-rich (Po+Pn>Ccp+Cb) and Cu-rich (Ccp+Cb>Po+Pn) ore types in zoned deposits (Dare et al., 2014; Dare et al., 2010a, 2011; Duran et al., 2017; Salim Amaral, 2017). As such, Cu-rich (N=19) and Fe-rich samples (N=18) from 3 zoned deposits were studied (Voisey's Bay, Noril'sk and Sudbury), whereas 28 samples were selected from the remaining 10 deposits that do not show mineralogical zonation on a large scale (unzoned deposits). In

addition, representative samples (N=12) from 5 Reef-type PGE deposits from 4 mafic-ultramafic layered intrusions were also selected. Table 1.1 summarizes the geologic information of the selected deposits.

Samples were also classified by sulfide texture (Fig. 1.2), according to a classification scheme simplified from Barnes et al. (2017) and Barnes et al. (2018), as follows: 1) disseminated (0-5% sulfides; N=15), 2) net-textured/globular (5-70% sulfides; N=16) and massive (>70% sulfides; N=46). The term net-textured includes patchy net-textured and net-textured samples, whereas massive comprises semi-massive (70 – 90%) and massive samples (>90%) (Annexe A1). As globular refers to convex, sub-spherical or ellipsoidal aggregates with variable diameters (Barnes et al., 2017), globular samples could belong to disseminated or net-textured/globular group.

1.4.2 Analytical Methods

Mineralogical composition and textures were determined from composite photographs of each polished thin section, considered representative of the sample, using a reflected light microscope, and modal percentages were calculated using ImageJ 1.52p. A Scanning Electron Microscope (SEM) model JEOL 840A, equipped with an energy-dispersive spectrometer (EDS) at Université Laval, was used to verify the presence of inclusions not detected under optical microscope and to select regions without inclusions in chalcopyrite (<10 μm) for geochemical analysis. Between five and seven grains of chalcopyrite and three to four grains for other sulfides (pyrrhotite, pentlandite and cubanite) were selected in each polished section for geochemical analysis, based on the amount and distribution of chalcopyrite, grain size and mineralogical association.

Chalcopyrite (n=39), pyrrhotite (n=25), pentlandite (n=30) and cubanite (n=32) were analyzed for major and minor elements with a CAMECA SX-100 EPMA, equipped with five wavelength-dispersive spectrometers (WDS) at Université Laval, Québec. Beam size was 10 μm with a voltage of 15 kV and a current of 20 nA. The background was measured for 15-20 s on both sides and a peak counting time of 10 s was carried out. Metallic cobalt standard (Co), Fe_2O_3 (Fe), FeS_2 (S), NiAs (Ni) and $CuFeS_2$ (Cu) were used for the calibration. The results are summarized in Annexe A2 and shows that the major element compositions are similar to stoichiometric values. Complete EPMA data are in Annexe A3.

A total of 556 chalcopyrite, 67 pyrrhotite, 44 pentlandite and 45 cubanite grains were analyzed for trace elements by LA-ICP-MS at LabMaTer (Université du Québec à Chicoutimi, UQAC) using an Excimer 193-nm RESOlution M-50 laser ablation system (Australian Scientific Instrument) equipped with a double volume cell S-155 (Laurin Technic) and coupled to an Agilent 7900 mass spectrometer. A beam size of 55 μm and 33 μm, depending on grain size, a line speed of 5 μm/s, a laser frequency of 15 Hz and a fluence of 3 J/cm^2 were used to analyze chalcopyrite. Additionally, cubanite (n=46), pyrrhotite (n=67) and pentlandite (n=44) were analyzed. Lines were made across the sulfide grains for a period of 20 to 60 s according to grain size, after measuring the gas blank for 30 s. The ablated material was carried into the ICP-MS by an argon-helium gas mix at a rate of 0.8 to 1 L/min

for Ar and 350 mL/min for He, and 2 mL/min of nitrogen was also added to the mixture. Data reduction was carried out using Iolite package for Igor Pro software (Paton et al., 2011).

A total of 36 isotopes measured were: ^{24}Mg, ^{29}Si, ^{34}S, ^{49}Ti, ^{51}V, ^{52}Cr, ^{55}Mn, ^{59}Co, ^{60}Ni, ^{65}Cu, ^{66}Zn, ^{71}Ga, ^{74}Ge, ^{75}As, ^{82}Se, ^{95}Mo, ^{101}Ru, ^{103}Rh, ^{107}Ag, ^{108}Pd, ^{111}Cd, ^{115}In, ^{118}Sn, ^{121}Sb, ^{128}Te, ^{137}Ba, ^{182}W, ^{185}Re, ^{189}Os, ^{193}Ir, ^{195}Pt, ^{197}Au, ^{202}Hg, ^{205}Tl, ^{208}Pb and ^{209}Bi. The polyatomic interference of ^{40}Ar^{63}Cu on ^{103}Rh was corrected in chalcopyrite and cubanite using a Cu-blank. However, the ^{103}Rh values of are not reported as the interference corrections are too large in chalcopyrite and cubanite (1% Cu produces about 0.1-0.2 ppm ^{103}Rh interference). Additionally, in most cases PGE were below detection limit in chalcopyrite. Interference of ^{40}Ar^{61}Ni on ^{101}Ru was corrected in pentlandite. Direct interference of ^{115}Sn on ^{115}In and ^{108}Cd on ^{108}Pd were corrected in chalcopyrite, cubanite, pyrrhotite and pentlandite manually from ^{118}Sn and ^{111}Cd. We used ^{57}Fe as the internal standard with stoichiometric iron values of chalcopyrite (30.43 %), whereas for cubanite, pyrrhotite and pentlandite the Fe value was determined by EPMA. Calibration was based on a combination of three international reference materials (RM): MASS-1 (Wilson et al., 2002), corresponding to a pressed powder pellet (ZnCuFeS) used to calibrate S, Cu, Zn, As, Se, Mo, Cd, Sn, Sb, Te, W, Hg and Pb; GSE-1g (Jochum et al., 2005), a Fe-rich natural basaltic glass used to calibrate Si, Ti, V, Cr, Mn, Co, Ni, Ga, Ge, Ag, In, Ba, Re, Tl and Bi; and Laflamme Po727, a synthetic FeS doped with PGE, used to calibrate Au and PGE. The RM used to monitor quality control of the analyses were: CCu-1e, a copper concentrate (certified by CCRMP-Canadian Certified Reference Materials project, CANMET, Canada); UQAC-FeS1, a synthetic sulfide developed at LabMaTer (UQAC) and PTC-1b, a Cu-Ni-sulfide concentrate powder (Jochum et al., 2005).

The results of analyses of reference materials used in the calibration and the range of detection limits are shown in Annexe A4. The majority of chalcophile elements (Ag, As, Au, Bi, Co, Ga, Ge, In, Ir, Mn, Mo, Ni, Os, Pb, Pd, Rh, Ru, Sb, Se, Sn, Te and Tl) have a moderate to high accuracy relative to their reference values (rel. diff.<10-15%) and a moderate to high precision (RSD<10-15%). Elements such as Ti and Cd show lower accuracy (rel. diff.>15%) and lower precision (RSD>15%; Annexe A4). Differences between working values in a few of RM and those measured in this study could be a result of heterogeneity and non-matrix matched materials or due to the low level of confidence of reported working values for some elements in RM (provisional/informative values). As polyatomic interferences were detected on ^{49}Ti (from ^{33}S^{16}O^{+}) and ^{74}Ge (from ^{40}Ar^{34}S^{+}, ^{36}Ar^{38}Ar^{+} and/or ^{38}Ar^{36}S^{+}), and Cd shows low accuracy and precision, these elements were not used for statistical analysis.

On each time-signal, only inclusion-free regions were selected for data reduction in order to have the most reliable composition of chalcopyrite (Annexe A9). The following elements were used to monitor for inclusions, i.e., Si (silicates), Zn-Cd (sphalerite), Pb (galena) and Ni (pentlandite).

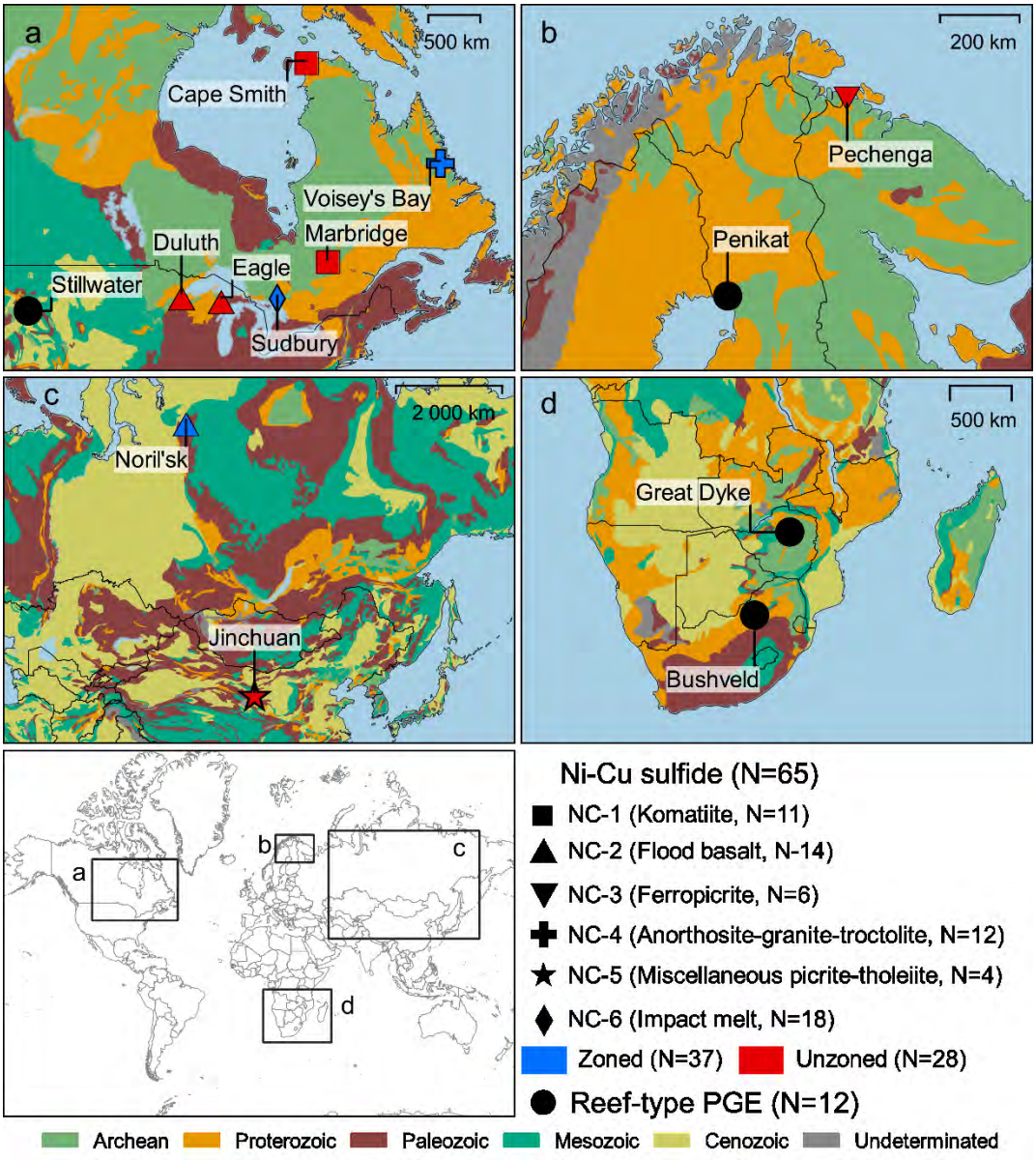

Fig. 1. 1 Location of selected magmatic sulfide deposits in this study. Ni-Cu sulfide deposits classification according to Naldrett (2004). Generalized geologic map of the world (Chorlton, 2007). N = number of samples.

1.4.3 Statistical Methods

1.4.3.1 Preliminary Data Analysis

The geochemical data was processed for the values below detection limit (censored values). Elements with more than 40% of values censored are banned from the database in order to reduce "noise" in statistical analysis. Additionally, most of imputation algorithms do not remain stable with higher degrees of censoring (Antweiler, 2015; Hron et al., 2010; Makvandi et al., 2016b). The log-ratio Expectation-Maximisation (lrEM) algorithm was applied to impute censored values, using zComposition R-package (Palarea-Albaladejo and Martín-Fernández, 2015). According to Palarea-Albaladejo and Martín-Fernández (2008), an alr-transformed component $y_{ij} =$

$ln(x_{ij}/x_{iD})$ from a compositional vector x_i is considered a censored value if $y_{ij} \leq \psi_{ij}$, where ψ_{ij} is alr-transformed threshold (detection limit). This adapted statistical iterative procedure ensures that censored values y_{ij} are replaced by values lower than threshold ψ_{ij} (Palarea-Albaladejo et al., 2007).

Statistical estimators were calculated to characterize different groups of data (arithmetic mean, standard deviation and median). With the aim to reduce effects of outliers on estimator calculation, a robust measure of location was incorporated: the trimmed mean. According to Wilcox (2011), a *γ*-trimmed mean is the mean of a truncated distribution at *γ* and 1- *γ* quantiles and is calculated as follows:

$$\mu_t = \frac{1}{1-2\gamma} \int_{x_\gamma}^{x_{1-\gamma}} x dF(x) \quad (1)$$

Hypothesis tests were performed in order to compare trimmed means between groups of data (ore types and deposit types) to determine if there are significant differences using Yuen's method (Wilcox, 2011) where null hypothesis is $H_0: \mu_{t1} = \mu_{t2}$ with *α*=0.05.

Compositional data describe quantitatively the parts of a whole, which sums to a constant (i.e., 100%), having thus a closed nature and restricting a free variation of variables (Egozcue and Pawlowsky-Glahn, 2011; Filzmoser et al., 2009; Pawlowsky-Glahn and Buccianti, 2011). The constant sum of closed data could lead to spurious correlations, such that compositional data was transformed using centered log-ratios according to Aitchison (1986).

1.4.3.2 Partial Least Squares Discriminant Analysis (PLS-DA)

Once imputed and clr-transformed, chalcopyrite LA-ICP-MS data was investigated with PLS-DA. This method consists of a supervised linear classification which models dependent variables *Y* from a set of predictor variables *X*, by reducing the multidimensionality of the data (Ruiz-Perez et al., 2020; Wold et al., 2001). Response variables *Y* in classification tasks is always categorical and recoding into continuous variables are necessary (Lee et al., 2018). Partial least squares discriminant analysis is based on the PLS algorithm, which was introduced originally for regression tasks (Lee et al., 2018) and searches for latent variables with a maximum covariance between *X* and *Y* variables (Ballabio and Consonni, 2013). Latent variables are linear combinations of the original variables which are modelled using PLS-DA and capture an underlying phenomenon (Ballabio and Consonni, 2013; Dunn, 2019).

PLS-DA is an iterative method consisting of five principal steps (Brereton and Lloyd, 2014). Starting with weight vector *w** estimation by maximizing the covariance between *X* and *Y*, the *t*, *p* and *q* coefficients (*X*-scores, *X*-loadings, *Y*-loadings, respectively) are calculated sequentially. Finally, residuals of *X* and *Y* replace original input

data in order to determinate the second PLS component (Lee et al., 2018). A PLS-DA model can be interpreted from two principal outputs, scores and loadings. After calculating latent variables, they can be used in a cartesian space (i.e. t_1-t_2) to project *X*-scores of the observations. The aim of these representations, called score plots, is to look for clusters indicating similar characteristics (Brereton and Lloyd, 2014). Likewise, distance between clusters can suggest differences in attributes.

On the other hand, loading plots show correlations between original variables. Superposing *X*-loadings (specifically *X*-weight, *w**) and *Y*-loadings in a same plot, relationship between *X*-variables (elements) and *Y*-variables (classes) can be inferred (Dunn, 2019; Wold et al., 2001). Variables positively correlated are shown grouped, whereas those with a negative correlation plot diametrically opposed. Location of variables in a loading plot is dependent on contribution in discrimination, therefore, *X*-variables near the correlation circle (radius=1) are interpreted to be highly variable between classes, in contrast, those located near the origin contribute weakly to classification, as variability is negligible.

Different estimators have been used to judge the importance of the *X*-variables on the classification model. Mehmood et al. (2012) described three filter methods (loading weights, regression coefficients and variable importance on projection) used to determine variable importance and consequently the selection of variables to improve PLS-DA models. Variable importance on projection (VIP) quantifies the influence on the model by accumulating the importance of each variable *j* reflected by the weight *w* from each latent variable (Favilla et al., 2013; Mehmood et al., 2012) according to:

$$v_j = \sqrt{\frac{M \sum_{a=1}^{A} [SS_a (\frac{w_{aj}}{||w_a| \quad |^2})}{\sum_{a=1}^{A} SS_a}} \quad (2)$$

where SS_a is the sum of squares of *Y* explained variance by the *a*th latent variable, $(w_{aj}/||w_a||)^2$ represents the importance of the *j*th variable, *M* is the total number of *X*-variables and *A* the total number of latent variables. The average of VIP scores is 1 and the sum of squares of all VIP scores is equal to *M*. Thus, variables with VIP scores>1.0 are considered highly influential on the discrimination model, whereas VIP between 0.8-1.0 indicate a variable moderately influential and VIP<0.8 represent less important variables (Chong and Jun, 2005; Gosselin et al., 2010; Mendez et al., 2020). A second, widely used method to assess the importance of *X*-variables on the classification model is the vector or matrix of regression coefficients (B_{pls}), which measures the association between predictor and responses variables (Mehmood et al., 2012). Partial least square discriminant analysis is based on a regression algorithm, thus, these coefficients are calculated for each modeled response or class (Ballabio and Consonni, 2013). Variables with a strong importance for a specific class have generally high absolute values of regression coefficients and those with small absolute values do not contribute importantly

and could be eliminated to improve the model (Ballabio and Consonni, 2013; Gosselin et al., 2010; Mehmood et al., 2012). A regression coefficient matrix is defined as

$$B_{pls} = W^{*}Q^{T} \quad (3) \text{ where } \quad W^{*} = W(P^{T}W)^{-1} \quad (4)$$

Q matrix corresponds to *Y*-loadings, *P* to *X*-loadings and *W* is *X*-loading weights. Dunn (2019) indicated that as regression coefficients derivation includes *W**, these are a function of all the latent variables. In order to optimize classification models, a cross-validation analysis was carried out to select the optimal number of latent variables. For variable selection, Chong and Jun (2005) and Wold et al. (2004) proposed a strategy which combines VIP scores and regression coefficients in which both should be low for a variable to be excluded. Once the number of latent variables is determined, the classification models were performed only with variables with VIP ≥ 1 and relatively high B_{pls}, and further an assessment of classification capability of the models was performed using the Receiver Operator Characteristic (ROC). A ROC curve plots the number of True positives (sensitivity) and number of False positives (1-specifity), both as percentages (Westerhuis et al., 2008). Area Under the ROC (AUROC) measures the quality of the classification, where values equal to 1 indicates a perfect separation, whereas AUROC values equal to 0.5 indicates a random classifier (no separation; Ballabio and Consonni, 2013; Westerhuis et al., 2008). For model testing using published data, confusion matrices were generated in order to judge the classification performance. The confusion matrix is a square matrix *C x C,* where *C* is the number of classes and collect the outputs of the classification model, allowing calculating multiple estimators, such as the accuracy, which measure the percentage of observations correctly classified (Ballabio and Consonni, 2013).

Table 1. 1 Summary of studied magmatic sulfide deposits in this study (details of sulfide textures and opaque mineralogy in Annexe A1). *In italic the sources of sample containing detailed descriptions and location maps. Abbreviations: M : mela, Km : komatiite, Troc : troctolite, Nor : norite, Gab: gabbro, Pdt : peridotite, Pxt : pyroxenite, Bst: basalt, Fpc: ferropicrite, Whl : wehrlite, Hzb : harzburgite, Lhz : lherzolite, Dn : dunite, Gphy : granophyre, Ol : olivine, Ant :anorthosite, Unmet: Unmetamorphosed. Classes according to Naldrett (2004). NC-1: komatiite; NC-2: flood basalt; NC-3: ferropicrite; NC-4: anorthosite-granite -troctolite; NC-5: picrite to tholeiite; NC-6: impact melt

Type		Class	Deposit name (number of samples)	Host igneous complex (age)	Location	Host rocks	Regional metamorphism	References*
Ni-Cu sulfide	Unzoned deposits	NC-1	Delta (2) Expo (1) Mesamax (1) Katinniq (1) Zone Frontier (5)	Cape Smith Belt (1.88 Ga)	Quebec, Canada	Bas-kom Kom Bas	Greenschist	*Boutroy et al. (2014); Dionne-Foster (2007);* Mungall (2007); Seabrook et al. (2004)
			Marbridge (1)	Abitibi Greenstone Belt (2.7 Ga)	Quebec, Canada	Kom	Amphibolite	*Barnes et al. (2007); Boutroy et al. (2014);* Sproule et al. (2005)
		NC-2	Dunka Road (2) Mesaba (2)	Duluth Complex (1.10 Ga)	Minnesota, USA	Troc, gab, nor	Unmet	Naldrett (2004); *Thériault (1999)*; (Samalens et al., 2017a)
			Eagle (3)	Eagle Intrusion (1.10 Ga)	Michigan, USA	Perid, M-troc, M-gab		Boutroy et al. (2014); Ding et al. (2010); Ripley (2014)
		NC-3	Kotselvaara (2) Semilekta (3)	Pechenga Complex (2.50 Ga)	Kola Peninsula, Russia	Gab-whl, Perid., Fe-pic	Greenschist	Barnes et al. (2001); Brügmann et al. (2000); Hanski et al. (2011); Lagueux (1999)
		NC-5	Jinchuan (4)	Jinchuan Complex (0.82 Ga)	Gansu, China	Hzb, lhz, dun	Greenschist	Chen et al. (2015); Song et al. (2009), Ripley et al. (2005), *UQAC*
	Zoned deposits	NC-2	Medvezhy Creek (2) Talnakh (5)	Noril'sk Intrusion (0.25 Ga)	Krasnoyarsk Krai, Russia	Gabnor, gab	Unmet	*Barnes et al. (2006); Boutroy et al. (2014); Duran et al. (2017a);* Krivolutskaya (2016); Naldrett (1997)
		NC-4	Eastern Deeps (1) Ovoid (11)	Voisey's Bay Nain Plutonic Suite (1.33 Ga)	Newfoundland, Canada	Ol-gab, troc, ferrogab		*Boutroy et al. (2014)*; Naldrett (2004); Ripley and Li (2011); *Salim Amaral (2017)*
		NC-6	Broken Hammer (2) Copper Cliff (1) Creighton (7) McCreedy (8)	Sudbury Igneous Complex (1.85 Ga)	Ontario, Canada	Nor, qz-gab, gphy	Greenschist	*Boutroy et al. (2014); Dare et al. (2012); Dare et al. (2014); Dare et al. (2010a); Dare et al. (2010b); Dare et al. (2011);* Naldrett (2004)
Reef-type PGE			Merensky reef (1) Rustenburg (5)	Bushveld Complex (2.05 Ga)	South Africa	M-nor	Unmet	*Godel et al. (2007), ULAVAL collection*
			Mimosa (2)	Great Dyke (2.57 Ga)	Zimbabwe	Nor		*Barnes et al. (2008)*
			PV reef (1)	Penikat (2.44Ga)	Finland	Ant, gabnor	Greenschist	
			East Boulder (3)	Stillwater Complex (2.70 Ga)	Montana, USA	Loganberry	hydrothermal-Greenschist	*Godel and Barnes (2008)*

1.5 Results

1.5.1 Petrography

The mineralogical and textural characteristics of the analyzed samples, and the proportions of major minerals are summarized in Figures 1.2, 1.3 and in Annexe A1. In zoned massive sulfide deposits (Sudbury, Voisey´s Bay and Noril'sk), Fe-rich samples represent MSS cumulates from which pyrrhotite and pentlandite exsolved. Most of these samples are massive sulfides (Fig. 1.2a-d), dominated by pyrrhotite (19-92 vol.%), pentlandite (2-36 vol.%) and chalcopyrite (1-44 vol.%). Chalcopyrite typically occurs as micrometric exsolutions in pyrrhotite and as anhedral grains filling interstitial spaces (Figs. 1.2a, b). Pentlandite occurs as aggregates between chalcopyrite and pyrrhotite and as exsolution flames in pyrrhotite (Figs. 1.2c, d). Magnetite (1- 42 vol.%) from these deposits has been studied in detail by Dare et al. (2012), Boutroy et al. (2014) and Duran et al. (2020). Accessory sulfide minerals include galena and sphalerite. Occasionally, exsolution lamellae of troilite are present in pyrrhotite (Fig. 1.2a). In addition there are two net-textured Fe-rich sulfide samples from Voisey´s Bay (VB7 and VB21; Salim Amaral, 2017) and one from Creighton with globular texture (CRTN6; Dare et al., 2010a).

The Cu-rich samples, on the other hand, represent ISS that crystallized from the residual Cu-rich liquid, from which chalcopyrite, cubanite (+pyrrhotite) and some pentlandite exsolved (Dare et al., 2014). The Cu-rich samples (Figs. 1.2e-h) are dominated by chalcopyrite (<97 vol.%), cubanite (<85 vol.%) with minor pyrrhotite (<45 vol.%) and pentlandite (<32 vol.%, except VB6). Cubanite commonly forms lamellae exsolutions in chalcopyrite (Fig. 1.2h). Magnetite ranges from 2-16 vol.% (Boutroy et al., 2014; Dare et al., 2012; Duran et al., 2020) and accessory minerals include galena, pyrite and sphalerite (star-like and skeletal inclusions; Annexe A10).

Samples from unzoned Ni-Cu deposits cover a range of sulfide textures (Figs. 1.2i-l). Globular texture comprises sulfides forming aggregates (Fig. 1.2l) composed by chalcopyrite, pentlandite and pyrrhotite in variable proportions. Net-textured sulfides form a connected framework around the silicates (Fig. 1.2j). The massive sulfide samples are mainly dominated by pyrrhotite (50-95 vol.%) associated with minor amounts of chalcopyrite, pentlandite and magnetite (Fig. 1.2l). Magnetite in massive samples is hosted principally within sulfide grains (Fig. 1.2l) and as subhedral grains at the sulfide-silicate contact (Fig. 1.2i-1.2k) in disseminated and net-textured samples. Magnetite from some of these unzoned deposits has been studied by Boutroy et al. (2014). Chromite occurs in trace amounts in some of the komatiite samples from Cape Smith (Zone Frontier and Katinniq).

Samples from the Reef -type PGE deposits, which contain disseminated sulfides only, are composed of chalcopyrite (5-62 vol.%), pyrrhotite (11-58 vol.%) and pentlandite (5-22 vol.%; Fig. 1.2m-p). Chalcopyrite occurs as isolated grains or forming aggregates with other sulfides (Figs. 1.2n, o). Chromite (ranging from 14-76%) occurs as micrometric to millimetric euhedral to subhedral isolated grains within silicates (Fig. 1.2m) and in

contact with sulfides (Fig. 1.2o). Magnetite is present only in veinlets in samples from Stillwater (Fig. 2o; Godel and Barnes, 2008).

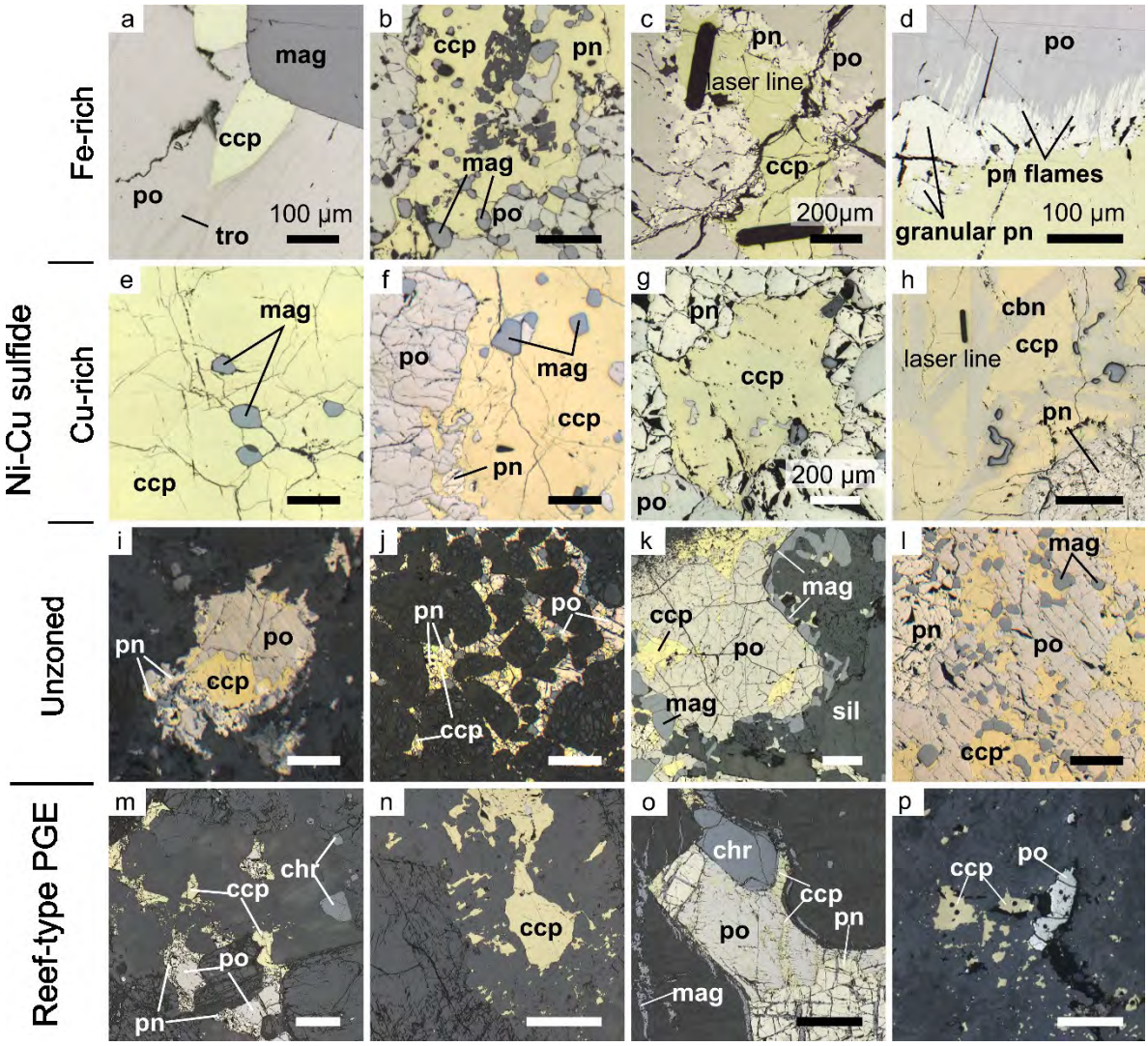

Fig. 1. 2 Reflected light photographs of chalcopyrite from different ore types and sulfide textures from Ni-Cu sulfide (a-l) and Reef-type PGE deposits (m-p). a-d: Chalcopyrite (ccp) from Fe-rich (MSS) sulfides consisting as (a) exsolutions in pyrrhotite (po) also containing troilite (tro) exsolution lamellae (Voisey´s Bay), (b) as interstitial aggregates (McCreedy East, Sudbury) and (c-d) interstitial aggregates in contact with pentlandite (pn) (Noril´sk). e-h: Chalcopyrite from Cu-rich (ISS) sulfides (>90% ccp) from (e) Broken Hammer, Sudbury, (f-g) associated with granular pyrrhotite and pentlandite (Copper Cliff and Creighton, Sudbury, respectively) and (h) with cubanite (cbn) exsolution lamellae (Noril´sk). i-l: Chalcopyrite from unzoned deposits (po-pn-ccp assemblage) showing principally disseminated sulfide textures (i-k), comprising (i) globular (Eagle) and (i) net-textured (Jinchuan), and (l) massive sulfides (Eagle). m-p: Chalcopyrite from Reef-type PGE deposits in disseminated sulfides as (m-n) isolated grains (Merensky reef) or (o-p) associated with pentlandite and pyrrhotite (Stillwater and Penikat, respectively). Chromite (chr) is present as anhedral grains in Reef-type PGE (m and o). Magnetite (mag) is commonly present as anhedral grains within most massive sulfides (i.e. b, e, f), in contact sulfides-silicates (k, Duluth) and as veins in silicates (o).

1.5.2 Trace Elements in Chalcopyrite

Only elements containing <40% of censored data (Mn, Co, Ni, Zn, Ga, Se, Ag, Cd, In, Sn, Sb, Te, Au, Tl, Pb and Bi) were used for statistical analysis. The remaining elements (PGE, As, Mo and Re) were typically below detection. The trace element composition of chalcopyrite is variable, with Co, Ag and In ranging from <1 to 50 ppm, whereas elements such as Te, Mn, Zn, Se, Sn and Pb are characterized by a wide variation (<0.1-800 ppm). In particular, Ni varies considerably from low (<1 ppm) to very high as 7900 ppm values (Noril'sk). Gallium, Sb, Au, Tl and Bi are typically in low concentrations (<1 ppm), close to or below the limit of detection. For most elements, data distribution is highly asymmetric with several outlier values (Fig. 1.4). Table 1.2 presents a statistical summary, and the complete database is in Annexe A5.

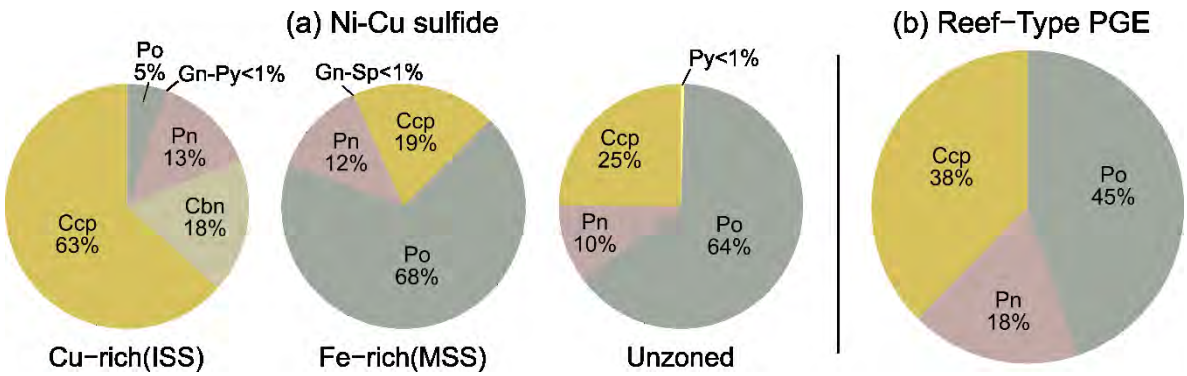

Fig. 1. 3 Pie charts summarizing relative modal proportions (%) of major sulfides, normalized to 100% sulfide) in the analyzed samples from (a) Ni-Cu sulfide and (b) Reef-type PGE deposits. Ccp: chalcopyrite, Cbn: cubanite, Po: pyrrhotite, Py: pyrite, Pn: pentla ndite. Detailed compositions given in Annexe A1.

According to hypothesis tests, chalcopyrite from Ni-Cu sulfide and Reef-type PGE deposits shows a significant difference for most elements (Fig. 1.4). Zinc, Ga and Se contents are higher in chalcopyrite from Reef-type PGE deposits, whereas the remaining elements are higher in that from Ni-Cu sulfide deposits, principally Bi, In, Sb, Sn and Te (Fig. 1.4).

The composition of chalcopyrite from Ni-Cu sulfide deposits (n=440) is highly variable, with significant differences between chalcopyrite from Cu-rich (ISS) and Fe-rich (MSS). In zoned deposits (Voisey's Bay, Noril'sk and Sudbury), chalcopyrite from Cu-rich massive sulfides is significatively higher in Ag, In, Se, Sn, Te and Tl, whereas Co and Zn are concentrated in chalcopyrite from Fe-rich massive sulfides (Fig. 1.4). Overall chalcopyrite from unzoned deposits is similar to that from Fe-rich (MSS), i.e. Cd, Co, In, Mn, Sn and Te. The content of the remaining elements (except for Sb, Pb and Se) in chalcopyrite from unzoned deposits, range between those from Cu-rich (ISS) and Fe-rich (MSS).

In Reef-type PGE deposits (Table 1.2), chalcopyrite in samples from Stillwater and a lesser extent Penikat are higher in Se than that from Bushveld and Great Dyke (Annexe A14A). The Bi content in chalcopyrite from the Great Dyke is higher than that in other deposits (Annexe A14B). Chalcopyrite from the Great Dyke and Merensky

reef (Bushveld) are richer in Sn than that in Rustenburg (Bushveld), Penikat and Stillwater PGE deposits. Nickel is considerably depleted in Penikat (<1 ppm) in comparison to other Reef-type PGE deposits (Annexe A14C). Indium contents in chalcopyrite from Penikat and Stillwater are slightly lower than in other deposits.

Elements significatively correlated are shown in Annexe A11-A14. The Pearson coefficient correlation (r) matrix is presented in Annexe A11-A13. Overall, elements show a low correlation (<0.3), with the following pairs of elements having the highest correlations: Se-Zn (0.6), Pb-Bi (-0.49), Ni-Te (-0.56), Te-Se (0.46), Sn-In (0.51) and Tl-Zn (-0.65). An imperfect grouping is shown between chalcopyrite from Cu-rich (ISS) and the remaining ores, principally in Tl vs. Zn (Annexe A14F).

1.5.3 Mantle-normalized Multi-Element Patterns

In order to compare the trace element signature of chalcopyrite from the different deposits, ore type and textures, the data were plotted on primitive mantle-normalized multi-element diagrams (Figs. 1.5 and 1.6). On these diagrams, the elements are ordered from slightly to highly chalcophile, according to Barnes (2016) and Barnes and Ripley (2016). Gallium, which is slightly chalcophile to lithophile, was placed on the left, before Zn, since it exhibits different behavior according to geological environments, with a systematic occurrence in a variety of sulfides (e.g. sphalerite; Belissont, 2016; Belissont et al., 2019; Frenzel et al., 2016; Rouxel and Luais, 2017). Manganese, nominally a lithophile element (Wood and Kiseeva, 2015) was placed at the far left of the diagram.

Table 1. 2 Summary of selected trace element composition (ppm) of chalcopyrite from Ni-Cu sulfide and Reef-type PGE deposits used for multivariate statistical analysis.

	Deposit	Region	Texture	n	Element	^{55}Mn	^{59}Co	^{60}Ni	^{66}Zn	^{71}Ga	^{82}Se	^{107}Ag	^{115}In	^{118}Sn	^{121}Sb	^{128}Te	^{197}Au	^{205}Tl	^{208}Pb	^{209}Bi
Median of detection limit					55µm	0.479	0.016	0.207	0.024	0.079	0.029	0.011	0.070	0.017	0.221	0.007	0.004	0.006	0.004	0.006
					33µm	1.03	0.028	0.410	0.051	0.149	0.030	0.026	0.147	0.027	0.501	0.012	0.007	0.011	0.007	0.004
Ni-Cu sulfide	Delta	Cape Smith Belt	Massive	15	μ_t	0.705	0.195	31.7	303	<dl	48.3	16.8	3.20	6.27	0.024	1.49	0.047	<dl	3.26	0.108
					sd_t	0.890	0.216	13.3	54.7	<dl	12.7	9.04	2.84	5.44	0.032	0.639	0.044	0.005	3.16	0.085
	Expo			9	μ_t	1.14	0.101	8.39	265	0.071	49.6	5.43	2.39	11.1	<dl	6.31	0.018	<dl	3.85	0.100
					sd_t	1.25	0.066	2.53	15.3	0.046	4.17	2.79	0.155	0.519	<dl	2.04	0.012	<dl	1.43	0.034
	Katinniq			8	μ_t	1.52	0.217	20.9	308	0.094	52.2	1.12	6.34	24.7	0.526	2.17	0.028	<dl	2.16	0.276
					sd_t	0.764	0.083	7.03	26.7	0.041	<dl	0.687	0.438	1.35	0.596	2.24	0.023	<dl	0.682	0.249
	Mesamax			7	μ_t	8.02	0.273	8.79	322	0.057	73.7	6.90	2.57	18.5	<dl	3.65	0.062	0.004	1.50	0.056
					sd_t	6.52	0.185	1.62	23.8	<dl	<dl	4.93	0.094	1.38	<dl	3.14	0.016	0.005	0.082	0.019
	Zone Frontier			24	μ_t	1.52	2.00	18.9	263	0.106	35.0	10.1	12.3	23.1	0.077	0.369	0.026	0.010	5.21	0.150
					sd_t	2.18	2.55	8.28	37.8	0.120	6.27	2.23	9.61	9.84	0.047	0.363	0.022	0.011	3.96	0.072
			Net-textured	11	μ_t	2.37	0.322	13.4	273	<dl	50.0	11.1	1.65	1.43	0.061	0.381	<dl	0.021	4.78	0.134
					sd_t	3.93	0.333	3.32	65.4	<dl	3.70	3.74	0.887	1.07	0.050	0.510	<dl	0.031	3.85	0.126
	Dunka Road	Duluth Complex	Net-textured	14	μ_t	0.63	0.414	22.0	245	0.466	50.5	1.74	1.39	3.39	0.026	2.90	<dl	<dl	8.02	0.264
					sd_t	<dl	0.330	13.7	40.2	0.086	10.3	1.95	0.206	1.60	0.019	1.11	<dl	<dl	2.93	0.225
	Mesaba		Disseminated	4	μ_t	<dl	0.018	78.6	38.5	0.359	133	2.42	1.26	11.8	<dl	1.43	<dl	<dl	6.52	0.038
					sd_t	<dl	0.021	14.8	4.04	0.030	45.9	2.54	0.218	4.83	<dl	<dl	<dl	<dl	3.97	0.016
			Net-textured	6	μ_t	1.12	0.671	8.31	256	0.196	53.6	2.43	0.591	0.546	<dl	3.59	<dl	0.009	1.29	0.154
					sd_t	<dl	0.253	3.34	78.7	0.101	5.56	1.12	0.126	0.274	<dl	0.814	<dl	0.009	0.349	0.056
	Eagle Intrusion		Disseminated	7	μ_t	<dl	0.167	11.6	310	<dl	84.4	6.78	2.21	0.692	0.069	8.46	<dl	0.020	6.64	0.932
					sd_t	<dl	0.156	4.44	79.3	<dl	16.2	1.78	0.315	0.434	0.073	5.33	0.010	0.020	4.32	0.636
			Massive	6	μ_t	0.684	0.418	65.1	502	<dl	105	11.5	3.25	32.9	0.031	15.7	0.017	0.068	22.5	1.36
					sd_t	0.735	0.423	65.8	127	<dl	17.0	5.99	0.278	1.20	<dl	21.1	0.008	0.092	38.3	1.64
	Kotselvaara	Pechenga Complex	Net-textured	11	μ_t	1.55	0.384	50.7	308	<dl	54.6	2.38	3.14	1.85	0.496	0.646	0.077	0.021	11.2	2.97
					sd_t	1.22	0.473	64.8	15.2	<dl	3.43	0.387	0.871	0.264	0.200	0.365	0.032	0.020	9.85	2.41
	Semilekta		Massive	12	μ_t	2.70	0.132	22.7	335	<dl	44.6	1.62	3.58	7.02	0.588	0.727	<dl	0.038	7.85	0.440
					sd_t	2.86	0.075	3.24	96.5	<dl	14.5	1.20	1.44	2.77	0.524	0.704	<dl	0.042	8.89	0.519
			Net-textured	7	μ_t	1.06	0.149	14.4	368	<dl	64.1	1.30	3.31	2.94	0.344	1.26	<dl	0.024	2.82	0.136
					sd_t	0.944	0.092	2.41	36.0	<dl	3.29	0.501	0.599	2.85	0.174	0.335	<dl	0.023	1.75	0.079
	Zhdanovskoe		Disseminated	5	μ_t	<dl	0.090	4.33	354	<dl	82.3	5.69	2.86	0.284	0.042	1.90	0.020	<dl	1.45	0.519
					sd_t	<dl	0.142	1.80	55.1	<dl	9.04	2.69	0.062	<dl	0.045	1.05	0.025	<dl	0.800	0.056

Table 1.2 continued

	Deposit	Region	Texture	n	Element	^{55}Mn	^{59}Co	^{60}Ni	^{66}Zn	^{71}Ga	^{82}Se	^{107}Ag	^{115}In	^{118}Sn	^{121}Sb	^{128}Te	^{197}Au	^{205}Tl	^{208}Pb	^{209}Bi
Median of detection limits					55um	0.479	0.016	0.207	0.024	0.079	0.029	0.011	0.070	0.017	0.221	0.007	0.004	0.006	0.004	0.006
					33um	1.03	0.028	0.410	0.051	0.149	0.030	0.026	0.147	0.027	0.501	0.012	0.007	0.011	0.007	0.004
Ni-Cu sulfide	Jinchuan Complex		Disseminated	7	µt	<dl	0.164	30.5	412	0.037	91.8	4.37	1.41	5.37	0.025	7.95	0.015	<dl	6.48	3.43
					sdt	<dl	0.090	7.32	50.5	<dl	9.53	0.99	0.336	2.42	0.026	1.11	0.015	<dl	2.06	2.03
			Net-textured	12	µt	2.16	0.129	13.1	286	<dl	66.7	8.47	1.66	0.338	<dl	2.59	0.016	0.006	13.6	0.918
					sdt	1.47	0.095	11.1	66.1	<dl	9.74	6.82	0.599	0.388	<dl	2.67	0.021	0.008	5.81	0.366
			Massive	2	µt	0.583	0.249	47.9	416	0.172	65.9	1.47	3.19	8.14	0.080	1.69	0.017	<dl	4.38	1.85
					sdt	<dl	0.141	1.88	44.8	0.039	6.26	0.596	0.923	2.99	0.056	0.634	0.022	<dl	0.939	0.354
	Marbridge		Net-textured	6	µt	0.583	0.249	47.9	416	0.172	65.9	1.46	3.19	8.14	0.080	1.69	0.017	<dl	4.38	1.85
					sdt	<dl	0.141	1.88	44.8	0.039	6.26	0.596	0.923	2.99	0.056	0.634	0.022	<dl	0.939	0.354
	Medvezhy Creek	Noril'sk Intrusion	Massive	12	µt	<dl	0.232	45.1	157	0.036	154	6.95	0.823	<dl	0.028	45.9	<dl	0.998	4.65	0.047
					sdt	<dl	0.338	9.10	131	<dl	132	3.97	0.622	<dl	0.019	51.6	<dl	1.19	8.07	0.051
	Talnakh			36	µt	6.68	0.189	1220	135	<dl	110	1.47	2.78	0.592	0.018	21.1	<dl	0.656	12.9	0.016
					sdt	6.00	0.207	2410	168	0.032	58.8	2.08	2.07	0.558	0.019	21.9	<dl	0.783	15.1	0.008
	Broken Hammer	Sudbury Igneous Complex	Massive	16	µt	<dl	0.823	<dl	81.9	0.081	192	1.04	9.25	64.7	0.026	0.539	0.192	0.008	3.15	2.16
					sdt	<dl	1.44	<dl	105	0.065	30.3	0.364	0.370	65.4	0.023	0.361	0.193	0.008	2.36	0.690
	Copper Cliff			8	µt	6.99	0.138	39.3	352	0.157	183	5.43	10.5	53.3	0.072	3.23	<dl	0.150	53.3	0.942
					sdt	5.95	0.070	9.57	23.3	0.080	14.1	1.40	2.69	15.4	0.028	1.96	<dl	0.089	62.7	0.110
	Creighton			47	µt	1.06	0.408	72.9	491	0.082	77.4	3.98	1.64	10.7	0.048	0.673	0.024	<dl	2.47	2.42
					sdt	0.504	0.228	26.1	84.0	0.050	7.36	2.44	1.17	8.35	0.042	0.694	0.042	<dl	1.07	0.748
			Net-textured	10	µt	1.06	0.481	57.7	493	0.114	94.0	3.49	1.95	6.48	0.040	1.15	<dl	<dl	3.07	0.451
					sdt	<dl	0.236	4.15	44.1	<dl	5.80	0.256	0.460	1.28	0.019	0.626	<dl	<dl	0.88	0.224
	McCreedy		Massive	73	µt	1.19	0.165	46.9	207	0.061	148	19.7	7.59	126	0.019	2.41	0.024	0.046	4.27	0.219
					sdt	1.12	0.118	9.54	91.1	0.033	73.7	18.1	2.88	102	0.020	2.39	0.028	0.060	2.36	0.103
	Eastern Deeps	Voisey's Bay Anorthosite Complex	Massive	5	µt	0.660	0.139	12.1	227	0.293	56.1	2.55	2.79	2.77	<dl	11.0	<dl	<dl	2.27	0.485
					sdt	0.725	0.070	4.19	50.1	0.129	5.51	1.89	0.745	0.539	<dl	3.55	<dl	<dl	1.17	0.404
	Ovoid			53	µt	0.803	0.132	5.53	187	<dl	72.9	4.81	6.43	11.4	<dl	10.9	<dl	0.037	9.92	0.174
					sdt	0.751	0.149	4.38	35.6	<dl	19.2	4.81	5.22	11.8	<dl	7.74	<dl	0.074	5.12	0.132
			Net-textured	7	µt	<dl	0.160	9.17	168	0.127	54.4	4.55	1.73	6.00	<dl	16.2	<dl	<dl	5.46	0.190
					sdt	<dl	0.088	3.17	29.3	<dl	2.98	2.73	0.260	1.15	<dl	1.68	<dl	<dl	1.41	0.052

Table 1.2 continued

	Deposit	Region	Texture	n	Element	^{55}Mn	^{59}Co	^{60}Ni	^{66}Zn	^{71}Ga	^{82}Se	^{107}Ag	^{115}In	^{118}Sn	^{121}Sb	^{128}Te	^{197}Au	^{205}Tl	^{208}Pb	^{209}Bi
Median of detection limits					55um	0.479	0.016	0.207	0.024	0.079	0.029	0.011	0.070	0.017	0.221	0.007	0.004	0.006	0.004	0.006
					33um	1.03	0.028	0.410	0.051	0.149	0.030	0.026	0.147	0.027	0.501	0.012	0.007	0.011	0.007	0.004
Reef-type PGE	Merensky Reef	Bushveld Complex	Disseminated	12	μt	1.34	0.101	14.5	519	0.489	132	4.08	1.69	3.81	<dl	<dl	<dl	<dl	103	0.019
					sdt	0.772	0.092	1.950	112	0.142	15.6	1.99	0.448	1.20	<dl	<dl	<dl	<dl	83.2	0.008
	Rustenburg			46	μt	2.08	0.071	20.6	310	0.059	103	2.97	1.95	0.123	<dl	<dl	<dl	0.014	5.49	0.017
					sdt	1.74	0.050	5.09	83.9	0.045	22.6	1.33	1.05	0.128	<dl	<dl	<dl	0.018	2.83	0.019
	Mimosa	Great Dyke		23	μt	1.04	0.182	31.9	599	0.182	132	2.40	1.51	4.05	<dl	0.536	0.018	<dl	1.16	0.445
					sdt	0.609	0.158	6.85	98.7	0.144	35.4	2.01	0.864	3.42	<dl	0.547	0.026	<dl	0.587	0.446
	PV Reef	Penikat		12	μt	1.21	0.033	1.07	363	0.080	188	3.46	0.346	0.113	<dl	1.39	<dl	<dl	1.35	0.029
					sdt	0.896	0.026	0.953	83.3	0.046	23.2	1.02	0.092	0.108	<dl	1.07	<dl	<dl	0.416	0.032
	East Boulder	Stillwater Complex		23	μt	1.34	0.299	29.4	407	0.085	252	5.68	0.852	<dl	<dl	<dl	<dl	0.018	7.73	0.010
					sdt	1.17	0.158	15.5	99.9	0.060	130	7.12	0.872	<dl	<dl	<dl	0.008	0.026	6.13	0.007
			Total	556																

<dl: below detection limit; n: number of analyzed grains; sd_t: 1 trimmed standard deviation; μ_t: γ-trimmed mean with γ=0.2

Overall, mantle-normalized patterns for chalcopyrite from different deposit and ore types are similar: they all increase from left to right of the diagram, with increasing chalcophile behavior. All chalcophile patterns have strong Co and Ni negative anomalies due to preferential partitioning of these elements into pentlandite and pyrrhotite. In detail, chalcopyrite is depleted in lithophile (Mn) and in slightly chalcophile to lithophile element (Ga) relative to mantle. Concentrations of chalcophile elements (Zn to Te) range from 1- to 10000-times mantle concentrations in zoned deposits (Fig. 1.5a-c) and from 50- to 1000-times mantle in unzoned deposits (Figs. 1.5g-j).

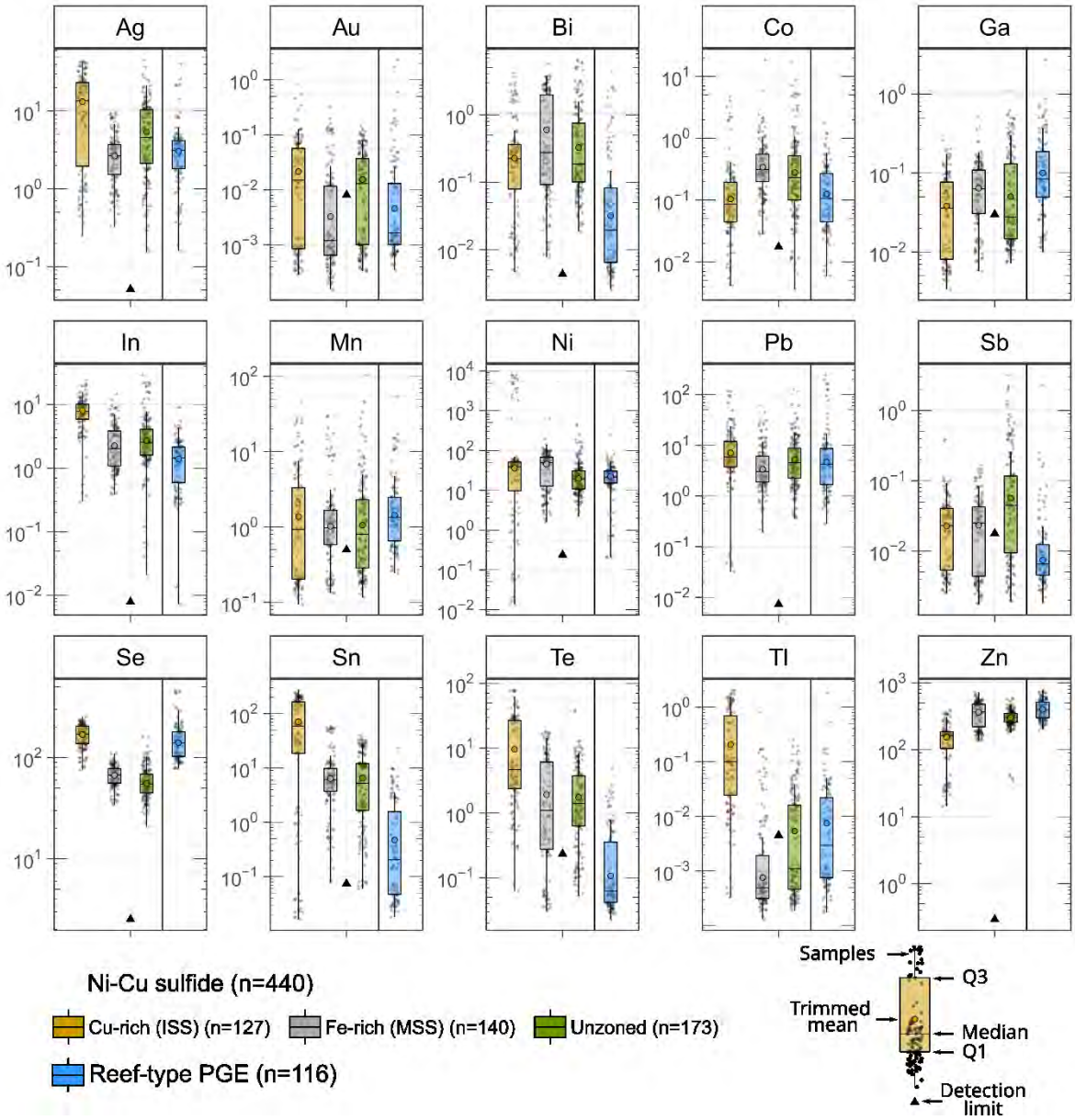

Fig. 1. 4 Boxplots showing trace elements in chalcopyrite from Ni-Cu sulfide and Reef-type PGE deposits. n: number of analyzed grains. Q1 and Q3 denote first and third quartiles, respectively.

Although the pattern is similar for chalcopyrite from Cu-rich (ISS) and Fe-rich (MSS) samples, with concentrations up to 10000- and 1000-times mantle concentration, respectively (Figs. 1.5d-f), the median of normalized values of Tl and Sn, and a lesser extent In, Se, Ag and Te are higher in chalcopyrite from Cu-rich (ISS) sulfides (Fig. 1.5f). Chalcopyrite from Cu-rich (ISS) samples from Broken Hammer, Sudbury, shows a slightly different pattern, with higher Bi and Au, and lower Tl, Ni, Ag and Te than the remaining chalcopyrite from Cu-rich (ISS) ores (Fig. 1.5d). In unzoned deposits, trace element patterns from chalcopyrite, plotted according to sulfide texture, are similar (Figs. 1.5g-j), with only Mn, Tl and Sn in higher concentrations in chalcopyrite from massive sulfides compared to chalcopyrite from disseminated sulfides. In contrast, Bi has higher contents in chalcopyrite from disseminated sulfides than that from massive ores (Fig. 1.5j). Furthermore, the signature of chalcopyrite from Fe-rich (MSS) samples is similar to that from unzoned deposits (Fig. 1.5j), with the median values from both massive and disseminated samples within the Fe-rich (MSS) field. A few elements have slightly different values that vary among the unzoned deposits, such as Mn (lower in chalcopyrite from disseminated samples from Mesaba), Sb (higher in chalcopyrite from massive samples from Semilekta, Pechenga) and In (lower in chalcopyrite from massive samples from Jinchuan).

Chalcopyrite from Reef-type PGE deposits has similar patterns to those from Ni-Cu sulfide (Fig. 1.6), including negative Co and Ni anomalies. The lithophile to slightly chalcophile elements (Mn, Ga) are slightly more abundant in chalcopyrite from Reef-type PGE deposits than those from Ni-Cu sulfide deposits (Fig. 1.6b). In addition, chalcopyrite from Reef-type PGE deposits is depleted relative to those from Ni-Cu sulfide in Sn, Bi, and Te.

1.5.4 Multivariate Data Analysis

1.5.4.1 PLS-DA on Trace Element Composition of Chalcopyrite

Preliminary PLS-DA was performed to assess the potential of the trace element composition of chalcopyrite to distinguish between deposit type (Ni-Cu sulfide and Reef-type PGE deposits), ore types (Cu-rich, Fe-rich and unzoned) and sulfide textures (massive to disseminated) in Ni-Cu sulfide deposits. Models were built with 15 elements selecting 14 latent variables, in order to obtain most of the relevant information from the dataset. A cross validation procedure was carried out to optimize classification models.

The PLS-DA results show that Ni-Cu sulfide vs. Reef-type PGE deposits form two clusters in scores plot corresponding to the assigned classes (Fig. 1.7a), indicating a constrained variation in their trace element compositions. The first two latent variables explain about 25.5% of the variance of the 15 independent chemical variables (t1=15.8%; t2=9.7%; Fig. 1.7a) and at least 5 latent variables are necessary to explain more than 50% of the data variance (Annexe A16). Figure 1.7b shows correlations among independent variables (elements) and, in turn, correlations between these and the dependent variables (deposit type). In this model, most of the

elements plot close to the center indicating little relevance in understanding the total variability in the system, supported by relatively low loading values on qw*1 and qw*2.

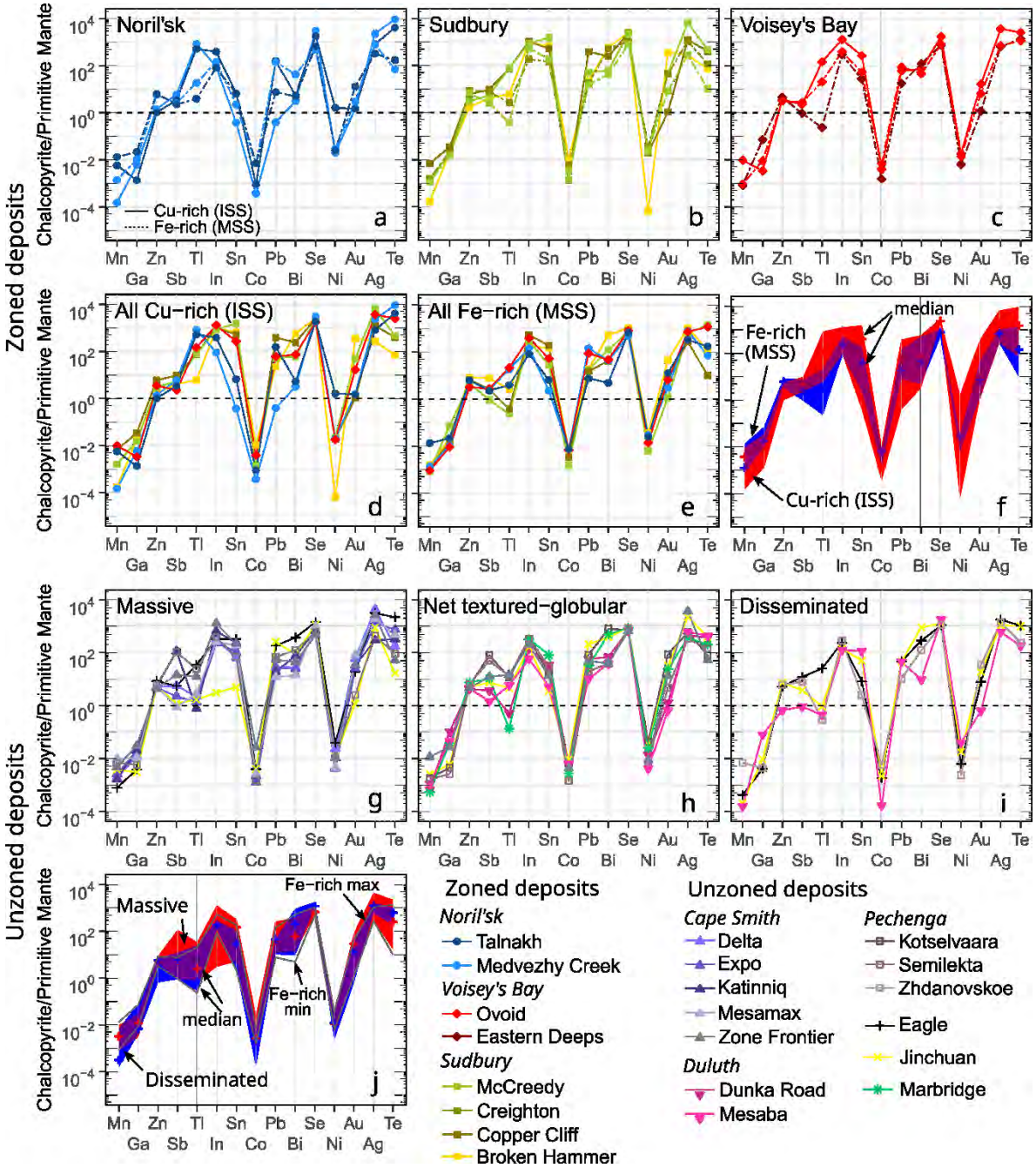

Fig. 1. 5 Multi-element diagrams of chalcopyrite from Ni-Cu sulfide deposits according to ore type and sulfide textures from zoned deposits (a-f) and unzoned deposits (g-j). Sulfide texture follows simplified classification from Barnes et al. (2017) and Barnes et al. (2018). Order of elements from slightly to highly chalcophile, according to Barnes and Ripley (2016) and Barnes (2016). Primitive mantle concentrations from Lyubetskaya and Korenaga (2007).

Tellurium is positively correlated with Ni-Cu sulfide deposits and to a lesser extent Se with Reef-type PGE deposits, which are located diametrically opposite (Fig. 1.7b). The positive correlation between Se and Reef-

type PGE deposits is confirmed by a highly positive value of the regression coefficient (Annexe A15A), indicating that this element is in higher concentration in chalcopyrite from these deposits (160 ppm on average) compared to those from Ni-Cu sulfide deposits (93 ppm). Tellurium shows similar characteristics in relation to chalcopyrite from Ni-Cu sulfide deposits, which have higher concentrations (6.6 ppm) than those from Reef-type PGE deposits (typically below detection limit). To a lesser extent, Co, Bi, Sn, In and Ni also have positive correlations with Ni-Cu deposits, whereas Au, Ga, and Zn are slightly positively correlated with Reef-type PGE deposits. Only Bi, In, Se, Sn, Te and Zn have a variable importance on projection (VIP) ≥1, suggesting that they have a higher influence in the discrimination between Ni-Cu sulfide and Reef-type PGE deposits than the remaining elements (Annexe A15B).

Comparing ore type PLS-DA reveals a grouping in t1-t2 scores plot (Fig. 1.7c) according to the assigned classes (Cu-rich, Fe-rich and unzoned). Chalcopyrite from Fe-rich (MSS) and unzoned deposits, with overall negative and positive t2 scores, respectively, and positive t1 scores, overlap significantly showing a high dispersion, indicating that trace element composition of chalcopyrite varies considerably by ore types; however, they show a clear separation from chalcopyrite from Cu-rich (ISS) samples, which shows positive t1 scores (Fig. 1.7c). The first two latent variables explain 29.2% of the variance (t1=19.5%; t2=9.7%; Fig. 1.7c) and at least 4 latent variables are necessary to explain more than 50% of the data variance (Annexe A17).

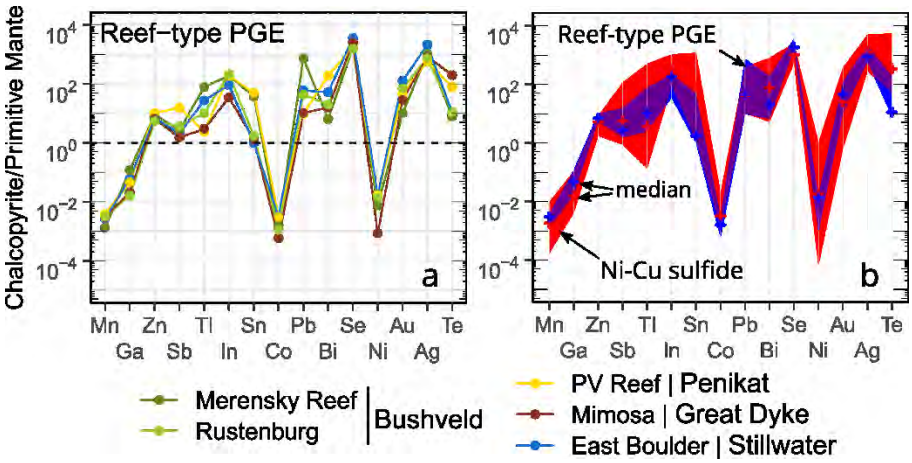

Fig. 1. 6 Multi-element diagram for chalcopyrite from Reef-type PGE deposits (a) and comparison with Ni-Cu sulfide deposits (b). Order of elements from slightly to highly chalcophile, according to Barnes and Ripley (2016) and Barnes (2016). Primitive mantle concentrations from Lyubetskaya and Korenaga (2007).

Thallium, Se, Sn show a positive correlation with Cu-rich (ISS) samples, whereas Zn, Co and a lesser extent Ga and Sb are positively correlated with Fe-rich/unzoned group (Fig. 1.7d). The positive correlations are confirmed by the respective high positive regression coefficients for the corresponding groups (e.g., positive in Se for Cu-rich; Annexe A15C). Nickel, Sb, Se, Sn, Tl and Zn have a VIP ≥1, suggesting a higher influence on discrimination than the remaining elements (Annexe A15D).

Although Te is positively correlated with Cu-rich ore type in Fig. 1.7b, the regression coefficient is negative, indicating low concentration in these Cu-rich samples relative to Fe-rich/unzoned samples (Annexe A15C). This apparent contradiction is explained by the fact that VIP scores and regression coefficients are calculated based on the entire model (comprising all original and latent variables), hence the t1-t2 and qw*1*-qw*2 plots show only a fraction of the variance of the whole data. Consequently, it is necessary to analyze more combinations between latent variables.

The composition of chalcopyrite by sulfide texture classes (Ni-Cu sulfide deposits) is shown in Figs. 1.7e and 7f. The score plot t1-t2 (Fig. 1.7e) displays grouping according to massive, net-textured and disseminated samples. Chalcopyrite from massive samples is widely dispersed, indicating a high variability of the trace element compositions. In contrast, trace elements in chalcopyrite from net-textured and disseminated sulfides show less variability, however, with considerable overlap with massive sulfides. First and second latent variables explain 26.4% of variance and at least 5 latent variables are necessary to explain more than 50% (Annexe A18). Overall, elements in the loading plots are concentrated in the center, with no significant correlation between them and the classes. Tin and Mn are positively correlated with chalcopyrite from massive samples, whereas Te and Bi show a slightly positive correlation with disseminated and net-textured sulfides (Fig. 1.7f). However, according to VIP scores and regression coefficients, In, Sn and Tl are the variables with more importance in discrimination (Annexe A15E, F).

Results of cross validation indicate that the optimal number of latent variables to obtain a classification error sufficiently low is three for the model by deposit type, four by ore type, and two by sulfide textures (Annexe A19). In element selection, we followed the strategy proposed by Chong and Jun (2005) and Wold et al. (2004), which combines VIP scores and regression coefficients indicating that both should be low for a variable to be excluded. To optimize PLS-DA model by deposit type, Bi, In, Se, Sn and Te were selected (high regression coefficients and VIP>1). Zinc was excluded as regression coefficients are low (despite VIP>1). For PLS-DA by ore type in Ni-Cu sulfide deposits, Sb, Se, Sn, Tl and Zn were selected. Nickel was excluded as its regression coefficients is low. The PLS-DA model by sulfide texture type was simplified to 3 trace elements (In, Sn and Tl).

An optimized PLS-DA model by deposit type (Fig. 1.8a-e), built with the five selected elements, improves the discrimination between chalcopyrite from Reef-type PGE and Ni-Cu sulfide deposits, displaying a better clustering and reduced overlap. The three selected latent variables explain 69.1% of the variance corresponding to the five selected trace elements. The positive correlation between Se and Reef-type PGE deposits is more obvious compared to the preliminary model, whereas Te, Bi, Sn and In remain positively correlated with Ni-Cu sulfide deposits (Figs. 1.8b, c and d). Cross validation of data suggests that this model discriminates almost perfectly between the two deposit types, supported by the AUROC value of 0.97 (Fig. 1.8e).

Optimized PLS-DA results according to ore type are shown in Figs. 1.8f-j. The four selected latent variables explain 94% of the variance of the selected trace elements. The separation between chalcopyrite from Cu-rich samples and those from Fe-rich/unzoned samples is enhanced (Fig. 1.8f). However, Fe-rich samples still overlap significantly with those from unzoned deposits. Some chalcopyrite from the unzoned sulfides at Duluth and six samples from Fe-rich ore at Voisey's Bay are located within the Cu-rich field (Fig. 1.8f). Indium, Se, Sn and Tl are positively correlated with chalcopyrite from Cu-rich samples, having positive regression coefficients, whereas Sb and Zn show a high positive correlation with Fe-rich/unzoned samples (Figs. 1.8g and h). Antimony and Sn are shown as the more relevant elements in discrimination for this model (VIP>1, Fig. 1.8i). The AUROC value (0.99) confirms that the improved model has a high reliability to discriminate between chalcopyrite from Cu-rich and other ore types. However, separation between Fe-rich (AUROC=0.71) and unzoned samples (AUROC=0.75) is not possible (Fig. 1.8j).

Although the PLS-DA model by sulfide texture was built with only 3 trace elements and simplified to 2 latent variables, which explain 74.3% of the total variance, overlapping of the textural groups remains significant (Fig. 1.8k). The massive sulfide group shows a notable separation according to ore type, with chalcopyrite from massive Cu-rich (ISS) samples on the left side, whereas those from massive Fe-rich (MSS) sulfides and from unzoned deposits are in the center (Fig. 1.8k). Thallium, Sn and to a lesser extent In are positively correlated with chalcopyrite from massive samples (Fig. 1.8l), and they are opposite to chalcopyrite from disseminated/net-textured samples. Chalcopyrite from massive Cu-rich (ISS) samples have a highly positive correlation with Tl and Sn (Fig. 1.8l). Discrimination by sulfide texture must be taken with caution for the following reasons: (1) AUROC values (ranging from 0.76-0.81; Fig. 1.8o) indicate moderate performance of the model, and (2) Tl, an important variable in this model, has at least 30% of values close or below to the detection limit.

1.5.5 Distribution of Trace Elements Between Chalcopyrite and Other Sulfides

As described previously, most of the studied Cu-rich samples from zoned deposits are characterized principally by chalcopyrite and pentlandite formed by exsolution from ISS (Barnes et al. 2006; Dare et al. 2014). Cubanite exsolved from chalcopyrite occurs as lamellae. Iron-rich samples typically consist of pyrrhotite, pentlandite and, to a lesser extent, by chalcopyrite formed by exsolution from MSS. However, interstitial chalcopyrite is the principal Cu-sulfide in these ores, exsolved from ISS, which crystallized from trapped Cu-rich liquid in MSS.

All these phases co-exist in textural equilibrium. Although the sulfides did not necessarily crystallize simultaneously, we calculated an elemental ratio between chalcopyrite and other sulfides in order to study how trace elements are distributed (Annexe A6; Annexe A22). This ratio, called in this study D, should not be confused with partition coefficients, used to measure quantitatively the equilibrium fractionation between solid/melt or co-crystallising minerals (Bédard, 2005; Sun, 2018).

Overall, our data agrees with previous studies (Dare et al., 2014; Dare et al., 2010b; Duran et al., 2016b; Mansur et al., 2020), except for Au ($D^{Au}_{ccp/po}$ and $D^{Au}_{ccp/cb}$ <1). Selenium is evenly distributed amongst all the sulfides, with ratios ranging from 0.97 to 1.4. Silver, Pb, and Ga also show roughly an even distribution between chalcopyrite and pentlandite ($D_{ccp/pn}$ 0.63-1.12; Annexe A22A), whereas Sn, In and Zn partition principally into chalcopyrite with high ratio values ($\mathrm{D_{ccp/pn}}$ $83.6\text{-}121$). Bismuth, Te, and Sb have a weak preference for pentlandite in comparison to chalcopyrite ($D_{ccp/pn}$ $0.31 - 0.55$). In contrast, Tl, Au and Mn show a strong preference for pentlandite ($D_{ccp/pn}$ $0.02 - 0.13$), and with Co and Ni having the strongest preference for pentlandite, with the lowest ratios ($D_{ccp/pn} < 10^{-4}$).

Antimony and Mn have ratios between chalcopyrite and pyrrhotite (Annexe A22B) close to 1, whereas Bi show a slight preference for chalcopyrite $D_{ccp/po}$ 1.92. However, In, Zn, Cd and Sn prefer chalcopyrite over pyrrhotite ($D_{ccp/po}$ $94.5 - 1269$). Co and Ni are enriched in pyrrhotite in comparison to chalcopyrite ($D_{ccp/po} < 0.008$), but less so than with pentlandite.

Chalcopyrite and cubanite (Annexe A22C) incorporate Bi, Se, Te, Tl and Zn uniformly, with ratios of around 1 ($D_{ccp/cbn}$ $0.81 - 1.05$). However, Pb, Co, Au, Sb ($D_{ccp/cbn}$ $0.24 - 0.43$) and to a lesser extent Ga, Mn, Ni and Ag ($D_{ccp/cbn}$ $0.50 - 0.0.58$) are preferentially concentred in cubanite ($D_{ccp/cbn}$ $0.28 - 0.58$), whereas Sn, Cd and In have a preference for chalcopyrite ($D_{ccp/cbn}$ $1.38 - 2.49$).

The distribution of trace elements between chalcopyrite and pentlandite shows a high variability for most of the elements, ranging for instance, from 0.55 to 756 for Sn or from 0.46 to 1085 for Zn. According to sample and ore type, pairs of adjacent chalcopyrite and pentlandite were plotted (Annexe A23). Pairs from Cu-rich (ISS) ores show systematically higher ratios ($\mathrm{D_{ccp/pn}} \gg 1$), indicating a higher enrichment of Bi, Pb and Ag in chalcopyrite in comparison to pentlandite. Chalcopyrite from Fe-rich (MSS) ores show two populations: 1) pairs with values higher than 1 (Annexe A23A-C), and 2) pairs with values lower than 1. The latter being normally associated with pentlandite in contact with pyrrhotite and chalcopyrite (Annexe A23D), and probably formed by a peritectic reaction of Fe-rich MSS with trapped Cu-rich sulfide liquid (Mansur et al., 2019).

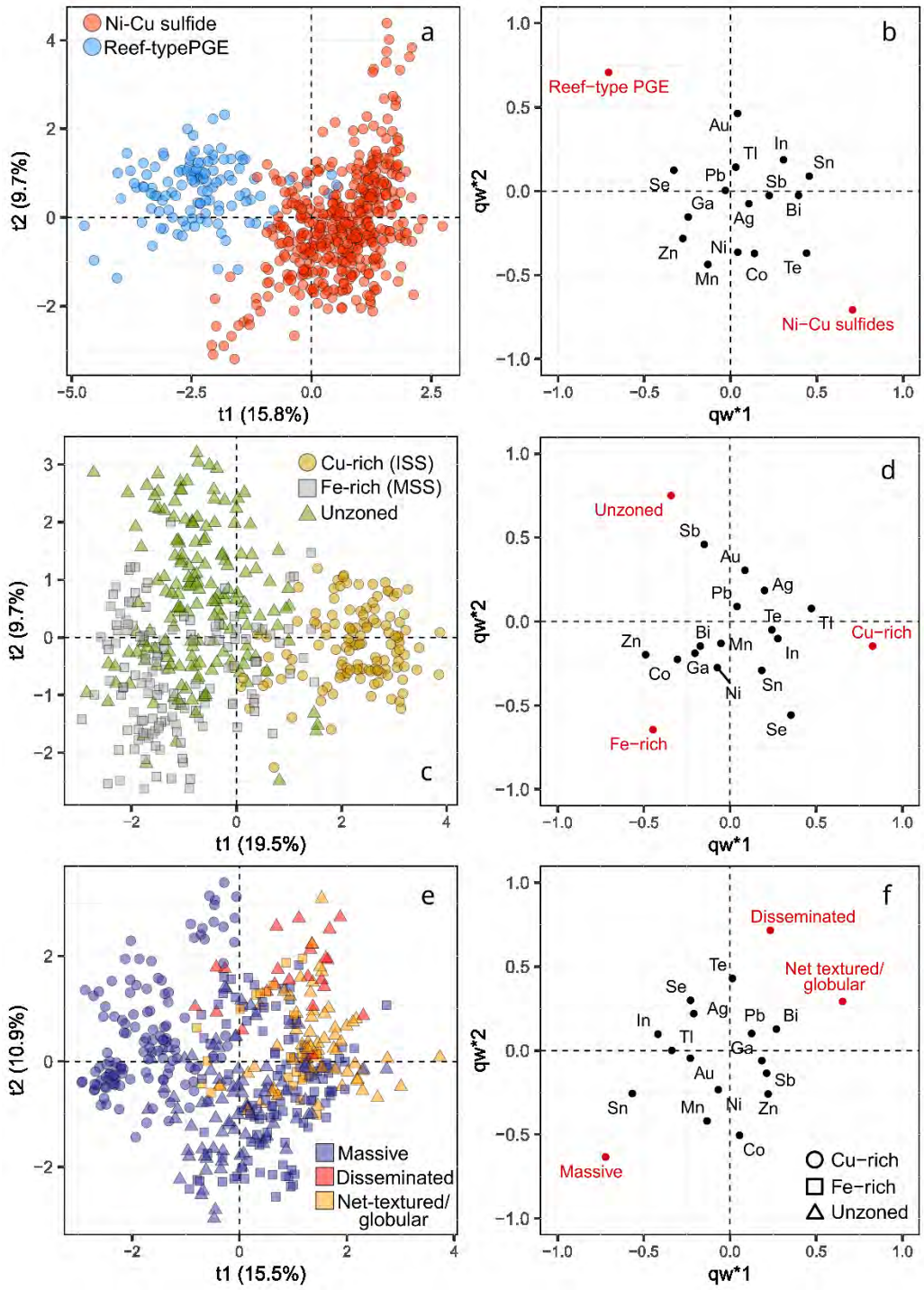

Fig. 1. 7 Preliminary PLS-DA models for trace element composition of chalcopyrite from magmatic sulfide deposits (Ni-Cu sulfide, Reef-type PGE). (a) score plot of first latent variable (t1) vs. second latent variable (t2) showing a marked separation of the samples by deposit type. (b) X-loadings (w*) and Y-loadings (q) in qw*1 vs. qw*2 space showing correlation between Se and Reef-type PGE deposits, whereas Te is highly correlated with Ni-Cu sulfide deposits. (c) Score plot on t1-t2 latent variable space reveals a marked separation between chalcopyrite from Cu-rich (ISS) sulfides from those from Fe-rich (MSS) and unzoned sulfides. (d) X-loadings (w*) and Y-loadings (q) in qw*1 vs. qw*2 space shows that chalcopyrite from Cu-rich (ISS) ores is correlated with Tl, In, Se and Sn and those from Fe-rich (MSS) and unzoned sulfides are correlated with Ni, Zn and Co. (e) Score plot shows important overlap between massive and net-textured/disseminated samples with a slight grouping in the right upper quadrant. According to loading plot (f), regression coefficients and VIP scores (see Annexe A15) only In, Sn, Tl show higher values.

1.6 Discussion

1.6.1 Overview of Processes that Control the Variation of Trace Elements in Chalcopyrite

Several processes can control the trace element content in chalcopyrite from magmatic sulfide deposits (see review by Mansur et al., 2021), such as 1) crustal contamination; 2) interaction between sulfide liquid and magma (R-factor); 3) crystallization of sulfide liquid (fractional vs. equilibrium); 4) reaction of trapped residual Cu-rich liquid with Fe-rich (MSS) cumulates (i.e. peritectic reaction); 5) competition with other phases, such as PGM, during crystallization and subsolidus exsolution, and 6) reaction with later hydrothermal/metamorphic fluids. As no evidence was found for the last process, it is not discussed further.

Based on results of optimized PLS-DA, we show that the trace element composition of chalcopyrite is significantly different between deposit types (Ni-Cu sulfide and Reef-type PGE) and between certain ore types in Ni-Cu sulfide deposits (Cu-rich from the rest). However, there is no significant difference among the sulfide textures (massive and disseminated). The potential effects of processes involved in the formation of magmatic sulfide deposits on the trace element composition of chalcopyrite do not seem to affect its discriminating capability, thus allowing to define compositional criteria for each group.

According to PLS-DA results by deposit type, Bi, Te, Sn and a lesser extent In and Se are the most important elements in classification by deposit type (Fig. 1.8a-e). Chalcopyrite from Reef-type PGE deposits are characterized by high values of Se (Figs. 1.4 and 1.6), whereas the remaining elements are low relative to chalcopyrite from Ni-Cu sulfide deposits. High contents of Se, a strongly to highly chalcophile element (Barnes, 2016), in chalcopyrite from Reef-type PGE deposits could be recording a higher R factor in comparison to Ni-Cu sulfide deposits. In contrast, high values of Te, Sn, In and Bi in chalcopyrite from Ni-Cu sulfide deposits could be affected by fractional crystallization (Barnes and Lightfoot, 2005; Dare et al., 2014; Mansur et al., 2020; Naldrett, 2004). The PLS-DA model by ore type (Ni-Cu sulfide deposits) suggests that Sn, Sb and partly Se, Tl and Zn have a high influence in discrimination. This agrees with previous work that shows that chalcopyrite records fractional crystallization, whereby elements incompatible with MSS, such as Sn, Tl and Se, are characteristically higher in chalcopyrite from Cu-rich (ISS) samples relative to those from Fe-rich (MSS)/unzoned ores (Fig. 1.4).

1.6.1.1 Crustal Contamination

It is widely accepted that Ni-Cu-PGE deposits form when sulfide saturation of a mafic-ultramafic magma is attained, forming an immiscible S-rich liquid (Naldrett, 2004). Saturation is thought to result from S-incorporation from xenoliths or by thermomechanical incorporation from S-rich country rocks, near the base of komatiite flows (Ripley and Li, 2013). In addition to S input during assimilation of black shales, other chalcophile elements can

be transferred to the magma, principally TABS (Te, As, Bi, Sb, Sn), Mo, and Pb via droplets of sulfide melt (Samalens et al., 2017a). On the basis that TABS would be expected to be high when external sources of S are assimilated, Mansur et al. (2021) proposed the use of As/Se and Sb/Se in pentlandite to indicate high degrees of crustal contamination, typical of some Ni-Cu sulfide deposits. They also observed high As, Bi and Sb contents of chalcopyrite in samples from Beni Bousera, Mirabela and Rosie prospect that they attributed to crustal contamination.

Tellurium, Bi, In, Sn and Sn are overall higher in chalcopyrite from Ni-Cu deposits compared to those from Reef-type PGE deposits (As and Mo are below detection; Fig. 1.6b). The high contents of Sb and Bi recorded in chalcopyrite from Pechenga, Marbridge, Katinniq and Eagle (Fig. 1.5g-i) are likely the result from important crustal contamination by S-rich metasediments (Barnes et al., 2001; Benson et al., 2020; Mungall, 2007; Ripley, 2014; Song et al., 2009). However, high concentrations of some of these 'contaminant' elements (Sn, Te, In ± Bi, Pb) in Cu-rich (ISS) compared to Fe-rich (MSS) samples (Fig. 1.4), such as those from Sudbury (Fig. 1.5b), suggest other processes (e.g., fractional crystallization) affecting the signature of trace elements in chalcopyrite.

Crustal contamination is also common in magmas that formed Reef-type PGE deposits, however, it does not necessarily involve an external source of S. Mansur et al. (2021) described samples from Great Dyke that probably record crustal contamination with high As/Se and Sb/Se ratios in pentlandite. Although the Bushveld magmas probably incorporated As and Sb from country rocks, the high R-factors increased Se contents because it is more chalcophile than As and Sb, thus leading to low As/Se and Sb/Se ratios (Mansur and Barnes, 2020a, b).

1.6.1.2 Sulfide liquid-magma interaction (R-factor)

The degree of interaction of the sulfide liquid with magma (R-factor) is well known to affect the composition of base metal sulfides (Mansur et al., 2021 and references therein) and is thought to be critical to increase the concentration of strongly to highly chalcophile elements (e.g. Se, PGE, Te, Ag and Au) in the sulfide liquid (Barnes and Lightfoot, 2005). Disseminated sulfides from Reef-type PGE and Ni-Cu sulfide deposits are considered to form at higher R-factors than massive Ni-Cu sulfide (Duran et al., 2016a; Mansur et al., 2021). Disseminated, net-textured and massive samples from the same deposit (e.g., Pechenga and Jinchuan) are compared to evaluate the possible effect of R-factor on the trace element composition in chalcopyrite from unzoned Ni-Cu sulfide deposits (Fig. 1.5g-i). At Pechenga, massive sulfides formed at unusually high R-factors (<1000, Brügmann et al., 2000), whereas disseminated samples formed at low R factor ≈ 250 (Barnes et al., 2001). At Jinchuan, R-factors are about 2000 for disseminated samples and 260 for massive samples (Li and Ripley, 2011).

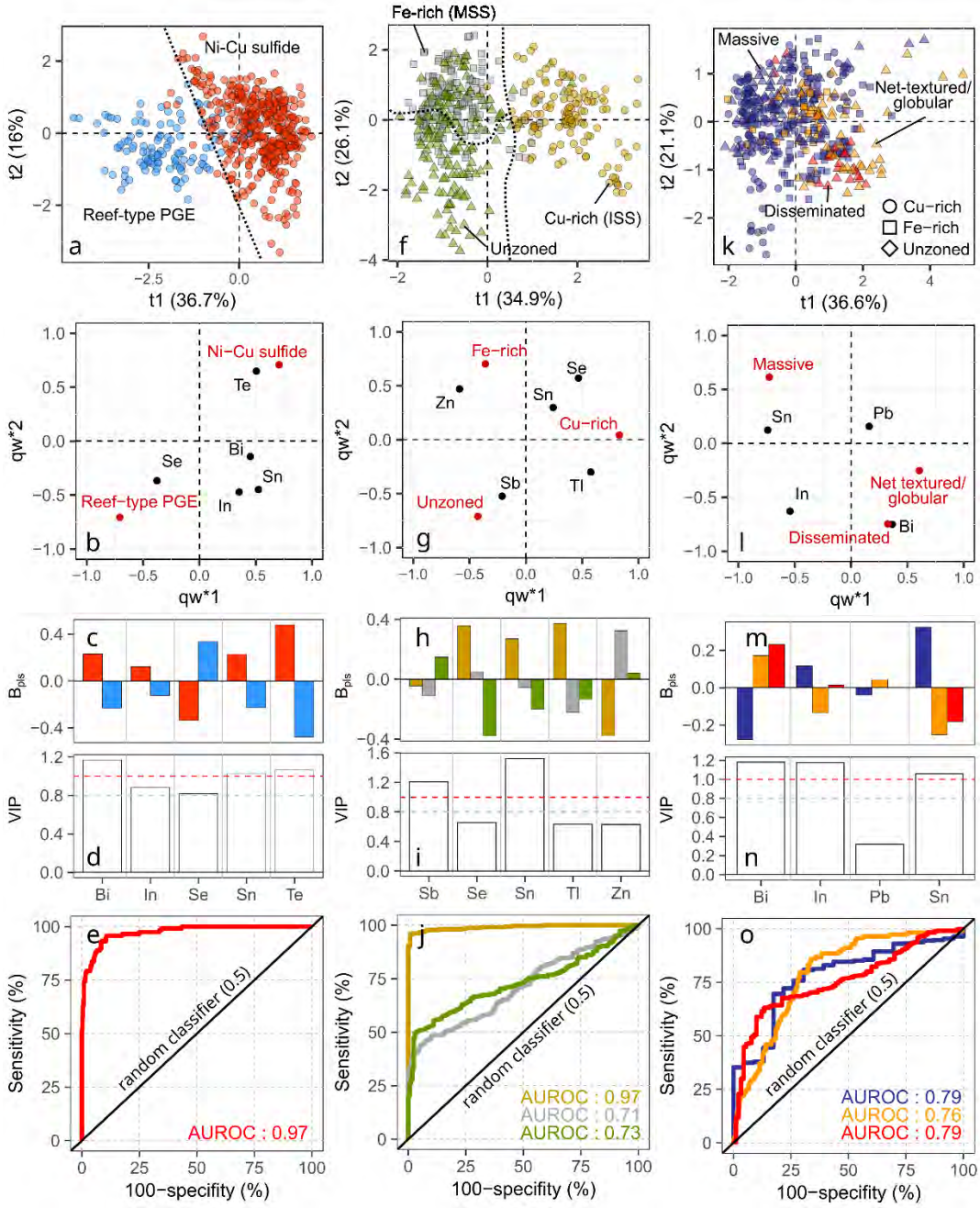

Fig. 1. 8 Optimized PLS-DA models for trace element composition of chalcopyrite from magmatic sulfide deposits (Ni-Cu sulfide, Reef-type PGE). (a) Score plot t1-t2 showing clustering by deposit type. (b) Correlations between independent (trace elements) and dependent (deposit type) variables are enhanced in this model. (c) Regression coefficients (B_{pls}) combined with VIP scores (d) suggest that Bi, Sn and Te are important in discrimination (VIP >1), and to a lesser extent In and Se (VIP <0.8). High performance of the model is supported by (E) AUROC value (0.97). (f) Separation of chalcopyrite from Cu-rich (ISS) and the Fe-rich (MSS) and unzoned ore types is more pronounced, but significant overlapping between chalcopyrite from Fe-rich (MSS) and unzoned remains. (g) Chalcopyrite from Cu-rich (ISS) sulfides are correlated with Se, Sn and Tl, whereas those Fe-rich (MSS) and unzoned sulfides are correlated positively with Zn and Sb. (h and i) Sn and Sb are the more relevant elements in discrimination. (j) High AUROC values (0.99) for the Cu-rich (ISS) group suggest a reliable model to discriminate chalcopyrite in Cu-rich ore bodies from the others. Moderate AUROC values for Fe-rich (MSS) and unzoned groups indicate that discrimination is not possible. (k) Score plot shows significant overlap between groups. (l) Thallium and Sn are correlated with chalcopyrite from massive samples, and to a lesser extent In. (m and n) Although this model comprises only 3 variables, only In seems more important in discrimination, and (o) AUROC values indicate a moderate performance of the model. Dotted lines in score plots draw boundary between classes, given by the model. Red dashed lines in VIP plots indicate threshold 1.

Our results show that at the deposit scale, the interaction between sulfide liquid and the magma is recorded by systematically high values of strongly chalcophile elements (Ag, Au and Te) in disseminated compared to massive sulfide samples and with net-textured samples having intermediate values (Fig. 1.5g-i) except for Pechenga. In spite of this, the dataset shows no systematic difference in these elements between disseminated and massive samples (Figs. 1.5j), probably due to other processes (contamination, fractionation, PGM crystallization) masking the effect from R-factor in unzoned deposits. Differences between these elements in chalcopyrite from Ni-Cu sulfide and Reef-type PGE deposits are not significant (Fig. 1.6b), except for Te being higher in chalcopyrite from the former. Selenium, a highly chalcophile element, shows higher values in chalcopyrite from Reef-type PGE (ave. 160 ppm) than those from Ni-Cu sulfide deposits (ave. 90 ppm). In Ni-Cu sulfide deposits, Se is concentrated preferentially in chalcopyrite from Cu-rich (ISS) to similar levels as those from Reef-type PGE deposits (Fig. 1.4). Thus, Se records two different processes, indicating that, in Ni-Cu sulfide deposits this element is controlled by fractional crystallization (incompatible with MSS) and, in Reef-type PGE deposits by high R-factor (collected from magma). In S-poor Reef-type PGE deposits, Te in sulfides would be expected to be higher than in Ni-Cu sulfide deposits as results of a higher interaction magma/sulfide liquid. The high Te values in chalcopyrite from Ni-Cu sulfide deposits probably are a consequence of fractional crystallization more important in the sulfide liquid, whereas Te, and a lesser extent Bi and Sn, are low in chalcopyrite from Reef-type PGE deposits as a result of the formation of PGM (Mansur et al., 2021) which depletes TABS (used to form PGM), as discussed later.

1.6.1.3 Fractional Crystallization of Sulfides in Ni-Cu Sulfide Deposits

Once sulfide liquid is formed, the crystallization of Fe-rich monosulfide solid solution (MSS) occurs at high temperatures (about 1190°C), collecting elements such as Co, Ni, Re and IPGE (Os, Ir, Ru, Rh). The residual liquid becomes Cu-rich and concentrates elements that are incompatible with MSS (Ag, Bi, Cd, Pb, Se, Sn, and Te), from which Cu-rich intermediate solid solution (ISS) crystallizes (850-890°C; Barnes and Lightfoot, 2005; Dare et al., 2014; Mansur et al., 2020; Naldrett, 2004). In some Ni-Cu sulfide deposits, separation of Cu-rich residual melt from MSS cumulates occurs by physical processes (i.e. fractional crystallization), leading to Cu-rich and Fe-rich zonation at the deposit scale (e.g., massive ore bodies at Voisey's Bay, Noril'sk and Sudbury) and in sulfide droplets (e.g. globular ore; Barnes et al., 2006). Fe-rich MSS cumulates may contain minor amounts of trapped Cu-rich liquid.

Previous work on zoned Ni-Cu sulfide deposits, such as Sudbury, Voisey's Bay and Noril'sk, has shown that chalcopyrite composition, in part, records the degree of fractional crystallization of the sulfide liquid (Dare et al., 2014; Dare et al., 2010b; Dare et al., 2011; Mansur et al., 2021; Mansur et al., 2020; Salim Amaral, 2017). In the 3 studied zoned deposits, elements incompatible with Fe-rich (MSS) during sulfide fractionation (Ag, In, Se, Te, Sn and Tl) are enriched in chalcopyrite from Cu-rich (ISS) ores relative to that from MSS ores (Fig. 1.5f;

Figs. 1.7a, b and c; Barnes and Ripley, 2016; Dare et al., 2014; Dare et al., 2010b; Dare et al., 2011; Duran et al., 2017; Duran et al., 2016a; Mansur et al., 2020; Naldrett, 2004; Piña et al., 2012b). Moreover, TABS are incompatible with MSS and ISS being enriched in the last residual sulfide liquid, from which PGM may crystallize (Dare et al., 2014; Duran et al., 2017; Mansur et al., 2020). However, even though TABS/PGE are incompatible in ISS, as they are enriched in chalcopyrite compared to those from MSS. Chalcopyrite from Fe-rich (MSS) cumulates that formed by equilibrium crystallization from trapped Cu-rich liquid, do not experience extreme fractionation, hence they are relatively depleted in incompatible elements compared to chalcopyrite from Cu-rich (ISS) ores. In turn, Co and Zn are enriched in chalcopyrite from Fe-rich (MSS) samples, indicating compatible behavior. Mansur et al. (2021) suggested that the decreasing content of Zn in chalcopyrite with whole rock (Pt+Pd)/IPGE ratio could be a result of dilution caused by crystallization of greater amounts of ISS from a fractionated liquid. Another process may also affect Zn concentrations in chalcopyrite, as discussed in the next section. The effect of fractionation of sulfide liquid on the composition of chalcopyrite from zoned deposits is shown in Fig. 1.9. In systems where the fractionation of sulfide liquid was higher (e.g., draining of Cu-rich liquid into footwall veins), the difference between chalcopyrite from Fe-rich (MSS) and Cu-rich (ISS) is more important (Noril´sk and Sudbury; Figs. 1.9a, b), whereas chalcopyrite from deposits displaying concentric zonation of ore types and where the separation is less marked, such as the Ovoid at Voisey´s Bay (Fig. 1.9c), show some overlap in composition. Chalcopyrite from unzoned deposits is similar to chalcopyrite from Fe-rich (MSS) samples (Figs. 1.4 and 1.5j), probably because it did not undergo the fractional crystallization that forms Cu-rich (ISS) zoned orebodies.

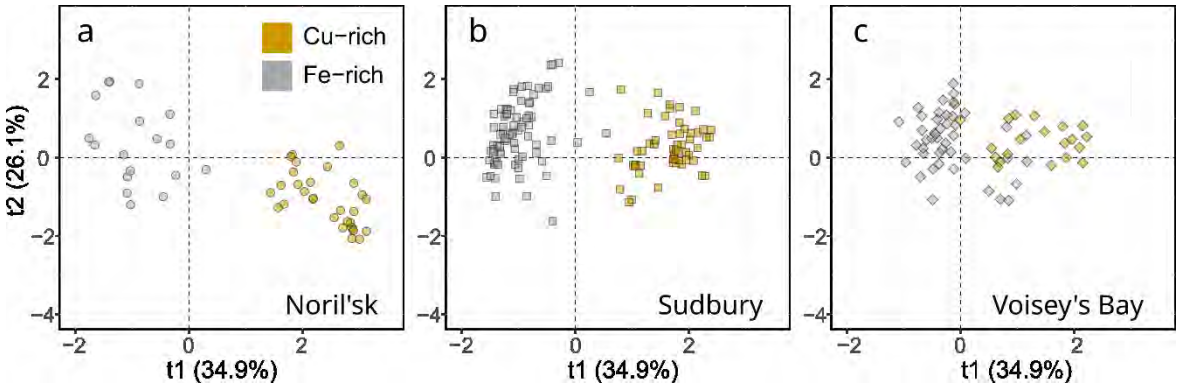

Fig. 1. 9 Effect of fractionation of sulfide liquid on PLS-DA in chalcopyrite from zoned deposits. Deposits with high to extreme fractionation show a marked difference between chalcopyrite from Cu-rich and Fe-rich samples (a, b). In deposits with fractionation less pronounced (b), difference between Fe-rich and Cu-rich less important.

1.6.1.4 Reaction with trapped liquid in Fe-rich (MSS): the peritectic reaction

Trapped residual Cu-rich liquid in both massive and disseminated sulfides (including Reef-type PGE deposits; Mansur and Barnes, 2020b), may react with Fe-rich MSS cumulates to form high temperature pentlandite via a peritectic reaction (Barnes et al., 2020; Kitakaze et al., 2016; Kosyakov and Sinyakova, 2012; Mansur et al.,

2019). Mansur et al. (2019) showed that pentlandite formed by peritectic reaction is enriched in Pd, Te, Bi and Pb close to the contact with chalcopyrite, whereas Ru, Rh, Ir, Os Re, and Mo are enriched close to pyrrhotite. In our study, a few samples from Voisey's Bay (VB25 and VB29) and McCreedy (MCR5 and MCR4B) show textural and chemical features of pentlandite formed by peritectic reaction (Annexe A23). These pentlandites are located in contact between chalcopyrite and pyrrhotite, forming discrete grains or rims around chalcopyrite grains (Figs. 1.2c, d). In addition to the textural relation, the elemental ratio between chalcopyrite and contact pentlandite is below 1 for Bi, Pb and Ag suggesting that, if pentlandite is peritectic, the reaction depleted the trapped Cu-rich liquid in these incompatible elements. These elements which are normally higher in chalcopyrite than in pentlandite (Annexe A22A) diffused from the Cu-rich liquid and were incorporated into pentlandite during the peritectic reaction resulting in their depletion in the trapped ISS liquid, from which chalcopyrite formed. Consequently, chalcopyrite from Fe-rich (MSS) samples, in particular those formed from trapped Cu-rich liquid involved in the peritectic reaction with pentlandite, has even lower contents of incompatible elements relative to those from highly fractionated Cu-rich (ISS) samples.

1.6.1.5 Competition with Other Phases During Crystallization and Subsolidus Exsolution

Although co-crystallization of other sulfide phases (e.g., magnetite, sphalerite) could also affect the composition of chalcopyrite, there is no clear evidence to demonstrate their effect on the trace element content of chalcopyrite. According to Mansur et al. (2021), a high content of PGE in pentlandite would lead to exsolution of PGM with subsequent sequestration and depletion of TABS in samples from Reef-type PGE deposits. Our results show that, in addition to high Se content, chalcopyrite from Reef-type PGE is lower in Te, Bi and Sn than chalcopyrite from Ni-Cu sulfide deposits, suggesting a PGM exsolution effect.

Sphalerite grains with characteristic star-like and skeletal forms (Annexe A10) occur in chalcopyrite from Cu-rich (ISS) samples from Medvezhy Creek (Noril'sk), McCreedy (Sudbury), Copper Cliff (Sudbury) and Ovoid (Voisey's Bay), interpreted as products of exsolution (Kojima and Sugaki, 1985; Ren et al., 2017; Sugaki et al., 1987; Vaughan, 2006). According to Kojima and Sugaki (1985) the solubility of Zn in solid solution in chalcopyrite is generally low, reaching up 0.9 wt.% at 500°C. In contrast, Zn has a higher solubility in ISS than in chalcopyrite, which can dissolve a maximum 3.3 wt.% Zn at 500°C (Kojima and Sugaki, 1985). Sphalerite exsolution, as well as the possible dilution of Zn caused by a high proportion if ISS from fractionated liquids, could have contributed to depleting of Zn in Cu-rich ISS and subsequently in exsolved chalcopyrite from Cu-rich samples.

Chalcopyrite forms at lower temperature (600-500°C) by subsolidus exsolution from Cu-rich (ISS). However, a minor amount of chalcopyrite may also exsolve directly from Fe-rich MSS (Fig. 1.2a), together with pyrrhotite and pentlandite, at around 650°C. Experiments in the Cu-Fe-S system show that Cu-rich ISS phases exsolve to from a high-Cu MSS (Naldrett, 2004; Vaughan, 2006). This, in addition to peritectic reaction with pentlandite,

could explain differences in trace element composition between chalcopyrite from Fe-rich (MSS) and Cu-rich (ISS) ores.

After exsolution of chalcopyrite and pyrrhotite from ISS at <550°C and <650°C, respectively, cubanite exsolves at lower temperatures (<210°C; Dare et al., 2014; Mansur et al., 2021). As shown by this study, as well as Dare et al. (2014) at McCreedy and by Mansur et al. (2020) at Norils'k, elements such as Co, Ni, Sb, Ag, Pb and Au show a preference for cubanite over chalcopyrite (Annexe A22C). However, the presence of this mineral does not seem to affect importantly the fractional crystallization effect.

1.6.2 Trace Element Composition of Chalcopyrite as an Exploration Tool

The PLS-DA model proposed to discriminate chalcopyrite by deposit type (Ni-Cu sulfide vs. Reef-type PGE) and ore type (Cu-rich vs. Fe-rich/unzoned) was tested using literature data, corresponding to individual chalcopyrite grains, where an extensive suite of chalcophile elements, including TABS, were analyzed. Therefore, only the recent studies (Mansur and Barnes, 2020b; Mansur et al., 2021; Mansur et al., 2020) can be tested on the PLS-DA models by deposit type (Fig. 1.10a, b) and ore type (Fig. 1.10c, d). According to confusion matrices (Annexe A7), classification by deposit type has an accuracy of 89.6%, correctly predicting 146 chalcopyrite grains of 163. However, Fig. 1.10a shows that 80% of chalcopyrite from Alexo, a komatiite-hosted Ni-Cu sulfide deposit, and 1% from Noril'sk, were predicted incorrectly as Reef-type PGE deposit (Fig. 1.10b), whereas 14% of chalcopyrite from Merensky Reef were predicted to belong to Ni-Cu sulfide deposits. On the other hand, prediction using the model by ore types from Ni-Cu sulfide deposits has an accuracy of 64% (Annexe A7). As chalcopyrite from Fe-rich (MSS) and unzoned deposits do not show a significative difference (Fig. 1.8f), we refer them as a group. Among chalcopyrite from Fe-rich/unzoned samples, only 3.5% were misclassified as Cu-rich (ISS), corresponding to two chalcopyrite from Alexo (Figs. 1.10c, d). In contrast, chalcopyrite from Cu-rich samples records a high proportion of misclassification (Figs. 1.10c, d). Chalcopyrite from Noril'sk (Oktaybr´sky and some from Medvezhy), Cu-rich ore (Duran et al., 2017; Mansur et al., 2020), were misclassified as Fe-rich/unzoned (74%). According to Zientek et al. (1994), massive sulfides at Oktaybr´sky display a complex concentric zonation of ore types, varying the BMS proportions and showing a continuum between the outer and lateral margins rich in pyrrhotite (with minor chalcopyrite and pentlandite), and inward zones rich in chalcopyrite and cubanite, which surrounds a core rich in mooihoekite-cubanite or talnakhite-cubanite. Although whole rock compositions (Duran et al., 2017; Mansur et al., 2020) of these samples indicate that they are Cu-rich, the (Pd+Pt)/IPGE ratio is intermediate between Fe-rich and Cu-rich samples. Moreover, Se and Zn values in chalcopyrite are comparable to those from Fe-rich ores, suggesting that probably they are Cu-rich transitional massive sulfides.

1.6.3 New Discriminant Binary Diagrams

In order to use elements commonly analyzed in previous studies, new discriminant binary diagrams are proposed based on the most important elements indicated by PLS-DA models (Bi, In, Sb, Se, Sn, Te, Tl, and Zn). Contrary

to PLS-DA models which calculate class prediction probabilities for each observation, prediction using binary diagrams is nominally visual; however, they could be complementary and a more accessible method. The diagram Se/(Te+Bi) vs. Se (Fig. 1.11a) discriminates efficiently chalcopyrite from Reef-type PGE and Ni-Cu sulfide deposits, showing only a small overlap. Chalcopyrite from Reef-type PGE deposits are higher in Se and as such have higher Se/(Te+Bi) ratios, likely as a result of higher R factors and PGM formation, as discussed above. On the other hand, the diagram 2Zn/(3Se+5Sn) vs. Se allows discrimination of chalcopyrite from Cu-rich ISS from Fe-rich (MSS) /unzoned Ni-Cu sulfide deposits (Fig. 1.11b).

Predictions of literature data by deposit type using the new binary diagrams are shown in Figs. 1.12a and 12b. The majority (91.9 %) of published chalcopyrite data from deposits studied in this paper (Fig. 1.12a, Annexe A8) plot in their corresponding fields, with the exception of some chalcopyrite from Great Dyke (Piña et al., 2016) and Bushveld (Mansur and Barnes, 2020a). Chalcopyrite from Ni-Cu deposits plot correctly, except for samples from Mirabela (Knight et al., 2017), and some disseminated and massive samples from Lac des Iles (Djon and Barnes, 2012; Duran et al., 2016b) that plot in the Reef-type PGE deposit field (Fig. 1.12b). Mansur et al. (2021) indicated that, although Mirabela is primarily a Ni-Cu sulfide deposit, the shape of strongly to highly chalcophile elements mantle-normalized patterns for BMS are similar to those from PGE-dominated deposits, suggesting a similarly high R-factor resulting in unusually high Se/(Te+Bi) ratios. The Lac des Iles Complex is known for its Pd-rich mineralization, classified as PGE-dominated (Djon and Barnes, 2012; Duran et al., 2016a; Mansur et al., 2021). Fig. 1.12b shows that the most chalcopyrite from massive sulfides from Lac des Iles plot in the Ni-Cu sulfide field or at its edge, whereas most chalcopyrite from disseminated samples plot in the Reef-type PGE zone, probably reflecting the effect of the R factor (Duran et al., 2016a).

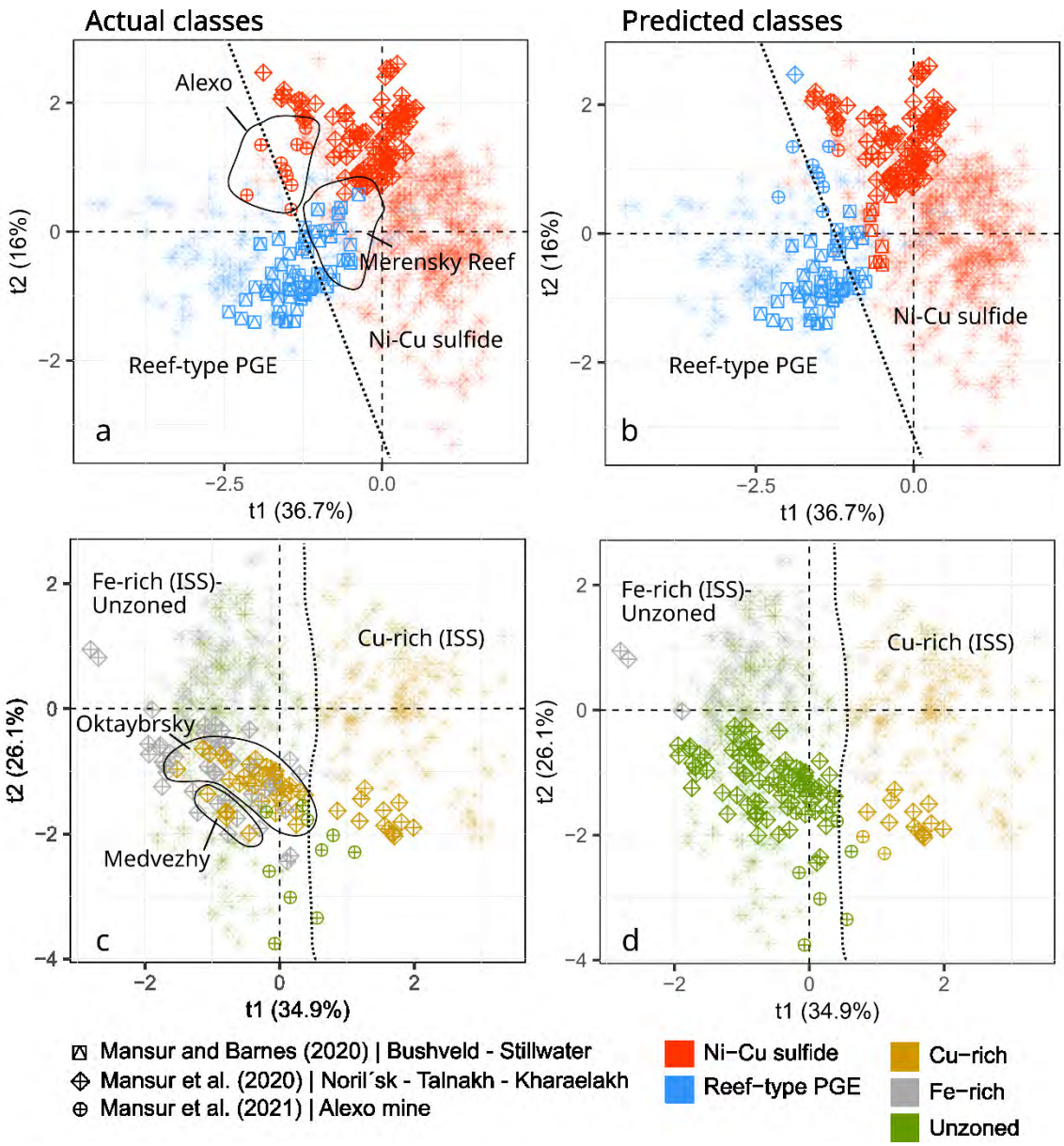

Fig. 1. 10 Prediction of published data on PLS-DA models. Model by deposit type (a-b) shows a high accuracy (89.6%) in classification, whereas for c and d classification is not possible between chalcopyrite Fe-rich and unzoned and moderate between Cu-rich and the remaining (61.7%).

Classification of literature data by ore type is shown in the Figs. 1.12c and 1.12d, with an accuracy of 67.6%. Similar to results from PLS-DA, chalcopyrite from Cu-rich samples from Oktaybr´sky plot in the Fe-rich/unzoned region, probably as a result, as discussed above, of the transition between Cu-rich and Fe-rich ores (Fig. 12c). Samples from Voisey's Bay, Sudbury and Duluth were classified correctly (Fig. 12c), whereas the most chalcopyrite from Lac des Iles massive sulfides were misclassified as Cu-rich (Fig. 12d).

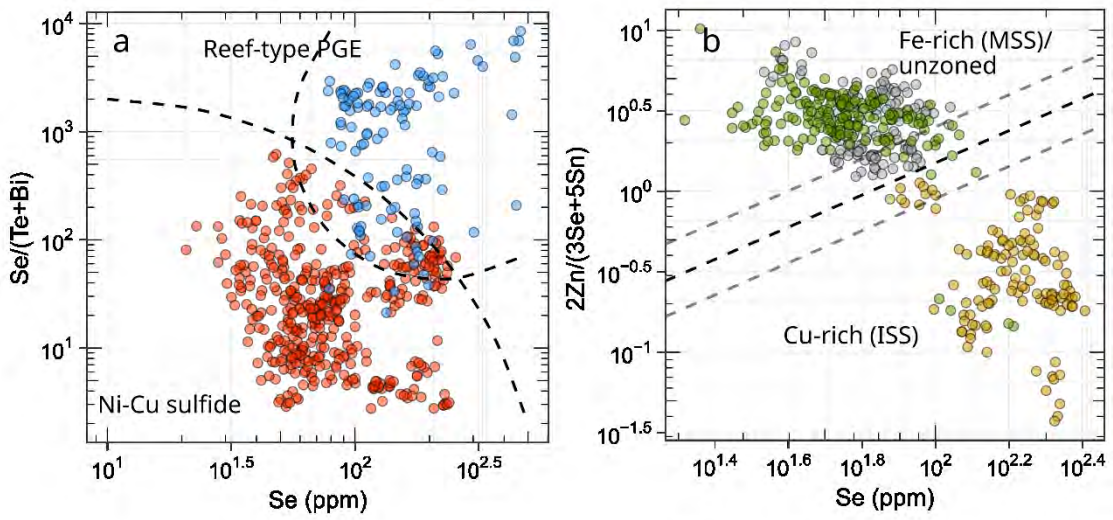

Fig. 1. 11 New discriminant binary diagrams, based on PLS-DS results from this study, that could be used as complementary tools in prediction tasks in addition to PLS-DA models. Both models show a marked separation between chalcopyrite from Ni-Cu sulfide and Reef-type PGE deposits (a) and chalcopyrite from Cu-rich (ISS) and Fe-rich (MSS)/unzoned (b) sulfide groups.

Chalcopyrite from massive sulfides from Lac des Iles has Se median values 1.5 times higher to those from chalcopyrite from Cu-rich (similar to Reef-type PGE deposits), Zn content about a half, and Sn values considerably lower relative to Cu-rich and Fe-rich samples (about 500x and 20x, respectively) resulting in low 2Zn/(3Se+5Sn) ratio. Probably, this result is the combination of two processes, the high R factors responsible of the enrichment of Se, and PGM crystallization, possibly responsible of depletion of Sn in chalcopyrite at Lac des Iles.

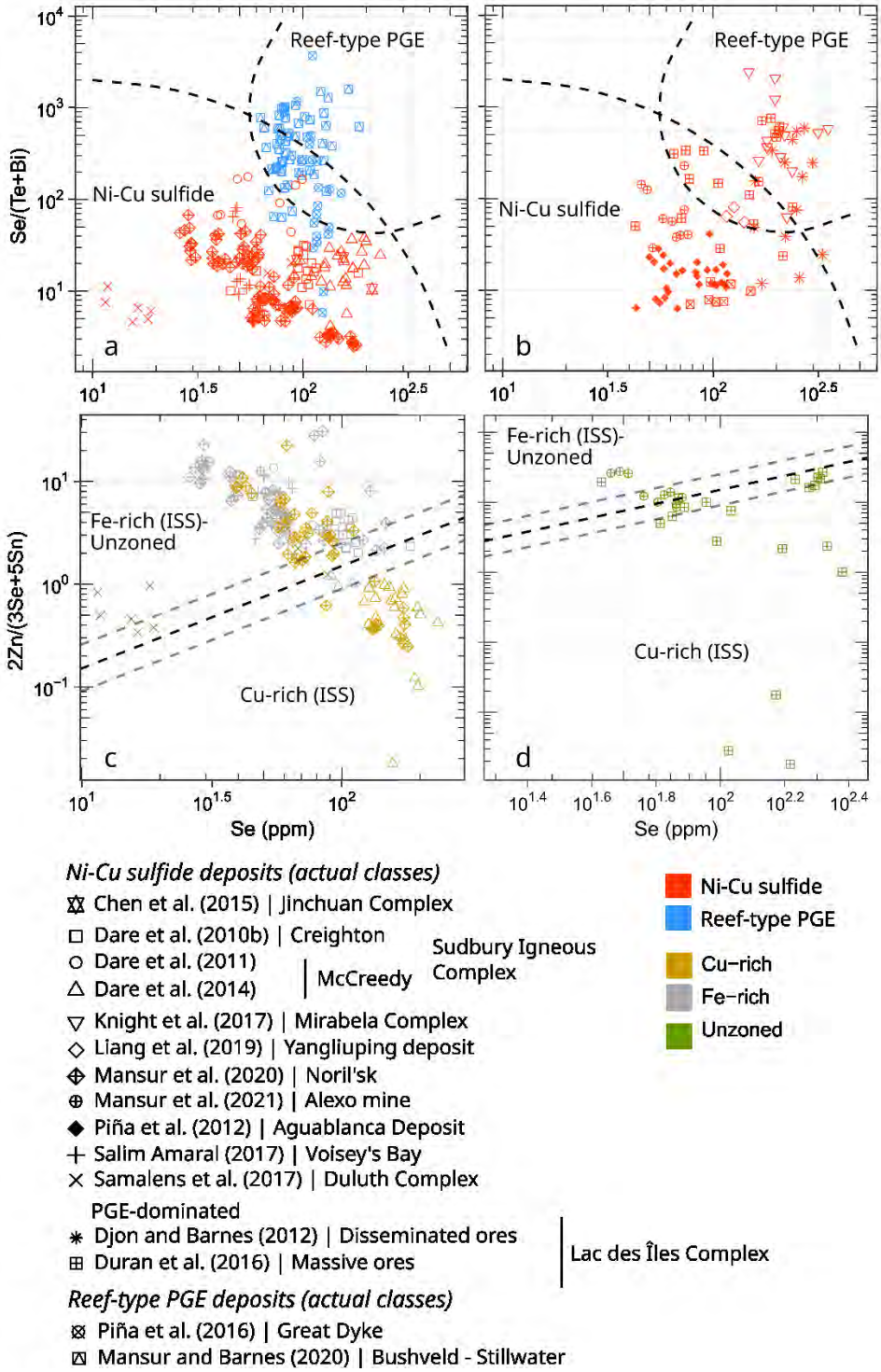

Fig. 1. 12 Evaluation of performance of the Se/(Te+Bi)/Se discriminant diagram by magmatic sulfide deposit type (accuracy 91.9%). (a) Literature data from deposits studied in this paper, (b) data from other deposits. (c-d) Evaluation of performance of the discriminant diagram by ore type showing actual classes. Accuracy for the model is 67.6%. Almost all chalcopyrite from Fe-rich/unzoned samples were correctly identified (c), whereas chalcopyrite from Lac des Iles Complex plots between Cu-rich (ISS) and Fe-rich (MSS)/unzoned classes. The database used includes chalcopyrite from Ni-Cu sulfide deposits, such as Sudbury (Dare et al., 2014; Dare et al., 2010b; Dare et al., 2011), Voisey's Bay (Salim Amaral, 2017), Duluth (Samalens et al., 2017a), Lac des Iles (Duran et al., 2016b), Noril'sk (Mansur et al., 2020), Jinchuan (Chen et al., 2015), Mirabela (Knight et al., 2017) and Alexo (Mansur et al., 2021); and from Reef-type PGE deposits: Bushveld (Mansur and Barnes, 2020a), Stillwater (Mansur and Barnes, 2020a) and Great Dyke (Piña et al., 2016).

1.7 Conclusions

This study highlights the potential of chalcopyrite chemistry as an indicator mineral for mineral exploration in magmatic sulfide systems (Ni-Cu-PGE), and demonstrates that multivariate statistical analysis, such as PLS-DA, combined with discriminant binary diagrams and the understanding of processes affecting composition of chalcopyrite is a reliable tool for discrimination of deposit type (Ni-Cu sulfide vs. Reef-type PGE) and ore type (Cu-rich vs. Fe-rich). Based on our results, we established that two processes have a major effect on the composition of chalcopyrite and on discrimination models: a) higher R factors lead to the enrichment of Se in chalcopyrite from Reef-type PGE deposits relative to Ni-Cu sulfide deposits and b) fractional crystallization of sulfide liquid in Ni-Cu sulfide deposits leads to Cu-rich ore chalcopyrite enriched in Ag, Bi, Pb, Se, Sn and Tl relative to those from Fe-rich/unzoned ore. Unusually high R factors in Ni-Cu sulfide deposits, such as Mirabela, could mask effects of fractional crystallization, leading to potential misclassification. Other processes, such as PGM crystallization in Reef-type PGE deposits, leading to a small depletion of Te, Bi, Sb and Sn in co-existing chalcopyrite, could enhance discrimination of Reef-type PGE deposits from chalcopyrite from Ni-Cu sulfide deposits.

Our PLS-DA model enables discrimination of chalcopyrite from Ni-Cu sulfide and Reef-type PGE deposits based on Bi, In, Se, Sn and Te. Chalcopyrite from Ni-Cu sulfide are characterized by high content in Te, Bi, In and Sn and low concentrations in Se relative to chalcopyrite from Reef-type PGE deposits. Our PLS-DA analysis also enables discrimination of chalcopyrite from Cu-rich (ISS) and Fe-rich (MSS)/unzoned ores based on Sb, Se, Sn, Tl and Zn. Chalcopyrite from Fe-rich (MSS)/unzoned are overall characterized by low Sn, Se and Tl, and high Zn in comparison to chalcopyrite from Cu-rich (ISS) ores.

We present a discriminant binary diagram Se/(Te+Bi) vs. Se, in which chalcopyrite from Ni-Cu sulfide deposits is characterized by low Se/(Te+Bi) ratios and low Se content relative to Reef-type PGE deposits, and a discriminant binary diagram 2Zn/(3Se+5Sn) vs. Se, wherein chalcopyrite from Cu-rich (ISS) has a low 2Zn/(3Se+5Sn) and high Se content relative to those from Fe-rich (MSS)/unzoned deposits.

1.8 Acknowledgements

This study was funded by the Natural Science and Engineering Research Council of Canada (NSERC), Agnico Eagle Mines Limited and le Ministère de l'Energie et des Ressources Naturelles du Québec. We thank the numerous colleagues that provided samples for this study, especially Sarah-Jane Barnes at UQAC for access to her extensive collection of magmatic sulfide deposits. We are very grateful to Dany Savard and Audrey Lavoie from LabMaTer, Université du Québec à Chicoutimi for their support with LA-ICP-MS analyses, to Marc Choquette and Suzie Coté from Université Laval for their assistance and support for SEM and EPMA analyzes and Edmond Rousseau for his support for sample preparation. We thank the referees, Eduardo Mansur and

Ruben Piña, and Associate Editor Wolfgang Maier for their judicious comments which helped improve the paper significantly.

Funding information The research is funded by Agnico Eagle Mines Ltd., the Ministère de l'Énergie et des Ressources Naturelles du Québec and the Natural Sciences and Engineering Research Council.

1.9 References

Agangi A, Reddy S, Plavsa D, Vieru C, Selvaraja V, LaFlamme C, Jeon H, Martin L, Nozaki T, Takaya Y (2018) Subsurface deposition of Cu-rich massive sulphide underneath a Palaeoproterozoic seafloor hydrothermal system—the Red Bore prospect, Western Australia. Mineralium Deposita:1-18.

Aitchison J (1986) The statistical analysis of compositional data. Chapman and Hall, London.

Antweiler RC (2015) Evaluation of Statistical Treatments of Left-Censored Environmental Data Using Coincident Uncensored Data Sets. II. Group Comparisons. Environmental Science & Technology 49:13439-13446. doi: 10.1021/acs.est.5b02385.

Averill S (2011) Viable indicator minerals in surficial sediments for two major base metal deposit types: Ni-Cu-PGE and porphyry Cu.

Bajwah ZU, Seccombe PK, Offler R (1987) Trace element distribution, Co: Ni ratios and genesis of the Big Cadia iron-copper deposit, New South Wales, Australia. Mineralium Deposita 22:292-300.

Balch SJ (2005) The geophysical signatures of platinum group element deposits In: Mungall JE (ed) Exploration for platinum-group element deposits: Mineralogical Association of Canada, Short-Course Series, Volume 35. pp 275-286.

Ballabio D, Consonni V (2013) Classification tools in chemistry. Part 1: linear models. PLS-DA. Analytical Methods 5:3790-3798.

Barnes S-J, Melezhik VA, Sokolov SV (2001) The composition and mode of formation of the Pechenga nickel deposits, Kola Peninsula, northwestern Russia. The Canadian Mineralogist 39:447-471.

Barnes S-J, Lightfoot PC (2005) Formation of magmatic nickel sulfide ore deposits and processes affecting their copper and platinum group element contents. Economic geology 100th anniversary volume 34:179-214.

Barnes S-J, Cox RA, Zientek ML (2006) Platinum-group element, gold, silver and base metal distribution in compositionally zoned sulfide droplets from the Medvezky Creek Mine, Noril'sk, Russia. Contributions to Mineralogy and Petrology 152:187-200.

Barnes S-J, Prichard HM, Cox RA, Fisher PC, Godel B (2008) The location of the chalcophile and siderophile elements in platinum-group element ore deposits (a textural, microbeam and whole rock geochemical study): Implications for the formation of the deposits. Chemical Geology 248:295-317.

Barnes S-J (2016) Chalcophile elements Encyclopedia of Geochemistry: A Comprehensive Reference Source on the Chemistry of the Earth. Springer International Publishing, pp 1-5.

Barnes S-J, Ripley EM (2016) Highly siderophile and strongly chalcophile elements in magmatic ore deposits. Reviews in Mineralogy and Geochemistry 81:725-774.

Barnes SJ, Mungall JE, Le Vaillant M, Godel B, Lesher CM, Holwell D, Lightfoot PC, Krivolutskaya N, Wei B (2017) Sulfide-silicate textures in magmatic Ni-Cu-PGE sulfide ore deposits: Disseminated and net-textured ores. American Mineralogist 102:473-506.

Barnes SJ, Staude S, Le Vaillant M, Piña R, Lightfoot PC (2018) Sulfide-silicate textures in magmatic Ni-Cu-PGE sulfide ore deposits: Massive, semi-massive and sulfide-matrix breccia ores. Ore Geology Reviews 101:629-651. doi: https://doi.org/10.1016/j.oregeorev.2018.08.011.

Barnes SJ, Taranovic V, Schoneveld LE, Mansur ET, Le Vaillant M, Dare S, Staude S, Evans NJ, Blanks D (2020) The Occurrence and Origin of Pentlandite-Chalcopyrite-Pyrrhotite Loop Textures in Magmatic Ni-Cu Sulfide Ores. Economic Geology 115:1777-1798. doi: 10.5382/econgeo.4757.

Bédard É, Goulet A, Sappin A-A, Makvandi S, Beaudoin G (2017) Chalcopyrite as an indicator mineral to fingerprint mineral deposit types: a preliminary study Mineral Resources to Discover- Proceedings of the 14th SGA Biennial Meeting. Québec City, Canada, pp 1115-1118.

Bédard JH (2005) Partitioning coefficients between olivine and silicate melts. Lithos 83:394-419. doi: https://doi.org/10.1016/j.lithos.2005.03.011.

Belissont R (2016) Germanium and related elements in sulphide minerals: crystal chemistry, incorporation and isotope fractionation.

Belissont R, Munoz M, Boiron M-C, Luais B, Mathon O (2019) Germanium crystal chemistry in Cu-bearing sulfides from micro-XRF mapping and micro-XANES spectroscopy. Minerals 9:227.

Benson EK, Ripley EM, Li C, Underwood BW, Mahin R (2020) Multiple S Isotopes and S Isotope Heterogeneity at the East Eagle Ni-Cu-Platinum Group Element Deposit, Northern Michigan. Economic Geology 115:527-541.

Boutroy E, Dare SA, Beaudoin G, Barnes S-J, Lightfoot PC (2014) Magnetite composition in Ni-Cu-PGE deposits worldwide: application to mineral exploration. Journal of Geochemical Exploration 145:64-81.

Brereton RG, Lloyd GR (2014) Partial least squares discriminant analysis: taking the magic away. Journal of Chemometrics 28:213-225.

Brügmann G, Hanski E, Naldrett A, Smolkin V (2000) Sulphide segregation in ferropicrites from the Pechenga Complex, Kola peninsula, Russia. Journal of Petrology 41:1721-1742.

Butler IB, Nesbitt RW (1999) Trace element distributions in the chalcopyrite wall of a black smoker chimney: insights from laser ablation inductively coupled plasma mass spectrometry (LA–ICP–MS). Earth and Planetary Science Letters 167:335-345.

Cabri LJ, Campbell JL, Laflamme JHG, Leigh RG, Maxwell JA, Scott JD (1985) Proton-microprobe analysis of trace elements in sulfides from some massive-sulfide deposits. The Canadian Mineralogist 23:133-148.

Cafagna F, Jugo PJ (2016) An experimental study on the geochemical behavior of highly siderophile elements (HSE) and metalloids (As, Se, Sb, Te, Bi) in a mss-iss-pyrite system at 650°C: A possible magmatic origin for Co-HSE-bearing pyrite and the role of metalloid-rich phases in the fractionation of HSE. Geochimica et Cosmochimica Acta 178:233-258. doi: https://doi.org/10.1016/j.gca.2015.12.035.

Chen L-M, Song X-Y, Danyushevsky LV, Wang Y-S, Tian Y-L, Xiao J-F (2015) A laser ablation ICP-MS study of platinum-group and chalcophile elements in base metal sulfide minerals of the Jinchuan Ni–Cu sulfide deposit, NW China. Ore Geology Reviews 65:955-967.

Chong I-G, Jun C-H (2005) Performance of some variable selection methods when multicollinearity is present. Chemometrics and intelligent laboratory systems 78:103-112.

Cook NJ, Ciobanu CL, Danyushevsky LV, Gilbert S (2011) Minor and trace elements in bornite and associated Cu–(Fe)-sulfides: A LA-ICP-MS studyBornite mineral chemistry. Geochimica et Cosmochimica Acta 75:6473-6496.

Czamanske GK, Kunilov VE, Zientek ML, Cabri LJ, Likhachev AP, Calk LC, Oscarson RL (1992) A proton microprobe study of magmatic sulfide ores from the Noril'sk-Talnakh District, Siberia. The Canadian Mineralogist 30:249-287.

Dare SA, Barnes S-J, Beaudoin G (2012) Variation in trace element content of magnetite crystallized from a fractionating sulfide liquid, Sudbury, Canada: Implications for provenance discrimination. Geochimica et Cosmochimica Acta 88:27-50.

Dare SA, Barnes S-J, Prichard HM, Fisher PC (2014) Mineralogy and geochemistry of Cu-rich ores from the McCreedy East Ni-Cu-PGE deposit (Sudbury, Canada): implications for the behavior of platinum group

and chalcophile elements at the end of crystallization of a sulfide liquid. Economic Geology 109:343-366.

Dare SAS, Barnes S-J, Prichard HM (2010a) The distribution of platinum group elements (PGE) and other chalcophile elements among sulfides from the Creighton Ni–Cu–PGE sulfide deposit, Sudbury, Canada, and the origin of palladium in pentlandite. Mineralium Deposita 45:765-793.

Dare SAS, Barnes S-J, Prichard HM, Fisher PC (2010b) The timing and formation of platinum-group minerals from the Creighton Ni-Cu-platinum-group element sulfide deposit, Sudbury, Canada: Early crystallization of PGE-rich sulfarsenides. Economic Geology 105:1071-1096.

Dare SAS, Barnes S-J, Prichard HM, Fisher PC (2011) Chalcophile and platinum-group element (PGE) concentrations in the sulfide minerals from the McCreedy East deposit, Sudbury, Canada, and the origin of PGE in pyrite. Mineralium Deposita 46:381-407.

De Bronac de Vazelhes V (2019) Étude de la dispersion d'un gisement d'or dans les sédiments glaciaires: le cas d'Amaruq (Nunavut, Canada).

Djon MLN, Barnes S-J (2012) Changes in sulfides and platinum-group minerals with the degree of alteration in the Roby, Twilight, and High Grade Zones of the Lac des Iles Complex, Ontario, Canada. Mineralium Deposita 47:875-896. doi: 10.1007/s00126-012-0401-z.

Dunn K (2019) Process improvement using data. Experimentation for Improvement Hamilton, Ontario, Canada Creative Commons Attribution-ShareAlike 4:325-404.

Duran C, Barnes S, Pleše P, Prašek MK, Zientek ML, Pagé P (2017) Fractional crystallization-induced variations in sulfides from the Noril'sk-Talnakh mining district (polar Siberia, Russia). Ore Geology Reviews 90:326-351.

Duran CJ, Barnes S-J, Corkery JT (2016a) Trace element distribution in primary sulfides and Fe–Ti oxides from the sulfide-rich pods of the Lac des Iles Pd deposits, Western Ontario, Canada: Constraints on processes controlling the composition of the ore and the use of pentlandite compositions in exploration. Journal of Geochemical Exploration 166:45-63.

Duran CJ, Barnes S-J, Corkery JT (2016b) Geology, petrography, geochemistry, and genesis of sulfide-rich pods in the Lac des Iles palladium deposits, western Ontario, Canada. Mineralium Deposita 51:509-532.

Duran CJ, Dubé-Loubert H, Pagé P, Barnes S-J, Roy M, Savard D, Cave BJ, Arguin J-P, Mansur ET (2019) Applications of trace element chemistry of pyrite and chalcopyrite in glacial sediments to mineral exploration targeting: Example from the Churchill Province, northern Quebec, Canada. Journal of Geochemical Exploration. doi: https://doi.org/10.1016/j.gexplo.2018.10.006.

Duran CJ, Barnes S-J, Mansur ET, Dare SAS, Bédard LP, Sluzhenikin SF (2020) Magnetite chemistry by LA-ICP-MS records sulfide fractional crystallization in massive nickel-copper-platinum group element ores from the Norilsk-Talnakh mining district (Siberia, Russia): Implications for trace element partitioning into magnetite. Economic Geology 115:1245-1266.

Egozcue JJ, Pawlowsky-Glahn V (2011) Análisis composicional de datos en Ciencias Geoambientales. Boletín Geológico y Minero 122:439-452.

Favilla S, Durante C, Vigni ML, Cocchi M (2013) Assessing feature relevance in NPLS models by VIP. Chemometrics and Intelligent Laboratory Systems 129:76-86.

Filzmoser P, Hron K, Reimann C (2009) Principal component analysis for compositional data with outliers. Environmetrics 20:621-632.

Frenzel M, Hirsch T, Gutzmer J (2016) Gallium, germanium, indium, and other trace and minor elements in sphalerite as a function of deposit type—A meta-analysis. Ore Geology Reviews 76:52-78.

George LL, Cook NJ, Ciobanu CL (2016) Partitioning of trace elements in co-crystallized sphalerite–galena–chalcopyrite hydrothermal ores. Ore Geology Reviews 77:97-116.

George LL, Cook NJ, Crowe BB, Ciobanu CLJMM (2018) Trace elements in hydrothermal chalcopyrite. 82:59-88.

Godel B, Barnes S-J, Maier WD (2006) 3-D distribution of sulphide minerals in the Merensky Reef (Bushveld Complex, South Africa) and the JM Reef (Stillwater Complex, USA) and their relationship to microstructures using X-ray computed tomography. Journal of Petrology 47:1853-1872.

Godel B, Barnes S-J, Maier WDJJoP (2007) Platinum-group elements in sulphide minerals, platinum-group minerals, and whole-rocks of the Merensky Reef (Bushveld Complex, South Africa): implications for the formation of the reef. 48:1569-1604.

Godel B, Barnes S-J (2008) Platinum-group elements in sulfide minerals and the whole rocks of the JM Reef (Stillwater Complex): Implication for the formation of the reef. Chemical Geology 248:272-294.

Godel B (2015) Platinum-group element deposits in layered intrusions: recent advances in the understanding of the ore forming processes. Layered intrusions:379-432.

Gosselin R, Rodrigue D, Duchesne C (2010) A Bootstrap-VIP approach for selecting wavelength intervals in spectral imaging applications. Chemometrics and Intelligent Laboratory Systems 100:12-21.

Goulet A (2016) Composition chimique de la chalcopyrite et application à l'exploration minérale In: Département de géologie et génie géologique UL (ed). pp 99.

Green T, Peck D (2005) Platinum group elements exploration: economic considerations and geological criteria In: Mungall JE (ed) Exploration For Platinum-Group Elements Deposits. Mineralogical Association of Canada. Short Course Series, Volume 35, pp 247-274.

Harris DC, Cabri LJ, Nobiling R (1984) Silver-bearing chalcopyrite, a principal source of silver in the Izok Lake massive-sulfide deposit; confirmation by electron-and proton-microprobe analyses. The Canadian Mineralogist 22:493-498.

Hashmi S, Ward BC, Plouffe A, Leybourne MI, Ferbey T (2015) Geochemical and mineralogical dispersal in till from the Mount Polley Cu-Au porphyry deposit, central British Columbia, Canada. Geochemistry: Exploration, Environment, Analysis 15:234-249.

Hawley J, Nichol I (1961) Trace elements in pyrite, pyrrhotite and chalcopyrite of different ores. Economic Geology 56:467-487.

Holwell DA, McDonald I (2007) Distribution of platinum-group elements in the Platreef at Overysel, northern Bushveld Complex: a combined PGM and LA-ICP-MS study. Contributions to Mineralogy and Petrology 154:171-190.

Hron K, Templ M, Filzmoser P (2010) Imputation of missing values for compositional data using classical and robust methods. Computational Statistics & Data Analysis 54:3095-3107.

Huston DL, Sie SH, Suter GF, Cooke DR, Both RA (1995) Trace elements in sulfide minerals from eastern Australian volcanic-hosted massive sulfide deposits; Part I, Proton microprobe analyses of pyrite, chalcopyrite, and sphalerite, and Part II, Selenium levels in pyrite; comparison with delta 34 S values and implications for the source of sulfur in volcanogenic hydrothermal systems. Economic Geology 90:1167-1196.

Jochum KP, Nohl U, Herwig K, Lammel E, Stoll B, Hofmann AW (2005) GeoReM: a new geochemical database for reference materials and isotopic standards. Geostandards and Geoanalytical Research 29:333-338.

Kase K (1987) Tin-bearing chalcopyrite from the Izumo vein, Toyoha mine, Hokkaido, Japan. The Canadian Mineralogist 25:9-13.

Kitakaze A, Machida T, Komatsu R (2016) Phase Relations in the Fe–ni–s System from 875 To 650° c. The Canadian Mineralogist 54:1175-1186.

Knight RD, Prichard HM, Ferreira Filho CF (2017) Evidence for As contamination and the partitioning of Pd into Pentlandite and Co+ platinum group elements into pyrite in the Fazenda Mirabela intrusion, Brazil. Economic Geology 112:1889-1912.

Kojima S, Sugaki AJEG (1985) Phase relations in the Cu-Fe-Zn-S system between 500 degrees and 300 degrees C under hydrothermal conditions. 80:158-171.

Kosyakov VI, Sinyakova EF (2012) Physicochemical prerequisites for the formation of primary orebody zoning at copper-nickel sulfide deposits (by the example of the systems Fe–Ni–S and Cu–Fe–S). Russian Geology and Geophysics 53:861-882.

Lazich BJ (2010) The trace-element chemistry of chalcopyrite and its potential application to discriminate ore deposit types: Application to the Archean, syenite-associated Upper Beaver Cu-Au deposit, Kirkland. Laurentian, University Sudbury, pp 45.

Lee LC, Liong C-Y, Jemain AA (2018) Partial least squares-discriminant analysis (PLS-DA) for classification of high-dimensional (HD) data: a review of contemporary practice strategies and knowledge gaps. Analyst 143:3526-3539.

Li C, Ripley EM (2011) The giant Jinchuan Ni-Cu-(PGE) deposit; tectonic setting, magma evolution, ore genesis, and exploration implications. Reviews in Economic Geology 17:163-180.

Liu H, Beaudoin G (2021) Geochemical signatures in native gold derived from Au-bearing ore deposits. Ore Geology Reviews:104066.

Liu H, Beaudoin G, Makvandi S, Jackson SE, Huang X (2021) Multivariate statistical analysis of trace element compositions of native gold from orogenic gold deposits: implication for mineral exploration. Ore Geology Reviews:104061.

Liu Y, Brenan J (2015) Partitioning of platinum-group elements (PGE) and chalcogens (Se, Te, As, Sb, Bi) between monosulfide-solid solution (MSS), intermediate solid solution (ISS) and sulfide liquid at controlled fO2–fS2 conditions. Geochimica et Cosmochimica Acta 159:139-161.

Lyubetskaya T, Korenaga J (2007) Chemical composition of Earth's primitive mantle and its variance: 1. Method and results. Journal of Geophysical Research: Solid Earth 112.

Makvandi S, Ghasemzadeh-Barvarz M, Beaudoin G, Grunsky EC, Beth McClenaghan M, Duchesne C (2016a) Principal component analysis of magnetite composition from volcanogenic massive sulfide deposits: Case studies from the Izok Lake (Nunavut, Canada) and Halfmile Lake (New Brunswick, Canada) deposits. Ore Geology Reviews 72:60-85. doi: https://doi.org/10.1016/j.oregeorev.2015.06.023.

Makvandi S, Ghasemzadeh-Barvarz M, Beaudoin G, Grunsky EC, McClenaghan MB, Duchesne C, Boutroy E (2016b) Partial least squares-discriminant analysis of trace element compositions of magnetite from various VMS deposit subtypes: Application to mineral exploration. Ore Geology Reviews 78:388-408.

Mansur ET, Barnes S-J, Duran CJ (2019) Textural and compositional evidence for the formation of pentlandite via peritectic reaction: Implications for the distribution of highly siderophile elements. Geology 47:351-354.

Mansur ET, Barnes S-J (2020a) Concentrations of Te, As, Bi, Sb and Se in the Marginal Zone of the Bushveld Complex: Evidence for crustal contamination and the nature of the magma that formed the Merensky Reef. Lithos 358:105407.

Mansur ET, Barnes S-J (2020b) The role of Te, As, Bi, Sn and Sb during the formation of platinum-group-element reef deposits: examples from the Bushveld and Stillwater complexes. Geochimica et Cosmochimica Acta 272:235-258.

Mansur ET, Barnes S-J, Duran CJ, Sluzhenikin SF (2020) Distribution of chalcophile and platinum-group elements among pyrrhotite, pentlandite, chalcopyrite and cubanite from the Noril'sk-Talnakh ores: Implications for the formation of platinum-group minerals. Mineralium Deposita 55:1215-1232.

Mansur ET, Barnes S-J, Duran CJ (2021) An overview of chalcophile element contents of pyrrhotite, pentlandite, chalcopyrite, and pyrite from magmatic Ni-Cu-PGE sulfide deposits. Mineralium Deposita:1-26.

Maslennikov V, Maslennikova S, Large R, Danyushevsky L (2009a) Study of trace element zonation in vent chimneys from the Silurian Yaman-Kasy volcanic-hosted massive sulfide deposit (Southern Urals, Russia) using laser ablation-inductively coupled plasma mass spectrometry (LA-ICPMS). Economic Geology 104:1111-1141.

Maslennikov VV, Maslennikova SP, Large RR, Danyushevsky LV (2009b) Study of trace element zonation in vent chimneys from the Silurian Yaman-Kasy volcanic-hosted massive sulfide deposit (Southern Urals, Russia) using laser ablation-inductively coupled plasma mass spectrometry (LA-ICPMS). Economic Geology 104:1111-1141.

McClenaghan MB (2005) Indicator mineral methods in mineral exploration. Geochemistry: Exploration, Environment, Analysis 5:233-245.

Mehmood T, Liland KH, Snipen L, Sæbø S (2012) A review of variable selection methods in partial least squares regression. Chemometrics and Intelligent Laboratory Systems 118:62-69.

Mendez KM, Broadhurst DI, Reinke SN (2020) Migrating from partial least squares discriminant analysis to artificial neural networks: a comparison of functionally equivalent visualisation and feature contribution tools using jupyter notebooks. Metabolomics 16:17. doi: 10.1007/s11306-020-1640-0.

Moggi-Cecchi V, Cipriani C, Rossi P, Ceccato D, Rudello V, Somacal H (2002) Trace element contents and distribution maps of chalcopyrite: a micro-PIXE study. Per Mineral 71:101-109.

Mungall JE (2007) Crustal contamination of picritic magmas during transport through dikes: the Expo Intrusive Suite, Cape Smith fold belt, New Quebec. Journal of Petrology 48:1021-1039.

Naldrett AJ (2004) Magmatic sulfide deposits: Geology, geochemistry and exploration. Springer Science & Business Media.

Palarea-Albaladejo J, Martín-Fernández JA, Gómez-García J (2007) A parametric approach for dealing with compositional rounded zeros. Mathematical Geology 39:625-645.

Palarea-Albaladejo J, Martín-Fernández JA (2008) A modified EM alr-algorithm for replacing rounded zeros in compositional data sets. Computers & Geosciences 34:902-917.

Palarea-Albaladejo J, Martín-Fernández JA (2015) zCompositions—R package for multivariate imputation of left-censored data under a compositional approach. Chemometrics and Intelligent Laboratory Systems 143:85-96.

Paton C, Hellstrom J, Paul B, Woodhead J, Hergt J (2011) Iolite: Freeware for the visualisation and processing of mass spectrometric data. Journal of Analytical Atomic Spectrometry 26:2508-2518.

Pawlowsky-Glahn V, Buccianti A (2011) Compositional data analysis: Theory and applications. John Wiley & Sons.

Perez DR, Narasimhan G (2018) So you think you can PLS-DA? bioRxiv:207225.

Piña R, Gervilla F, Barnes S-J, Ortega L, Lunar R (2012a) Distribution of platinum-group and chalcophile elements in the Aguablanca Ni–Cu sulfide deposit (SW Spain): evidence from a LA-ICP-MS study. Chemical Geology 302:61-75.

Piña R, Gervilla F, Barnes S-J, Ortega L, Lunar RJCG (2012b) Distribution of platinum-group and chalcophile elements in the Aguablanca Ni–Cu sulfide deposit (SW Spain): evidence from a LA-ICP-MS study. 302:61-75.

Piña R, Gervilla F, Barnes SJ, Oberthür T, Lunar R (2016) Platinum-group element concentrations in pyrite from the Main Sulfide Zone of the Great Dyke of Zimbabwe. Mineralium Deposita 51:853-872.

Plouffe A, Ferbey T, Hashmi S, Ward B (2016) Till geochemistry and mineralogy: vectoring towards Cu porphyry deposits in British Columbia, Canada. Geochemistry: Exploration, Environment, Analysis 16:213-232.

Reich M, Palacios C, Barra F, Chryssoulis SJEJoM (2013) "Invisible" silver in chalcopyrite and bornite from the Mantos Blancos Cu deposit, northern Chile. 25:453-460.

Ren Y, Huang F, Li Y, Zhu J, Wan Q, Yu L, Zhang Z, Gao S (2017) Genesis Study of the Nano-Micron Sphalerite Exsolution in Chalcopyrite from the Gengzhuang Gold Deposit in China. Journal of Nanoscience and Nanotechnology 17:6677-6685.

Ripley EM, Li C (2011) A review of conduit-related Ni-Cu-(PGE) sulfide mineralization at the Voisey's Bay Deposit, Labrador, and the Eagle Deposit, northern Michigan. Reviews in Economic Geology 17:181-197.

Ripley EM, Li C (2013) Sulfide Saturation in Mafic Magmas: Is External Sulfur Required for Magmatic Ni-Cu-(PGE) Ore Genesis? Economic Geology 108:45-58. doi: 10.2113/econgeo.108.1.45.

Ripley EM (2014) Ni-Cu-PGE Mineralization in the Partridge River, South Kawishiwi, and Eagle Intrusions: A Review of Contrasting Styles of Sulfide-Rich Occurrences in the Midcontinent Rift System. Economic Geology 109:309-324. doi: 10.2113/econgeo.109.2.309.

Rose AW (1967) Trace elements in solflde minerals from the Central district, New Mexico and the Bingham district, Utah. Geochimica et Cosmochimica Acta 31:547-585.

Rouxel OJ, Luais B (2017) Germanium isotope geochemistry. Reviews in Mineralogy and Geochemistry 82:601-656.

Salim Amaral LF (2017) The distribution of platinum-group elements and other chalcophile elements among sulfide minerals from the Ovoid ore body of the Voisey's Bay Ni-Cu sulfide deposit, Canada.

Samalens N, Barnes S-J, Sawyer EW (2017) The role of black shales as a source of sulfur and semimetals in magmatic nickel-copper deposits: Example from the Partridge River Intrusion, Duluth Complex, Minnesota, USA. Ore Geology Reviews 81:173-187.

Schulz KJ, Woodruff LG, Nicholson SW, Seal Ii RR, Piatak NM, Chandler VW, Mars JL (2014) Occurrence model for magmatic sulfide-rich nickel-copper-(platinum-group element) deposits related to mafic and ultramafic dike-sill complexes: Chapter I in Mineral deposit models for resource assessment. US Geological Survey.

Sciuba M, Beaudoin G, Grzela D, Makvandi S (2019) Trace element composition of scheelite in orogenic gold deposits. Mineralium Deposita:1-24.

Sciuba M, Beaudoin G, Makvandi S (2021) Chemical composition of tourmaline in orogenic gold deposits. Mineralium Deposita 56:537-560.

Song X-Y, Keays RR, Zhou M-F, Qi L, Ihlenfeld C, Xiao J-F (2009) Siderophile and chalcophile elemental constraints on the origin of the Jinchuan Ni-Cu-(PGE) sulfide deposit, NW China. Geochimica et Cosmochimica Acta 73:404-424. doi: https://doi.org/10.1016/j.gca.2008.10.029.

Sugaki A, Kitakaze A, Kojima S (1987) Bulk compositions of intimate intergrowths of chalcopyrite and sphalerite and their genetic implications. Mineralium deposita 22:26-32.

Sun C (2018) Partitioning and partition coefficients In: White WM (ed) Encyclopedia of geochemistry Encyclopedia of earth sciences series. Springer, pp 1186-1197.

Vaughan DJ (2006) Sulfide mineralogy and geochemistry: introduction and overview. Reviews in Mineralogy and Geochemistry 61:1-5.

Wang Z, Xu D, Zhang Z, Zou F, Wang L, Yu L, Hu M (2015) Mineralogy and trace element geochemistry of the Co-and Cu-bearing sulfides from the Shilu Fe–Co–Cu ore district in Hainan Province of South China. Journal of Asian Earth Sciences 113:980-997.

Westerhuis JA, Hoefsloot HCJ, Smit S, Vis DJ, Smilde AK, van Velzen EJJ, van Duijnhoven JPM, van Dorsten FA (2008) Assessment of PLSDA cross validation. Metabolomics 4:81-89.

Wilcox RR (2011) Introduction to robust estimation and hypothesis testing. Academic press.

Wilson SA, Ridley WI, Koenig AE (2002) Development of sulfide calibration standards for the laser ablation inductively-coupled plasma mass spectrometry technique. Journal of Analytical Atomic Spectrometry 17:406-409.

Wohlgemuth-Ueberwasser CC, Viljoen F, Petersen S, Vorster C (2015) Distribution and solubility limits of trace elements in hydrothermal black smoker sulfides: An in-situ LA-ICP-MS study. Geochimica et Cosmochimica Acta 159:16-41.

Wold S, Sjöström M, Eriksson L (2001) PLS-regression: a basic tool of chemometrics. Chemometrics and intelligent laboratory systems 58:109-130.

Wold S, Eriksson L, Trygg J, Kettaneh N (2004) The PLS method–partial least squares projections to latent structures–and its applications in industrial RDP (research, development, and production). Unea University.

Wood BJ, Kiseeva ES (2015) Trace element partitioning into sulfide: How lithophile elements become chalcophile and vice versa†. American Mineralogist 100:2371-2379. doi: 10.2138/am-2015-5358CCBYNCND.

Zientek ML, Likhachev AP, Kunilov VE, Barnes S-J, Meier AL, Carlson RR, Briggs PH, Fries TL, Adrian BM, Lightfoot PC (1994) Cumulus processes and the composition of magmatic ore deposits: examples from the Talnakh district, Russia. Ont Geol Surv Spec Publ 5:373-392.

Chapitre 2 Trace element composition of chalcopyrite from volcanogenic massive sulfide deposits: variation and implications for provenance recognition

Enzo Caraballo[1,*], Georges Beaudoin[1], Sarah Dare[2], Dominique Genna[2,3], Sven Petersen[4], Jorge M.R.S. Relvas[5], Stephen J. Piercey[6]

[1]Département de géologie et génie géologique, Université Laval, 1065 avenue de la Médecine, Québec, Québec C G1V 0A6, Canada; [2] Département des Sciences Appliquées, Université du Québec à Chicoutimi, 555, boul. de l'Université, Saguenay, Québec G7H 2B1, Canada; [3]CONSOREM, 555, boul. de l'Université, Saguenay, Québec G7H 2B1, Canada; [4]Helmholtz Centre for Ocean Research Kiel, Wischhofstr 1-3, 24148 Kiel, Germany; [5]Instituto Dom Luiz, Faculdade de Ciências, Universidade de Lisboa, 1749-016 Lisbon, Portugal; [6]Memorial University of Newfoundland, 300 Prince Philip Drive, St. John's, Newfoundland and Labrador A1B 3X5, Canada

2.1 Résumé

De la chalcopyrite provenant de 51 dépôts de sulfures massifs volcanogènes (SMV) et de sulfures massifs des fond marins (SMS) appartenant à 6 contextes lithostratigraphiques, ont été analysées pour les éléments traces par ablation laser et spectrométrie de masse à plasma à couplage inductif (LA-ICP-MS) pour évaluer son potentiel comme minéral indicateur pour l'exploration. L'analyse discriminante par les moindres carrés partiels (PLS-DA) a révélé que la chalcopyrite provenant de différents sous-types lithostratigraphiques a une composition différente, comme résultat des assemblages lithologiques encaissantes et de la composition du fluide. Trois modèles Random Forest (RF) ont été développés pour distinguer la chalcopyrite selon les sous-types de SVM avec une approche hiérarchique descendante. Cette méthode, laquelle premièrement classifie selon les affinités lithologiques majeures, et ultérieurement selon le sous-type de SMV, a rapporté une proportion d'échantillons classifiés correctement (accuracy) sur le 0.96 avec les données de test. La validation des modèles avec des données de la littérature avec les mêmes éléments requis pour les modèles a rapporté les proportions d'échantillons classifiés correctement les plus élevées (>0.90). La validation en utilisant des données incomplètes a rapporté une proportion de modérée à élevée (0.60-1); néanmoins, les performances diminuent significativement (<0.50) lorsque les éléments les plus importants sont manquants. Les modèles de régression, développés en utilisant tous les éléments analysés, pour déterminer le rapport ccp/(ccp+sp) dans la chalcopyrite dans un sous-type SMV ont rapporté des performances élevées, et démontre le potentiel pour prédire le rapport Cu/Zn de la minéralisation basé sur la composition de la chalcopyrite. Cette étude démontre que les éléments traces dans la chalcopyrite sont contrôlés principalement par la configuration lithostratigraphique et qu'ils peuvent être utilisés comme des variables prédictives dans un modèle RF pour distinguer les différents sous-types de SMV.

2.2 Abstract

Chalcopyrite from 51 volcanogenic massive sulfide (VMS) and seafloor massive sulfide (SMS) deposits from 6 lithostratigraphic settings, were analyzed for trace elements by laser ablation-inductively coupled plasma-mass spectrometry (LA-ICP-MS) to evaluate its potential as an indicator mineral for exploration. Partial least squares discriminant analysis (PLS-DA) results reveal that chalcopyrite from different lithostratigraphic settings have different compositions reflecting their host rock assemblages and fluid composition. Three random forest (RF) classifiers were developed to distinguish chalcopyrite from the six lithostratigraphic settings with a divisive approach. This method, which primarily classifies according to the major host rock affinity, and subsequently according to VMS settings, yielded an overall accuracy higher than 0.96 on test data. The model validation with literature data having the same elements required by the models yielded the highest accuracies (>0.90). Validation using published data with missing elements the accuracy is moderate to high (0.60-1), however; the

performances decrease significantly (<0.50) when the most important elements are missing. Similarly, RF regression models developed using all sets of analyzed elements to determine ccp/(ccp+sp) ratio in chalcopyrite within a single VMS setting reported high performances, thus showing a potential to predict the Cu/Zn ratio (Cu-rich vs. Zn-rich) of the mineralization based on chalcopyrite composition. This study demonstrates that trace element concentrations in chalcopyrite are primarily controlled by lithotectonic setting and can be used as predictors in a random forest classifier to distinguish the different VMS subtypes.

2.3 Introduction

Chalcopyrite occurs in numerous mineral deposit types, from magmatic to hydrothermal systems. Its trace element composition is highly variable, as shown by several studies of magmatic Ni-Cu-PGE deposits (Barnes et al., 2008; Caraballo et al., 2022; Czamanske et al., 1992; Dare et al., 2014; Dare et al., 2010b; Dare et al., 2011; Duran et al., 2016b; Godel and Barnes, 2008; Mansur et al., 2020; Piña et al., 2012a) and hydrothermal environments (Agangi et al., 2018; Bajwah et al., 1987; Butler and Nesbitt, 1999; Cabri et al., 1985; Cook et al., 2011; George et al., 2018b; Harris et al., 1984; Hawley and Nichol, 1961b; Huston et al., 1995; Kase, 1987; Moggi-Cecchi et al., 2002; Reich et al., 2013b; Rose, 1967; Wang et al., 2015; Wohlgemuth-Ueberwasser et al., 2015). The crystal structure, partitioning with co-crystallizing minerals, and magma/fluid composition are the principal factors controlling the trace element content of chalcopyrite (Caraballo et al., 2022; George et al., 2016). Thus, the trace element composition of chalcopyrite can be used for provenance studies (Caraballo et al., 2022; Duran et al., 2019b; Hashmi et al., 2015a).

An indicator mineral provides evidence on the presence of a type of mineralization, hydrothermal alteration, or lithology in bedrock; their morphology, textures and/or geochemistry may be investigated in order to obtain information about transport and nature of mineralization (McClenaghan, 2005). The characteristics to consider a mineral as indicator in exploration are: a) a specific gravity relatively high (G>3.2) to be separated from sample media; b) distinctive visual properties with minimal size about of 0.25 mm to be recuperated efficiently from sediments (e.g., till, soils, fluvial); c) high resistance to weathering (e.g., oxidation) and/or mechanical transport; d) a wide range of trace element compositions that is sensitive to the environment of crystallization, including important genetic information about mineralization and host rocks (Averill, 2001; Averill, 2011b; McClenaghan, 2005). With a specific gravity of 4.1-4.3, chalcopyrite is easily separated by density, and its physical properties enable recognition by optic microscope. In addition, chalcopyrite is among the sulfides the most resistant to dissolution in the weathering environment, and several hypotheses have been proposed to explain the mechanisms leading to slow dissolution kinetic (Crundwell et al., 2021; Rimstidt et al., 1993). Averill (2011b), based on stability in surficial sediments under temperate and humid tropical conditions, and Crundwell (2021), based on the electronic structure of the most common sulfides, proposed a relative scale of dissolution resistance/stability, which places chalcopyrite as one of the most resistant sulfide.

Multivariate statistical analysis, such as principal component analysis (PCA), partial least square-discriminant analysis (PLS-DA), and machine learning methods, such as random forest, are useful to investigate the chemical variations of large datasets of trace elements in indicator minerals, such as gold (Liu and Beaudoin, 2021; Liu et al., 2021), pyrite (Gregory et al., 2019), magnetite (Bédard et al., 2022; Duran et al., 2020; Makvandi et al., 2016a; Makvandi et al., 2016b), scheelite (Grzela et al., 2019; Manéglia et al., 2018; Miranda et al., 2022; Sciuba et al., 2020), sphalerite (Frenzel et al., 2016; Zhang et al., 2022a), rutile (Sciuba and Beaudoin, 2021) and tourmaline (Sciuba et al., 2021). However, studies on chalcopyrite using this approach are scarce and previous work relied more on empirical discrimination diagrams (Duran et al., 2019a; George et al., 2018b). Bédard et al. (2017) investigated trace element compositions of chalcopyrite from different ore deposit types using principal component analysis (PCA) and demonstrated its potential for recognizing chalcopyrite from different deposit types. They showed that trace element signatures discriminate chalcopyrite from volcanogenic massive sulfide (VMS: Ag, Sn, Zn and Se), Ni-Cu-PGE (Ni, Te and Pd), orogenic gold and red beds (Au and As), porphyry and skarn (Sb, In and Se), and IOCG (Zn and Ba) deposits. Caraballo et al. (2022) demonstrated, using PLS-DA, that chalcopyrite from Ni-Cu sulfide and reef-type PGE deposits can be distinguished using Bi, In, Se, Sn and Te. Furthermore, they showed that in Ni-Cu sulfide deposits, it was possible to discriminate chalcopyrite according to ore type (Cu-rich vs. Fe-rich) using the assemblage Sb, Se, Sn, Tl and Zn. Based on cluster analysis and classification tree approach on trace elements in chalcopyrite from a single Ni-Cu-PGE deposit (Norilsk-Talnakh), Marfin et al. (2020) showed that there are chemical differences between massive vs. disseminated ore types. This study focusses on another single deposit-type, that of VMS, to determine the intra-deposit scale variation of chalcopyrite composition according to both ore type and lithostratigraphic setting.

Volcanogenic massive sulfides occur as ancient accumulations of sulfide minerals (sphalerite, chalcopyrite, pyrite ± pyrrhotite, galena) that precipitated at, or below, the seafloor from convective hydrothermal fluids, in spatial relationship with volcano-sedimentary sequences and usually coeval with volcanic host rocks (Barrie and Hannington, 1999; Franklin et al., 2005; Hannington, 2014; Lydon, 1988). They are important sources of Zn, Cu, Pb, Ag and Au, and of critical and strategic metal by-products, such as Co, Sn, Se, Mn, Cd, In, Bi, Te, Ga and Ge (Galley et al., 2007). The modern equivalent of VMS deposits are seafloor massive sulfides (SMS), which form in active submarine hydrothermal systems, where high-temperature (≈350°C) black smoker vents are the most recognizable features and occur in extensional environments, principally at mid-ocean ridges, in back-arc basins and along submarine volcanic arcs (Fuchs et al., 2019; Hannington et al., 2005).

This deposit type typically comprises a mound-shaped to tabular, stratabound body of massive sulfides (>60% sulfides), with altered silicates, with some underlain by a discordant stockwork or stringer veins composed of Cu-rich sulfides (Barrie and Hannington, 1999; Galley et al., 2007; Hannington, 2014; Lydon, 1988). In some VMS deposits, a zonation is present, with a systematic decrease of chalcopyrite/(sphalerite+galena) ratio from the inner, underlying stockwork zones to the outer margins (Galley et al., 2007; Hannington, 2014; Lydon, 1988).

This zoning is principally a result of several high temperature events, with replacement of early sulfides (Zn-Pb-rich) by Cu-rich ores as the system increase temperature in the lower parts, and a reprecipitation of Zn-Pb minerals in the outer zones of the growing orebody (Eldridge et al., 1983; Ohmoto, 1996). The spatial distribution of these minerals could also be affected by the cooling path and the solubility of chalcopyrite and sphalerite, precipitating initially chalcopyrite and then sphalerite (Hannington, 2014; Hannington et al., 1995). Chalcopyrite precipitates at relatively high temperatures, between 270°C and 360°C, at the base, whereas sphalerite is deposited at lower temperatures (175°C-250°C) in the outer margins (Franklin et al., 2005; Hannington, 2014; Hannington et al., 1995; Lydon, 1988). In conductive cooling processes, pH variation in the fluid is limited, which could inhibit precipitation of sphalerite and triggering chalcopyrite precipitation at the base, whereas in a mixing cooling history, the pH variation is larger, leading to co-crystallization of chalcopyrite and sphalerite (Hannington et al., 1995). In hydrothermal systems, the behavior of elements is controlled principally by the stability of aqueous complexes of chlorine and sulfur (Hannington, 2014; Seward et al., 2014). Hannington (2014) indicates that there are two principal trace element associations according to temperature: a) a low temperature assemblage, comprising Zn, Pb, Ag, Cd, Sn, Sb, As, Hg, ±Tl, ±W, in the outer margin; and b) higher temperature association of Cu, Co, Bi, Se, In, ±Ni and ±Mo in the deeper roots of the system. The composition of chalcopyrite is also determined by partitioning in co-crystallizing sulfides, such as pyrite, sphalerite and galena (Genna and Gaboury, 2015; George et al., 2016; George et al., 2018b).

Although several studies have analyzed chalcopyrite from VMS-SMS deposits (e.g., George et al., 2018b; Hawley and Nichol, 1961b; Martin et al., 2019; Wang et al., 2018), only a few have been focused on variability of the trace element composition at deposit scale (Butler and Nesbitt, 1999; Maslennikov et al., 2017; Revan et al., 2014; Torró et al., 2022). Torró et al. (2022) showed that the increase of Se and Bi contents in chalcopyrite from Zn-rich to Cu-rich zone suggests an increase in temperature at the Sofía-D massive sulfide body in the María Teresa VMS deposit (Perú). Furthermore, at chimney scale, the same behavior is observed in the Broken Spur SMS deposit (Mid-Atlantic Ridge; Butler and Nesbitt, 1999), Çayeli¸-Kutlular (Turkey; Revan et al., 2014), and in Urals deposits (Russia; Maslennikov et al., 2009b; Maslennikov et al., 2017), where chalcopyrite from inner zones is higher in Se than those from outer parts of the chimney, likewise supporting the model of temperature-controlled precipitation. However, more studies are needed to fully understand the chemical behavior of chalcopyrite in VMS deposits.

Based on the volcano-sedimentary assemblage within a district, delimited by major time breaks, faults or major intrusions, metal proportions and associated with specific tectonic settings, VMS deposits are classified into five lithostratigraphic types (Barrie and Hannington, 1999; Franklin et al., 2005). Furthermore, the sulfide mineralogy and abundance vary according to the composition of ore-forming hydrothermal fluids and the interaction with the underlying rocks (Hannington, 2014; Hannington et al., 2005; Shanks et al., 2012), such that mafic-hosted deposits are typically Cu-rich, whereas bimodal-felsic deposits are higher in Zn and siliciclastic-felsic in Pb

(Galley et al., 2007; Hannington, 2014). The five VMS lithostratigraphic types comprise: 1) mafic, associated with ophiolite assemblages in mature intra-oceanic back-arc basins, dominated by MORB successions; 2) siliciclastic-mafic, related to mature backarc settings in basalt-pelite or pelite dominant sequences; 3) bimodal-mafic, associated with incipient-rifted bimodal volcanic arcs and basalt-dominated with up to 25% felsic volcanic strata; 4) bimodal-felsic, in continental margin arcs and related back-arcs, with felsic volcanics up to 35-75% and basalt 20-50%, and 5) siliciclastic-felsic, associated to mature epicontinental back-arc and dominated by siliciclastic rocks (~80%). Patten et al. (2022) suggested there is also an ultramafic-hosted subgroup of VMS deposits given their unique lithostratigraphic setting and metal endowment (*e.g.,* Cu, Zn, Co, Ni). They form principally in slow to ultra-slow spreading mid-ocean ridges with limited effusive magmatic activity. Although chalcopyrite is present in all the subtypes of VMS deposits, there is not a systematic study that has compared the signatures between these different settings. Therefore, the ability to predict the VMS lithostratigraphic setting using chalcopyrite as an indicator mineral from till or river sediments at an early exploration stage, could be an important tool to guide exploration strategies in covered terrains in addition to geophysical techniques.

This study aims to evaluate the potential of chalcopyrite chemistry from ancient VMS deposits (Archean to Tertiary) and seafloor massive sulfide (SMS) deposits, to be used as an indicator mineral for exploration. We systematically investigated the variation of 36 trace elements in chalcopyrite from worldwide VMS-SMS deposits, as a function of the deposit lithostratigraphic subtype (Franklin et al., 2005; Patten et al., 2022), ore type (massive/stockwork) and sulfide proportions. We show that the chalcopyrite chemical composition varies as a function of lithostratigraphic setting and that, by using multivariate statistical analysis and a random forest classification model combined with an understanding of the processes that control the trace element content of chalcopyrite, it is possible to distinguish chalcopyrite from different lithostratigraphic subtypes and to classify accurately unknown chalcopyrite samples by VMS-SMS subtypes. In addition, we tested the models on literature data, demonstrating that internal variation in a deposit scale or in a single VMS subtype is considerably less important that the variation between VMS subtypes.

2.4 Methodology

2.4.1 Sample Selection

A total of one hundred chalcopyrite-bearing samples (N=100) were selected from 51 VMS-SMS deposits from around the world (Fig. 2.1). The deposits belong to 6 lithostratigraphic types of settings according to the classification for VMS-SMS (Franklin et al., 2005; Patten et al., 2022), as follows (Table 2.1): a) ultramafic (UM, N=8); b) mafic (M, N=6); c) siliciclastic-mafic (SM, N=3); d) bimodal-mafic (BM, N=27); e) bimodal-felsic (BF, N=30) and f) siliciclastic-felsic (SF, N=22). The VMS samples (N=89) comprise all of the lithostratigraphic types, except for the ultramafic type. The SMS samples (N=11) are related to the ultramafic (N=8; from the Logatchev

and Irinovskoe vent fields) and bimodal-felsic type (N=3; PacManus vent field). The sulfide proportions in each sample are reported as ccp/(ccp+sp), po/(po+sp+py) and ccp/(ccp+po) ratios. The sulfide proportion was calculated for each sample from percentage of sulfides in thin section and in macroscopic sample, and from information on position in deposit. Since this study focusses on chalcopyrite, samples from the Cu-rich areas of mineralization were targeted. However, chalcopyrite from the Matagami district comprises samples of both Cu-rich (N=7) and Zn-rich (N=6) ores and represents the most balanced sample set according to Cu/Zn ratio. Furthermore, according to microscopic and megascopic sample observations, we classified the samples into massive ore (>60% opaque minerals and massive structure) and stockwork ores (stringer/vein mineralization, Annexe B1).

Most of studied deposits are metamorphosed, from prehnite-pumpellyite to principally greenschist conditions, and only one has undergone amphibolite grade metamorphism (Tétrault, Québec). Among unmetamorphosed deposits are those from Semail (Lasail) and VMS-SMS deposits (Table 2.1; Annexe B1). Siliciclastic-felsic group presents the greater diversity of the metamorphic grades, whereas the siliciclastic-mafic subtype is at upper greenschist metamorphic facies.

The selected samples are representative of the different subtypes of VMS-SMS deposits. For 10 deposits, we analyzed more than 4 samples, whereas we analyzed 2-3 samples in 10 other deposits, and 1 in the remaining 31 deposits (Table 2.1). According to the compilation included in Franklin et al. (2005), among a total of 646 VMS deposits only 63 (10%) correspond to mafic and 80 (12%) to siliciclastic-mafic settings. An underlying class imbalance problem is present as result of rarity of deposits belonging to these settings. In our data, deposits from the mafic subtype represent about 12% (12 samples from 6 deposits; Fig. 2.1), belonging to 4 host tectonostratigraphic complexes with a total of 42 analyses (7.4%). Based on these sampling statistics, the mafic subtype would be considered representative, since its distribution is similar to the deposit distribution from Franklin et al. (2005). Concerning the siliciclastic-mafic subtype, according to Franklin et al. (2005) it represents 12% of compiled deposits. In our data, deposits from this setting represent about 4%, belonging to the same host tectonostratigraphic complex. The representative nature of the selected samples and deposits ensures that the analytical data will capture the more important characteristics of chalcopyrite composition in VMS-SMS deposits, but it is possible that some intra-deposit variance or less common features will require detailed deposit-scale studies and investigation of other VMS-SMS deposits in future.

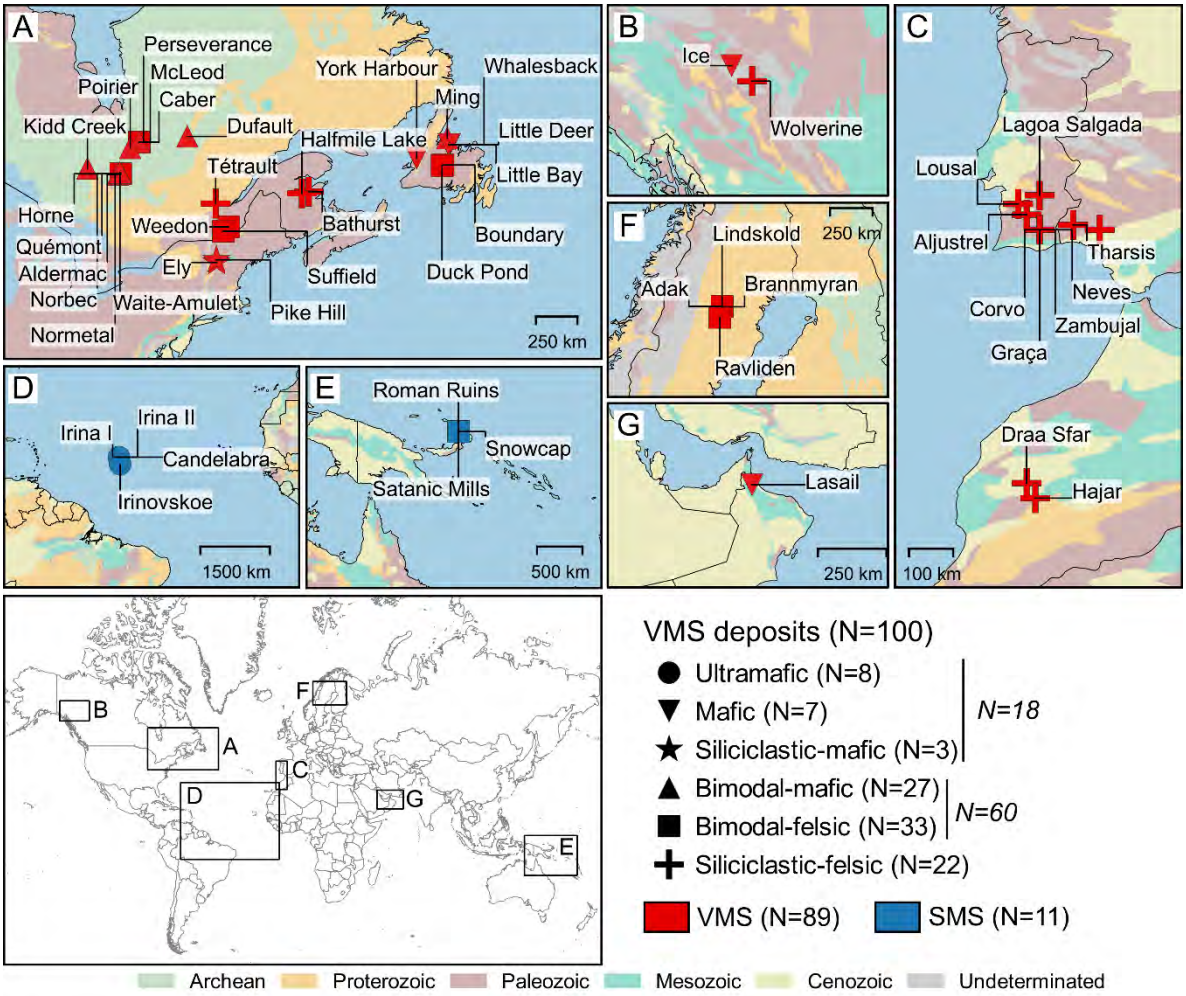

Fig. 2. 1 Location of selected VMS-SMS deposits in this study. Classification according to Franklin et al. (2005) and Patten et al. (2022). Generalized geologic map of the world (Chorlton, 2007). N= number of samples.

2.4.2 Petrography

Mineralogical composition and detailed textural descriptions of each thin section, considered representative of the sample, were carried out using a reflected light microscope. From this information, paragenetic sequences were determined in each sample. Modal percentages were calculated using ImageJ 1.52p based on a mosaic of photomicrographs. To verify the presence of inclusions not detected under optical microscope, and to select regions without inclusions (<10 µm) for geochemical analysis, scanning electron microscopy (SEM) was used (model FEI Inspect F50, equipped with an energy-dispersive spectrometer (EDS) at Université Laval; Annexe B6). Between five and seven grains of chalcopyrite were selected in each polished section for geochemical analysis, based on the amount and distribution of chalcopyrite, grain size and mineralogical association.

2.4.3 Analytical Methods

Major elements in 296 grains of chalcopyrite (n=296) were analyzed by electron probe microanalysis (EPMA), using a CAMECA SX-100 equipped with five wavelength-dispersive spectrometers (WDS) at Université Laval,

Québec. Beam size was 10 μm with a voltage of 15 kV and a current of 20 nA. The background was measured for 15-20 s on both sides and a peak counting time of 10 s was carried out. Standard Fe_2O_3 (Fe), FeS_2 (S) and $CuFeS_2$ (Cu) were used for the calibration. The results are given in Annexe B2 and show that the major element composition of all chalcopyrite is close to stoichiometric values.

Trace elements in 561 grains of chalcopyrite (n=561) were analyzed by laser ablation inductively coupled plasma mass spectrometry (LA-ICP-MS) at LabMaTer (Université du Québec à Chicoutimi, UQAC) using an Excimer 193-nm RESOlution M-50 laser ablation system (Australian Scientific Instrument) equipped with a double volume cell S-155 (Laurin Technic) and coupled to an Agilent 7900 ICP-MS following the protocol described in Caraballo et al. (2022). Depending on grain size, a beam size of 55 μm and 33 μm, a line speed of 5 μm/s, a laser frequency of 15 Hz and a fluence of 3 J/cm^2 were used to analyze chalcopyrite. Lines were made across the sulfide grains for a period of 20 to 60 s according to grain size, after measuring the gas blank for 30 s. The ablated material was carried into the ICP-MS by an argon-helium gas mix at a rate of 0.8 to 1 L/min for Ar and 350 mL/min for He, and 2 mL/min of nitrogen was also added to the mixture. Data reduction was carried out using Iolite package for Igor Pro software (Paton et al., 2011). Full results are given in Annexe B3.

Thirty-six isotopes were measured: ^{24}Mg, ^{29}Si, ^{34}S, ^{49}Ti, ^{51}V, ^{52}Cr, ^{55}Mn, ^{59}Co, ^{60}Ni, ^{65}Cu, ^{66}Zn, ^{71}Ga, ^{74}Ge, ^{75}As, ^{82}Se, ^{95}Mo, ^{101}Ru, ^{103}Rh, ^{107}Ag, ^{108}Pd, ^{111}Cd, ^{115}In, ^{118}Sn, ^{121}Sb, ^{128}Te, ^{137}Ba, ^{182}W, ^{185}Re, ^{189}Os, ^{193}Ir, ^{195}Pt, ^{197}Au, ^{202}Hg, ^{205}Tl, ^{208}Pb and ^{209}Bi. The polyatomic interference of ^{40}Ar^{63}Cu on ^{103}Rh was corrected in chalcopyrite using a Cu-blank. However, the ^{103}Rh values of are not reported as the interference corrections are too large in chalcopyrite (1% Cu produces about 0.1-0.2 ppm ^{103}Rh interference). Additionally, in most cases PGE were below detection limit in chalcopyrite. Direct interference of ^{115}Sn on ^{115}In and ^{108}Cd on ^{108}Pd were corrected in chalcopyrite manually from ^{118}Sn and ^{111}Cd. We used ^{57}Fe as the internal standard with stoichiometric iron value of chalcopyrite (30.43 %). Calibration was based on a combination of three international reference materials (RM): MASS-1 (Wilson et al., 2002), corresponding to a pressed powder pellet (ZnCuFeS) used to calibrate S, Cu, Zn, As, Se, Mo, Cd, Sn, Sb, Te, W, Hg, Tl and Pb; GSE-1g (Jochum et al., 2005), a Fe-rich natural basaltic glass used to calibrate Si, Ti, V, Cr, Mn, Co, Ni, Ga, Ge, Ag, In, Ba, Re and Bi; and Laflamme Po727, a synthetic FeS doped with PGE, used to calibrate Au and PGE. The RM used to monitor quality control of the analyses were: CCu-1e, a copper concentrate (certified by CCRMP-Canadian Certified Reference Materials project, CANMET, Canada); UQAC-FeS1, a synthetic sulfide developed at LabMaTer (UQAC) and PTC-1b, a Cu-Ni-sulfide concentrate powder (Jochum et al., 2005). The results of analyses of reference materials and the range of detection limits are shown in Annexe B4. Most elements (Ag, As, Au, Bi, Co, Ga, In, Ir, Mn, Mo, Ni, Os, Pb, Rh, Ru, Sb, Se, Sn, Te, Tl and Zn) have a moderate to high accuracy relative to their reference values (rel. diff.<10-15%) and a moderate to high precision (RSD<10-15%). Elements such as Ti, Ge and Cd show lower accuracy (rel. diff.>15%) and lower precision (RSD>15%; Annexe B4). Differences between working values in a few of RM and those measured in this study could be a result of heterogeneity and non-matrix matched materials

or due to the low level of confidence of reported working values for some elements in RM (provisional/informative values). As polyatomic interferences were detected on ^{49}Ti (from $^{33}S^{16}O^{+}$) and ^{74}Ge (from $^{40}Ar^{34}S^{+}$, $^{36}Ar^{38}Ar^{+}$ and/or $^{38}Ar^{36}S^{+}$), and Cd shows low accuracy and precision, these elements were not used for statistical analysis.

Elements such as Si (silicates), Zn-Cd (sphalerite), Pb (galena), Ni (pentlandite), Ba (barite) were used to monitor for inclusions. On each time-signal, only micrometric inclusion-free regions were selected for data reduction in order to have the most reliable composition of chalcopyrite (Annexe B6).

2.4.4 Statistical Methods

2.4.4.1 Data pre-Processing

Before statistical analysis, the geochemical data were pre-processed for the values below detection limit (*i.e.,* censored values). Since most imputation algorithms do not remain stable with higher degrees of censoring (Antweiler, 2015; Hron et al., 2010; Makvandi et al., 2016b), elements with more than 40% of censored values were excluded from the database. The log-ratio expectation-maximization (lrEM) algorithm was applied to impute censored values, using zComposition R-package (Palarea-Albaladejo and Martín-Fernández, 2015). According to Palarea-Albaladejo and Martín-Fernández (2008), an alr-transformed component $y_{ij} = ln(x_{ij}/x_{iD})$ from a compositional vector x_i is considered a censored value if $y_{ij} \leq \psi_{ij}$, where ψ_{ij} is alr-transformed threshold (detection limit). This adapted statistical iterative procedure ensures that censored values y_{ij} are replaced by values lower than threshold ψ_{ij} (Palarea-Albaladejo et al., 2007).

Compositional data describe quantitatively the parts of a whole, which sum to a constant (*i.e.*, 100%), having thus a closed nature, thus leading to potential spurious correlations (Egozcue and Pawlowsky-Glahn, 2011; Filzmoser et al., 2009; Pawlowsky-Glahn and Buccianti, 2011). In order to avoid this problem, the data was transformed using centered log-ratios following Aitchison (1986).

Table 2. 1 Summary of studied VMS and SMS deposits (details of sulfide textures and opaque mineralogy in Annexe B1)

Setting[1]	Affinity[2]	Deposit name (number of samples)	Host tectonostratigraphic complex (age)	Location	Host rocks composition	Regional metamorphism	References
Ultramafic	Mafic-ultramafic	Irinovskoe (4)	Mid-Atlantic Ridge (?)	Irinovskoe field, Atlantic Ocean	Pdt-Gabnor	Unmetamorphosed	Cherkashev et al. (2013); Petersen et al. (2009); Wohlgemuth-Ueberwasser et al. (2015)
		Candelabra (2)	Mid-Atlantic Ridge (1-60 ka)	Logatchev-1 field, Atlantic Ocean			
		Irina I (1)					
		Irina II (1)					
Mafic		Lasail (2)	Semail Ophiolite (95 Ma)	Al Batinah North, Oman	Bas and basaltic And		Gilgen et al. (2014); Stakes and Taylor (2003)
		Little Deer (1)	Dunnage Zone - Notre Dame Subzone (0.48 Ga)	Newfoundland, Canada	Pillow Bas	Lower greenschist	Kean et al. (1995); Piercey (2007)
		Whalesback (1)					Cloutier et al. (2015); Piercey (2007)
		Little Bay (1)					Kean et al. (1995); Piercey (2007)
		York Harbour (1)	Humber Zone - Bay of Islands Ophiolite (0.48 Ga)				Lode et al. (2015); Piercey (2007)
		Ice (1)	Slide Mountain terrane (0.28 Ga)	Yukon, Canada	Bas		Piercey et al. (2008)
Siliciclastic-mafic		Ely (1)	Vermont Copper Belt (0.41 Ga)	Vermont, USA	Meta-Bas / Meta-Sed / minor Meta-Mafic-volc	Upper greenschist	McWilliams et al. (2010); Slack et al. (2001)
		Pike Hill (2)					
Bimodal-mafic	Bimodal	Poirier (1)	Abitibi Greenstone Belt (2.7 Ga)	Joutel, Quebec, Canada	Rhy-Dac / And-Bas	Lower greenschist	Barrie et al. (1999); Dubé et al. (2007); Gaboury and Pearson (2008); Lafrance et al. (2000); Mercier-Langevin et al. (2007); Shriver and MacLean (1993); Taylor et al. (2014); Genna et al. (2014a); Genna et al. (2014b); Ioannou et al. (2007)
		Caber (3)		Matagami, Quebec, Canada	Rhy		
		Aldermac (3)		Noranda, Quebec, Canada	Rhy-And		
		Dufault (3)					
		Norbec (2)					
		Normetal (1)					
		Aldermac (3)					
		Dufault (3)					

Setting[1]	Affinity[2]	Deposit name (number of samples)	Host tectonostratigraphic complex (age)	Location	Host rocks composition	Regional metamorphism	References
Bimodal-mafic	Bimodal	Norbec (2) Normetal (1) Waite-Amulet (5)	Abitibi Greenstone Belt (2.7 Ga)	Noranda, Quebec, Canada	Rhy-And	Lower greenschist	Barrie et al. (1999); Dubé et al. (2007); Gaboury and Pearson (2008); Lafrance et al. (2000); Mercier-Langevin et al. (2007); Shriver and MacLean (1993); Taylor et al. (2014); Genna et al. (2014a); Genna et al. (2014b); Ioannou et al. (2007)
		Kidd Creek (4)		Timmins, Ontario, Canada	Rhy-Um		
		Ming (5)	Dunnage Zone - Notre Dame Subzone (0.48 Ga)	Newfoundland, Canada	Bon / Bas / Rhy	Upper greenschist	Brueckner et al. (2014); Brueckner et al. (2015); Pilote et al. (2020); Pilote and Piercey (2013)
Bimodal-felsic		Suffield Mine (1) Weedon (1)	Ascot-Weedon Complex (0.45 Ga)	Cantons de l'Est, Quebec, Canada	Felsic-volc	Lower greenschist	Gauthier et al. (1994)
		McLeod (4) Perseverance (6)	Abitibi Greenstone Belt (2.7 Ga)	Matagami, Quebec, Canada	Rhy-Rhydac		Barrie et al. (1999); Dubé et al. (2007); Gaboury and Pearson (2008); Lafrance et al. (2000); Mercier-Langevin et al. (2007); Shriver and MacLean (1993); Taylor et al. (2014); Genna et al. (2014a); Genna et al. (2014b); Ioannou et al. (2007)
		Horne (4)		Noranda, Quebec, Canada	Rhy-And		
		Boundary (1)	Dunnage Zone - Exploits Subzone (0.51 Ga)	Newfoundland, Canada	Dac-Rhy / Bas		Buschette and Piercey (2016); Piercey (2007)
		Duck Pond (1)					McNicoll et al. (2010); Piercey (2007)
		Roman Ruins (1) Satanic Mills (1) Snowcap (1)	Pual Ridge (20-50 ka)	Pacmanus field, Papua New Guinea	Dac-Rhy	Unmetamorphosed	Binns et al. (2007); Hannington et al. (2005); Reeves et al. (2011)
		Adak (2) Brannmyran (1) Lindsköld (3)	Bothnia-Skelleftea Unit (1.8 Ga)	Västerbotten, Sweden	Felsic-volc	Lower greenschist	Allen et al. (1996); Årebäck et al. (2005); Johansson (2017); Skyttä et al. (2020)
		Rävliden (1)			Felsic-volc to Mafic-volc / argilites		
Siliciclastic-felsic		Aznalcollar (1) Tharsis (1)	Iberian Pyrite Belt (0.34-0.38 Ga)	Andalucia, Spain	Rhy-Dac/ phyllite-quartzite	Prehnite-pumpellyite	Almodóvar et al. (2019); Barrie et al. (2002); Inverno et al. (2015); Relvas et al. (2001); Relvas et al. (2006); Sáez et al. (1999); Tornos (2006)
		Aljustrel (1)		Beja, Portugal			

Setting[1]	Affinity[2]	Deposit name (number of samples)	Host tectonostratigraphic complex (age)	Location	Host rocks composition	Regional metamorphism	References
Siliciclastic-felsic		Corvo (4)	Iberian Pyrite Belt (0.34-0.38 Ga)	Beja, Portugal	Rhy-Dac/ phyllite-quartzite	Prehnite-pumpellyite	Almodóvar et al. (2019); Barrie et al. (2002); Inverno et al. (2015); Relvas et al. (2001); Relvas et al. (2006); Sáez et al. (1999); Tornos (2006)
		Graça (1)					
		Neves (2)					
		Zambujal (1)					
		Lagoa Salgada (1)		Setúbal, Portugal			
		Lousal (1)					
		Hajar (1)	Guemassa Massif (0.34 Ga)	Marrakech-Safi, Morocco	Rhy-Rhydac	Lower greenschist	Admou et al. (2018); Marcoux et al. (2008); Moreno et al. (2008)
		Draa Sfar (1)	Jebilet Massif (0.34 Ga)				
		Tétrault (1)	Greenville Province	Montauban, Quebec, Canada	Gneiss	Amphibolite	Tomkins (2007); Stamatelopoulou-Seymour and MacLean (1984)
		Bathurst (4)	Bathurst Mining Camp (0.47 Ga)	New Brunswick, Canada	Rhy-Rhydac	Upper greenschist	Goodfellow (2007); Mireku and Stanley (2006)
		Halfmile Lake (1)					
		Wolverine (1)	Yukon-Tanana Terrane (0.34 Ga)	Yukon, Canada	Maf-volc and Fel-volc / dark Sed	Middle greenschist	Piercey et al. (2008)

[1]: classification according to Franklin et al. (2005)

[2]: classification according to major host rocks composition

Volc: volcanic; Felsic-volc: felsic volcanic rocks rocks; Mafic-volc: mafic volcanic rocks; Sed: sedimentary rocks.

Dac: dacite; And: andesite; rhy: rhyolite; Rhydac: rhyodacite; Maf-volc: mafic volcanic rocks; Fel-volc:felsic volcanic rocks; Pdt: peridotite; Gabnor: gabbronorite; Nor: norite; Bas: basalte; Bon: bonninite; Um: ultramafic rocks; Phy: phyllite; Qtz: quartzite.

2.4.4.2 Exploratory Data Analysis

The exploratory analysis comprised univariate, bivariate and multivariate methods to identify systematic variations in the data before building discrimination models. Univariate analysis (boxplots) explores each variable in a data set, separately. In this phase, to characterize different variables, the trimmed mean (μ_t) and the trimmed standard deviation (sd_t), two robust measures of location and dispersion with the aim to reduce effects of outliers on estimator calculation was used (Wilcox, 2011). These statistic estimators are presented for each variable (trace elements and mineralogical composition) in the format $\mu_t \pm sd_t$ plus the respective unit (ppm or vol.%). The bivariate analysis was conducted to determine whether a statistical association exists between two variables and verify clusters in the data using, respectively, Pearson correlation coefficients and binary diagrams.

A PLS-DA based on clr-transformed and auto-scaled data was performed. Previous studies have used PLS-DA on indicator minerals as a tool to classify unknown data (Caraballo et al., 2022; Liu and Beaudoin, 2021; Liu et al., 2021; Makvandi et al., 2016b; Miranda et al., 2022; Sciuba et al., 2020; Sciuba et al., 2021). However, since in this study the PLS-DA recorded lower performance than Random Forest model, as presented below, this was used as a multivariate exploratory method. This method consists of a supervised linear classification, which models dependent variables *Y* from a set of predictor variables *X*, by reducing the multidimensionality of the data (Ruiz-Perez et al., 2020; Wold et al., 2001). A PLS-DA model can be interpreted from two principal outputs, scores and loadings. After calculating latent variables, they can be used in a cartesian space (*i.e.,* t_1-t_2) to project *X*-scores of the observations. The aim of these representations, called score plots, is to look for clusters indicating similar characteristics (Brereton and Lloyd, 2014). Likewise, the distance between clusters can suggest differences in attributes. On the other hand, loading plots show correlations between original variables. Superposing *X*-loadings (specifically *X*-weight, w^*) and *Y*-loadings in the same plot, the relationship between *X*-variables (elements) and *Y*-variables (classes) can be inferred (Dunn, 2019; Wold et al., 2001). Variables positively correlated are shown grouped, whereas those with a negative correlation plot diametrically opposed. Location of variables in a loading plot is dependent on contributions in discrimination, therefore, *X*-variables near the correlation circle (radius=1) are interpreted to be highly variable between classes; in contrast, those located near the origin contribute weakly to classification, as variability is negligible. Since dummy variables are required to use PLS-DA on categorical data, the encoding, which consisted in binary integers where 1 is in class, and 0 out of class, was performed automatically by CARET package in R.

Different estimators have been used to judge the importance of the *X*-variables on the classification model. Mehmood et al. (2012) described three filter methods (loading weights, regression coefficients and variable importance on projection) used to determine variable importance. Variable importance on projection (VIP) quantifies the influence on the model by accumulating the importance of each variable *j* reflected by the weight *w* from each latent variable (Favilla et al., 2013; Mehmood et al., 2012). The average of VIP scores is 1 and the

sum of squares of all VIP scores is equal to *M*. Thus, variables with VIP scores>1.0 are considered highly influential on the discrimination model, whereas VIP between 0.8-1.0 indicate a variable moderately influential and VIP<0.8 represent less important variables (Chong and Jun, 2005; Gosselin et al., 2010; Mendez et al., 2020).

A second, widely used method to assess the importance of *X*-variables on the classification model is the vector or matrix of regression coefficients (B_{pls}), which measures the association between predictor and responses variables (Mehmood et al., 2012). Partial least square discriminant analysis is based on a regression algorithm, thus, these coefficients are calculated for each modeled response or class (Ballabio and Consonni, 2013). Variables with a strong importance for a specific class have generally high absolute values of regression coefficients, whereas those with small absolute values do not contribute importantly (Ballabio and Consonni, 2013; Gosselin et al., 2010; Mehmood et al., 2012).

2.4.4.3 Random Forest

In order to test the trace element composition of chalcopyrite to discriminate different lithostratigraphic settings of VMS deposits, a supervised classification was performed using the random forest (RF) algorithm. In addition to classification model, a preliminary RF regression model was developed using trace elements in chalcopyrite to predict ccp/(ccp+sp) ratio. Random forest consists of an ensemble of methods using tree-type classifiers, which generates predictions based on class membership probabilities for individual predictions (Breiman, 2001). This algorithm is random in two ways: 1) each tree is based on a random subsample of the observations, and 2) each split within each tree is created based on a random subset of independent variables or predictors (Breiman, 2001; Gislason et al., 2006; Harris and Grunsky, 2015). The random subsamples are created from an internal resampling in the training set through a bootstrapping procedure, which provides a stable estimate of classification accuracy from out-of-bag (OOB) data (Harris and Grunsky, 2015). Random forest algorithm is considered a non-parametric classifier, it is insensitive to outliers and requires minimal input parameters: the number of decision trees and the number of random variables for each decision tree, called *mtry* (Harris and Grunsky, 2015). For classification problems, the dependent variable *Y* is categorical (classes), and the prediction is based on a majority class vote, whereas in regression, the outcome *Y* is numerical (*e.g.*, sulfide ratio), and the final prediction is the average of the individual tree values (Barker et al., 2021; Brownlee, 2018; Grömping, 2009; Svetnik et al., 2003).

Before building the classification and regression models, a recursive feature elimination (RFE) incorporating resampling, was performed to determinate the optimal number of variables using an exploratory random forest model. When the model is created, a measure of variable importance is calculated; thus, the least important predictor is iteratively eliminated prior to rebuilding the new model (Kuhn, 2008; Kuhn and Johnson, 2013). Thus, an optimal number of important variables are chosen and used to train the RF model.

The dataset in this study presents a class imbalance problem, where the ultramafic (UM), mafic (M) and particularly siliciclastic-mafic (SM) classes, have the lowest number of samples. The class imbalance ratio between the over- represented (BF) and under-represented (SM) classes is ≈9. Class imbalance in a dataset degrades the performance of machine learning models, leading to misclassifying the minority class samples (Abd Elrahman and Abraham, 2013). This problem has been discussed in several studies, and different approaches have been proposed to counteract its negative effect (e.g., Abd Elrahman and Abraham, 2013; Kuhn and Johnson, 2013; Megahed et al., 2021; Thabtah et al., 2020; Weiss, 2013). The sampling methods are mostly used to overcome the class imbalance, which include preprocessing of data by creating a balanced training dataset, either by under sampling the majority class and/or over sampling the minority class (Abd Elrahman and Abraham, 2013). However, Tarawneh et al. (2022) evaluated more than 70 oversampling methods, of which only 6 were developed to multiclass problems, and concluded that in the current forms, the sampling methods are unreliable for learning from imbalance data. Oversampling methods create fictitious samples, adding more samples to the minority class and can result in an overfitting (Abd Elrahman and Abraham, 2013; Megahed et al., 2021). In contrast, undersampling methods randomly remove samples from the majority class, which can result in a loss of important information (Abd Elrahman and Abraham, 2013; Megahed et al., 2021). According to Weiss (2013), there is no standard on the degree of class imbalance in a dataset to be considered unbalanced, indicating that overall a class imbalance ratio IR≤2 would be considered as marginally unbalanced, whereas IR≈10 modestly unbalanced, and a IR≈1000 would be considered extremely unbalanced. To avoid the problem of class imbalance, the problem was redefined with a divisive approach by classifying the samples according to major host rocks affinity and train a RF model as a first step. In this method, samples are separated into three major classes, as follows, as follows (Table 2.1): a) mafic-ultramafic (M-UM) class: it contains all samples from subtypes constituted principally by mafic-ultramafic host rocks. It comprises ultramafic, mafic and siliciclastic-mafic subtypes; b) bimodal-mafic-felsic (BMF) class: is contains all samples from bimodal-felsic and bimodal-mafic subtypes; and c) siliciclastic-felsic (SF) class: this class correspond to the original siliciclastic-felsic setting. Once the samples are classified by the affinity model (RFmodel.01), two models will be used to reclassify between ultramafic, mafic and siliciclastic-mafic subtypes (RFmodel.02-A), and between bimodal-mafic and bimodal-felsic subtypes (RFmodel.02-B).

For each RF model, the dataset was split into training (70%) and test (30%) subsets using stratified sampling to obtain balanced classes. In order to improve the classification model, the optimal number of randomly selected variables in each split (mtry) was determined using a hyperparameter grid search function, implemented by Caret package in R software. Performances were determined through 10-fold cross-validation with 10 repetitions during training and different metrics were used to evaluate the model efficacy (accuracy, kappa, recall, specificity, precision, F1 and balanced accuracy). For the RF regression model, performance estimators were the root mean squared error (RMSE), the mean absolute error (MAE) and the coefficient of determination (R^2)

in training and test data. Details of performance estimators and calculation are shown in Annexe B14-B15. The variable importance in classification and regression models was measured with the mean decrease in accuracy (MDA) and mean decrease Gini (MDG) coefficients (Han et al., 2016). The index MDA uses permuting OOB samples to compute the importance of the variable, whereas the MDG index determines the impurity at each node (Gregory et al., 2019; Harris and Grunsky, 2015).

To verify the model classification accuracy, we used the remaining 30% of the total dataset to compare the predicted classes with the actual classes (*i.e.,* known classes) in a confusion matrix. Confusion matrices allow an evaluation of the classification performance, consisting of a square matrix *C x C,* where *C* is the number of classes and collects the outputs of the classification model. This allowed the calculation of multiple estimators, such as the accuracy, , which measures the percentage of observations correctly classified (Ballabio and Consonni, 2013).

2.5 Results

2.5.1 Petrography

Mineralogical composition and textural features are summarized in Figure 2.2 and in Annexe B1. Most samples contain an assemblage of chalcopyrite, pyrrhotite, pyrite and sphalerite in different proportions and textural relations, with minor and trace minerals (*i.e.,* magnetite, cassiterite, tennantite). Chalcopyrite (66±32 vol.%) occurs in varying proportions, coexisting principally with anhedral pyrrhotite (4.2±7.9 vol.%; Figs. 2.2A), and commonly replacing pyrite (Fig. 2.2C) and/or sphalerite (Figs. 2.2C, D, E). Pyrite (8.7±13vol.%) is present in most samples, occurring principally as subhedral to anhedral grains (Figs. 2.2C, D, E, G, I). Sphalerite (3.2±4.1 vol.%) is present as anhedral grains, often showing replacement textures by chalcopyrite in different proportions (Figs. 2.2C-F). In some cases, sphalerite occurs in fractured pyrite (Fig. 2.2D). Rarely, exsolutions of pyrite in cubanite lamellae are present in chalcopyrite (Fig. 2.2B).

Magnetite is the most abundant iron oxide (1.9±9.9 vol.%), forming mainly anhedral to subhedral grains (Fig. 2.2G). Occasionally, magnetite is present in high concentrations, such as at Quémont (≈81 vol.%) and Caber (≈45 vol.%) deposits (Annexe B1). Cassiterite (<1.5 vol.%) and tennantite (<1.5 vol.%), are present in samples from Iberian Pyrite Belt (IPB), principally in the stringer mineralization (Fig. 2.2H). Other Cu-minerals, such as bornite (<3 vol.%) occur with chalcopyrite (Ice deposit, Fig. 2.2I), whereas covellite (<2.5 vol.%) and digenite (<3 vol.%) occur dominantly in SMS samples, where they are typically layered, intergrown with coarse- to fine-grained chalcopyrite and occasionally minor anhydrite and opal-A (*i.e.*, amorphous silica; Figs. 2.2J-L).

2.5.2 Trace Element Composition of Chalcopyrite

Among the analyzed trace elements, Mn, Co, Ni, Zn, Ga, Se, Ag, In, Sn, Sb, Te, Au, Tl, Pb and Bi have <40% censored data. Arsenic, PGE, Mo and Re were below detection limits (<dl) in most samples. Of the elements used for statistical analysis, Zn and Se show the highest mean concentration values (312 and 260 ppm, respectively), whereas Ag, In and Sn vary typically between 40 and 100 ppm. Elements such as Pb, Ga, Mn, Bi and Co have a range between 1-5 ppm, whereas the concentrations of Sb, Ni, Te, Au and Tl are typically below 1 ppm. The data distribution is highly asymmetric with a large range of values and outliers (Fig. 2.3). Table 2.2 presents a statistical summary, and the complete database is given in Annexe B3.

The boxplots (Fig. 2.3) show that only a few elements have a significant difference amongst the VMS-SMS subtypes according to lithostratigraphy. In chalcopyrite from ultramafic deposits (n=50), Co (275±140 ppm) and Te (26±19 ppm), and to a lesser extent Se (718±526 ppm) and Ni (38±81 ppm) contents, are higher than that in chalcopyrite from the other VMS-SMS subtypes. In contrast, chalcopyrite from ultramafic settings shows low values of In (4.1±2.9 ppm), Sb (0.07±0.14 ppm), Tl (<dl), Bi (0.19±0.16 ppm), and the lowest content of Pb (0.13±0.15 ppm). Chalcopyrite from mafic settings (n=42) has a slightly higher concentration of Pb (9.3±8.2 ppm) and the lowest Sn (1.5±1.5 ppm) concentrations than chalcopyrite from other VMS-SMS subtypes. In bimodal-mafic deposits (n=163), chalcopyrite is slightly enriched in Ag (95±113 ppm); however, this value is highly biased by the values from samples from the Kidd Creek (sample 2369) and Normétal (sample 52) deposits, which have a trimmed mean of 1491 ppm and 940 ppm of Ag, respectively (Table 2.2, Annexe B1, B3). Chalcopyrite from the bimodal-felsic subtype (n=168) has no significant differences compared to other VMS-SMS settings for most of the elements except for slightly higher Au concentrations (0.09±0.14 ppm). However, the data shows a considerable dispersion. Chalcopyrite from the siliciclastic-mafic subtype (n=18) shows higher content in Mn (92±63 ppm), the lowest concentrations of Au (<dl) and the second-lowest values in Pb (0.66±0.47 ppm), after ultramafic settings. In siliciclastic-felsic deposits (n=127), chalcopyrite is substantially higher in Sn (467±414 ppm) than the other subtypes, and to a lesser extent Bi (4.4±5.5 ppm), In (140±152 ppm) and Sb (3.4±3.8 ppm), whereas Ag (9.6±11 ppm) and Te (<dl) have the lowest values.

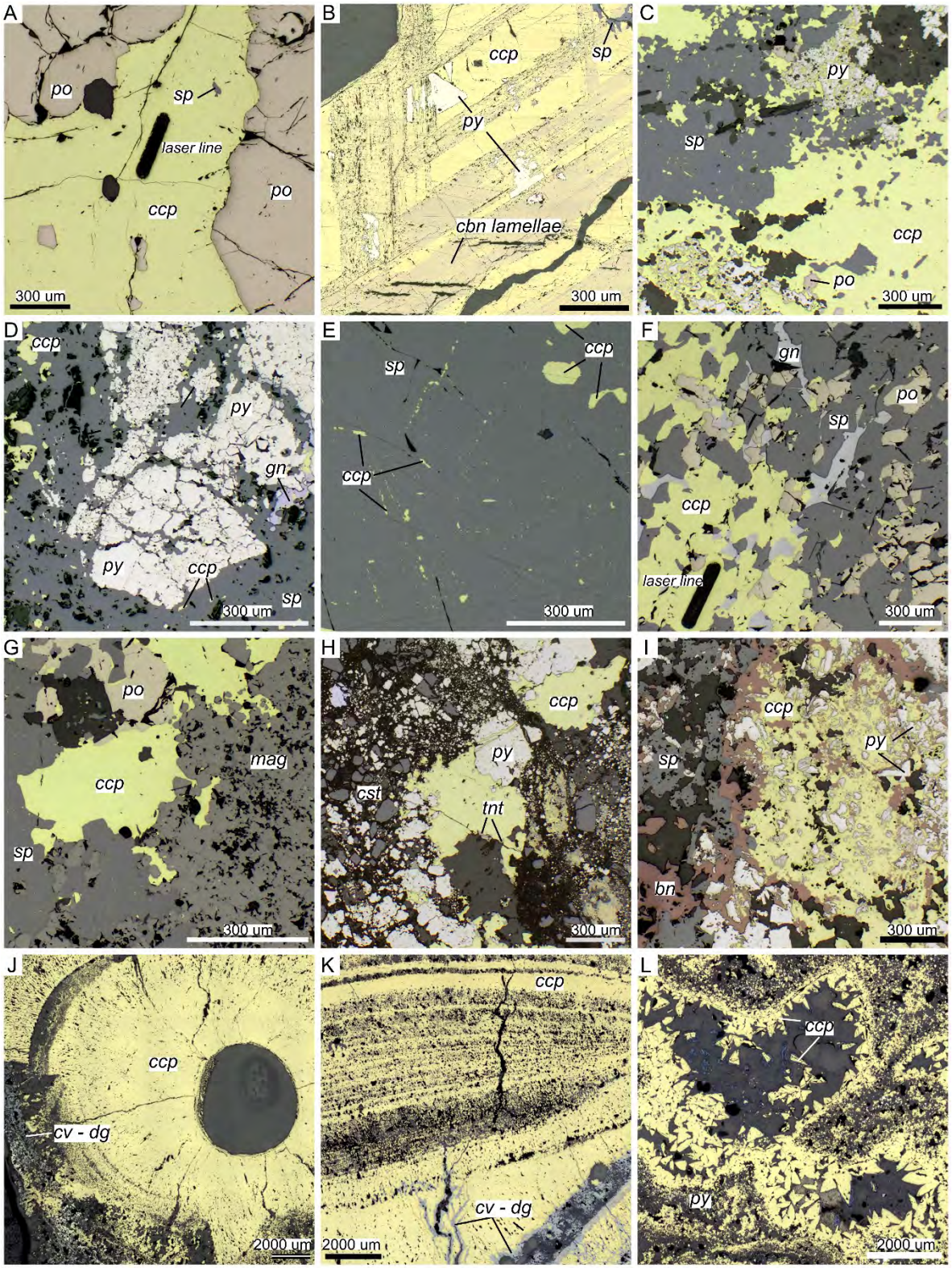

Fig. 2. 2 Reflected light micro-photographs of chalcopyrite from VMS-SMS deposits from Cu-rich (A-C) and Zn-rich (D-F) samples. (A) pyrrhotite (po) coexisting with chalcopyrite (ccp) from Aldermac deposit. (B) star-like sphalerite (sp) and cubanite (cbn) lamellae exsolutions in chalcopyrite in association with pyrrhotite (Pike Hill deposit). (C) pyrite (py) and sphalerite replaced by chalcopyrite (chalcopyrite disease) and (D) pyrite replaced by sphalerite, in addition, chalcopyrite replaces sphalerite and pyrite in samples from Kidd

Creek deposit. (E) chalcopyrite replacing sphalerite (chalcopyrite disease) in sample from Waite-Amulet. (F) galena, sphalerite, chalcopyrite and pyrrhotite assemblage in sample from Hajar deposit. (G) Magnetite-rich sample from Quémont deposit, in association with chalcopyrite, pyrite, pyrrhotite and sphalerite. (H) anhedral cassiterite (cst) and euhedral tennantite (tnt) with pyrite and chalcopyrite in Sn-rich sample (Corvo deposit). (I) sphalerite and pyrite replaced by chalcopyrite and bornite (Ice deposit). (J, K) layered covellite – digenite and chalcopyrite in sample from Roman Ruins (J) and Satanic Mills (PacManus field, K). (L) subhedral chalcopyrite with minor pyrite from the Irinovskoe hydrothermal field.

Pearson correlation coefficients for chalcopyrite from the VMS-SMS settings show the positive correlation between Pb and Tl ($r = 0.50$) and to a lesser extent Te and Co ($r = 0.41$; Figs. 2.4A, B). Antimony-Co and Pb-Ni have dispersed, negative correlations (Figs. 2.4C, D). These binary diagrams confirm that chalcopyrite from ultramafic deposits is significantly different from the other settings. Although an imperfect grouping is shown between chalcopyrite in the remaining deposits, samples from siliciclastic-felsic form a cluster in the Te-Co diagram with the lowest content of Te (Fig. 2.4B). Correlation matrices by deposit setting are shown in Annexe B7. Chalcopyrite from bimodal-mafic subtype shows a bimodal distribution of Te and Co, and to a lesser extent Ni (Figs. 2.3 and 2.4). These samples correspond to different host tectonostratigraphic complexes (Abitibi Belt vs. Dunnage Zone - Notre Dame Subzone). Chalcopyrite from Dunnage Zone - Notre Dame Subzone Complex (Newfoundland) has a higher concentration of Te than the most of chalcopyrite from Abitibi Belt. Furthermore, bimodality in Co and Ni is overall related to the deposit; however, it is less systematic.

Deposits showing differences as a function of the ccp/(ccp+sp) ratio and ore type (massive vs stockwork) are presented in binary diagrams in Figure 2.5. Overall, chalcopyrite from samples with low ccp/(ccp+sp) ratio (*i.e.,* Zn-rich samples) are higher in Ga, In and Sn, and lower in Bi and Co than those from samples with high ccp/(ccp+sp) ratios (*i.e.,* Cu-rich samples; Fig. 2.5A-I). Gold, (except Ascot-Weedon; Fig. 2.5I), Zn (except Kidd Creek; Fig 2.5F), and Tl show no differences as a function of this ratio. Chalcopyrite from the Perseverance and McLeod deposits (Matagami; Fig. 2.5A-D) shows the same variations, except for Sn, whose concentrations are similar in chalcopyrite from Zn-rich and Cu-rich samples (Fig. 2.5C). From Matagami, only one analysis is from a stockwork sample, consequently, comparison between ore types is not possible.

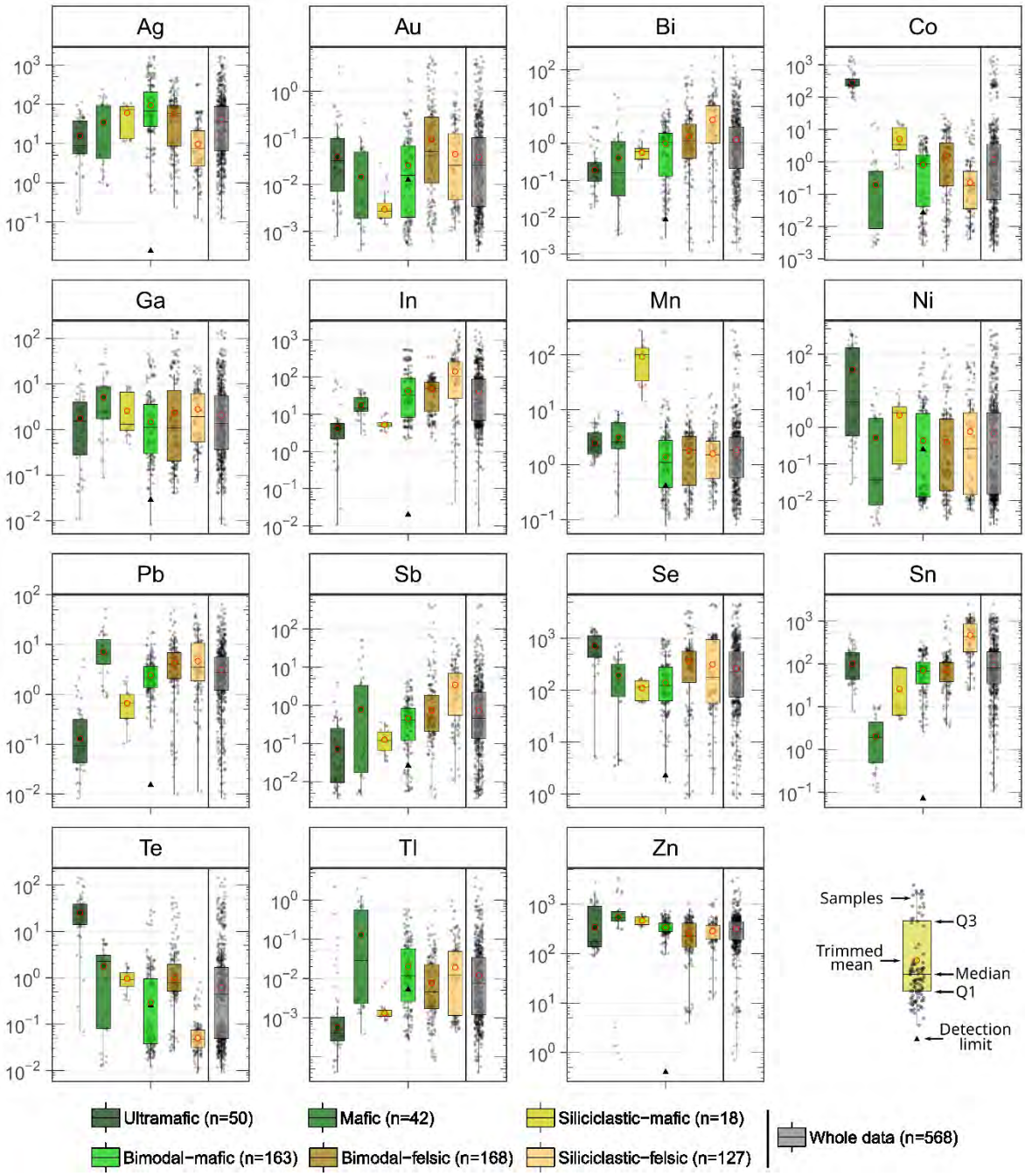

Fig. 2. 3 Boxplots showing the variation of selected trace elements (in ppm) in chalcopyrite according to the geological setting of the deposit. n: number of analyses. Q1 and Q3 indicate first and third quartiles, respectively.

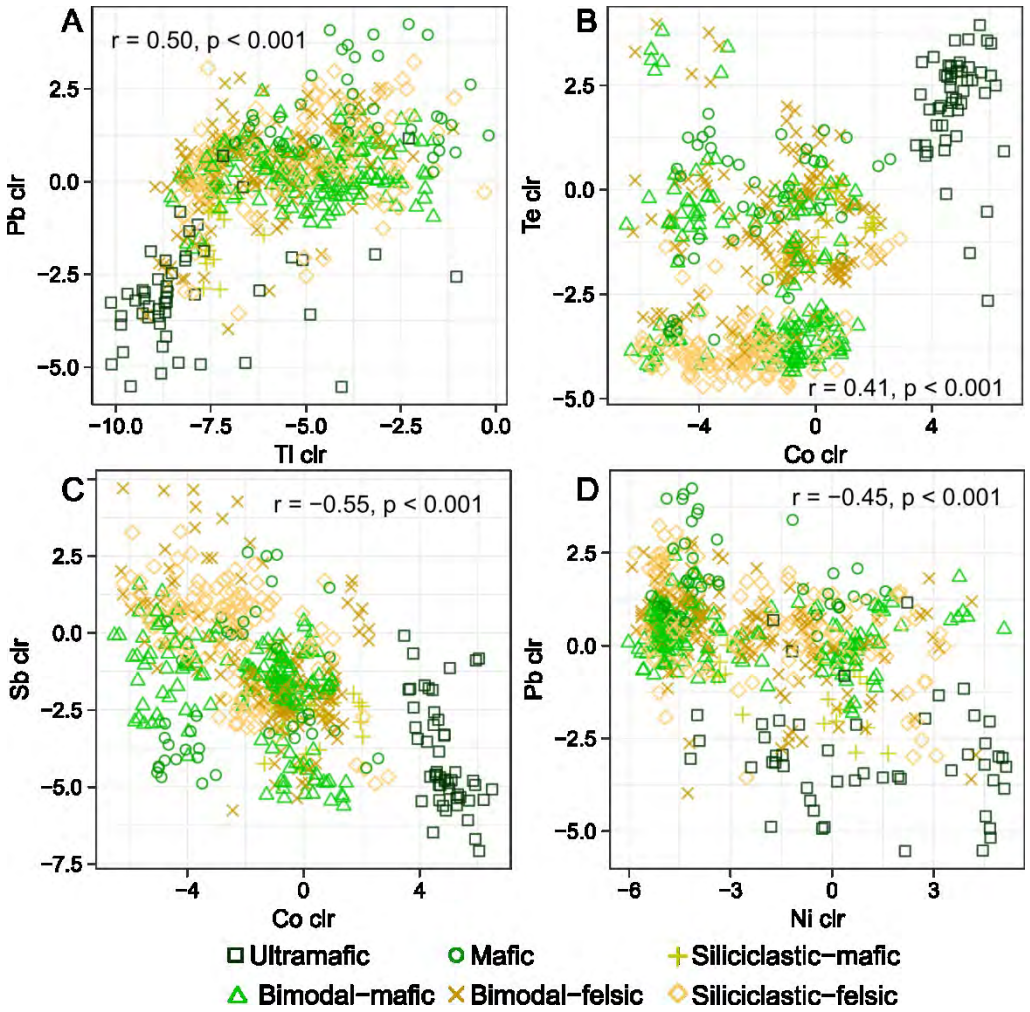

Fig. 2. 4 Binary diagrams of elements with highest Pearson correlation coefficients showing grouping in function of the geological setting of the deposit. Chalcopyrite from ultramafic deposits is separated from the remaining classes in most diagrams, in a lesser extent mafic and siliciclastic-felsic subtypes. clr: centered-log transformation; r: Pearson correlation coefficient; p: p-value.

In chalcopyrite from Kidd Creek (Fig. 2.5E-H), the differences are defined by ccp/(ccp+sp) ratio but not ore type. In particular, chalcopyrite from Zn-rich samples is considerably higher in Zn than in other deposits (Fig. 2.5F). The diagram of Tl-Co, however, shows no grouping as a function of ccp/(ccp+sp) (Fig. 2.5H), except for the Matagami and Ascot-Weedon samples. Furthermore, chalcopyrite from Ascot-Weedon (Suffield and Weedon deposits) form separate groups according to ccp/(ccp+sp) ratios (Fig. 2.5I-L). Chalcopyrite from Cu-rich samples is depleted in Ga and Sn compared to chalcopyrite in Zn-rich samples (Fig. 2.5I). Other elements such as Ag and occasionally Se, Te and Ni are enriched in chalcopyrite from Cu-rich samples, whereas Sb is principally higher in those from Zn-rich samples (Annexe B8). Manganese and Pb do not show systematic variations. However, Pb has a high positive correlation with Sb at Kidd Creek, with a relative enrichment in Pb in Zn-rich samples (r = 0.83; Annexe B8H). According to ore type, chalcopyrite from Ming deposit shows significant differences between massive and stockwork ores, in which that from massive ores is higher in Au, Bi and Co, and lower in In, Sn and Tl (Fig. 2.5M-P). Successive remobilization of these elements from sulfides previously

formed at lower temperature (e.g., sphalerite, galena, or pyrite) suggests that the trace element composition of chalcopyrite is inherited from replaced assemblages.

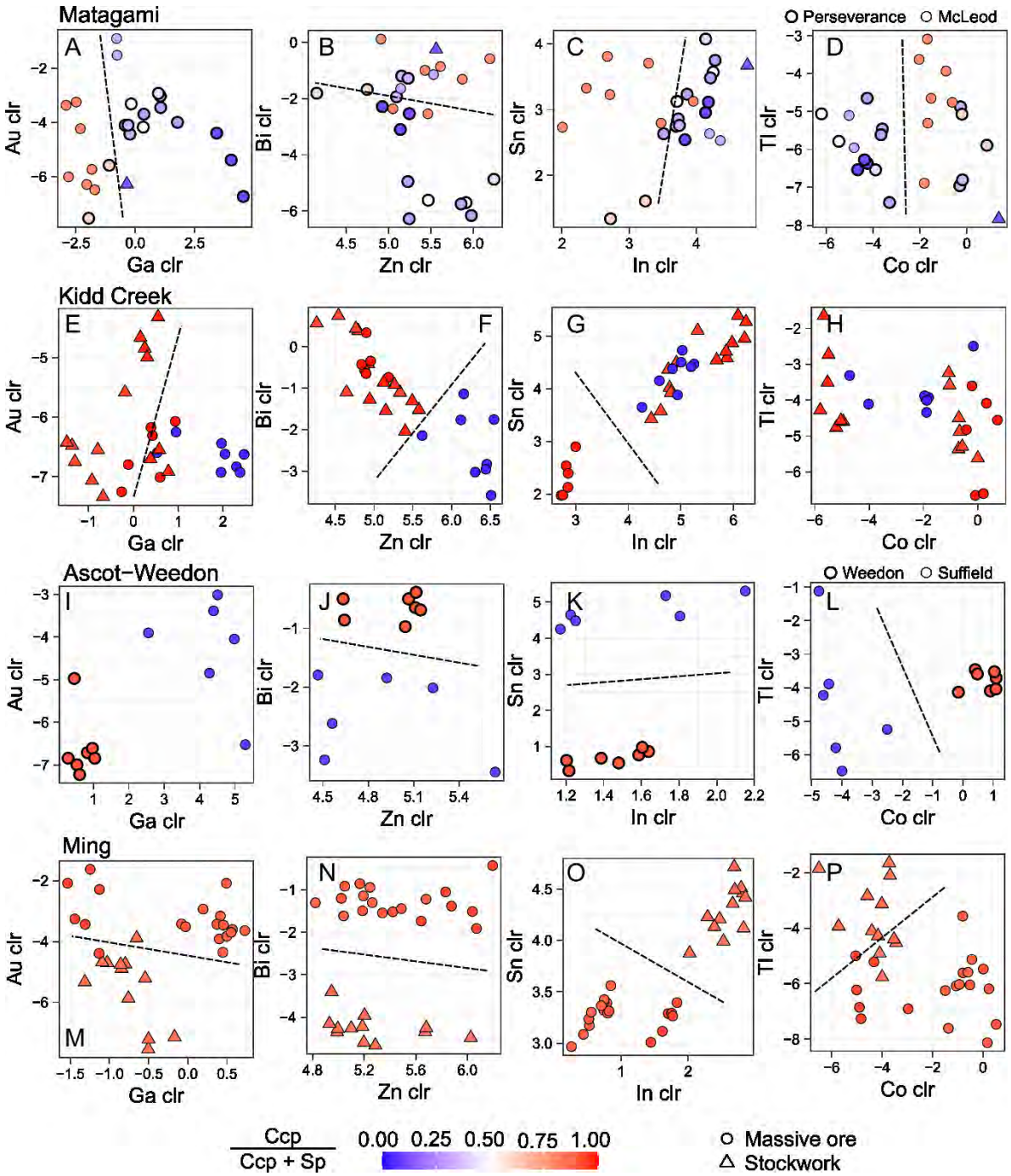

Fig. 2. 5 Binary diagrams by deposit showing differences between chalcopyrite in function of ccp/(ccp+sp) ratio and ore type. Dashed lines show approximately limits between groups.

2.5.3 Exploratory PLS-DA

The PLS-DA using all elements with less than 40% of censured values confirms that chalcopyrite can be grouped according to VMS-SMS settings (Fig. 2.6A). The first two latent variables explain about 36.5% of the variance of

the 15 chemical variables (t1=24.7%; t2=11.8%; Fig. 2.6A) and at least 6 latent variables are necessary to explain more than 60% of the data variance (Annexe B10G). Estimators indicate a moderate to low performance of the model with an accuracy of 0.48 and kappa 0.29 (Annexe B10G). Chalcopyrite from ultramafic, mafic and to a lesser extent siliciclastic-felsic shows significant differences from the other settings (Figs. 2.6A). Chalcopyrite from ultramafic deposits forms a group separated from the other subtypes, and it exists a positive correlation with Co, Te (±Sn) and to a lesser extent with Ni according to the score plot t1-t2 and loading plot qw*1-qw*2 (Fig. 2.6A, B), respectively. In contrast, Ag, Pb, Bi and Sb are situated opposed to the UM (ultramafic) pole, suggesting a negative correlation with chalcopyrite from the ultramafic subtype (Fig. 2.6B). Relative high regression coefficients of Co, Te, Ag, Pb, Bi and Sb confirm a high correlation with chalcopyrite from ultramafic subtype (Fig. 2.6C).

Samples from mafic deposits form a group associated to positive scores on latent variable t2 separated from the remaining subtypes (Fig. 2.6A), and is positively correlated with Pb and Ga, and negatively correlated with Sn (Fig. 2.6B, C). The positive correlation between Pb and Ga and the mafic subtype is shown in the loading plots qw*3-qw*4 (Pb; Annexe B10A) as well as loading plots qw*7-qw*8 and qw*9-qw*10 (Ga; Annexe B10C, B10D), and by their higher concentrations than in the other deposit sub-types (Table 2.2). Also, regression coefficients show that Ag, Bi and Co have a moderate negative correlation with chalcopyrite from mafic deposits (Fig. 2.6C). These relations are evidenced by the loading plots in Annexe B10, where Ag, Bi and Co tend to be opposed to M (mafic) pole. Chalcopyrite from siliciclastic-mafic deposits forms a compact group in upper left part of the score plot t1-t2, relatively near to the center (Fig. 2.6A). These samples are principally correlated with Mn, which records a high positive regression coefficient (Fig. 2.6C). Lead, Tl, Sn and Au have moderate negative regression coefficients, which is evidenced by loading plots in Annexe B10, which show a relative opposed position to SM (siliciclastic-mafic) pole. Chalcopyrite from bimodal-mafic and bimodal-felsic deposits overlap considerably, plotting principally at the center of the score plot t1-t2 and loading plot qw*1-qw*2 (Fig. 2.6A, B). However, according to the regression coefficients, chalcopyrite from the bimodal-mafic subtype has a high positive correlation with Ag, and moderate with Tl and Zn, whereas Pb, and to a lesser extent Co, Mn, Sb and Te record a moderate negative correlation. Loading plots qw*3-qw*4, qw*7-qw*8 and qw*9-qw*10 illustrate these relations (Annexe B10A, C and D, respectively). On the other hand, chalcopyrite from bimodal-felsic subtype records high positive regression coefficients in Te and Pb, whereas Ag, Au and Sb show moderate positive values. In contrast, Tl and Zn show negative regression coefficients (Fig. 2.6C). The association between Te, Pb and chalcopyrite from bimodal-felsic setting is evidenced in loading plot in Annexe B10. Chalcopyrite from the siliciclastic-felsic subtype is grouped in the lower right quadrant (Fig. 2.6A), positively correlated with Sn and to a lesser extent Se, and negatively correlated with Ag and Te (Figs. 2.6B, C).

In order to evaluate the impact of metamorphism, the sulfide proportion and the ore type on PLS-DA results by VMS setting (Fig. 2.6), each factor was projected on score plot t1-t2 (Fig. 2.7, Fig. 2.8, Annexe B11-B13). Among

the studied VMS subtypes, only mafic, bimodal-mafic, bimodal-felsic and siliciclastic-felsic have samples from different metamorphic facies. Chalcopyrite records similar trace element composition within each VMS subtype, independently of the metamorphic facies, although a certain grouping is observed within siliciclastic-felsic subtype (Fig. 2.7B-F). In mafic subtype, chalcopyrite from unmetamorphosed deposits has not significant difference from those from deposits with lower greenschist metamorphism (Fig. 2.7B). In bimodal-mafic subtype, chalcopyrite from deposits with lower and upper greenschist metamorphism shows similar trace element composition, with a considerable overlapping at the center of score plot (Fig. 2.7D). In bimodal-felsic subtype, chalcopyrite from unmetamorphosed deposits (SMS deposits from PACMANUS) forms a group plotting at the edge and outside of the 95% confidence ellipse (Fig. 2.7E), which enclose approximately 95% data points (Michael et al., 2013). Chalcopyrite in unmetamorphosed deposits from bimodal-felsic subtype plotting outside of the confidence ellipse has similar composition to those from siliciclastic-felsic deposits with prehnite-pumpellyite metamorphism (Fig. 2.7E).

In siliciclastic-felsic subtype, chalcopyrite from deposits with upper and lower greenschist forms a group from those with prehnite-pumpellyite and to a lesser extent middle greenschist metamorphism, whereas chalcopyrite from deposits with amphibolite metamorphism plots outside of the confidence ellipse (Fig. 2.7F). Although metamorphism has an effect the trace element contents in chalcopyrite, the modifications are smaller than the much larger variation in composition due to the different lithotectonic subtypes of VMS deposits, such that it does not significantly affect the trace element signature.

Similarly, trace element composition of chalcopyrite from samples with different sulfide proportions shows variation within each VMS subtype (Fig. 2.8, Annexe B11-B13). Chalcopyrite from samples with different ccp/(ccp+sp) ratios in bimodal-mafic and bimodal-felsic VMS subtypes has similar trace element composition, with an important overlap at the center of the score plot (Fig. 2.8D, E). Although samples with different ccp/(ccp+sp), po/(po+py+py) and ccp/(ccp+po) ratios, and different ore types, show a slight grouping within each VMS subtype (Annexe B11-B13), the trace element composition of chalcopyrite remains constrained to the groups defined by the PLS-DA by VMS setting.

Table 2. 2 Summary of selected trace elements (ppm) in chalcopyrite from volcanogenic massive deposits used for multivariate statistical analysis and machine learning.

Setting	Name	Host complex	n		^{55}Mn	^{59}Co	^{60}Ni	^{66}Zn	^{71}Ga	^{82}Se	^{107}Ag	^{115}In	^{118}Sn	^{121}Sb	^{128}Te	^{197}Au	^{205}Tl	^{208}Pb	^{209}Bi
				55um	0.479	0.016	0.207	0.024	0.079	0.029	0.011	0.070	0.017	0.221	0.007	0.004	0.006	0.004	0.006
				33um	1.030	0.028	0.410	0.051	0.149	0.030	0.026	0.147	0.027	0.501	0.012	0.007	0.011	0.007	0.004
Ultramafic	Candelabra	Mid-Atlantic Ridge	11	μ_t	3.41	678	266	755	0.23	1371	9.30	33.5	52.6	<dl	57.5	0.09	<dl	0.15	0.29
				sd_t	2.78	706	132	723	0.28	163	5.88	39.8	28.2	na	63.6	0.08	na	0.20	0.60
	Irina I		6	μ_t	3.36	206	163	124	<dl	1195	2.94	5.78	44.9	<dl	24.9	0.01	<dl	0.05	0.04
				sd_t	0.94	59.9	114	13.6	na	129	3.92	1.35	9.02	0.34	11.8	0.01	na	0.02	0.03
	Irina II		6	μ_t	3.83	829	0.64	1296	1.22	375	1.51	1.75	216	<dl	19.3	0.03	<dl	0.14	0.16
				sd_t	1.65	476	0.98	824	1.56	496	1.66	2.54	42.8	na	31.4	0.02	na	0.14	0.08
	Irinovskoe		27	μ_t	1.80	240	2.09	201	3.77	503	32.3	3.36	123	<dl	23.3	0.05	<dl	0.16	0.28
				sd_t	0.63	53.3	2.54	83.4	2.90	222	25.7	2.30	101	na	14.8	0.05	na	0.16	0.23
		Summary (50)		μ_t	2.45	275	38.2	345	1.74	719	15.6	4.16	100	0.07	25.5	0.04	na	0.13	0.19
				sd_t	1.35	141	81.3	420	2.19	526	19.6	2.93	91.1	0.14	19.3	0.05	na	0.15	0.16
				med	2.17	245	4.95	178	1.53	669	8.82	4.18	78.4	0.02	25.4	0.03	na	0.09	0.17
Mafic	Little Bay	Dunnage Zone - Notre Dame Subzone	6	μ_t	2.38	0.04	0.77	646	2.50	110	1.95	12.4	2.12	<dl	5.64	0.02	0.03	7.60	7.96
				sd_t	0.35	0.02	1.28	127	0.13	59.4	1.34	1.4	0.39	na	0.90	0.06	0.03	1.89	11.0
	Little Deer		6	μ_t	6.00	0.32	1.84	406	1.89	378	94.8	36.3	0.17	3.88	2.08	<dl	0.76	7.14	1.12
				sd_t	1.21	0.16	2.18	153	0.43	54.6	9.64	3.49	0.09	1.26	2.33	na	0.21	3.09	0.37
	Whalesback		5	μ_t	7.55	1.05	0.60	493	8.65	549	70.2	7.78	3.28	34.2	2.27	<dl	0.83	17.4	<dl
				sd_t	2.38	0.45	1.29	51.2	0.39	265	48.0	6.28	3.26	24.0	0.17	na	0.55	2.53	na
	York Harbour	Humber Zone - Bay of Islands Ophiolite	6	μ_t	2.51	3.40	0.92	521	0.48	264	120	17.8	1.81	<dl	2.63	0.03	<dl	5.74	0.25
				sd_t	0.53	9.43	1.54	54.3	0.32	7.15	141	14.2	0.54	na	0.33	0.04	na	2.16	0.55
	Lasail	Semail Ophiolite	14	μ_t	1.58	0.40	<dl	926	5.43	40.0	13.2	10.2	4.69	<dl	0.71	0.03	0.01	15.2	0.22
				sd_t	1.86	0.58	na	1414	7.08	54.8	10.2	6.22	6.72	na	1.02	0.04	0.01	22.3	0.23
	Ice	Slide Mountain terrane	5	μ_t	3.73	0.16	<dl	1.24	17.8	112	8.3	29.3	0.44	0.40	0.08	<dl	0.02	11.4	0.16
				sd_t	2.64	0.35	na	0.54	15.0	29.5	7.45	18.2	0.17	0.35	0.01	na	0.04	14.4	0.19
		Summary (42)		μ_t	3.23	0.34	0.35	443	3.84	160	29.5	14.9	1.48	0.48	1.81	0.01	0.08	9.26	0.39
				sd_t	2.70	0.48	0.82	412	4.74	154	42.5	11.1	1.55	1.18	1.89	0.02	0.19	8.19	0.51
				med	2.63	0.25	0.03	496	2.41	130	20.5	13.9	1.32	0.05	2.22	0.004	0.02	7.57	0.29
Bimodal-mafic	Aldermac	Abitibi Greenstone Belt	18	μ_t	4.04	2.18	1.80	421	1.93	149	124	35.7	42.9	0.34	0.54	0.02	0.01	1.98	1.10
				sd_t	1.89	1.81	2.08	84.4	2.06	32.7	86.1	43.6	51.5	0.39	0.52	0.02	0.01	1.23	1.08
	Caber		10	μ_t	<dl	<dl	<dl	176	0.29	461	9.01	16.4	12.4	0.99	13.9	0.01	0.01	2.64	0.09
				sd_t	na	na	na	95.1	0.22	460	25.3	16.7	4.07	0.69	13.3	0.02	0.02	1.93	0.08
	Dufault		20	μ_t	1.51	0.89	<dl	285	2.96	271	88.4	179	88.9	0.42	0.05	0.04	0.05	2.37	1.94
				sd_t	1.93	1.14	na	38.9	6.16	399	57.3	140	26.9	0.24	0.01	0.06	0.06	1.08	1.60
	Kidd Creek		28	μ_t	0.87	0.64	<dl	302	2.55	114	170	211	93.3	<dl	0.05	<dl	0.02	3.39	0.77
				sd_t	0.91	0.92	na	49.5	1.82	98.9	283	216	83.6	na	0.05	na	0.02	2.95	0.90
	Norbec		12	μ_t	0.80	0.38	2.03	331	0.35	259	222	61.1	140	<dl	0.02	0.01	<dl	0.93	0.88
				sd_t	0.61	0.41	1.34	24.8	0.19	309	327	90.1	110	na	0.01	0.01	na	0.50	1.32

Setting	Name	Host complex	n		^{55}Mn	^{59}Co	^{60}Ni	^{66}Zn	^{71}Ga	^{82}Se	^{107}Ag	^{115}In	^{118}Sn	^{121}Sb	^{128}Te	^{197}Au	^{205}Tl	^{208}Pb	^{209}Bi
Bimodal-mafic	Normetal	Abitibi Greenstone Belt	5	μ_t	<dl	2.29	<dl	288	4.03	139	1491	19.6	35.2	1.96	0.09	<dl	0.01	2.86	3.90
				sd_t	na	0.19	na	61.7	0.53	38.3	182	1.11	1.81	1.36	0.02	na	0.01	2.1	1.81
	Poirier		6	μ_t	2.52	0.03	6.78	161	<dl	76.6	32.0	6.72	21.4	<dl	0.76	0.06	<dl	3.82	1.65
				sd_t	0.22	0.03	2.83	11.1	na	3.86	3.71	0.36	4.12	na	0.22	0.04	na	0.77	0.53
	Waite-Amulet		33	μ_t	1.64	1.40	<dl	325	6.16	60.6	91.0	30.0	70.1	0.43	0.05	0.12	0.06	2.27	1.89
				sd_t	1.38	1.22	na	58.2	11.7	41.5	73.8	11.1	28.1	0.51	0.02	0.18	0.07	1.06	1.68
	Ming	Dunnage Zone - Notre Dame	31	μ_t	1.11	0.37	1.75	513	1.99	230	187	14.9	99.2	1.15	1.86	0.05	0.02	2.72	0.35
				sd_t	0.64	0.65	3.38	95.7	1.67	188	352	18.4	83.2	0.90	0.88	0.04	0.03	1.83	0.38
		Summary (163)		μ_t	1.37	0.80	0.43	339	1.48	140	94.8	41.8	69.9	0.45	0.29	0.03	0.02	2.41	0.99
				sd_t	1.41	1.00	1.13	104	1.80	123	113	49.5	58.6	0.46	0.51	0.04	0.03	1.57	1.11
				med	1.09	0.87	0.02	330	1.11	122	67.5	32.0	68.3	0.41	0.08	0.02	0.01	2.25	1.07
Bimodal-felsic	Horne	Abitibi Greenstone Belt	24	μ_t	1.45	3.64	0.68	243	7.46	1349	61.5	57.4	82.2	0.36	5.43	0.29	0.02	4.52	6.36
				sd_t	1.59	2.23	1.02	133	9.83	1193	16.3	67.5	27.8	0.29	4.09	0.20	0.02	2.92	6.35
	McLeod		10	μ_t	2.89	0.21	<dl	232	0.18	57.2	35.0	37.0	22.0	<dl	0.53	0.02	0.01	1.84	0.31
				sd_t	4.51	0.25	na	43.0	0.26	67.6	13.3	47.7	6.32	na	0.20	0.03	0.01	1.09	0.19
	Perseverance		15	μ_t	<dl	0.23	<dl	235	1.90	782	3.98	53.3	23.0	1.04	8.43	0.02	<dl	2.79	0.10
				sd_t	na	0.58	na	42.9	2.28	482	4.44	13.0	7.24	0.98	11.2	0.01	na	2.07	0.17
	Quémont		32	μ_t	1.48	5.65	2.39	162	0.16	392	204	51.3	79.6	0.30	0.51	0.83	0.01	3.95	2.04
				sd_t	1.50	6.79	4.46	58.4	0.06	104	150	26.0	37.0	0.19	0.29	1.03	0.01	2.08	2.04
	Suffield Mine	Ascot-Weedon Complex	6	μ_t	<dl	<dl	<dl	145	129	31.9	16.7	5.44	134	6.16	0.06	0.03	0.02	4.88	0.11
				sd_t	na	na	na	9.31	19.4	3.92	10.1	0.92	26.2	8.01	0.02	0.03	0.02	2.65	0.09
	Weedon		7	μ_t	0.54	4.73	0.45	306	4.35	42.3	123	9.13	4.32	0.39	1.35	<dl	0.05	7.45	1.14
				sd_t	0.33	1.41	0.58	24.0	0.63	2.65	2.61	0.36	0.73	0.04	0.24	na	0.01	6.61	0.18
	Adak	Bothnia-Skelleftea Unit	11	μ_t	3.20	1.30	0.57	454	0.74	509	84.7	85.8	81.6	0.38	0.48	0.04	<dl	8.06	1.08
				sd_t	0.81	0.57	1.27	93.8	0.45	47.5	6.39	18.7	21.4	0.32	0.16	0.05	na	3.58	0.55
	Brannmyran		6	μ_t	3.70	2.02	0.36	576	1.46	428	87.3	68.4	179	1.05	0.46	0.07	<dl	4.5	2.26
				sd_t	0.39	0.82	0.83	51.2	0.14	35.8	1.97	9.60	26.1	0.88	0.07	0.07	na	1.98	1.18
	Lindsköld		18	μ_t	3.75	2.73	0.78	483	1.17	329	85.4	47.9	104	1.91	0.82	0.02	0.01	4.83	0.78
				sd_t	1.47	2.82	1.20	87.8	1.46	156	53.2	31.8	45.0	1.91	0.28	0.02	0.01	3.17	0.43
	Rävliden		6	μ_t	3.58	1.76	<dl	492	0.52	599	79.9	73.5	73.3	0.34	0.77	0.09	<dl	7.73	1.00
				sd_t	0.50	0.68	na	68.3	0.11	23.2	2.37	13.5	8.24	0.12	0.20	0.08	na	2.14	0.53
	Boundary	Dunnage Zone - Exploits Subzone	5	μ_t	2.34	13.3	<dl	486	0.26	271	1.11	6.78	45.2	8.33	1.35	0.02	0.02	16.0	0.80
				sd_t	0.42	2.31	na	64.9	0.12	18.4	0.74	0.94	3.78	5.71	0.59	0.02	0.03	16.1	0.40
	Duck Pond		7	μ_t	<dl	<dl	<dl	135	47.4	33.8	6.34	48.3	41.0	4.51	0.27	<dl	0.03	8.54	6.44
				sd_t	na	na	na	29.1	6.61	11.5	1.99	2.99	1.76	3.30	0.35	na	0.03	6.66	4.55
	Roman Ruins	Pual Ridge	8	μ_t	1.97	0.47	0.51	60.8	1.62	305	5.87	10.4	26.4	<dl	1.43	0.05	<dl	0.05	0.34
				sd_t	0.33	0.22	0.62	8.19	0.70	31.9	3.77	2.06	20.1	na	1.08	0.06	na	0.02	0.23
	Satanic Mills		7	μ_t	1.30	0.14	2.17	7.68	21.2	4.87	2.96	49.9	734	29.7	1.52	0.12	<dl	0.29	21.7
				sd_t	0.40	0.14	2.65	0.73	3.78	2.04	0.59	21.0	176	27.8	0.88	0.14	na	0.27	20.8

Setting	Name	Host complex	n		^{55}Mn	^{59}Co	^{60}Ni	^{66}Zn	^{71}Ga	^{82}Se	^{107}Ag	^{115}In	^{118}Sn	^{121}Sb	^{128}Te	^{197}Au	^{205}Tl	^{208}Pb	^{209}Bi
	Snowcap		6	μ_t	1.28	0.06	8.90	6.51	29.5	1.02	4.76	68.7	148	302	3.74	2.67	0.01	5.19	29.7
				sd_t	0.41	0.07	9.79	0.77	3.55	0.18	1.41	18.8	52.1	245	2.96	2.63	0.01	4.92	23.4
		Summary (186)		μ_t	1.80	1.55	0.40	255	2.34	361	56.7	47.1	72.1	0.74	1.01	0.09	0.01	4.25	1.52
				sd_t	1.79	2.24	0.82	192	4.61	309	58.0	40.1	51.8	0.94	0.95	0.14	0.01	3.5	1.73
				med	1.84	1.19	0.09	225	1.08	385	58.2	49.2	69.0	0.46	0.78	0.05	0.005	4.01	1.16
Siliciclastic-mafic	Ely	Vermont Copper Belt	6	μ_t	27.5	3.08	2.90	375	0.81	158	12.1	4.05	5.89	<dl	1.55	<dl	<dl	1.07	0.39
				sd_t	10.5	1.01	2.25	28.2	0.31	9.18	0.68	0.92	1.25	na	0.35	na	na	0.83	0.32
	Pike Hill		12	μ_t	119	7.44	1.79	519	4.17	85.2	83.3	5.90	45.0	<dl	0.70	<dl	<dl	0.52	0.62
				sd_t	26.7	8.31	2.16	62.7	4.41	36.5	18.3	0.97	55.6	na	0.32	na	na	0.43	0.21
		Summary (18)		μ_t	92.0	5.12	2.16	466	2.55	110	60.5	5.21	25.9	0.13	0.96	0.003	0.001	0.66	0.56
				sd_t	62.7	5.42	2.35	107	3.16	55	48.8	1.17	41.4	0.09	0.56	0.001	na	0.47	0.27
				med	99.9	3.46	2.53	457	1.31	114	72.5	5.06	8.55	0.12	0.92	0.003	0.001	0.66	0.61
Siliciclastic-felsic	Bathurst	Bathurst Mining Camp	21	μ_t	1.94	0.31	<dl	324	3.06	936	25.2	78.9	165	0.22	0.06	0.25	<dl	2.55	7.04
				sd_t	0.58	0.14	na	30.9	3.57	184	10.0	22.1	70.6	0.12	0.01	0.20	na	1.51	7.48
	Halfmile Lake		5	μ_t	1.17	1.05	1.15	415	0.30	56.4	63.5	22.4	543	1.22	0.03	0.11	0.02	5.25	7.09
				sd_t	0.09	0.07	0.25	30.4	0.04	2.92	3.64	6.53	175	1.02	na	0.16	0.03	1.65	4.98
	Tétrault	Greenville Province	5	μ_t	2.57	14.6	3.03	159	0.09	43.3	35.5	2.01	141	<dl	0.34	0.05	<dl	3.11	0.79
				sd_t	0.31	6.28	3.69	32.9	0.02	1.90	28.4	1.48	94.6	na	0.05	0.06	na	0.76	0.52
	Aljustrel	Iberian Pyrite Belt	6	μ_t	4.23	0.17	0.35	367	4.36	51.7	4.60	77.5	321	4.56	0.05	0.02	0.21	2.29	0.85
				sd_t	5.79	0.32	0.89	25.5	3.10	9.05	2.02	9.30	198	6.10	0.03	0.03	0.33	2.97	0.88
	Aznalcollar		6	μ_t	0.72	0.06	19.5	256	0.61	84.0	0.32	238	375	3.03	0.03	<dl	0.04	2.63	0.18
				sd_t	0.39	0.08	30.2	34.6	0.08	5.22	0.33	5.59	27.2	1.95	0.01	na	0.04	2.52	0.20
	Corvo		28	μ_t	1.00	0.19	0.76	197	7.35	407	3.84	278	771	5.35	0.07	0.02	0.04	7.89	8.45
				sd_t	0.94	0.24	1.03	166	5.96	484	3.21	124	349	4.58	0.04	0.03	0.07	7.26	7.96
	Graça		6	μ_t	0.62	0.07	0.60	314	3.33	267	5.36	320	1007	6.00	0.04	0.01	0.04	4.14	1.66
				sd_t	0.65	0.10	1.59	74.9	1.41	132	3.02	134	415	5.85	0.02	0.01	0.05	4.25	1.54
	Lagoa Salgada		7	μ_t	0.82	0.03	0.35	225	0.43	187	8.75	54	714	18.5	0.03	0.09	0.09	10.8	3.95
				sd_t	0.44	0.01	0.46	60.2	0.23	29.8	9.14	34.1	301	17.6	0.01	0.11	0.11	8.98	2.88
	Lousal		7	μ_t	1.74	0.46	0.95	216	0.30	97.4	5.31	549	312	21.2	0.05	0.04	0.03	17.9	16.2
				sd_t	2.04	0.63	1.32	27	0.16	24.9	2.24	147	43.3	9.67	0.03	0.08	0.02	5.96	6.36
	Neves		7	μ_t	2.39	0.05	2.73	192	1.39	48.5	5.44	421	700	3.46	0.02	0.005	<dl	2.72	0.35
				sd_t	0.49	0.04	2.93	126	0.8	51.5	1.95	233	700	2.98	0.01	0.002	na	1.77	0.47
	Tharsis		4	μ_t	<dl	<dl	<dl	449	4.66	2.40	315	0.43	434	0.52	0.02	0.02	0.05	0.85	<dl
				sd_t	na	na	na	107	0.26	1.01	15.4	0.29	189	0.46	0.01	0.01	0.04	0.89	na
	Zambujal		7	μ_t	3.42	0.23	20.4	178	7.85	1097	0.73	235	1058	5.00	0.04	0.006	0.01	4.45	4.90
				sd_t	3.72	0.27	23.7	19.2	1.08	56.9	0.13	21.0	79.7	1.73	0.01	0.005	0.01	3.27	1.66

Setting	Name	Host complex	n		^{55}Mn	^{59}Co	^{60}Ni	^{66}Zn	^{71}Ga	^{82}Se	^{107}Ag	^{115}In	^{118}Sn	^{121}Sb	^{128}Te	^{197}Au	^{205}Tl	^{208}Pb	^{209}Bi
Siliciclastic-felsic	Draa Sfar	Jebilet Massif	6	μ_t	0.94	0.19	<dl	273	0.28	98.7	3.26	7.68	35	4.18	0.07	0.28	0.02	23.3	28.7
				sd_t	1.10	0.1	na	22.9	0.05	2.22	0.93	2.15	15	2.71	0.01	0.10	0.01	7.77	13.3
	Hajar		6	μ_t	3.88	0.19	<dl	466	12.6	8.38	61.4	5.56	856	7.90	0.03	0.03	0.03	11.1	0.17
				sd_t	2.47	0.02	na	51.1	4.12	5.79	4.69	1.26	64.6	7.15	0.01	0.02	0.03	6.84	0.15
	Wolverine	Yukon-Tanana Terrane	6	μ_t	2.68	5.42	43.4	1002	0.61	4310	10.1	1.61	101	2.81	0.08	0.02	0.02	0.36	1.85
				sd_t	0.45	1.70	7	120	0.07	236	2.27	0.18	13.3	2.06	0.01	0.01	0.03	0.32	0.65
		Summary (172)		μ_t	1.57	0.23	0.76	286	2.79	316	9.62	140	467	3.39	0.05	0.05	0.02	4.65	4.36
				sd_t	1.37	0.29	1.35	130	3.43	466	10.9	153	415	3.81	0.03	0.07	0.03	4.8	5.49
				med	1.51	0.18	0.26	286	1.92	178	7.38	104	437	2.92	0.05	0.03	0.01	3.5	3.13

μ_t: trimmed mean (0.2); *sdt*: trimmed standard deviation; med: median

n: number of analyses

<dl: below detection limit

na: not apply

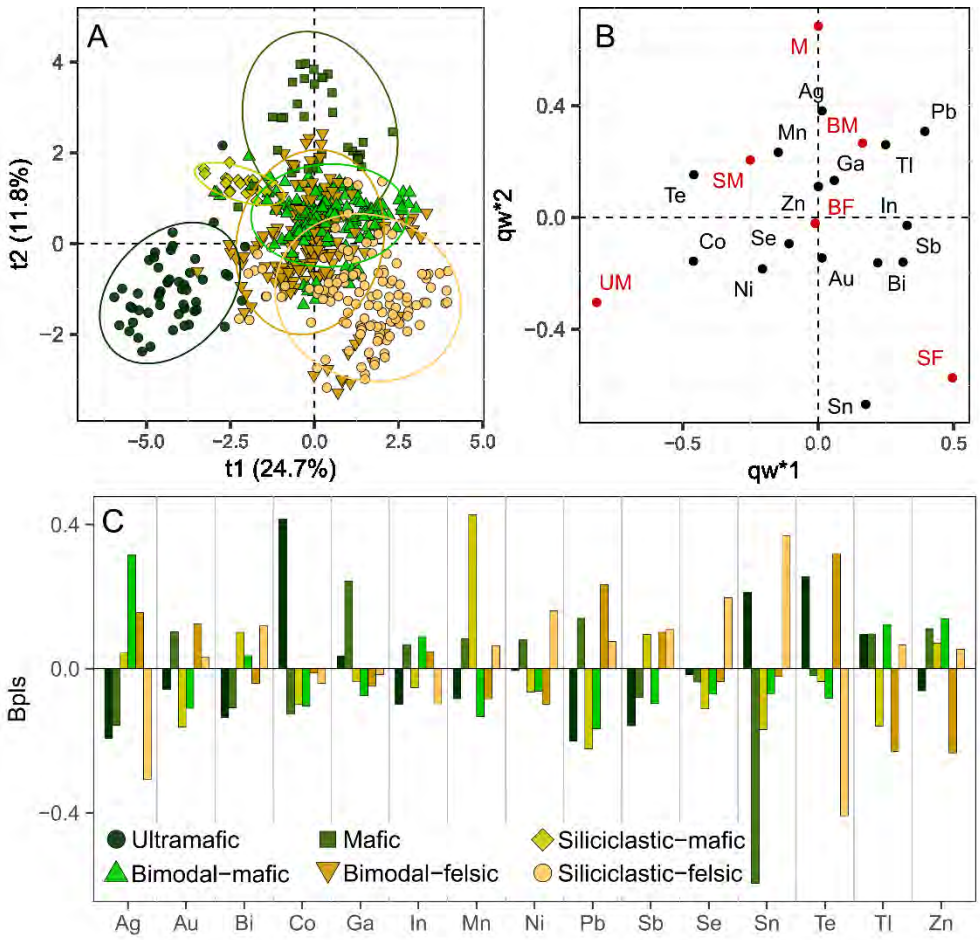

Fig. 2. 6 PLS-DA on trace elements in chalcopyrite by geological setting of the deposit. Chalcopyrite from ultramafic, mafic, and siliciclastic-felsic settings show an important separation from the other subtypes in score plot t1-t2 (A). According to loading plot (B) and regression coefficients (C), chalcopyrite from the ultramafic subtype is associated with a high content of Co (±Te), whereas chalcopyrite from mafic settings is correlated to high Ag and low Sn concentrations. In contrast, chalcopyrite from siliciclastic-felsic settings is associated with high Sn and low Ag concentrations. B_{pls}: regression coefficients. UM: ultramafic, M: mafic, BM: bimodal-mafic, SM: siliciclastic-mafic, BF: bimodal-felsic, SF: siliciclastic-felsic. Confidence ellipses enclose approximately 95% of the data.

Since the ccp/(ccp+sp) ratio provides important information on location in the deposit, and its distribution is skewed in whole data, a PLS-DA was carried out separately on chalcopyrite from bimodal-mafic (Figs. 2.9A, B), bimodal-felsic (Figs. 2.9C, D) and siliciclastic-felsic settings (Figs. 2.9E, F), as a preliminary approach. The PLS-DA results show that Ga, Sn, Tl, In and to a lesser extent Sb and Zn are positively correlated with samples with low ccp/(ccp+sp) ratio, whereas Bi, Co, Ni, Au, Se, Mn and Te are associated with samples with high ccp/(ccp+sp) ratio. Results for bimodal-mafic setting show two clusters in the score plot t1-t2: 1) where chalcopyrite from samples with low ccp/(ccp+sp) ratio is associated with Ga, Sn, Tl, In, and to a lesser extent Sb and Zn, whereas 2) chalcopyrite from samples with high ccp/(ccp+sp) ratio is principally associated with Te, Au, Se, Bi, Mn, Ni and Co (Figs. 2.9A, B). Chalcopyrite from Cu-rich stockwork ores plot mainly with chalcopyrite from low ccp/(ccp+sp) ratio massive samples. Chalcopyrite from bimodal-felsic settings show similar relations according to ccp/(ccp+sp) ratios (Figs. 2.9C, D). Indium, Ga, Sn and to a lesser extent Zn, Sb and Pb are

positively correlated with Zn-rich samples (Fig. 2.9D). To a lesser extent, in siliciclastic-felsic settings, chalcopyrite from Zn-rich samples (Fig. 2.9E), with relatively low ccp/(ccp+sp) ratios, is associated with Ga, Mn, Zn, Sb and marginally Pb and Ag (Fig. 2.9F).

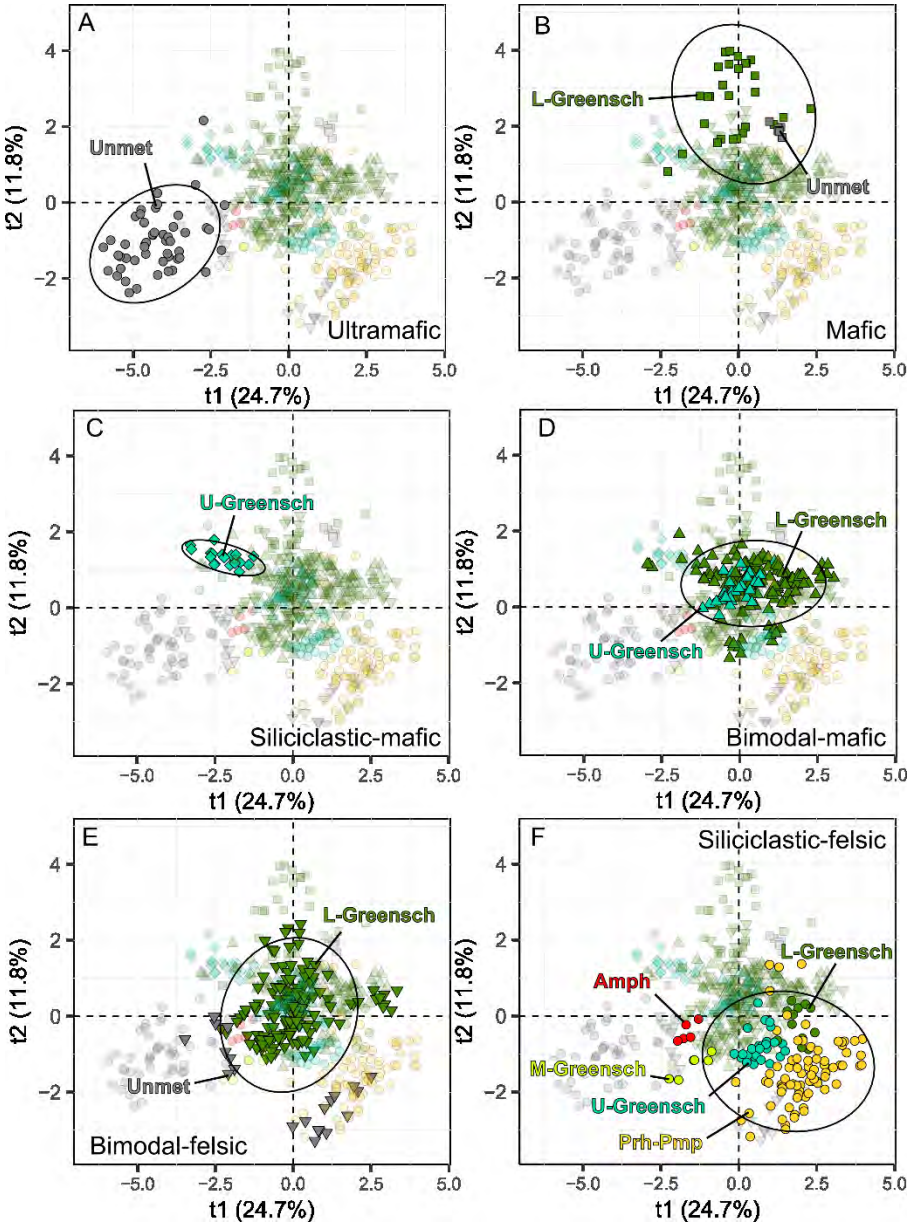

Fig. 2. 7 Metamorphic grades of samples projected on PLS-DA results according to lithotectonic settings. (A) samples from unmetamorphosed SMS ultramafic-hosted deposits. (B) Mafic subtype group comprising samples from deposits with different metamorphic grades, show similar trace element composition. (C) Samples from siliciclastic-mafic setting have upper greenschist metamorphism. (D, E) Chalcopyrite from bimodal subtypes showing similar trace element composition independent of metamorphic grade. (F) In siliciclastic-felsic setting, chalcopyrite from deposits with prehnite-pumpellyite, lower greenschist, upper greenschist and, to a lesser extent middle greenschist and amphibolite metamorphism, have similar trace element composition. Unmet: unmetamorphosed; Prh-Pmp: prehnite-pumpellyite; L-Greensch: lower greenschist; M-Greensch: middle greenschist; U-Greensch: upper greenschist; Amp: amphibolite.

2.5.4 Supervised Classification and Regression with Random Forest

Performance estimators in the optimized models, calculated from cross validation during training, are summarized in Table 2.3. Figure 2.10 shows results of recursive feature elimination, indicating that the optimal variables are Sn, Co, Te, In, Zn, Se, Ag, Sb and Pb for the RFmodel.01 (affinity), Co, Sn, Mn, Te, In, Pb, Se, Tl, Ni, Ag Zn and Bi for the RFmodel.02-A (ultramafic vs. mafic vs. siliciclastic-mafic subtypes), and Te, Se, Zn, In, Ag, Sb, Co, Ga, Sn and Ni for the RFmodel.02-B (bimodal-mafic vs. bimodal-felsic subtypes). All models resulted in kappa values greater than 0.90. Minimum training accuracy was 0.95, recorded by the RFmodel.02-B, whereas maximum training accuracy was 0.99, reported by RFmodel.02-A. Classification outcomes for the test data are presented in Table 2.4, 2.5 and 2.6 for each model. Random Forest model.01 correctly identified the classes from chalcopyrite trace element composition with an overall accuracy of 0.98, whereas RFmodel.02-A recorded an accuracy of 0.97 and RFmodel.02-B of 0.96.

Table 2. 3 Classification performance estimators of the Random Forest models.

	RFmodel.01 (Affinity)		RFmodel.02-A (M-UM)		RFmodel.02-B (BMF)	
Estimator	μ	sd	μ	sd	μ	sd
Accuracy (Acc)	0.97	0.03	0.99	0.04	0.95	0.04
Kappa (K)	0.95	0.05	0.98	0.06	0.91	0.07
F1-score (F1)	0.97	0.03	0.99	0.04	0.95	0.04
Specificity (Spe)	0.98	0.02	0.99	0.02	0.97	0.05
Precision (Pre)	0.98	0.02	0.99	0.02	0.97	0.05
Recall (Recall)	0.96	0.04	0.98	0.07	0.94	0.06
Balanced accuracy (Bacc)	0.97	0.03	0.99	0.04	0.95	0.04

M: mafic; UM: ultramafic; BMF: bimodal-mafic-felsic. μ: mean. sd: standard deviation

In addition to classifying chalcopyrite by VMS setting using trace elements, a random forest regression model was developed for bimodal-mafic, bimodal-felsic and siliciclastic-felsic to predict the ccp/(ccp+sp) ratio in samples. Figure 2.11 summarises the performance and shows the variable importance for each model. The regression model performs better for chalcopyrite from bimodal-mafic VMS setting, (Figs. 2.11A, B), reporting the lowest errors in training ($RMSE_{tr}$: 0.09; MAE_{tr}: 0.06) and test data ($RMSE_{test}$: 0.06; MAE_{test}: 0.06), and the higher coefficient of determination (R^2_{tr}: 0.84; R^2_{test}: 0.93). In bimodal-felsic settings (Figs. 2.11C, D), RF regression model errors for training ($RMSE_{tr}$: 0.12; MAE_{tr}: 0.08) and test data ($RMSE_{test}$: 0.12; MAE_{test}: 0.07) are slightly higher, whereas coefficient of determination is lower (R^2_{tr}: 0.78; R^2_{test}: 0.79), indicating a performance slightly lower than bimodal-mafic. Finally, in siliciclastic-felsic setting (Figs. 2.11E, F), the performance of the RF regression model is the lowest, reporting the highest errors in training ($RMSE_{tr}$: 0.13; MAE_{tr}: 0.09) and test data ($RMSE_{test}$: 0.14; MAE_{test}: 0.10), as well as the lowest coefficient of determination (R^2_{tr}: 0.50; R^2_{test}: 0.55). The results of RF regression models confirm that there is potential to predict ccp/(ccp+sp) ratio and determinate Cu-rich and Zn-rich zones in bimodal-mafic, bimodal-felsic and siliciclastic-felsic VMS settings, as suggested by PLS-DA results.

Table 2. 4 Confusion matrix and performance estimators for RFmodel.01 on test data.

		Actual			
		Mafic-ultramafic	Bimodal	Felsic	*Total*
Predicted	Mafic-ultramafic	31	0	0	31
	Bimodal	0	99	3	102
	Felsic	0	0	35	35
	Total	31	99	38	168
	Accuracy by class	*1.00*	*1.00*	*0.92*	
	Overall accuracy	*0.98*			
	Recall	*0.97*			
	Kappa	*0.97*			

2.6 Discussion

Numerous parameters affect the trace element composition of sulfides in VMS deposits, such as host rock composition, temperature, fO_2, aS_2 and pH of the fluid in the reaction zone, volatile content, as well as cooling, mixing with seawater, and boiling (Barrie and Hannington, 1999; Franklin et al., 2005; Fuchs et al., 2019; Galley et al., 2007; Hannington, 2014). During precipitation, trace elements partition between chalcopyrite and co-precipitating sulfides, such as sphalerite, galena, and pyrite/pyrrhotite (Carvalho et al., 2018; Genna and Gaboury, 2015; George et al., 2015; George et al., 2016; George et al., 2018b; Lockington et al., 2014; Reich et al., 2013a; Torró et al., 2022; Xing et al., 2022). Although the Cu-Zn zonation model is consistent in most deposits and at a variety of scales, locally VMS and SMS are often paragenetically complex (Hannington, 2014). Deposits can be affected by different thermal histories involving continuous dissolution and precipitation processes (*i.e.*, zone refining), and potentially trace element remobilization, as shown by replacement of pre-existing sulfides (Eldridge et al., 1983; Hannington, 2014; Ohmoto, 1996).

Table 2. 5 Confusion matrix and performance estimators for RFmodel.02-A on test data.

		Actual			
		Ultramafic	Mafic	Siliciclastic-mafic	*Total*
Predicted	Ultramafic	15	1	0	10
	Mafic	0	10	0	1
	Siliciclastic-mafic	0	0	5	5
	Total	15	11	5	31
	Accuracy by class	*1.00*	*0.91*	*1.00*	
	Overall accuracy	*0.97*			
	Recall	*0.97*			
	Kappa	*0.96*			

Table 2. 6 Confusion matrix and performance estimators for RFmodel.02-B on test data.

		Actual		
		Bimodal-mafic	Bimodal-felsic	*Total*
Predicted	Bimodal-mafic	48	3	47
	Bimodal-felsic	1	47	3
	Total	49	50	99
	Accuracy by class	*0.98*	*0.94*	
	Overall accuracy	*0.96*		
	Recall	*0.96*		
	Kappa	*0.95*		

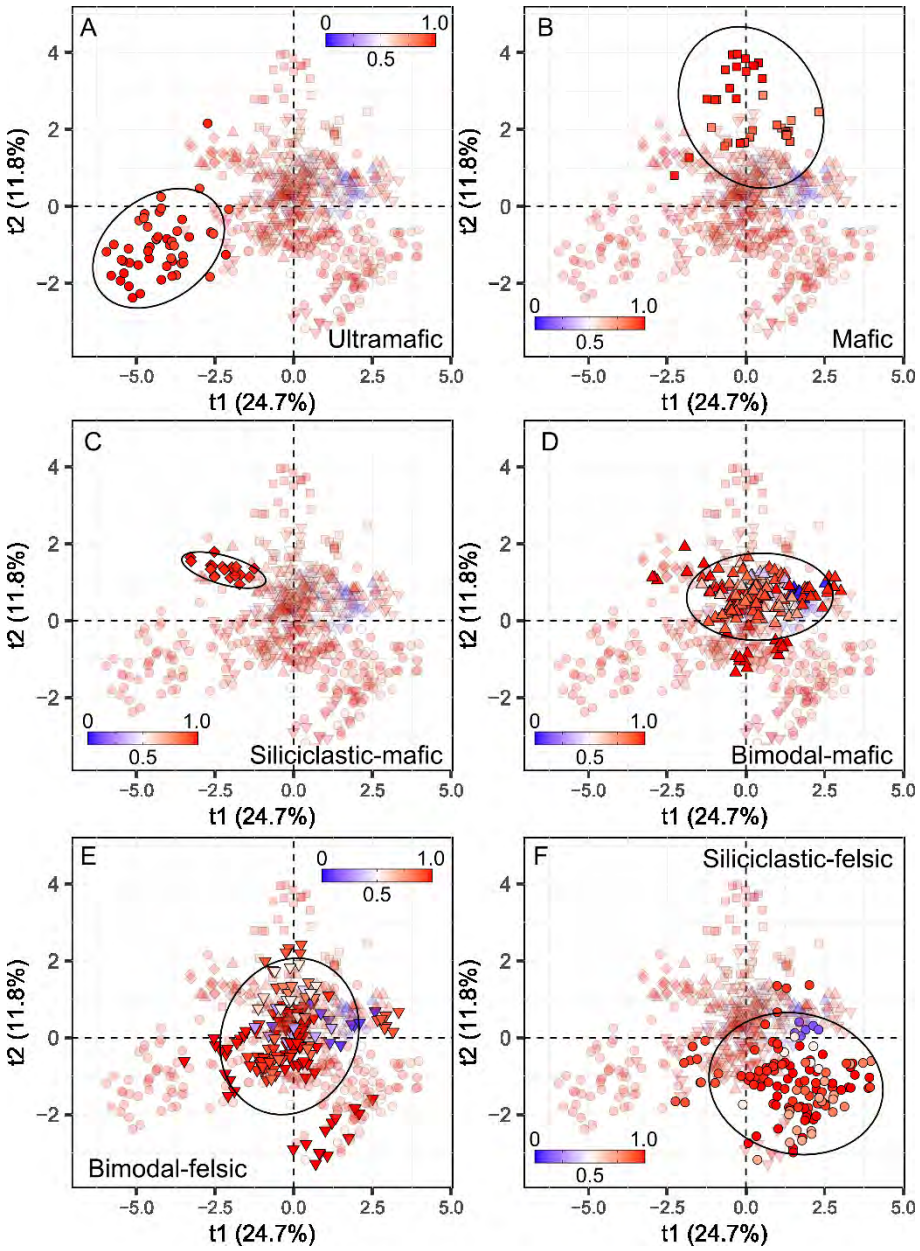

Fig. 2. 8 The ccp/(ccp+sp) ratio of the samples projected on PLS-DA results, showing that sulfide proportions have no impact on grouping according to lithotectonic settings.

2.6.1 Trace Element Composition of Chalcopyrite as a Tool to Sulfide Assemblage Recognition

Based on our PLS-DA results, at the deposit scale, chalcopyrite from Cu-rich samples with high ccp/(ccp+sp) ratio is enriched in Bi, Co, Ni, Au, Ag, Te and Se (Figs. 2.5, 2.9 and Annexe B8, B9). According to Hannington (2014), these elements correspond to a typical high-temperature polymetallic assemblage, including Ag transport under reducing conditions. Similar results are reported in pyrite from high-temperature Cu-rich VMS ore zones, which also are enriched in Se, Bi and Co (Genna and Gaboury, 2015). Silver-bearing chalcopyrite has been reported in VMS deposits (Broken Spur vent field: Butler and Nesbitt, 1999; Izok Lake: Harris et al., 1984) and other hydrothermal systems (Cook and Chryssoulis, 1990; Cook et al., 2011; Reich et al., 2013b; Reich et al., 2020), incorporated in solid solution. In contrast, chalcopyrite from Zn-rich samples, with low ccp/(ccp+sp) ratio is high in Ga, Sn, In, Sb and to a lesser extent Tl (Figs. 2.5, 2.9, and Annexe B8, B9), typical of low-temperature assemblages (Hannington, 2014). In Zn-rich samples, chalcopyrite commonly replaces pyrite and sphalerite, with the latter showing typical replacement textures such as chalcopyrite disease (Figs. 2.2D, E; Barton and Bethke, 1987; Bortnikov et al., 1991; Hannington, 2014; Nagase and Kojima, 1997). Previous studies have demonstrated that sphalerite and galena are the principal host of elements such as Ga, In, Sb and Tl in hydrothermal deposits (Carvalho et al., 2018; George et al., 2015; George et al., 2016; Lockington et al., 2014; Torró et al., 2022; Xing et al., 2022). Likewise, pyrite is also known to be an important sink of Tl and Sb, in particular in Zn-rich zones, among others (Dehnavi et al., 2018; Genna and Gaboury, 2015; Ren et al., 2021). Probably during the zone refining process, a successive remobilization of these elements from sulfides previously formed at lower temperature (*e.g.,* sphalerite, galena, or pyrite) led to their incorporation into chalcopyrite at different replacement degrees. Chalcopyrite still forms at high temperature; however, it overprints the low temperature assemblage. The differences between chalcopyrite composition from massive and stockwork ores in some deposits are not systematic, suggesting that conditions of precipitation are similar.

2.6.2 Trace Element Composition of Chalcopyrite as a Tool to VMS Setting Recognition

Partial least square-discriminant analysis results demonstrate that lithostratigraphic setting of the VMS-SMS deposits (*e.g.*, Franklin et al., 2005; Patten et al., 2022), is the main control on the trace element content in chalcopyrite (Fig. 2.6). Moreover, PLS-DA allows for determination of the element association for each lithostratigraphic setting, information not provided by random forest classification model. Our results show that chalcopyrite from ultramafic-hosted SMS deposits (Logatchev and Irinovskoe hydrothermal fields) is significantly enriched in Co, Ni and Te when compared to other subtypes (Figs. 2.3, 2.4). This is in agreement with results previously published from Logatchev (Wohlgemuth-Ueberwasser et al., 2015). Previous studies on tourmaline reported unusually high Ni and Co concentrations in orogenic gold deposits that are hosted in mafic-ultramafic rocks (Hazarika et al., 2015; Sciuba et al., 2021), possibly indicating a common enrichment process related to

the host rock lithology. Ultramafic rocks have abundant ferromagnesian minerals and minor Ni-Co-enriched magmatic sulfides (e.g., olivine; Vasyukova and Williams-Jones, 2022).

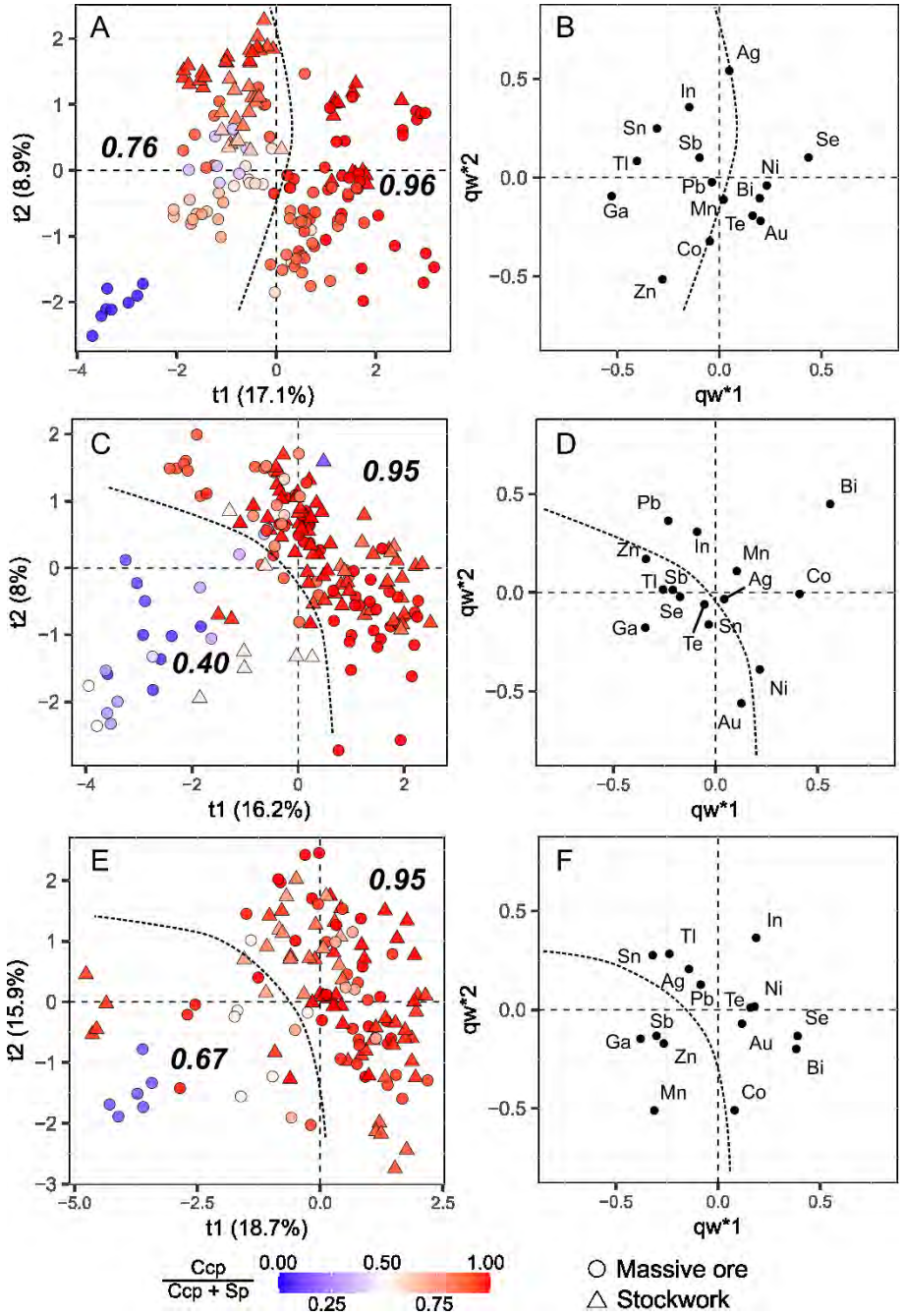

Fig. 2. 9 PLS-DA on trace elements in chalcopyrite from bimodal-mafic (A, B), bimodal-felsic (C, D) and siliciclastic-felsic deposits (E, F) according to ccp/(ccp+sp) ratio. In bold-italic trimmed means of chalcopyrite-sphalerite proportion of each group delineated by the dotted lines.

During fluid-rock interaction Ni and Co can be leached, transported, and precipitated in the massive sulfide deposits (Barrie and Hannington, 1999; Hannington, 2014). High values of Te in chalcopyrite from ultramafic-hosted deposits may also have been derived from sulfide droplets in ultramafic rocks (Hattori et al., 2002). In

contrast, Pb is significantly depleted in chalcopyrite from ultramafic-hosted deposits relative to other settings (Figs. 2.3, 2.4 and 2.6). Chalcopyrite from Cu-rich samples shows negative correlation coefficients between Pb-Se (r = -0.41) and Pb-In (r = -0.39), whereas Pb is positively correlated with Tl (r = 0.35) (Annexe B7B), suggesting that temperature could be a factor controlling concentration of Pb and Tl (Hannington, 2014). Selenium and In show strong correlation with Cu in most of VMS deposits, which form stable H_2Se and $InCl_3$ complexes at high temperatures, respectively (Carvalho et al., 2018; Hannington, 2014; Ishihara and Endo, 2007). Additionally, ultramafic rocks are characterized by low Pb concentrations compared to the other rock types (Digis Team, 2022; Hofmann, 1988; Workman and Hart, 2005), which also influences the low Pb contents of the ultramafic VMS subtype.

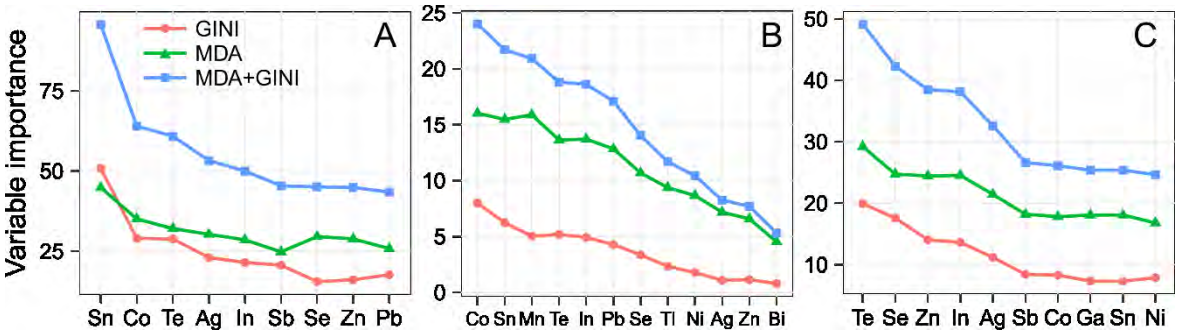

Fig. 2. 10 Variable importance measures of the optimal elements after recursive feature elimination for the (A) RFmodel.01 (affinity), (B) RFmodel.02-A (mafic-ultramafic-siliciclastic mafic), and (C) RFmodel.02-B (bimodal mafic-bimodal felsic). MDA: Mean Decrease in Accuracy; GINI: Gini index; MDA+GINI: total scores.

Most trace elements in chalcopyrite from the mafic subtype of VMS deposits do not show significant differences to chalcopyrite from the other settings (Fig. 2.3). Although Pb has a low average concentration in mafic rocks (3.6 ppm in basalt; 4.2 ppm in gabbro, Digis Team (2022) database), it is the only element showing a trimmed mean in chalcopyrite higher than for the other subtypes (9.26 ppm; Table 2.2; Fig. 2.3). The association between Pb and mafic-hosted deposits is also evidenced by high positive regression coefficients from PLS-DA (Fig. 2.6C) and loading plot qw*3-qw*4 (Annexe B10A). According to our results, chalcopyrite from Whalesback (17.4 ppm, n=5), Lasail (15.2 ppm, n=14) and to a lesser extent the Ice (11.4 ppm, n=5) deposit has higher concentration of Pb than the remaining mafic VMS deposits (Table 2.2). Mafic VMS deposits are on average dominated by Cu-rich and Pb-Zn poor sulfide assemblages with scarce to absent galena (Franklin et al., 2005; Galley et al., 2007; Hannington, 2014). According to George et al. (2016), chalcopyrite may be an important trace element host of Pb in the absence of sphalerite and/or galena. The high Pb content in chalcopyrite from the mafic subtype could be related to the near absence of galena, which led to more availability of Pb to partition onto chalcopyrite. In addition, Pb can be efficiently mobilized not only from the sheeted dyke zones (*i.e.*, epidosite zones) but also from Sb- and Pb-enriched plagiogranites during hydrothermal alteration of the oceanic crust, such as that at Troodos ophiolite, Cyprus (Patten et al., 2017; Patten et al., 2016). As such, Martin et al. (2019) reported high concentrations of Pb in chalcopyrite from Troodos mafic-hosted VMS deposit. In the Lasail deposit of the Oman

ophiolite, Stakes and Taylor (2003) demonstrated the existence of multiple superimposed magmatic and hydrothermal events, and that the large plagiogranite bodies and associated gabbroic rocks found with the contemporaneous late mafic dykes played an important role as a source of heat and metals (such as Pb) for massive sulfide formation.

In the bimodal-mafic subtype, chalcopyrite shows a slightly higher trimmed mean of Ag (94.8 ppm) than the other subtypes (Fig. 2.3) and a high positive regression coefficient from PLS-DA (Fig. 2.6C). The high concentration of Ag in chalcopyrite from bimodal-mafic setting is significatively biased by samples from Normétal (sample 51) and Kidd Creek (sample 2369), with maximum of 1640 ppm and 1031 ppm, respectively (Annexe B3). The bias is also evidenced by the median of Ag in chalcopyrite from bimodal-mafic deposits (68 ppm Ag), which is significatively different from the mean value (95 ppm Ag; Table 2.2). Except for Au, Se, and Pb, chalcopyrite from bimodal-mafic and bimodal-felsic subtypes do not show significative differences to each other (Fig. 2.1). Bimodal deposits are characterized by a variable proportion of mafic and felsic volcanic rocks, representing a transition of host rock composition (Franklin et al., 2005), leading to similar trace element composition in chalcopyrite, as shown by important overlapping of chalcopyrite composition from these settings in our PLS-DA results (Fig. 2.6A).

Chalcopyrite from bimodal-felsic settings has higher concentrations of Au than the remaining subtypes. Chalcopyrite from Quémont (0.83±1.0 ppm) and Horne (0.29±0.20 ppm) deposits is enriched in gold compared to the other deposits (<0.05 ppm), reaching a maximum of 5.6 ppm and 1.1 ppm Au, respectively (Table 2.2, Annexe B3). The Quémont and Horne deposits are considered two of the largest and richest gold-rich VMS deposits worldwide (Dubé et al., 2007; Mercier-Langevin et al., 2007; Mercier-Langevin et al., 2011), which is clearly recorded in the chalcopyrite composition. Chalcopyrite from Snowcap bimodal-felsic-hosted SMS occurrence, in the PACMANUS hydrothermal field, also records high concentration in Au (2.7±2.6 ppm) with a maximum of 4.8 ppm. Studies have reported that chalcopyrite-rich chimneys in PACMANUS are enriched in Au (Binns et al., 2007; Binns et al., 2004; Fuchs et al., 2019; Hannington et al., 2005). In addition, chalcopyrite from bimodal-felsic compared to bimodal-mafic settings has a higher content of Pb, which may be explained by a larger proportion of felsic volcanic host rocks. Lead is principally derived from the destruction of feldspar, particularly abundant in felsic rocks from subduction-related volcanic arc systems floored by continental basement (Hannington, 2014; Hannington et al., 1995).

The trace element composition in chalcopyrite from siliciclastic-mafic settings has the highest values of Mn (Fig. 2.3), particularly those from Pike Hill mine in the Vermont Copper Belt (119 ppm; Table 2.2). The association between Mn and siliciclastic-mafic subtype is supported by a high positive regression coefficient and the loading plot qw*1-qw*2 and qw*3-qw*4 (Fig. 2.6B, C and Annexe B10A).

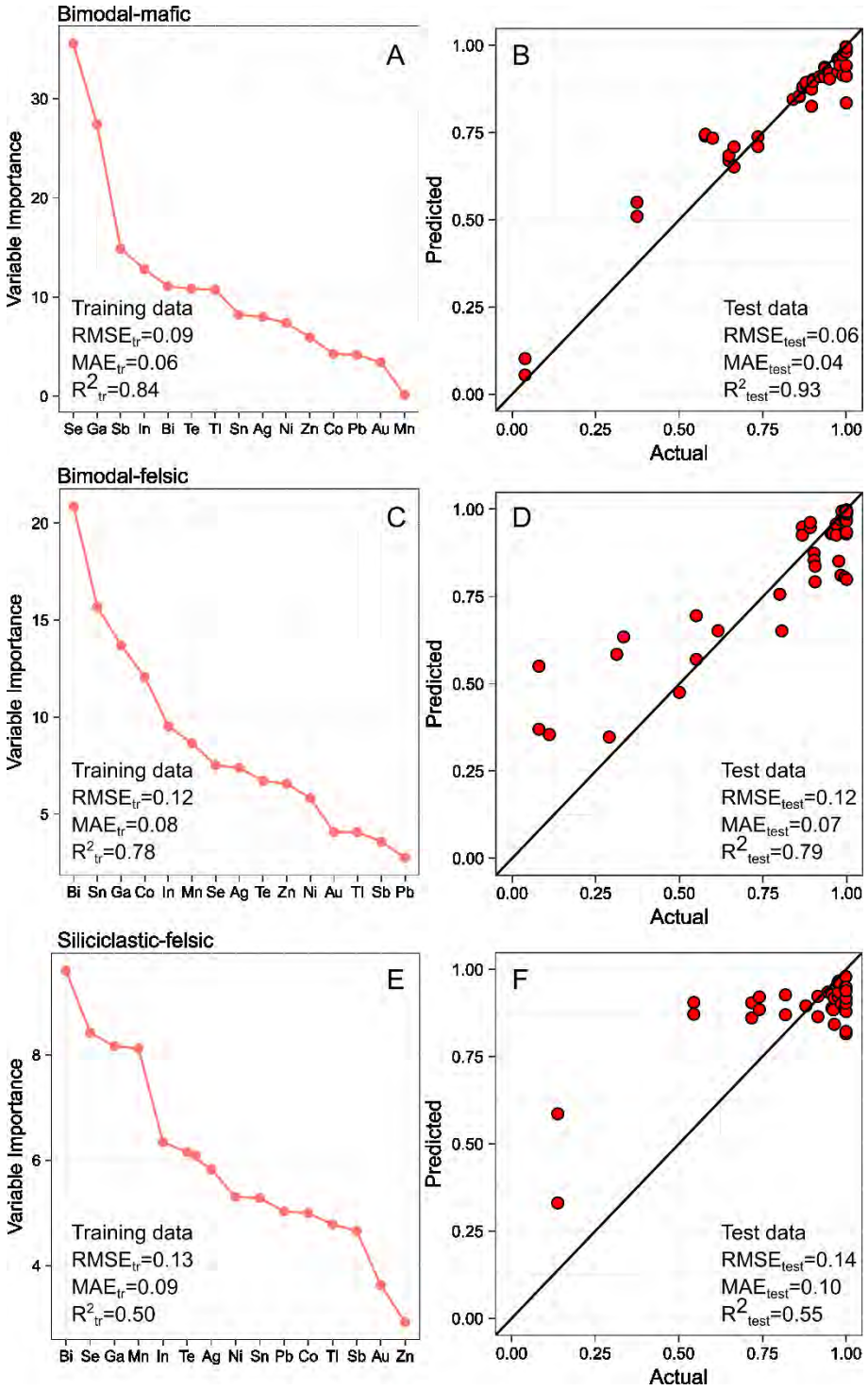

Fig. 2. 11 Random Forest regression model results for chalcopyrite from bimodal-mafic (A, B), bimodal-felsic (C, D) and siliciclastic-felsic (E, F) settings. Variable importance is shown at the left side with the performance metrics for training data. Actual and predicted ccp/(ccp+sp) ratio values for test data are shown at the right side with their corresponding performance metrics. RMSE: Root Mean Square Error; MAE: Mean Absolute Error; R^2: Coefficient of determination.

In metamorphosed hydrothermal systems, Mn-rich siliciclastic sedimentary rocks (*i.e.*, coticule) that are usually intercalated with other meta-exhalites are typically found in rift-hosted volcanosedimentary base metal sulfide

deposits, typical for the siliciclastic-mafic type (Spry et al., 1998). Slack et al. (2001) also reported the presence of Mn-rich garnet-quartz rocks in Elizabeth and Pike Hill mines in the Vermont Copper Belt and suggest that they have formed as exhalative chemical precipitates on the seafloor. According to Hannington (2014), Mn is common at high concentrations in the most reduced fluids involved in the formation of VMS deposits. However, it rarely forms stable sulfides and is lost to distal hydrothermal facies, such as exhalites. The presence of coticules in Pike Hill mine suggests mobilization of Mn by hydrothermal fluids during VMS deposit formation, which was in part incorporated in chalcopyrite.

Finally, our results show that chalcopyrite from siliciclastic-felsic setting has higher concentrations of Sn, Sb, Bi and In than the other subtypes (Figs. 2.3, 2.6). In particular, chalcopyrite from Neves-Corvo is enriched in Sn (1058 ppm) and to a lesser extent In (Table 2.2), in agreement with the study of Carvalho et al. (2018). Likewise, chalcopyrite from Halfmile Lake (5643 ppm) and Hajar (856 ppm) deposits also shows high values of Sn (Table 2.2). Several studies have proposed a model for ore formation at Neves-Corvo involving direct magmatic contributions of Sn in addition to footwall metasediments (Carvalho et al., 2018; Huston et al., 2011; Li et al., 2019; Marques et al., 2020; Relvas et al., 2001; Relvas et al., 2006). Similarly, Goodfellow (2007) reported Sn enrichment at Bathurst, also proposing a magmatic component for the metal source, based on radiogenic Pb isotopes. The high concentration of Bi in chalcopyrite from siliciclastic-felsic settings may therefore also be explained by the presence of a magmatic component, since significant co-enrichment of Bi and In have been used as evidence of direct contributions of metal from magmatic fluids (Hannington, 2014).

2.6.3 Predicting Lithostratigraphic Setting of VMS-SMS Deposits with Random Forest (from affinity to VMS subtype)

The results of the predictions of literature data are summarized in Table 2.7 and Table 2.8. All analyses were classified primarily by affinity with the model RFmodel.01, subsequent analyses correctly predicted were reclassified by subtype with the RFmodel.02-A or RFmodel.02-B models for those predicted as belonging to mafic-ultramafic or bimodal classes, respectively. Literature data with complete set of elements analyzed by LA-ICP-MS required by the models correspond to George et al. (2018b), Wang et al. (2018) and Melekestseva et al. (2020a) (Table 2.7). The highest rates of analyses correctly classified according to the affinity (RFmodel.01) were recorded for the ultramafic-hosted SMS deposits Ashadze-2 hydrothermal field, Mid-Atlantic Ridge (Melekestseva et al., 2020a) and Kairei Vent Field, Central Indian Ridge from Wang et al. (2018), with 100%, followed by the mafic-hosted Vorta deposit, Romania (George et al., 2018b) with 87.5% (Table 2.7). Similarly, Ashadze-2 and Kairei deposits reported the highest rates of analyses correctly classified according to VMS subtype (RFmodel.02-A), with 100% and 93.8%, respectively, followed by Vorta deposit which registered an accuracy of 87.5%. Sulitjelma deposit has an imprecise classification using literature data, and although several studies indicate that the host rocks show characteristics similar to the mafic subtype (Barrie et al., 2010; Cook, 1996; Cook and Halls, 1990), Pedersen et al. (1991) proposed that Sulitjelma formed during the initial stages of

back-arc spreading in the late Ordovician, more akin to the bimodal-mafic setting. Considering this uncertainty of the lithostratigraphic setting of the Sulitjelma deposit, the RF classification model yields results more consistent with a bimodal affinity (96.4%) and bimodal-mafic subtype (60.4%).

Table 2. 7 Results of the predictions of literature data with all elements required by the RF models.

	Author	Melekestseva et al. (2020a)	Wang et al. (2018)	George et al. (2018)	George et al. (2018)
Actual	Deposit	Ashadze-2 (SMS)	Kairei (SMS)	Vorta, Romania	Sulitjelma, Norway
	Metamorphism	Unmet		Low grade	U-greensch
	n	7	16	8	111
	Subtype	UM		M	BM[1]
	Affinity	M-UM			
RFmodel.01 (affinity) Sn-Co-Te-Ag-In-Sb-Se-Zn-Pb					
Predicted	Number correct[2]	7	16	7	107
	M-UM	100.0%	100.0%	87.5%	3.6%
	BMF	0.0%	0.0%	12.5%	96.4%
	SF	0.0%	0.0%	0.0%	0.0%
RFmodel.02-A (M-UM) Co-Sn-Mn-Te-In-Pb-Se-Tl-Ni-Ag-Zn-Bi					
Predicted	Number correct	7	15	7	
	UM	100.0%	93.8%	0.0%	
	M	0.0%	6.2%	87.5%	
	SM	0.0%	0.0%	0.0%	
RFmodel.02-B (BMF) Te-Se-Zn-In-Ag-Sb-Co-Ga-Sn-Ni					
Predicted	Number correct				67
	BM				60.4%
	BF				36.0%

n: number of analyses. [1]imprecise classification in literature. [2]number of samples correctly classified. Percentage in bolt: percentage of analyses correctly classified on total of samples (n). Unmet: umetamorphosed, U-greensch: upper greenschist. UM: ultramafic, M: mafic, BM: bimodal-mafic, SMS: seafloor massive sulfides.

2.6.3.1 Predicting Samples with Missing Elements

Published trace element data of chalcopyrite is scarce for VMS-SMS deposits. This is especially true for analyses of the elements required by our RF classification models. Machine learning algorithms provide some techniques to deal with missing predictors, such as bagged classification trees or k-Nearest Neighbor (kNN; (Kuhn and Johnson, 2013; Provost and Saar-Tsechanski, 2007). We tested bagged classification trees to impute missing predictors in studies where one or multiple elements were not analyzed. During our RF model training, bagged classification trees can be built for each predictor in order to use them for imputation of missing data (Kuhn and Johnson, 2013; Provost and Saar-Tsechanski, 2007).

Among studies with missing variables, those with low number of no analyzed elements (<2) and of moderate to low variable importance in classification (e.g., Ga, In), recorded the highest rate of chalcopyrite correctly classified (Table 2.8). The highest proportion of correct prediction according to affinity (Table 2.8) were obtained for the bimodal-felsic María Teresa deposit, Peru (100%; Torró et al., 2022), the bimodal-felsic Çayeli-Kutlular deposit (82.1%; Revan et al., 2014) and the ultramafic-hosted Dergamysh deposit, Russia (77.3%; Melekestseva et al., 2020b). The remaining deposits, except for the bimodal-felsic SMS Roman Ruins, Papua New Guinea (74.1%; Wohlgemuth-Ueberwasser et al., 2015), which have at least half of the key elements missing, reported an overall accuracy lower than 65% with a minimum of 24.1% for the mafic-hosted Troodos deposits, Cyprus (Table 2.8; Martin et al., 2019). According to RF models by VMS settings, the highest percentage of analyses corrected classified were reported for bimodal-felsic María Teresa (89.6%), the bimodal-felsic Çayeli-Kutlular deposit (79.1%) and the ultramafic-hosted Dergamysh deposit (63.7%). Furthermore, the ultramafic-hosted SMS Logatchev deposit, the bimodal-felsic SMS Roman Ruins and Satanic Mills deposits, and the mafic-hosted Troodos deposits registered an overall accuracy lower than 60%. An increase of the number of non-analyzed elements, particularly those with a moderate to high variable importance, degrades considerably the performance of the classifier, since less information is available to determine the provenance of the analyses. In addition to the number of missing elements, another important factor impacting the performance of the models is the percentage of censured values in the original data. This is the case of the dataset from Martin et al. (2019), which has more than 30% of values below detection limit (in addition to the missing elements), decreasing the precision of the imputation, and consequently the performance of the prediction. On the other hand, although all samples from Cerro de Maimón deposit (Torró et al., 2022) were predicted as mafic subtype, its classification in the literature is inconclusive, since it is considerably deformed. The RF classification model (RFmodel.02-B) yields results more consistent with a mafic subtype, with 100% of samples predicted as belonging to this setting.

2.6.4 Effects of Metamorphism on Classifier Predictions

Several studies have documented the textural and chemical effects of deformation and remobilization on sulfides from VMS settings during metamorphism, principally on pyrite (Barrie et al., 2010; Barrie et al., 2009; Conn et al., 2019; George et al., 2018a; Zhao et al., 2021b), sphalerite (George et al., 2016; Zhao et al., 2021b), galena (George et al., 2015) and pyrrhotite (Steadman and Large, 2016). Solid mechanical transfer, liquid-state chemical transfer, and/or partial melting are the principal mechanisms involved in metamorphic remobilization of massive sulfide ores (Andersson et al., 2016; Marshall et al., 1998; Tomkins, 2007; Tomkins et al., 2007). Although little is known about the effect on chalcopyrite, some studies suggest that at high grades of metamorphism (upper amphibolite to granulite facies) Sn, In, Ga and Ag are preferentially incorporated into chalcopyrite, especially when it co-exists with sphalerite, probably through partial melting, as well as a chemical remobilization mechanism combined with mechanical processes (George et al., 2016; Zhao et al., 2021b).

Table 2. 8 Results of the predictions of literature data with missing elements using RF models.

	Author	Melekestseva et al. (2020b)	Wohlgemuth-Ueberwasser et al. (2015)	Martin et al. (2019)	Torró et al. (2022)		Revan et al. (2014)	Wohlgemuth-Ueberwasser et al. (2015)	
	Deposit	Dergamysh, Russia	Logatchev (SMS)	Troodos, Cyprus	Cerro de Maimón, DR	María Teresa, Peru	Çayeli-Kutlular, Turkey	Roman Ruins (SMS)	Satanic Mills (SMS)
	Meta	Greensch	Unmet	Unmet	Greensch/ bluesch	Contact		Unmet	
	Missing elements	Ga-In	Co-Ni-Zn-Ga-Ag-In-Tl-Pb-Bi	Tl-Mn-Ga-In-Sn	Te	Te	Ga-In	Co-Ni-Zn-Ga-Ag-In-Tl-Pb-Bi	
	n	22	29	41	11	29	67	77	25
Actual	Subtype	UM		M	M[1]		BF		
	Affinity	M-UM			BMF				
	RFmodel.01 (affinity) Sn-Co-Te-Ag-In-Sb-Se-Zn-Pb								
Predicted	Number correct[2]	17	15	10	11	29	55	55	16
	M-UM	77.3%	51.7%	24.1%	100.0%	0.0%	17.9%	0.0%	0.0%
	BMF	18.2%	48.3%	59.3%	0.0%	100.0%	82.1%	71.4%	64.0%
	SF	4.5%	0.0%	16.6%	0.0%	0.0%	0.0%	28.6%	36.0%
	RFmodel.02-A (M-UM) Co-Sn-Mn-Te-In-Pb-Se-Tl-Ni-Ag-Zn-Bi								
Predicted	Number correct	14	15	1	11				
	UM	63.7%	51.7%	20.3%	0.0%				
	M	13.6%	0.0%	1.9%	100.0%				
	SM	0.0%	0.0%	1.9%	0.0%				
	RFmodel.02-B (BMF) Te-Se-Zn-In-Ag-Sb-Co-Ga-Sn-Ni								
Predicted	Number correct					26	53	34	15
	BM					10.4%	3.0%	27.3%	4.0%
	BF					89.6%	79.1%	44.1%	60.0%

n: number of analyses. [1]imprecise classification in literature. [2]number of samples correctly classified. Percentage in bolt: percentage of analyses correctly classified on total of samples (n). Greensch: greenschist, Unmet: unmetamorphosed, Bluesch: blueschist. UM: ultramafic, M: mafic, BM: bimodal-mafic, SM: siliciclastic-mafic. SMS: seafloor massive sulfides.

In this study, samples come from a range of low metamorphic grades (Table 2.1). The majority of deposits underwent low-grade prehnite-pumpellyite (Iberian Pyrite Belt (IPB)) and lower greenschist (Abitibi Greenstone Belt). In the IPB deposits, studies have reported tectonic stacking of massive sulfide lenses, metal remobilization and local enrichment associated to Variscan deformation and metamorphism (Almodóvar et al., 2019; Castroviejo et al., 2011; Marignac et al., 2003; Tornos, 2006). Moreover, Almodóvar et al. (2019) suggested that post-mineralization and pre-Variscan deformation sill emplacement in some IPB deposits (e.g., Aguas Teñidas),

conducted to a local increase of temperature leading to a Cu remobilization, probably by a liquid-state mechanism. Few studies have been conducted on remobilization mechanisms in sulfides at greenschist facies. For the McLeod deposit (Matagami, Québec) Genna and Gaboury (2019) suggested that semi-volatile elements, principally hosted in pyrite (e.g., Sb, Tl, W, Sn), could be remobilized from the massive sulfide lens to the host rhyolite during prograde greenschist metamorphism, by the transformation of pyrite to pyrrhotite. Concerning the deposits from Bothnia-Skelleftea Unit, Skyttä et al. (2020) indicated that they have been affected by polyphase ductile deformation and metamorphism at variable temperature and low-pressure conditions, the later event under lower greenschist conditions. In these deposits, both solid-state remobilization, which includes fold hinge sulfide thickening and limb attenuation, and liquid-state remobilization has led to gold enrichment (Weihed et al., 2002). Samples from Ming, Bathurst and Vermont Copper Belt have undergone upper greenschist metamorphism (Table 2.1; Annexe B1). At Ming, minor metal remobilization by metamorphism and deformation has been recorded (Brueckner et al., 2015; Brueckner et al., 2016; Pilote et al., 2020). On the other hand, the Bathurst and Halfmile Lake deposits show textural characteristics typically related to remobilization of sulfides (Dehnavi et al., 2018), by solution transfer, principally in pyrite but also probably in pyrrhotite, sphalerite and chalcopyrite (Roo and Staal, 2003). Samples from the Tétrault deposit of Montauban (Grenville Province, Québec) reached the lower amphibolite facies. In this deposit, Tomkins (2007) demonstrated that mechanical remobilization of sulfides was the most important mechanism for controlling the distribution of Zn-Pb mineralization, whereas a combination of partial melting and prograde hydrothermal mechanisms were responsible for Ag-Au remobilization.

Our PLS-DA results (Fig. 2.7) demonstrate that any modification of the trace element composition of chalcopyrite due to variable metamorphic grade is in fact smaller than the much larger variation in composition due to the different lithotectonic subtypes of VMS deposits. This is particularly well-shown for the mafic subtype, where chalcopyrite from unmetamorphosed and lower greenschist grade deposits plot within the limits of the 95% confidence ellipse, indicating no significant differences in trace element composition (Fig. 2.7B). For the siliciclastic-felsic subtype, although chalcopyrite from deposits at greenschist and amphibolite facies form a group separated from those at prehnite-pumpellyite and to a lesser extent middle greenschist metamorphism, the signature of chalcopyrite from this subtype as a whole is still distinctive from all other VMS sub-types (Fig. 2.7F). As such, the RF model remains robust even when metamorphic grade varies, i.e., the prediction is not significantly affected. The literature data used to validate the RF models also comprise samples from deposits that have undergone metamorphism at different conditions (Tables 2.7, 2.8). Yet, the RF models reported a high accuracy for prediction (>60%) in samples from the ultramafic-hosted Dergamysh deposit (Melekestseva et al., 2020b), affected by greenschist metamorphism (Table 2.8), in spite of the fact that the ultramafic class was trained exclusively with chalcopyrite from unmetamorphosed SMS deposits. Similarly, literature data from unmetamorphosed deposits, such as the bimodal-felsic Çayeli-Kutlular deposit (Revan et al., 2014), reported

more than 79% of samples correctly classified (Table 2.8), although the training set was mostly from deposits at the lower greenschist facies.

2.7 Conclusions

This study shows that trace element composition of chalcopyrite is principally controlled by the lithostratigraphic setting, which is affected by the host rock composition, but with a second order variation due to the temperature of the sulfide assemblage (Cu-rich vs. Zn-rich), in which chalcopyrite is replacing/precipitating. In addition, results demonstrate that metamorphic grade does not impact significantly on PLS-DA results nor on the ability of Random Forest models to identify VMS subtype. Chalcopyrite from ultramafic-hosted SMS setting is characterized by high content in Co, Ni and Te most likely as a result of leaching of these elements by the fluids during the alteration of the ferromagnesian minerals and magmatic sulfides of the footwall ultramafic rocks. Chalcopyrite from mafic-hosted VMS, although does not show significant differences in the most trace elements from the other subtypes, has higher concentrations of Pb, which could be derived from alteration of plagiogranites in the oceanic crust and/or result from the lack of galena co-precipitating in mafic-hosted deposits. Chalcopyrite from bimodal settings of VMS shows similar content for most elements since they are constituted by a variable proportion of mafic and felsic volcanic rocks, representing a transition of host rock composition. However, Au and Pb are enriched in chalcopyrite from the bimodal-felsic subtype, with Pb likely derived from the destruction of feldspar in felsic volcanic rocks. In siliciclastic-mafic deposits, chalcopyrite is particularly enriched in Mn. The presence of Mn-rich meta-exhalites in this deposit type suggests that Mn-rich hydrothermal fluids were involved in forming siliciclastic-mafic deposits, as recorded by chalcopyrite. Finally, in siliciclastic-felsic setting, chalcopyrite is characterized by high content of Sn, Sb, Bi and In, associated with a magmatic component in addition to footwall metasediments. On the other hand, chalcopyrite from Cu-rich samples is associated with high content of high-temperature elements (Bi, Co, Ni, Au, Ag, Te and Se), whereas those from Zn-rich samples are associated with high Ga, Sn, In, Sb and Tl, typical low-temperature assemblage, suggesting that during the zone refining process, a successive remobilization of these elements from sulfides previously formed at lower temperature (*e.g.,* sphalerite, galena, or pyrite) led to their incorporation into chalcopyrite at different replacement degrees.

We developed a set of three random forest models to classify chalcopyrite from VMS deposits according to the 6 lithostratigraphic subtypes proposed in the literature. Our approach consisting of one RF model to first classify chalcopyrite according to major host rock affinity and two subsequent RF models to reclassify chalcopyrite according to VMS subtype recorded an overall accuracy higher than 0.95. Further testing using data from the literature illustrates that the performance of the prediction of our classification model is determined by the deposit setting, number and importance of the variables used (quality of the data). Chalcopyrite from the ultramafic subtype shows the highest classification rates because this subtype is significantly different in trace element

composition from all others. The prediction results show the highest performance in prediction with literature data containing all elements required by the RF models. In studies with missing elements, the classification accuracy decreases significatively especially when a high number or the most important variables are missing. Finally, RF regression models indicate that there is a potential to predict ccp/(ccp+sp) ratio from trace element composition, and we suggest further studies involving a wider range of samples.

2.8 Acknowledgements

This study was funded by the Natural Science and Engineering Research Council of Canada (NSERC), Agnico Eagle Mines Limited, le Ministère de l'Energie et des Ressources Naturelles du Québec and the Portuguese Fundação para a Ciência e a Tecnologia (FCT) I.P./MCTES, through national funds (PIDDAC) – UIDB/50019/2020. We are very grateful to Dany Savard and Audrey Lavoie from LabMaTer, Université du Québec à Chicoutimi for their support with LA-ICP-MS analyses, to Marc Choquette and Suzie Coté from Université Laval for their assistance and support for SEM and EPMA analyzes and Edmond Rousseau for his support for sample preparation. Seafloor samples were taken during RV Sonne cruise SO216 to the Manus Basin (chief scientist W. Bach), RV Pourquoi Pas? cruise ODEMAR to Irinovskoe (chief scientist J. Escartin), and RV Meteor cruise M60/3 to Logatchev (chief scientist T. Kuhn). Officers and crews of these cruises, especially the ROV pilots, are gratefully acknowledged. We also thank Lisard Torró for fruitful discussions on the geodynamic and geologic setting of Cerro Maimón VMS deposit.

2.9 References

Abd Elrahman, S. M., and Abraham, A., 2013, A review of class imbalance problem: Journal of Network and Innovative Computing, v. 1, p. 332-340.

Agangi, A., Reddy, S., Plavsa, D., Vieru, C., Selvaraja, V., LaFlamme, C., Jeon, H., Martin, L., Nozaki, T., and Takaya, Y., 2018, Subsurface deposition of Cu-rich massive sulphide underneath a Palaeoproterozoic seafloor hydrothermal system—the Red Bore prospect, Western Australia: Mineralium Deposita, p. 1-18.

Aitchison, J., 1986, The statistical analysis of compositional data: London, Chapman and Hall, 416 p p.

Almodóvar, G. R., Yesares, L., Sáez, R., Toscano, M., González, F., and Pons, J. M., 2019, Massive Sulfide Ores in the Iberian Pyrite Belt: Mineralogical and Textural Evolution: Minerals, v. 9, p. 653.

Andersson, S. S., Jonsson, E., and Högdahl, K., 2016, Metamorphism and deformation of a Palaeoproterozoic polymetallic sulphide–oxide mineralisation: Hornkullen, Bergslagen, Sweden: GFF, v. 138, p. 410-423.

Antweiler, R. C., 2015, Evaluation of Statistical Treatments of Left-Censored Environmental Data Using Coincident Uncensored Data Sets. II. Group Comparisons: Environmental Science & Technology, v. 49, p. 13439-13446.

Averill, S. A., 2001, The application of heavy indicator mineralogy in mineral exploration with emphasis on base metal indicators in glaciated metamorphic and plutonic terrains: Geological Society, London, Special Publications, v. 185, p. 69-81.

Averill, S. A., 2011, Viable indicator minerals in surficial sediments for two major base metal deposit types: Ni-Cu-PGE and porphyry Cu: Geochemistry: Exploration, Environment, Analysis, v. 11, p. 279-291.

Bajwah, Z. U., Seccombe, P. K., and Offler, R., 1987, Trace element distribution, Co: Ni ratios and genesis of the Big Cadia iron-copper deposit, New South Wales, Australia: Mineralium Deposita, v. 22, p. 292-300.

Ballabio, D., and Consonni, V., 2013, Classification tools in chemistry. Part 1: linear models. PLS-DA: Analytical Methods, v. 5, p. 3790-3798.

Barker, R. D., Barker, S. L. L., Cracknell, M. J., Stock, E. D., and Holmes, G., 2021, Quantitative Mineral Mapping of Drill Core Surfaces II: Long-Wave Infrared Mineral Characterization Using µXRF and Machine Learning: Economic Geology, v. 116, p. 821-836.

Barnes, S.-J., Prichard, H. M., Cox, R. A., Fisher, P. C., and Godel, B., 2008, The location of the chalcophile and siderophile elements in platinum-group element ore deposits (a textural, microbeam and whole rock geochemical study): Implications for the formation of the deposits: Chemical Geology, v. 248, p. 295-317.

Barrie, C. D., Boyle, A. P., Cook, N. J., and Prior, D. J., 2010a, Pyrite deformation textures in the massive sulfide ore deposits of the Norwegian Caledonides: Tectonophysics, v. 483, p. 269-286.

Barrie, C. D., Boyle, A. P., Cook, N. J., and Prior, D. J., 2010b, Pyrite deformation textures in the massive sulfide ore deposits of the Norwegian Caledonides: Tectonophysics, v. 483, p. 269-286.

Barrie, C. D., Boyle, A. P., and Salter, M., 2009, How low can you go? - Extending downwards the limits of plastic deformation in pyrite: Mineralogical Magazine, v. 73, p. 895-913.

Barrie, C. T., and Hannington, M. D., 1999, Classification of volcanic-associated massive sulfide deposits based on host-rock composition: Reviews in Economic Geology, v. 8, p. 1-11.

Barton, P. B., and Bethke, P. M., 1987, Chalcopyrite disease in sphalerite; pathology and epidemiology: American Mineralogist, v. 72, p. 451-467.

Bédard, É., De Bronac de Vazelhes, V., and Beaudoin, G., 2022, Performance of predictive supervised classification models of trace elements in magnetite for mineral exploration: Journal of Geochemical Exploration, v. 236, p. 106959.

Bédard, É., Goulet, A., Sappin, A.-A., Makvandi, S., and Beaudoin, G., 2017, Chalcopyrite as an indicator mineral to fingerprint mineral deposit types: a preliminary study: Mineral Resources to Discover-Proceedings of the 14th SGA Biennial Meeting, Québec City, Canada, 2017, p. 1115-1118.

Binns, R. A., Barriga, F., and Miller, D. J., 2007, Leg 193 synthesis; anatomy of an active felsic hosted hydrothermal system, eastern Manus Basin, Papua New Guinea: Proceedings of the Ocean Drilling Program, Scientific Results (CD ROM), v. 193, p. 71.

Binns, R. A., McConachy, T., and McInnes, B., 2004, Eastern Manus basin, Papua New Guinea: Guides for volcanogenic massive sulphide exploration from a modern seafloor analogue: CSIRO Explores, v. 2, p. 59-80.

Bortnikov, N. S., Genkin, A. D., Dobrovol'Skaya, M. G., Muravitskaya, G. N., and Filimonova, A. A., 1991, The nature of chalcopyrite inclusions in sphalerite; exsolution, coprecipitation, or" disease"?: Economic Geology, v. 86, p. 1070-1082.

Breiman, L., 2001, Random Forests: Machine Learning, v. 45, p. 5-32.

Brereton, R. G., and Lloyd, G. R., 2014, Partial least squares discriminant analysis: taking the magic away: Journal of Chemometrics, v. 28, p. 213-225.

Brownlee, J., 2018, Master machine learning algorithms: Discover how they work and implement them from scratch, Melbourne, Machine Learning Mastery.

Brueckner, S. M., Piercey, S. J., Layne, G. D., Piercey, G., and Sylvester, P. J., 2015, Variations of sulphur isotope signatures in sulphides from the metamorphosed Ming Cu(−Au) volcanogenic massive sulphide deposit, Newfoundland Appalachians, Canada: Mineralium Deposita, v. 50, p. 619-640.

Brueckner, S. M., Piercey, S. J., Pilote, J.-L., Layne, G. D., and Sylvester, P. J., 2016, Mineralogy and mineral chemistry of the metamorphosed and precious metal-bearing Ming deposit, Canada: Ore Geology Reviews, v. 72, p. 914-939.

Butler, I. B., and Nesbitt, R. W., 1999, Trace element distributions in the chalcopyrite wall of a black smoker chimney: insights from laser ablation inductively coupled plasma mass spectrometry (LA–ICP–MS): Earth and Planetary Science Letters, v. 167, p. 335-345.

Cabri, L. J., Campbell, J. L., Laflamme, J. H. G., Leigh, R. G., Maxwell, J. A., and Scott, J. D., 1985, Proton-microprobe analysis of trace elements in sulfides from some massive-sulfide deposits: The Canadian Mineralogist, v. 23, p. 133-148.

Caraballo, E., Dare, S., and Beaudoin, G., 2022, Variation of trace elements in chalcopyrite from worldwide Ni-Cu sulfide and Reef-type PGE deposits: implications for mineral exploration: Mineralium Deposita, v. 57, p. 1293-1321.

Carvalho, J. R. S., Relvas, J., Pinto, A. M. M., Frenzel, M., Krause, J., Gutzmer, J., Pacheco, N., Fonseca, R., Santos, S., and Caetano, P., 2018, Indium and selenium distribution in the Neves-Corvo deposit, Iberian Pyrite Belt, Portugal: Mineralogical Magazine, v. 82, p. S5-S41.

Castroviejo, R., Quesada, C., and Soler, M., 2011, Post-depositional tectonic modification of VMS deposits in Iberia and its economic significance: Mineralium Deposita, v. 46, p. 615-637.

Chong, I.-G., and Jun, C.-H., 2005, Performance of some variable selection methods when multicollinearity is present: Chemometrics and intelligent laboratory systems, v. 78, p. 103-112.

Chorlton, L. B., 2007, Generalized geology of the world: bedrock domains and major faults in GIS format: Geological Survey of Canada, Open File, v. 5529.

Conn, C. D., Spry, P. G., Layton-Matthews, D., Voinot, A., and Koenig, A., 2019, The effects of amphibolite facies metamorphism on the trace element composition of pyrite and pyrrhotite in the Cambrian Nairne Pyrite Member, Kanmantoo Group, South Australia: Ore Geology Reviews, v. 114, p. 103128.

Cook, N. J., 1996, Mineralogy of the sulphide deposits at Sulitjelma, northern Norway: Ore Geology Reviews, v. 11, p. 303-338.

Cook, N. J., and Chryssoulis, S. L., 1990, Concentrations of invisible gold in the common sulfides: The Canadian Mineralogist, v. 28, p. 1-16.

Cook, N. J., Ciobanu, C. L., Danyushevsky, L. V., and Gilbert, S., 2011, Minor and trace elements in bornite and associated Cu–(Fe)-sulfides: A LA-ICP-MS studyBornite mineral chemistry: Geochimica et Cosmochimica Acta, v. 75, p. 6473-6496.

Cook, N. J., and Halls, C., 1990, Coticules at Sulitjalma, Norway and their possible origin: Norsk geologisk tidsskrift, v. 70, p. 153-158.

Crundwell, F. K., 2021, The impact of light on understanding the mechanism of dissolution and leaching of sphalerite (ZnS), pyrite (FeS2) and chalcopyrite (CuFeS2): Minerals Engineering, v. 161, p. 106728.

Crundwell, F. K., Bryson, L. J., van Aswegen, A., and Knights, B. D. H., 2021, Effect of chopped light on the dissolution and leaching of chalcopyrite: Minerals Engineering, v. 160, p. 106703.

Czamanske, G. K., Kunilov, V. E., Zientek, M. L., Cabri, L. J., Likhachev, A. P., Calk, L. C., and Oscarson, R. L., 1992, A proton microprobe study of magmatic sulfide ores from the Noril'sk-Talnakh District, Siberia: The Canadian Mineralogist, v. 30, p. 249-287.

Dare, S. A., Barnes, S.-J., Prichard, H. M., and Fisher, P. C., 2014, Mineralogy and geochemistry of Cu-rich ores from the McCreedy East Ni-Cu-PGE deposit (Sudbury, Canada): implications for the behavior of platinum group and chalcophile elements at the end of crystallization of a sulfide liquid: Economic Geology, v. 109, p. 343-366.

Dare, S. A. S., Barnes, S.-J., and Prichard, H. M., 2010, The distribution of platinum group elements (PGE) and other chalcophile elements among sulfides from the Creighton Ni–Cu–PGE sulfide deposit, Sudbury, Canada, and the origin of palladium in pentlandite: Mineralium Deposita, v. 45, p. 765-793.

Dare, S. A. S., Barnes, S.-J., Prichard, H. M., and Fisher, P. C., 2011, Chalcophile and platinum-group element (PGE) concentrations in the sulfide minerals from the McCreedy East deposit, Sudbury, Canada, and the origin of PGE in pyrite: Mineralium Deposita, v. 46, p. 381-407.

Dehnavi, A. S., McFarlane, C. R. M., Lentz, D. R., and Walker, J. A., 2018, Assessment of pyrite composition by LA-ICP-MS techniques from massive sulfide deposits of the Bathurst Mining Camp, Canada: from textural and chemical evolution to its application as a vectoring tool for the exploration of VMS deposits: Ore Geology Reviews, v. 92, p. 656-671.

Digis Team, 2022, GEOROC Compilation: Rock Types, Goettingen Research Online.data.

Dubé, B., Gosselin, P., Mercier-Langevin, P., Hannington, M., and Galley, A., 2007, Gold-rich volcanogenic massive sulphide deposits: Geological Association of Canada, Mineral Deposits Division, p. 75-94.

Dunn, K., 2019, Process improvement using data: Experimentation for Improvement. Hamilton, Ontario, Canada. Creative Commons Attribution-ShareAlike, v. 4, p. 325-404.

Duran, C. J., Barnes, S.-J., and Corkery, J. T., 2016, Trace element distribution in primary sulfides and Fe–Ti oxides from the sulfide-rich pods of the Lac des Iles Pd deposits, Western Ontario, Canada: Constraints

on processes controlling the composition of the ore and the use of pentlandite compositions in exploration: Journal of Geochemical Exploration, v. 166, p. 45-63.

Duran, C. J., Barnes, S.-J., Mansur, E. T., Dare, S. A. S., Bédard, L. P., and Sluzhenikin, S. F., 2020, Magnetite chemistry by LA-ICP-MS records sulfide fractional crystallization in massive nickel-copper-platinum group element ores from the Norilsk-Talnakh mining district (Siberia, Russia): Implications for trace element partitioning into magnetite: Economic Geology, v. 115, p. 1245-1266.

Duran, C. J., Dubé-Loubert, H., Pagé, P., Barnes, S.-J., Roy, M., Savard, D., Cave, B. J., Arguin, J.-P., and Mansur, E. T., 2019a, Applications of trace element chemistry of pyrite and chalcopyrite in glacial sediments to mineral exploration targeting: Example from the Churchill Province, northern Quebec, Canada: Journal of Geochemical Exploration, v. 196, p. 105-130.

Duran, C. J., Dubé-Loubert, H., Pagé, P., Barnes, S.-J., Roy, M., Savard, D., Cave, B. J., Arguin, J.-P., and Mansur, E. T., 2019b, Applications of trace element chemistry of pyrite and chalcopyrite in glacial sediments to mineral exploration targeting: Example from the Churchill Province, northern Quebec, Canada: Journal of Geochemical Exploration.

Egozcue, J. J., and Pawlowsky-Glahn, V., 2011, Análisis composicional de datos en Ciencias Geoambientales: Boletín Geológico y Minero, v. 122, p. 439-452.

Eldridge, C. S., Barton, P. B., Jr., and Ohmoto, H., 1983, Mineral Textures and Their Bearing on Formation of the Kuroko Orebodies, *in* Ohmoto, H., and Skinner, B. J., eds., The Kuroko and Related Volcanogenic Massive Sulfide Deposits, 5, Society of Economic Geologists, p. 0.

Favilla, S., Durante, C., Vigni, M. L., and Cocchi, M., 2013, Assessing feature relevance in NPLS models by VIP: Chemometrics and Intelligent Laboratory Systems, v. 129, p. 76-86.

Filzmoser, P., Hron, K., and Reimann, C., 2009, Principal component analysis for compositional data with outliers: Environmetrics, v. 20, p. 621-632.

Franklin, J., Gibson, H., and Jonasson, G., 2005, Volcanogenic massive sulfide deposit: Economic Geology 100th Anniversary Volume, p. 523-560.

Frenzel, M., Hirsch, T., and Gutzmer, J., 2016, Gallium, germanium, indium, and other trace and minor elements in sphalerite as a function of deposit type—A meta-analysis: Ore Geology Reviews, v. 76, p. 52-78.

Fuchs, S., Hannington, M. D., and Petersen, S., 2019, Divining gold in seafloor polymetallic massive sulfide systems: Mineralium Deposita, v. 54, p. 789-820.

Galley, A. G., Hannington, M. D., and Jonasson, I., 2007, Volcanogenic massive sulphide deposits: Mineral deposits of Canada: A synthesis of major deposit-types, district metallogeny, the evolution of geological provinces, and exploration methods: Geological Association of Canada, Mineral Deposits Division, Special Publication, v. 5, p. 141-161.

Genna, D., and Gaboury, D., 2015, Deciphering the hydrothermal evolution of a VMS system by LA-ICP-MS using trace elements in pyrite: an example from the Bracemac-McLeod deposits, Abitibi, Canada, and implications for exploration: Economic Geology, v. 110, p. 2087-2108.

Genna, D., and Gaboury, D., 2019, Use of semi-volatile metals as a new vectoring tool for VMS exploration: Example from the Zn-rich McLeod deposit, Abitibi, Canada: Journal of Geochemical Exploration, v. 207, p. 106358.

George, L., Cook, N. J., Ciobanu, C. L., and Wade, B. P., 2015, Trace and minor elements in galena: A reconnaissance LA-ICP-MS study: American Mineralogist, v. 100, p. 548-569.

George, L. L., Biagioni, C., D'Orazio, M., and Cook, N. J., 2018a, Textural and trace element evolution of pyrite during greenschist facies metamorphic recrystallization in the southern Apuan Alps (Tuscany, Italy): Influence on the formation of Tl-rich sulfosalt melt: Ore Geology Reviews, v. 102, p. 59-105.

George, L. L., Cook, N. J., and Ciobanu, C. L., 2016, Partitioning of trace elements in co-crystallized sphalerite–galena–chalcopyrite hydrothermal ores: Ore Geology Reviews, v. 77, p. 97-116.

George, L. L., Cook, N. J., Crowe, B. B., and Ciobanu, C. L., 2018b, Trace elements in hydrothermal chalcopyrite: Mineralogical Magazine, v. 82, p. 59-88.

Gislason, P. O., Benediktsson, J. A., and Sveinsson, J. R., 2006, Random forests for land cover classification: Pattern recognition letters, v. 27, p. 294-300.

Godel, B., and Barnes, S.-J., 2008, Platinum-group elements in sulfide minerals and the whole rocks of the JM Reef (Stillwater Complex): Implication for the formation of the reef: Chemical Geology, v. 248, p. 272-294.

Goodfellow, W. D., 2007, Metallogeny of the Bathurst mining camp, northern New Brunswick: Mineral deposits of Canada. A synthesis of major deposit-type, district metallogeny, the evolution of geological provinces and exploration methods. Edited by WD Goodfellow. Geological Association of Canada, Mineral Deposits Division, Special Publication, v. 5, p. 449-469.

Gosselin, R., Rodrigue, D., and Duchesne, C., 2010, A Bootstrap-VIP approach for selecting wavelength intervals in spectral imaging applications: Chemometrics and Intelligent Laboratory Systems, v. 100, p. 12-21.

Gregory, D. D., Cracknell, M. J., Large, R. R., McGoldrick, P., Kuhn, S., Maslennikov, V. V., Baker, M. J., Fox, N., Belousov, I., Figueroa, M. C., Steadman, J. A., Fabris, A. J., and Lyons, T. W., 2019, Distinguishing Ore Deposit Type and Barren Sedimentary Pyrite Using Laser Ablation-Inductively Coupled Plasma-Mass Spectrometry Trace Element Data and Statistical Analysis of Large Data Sets: Economic Geology, v. 114, p. 771-786.

Grömping, U., 2009, Variable Importance Assessment in Regression: Linear Regression versus Random Forest: The American Statistician, v. 63, p. 308-319.

Grzela, D., Beaudoin, G., and Bédard, É., 2019, Tourmaline, scheelite, and magnetite compositions from orogenic gold deposits and glacial sediments of the Val-d'Or district (Quebec, Canada): Applications to mineral exploration: Journal of Geochemical Exploration, v. 206, p. 106355.

Han, H., Guo, X., and Yu, H., 2016, Variable selection using mean decrease accuracy and mean decrease gini based on random forest: 7th IEEE International Conference on Software Engineering And Service Science (ICSESS), 2016, p. 219-224.

Hannington, M. D., 2014, 13.18 - Volcanogenic Massive Sulfide Deposits, *in* Holland, H. D., and Turekian, K. K., eds., Treatise on Geochemistry (Second Edition): Oxford, Elsevier, p. 463-488.

Hannington, M. D., de Ronde, C. D., and Petersen, S., 2005, Sea-Floor Tectonics and Submarine Hydrothermal Systems, One Hundredth Anniversary Volume, Society of Economic Geologists, p. 111–141.

Hannington, M. D., Jonasson, I. R., Herzig, P. M., and Petersen, S., 1995, Physical and chemical processes of seafloor mineralization at mid-ocean ridges: Seafloor hydrothermal systems: Physical, chemical, biological, and geological interactions, v. 91, p. 115-157.

Harris, D. C., Cabri, L. J., and Nobiling, R., 1984, Silver-bearing chalcopyrite, a principal source of silver in the Izok Lake massive-sulfide deposit; confirmation by electron-and proton-microprobe analyses: The Canadian Mineralogist, v. 22, p. 493-498.

Harris, J. R., and Grunsky, E. C., 2015, Predictive lithological mapping of Canada's North using Random Forest classification applied to geophysical and geochemical data: Computers & Geosciences, v. 80, p. 9-25.

Hashmi, S., Ward, B., Plouffe, A., Leybourne, M., and Ferbey, T., 2015, Geochemical and mineralogical dispersal in till from the Mount Polley Cu-Au porphyry deposit, central British Columbia, Canada: Geochemistry: Exploration, Environment, Analysis, v. 15, p. 234-249.

Hattori, K. H., Arai, S., and Clarke, D. B., 2002, Selenium, tellurium, arsenic and antimony contents of primary mantle sulfides: The Canadian Mineralogist, v. 40, p. 637-650.

Hawley, J. E., and Nichol, I., 1961, Trace elements in pyrite, pyrrhotite and chalcopyrite of different ores: Economic Geology, v. 56, p. 467-487.

Hazarika, P., Mishra, B., and Pruseth, K. L., 2015, Diverse tourmaline compositions from orogenic gold deposits in the Hutti-Maski greenstone belt, India: implications for sources of ore-forming fluids: Economic Geology, v. 110, p. 337-353.

Hofmann, A. W., 1988, Chemical differentiation of the Earth: the relationship between mantle, continental crust, and oceanic crust: Earth and Planetary Science Letters, v. 90, p. 297-314.

Hron, K., Templ, M., and Filzmoser, P., 2010, Imputation of missing values for compositional data using classical and robust methods: Computational Statistics & Data Analysis, v. 54, p. 3095-3107.

Huston, D. L., Relvas, J. M. R. S., Gemmell, J. B., and Drieberg, S., 2011, The role of granites in volcanic-hosted massive sulphide ore-forming systems: an assessment of magmatic–hydrothermal contributions: Mineralium Deposita, v. 46, p. 473-507.

Huston, D. L., Sie, S. H., Suter, G. F., Cooke, D. R., and Both, R. A., 1995, Trace elements in sulfide minerals from eastern Australian volcanic-hosted massive sulfide deposits; Part I, Proton microprobe analyses of pyrite, chalcopyrite, and sphalerite, and Part II, Selenium levels in pyrite; comparison with delta 34 S values and implications for the source of sulfur in volcanogenic hydrothermal systems: Economic Geology, v. 90, p. 1167-1196.

Ishihara, S., and Endo, Y., 2007, Indium and other trace elements in volcanogenic massive sulfide ores from the Kuroko, Besshi and other types in Japan: Bull. Geol. Surv. Japan, v. 58, p. 7-22.

Jochum, K. P., Nohl, U., Herwig, K., Lammel, E., Stoll, B., and Hofmann, A. W., 2005, GeoReM: a new geochemical database for reference materials and isotopic standards: Geostandards and Geoanalytical Research, v. 29, p. 333-338.

Kase, K., 1987, Tin-bearing chalcopyrite from the Izumo vein, Toyoha mine, Hokkaido, Japan: The Canadian Mineralogist, v. 25, p. 9-13.

Kuhn, M., 2008, Building Predictive Models in R Using the caret Package: Journal of Statistical Software, v. 28, p. 1 - 26.

Kuhn, M., and Johnson, K., 2013, Applied predictive modeling: New York, Springer, 600 p.

Li, X., Zhao, K.-D., Jiang, S.-Y., and Palmer, M. R., 2019, In-situ U-Pb geochronology and sulfur isotopes constrain the metallogenesis of the giant Neves Corvo deposit, Iberian Pyrite Belt: Ore Geology Reviews, v. 105, p. 223-235.

Liu, H., and Beaudoin, G., 2021, Geochemical signatures in native gold derived from Au-bearing ore deposits: Ore Geology Reviews, p. 104066.

Liu, H., Beaudoin, G., Makvandi, S., Jackson, S. E., and Huang, X., 2021, Multivariate statistical analysis of trace element compositions of native gold from orogenic gold deposits: implication for mineral exploration: Ore Geology Reviews, p. 104061.

Lockington, J. A., Cook, N. J., and Ciobanu, C. L., 2014, Trace and minor elements in sphalerite from metamorphosed sulphide deposits: Mineralogy and Petrology, v. 108, p. 873-890.

Lydon, J., 1988, Ore deposit models# 14. Volcanogenic massive sulphide deposits Part 2: Genetic models: Geoscience Canada, v. 15, p. 43-65.

Makvandi, S., Ghasemzadeh-Barvarz, M., Beaudoin, G., Grunsky, E. C., Beth McClenaghan, M., and Duchesne, C., 2016a, Principal component analysis of magnetite composition from volcanogenic

massive sulfide deposits: Case studies from the Izok Lake (Nunavut, Canada) and Halfmile Lake (New Brunswick, Canada) deposits: Ore Geology Reviews, v. 72, p. 60-85.

Makvandi, S., Ghasemzadeh-Barvarz, M., Beaudoin, G., Grunsky, E. C., McClenaghan, M. B., Duchesne, C., and Boutroy, E., 2016b, Partial least squares-discriminant analysis of trace element compositions of magnetite from various VMS deposit subtypes: Application to mineral exploration: Ore Geology Reviews, v. 78, p. 388-408.

Manéglia, N., Beaudoin, G., and Simard, M., 2018, Indicator minerals of the Meliadine orogenic gold deposits, Nunavut (Canada), and application to till surveys: Geochemistry: Exploration, Environment, Analysis, v. 18, p. 241-251.

Mansur, E. T., Barnes, S.-J., Duran, C. J., and Sluzhenikin, S. F., 2020, Distribution of chalcophile and platinum-group elements among pyrrhotite, pentlandite, chalcopyrite and cubanite from the Noril'sk-Talnakh ores: Implications for the formation of platinum-group minerals: Mineralium Deposita, v. 55, p. 1215-1232.

Marfin, A. E., Ivanov, A. V., Abramova, V. D., Anziferova, T. N., Radomskaya, T. A., Yakich, T. Y., and Bestemianova, K. V., 2020, A Trace Element Classification Tree for Chalcopyrite from Oktyabrsk Deposit, Norilsk–Talnakh Ore District, Russia: LA-ICPMS Study: Minerals, v. 10, p. 716.

Marignac, C., Diagana, B., Cathelineau, M., Boiron, M.-C., Banks, D., Fourcade, S., and Vallance, J., 2003, Remobilisation of base metals and gold by Variscan metamorphic fluids in the south Iberian pyrite belt: evidence from the Tharsis VMS deposit: Chemical Geology, v. 194, p. 143-165.

Marques, A. F. A., Relvas, J. M. R. S., Scott, S. D., Rosa, C., and Guillong, M., 2020, Melt inclusions in quartz from felsic volcanic rocks of the Iberian Pyrite Belt: clues for magmatic ore metal transfer towards VMS-forming systems: Ore Geology Reviews, v. 126, p. 103743.

Marshall, B., Vokes, F. M., and Larocque, A. C. L., 1998, Regional Metamorphic Remobilization: Upgrading and Formation of Ore Deposits, *in* Vokes, F. M., Marshall, B., and Spry, P. G., eds., Metamorphic and Metamorphogenic Ore Deposits, 11, Society of Economic Geologists, p. 0.

Martin, A. J., Keith, M., McDonald, I., Haase, K. M., McFall, K. A., Klemd, R., and MacLeod, C. J., 2019, Trace element systematics and ore-forming processes in mafic VMS deposits: Evidence from the Troodos ophiolite, Cyprus: Ore Geology Reviews, v. 106, p. 205-225.

Maslennikov, V. V., Maslennikova, S. P., Large, R. R., and Danyushevsky, L. V., 2009, Study of trace element zonation in vent chimneys from the Silurian Yaman-Kasy volcanic-hosted massive sulfide deposit (Southern Urals, Russia) using laser ablation-inductively coupled plasma mass spectrometry (LA-ICPMS): Economic Geology, v. 104, p. 1111-1141.

Maslennikov, V. V., Maslennikova, S. P., Large, R. R., Danyushevsky, L. V., Herrington, R. J., Ayupova, N. R., Zaykov, V. V., Lein, A. Y., Tseluyko, A. S., Melekestseva, I. Y., and Tessalina, S. G., 2017, Chimneys in Paleozoic massive sulfide mounds of the Urals VMS deposits: Mineral and trace element comparison with modern black, grey, white and clear smokers: Ore Geology Reviews, v. 85, p. 64-106.

McClenaghan, M. B., 2005, Indicator mineral methods in mineral exploration: Geochemistry: Exploration, Environment, Analysis, v. 5, p. 233-245.

Megahed, F. M., Chen, Y.-J., Megahed, A., Ong, Y., Altman, N., and Krzywinski, M., 2021, The class imbalance problem: Nature Methods, v. 18, p. 1270-1272.

Mehmood, T., Liland, K. H., Snipen, L., and Sæbø, S., 2012, A review of variable selection methods in partial least squares regression: Chemometrics and Intelligent Laboratory Systems, v. 118, p. 62-69.

Melekestseva, I., Maslennikov, V., Tret'yakov, G., Maslennikova, S., Danyushevsky, L., Kotlyarov, V., Large, R., Beltenev, V., and Khvorov, P., 2020a, Trace Element Geochemistry of Sulfides from the Ashadze-2

Hydrothermal Field (12°58' N, Mid-Atlantic Ridge): Influence of Host Rocks, Formation Conditions or Seawater?: Minerals, v. 10.

Melekestseva, I. Y., Maslennikov, V. V., and Maslennikova, S. P., 2020b, Trace-elements in sulfides of the Dergamysh cobalt-bearing massive sulfide deposit, the Southern Urals: Mode of occurrence and matter sources: Lithosphere (Russia), v. 20, p. 499-516.

Mendez, K. M., Broadhurst, D. I., and Reinke, S. N., 2020, Migrating from partial least squares discriminant analysis to artificial neural networks: a comparison of functionally equivalent visualisation and feature contribution tools using jupyter notebooks: Metabolomics, v. 16, p. 17.

Mercier-Langevin, P., Dubé, B., Hannington, M. D., Davis, D. W., Lafrance, B., and Gosselin, G., 2007, The LaRonde Penna Au-Rich Volcanogenic Massive Sulfide Deposit, Abitibi Greenstone Belt, Quebec: Part I. Geology and Geochronology*: Economic Geology, v. 102, p. 585-609.

Mercier-Langevin, P., Hannington, M. D., Dubé, B., and Bécu, V., 2011, The gold content of volcanogenic massive sulfide deposits: Mineralium Deposita, v. 46, p. 509-539.

Michael, F., Georges, M., and John, F., 2013, Elliptical Insights: Understanding Statistical Methods through Elliptical Geometry: Statistical Science, v. 28, p. 1-39.

Miranda, A. C. R., Beaudoin, G., and Rottier, B., 2022, Scheelite chemistry from skarn systems: implications for ore-forming processes and mineral exploration: Mineralium Deposita.

Moggi-Cecchi, V., Cipriani, C., Rossi, P., Ceccato, D., Rudello, V., and Somacal, H., 2002, Trace element contents and distribution maps of chalcopyrite: a micro-PIXE study: PERIODICO di MINERALOGIA, v. 71, p. 101-9.

Nagase, T., and Kojima, S., 1997, An SEM examination of the chalcopyrite disease texture and its genetic implications: Mineralogical Magazine, v. 61, p. 89-97.

Ohmoto, H., 1996, Formation of volcanogenic massive sulfide deposits: the Kuroko perspective: Ore Geology Reviews, v. 10, p. 135-177.

Palarea-Albaladejo, J., and Martín-Fernández, J. A., 2008, A modified EM alr-algorithm for replacing rounded zeros in compositional data sets: Computers & Geosciences, v. 34, p. 902-917.

Palarea-Albaladejo, J., and Martín-Fernández, J. A., 2015, zCompositions—R package for multivariate imputation of left-censored data under a compositional approach: Chemometrics and Intelligent Laboratory Systems, v. 143, p. 85-96.

Palarea-Albaladejo, J., Martín-Fernández, J. A., and Gómez-García, J., 2007, A parametric approach for dealing with compositional rounded zeros: Mathematical Geology, v. 39, p. 625-645.

Paton, C., Hellstrom, J., Paul, B., Woodhead, J., and Hergt, J., 2011, Iolite: Freeware for the visualisation and processing of mass spectrometric data: Journal of Analytical Atomic Spectrometry, v. 26, p. 2508-2518.

Patten, C. G. C., Coltat, R., Junge, M., Peillod, A., Ulrich, M., Manatschal, G., and Kolb, J., 2022, Ultramafic-hosted volcanogenic massive sulfide deposits: an overlooked sub-class of VMS deposit forming in complex tectonic environments: Earth-Science Reviews, v. 224, p. 103891.

Patten, C. G. C., Pitcairn, I. K., and Teagle, D. A. H., 2017, Hydrothermal mobilisation of Au and other metals in supra-subduction oceanic crust: Insights from the Troodos ophiolite: Ore Geology Reviews, v. 86, p. 487-508.

Patten, C. G. C., Pitcairn, I. K., Teagle, D. A. H., and Harris, M., 2016, Mobility of Au and related elements during the hydrothermal alteration of the oceanic crust: implications for the sources of metals in VMS deposits: Mineralium Deposita, v. 51, p. 179-200.

Pawlowsky-Glahn, V., and Buccianti, A., 2011, Compositional data analysis: Theory and applications, John Wiley & Sons, 378 p, 378 p.

Pedersen, R.-B., Furnes, H., and Dunning, G., 1991, A U/Pb age for the Sulitjelma Gabbro, North Norway: further evidence for the development of a Caledonian marginal basin in Ashgill–Llandovery time: Geological Magazine, v. 128, p. 141-153.

Pilote, J.-L., Piercey, S. J., and Mercier-Langevin, P., 2020, Evolution of the subseafloor hydrothermal system associated with the Ming VMS deposit, Newfoundland Appalachians, and its controls on base and precious metal distribution: Mineralium Deposita, v. 55, p. 913-936.

Piña, R., Gervilla, F., Barnes, S.-J., Ortega, L., and Lunar, R., 2012, Distribution of platinum-group and chalcophile elements in the Aguablanca Ni–Cu sulfide deposit (SW Spain): evidence from a LA-ICP-MS study: Chemical Geology, v. 302, p. 61-75.

Plouffe, A., Ferbey, T., Hashmi, S., and Ward, B., 2016, Till geochemistry and mineralogy: vectoring towards Cu porphyry deposits in British Columbia, Canada: Geochemistry: Exploration, Environment, Analysis, v. 16, p. 213-232.

Provost, F., and Saar-Tsechanski, M., 2007, Handling Missing Values when Applying Classification Models: Journal of Machine Learning Research, v. 8, p. 1625-1657.

Reich, M., Deditius, A., Chryssoulis, S., Li, J.-W., Ma, C.-Q., Parada, M. A., Barra, F., and Mittermayr, F., 2013a, Pyrite as a record of hydrothermal fluid evolution in a porphyry copper system: A SIMS/EMPA trace element study: Geochimica et Cosmochimica Acta, v. 104, p. 42-62.

Reich, M., Palacios, C., Barra, F., and Chryssoulis, S., 2013b, "Invisible" silver in chalcopyrite and bornite from the Mantos Blancos Cu deposit, northern Chile: European Journal of Mineralogy, v. 25, p. 453-460.

Reich, M., Román, N., Barra, F., and Morata, D., 2020, Silver-rich chalcopyrite from the active Cerro Pabellón geothermal system, Northern Chile: Minerals, v. 10, p. 113.

Relvas, J. M., Tassinari, C. C., Munhá, J., and Barriga, F. J., 2001, Multiple sources for ore-forming fluids in the Neves Corvo VHMS Deposit of the Iberian Pyrite Belt (Portugal): strontium, neodymium and lead isotope evidence: Mineralium Deposita, v. 36, p. 416-427.

Relvas, J. M. R. S., Barriga, F. J. A. S., Ferreira, A., Noiva, P. C., Pacheco, N., and Barriga, G., 2006, Hydrothermal alteration and mineralization in the Neves-Corvo volcanic-hosted massive sulfide deposit, Portugal. I. Geology, mineralogy, and geochemistry: Economic Geology, v. 101, p. 753-790.

Ren, Y., Wohlgemuth-Ueberwasser, C. C., Huang, F., Shi, X., Li, B., Oelze, M., Schreiber, A., and Wirth, R., 2021, Distribution of trace elements in sulfides from Deyin hydrothermal field, Mid-Atlantic Ridge – Implications for its mineralizing processes: Ore Geology Reviews, v. 128, p. 103911.

Revan, M. K., Genç, Y., Maslennikov, V. V., Maslennikova, S. P., Large, R. R., and Danyushevsky, L. V., 2014, Mineralogy and trace-element geochemistry of sulfide minerals in hydrothermal chimneys from the Upper-Cretaceous VMS deposits of the eastern Pontide orogenic belt (NE Turkey): Ore Geology Reviews, v. 63, p. 129-149.

Rimstidt, J. D., Chermak, J. A., and Gagen, P. M., 1993, Rates of Reaction of Galena, Sphalerite, Chalcopyrite, and Arsenopyrite with Fe(III) in Acidic Solutions, Environmental Geochemistry of Sulfide Oxidation, 550. ACS Symposium Series, American Chemical Society, p. 2-13.

Roo, J. A. d., and Staal, C. R. v., 2003, Sulfide Remobilization and Sulfide Breccias in the Heath Steele and Brunswick Deposits, Bathurst Mining Camp, New Brunswick*, *in* Goodfellow, W. D., McCutcheon, S. R., and Peter, J. M., eds., Massive Sulfide Deposits of the Bathurst Mining Camp, New Brunswick, and Northern Maine, 11, Society of Economic Geologists, p. 0.

Rose, A. W., 1967, Trace elements in solflde minerals from the Central district, New Mexico and the Bingham district, Utah: Geochimica et Cosmochimica Acta, v. 31, p. 547-585.

Ruiz-Perez, D., Guan, H., Madhivanan, P., Mathee, K., and Narasimhan, G., 2020, So you think you can PLS-DA?: BMC Bioinformatics, v. 21, p. 207225.

Sciuba, M., and Beaudoin, G., 2021, Texture and Trace Element Composition of Rutile in Orogenic Gold Deposits: Economic Geology, v. 116, p. 1865-1892.

Sciuba, M., Beaudoin, G., Grzela, D., and Makvandi, S., 2020, Trace element composition of scheelite in orogenic gold deposits: Mineralium Deposita, v. 55, p. 1149–1172.

Sciuba, M., Beaudoin, G., and Makvandi, S., 2021, Chemical composition of tourmaline in orogenic gold deposits: Mineralium Deposita, v. 56, p. 537-560.

Seward, T. M., Williams-Jones, A. E., and Migdisov, A. A., 2014, The chemistry of metal transport and deposition by ore-forming hydrothermal fluids, *in* Holland, H. D., and Tukerian, K. K., eds., Treatise on geochemistry, 13, Elsevier Oxford, p. 29-57.

Shanks, W. C., Koski, R. A., Mosier, D. L., Schulz, K. J., Morgan, L. A., Slack, J. F., Ridley, W. I., Dusel-Bacon, C., Seal Ii, R. R., and Piatak, N. M., 2012, Volcanogenic massive sulfide occurrence model: Chapter C in Mineral deposit models for resource assessment, *in* Shanks, W. C., and Thurston, R., eds., Scientific Investigations Report: Reston, VA, US Department of the Interior, US Geological Survey.

Skyttä, P., Weihed, P., Högdahl, K., Bergman, S., and Stephens, M. B., 2020, Paleoproterozoic (2.0–1.8 Ga) syn-orogenic sedimentation, magmatism and mineralization in the Bothnia–Skellefteå lithotectonic unit, Svecokarelian orogen, Sweden: Lithotectonic Framework, Tectonic Evolution and Mineral Resources, 50, Geological Society of London, p. 0.

Slack, J. F., Offield, T. W., Woodruff, L. G., and Shanks, W. C., 2001, Geology and geochemistry of Besshi-type massive sulfide deposits of the Vermont copper belt: Part II. Environmental Geochemistry and Mining History of Massive Sulfide Deposits in the Vermont Copper Belt: Society of Economic Geologists Guidebook Series, v. 35, p. 193-211.

Spry, P. G., Peter, J. M., and Slack, J. F., 1998, Meta-exhalites as exploration guides to ore: Reviews in Economic Geology, v. 11, p. 163-201.

Stakes, D. S., and Taylor, H. P., 2003, Oxygen isotope and chemical studies on the origin of large plagiogranite bodies in northern Oman, and their relationship to the overlying massive sulphide deposits: Geological Society, London, Special Publications, v. 218, p. 315.

Steadman, J. A., and Large, R. R., 2016, Synsedimentary, Diagenetic, and Metamorphic Pyrite, Pyrrhotite, and Marcasite at the Homestake BIF-Hosted Gold Deposit, South Dakota, USA: Insights on Au-As Ore Genesis from Textural and LA-ICP-MS Trace Element Studies: Economic Geology, v. 111, p. 1731-1752.

Svetnik, V., Liaw, A., Tong, C., Culberson, J. C., Sheridan, R. P., and Feuston, B. P., 2003, Random Forest: A Classification and Regression Tool for Compound Classification and QSAR Modeling: Journal of Chemical Information and Computer Sciences, v. 43, p. 1947-1958.

Tarawneh, A. S., Hassanat, A. B., Altarawneh, G. A., and Almuhaimeed, A., 2022, Stop Oversampling for Class Imbalance Learning: A Review: IEEE Access, v. 10, p. 47643-47660.

Thabtah, F., Hammoud, S., Kamalov, F., and Gonsalves, A., 2020, Data imbalance in classification: Experimental evaluation: Information Sciences, v. 513, p. 429-441.

Tomkins, A. G., 2007, Three mechanisms of ore re-mobilisation during amphibolite facies metamorphism at the Montauban Zn–Pb–Au–Ag deposit: Mineralium Deposita, v. 42, p. 627-637.

Tomkins, A. G., Pattison, D. R. M., and Frost, B. R., 2007, On the initiation of metamorphic sulfide anatexis: Journal of Petrology, v. 48, p. 511-535.

Tornos, F., 2006, Environment of formation and styles of volcanogenic massive sulfides: The Iberian Pyrite Belt: Ore Geology Reviews, v. 28, p. 259-307.

Torró, L., Benites, D., Vallance, J., Laurent, O., Ortiz-Benavente, B. A., Chelle-Michou, C., Proenza, J. A., and Fontboté, L., 2022, Trace element geochemistry of sphalerite and chalcopyrite in arc-hosted VMS deposits: Journal of Geochemical Exploration, v. 232, p. 106882.

Vasyukova, O. V., and Williams-Jones, A. E., 2022, Constraints on the Genesis of Cobalt Deposits: Part II. Applications to Natural Systems: Economic Geology, v. 117, p. 529-544.

Wang, Y., Han, X., Petersen, S., Frische, M., Qiu, Z., Cai, Y., and Zhou, P., 2018, Trace Metal Distribution in Sulfide Minerals from Ultramafic-Hosted Hydrothermal Systems: Examples from the Kairei Vent Field, Central Indian Ridge: Minerals, v. 8, p. 526.

Wang, Z., Xu, D., Zhang, Z., Zou, F., Wang, L., Yu, L., and Hu, M., 2015, Mineralogy and trace element geochemistry of the Co-and Cu-bearing sulfides from the Shilu Fe–Co–Cu ore district in Hainan Province of South China: Journal of Asian Earth Sciences, v. 113, p. 980-997.

Weihed, P., Weihed, J. B., Sorjonen-Ward, P., and Matsson, B., 2002, Post-deformation, sulphide-quartz vein hosted gold ore in the footwall alteration zone of the Palaeoproterozoic Långdal VHMS deposit, Skellefte District, northern Sweden: GFF, v. 124, p. 201-210.

Weiss, G. M., 2013, Foundations of imbalanced learning, *in* He, H., and Ma, Y., eds., Imbalanced Learning: Foundations, Algorithms, and Applications, Wiley Online Library, p. 13-41.

Wilcox, R. R., 2011, Introduction to robust estimation and hypothesis testing, Academic press, 608 p.

Wilson, S. A., Ridley, W. I., and Koenig, A. E., 2002, Development of sulfide calibration standards for the laser ablation inductively-coupled plasma mass spectrometry technique: Journal of Analytical Atomic Spectrometry, v. 17, p. 406-409.

Wohlgemuth-Ueberwasser, C. C., Viljoen, F., Petersen, S., and Vorster, C., 2015, Distribution and solubility limits of trace elements in hydrothermal black smoker sulfides: An in-situ LA-ICP-MS study: Geochimica et Cosmochimica Acta, v. 159, p. 16-41.

Wold, S., Sjöström, M., and Eriksson, L., 2001, PLS-regression: a basic tool of chemometrics: Chemometrics and intelligent laboratory systems, v. 58, p. 109-130.

Workman, R. K., and Hart, S. R., 2005, Major and trace element composition of the depleted MORB mantle (DMM): Earth and Planetary Science Letters, v. 231, p. 53-72.

Xing, B., Mao, J., Xiao, X., Liu, H., Zhang, C., Guo, S., Li, H., Huang, W., and Lai, C., 2022, Metallogenic discrimination by sphalerite trace element geochemistry: An example from the Fengyan Zn-Pb deposit in central Fujian, SE China: Ore Geology Reviews, v. 141, p. 104651.

Zhang, J., Shao, Y., Liu, Z., and Chen, K., 2022, Sphalerite as a record of metallogenic information using multivariate statistical analysis: Constraints from trace element geochemistry: Journal of Geochemical Exploration, v. 232, p. 106883.

Zhao, Z., Wei, J., Liang, S., and Gao, T., 2021, Sulfide remobilization and trace element redistribution during metamorphism and deformation at the Xitieshan Pb-Zn deposit, NW China: Ore Geology Reviews, v. 136, p. 104170.

Chapitre 3 Trace element composition of chalcopyrite as a tool for deposit type discrimination: a machine learning approach

Enzo Caraballo[1], Georges Beaudoin[1], Sarah Dare[2]

[1]Université Laval, QC; [2]Université du Québec à Chicoutimi, QC

3.1 Résumé

La chalcopyrite se forme dans différents types de dépôts, de magmatiques à hydrothermaux. Cette étude a pour but le développement d'un modèle optimal d'apprentissage automatique pour prédire la provenance de la chalcopyrite à partir de sa composition en éléments traces et fournir un outil robuste pour l'exploration. La base des données des éléments traces, mesurés par ablation laser et spectrométrie de masse à plasma à couplage inductif (LA-ICP-MS), comprend 2562 analyses, desquelles 1832 ont été obtenues de cette étude et 730 ont été compilées de la littérature, provenant de 155 dépôts représentatifs à l'échelle mondiale appartenant à 8 types deépôts (Ni-Cu-EGP, porphyres, skarn, iron oxide copper-gold (IOCG), sulfures massifs volcanogènes (SMV), or épithermal et or orogénique). Trois collections de modèles prédictifs, chacune comparant 4 algorithmes d'apprentissage automatique (Random Forest (RF), Artificial Neural Network (ANN), K-Nearest Neighbors (KNN), and Naive Bayes (NB)) et une méthode statistique de classification supervisée (partial least square-discriminant analysis (PLS-DA)), ont été testés pour : 1) discriminer entre dépôts magmatiques et hydrothermaux; 2) discriminer entre les types de dépôts magmatiques (sulfures à Ni-Cu et EGP lités), et 3) discriminer parmi les différents types de dépôt hydrothermaux. L'algorithme RF a rapporté les performances les plus élevées dans les trois contextes, avec les données de test. Le premier modèle RF, lequel discrimine entre dépôts magmatiques et hydrothermaux avec le Ni, Ga, In, Sb, Se, Ag, Zn, Pb, Sn et Bi comme des prédicteurs, rapporte une proportion générale d'analyses correctement classifiées (accuracy) de 97.2%. Le deuxième modèle RF pour les dépôts magmatiques utilise Te, Sn, Se, In, Bi et Zn comme des prédicteurs, rapporte une proportion générale d'analyses correctement classifiées de 98.3%. Le troisième modèle RF discrimine la chalcopyrite parmi 6 types de dépôts hydrothermaux avec une proportion générale d'analyses correctement classifiées de 93% (99.6% pour SMV, 91.9% pour or épithermal, 90.5% pour IOCG, 85.7% for or orogénique, 85.7% pour porphyre and 79.5% pour skarn), avec le Se, Zn, Sn, In, Ga, Te, Ag, Sb, Bi, Co, Ni et Pb comme les variables prédictives. Les trois modèles RF ont été testés également avec des données de la littérature non incluses dans la phase d'entrainement (blind data) afin d'évaluer la robustesse pendant la prédiction, en rapportant >75% d'analyses correctement classifiées. Comme un exemple d'application, les modèles RF ont été utilisés pour classifier des données de chalcopyrite de la littérature, provenant de sédiments de tills et eskers couvrant la Province de Churchill, Canada. Les modèles suggèrent que 59.8? des grains de chalcopyrite ont une origine hydrothermale, principalement porphyre (31.3%), IOCG (33.2%) et SMV (26.8%), tandis que 40.2% des échantillons ont une provenance magmatique (72.3% sulfure à Ni-Cu et 27.7% EGP lités). Les modèles RF fournissent un outil robuste et précis pour identifier les types de dépôts en utilisant la composition en éléments traces de la chalcopyrite pour l'exploration minérale.

3.2 Abstract

Chalcopyrite occurs in several types of deposits, from magmatic to hydrothermal systems. This study aims to develop an optimal machine learning classifier to predict chalcopyrite provenance using trace element composition and to provide a robust indicator mineral tool for exploration. The trace element dataset, measured by laser ablation-inductively coupled plasma-mass spectrometry (LA-ICP-MS), comprises 2562 analyses, of which 1832 are from this study and 730 analyses are compiled from literature, from 155 representative deposits worldwide belonging to 8 major deposit types (Ni-Cu-PGE, porphyry, skarn, iron oxide copper-gold (IOCG), volcanogenic massive sulfides (VMS), epithermal gold and orogenic gold). Four supervised machine learning algorithms (Random Forest (RF), Artificial Neural Network (ANN), K-Nearest Neighbors (KNN), and Naive Bayes (NB)) and a supervised classification statistical method (partial least square-discriminant analysis (PLS-DA)), were tested in three context for: 1) discrimination between magmatic and hydrothermal deposits, 2) discrimination between types of magmatic deposits (Ni-Cu sulfide and Reef-type PGE), and 3) discrimination between different types of hydrothermal deposits. The RF algorithm yields the highest performance in the three contexts with test data. The first RF model, discriminating magmatic from hydrothermal deposits with Ni, Ga, In, Sb, Se, Ag, Zn, Pb, Sn and Bi as predictors, yields an overall accuracy of 97.2%. The second RF model to discriminate magmatic deposit types uses Te, Sn, Se, In, Bi and Zn as predictors, and reports an overall accuracy of 98.3%. The third RF model discriminates chalcopyrite among 6 hydrothermal deposit types with an overall accuracy on test data of 93 % (99.6% for VMS, 91.9% for epithermal gold, 90.5% for IOCG, 85.7% for orogenic gold, 85.7% for porphyry and 79.5% for skarn), using Se, Zn, Sn, In, Ga, Te, Ag, Sb, Bi, Co, Ni and Pb as predictors. Additionally, the three classifiers were tested with literature data not included in the training phase (blind data) to assess the robustness in prediction, yielding a mean accuracy >75%. As an example of an application, the RF models were used to classify literature chalcopyrite data from glacial till and esker sediments overlying the Churchill Province, Canada. Our models suggest that 59.8% of the detrital grains belong to hydrothermal deposits, primarily with porphyry (31.3%), IOCG (33.2%) and VMS (26.8%) sources, whereas 40.2% of samples are from a magmatic provenance (72.3% Ni-Cu sulfide and 27.7% Reef-type PGE deposits). Our Random Forest models provide an accurate and robust tool to fingerprint deposit types using trace element composition of chalcopyrite for mineral exploration.

3.3 Introduction

Chalcopyrite forms in a wide variety of mineral deposits, as a minor to major sulfide, from hydrothermal (porphyry, iron oxide copper-gold (IOCG), volcanogenic massive sulfides (VMS), orogenic gold, epithermal gold, Cu-skarn, sedimentary exhalative sulfides, and red beds) to magmatic systems (Ni-Cu-platinum group element (PGE) sulfide systems). Studies on chalcopyrite for petrogenetic and exploration purposes, have shown that its

trace element composition varies in both magmatic (Barnes et al., 2006; Barnes et al., 2008; Caraballo et al., 2022; Chen et al., 2015; Czamanske et al., 1992; Dare et al., 2014; Dare et al., 2010b; Dare et al., 2010a, 2011; Djon and Barnes, 2012; Duran et al., 2016b; Godel and Barnes, 2008; Godel et al., 2007; Holwell and McDonald, 2007; Mansur et al., 2020; Marfin et al., 2020; Piña et al., 2012a) and in hydrothermal ore environments (Agangi et al., 2018; Bajwah et al., 1987; Butler and Nesbitt, 1999; Cabri et al., 1985; Chowdhury et al., 2020; Cook et al., 2011; George et al., 2016; George et al., 2018b; Harris et al., 1984; Hawley and Nichol, 1961a; Huston et al., 1995; Kase, 1987; Martin et al., 2019; Martin et al., 2018; Maslennikov et al., 2009a; Maslennikov et al., 2009b; Moggi-Cecchi et al., 2002; Reich et al., 2013b; Reich et al., 2020; Rose, 1967; Wang et al., 2015; Wohlgemuth-Ueberwasser et al., 2015; Xie et al., 2020; Yang et al., 2022; Yano, 2012; Yuan et al., 2018; Zhao et al., 2020; Zhao et al., 2021a). Similar to other minerals, the trace element composition of chalcopyrite reflects the physico-chemical conditions of the geological/ore-forming environment, and its variability is principally controlled by its crystal structure, partition coefficients between mineral and fluid/magma, partitioning with co-crystallizing minerals, fO_2, aS_2 and pH of the fluid, volatile content and magma/fluid composition (Caraballo et al., 2023 in press; Caraballo et al., 2022; George et al., 2016; George et al., 2018b). In contrast, its major element composition is almost always near stoichiometric (Caraballo et al., 2023 in press; Caraballo et al., 2022; George et al., 2016; George et al., 2018b).

As such, trace elements in chalcopyrite potentially can be used as an indicator mineral for deposit type recognition (Caraballo et al. 2023 in press; Bédard et al., 2017; Caraballo et al., 2022; Duran et al., 2019a; Goulet, 2016; Mansur et al., 2021). An indicator mineral provides evidence on the presence of a type of mineralization, hydrothermal alteration, or lithology of bedrock, hence their morphology, textures and/or geochemistry may be investigated in order to obtain information nature of mineralization and clastic transport (McClenaghan, 2005). Chalcopyrite is considered as an indicator mineral for its high specific gravity (4.1-4.3) and physical properties, which enable a simple separation by density and recognition by optical microscope, respectively from sediments (e.g., till, soils, fluvial) in comparation to other sulfides (e.g., pentlandite, pyrrhotite). In addition, chalcopyrite is the most resistant sulfide to dissolution (Crundwell et al., 2021; Rimstidt et al., 1993). Averill (2011b), based on the stability in surficial sediments under temperate and humid tropical conditions, and Crundwell (2021), based on the electronic structure of the most common sulfides, proposed a relative scale of dissolution resistance/stability, which places chalcopyrite as one of the most resistant sulfides. Moreover, the potential of chalcopyrite as an indicator mineral has been highlighted by several studies on surficial sediment heavy mineral fraction from glacial environments associated with several mineralization styles, such as VMS, skarn and Ni-Cu-PGE (Averill, 2001; Averill, 2011b), and porphyry Cu-Au and Cu-Mo (Hashmi et al., 2015a; Plouffe et al., 2016; Plouffe et al., 2022). In addition, Duran et al. (2019a) showed that the 0.25-1 mm non-ferromagnetic heavy mineral concentrates of Quaternary till and esker samples from the Churchill Province

(Québec, Canada) can contain up to thousands of chalcopyrite grains, of which their trace element composition may be used to determine provenance.

The study of the variation of trace element composition with multivariate statistical methods, such as partial-least square discriminant analysis (PLS-DA) or principal component analysis (PCA), has been used to explore a wide variety of indicator minerals, such as apatite (Tan et al., 2023), gold (Liu and Beaudoin, 2021; Liu et al., 2021), pyrite (Dmitrijeva et al., 2020; Mishra et al., 2021), magnetite (Makvandi et al., 2016a; Makvandi et al., 2016b), scheelite (Grzela et al., 2019; Miranda et al., 2022; Sciuba et al., 2020), sphalerite (Frenzel et al., 2016; Mishra et al., 2021; Zhang et al., 2022a), rutile (Sciuba and Beaudoin, 2021), tourmaline (Grzela et al., 2019; Sciuba et al., 2021) and chalcopyrite (Bédard et al., 2022; Caraballo et al., 2022; Marfin et al., 2020). PLS-DA considers the complex relations between variables, revealing the underlaying data structure and determine the compositional criteria for mineral exploration, and represents an efficient alternative to binary diagrams, which are built with a limited number of elements (Bédard et al., 2022). In contrast, indicator mineral studies with a machine learning approach are scarce: sphalerite (Li et al., 2023; Sun and Zhou, 2022), pyrite (Cui et al., 2023; Gregory et al., 2019; Sun et al., 2022; Winderbaum et al., 2012), magnetite (Bédard et al., 2022; Hong et al., 2021; Hu et al., 2022; Zhang et al., 2022b) and quartz (Wang et al., 2021). However, previous studies on chalcopyrite relied mainly on empirical discrimination diagrams (Duran et al., 2019a; George et al., 2018b; Goulet, 2016), PCA (Bédard et al., 2017), PLS-DA (Caraballo et al., 2023 in press; Caraballo et al., 2022;), and cluster analysis (Marfin et al., 2020), rather than machine learning (Caraballo et al., 2023, in press). However, Caraballo et al. (2023, in press) demonstrated that machine learning, RF in particular, was more performant discriminating chalcopyrite trace element composition from different lithotectonic settings in VMS deposits than PLS-DA, enabling its use as an indicator mineral for exploration.

The aim of this study is to develop an efficient machine learning classifier to predict the source of chalcopyrite grains from 8 major deposit types using trace element compositions and apply it to published data from several deposits and to detrital grains recovered from overburden in Churchill Province. We show that the chalcopyrite chemical composition varies significantly from hydrothermal to magmatic systems. Among the tested machine learning algorithms, the Random Forest algorithm reports the highest performance, classifying accurately unknown chalcopyrite samples by deposit type.

3.4 Methodology

3.4.1 Trace Element Dataset of Chalcopyrite

The complete dataset is constituted by Dataset A, which comprises 1832 analyses of chalcopyrite, and Dataset B, with 730 analyses compiled from literature, from 426 samples belonging to 155 representative worldwide ore deposits (Fig. 3.1). The complete dataset (Dataset C, n=2562) belong to 8 different deposit types, ranging from

magmatic: a) Ni-Cu sulfide (N=106), and b) Reef-type PGE (N=45) to hydrothermal systems: c) Porphyry (N=34); d) Skarn (N=20); e) Iron oxide copper-gold (IOCG, N=48); f) Volcanogenic massive sulfides (VMS, N=124); g) Epithermal gold (N=26), and h) Orogenic gold (N=23). Dataset A includes data from this contribution (porphyry, skarn, IOCG, epithermal and orogenic gold) and from our recent papers on magmatic sulfide (Ni-Cu sulfide and Reef-type PGE: Caraballo et al., 2022) and VMS deposits (Caraballo et al. 2023, in press), which were all collected using the same analytical protocol (Annexe C1). Annexe C1 summarizes the geologic information of the selected deposits and their samples. Dataset B comprises literature data from 11 studies (Annexe C2), in which chalcopyrite was analyzed by comparable analytical methods (i.e., *in situ* LA-ICP-MS) using sulfide reference materials (e.g., MASS1, GSE-1g, Po-727, UQAC-FeS, and Fe or Cu as internal standard). The total of missing values in datasets from compiled studies, calculated as the sum of censored values (*i.e.,* values below detection limit) and missing values sensu stricto (not-analyzed elements), was used as a parameter of selection. Only literature data with less than 30% of total of missing values were used in dataset B (Annexe C2). Among studies used to build Dataset B, only a few analyzed the exact same elements as those in Dataset A (George et al., 2018b; Melekestseva et al., 2020a; Yang et al., 2022). The remaining studies commonly did not analyze Ga, Mn and to a lesser extent In (Duran et al., 2016b; Li et al., 2018; Mansur and Barnes, 2020b).

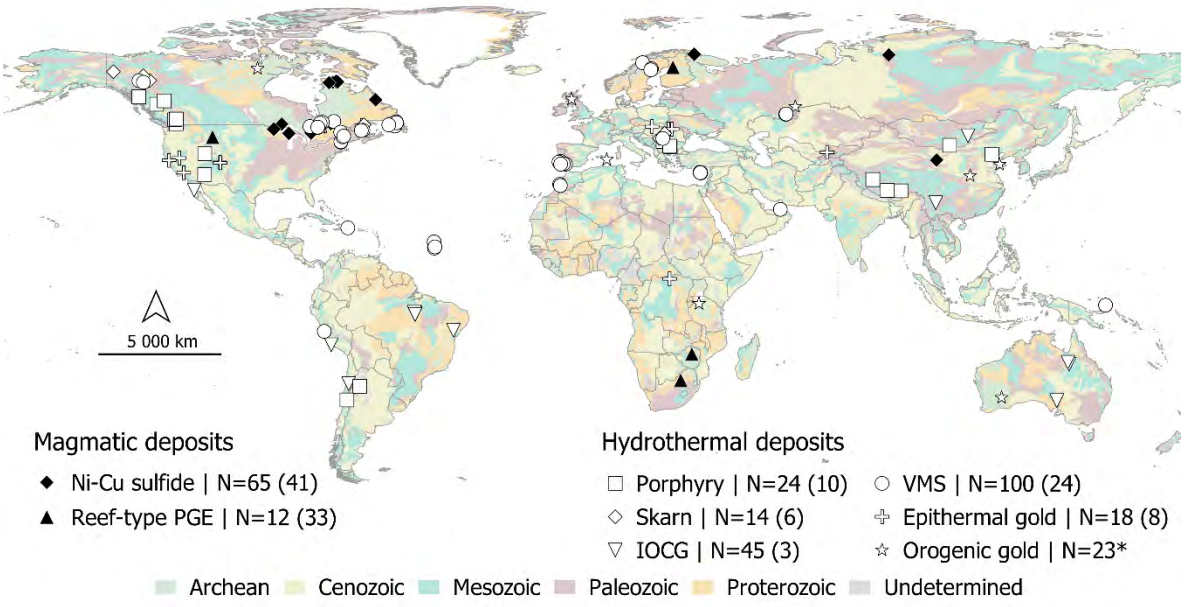

Figure 3. 1 Location of selected deposits. Generalized geologic map of the world (Chorlton, 2007). N= number of samples for this study (number of samples from literature in brackets).

Dataset from studies which did not satisfy Dataset B criteria (named Dataset D) were utilized to not only test the models, but also to evaluate the data quality and its impact on predictions (blind test). Dataset D is a compilation of 29 studies, of which 14 are from magmatic deposits and 15 from hydrothermal deposits, with different percentages of censored values, number and type of missing elements (Annexe C3). The chalcopyrite data from

glacial till and esker sediments overlying the Churchill Province (Duran et al., 2019a) was classified to assess the provenance in this regional survey. Gallium is the only missing element in Duran et al. (2019a) and with a total of 14% of censored values.

Most of the deposits included in Dataset C are metamorphosed. A wide range of metamorphic grades are represented in each deposit type, from prehnite-pumpellyite to amphibolite; however, the majority presents greenschist grade metamorphism (Annexe C1). Some unmetamorphosed deposits are also included, principally from VMS (e.g., SMS Roman Ruins, Papua New Guinea), epithermal gold (e.g., Palisades, USA), IOCG (e.g., Candelaria, Chile), porphyry (e.g., Granisle, Canada), skarn (e.g., Mactung, Canada) and Ni-Cu-PGE (e.g., Noril'sk, Russia). The VMS deposit class contains the wider variety of metamorphic grades, from unmetamorphosed deposits to amphibolite grades (e.g., Caraballo et al., 2023 in press). The representativity of the different metamorphic grades of the selected samples and deposits in Dataset C contributes to ensure that the analytical data captures the more important characteristics of chalcopyrite composition in the deposit types studied in more details.

3.4.2 Analytical Methods

Major elements in 342 grains of chalcopyrite from 58 samples belonging to 26 deposits, were analyzed with a CAMECA SX-100 Electron Probe Microanalysis (EPMA), equipped with five wavelength-dispersive spectrometers (WDS) at Université Laval, Québec. The results and analytical conditions are given in Annexe C4 and show that the major element composition of all chalcopyrite is close to stoichiometric values. To verify the presence of inclusions not detected under optical microscope, and to select regions without inclusions (<10 μm) for geochemical analysis, scanning electron microscopy (SEM) was used (FEI Inspect F50, equipped with an energy-dispersive spectrometer (EDS) at Université Laval; Annexe C17). Between five and seven grains of chalcopyrite were selected in each polished section for geochemical analysis, based on the amount and distribution of chalcopyrite, grain size and mineralogical association.

Trace elements in 1832 grains of chalcopyrite were analyzed by LA-ICP-MS at LabMaTer (Université du Québec à Chicoutimi, UQAC) using an Excimer 193-nm RESOlution M-50 laser ablation system (Australian Scientific Instrument) equipped with a double volume cell S-155 (Laurin Technic) and coupled to an Agilent 7900 ICP-MS, following the protocol described in Caraballo et al. (2022). Beam size used for analysis were 33 μm and 55 μm, based on grain size of chalcopyrite. A laser frequency of 15 Hz and a fluence of 3 J/cm^2 were used. After 30 seconds of gas blank measurement, line profiles were made across the sulfide grains for 20 to 60 seconds. The ablated material was carried into the ICP-MS by an argon-helium gas mix at a rate of 0.8 to 1 L/min for Ar and 350 mL/min for He, and 2 mL/min of nitrogen was also added to the mixture. Data reduction was carried out using Iolite package for Igor Pro software (Paton et al., 2011). Full results are given in Annexe C5.

Thirty-six isotopes (36) were measured: ^{24}Mg, ^{29}Si, ^{34}S, ^{49}Ti, ^{51}V, ^{52}Cr, ^{55}Mn, ^{59}Co, ^{60}Ni, ^{65}Cu, ^{66}Zn, ^{71}Ga, ^{74}Ge, ^{75}As, ^{82}Se, ^{95}Mo, ^{101}Ru, ^{103}Rh, ^{107}Ag, ^{108}Pd, ^{111}Cd, ^{115}In, ^{118}Sn, ^{121}Sb, ^{128}Te, ^{137}Ba, ^{182}W, ^{185}Re, ^{189}Os, ^{193}Ir, ^{195}Pt, ^{197}Au, ^{202}Hg, ^{205}Tl, ^{208}Pb and ^{209}Bi. The polyatomic interference of ^{40}Ar^{63}Cu on ^{103}Rh was corrected in chalcopyrite using a Cu-blank. However, the ^{103}Rh values of are not reported as the interference corrections are too large in chalcopyrite (1% Cu produces about 0.1-0.2 ppm ^{103}Rh interference). In most cases PGE were below detection limit in chalcopyrite. Direct interference of ^{115}Sn on ^{115}In and ^{108}Cd on ^{108}Pd were corrected in chalcopyrite manually from ^{118}Sn and ^{111}Cd. The internal standard used was ^{57}Fe with the stoichiometric iron value of chalcopyrite (30.43 %). A combination of three international reference materials (RM) for calibration was used to cover all elements: i) MASS-1 (Wilson et al., 2002), a pressed powder pellet (ZnCuFeS), was used to calibrate S, Cu, Zn, As, Se, Mo, Cd, Sn, Sb, Te, Hg, Tl and Pb; ii) GSE-1g (Jochum et al., 2005), a Fe-rich natural basaltic glass, was used to calibrate Cr, Mn, Co, Ni, Ga, Ge, Ag, In, Re and Bi; and iii) Laflamme Po727, a synthetic FeS doped with PGE, used to calibrate Au and PGE. The RM used to monitor quality control of the analyses were: 1) UQAC-FeS1, a synthetic sulfide developed at LabMaTer (UQAC); 2) CCu-1e, a copper concentrate (certified by CCRMP-Canadian Certified Reference Materials project, CANMET, Canada); and 3) PTC-1b, a Cu-Ni-sulfide concentrate powder (Jochum et al., 2005). The results of analyses of these reference materials and the range of detection limits are shown in Annexe C6. Most elements (Ag, As, Au, Bi, Co, Ga, In, Ir, Mn, Mo, Ni, Os, Pb, Rh, Ru, Sb, Se, Sn, Te, Tl and Zn) have a moderate to high accuracy relative to their reference values (rel. diff.<10-15%) and a moderate to high precision (RSD<10-15%). Elements such as Ge, Tl and Cd show lower accuracy (rel. diff.>15%) and lower precision (RSD>15%; Annexe C6). Differences between working values in a few of RM and those measured in this study could be a result of heterogeneity of non-matrix matched materials, or due to the low level of confidence of reported working values (provisional/informative values). As polyatomic interferences were detected on ^{74}Ge (from ^{40}Ar^{34}S^{+}, ^{36}Ar^{38}Ar^{+} and/or ^{38}Ar^{36}S^{+}) and Tl reported low accuracy and precision, such that these elements were not used for statistical analysis. Although Cd also reported low accuracy and precision, it was exclusively used to compare with ternary diagram Ni-Cd-Se from Duran et al. (2019a), but not for statistical analyses and machine learning development and testing.

Elements such as Si and Mg (silicates), Ti (Fe-Ti oxides), Zn and Cd (sphalerite), Pb (galena), Ni (pentlandite), Ba (barite), W (scheelite) were used to monitor for mineral inclusions. On each time-signal, only regions free of micrometric inclusions were selected for data reduction in order to have the most reliable composition of chalcopyrite (Annexe C17).

3.4.3 Statistical Methods

Data pre-processing: The geochemical data obtained from this study (Dataset A) and the compiled literature data (Dataset B) were separately pre-processed for the values below detection limit (*i.e.,* censored values) following protocol from Caraballo et al. (2023, in press) and Caraballo et al. (2022). After datasets were

separately imputed for censored values with lrEM (log-ratio expectation-maximization) algorithm (Palarea-Albaladejo and Martín-Fernández, 2015), they were merged in Dataset C, and then missing values for not-analyzed elements were imputed by deposit type using package missForest (Stekhoven and Bühlmann, 2012). Dataset D was used to test the selected classifiers and evaluate the data quality and its impact on predictions. Dataset D has censored values and missing elements (not analyzed), thus requiring imputation. Furthermore, detection limits are not provided in some studies, or these limits are averaged such that imputation with lrEM could potentially give imprecise results and affect prediction accuracy. Therefore, we implemented a K-Nearest Neighbor (KNN) algorithm to impute missing values in Dataset D. The KNN is developed during model training which use information of the 5-nearest neighbors from Dataset C (Kuhn and Johnson, 2013; Provost and Saar-Tsechanski, 2007).

In addition, compositional data describe quantitatively the parts of a whole, which sum to a constant (*i.e.*, 100%), having thus a closed nature, leading to potential spurious correlations (Egozcue and Pawlowsky-Glahn, 2011; Filzmoser et al., 2009; Pawlowsky-Glahn and Buccianti, 2011). In order to avoid this problem in exploratory data analysis (binary and ternary plots), the data was transformed using centered log-ratios following Aitchison (1986).

Exploratory data analysis: The exploratory analysis comprised univariate, bivariate and multivariate methods in order to identify systematic variations in the data before building discrimination models. Univariate analysis (boxplots) explores each variable, separately. The trimmed mean (μ_t) and the trimmed standard deviation (sd_t), two robust measures of location and dispersion with the aim to reduce effects of outliers on estimator calculation were used (Wilcox, 2011). These statistic estimators are presented for each variable in the format μt[sdt] plus the respective unit (ppm). Bivariate analysis was conducted to determine whether a statistical association exists between two variables and verify clusters in the data using, respectively, Pearson correlation coefficients and binary diagrams. Ternary plots with a compositional data approach were also built. In the compositional ternary diagram, the data is centered to the geometric mean (*g*) and scaled by powering it with total variance (Aitchison, 1986; Pawlowsky-Glahn et al., 2015; Von Eynatten et al., 2002). For a sample *X* with a center *g* (geometric mean) and total variance *totvar(X)*, the standardised data X_s is:

$$\left(1/\sqrt{totvar(X)}\right)\odot(X \oplus g)$$

where $\odot$ is the operation of powering and $\oplus$ perturbation defined by Aitchison (1986). This representation improves visualisation and interpretation, and avoids problems when the data is close to the boundaries of the ternary diagram (Daunis-i-Estadella et al., 2006; Von Eynatten et al., 2002).

Supervised Classification Models: Dataset C has a class imbalance ratio between the over-represented (VMS n=755) and under-represented (epithermal gold, n=124) classes of ≈6. Class imbalance in a dataset potentially

may degrade the performance of machine learning models, leading to misclassification of the minority class samples (Abd Elrahman and Abraham, 2013). According to Weiss (2013), there is no standard on the degree of class imbalance in a dataset to be considered unbalanced, indicating that overall, a class imbalance ratio IR≤2 would be considered as marginally unbalanced, whereas IR≈10 modestly unbalanced, and IR≈1000 would be considered extremely unbalanced. In addition, the classification problem in this study involves 8 deposit types, in many of which chalcopyrite shows similar trace element composition. To decrease complexity in classification, the problem was redefined with a divisive approach by classifying the samples according to: a) two major geological systems (magmatic and hydrothermal): from which the models are trained with all Dataset C; b) deposit type in magmatic environments (Ni-Cu sulfide and Reef-type PGE): from which the models are trained using only magmatic analyses from Dataset C; and c) deposit type in hydrothermal systems (porphyry, skarn, IOCG, VMS, epithermal and orogenic gold): comprising only hydrothermal analyses from Dataset C to train the models. Once the samples are classified by the major geological system model (magmatic vs. hydrothermal; mag-hyd.model), two models are subsequently used to reclassify them according to magmatic (mag model), and hydrothermal (hyd model) deposit types.

For each context presented previously and based on trace element composition of chalcopyrite in Dataset C, were tested and compared four machine learning algorithms (following Caraballo et al. 2023, in press): 1) Random Forest (RF), 2) Artificial Neural Network (ANN), 3) Naïves Bayes (NB), and 4) K-Nearest Neighbors (KNN), and one supervised classification multivariate statistical method, partial least squares-discriminant analysis (PLS-DA). Dataset C in each case was split into training (70%) and test (30%) subsets using stratified sampling. Classification models were tuned using a hyperparameter grid search function, implemented by Caret package in R software (Kuhn, 2012). In addition, several variable transformations were applied in order to test for improvements during the training step for each context and model, which include: a) standardization: centering (subtracting each predictor by its mean) and scaling (dividing each predictor by their standard deviation); b) YeoJohnson: a power transformation belonging to Box-Cox family, which improves normality or symmetry of the data (Yeo and Johnson, 2000); and c) Centered log-ratio following Aitchison (1986). The workflow is summarized in Annexe C18.

Furthermore, the models were validated using the test data to compare the predicted classes with the known classes in a confusion matrix. Confusion matrices allow an evaluation of the classification performance, consisting of a square matrix *C x C,* where *C* is the number of classes and collect the outputs of the classification model (Ballabio and Consonni, 2013; Sokolova and Lapalme, 2009). In binary classification, the hydrothermal class in the mag-hyd models, and the Ni-Cu sulfide class in the mag models are referred as the positive classes, whereas magmatic and Reef-type PGE labels correspond to the negative classes, thus items in the confusion matrices were defined and performance metrics were calculated (Annexe C9F, C10F). For multiclass

classification (hyd models), the metrics were calculated with a “one-versus-all" approach following Caraballo et al. (2023, in press) (Annexe C11F).

Performance measures, appropriated for imbalanced data, such as Matthew’s Correlation Coefficient (MCC), kappa and F1-score (Bolton et al., 2020; Bowes et al., 2012; Delgado and Tibau, 2019; Yilmaz and Demirhan, 2023), were determined from confusion matrices derived from cross-validation during training and from validation on test data, and used to compare the models. The Matthew’s Correlation Coefficient (MCC) measures the degree of correlation between the predicted and actual class memberships using the cell counts of the confusion matrix, and it returns values from -1 (lowest performance) to 1 (perfect classification performance; Yilmaz and Demirhan, 2023). Kappa is defined as a measure of agreement between observed and predicted classes based on the corrected accuracy, which is the proportion of the observed and expected of samples correctly classified, the larger the metric value (near 1), the better the classifier performance (Delgado and Tibau, 2019; Yilmaz and Demirhan, 2023). F1-score represents the harmonic mean between the effectiveness to identify the truly positive labels (precision) and the effectiveness to identify positive labels (recall), in which a value near to 1 indicates high performance (Sokolova and Lapalme, 2009; Yilmaz and Demirhan, 2023). The model with the highest performance metrics was used for testing on blind data (Dataset D), which consists of data not included in the training and testing phases. Performance of the selected models in prediction during blind tests was measured using principally the accuracy, which is calculated as the ratio of analyses correctly classified to the number of observations (Sokolova and Lapalme, 2009; Yilmaz and Demirhan, 2023). The variable importance in classification was measured with the Gini index (Han et al., 2016), which gives the contribution of a variable to correctly classify training data by comparing the average total decrease in node impurity (Gregory et al., 2019; Menze et al., 2009).

Random Forest (RF): Random Forest is defined as an ensemble of decision trees, which generates predictions based on class membership probabilities for individual predictions (Breiman, 2001). In this algorithm each tree is based on a random subsample of the observations, and each split within each tree is created based on a random subset of independent variables (Breiman, 2001; Gislason et al., 2006; Harris and Grunsky, 2015). The random subsamples are created through a bootstrapping procedure, providing a stable estimate of classification accuracy from out-of-bag (OOB) data (Harris and Grunsky, 2015). In classification problems, the dependent variable Y is categorical (classes), and the prediction is based on a majority class vote (Barker et al., 2021; Brownlee, 2018; Grömping, 2009; Svetnik et al., 2003).

Artificial Neural Network (ANN): Artificial neural network is a machine learning algorithm inspired by the characteristics and mechanisms of biological neural systems, and it simulates the pattern recognition ability of the human brain, which has been applied to classification, regression, and prediction problems (Liu et al., 2020; Sun et al., 2020). The artificial neuron is the most fundamental unit that processes the received information by

using a sigmoid activation function (Sun et al., 2020). Artificial neural network is a layered structure, where neurons are arranged, and it consists of an input layer, one or more hidden layers, and an output layer (Sun et al., 2020). The most used neural network is feed-forward network, as employed in this study, in which the neurons of different layers are fully interconnected to each other, but the information is unidirectional starting from the input layer through hidden layers to the output layer (Liu et al., 2020; Sun et al., 2020).

Naïves Bayes (NB): Naïves Bayes learning refers to the construction of a Bayesian probabilistic model, which uses Bayes theorem to evaluate the probability of an event (class) to occur given the negative class has been randomly undersampled to match positive class (Berrar, 2018; Caté et al., 2017). Class-conditional probabilities are computed by "naively" assuming that for a given class the inputs or predictors are independent of each other; thus, an observation is labelled using the class with the highest probability (Bédard et al., 2022; Cracknell and Reading, 2014).

K-Nearest Neighbors (KNN): The K-Nearest Neighbors algorithm is based on the principle that the observations in a dataset should be in close proximity to other observations that have similar properties (Kotsiantis et al., 2007). The KNN searches for the *k* nearest observations to the queried observation and determines the class by identifying the single most frequent class label (Kotsiantis et al., 2007). The relative distance between observations is determined by using a distance metric, such as the Euclidean distance (Kotsiantis et al., 2007).

Partial Least-Squares Discriminant Analysis (PLS-DA): PLS-DA is an iterative method consisting of five principal steps (Brereton and Lloyd, 2014). Starting with weight vector w^* estimation by maximizing the covariance between X and Y, the t, p and q coefficients (X-scores, X-loadings, Y-loadings, respectively) are calculated sequentially. Finally, residuals of X and Y replace original input data in order to determine the second PLS component (Lee et al., 2018). A PLS-DA model can be interpreted from two principal outputs, scores and loadings. After calculating latent variables, they can be used in a cartesian space to project X-scores of the observations (i.e. t_1-t_2). The aim of these representations, called score plots, is to look for clusters indicating similar characteristics (Brereton and Lloyd, 2014). Likewise, distance between clusters can suggest differences in attributes. On the other hand, loading plots show correlations between original variables. Superposing X-loadings (specifically X-weight, w^*) and Y-loadings in the same plot, the relationships between X-variables (elements) and Y-variables (classes) can be inferred (Dunn, 2019; Wold et al., 2001). Variables positively correlated are shown grouped together, whereas those with a negative correlation plot diametrically opposed. Location of variables in a loading plot is dependent on their contribution to the discrimination, therefore, X-variables near the correlation circle (radius=1) are interpreted to be highly variable between classes, in contrast, those located near the origin contribute weakly to classification, as variability is negligible.

3.5 Results

3.5.1 Trace Elements in Chalcopyrite

After preprocessing the chalcopyrite dataset from this study (Dataset A, Annexe C5) for censored values, Mn, Co, Ni, Zn, Ga, Se, Ag, In, Sn, Sb, Te, Au, Pb and Bi were selected for further statistical analysis and machine learning modeling. Arsenic, PGE, Mo and Re were below detection limits (<dl) in most samples. Selected literature data (Dataset B) is presented in Annexe C2. The statistical summary of preprocessed Dataset C (the complete dataset) is presented in Annexe C7 and described below. Variable distribution in Dataset C is highly asymmetric with a large range of values and outliers (Fig. 3.2). In detail, Zn and Se show the highest mean concentrations values (234[293] ppm and 83[81] ppm, respectively). Tin, Ag and Ni averages have a range between 15 and 40 ppm, whereas In, Pb, Mn and Te vary between 1 and 15 ppm. Cobalt, Ga, Bi and Sb have concentrations typically below 1 ppm.

Gallium, In, Ni, Sb, Sn, and to a lesser extent Ag and Pb, show significant differences between chalcopyrite from hydrothermal and magmatic deposits (Fig. 3.2). Silver (31[42] ppm), Sn (28[39] ppm), In (14[18] ppm), Ga (0.79[1.1] ppm) and Sb (0.39[0.60] ppm) typically are higher in chalcopyrite from hydrothermal deposits, whereas Ni (38[30] ppm) shows considerably higher mean concentrations in chalcopyrite from magmatic systems (Fig. 2, Appendix A Table A.7). In magmatic deposits (Fig. 2), chalcopyrite from Ni-Cu sulfide deposits shows higher concentrations of Ni (41[37] ppm), Sn (6.7[8.7] ppm), Ag (5.7[5.8] ppm), In (3.1[2.2] ppm) and Te (3.9[4.9] ppm) than chalcopyrite from Reef-type PGE deposits, which have higher concentrations of Se (113[47] ppm) and Mn (4.1[3.2] ppm). Among hydrothermal deposits, chalcopyrite does not show significant differences in concentration for most trace elements. However, chalcopyrite from VMS deposits is richer in Se (219[250] ppm), Sn (64[72] ppm), Ag (46[56] ppm) and In (30[38] ppm) than the other hydrothermal deposits, whereas chalcopyrite from epithermal and orogenic gold deposits shows lower mean concentrations of Co, Se and Te (Fig. 2, Appendix A Table A.7). Moreover, chalcopyrite from porphyry deposits reports the lowest concentrations of Zn (28[37] ppm) among all deposit types.

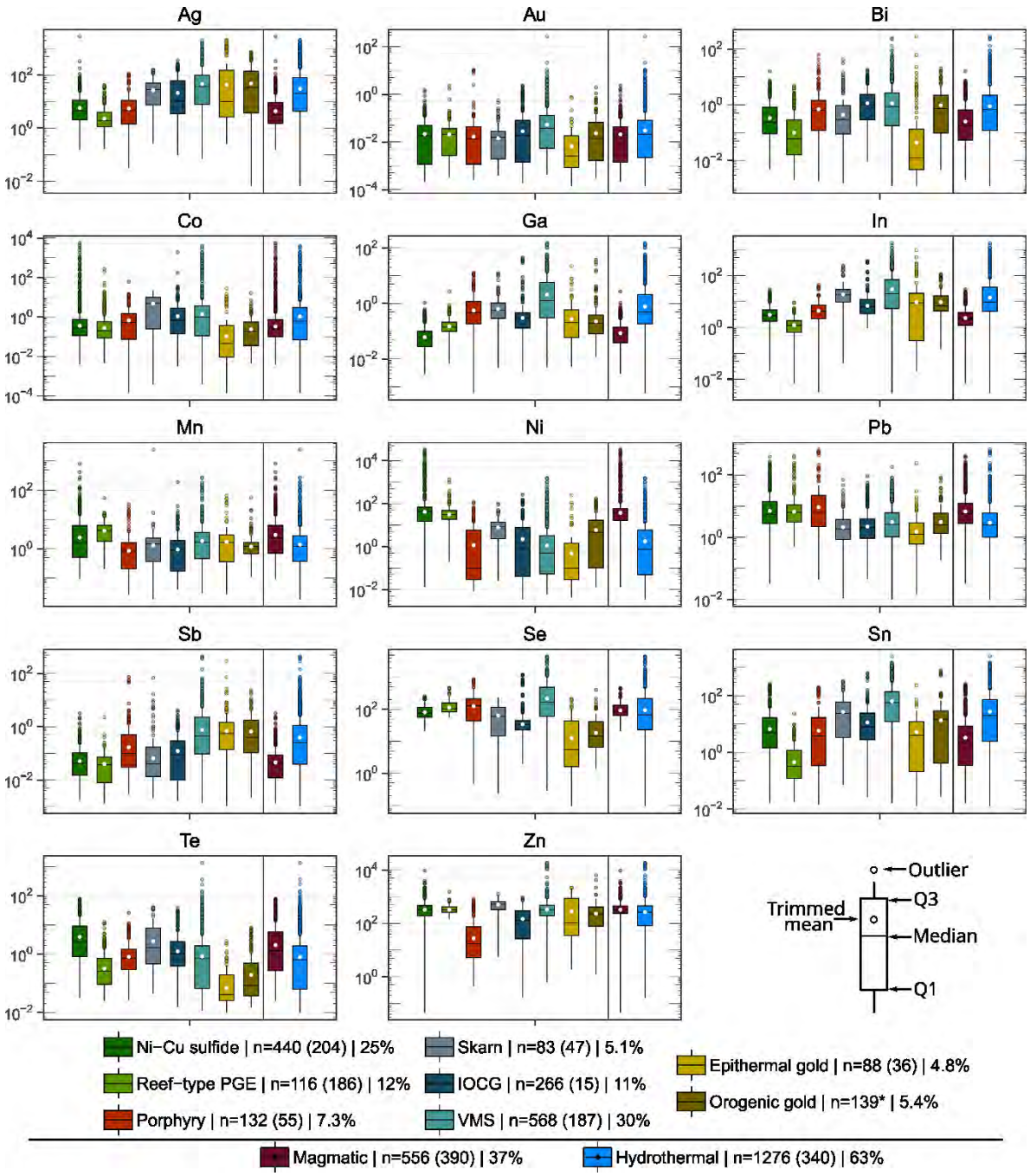

Figure 3. 2 Boxplots showing the variation of selected trace elements (in ppm) in chalcopyrite according to the deposit type. n: number of analyses for this study (Dataset A); number of analyses compiled from the literature given in brackets (Dataset B). Q1 and Q3 indicate first and third quartiles, respectively. Percentage represents the proportion of each deposit with respect to all analyses, including literature data.

Binary diagrams in Figure 3.3 show that, despite overlapping, chalcopyrite from magmatic and hydrothermal deposits forms separate groupings, with the latter being more dispersed. Density plots show that chalcopyrite from magmatic deposits is enriched in Ni (>3.5 ppm) and relatively depleted in Ga (<0.25 ppm), In (<4 ppm) and Sb (<0.20 ppm; Fig. 3.3). Hydrothermal deposits show a bimodal distribution of Ni, present principally in density

diagrams Ga-Ni and Se-Ni (Figs. 3.3F, H). These differences are larger in ternary diagrams (Fig. 3.4), where chalcopyrite from magmatic deposits shows less overlapping with chalcopyrite from hydrothermal deposits. This is better shown in the density ternary diagrams of Ni-Sb-Co (Figs. 3.4A-B), Ni-Ga-In (Figs. 3.4C-D) and Ni-Cd-Se (Figs. 3.4E-F), which enable an imperfect discrimination between chalcopyrite from both environments. Overall, chalcopyrite from magmatic deposits has Ni/(Sb+Co) and Ni/(Ga+In) ratios higher than 2.5 and 1.5, respectively, whereas the Ni/Se ratio is higher than 0.12 (Fig. 3.4). In summary, the exploratory statistical methods do not show robust or systematic discrimination by deposit type based on the trace element composition of chalcopyrite. Only Ni determines of marked differences between magmatic and hydrothermal chalcopyrite (Figs. 3.2, 3.3 and 3.4).

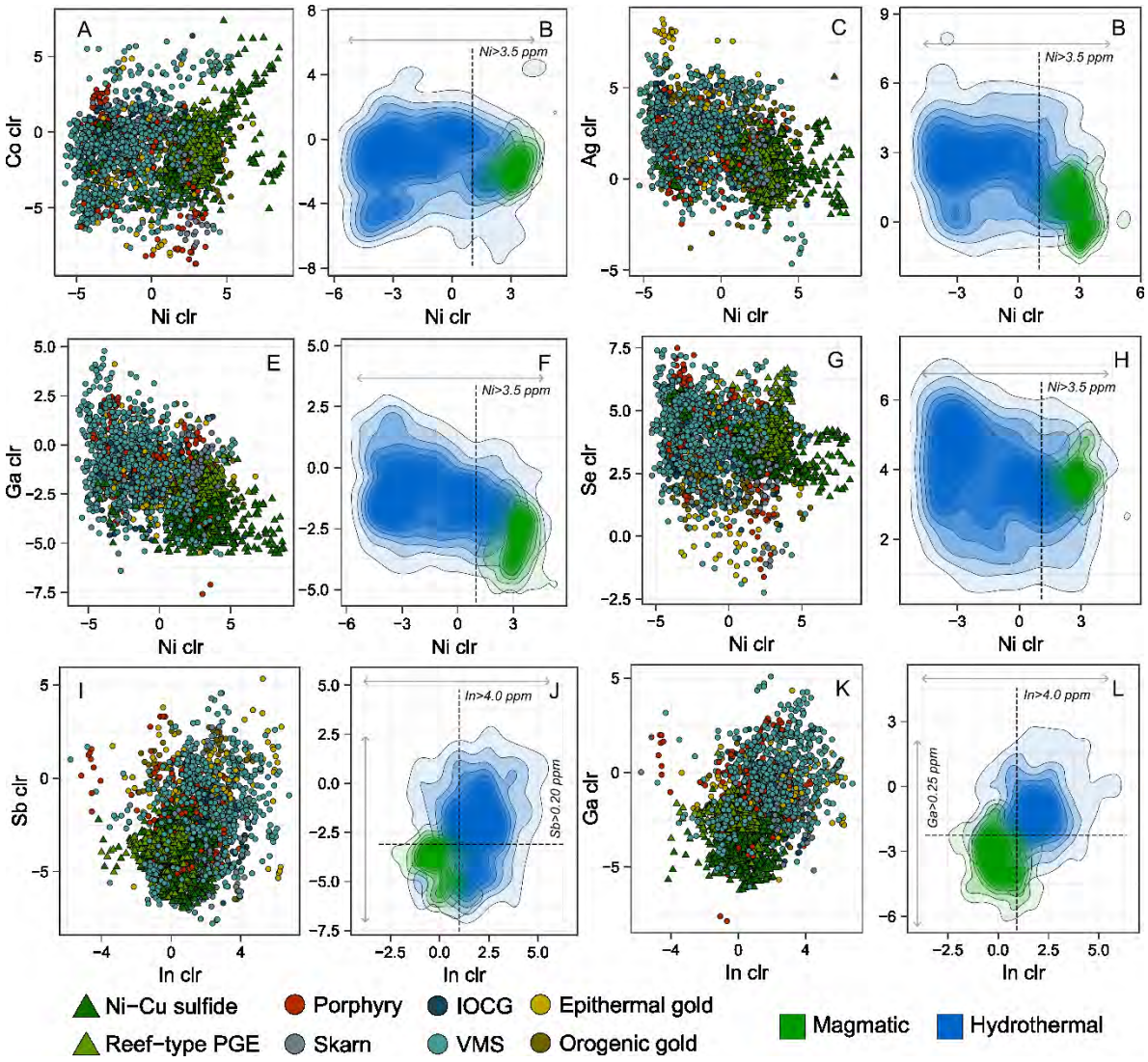

Figure 3. 3 Binary diagrams showing data points of chalcopyrite (left) and density binary plot using centred-log-ratio (clr) values (right) for elements that best show a marked difference between chalcopyrite from magmatic and hydrothermal deposits: Co-Ni (A-B), Ag-Ni (B-C), Ga-Ni (E-F), Se-Ni (G-H), Sb-In (I-J) and Ga-In (K-L). Note, there is considerable overlap among the different hydrothermal deposits.

Primitive mantle-normalized data for chalcopyrite from different deposit types yield similar patterns: they all increase from left to right of the diagram, with increasing chalcophile behavior (Fig. 3.5), according to Barnes (2016) and Barnes and Ripley (2016), which enables visualisation of all trace elements in a single diagram (Caraballo et al., 2022). All patterns have strong Co and Ni negative anomalies due to partitioning of these elements into other sulfides (e.g., pentlandite, pyrrhotite, sphalerite and pyrite). In detail, chalcopyrite is depleted in lithophile (Mn) and in slightly chalcophile to lithophile element (Ga) relative to mantle. Concentrations of chalcophile elements (Zn to Te) range from 1- to 10,000-times primitive mantle concentrations in magmatic deposits (Fig. 3.5A) and from 1- to 100,000-times in hydrothermal deposits (Fig. 3.5B). Overall, signatures are similar with no discrimination by deposit type, with important overlap of mean and data range (Fig. 3.5C).

3.5.2 Classifier Performances

Since boxplots, binary and ternary diagrams do not discriminate chalcopyrite from the 8 selected deposit types, supervised classification models are compared in order to determine the most adapted algorithm for each context. Random Forest model with Yeo-Johnson transformation yielded the highest performance. The results of the other models with other data transformations are reported in Annexe C8. Figure 3.6 shows the comparison between RF, KNN, ANN, NB and PLS-DA model performances with transformed predictors (Yeo-Johnson) on training and test data (Dataset C) to discriminate 1) between chalcopyrite from magmatic and hydrothermal chalcopyrite (mag-hyd.models; Fig. 3.6A), 2) between chalcopyrite from magmatic deposits (mag.models; Ni-Cu sulfide vs. Reef-type PGE; Fig. 3.6B), and 3) among chalcopyrite from different hydrothermal deposits (hyd.models; Fig. 3.6C). Confusion matrices of the models with Yeo-Johnson transformation evaluated on test data are presented in Annexe C9, C10 and C11.

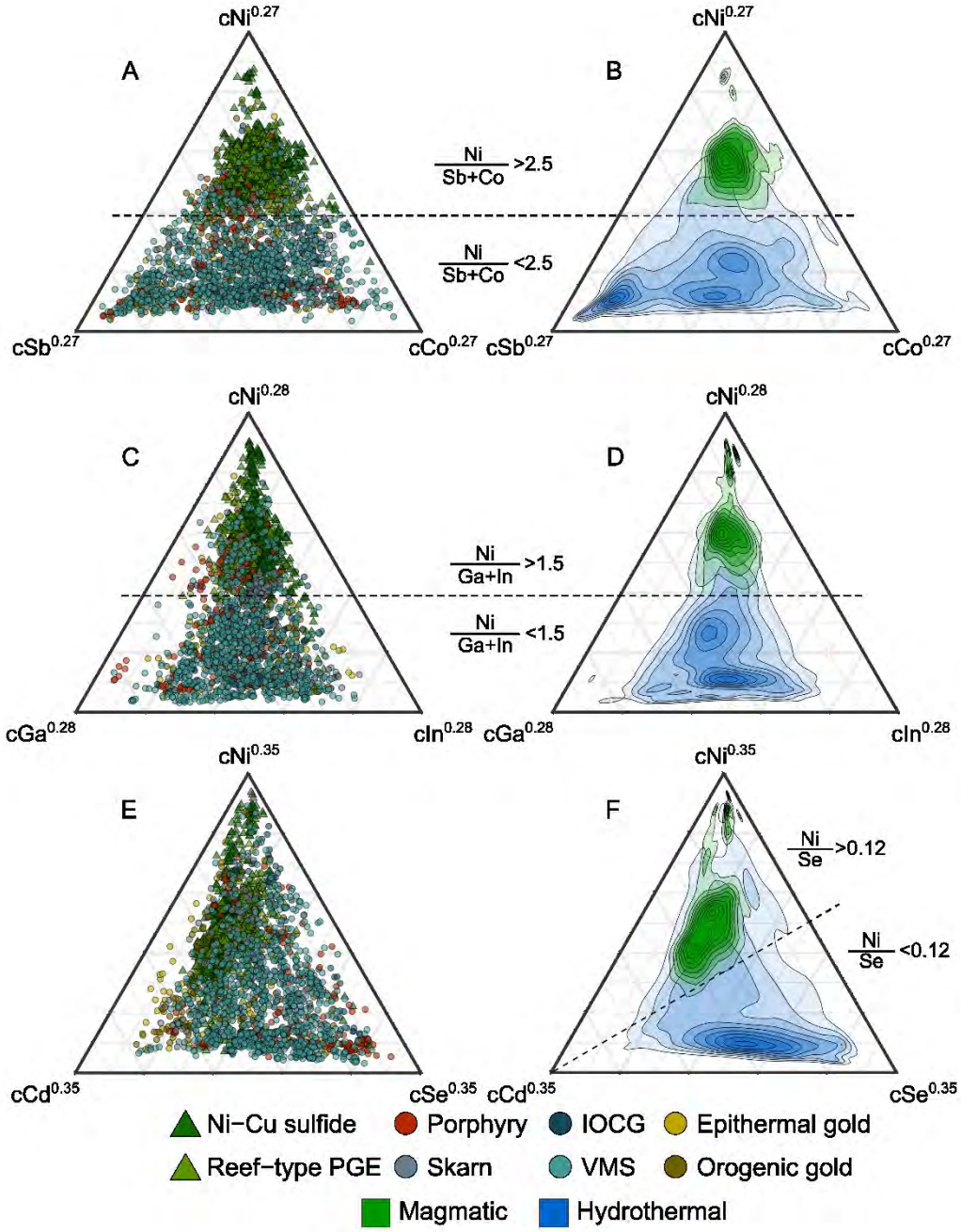

Figure 3. 4 Ternary diagrams of trace element composition of chalcopyrite (left) and data density ternary diagrams (right) showing the relative proportion amongst Ni-Sb-Co (A-B), Ni-Ga-In (C-D), Ni-Cd-Se (E-F). Data is centred to geometric mean (c) and standardised to the total variance (superscript).

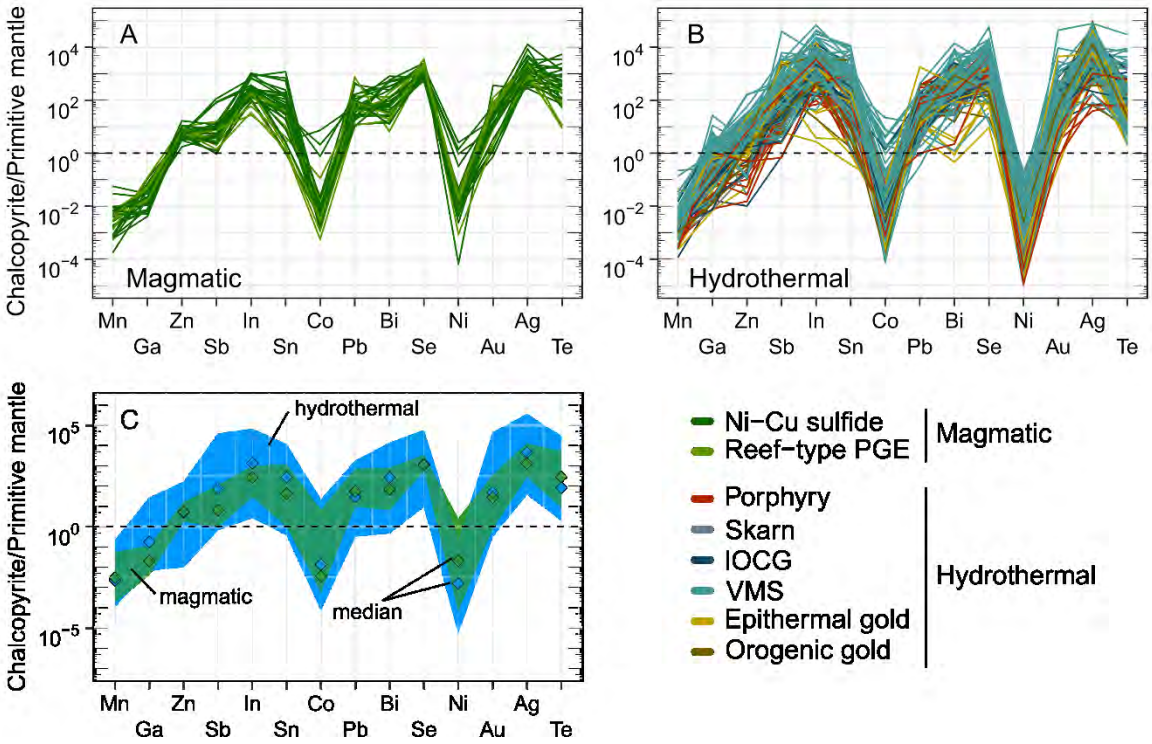

Figure 3. 5 Multi-element diagrams, normalized to primitive mantle of chalcopyrite from magmatic deposits (A) (after Caraballo et al., 2022), hydrothermal deposits (B) and comparison of medians for both classes (C). Chalcopyrite from magmatic and hydrothermal deposits show similar patterns and considerable overlap on these diagrams. Order of elements from slightly to highly chalcophile, according to Barnes and Ripley (2016) and Barnes (2016). Primitive mantle concentrations from Lyubetskaya and Korenaga (2007).

Models to discriminate between chalcopyrite from magmatic and hydrothermal deposits (mag-hyd models): This RF model registered the highest performance on training and test data (Fig. 3.6A) reporting MCC, kappa and F1-score values between 0.976-0.992. The ANN model also reported high, but slightly lower values than the RF model of MCC, kappa and F1-score from training and test data evaluation (0.966-0.987; Fig. 3.6A). Although the KNN model reported high performance values from training (0.946-979), these estimators decrease considerably on test data with MCC and kappa 0.00, and intermediate F1-score of 0.774 (Fig. 3.6A). The Naïve Bayes model showed a high performance on training and test data with similar values of MCC (0.902-0.907), kappa (0.902-0.906) and an F1-score of 0.963-0.964 (Fig. 3.6A). PLS-DA model showed a high performance on training data (0.872-0.949), but low values of MCC and kappa (0.00), and F1-score on test data (0.774; Fig. 3.6A). The low values of MCC and kappa (0.00) in the KNN and PLS-DA models on test data indicate that they have the lowest overall performances; however, both models show an intermediate performance detecting correctly positive class (hydrothermal), shown by F1-score (0.774). Since the RF classifier (RF mag-hyd model) reported the highest performance on training and test data, it was selected for application on blind data (Dataset D). Variable importance was determined for predictors in RF mag-hyd model and are shown in Figure 3.7A. According to Gini index, Ni and Ga are the most important elements in classification, followed by In, whereas Sb, Se, Ag, Zn, Pb, Sn and Bi have lower influence (Fig. 3.7A).

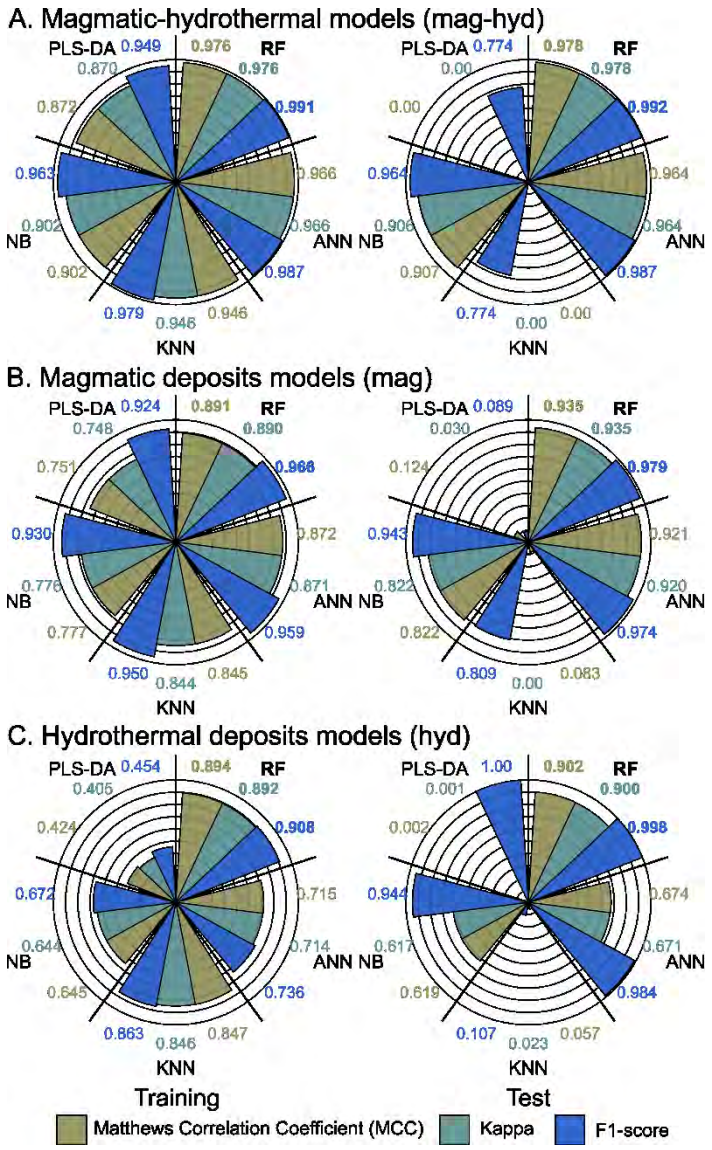

Figure 3. 6 Performances on training and test data of supervised classification algorithms with transformed data (Yeo-Johnson). A) Models to discriminate between chalcopyrite from magmatic and hydrothermal deposits, and B) Models to discriminate chalcopyrite by magmatic deposit type, and C) Models to discriminate chalcopyrite by hydrothermal deposit type. RF: Random Forest; KNN: K-Nearest neighbors; ANN: artificial neural network; NB: Naïve Bayes; PLS-DA: Partial Least-Square-Discriminant Analysis.

Models to discriminate chalcopyrite by magmatic deposit type (mag models): Overall, the RF and ANN models recorded the highest metrics on training and test data, ranging from 0.871 to 0.974 with low differences between both models (Fig. 3.7B). The KNN model reported high values in MCC (0.845), kappa (0.844) and F1-score (0.950) on training data; however, performance on test data decrease significantly with the lowest values of MMC and kappa (0.083 and 0.00, respectively), whereas F1-score has an high value of 0.809 (Fig. 3.7B), indicating a high performance in detecting correctly positive class (Ni-Cu sulfide) (Annexe C10C). The NB model reported values of MCC (0.777-0.822), kappa (0.776-0.822), and F1-score (0.930-0.943) on training and test data (Figure 3.6B). The PLS-DA model showed an intermediate performance on training data (0.748-0.924);

however, it reported low values of MCC (0.124), kappa (0.030) and F1-score (0.089) on test data (Fig. 3.6B). Since the RF classifier (RF mag model) reported the highest performance on training and test data, it was selected for application on blind data (Dataset D). Variable importance was determined for predictors in RF.mag.model and are shown in Figure 3.7B. According to Gini index, Te, Sn and Se and In are the most relevant elements for classification, whereas Bi and Zn have a lower influence in prediction (Fig. 3.7B).

Models to discriminate chalcopyrite by hydrothermal deposit type (hyd models): Unlike the previous models, the hydrothermal deposit models reported an important decrease in performance on training data from RF to PLS-DA (Fig. 3.6C). The RF model recorded the highest values of MCC (0.894-0.902), kappa (0.892-0.900) and F1-score (0.908-0.998) on training and test data (Fig. 3.6C). The RF showed the highest accuracy (>80%) in each deposit type on test data (Annexe C11A). The other models reported metrics lower than 0.70, with the lowest values of MCC and kappa for KNN and PLS-DA on test data (<0.1; Fig. 3.6C). Consequently, the RF model was selected to classification of blind data (Dataset D). Variable importance of predictors in RF hyd model is shown in Figure 3.7C, which Se, Zn and Sn are the most important variables, and to a lesser extent In and Ga according to Gini index.

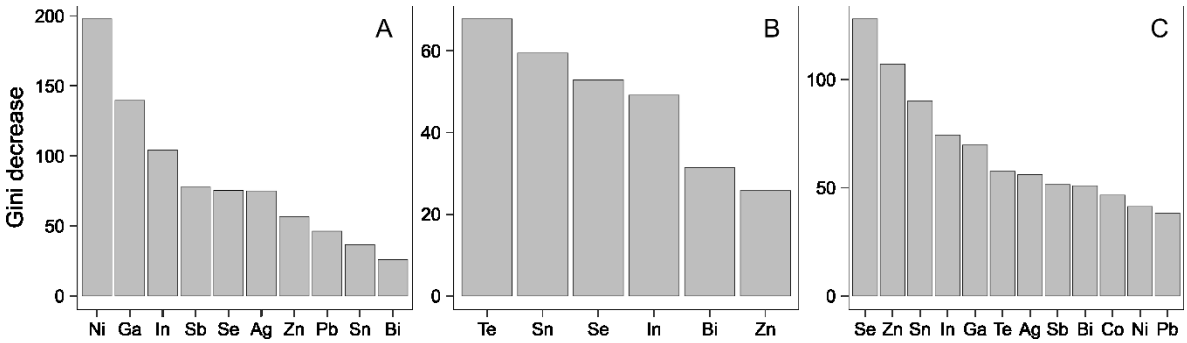

Figure 3. 7 Variable importance coefficients according to Gini index. A) RF model to discriminate between chalcopyrite from magmatic and hydrothermal deposits, and B) RF model to discriminate chalcopyrite according to magmatic deposit type, and C) RF model to discriminate chalcopyrite according to hydrothermal deposit type.

3.6 Discussion

Since chalcopyrite forms in a wide variety of deposit types, its trace element composition should reflect the diversity of physico-chemical conditions of the different ore-forming environments where the mineral deposits form. In magmatic sulfide deposits, variation of chalcopyrite trace element composition reflects the changing melt composition during sulfide fractionation (Caraballo et al., 2022; Dare et al., 2014), whereas in hydrothermal environments variation of chalcopyrite composition reflects the fluid composition (George et al., 2018b; Hannington, 2014), which in the case of VMS settings is a function of host rock composition and temperature (Caraballo et al., 2023 in press; George et al., 2016; George et al., 2018b). Bédard et al. (2017) investigated trace element composition of chalcopyrite from different mineral deposit types using PCA and demonstrated its

potential in recognizing the principal deposit types. They showed that specific trace element signatures discriminate chalcopyrite from volcanogenic massive sulfide (Ag, Sn, Zn and Se), Ni-Cu-PGE (Ni, Te and Pd), orogenic gold and red beds (Au and As), porphyry and skarn (Sb, In and Se), and IOCG (Zn and Ba) deposits. Caraballo et al. (2022) demonstrated, using PLS-DA, that chalcopyrite from representative Ni-Cu sulfide and Reef-type PGE deposits can be distinguished using Bi, In, Se, Sn and Te. Furthermore, they showed that in Ni-Cu sulfide deposits, it was possible to discriminate chalcopyrite according to ore type (Cu-rich vs. Fe-rich) using the assemblage Sb, Se, Sn, Tl and Zn. Based on cluster analysis and classification tree approach on trace elements in chalcopyrite from a single Ni-Cu-PGE deposit (Norilsk-Talnakh), Marfin et al. (2020) showed that there are chemical differences between massive and disseminated ore types. Most of these studies focused on a single deposit, or deposit type in order to show how the trace element composition of chalcopyrite varies. Our results show that although variations in chalcopyrite composition do occur within deposits, there is a significant variation between deposit types, and this can be useful to distinguish different deposit types through RF models.

Boxplots, binary and ternary diagrams show that the most important differences in trace element composition are found between chalcopyrite from magmatic and hydrothermal deposits, as two major classes. Nickel determines the difference between the two classes, which is enriched in chalcopyrite from Ni-Cu sulfide and Reef-type PGE deposits (38±31 ppm; Figs. 3.2, 3.3, 3.4; Annexe C7; Annexe C19). Nickel-rich sulfide deposits are found principally at the base of mafic and ultramafic intrusions (or komatiite lavas), that formed from mantle-derived melts as a result of partial melting of the mantle, and consequently enriching the silicate magma, and subsequent immiscible sulfide melt, in Ni, Cu and PGE (Barnes and Lightfoot, 2005; Naldrett, 2004). In contrast, the average Ni concentration in chalcopyrite from hydrothermal deposits is about 20x lower than that in chalcopyrite from magmatic deposits (1.8±3.3 ppm; Figs. 3.2, 3.3, 3.4; Annexe C7). Nickel solubility in hydrothermal systems are poorly understood (González-Álvarez et al., 2013; Seward et al., 2014) and hydrothermal deposits of Ni are rare and small. Liu et al. (2012) demonstrated experimentally that the solubility of Ni in aqueous solutions is substantially lower than that of Co. Chloride species, such as $NiCl^+$, $NiCl_{2(aq)}$ and $(NiCl_3)^-$ are thought to be responsible of transport of Ni in hydrothermal environments, which occurs most commonly as a trace element in pyrite, Co-pentlandite and massive chalcopyrite and chalcopyrite stringers ores (Hannington, 2014; Tian et al., 2012). However, chalcopyrite from some hydrothermal deposits can contain unusually high Ni contents, similar to those from magmatic deposits (Annexe C19). In these cases, the deposits are hosted by mafic and ultramafic rocks from which Ni was most likely leached, such as some porphyry Cu deposits (e.g., Elatsite; Strashimirov et al., 2002; Annexe C19A), gabbro-hosted skarn deposit (Oravite; Dupont et al., 2002; Annexe C19B), IOCG deposits (Igarapé Bahia/Alemao; Jaguar: Mansur et al., 2023; Annexe C19C), mafic and ultramafic-hosted VMS deposits (e.g., Troodos, Cyprus: Martin et al., 2019; Dergamysh, Urals: Melekestseva et al., 2020b; Irinovskoe and Candelabra hydrothermal fields, Mid-Atlantic Ridge: Wohlgemuth-

Ueberwasser et al., 2015; Annexe C19D) and some orogenic gold deposits hosted in country rocks containing mafic to ultramafic rocks (e.g., Kochkar, Bulyanhulu, Amaruq, Lega Dembi: Sciuba et al., 2021; Annexe C19F).

Given the complexity of the ore-forming processes and the large number of classes used for classification, it is not surprising that univariate and bivariate statistical methods, and ternary plots cannot provide accurate prediction of the chalcopyrite provenance. The overlap between most hydrothermal and magmatic chalcopyrite (Figs. 3.2, 3.3, 3.4 and 3.5) enables use of these diagrams only as preliminary tools to identify broad provenance, but with no probabilistic application in classification. Ternary diagrams (Fig. 3.4) show similar groupings with considerable overlap between magmatic and hydrothermal chalcopyrite, including the Ni-Cd-Se diagram suggested by Duran et al. (2019a), which decrease significantly their potential as a discriminator tool. In this context, machine learning algorithms are better to predict chalcopyrite provenance using its trace element composition. Caraballo et al. (2023, in press), demonstrated that Random Forest is better than PLS-DA to discriminate chalcopyrite provenance according to the lithotectonic settings in VMS deposits.

The selected RF models were tested with blind data (Dataset D; Annexe C3), which consists of literature chalcopyrite data that was not included in the training phase. This dataset allows to test the robustness of the models on compiled data from the literature and show how the predictions are affected by different proportions of censored values, missing elements, and different analytical conditions. The percentage of censored values, the proportion and importance of missing variables in blind data vary according to the study. The K-Nearest Neighbor (KNN) algorithm uses available compositional data, such that a database with high proportion of censored values or missing elements potentially can result in biased imputation, and consequently affect the accuracy in prediction. Furthermore, some datasets do not identify censored values, which may have been imputed by undocumented arbitrary values (e.g., 0.65 x dl). In some studies, in which censored values have not been imputed, the values below detection limit are indicated as <dl or any other term (e.g., bdl). In these cases, cells with <dl or bdl values are imputed by KNN algorithm during prediction. Chalcopyrite analyses in Dataset D with anomalous concentrations (>2 wt.%) of elements, such as Zn (sphalerite), Pb (galena) and Ni (pentlandite) were removed to avoid potential impact of inclusions.

3.6.1 Trace Element Composition of Chalcopyrite as a Tool to Fingerprint Deposit Types

Among the models tested in this study to determine chalcopyrite provenance using its trace element composition, the RF algorithm reported the highest performance during the training and test phase (Fig. 3.6A, B and C). Random Forest models developed in each context (mag-hyd model, mag model and hyd model) were tested with blind data (Dataset D, Annexe C3), which includes analyses from: a) magmatic deposits (n=255): Ni-Cu sulfide (Barnes et al., 2008; Chen et al., 2015; Dare et al., 2014; Dare et al., 2010b; Djon and Barnes, 2012; Knight et al., 2017; Liang et al., 2019; Piña et al., 2012a; Piña et al., 2015; Salim Amaral, 2017; Samalens et al.,

2017b) and Reef-type PGE deposits (Barnes et al., 2008; Godel and Barnes, 2008; Piña et al., 2016); and b) hydrothermal deposits (n=718): VMS (Agangi et al., 2018; Martin et al., 2018; Maslennikov et al., 2017; Revan et al., 2014; Wang et al., 2018; Wohlgemuth-Ueberwasser et al., 2015), porphyry (Lobo, 2022; Stefanova et al., 2023; Yu et al., 2022), skarn (Chen et al., 2022; Xie et al., 2020), IOCG (Liang et al., 2021; Mansur et al., 2023), epithermal gold (Reich et al., 2020) and orogenic gold deposits (Vasilopoulos et al., 2023). Prediction probabilities, confusion matrices and performance metrics for each model on blind data are summarized in Annexe C12 and C13. Results of predictions by study are shown in Figures 3.8, 3.9 and 3.10.

The RF mag-hyd and the RF mag models show the highest performance on the blind data test with an overall accuracy of 86% and 82%, respectively (Figs. 3.8 and 3.9; Annexe C13A, C13B). However, both models show low to intermediate values of MCC and kappa, between 0.30 and 0.65 (Annexe C13A, C13B). The class imbalance ratio between hydrothermal and magmatic deposits (≈3), and between Ni-Cu sulfide and Reef-type PGE deposits (≈4.6) in blind data affects MCC and kappa values, since these are calculated using all information provided by the matrix confusion. Both models show high F1-scores (>0.89), indicating high performance detecting chalcopyrite from hydrothermal (RF mag-hyd model) and that from Ni-Cu sulfide deposits (RF mag model) in blind data. The RF hyd model shows lower overall accuracy than the other models (65%) on blind data (Fig. 3.10; Annexe C13C). Similarly, MCC, kappa and F1-score are low (0.42-0.43), probably as a result of high class imbalance ratio between hydrothermal deposit types in blind data. The blind data used to test the models are heterogeneous. Therefore, the assessment of the performance of each model requires an integrated approach that takes into account the factors that can potentially affect the results of the predictions, such as the proportion of censored values, missing values and not analyzed elements.

3.6.2 Effect of the Proportion of Censored Values and Missing Elements on Predictions

To explore the impact on predictions, correlation coefficients (r) were calculated for each model between accuracy and the proportion of censored values per element, the proportion of missing elements, and the proportion of elements without censored values (Annexe C14). Overall, the main factor that positively affects prediction accuracy in most of the models is the proportion of elements without censored values. The positive correlation coefficients (0.47-0.84) indicate that in the three RF models, the accuracy of the prediction increases with the number of elements whose values are all above the detection limits. The proportion of missing elements locally degrades the prediction. This is especially true for the RF mag-hyd model ($r = -0.64$, p-value = 0.024 in magmatic deposits) and the RF mag model ($r = -0.66$, p-value = 0.019).

Furthermore, the impact of the proportion of censored values per element on predictions varies according to the deposit type. For example, in magmatic deposits, the accuracy decreases as the percentage of censored values in Se and Bi increase in the RF mag-hyd and RF mag models. In addition to Se and Bi, the proportion of censored

values in Te is negatively correlated with the accuracy of the RF mag model. Similarly, the percentage of censored values in Sb negatively correlates with the accuracy of predicting chalcopyrite from hydrothermal (RF mag-hyd model) and VMS (RF hyd model) deposits.

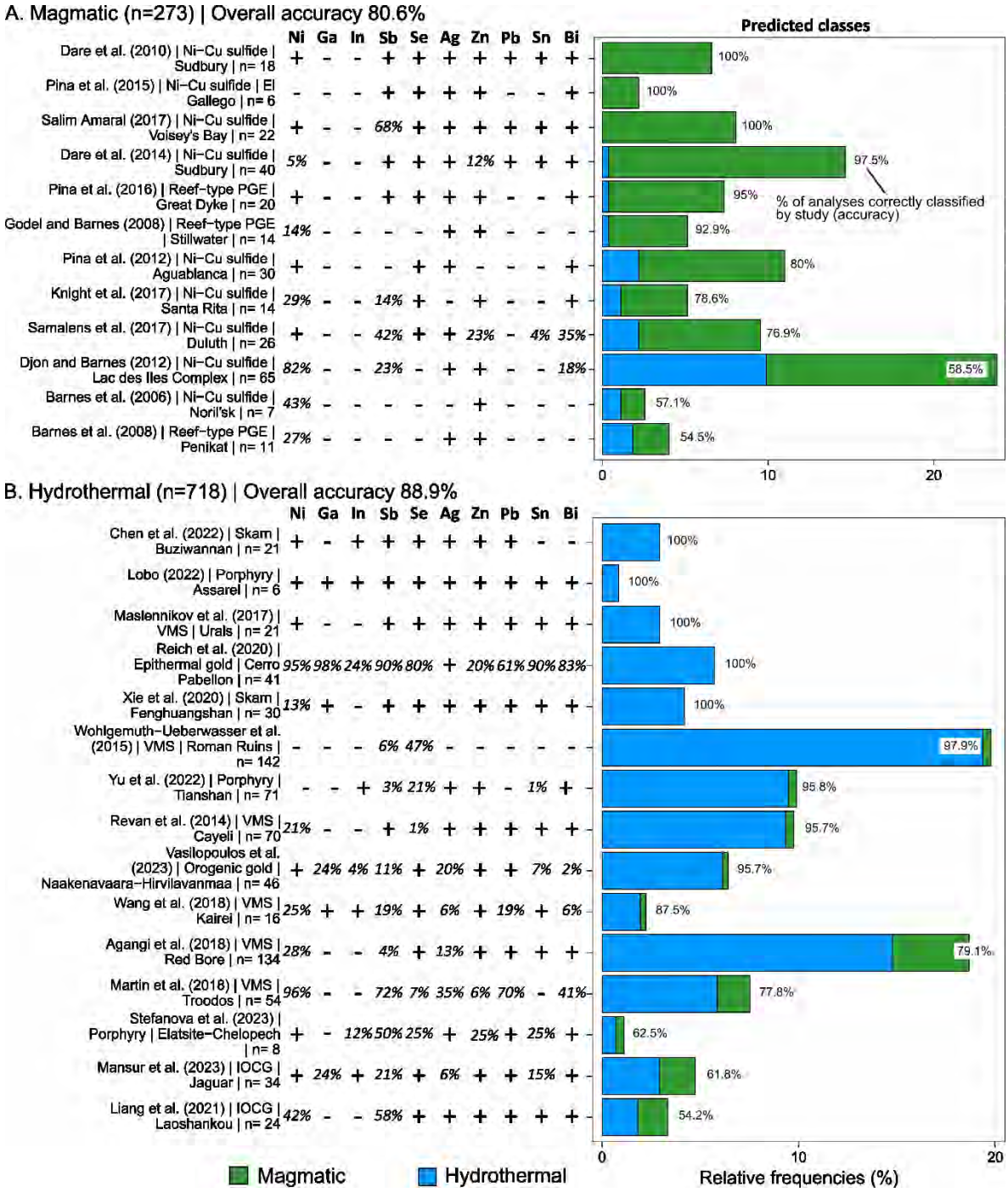

Figure 3. 8 Predictions of blind chalcopyrite data using RF mag-hyd model. A) Prediction of magmatic chalcopyrite, B) prediction of hydrothermal chalcopyrite. Relative frequencies: proportion of the number of analyses of each study in the set of all magmatic (A) and hydrothermal analyses (B). n: number of analyses. Cross symbol: analyzed element without censored values; dash symbol: not analyzed element; percentages in italic: proportion of censored values per element.

3.6.3 Other Factors Potentially Affecting the Predictions

Some of the deposits from blind data used to test the RF models have special geological characteristics that lead to high rates of misclassification. These include the Elatsite-Chelopech porphyry deposits (Stefanova et al., 2023), the Jaguar (Mansur et al., 2023) and the Laoshankou IOCG deposits (Liang et al., 2021), which reported a misclassification as magmatic deposits between 38% and 46% (Fig. 3.8B), using the RF mag-hyd model. In the case of Elatsite-Chelopech porphyry deposits, most are hosted by mafic and ultramafic rocks and are characterized by the presence of PGE and Co-Ni rich assemblages (Strashimirov et al., 2002), resulting in unusual high concentrations of Ni in chalcopyrite (characteristic of magmatic deposits). Chalcopyrite from the Jaguar IOCG deposit (Brazil, Mansur et al., 2023) reported a prediction accuracy of 61.8% as hydrothermal deposit, despite the fact that all elements required by the model were analyzed with with a dataset having low percentage of censored values. The Jaguar deposit is an unusually Ni-rich IOCG deposit (Ferreira Filho et al., 2021; Mansur et al., 2023), probably related to mafic-ultramafic host rocks (Mansur et al., 2023) resulting in chalcopyrite with high Ni, which explains the 38.2% of chalcopyrite predicted as belonging to magmatic deposits rather than the hydrothermal class. Similarly, chalcopyrite from the Laoshankou IOCG deposit inherited part of the trace element signature of Ni-rich pyrite during replacement, previously formed from Ni-rich fluids (Liang et al., 2021), which combined with the high percentage of censored values in Ni and especially Sb, results in low predictive accuracy.

Other factors concern the possibility of a mismatch between the deposit type assignments and the descriptions from the studies, particularly those with high rates of misclassified analyses (epithermal gold, skarn and orogenic gold) in RF hyd model. The Cerro Pabellón epithermal gold deposit (Chile; Reich et al., 2020), from which only 24% of chalcopyrite was correctly classified as epithermal, represents a modern analogue of low- to intermediate-sulfidation epithermal Au-Ag. According to Reich et al. (2020), based on petrological, geophysical, and geochemical studies, an epithermal system with a magmatic high-temperature heat source has been proposed. Therefore, a discrepancy between deposit type assignment and deposit description is not plausible as the cause of the high rate of misclassification of chalcopyrite from the Cerro Pabellón deposit. A possible cause may be the structure of data used to train the RF hyd model (Dataset C), as explained below. Concerning the skarn deposits tested in the RF hyd model, Xie et al. (2020) indicates that Fenghuangshan deposit is a skarn Cu (Au), whereby four stages of mineral precipitation were identified according to the crosscutting relationships, ore mineralogy, mineral assemblages and mode of occurrences. However, skarn-like alteration is prominent in some orogenic and post-orogenic IOCG deposits, characterized by the presence of clinopyroxene or amphibole ± garnet (Skirrow, 2022), which may explain the high proportion of chalcopyrite from skarn classified as IOCG origin (Fig. 3.10E). On the other hand, the Buziwannan deposit type assignment is mainly based on the trace element signature of co-crystallising magnetite and chalcopyrite. According to mineral assemblage and paragenesis (Chen et al., 2022), a skarn and hydrothermal stages were identified in the Buziwannan deposit.

Chen et al. (2022) used Cd/Zn ratio and Cd-Se-Ni ternary diagram to determine the origin of chalcopyrite. Although the Cd-Se-Ni ternary diagram indicates that chalcopyrite from Buziwannan deposit is of hydrothermal origin, the Cd-Zn diagram is less clear, ranging from epithermal, skarn to recrystallized VMS deposit (Chen et al., 2022). These results may explain the misclassification, principally as VMS, of chalcopyrite from this deposit using the RF hyd model.

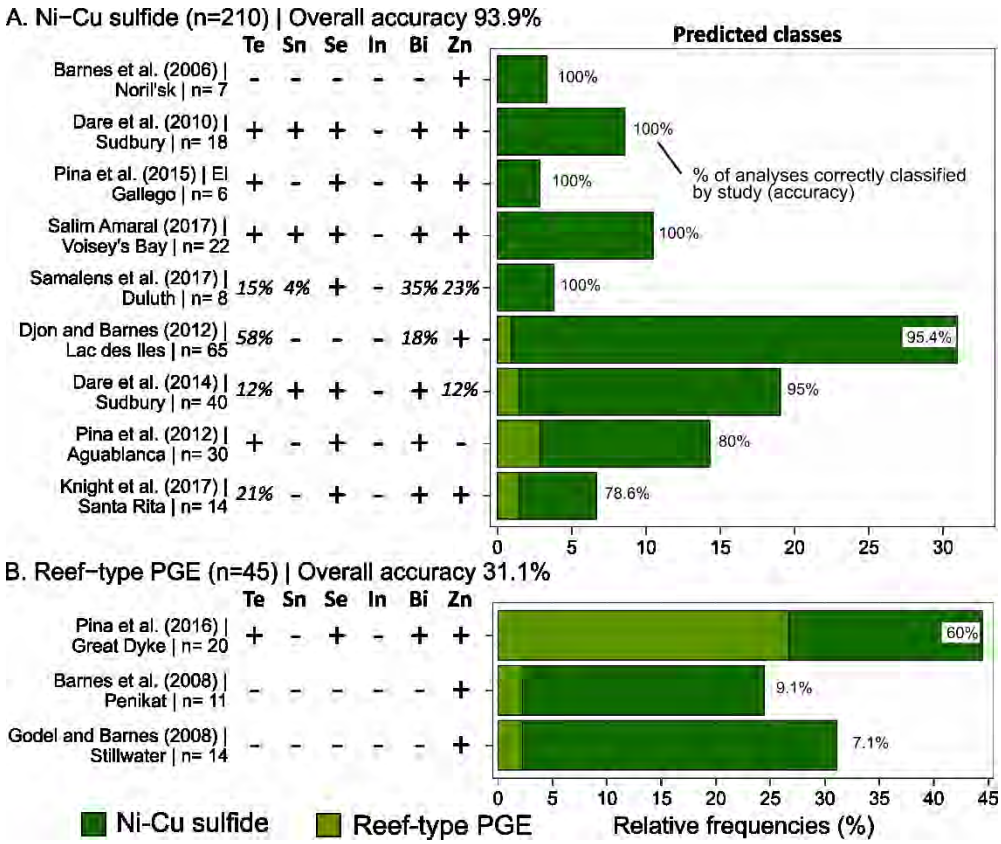

Figure 3. 9 Predictions of blind chalcopyrite data using RF mag model. A) Prediction of chalcopyrite from Ni-Cu sulfide deposits, B) prediction of chalcopyrite from Reef-type PGE deposits. Relative frequencies: proportion of the number of analyses of each study in the set of all Ni-Cu sulfide (A) and Reef-type PGE analyses (B). n: number of analyses. Cross symbol: analyzed element without censored values; dash symbol: not analyzed element; percentages in italic: proportion of censored values per element.

The Dataset C structure used to train the RF models probably also affects the prediction accuracy, particularly in the RF hyd model (Fig. 3.10). For example, VMS performs best because it represents 47% of hydrothermal deposits in Dataset C, whereas IOCG corresponds to 17%, followed by porphyry (12%), orogenic gold (8.6%), skarn (8.0%), and epithermal gold deposits (7.7%). This difference in number of analyses used to build the RF model could lead to class imbalance and decrease the accuracy of the model for some minority deposit classes (Bédard et al., 2022; Weiss, 2013). Another hypothesis that could explain the high misclassification rate of chalcopyrite from skarn, epithermal and orogenic gold deposits is related to geochemical background values associated with differences in geotectonic and geological settings. Probably, calibration of the training data according to the geotectonic environment may improve the classification performance.

In summary, this study shows that there is a high potential to use Random Forest to successfully discriminate chalcopyrite from different mineral deposits. However, future work should concentrate on addressing the class imbalance problem for the minority deposit classes by analyzing chalcopyrite with the suite of elements analyzed in this study to limit the proportion of censored values and missing elements.

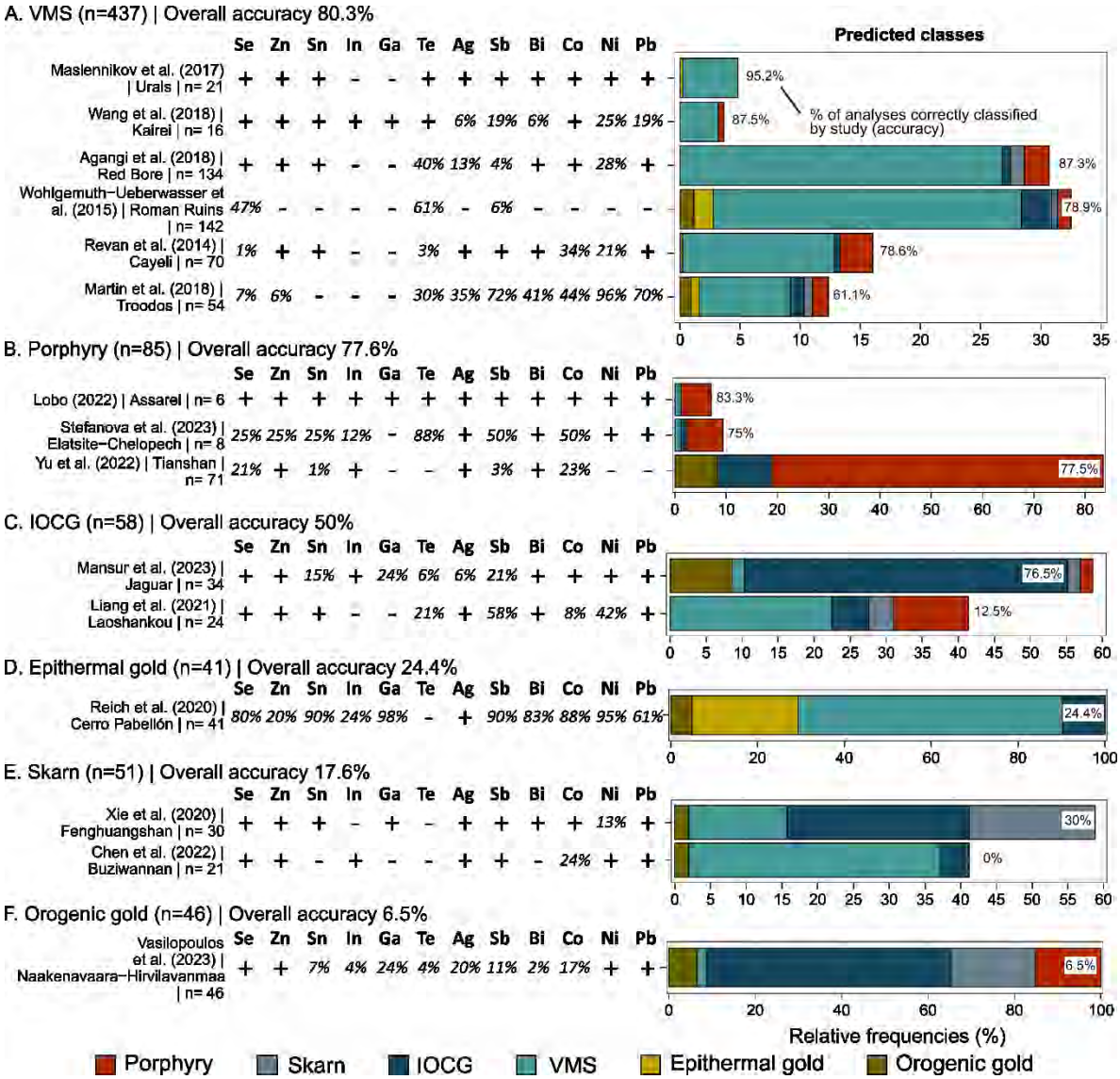

Figure 3. 10 Predictions of blind chalcopyrite data using RF hyd model. Predictions of chalcopyrite from (A) volcanogenic massive sulfides (VMS), (B) porphyry, (C) Iron Oxide-Copper Gold (IOCG) and (D) epithermal gold, (E) skarn and (F) orogenic gold deposits. Relative frequencies: proportion of the number of analyses of each study in relation to all analyses in each class. SMS: seafloor massive sulfides deposits. n: number of analyses. Cross symbol: analyzed element without censored values; dash symbol: not analyzed element; percentages in italic: proportion of censored values per element.

3.6.4 Application of RF Models to Detrital Chalcopyrite from Glacial Sediments

We also tested the Random Forest classifiers using the trace element data (n=630) of detrital chalcopyrite recovered from glacial sediments overlying the Churchill Province in Nunavik, Canada (Duran et al., 2019a).

The chalcopyrite analyses from Duran et al. (2019a) were carried out under the same analytical conditions and reference materials (MASS-1, GSE-1g and Po-727) at the same laboratory (LabMater, UQAC) as this study. This chalcopyrite dataset has 15% of censored values and one missing element (Ga) making it ideal to test the application of our RF models for mineral exploration. The RF models improve the classification from Duran et al. (2019a), which used a Se-Cd-Ni ternary diagram (Fig. 3.4F) to distinguish chalcopyrite from magmatic and hydrothermal deposits. The use of the RF models on detrital chalcopyrite from glacial sediments enables to test application for mineral exploration, and although chalcopyrite from barren rocks can be present in trace amounts, our models can be a guide on the dominant mineralisation type/s present in the region. Sediment till and esker samples from Duran et al. (2019a) were collected over an area covering about 31,250 km^2, which contained between 1-61 grains of pyrite and chalcopyrite ± sulfarsenide grains per sample (Duran et al., 2019a). Chalcopyrite in till sediments is characterized by subhedral to anhedral morphology with angular shapes and presence of inclusions, coronas and probably cubanite-pentlandite exsolutions (Duran et al., 2019a).

The Churchill Province bedrock principally comprises of Archean to Mesoproterozoic rocks, which is divided into: 1) the Labrador Trough, a basin of over 850 km in length mainly composed of Archean to Paleoproterozoic volcanic and metasedimentary rocks (Lafrance et al., 2014), 2) the Core Zone, comprising Archean to Paleoproterozoic granitoid, gneiss, paragneiss, migmatite, and amphibolite rocks (Lafrance et al., 2014), and 3) the Torngat Orogen, consisting of lithotectonic domains of intrusive rocks in a high-grade metamorphic context (Houle and Perreault, 2007; Lafrance et al., 2014). Mineralisation in the area, consist of: 1) Ni-Cu ± PGE magmatic sulfides mineralisation associated with mafic-ultramafic rocks (Charette et al., 2015; Lafrance et al., 2014; Lafrance et al., 2020), 2) Ni-Cr-PGE mineralisation (Reef-type PGE) associated with ultramafic intrusions (Charette et al., 2015; Lafrance et al., 2014; Lafrance et al., 2020), 3) Cu-Au-Mo porphyry mineralization associated with porphyritic intrusions (Lafrance et al., 2020), 4) Cu-Zn VMS mineralisation associated with volcano-sedimentary rocks (Charette et al., 2015; Lafrance et al., 2014; Lafrance et al., 2020), 5) epithermal Au-Cu-Ag vein mineralization associated with mafic-felsic metavolcanic rocks (Lafrance et al., 2020), 6) Cu-Zn ± Ag ± Ni associated with migmatite paragneiss (Lafrance et al., 2014), and 7) U-Th ± Y ± PGE associated with granite (Charette et al., 2015; Lafrance et al., 2014; Lafrance et al., 2020). McClenaghan (2017) reported gold grains in till sediments, suggesting a potential for undiscovered Au mineralisation. Duran et al. (2019a) used a Se-Ni-Cd ternary plot for chalcopyrite to discriminate magmatic and hydrothermal provenance, and suggested that 25% had a magmatic source, whereas 14% were from a hydrothermal origin, and the rest (61%) having unknown provenance. Duran et al. (2019a) also suggested that chalcopyrite identified as hydrothermal have relatively high Cd/Zn ratios, originating from skarn or metamorphosed exhalative deposits, such as recrystallised VMS deposits (George et al., 2018b).

The RF mag-hyd model applied to the complete dataset from Duran et al. (2019a) shows that chalcopyrite originated from magmatic (40.2%) and hydrothermal (59.8%) systems (Fig. 3.11). Among the grains predicted

to belong to magmatic deposits, 72.3% were classified as Ni-Cu sulfide and 27.7% as Reef-type PGE deposits (Fig. 3.11A). Although Ga is missing from the dataset and it has a high variable importance in the RF mag-hyd model, Ni is the element most strongly affecting the prediction between chalcopyrite from magmatic and hydrothermal deposits (Fig. 3.7A). In addition, Ga is not used in classification between Ni-Cu sulfide and Reef-type PGE deposits (RF mag model; Fig. 3.7B). For those grains identified as hydrothermal in origin, the RF hyd model classified 33.2% of the grains from IOCG, 31.3% from porphyry, 26.8% from VMS, 4.2% as epithermal gold, 2.4% as orogenic gold, and 2.1% as skarn (Fig. 3.11B). Although Ga is missing, it is only of intermediate importance for discriminating chalcopyrite among hydrothermal deposits (RF hyd model; Fig. 3.7C). Our classification is consistent with known types of mineralization in the area, in particular Cu-porphyry, VMS and Ni-Cu sulfide and Reef-type PGE deposits; however, the model classified a high proportion of chalcopyrite grains to be sourced from IOCG deposits, which are unknown so far for the Churchill Province of Quebec. Results of predictions of chalcopyrite grains from Churchill Province, including prediction probabilities, are shown in Annexe C15.

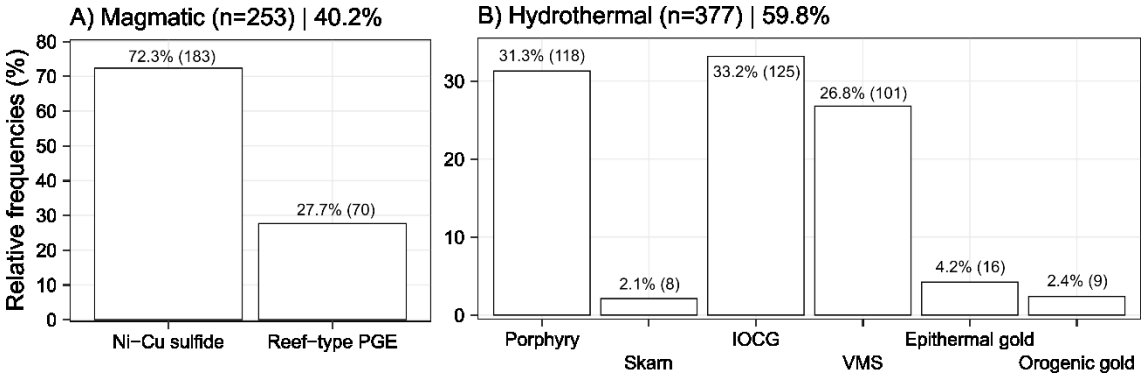

Figure 3. 11 Application of the three RF models on data of detrital chalcopyrite grains (n=630; Duran et al., 2019) from glacial sediment and eskers overlying the Churchill Province, Canada. A) Chalcopyrite predicted as belonging to magmatic source using RF mag-hyd model, and specific deposit types according to RF mag model, B) Chalcopyrite predicted as belonging to hydrothermal sources using RF mag-hyd model and their specific deposit types according to RF hyd model. Relative frequencies: proportion of the number of analyses in the set of all magmatic (A) and hydrothermal analyses (B). n: number of analyses.

To assess the behavior of the models in relation to ambiguous classifications, we tested their effectiveness considering only predictions with a high confidence, according to three uncertainty thresholds based on the difference between the first and second highest probabilities by sample. Random Forest model generates class predictions based on a majority of votes cast by all decision trees (Annexe C11, C15), providing an opportunity to evaluate the confidence of individual classifications (Gregory et al., 2019). In binary classification, the class membership of a sample is attributed to the class with a probability higher than 0.5, thus predictions when probabilities are similar can be considered as uncertain or inconclusive. Therefore, we used the difference between the first highest and the second highest probability as it can be applied to two-class and multiclass problems, hence, higher thresholds remove increasingly ambiguous predictions. Annexe C16 shows results of: a) Case 1: corresponding to original classification shown in Figure 11, in which no analyses were removed and

it is used as reference; b) Case 2: removing analyses with a difference between the first and second highest probability <0.1; c) Case 3: when analyses with a difference between the first and second highest probability <0.2 are removed; and d) Case 4: when analyses with a probability difference <0.3 are removed. When removing analyses with probability differences lower than 0.3, Ni-Cu-PGE, porphyry, VMS and IOCG deposits remain the major classes predicted (Annexe C16) with high level of confidence. In contrast, chalcopyrite predicted to come from skarn, epithermal gold and orogenic gold deposits are negligible or removed as they were inconclusive according to this threshold.

3.6.5 Metamorphism and Potential Effect on Model Predictions

The RF models, trained with Dataset C, comprises samples from deposits with a wide diversity of metamorphism grades, from prehnite-pumpellyite to granulite (Annexe C1 and C2). Samples from unmetamorphosed deposits are present in almost all deposit types. The volcanogenic massive sulfide class contains the widest variety of metamorphic grades, from unmetamorphosed deposits (e.g., SMS Logatchev-1, Mid-Atlantic Ridge) to prehnite-pumpellyite (IPB deposits, Spain), greenschist and amphibolite grades (Tétrault deposit, Canada). Therefore, our RF models can classify chalcopyrite from different metamorphic grades, as a wide range of trace element composition is covered (Figs. 3.8, 3.9 and 3.10). Although accuracy in prediction of blind data is multifactor-dependent, principally on the proportion of censored values and missing elements, no correlation between accuracy and metamorphic grade was evidenced. For instance, dataset from Agangi et al. (2018) in Red Bore (Australia) and from Revan et al. (2014) in Çayeli (Turkey) VMS deposits, which present similar characteristics (low percentage of censored values and same missing elements), reported high proportion of samples correctly classified (>80%), despite Red Bore deposit being metamorphosed to the greenschist, whereas Çayeli is unmetamorphosed (Fig. 3.10A).

3.7 Conclusions

This study highlights the potential of chalcopyrite trace element chemistry as an indicator mineral for mineral exploration and proposes a reliable methodology involving Machine Learning models to distinguish chalcopyrite from Ni-Cu-PGE, porphyry, IOCG, skarn, VMS, epithermal and orogenic gold deposits. Among the tested supervised classification algorithms, Random Forest is the most adapted algorithm to predict deposit types based on chalcopyrite composition. Application of our models to literature data of chalcopyrite demonstrates a high effectivity in predicting deposit types, principally for Ni-Cu sulfide, VMS and porphyry deposits. The RF model for chalcopyrite from magmatic and hydrothermal deposits, based on Ni, Ga, In, Sb, Se, Ag, Zn, Pb, Sn and Bi, yielded an overall accuracy of 86% for the blind test data. The RF model to discriminate chalcopyrite by magmatic (based on Te, Sn, Se, In, Bi and Zn) and hydrothermal deposit types (based on Se, Zn, Sn, In, Ga, Te, Ag, Sb, Bi, Co, Ni and Pb) reported overall accuracy of 82% and 65%, respectively. The main factors that

could affect the predictive accuracy are the percentage of censured values in the dataset, number of missing variables and the proportion of elements without censored values. Binary and ternary diagrams presented in this study could be used as preliminary tool to discern the possible source (magmatic vs. hydrothermal) based on elemental ratios. Finally, model prediction accuracy should be increased with the addition of new data to the training dataset, principally for underrepresented classes.

3.8 Acknowledgements

This study was funded by the Natural Science and Engineering Research Council of Canada (NSERC), Agnico Eagle Mines Limited, and Ministère de l'Energie et des Ressources Naturelles of Québec. We are very grateful to Dany Savard and Audrey Lavoie from LabMaTer, Université du Québec à Chicoutimi for their support with LA-ICP-MS analyses, to Marc Choquette and Suzie Coté from Université Laval for their assistance and support for SEM and EPMA analyzes and Edmond Rousseau for his support for sample preparation. Special thanks to those who provided chalcopyrite samples for analysis: Dominique Genna (CONSOREM, Canada), Sven Petersen (Helmholtz Centre for Ocean Research Kiel, Germany), Jorge M.R.S. Relvas (Instituto Dom Luiz, Faculdade de Ciências, Universidade de Lisboa, Portugal), Stephen J. Piercey (Memorial University of Newfoundland, Canada) for samples from VMS deposits, Sarah-Jane Barnes (UQAC, Canada) for samples from magmatic sulfide deposits, Daniel Gregory (University of Toronto, Canada) for representative samples from IOCG deposits, and Mikael Vasilopoulos (University of Oulu, Finland) for chalcopyrite samples from orogenic gold deposits.

Funding information The research is funded by Agnico Eagle Mines Ltd., the Ministère de l'Énergie et des Ressources Naturelles du Québec and the Natural Sciences and Engineering Research Council.

3.9 References

Abd Elrahman, S. M., and Abraham, A., 2013, A review of class imbalance problem: Journal of Network and Innovative Computing, v. 1, p. 332-340.

Agangi, A., Reddy, S., Plavsa, D., Vieru, C., Selvaraja, V., LaFlamme, C., Jeon, H., Martin, L., Nozaki, T., and Takaya, Y., 2018, Subsurface deposition of Cu-rich massive sulphide underneath a Palaeoproterozoic seafloor hydrothermal system—the Red Bore prospect, Western Australia: Mineralium Deposita, p. 1-18.

Aitchison, J., 1986, The statistical analysis of compositional data: London, Chapman and Hall, 416 p p.

Averill, S. A., 2001, The application of heavy indicator mineralogy in mineral exploration with emphasis on base metal indicators in glaciated metamorphic and plutonic terrains: Geological Society, London, Special Publications, v. 185, p. 69-81.

Averill, S. A., 2011, Viable indicator minerals in surficial sediments for two major base metal deposit types: Ni-Cu-PGE and porphyry Cu: Geochemistry: Exploration, Environment, Analysis, v. 11, p. 279-291.

Bajwah, Z. U., Seccombe, P. K., and Offler, R., 1987, Trace element distribution, Co: Ni ratios and genesis of the Big Cadia iron-copper deposit, New South Wales, Australia: Mineralium Deposita, v. 22, p. 292-300.

Ballabio, D., and Consonni, V., 2013, Classification tools in chemistry. Part 1: linear models. PLS-DA: Analytical Methods, v. 5, p. 3790-3798.

Barker, R. D., Barker, S. L. L., Cracknell, M. J., Stock, E. D., and Holmes, G., 2021, Quantitative Mineral Mapping of Drill Core Surfaces II: Long-Wave Infrared Mineral Characterization Using μXRF and Machine Learning: Economic Geology, v. 116, p. 821-836.

Barnes, S.-J., 2016, Chalcophile elements, Encyclopedia of Geochemistry: A Comprehensive Reference Source on the Chemistry of the Earth, Springer International Publishing, p. 1-5.

Barnes, S.-J., Cox, R. A., and Zientek, M. L., 2006, Platinum-group element, gold, silver and base metal distribution in compositionally zoned sulfide droplets from the Medvezky Creek Mine, Noril'sk, Russia: Contributions to Mineralogy and Petrology, v. 152, p. 187-200.

Barnes, S.-J., and Lightfoot, P. C., 2005, Formation of magmatic nickel sulfide ore deposits and processes affecting their copper and platinum group element contents: Economic geology 100th anniversary volume, v. 34, p. 179-214.

Barnes, S.-J., Prichard, H. M., Cox, R. A., Fisher, P. C., and Godel, B., 2008, The location of the chalcophile and siderophile elements in platinum-group element ore deposits (a textural, microbeam and whole rock geochemical study): Implications for the formation of the deposits: Chemical Geology, v. 248, p. 295-317.

Barnes, S.-J., and Ripley, E. M., 2016, Highly siderophile and strongly chalcophile elements in magmatic ore deposits: Reviews in Mineralogy and Geochemistry, v. 81, p. 725-774.

Bédard, É., De Bronac de Vazelhes, V., and Beaudoin, G., 2022, Performance of predictive supervised classification models of trace elements in magnetite for mineral exploration: Journal of Geochemical Exploration, v. 236, p. 106959.

Bédard, É., Goulet, A., Sappin, A.-A., Makvandi, S., and Beaudoin, G., 2017, Chalcopyrite as an indicator mineral to fingerprint mineral deposit types: a preliminary study: Mineral Resources to Discover-Proceedings of the 14th SGA Biennial Meeting, Québec City, Canada, 2017, p. 1115-1118.

Berrar, D., 2018, Bayes' theorem and naive Bayes classifier: Encyclopedia of Bioinformatics and Computational Biology: ABC of Bioinformatics, v. 403.

Bolton, M. S. M., Jensen, B. J. L., Wallace, K., Praet, N., Fortin, D., Kaufman, D., and De Batist, M., 2020, Machine learning classifiers for attributing tephra to source volcanoes: an evaluation of methods for Alaska tephras: Journal of Quaternary Science, v. 35, p. 81-92.

Bowes, D., Hall, T., and Gray, D., 2012, Comparing the performance of fault prediction models which report multiple performance measures: recomputing the confusion matrix: Proceedings of the 8th international conference on predictive models in software engineering, 2012, p. 109-118.

Breiman, L., 2001, Random Forests: Machine Learning, v. 45, p. 5-32.

Brereton, R. G., and Lloyd, G. R., 2014, Partial least squares discriminant analysis: taking the magic away: Journal of Chemometrics, v. 28, p. 213-225.

Brownlee, J., 2018, Master machine learning algorithms: Discover how they work and implement them from scratch, Melbourne, Machine Learning Mastery.

Butler, I. B., and Nesbitt, R. W., 1999, Trace element distributions in the chalcopyrite wall of a black smoker chimney: insights from laser ablation inductively coupled plasma mass spectrometry (LA–ICP–MS): Earth and Planetary Science Letters, v. 167, p. 335-345.

Cabri, L. J., Campbell, J. L., Laflamme, J. H. G., Leigh, R. G., Maxwell, J. A., and Scott, J. D., 1985, Proton-microprobe analysis of trace elements in sulfides from some massive-sulfide deposits: The Canadian Mineralogist, v. 23, p. 133-148.

Caraballo, E., Dare, S., and Beaudoin, G., 2022, Variation of trace elements in chalcopyrite from worldwide Ni-Cu sulfide and Reef-type PGE deposits: implications for mineral exploration: Mineralium Deposita, v. 57, p. 1293-1321.

Caté, A., Perozzi, L., Gloaguen, E., and Blouin, M., 2017, Machine learning as a tool for geologists: The Leading Edge, v. 36, p. 215-219.

Charette, B., Lafrance, I., and Mathieu, G., 2015, Géologie de la région du lac Jeannin (SNRC 24B): Ministère de l'Énergie et des Ressources naturelles, Québec, BG, v. 1.

Chen, L.-M., Song, X.-Y., Danyushevsky, L. V., Wang, Y.-S., Tian, Y.-L., and Xiao, J.-F., 2015, A laser ablation ICP-MS study of platinum-group and chalcophile elements in base metal sulfide minerals of the Jinchuan Ni–Cu sulfide deposit, NW China: Ore Geology Reviews, v. 65, p. 955-967.

Chen, P., Zeng, Q., Zhou, L., Liu, B., Fu, Y., Sun, G., Yu, B., and Long, Z., 2022, Genesis and prospecting significance of the Buziwannan gold-polymetallic ore deposit in the West Kunlun Orogen Belt, China: Constraints from mineral geochemistry and in situ S–Pb isotope analyses of sulfides: Journal of Geochemical Exploration, p. 107125.

Chorlton, L. B., 2007, Generalized geology of the world: bedrock domains and major faults in GIS format: Geological Survey of Canada, Open File, v. 5529.

Chowdhury, S., Pal, D. C., Papineau, D., and Lentz, D. R., 2020, Major and trace element and multiple sulfur isotope composition of sulfides from the Paleoproterozoic Surda copper deposit, Singhbhum shear Zone, India: Implications for the mineralization processes: Ore Geology Reviews, v. 120, p. 103396.

Cook, N. J., Ciobanu, C. L., Danyushevsky, L. V., and Gilbert, S., 2011, Minor and trace elements in bornite and associated Cu–(Fe)-sulfides: A LA-ICP-MS studyBornite mineral chemistry: Geochimica et Cosmochimica Acta, v. 75, p. 6473-6496.

Cracknell, M. J., and Reading, A. M., 2014, Geological mapping using remote sensing data: A comparison of five machine learning algorithms, their response to variations in the spatial distribution of training data and the use of explicit spatial information: Computers & Geosciences, v. 63, p. 22-33.

Crundwell, F. K., 2021, The impact of light on understanding the mechanism of dissolution and leaching of sphalerite (ZnS), pyrite (FeS2) and chalcopyrite (CuFeS2): Minerals Engineering, v. 161, p. 106728.

Crundwell, F. K., Bryson, L. J., van Aswegen, A., and Knights, B. D. H., 2021, Effect of chopped light on the dissolution and leaching of chalcopyrite: Minerals Engineering, v. 160, p. 106703.

Cui, H., Zhong, R., Li, W., Yu, C., Danyushevsky, L. V., Belousov, I., Liu, C., and Li, Z., 2023, Revealing the orogenic genesis of Huogeqi Cu-Pb-Zn deposit: Evidence from the machine learning-based data interpretation of pyrite geochemistry: Ore Geology Reviews, v. 154, p. 105350.

Czamanske, G. K., Kunilov, V. E., Zientek, M. L., Cabri, L. J., Likhachev, A. P., Calk, L. C., and Oscarson, R. L., 1992, A proton microprobe study of magmatic sulfide ores from the Noril'sk-Talnakh District, Siberia: The Canadian Mineralogist, v. 30, p. 249-287.

Dare, S. A., Barnes, S.-J., Prichard, H. M., and Fisher, P. C., 2014, Mineralogy and geochemistry of Cu-rich ores from the McCreedy East Ni-Cu-PGE deposit (Sudbury, Canada): implications for the behavior of

platinum group and chalcophile elements at the end of crystallization of a sulfide liquid: Economic Geology, v. 109, p. 343-366.

Dare, S. A. S., Barnes, S.-J., and Prichard, H. M., 2010b, The distribution of platinum group elements (PGE) and other chalcophile elements among sulfides from the Creighton Ni–Cu–PGE sulfide deposit, Sudbury, Canada, and the origin of palladium in pentlandite: Mineralium Deposita, v. 45, p. 765-793.

Dare, S. A. S., Barnes, S.-J., Prichard, H. M., and Fisher, P. C., 2010a, The timing and formation of platinum-group minerals from the Creighton Ni-Cu-platinum-group element sulfide deposit, Sudbury, Canada: Early crystallization of PGE-rich sulfarsenides: Economic Geology, v. 105, p. 1071-1096.

Dare, S. A. S., Barnes, S.-J., Prichard, H. M., and Fisher, P. C., 2011, Chalcophile and platinum-group element (PGE) concentrations in the sulfide minerals from the McCreedy East deposit, Sudbury, Canada, and the origin of PGE in pyrite: Mineralium Deposita, v. 46, p. 381-407.

Daunis-i-Estadella, J., Barceló-Vidal, C., and Buccianti, A., 2006, Exploratory compositional data analysis: Geological Society, London, Special Publications, v. 264, p. 161-174.

Delgado, R., and Tibau, X.-A., 2019, Why Cohen's Kappa should be avoided as performance measure in classification: PloS one, v. 14, p. e0222916.

Djon, M. L. N., and Barnes, S.-J., 2012, Changes in sulfides and platinum-group minerals with the degree of alteration in the Roby, Twilight, and High Grade Zones of the Lac des Iles Complex, Ontario, Canada: Mineralium Deposita, v. 47, p. 875-896.

Dmitrijeva, M., Cook, N. J., Ehrig, K., Ciobanu, C. L., Metcalfe, A. V., Kamenetsky, M., Kamenetsky, V. S., and Gilbert, S., 2020, Multivariate Statistical Analysis of Trace Elements in Pyrite: Prediction, Bias and Artefacts in Defining Mineral Signatures: Minerals, v. 10, p. 61.

Dunn, K., 2019, Process improvement using data, 325-404 p.

Dupont, A., Vander Auwera, J., Pin, C., Marincea, S., and Berza, T., 2002, Trace element and isotope (Sr, Nd) geochemistry of porphyry-and skarn-mineralising Late Cretaceous intrusions from Banat, western South Carpathians, Romania: Mineralium Deposita, v. 37, p. 568.

Duran, C. J., Barnes, S.-J., and Corkery, J. T., 2016, Trace element distribution in primary sulfides and Fe–Ti oxides from the sulfide-rich pods of the Lac des Iles Pd deposits, Western Ontario, Canada: Constraints on processes controlling the composition of the ore and the use of pentlandite compositions in exploration: Journal of Geochemical Exploration, v. 166, p. 45-63.

Duran, C. J., Dubé-Loubert, H., Pagé, P., Barnes, S.-J., Roy, M., Savard, D., Cave, B. J., Arguin, J.-P., and Mansur, E. T., 2019, Applications of trace element chemistry of pyrite and chalcopyrite in glacial sediments to mineral exploration targeting: Example from the Churchill Province, northern Quebec, Canada: Journal of Geochemical Exploration, v. 196, p. 105-130.

Egozcue, J. J., and Pawlowsky-Glahn, V., 2011, Análisis composicional de datos en Ciencias Geoambientales: Boletín Geológico y Minero, v. 122, p. 439-452.

Ferreira Filho, C. F., Ferraz de Oliveira, M. M., Mansur, E. T., and Rosa, W. D., 2021, The Jaguar hydrothermal nickel sulfide deposit: Evidence for a nickel-rich member of IOCG-type deposits in the Carajás Mineral Province, Brazil: Journal of South American Earth Sciences, v. 111, p. 103501.

Filzmoser, P., Hron, K., and Reimann, C., 2009, Principal component analysis for compositional data with outliers: Environmetrics, v. 20, p. 621-632.

Frenzel, M., Hirsch, T., and Gutzmer, J., 2016, Gallium, germanium, indium, and other trace and minor elements in sphalerite as a function of deposit type—A meta-analysis: Ore Geology Reviews, v. 76, p. 52-78.

George, L. L., Cook, N. J., and Ciobanu, C. L., 2016, Partitioning of trace elements in co-crystallized sphalerite–galena–chalcopyrite hydrothermal ores: Ore Geology Reviews, v. 77, p. 97-116.

George, L. L., Cook, N. J., Crowe, B. B., and Ciobanu, C. L., 2018, Trace elements in hydrothermal chalcopyrite: Mineralogical Magazine, v. 82, p. 59-88.

Gislason, P. O., Benediktsson, J. A., and Sveinsson, J. R., 2006, Random forests for land cover classification: Pattern recognition letters, v. 27, p. 294-300.

Godel, B., and Barnes, S.-J., 2008, Platinum-group elements in sulfide minerals and the whole rocks of the JM Reef (Stillwater Complex): Implication for the formation of the reef: Chemical Geology, v. 248, p. 272-294.

Godel, B., Barnes, S.-J., and Maier, W. D. J. J. o. P., 2007, Platinum-group elements in sulphide minerals, platinum-group minerals, and whole-rocks of the Merensky Reef (Bushveld Complex, South Africa): implications for the formation of the reef, v. 48, p. 1569-1604.

González-Álvarez, I., Pirajno, F., and Kerrich, R., 2013, Hydrothermal nickel deposits: Secular variation and diversity, 52, Elsevier, p. 1-3.

Goulet, A., 2016, Composition chimique de la chalcopyrite et application à l'exploration minérale, *in* Département de géologie et génie géologique, U. L., ed., p. 99.

Gregory, D. D., Cracknell, M. J., Large, R. R., McGoldrick, P., Kuhn, S., Maslennikov, V. V., Baker, M. J., Fox, N., Belousov, I., Figueroa, M. C., Steadman, J. A., Fabris, A. J., and Lyons, T. W., 2019, Distinguishing Ore Deposit Type and Barren Sedimentary Pyrite Using Laser Ablation-Inductively Coupled Plasma-Mass Spectrometry Trace Element Data and Statistical Analysis of Large Data Sets: Economic Geology, v. 114, p. 771-786.

Grömping, U., 2009, Variable Importance Assessment in Regression: Linear Regression versus Random Forest: The American Statistician, v. 63, p. 308-319.

Grzela, D., Beaudoin, G., and Bédard, É., 2019, Tourmaline, scheelite, and magnetite compositions from orogenic gold deposits and glacial sediments of the Val-d'Or district (Quebec, Canada): Applications to mineral exploration: Journal of Geochemical Exploration, v. 206, p. 106355.

Hannington, M. D., 2014, 13.18 - Volcanogenic Massive Sulfide Deposits, *in* Holland, H. D., and Turekian, K. K., eds., Treatise on Geochemistry (Second Edition): Oxford, Elsevier, p. 463-488.

Harris, D. C., Cabri, L. J., and Nobiling, R., 1984, Silver-bearing chalcopyrite, a principal source of silver in the Izok Lake massive-sulfide deposit; confirmation by electron-and proton-microprobe analyses: The Canadian Mineralogist, v. 22, p. 493-498.

Harris, J. R., and Grunsky, E. C., 2015, Predictive lithological mapping of Canada's North using Random Forest classification applied to geophysical and geochemical data: Computers & Geosciences, v. 80, p. 9-25.

Hashmi, S., Ward, B., Plouffe, A., Leybourne, M., and Ferbey, T., 2015, Geochemical and mineralogical dispersal in till from the Mount Polley Cu-Au porphyry deposit, central British Columbia, Canada: Geochemistry: Exploration, Environment, Analysis, v. 15, p. 234-249.

Hawley, J., and Nichol, I., 1961, Trace elements in pyrite, pyrrhotite and chalcopyrite of different ores: Economic Geology, v. 56, p. 467-487.

Holwell, D. A., and McDonald, I., 2007, Distribution of platinum-group elements in the Platreef at Overysel, northern Bushveld Complex: a combined PGM and LA-ICP-MS study: Contributions to Mineralogy and Petrology, v. 154, p. 171-190.

Hong, S., Zuo, R., Huang, X., and Xiong, Y., 2021, Distinguishing IOCG and IOA deposits via random forest algorithm based on magnetite composition: Journal of Geochemical Exploration, v. 230, p. 106859.

Houle, P., and Perreault, S., 2007, Les Orogènes du Nouveau-Québec et des Torngat, la Province de Churchill Sud-Est (Zone noyau) et l'Orogène de l'Ungava (région administrative 10, Nord-du-Québec): Ministère des Ressources naturelles et de la Faune du Québec: Rapport sur les activités d'exploration minière au Québec 2007, p. 35-40.

Hu, B., Zeng, L.-P., Liao, W., Wen, G., Hu, H., Li, M. Y. H., and Zhao, X.-F., 2022, The Origin and Discrimination of High-Ti Magnetite in Magmatic-Hydrothermal Systems: Insight from Machine Learning Analysis: Economic Geology, v. 117, p. 1613-1627.

Huston, D. L., Sie, S. H., Suter, G. F., Cooke, D. R., and Both, R. A., 1995, Trace elements in sulfide minerals from eastern Australian volcanic-hosted massive sulfide deposits; Part I, Proton microprobe analyses of pyrite, chalcopyrite, and sphalerite, and Part II, Selenium levels in pyrite; comparison with delta 34 S values and implications for the source of sulfur in volcanogenic hydrothermal systems: Economic Geology, v. 90, p. 1167-1196.

Jochum, K. P., Nohl, U., Herwig, K., Lammel, E., Stoll, B., and Hofmann, A. W., 2005, GeoReM: a new geochemical database for reference materials and isotopic standards: Geostandards and Geoanalytical Research, v. 29, p. 333-338.

Kase, K., 1987, Tin-bearing chalcopyrite from the Izumo vein, Toyoha mine, Hokkaido, Japan: The Canadian Mineralogist, v. 25, p. 9-13.

Knight, R. D., Prichard, H. M., and Ferreira Filho, C. F., 2017, Evidence for As contamination and the partitioning of Pd into Pentlandite and Co+ platinum group elements into pyrite in the Fazenda Mirabela intrusion, Brazil: Economic Geology, v. 112, p. 1889-1912.

Kotsiantis, S. B., Zaharakis, I., and Pintelas, P., 2007, Supervised machine learning: A review of classification techniques: Emerging artificial intelligence applications in computer engineering, v. 160, p. 3-24.

Kuhn, M., 2012, The caret package: R Foundation for Statistical Computing, Vienna, Austria. URL https://cran. r-project. org/package= caret.

Kuhn, M., and Johnson, K., 2013, Applied predictive modeling: New York, Springer, 600 p.

Lafrance, I., Simard, M., and Bandyayera, D., 2014, Géologie de la région du lac Saffray (SNRC 24G, 24F), Géologie Québec.

Lafrance, I., Vanier, M.-A., and Charette, B., 2020, Baleine Lithotectonic Domain, Southeastern Churchill Province, Nunavik, Quebec, Canada: Geological Synthesis (BG 2020-07), Ministère de l'Énergie et des Ressources naturelles, Québec, BG, 1.

Lee, L. C., Liong, C.-Y., and Jemain, A. A., 2018, Partial least squares-discriminant analysis (PLS-DA) for classification of high-dimensional (HD) data: a review of contemporary practice strategies and knowledge gaps: Analyst, v. 143, p. 3526-3539.

Li, R., Chen, H., Xia, X., Yang, Q., Danyushevsky, L. V., and Lai, C., 2018, Using integrated in-situ sulfide trace element geochemistry and sulfur isotopes to trace ore-forming fluids: Example from the Mina Justa IOCG deposit (southern Perú): Ore Geology Reviews, v. 101, p. 165-179.

Li, X.-M., Zhang, Y.-X., Li, Z.-K., Zhao, X.-F., Zuo, R.-G., Xiao, F., and Zheng, Y., 2023, Discrimination of Pb-Zn deposit types using sphalerite geochemistry: New insights from machine learning algorithm: Geoscience Frontiers, v. 14, p. 101580.

Liang, P., Chen, L., Li, R., Xie, Y., Wu, C., and Lai, C.-K., 2021, In-situ element geochemical and sulfur isotope signature of pyrite and chalcopyrite: Constraints on ore-forming processes of the Laoshankou iron oxide-copper (-gold) deposit, northern East Junggar: Ore Geology Reviews, v. 139, p. 104510.

Liang, Q.-L., Song, X.-Y., Wirth, R., Chen, L.-M., and Dai, Z.-H., 2019, Implications of nano- and micrometer-size platinum-group element minerals in base metal sulfides of the Yangliuping Ni-Cu-PGE sulfide deposit, SW China: Chemical Geology, v. 517, p. 7-21.

Liu, B., Gao, L., Li, B., Marcos-Martinez, R., and Bryan, B. A., 2020, Nonparametric machine learning for mapping forest cover and exploring influential factors: Landscape Ecology, v. 35, p. 1683-1699.

Liu, H., and Beaudoin, G., 2021, Geochemical signatures in native gold derived from Au-bearing ore deposits: Ore Geology Reviews, p. 104066.

Liu, H., Beaudoin, G., Makvandi, S., Jackson, S. E., and Huang, X., 2021, Multivariate statistical analysis of trace element compositions of native gold from orogenic gold deposits: implication for mineral exploration: Ore Geology Reviews, p. 104061.

Liu, W., Migdisov, A., and Williams-Jones, A., 2012, The stability of aqueous nickel (II) chloride complexes in hydrothermal solutions: Results of UV–Visible spectroscopic experiments: Geochimica et Cosmochimica Acta, v. 94, p. 276-290.

Lobo, L., 2022, Geochemical Study of Trace and Critical Elements in Chalcopyrite and Pyrite from the Assarel Porphyry-Cu-Au Deposit, Bulgaria, Uppsala University 108 p.

Lyubetskaya, T., and Korenaga, J., 2007, Chemical composition of Earth's primitive mantle and its variance: 1. Method and results: Journal of Geophysical Research: Solid Earth, v. 112.

Makvandi, S., Ghasemzadeh-Barvarz, M., Beaudoin, G., Grunsky, E. C., Beth McClenaghan, M., and Duchesne, C., 2016a, Principal component analysis of magnetite composition from volcanogenic massive sulfide deposits: Case studies from the Izok Lake (Nunavut, Canada) and Halfmile Lake (New Brunswick, Canada) deposits: Ore Geology Reviews, v. 72, p. 60-85.

Makvandi, S., Ghasemzadeh-Barvarz, M., Beaudoin, G., Grunsky, E. C., McClenaghan, M. B., Duchesne, C., and Boutroy, E., 2016b, Partial least squares-discriminant analysis of trace element compositions of magnetite from various VMS deposit subtypes: Application to mineral exploration: Ore Geology Reviews, v. 78, p. 388-408.

Mansur, E. T., and Barnes, S.-J., 2020, The role of Te, As, Bi, Sn and Sb during the formation of platinum-group-element reef deposits: examples from the Bushveld and Stillwater complexes: Geochimica et Cosmochimica Acta, v. 272, p. 235-258.

Mansur, E. T., Barnes, S.-J., and Duran, C. J., 2021, An overview of chalcophile element contents of pyrrhotite, pentlandite, chalcopyrite, and pyrite from magmatic Ni-Cu-PGE sulfide deposits: Mineralium Deposita, p. 1-26.

Mansur, E. T., Barnes, S.-J., Duran, C. J., and Sluzhenikin, S. F., 2020, Distribution of chalcophile and platinum-group elements among pyrrhotite, pentlandite, chalcopyrite and cubanite from the Noril'sk-Talnakh ores: Implications for the formation of platinum-group minerals: Mineralium Deposita, v. 55, p. 1215-1232.

Mansur, E. T., Dare, S. A. S., Filho, C. F. F., Miranda, A. C. R., and Monteiro, L. V. S., 2023, The distribution of trace elements in sulfides and magnetite from the Jaguar hydrothermal nickel deposit: Exploring the link with IOA and IOCG deposits within the Carajás Mineral Province, Brazil: Ore Geology Reviews, v. 152, p. 105256.

Marfin, A. E., Ivanov, A. V., Abramova, V. D., Anziferova, T. N., Radomskaya, T. A., Yakich, T. Y., and Bestemianova, K. V., 2020, A Trace Element Classification Tree for Chalcopyrite from Oktyabrsk Deposit, Norilsk–Talnakh Ore District, Russia: LA-ICPMS Study: Minerals, v. 10, p. 716.

Martin, A. J., Keith, M., McDonald, I., Haase, K. M., McFall, K. A., Klemd, R., and MacLeod, C. J., 2019, Trace element systematics and ore-forming processes in mafic VMS deposits: Evidence from the Troodos ophiolite, Cyprus: Ore Geology Reviews, v. 106, p. 205-225.

Martin, A. J., McDonald, I., MacLeod, C. J., Prichard, H. M., and McFall, K., 2018, Extreme enrichment of selenium in the Apliki Cyprus-type VMS deposit, Troodos, Cyprus: Mineralogical Magazine, v. 82, p. 697-724.

Maslennikov, V., Maslennikova, S., Large, R., and Danyushevsky, L., 2009a, Study of trace element zonation in vent chimneys from the Silurian Yaman-Kasy volcanic-hosted massive sulfide deposit (Southern Urals, Russia) using laser ablation-inductively coupled plasma mass spectrometry (LA-ICPMS): Economic Geology, v. 104, p. 1111-1141.

Maslennikov, V. V., Maslennikova, S. P., Large, R. R., and Danyushevsky, L. V., 2009b, Study of trace element zonation in vent chimneys from the Silurian Yaman-Kasy volcanic-hosted massive sulfide deposit (Southern Urals, Russia) using laser ablation-inductively coupled plasma mass spectrometry (LA-ICPMS): Economic Geology, v. 104, p. 1111-1141.

Maslennikov, V. V., Maslennikova, S. P., Large, R. R., Danyushevsky, L. V., Herrington, R. J., Ayupova, N. R., Zaykov, V. V., Lein, A. Y., Tseluyko, A. S., Melekestseva, I. Y., and Tessalina, S. G., 2017, Chimneys in Paleozoic massive sulfide mounds of the Urals VMS deposits: Mineral and trace element comparison with modern black, grey, white and clear smokers: Ore Geology Reviews, v. 85, p. 64-106.

McClenaghan, M. B., 2005, Indicator mineral methods in mineral exploration: Geochemistry: Exploration, Environment, Analysis, v. 5, p. 233-245.

McClenaghan, M. B., 2017, Gold grains in till samples from the southern Core Zone, Quebec and Newfoundland and Labrador (NTS 23-P and 23-I): potential for undiscovered mineralization, Natural Resources Canada, Geological Survey of Canada.

Melekestseva, I., Maslennikov, V., Tret'yakov, G., Maslennikova, S., Danyushevsky, L., Kotlyarov, V., Large, R., Beltenev, V., and Khvorov, P., 2020a, Trace Element Geochemistry of Sulfides from the Ashadze-2 Hydrothermal Field (12°58' N, Mid-Atlantic Ridge): Influence of Host Rocks, Formation Conditions or Seawater?: Minerals, v. 10.

Melekestseva, I. Y., Maslennikov, V. V., and Maslennikova, S. P., 2020b, Trace-elements in sulfides of the Dergamysh cobalt-bearing massive sulfide deposit, the Southern Urals: Mode of occurrence and matter sources: Lithosphere (Russia), v. 20, p. 499-516.

Menze, B. H., Kelm, B. M., Masuch, R., Himmelreich, U., Bachert, P., Petrich, W., and Hamprecht, F. A., 2009, A comparison of random forest and its Gini importance with standard chemometric methods for the feature selection and classification of spectral data: BMC Bioinformatics, v. 10, p. 213.

Miranda, A. C. R., Beaudoin, G., and Rottier, B., 2022, Scheelite chemistry from skarn systems: implications for ore-forming processes and mineral exploration: Mineralium Deposita.

Mishra, B. P., Pati, P., Dora, M. L., Baswani, S. R., Meshram, T., Shareef, M., Pattanayak, R. S., Suryavanshi, H., Mishra, M., and Raza, M. A., 2021, Trace-element systematics and isotopic characteristics of sphalerite-pyrite from volcanogenic massive sulfide deposits of Betul belt, central Indian Tectonic Zone: Insight of ore genesis to exploration: Ore Geology Reviews, v. 134, p. 104149.

Moggi-Cecchi, V., Cipriani, C., Rossi, P., Ceccato, D., Rudello, V., and Somacal, H., 2002, Trace element contents and distribution maps of chalcopyrite: a micro-PIXE study: PERIODICO di MINERALOGIA, v. 71, p. 101-9.

Naldrett, A. J., 2004, Magmatic sulfide deposits: Geology, geochemistry and exploration, Springer, Berlin, Heidelberg, 728 p, 728 p.

Palarea-Albaladejo, J., and Martín-Fernández, J. A., 2015, zCompositions—R package for multivariate imputation of left-censored data under a compositional approach: Chemometrics and Intelligent Laboratory Systems, v. 143, p. 85-96.

Pawlowsky-Glahn, V., and Buccianti, A., 2011, Compositional data analysis: Theory and applications, John Wiley & Sons, 378 p, 378 p.

Pawlowsky-Glahn, V., Egozcue, J. J., and Tolosana-Delgado, R., 2015, Modeling and analysis of compositional data, John Wiley & Sons.

Piña, R., Gervilla, F., Barnes, S.-J., Ortega, L., and Lunar, R., 2012, Distribution of platinum-group and chalcophile elements in the Aguablanca Ni–Cu sulfide deposit (SW Spain): evidence from a LA-ICP-MS study: Chemical Geology, v. 302, p. 61-75.

Piña, R., Gervilla, F., Barnes, S. J., Oberthür, T., and Lunar, R., 2016, Platinum-group element concentrations in pyrite from the Main Sulfide Zone of the Great Dyke of Zimbabwe: Mineralium Deposita, v. 51, p. 853-872.

Piña, R., Gervilla, F., Barnes, S. J., Ortega, L., and Lunar, R., 2015, Liquid immiscibility between arsenide and sulfide melts: evidence from a LA-ICP-MS study in magmatic deposits at Serranía de Ronda (Spain): Mineralium Deposita, v. 50, p. 265-279.

Plouffe, A., Ferbey, T., Hashmi, S., and Ward, B., 2016, Till geochemistry and mineralogy: vectoring towards Cu porphyry deposits in British Columbia, Canada: Geochemistry: Exploration, Environment, Analysis, v. 16, p. 213-232.

Plouffe, A., Kjarsgaard, I. M., Ferbey, T., Wilton, D. H. C., Petts, D. C., Percival, J. B., Kobylinski, C. H., and McNeil, R., 2022, Detecting Buried Porphyry Cu Mineralization in a Glaciated Landscape: A Case Study from the Gibraltar Cu-Mo Deposit, British Columbia, Canada: Economic Geology, v. 117, p. 777-799.

Provost, F., and Saar-Tsechanski, M., 2007, Handling Missing Values when Applying Classification Models: Journal of Machine Learning Research, v. 8, p. 1625-1657.

Reich, M., Palacios, C., Barra, F., and Chryssoulis, S., 2013, "Invisible" silver in chalcopyrite and bornite from the Mantos Blancos Cu deposit, northern Chile: European Journal of Mineralogy, v. 25, p. 453-460.

Reich, M., Román, N., Barra, F., and Morata, D., 2020, Silver-rich chalcopyrite from the active Cerro Pabellón geothermal system, Northern Chile: Minerals, v. 10, p. 113.

Revan, M. K., Genç, Y., Maslennikov, V. V., Maslennikova, S. P., Large, R. R., and Danyushevsky, L. V., 2014, Mineralogy and trace-element geochemistry of sulfide minerals in hydrothermal chimneys from the Upper-Cretaceous VMS deposits of the eastern Pontide orogenic belt (NE Turkey): Ore Geology Reviews, v. 63, p. 129-149.

Rimstidt, J. D., Chermak, J. A., and Gagen, P. M., 1993, Rates of Reaction of Galena, Sphalerite, Chalcopyrite, and Arsenopyrite with Fe(III) in Acidic Solutions, Environmental Geochemistry of Sulfide Oxidation, 550. ACS Symposium Series, American Chemical Society, p. 2-13.

Rose, A. W., 1967, Trace elements in solflde minerals from the Central district, New Mexico and the Bingham district, Utah: Geochimica et Cosmochimica Acta, v. 31, p. 547-585.

Salim Amaral, L. F., 2017, The distribution of platinum-group elements and other chalcophile elements among sulfide minerals from the Ovoid ore body of the Voisey's Bay Ni-Cu sulfide deposit, Canada (Master's thesis): Unpub. Master's thesis thesis, Université du Québec à Chicoutimi, 154 p.

Samalens, N., Barnes, S. J., and Sawyer, E. W., 2017, A laser ablation inductively coupled plasma mass spectrometry study of the distribution of chalcophile elements among sulfide phases in sedimentary and magmatic rocks of the Duluth Complex, Minnesota, USA: Ore Geology Reviews, v. 90, p. 352-370.

Sciuba, M., and Beaudoin, G., 2021, Texture and Trace Element Composition of Rutile in Orogenic Gold Deposits: Economic Geology, v. 116, p. 1865-1892.

Sciuba, M., Beaudoin, G., Grzela, D., and Makvandi, S., 2020, Trace element composition of scheelite in orogenic gold deposits: Mineralium Deposita, v. 55, p. 1149–1172.

Sciuba, M., Beaudoin, G., and Makvandi, S., 2021, Chemical composition of tourmaline in orogenic gold deposits: Mineralium Deposita, v. 56, p. 537-560.

Seward, T. M., Williams-Jones, A. E., and Migdisov, A. A., 2014, The chemistry of metal transport and deposition by ore-forming hydrothermal fluids, *in* Holland, H. D., and Tukerian, K. K., eds., Treatise on geochemistry, 13, Elsevier Oxford, p. 29-57.

Skirrow, R. G., 2022, Iron oxide copper-gold (IOCG) deposits – A review (part 1): Settings, mineralogy, ore geochemistry and classification: Ore Geology Reviews, v. 140, p. 104569.

Sokolova, M., and Lapalme, G., 2009, A systematic analysis of performance measures for classification tasks: Information Processing & Management, v. 45, p. 427-437.

Stefanova, E., Georgiev, S., Peytcheva, I., Marchev, P., Quadt, A. V., Raicheva, R., Gerdjikov, I., Kouzmanov, K., Boyce, A., and Vennemann, T., 2023, Sulfide Trace Element Signatures and S-and Pb-Isotope Geochemistry of Porphyry Copper and Epithermal Gold-Base Metal Mineralization in the Eletsite–Chelopech Ore Field (Bulgaria): Minerals, v. 13, p. 630.

Stekhoven, D. J., and Bühlmann, P., 2012, MissForest—non-parametric missing value imputation for mixed-type data: Bioinformatics, v. 28, p. 112-118.

Strashimirov, S., Petrunov, R., and Kanazirski, M., 2002, Porphyry-copper mineralisation in the central Srednogorie zone, Bulgaria: Mineralium Deposita, v. 37, p. 587-598.

Sun, G.-T., and Zhou, J.-X., 2022, Application of Machine Learning Algorithms to Classification of Pb–Zn Deposit Types Using LA–ICP–MS Data of Sphalerite: Minerals, v. 12, p. 1293.

Sun, G., Zeng, Q., and Zhou, J.-X., 2022, Machine learning coupled with mineral geochemistry reveals the origin of ore deposits: Ore Geology Reviews, v. 142, p. 104753.

Sun, T., Li, H., Wu, K., Chen, F., Zhu, Z., and Hu, Z., 2020, Data-Driven Predictive Modelling of Mineral Prospectivity Using Machine Learning and Deep Learning Methods: A Case Study from Southern Jiangxi Province, China: Minerals, v. 10.

Svetnik, V., Liaw, A., Tong, C., Culberson, J. C., Sheridan, R. P., and Feuston, B. P., 2003, Random Forest: A Classification and Regression Tool for Compound Classification and QSAR Modeling: Journal of Chemical Information and Computer Sciences, v. 43, p. 1947-1958.

Tan, H. M. R., Huang, X.-W., Meng, Y.-M., Xie, H., and Qi, L., 2023, Multivariate statistical analysis of trace elements in apatite: Discrimination of apatite with different origins: Ore Geology Reviews, v. 153, p. 105269.

Tian, Y., Etschmann, B., Liu, W., Borg, S., Mei, Y., Testemale, D., O'Neill, B., Rae, N., Sherman, D. M., Ngothai, Y., Johannessen, B., Glover, C., and Brugger, J., 2012, Speciation of nickel (II) chloride complexes in hydrothermal fluids: In situ XAS study: Chemical Geology, v. 334, p. 345-363.

Vasilopoulos, M., Molnár, F., Ranta, J.-P., and O'Brien, H., 2023, Mineralogical, lithogeochemical and sulfide trace element characteristics of the Hirvilavanmaa Au-only and the base metal-rich Naakenavaara orogenic gold deposits in the Central Lapland belt, northern Finland: Journal of Geochemical Exploration, v. 244, p. 107132.

Von Eynatten, H., Pawlowsky-Glahn, V., and Egozcue, J. J., 2002, Understanding perturbation on the simplex: A simple method to better visualize and interpret compositional data in ternary diagrams: Mathematical Geology, v. 34, p. 249-257.

Wang, Y., Han, X., Petersen, S., Frische, M., Qiu, Z., Cai, Y., and Zhou, P., 2018, Trace Metal Distribution in Sulfide Minerals from Ultramafic-Hosted Hydrothermal Systems: Examples from the Kairei Vent Field, Central Indian Ridge: Minerals, v. 8, p. 526.

Wang, Y., Qiu, K.-F., Müller, A., Hou, Z.-L., Zhu, Z.-H., and Yu, H.-C., 2021, Machine Learning Prediction of Quartz Forming-Environments: Journal of Geophysical Research: Solid Earth, v. 126, p. e2021JB021925.

Wang, Z., Xu, D., Zhang, Z., Zou, F., Wang, L., Yu, L., and Hu, M., 2015, Mineralogy and trace element geochemistry of the Co-and Cu-bearing sulfides from the Shilu Fe–Co–Cu ore district in Hainan Province of South China: Journal of Asian Earth Sciences, v. 113, p. 980-997.

Weiss, G. M., 2013, Foundations of imbalanced learning, *in* He, H., and Ma, Y., eds., Imbalanced Learning: Foundations, Algorithms, and Applications, Wiley Online Library, p. 13-41.

Wilcox, R. R., 2011, Introduction to robust estimation and hypothesis testing, Academic press, 608 p.

Wilson, S. A., Ridley, W. I., and Koenig, A. E., 2002, Development of sulfide calibration standards for the laser ablation inductively-coupled plasma mass spectrometry technique: Journal of Analytical Atomic Spectrometry, v. 17, p. 406-409.

Winderbaum, L., Ciobanu, C. L., Cook, N. J., Paul, M., Metcalfe, A., and Gilbert, S., 2012, Multivariate analysis of an LA-ICP-MS trace element dataset for pyrite: Mathematical Geosciences, v. 44, p. 823-842.

Wohlgemuth-Ueberwasser, C. C., Viljoen, F., Petersen, S., and Vorster, C., 2015, Distribution and solubility limits of trace elements in hydrothermal black smoker sulfides: An in-situ LA-ICP-MS study: Geochimica et Cosmochimica Acta, v. 159, p. 16-41.

Wold, S., Sjöström, M., and Eriksson, L., 2001, PLS-regression: a basic tool of chemometrics: Chemometrics and intelligent laboratory systems, v. 58, p. 109-130.

Xie, J., Tang, D., Qian, L., Wang, Y., and Sun, W., 2020, Geochemistry of sulfide minerals from skarn Cu (Au) deposits in the Fenghuangshan ore field, Tongling, eastern China: Insights into ore-forming process: Ore Geology Reviews, v. 122, p. 103537.

Yang, C., Beaudoin, G., Tang, J.-X., Song, Y., Wang, L.-Q., and Huang, X.-W., 2022, Cu-sulfide mineralogy, texture, and geochemistry in the Tiegelongnan porphyry-epithermal copper system, Tibet, China: Mineralium Deposita, v. 57, p. 759-779.

Yano, R. I., 2012, Trace element distribution in chalcopyrite-bearing porphyry and skarn deposits, University of Nevada, Reno.

Yeo, I.-K., and Johnson, R. A., 2000, A New Family of Power Transformations to Improve Normality or Symmetry: Biometrika, v. 87, p. 954-959.

Yilmaz, A. E., and Demirhan, H., 2023, Weighted kappa measures for ordinal multi-class classification performance: Applied Soft Computing, v. 134, p. 110020.

Yu, J., Li, N., Zhang, B., Ulrich, T., Chen, X., Hand, M., Morrissey, L. J., Payne, J. L., and Chen, Y.-J., 2022, Perspective of Permian porphyry Cu-Au mineralization in Chinese Western Tianshan: Constraints from sulfide Re-Os dating and trace element study of the Kuruer deposit, Xinjiang: Ore Geology Reviews, v. 142, p. 104707.

Yuan, B., Yang, Y., Yu, H., Zhao, Y., Ding, Q., Yang, J., and Tang, X., 2018, Geochemistry of pyrite and chalcopyrite from an active black smoker in 49.6°E Southwest Indian Ridge: Marine Geophysical Research, v. 39, p. 441-461.

Zhang, J., Shao, Y., Liu, Z., and Chen, K., 2022a, Sphalerite as a record of metallogenic information using multivariate statistical analysis: Constraints from trace element geochemistry: Journal of Geochemical Exploration, v. 232, p. 106883.

Zhang, P., Zhang, Z., Yang, J., and Cheng, Q., 2022b, Machine Learning Prediction of Ore Deposit Genetic Type Using Magnetite Geochemistry: Natural Resources Research.

Zhao, X.-Y., Zhong, H., Mao, W., Bai, Z.-J., and Xue, K., 2020, Molybdenite Re-Os dating and LA-ICP-MS trace element study of sulfide minerals from the Zijinshan high-sulfidation epithermal Cu-Au deposit, Fujian Province, China: Ore Geology Reviews, v. 118, p. 103363.

Zhao, Y., Chen, S., Tian, H., Zhao, J., Tong, X., and Chen, X., 2021, Trace element and S isotope characterization of sulfides from skarn Cu ore in the Laochang Sn-Cu deposit, Gejiu district, Yunnan, China: Implications for the ore-forming process: Ore Geology Reviews, v. 134, p. 104155.

Conclusion générale

Cette thèse a pour but évaluer la chalcopyrite comme un minéral indicateur et développer une méthodologie permettant la discrimination des différents types de dépôts en utilisant sa composition en éléments traces. Les études sur la composition en éléments traces de la chalcopyrite comme minéral indicateur sont rares (Bédard et al., 2017; Duran et al., 2019a; George et al., 2018b; Goulet, 2016; Mansur et al., 2021; Marfin et al., 2020) et jusqu'alors, très peu étaient centrées sur l'application à l'exploration minérale (Bédard et al., 2017; Duran et al., 2019a; Goulet, 2016; Mansur et al., 2021), dont seulement Bédard et al. (2017) propose une approche statistique multivariée (ACP). Cette étude est la première de son type à faire une analyse systématique sur la composition en éléments traces de la chalcopyrite, laquelle rassemble des méthodes statistiques multivariées et l'apprentissage automatique et développe des modèles de prédiction de types de dépôts aux fins d'application en exploration minérale.

Composition en éléments traces de la chalcopyrite comme indicateur du type de dépôt magmatique

La chalcopyrite des dépôts de sulfures à Ni-Cu montre des différences significatives dans sa composition en éléments traces par rapport à celle de dépôts d'EGP lités. En outre, dans les dépôts de sulfures à Ni-Cu, les éléments traces de la chalcopyrite varient systématiquement d'après le type de minerais (riche en Cu vs riche en Fe). Néanmoins, il n'y a aucun rapport entre les textures des échantillons et la composition en éléments traces de la chalcopyrite. Les effets potentiels des processus ayant lieu pendant la formation des dépôts de sulfures magmatiques sur les éléments traces dans la chalcopyrite n'impactent pas significativement sa capacité de discrimination.

D'après les résultats de la PLS-DA, le Bi, Te, Sn, In et Se sont les éléments les plus importants pour la classification par type de dépôt. Dans les dépôts d'EGP lités, la chalcopyrite a une concentration plus élevée de Se, tandis que le Bi, Te, Sn et In sont principalement élevés dans la chalcopyrite des dépôts de sulfures à Ni-Cu. Le Se est un élément fortement chalcophile (Barnes 2016), par conséquence son incorporation dans la chalcopyrite est favorisée dans des systèmes magmatiques avec un rapport liquide silicaté/liquide sulfuré élevé (facteur R). Ces conditions sont typiques des dépôts d'EGP lités. D'autre part, dans les dépôts de sulfures à Ni-Cu le Se est principalement contrôlé par la cristallisation fractionnée, en étant un élément incompatible avec la solution solide de monosulfure (mss). Par conséquence, le Se et d'autres éléments incompatibles (Ag, Bi, Cd, Pb, Sn, Te) sont enrichis dans la chalcopyrite des minerais riches en Cu, par rapport à celle des minerais riches en Fe. Ainsi, le Se trace deux processus différents. Le Te dans la chalcopyrite est également contrôlé par la cristallisation fractionnée dans les dépôts de sulfures à Ni-Cu,

principalement concentré dans celle des minerais riches en Cu. Cet élément présente des concentrations faibles dans la chalcopyrite des dépôts d'EGP lités par rapport les dépôts de sulfures à Ni-Cu, bien qu'il s'agisse d'un élément hautement chalcophile. Cela est le résultat de la cristallisation de minéraux du group du platine dans les EGP lités, ce qui conduit à une diminution de la disponibilité du TABS (Te, As, Bi et Sn).

Les éléments traces de la chalcopyrite comme critère de discrimination de sous-types de SMV

Dans un système hydrothermal menant la formation de dépôts de sulfures massifs volcanogènes (SMV), plusieurs facteurs peuvent impacter la composition de la chalcopyrite, tels que la composition des roches encaissantes, la température, fO_2, aS_2 et le pH du fluide dans la zone de réaction, la teneur de volatiles, mais aussi l'interaction avec l'eau marine (Barrie and Hannington, 1999; Franklin et al., 2005; Fuchs et al., 2019; Galley et al., 2007; Hannington, 2014). Pendant la précipitation, les éléments traces se partagent entre la chalcopyrite et les sulfures qui co-cristallisent, tels que la sphalérite, la galène, la pyrite et la pyrrhotite (Carvalho et al., 2018; Genna and Gaboury, 2015; George et al., 2015; George et al., 2016; George et al., 2018b; Lockington et al., 2014; Reich et al., 2013a; Torró et al., 2022; Xing et al., 2022). En plus, les dépôts peuvent être affectés par des différents épisodes thermales impliquant des processus de dissolution, re-précipitation et potentiellement remobilisation des éléments traces (Eldridge et al., 1983; Hannington, 2014; Ohmoto, 1996).

D'après les résultats de la PLS-DA dans une échelle de dépôt, la chalcopyrite provenant des zones riches en Cu est enrichie en Bi, Co, Ni, Au, Ag, Te et Se, un assemblage typique de haute température (Hannington, 2014). Cependant, la chalcopyrite provenant des zones riches en Zn et enrichie en Ga, Sn, In, Sb et Tl, un assemblage de basse température d'après Hannington (2014). Cela est une évidence des processus de remobilisation des éléments traces des sulfures précédemment formés à plus basses températures (e.g., sphalérite, galène ou pyrite), et qui sont ultérieurement incorporés dans la chalcopyrite durant le processus de remplacement.

La composition en éléments trace dans la chalcopyrite varie à une échelle régionale selon la configuration lithostratigraphique des dépôts SMV (*e.g.*, Franklin et al., 2005; Patten et al., 2022). La composition des roches encaissantes contrôle celle de la chalcopyrite. Ainsi, dans les dépôts SMV en contexte ultramafique, le Ni-Co sont lixiviés des minéraux ferromagnésiens qui constituent les roches mafiques-ultramafiques, transportés et incorporés dans les dépôts de sulfures massifs. Dans les SMV en contexte mafique, la chalcopyrite présente les valeurs les plus élevées de Pb, probablement à cause de l'absence de galène dans ce type de dépôts, ce qui favorise son incorporation dans la chalcopyrite. La chalcopyrite provenant des dépôts SMV en contexte bimodal-mafique et bimodal-felsique ne rapporte pas une différence

significative dans la composition en éléments traces. Les deux contextes sont caractérisés par une proportion variable de roches volcaniques mafiques et felsiques (Franklin et al., 2005), ce qui résulte en une composition en éléments traces de la chalcopyrite similaire. Dans les dépôts SMV dans un contexte siliciclastique-mafique, la chalcopyrite a des valeurs élevées de Mn, probablement liées à la présence de roches riches en cet élément (*i.e.,* cuticule) associées à des meta-exhalites (Spry et al., 1998). La chalcopyrite des dépôts SMV de contexte siliciclastique-felsique montre des concentrations élevées de Sn, Sb, Bi et In. Les valeurs élevées de ces éléments sont associées à une contribution magmatique et à la présence de roches méta sédimentaires sous-jacentes (e.g., Neves-Corvo; Carvalho et al., 2018; Huston et al., 2011).

Discrimination de types de dépôts avec les éléments traces de la chalcopyrite et une approche d'apprentissage automatique

Dans les systèmes magmatiques, la variation des éléments traces dans la chalcopyrite est le résultat des changements ayant lieu pendant la cristallisation du liquide sulfuré au sein d'un magma, tandis que dans les systèmes hydrothermaux la composition de la chalcopyrite reflète celle du fluide. Bien que la chalcopyrite se forme dans une ample variété de types de dépôts, et que des variations dans sa composition des éléments traces ont lieu localement, nos résultats démontrent qu'il y a une variation significative parmi les différents types, permettant son utilisation pour la discrimination avec des modèles de Random Forest. La différence la plus importante entre la chalcopyrite d'origine hydrothermale et magmatique est déterminée par le Ni, enrichi dans la chalcopyrite des dépôts de sulfures à Ni-Cu et les EGP lités par rapport les dépôts hydrothermaux. Les dépôts riches en Ni sont principalement associés à des intrusions mafiques-ultramafiques formées à partir de la fusion partielle du manteau. Contrairement, dans des systèmes hydrothermaux, la solubilité du Ni est peu connue et les dépôts riches en Ni d'origine hydrothermale sont rares.

La complexité des processus de formation impliqués et le nombre de types de dépôts considéré pour la classification, les méthodes statistiques classiques univariées, bivariées et les diagrammes ternaires ne permettent pas une prédiction efficace de la provenance de la chalcopyrite. Pour cela, une approche d'apprentissage automatique a été réalisée, dont le Random Forest s'est avéré comme l'algorithme le plus performant. La qualité de la prédiction des modèles développées pour discriminer les 8 types de dépôts dépend de trois facteurs : a) le pourcentage de valeurs censurées, b) le nombre de variables manquantes, et c) la proportion d'éléments sans valeurs censurées.

Ainsi, sur la base de ces résultats, les conclusions suivantes ont été tirées:

1. Cette étude a analysé la composition en éléments traces de la chalcopyrite dans des systèmes magmatiques et a démontré que sa variation est une fonction du type de dépôt (sulfures à Ni-Cu et EGP lités) et du type de minerais (riche en Cu et riche en Fe). La variabilité de la concentration des éléments traces selon le type de dépôt est déterminée par le rapport entre le liquide silicaté et le liquide sulfuré pendant la cristallisation (facteur-R). Les valeurs élevées du facteur R dans les dépôts d'EGP lités conduisent à un enrichissement systématique des éléments fortement chalcophiles dans la chalcopyrite, tel que le Se, alors la concentration des éléments tels que le Te, Sn, Bi et In diminue par rapport aux dépôts de sulfures à Ni-Cu. Par ailleurs, dans les dépôts de sulfures à Ni-Cu, la concentration des éléments traces dans la chalcopyrite répond à un processus différent, la cristallisation fractionnée du liquide sulfuré. Dans ce contexte, la chalcopyrite formée à partir de la solution solide intermédiaire (iss), laquelle cristallise en dernier à partir d'un liquide résiduel riche en Cu, est enrichie en Ag, Bi, Cd, Pb, Se, Sn et Tl, par rapport à celle formée à partir d'une solution solide de monosulfure (mss) riche en Fe.
2. Cette étude est la première à caractériser de manière systématique la composition en éléments traces de la chalcopyrite dans les dépôts SMV. En tant que dépôt d'affiliation hydrothermale, la variabilité des éléments traces dépend de plusieurs facteurs, tels que, la composition du fluide hydrothermal, conditionnée à son tour par la composition de la roche encaissante, la température et la nature de la source de ces fluides. La chalcopyrite capture de façon systématique la variation de la concentration des éléments traces en fonction de la configuration lithostratigraphique établie par Franklin et al. (2005). La chalcopyrite formée dans les SMV en contexte ultramafiques est enrichie en Ni, Co et Te, alors que celle des SMV en contexte siliciclastique-felsique a des teneurs élevées en Sb, Bi et In. Dans les SMV du sous-type mafique et siliciclastique-mafique, la chalcopyrite est respectivement enrichie en Pb et Mn, tandis que celle formée dans les dépôts du sous-type bimodal-mafique montre une composition similaire à celle des dépôts formés en contexte bimodal-felsique. Des potentielles modifications de la composition en éléments traces de la chalcopyrite à cause du métamorphisme n'ont aucun impact sur la variation en la composition dû au sous-type de VMS.
3. Cette étude fourni une méthodologie systématique d'analyse statistique pour les données géochimiques, de l'analyse exploratoire uni- et bivariée jusqu'à le développement de modèles de discrimination avec la PLS-DA. Une méthodologie avec une approche d'analyse de données compositionnelles est présentée, avec des critères pour traiter leur nature fermée et les valeurs censurées. La transformation clr (centered log ratio) a été utilisée afin de supprimer la nature fermée des données compositionnelles, ce qui supprime la possibilité de possibles fausses corrélations. En plus, l'imputation des données censurées a été réalisée avec la procédure lrEM (log ratio Expectation–

Maximization), un algorithme qui permet d'établir comme plafond la limite de détection et par conséquence l'obtention de valeurs imputées fiables.

4. Cette étude démontre la capacité de la PLS-DA, une méthode statistique de classification supervisée, pour discerner la structure des bases des données complexes et de développer des modèles de classification performants. Dans ce contexte, dans cette étude des modèles PLS-DA ont été développés pour prédire le type de dépôt magmatique (sulfure à Ni-Cu vs. EGP lités) en utilisant le Se, Te, Bi, Sn, et In; ainsi qu'un modèle pour déterminer le type de minerais dans les dépôts de sulfure à Ni-Cu (riche en Cu vs. riche en Fe) avec le Sb, Se, Sn, Tl et le Zn dans la chalcopyrite.
5. Cette étude présente, pour la première fois, une approche d'apprentissage automatique pour la classification de la chalcopyrite à partir de sa composition en éléments traces. Une méthodologie systématique basée sur 3 modèles RF a été développé pour déterminer le sous-type lithostratigraphique dans les dépôts SMV. Ainsi, un premier modèle permet de discriminer parmi les trois principales affinités lithologiques (mafique-ultramafique, bimodaux et siliciclastique-felsique) en utilisant le Sn, Co, Te, Ag, In, Sb, Se, Zn et le Pb; ensuite un deuxième modèle permet de discriminer parmi les sous-types ultramafique, mafique et siliciclastique-mafique avec le Co, Sn, Mn, Te, In, Pb, Se, Tl, Ni, Ag, Zn et le Bi. Finalement, un troisième modèle basé sur le Te, Se, Zn, In, Ag, Sb, Co, Ga, Sn et In permet la discrimination entre les sous-types bimodal-mafique bimodal-felsique.
6. Une méthodologie similaire a été proposée afin de prédire la provenance de la chalcopyrite parmi 8 types de dépôts différents en utilisant sa composition en éléments traces. Ce schéma est constitué par trois modèles, dont le premier permet de discerner entre une source magmatique et hydrothermale à partir du Ni, Ga, In, Sb, Se, Ag, Zn, Sb, Sn and Bi. Le deuxième, basé sur le Te, Sn, Se, In, Bi et le Zn classifie la chalcopyrite selon le type de dépôt magmatique (sulfure à Ni-Cu vs. EGP lité) et représente un complément du modèle PLS-DA déjà proposé. Pour les dépôts hydrothermaux, un modèle Random Forest basé sur le Se, Zn, Sn, In, Ga, Te, Ag, Sb, Bi, Co, Ni et le Pb a été développé.
7. L'application sur les données de la littérature montrent une efficacité élevée des modèles Random Forest pour prédire le type de dépôt. Principalement pour les dépôts du type sulfure à Ni-Cu, SMV et porphyres. La prédiction de la chalcopyrite d'après son origine hydrothermal ou magmatique est très efficace, avec un pourcentage d'analyses classifiées correctement de 86%. Parmi les facteurs qui réduisent la qualité des prédictions se trouvent le pourcentage de valeurs censurées, le nombre de variables non analysées et la proportion d'éléments sans valeurs censurées.
8. Les modèles Random Forest ont été appliqués sur des données d'éléments trace de grains de chalcopyrite provenant de sédiments de till et eskers de la Province de Churchill au Nunavik, Canada (Durand et al. 2019). La classification avec nos modèles sont consistent avec les types de minéralisation de la région, particulièrement de porphyres, SMV, sulfures à Ni-Cu et EGP lités.

Néanmoins, il y a une proportion élevée de chalcopyrite provenant de dépôts IOCG, un type de minéralisation non connue jusqu'alors.

Limitations et recommandations

Une collection de modèles de classification PLS-DA et RF sont proposés dans cette étude, basés sur la composition en éléments traces de la chalcopyrite. Toute classification est susceptible de présenter de problèmes liés à l'échantillonnage et aux éléments mesurés, ce qui pourrait éventuellement réduire la performance des modèles de classification. Ce problème, principalement associé à un échantillonnage non balancé parmi les classes, est traduit par une sur-représentation et une sous-représentation de certains groupes. Dans le contexte de cette étude, afin de réduire au maximum l'effet de ce problème sur la performance, des stratégies ont été mises en place, telle que le regroupement des échantillons dans des classes plus générales. La définition des classes par affinité lithologiques dans les dépôts SVM avant de discriminer par sous-type, ou le développement d'un modèle permettant déterminer entre une source magmatique ou hydrothermale, a permis de réduire cet effet sur la performance. Néanmoins, il est conseillé d'augmenter le nombre d'échantillons, principalement dans les sous-types mafique et siliciclastique-mafique pour les dépôts SMV, ainsi que dans les classes porphyres, or orogénique, or épithermal et skarn. Par ailleurs, il est conseillé d'analyser les mêmes éléments traces requis par les modèles de prédiction, afin de réduire les biais potentiels comme résultat de l'imputation des valeurs manquantes

Bibliographie

Abd Elrahman SM, Abraham A (2013) A review of class imbalance problem. Journal of Network and Innovative Computing 1:332-340.

Agangi A, Reddy S, Plavsa D, Vieru C, Selvaraja V, LaFlamme C, Jeon H, Martin L, Nozaki T, Takaya Y (2018) Subsurface deposition of Cu-rich massive sulphide underneath a Palaeoproterozoic seafloor hydrothermal system—the Red Bore prospect, Western Australia. Mineralium Deposita:1-18.

Aitchison J (1986) The statistical analysis of compositional data. Chapman and Hall, London.

Almodóvar GR, Yesares L, Sáez R, Toscano M, González F, Pons JM (2019) Massive Sulfide Ores in the Iberian Pyrite Belt: Mineralogical and Textural Evolution. Minerals 9:653.

Andersson SS, Jonsson E, Högdahl K (2016) Metamorphism and deformation of a Palaeoproterozoic polymetallic sulphide–oxide mineralisation: Hornkullen, Bergslagen, Sweden. GFF 138:410-423. doi: 10.1080/11035897.2015.1135187.

Antweiler RC (2015) Evaluation of Statistical Treatments of Left-Censored Environmental Data Using Coincident Uncensored Data Sets. II. Group Comparisons. Environmental Science & Technology 49:13439-13446. doi: 10.1021/acs.est.5b02385.

Averill S (2011a) Viable indicator minerals in surficial sediments for two major base metal deposit types: Ni-Cu-PGE and porphyry Cu.

Averill SA (2001) The application of heavy indicator mineralogy in mineral exploration with emphasis on base metal indicators in glaciated metamorphic and plutonic terrains. Geological Society, London, Special Publications 185:69-81. doi: 10.1144/gsl.sp.2001.185.01.04.

Averill SA (2011b) Viable indicator minerals in surficial sediments for two major base metal deposit types: Ni-Cu-PGE and porphyry Cu. Geochemistry: Exploration, Environment, Analysis 11:279-291. doi: 10.1144/1467-7873/10-IM-022.

Bajwah ZU, Seccombe PK, Offler R (1987) Trace element distribution, Co: Ni ratios and genesis of the Big Cadia iron-copper deposit, New South Wales, Australia. Mineralium Deposita 22:292-300.

Balch SJ (2005) The geophysical signatures of platinum group element deposits In: Mungall JE (ed) Exploration for platinum-group element deposits: Mineralogical Association of Canada, Short-Course Series, Volume 35. pp 275-286.

Ballabio D, Consonni V (2013) Classification tools in chemistry. Part 1: linear models. PLS-DA. Analytical Methods 5:3790-3798.

Barker RD, Barker SLL, Cracknell MJ, Stock ED, Holmes G (2021) Quantitative Mineral Mapping of Drill Core Surfaces II: Long-Wave Infrared Mineral Characterization Using µXRF and Machine Learning. Economic Geology 116:821-836. doi: 10.5382/econgeo.4804.

Barnes S-J, Melezhik VA, Sokolov SV (2001) The composition and mode of formation of the Pechenga nickel deposits, Kola Peninsula, northwestern Russia. The Canadian Mineralogist 39:447-471.

Barnes S-J, Lightfoot PC (2005) Formation of magmatic nickel sulfide ore deposits and processes affecting their copper and platinum group element contents. Economic geology 100th anniversary volume 34:179-214.

Barnes S-J, Cox RA, Zientek ML (2006) Platinum-group element, gold, silver and base metal distribution in compositionally zoned sulfide droplets from the Medvezky Creek Mine, Noril'sk, Russia. Contributions to Mineralogy and Petrology 152:187-200.

Barnes S-J, Prichard HM, Cox RA, Fisher PC, Godel B (2008) The location of the chalcophile and siderophile elements in platinum-group element ore deposits (a textural, microbeam and whole rock geochemical study): Implications for the formation of the deposits. Chemical Geology 248:295-317.

Barnes S-J (2016) Chalcophile elements Encyclopedia of Geochemistry: A Comprehensive Reference Source on the Chemistry of the Earth. Springer International Publishing, pp 1-5.

Barnes S-J, Ripley EM (2016) Highly siderophile and strongly chalcophile elements in magmatic ore deposits. Reviews in Mineralogy and Geochemistry 81:725-774.

Barnes SJ, Mungall JE, Le Vaillant M, Godel B, Lesher CM, Holwell D, Lightfoot PC, Krivolutskaya N, Wei B (2017) Sulfide-silicate textures in magmatic Ni-Cu-PGE sulfide ore deposits: Disseminated and net-textured ores. American Mineralogist 102:473-506.

Barnes SJ, Staude S, Le Vaillant M, Piña R, Lightfoot PC (2018) Sulfide-silicate textures in magmatic Ni-Cu-PGE sulfide ore deposits: Massive, semi-massive and sulfide-matrix breccia ores. Ore Geology Reviews 101:629-651. doi: https://doi.org/10.1016/j.oregeorev.2018.08.011.

Barnes SJ, Taranovic V, Schoneveld LE, Mansur ET, Le Vaillant M, Dare S, Staude S, Evans NJ, Blanks D (2020) The Occurrence and Origin of Pentlandite-Chalcopyrite-Pyrrhotite Loop Textures in Magmatic Ni-Cu Sulfide Ores. Economic Geology 115:1777-1798. doi: 10.5382/econgeo.4757.

Barrie CD, Boyle AP, Salter M (2009) How low can you go? - Extending downwards the limits of plastic deformation in pyrite. Mineralogical Magazine 73:895-913. doi: 10.1180/minmag.2009.073.6.895.

Barrie CD, Boyle AP, Cook NJ, Prior DJ (2010a) Pyrite deformation textures in the massive sulfide ore deposits of the Norwegian Caledonides. Tectonophysics 483:269-286.

Barrie CD, Boyle AP, Cook NJ, Prior DJ (2010b) Pyrite deformation textures in the massive sulfide ore deposits of the Norwegian Caledonides. Tectonophysics 483:269-286. doi: https://doi.org/10.1016/j.tecto.2009.10.024.

Barrie CT, Hannington MD (1999) Classification of volcanic-associated massive sulfide deposits based on host-rock composition. Reviews in Economic Geology 8:1-11.

Barton PB, Bethke PM (1987) Chalcopyrite disease in sphalerite; pathology and epidemiology. American Mineralogist 72:451-467.

Bédard É, Goulet A, Sappin A-A, Makvandi S, Beaudoin G (2017) Chalcopyrite as an indicator mineral to fingerprint mineral deposit types: a preliminary study Mineral Resources to Discover- Proceedings of the 14th SGA Biennial Meeting. Québec City, Canada, pp 1115-1118.

Bédard É, De Bronac de Vazelhes V, Beaudoin G (2022) Performance of predictive supervised classification models of trace elements in magnetite for mineral exploration. Journal of Geochemical Exploration 236:106959. doi: https://doi.org/10.1016/j.gexplo.2022.106959.

Bédard JH (2005) Partitioning coefficients between olivine and silicate melts. Lithos 83:394-419. doi: https://doi.org/10.1016/j.lithos.2005.03.011.

Belissont R (2016) Germanium and related elements in sulphide minerals: crystal chemistry, incorporation and isotope fractionation (Doctoral dissertation, Université de Lorraine, France). Available from INIS: http://inis.iaea.org/search/search.aspx?orig_q=RN:51079040.

Belissont R, Munoz M, Boiron M-C, Luais B, Mathon O (2019) Germanium crystal chemistry in Cu-bearing sulfides from micro-XRF mapping and micro-XANES spectroscopy. Minerals 9:227.

Benson EK, Ripley EM, Li C, Underwood BW, Mahin R (2020) Multiple S Isotopes and S Isotope Heterogeneity at the East Eagle Ni-Cu-Platinum Group Element Deposit, Northern Michigan. Economic Geology 115:527-541.

Berrar D (2018) Bayes' theorem and naive Bayes classifier. Encyclopedia of Bioinformatics and Computational Biology: ABC of Bioinformatics 403.

Binns RA, McConachy T, McInnes B (2004) Eastern Manus basin, Papua New Guinea: Guides for volcanogenic massive sulphide exploration from a modern seafloor analogue. CSIRO Explores 2:59-80.

Binns RA, Barriga F, Miller DJ (2007) Leg 193 synthesis; anatomy of an active felsic hosted hydrothermal system, eastern Manus Basin, Papua New Guinea. Proceedings of the Ocean Drilling Program, Scientific Results (CD ROM) 193:71.

Bolton MSM, Jensen BJL, Wallace K, Praet N, Fortin D, Kaufman D, De Batist M (2020) Machine learning classifiers for attributing tephra to source volcanoes: an evaluation of methods for Alaska tephras. Journal of Quaternary Science 35:81-92.

Bortnikov NS, Genkin AD, Dobrovol'Skaya MG, Muravitskaya GN, Filimonova AA (1991) The nature of chalcopyrite inclusions in sphalerite; exsolution, coprecipitation, or" disease"? Economic Geology 86:1070-1082.

Boutroy E, Dare SA, Beaudoin G, Barnes S-J, Lightfoot PC (2014) Magnetite composition in Ni-Cu-PGE deposits worldwide: application to mineral exploration. Journal of Geochemical Exploration 145:64-81.

Bowes D, Hall T, Gray D (2012) Comparing the performance of fault prediction models which report multiple performance measures: recomputing the confusion matrix In: Machinery AfC (ed) Proceedings of the 8th international conference on predictive models in software engineering. pp 109-118.

Breiman L (2001) Random Forests. Machine Learning 45:5-32. doi: 10.1023/A:1010933404324.

Brereton RG, Lloyd GR (2014) Partial least squares discriminant analysis: taking the magic away. Journal of Chemometrics 28:213-225.

Brownlee J (2018) Master machine learning algorithms: Discover how they work and implement them from scratch. Melbourne, Machine Learning Mastery.

Brueckner SM, Piercey SJ, Layne GD, Piercey G, Sylvester PJ (2015) Variations of sulphur isotope signatures in sulphides from the metamorphosed Ming Cu(−Au) volcanogenic massive sulphide deposit, Newfoundland Appalachians, Canada. Mineralium Deposita 50:619-640. doi: 10.1007/s00126-014-0567-7.

Brueckner SM, Piercey SJ, Pilote J-L, Layne GD, Sylvester PJ (2016) Mineralogy and mineral chemistry of the metamorphosed and precious metal-bearing Ming deposit, Canada. Ore Geology Reviews 72:914-939. doi: https://doi.org/10.1016/j.oregeorev.2015.09.016.

Brügmann G, Hanski E, Naldrett A, Smolkin V (2000) Sulphide segregation in ferropicrites from the Pechenga Complex, Kola peninsula, Russia. Journal of Petrology 41:1721-1742.

Butler IB, Nesbitt RW (1999) Trace element distributions in the chalcopyrite wall of a black smoker chimney: insights from laser ablation inductively coupled plasma mass spectrometry (LA–ICP–MS). Earth and Planetary Science Letters 167:335-345.

Cabri LJ, Campbell JL, Laflamme JHG, Leigh RG, Maxwell JA, Scott JD (1985) Proton-microprobe analysis of trace elements in sulfides from some massive-sulfide deposits. The Canadian Mineralogist 23:133-148.

Cafagna F, Jugo PJ (2016) An experimental study on the geochemical behavior of highly siderophile elements (HSE) and metalloids (As, Se, Sb, Te, Bi) in a mss-iss-pyrite system at 650°C: A possible magmatic origin for Co-HSE-bearing pyrite and the role of metalloid-rich phases in the fractionation of HSE. Geochimica et Cosmochimica Acta 178:233-258. doi: https://doi.org/10.1016/j.gca.2015.12.035.

Caraballo E, Dare S, Beaudoin G (2022) Variation of trace elements in chalcopyrite from worldwide Ni-Cu sulfide and Reef-type PGE deposits: implications for mineral exploration. Mineralium Deposita 57:1293-1321. doi: https://doi.org/10.1007/s00126-021-01091-y.

Carvalho JRS, Relvas J, Pinto AMM, Frenzel M, Krause J, Gutzmer J, Pacheco N, Fonseca R, Santos S, Caetano P (2018) Indium and selenium distribution in the Neves-Corvo deposit, Iberian Pyrite Belt, Portugal. Mineralogical Magazine 82:S5-S41.

Castroviejo R, Quesada C, Soler M (2011) Post-depositional tectonic modification of VMS deposits in Iberia and its economic significance. Mineralium Deposita 46:615-637. doi: 10.1007/s00126-010-0306-7.

Caté A, Perozzi L, Gloaguen E, Blouin M (2017) Machine learning as a tool for geologists. The Leading Edge 36:215-219.

Charette B, Lafrance I, Mathieu G (2015) Géologie de la région du lac Jeannin (SNRC 24B). Ministère de l'Énergie et des Ressources naturelles, Québec, BG 1.

Chen L-M, Song X-Y, Danyushevsky LV, Wang Y-S, Tian Y-L, Xiao J-F (2015) A laser ablation ICP-MS study of platinum-group and chalcophile elements in base metal sulfide minerals of the Jinchuan Ni–Cu sulfide deposit, NW China. Ore Geology Reviews 65:955-967.

Chen P, Zeng Q, Zhou L, Liu B, Fu Y, Sun G, Yu B, Long Z (2022) Genesis and prospecting significance of the Buziwannan gold-polymetallic ore deposit in the West Kunlun Orogen Belt, China: Constraints from mineral geochemistry and in situ S–Pb isotope analyses of sulfides. Journal of Geochemical Exploration:107125. doi: https://doi.org/10.1016/j.gexplo.2022.107125.

Chong I-G, Jun C-H (2005) Performance of some variable selection methods when multicollinearity is present. Chemometrics and intelligent laboratory systems 78:103-112.

Chowdhury S, Pal DC, Papineau D, Lentz DR (2020) Major and trace element and multiple sulfur isotope composition of sulfides from the Paleoproterozoic Surda copper deposit, Singhbhum shear Zone, India: Implications for the mineralization processes. Ore Geology Reviews 120:103396. doi: https://doi.org/10.1016/j.oregeorev.2020.103396.

Conn CD, Spry PG, Layton-Matthews D, Voinot A, Koenig A (2019) The effects of amphibolite facies metamorphism on the trace element composition of pyrite and pyrrhotite in the Cambrian Nairne Pyrite Member, Kanmantoo Group, South Australia. Ore Geology Reviews 114:103128. doi: https://doi.org/10.1016/j.oregeorev.2019.103128.

Cook NJ, Chryssoulis SL (1990) Concentrations of invisible gold in the common sulfides. The Canadian Mineralogist 28:1-16.

Cook NJ, Halls C (1990) Coticules at Sulitjalma, Norway and their possible origin. Norsk geologisk tidsskrift 70:153-158.

Cook NJ (1996) Mineralogy of the sulphide deposits at Sulitjelma, northern Norway. Ore Geology Reviews 11:303-338. doi: https://doi.org/10.1016/S0169-1368(96)00009-1.

Cook NJ, Ciobanu CL, Danyushevsky LV, Gilbert S (2011) Minor and trace elements in bornite and associated Cu–(Fe)-sulfides: A LA-ICP-MS studyBornite mineral chemistry. Geochimica et Cosmochimica Acta 75:6473-6496.

Cracknell MJ, Reading AM (2014) Geological mapping using remote sensing data: A comparison of five machine learning algorithms, their response to variations in the spatial distribution of training data and the use of explicit spatial information. Computers & Geosciences 63:22-33. doi: https://doi.org/10.1016/j.cageo.2013.10.008.

Crundwell FK (2021) The impact of light on understanding the mechanism of dissolution and leaching of sphalerite (ZnS), pyrite (FeS2) and chalcopyrite (CuFeS2). Minerals Engineering 161:106728. doi: https://doi.org/10.1016/j.mineng.2020.106728.

Crundwell FK, Bryson LJ, van Aswegen A, Knights BDH (2021) Effect of chopped light on the dissolution and leaching of chalcopyrite. Minerals Engineering 160:106703. doi: https://doi.org/10.1016/j.mineng.2020.106703.

Cui H, Zhong R, Li W, Yu C, Danyushevsky LV, Belousov I, Liu C, Li Z (2023) Revealing the orogenic genesis of Huogeqi Cu-Pb-Zn deposit: Evidence from the machine learning-based data interpretation of pyrite geochemistry. Ore Geology Reviews 154:105350. doi: https://doi.org/10.1016/j.oregeorev.2023.105350.

Czamanske GK, Kunilov VE, Zientek ML, Cabri LJ, Likhachev AP, Calk LC, Oscarson RL (1992) A proton microprobe study of magmatic sulfide ores from the Noril'sk-Talnakh District, Siberia. The Canadian Mineralogist 30:249-287.

Dare SA, Barnes S-J, Beaudoin G (2012) Variation in trace element content of magnetite crystallized from a fractionating sulfide liquid, Sudbury, Canada: Implications for provenance discrimination. Geochimica et Cosmochimica Acta 88:27-50.

Dare SA, Barnes S-J, Prichard HM, Fisher PC (2014) Mineralogy and geochemistry of Cu-rich ores from the McCreedy East Ni-Cu-PGE deposit (Sudbury, Canada): implications for the behavior of platinum group and chalcophile elements at the end of crystallization of a sulfide liquid. Economic Geology 109:343-366.

Dare SAS, Barnes S-J, Prichard HM, Fisher PC (2010a) The timing and formation of platinum-group minerals from the Creighton Ni-Cu-platinum-group element sulfide deposit, Sudbury, Canada: Early crystallization of PGE-rich sulfarsenides. Economic Geology 105:1071-1096.

Dare SAS, Barnes S-J, Prichard HM (2010b) The distribution of platinum group elements (PGE) and other chalcophile elements among sulfides from the Creighton Ni–Cu–PGE sulfide deposit, Sudbury, Canada, and the origin of palladium in pentlandite. Mineralium Deposita 45:765-793.

Dare SAS, Barnes S-J, Prichard HM, Fisher PC (2011) Chalcophile and platinum-group element (PGE) concentrations in the sulfide minerals from the McCreedy East deposit, Sudbury, Canada, and the origin of PGE in pyrite. Mineralium Deposita 46:381-407.

Daunis-i-Estadella J, Barceló-Vidal C, Buccianti A (2006) Exploratory compositional data analysis. Geological Society, London, Special Publications 264:161-174.

De Bronac de Vazelhes V (2019) Étude de la dispersion d'un gisement d'or dans les sédiments glaciaires: le cas d'Amaruq (Nunavut, Canada) (Master's thesis). Université Laval, pp 199.

Dehnavi AS, McFarlane CRM, Lentz DR, Walker JA (2018) Assessment of pyrite composition by LA-ICP-MS techniques from massive sulfide deposits of the Bathurst Mining Camp, Canada: from textural and chemical evolution to its application as a vectoring tool for the exploration of VMS deposits. Ore Geology Reviews 92:656-671.

Delgado R, Tibau X-A (2019) Why Cohen's Kappa should be avoided as performance measure in classification. PloS one 14:e0222916.

Digis Team (2022) GEOROC Compilation: Rock Types. V3 edn. Goettingen Research Online.data.

Djon MLN, Barnes S-J (2012) Changes in sulfides and platinum-group minerals with the degree of alteration in the Roby, Twilight, and High Grade Zones of the Lac des Iles Complex, Ontario, Canada. Mineralium Deposita 47:875-896. doi: 10.1007/s00126-012-0401-z.

Dmitrijeva M, Cook NJ, Ehrig K, Ciobanu CL, Metcalfe AV, Kamenetsky M, Kamenetsky VS, Gilbert S (2020) Multivariate Statistical Analysis of Trace Elements in Pyrite: Prediction, Bias and Artefacts in Defining Mineral Signatures. Minerals 10:61.

Dubé B, Gosselin P, Mercier-Langevin P, Hannington M, Galley A (2007) Gold-rich volcanogenic massive sulphide deposits. Geological Association of Canada, Mineral Deposits Division:75-94.

Dunn K (2019) Process improvement using data.

Dupont A, Vander Auwera J, Pin C, Marincea S, Berza T (2002) Trace element and isotope (Sr, Nd) geochemistry of porphyry-and skarn-mineralising Late Cretaceous intrusions from Banat, western South Carpathians, Romania. Mineralium Deposita 37:568.

Duran C, Barnes S, Pleše P, Prašek MK, Zientek ML, Pagé P (2017) Fractional crystallization-induced variations in sulfides from the Noril'sk-Talnakh mining district (polar Siberia, Russia). Ore Geology Reviews 90:326-351.

Duran CJ, Barnes S-J, Corkery JT (2016a) Trace element distribution in primary sulfides and Fe–Ti oxides from the sulfide-rich pods of the Lac des Iles Pd deposits, Western Ontario, Canada: Constraints on processes controlling the composition of the ore and the use of pentlandite compositions in exploration. Journal of Geochemical Exploration 166:45-63.

Duran CJ, Barnes S-J, Corkery JT (2016b) Geology, petrography, geochemistry, and genesis of sulfide-rich pods in the Lac des Iles palladium deposits, western Ontario, Canada. Mineralium Deposita 51:509-532.

Duran CJ, Dubé-Loubert H, Pagé P, Barnes S-J, Roy M, Savard D, Cave BJ, Arguin J-P, Mansur ET (2019a) Applications of trace element chemistry of pyrite and chalcopyrite in glacial sediments to mineral exploration targeting: Example from the Churchill Province, northern Quebec, Canada. Journal of Geochemical Exploration 196:105-130. doi: https://doi.org/10.1016/j.gexplo.2018.10.006.

Duran CJ, Dubé-Loubert H, Pagé P, Barnes S-J, Roy M, Savard D, Cave BJ, Arguin J-P, Mansur ET (2019b) Applications of trace element chemistry of pyrite and chalcopyrite in glacial sediments to mineral exploration targeting: Example from the Churchill Province, northern Quebec, Canada. Journal of Geochemical Exploration. doi: https://doi.org/10.1016/j.gexplo.2018.10.006.

Duran CJ, Barnes S-J, Mansur ET, Dare SAS, Bédard LP, Sluzhenikin SF (2020) Magnetite chemistry by LA-ICP-MS records sulfide fractional crystallization in massive nickel-copper-platinum group element ores from the Norilsk-Talnakh mining district (Siberia, Russia): Implications for trace element partitioning into magnetite. Economic Geology 115:1245-1266.

Egozcue JJ, Pawlowsky-Glahn V (2011) Análisis composicional de datos en Ciencias Geoambientales. Boletín Geológico y Minero 122:439-452.

Eldridge CS, Barton PB, Jr., Ohmoto H (1983) Mineral Textures and Their Bearing on Formation of the Kuroko Orebodies In: Ohmoto H, Skinner BJ (eds) The Kuroko and Related Volcanogenic Massive Sulfide Deposits. Society of Economic Geologists, pp 0.

Favilla S, Durante C, Vigni ML, Cocchi M (2013) Assessing feature relevance in NPLS models by VIP. Chemometrics and Intelligent Laboratory Systems 129:76-86.

Ferreira Filho CF, Ferraz de Oliveira MM, Mansur ET, Rosa WD (2021) The Jaguar hydrothermal nickel sulfide deposit: Evidence for a nickel-rich member of IOCG-type deposits in the Carajás Mineral Province, Brazil. Journal of South American Earth Sciences 111:103501. doi: https://doi.org/10.1016/j.jsames.2021.103501.

Filzmoser P, Hron K, Reimann C (2009) Principal component analysis for compositional data with outliers. Environmetrics 20:621-632.

Franklin J, Gibson H, Jonasson G (2005) Volcanogenic massive sulfide deposit. Economic Geology 100th Anniversary Volume:523-560.

Frenzel M, Hirsch T, Gutzmer J (2016) Gallium, germanium, indium, and other trace and minor elements in sphalerite as a function of deposit type—A meta-analysis. Ore Geology Reviews 76:52-78.

Fuchs S, Hannington MD, Petersen S (2019) Divining gold in seafloor polymetallic massive sulfide systems. Mineralium Deposita 54:789-820. doi: 10.1007/s00126-019-00895-3.

Galley AG, Hannington MD, Jonasson I (2007) Volcanogenic massive sulphide deposits. Mineral deposits of Canada: A synthesis of major deposit-types, district metallogeny, the evolution of geological provinces, and exploration methods: Geological Association of Canada, Mineral Deposits Division, Special Publication 5:141-161.

Genna D, Gaboury D (2015) Deciphering the hydrothermal evolution of a VMS system by LA-ICP-MS using trace elements in pyrite: an example from the Bracemac-McLeod deposits, Abitibi, Canada, and implications for exploration. Economic Geology 110:2087-2108.

Genna D, Gaboury D (2019) Use of semi-volatile metals as a new vectoring tool for VMS exploration: Example from the Zn-rich McLeod deposit, Abitibi, Canada. Journal of Geochemical Exploration 207:106358.

George L, Cook NJ, Ciobanu CL, Wade BP (2015) Trace and minor elements in galena: A reconnaissance LA-ICP-MS study. American Mineralogist 100:548-569. doi: 10.2138/am-2015-4862.

George LL, Cook NJ, Ciobanu CL (2016) Partitioning of trace elements in co-crystallized sphalerite–galena–chalcopyrite hydrothermal ores. Ore Geology Reviews 77:97-116.

George LL, Biagioni C, D'Orazio M, Cook NJ (2018a) Textural and trace element evolution of pyrite during greenschist facies metamorphic recrystallization in the southern Apuan Alps (Tuscany, Italy): Influence on the formation of Tl-rich sulfosalt melt. Ore Geology Reviews 102:59-105. doi: https://doi.org/10.1016/j.oregeorev.2018.08.032.

George LL, Cook NJ, Crowe BB, Ciobanu CL (2018b) Trace elements in hydrothermal chalcopyrite. Mineralogical Magazine 82:59-88.

Gislason PO, Benediktsson JA, Sveinsson JR (2006) Random forests for land cover classification. Pattern recognition letters 27:294-300.

Godel B, Barnes S-J, Maier WD (2006) 3-D distribution of sulphide minerals in the Merensky Reef (Bushveld Complex, South Africa) and the JM Reef (Stillwater Complex, USA) and their relationship to microstructures using X-ray computed tomography. Journal of Petrology 47:1853-1872.

Godel B, Barnes S-J, Maier WDJJoP (2007) Platinum-group elements in sulphide minerals, platinum-group minerals, and whole-rocks of the Merensky Reef (Bushveld Complex, South Africa): implications for the formation of the reef. 48:1569-1604.

Godel B, Barnes S-J (2008) Platinum-group elements in sulfide minerals and the whole rocks of the JM Reef (Stillwater Complex): Implication for the formation of the reef. Chemical Geology 248:272-294.

Godel B (2015) Platinum-group element deposits in layered intrusions: recent advances in the understanding of the ore forming processes. Layered intrusions:379-432.

González-Álvarez I, Pirajno F, Kerrich R (2013) Hydrothermal nickel deposits: Secular variation and diversity. Elsevier, pp 1-3.

Goodfellow WD (2007) Metallogeny of the Bathurst mining camp, northern New Brunswick. Mineral deposits of Canada A synthesis of major deposit-type, district metallogeny, the evolution of geological provinces and exploration methods Edited by WD Goodfellow Geological Association of Canada, Mineral Deposits Division, Special Publication 5:449-469.

Gosselin R, Rodrigue D, Duchesne C (2010) A Bootstrap-VIP approach for selecting wavelength intervals in spectral imaging applications. Chemometrics and Intelligent Laboratory Systems 100:12-21.

Goulet A (2016) Composition chimique de la chalcopyrite et application à l'exploration minérale In: Département de géologie et génie géologique UL (ed). pp 99.

Green T, Peck D (2005) Platinum group elements exploration: economic considerations and geological criteria In: Mungall JE (ed) Exploration For Platinum-Group Elements Deposits. Mineralogical Association of Canada. Short Course Series, Volume 35, pp 247-274.

Gregory DD, Cracknell MJ, Large RR, McGoldrick P, Kuhn S, Maslennikov VV, Baker MJ, Fox N, Belousov I, Figueroa MC, Steadman JA, Fabris AJ, Lyons TW (2019) Distinguishing Ore Deposit Type and Barren Sedimentary Pyrite Using Laser Ablation-Inductively Coupled Plasma-Mass Spectrometry Trace Element Data and Statistical Analysis of Large Data Sets. Economic Geology 114:771-786. doi: 10.5382/econgeo.4654.

Grömping U (2009) Variable Importance Assessment in Regression: Linear Regression versus Random Forest. The American Statistician 63:308-319. doi: 10.1198/tast.2009.08199.

Grzela D, Beaudoin G, Bédard É (2019) Tourmaline, scheelite, and magnetite compositions from orogenic gold deposits and glacial sediments of the Val-d'Or district (Quebec, Canada): Applications to mineral exploration. Journal of Geochemical Exploration 206:106355.

Han H, Guo X, Yu H (2016) Variable selection using mean decrease accuracy and mean decrease gini based on random forest 7th IEEE International Conference on Software Engineering And Service Science (ICSESS). IEEE, pp 219-224.

Hannington MD, Jonasson IR, Herzig PM, Petersen S (1995) Physical and chemical processes of seafloor mineralization at mid-ocean ridges. Seafloor hydrothermal systems: Physical, chemical, biological, and geological interactions 91:115-157.

Hannington MD, de Ronde CD, Petersen S (2005) Sea-Floor Tectonics and Submarine Hydrothermal Systems One Hundredth Anniversary Volume. Society of Economic Geologists, pp 111–141.

Hannington MD (2014) 13.18 - Volcanogenic Massive Sulfide Deposits In: Holland HD, Turekian KK (eds) Treatise on Geochemistry (Second Edition). Elsevier, Oxford, pp 463-488.

Harris DC, Cabri LJ, Nobiling R (1984) Silver-bearing chalcopyrite, a principal source of silver in the Izok Lake massive-sulfide deposit; confirmation by electron-and proton-microprobe analyses. The Canadian Mineralogist 22:493-498.

Harris JR, Grunsky EC (2015) Predictive lithological mapping of Canada's North using Random Forest classification applied to geophysical and geochemical data. Computers & Geosciences 80:9-25. doi: https://doi.org/10.1016/j.cageo.2015.03.013.

Hashmi S, Ward B, Plouffe A, Leybourne M, Ferbey T (2015a) Geochemical and mineralogical dispersal in till from the Mount Polley Cu-Au porphyry deposit, central British Columbia, Canada. Geochemistry: Exploration, Environment, Analysis 15:234-249.

Hashmi S, Ward BC, Plouffe A, Leybourne MI, Ferbey T (2015b) Geochemical and mineralogical dispersal in till from the Mount Polley Cu-Au porphyry deposit, central British Columbia, Canada. Geochemistry: Exploration, Environment, Analysis 15:234-249.

Hattori KH, Arai S, Clarke DB (2002) Selenium, tellurium, arsenic and antimony contents of primary mantle sulfides. The Canadian Mineralogist 40:637-650.

Hawley J, Nichol I (1961a) Trace elements in pyrite, pyrrhotite and chalcopyrite of different ores. Economic Geology 56:467-487.

Hawley JE, Nichol I (1961b) Trace elements in pyrite, pyrrhotite and chalcopyrite of different ores. Economic Geology 56:467-487.

Hazarika P, Mishra B, Pruseth KL (2015) Diverse tourmaline compositions from orogenic gold deposits in the Hutti-Maski greenstone belt, India: implications for sources of ore-forming fluids. Economic Geology 110:337-353.

Hofmann AW (1988) Chemical differentiation of the Earth: the relationship between mantle, continental crust, and oceanic crust. Earth and Planetary Science Letters 90:297-314. doi: https://doi.org/10.1016/0012-821X(88)90132-X.

Holwell DA, McDonald I (2007) Distribution of platinum-group elements in the Platreef at Overysel, northern Bushveld Complex: a combined PGM and LA-ICP-MS study. Contributions to Mineralogy and Petrology 154:171-190.

Hong S, Zuo R, Huang X, Xiong Y (2021) Distinguishing IOCG and IOA deposits via random forest algorithm based on magnetite composition. Journal of Geochemical Exploration 230:106859. doi: https://doi.org/10.1016/j.gexplo.2021.106859.

Houle P, Perreault S (2007) Les Orogènes du Nouveau-Québec et des Torngat, la Province de Churchill Sud-Est (Zone noyau) et l'Orogène de l'Ungava (région administrative 10, Nord-du-Québec). Ministère des Ressources naturelles et de la Faune du Québec: Rapport sur les activités d'exploration minière au Québec 2007:35-40.

Hron K, Templ M, Filzmoser P (2010) Imputation of missing values for compositional data using classical and robust methods. Computational Statistics & Data Analysis 54:3095-3107.

Hu B, Zeng L-P, Liao W, Wen G, Hu H, Li MYH, Zhao X-F (2022) The Origin and Discrimination of High-Ti Magnetite in Magmatic-Hydrothermal Systems: Insight from Machine Learning Analysis. Economic Geology 117:1613-1627. doi: 10.5382/econgeo.4946.

Huston DL, Sie SH, Suter GF, Cooke DR, Both RA (1995) Trace elements in sulfide minerals from eastern Australian volcanic-hosted massive sulfide deposits; Part I, Proton microprobe analyses of pyrite, chalcopyrite, and sphalerite, and Part II, Selenium levels in pyrite; comparison with delta 34 S values and implications for the source of sulfur in volcanogenic hydrothermal systems. Economic Geology 90:1167-1196.

Huston DL, Relvas JMRS, Gemmell JB, Drieberg S (2011) The role of granites in volcanic-hosted massive sulphide ore-forming systems: an assessment of magmatic–hydrothermal contributions. Mineralium Deposita 46:473-507. doi: 10.1007/s00126-010-0322-7.

Ishihara S, Endo Y (2007) Indium and other trace elements in volcanogenic massive sulfide ores from the Kuroko, Besshi and other types in Japan. Bull Geol Surv Japan 58:7-22.

Jochum KP, Nohl U, Herwig K, Lammel E, Stoll B, Hofmann AW (2005) GeoReM: a new geochemical database for reference materials and isotopic standards. Geostandards and Geoanalytical Research 29:333-338.

Kase K (1987) Tin-bearing chalcopyrite from the Izumo vein, Toyoha mine, Hokkaido, Japan. The Canadian Mineralogist 25:9-13.

Kitakaze A, Machida T, Komatsu R (2016) Phase Relations in the Fe–ni–s System from 875 To 650° c. The Canadian Mineralogist 54:1175-1186.

Knight RD, Prichard HM, Ferreira Filho CF (2017) Evidence for As contamination and the partitioning of Pd into Pentlandite and Co+ platinum group elements into pyrite in the Fazenda Mirabela intrusion, Brazil. Economic Geology 112:1889-1912.

Kojima S, Sugaki AJEG (1985) Phase relations in the Cu-Fe-Zn-S system between 500 degrees and 300 degrees C under hydrothermal conditions. 80:158-171.

Kosyakov VI, Sinyakova EF (2012) Physicochemical prerequisites for the formation of primary orebody zoning at copper-nickel sulfide deposits (by the example of the systems Fe–Ni–S and Cu–Fe–S). Russian Geology and Geophysics 53:861-882.

Kotsiantis SB, Zaharakis I, Pintelas P (2007) Supervised machine learning: A review of classification techniques. Emerging artificial intelligence applications in computer engineering 160:3-24.

Kuhn M (2008) Building Predictive Models in R Using the caret Package. Journal of Statistical Software 28:1 - 26. doi: 10.18637/jss.v028.i05.

Kuhn M (2012) The caret package. R Foundation for Statistical Computing, Vienna, Austria URL https://cran r-project org/package= caret.

Kuhn M, Johnson K (2013) Applied predictive modeling. Springer, New York.

Lafrance I, Simard M, Bandyayera D (2014) Géologie de la région du lac Saffray (SNRC 24G, 24F). Géologie Québec.

Lafrance I, Vanier M-A, Charette B (2020) Baleine Lithotectonic Domain, Southeastern Churchill Province, Nunavik, Quebec, Canada: Geological Synthesis (BG 2020-07) Ministère de l'Énergie et des Ressources naturelles, Québec, BG.

Lazich BJ (2010) The trace-element chemistry of chalcopyrite and its potential application to discriminate ore deposit types: Application to the Archean, syenite-associated Upper Beaver Cu-Au deposit, Kirkland. Laurentian, University Sudbury, pp 45.

Lee LC, Liong C-Y, Jemain AA (2018) Partial least squares-discriminant analysis (PLS-DA) for classification of high-dimensional (HD) data: a review of contemporary practice strategies and knowledge gaps. Analyst 143:3526-3539.

Li C, Ripley EM (2011) The giant Jinchuan Ni-Cu-(PGE) deposit; tectonic setting, magma evolution, ore genesis, and exploration implications. Reviews in Economic Geology 17:163-180.

Li R, Chen H, Xia X, Yang Q, Danyushevsky LV, Lai C (2018) Using integrated in-situ sulfide trace element geochemistry and sulfur isotopes to trace ore-forming fluids: Example from the Mina Justa IOCG deposit (southern Perú). Ore Geology Reviews 101:165-179. doi: https://doi.org/10.1016/j.oregeorev.2018.06.010.

Li X-M, Zhang Y-X, Li Z-K, Zhao X-F, Zuo R-G, Xiao F, Zheng Y (2023) Discrimination of Pb-Zn deposit types using sphalerite geochemistry: New insights from machine learning algorithm. Geoscience Frontiers 14:101580. doi: https://doi.org/10.1016/j.gsf.2023.101580.

Li X, Zhao K-D, Jiang S-Y, Palmer MR (2019) In-situ U-Pb geochronology and sulfur isotopes constrain the metallogenesis of the giant Neves Corvo deposit, Iberian Pyrite Belt. Ore Geology Reviews 105:223-235.

Liang P, Chen L, Li R, Xie Y, Wu C, Lai C-K (2021) In-situ element geochemical and sulfur isotope signature of pyrite and chalcopyrite: Constraints on ore-forming processes of the Laoshankou iron oxide-copper (-gold) deposit, northern East Junggar. Ore Geology Reviews 139:104510. doi: https://doi.org/10.1016/j.oregeorev.2021.104510.

Liang Q-L, Song X-Y, Wirth R, Chen L-M, Dai Z-H (2019) Implications of nano- and micrometer-size platinum-group element minerals in base metal sulfides of the Yangliuping Ni-Cu-PGE sulfide deposit, SW China. Chemical Geology 517:7-21. doi: https://doi.org/10.1016/j.chemgeo.2019.04.015.

Liu B, Gao L, Li B, Marcos-Martinez R, Bryan BA (2020) Nonparametric machine learning for mapping forest cover and exploring influential factors. Landscape Ecology 35:1683-1699. doi: 10.1007/s10980-020-01046-0.

Liu H, Beaudoin G (2021) Geochemical signatures in native gold derived from Au-bearing ore deposits. Ore Geology Reviews:104066.

Liu H, Beaudoin G, Makvandi S, Jackson SE, Huang X (2021) Multivariate statistical analysis of trace element compositions of native gold from orogenic gold deposits: implication for mineral exploration. Ore Geology Reviews:104061.

Liu W, Migdisov A, Williams-Jones A (2012) The stability of aqueous nickel (II) chloride complexes in hydrothermal solutions: Results of UV–Visible spectroscopic experiments. Geochimica et Cosmochimica Acta 94:276-290.

Liu Y, Brenan J (2015) Partitioning of platinum-group elements (PGE) and chalcogens (Se, Te, As, Sb, Bi) between monosulfide-solid solution (MSS), intermediate solid solution (ISS) and sulfide liquid at controlled fO2–fS2 conditions. Geochimica et Cosmochimica Acta 159:139-161.

Lobo L (2022) Geochemical Study of Trace and Critical Elements in Chalcopyrite and Pyrite from the Assarel Porphyry-Cu-Au Deposit, Bulgaria Department of Earth Sciences. Uppsala University Uppsala, pp 108.

Lockington JA, Cook NJ, Ciobanu CL (2014) Trace and minor elements in sphalerite from metamorphosed sulphide deposits. Mineralogy and Petrology 108:873-890. doi: 10.1007/s00710-014-0346-2.

Lydon J (1988) Ore deposit models# 14. Volcanogenic massive sulphide deposits Part 2: Genetic models. Geoscience Canada 15:43-65.

Makvandi S, Ghasemzadeh-Barvarz M, Beaudoin G, Grunsky EC, Beth McClenaghan M, Duchesne C (2016a) Principal component analysis of magnetite composition from volcanogenic massive sulfide deposits: Case studies from the Izok Lake (Nunavut, Canada) and Halfmile Lake (New Brunswick, Canada) deposits. Ore Geology Reviews 72:60-85. doi: https://doi.org/10.1016/j.oregeorev.2015.06.023.

Makvandi S, Ghasemzadeh-Barvarz M, Beaudoin G, Grunsky EC, McClenaghan MB, Duchesne C, Boutroy E (2016b) Partial least squares-discriminant analysis of trace element compositions of magnetite from various VMS deposit subtypes: Application to mineral exploration. Ore Geology Reviews 78:388-408.

Manéglia N, Beaudoin G, Simard M (2018) Indicator minerals of the Meliadine orogenic gold deposits, Nunavut (Canada), and application to till surveys. Geochemistry: Exploration, Environment, Analysis 18:241-251.

Mansur ET, Barnes S-J, Duran CJ (2019) Textural and compositional evidence for the formation of pentlandite via peritectic reaction: Implications for the distribution of highly siderophile elements. Geology 47:351-354.

Mansur ET, Barnes S-J (2020a) Concentrations of Te, As, Bi, Sb and Se in the Marginal Zone of the Bushveld Complex: Evidence for crustal contamination and the nature of the magma that formed the Merensky Reef. Lithos 358:105407.

Mansur ET, Barnes S-J (2020b) The role of Te, As, Bi, Sn and Sb during the formation of platinum-group-element reef deposits: examples from the Bushveld and Stillwater complexes. Geochimica et Cosmochimica Acta 272:235-258.

Mansur ET, Barnes S-J, Duran CJ, Sluzhenikin SF (2020) Distribution of chalcophile and platinum-group elements among pyrrhotite, pentlandite, chalcopyrite and cubanite from the Noril'sk-Talnakh ores: Implications for the formation of platinum-group minerals. Mineralium Deposita 55:1215-1232.

Mansur ET, Barnes S-J, Duran CJ (2021) An overview of chalcophile element contents of pyrrhotite, pentlandite, chalcopyrite, and pyrite from magmatic Ni-Cu-PGE sulfide deposits. Mineralium Deposita:1-26.

Mansur ET, Dare SAS, Filho CFF, Miranda ACR, Monteiro LVS (2023) The distribution of trace elements in sulfides and magnetite from the Jaguar hydrothermal nickel deposit: Exploring the link with IOA and

IOCG deposits within the Carajás Mineral Province, Brazil. Ore Geology Reviews 152:105256. doi: https://doi.org/10.1016/j.oregeorev.2022.105256.

Marfin AE, Ivanov AV, Abramova VD, Anziferova TN, Radomskaya TA, Yakich TY, Bestemianova KV (2020) A Trace Element Classification Tree for Chalcopyrite from Oktyabrsk Deposit, Norilsk–Talnakh Ore District, Russia: LA-ICPMS Study. Minerals 10:716.

Marignac C, Diagana B, Cathelineau M, Boiron M-C, Banks D, Fourcade S, Vallance J (2003) Remobilisation of base metals and gold by Variscan metamorphic fluids in the south Iberian pyrite belt: evidence from the Tharsis VMS deposit. Chemical Geology 194:143-165.

Marques AFA, Relvas JMRS, Scott SD, Rosa C, Guillong M (2020) Melt inclusions in quartz from felsic volcanic rocks of the Iberian Pyrite Belt: clues for magmatic ore metal transfer towards VMS-forming systems. Ore Geology Reviews 126:103743.

Marshall B, Vokes FM, Larocque ACL (1998) Regional Metamorphic Remobilization: Upgrading and Formation of Ore Deposits In: Vokes FM, Marshall B, Spry PG (eds) Metamorphic and Metamorphogenic Ore Deposits. Society of Economic Geologists, pp 0.

Martin AJ, McDonald I, MacLeod CJ, Prichard HM, McFall K (2018) Extreme enrichment of selenium in the Apliki Cyprus-type VMS deposit, Troodos, Cyprus. Mineralogical Magazine 82:697-724.

Martin AJ, Keith M, McDonald I, Haase KM, McFall KA, Klemd R, MacLeod CJ (2019) Trace element systematics and ore-forming processes in mafic VMS deposits: Evidence from the Troodos ophiolite, Cyprus. Ore Geology Reviews 106:205-225. doi: https://doi.org/10.1016/j.oregeorev.2019.01.024.

Maslennikov V, Maslennikova S, Large R, Danyushevsky L (2009a) Study of trace element zonation in vent chimneys from the Silurian Yaman-Kasy volcanic-hosted massive sulfide deposit (Southern Urals, Russia) using laser ablation-inductively coupled plasma mass spectrometry (LA-ICPMS). Economic Geology 104:1111-1141.

Maslennikov VV, Maslennikova SP, Large RR, Danyushevsky LV (2009b) Study of trace element zonation in vent chimneys from the Silurian Yaman-Kasy volcanic-hosted massive sulfide deposit (Southern Urals, Russia) using laser ablation-inductively coupled plasma mass spectrometry (LA-ICPMS). Economic Geology 104:1111-1141.

Maslennikov VV, Maslennikova SP, Large RR, Danyushevsky LV, Herrington RJ, Ayupova NR, Zaykov VV, Lein AY, Tseluyko AS, Melekestseva IY, Tessalina SG (2017) Chimneys in Paleozoic massive sulfide mounds of the Urals VMS deposits: Mineral and trace element comparison with modern black, grey, white and clear smokers. Ore Geology Reviews 85:64-106. doi: https://doi.org/10.1016/j.oregeorev.2016.09.012.

McClenaghan MB (2005) Indicator mineral methods in mineral exploration. Geochemistry: Exploration, Environment, Analysis 5:233-245.

McClenaghan MB (2017) Gold grains in till samples from the southern Core Zone, Quebec and Newfoundland and Labrador (NTS 23-P and 23-I): potential for undiscovered mineralization. Natural Resources Canada, Geological Survey of Canada.

Megahed FM, Chen Y-J, Megahed A, Ong Y, Altman N, Krzywinski M (2021) The class imbalance problem. Nature Methods 18:1270-1272. doi: 10.1038/s41592-021-01302-4.

Mehmood T, Liland KH, Snipen L, Sæbø S (2012) A review of variable selection methods in partial least squares regression. Chemometrics and Intelligent Laboratory Systems 118:62-69.

Melekestseva I, Maslennikov V, Tret'yakov G, Maslennikova S, Danyushevsky L, Kotlyarov V, Large R, Beltenev V, Khvorov P (2020a) Trace Element Geochemistry of Sulfides from the Ashadze-2 Hydrothermal Field

(12°58' N, Mid-Atlantic Ridge): Influence of Host Rocks, Formation Conditions or Seawater? Minerals 10. doi: 10.3390/min10090743.

Melekestseva IY, Maslennikov VV, Maslennikova SP (2020b) Trace-elements in sulfides of the Dergamysh cobalt-bearing massive sulfide deposit, the Southern Urals: Mode of occurrence and matter sources. Lithosphere (Russia) 20:499-516.

Mendez KM, Broadhurst DI, Reinke SN (2020) Migrating from partial least squares discriminant analysis to artificial neural networks: a comparison of functionally equivalent visualisation and feature contribution tools using jupyter notebooks. Metabolomics 16:17. doi: 10.1007/s11306-020-1640-0.

Menze BH, Kelm BM, Masuch R, Himmelreich U, Bachert P, Petrich W, Hamprecht FA (2009) A comparison of random forest and its Gini importance with standard chemometric methods for the feature selection and classification of spectral data. BMC Bioinformatics 10:213. doi: 10.1186/1471-2105-10-213.

Mercier-Langevin P, Dubé B, Hannington MD, Davis DW, Lafrance B, Gosselin G (2007) The LaRonde Penna Au-Rich Volcanogenic Massive Sulfide Deposit, Abitibi Greenstone Belt, Quebec: Part I. Geology and Geochronology*. Economic Geology 102:585-609. doi: 10.2113/gsecongeo.102.4.585.

Mercier-Langevin P, Hannington MD, Dubé B, Bécu V (2011) The gold content of volcanogenic massive sulfide deposits. Mineralium Deposita 46:509-539.

Michael F, Georges M, John F (2013) Elliptical Insights: Understanding Statistical Methods through Elliptical Geometry. Statistical Science 28:1-39. doi: 10.1214/12-STS402.

Miranda ACR, Beaudoin G, Rottier B (2022) Scheelite chemistry from skarn systems: implications for ore-forming processes and mineral exploration. Mineralium Deposita. doi: https://doi.org/10.1007/s00126-022-01118-y.

Mishra BP, Pati P, Dora ML, Baswani SR, Meshram T, Shareef M, Pattanayak RS, Suryavanshi H, Mishra M, Raza MA (2021) Trace-element systematics and isotopic characteristics of sphalerite-pyrite from volcanogenic massive sulfide deposits of Betul belt, central Indian Tectonic Zone: Insight of ore genesis to exploration. Ore Geology Reviews 134:104149. doi: https://doi.org/10.1016/j.oregeorev.2021.104149.

Moggi-Cecchi V, Cipriani C, Rossi P, Ceccato D, Rudello V, Somacal H (2002) Trace element contents and distribution maps of chalcopyrite: a micro-PIXE study. PERIODICO di MINERALOGIA 71:101-109.

Mungall JE (2007) Crustal contamination of picritic magmas during transport through dikes: the Expo Intrusive Suite, Cape Smith fold belt, New Quebec. Journal of Petrology 48:1021-1039.

Nagase T, Kojima S (1997) An SEM examination of the chalcopyrite disease texture and its genetic implications. Mineralogical Magazine 61:89-97. doi: 10.1180/minmag.1997.061.404.09.

Naldrett AJ (2004) Magmatic sulfide deposits: Geology, geochemistry and exploration. Springer, Berlin, Heidelberg, 728 p.

Ohmoto H (1996) Formation of volcanogenic massive sulfide deposits: the Kuroko perspective. Ore Geology Reviews 10:135-177.

Palarea-Albaladejo J, Martín-Fernández JA, Gómez-García J (2007) A parametric approach for dealing with compositional rounded zeros. Mathematical Geology 39:625-645.

Palarea-Albaladejo J, Martín-Fernández JA (2008) A modified EM alr-algorithm for replacing rounded zeros in compositional data sets. Computers & Geosciences 34:902-917.

Palarea-Albaladejo J, Martín-Fernández JA (2015) zCompositions—R package for multivariate imputation of left-censored data under a compositional approach. Chemometrics and Intelligent Laboratory Systems 143:85-96.

Paton C, Hellstrom J, Paul B, Woodhead J, Hergt J (2011) Iolite: Freeware for the visualisation and processing of mass spectrometric data. Journal of Analytical Atomic Spectrometry 26:2508-2518.

Patten CGC, Pitcairn IK, Teagle DAH, Harris M (2016) Mobility of Au and related elements during the hydrothermal alteration of the oceanic crust: implications for the sources of metals in VMS deposits. Mineralium Deposita 51:179-200.

Patten CGC, Pitcairn IK, Teagle DAH (2017) Hydrothermal mobilisation of Au and other metals in supra-subduction oceanic crust: Insights from the Troodos ophiolite. Ore Geology Reviews 86:487-508. doi: https://doi.org/10.1016/j.oregeorev.2017.02.019.

Patten CGC, Coltat R, Junge M, Peillod A, Ulrich M, Manatschal G, Kolb J (2022) Ultramafic-hosted volcanogenic massive sulfide deposits: an overlooked sub-class of VMS deposit forming in complex tectonic environments. Earth-Science Reviews 224:103891. doi: https://doi.org/10.1016/j.earscirev.2021.103891.

Pawlowsky-Glahn V, Buccianti A (2011) Compositional data analysis: Theory and applications. John Wiley & Sons, 378 p.

Pawlowsky-Glahn V, Egozcue JJ, Tolosana-Delgado R (2015) Modeling and analysis of compositional data. John Wiley & Sons.

Pedersen R-B, Furnes H, Dunning G (1991) A U/Pb age for the Sulitjelma Gabbro, North Norway: further evidence for the development of a Caledonian marginal basin in Ashgill–Llandovery time. Geological Magazine 128:141-153. doi: 10.1017/S0016756800018331.

Pilote J-L, Piercey SJ, Mercier-Langevin P (2020) Evolution of the subseafloor hydrothermal system associated with the Ming VMS deposit, Newfoundland Appalachians, and its controls on base and precious metal distribution. Mineralium Deposita 55:913-936.

Piña R, Gervilla F, Barnes S-J, Ortega L, Lunar R (2012a) Distribution of platinum-group and chalcophile elements in the Aguablanca Ni–Cu sulfide deposit (SW Spain): evidence from a LA-ICP-MS study. Chemical Geology 302:61-75.

Piña R, Gervilla F, Barnes S-J, Ortega L, Lunar RJCG (2012b) Distribution of platinum-group and chalcophile elements in the Aguablanca Ni–Cu sulfide deposit (SW Spain): evidence from a LA-ICP-MS study. 302:61-75.

Piña R, Gervilla F, Barnes SJ, Ortega L, Lunar R (2015) Liquid immiscibility between arsenide and sulfide melts: evidence from a LA-ICP-MS study in magmatic deposits at Serranía de Ronda (Spain). Mineralium Deposita 50:265-279. doi: 10.1007/s00126-014-0534-3.

Piña R, Gervilla F, Barnes SJ, Oberthür T, Lunar R (2016) Platinum-group element concentrations in pyrite from the Main Sulfide Zone of the Great Dyke of Zimbabwe. Mineralium Deposita 51:853-872.

Plouffe A, Ferbey T, Hashmi S, Ward B (2016) Till geochemistry and mineralogy: vectoring towards Cu porphyry deposits in British Columbia, Canada. Geochemistry: Exploration, Environment, Analysis 16:213-232.

Plouffe A, Kjarsgaard IM, Ferbey T, Wilton DHC, Petts DC, Percival JB, Kobylinski CH, McNeil R (2022) Detecting Buried Porphyry Cu Mineralization in a Glaciated Landscape: A Case Study from the Gibraltar Cu-Mo Deposit, British Columbia, Canada. Economic Geology 117:777-799.

Provost F, Saar-Tsechanski M (2007) Handling Missing Values when Applying Classification Models. Journal of Machine Learning Research 8:1625-1657.

Reich M, Deditius A, Chryssoulis S, Li J-W, Ma C-Q, Parada MA, Barra F, Mittermayr F (2013a) Pyrite as a record of hydrothermal fluid evolution in a porphyry copper system: A SIMS/EMPA trace element study. Geochimica et Cosmochimica Acta 104:42-62. doi: https://doi.org/10.1016/j.gca.2012.11.006.

Reich M, Palacios C, Barra F, Chryssoulis S (2013b) “Invisible” silver in chalcopyrite and bornite from the Mantos Blancos Cu deposit, northern Chile. European Journal of Mineralogy 25:453-460.

Reich M, Román N, Barra F, Morata D (2020) Silver-rich chalcopyrite from the active Cerro Pabellón geothermal system, Northern Chile. Minerals 10:113.

Relvas JM, Tassinari CC, Munhá J, Barriga FJ (2001) Multiple sources for ore-forming fluids in the Neves Corvo VHMS Deposit of the Iberian Pyrite Belt (Portugal): strontium, neodymium and lead isotope evidence. Mineralium Deposita 36:416-427.

Relvas JMRS, Barriga FJAS, Ferreira A, Noiva PC, Pacheco N, Barriga G (2006) Hydrothermal alteration and mineralization in the Neves-Corvo volcanic-hosted massive sulfide deposit, Portugal. I. Geology, mineralogy, and geochemistry. Economic Geology 101:753-790.

Ren Y, Huang F, Li Y, Zhu J, Wan Q, Yu L, Zhang Z, Gao S (2017) Genesis Study of the Nano-Micron Sphalerite Exsolution in Chalcopyrite from the Gengzhuang Gold Deposit in China. Journal of Nanoscience and Nanotechnology 17:6677-6685.

Ren Y, Wohlgemuth-Ueberwasser CC, Huang F, Shi X, Li B, Oelze M, Schreiber A, Wirth R (2021) Distribution of trace elements in sulfides from Deyin hydrothermal field, Mid-Atlantic Ridge – Implications for its mineralizing processes. Ore Geology Reviews 128:103911. doi: https://doi.org/10.1016/j.oregeorev.2020.103911.

Revan MK, Genç Y, Maslennikov VV, Maslennikova SP, Large RR, Danyushevsky LV (2014) Mineralogy and trace-element geochemistry of sulfide minerals in hydrothermal chimneys from the Upper-Cretaceous VMS deposits of the eastern Pontide orogenic belt (NE Turkey). Ore Geology Reviews 63:129-149. doi: https://doi.org/10.1016/j.oregeorev.2014.05.006.

Rimstidt JD, Chermak JA, Gagen PM (1993) Rates of Reaction of Galena, Sphalerite, Chalcopyrite, and Arsenopyrite with Fe(III) in Acidic Solutions Environmental Geochemistry of Sulfide Oxidation. American Chemical Society, pp 2-13.

Ripley EM, Li C (2011) A review of conduit-related Ni-Cu-(PGE) sulfide mineralization at the Voisey's Bay Deposit, Labrador, and the Eagle Deposit, northern Michigan. Reviews in Economic Geology 17:181-197.

Ripley EM, Li C (2013) Sulfide Saturation in Mafic Magmas: Is External Sulfur Required for Magmatic Ni-Cu-(PGE) Ore Genesis? Economic Geology 108:45-58. doi: 10.2113/econgeo.108.1.45.

Ripley EM (2014) Ni-Cu-PGE Mineralization in the Partridge River, South Kawishiwi, and Eagle Intrusions: A Review of Contrasting Styles of Sulfide-Rich Occurrences in the Midcontinent Rift System. Economic Geology 109:309-324. doi: 10.2113/econgeo.109.2.309.

Roo JAd, Staal CRv (2003) Sulfide Remobilization and Sulfide Breccias in the Heath Steele and Brunswick Deposits, Bathurst Mining Camp, New Brunswick* In: Goodfellow WD, McCutcheon SR, Peter JM (eds) Massive Sulfide Deposits of the Bathurst Mining Camp, New Brunswick, and Northern Maine. Society of Economic Geologists, pp 0.

Rose AW (1967) Trace elements in solflde minerals from the Central district, New Mexico and the Bingham district, Utah. Geochimica et Cosmochimica Acta 31:547-585.

Rouxel OJ, Luais B (2017) Germanium isotope geochemistry. Reviews in Mineralogy and Geochemistry 82:601-656.

Ruiz-Perez D, Guan H, Madhivanan P, Mathee K, Narasimhan G (2020) So you think you can PLS-DA? BMC Bioinformatics 21:207225. doi: 10.1186/s12859-019-3310-7.

Salim Amaral LF (2017) The distribution of platinum-group elements and other chalcophile elements among sulfide minerals from the Ovoid ore body of the Voisey's Bay Ni-Cu sulfide deposit, Canada (Master's thesis) Département des sciences appliquées. Université du Québec à Chicoutimi, Chicoutimi, pp 154.

Samalens N, Barnes S-J, Sawyer EW (2017a) The role of black shales as a source of sulfur and semimetals in magmatic nickel-copper deposits: Example from the Partridge River Intrusion, Duluth Complex, Minnesota, USA. Ore Geology Reviews 81:173-187.

Samalens N, Barnes SJ, Sawyer EW (2017b) A laser ablation inductively coupled plasma mass spectrometry study of the distribution of chalcophile elements among sulfide phases in sedimentary and magmatic rocks of the Duluth Complex, Minnesota, USA. Ore Geology Reviews 90:352-370.

Schulz KJ, Woodruff LG, Nicholson SW, Seal Ii RR, Piatak NM, Chandler VW, Mars JL (2014) Occurrence model for magmatic sulfide-rich nickel-copper-(platinum-group element) deposits related to mafic and ultramafic dike-sill complexes: Chapter I in Mineral deposit models for resource assessment (Scientific Investigations Report 2010-5070-I). US Geological Survey, pp 80.

Sciuba M, Beaudoin G, Grzela D, Makvandi S (2020) Trace element composition of scheelite in orogenic gold deposits. Mineralium Deposita 55:1149–1172.

Sciuba M, Beaudoin G (2021) Texture and Trace Element Composition of Rutile in Orogenic Gold Deposits. Economic Geology 116:1865-1892. doi: 10.5382/econgeo.4857.

Sciuba M, Beaudoin G, Makvandi S (2021) Chemical composition of tourmaline in orogenic gold deposits. Mineralium Deposita 56:537-560.

Seward TM, Williams-Jones AE, Migdisov AA (2014) The chemistry of metal transport and deposition by ore-forming hydrothermal fluids In: Holland HD, Tukerian KK (eds) Treatise on geochemistry. Elsevier Oxford, pp 29-57.

Shanks WC, Koski RA, Mosier DL, Schulz KJ, Morgan LA, Slack JF, Ridley WI, Dusel-Bacon C, Seal Ii RR, Piatak NM (2012) Volcanogenic massive sulfide occurrence model: Chapter C in Mineral deposit models for resource assessment In: Shanks WC, Thurston R (eds) Scientific Investigations Report. US Department of the Interior, US Geological Survey, Reston, VA.

Skirrow RG (2022) Iron oxide copper-gold (IOCG) deposits – A review (part 1): Settings, mineralogy, ore geochemistry and classification. Ore Geology Reviews 140:104569. doi: https://doi.org/10.1016/j.oregeorev.2021.104569.

Skyttä P, Weihed P, Högdahl K, Bergman S, Stephens MB (2020) Paleoproterozoic (2.0–1.8 Ga) syn-orogenic sedimentation, magmatism and mineralization in the Bothnia–Skellefteå lithotectonic unit, Svecokarelian orogen Sweden: Lithotectonic Framework, Tectonic Evolution and Mineral Resources. Geological Society of London, pp 0.

Slack JF, Offield TW, Woodruff LG, Shanks WC (2001) Geology and geochemistry of Besshi-type massive sulfide deposits of the Vermont copper belt. Part II Environmental Geochemistry and Mining History of Massive Sulfide Deposits in the Vermont Copper Belt: Society of Economic Geologists Guidebook Series 35:193-211.

Sokolova M, Lapalme G (2009) A systematic analysis of performance measures for classification tasks. Information Processing & Management 45:427-437. doi: https://doi.org/10.1016/j.ipm.2009.03.002.

Song X-Y, Keays RR, Zhou M-F, Qi L, Ihlenfeld C, Xiao J-F (2009) Siderophile and chalcophile elemental constraints on the origin of the Jinchuan Ni-Cu-(PGE) sulfide deposit, NW China. Geochimica et Cosmochimica Acta 73:404-424. doi: https://doi.org/10.1016/j.gca.2008.10.029.

Spry PG, Peter JM, Slack JF (1998) Meta-exhalites as exploration guides to ore. Reviews in Economic Geology 11:163-201.

Stakes DS, Taylor HP (2003) Oxygen isotope and chemical studies on the origin of large plagiogranite bodies in northern Oman, and their relationship to the overlying massive sulphide deposits. Geological Society, London, Special Publications 218:315. doi: 10.1144/GSL.SP.2003.218.01.17.

Steadman JA, Large RR (2016) Synsedimentary, Diagenetic, and Metamorphic Pyrite, Pyrrhotite, and Marcasite at the Homestake BIF-Hosted Gold Deposit, South Dakota, USA: Insights on Au-As Ore Genesis from Textural and LA-ICP-MS Trace Element Studies. Economic Geology 111:1731-1752. doi: 10.2113/econgeo.111.7.1731.

Stefanova E, Georgiev S, Peytcheva I, Marchev P, Quadt AV, Raicheva R, Gerdjikov I, Kouzmanov K, Boyce A, Vennemann T (2023) Sulfide Trace Element Signatures and S-and Pb-Isotope Geochemistry of Porphyry Copper and Epithermal Gold-Base Metal Mineralization in the Eletsite–Chelopech Ore Field (Bulgaria). Minerals 13:630.

Stekhoven DJ, Bühlmann P (2012) MissForest—non-parametric missing value imputation for mixed-type data. Bioinformatics 28:112-118. doi: 10.1093/bioinformatics/btr597.

Strashimirov S, Petrunov R, Kanazirski M (2002) Porphyry-copper mineralisation in the central Srednogorie zone, Bulgaria. Mineralium Deposita 37:587-598. doi: 10.1007/s00126-002-0275-6.

Sugaki A, Kitakaze A, Kojima S (1987) Bulk compositions of intimate intergrowths of chalcopyrite and sphalerite and their genetic implications. Mineralium deposita 22:26-32.

Sun C (2018) Partitioning and partition coefficients In: White WM (ed) Encyclopedia of geochemistry Encyclopedia of earth sciences series. Springer, pp 1186-1197.

Sun G-T, Zhou J-X (2022) Application of Machine Learning Algorithms to Classification of Pb–Zn Deposit Types Using LA–ICP–MS Data of Sphalerite. Minerals 12:1293.

Sun G, Zeng Q, Zhou J-X (2022) Machine learning coupled with mineral geochemistry reveals the origin of ore deposits. Ore Geology Reviews 142:104753. doi: https://doi.org/10.1016/j.oregeorev.2022.104753.

Sun T, Li H, Wu K, Chen F, Zhu Z, Hu Z (2020) Data-Driven Predictive Modelling of Mineral Prospectivity Using Machine Learning and Deep Learning Methods: A Case Study from Southern Jiangxi Province, China. Minerals 10. doi: 10.3390/min10020102.

Svetnik V, Liaw A, Tong C, Culberson JC, Sheridan RP, Feuston BP (2003) Random Forest: A Classification and Regression Tool for Compound Classification and QSAR Modeling. Journal of Chemical Information and Computer Sciences 43:1947-1958. doi: 10.1021/ci034160g.

Tan HMR, Huang X-W, Meng Y-M, Xie H, Qi L (2023) Multivariate statistical analysis of trace elements in apatite: Discrimination of apatite with different origins. Ore Geology Reviews 153:105269. doi: https://doi.org/10.1016/j.oregeorev.2022.105269.

Tarawneh AS, Hassanat AB, Altarawneh GA, Almuhaimeed A (2022) Stop Oversampling for Class Imbalance Learning: A Review. IEEE Access 10:47643-47660. doi: 10.1109/ACCESS.2022.3169512.

Thabtah F, Hammoud S, Kamalov F, Gonsalves A (2020) Data imbalance in classification: Experimental evaluation. Information Sciences 513:429-441. doi: https://doi.org/10.1016/j.ins.2019.11.004.

Tian Y, Etschmann B, Liu W, Borg S, Mei Y, Testemale D, O'Neill B, Rae N, Sherman DM, Ngothai Y, Johannessen B, Glover C, Brugger J (2012) Speciation of nickel (II) chloride complexes in hydrothermal fluids: In situ XAS study. Chemical Geology 334:345-363. doi: https://doi.org/10.1016/j.chemgeo.2012.10.010.

Tomkins AG (2007) Three mechanisms of ore re-mobilisation during amphibolite facies metamorphism at the Montauban Zn–Pb–Au–Ag deposit. Mineralium Deposita 42:627-637.

Tomkins AG, Pattison DRM, Frost BR (2007) On the initiation of metamorphic sulfide anatexis. Journal of Petrology 48:511-535.

Tornos F (2006) Environment of formation and styles of volcanogenic massive sulfides: The Iberian Pyrite Belt. Ore Geology Reviews 28:259-307.

Torró L, Benites D, Vallance J, Laurent O, Ortiz-Benavente BA, Chelle-Michou C, Proenza JA, Fontboté L (2022) Trace element geochemistry of sphalerite and chalcopyrite in arc-hosted VMS deposits. Journal of Geochemical Exploration 232:106882.

Vasilopoulos M, Molnár F, Ranta J-P, O'Brien H (2023) Mineralogical, lithogeochemical and sulfide trace element characteristics of the Hirvilavanmaa Au-only and the base metal-rich Naakenavaara orogenic gold deposits in the Central Lapland belt, northern Finland. Journal of Geochemical Exploration 244:107132. doi: https://doi.org/10.1016/j.gexplo.2022.107132.

Vasyukova OV, Williams-Jones AE (2022) Constraints on the Genesis of Cobalt Deposits: Part II. Applications to Natural Systems. Economic Geology 117:529-544. doi: 10.5382/econgeo.4888.

Vaughan DJ (2006) Sulfide mineralogy and geochemistry: introduction and overview. Reviews in Mineralogy and Geochemistry 61:1-5.

Von Eynatten H, Pawlowsky-Glahn V, Egozcue JJ (2002) Understanding perturbation on the simplex: A simple method to better visualize and interpret compositional data in ternary diagrams. Mathematical Geology 34:249-257.

Wang Y, Han X, Petersen S, Frische M, Qiu Z, Cai Y, Zhou P (2018) Trace Metal Distribution in Sulfide Minerals from Ultramafic-Hosted Hydrothermal Systems: Examples from the Kairei Vent Field, Central Indian Ridge. Minerals 8:526.

Wang Y, Qiu K-F, Müller A, Hou Z-L, Zhu Z-H, Yu H-C (2021) Machine Learning Prediction of Quartz Forming-Environments. Journal of Geophysical Research: Solid Earth 126:e2021JB021925. doi: https://doi.org/10.1029/2021JB021925.

Wang Z, Xu D, Zhang Z, Zou F, Wang L, Yu L, Hu M (2015) Mineralogy and trace element geochemistry of the Co-and Cu-bearing sulfides from the Shilu Fe–Co–Cu ore district in Hainan Province of South China. Journal of Asian Earth Sciences 113:980-997.

Weihed P, Weihed JB, Sorjonen-Ward P, Matsson B (2002) Post-deformation, sulphide-quartz vein hosted gold ore in the footwall alteration zone of the Palaeoproterozoic Långdal VHMS deposit, Skellefte District, northern Sweden. GFF 124:201-210. doi: 10.1080/11035890201244201.

Weiss GM (2013) Foundations of imbalanced learning In: He H, Ma Y (eds) Imbalanced Learning: Foundations, Algorithms, and Applications. First edn. Wiley Online Library, pp 13-41.

Westerhuis JA, Hoefsloot HCJ, Smit S, Vis DJ, Smilde AK, van Velzen EJJ, van Duijnhoven JPM, van Dorsten FA (2008) Assessment of PLSDA cross validation. Metabolomics 4:81-89.

Wilcox RR (2011) Introduction to robust estimation and hypothesis testing. Academic press.

Wilson SA, Ridley WI, Koenig AE (2002) Development of sulfide calibration standards for the laser ablation inductively-coupled plasma mass spectrometry technique. Journal of Analytical Atomic Spectrometry 17:406-409.

Winderbaum L, Ciobanu CL, Cook NJ, Paul M, Metcalfe A, Gilbert S (2012) Multivariate analysis of an LA-ICP-MS trace element dataset for pyrite. Mathematical Geosciences 44:823-842.

Wohlgemuth-Ueberwasser CC, Viljoen F, Petersen S, Vorster C (2015) Distribution and solubility limits of trace elements in hydrothermal black smoker sulfides: An in-situ LA-ICP-MS study. Geochimica et Cosmochimica Acta 159:16-41.

Wold S, Sjöström M, Eriksson L (2001) PLS-regression: a basic tool of chemometrics. Chemometrics and intelligent laboratory systems 58:109-130.

Wold S, Eriksson L, Trygg J, Kettaneh N (2004) The PLS method–partial least squares projections to latent structures–and its applications in industrial RDP (research, development, and production). Unea University.

Wood BJ, Kiseeva ES (2015) Trace element partitioning into sulfide: How lithophile elements become chalcophile and vice versa†. American Mineralogist 100:2371-2379. doi: 10.2138/am-2015-5358CCBYNCND.

Workman RK, Hart SR (2005) Major and trace element composition of the depleted MORB mantle (DMM). Earth and Planetary Science Letters 231:53-72.

Xie J, Tang D, Qian L, Wang Y, Sun W (2020) Geochemistry of sulfide minerals from skarn Cu (Au) deposits in the Fenghuangshan ore field, Tongling, eastern China: Insights into ore-forming process. Ore Geology Reviews 122:103537. doi: https://doi.org/10.1016/j.oregeorev.2020.103537.

Xing B, Mao J, Xiao X, Liu H, Zhang C, Guo S, Li H, Huang W, Lai C (2022) Metallogenic discrimination by sphalerite trace element geochemistry: An example from the Fengyan Zn-Pb deposit in central Fujian, SE China. Ore Geology Reviews 141:104651. doi: https://doi.org/10.1016/j.oregeorev.2021.104651.

Yang C, Beaudoin G, Tang J-X, Song Y, Wang L-Q, Huang X-W (2022) Cu-sulfide mineralogy, texture, and geochemistry in the Tiegelongnan porphyry-epithermal copper system, Tibet, China. Mineralium Deposita 57:759-779. doi: 10.1007/s00126-021-01075-y.

Yano RI (2012) Trace element distribution in chalcopyrite-bearing porphyry and skarn deposits. University of Nevada, Reno.

Yeo I-K, Johnson RA (2000) A New Family of Power Transformations to Improve Normality or Symmetry. Biometrika 87:954-959.

Yilmaz AE, Demirhan H (2023) Weighted kappa measures for ordinal multi-class classification performance. Applied Soft Computing 134:110020. doi: https://doi.org/10.1016/j.asoc.2023.110020.

Yu J, Li N, Zhang B, Ulrich T, Chen X, Hand M, Morrissey LJ, Payne JL, Chen Y-J (2022) Perspective of Permian porphyry Cu-Au mineralization in Chinese Western Tianshan: Constraints from sulfide Re-Os dating and trace element study of the Kuruer deposit, Xinjiang. Ore Geology Reviews 142:104707. doi: https://doi.org/10.1016/j.oregeorev.2022.104707.

Yuan B, Yang Y, Yu H, Zhao Y, Ding Q, Yang J, Tang X (2018) Geochemistry of pyrite and chalcopyrite from an active black smoker in 49.6°E Southwest Indian Ridge. Marine Geophysical Research 39:441-461. doi: 10.1007/s11001-017-9324-5.

Zhang J, Shao Y, Liu Z, Chen K (2022a) Sphalerite as a record of metallogenic information using multivariate statistical analysis: Constraints from trace element geochemistry. Journal of Geochemical Exploration 232:106883. doi: https://doi.org/10.1016/j.gexplo.2021.106883.

Zhang P, Zhang Z, Yang J, Cheng Q (2022b) Machine Learning Prediction of Ore Deposit Genetic Type Using Magnetite Geochemistry. Natural Resources Research. doi: 10.1007/s11053-022-10146-4.

Zhao X-Y, Zhong H, Mao W, Bai Z-J, Xue K (2020) Molybdenite Re-Os dating and LA-ICP-MS trace element study of sulfide minerals from the Zijinshan high-sulfidation epithermal Cu-Au deposit, Fujian Province, China. Ore Geology Reviews 118:103363. doi: https://doi.org/10.1016/j.oregeorev.2020.103363.

Zhao Y, Chen S, Tian H, Zhao J, Tong X, Chen X (2021a) Trace element and S isotope characterization of sulfides from skarn Cu ore in the Laochang Sn-Cu deposit, Gejiu district, Yunnan, China: Implications for the ore-forming process. Ore Geology Reviews 134:104155. doi: https://doi.org/10.1016/j.oregeorev.2021.104155.

Zhao Z, Wei J, Liang S, Gao T (2021b) Sulfide remobilization and trace element redistribution during metamorphism and deformation at the Xitieshan Pb-Zn deposit, NW China. Ore Geology Reviews 136:104170.

Zientek ML, Likhachev AP, Kunilov VE, Barnes S-J, Meier AL, Carlson RR, Briggs PH, Fries TL, Adrian BM, Lightfoot PC (1994) Cumulus processes and the composition of magmatic ore deposits: examples from the Talnakh district, Russia. Ont Geol Surv Spec Publ 5:373-392.

Annexe A

Annexes correspondant à l'article: Variation of trace elements in chalcopyrite from worldwide Ni-Cu sulfide and Reef-type PGE deposits: implications for mineral exploration

Annexe A1 Samples list of chalcopyrite-bearing magmatic sulfides from Ni-Cu sulfide and Reef-type PGE deposits with details of location, ore type, texture and mineralogical composition.

Type	Subtype[1]	Sample	n	Deposit name	Host igneous complex (age)	Location	Orebody type	Sulfide texture[2]	Sulfide texture[3]	Metamorphism	Sulfide content (%)[4]	Ccp (%)	Cbn (%)	Po (%)	Py (%)	Pn (%)	Sp (%)	Gn (%)	PGM (%)[5]	Mag (%)	Chr (%)
Ni-Cu sulfide	NC-1	TR15	7	Delta	Cape Smith Belt (1.88 Ga)	Northen Quebec, Canada	Unzoned	Massive	Massive	Greensc	93.6	6.5	*np*	79.7	*np*	13.8	*np*	*np*	*np*	*np*	*np*
		TR20	8				Unzoned	Semi-massive	Massive		70.1	6.6	*np*	91.9	*np*	1.6	*np*	*np*	*np*	*np*	*np*
		EX0301	9	Expo			Unzoned	Massive	Massive		92.9	17.6	*np*	67.2	*np*	7.1	*np*	*np*	*np*	8.2	*np*
		MXNW	7	Mesamax			Unzoned	Massive	Massive		91.4	24.6	*np*	62.6	*np*	6.5	*np*	*np*	*np*	6.3	*np*
		K2	8	Katinniq			Unzoned	Massive	Massive		92.0	6.7	*np*	81.2	*np*	12.1	*np*	*np*	*np*	*np*	<1
		C0423	8				Unzoned	Semi-massive	Massive		75.5	10.3	*np*	82.8	*np*	5.5	*np*	*np*	*np*	1.4	*np*
		C0424	7				Unzoned	Massive	Massive		81.5	6.6	*np*	89.7	*np*	3.7	*np*	*np*	*np*	*np*	<1
		C0425	9	Zone Frontier			Unzoned	Semi-massive	Massive		73.5	4.9	*np*	90.9	*np*	4.2	*np*	*np*	*np*	*np*	<1
		C0438	3				Unzoned	Patchy net textured	Net textured/globular		24.3	9.5	*np*	84.2	*np*	*np*	*np*	*np*	*np*	6.3	*np*
		C0443	8				Unzoned	Patchy net textured	Net textured/globular		32.9	31.2	*np*	44.6	*np*	18.6	*np*	*np*	*np*	5.6	<1
		2523	6	Marbridge	Kidd-Munro assemblage (2.71 Ga)	Abitibi, Quebec, Canada	Unzoned	Patchy net textured	Net textured/globular	Amph	46.5	42.9	*np*	42.9	*np*	14.3	*np*	*np*	*np*	*np*	*np*
	NC-2	A2	7	Medvezhy Creek	Noril'sk-Talnakh Intrusion (0.25 Ga)	Krasnoyarsk Krai, Russia	Cu-rich	Massive	Massive	Unmet	94.5	94.6	*np*	*np*	*np*	5.4	<1	*np*	*np*	*np*	*np*
		NR6	5				Fe-rich	Massive	Massive		96.1	6.8	*np*	93.2	*np*	*np*	*np*	*np*	*np*	*np*	*np*
		T11	8	Talnakh			Cu-rich	Massive	Massive		90.6	16.0	43.3	*np*	*np*	32.0	*np*	*np*	*np*	8.7	*np*
		T3	7				Cu-rich	Massive	Massive		91.2	24.3	69.1	*np*	*np*	1.0	*np*	*np*	*np*	5.5	*np*
		T4	8				Cu-rich	Massive	Massive		93.6	26.5	65.7	*np*	*np*	7.8	*np*	*np*	*np*	*np*	*np*
		T1	5				Fe-rich	Semi-massive	Massive		73.0	12.3	*np*	68.6	*np*	12.7	*np*	*np*	*np*	6.4	*np*
		T2	8				Fe-rich	Massive	Massive		90.1	8.8	*np*	85.8	*np*	2.1	*np*	*np*	*np*	3.2	*np*
		DC18	7	Dunka Road	Duluth Complex (1.10 Ga)	Minnesota, USA	Unzoned	Net textured	Net textured/globular	Unmet	38.1	11.2	*np*	69.2	*np*	<1	*np*	*np*	*np*	18.7	*np*
		DC69	7				Unzoned	Patchy net textured	Net textured/globular		20.8	13.0	*np*	76.3	*np*	2.8	*np*	*np*	*np*	7.9	*np*
		B138405	4	Mesaba			Unzoned	Globular	Net textured/globular		1.9	59.5	*np*	*np*	*np*	40.5	*np*	*np*	*np*	*np*	*np*
		B138439	6				Unzoned	Patchy net textured	Net textured/globular		51.0	40.4	*np*	47.6	*np*	*11.9*	*np*	*np*	*np*	*np*	*np*
		E1	4	Eagle	Eagle Intrusion (1.10 Ga)	Michigan,USA	Unzoned	Globular	Disseminated	Unmet	5.5	37.3	*np*	25.5	*np*	3.9	*np*	*np*	*np*	33.3	*np*
		E13	3				Unzoned	Globular	Disseminated		3.2	23.5	*np*	70.6	*np*	5.9	*np*	*np*	*np*	*np*	*np*
		E4	6				Unzoned	Massive	Massive		91.9	31.9	*np*	53.1	*np*	6.8	*np*	*np*	*np*	8.2	*np*

Type	Subtype[1]	Sample	n	Deposit name	Host igneous complex (age)	Location	Orebody type	Sulfide texture[2]	Sulfide texture[3]	Metamorphism	Sulfide content (%)[4]	Ccp (%)	Cbn (%)	Po (%)	Py (%)	Pn (%)	Sp (%)	Gn (%)	PGM (%)[5]	Mag (%)	Chr (%)
	NC-3	MS2	7	Kotselvaara	Pechenga Complex (2.50 Ga)	Kola Peninsula, Russia	Unzoned	Patchy net textured	Net textured/globular	Pr-Pm	11.2	29.7	*np*	*np*	*np*	22.1	*np*	*np*	*np*	48.3	*np*
		MS3	4				Unzoned	Patchy net textured	Net textured/globular		18.3	31.4	*np*	*np*	*np*	21.6	*np*	*np*	*np*	47.0	*np*
		MS10	7	Semilekta			Unzoned	Breccia-matrix	Net textured/globular		31.7	28.9	*np*	64.7	*np*	6.5	*np*	*np*	*np*	*np*	*np*
		MS12	5				Unzoned	Massive	Massive		66.5	18.9	*np*	59.7	*np*	4.7	*np*	*np*	*np*	16.6	*np*
		MS8	7				Unzoned	Massive	Massive		90.9	10.8	*np*	73.9	*np*	15.3	*np*	*np*	*np*	*np*	*np*
		IGCP4	5	Zhdanovskoe			Unzoned	Disseminated	Disseminated		5.2	76.7	*np*	23.3	*np*	*np*	*np*	*np*	*np*	*np*	*np*
	NC-4	EDEEP	5	Eastern Deeps	Voisey's Bay Nain Plutonic Suite (1.33 Ga)	Newfoundland, Canada	Fe-rich	Massive	Massive	Unmet	45.3	5.9	*np*	82.5	*np*	3.3	*np*	*np*	*np*	8.2	*np*
		VB27	4	Ovoid			Cu-rich	Massive	Massive		91.5	3.7	44.7	45.7	*np*	1.6	*np*	*np*	*np*	4.3	*np*
		VB34	2				Cu-rich	Massive	Massive		92.8	1.4	85.2	10.2	*np*	*np*	<1	*np*	*np*	<1	*np*
		VB5	3				Cu-rich	Massive	Massive		91.4	2.7	70.6	24.1	*np*	*np*	<1	<1	*np*	2.6	*np*
		VB6	11				Cu-rich	Massive	Massive		77.2	12.9	1.3	9.2	*np*	<1	<1	*np*	*np*	13.9	*np*
		OVOID	7				Fe-rich	Massive	Massive		90.6	1.8	*np*	86.5	*np*	2.3	*np*	*np*	*np*	9.5	*np*
		VB21	6				Fe-rich	Net textured	Net textured/globular		37.7	2.5	*np*	20.5	*np*	35.1	*np*	*np*	*np*	42.0	*np*
		VB25	5				Fe-rich	Massive	Massive		92.1	1.3	*np*	83.0	*np*	5.9	*np*	*np*	*np*	9.9	*np*
		VB29	2				Fe-rich	Massive	Massive		93.2	<1	*np*	53.7	*np*	39.5	*np*	*np*	*np*	6.1	*np*
		VB30	6				Fe-rich	Massive	Massive		80.9	34.6	*np*	46.8	*np*	3.4	*np*	*np*	*np*	15.3	*np*
		VB31	7				Fe-rich	Massive	Massive		94.8	30.0	<1	63.5	*np*	3.6	*np*	*np*	*np*	*np*	*np*
		VB7	7				Fe-rich	Net textured	Net textured/globular		36.2	4.1	*np*	92.0	*np*	3.9	*np*	*np*	*np*	*np*	*np*
	NC-5	J12	7	Jinchuan	Jinchuan Complex (0.82 Ga)	Gansu, China	Unzoned	Globular	Net textured/globular	Greensch	8.0	43.2	*np*	40.5	*np*	16.2	*np*	*np*	*np*	*np*	*np*
		J2	2				Unzoned	Massive	Massive		97.2	4.6	*np*	84.6	*np*	10.8	*np*	*np*	*np*	*np*	*np*
		J3	6				Unzoned	Patchy net textured	Net textured/globular		48.0	16.4	*np*	70.6	*np*	13.0	*np*	*np*	*np*	*np*	*np*
		J9B	6				Unzoned	Net textured	Net textured/globular		14.7	43.9	*np*	35.7	*np*	20.4	*np*	*np*	*np*	*np*	*np*
	NC-6	06MPBR15	9	Broken Hammer	Sudbury Igneous Complex (1.85 Ga)	Ontario, Canada	Cu-rich	Semi-massive	Massive	Greensch	72.0	97.2	*np*	*np*	<1	*np*	*np*	*np*	*np*	2.3	*np*
		06MPBR16	7				Cu-rich	Massive	Massive		92.8	97.9	*np*	*np*	*np*	*np*	*np*	*np*	*np*	2.1	*np*
		1533	8	Copper Cliff			Cu-rich	Massive	Massive		92.2	70.2	*np*	26.7	*np*	*np*	<1	*np*	*np*	3.1	*np*
		CRTN18	5	Creighton			Fe-rich	Massive	Massive		92.2	49.9	*np*	26.7	*np*	20.7	*np*	*np*	*np*	2.8	*np*
		CRTN12	10				Fe-rich	Massive	Massive		97.3	1.9	*np*	71.2	1.1	25.0	*np*	*np*	*np*	<1	*np*
		CRTN13	10				Fe-rich	Massive	Massive		96.6	4.0	*np*	81.3	*np*	14.7	<1	<1	*np*	*np*	*np*
		CRTN14	8				Fe-rich	Massive	Massive		91.3	39.1	*np*	19.2	<1	36.3	*np*	*np*	*np*	*5.4*	*np*
		CRTN19	6				Fe-rich	Massive	Massive		93.9	34.9	*np*	52.3	*np*	10.6	*np*		*np*	2.2	*np*
		CRTN6	10				Fe-rich	Globular	Net textured/globular		16.0	5.9	*np*	88.0	<1	6.1	<1	<1	*np*	*np*	*np*
		CRTN9B	8				Fe-rich	Massive	Massive		89.5	47.0	*np*	36.5	*np*	12.2	*np*	*np*	*np*	*4.4*	*np*
		MCR10A	16	McCreedy			Cu-rich	Massive	Massive		94.8	92.4	3.0	2.5	*np*	*np*	*np*	*np*	*np*	2.1	*np*
		MCR10B	10				Cu-rich	Massive	Massive		90.0	49.4	8.3	*np*	*np*	35.2	*np*	*np*	*np*	7.0	*np*
		MCR13	12				Cu-rich	Massive	Massive		91.3	80.8	2.3	*np*	*np*	15.8	*np*	*np*	*np*	1.1	*np*
		RX162	5				Cu-rich	Massive	Massive		92.0	85.6	11.5	*np*	*np*	*np*	*np*	<1	*np*	2.9	*np*
		RX164	10				Cu-rich	Semi-massive	Massive		72.0	80.7	1.3	*np*	*np*	2.1	*np*	*np*	*np*	15.9	*np*

Type	Subtype[1]	Sample	n	Deposit name	Host igneous complex (age)	Location	Orebody type	Sulfide texture[2]	Sulfide texture[3]	Metamorphism	Sulfide content (%)[4]	Ccp (%)	Cbn (%)	Po (%)	Py (%)	Pn (%)	Sp (%)	Gn (%)	PGM (%)[5]	Mag (%)	Chr (%)
Reef-type PGE		MCR3	8				Fe-rich	Massive	Massive		92.6	20.9	*np*	67.6	*np*	3.9	<1	*np*	*np*	7.6	*np*
		MCR4B	7				Fe-rich	Massive	Massive		93.8	48.4	*np*	37.8	2.5	7.6	*np*	*np*	*np*	3.7	*np*
		MCR5	5				Fe-rich	Massive	Massive		90.5	16.4	*np*	69.3	*np*	8.3	*np*	*np*	*np*	6.1	*np*
		2938	12	Merensky Reef	Bushveld Complex (2.05 Ga)	South Africa			Disseminated	Unmet	2.1	45.9	*np*	24.9	*np*	11.2	*np*	*np*	<1	*np*	18.0
		CGMA	9	Rustenburg					Disseminated		7.5	9.1	*np*	58.2	*np*	9.9	*np*	*np*	<1	*np*	22.8
		CGMB	8						Disseminated		5.6	7.5	*np*	55.4	*np*	22.2	*np*	*np*	*np*	*np*	15.0
		M1	9						Disseminated		6.2	32.2	*np*	35.2	*np*	15.3	<1	*np*	*np*	<1	17.3
		M2	11						Disseminated		4.1	8.9	*np*	26.7	*np*	6.0	<1	*np*	*np*	*np*	58.4
		MR2	9						Disseminated		2.8	5.3	*np*	11.0	*np*	7.4	<1	*np*	*np*	*np*	76.3
		GD10	14	Mimosa	Great Dyke (2.57 Ga)	Mashonaland West, Zimbabwe			Disseminated		3.1	28.9	*np*	58.4	*np*	5.8	<1	*np*	*np*	*np*	<1
		GDN4	9						Disseminated		0.6	35.0	*np*	46.9	*np*	18.1	*np*	*np*	*np*	*np*	*np*
		F10304	12	PV Reef	Penikat (2.44Ga)	Finland			Disseminated	Greensch	3.3	62.4	*np*	*np*	*np*	37.6	<1	*np*	*np*	*np*	*np*
		ST12	3	East Boulder	Stillwater Complex (2.70 Ga)	Montana, USA			Disseminated		5.4	19.4	*np*	21.8	*np*	14.8	*np*	*np*	*np*	24.0	20.0
		T10T	8						Disseminated		1.8	50.5	*np*	41.6	*np*	7.9	*np*	*np*	*np*	*np*	*np*
		T11T	12						Disseminated		2.9	37.7	*np*	48.6	*np*	13.7	<1	*np*	*np*	*np*	*np*

1 Classification according to Naldrett (2004). NC-1: komatiite; NC-2: flood basalt; NC-3: ferropicrite; NC-4: anorthosite-granite -troctolite; NC-5: picrite to tholeiite; NC-6: impact melt
2 Texture defined according to classification from Barnes et al. (2017) and Barnes et al. (2018) based on modal percent of sulfides in the sample. Disseminated (0-5%); Patchy net textured (5-40%); Net textured (40-70%) or matrix; Semi-massive (70-90%) with variable abundance of silicate inclusions, Massive (>90%) with variable but typically low content of magnetite
3 Simplified texture classification according to classification from Barnes et al (2017) and Barnes et al (2018) based on modal percent of sulfides in the sample. Disseminated (0-5%); Net textured/globular (5-70%); Massive (>70%)
4 Normalised to 100% opaques
5 Not present in region analysis.
np: not present
n: number of analyses
Mineral abbreviations from Whitney & Evans (2010). Ccp: chalcopyrite; Cbn: cubanite; Po: pyrrhotite; Py: pyrite; Pn: pentlandite; Sp: sphalerite; Gn: galena; Mag: magnetite; Chr; chromite; : PGM: Platinum Group Minerals

Annexe A2 Electron microprobe results for pyrrhotite, pentlandite, cubanite and chalcopyrite.

Sulfide		S (wt%)	Cu (wt%)	Fe (wt%)	Co (wt%)	Ni (wt%)	Total (wt%)	S (at%)	Cu (at%)	Fe (at%)	Co (at%)	Ni (at%)
Detection limit		0.031	0.04	0.056	0.029	0.027						
Po	*mean*	39.4	<dl	59.9	<dl	0.371	99.7	53.2	<dl	46.5	<dl	0.273
n=25	*sd*	0.879		1.02		0.3		0.93		1.01		0.223
Pn	*mean*	32.8	<dl	32.7	1.51	32.8	99.8	46.6	<dl	26.7	1.17	25.5
n=30	*sd*	0.146		1.62	1.03	1.47		0.162		1.3	0.777	1.15
Cbn	*mean*	35.6	22.3	41.8	<dl	<dl	99.7	50.3	15.9	33.9	<dl	<dl
n=32	*sd*	0.235	1.74	2.05				0.297	1.34	1.48		
Ccp	*mean*	35.2	34.4	30.3	<dl	<dl	99.8	50.3	24.8	24.8	<dl	<dl
n=39	*sd*	0.195	0.281	0.281				0.165	0.136	0.19		

n: number of grains analyzed, mean: arithmetic mean, sd: 1 standard deviation, <dl: below detection limit, po : pyrrhotite, pn : pentlandite, cbn : cubanite, ccp : chalcopyrite

Annexe A3 Electron Probe Micro Analysis results for chalcopyrite, pentlandite, pyrrhotite and cubanite. <dl: below detection limit

Chalcopyrite	Weight percent (%)						Atomic proportions (at%)						Detection limits (%)				
Grain	S (%)	Cu	Fe	Ni	Co	Total	S	Cu	Fe	Ni	Co	Total	S_DL	Cu_DL	Fe_DL	Ni_DL	Co_DL
E13 02 ccp	35.2	34.5	30.2	0.028	<dl	99.9	50.4	24.9	24.8	<dl	<dl	100.0	0.026	0.039	0.056	0.026	0.028
E13 03 ccp	35.2	34.4	30.2	<dl	<dl	99.8	50.3	24.8	24.8	<dl	<dl	100.0	0.026	0.041	0.054	0.028	0.028
E13 04 ccp	35.3	34.6	30.5	<dl	<dl	100.3	50.2	24.8	24.9	<dl	<dl	99.9	0.026	0.039	0.056	0.028	0.027
E13 06 ccp	35.2	34.9	30.2	<dl	<dl	100.4	50.1	25.1	24.7	<dl	<dl	99.9	0.026	0.040	0.056	0.028	0.027
E-DEEP 03 ccp	35.3	34.4	30.2	<dl	<dl	99.9	50.4	24.8	24.7	<dl	<dl	99.8	0.026	0.040	0.051	0.028	0.028
E-DEEP 04 ccp	35.2	34.6	30.1	0.039	<dl	99.9	50.3	24.9	24.6	0.031	<dl	99.9	0.026	0.040	0.055	0.026	0.028
E-DEEP 05 ccp	35.0	34.3	30.1	<dl	<dl	99.4	50.3	24.9	24.8	<dl	<dl	100.0	0.027	0.039	0.055	0.028	0.028
E-DEEP 08 ccp	35.1	34.5	30.8	<dl	<dl	100.4	50.0	24.7	25.2	<dl	<dl	99.9	0.026	0.039	0.054	0.027	0.027
E-DEEP 09 ccp	35.1	34.7	30.1	<dl	<dl	99.9	50.2	25.1	24.7	<dl	<dl	100.0	0.026	0.039	0.055	0.029	0.028
E-DEEP 10 ccp	35.3	34.6	30.3	<dl	<dl	100.2	50.2	24.9	24.8	<dl	<dl	99.9	0.026	0.039	0.045	0.027	0.028
DC69 02 ccp	35.1	34.4	30.1	<dl	<dl	99.5	50.3	24.9	24.8	<dl	<dl	99.9	0.026	0.039	0.058	0.029	0.028
DC69 03 ccp	35.2	34.5	29.7	<dl	<dl	99.4	50.5	24.9	24.5	<dl	<dl	99.9	0.026	0.039	0.052	0.028	0.027
DC69 04 ccp	35.2	34.5	31.1	<dl	<dl	100.7	49.9	24.7	25.3	<dl	<dl	100.0	0.025	0.040	0.055	0.028	0.028
DC69 05 ccp	35.3	34.3	30.3	<dl	<dl	99.8	50.4	24.7	24.8	<dl	<dl	99.9	0.025	0.040	0.053	0.028	0.028
DC69 08 ccp	35.0	34.5	30.1	<dl	<dl	99.6	50.2	25.0	24.8	<dl	<dl	100.0	0.026	0.040	0.044	0.028	0.028
DC69 09 ccp	35.2	34.5	29.6	<dl	<dl	99.3	50.5	25.0	24.4	<dl	<dl	99.9	0.026	0.039	0.053	0.028	0.028
DC69 10 ccp	35.1	34.3	29.9	<dl	<dl	99.4	50.4	24.9	24.7	<dl	<dl	99.9	0.026	0.040	0.055	0.028	0.027
DC69 11 ccp	35.0	34.1	30.3	<dl	<dl	99.4	50.2	24.7	25.0	<dl	<dl	99.9	0.026	0.040	0.053	0.027	0.028
T1 01 ccp	35.4	34.5	30.2	<dl	<dl	100.1	50.5	24.8	24.7	<dl	<dl	100.0	0.025	0.039	0.046	0.027	0.028
T1 02 ccp	34.0	32.9	29.5	<dl	<dl	96.4	50.3	24.6	25.0	<dl	<dl	99.9	0.025	0.040	0.054	0.027	0.028
T1 03 ccp	35.1	34.7	30.5	<dl	<dl	100.3	50.0	24.9	25.0	<dl	<dl	100.0	0.026	0.040	0.048	0.028	0.028
T1 04 ccp	35.3	34.6	30.3	<dl	<dl	100.2	50.3	24.9	24.8	<dl	<dl	100.0	0.026	0.039	0.051	0.028	0.028
T1 05 ccp	35.2	34.0	30.4	0.388	<dl	100.0	50.2	24.5	24.9	0.303	<dl	99.9	0.026	0.039	0.051	0.028	0.029
T1 06 ccp	35.3	34.5	30.7	<dl	<dl	100.5	50.1	24.7	25.0	<dl	<dl	99.9	0.026	0.040	0.048	0.029	0.027
T1 07 ccp	35.4	34.4	30.1	<dl	<dl	99.9	50.5	24.7	24.7	<dl	<dl	99.9	0.027	0.038	0.056	0.028	0.027
T1 08 ccp	35.2	34.3	30.1	<dl	<dl	99.7	50.4	24.8	24.7	<dl	<dl	99.8	0.026	0.040	0.049	0.030	0.027
T1 09 ccp	35.1	34.0	30.1	<dl	<dl	99.2	50.4	24.7	24.9	<dl	<dl	100.0	0.026	0.039	0.055	0.028	0.028
2523 01 ccp	35.3	34.0	30.6	0.031	<dl	99.2	50.4	24.5	25.0	<dl	<dl	100.0	0.026	0.039	0.049	0.027	0.028
2523 02 ccp	35.3	34.5	30.2	<dl	<dl	99.2	50.4	24.8	24.7	<dl	<dl	100.0	0.026	0.039	0.046	0.027	0.027
2523 03 ccp	35.5	34.4	30.2	0.038	<dl	99.2	50.5	24.7	24.7	0.029	<dl	100.0	0.026	0.039	0.054	0.027	0.028
2523 04 ccp	35.2	34.1	30.5	0.040	<dl	99.2	50.4	24.6	25.0	0.031	<dl	100.0	0.027	0.039	0.056	0.026	0.028
2523 07 ccp	35.3	34.0	30.4	<dl	<dl	99.2	50.4	24.5	25.0	<dl	<dl	100.0	0.026	0.040	0.052	0.028	0.028
2523 09 ccp	35.2	34.4	30.0	<dl	<dl	99.2	50.5	24.8	24.7	<dl	<dl	100.0	0.027	0.040	0.052	0.028	0.027
2523 10 ccp	35.3	34.6	30.7	<dl	<dl	99.2	50.1	24.8	25.0	<dl	<dl	100.0	0.026	0.038	0.048	0.028	0.028
NR6 01 ccp	35.1	34.2	30.7	<dl	<dl	100.0	50.1	24.6	25.1	<dl	<dl	99.9	0.026	0.039	0.050	0.028	0.028
NR6 02 ccp	35.1	34.2	30.7	<dl	<dl	100.0	50.0	24.7	25.2	<dl	<dl	99.9	0.025	0.040	0.048	0.029	0.029
NR6 06 ccp	35.2	34.3	30.2	0.062	<dl	99.8	50.3	24.8	24.8	0.049	<dl	99.9	0.026	0.039	0.049	0.028	0.028
NR6 07 ccp	35.1	34.6	30.4	<dl	<dl	100.2	50.1	24.9	24.9	<dl	<dl	99.9	0.026	0.040	0.052	0.028	0.027
NR6 08 ccp	35.4	34.6	30.2	<dl	<dl	100.2	50.4	24.9	24.7	<dl	<dl	100.0	0.026	0.039	0.056	0.028	0.029

Pentlandite	Weight percent (%)						Atomic proportions (at%)						Detection limits (%)				
Grain	S	Cu	Fe	Ni	Co	Total	S	Cu	Fe	Ni	Co	Total	S_DL	Cu_DL	Fe_DL	Ni_DL	Co_DL
VB7-PN001	33.0	<dl	34.5	30.9	1.46	99.8	46.8	<dl	28.1	23.9	1.13	99.8	0.032	0.041	0.058	0.030	0.029
VB7-PN002	32.7	<dl	35.1	31.3	1.51	100.7	46.2	<dl	28.4	24.1	1.16	100.0	0.031	0.040	0.053	0.030	0.028
VB7-PN003	33.0	<dl	34.1	31.2	1.62	99.9	46.8	<dl	27.8	24.1	1.25	99.9	0.031	0.040	0.062	0.030	0.028
VB7-PN004	32.7	<dl	34.6	30.9	1.72	99.9	46.4	<dl	28.3	23.9	1.33	99.9	0.031	0.041	0.059	0.029	0.028
VB7-PN005	33.1	<dl	34.6	31.2	1.51	100.4	46.7	<dl	28.0	24.0	1.16	99.9	0.031	0.040	0.059	0.031	0.028
MCR4B-PN001	33.1	<dl	32.1	34.3	0.808	100.3	46.7	<dl	26.1	26.5	0.622	99.9	0.030	0.041	0.052	0.030	0.028
MCR4B-PN002	33.0	<dl	32.3	34.6	0.892	100.7	46.4	<dl	26.1	26.6	0.684	99.9	0.031	0.039	0.057	0.030	0.028
MCR4B-PN003	32.9	<dl	32.5	34.3	0.829	100.6	46.5	<dl	26.4	26.5	0.637	99.9	0.031	0.041	0.054	0.030	0.029
MCR4B-PN004	33.1	<dl	32.0	34.2	0.849	100.2	46.9	<dl	26.0	26.4	0.654	100.0	0.031	0.040	0.058	0.031	0.028
CRTN18-PN001	33.0	<dl	31.7	34.5	0.568	99.8	46.8	<dl	25.9	26.8	0.439	99.9	0.031	0.040	0.058	0.029	0.028
CRTN18-PN002	33.1	<dl	32.3	34.5	0.541	100.4	46.7	<dl	26.2	26.6	0.415	99.9	0.031	0.039	0.060	0.030	0.028
CRTN18-PN003	32.9	<dl	32.1	34.7	0.557	100.3	46.6	<dl	26.1	26.8	0.429	99.9	0.031	0.040	0.060	0.030	0.027
CRTN18-PN004	33.0	<dl	32.4	34.4	0.495	100.3	46.7	<dl	26.3	26.6	0.381	100.0	0.032	0.039	0.052	0.030	0.029
CRTN18-PN005	32.9	<dl	32.1	34.2	0.565	99.8	46.8	<dl	26.2	26.5	0.436	99.9	0.032	0.041	0.055	0.030	0.029
E13-PN001	32.2	<dl	35.9	29.4	0.591	98.1	46.5	<dl	29.8	23.2	0.464	100.0	0.032	0.039	0.057	0.030	0.028
E13-PN002	32.4	<dl	35.9	29.7	0.639	98.6	46.5	<dl	29.6	23.3	0.500	99.9	0.032	0.040	0.055	0.031	0.029
E13-PN003	32.5	<dl	35.6	30.5	0.653	99.2	46.5	<dl	29.2	23.8	0.507	99.9	0.032	0.038	0.055	0.030	0.029
DC69-PN001	32.9	<dl	31.4	32.8	3.52	100.7	46.5	<dl	25.5	25.3	2.71	99.9	0.032	0.040	0.054	0.030	0.030
DC69-PN002	33.0	<dl	30.7	33.3	3.60	100.6	46.6	<dl	24.9	25.7	2.77	100.0	0.032	0.040	0.051	0.030	0.030
DC69-PN003	32.9	<dl	31.1	32.9	3.88	100.8	46.4	<dl	25.2	25.4	2.98	100.0	0.032	0.040	0.060	0.030	0.028
DC69-PN004	33.1	<dl	31.2	33.2	3.84	101.4	46.4	<dl	25.1	25.5	2.93	99.9	0.032	0.041	0.051	0.030	0.029
EDEEP-PN001	32.5	<dl	31.7	32.6	2.05	98.9	46.6	<dl	26.1	25.6	1.60	99.9	0.031	0.039	0.050	0.030	0.029
EDEEP-PN002	32.5	<dl	31.9	32.9	2.08	99.4	46.5	<dl	26.2	25.7	1.62	99.9	0.032	0.038	0.056	0.031	0.028
EDEEP-PN003	32.7	<dl	32.0	32.6	2.14	99.5	46.7	<dl	26.2	25.4	1.66	100.0	0.032	0.038	0.059	0.029	0.029
EDEEP-PN004	32.5	0.014	31.8	32.4	2.14	98.8	46.7	0.010	26.2	25.4	1.67	100.0	0.031	0.038	0.055	0.030	0.028
EDEEP-PN005	32.5	<dl	32.1	32.5	2.00	99.0	46.6	<dl	26.4	25.4	1.56	100.0	0.032	0.041	0.053	0.030	0.029
2523-PN001	32.9	dl	31.9	34.1	1.06	100.1	46.7	dl	26.0	26.4	0.817	99.9	0.032	0.041	0.050	0.030	0.029
2523-PN002	32.8	dl	32.3	34.3	1.13	100.5	46.4	dl	26.2	26.5	0.871	100.0	0.033	0.040	0.059	0.030	0.028
2523-PN003	32.9	dl	33.0	34.2	1.08	101.2	46.3	dl	26.6	26.2	0.825	99.9	0.032	0.041	0.057	0.030	0.028
2523-PN004	33.0	dl	32.4	34.3	1.06	100.7	46.5	dl	26.2	26.4	0.810	99.9	0.033	0.041	0.058	0.031	0.029

Pyrrhotite	Weight percent (%)						Atomic proportions (at%)						Detection limits (%)				
Grain	S	Cu	Fe	Ni	Co	Total	S	Cu	Fe	Ni	Co	Total	S_DL	Cu_DL	Fe_DL	Ni_DL	Co_DL
E13 01 po	36.9	<dl	62.5	<dl	<dl	99.4	50.6	<dl	49.3	<dl	<dl	99.9	0.027	0.035	0.060	0.027	0.029
E13 05 po	37.0	<dl	63.1	<dl	<dl	100.0	50.5	<dl	49.5	<dl	<dl	99.9	0.027	0.035	0.054	0.026	0.029
E-DEEP 01 po	39.0	<dl	60.6	0.470	<dl	100.1	52.7	<dl	47.0	0.346	<dl	100.0	0.028	0.036	0.059	0.026	0.028
E-DEEP 02 po	39.0	<dl	60.2	0.463	<dl	99.6	52.8	<dl	46.8	0.342	<dl	99.9	0.028	0.035	0.056	0.026	0.029
E-DEEP 06 po	39.0	<dl	60.6	0.499	<dl	100.0	52.6	<dl	46.9	0.368	<dl	99.8	0.028	0.035	0.051	0.026	0.029
E-DEEP 07 po	38.7	<dl	60.3	0.444	<dl	99.5	52.6	<dl	47.0	0.329	<dl	99.9	0.027	0.034	0.051	0.027	0.031
DC69 01 po	39.2	<dl	60.1	0.515	<dl	99.8	52.9	<dl	46.6	0.380	<dl	99.9	0.028	0.036	0.062	0.027	0.029
DC69 06 po	39.4	<dl	59.8	0.541	<dl	99.7	53.1	<dl	46.4	0.399	<dl	99.9	0.028	0.035	0.052	0.027	0.030
DC69 07 po	39.4	<dl	59.5	0.475	<dl	99.4	53.3	<dl	46.2	0.351	<dl	99.8	0.028	0.035	0.050	0.027	0.029
2523 11 po	39.5	<dl	59.0	0.817	<dl	99.3	53.5	<dl	45.9	0.604	<dl	99.9	0.028	0.036	0.060	0.026	0.029
T1 10 po	39.9	<dl	59.5	0.275	<dl	99.7	53.7	<dl	46.0	0.202	<dl	99.9	0.028	0.035	0.054	0.026	0.028
T1 11 po	40.2	<dl	59.4	0.540	<dl	100.1	53.9	<dl	45.7	0.395	<dl	99.9	0.027	0.035	0.060	0.027	0.029
NR6 03 po	39.8	<dl	59.7	0.915	<dl	100.5	53.3	<dl	45.9	0.669	<dl	99.9	0.028	0.034	0.057	0.026	0.030
NR6 04 po	39.9	<dl	59.1	0.760	0.031	99.8	53.7	<dl	45.6	0.558	<dl	99.8	0.028	0.035	0.050	0.027	0.029
NR6 05 po	40.0	<dl	59.3	0.794	<dl	100.0	53.7	<dl	45.7	0.582	<dl	99.9	0.028	0.034	0.057	0.027	0.029
NR6 09 po	40.0	<dl	59.2	0.789	0.044	100.1	53.7	<dl	45.7	0.578	0.032	100.0	0.028	0.035	0.056	0.026	0.028
2523 05 po	40.1	<dl	59.9	0.295	<dl	100.3	53.7	<dl	46.1	0.216	<dl	100.0	0.028	0.035	0.053	0.025	0.029
2523 06 po	40.1	<dl	58.9	0.335	<dl	99.3	54.1	<dl	45.6	0.247	<dl	99.9	0.029	0.036	0.052	0.026	0.030
2523 08 po	40.0	<dl	59.6	0.303	<dl	99.9	53.7	<dl	46.0	0.223	<dl	99.9	0.028	0.035	0.059	0.027	0.028
2523 11 po	39.5	<dl	59.0	0.817	<dl	99.3	53.5	<dl	45.9	0.604	<dl	99.9	0.028	0.036	0.060	0.026	0.029

Cubanite	Weight percent (%)						Atomic proportions (at%)						Detection limits (%)				
Grain	S	Cu	Fe	Ni	Co	Total	S	Cu	Fe	Ni	Co	Total	S_DL	Cu_DL	Fe_DL	Ni_DL	Co_DL
T4 cb01	35.1	22.6	41.6	<dl	<dl	99.4	49.9	16.2	33.9	<dl	<dl	100	0.036	0.090	0.060	0.025	0.031
T4 cb02	35.7	22.4	43.0	<dl	<dl	101	49.8	15.8	34.4	<dl	<dl	100	0.037	0.090	0.059	0.025	0.033
T4 cb03	35.6	22.2	42.6	<dl	0.036	100.4	50.0	15.7	34.3	<dl	<dl	100	0.037	0.092	0.059	0.024	0.032
T4 cb04	35.8	22.3	42.5	<dl	<dl	100.6	50.1	15.7	34.2	<dl	<dl	100	0.036	0.089	0.059	0.025	0.032
T3 cb01	35.7	21.9	43.1	<dl	0.043	100.7	49.9	15.5	34.6	<dl	0.032	100	0.036	0.087	0.060	0.025	0.030
T3 cb02	35.9	22.4	43.2	<dl	0.030	101.6	49.9	15.7	34.4	<dl	<dl	100	0.036	0.086	0.060	0.025	0.030
T3 cb03	35.8	21.9	42.3	<dl	0.031	99.9	50.3	15.5	34.1	<dl	<dl	100	0.036	0.092	0.058	0.025	0.030
T3 cb04	35.7	22.2	43.3	<dl	<dl	101.1	49.8	15.6	34.6	<dl	<dl	100	0.036	0.089	0.058	0.025	0.031
RX164 cb01	35.6	21.8	41.8	<dl	<dl	99.2	50.4	15.6	34.0	<dl	<dl	100	0.037	0.092	0.056	0.026	0.030
RX164 cb02	35.8	21.8	42.5	<dl	<dl	100.1	50.3	15.5	34.3	<dl	<dl	100	0.037	0.086	0.058	0.025	0.031
RX164 cb03	35.8	22.0	43.1	<dl	<dl	100.8	50.0	15.5	34.5	<dl	<dl	100	0.036	0.087	0.061	0.025	0.031
RX164 cb04	35.8	22.5	42.7	<dl	<dl	100.9	49.9	15.8	34.2	<dl	<dl	100	0.036	0.084	0.060	0.025	0.030
RX164 cb05	35.9	22.0	43.1	<dl	<dl	100.9	50.0	15.5	34.5	<dl	<dl	100	0.036	0.086	0.061	0.025	0.031
VB6 cb01	35.5	21.7	41.6	<dl	<dl	98.8	50.4	15.6	34.0	<dl	<dl	100	0.036	0.085	0.057	0.025	0.031
VB6 cb02	35.7	21.9	41.7	<dl	<dl	99.3	50.5	15.6	33.9	<dl	<dl	100	0.036	0.092	0.058	0.025	0.031
VB6 cb03	35.7	21.7	41.9	<dl	<dl	99.3	50.5	15.5	34.0	<dl	<dl	100	0.036	0.097	0.059	0.025	0.031
VB6 cb04	35.8	21.8	41.8	<dl	<dl	99.4	50.6	15.5	33.9	<dl	<dl	100	0.037	0.093	0.057	0.024	0.031
VB6 cb05	35.7	21.5	41.3	<dl	<dl	98.5	50.8	15.4	33.7	<dl	<dl	100	0.036	0.082	0.061	0.025	0.031
MCR10A cb01	35.4	21.9	42.1	<dl	<dl	99.4	50.1	15.7	34.3	<dl	<dl	100	0.036	0.087	0.057	0.025	0.032
MCR10A cb02	35.4	21.6	41.9	<dl	<dl	98.9	50.3	15.5	34.2	<dl	<dl	100	0.036	0.082	0.057	0.025	0.032
MCR10A cb03	35.5	22.3	41.8	<dl	<dl	99.6	50.2	15.9	33.9	<dl	<dl	100	0.036	0.086	0.056	0.024	0.032
MCR10A cb04	35.3	21.7	41.9	<dl	<dl	98.9	50.3	15.5	34.2	<dl	<dl	100	0.036	0.092	0.054	0.025	0.032
MCR10A cb05	35.1	21.3	41.2	<dl	<dl	97.5	50.5	15.5	34.0	<dl	<dl	100	0.035	0.087	0.056	0.025	0.031
MCR10A cb06	35.3	21.9	40.8	<dl	<dl	98.0	50.6	15.8	33.6	<dl	<dl	100	0.036	0.088	0.055	0.025	0.031
VB31 cb01	35.3	21.6	42.0	<dl	<dl	99.2	50.1	15.5	34.2	<dl	<dl	100	0.035	0.091	0.060	0.025	0.032
VB31 cb02	35.5	22.1	41.7	<dl	0.041	99.3	50.3	15.8	33.9	<dl	0.032	100	0.036	0.095	0.058	0.024	0.032
VB31 cb03	35.6	22.2	41.7	<dl	0.030	99.5	50.3	15.8	33.9	<dl	<dl	100	0.037	0.098	0.054	0.025	0.030
MCR13 cb01	35.8	21.5	42.5	<dl	<dl	99.8	50.4	15.3	34.4	<dl	<dl	100	0.037	0.087	0.053	0.024	0.031
MCR13 cb02	35.1	31.6	31.1	<dl	<dl	97.8	50.9	23.2	25.9	<dl	<dl	100	0.036	0.096	0.055	0.024	0.031
MCR13 cb03	35.7	22.0	41.6	<dl	<dl	99.2	50.5	15.7	33.8	<dl	<dl	100	0.036	0.095	0.065	0.024	0.032
MCR13 cb04	35.9	22.1	41.8	<dl	<dl	99.8	50.5	15.7	33.8	<dl	<dl	100	0.036	0.085	0.056	0.025	0.030
MCR13 cb05	35.8	22.5	42.7	<dl	<dl	101	50.0	15.8	34.2	<dl	<dl	100	0.038	0.079	0.057	0.024	0.032

Annexe A4 Analyses of reference materials used in the calibration of the LA-ICP-MS and in-house reference materials used to monitor the data quality. Concentrations in ppm.

	Element	Ti	Mn	Co	Ni	Cu	Zn	Ga	Ge	As	Se	Mo	Ru	Rh	Ag
	Isotope	49	55	59	60	65	66	71	74	75	82	95	101	103	107
Median of detection limits	55um	0.553	0.479	0.016	0.207	0.270	0.024	0.079	0.348	2.41	0.029	0.020	0.004	0.049	0.011
(ccp)	33um	0.661	1.03	0.028	0.410	0.526	0.051	0.149	0.582	5.31	0.030	0.020	0.007	0.100	0.026
Reference materials used for calibration		GSE-1g	GSE-1g	GSE-1g	GSE-1g	MASS1	MASS1	GSE-1g	GSE-1g	MASS1	MASS1	MASS1	Po-727	Po-727	GSE-1g
	Working value	450	590	380	440	134000	210000	490	320	65	51	59	36.5	41.6	200
	sd	42	20	20	30	500	5000	70	80	3	4	9	0.3	0.3	20
Values obtained for reference materials used as monitors															
UQAC-FeS1	Working value	298	56.3	643	25680	22542	260	*9.26*		1056	346	65.5	68.5	63.7	176
	Uncertainty	18.8	7.50	19.4	1769	902	31.9	1.00		116	42.0	3.70	5.00	3.50	19.6
This study	Average	421	55.9	646	25590	22160	287	9.59		1145	306	65.9	69.8	62.4	168
n = 83	sd	137	5.73	29.2	3378	836	53.8	0.579		146	45.2	3.48	3.37	3.36	16.1
	RSD (%)	32.5	10.3	4.52	13.2	3.77	18.7	6.04		12.7	14.7	5.28	4.83	5.38	9.60
	rel. diff (%)	41.5	-0.689	0.511	-0.350	-1.70	10.5	3.51		8.43	-11.4	0.595	1.88	-2.07	-4.51
PTC-1b	Working value	696	193	3253	112900	79700	2083			222	120	*11.0*		*0.500*	53.1
	Uncertainty	4.10	1.80	38.0	1000	1000	38.0			17.0	11.0	1.00		1.00	1.00
This study	Average	692	177	3140	108275	83545	2647			279	118	9.17		1.03	56.8
n = 48	sd	139	15.5	104	11359	3507	678			97.9	19.1	12.6		0.522	17.7
	RSD (%)	20.0	8.75	3.30	10.5	4.20	25.6			35.1	16.2	137		50.9	31.2
	rel. diff (%)	-0.541	-8.26	-3.49	-4.10	4.82	27.1			25.5	-1.27	-16.6		105	6.95
CCu-1e	Working value	*54.9*	96.0	301	*7.27*	230700	30200	*3.00*	*1.00*	1010	*304*	*16.1*			205
	Uncertainty	1.90	4.00	6.00	0.430	2400	300	nd	nd	30.0	8.00	0.700			3.40
This study	Average	132	85.7	324	172	214069	38649	2.83	3.30	1190	274	12.0			206
n = 53	sd	125	10.0	20.4	392	7092	6004	0.436	0.796	184	33.1	12.0			40.6
	RSD (%)	94.8	11.7	6.31	229	3.31	15.5	15.4	24.1	15.5	12.1	100			19.7
	rel. diff (%)	141	-10.7	7.52	2261	-7.21	28.0	-5.67	230	17.8	-10.0	-25.7			0.304
	Others		MASS1	MASS1	MASS1		GSE-1g					GSE-1g			MASS1
	Working value		280	60.0	97.0		460					390			50.0
	Uncertainty		80.0	10.0	15.0		10.0					30.0			5.00
This study	Average		245	68.8	122		428					382			65.9
n = 49 (MASS1)	sd		13.9	1.54	35.7		70.6					12.5			4.78
n = 39 (GSE-1g)	RSD (%)		5.68	2.24	29.4		16.5					3.28			7.25
	rel. diff (%)		-12.5	14.7	25.4		-6.86					-2.00			31.8

	Element	Pd	Cd	In	Sn	Sb	Te	Re	Os	Ir	Pt	Au	Tl	Pb	Bi
	Isotope	108	111	115	118	121	128	185	189	193	195	197	205	208	209
Median of detection limits	55um	0.061	0.007	0.070	0.017	0.221	0.007	0.016	0.004	0.010	0.006	0.004	0.006	0.004	0.006
(ccp)	33um	0.118	0.012	0.147	0.027	0.501	0.012	0.028	0.007	0.018	0.014	0.007	0.011	0.007	0.004
Reference materials used for calibration		Po-727	MASS1	GSE-1g	MASS1	MASS1	MASS1	GSE-1g	Po-727	Po-727	Po-727	Po-727	GSE-1g	MASS1	GSE-1g
	Working value	43.4	60	370	59	60	15	78.9	46.7	48	35.5	45.8	2	68	320
	sd	0.3	7	60	6	9	-	7.7	2.6	1.2	0.8	2.4	0.2	7.0	30
Values obtained for reference materials used as monitors															
UQAC-FeS1	Working value	52.4		9.50	183	92.6	151	65.2	86.6	62.8	60.1	66.2		91.1	120
	Uncertainty	8.70		1.10	18.3	15.3	24.7	11.6	11.8	10.1	13.6	9.70		7.70	16.6
This study	Average	44.3		10.4	182	80.7	137	54.6	89.7	55.4	45.5	60.9		83.0	123
n = 83	sd	4.00		0.665	10.2	9.40	18.3	3.84	3.72	4.32	6.03	7.18		10.2	10.9
	RSD (%)	9.04		6.40	5.60	11.7	13.4	7.02	4.15	7.80	13.3	11.8		12.3	8.86
	rel. diff (%)	-15.5		9.35	-0.651	-12.9	-9.50	-16.2	3.59	-11.8	-24.4	-8.06		-8.85	3.05
PTC-1b	Working value	9.46	*38.0*		*120*	*6.00*	*30.0*							795	
	Uncertainty	0.200	1.00		1.00	1.00	1.00							1.50	
This study	Average	8.66	72.4		124	6.58	29.7							938	
n = 48	sd	7.60	19.4		14.5	5.05	8.98							123	
	RSD (%)	87.7	26.8		11.7	76.8	30.3							13.1	
	rel. diff (%)	-8.44	90.5		3.19	9.66	-1.05							18.0	
CCu-1e	Working value		74.2	*6.00*	*13.7*	104	61.8					20.3	2.70	7030	*3.00*
	Uncertainty		1.90	nd	nd	3.00	2.60					0.520	0.090	90.0	nd
This study	Average		119	5.65	17.7	108	58.2					9.89	3.07	7201	2.56
n = 53	sd		32.4	0.617	10.6	38.6	22.0					6.02	0.430	833	0.446
	RSD (%)		27.1	10.9	59.9	35.7	37.9					60.9	14.0	11.6	17.4
	rel. diff (%)		61.0	-5.78	29.0	3.89	-5.90					-51.3	13.6	2.43	-14.5
	Others			MASS1								MASS1	MASS1	GSE-1g	MASS1
	Working value			50.0								47.0	50.0	378	60.0
	Uncertainty			nd								nd	1.00	12.0	nd
This study	Average			61.4								48.3	78.4	324	64.8
n = 49 (MASS1)	sd			2.28								3.14	13.5	21.8	2.93
n = 39 (GSE-1g)	RSD (%)			3.72								6.50	17.2	6.74	4.52
	rel. diff (%)			22.9								2.74	56.9	-14.2	7.98

italic: informational/provisional values. Interference of ^{115}Sn on ^{115}In on calibrant (GSE-1g) is negligible (0.27 %) and therefore correction not applied. Interference of $^{40}Ar^{63}Cu$ on ^{103}Rh on calibrant (Po-727) is negligible (4.63%) and therefore correction not applied. Interference of $^{40}Ar^{61}Ni$ on ^{101}Ru on calibrant (Po-727) is negligible (7.84%) and therefore correction not applied. Interference of ^{115}Sn on ^{115}In on UQAC-FeS1 is negligible (6.22%) and therefore correction not applied. Interference of $^{40}Ar^{63}Cu$ on ^{103}Rh on UQAC-FeS1 is negligible (3.55%) and therefore correction not applied.Interference of $^{40}Ar^{61}Ni$ on ^{101}Ru on UQAC-FeS1 is negligible (0.73%) and therefore correction not applied. RSD (%) : relative standard deviation. sd: standard deviation. rel. diff (%): relative difference. n: number of analyses

Annexe A5 Full LA-ICP-MS results for trace elements (in ppm) of chalcopyrite, pentlandite, pyrrhotite and cubanite. In red: values below detection limit, calculated with IrEM imputation algorithm considering detection limit in each analysis.

Grain ID (chalcopyrite)	Ti 49	Mn 55	Co 59	Ni 60	Zn 66	Ga 71	Ge 74	As 75	Se 82	Mo 95	Ru 101	Rh 103	Ag 107	Pd 108	Cd 111	In 115	Sn 118	Sb 121	Te 128	Re 185	Os 189	Ir 193	Pt 195	Au 197	Tl 205	Pb 208	Bi 209
55um	0.553	0.479	0.016	0.207	0.270	0.024	0.079	0.348	2.409	0.029	0.020	0.004	0.049	0.011	0.061	0.007	0.070	0.017	0.221	0.007	0.016	0.004	0.010	0.006	0.004	0.006	0.004
33um	0.661	1.030	0.028	0.410	0.526	0.051	0.149	0.582	5.311	0.030	0.020	0.007	0.100	0.026	0.118	0.012	0.147	0.027	0.501	0.012	0.028	0.007	0.018	0.014	0.007	0.011	0.007
06-MPB-R15-1d	4.30	0.159	0.145	0.014	15.5	0.160	0.950	0.245	211	0.018	0.012	n.r.	1.96	0.007	0.210	9.11	39.1	0.093	0.310	0.003	0.007	0.002	0.005	0.103	0.049	5.18	4.18
06-MPB-R15-2.d	2.90	0.113	0.086	0.017	30.1	0.124	0.950	0.228	218	0.032	0.012	n.r.	1.25	0.009	0.180	9.15	35.5	0.021	0.540	0.003	0.007	0.002	0.006	0.106	0.006	1.24	1.68
06-MPB-R15-3.d	2.10	0.121	0.029	0.017	14.3	0.097	1.55	0.182	215	0.018	0.012	n.r.	0.980	0.007	0.026	9.33	13.7	0.019	0.330	0.003	0.007	0.002	0.005	0.124	0.015	2.20	3.00
06-MPB-R15-4.d	2.70	0.126	0.029	0.360	18.0	0.045	1.24	0.255	218	0.018	0.012	n.r.	1.12	0.048	0.034	9.13	19.7	0.030	0.350	0.003	0.007	0.002	0.011	0.075	0.012	1.43	2.69
06-MPB-R15-5.d	0.366	0.169	0.009	0.570	24.0	0.200	0.740	0.228	200	0.018	0.012	n.r.	1.20	0.009	0.047	9.27	46.0	0.004	0.630	0.003	0.007	0.002	0.005	0.094	0.026	1.80	2.20
06-MPB-R15-6.d	2.89	0.153	0.005	0.021	27.0	0.008	1.10	0.278	188	0.018	0.012	n.r.	1.14	0.009	0.048	8.56	28.6	0.039	0.063	0.003	0.007	0.002	0.005	0.190	3.E-04	1.48	2.06
06-MPB-R15-7.d	3.00	0.148	0.080	0.029	26.8	0.023	1.24	0.237	208	0.018	0.012	n.r.	0.920	0.045	0.063	9.70	26.6	0.045	0.076	0.003	0.007	0.002	0.005	0.086	0.008	1.38	1.50
06-MPB-R15-8.d	2.55	0.094	0.055	0.014	25.7	0.058	1.21	0.220	210	0.018	0.020	n.r.	1.50	0.142	0.117	9.47	24.9	0.059	0.970	0.003	0.007	0.002	0.004	0.127	0.007	2.07	1.97
06-MPB-R15-9.d	3.80	0.112	0.049	0.180	31.7	0.118	1.18	0.201	212	0.018	0.012	n.r.	0.630	0.009	0.130	9.23	18.6	0.023	0.310	0.003	0.007	0.002	0.005	0.067	0.009	1.76	1.97
06-MPB-R16-11d	3.70	0.257	2.21	0.053	165	0.010	0.730	0.284	176	0.021	0.018	n.r.	1.07	0.007	15.8	9.45	97.9	0.004	0.570	0.003	0.007	0.002	0.004	0.857	7.E-04	6.31	3.66
06-MPB-R16-12.d	3.30	0.252	2.59	0.075	283	0.130	0.930	0.216	148	0.021	0.033	n.r.	0.460	0.007	32.0	9.94	115	0.005	1.03	0.003	0.007	0.002	0.007	0.078	0.036	4.00	1.59
06-MPB-R16-2.d	3.80	0.232	3.95	0.440	169	0.100	0.710	0.237	181	0.024	0.018	n.r.	0.680	0.007	17.5	8.92	133	0.040	0.580	0.003	0.007	0.002	0.006	0.282	0.005	4.74	2.87
06-MPB-R16-3.d	3.60	0.217	2.19	0.079	170	0.045	0.760	0.291	151	0.021	0.018	n.r.	0.800	0.015	9.80	9.07	123	0.008	0.810	0.003	0.007	0.002	0.007	0.550	4.E-04	3.39	1.69
06-MPB-R16-4.d	4.00	0.210	1.97	0.068	185	0.060	0.760	0.252	156	0.020	0.030	n.r.	0.950	0.007	10.5	8.79	137	0.041	0.640	0.003	0.007	0.002	0.004	0.345	0.012	4.90	2.18
06-MPB-R16-6.d	3.40	0.196	1.42	0.061	151	0.067	1.07	0.237	165	0.021	0.030	n.r.	1.00	0.007	6.61	9.32	110	0.031	0.630	0.003	0.007	0.002	0.005	0.462	0.007	5.48	2.29
06-MPB-R16-9.d	3.00	0.186	3.24	0.057	274	0.040	0.990	0.198	173	0.021	0.018	n.r.	1.85	0.007	18.7	9.85	169	0.004	1.30	0.003	0.007	0.002	0.004	1.52	0.003	5.50	1.56
1533-1d	3.20	12.1	0.136	33.0	337	0.080	1.09	0.133	188	0.018	0.012	n.r.	5.49	0.007	39.3	13.2	77.2	0.038	5.09	0.003	0.007	0.002	0.004	9.E-04	0.210	96.4	1.06
1533-11d	5.20	3.52	0.129	47.0	393	0.157	0.800	0.287	181	0.018	0.021	n.r.	6.10	0.007	36.3	10.2	59.3	0.071	4.79	0.003	0.007	0.002	0.005	1.E-03	0.227	16.0	1.55
1533-13.d	4.80	1.25	0.230	39.9	307	0.175	0.890	0.470	191	0.018	0.012	n.r.	6.70	0.007	32.4	8.59	43.0	0.101	2.31	0.003	0.007	0.002	0.005	8.E-04	0.049	7.00	0.980
1533-14.d	7.80	11.9	0.065	31.9	344	0.190	0.880	0.340	194	0.018	0.018	n.r.	6.29	0.009	41.6	8.74	41.6	0.088	3.52	0.003	0.007	0.002	0.044	9.E-04	0.140	118	0.920
1533-16.d	3.70	7.20	0.074	26.9	351	0.202	1.24	0.294	208	0.014	0.027	n.r.	6.14	0.007	33.8	8.19	42.2	0.071	4.66	0.005	0.011	0.003	0.008	0.001	0.168	115	0.920
1533-3.d	4.30	0.950	0.105	46.9	378	0.008	0.950	0.290	174	0.018	0.037	n.r.	1.52	0.009	29.7	12.6	63.4	0.063	1.05	0.003	0.007	0.002	0.005	1.E-03	0.104	16.7	0.836
1533-6.d	4.10	6.50	0.169	47.7	364	0.085	1.12	0.166	170	0.018	0.012	n.r.	1.97	0.009	35.0	12.9	66.2	0.006	1.38	0.003	0.007	0.002	0.090	8.E-04	0.053	5.10	0.555
1533-8.d	4.80	11.6	0.215	37.2	339	0.260	0.650	0.261	160	0.018	0.012	n.r.	6.58	0.009	38.5	9.84	45.7	0.098	2.72	0.003	0.007	0.002	0.005	9.E-04	0.233	68.7	0.930
2523-10.d	3.90	0.520	0.161	48.3	410	0.158	0.340	0.218	59.8	0.021	0.034	n.r.	1.02	0.007	10.4	3.95	10.5	0.116	1.07	0.003	0.007	0.002	0.004	0.018	3.E-04	4.53	1.54
2523-2.d	5.80	0.680	0.155	45.8	380	0.153	0.430	0.250	58.0	0.050	0.018	n.r.	1.28	0.007	9.90	2.91	7.80	0.097	1.94	0.002	0.007	0.002	0.004	0.016	2.E-04	3.87	1.89
2523-3.d	5.30	0.780	0.361	47.8	436	0.190	0.370	0.246	69.7	0.021	0.018	n.r.	1.82	0.007	10.5	2.79	6.98	0.057	1.82	0.003	0.007	0.002	0.004	0.001	3.E-04	5.05	1.92
2523-4.d	4.90	0.650	0.279	47.1	437	0.154	0.371	0.248	68.8	0.021	0.018	n.r.	1.86	0.007	11.4	3.14	7.30	0.048	2.07	0.002	0.007	0.002	0.004	0.034	2.E-04	3.58	2.03
2523-7.d	5.40	0.480	0.580	62.0	382	0.127	0.310	0.470	67.3	0.021	0.018	n.r.	1.74	0.007	11.8	2.42	5.46	0.004	1.94	0.003	0.007	0.002	0.004	7.E-04	3.E-04	4.08	1.58
2523-9.d	5.00	0.186	0.193	48.6	510	0.213	0.280	0.229	67.6	0.021	0.018	n.r.	1.01	0.007	12.4	4.37	12.5	0.126	0.810	0.003	0.007	0.002	0.004	0.058	3.E-04	7.30	2.70
2938CCP-01d	226	2.46	0.120	14.9	622	0.540	0.750	0.114	114	0.645	0.022	n.r.	1.96	0.004	23.5	1.43	2.79	0.008	0.042	0.003	0.007	0.370	0.044	0.033	6.E-04	93.9	0.022
2938CCP-03.d	216	1.00	0.190	14.9	492	0.372	0.800	0.325	123	2.90	0.008	n.r.	2.61	0.004	21.6	1.99	2.63	0.008	0.124	0.003	0.067	0.002	0.014	6.E-04	1.80	4.48	0.019
2938CCP-04.d	211	1.80	0.360	13.3	715	0.690	1.01	0.325	127	0.200	0.500	n.r.	4.64	0.004	25.6	1.47	5.05	0.049	0.057	0.005	0.008	0.002	0.005	7.E-04	0.002	196	0.018
2938CCP-05.d	223	1.86	0.800	18.1	555	0.630	0.940	0.312	126	0.090	0.038	n.r.	4.97	0.004	24.4	1.52	4.67	0.063	0.049	0.007	0.008	0.002	0.039	0.013	0.070	125	0.005
2938CCP-06.d	218	1.43	0.210	10.5	731	0.370	0.780	0.142	129	0.009	0.025	n.r.	6.18	0.004	23.7	4.18	3.53	0.010	0.038	0.003	0.008	0.002	0.011	0.026	0.002	162	0.012
2938CCP-07.d	218	1.86	0.055	14.1	513	0.232	0.820	0.141	130	0.055	0.045	n.r.	8.16	0.004	18.7	1.39	2.93	0.013	0.053	0.003	0.062	0.012	0.015	0.007	0.001	43.0	0.080
2938CCPr-01d	212	0.630	0.039	22.7	356	0.740	1.11	0.184	106	0.106	0.071	n.r.	2.00	0.007	22.1	1.20	2.92	0.015	0.071	0.007	0.033	0.004	0.018	0.011	0.003	165	0.070
2938CCPr-02.d	238	0.570	0.071	16.7	470	0.400	1.55	0.640	149	0.036	0.075	n.r.	3.53	0.007	27.0	2.19	5.26	0.010	0.057	0.007	0.018	0.004	0.017	9.E-04	0.002	34.4	0.020
2938CCPr-03.d	224	1.66	0.066	12.1	449	0.410	1.80	0.148	133	0.032	0.068	n.r.	1.98	0.007	21.2	2.75	3.17	0.008	0.052	0.007	0.018	0.004	0.016	0.011	9.E-04	3.47	0.006

Grain ID (chalcopyrite)	Ti 49	Mn 55	Co 59	Ni 60	Zn 66	Ga 71	Ge 74	As 75	Se 82	Mo 95	Ru 101	Rh 103	Ag 107	Pd 108	Cd 111	In 115	Sn 118	Sb 121	Te 128	Re 185	Os 189	Ir 193	Pt 195	Au 197	Tl 205	Pb 208	Bi 209
55um	0.553	0.479	0.016	0.207	0.270	0.024	0.079	0.348	2.409	0.029	0.020	0.004	0.049	0.011	0.061	0.007	0.070	0.017	0.221	0.007	0.016	0.004	0.010	0.006	0.004	0.006	0.004
33um	0.661	1.030	0.028	0.410	0.526	0.051	0.149	0.582	5.311	0.030	0.020	0.007	0.100	0.026	0.118	0.012	0.147	0.027	0.501	0.012	0.028	0.007	0.018	0.014	0.007	0.011	0.007
2938CCPr-04.d	245	0.302	0.035	14.1	325	0.590	1.81	0.231	157	0.073	0.091	n.r.	4.43	0.022	23.8	1.73	5.81	0.022	0.081	0.007	0.042	0.004	0.007	0.001	0.001	244	0.022
2938CCPr-05.d	242	0.487	0.054	13.3	515	0.510	1.65	0.240	143	0.106	0.145	n.r.	5.12	0.007	25.2	1.76	4.00	0.009	0.065	0.007	0.028	0.004	0.007	0.001	0.002	77.1	0.019
2938CCPr-06.d	249	1.75	0.007	14.8	543	0.460	2.02	0.168	160	0.106	0.092	n.r.	5.32	0.032	26.4	1.25	4.21	0.012	0.081	0.007	0.018	0.007	0.018	0.001	0.001	126	0.019
a2-1d	7.90	0.156	0.054	36.9	79.7	0.028	1.14	0.314	240	0.047	0.024	n.r.	9.35	2.68	6.37	0.550	0.050	0.019	76.8	0.004	0.011	0.003	0.217	5.E-04	1.97	0.048	0.011
a2-10.d	4.50	0.129	0.046	41.4	105	0.003	1.21	0.251	227	0.084	0.013	n.r.	8.17	1.84	7.38	0.720	0.026	0.031	77.0	0.004	0.005	0.003	0.044	0.006	1.40	0.073	0.005
a2-2.d	4.80	0.143	0.036	36.7	89.0	0.034	0.930	0.540	228	0.170	0.045	n.r.	9.77	4.05	7.90	0.406	0.036	0.034	77.0	0.004	0.006	0.003	0.218	4.E-04	1.73	0.048	0.015
a2-4.d	6.40	0.168	0.031	37.1	75.5	0.010	1.24	0.368	230	0.019	0.030	n.r.	9.59	1.20	6.80	0.367	0.040	0.076	61.5	0.004	0.007	0.003	0.063	7.E-04	1.99	0.042	0.013
a2-5.d	4.40	0.153	0.043	36.5	72.4	0.033	1.08	0.315	208	0.072	0.013	n.r.	9.21	2.17	6.88	0.299	0.039	0.003	75.3	0.004	0.011	0.003	0.071	8.E-04	1.77	0.032	0.032
a2-7.d	4.40	0.179	0.045	46.5	76.5	0.029	1.15	0.364	236	0.081	0.013	n.r.	9.67	3.19	6.78	1.49	0.048	0.050	78.7	0.006	0.011	0.003	0.019	7.E-04	1.48	0.063	0.008
a2-9.d	5.00	0.144	0.018	45.4	83.6	0.038	0.990	0.325	232	0.087	0.028	n.r.	8.78	4.46	7.80	2.63	0.035	0.084	75.0	0.004	0.011	0.003	0.035	4.E-04	1.46	0.092	0.005
B1-384-05-2.d	3.80	0.146	0.033	83.3	37.1	0.370	0.560	2.80	102	0.020	0.013	n.r.	1.23	0.017	0.500	1.60	7.63	0.003	1.29	0.008	0.020	0.005	0.004	3.E-04	3.E-04	3.17	0.048
B1-384-05-5.d	4.70	0.182	0.028	92.6	34.9	0.318	0.630	0.270	110	0.020	0.013	n.r.	6.70	0.017	0.610	1.22	10.8	0.006	1.34	0.004	0.020	0.005	0.011	7.E-04	0.001	5.12	0.025
B1-384-05-6.d	4.20	0.116	0.004	66.8	42.4	0.315	0.750	0.338	163	0.020	0.013	n.r.	0.880	0.017	2.29	1.09	19.0	0.011	1.47	0.008	0.007	0.005	0.011	7.E-04	8.E-04	5.11	0.048
B1-384-05-7.d	4.00	0.195	0.007	71.5	39.5	0.340	1.05	0.231	158	0.020	0.032	n.r.	0.870	0.017	0.910	1.16	9.90	0.005	1.63	0.008	0.020	0.005	0.004	6.E-04	0.001	12.7	0.031
B1-384-39-3.d	5.30	1.26	0.795	10.9	191	0.270	0.201	0.371	53.6	0.020	0.013	n.r.	3.12	0.017	18.4	0.538	0.265	0.002	2.93	0.005	0.009	0.005	0.006	6.E-04	0.034	1.30	0.179
B1-384-39-4.d	3.60	1.60	0.520	11.4	385	0.134	0.300	0.244	50.0	0.024	0.018	n.r.	3.47	0.007	24.1	0.636	0.830	0.026	4.29	0.003	0.007	0.002	0.007	5.E-04	0.006	1.33	0.115
B1-384-39-5.d	4.60	0.690	0.630	7.80	323	0.290	0.273	0.450	53.6	0.024	0.018	n.r.	2.34	0.007	21.7	0.701	0.382	0.003	2.72	0.003	0.007	0.002	0.006	5.E-04	0.004	1.38	0.180
B1-384-39-6.d	4.60	0.850	0.410	7.25	232	0.169	0.260	0.271	58.6	0.024	0.018	n.r.	2.55	0.007	23.0	0.527	0.670	0.024	3.90	0.003	0.007	0.002	0.004	6.E-04	4.E-04	2.82	0.202
B1-384-39-7.d	5.60	1.21	0.740	5.24	244	0.170	0.360	0.308	57.3	0.024	0.018	n.r.	1.14	0.007	21.5	0.665	0.600	0.002	3.87	0.004	0.015	0.002	0.004	8.E-04	0.013	0.870	0.104
B1-384-39-9.d	5.10	1.15	0.920	7.30	228	0.117	0.260	0.229	48.4	0.024	0.018	n.r.	1.71	0.007	22.4	0.482	0.533	0.002	3.67	0.003	0.007	0.002	0.004	5.E-04	0.013	1.19	0.143
C-04-23-1d	5.50	0.162	5.20	12.8	329	0.228	0.120	11.7	32.7	10.3	0.095	n.r.	9.29	0.006	6.86	21.9	28.1	0.029	1.13	0.224	0.020	0.022	0.071	0.021	7.E-04	2.27	0.187
C-04-23-2.d	2.80	0.225	5.20	24.7	314	0.320	0.330	9.60	31.7	9.90	0.110	n.r.	9.66	0.017	12.7	18.9	29.0	0.049	0.900	0.214	0.037	0.049	0.051	0.035	0.008	1.42	0.177
C-04-23-3.d	5.60	17.0	2.90	15.1	271	0.570	0.260	7.80	39.8	10.1	0.061	n.r.	11.2	0.017	4.68	21.2	29.1	0.083	0.079	0.203	0.020	0.033	0.102	0.064	0.020	4.55	0.187
C-04-23-4.d	4.30	0.191	7.10	22.3	308	0.176	0.162	18.3	34.5	10.1	0.112	n.r.	13.6	0.017	9.55	19.6	26.7	0.122	0.330	0.181	0.020	0.016	0.660	0.014	0.016	7.44	0.261
C-04-23-5.d	3.70	0.193	4.60	31.0	273	0.162	0.157	10.8	34.1	9.60	0.075	n.r.	11.5	0.017	9.76	19.8	27.3	0.066	0.440	0.215	0.020	0.017	0.124	0.001	0.017	3.19	0.185
C-04-23-6.d	3.90	0.242	4.80	17.4	308	0.300	0.160	10.4	30.4	9.60	0.068	n.r.	20.8	0.017	9.30	29.1	31.3	0.093	0.660	0.151	0.020	0.026	0.880	0.027	8.E-04	1.64	0.110
C-04-23-7.d	6.00	6.60	5.00	11.8	312	0.258	0.310	7.10	34.8	10.4	0.042	n.r.	11.1	0.010	7.40	21.9	24.8	0.037	0.820	0.093	0.019	0.019	0.033	0.042	0.016	2.08	0.143
C-04-23-8.d	4.70	0.214	16.9	16.9	276	0.137	0.270	32.0	34.6	15.2	0.099	n.r.	8.31	0.017	3.83	22.2	26.7	0.109	0.750	0.171	0.047	0.020	1.11	0.101	0.032	3.90	0.275
C-04-24-1d	4.60	2.00	1.51	80.0	242	0.027	0.250	5.30	33.0	3.70	0.029	n.r.	11.3	0.017	3.89	4.33	11.2	0.114	0.400	0.044	0.018	0.049	0.023	0.016	0.015	12.4	0.230
C-04-24-2.d	4.40	0.336	0.160	10.8	228	0.026	0.100	0.590	38.0	2.10	0.050	n.r.	9.27	0.017	3.40	3.88	12.0	0.008	0.089	0.071	0.018	0.005	0.014	0.046	0.001	6.40	0.089
C-04-24-3.d	3.80	0.502	0.460	8.50	238	0.031	0.330	2.70	29.0	1.09	0.350	n.r.	11.0	0.017	2.40	4.65	11.2	0.038	0.169	0.023	0.022	0.027	0.016	0.002	1.E-03	8.49	0.113
C-04-24-4.d	7.20	3.90	0.870	38.0	250	0.030	0.240	2.80	45.0	1.40	0.100	n.r.	8.85	0.017	3.33	4.15	11.0	0.081	0.600	0.050	0.018	0.020	0.012	0.033	0.002	17.7	0.085
C-04-24-5.d	3.10	5.00	0.500	12.3	178	0.015	0.170	0.529	30.0	21.3	0.011	n.r.	15.4	0.017	2.15	4.61	9.90	0.117	0.141	0.124	0.018	0.005	0.110	0.003	0.195	22.8	0.270
C-04-24-6.d	2.20	2.30	0.890	51.0	226	0.024	0.170	0.470	28.0	2.00	0.011	n.r.	9.29	0.017	7.50	3.51	12.7	0.082	0.310	0.021	0.018	0.008	0.012	0.042	0.001	8.80	0.143
C-04-24-7.d	6.60	0.442	1.39	11.9	250	0.035	0.620	2.10	39.8	3.40	0.050	n.r.	9.27	0.017	7.70	4.09	10.5	0.010	0.169	0.059	0.034	0.019	0.032	0.058	8.E-04	5.39	0.096
C-04-25-1d	5.30	0.370	0.900	20.0	247	0.012	0.086	2.90	46.0	1.50	0.070	n.r.	8.25	0.007	1.89	6.84	19.7	0.111	0.660	0.200	0.014	0.019	0.019	0.020	0.068	3.40	0.119
C-04-25-2.d	2.00	1.60	0.440	13.8	275	0.013	0.230	3.00	20.8	0.510	0.018	n.r.	7.16	0.007	2.46	12.3	27.4	0.380	0.125	0.097	0.023	0.029	2.30	0.079	8.E-04	3.70	0.133

Grain ID (chalcopyrite)	Ti 49	Mn 55	Co 59	Ni 60	Zn 66	Ga 71	Ge 74	As 75	Se 82	Mo 95	Ru 101	Rh 103	Ag 107	Pd 108	Cd 111	In 115	Sn 118	Sb 121	Te 128	Re 185	Os 189	Ir 193	Pt 195	Au 197	Tl 205	Pb 208	Bi 209
55um	0.553	0.479	0.016	0.207	0.270	0.024	0.079	0.348	2.409	0.029	0.020	0.004	0.049	0.011	0.061	0.007	0.070	0.017	0.221	0.007	0.016	0.004	0.010	0.006	0.004	0.006	0.004
33um	0.661	1.030	0.028	0.410	0.526	0.051	0.149	0.582	5.311	0.030	0.020	0.007	0.100	0.026	0.118	0.012	0.147	0.027	0.501	0.012	0.028	0.007	0.018	0.014	0.007	0.011	0.007
C-04-25-3.d	3.10	0.404	0.690	25.4	254	0.014	0.220	2.50	42.3	2.30	0.018	n.r.	6.89	0.007	3.26	7.29	27.9	0.044	0.135	0.107	0.007	0.008	0.034	0.025	0.009	2.12	0.071
C-04-25-4.d	5.50	5.40	0.280	33.8	226	0.070	0.102	0.613	42.1	7.30	0.600	n.r.	8.73	0.007	1.78	6.98	25.0	0.250	0.770	0.230	0.007	0.033	0.090	0.027	0.031	28.1	0.470
C-04-25-5.d	1.70	22.0	0.240	19.9	205	0.075	0.158	0.619	36.5	0.024	0.018	n.r.	13.9	0.007	1.46	16.0	17.9	0.360	0.820	0.003	0.007	0.002	0.007	0.003	0.159	27.1	0.621
C-04-25-6.d	4.00	0.333	5.10	17.6	255	0.013	0.220	9.60	28.0	1.60	0.450	n.r.	11.3	0.007	2.38	10.5	24.6	0.046	0.104	0.029	0.029	0.052	0.160	8.E-04	5.E-04	1.33	0.107
C-04-25-7.d	2.80	0.540	0.390	12.7	291	0.145	0.220	0.430	43.7	1.70	0.048	n.r.	10.7	0.007	4.65	12.4	28.7	0.046	0.250	0.070	0.007	0.009	0.004	0.013	5.E-04	3.56	0.112
C-04-25-8.d	3.20	45.0	0.670	19.2	269	0.190	0.148	4.10	35.0	4.80	0.089	n.r.	10.4	0.007	2.07	15.5	31.6	0.097	0.153	0.060	0.044	0.025	0.016	0.020	0.001	5.60	0.093
C-04-25-9.d	6.10	0.392	1.28	22.2	280	0.210	0.210	5.80	34.2	4.00	0.070	n.r.	6.07	0.007	4.35	15.5	37.8	0.063	0.126	0.220	0.083	0.053	0.080	0.030	5.E-04	1.97	0.101
C-04-38-1d	25.7	104	1.52	37.0	190	1.06	0.390	0.620	51.6	0.024	0.018	n.r.	24.1	0.007	8.00	0.569	0.160	0.255	0.560	0.003	0.007	0.002	0.004	0.001	0.062	15.3	0.368
C-04-38-2.d	7.80	3.10	0.520	12.5	270	0.010	0.220	0.486	48.3	0.070	0.018	n.r.	7.26	0.007	15.7	1.47	0.074	0.246	1.06	0.007	0.007	0.002	0.008	0.011	0.105	25.6	0.369
C-04-38-3.d	4.80	8.40	1.20	37.0	212	0.054	0.410	0.501	48.2	0.018	0.067	n.r.	45.5	0.017	7.20	0.640	0.068	0.107	0.122	0.008	0.018	0.005	0.015	0.002	0.023	6.80	0.110
C-04-43-1d	4.40	0.383	0.380	12.4	240	0.012	0.240	1.25	55.0	4.80	0.480	n.r.	6.83	0.007	1.80	6.19	1.00	0.010	0.099	0.280	0.102	0.068	0.440	0.017	0.014	3.25	0.136
C-04-43-2.d	4.90	0.259	0.134	11.1	322	0.013	0.210	0.443	56.3	0.024	0.066	n.r.	8.99	0.007	3.06	2.77	1.85	0.055	0.076	0.005	0.007	0.002	0.012	0.078	5.E-04	4.15	0.110
C-04-43-3.d	6.20	0.272	0.093	11.7	322	0.012	0.240	0.514	46.8	0.024	0.018	n.r.	12.4	0.007	3.07	2.08	1.93	0.004	0.057	0.006	0.007	0.002	0.011	6.E-04	6.E-04	1.70	0.023
C-04-43-4.d	4.80	2.00	0.610	14.4	248	0.016	0.300	3.80	49.4	0.740	1.11	n.r.	13.1	0.007	1.81	1.86	1.53	0.059	0.104	0.312	0.112	0.104	0.370	8.E-04	0.073	7.81	0.304
C-04-43-5.d	5.20	1.74	0.330	18.1	334	0.011	0.230	0.750	50.8	1.08	0.200	n.r.	10.5	0.007	7.70	1.48	2.36	0.042	0.900	0.390	0.095	0.136	0.350	7.E-04	4.E-04	0.900	0.063
C-04-43-6.d	6.30	0.267	0.170	12.2	338	0.016	0.140	0.780	44.0	0.024	0.018	n.r.	9.42	0.017	3.33	1.77	2.18	0.062	0.950	0.003	0.007	0.003	0.004	0.006	4.E-04	1.68	0.071
C-04-43-7.d	6.00	8.10	0.110	12.3	259	0.014	0.210	0.443	50.7	0.024	0.018	n.r.	10.8	0.007	1.77	1.24	1.67	0.048	0.100	0.003	0.007	0.002	0.004	0.011	0.024	5.41	0.127
C-04-43-8.d	3.20	0.970	0.010	12.1	252	0.058	0.260	0.424	51.2	0.024	0.038	n.r.	12.4	0.007	1.23	1.69	1.93	0.054	0.740	0.003	0.007	0.002	0.010	7.E-04	0.021	4.36	0.077
CGMACCPr-01d	240	1.80	0.047	14.5	373	0.096	1.46	0.129	112	0.040	0.149	n.r.	2.73	0.007	5.05	1.55	0.028	0.008	0.045	0.010	0.018	0.008	0.028	8.E-04	9.E-04	8.32	0.020
CGMACCPr-02.d	250	0.269	0.068	19.7	235	0.028	1.65	0.330	139	0.073	0.210	n.r.	2.61	0.007	5.70	1.12	0.210	0.011	0.078	0.007	0.038	0.060	0.079	0.002	0.002	9.46	0.009
CGMACCPr-03.d	259	10.8	0.190	37.6	203	0.160	1.94	0.205	112	0.047	0.110	n.r.	2.20	0.007	10.3	4.76	0.046	0.012	0.070	0.007	0.018	0.009	0.039	0.002	0.048	7.89	0.046
CGMBCCP-01d	42.1	1.67	0.060	15.3	284	0.026	0.570	0.101	90.1	0.019	0.041	n.r.	1.54	0.007	7.37	1.54	0.028	0.004	0.048	0.008	0.018	0.005	0.011	8.E-04	0.001	5.28	0.005
CGMBCCP-03.d	40.8	1.05	0.056	15.2	236	0.012	0.800	0.104	95.3	0.024	0.041	n.r.	1.80	0.009	6.20	1.87	0.037	0.005	0.057	0.010	0.018	0.009	0.007	0.011	8.E-04	2.66	0.004
CGMBCCP-05.d	47.9	1.74	0.046	16.7	246	0.051	0.670	0.102	103	0.106	0.041	n.r.	1.43	0.007	6.93	1.57	0.065	0.004	0.037	0.007	0.023	0.004	0.007	4.E-04	0.019	4.30	0.008
CRTN12CCP-01d	360	1.80	0.530	61.5	619	0.114	0.570	0.079	82.3	0.062	0.006	n.r.	9.24	0.005	12.5	0.913	6.13	0.005	0.900	0.149	0.008	0.020	0.006	0.002	3.E-04	1.05	2.39
CRTN12CCP-02.d	366	2.40	0.422	52.1	678	0.173	0.580	0.126	73.5	0.047	0.036	n.r.	9.01	0.007	13.0	1.07	6.44	0.016	0.620	0.009	0.008	0.021	0.170	0.008	5.E-04	2.56	3.03
CRTN12CCP-03.d	358	1.67	0.305	44.1	494	0.185	0.290	0.325	72.4	0.070	0.006	n.r.	8.92	0.005	9.40	1.09	5.05	0.037	0.390	0.337	0.008	0.002	0.128	0.014	5.E-04	3.46	2.33
CRTN12CCP-04.d	353	0.248	0.310	48.0	476	0.032	0.280	0.325	69.2	0.180	0.028	n.r.	8.14	0.005	9.60	0.984	4.74	0.024	0.240	0.370	0.008	0.002	0.141	0.008	4.E-04	1.70	1.41
CRTN12CCP-05.d	375	1.49	0.382	49.7	489	0.155	0.420	0.135	66.5	0.031	0.022	n.r.	9.43	0.015	12.9	0.909	6.14	0.045	0.052	0.006	0.019	0.015	0.011	0.003	0.002	3.63	2.48
CRTN13CCP-01d	351	0.890	0.280	49.4	506	0.140	0.640	0.690	70.7	0.065	0.230	n.r.	5.85	0.016	12.1	2.15	12.4	0.167	0.250	0.033	0.270	0.010	0.020	0.012	1.E-03	6.19	3.34
CRTN13CCP-02.d	366	1.27	0.277	55.4	628	0.109	2.10	0.140	67.1	0.038	0.200	n.r.	6.24	0.012	15.1	1.37	6.02	0.050	0.250	0.009	0.034	0.027	0.060	0.019	7.E-04	3.03	3.80
CRTN13CCP-03.d	362	1.33	0.244	50.1	585	0.086	0.740	0.240	72.3	0.083	0.028	n.r.	6.06	0.016	14.9	0.786	5.29	0.111	0.323	0.011	0.034	0.010	0.020	0.160	0.170	3.32	2.57
CRTN13CCP-04.d	355	2.17	0.211	56.5	730	0.076	0.560	0.147	76.4	0.540	0.028	n.r.	5.41	0.200	16.7	0.973	5.46	0.082	0.052	5.00	0.056	0.003	0.037	0.016	0.030	4.99	3.38
CRTN13CCP-05.d	374	1.71	0.223	50.4	573	0.071	0.820	0.230	83.9	0.038	0.028	n.r.	5.58	0.016	14.1	2.17	5.60	0.100	0.054	0.011	0.034	0.060	0.020	0.120	8.E-04	4.60	2.96
CRTN13CCPr-01d	48.9	0.840	0.242	54.8	564	0.109	0.665	0.064	71.1	0.106	0.041	n.r.	6.35	0.007	12.1	0.975	5.89	0.050	0.330	0.007	0.018	0.004	0.012	0.032	6.E-04	3.36	2.97
CRTN13CCPr-02.d	46.5	0.990	0.226	51.0	484	0.085	0.590	0.069	73.0	0.025	0.041	n.r.	5.39	0.005	10.5	0.859	5.17	0.046	0.280	0.008	0.016	0.004	0.009	0.132	5.E-04	3.69	3.26
CRTN13CCPr-03.d	45.9	0.850	0.291	63.5	532	0.081	0.613	0.066	77.7	0.024	0.041	n.r.	3.77	0.005	10.4	1.03	5.12	0.028	0.260	0.008	0.015	0.004	0.009	0.001	4.E-04	2.87	1.63

Grain ID (chalcopyrite)	Ti 49	Mn 55	Co 59	Ni 60	Zn 66	Ga 71	Ge 74	As 75	Se 82	Mo 95	Ru 101	Rh 103	Ag 107	Pd 108	Cd 111	In 115	Sn 118	Sb 121	Te 128	Re 185	Os 189	Ir 193	Pt 195	Au 197	Tl 205	Pb 208	Bi 209
55um	0.553	0.479	0.016	0.207	0.270	0.024	0.079	0.348	2.409	0.029	0.020	0.004	0.049	0.011	0.061	0.007	0.070	0.017	0.221	0.007	0.016	0.004	0.010	0.006	0.004	0.006	0.004
33um	0.661	1.030	0.028	0.410	0.526	0.051	0.149	0.582	5.311	0.030	0.020	0.007	0.100	0.026	0.118	0.012	0.147	0.027	0.501	0.012	0.028	0.007	0.018	0.014	0.007	0.011	0.007
CRTN13CCPr-04.d	49.1	1.15	0.284	63.6	508	0.062	0.570	0.074	71.7	0.011	0.041	n.r.	4.13	0.007	10.3	0.775	4.80	0.084	0.048	0.007	0.018	0.004	0.014	0.113	7.E-04	4.77	2.85
CRTN13CCPr-05.d	46.8	1.11	0.234	58.8	546	0.082	0.622	0.054	78.1	0.106	0.041	n.r.	4.76	0.007	10.8	1.14	5.72	0.045	0.361	0.007	0.012	0.004	0.007	0.045	4.E-04	4.03	2.44
CRTN14-11CCP.d	4.42	0.870	0.613	65.2	465	0.036	0.480	0.181	84.0	0.019	0.013	n.r.	3.06	0.006	9.57	0.776	7.62	0.114	0.250	0.002	0.011	0.003	0.007	0.199	0.002	4.29	2.86
CRTN14-12CCP.d	3.60	0.680	0.450	64.0	458	0.023	0.490	0.560	77.8	0.019	0.190	n.r.	3.38	0.006	9.90	3.28	16.7	0.146	0.260	0.004	0.038	0.003	0.005	0.323	3.E-04	3.34	3.68
CRTN14-2CCP.d	4.50	0.640	1.90	87.0	423	0.071	0.420	0.213	76.1	0.019	0.023	n.r.	3.57	0.006	10.3	1.26	10.7	0.131	0.340	0.004	0.011	0.003	0.004	0.123	0.002	2.55	1.66
CRTN14-3CCP.d	4.50	0.700	0.499	72.0	478	0.036	0.450	0.258	77.9	0.019	0.076	n.r.	4.12	0.006	10.2	0.797	7.70	0.126	0.260	0.013	0.011	0.001	0.007	0.120	3.E-04	1.94	2.37
CRTN14-4CCP.d	5.40	0.910	2.13	74.3	463	0.120	0.346	0.230	82.2	0.019	0.021	n.r.	3.29	0.006	14.6	1.44	12.1	0.150	0.400	0.004	0.011	0.003	0.008	0.035	3.E-04	2.94	2.69
CRTN14-6CCP.d	4.20	0.840	0.790	73.7	475	0.030	0.390	0.248	75.4	0.019	0.022	n.r.	3.27	0.006	9.92	1.20	9.44	0.110	0.510	0.002	0.011	0.003	0.003	0.130	3.E-04	2.24	2.00
CRTN14-8CCP.d	5.60	1.18	1.43	94.3	469	0.135	0.480	0.470	73.8	0.019	0.013	n.r.	2.83	0.006	15.1	1.60	14.2	0.081	0.540	0.004	0.011	0.003	0.007	0.104	2.E-04	1.95	2.36
CRTN14-9CCP.d	4.00	0.880	1.05	86.2	434	0.160	0.380	0.224	69.0	0.019	0.030	n.r.	2.99	0.006	11.3	1.74	12.8	0.111	0.860	0.004	0.011	0.003	0.007	0.122	3.E-04	3.08	3.69
CRTN18-10.d	4.20	1.15	0.315	101	317	0.054	0.303	0.620	82.8	0.018	0.580	n.r.	1.70	0.009	23.1	3.17	19.9	0.019	0.680	0.011	0.058	0.002	0.005	7.E-04	0.008	1.80	0.895
CRTN18-2.d	3.48	0.440	0.900	106	515	0.045	0.373	0.203	79.7	0.019	0.029	n.r.	1.82	0.006	30.7	3.28	27.7	0.038	0.910	0.002	0.011	0.003	0.007	5.E-04	2.E-04	1.67	0.646
CRTN18-5.d	2.60	0.670	0.351	117	404	0.046	0.580	0.312	78.0	0.018	0.021	n.r.	2.67	0.009	27.3	3.55	24.7	0.029	2.03	0.003	0.009	0.002	0.005	9.E-04	3.E-04	2.54	2.22
CRTN18-6.d	3.40	0.217	0.257	96.4	550	0.014	0.620	0.241	80.9	0.018	0.034	n.r.	3.23	0.009	30.2	3.56	23.3	0.040	2.28	0.003	0.007	0.002	0.005	8.E-04	3.E-04	2.19	1.85
CRTN18-7.d	4.60	0.235	0.261	96.4	360	0.084	0.600	0.276	83.0	0.022	0.034	n.r.	2.45	0.010	26.4	3.78	24.5	0.025	1.95	0.003	0.007	0.002	0.008	8.E-04	3.E-04	2.20	1.25
CRTN19-1d	3.60	0.210	0.370	89.7	308	0.054	0.410	0.627	78.7	0.024	0.018	n.r.	2.54	0.010	19.8	1.99	11.9	0.037	1.22	0.003	0.007	0.002	0.007	0.002	3.E-04	2.37	2.46
CRTN19-10.d	1.40	1.24	0.920	99.0	311	0.008	0.256	0.277	77.0	0.024	0.140	n.r.	1.95	0.007	21.9	0.817	6.65	0.002	0.088	0.003	0.007	0.002	0.007	1.E-03	3.E-04	1.48	1.60
CRTN19-11d	3.90	0.590	0.261	95.1	520	0.010	0.630	0.255	61.0	0.024	0.060	n.r.	2.89	0.007	28.8	0.893	7.35	0.004	1.90	0.003	0.007	0.002	0.005	0.001	3.E-04	1.89	2.60
CRTN19-2.d	3.00	0.188	0.268	100	296	0.130	0.250	0.325	53.2	0.024	0.018	n.r.	3.28	0.007	20.9	2.06	11.6	0.008	2.11	0.007	0.007	0.002	0.004	0.002	3.E-04	2.23	3.69
CRTN19-8.d	4.30	0.730	0.250	95.6	341	0.048	0.270	0.254	61.4	0.024	0.018	n.r.	2.45	0.007	22.0	1.24	7.75	0.003	1.70	0.003	0.007	0.002	0.009	0.001	3.E-04	1.67	2.28
CRTN19-9.d	3.70	0.990	0.800	94.8	280	0.031	0.590	2.00	72.0	0.190	0.018	n.r.	2.31	0.007	19.0	1.38	9.80	0.004	1.45	0.013	0.007	0.002	0.006	0.001	0.039	2.04	2.84
CRTN6CCP-01d	227	1.41	0.670	57.3	575	0.023	0.680	0.083	110	0.077	0.031	n.r.	3.63	0.004	5.70	1.35	3.32	0.047	0.210	0.038	0.008	0.003	0.005	9.E-04	0.010	3.01	0.276
CRTN6CCP-02.d	222	1.19	6.00	67.4	495	0.133	0.720	0.061	87.9	0.033	0.056	n.r.	3.80	0.004	4.40	1.77	7.62	0.052	2.20	0.003	0.026	0.008	0.005	0.060	3.E-04	3.27	0.458
CRTN6CCP-03.d	223	1.42	0.570	62.0	533	0.111	0.600	0.200	90.2	0.019	0.043	n.r.	3.96	0.004	5.26	2.59	7.33	0.025	1.31	0.080	0.008	0.110	1.80	1.E-03	5.E-04	3.92	0.627
CRTN6CCP-04.d	220	1.36	0.310	52.4	495	0.127	0.630	0.063	94.1	0.009	0.008	n.r.	3.28	0.004	4.39	3.97	6.72	0.043	1.07	0.003	0.008	0.033	0.005	0.012	3.E-04	3.26	0.587
CRTN6CCP-05.d	237	1.17	0.680	57.2	541	0.095	0.320	0.150	95.3	0.009	0.021	n.r.	3.11	0.004	4.29	1.82	6.63	0.028	1.41	0.020	0.008	0.011	0.008	0.009	0.004	2.54	0.500
CRTN6CCPr-01d	48.6	0.850	0.269	56.1	480	0.112	0.710	0.065	94.1	0.018	0.041	n.r.	3.33	0.005	3.79	2.05	7.68	0.036	2.34	0.007	0.018	0.004	0.007	0.001	5.E-04	3.85	0.541
CRTN6CCPr-02.d	45.5	0.640	0.433	59.2	492	0.105	0.730	0.088	98.9	0.013	0.041	n.r.	3.40	0.009	3.88	1.61	5.27	0.069	0.890	0.007	0.020	0.005	0.007	0.001	6.E-04	2.50	0.222
CRTN6CCPr-03.d	47.9	1.06	0.355	60.9	465	0.141	0.670	0.092	89.6	0.013	0.041	n.r.	3.55	0.009	4.10	2.00	6.83	0.018	1.31	0.008	0.021	0.005	0.007	0.001	5.E-04	2.49	0.346
CRTN6CCPr-04.d	43.2	0.600	0.293	56.0	404	0.135	0.750	0.270	91.6	0.012	0.037	n.r.	3.55	0.006	3.40	2.26	5.88	0.137	0.890	0.013	0.018	0.004	0.020	0.001	1.E-03	5.31	0.750
CRTN6CCPr-05.d	46.5	0.750	0.550	53.7	460	0.075	0.870	1.40	109	0.013	0.011	n.r.	3.48	0.006	3.09	1.78	5.49	0.031	0.920	0.014	0.019	1.00	0.070	0.001	6.E-04	0.960	0.160
CRTN9B-1d	7.20	1.59	1.80	105	552	0.079	0.450	0.375	87.4	0.019	0.013	n.r.	1.44	0.007	28.1	3.12	48.6	0.077	1.32	0.004	0.011	0.003	0.007	0.020	3.E-04	2.38	2.11
CRTN9B-2.d	4.87	1.72	0.280	85.9	506	0.074	0.497	0.317	85.5	0.019	0.025	n.r.	2.08	0.007	26.4	3.38	51.3	0.062	1.86	0.004	0.011	0.003	0.009	0.139	3.E-04	0.833	2.77
CRTN9B-3.d	5.10	1.23	0.355	81.9	471	0.082	0.510	0.520	84.1	0.019	0.013	n.r.	1.74	0.005	26.9	3.36	53.4	0.081	1.50	0.004	0.011	0.003	0.007	0.064	4.E-04	2.58	2.30
CRTN9B-4.d	4.80	1.77	0.465	94.3	468	0.088	0.450	0.317	86.2	0.019	0.013	n.r.	2.47	0.006	25.7	3.29	54.4	0.059	2.59	0.004	0.011	0.003	0.007	0.018	3.E-04	1.25	2.33
CRTN9B-5.d	4.70	1.26	1.12	104	401	0.158	0.660	0.292	91.0	0.019	0.029	n.r.	1.33	0.009	24.7	3.30	51.4	0.038	1.25	0.004	0.011	0.003	0.004	0.010	3.E-04	1.40	1.08
CRTN9B-7.d	7.40	1.13	0.730	75.2	484	0.114	0.470	0.290	86.0	0.019	0.013	n.r.	3.04	0.006	26.7	3.14	54.5	0.005	4.10	0.004	0.011	0.003	0.007	0.001	3.E-04	1.30	5.70

Grain ID (chalcopyrite)	Ti 49	Mn 55	Co 59	Ni 60	Zn 66	Ga 71	Ge 74	As 75	Se 82	Mo 95	Ru 101	Rh 103	Ag 107	Pd 108	Cd 111	In 115	Sn 118	Sb 121	Te 128	Re 185	Os 189	Ir 193	Pt 195	Au 197	Tl 205	Pb 208	Bi 209
55um	0.553	0.479	0.016	0.207	0.270	0.024	0.079	0.348	2.409	0.029	0.020	0.004	0.049	0.011	0.061	0.007	0.070	0.017	0.221	0.007	0.016	0.004	0.010	0.006	0.004	0.006	0.004
33um	0.661	1.030	0.028	0.410	0.526	0.051	0.149	0.582	5.311	0.030	0.020	0.007	0.100	0.026	0.118	0.012	0.147	0.027	0.501	0.012	0.028	0.007	0.018	0.014	0.007	0.011	0.007
CRTN9B-8-2.d	7.00	30.0	1.26	86.0	441	0.055	0.375	0.240	89.1	0.019	0.021	n.r.	1.48	0.006	26.8	3.02	52.5	0.042	1.48	0.002	0.004	0.003	0.007	0.010	4.E-04	1.74	1.59
CRTN9B-9.d	4.50	1.10	0.474	71.6	496	0.070	0.470	0.440	84.4	0.019	0.023	n.r.	1.54	0.006	27.3	3.21	55.4	0.064	1.37	0.004	0.011	0.003	0.007	0.030	0.002	1.76	2.32
CRTN12CCPr-01d	43.7	1.07	0.210	46.3	541	0.122	0.686	0.054	73.0	0.107	0.037	n.r.	8.23	0.007	10.8	0.743	3.60	0.028	0.400	0.012	0.045	0.003	0.014	0.002	6.E-04	3.39	2.81
CRTN12CCPr-02.d	46.0	1.01	0.329	54.9	582	0.162	0.570	0.086	77.1	0.015	0.025	n.r.	8.06	0.008	12.4	1.37	7.08	0.004	0.540	0.012	0.024	0.004	0.020	0.002	6.E-04	2.43	1.98
CRTN12CCPr-03.d	44.3	1.16	0.264	46.7	476	0.140	0.570	0.074	79.3	0.107	0.016	n.r.	8.54	0.007	9.40	0.700	4.15	0.042	0.061	0.008	0.045	0.005	0.013	0.007	0.017	3.63	2.19
CRTN12CCPr-04.d	42.0	1.18	0.330	50.9	547	0.110	0.620	0.083	74.6	0.107	0.043	n.r.	8.30	0.006	10.3	0.817	5.66	0.005	0.230	0.007	0.020	0.005	0.016	0.001	3.E-04	0.790	1.30
CRTN12CCPr-05.d	46.0	1.91	0.550	55.9	650	0.051	0.710	0.226	88.5	0.107	0.460	n.r.	8.01	0.005	14.3	0.775	3.48	0.035	0.220	0.021	0.199	0.004	0.016	0.002	4.E-04	1.67	2.26
DC-18-07.d	3.20	0.560	0.125	12.5	261	0.403	0.450	0.192	61.4	0.021	0.018	n.r.	3.46	0.007	8.02	1.32	2.81	0.025	2.64	0.003	0.007	0.002	0.003	5.E-04	3.E-04	8.43	0.232
DC-18-08.d	3.50	0.520	0.159	12.9	243	0.430	0.330	0.229	56.9	0.021	0.018	n.r.	3.27	0.007	7.18	1.61	2.71	0.005	1.94	0.003	0.007	0.002	0.004	5.E-04	4.E-04	15.7	0.130
DC-18-09.d	2.91	0.176	0.296	19.2	199	0.428	0.319	0.229	57.1	0.021	0.018	n.r.	3.06	0.007	5.50	1.07	2.15	0.003	1.84	0.003	0.007	0.002	0.004	4.E-04	3.E-04	3.67	0.084
DC-18-10.d	2.50	0.182	0.056	8.17	197	0.500	0.360	0.175	53.4	0.021	0.018	n.r.	3.57	0.007	6.37	1.36	2.19	0.015	2.37	0.007	0.007	0.002	0.004	4.E-04	3.E-04	11.1	0.053
DC-18-11d	3.20	0.470	0.128	9.70	211	0.480	0.300	0.200	64.5	0.021	0.018	n.r.	3.55	0.007	6.93	1.35	2.37	0.014	2.54	0.003	0.007	0.002	0.007	4.E-04	4.E-04	6.51	0.059
DC-18-12.d	1.99	0.182	0.350	14.6	206	0.400	0.270	0.290	59.5	0.021	0.018	n.r.	2.53	0.007	5.80	1.64	2.18	0.018	2.46	0.003	0.007	0.002	0.004	4.E-04	0.003	8.06	0.085
DC-18-13.d	3.80	0.480	0.438	12.2	231	0.425	0.360	0.183	55.0	0.021	0.018	n.r.	2.37	0.007	5.99	1.26	2.12	0.019	2.18	0.003	0.007	0.002	0.004	0.007	3.E-04	8.49	0.178
DC69-10.d	4.00	1.46	0.454	26.2	273	0.540	0.089	0.243	45.4	0.020	0.013	n.r.	0.523	0.017	17.4	1.81	5.04	0.057	4.06	0.008	0.020	0.005	0.011	1.E-03	9.E-04	8.62	0.382
DC69-11d	3.20	0.810	2.99	103	225	0.330	0.230	15.0	36.9	0.220	0.013	n.r.	0.750	0.017	14.9	1.37	4.65	0.029	2.58	0.105	0.007	0.005	0.011	0.001	1.E-03	14.3	0.655
DC69-3.d	4.40	1.22	1.53	37.8	348	0.500	0.260	0.248	46.1	0.020	0.013	n.r.	0.153	0.017	22.5	1.29	5.47	0.044	3.74	0.008	0.006	0.005	0.011	1.E-03	6.E-04	5.52	0.490
DC69-4.d	3.90	0.430	0.376	28.7	258	0.278	0.162	0.217	40.5	0.020	0.032	n.r.	0.336	0.017	16.5	1.15	3.31	0.004	5.21	0.003	0.020	0.005	0.011	8.E-04	6.E-04	7.88	0.377
DC69-5.d	4.70	0.720	0.870	31.8	277	0.375	0.278	0.206	44.3	0.031	0.013	n.r.	0.298	0.017	14.6	1.35	4.01	0.035	4.93	0.008	0.020	0.005	0.005	9.E-04	2.E-04	8.25	0.416
DC69-8.d	3.80	1.08	0.730	38.1	274	0.490	0.138	0.233	42.9	0.020	0.013	n.r.	0.460	0.008	19.0	1.56	5.82	0.043	2.42	0.007	0.020	0.005	0.016	1.E-03	8.E-04	7.34	0.478
DC69-9.d	5.70	1.09	0.338	24.1	275	0.620	0.123	0.268	44.6	0.020	0.021	n.r.	0.610	0.017	16.9	1.53	4.66	0.053	4.02	0.008	0.020	0.005	0.011	1.E-03	0.006	1.77	0.274
E13-2.d	7.60	0.800	0.180	25.0	221	0.015	0.270	0.371	51.0	0.340	0.013	n.r.	8.27	0.017	7.30	2.40	1.63	0.004	2.98	0.021	0.020	0.062	0.011	7.E-04	0.048	3.51	0.199
E13-3.d	6.90	0.178	0.400	9.70	192	0.047	0.430	0.326	97.3	0.020	0.013	n.r.	7.96	0.017	6.58	2.19	2.12	0.019	10.3	0.008	0.020	0.005	0.011	0.019	3.E-04	1.77	0.570
E13-6.d	5.60	0.189	0.041	4.30	309	0.014	0.480	0.292	100	0.017	0.034	n.r.	5.38	0.017	4.73	1.90	0.301	0.013	4.87	0.005	0.020	0.005	0.025	0.013	0.258	7.47	1.49
E1-4.d	3.40	0.243	0.042	9.60	305	0.008	0.430	0.272	73.0	1.91	0.018	n.r.	5.02	0.011	14.9	2.12	0.470	0.243	4.02	0.153	0.081	0.087	0.006	0.013	0.020	12.5	3.12
E1-5.d	2.80	0.190	0.035	9.12	353	0.024	0.440	0.390	76.1	2.18	0.018	n.r.	6.09	0.007	11.9	1.76	0.450	0.093	10.3	0.076	0.025	0.098	0.009	9.E-04	8.E-04	4.55	0.560
E1-8.d	3.90	1.15	0.490	16.5	366	0.008	0.450	0.270	79.4	1.40	0.035	n.r.	10.9	0.007	12.0	3.92	0.400	0.170	12.8	0.029	0.038	0.120	0.009	0.001	0.020	11.4	1.35
E1-9.d	4.50	0.263	0.172	13.0	399	0.007	0.570	0.218	96.0	2.48	0.018	n.r.	6.21	0.007	11.1	2.45	0.510	0.051	12.8	0.216	0.098	0.154	0.024	9.E-04	0.010	6.31	0.690
E4-10.d	5.90	0.250	0.760	118	364	0.020	0.580	0.393	129	0.020	0.013	n.r.	10.2	0.010	12.4	3.38	33.7	0.026	37.0	0.008	0.020	0.005	0.005	0.025	0.089	64.2	3.17
E4-11d	7.70	1.06	0.390	33.8	570	0.016	0.510	0.276	116	0.020	0.013	n.r.	21.4	0.008	21.3	2.96	32.2	0.086	39.1	0.008	0.007	0.005	0.004	0.015	0.138	61.6	2.95
E4-3.d	6.40	1.15	0.113	26.5	578	0.013	0.560	0.281	93.3	0.064	0.013	n.r.	16.9	0.007	20.0	3.81	40.2	0.030	8.31	0.003	0.020	0.005	0.005	0.023	0.137	6.41	0.467
E4-5.d	5.20	1.85	0.460	82.0	580	0.017	0.480	0.297	92.3	0.020	0.013	n.r.	10.5	0.017	17.6	3.17	32.0	0.024	6.64	0.008	0.020	0.005	0.011	0.007	4.E-04	5.63	0.689
E4-6.d	7.90	0.242	0.710	190	450	0.017	0.450	0.326	100	0.020	0.013	n.r.	7.24	0.017	13.7	3.15	33.4	0.027	4.44	0.008	0.020	0.005	0.007	0.015	0.008	4.14	0.508
E4-9.d	4.90	0.224	0.072	24.6	412	0.016	0.360	0.347	111	0.020	0.023	n.r.	8.50	0.017	15.3	3.33	32.6	0.040	11.1	0.005	0.008	0.005	0.011	0.016	0.038	16.4	1.31
EDEEP-10.d	5.90	1.28	0.330	17.0	197	0.350	0.310	0.648	63.0	0.024	0.041	n.r.	0.960	0.007	22.4	2.23	2.49	0.014	10.0	0.003	0.007	0.002	0.019	8.E-04	4.E-04	1.21	0.301
EDEEP-4.d	6.40	0.330	0.067	9.20	255	0.250	0.300	0.563	57.3	0.024	0.040	n.r.	1.84	0.018	30.7	2.68	2.48	0.004	9.60	0.003	0.007	0.002	0.004	8.E-04	4.E-04	1.89	0.201
EDEEP-5.d	5.60	0.373	0.120	8.90	187	0.510	0.450	0.325	55.0	0.220	0.018	n.r.	2.07	0.007	22.9	2.39	3.21	0.004	8.20	0.370	0.015	0.002	0.012	9.E-04	4.E-04	1.97	0.374

Grain ID (chalcopyrite)	Ti 49	Mn 55	Co 59	Ni 60	Zn 66	Ga 71	Ge 74	As 75	Se 82	Mo 95	Ru 101	Rh 103	Ag 107	Pd 108	Cd 111	In 115	Sn 118	Sb 121	Te 128	Re 185	Os 189	Ir 193	Pt 195	Au 197	Tl 205	Pb 208	Bi 209
55um	0.553	0.479	0.016	0.207	0.270	0.024	0.079	0.348	2.409	0.029	0.020	0.004	0.049	0.011	0.061	0.007	0.070	0.017	0.221	0.007	0.016	0.004	0.010	0.006	0.004	0.006	0.004
33um	0.661	1.030	0.028	0.410	0.526	0.051	0.149	0.582	5.311	0.030	0.020	0.007	0.100	0.026	0.118	0.012	0.147	0.027	0.501	0.012	0.028	0.007	0.018	0.014	0.007	0.011	0.007
EDEEP-8.d	4.40	0.364	0.166	13.2	229	0.170	0.310	0.647	50.0	0.024	0.018	n.r.	4.49	0.007	27.9	4.26	3.44	0.005	14.1	0.003	0.007	0.004	0.011	0.001	5.E-04	4.81	0.790
EDEEP-9.d	3.30	1.89	0.132	13.9	432	0.250	0.530	0.527	56.0	0.024	0.018	n.r.	3.74	0.007	36.2	3.29	2.61	0.006	13.4	0.003	0.007	0.002	0.004	0.001	6.E-04	2.94	0.781
EX0301-1d	5.45	15.8	0.460	10.6	257	0.234	0.270	0.524	48.7	0.021	0.091	n.r.	0.750	0.007	16.9	2.63	12.2	0.004	0.930	0.003	0.154	0.266	0.229	0.070	5.E-04	2.34	0.063
EX0301-10.d	5.80	2.36	0.128	7.49	259	0.064	0.270	0.433	46.4	0.021	0.018	n.r.	6.84	0.009	12.7	2.22	9.98	0.003	6.11	0.003	0.007	0.002	0.004	0.020	0.004	4.58	0.124
EX0301-11.d	5.75	0.179	0.098	11.3	255	0.013	0.275	0.404	54.3	0.021	0.018	n.r.	2.69	0.007	11.2	2.32	10.6	0.028	5.06	0.006	0.007	0.002	0.005	0.010	3.E-04	3.06	0.084
EX0301-12.d	6.20	0.174	0.034	6.21	265	0.094	0.350	0.327	57.8	0.018	0.018	n.r.	8.20	0.007	13.0	2.54	11.4	0.003	7.84	0.003	0.007	0.002	0.006	0.015	4.E-04	5.72	0.119
EX0301-13.d	4.30	1.66	0.049	6.60	247	0.054	0.210	0.343	41.8	0.021	0.018	n.r.	6.18	0.007	13.3	2.45	10.9	0.014	8.20	0.004	0.007	0.002	0.004	0.007	0.009	4.44	0.126
EX0301-2.d	6.15	1.02	0.068	8.75	264	0.097	0.225	0.332	47.8	0.021	0.050	n.r.	6.12	0.007	13.4	2.41	11.1	0.016	9.15	0.003	0.009	0.002	0.004	0.005	0.005	5.59	0.129
EX0301-4.d	6.40	0.510	0.075	8.80	300	0.013	0.380	0.427	50.7	0.021	0.018	n.r.	7.26	0.007	15.6	2.45	11.6	0.018	6.24	0.003	0.007	0.002	0.004	0.044	5.E-04	2.98	0.097
EX0301-5.d	4.90	0.199	0.053	4.98	262	0.102	0.470	0.415	52.0	0.021	0.018	n.r.	2.82	0.007	12.8	2.36	10.8	0.022	4.37	0.003	0.007	0.002	0.005	0.013	4.E-04	2.95	0.079
EX0301-9.d	5.10	2.06	0.233	10.3	343	0.073	0.200	8.00	47.6	0.021	0.018	n.r.	6.10	0.008	15.2	2.22	11.3	0.033	6.38	0.003	0.014	0.042	0.022	0.016	0.004	3.38	0.071
F10304CCP-01d	334	0.516	0.028	2.50	408	0.083	1.22	0.127	205	0.151	0.007	n.r.	5.13	0.007	13.7	0.309	0.069	0.003	0.310	0.003	0.008	0.007	0.007	9.E-04	0.005	1.25	0.007
F10304CCP-02.d	348	2.02	0.090	0.710	548	0.033	1.54	0.076	206	0.410	0.078	n.r.	3.70	0.013	23.6	0.378	0.041	0.003	2.10	0.162	0.580	0.056	0.017	1.E-03	3.E-04	0.280	0.017
F10304CCP-03.d	346	15.0	0.038	0.214	600	0.166	1.16	0.325	198	0.687	0.041	n.r.	2.17	0.186	20.8	0.234	0.064	0.008	4.90	0.498	0.041	0.030	0.035	0.009	5.E-04	1.49	0.290
F10304CCP-04.d	350	1.08	0.030	1.27	393	0.066	1.26	0.325	173	0.537	0.500	n.r.	1.76	0.029	18.7	0.472	0.160	0.003	2.70	0.187	0.019	0.003	0.008	0.001	3.E-04	1.86	0.230
F10304CCP-06.d	354	1.21	0.032	0.207	408	0.028	1.04	0.440	161	0.025	0.009	n.r.	3.81	0.096	21.6	0.411	0.197	0.002	1.52	0.004	0.073	0.025	0.221	0.004	5.E-04	1.23	0.009
F10304CCP-07.d	359	1.21	0.250	0.208	458	0.060	1.13	0.325	176	0.043	0.022	n.r.	3.98	0.100	21.6	0.328	0.294	0.029	1.99	0.060	0.412	0.175	0.109	0.280	5.E-04	1.49	0.048
FI0304CCP-01d	229	0.379	0.006	0.720	315	0.079	2.87	0.119	225	0.076	0.134	n.r.	4.15	0.017	14.1	0.260	0.027	0.005	0.770	0.027	0.057	0.015	0.018	0.001	6.E-04	1.26	0.004
FI0304CCP-02.d	231	2.20	0.024	0.730	288	0.092	1.87	0.197	145	0.057	0.155	n.r.	4.53	0.017	18.5	0.283	0.033	0.005	0.720	0.027	0.057	0.015	0.028	0.001	7.E-04	0.680	0.005
FI0304CCP-03.d	223	10.5	0.210	8.90	300	0.120	2.81	0.184	226	0.075	0.090	n.r.	3.06	0.017	12.8	0.277	0.031	0.009	0.064	0.027	0.057	0.015	0.033	0.002	0.032	1.70	0.006
FI0304CCP-04.d	225	0.412	0.006	0.580	300	0.015	2.38	0.167	178	0.050	0.170	n.r.	3.36	0.015	19.5	0.468	0.390	0.005	2.21	0.027	0.057	0.015	0.033	0.001	6.E-04	0.920	0.085
FI0304CCP-05.d	220	0.544	0.009	2.76	308	0.107	2.58	0.171	179	0.071	0.340	n.r.	3.44	0.017	18.1	0.343	0.300	0.005	1.31	0.027	0.047	0.015	0.033	0.001	0.018	1.45	0.050
FI0304CCP-06.d	220	0.900	0.010	1.82	318	0.200	2.06	0.202	193	0.084	0.085	n.r.	1.81	0.007	21.8	0.439	0.047	0.052	0.520	0.007	0.055	0.004	0.007	0.002	0.013	4.13	0.009
GCMACCP-01d	354	11.2	0.033	22.9	223	0.100	0.910	0.146	113	0.023	0.039	n.r.	1.37	0.004	5.50	2.53	0.068	0.009	0.051	0.003	0.008	0.005	0.016	1.70	0.015	4.19	0.250
GCMACCP-02.d	343	14.0	0.180	24.6	273	0.044	0.750	0.115	103	0.048	0.343	n.r.	1.70	0.004	6.58	2.62	0.074	0.006	0.032	0.003	0.017	0.002	0.071	0.600	0.013	6.23	0.029
GCMACCP-03.d	347	12.0	0.062	21.6	284	0.240	0.740	3.70	114	0.055	0.012	n.r.	1.61	0.004	6.31	2.62	0.039	0.006	0.033	0.011	0.008	0.002	0.008	0.011	0.003	6.25	0.007
GCMACCP-04.d	360	5.20	0.107	14.4	355	0.040	1.40	0.340	121	0.020	0.008	n.r.	2.67	0.010	6.80	2.01	0.023	0.200	0.034	0.049	0.008	0.002	0.005	7.E-04	0.007	4.43	0.045
GCMACCP-05.d	370	5.20	0.150	20.9	411	0.062	0.740	0.170	113	0.023	0.008	n.r.	2.71	0.011	6.57	2.61	0.072	0.006	0.041	0.003	0.008	0.018	0.005	0.039	0.031	8.62	0.003
GCMACCP-06.d	376	1.16	0.097	14.8	237	0.025	1.17	0.124	180	0.420	0.183	n.r.	3.15	0.255	3.07	1.20	0.140	0.028	0.029	0.190	0.018	0.079	0.060	7.E-04	0.038	20.2	0.025
GCMBCCP-01d	248	3.40	0.080	23.9	452	0.060	0.730	0.074	96.7	0.032	0.015	n.r.	1.94	0.012	9.20	2.11	0.029	0.007	0.051	0.007	0.008	0.045	0.009	7.E-04	0.022	11.2	0.037
GCMBCCP-02.d	235	11.0	0.079	20.7	307	0.014	0.650	0.340	93.7	1.10	0.008	n.r.	1.66	0.011	6.80	1.88	0.027	0.009	0.036	0.003	0.008	0.039	0.005	4.E-04	0.015	4.98	0.011
GCMBCCP-03.d	209	2.90	0.112	32.0	253	0.048	0.660	0.340	87.9	1.80	0.008	n.r.	3.10	0.007	6.00	1.74	0.032	0.060	0.098	0.003	0.023	0.002	0.031	0.002	3.E-04	2.38	0.022
GCMBCCP-04.d	234	1.09	0.109	25.2	389	0.013	0.660	0.060	79.1	0.009	0.008	n.r.	1.88	0.007	8.40	1.87	0.140	0.005	0.023	0.014	0.027	0.025	0.005	0.003	0.006	3.57	0.004
GCMBCCP-05.d	216	0.660	0.059	19.6	399	0.061	0.520	0.140	91.4	0.033	0.031	n.r.	1.93	0.007	7.98	2.67	0.036	0.019	0.032	0.003	0.008	0.091	0.046	0.170	9.E-04	1.66	0.007
GD10CCP-01d	233	1.19	0.071	29.3	621	0.055	1.05	0.087	148	0.428	0.016	n.r.	3.94	0.004	77.1	1.17	0.890	0.003	0.780	0.040	0.008	0.002	0.320	0.009	0.004	0.549	0.480
GD10CCP-02.d	230	1.42	0.123	27.5	622	0.140	1.00	0.092	140	0.009	0.008	n.r.	4.48	0.010	75.3	1.12	0.980	2.30	0.039	0.005	0.008	0.007	0.005	0.001	3.E-04	0.492	0.700
GD10CCP-03.d	234	2.10	0.290	38.5	588	0.335	0.890	0.083	128	0.018	0.017	n.r.	2.54	0.004	49.4	1.30	6.20	0.007	0.046	0.003	0.008	0.060	0.005	0.200	0.004	2.67	0.777

Grain ID (chalcopyrite)	Ti 49	Mn 55	Co 59	Ni 60	Zn 66	Ga 71	Ge 74	As 75	Se 82	Mo 95	Ru 101	Rh 103	Ag 107	Pd 108	Cd 111	In 115	Sn 118	Sb 121	Te 128	Re 185	Os 189	Ir 193	Pt 195	Au 197	Tl 205	Pb 208	Bi 209
55um	0.553	0.479	0.016	0.207	0.270	0.024	0.079	0.348	2.409	0.029	0.020	0.004	0.049	0.011	0.061	0.007	0.070	0.017	0.221	0.007	0.016	0.004	0.010	0.006	0.004	0.006	0.004
33um	0.661	1.030	0.028	0.410	0.526	0.051	0.149	0.582	5.311	0.030	0.020	0.007	0.100	0.026	0.118	0.012	0.147	0.027	0.501	0.012	0.028	0.007	0.018	0.014	0.007	0.011	0.007
GD10CCP-04.d	232	1.61	0.146	37.8	651	0.230	0.950	0.170	128	0.019	0.049	n.r.	3.80	0.004	50.4	1.73	6.90	0.003	0.190	0.006	0.008	0.002	0.021	0.160	0.012	0.770	0.222
GD10CCP-05.d	249	0.990	0.242	66.0	703	0.327	0.930	0.180	132	0.009	0.016	n.r.	4.08	0.004	50.4	1.82	5.64	0.004	0.031	0.014	0.008	0.007	0.007	0.012	0.012	2.15	0.388
GD10CCP-06.d	231	1.08	0.450	39.2	637	0.050	1.02	0.099	134	0.021	0.016	n.r.	3.75	0.004	68.3	4.30	2.81	0.017	1.81	0.330	0.008	0.007	0.005	0.180	0.005	0.790	4.50
GD10CCP-07.d	234	1.54	1.00	44.5	571	0.082	0.890	0.122	144	0.009	0.008	n.r.	3.24	0.004	76.0	4.30	3.43	0.016	1.71	0.070	0.008	0.002	0.029	0.124	0.022	0.620	2.60
GD10CCPr-01d	237	0.541	0.062	28.3	589	0.140	1.95	0.139	174	0.047	0.071	n.r.	3.24	0.020	84.5	1.08	0.780	0.007	0.102	0.007	0.018	0.004	0.007	0.002	4.E-04	2.35	0.890
GD10CCPr-02.d	251	0.548	0.130	26.1	546	0.117	2.51	0.180	176	0.041	0.100	n.r.	4.46	0.007	96.0	1.22	1.21	0.006	0.560	0.007	0.018	0.004	0.310	0.001	6.E-04	0.800	0.620
GD10CCPr-03.d	268	0.262	0.030	36.2	554	0.330	1.77	0.213	180	0.106	0.104	n.r.	2.74	0.007	68.3	1.65	9.60	0.010	0.094	0.007	0.018	0.017	0.220	0.001	0.009	1.04	0.400
GD10CCPr-04.d	262	0.535	0.280	49.3	660	0.210	2.13	0.850	177	0.120	1.20	n.r.	2.29	0.007	65.0	1.28	7.10	0.076	0.078	0.470	0.130	0.900	0.350	0.002	0.031	1.59	0.460
GD10CCPr-05.d	262	0.552	0.184	31.1	740	0.145	2.00	0.131	148	0.042	0.120	n.r.	3.82	0.007	64.3	1.61	6.81	0.007	0.071	0.007	0.018	0.004	0.007	0.003	9.E-04	1.28	0.341
GD10CCPr-06.d	266	0.292	0.440	48.8	583	0.030	2.87	0.233	189	0.058	0.120	n.r.	3.04	0.025	88.0	4.56	4.55	0.010	1.69	0.007	0.018	0.004	0.040	0.048	0.001	0.890	2.30
GD10CCPr-07.d	236	1.20	0.187	31.2	780	0.039	2.58	0.188	181	0.054	0.090	n.r.	3.56	0.007	88.0	5.53	4.11	0.011	1.24	0.007	0.018	0.004	0.026	0.033	8.E-04	0.920	1.35
GDN4CCP-01d	215	0.267	1.80	23.6	561	0.270	0.700	0.124	104	0.016	0.016	n.r.	0.160	0.004	24.6	1.32	2.82	0.004	0.780	0.003	0.100	0.021	0.010	0.051	2.E-04	1.51	0.072
GDN4CCP-02.d	224	1.26	0.053	30.4	429	0.140	0.770	0.182	103	0.009	0.008	n.r.	1.04	0.004	28.2	3.59	2.36	0.009	0.440	0.003	0.068	0.033	0.016	8.E-04	0.001	1.36	0.048
GDN4CCP-03.d	216	1.28	1.20	30.4	523	0.407	0.640	0.467	105	0.009	0.045	n.r.	0.571	0.004	20.8	0.732	9.62	0.004	0.910	0.003	0.008	0.002	0.380	8.E-04	2.E-04	0.750	0.053
GDN4CCP-04.d	216	14.8	0.330	32.3	472	0.250	0.730	0.528	106	0.120	0.022	n.r.	0.890	0.004	19.6	0.616	3.09	0.006	0.700	1.60	0.050	0.036	0.005	0.021	5.E-04	1.11	0.092
GDN4CCP-05.d	223	1.35	0.104	30.4	710	0.510	0.960	0.420	96.5	0.056	0.044	n.r.	0.576	0.004	39.8	0.958	23.3	0.007	1.27	0.009	0.008	0.002	0.005	0.016	0.005	0.896	0.043
GDN4CCP-06.d	221	1.23	0.038	21.3	710	0.370	0.660	0.108	102	0.014	0.012	n.r.	0.920	0.004	93.0	2.09	9.52	0.012	0.650	0.241	0.008	0.002	0.005	0.060	2.E-04	0.960	0.144
GDN4CCPr-01d	59.5	0.570	0.044	27.3	580	0.197	0.910	0.071	104	0.106	0.047	n.r.	0.454	0.006	13.9	0.532	2.78	0.003	0.730	0.010	0.018	0.004	0.014	8.E-04	4.E-04	1.85	0.149
GDN4CCPr-02.d	61.5	0.820	0.073	26.5	329	0.061	0.950	0.104	109	0.013	0.012	n.r.	0.530	0.007	14.6	0.627	0.950	0.004	0.055	0.008	0.018	0.005	0.020	0.002	5.E-04	1.69	0.086
GDN4CCPr-04.d	60.7	54.0	0.072	29.5	465	0.086	0.940	0.144	115	0.025	0.041	n.r.	0.500	0.009	12.1	0.490	0.600	0.006	0.710	0.007	0.018	0.007	0.007	0.001	0.001	4.90	0.920
IGCP4-1d	3.60	0.287	0.053	5.40	351	0.016	0.390	0.523	87.0	0.018	0.011	n.r.	5.63	0.017	13.9	3.09	0.330	0.056	2.76	0.008	0.018	0.005	0.022	0.036	3.E-04	0.850	0.366
IGCP4-2.d	3.20	0.404	2.70	4.30	316	0.029	0.630	0.483	76.0	0.018	0.011	n.r.	2.71	0.017	14.0	2.86	0.080	0.060	1.48	0.008	0.018	0.005	0.012	0.003	5.E-04	2.26	0.519
IGCP4-3.d	8.50	33.6	0.204	7.20	320	0.011	0.490	0.384	75.8	0.018	0.011	n.r.	6.98	0.017	13.4	2.85	0.273	0.058	1.53	0.005	0.013	0.005	0.025	0.003	8.E-04	2.01	0.536
IGCP4-4.d	2.90	0.670	0.012	3.30	400	0.013	0.220	0.270	84.0	0.018	0.011	n.r.	4.46	0.017	15.0	2.90	0.340	0.023	1.17	0.008	0.018	0.025	0.012	0.019	5.E-04	1.10	0.578
IGCP4-5.d	4.30	0.151	0.012	2.90	391	0.023	0.820	0.099	91.0	0.018	0.011	n.r.	8.20	0.017	18.8	2.81	0.250	0.085	2.69	0.008	0.018	0.005	0.012	0.091	8.E-04	1.25	0.501
J12-10.d	6.70	0.191	0.062	21.7	532	0.014	0.520	0.273	96.7	0.021	0.035	n.r.	5.20	0.007	10.5	1.19	3.74	0.005	7.73	0.003	0.006	0.002	0.004	7.E-04	4.E-04	9.85	2.19
J12-2.d	6.00	0.204	0.155	26.4	395	0.046	0.450	0.493	90.0	0.021	0.056	n.r.	5.20	0.007	6.05	1.39	6.28	0.023	8.80	0.003	0.007	0.002	0.005	0.013	5.E-04	7.27	2.13
J12-3.d	8.70	0.219	0.123	34.7	430	0.092	0.440	0.451	86.2	0.021	0.018	n.r.	4.15	0.007	12.6	1.88	6.66	0.006	8.73	0.003	0.007	0.002	0.005	0.009	0.006	4.67	2.29
J12-6.d	6.90	0.215	0.730	73.0	389	0.013	0.580	0.389	83.8	0.021	0.034	n.r.	3.46	0.007	5.45	1.15	3.12	0.007	7.07	0.003	0.007	0.002	0.004	0.032	4.E-04	3.61	5.15
J12-7.d	7.50	0.203	0.101	23.4	374	0.039	0.410	0.578	84.0	0.021	0.018	n.r.	3.67	0.007	4.36	1.11	2.82	0.045	6.58	0.003	0.007	0.002	0.004	0.042	0.004	5.78	6.12
J12-8.d	7.60	0.186	0.151	33.8	473	0.014	0.520	0.740	111	0.044	0.014	n.r.	4.27	0.007	17.1	1.66	7.31	0.042	9.72	0.033	0.007	0.002	0.004	0.001	5.E-04	8.49	5.10
J12-9.d	4.70	0.258	0.290	34.0	362	0.061	0.420	0.407	102	0.700	0.018	n.r.	4.57	0.007	11.4	1.63	7.07	0.061	7.40	0.016	0.007	0.014	0.009	0.019	4.E-04	6.20	2.44
J2-3.d	3.20	3.22	0.412	18.2	346	0.012	0.440	0.610	77.0	0.018	0.520	n.r.	4.34	0.017	2.16	0.041	0.620	0.008	0.137	0.025	0.650	0.140	0.012	0.001	0.006	32.5	0.326
J2-4.d	4.70	4.51	0.460	29.0	275	0.014	0.450	0.524	95.1	0.220	0.076	n.r.	2.83	0.017	1.96	0.021	0.420	0.009	0.136	0.160	0.180	0.065	0.012	0.001	0.001	42.6	0.356
J3-1d	6.60	4.78	0.072	17.6	348	0.025	0.430	0.325	56.0	0.018	0.011	n.r.	1.41	0.017	2.65	1.47	0.700	0.008	3.30	0.014	0.018	0.005	0.012	7.E-04	5.E-04	4.18	0.383
J3-2.d	6.80	1.49	0.150	20.8	340	0.026	0.810	0.325	75.0	0.018	0.011	n.r.	2.37	0.025	3.26	1.32	0.750	0.009	1.03	0.008	0.038	0.005	0.018	0.018	0.001	16.1	0.820
J3-3.d	5.70	0.309	0.193	20.4	293	0.012	0.460	0.577	68.0	0.018	0.059	n.r.	3.23	0.017	3.53	1.83	0.550	0.006	1.67	0.008	0.018	0.005	0.011	0.016	0.008	11.3	1.25

Grain ID (chalcopyrite)	Ti 49	Mn 55	Co 59	Ni 60	Zn 66	Ga 71	Ge 74	As 75	Se 82	Mo 95	Ru 101	Rh 103	Ag 107	Pd 108	Cd 111	In 115	Sn 118	Sb 121	Te 128	Re 185	Os 189	Ir 193	Pt 195	Au 197	Tl 205	Pb 208	Bi 209
55um	0.553	0.479	0.016	0.207	0.270	0.024	0.079	0.348	2.409	0.029	0.020	0.004	0.049	0.011	0.061	0.007	0.070	0.017	0.221	0.007	0.016	0.004	0.010	0.006	0.004	0.006	0.004
33um	0.661	1.030	0.028	0.410	0.526	0.051	0.149	0.582	5.311	0.030	0.020	0.007	0.100	0.026	0.118	0.012	0.147	0.027	0.501	0.012	0.028	0.007	0.018	0.014	0.007	0.011	0.007
J3-4.d	4.00	1.54	0.128	21.3	413	0.075	0.390	0.325	72.0	0.018	0.011	n.r.	4.24	0.017	4.20	2.30	0.850	0.008	3.60	0.008	0.018	0.005	0.023	0.039	0.001	13.9	1.14
J3-7.d	5.90	1.91	8.70	422	389	0.011	0.210	0.530	60.2	0.120	0.480	n.r.	11.1	0.023	5.50	0.062	0.350	0.440	1.29	0.640	0.440	0.083	0.012	0.122	0.035	117	5.78
J3-8.d	2.60	2.05	2.23	250	268	0.017	0.580	0.325	86.0	0.018	0.011	n.r.	16.7	0.017	7.80	0.067	0.860	0.120	0.248	0.008	0.018	0.005	0.026	0.081	0.028	128	4.59
J9B-1d	3.80	2.23	0.008	7.60	276	0.025	0.410	0.267	60.0	0.050	0.011	n.r.	3.49	0.017	14.0	3.45	0.078	0.008	0.207	0.090	0.018	0.005	0.013	0.037	6.E-04	4.56	0.511
J9B-3.d	3.50	0.481	0.120	4.70	231	0.018	0.390	0.424	64.0	0.018	0.032	n.r.	7.10	0.017	13.4	1.34	0.068	0.006	0.231	0.008	0.018	0.005	0.012	0.003	0.013	15.5	1.01
J9B-4.d	4.50	8.90	0.100	7.30	201	0.024	0.300	0.512	82.0	0.018	0.011	n.r.	13.2	0.017	11.1	1.47	0.084	0.007	4.60	0.008	0.018	0.005	0.018	0.003	0.012	11.1	0.850
J9B-5.d	3.50	1.19	0.015	2.25	212	0.012	0.125	0.476	45.0	0.018	0.011	n.r.	13.1	0.017	13.2	1.55	0.069	0.005	7.60	0.008	0.018	0.005	0.014	0.002	8.E-04	16.6	0.562
J9B-6.d	5.20	2.20	0.055	5.20	270	0.028	0.510	0.486	62.0	0.018	0.023	n.r.	12.3	0.017	14.9	2.03	0.060	0.009	5.00	0.008	0.018	0.005	0.012	0.022	0.011	14.4	0.960
J9B-7.d	5.60	4.70	0.210	5.10	268	0.028	0.410	0.562	72.0	0.050	0.045	n.r.	15.0	0.026	16.4	2.35	0.080	0.008	9.90	0.008	0.018	0.005	0.012	0.002	0.001	9.84	0.753
K2-10.d	3.90	3.87	0.440	30.0	338	0.120	0.290	0.820	52.3	0.018	0.080	n.r.	1.13	0.017	31.4	6.71	26.3	0.189	1.58	0.066	0.133	0.150	0.045	0.045	4.E-04	1.61	0.135
K2-11.d	6.10	0.810	0.149	8.75	315	0.131	0.252	0.810	58.6	0.080	0.056	n.r.	0.601	0.007	24.0	8.86	28.9	0.039	0.620	0.390	0.121	0.137	0.095	0.004	2.E-04	2.69	0.100
K2-2.d	4.80	0.710	0.250	17.7	282	0.016	0.320	2.60	50.4	0.021	0.094	n.r.	2.24	0.007	25.8	6.68	25.4	3.20	6.00	0.003	0.250	0.330	1.60	0.066	4.E-04	1.45	0.710
K2-4.d	4.60	1.54	0.179	16.2	369	0.107	0.310	1.15	51.6	0.021	0.173	n.r.	2.12	0.007	30.7	6.12	24.8	2.10	7.50	0.052	0.168	0.171	0.078	0.037	5.E-04	2.53	0.640
K2-5.d	6.90	2.30	0.280	20.7	300	0.070	0.360	2.60	53.5	7.00	0.180	n.r.	1.42	0.007	31.9	5.85	24.1	0.480	3.44	0.210	0.500	0.270	0.226	0.042	0.010	2.07	0.161
K2-6.d	5.50	1.07	0.171	19.6	238	0.091	0.300	0.203	51.7	0.021	0.018	n.r.	0.620	0.007	22.8	6.18	21.7	0.220	0.670	0.003	0.007	0.022	0.040	0.011	6.E-04	7.86	0.469
K2-7.d	5.20	1.71	0.273	20.9	308	0.046	0.265	0.580	54.0	0.021	0.108	n.r.	0.473	0.007	28.6	5.99	24.0	0.069	0.390	0.003	0.097	0.192	0.080	0.024	2.E-04	1.62	0.114
K2-9.d	4.50	1.69	0.100	30.1	309	0.105	0.400	1.32	46.9	0.021	0.018	n.r.	0.800	0.007	30.6	6.38	24.0	0.096	0.710	0.023	0.163	0.320	0.173	0.008	3.E-04	2.44	0.137
M1CCP-01d	157	1.37	0.054	18.6	376	0.075	0.765	0.109	91.5	0.011	0.061	n.r.	3.17	0.006	9.55	2.93	0.029	0.005	0.036	0.016	0.013	0.003	0.009	0.002	0.030	8.37	0.017
M1CCP-02.d	237	1.66	0.111	24.3	401	0.073	0.590	0.270	77.9	0.020	0.037	n.r.	4.30	0.004	14.7	2.08	0.140	0.160	0.028	0.037	0.066	0.440	0.016	0.034	0.044	4.39	0.005
M1CCP-03.d	250	4.20	0.740	246	474	0.067	0.620	0.148	79.9	0.049	0.014	n.r.	4.77	0.004	19.4	1.03	0.213	0.005	0.060	0.003	0.008	0.002	0.057	0.013	0.026	9.10	0.042
M1CCP-04.d	257	2.87	0.041	22.5	291	0.051	0.490	0.157	87.5	0.074	0.075	n.r.	2.84	0.004	9.30	0.783	0.024	0.004	0.029	0.018	0.008	0.002	0.010	4.E-04	0.011	6.50	0.008
M1CCP-05.d	243	3.36	0.130	22.0	261	0.063	0.650	0.530	78.4	0.028	0.016	n.r.	2.71	0.004	6.46	0.923	1.30	0.250	0.028	0.003	0.008	0.011	0.010	0.013	0.026	5.51	2.20
M1CCP-06.d	242	1.03	0.310	38.8	365	0.016	0.920	0.180	130	0.150	0.410	n.r.	3.09	0.004	9.10	0.340	0.034	0.003	0.040	0.137	0.670	0.215	0.028	1.E-03	7.E-04	3.73	0.010
M1CCPr-02.d	57.2	4.60	0.087	25.0	313	0.026	0.690	0.071	87.8	0.014	0.041	n.r.	2.76	0.007	8.40	0.742	0.152	0.005	0.057	0.007	0.023	0.004	0.024	6.E-04	0.051	7.28	0.019
M1CCPr-04.d	63.0	0.448	0.037	20.1	320	0.047	1.43	0.124	197	0.106	0.041	n.r.	3.54	0.016	9.70	0.366	0.038	0.005	0.070	0.230	0.290	0.270	0.057	0.002	0.024	6.50	0.005
M1CCPr-07.d	53.0	1.37	0.029	17.6	255	0.015	1.46	0.098	201	0.106	0.041	n.r.	3.27	0.007	9.20	0.289	0.023	0.004	0.054	0.009	0.018	0.006	0.014	7.E-04	0.017	8.57	0.023
M2CCP-01d	359	7.50	0.035	15.7	370	0.143	1.07	0.094	112	0.009	0.023	n.r.	4.43	0.004	11.6	2.59	0.310	0.006	0.038	0.003	0.015	0.002	0.005	7.E-04	0.034	10.6	0.081
M2CCP-02.d	310	1.09	0.360	15.6	361	0.055	0.580	0.900	94.6	0.009	0.008	n.r.	4.42	0.004	11.2	2.53	0.225	0.030	0.042	0.003	0.008	0.002	0.015	0.150	0.009	4.36	0.007
M2CCP-03.d	367	1.34	0.035	18.1	337	0.099	7.00	3.40	111	0.042	0.008	n.r.	6.12	0.004	14.0	3.30	0.140	0.007	0.510	0.003	0.008	0.002	0.016	7.E-04	0.170	16.9	0.027
M2CCP-04.d	346	2.33	0.340	20.4	374	0.097	0.640	0.116	101	0.022	0.061	n.r.	3.67	0.004	12.0	2.89	0.154	0.004	0.033	0.003	0.194	0.002	0.070	0.036	0.014	3.74	0.011
M2CCP-05.d	344	2.53	0.086	20.9	450	0.090	0.560	0.079	87.6	0.015	0.015	n.r.	3.14	0.004	6.77	2.19	0.380	0.004	0.037	0.003	0.027	0.002	0.005	7.E-04	0.013	4.75	0.035
M2CCP-06.d	360	3.00	0.033	15.9	444	0.127	0.790	2.40	101	1.00	0.008	n.r.	4.09	0.004	13.3	2.73	0.262	0.017	0.147	0.020	0.008	0.002	0.005	0.009	8.E-04	4.23	0.005
M2CCP-07.d	346	1.34	0.061	16.8	486	0.130	0.570	0.131	90.3	0.009	0.008	n.r.	4.12	0.004	12.2	2.55	0.218	0.004	0.380	0.011	0.008	0.002	0.025	0.011	0.046	3.62	0.004
M2CCPr-01d	47.9	1.20	0.032	18.7	297	0.078	0.960	0.086	103	0.013	0.066	n.r.	4.03	0.007	12.1	2.33	0.220	0.005	0.510	0.007	0.018	0.004	0.007	0.001	0.041	5.54	0.004
M2CCPr-02.d	51.5	3.31	0.023	17.9	324	0.119	0.820	0.103	102	0.012	0.048	n.r.	3.99	0.006	11.4	2.34	0.288	0.005	0.040	0.007	0.019	0.004	0.011	0.012	0.036	8.62	0.016
M2CCPr-03.d	48.2	1.09	0.019	16.5	266	0.068	0.940	0.118	99.0	0.106	0.220	n.r.	3.75	0.007	11.4	2.14	0.033	0.005	0.410	0.007	0.025	0.004	0.014	0.001	0.001	4.69	0.004
M2CCPr-06.d	50.3	0.670	0.022	15.2	431	0.010	0.776	0.081	90.0	0.010	0.041	n.r.	3.28	0.005	5.31	1.52	0.018	0.003	0.033	0.007	0.015	0.004	0.060	8.E-04	0.009	3.46	0.004

Grain ID (chalcopyrite)	Ti 49	Mn 55	Co 59	Ni 60	Zn 66	Ga 71	Ge 74	As 75	Se 82	Mo 95	Ru 101	Rh 103	Ag 107	Pd 108	Cd 111	In 115	Sn 118	Sb 121	Te 128	Re 185	Os 189	Ir 193	Pt 195	Au 197	Tl 205	Pb 208	Bi 209
55um	0.553	0.479	0.016	0.207	0.270	0.024	0.079	0.348	2.409	0.029	0.020	0.004	0.049	0.011	0.061	0.007	0.070	0.017	0.221	0.007	0.016	0.004	0.010	0.006	0.004	0.006	0.004
33um	0.661	1.030	0.028	0.410	0.526	0.051	0.149	0.582	5.311	0.030	0.020	0.007	0.100	0.026	0.118	0.012	0.147	0.027	0.501	0.012	0.028	0.007	0.018	0.014	0.007	0.011	0.007
MCR10a-10.d	3.50	1.55	0.078	43.9	177	0.049	0.990	0.260	223	0.019	0.043	n.r.	28.7	0.009	46.0	7.65	173	0.028	2.43	0.003	0.007	0.002	0.009	0.034	0.088	5.10	0.425
MCR10a-11d	5.50	1.95	0.190	52.5	175	0.086	1.28	0.282	213	0.018	0.012	n.r.	30.5	0.009	44.2	7.60	189	0.018	4.03	0.003	0.007	0.002	0.005	0.035	0.116	4.64	0.167
MCR10a-12.d	5.70	1.90	0.104	48.9	185	0.029	0.920	0.374	175	0.018	0.012	n.r.	27.0	0.012	44.9	7.24	192	0.025	1.19	0.003	0.007	0.002	0.005	0.069	0.100	4.30	0.198
MCR10a-13.d	4.70	2.55	0.190	69.4	171	0.036	1.18	0.414	209	0.018	0.012	n.r.	32.6	0.009	45.4	7.28	205	0.044	3.66	0.003	0.007	0.002	0.005	0.027	0.069	3.58	0.140
MCR10a-14.d	4.49	1.54	0.071	51.5	158	0.049	1.11	0.234	199	0.013	0.012	n.r.	29.6	0.009	45.3	6.91	192	0.043	1.77	0.003	0.007	0.002	0.005	0.070	0.061	3.04	0.238
MCR10a-15.d	4.00	1.92	0.079	50.7	192	0.065	1.09	0.304	200	0.018	0.012	n.r.	30.4	0.009	48.1	6.85	211	0.031	2.95	0.003	0.007	0.002	0.009	0.070	0.106	4.80	0.141
MCR10a-16.d	4.10	2.13	0.043	48.2	170	0.056	1.40	0.279	255	0.018	0.012	n.r.	40.2	0.009	46.9	7.17	223	0.035	3.60	0.003	0.007	0.002	0.004	0.007	0.095	4.45	0.105
MCR10a-1b.d	4.90	1.71	0.051	45.8	167	0.084	1.00	0.284	201	0.019	0.013	n.r.	43.1	0.006	51.8	7.20	204	0.064	2.67	0.004	0.011	0.003	0.007	0.015	0.166	3.61	0.130
MCR10a-2.d	6.60	1.60	0.083	56.4	178	0.011	1.07	0.282	189	0.045	0.041	n.r.	37.1	0.006	48.7	7.05	195	0.004	1.83	0.004	0.006	0.003	0.005	0.014	0.095	4.60	0.298
MCR10a-3.d	5.50	2.13	0.112	54.0	162	0.094	1.23	0.299	219	0.019	0.013	n.r.	42.2	0.008	47.5	6.92	226	0.034	5.20	0.004	0.011	0.003	0.006	0.036	0.199	7.40	0.164
MCR10a-4.d	6.40	2.35	0.238	60.4	176	0.074	1.27	0.320	228	0.019	0.013	n.r.	43.7	0.009	52.4	7.03	218	0.008	5.10	0.004	0.011	0.003	0.005	0.030	0.116	9.60	0.271
MCR10a-5.d	7.20	2.30	0.211	57.3	171	0.105	1.17	0.311	235	0.018	0.012	n.r.	42.0	0.009	46.8	6.71	215	0.006	4.60	0.003	0.007	0.002	0.005	0.072	0.128	5.30	0.169
MCR10a-6.d	5.00	2.29	0.064	46.3	167	0.016	1.35	0.384	220	0.018	0.012	n.r.	35.4	0.008	45.2	6.98	174	0.066	2.72	0.003	0.007	0.002	0.007	0.054	0.071	3.74	0.203
MCR10a-7.d	5.20	2.62	0.239	61.4	339	0.043	1.38	0.302	223	0.018	0.051	n.r.	37.8	0.009	68.2	7.04	209	0.040	3.23	0.003	0.007	0.002	0.006	0.057	0.088	5.05	0.170
MCR10a-8.d	4.45	1.86	0.068	48.4	167	0.061	1.17	0.335	193	0.018	0.012	n.r.	32.7	0.009	46.9	7.39	196	0.007	2.86	0.003	0.007	0.002	0.005	0.027	0.383	5.73	0.332
MCR10a-9.d	4.25	1.66	0.106	55.5	162	0.078	1.04	0.291	210	0.018	0.012	n.r.	35.8	0.009	44.8	6.99	207	0.020	2.33	0.003	0.007	0.002	0.005	0.067	0.119	2.87	0.399
MCR10b-1d	4.45	2.38	0.148	58.3	173	0.096	1.33	0.320	236	0.018	0.012	n.r.	38.4	0.009	47.4	7.31	218	0.026	3.90	0.003	0.007	0.002	0.004	0.007	0.214	4.55	0.208
MCR10b-10.d	4.20	0.990	0.064	34.9	178	0.134	0.660	0.580	140	0.018	0.012	n.r.	26.9	0.009	41.6	10.5	271	0.022	6.16	0.003	0.007	0.002	0.005	0.183	0.180	3.91	0.358
MCR10b-11d	5.00	0.227	0.057	26.6	172	0.058	0.870	0.299	143	0.018	0.012	n.r.	21.2	0.009	41.1	10.9	240	0.016	4.68	0.003	0.007	0.002	0.005	0.027	0.121	4.01	0.367
MCR10b-2.d	2.30	2.17	0.111	51.7	165	0.054	1.19	0.291	207	0.018	0.012	n.r.	35.7	0.021	45.2	7.16	189	0.041	2.95	0.003	0.007	0.002	0.005	0.038	0.098	2.95	0.321
MCR10b-3.d	4.00	2.19	0.152	58.1	161	0.088	1.14	0.248	204	0.018	0.012	n.r.	34.6	0.009	41.0	7.61	200	0.021	2.76	0.005	0.007	0.002	0.005	0.008	0.113	2.27	0.175
MCR10b-4.d	6.10	2.08	0.044	41.3	189	0.054	1.21	0.293	224	0.018	0.025	n.r.	41.9	0.009	53.6	7.83	154	0.032	6.11	0.003	0.007	0.002	0.005	0.057	0.103	5.94	0.196
MCR10b-5.d	4.80	3.11	0.158	61.9	174	0.059	1.23	0.192	207	0.018	0.034	n.r.	38.2	0.009	46.6	8.10	182	0.006	3.80	0.003	0.007	0.002	0.005	0.020	0.276	4.44	0.217
MCR10b-6.d	3.85	0.765	0.160	38.8	162	0.040	0.985	0.339	173	0.043	0.012	n.r.	24.8	0.009	42.0	9.40	208	0.004	2.97	0.006	0.007	0.002	0.008	0.070	0.356	3.01	0.405
MCR10b-7.d	4.50	1.03	0.111	29.9	163	0.031	0.805	0.301	163	0.018	0.012	n.r.	21.3	0.009	41.0	13.3	151	0.017	1.84	0.003	0.008	0.002	0.005	0.037	0.092	3.79	0.260
MCR10b-9.d	3.80	0.204	0.070	25.2	211	0.103	0.670	0.262	141	0.018	0.012	n.r.	17.9	0.009	46.8	11.8	240	0.029	0.680	0.003	0.007	0.002	0.005	0.101	0.061	3.37	0.203
MCR13-1d	4.10	0.199	0.413	52.6	160	0.056	0.770	0.313	155	0.018	0.012	n.r.	21.8	0.009	18.1	9.49	64.9	0.025	4.30	0.003	0.007	0.002	0.005	0.011	0.014	3.88	0.120
MCR13-11d	3.30	0.192	0.199	45.5	157	0.050	0.780	0.221	139	0.016	0.012	n.r.	15.7	0.009	19.1	11.6	64.6	0.040	3.12	0.003	0.007	0.002	0.004	0.031	0.107	10.5	0.456
MCR13-11b.d	4.10	0.460	0.340	51.9	188	0.028	0.710	0.212	152	0.018	0.012	n.r.	19.6	0.008	21.2	10.9	62.1	0.005	4.55	0.003	0.007	0.002	0.006	0.036	0.011	3.69	0.291
MCR13-13.d	3.50	0.155	0.095	44.4	157	0.097	0.740	0.152	138	0.018	0.012	n.r.	17.2	0.009	19.6	10.4	68.9	0.005	2.73	0.004	0.007	0.002	0.007	0.019	0.055	11.4	0.586
MCR13-2.d	5.30	0.550	0.172	46.9	151	0.010	0.920	0.249	162	0.018	0.012	n.r.	24.1	0.009	19.8	9.72	67.8	0.066	5.10	0.003	0.007	0.002	0.005	0.007	0.009	5.40	0.291
MCR13-3.d	2.70	0.209	0.212	50.2	176	0.086	0.810	0.233	139	0.018	0.012	n.r.	21.2	0.009	19.7	10.0	69.8	0.046	3.67	0.003	0.007	0.002	0.005	0.011	0.023	8.29	0.184
MCR13-4.d	3.50	1.21	0.120	45.2	149	0.008	0.540	0.279	144	0.018	0.012	n.r.	22.4	0.009	18.1	9.40	64.2	0.004	2.15	0.003	0.011	0.002	0.022	0.015	5.E-04	5.40	0.313
MCR13-5.d	4.00	0.166	0.234	41.6	140	0.170	0.600	0.360	122	0.018	0.023	n.r.	17.4	0.009	17.3	10.9	65.0	0.029	3.45	0.003	0.007	0.002	0.007	0.092	0.003	3.07	0.271
MCR13-6.d	4.60	0.217	0.261	46.5	146	0.100	0.580	0.259	116	0.018	0.023	n.r.	16.8	0.009	17.6	10.6	64.6	0.110	3.21	0.003	0.007	0.002	0.005	0.055	0.013	3.72	0.323
MCR13-7.d	3.60	0.159	0.181	49.2	162	0.049	0.600	0.188	133	0.018	0.012	n.r.	19.3	0.009	20.3	11.1	71.6	0.019	4.29	0.003	0.007	0.002	0.005	0.029	0.012	6.58	0.259
MCR13-8.d	5.90	0.213	0.370	52.1	159	0.148	0.840	0.227	145	0.018	0.035	n.r.	21.2	0.008	19.4	11.8	69.7	0.029	5.65	0.003	0.007	0.002	0.005	0.050	0.017	6.58	0.264

Grain ID (chalcopyrite)	Ti 49	Mn 55	Co 59	Ni 60	Zn 66	Ga 71	Ge 74	As 75	Se 82	Mo 95	Ru 101	Rh 103	Ag 107	Pd 108	Cd 111	In 115	Sn 118	Sb 121	Te 128	Re 185	Os 189	Ir 193	Pt 195	Au 197	Tl 205	Pb 208	Bi 209
55um	0.553	0.479	0.016	0.207	0.270	0.024	0.079	0.348	2.409	0.029	0.020	0.004	0.049	0.011	0.061	0.007	0.070	0.017	0.221	0.007	0.016	0.004	0.010	0.006	0.004	0.006	0.004
33um	0.661	1.030	0.028	0.410	0.526	0.051	0.149	0.582	5.311	0.030	0.020	0.007	0.100	0.026	0.118	0.012	0.147	0.027	0.501	0.012	0.028	0.007	0.018	0.014	0.007	0.011	0.007
MCR13-9.d	5.20	0.203	0.280	49.1	157	0.125	0.850	0.242	151	0.018	0.012	n.r.	22.4	0.009	18.5	12.4	73.7	0.039	5.50	0.003	0.007	0.002	0.270	0.069	0.011	4.63	0.283
MCR3CCP-01d	381	2.14	0.400	51.3	520	0.160	0.390	0.170	60.0	0.878	0.022	n.r.	0.670	0.013	11.1	4.60	13.4	0.060	0.031	0.006	0.019	0.006	0.011	0.004	4.E-04	1.52	0.130
MCR3CCP-03.d	351	1.86	0.290	46.4	427	0.110	0.434	0.325	50.3	0.026	0.440	n.r.	0.894	0.013	10.2	4.89	11.7	0.004	0.035	0.006	0.019	0.007	0.011	0.110	4.E-04	1.76	0.131
MCR3CCP-04.d	378	2.18	0.420	50.6	481	0.067	0.640	0.107	57.8	0.020	0.022	n.r.	0.710	0.007	10.3	4.76	13.6	0.005	0.035	0.460	0.019	0.004	0.012	0.001	4.E-04	1.95	0.129
MCR3CCP-05.d	389	1.91	0.028	41.5	491	0.028	0.400	0.117	59.7	0.412	0.022	n.r.	2.60	0.013	10.0	4.91	12.7	0.039	0.033	0.700	0.021	0.006	0.011	0.001	5.E-04	2.61	0.258
MCR3CCPr-01d	46.3	2.58	0.540	68.6	459	0.046	0.414	0.060	61.5	0.107	0.041	n.r.	2.07	0.117	9.79	3.71	11.4	0.003	0.036	0.012	0.045	0.011	0.009	0.003	6.E-04	2.35	0.133
MCR3CCPr-03.d	43.3	1.66	0.261	48.4	427	0.082	0.380	0.102	51.7	0.023	0.027	n.r.	0.590	0.008	10.4	3.97	11.7	0.002	0.055	0.012	0.045	0.011	0.021	0.002	4.E-04	1.86	0.220
MCR3CCPr-04.d	41.1	1.33	0.278	47.5	390	0.067	0.390	0.069	52.5	0.013	0.068	n.r.	0.810	0.117	8.12	4.40	11.7	0.005	0.039	0.013	0.045	0.005	0.023	0.001	6.E-04	2.41	0.236
MCR3CCPr-05.d	44.9	1.58	0.292	48.9	432	0.034	0.350	0.094	53.3	0.014	0.056	n.r.	0.840	0.007	9.94	4.47	12.6	0.003	0.045	0.012	0.045	0.005	0.016	0.002	3.E-04	1.40	0.086
MCR4b-10.d	5.00	0.800	0.270	48.3	350	0.044	0.280	0.243	48.0	0.018	0.030	n.r.	0.840	0.009	6.02	4.32	5.49	0.035	0.046	0.003	0.007	0.002	0.029	3.E-04	1.E-04	0.500	0.032
MCR4b-12.d	4.10	0.167	0.142	44.1	366	0.045	0.230	0.353	53.3	0.018	0.012	n.r.	0.700	0.009	6.20	4.32	5.67	0.029	0.220	0.003	0.007	0.002	0.038	3.E-04	2.E-04	1.22	0.087
MCR4b-2.d	4.30	0.580	0.131	47.3	284	0.034	0.200	0.400	51.5	0.020	0.029	n.r.	0.900	0.009	4.43	5.48	7.30	0.027	0.220	0.100	0.007	0.002	0.005	4.E-04	0.005	5.50	0.133
MCR4b-3.d	4.00	0.790	0.124	38.0	337	0.087	0.281	0.241	54.2	0.380	0.012	n.r.	0.840	0.009	5.19	3.83	5.29	0.026	0.039	0.018	0.007	0.002	0.005	3.E-04	2.E-04	1.55	0.066
MCR4b-4.d	4.30	0.680	0.155	46.0	363	0.073	0.420	0.800	63.5	0.018	0.012	n.r.	0.910	0.009	5.60	4.95	6.34	0.031	0.067	0.003	0.007	0.002	0.005	4.E-04	3.E-04	0.830	0.093
MCR4b-7.d	3.90	1.16	0.247	47.9	328	0.023	0.370	0.304	59.7	0.018	0.012	n.r.	0.880	0.009	6.60	3.16	3.68	0.028	0.330	0.003	0.007	0.002	0.005	4.E-04	2.E-04	0.730	0.077
MCR4b-9.d	4.30	0.450	0.089	42.4	331	0.072	0.280	0.180	55.0	0.018	0.012	n.r.	0.800	0.013	5.30	3.15	4.05	0.036	0.047	0.003	0.007	0.002	0.004	5.E-04	3.E-04	3.72	0.124
MCR5-10.d	4.00	0.940	0.600	71.6	341	0.010	0.350	0.243	84.3	0.024	0.018	n.r.	1.40	0.007	9.10	8.05	44.9	0.014	0.059	0.003	0.007	0.002	0.012	6.E-04	3.E-04	1.99	0.270
MCR5-2.d	2.40	0.780	0.300	59.7	382	0.068	0.430	0.249	67.7	0.024	0.018	n.r.	1.15	0.007	7.79	9.69	58.0	0.003	0.091	0.003	0.007	0.002	0.004	0.001	4.E-04	3.28	0.263
MCR5-4.d	5.10	0.168	0.362	59.4	367	0.053	0.620	0.200	77.4	0.024	0.018	n.r.	1.38	0.009	8.68	9.20	44.4	0.002	0.054	0.003	0.007	0.002	0.005	9.E-04	4.E-04	3.43	0.310
MCR5-5.d	5.20	0.910	1.29	80.0	417	0.062	0.350	0.260	88.8	0.024	0.018	n.r.	1.92	0.007	11.6	8.53	51.2	0.002	0.064	0.003	0.007	0.002	0.008	0.012	3.E-04	2.57	0.338
MCR5-8.d	3.90	1.02	1.00	75.2	356	0.085	0.560	0.179	87.2	0.024	0.018	n.r.	1.50	0.007	9.33	7.08	47.7	0.003	0.059	0.003	0.007	0.002	0.004	7.E-04	0.004	3.03	0.215
MR2CCP-01d	208	0.980	0.057	21.5	274	0.030	2.50	0.639	198	0.051	0.070	n.r.	4.56	0.017	5.57	0.601	0.147	0.003	0.042	0.008	0.016	0.004	0.012	8.E-04	7.E-04	3.97	0.024
MR2CCP-02.d	217	3.30	0.120	27.3	224	0.046	1.59	0.325	221	0.780	0.620	n.r.	4.99	0.017	6.45	0.599	0.365	0.018	0.054	0.710	1.19	1.32	11.0	0.026	0.038	5.94	0.320
MR2CCP-05.d	230	1.55	0.350	52.7	237	0.017	0.970	0.102	161	0.051	0.035	n.r.	2.78	0.038	6.70	1.84	0.360	0.180	0.370	0.010	0.016	0.046	0.640	0.001	0.056	16.8	0.051
MR2CCP-06.d	214	0.690	0.580	57.0	309	0.017	1.37	0.200	155	0.219	1.92	n.r.	2.37	0.017	8.40	1.82	0.053	0.006	0.070	0.017	1.51	0.580	0.243	0.001	0.010	3.13	0.047
MR2CCPr-01d	57.2	0.710	0.037	21.9	276	0.011	1.64	0.097	218	0.106	0.117	n.r.	4.37	0.007	4.93	0.624	0.350	0.019	0.056	0.027	0.043	0.118	0.014	0.001	0.001	5.04	0.048
MR2CCPr-02.d	59.1	0.880	0.031	21.6	207	0.051	2.04	0.170	251	0.106	0.069	n.r.	3.96	0.007	4.17	0.586	0.380	0.004	0.056	0.137	0.280	0.250	0.053	0.001	0.001	3.66	0.055
MR2CCPr-03.d	52.2	4.10	0.067	32.6	264	0.097	0.790	0.077	87.8	0.106	0.041	n.r.	1.93	0.005	7.89	2.88	0.496	0.004	0.030	0.006	0.017	0.004	0.025	5.E-04	9.E-04	2.52	0.009
MR2CCPr-04.d	55.5	0.243	0.021	22.0	270	0.184	0.620	0.105	89.4	0.024	0.090	n.r.	1.38	0.007	5.30	9.13	0.171	0.005	0.039	0.007	0.045	0.004	0.013	6.E-04	9.E-04	5.00	0.005
MR2CCPr-05.d	55.4	1.27	0.045	20.2	264	0.158	0.780	0.098	98.5	0.022	0.041	n.r.	1.57	0.007	4.51	8.80	0.590	0.005	0.042	0.007	0.042	0.004	0.013	6.E-04	7.E-04	3.93	0.004
MS10-1d	3.50	6.30	0.180	10.6	425	0.016	0.370	0.639	66.3	2.20	0.018	n.r.	2.27	0.007	17.8	5.03	6.90	0.310	1.81	0.250	0.012	0.023	0.012	0.002	0.056	2.44	0.092
MS10-2.d	4.20	0.381	0.260	15.7	353	0.010	0.140	0.890	60.4	1.40	0.018	n.r.	1.81	0.007	19.0	3.43	2.55	0.700	1.04	0.018	0.021	0.034	0.015	0.001	0.062	5.30	0.370
MS10-3.d	5.00	2.50	0.058	11.5	346	0.011	0.520	0.581	66.7	0.024	0.018	n.r.	1.40	0.007	17.8	2.71	0.230	0.034	0.107	0.003	0.007	0.002	0.010	0.023	3.E-04	0.401	0.040
MS10-4.d	3.10	0.365	0.230	15.6	330	0.009	0.081	0.494	57.2	1.43	0.080	n.r.	0.690	0.007	18.9	2.85	0.820	0.390	1.60	0.037	0.031	0.028	0.009	9.E-04	0.023	4.68	0.187
MS10-5.d	3.20	0.379	0.160	18.2	378	0.012	0.360	0.540	63.0	0.700	0.018	n.r.	0.830	0.007	20.5	3.58	5.18	0.340	1.16	0.022	0.007	0.002	0.018	7.E-04	0.009	2.90	0.150
MS10-6.d	1.90	0.447	0.118	14.5	414	0.009	0.450	0.545	67.0	0.670	0.018	n.r.	1.28	0.007	23.2	2.89	1.25	0.510	1.41	0.007	0.007	0.002	0.016	0.002	0.025	2.87	0.187
MS10-7.d	5.00	1.46	0.031	14.7	353	0.010	0.490	0.598	63.9	0.024	0.062	n.r.	1.18	0.007	19.8	3.81	4.92	0.170	1.09	0.003	0.018	0.002	0.017	6.E-04	0.008	1.22	0.064

Grain ID (chalcopyrite)	Ti 49	Mn 55	Co 59	Ni 60	Zn 66	Ga 71	Ge 74	As 75	Se 82	Mo 95	Ru 101	Rh 103	Ag 107	Pd 108	Cd 111	In 115	Sn 118	Sb 121	Te 128	Re 185	Os 189	Ir 193	Pt 195	Au 197	Tl 205	Pb 208	Bi 209
55um	0.553	0.479	0.016	0.207	0.270	0.024	0.079	0.348	2.409	0.029	0.020	0.004	0.049	0.011	0.061	0.007	0.070	0.017	0.221	0.007	0.016	0.004	0.010	0.006	0.004	0.006	0.004
33um	0.661	1.030	0.028	0.410	0.526	0.051	0.149	0.582	5.311	0.030	0.020	0.007	0.100	0.026	0.118	0.012	0.147	0.027	0.501	0.012	0.028	0.007	0.018	0.014	0.007	0.011	0.007
MS12-2.d	5.40	0.352	0.110	26.2	297	0.023	0.118	0.325	61.0	0.800	0.011	n.r.	0.170	0.017	18.2	4.45	9.80	0.220	1.28	0.031	0.018	0.005	0.044	0.015	5.E-04	2.69	0.139
MS12-4.d	5.90	6.90	0.100	22.8	241	0.032	0.135	0.810	41.0	0.740	0.011	n.r.	2.04	0.028	18.0	3.87	9.18	1.37	1.35	0.050	0.018	0.010	0.055	0.002	0.188	34.2	1.32
MS12-6.d	3.10	2.40	0.082	25.0	270	0.014	0.250	0.644	34.0	0.310	0.011	n.r.	0.290	0.017	15.8	3.53	10.5	0.390	0.136	0.030	0.018	0.005	0.012	0.001	0.056	10.6	0.750
MS12-7.d	5.20	13.9	0.116	20.0	279	0.015	0.113	0.610	45.0	0.170	0.011	n.r.	0.450	0.017	17.6	3.50	11.1	0.610	0.141	0.030	0.016	0.005	0.170	0.001	0.051	8.50	0.490
MS12-8.d	5.10	47.0	0.136	21.4	272	0.035	0.490	0.800	46.0	0.700	0.011	n.r.	0.820	0.017	19.3	4.35	7.19	0.810	1.20	0.026	0.018	0.005	0.078	0.001	0.095	22.0	0.860
MS2-1d	4.20	0.561	3.37	444	293	0.015	0.150	0.486	56.0	0.018	0.011	n.r.	2.35	0.017	54.2	1.61	1.67	0.750	0.660	0.008	0.018	0.004	0.011	0.104	0.069	20.7	4.90
MS2-2.d	3.00	2.30	0.150	30.0	301	0.014	0.230	0.325	66.0	0.018	0.011	n.r.	2.28	0.017	44.4	2.07	1.99	0.440	0.118	0.008	0.018	0.005	0.014	0.050	0.014	12.7	2.73
MS2-3.d	4.30	0.500	0.870	129	333	0.019	0.310	0.609	52.0	0.018	0.043	n.r.	1.79	0.017	60.4	2.21	1.85	0.470	0.146	0.008	0.017	0.005	0.500	0.068	0.038	3.64	1.05
MS2-4.d	3.40	1.66	0.011	9.30	315	0.019	0.240	0.325	55.0	0.018	0.080	n.r.	2.51	0.017	52.5	3.03	1.62	0.440	0.830	0.008	0.018	0.005	0.027	0.099	0.009	6.90	2.40
MS2-5.d	5.10	5.60	0.080	10.2	291	0.024	0.250	0.325	52.0	0.018	0.060	n.r.	3.30	0.017	43.0	3.16	1.88	0.880	0.730	0.008	0.018	0.005	0.016	0.030	0.048	21.9	4.77
MS2-6.d	4.20	2.30	0.200	25.0	311	0.023	0.380	0.499	49.0	0.018	0.011	n.r.	2.33	0.017	48.8	3.56	2.00	0.460	0.980	0.008	0.018	0.005	0.019	0.064	0.001	11.1	3.17
MS2-7.d	2.70	1.47	0.580	57.0	334	0.017	0.310	0.518	56.3	0.018	0.011	n.r.	2.52	0.017	65.0	3.46	2.05	0.470	1.08	0.008	0.018	0.005	0.016	0.114	0.026	5.10	1.56
MS3-2.d	4.30	0.464	0.580	84.0	318	0.018	0.260	0.502	51.7	0.018	0.027	n.r.	1.83	0.017	57.4	3.86	1.59	0.280	0.620	0.008	0.018	0.005	0.012	0.080	0.013	5.34	1.26
MS3-4.d	5.80	1.80	1.09	157	306	0.023	0.390	0.418	58.0	0.018	0.011	n.r.	2.56	0.017	40.7	3.84	1.98	1.23	0.670	0.008	0.018	0.005	0.044	0.075	0.033	22.3	6.00
MS3-5.d	1.40	0.667	0.230	20.0	305	0.015	0.330	0.325	55.6	0.018	0.160	n.r.	2.63	0.017	38.4	2.84	1.62	0.440	0.298	0.010	0.030	0.005	0.031	0.051	0.002	16.7	6.50
MS3-6.d	8.00	3.00	0.067	10.1	304	0.023	0.330	0.603	55.4	0.018	0.011	n.r.	2.13	0.017	47.9	3.72	2.40	0.380	0.700	0.008	0.018	0.005	0.019	0.102	0.001	3.40	1.02
MS8-2.d	5.95	3.01	0.430	14.0	366	0.080	0.385	0.790	47.4	2.62	0.013	n.r.	2.53	0.017	22.8	4.36	7.13	0.670	1.04	0.196	0.020	0.023	0.011	8.E-04	0.040	4.49	0.254
MS8-4.d	4.90	3.50	0.240	20.6	259	0.014	0.100	0.306	37.6	4.00	0.071	n.r.	4.61	0.017	17.9	5.45	5.72	1.97	1.37	0.140	0.020	0.005	0.011	0.002	0.103	16.5	1.15
MS8-5.d	4.70	4.29	0.340	8.16	323	0.039	0.300	0.650	41.8	5.80	0.032	n.r.	3.11	0.007	23.5	7.79	6.55	2.23	1.10	0.410	0.020	0.033	0.011	0.002	0.045	16.2	0.870
MS8-6.d	5.60	0.176	0.156	23.6	462	0.009	0.160	0.258	22.9	0.020	0.013	n.r.	1.20	0.017	25.5	2.02	4.36	0.537	0.052	0.008	0.020	0.005	0.004	4.E-04	0.010	2.96	0.119
MS8-7.d	4.80	0.480	0.056	30.5	415	0.010	0.280	0.286	68.4	0.020	0.013	n.r.	1.92	0.017	25.0	2.03	6.25	0.071	0.490	0.008	0.020	0.005	0.011	4.E-04	6.E-04	0.900	0.035
MS8-8.d	4.80	0.130	0.030	22.7	460	0.008	0.310	0.254	61.0	0.020	0.013	n.r.	2.22	0.017	25.1	2.49	4.38	0.050	0.300	0.008	0.020	0.005	0.003	5.E-04	2.E-04	0.394	0.024
MS8-9.d	4.10	0.660	0.118	25.5	471	0.011	0.224	0.184	36.8	0.020	0.013	n.r.	1.76	0.017	26.9	2.09	3.64	0.097	0.230	0.008	0.020	0.005	0.004	3.E-04	3.E-04	0.510	0.025
MXNW-01-51-10.d	3.70	4.42	0.520	10.6	302	0.074	0.410	0.272	69.7	0.020	0.013	n.r.	4.06	0.017	14.2	2.54	17.0	0.003	1.13	0.004	0.020	0.005	0.011	0.069	3.E-04	1.54	0.044
MXNW-01-51-11.d	3.90	7.02	0.115	6.53	335	0.052	0.470	0.240	75.1	0.020	0.013	n.r.	17.3	0.007	13.2	2.62	19.0	0.014	7.39	0.003	0.007	0.005	0.077	0.046	0.015	1.58	0.068
MXNW-03-51-1.d	4.70	27.0	0.306	12.6	355	0.067	0.300	0.230	75.2	0.020	0.013	n.r.	4.90	0.007	15.7	2.49	28.0	0.005	1.77	0.008	0.020	0.005	0.012	0.047	3.E-04	1.09	0.050
MXNW-03-51-2.d	5.70	2.04	0.240	8.00	330	0.011	0.380	0.281	72.6	0.020	0.013	n.r.	4.16	0.017	14.7	2.43	19.5	0.002	3.61	0.008	0.020	0.005	0.011	0.062	3.E-04	1.47	0.042
MXNW-03-51-4.d	4.80	3.98	0.182	9.30	278	0.030	0.370	0.307	73.3	0.020	0.034	n.r.	9.70	0.017	12.9	2.71	19.1	0.003	5.97	0.008	0.020	0.005	0.039	0.147	0.022	1.44	0.075
MXNW-03-51-5.d	5.80	21.1	0.089	8.03	338	0.058	0.490	0.240	74.5	0.020	0.013	n.r.	11.7	0.007	15.3	2.56	18.2	0.006	5.79	0.008	0.020	0.005	0.077	0.057	0.001	1.47	0.076
MXNW-03-51-6.d	5.10	3.59	0.530	8.04	306	0.027	0.430	0.152	73.0	0.080	0.079	n.r.	2.27	0.007	14.4	2.66	16.1	0.010	0.850	0.031	0.058	0.007	0.011	0.077	0.001	3.56	0.043
NR6-1d	3.80	0.257	0.590	85.0	383	0.060	0.250	0.238	37.8	0.014	0.012	n.r.	4.62	0.007	20.8	0.805	0.085	0.021	0.490	0.005	0.011	0.003	0.280	8.E-04	0.033	45.7	0.400
NR6-2.d	4.30	2.56	0.560	49.3	472	0.042	0.264	0.209	38.9	0.014	0.012	n.r.	2.87	0.007	19.2	0.558	0.141	0.025	0.610	0.005	0.011	0.003	0.052	3.E-04	0.031	11.8	0.076
NR6-6.d	2.80	3.16	0.640	58.0	287	0.048	0.216	0.195	36.2	0.014	0.012	n.r.	2.70	0.007	11.5	3.90	0.520	0.025	0.560	0.003	0.011	0.003	0.076	6.E-04	0.066	13.7	0.156
NR6-7.d	3.30	0.600	1.50	59.0	258	0.029	0.270	0.259	35.6	0.014	0.012	n.r.	2.61	0.007	10.0	1.67	0.347	0.004	0.450	0.005	0.011	0.002	0.096	0.011	0.046	20.7	0.159
NR6-8.d	3.40	0.550	0.478	46.4	283	0.038	0.232	0.148	34.2	0.014	0.012	n.r.	2.97	0.007	13.1	0.384	0.078	0.016	0.710	0.005	0.011	0.003	0.029	5.E-04	0.009	11.4	0.064
OVOID-1d	4.30	0.180	0.147	2.48	162	0.043	0.370	0.214	64.3	0.021	0.018	n.r.	2.57	0.007	10.1	2.25	3.06	0.003	9.52	0.003	0.007	0.002	0.004	6.E-04	5.E-04	10.2	0.057
OVOID-2.d	4.10	0.227	0.310	7.30	270	0.013	0.270	0.214	54.3	0.059	0.018	n.r.	1.24	0.007	14.3	1.25	2.49	0.005	1.13	0.037	0.008	0.002	0.007	4.E-04	4.E-04	24.4	0.044

Grain ID (chalcopyrite)	Ti 49	Mn 55	Co 59	Ni 60	Zn 66	Ga 71	Ge 74	As 75	Se 82	Mo 95	Ru 101	Rh 103	Ag 107	Pd 108	Cd 111	In 115	Sn 118	Sb 121	Te 128	Re 185	Os 189	Ir 193	Pt 195	Au 197	Tl 205	Pb 208	Bi 209
55um	0.553	0.479	0.016	0.207	0.270	0.024	0.079	0.348	2.409	0.029	0.020	0.004	0.049	0.011	0.061	0.007	0.070	0.017	0.221	0.007	0.016	0.004	0.010	0.006	0.004	0.006	0.004
33um	0.661	1.030	0.028	0.410	0.526	0.051	0.149	0.582	5.311	0.030	0.020	0.007	0.100	0.026	0.118	0.012	0.147	0.027	0.501	0.012	0.028	0.007	0.018	0.014	0.007	0.011	0.007
OVOID-3.d	2.70	0.188	0.240	8.20	179	0.011	0.320	0.220	66.9	0.021	0.018	n.r.	2.53	0.007	7.80	1.84	2.60	0.003	11.3	0.003	0.007	0.002	0.004	4.E-04	6.E-04	7.32	0.027
OVOID-4.d	4.00	0.202	0.106	4.10	138	0.011	0.410	0.192	67.6	0.021	0.018	n.r.	3.92	0.007	10.5	1.50	3.23	0.004	15.1	0.003	0.007	0.002	0.004	0.013	6.E-04	13.7	0.086
OVOID-5.d	3.80	0.173	0.156	4.41	189	0.026	0.420	0.195	69.2	0.021	0.018	n.r.	2.57	0.007	11.2	2.17	3.77	0.002	9.07	0.003	0.007	0.002	0.004	0.010	4.E-04	14.3	0.075
OVOID-6.d	4.30	0.152	0.480	16.7	180	0.008	0.320	0.165	66.5	0.021	0.018	n.r.	1.65	0.007	10.1	2.18	3.78	0.018	5.88	0.004	0.007	0.002	0.004	4.E-04	4.E-04	9.76	0.038
OVOID-8.d	3.30	0.167	0.099	1.96	180	0.010	0.310	0.189	62.5	0.021	0.042	n.r.	2.56	0.007	10.5	1.55	2.26	0.004	10.5	0.003	0.007	0.002	0.012	0.006	4.E-04	9.19	0.114
RX162CCP-01d	233	2.30	0.110	15.0	267	0.049	1.40	0.220	196	0.009	0.008	n.r.	20.8	0.004	40.3	16.9	162	0.010	6.94	0.003	0.008	0.012	0.005	0.001	0.047	7.39	0.294
RX162CCP-02.d	209	3.36	0.069	16.8	255	0.021	1.27	0.151	186	0.009	0.020	n.r.	21.4	0.004	38.6	14.2	144	0.370	6.40	0.531	0.210	0.002	0.005	0.001	0.090	9.61	0.233
RX162CCP-03.d	222	4.36	0.117	17.9	268	0.046	1.55	0.083	211	0.359	0.150	n.r.	17.4	0.004	38.5	11.6	129	0.390	5.30	0.467	0.194	0.380	0.500	0.015	0.071	5.72	0.332
RX162CCP-04.d	235	10.2	0.032	19.4	262	0.068	1.73	4.20	199	0.065	0.020	n.r.	19.2	0.007	38.7	14.8	165	0.006	3.31	0.008	0.008	0.173	0.005	0.040	2.05	13.7	0.228
RX162CCP-05.d	215	13.6	0.064	17.5	272	0.082	1.33	0.106	215	0.022	0.025	n.r.	43.1	0.004	40.9	14.0	183	0.009	18.1	0.003	0.070	0.002	0.005	0.015	1.72	92.6	0.288
RX164-1d	4.80	0.351	0.100	37.5	100	0.012	0.520	0.316	99.0	0.024	0.040	n.r.	14.2	0.015	31.2	6.42	158	0.004	0.288	0.005	0.007	0.002	0.004	0.011	0.026	13.6	0.210
RX164-10.d	5.30	0.175	0.060	37.3	146	0.060	1.05	0.170	161	0.024	0.018	n.r.	14.8	0.007	39.9	5.81	145	0.004	2.50	0.007	0.007	0.002	0.004	0.091	0.072	10.5	0.386
RX164-2.d	4.70	0.790	0.123	39.6	123	0.128	0.840	0.224	134	0.024	0.034	n.r.	19.9	0.007	35.7	6.58	175	0.004	1.47	0.005	0.012	0.002	0.008	0.020	0.038	10.5	0.192
RX164-3.d	3.50	0.270	0.263	39.5	137	0.052	0.800	0.200	112	0.024	0.018	n.r.	24.1	0.007	33.7	6.77	142	0.003	3.70	0.005	0.009	0.002	0.006	0.033	0.016	2.91	0.092
RX164-4.d	3.20	0.730	0.290	40.8	153	0.041	1.01	0.164	131	0.024	0.018	n.r.	25.5	0.009	41.2	6.31	213	0.003	2.04	0.003	0.007	0.002	0.005	0.022	0.017	4.11	0.161
RX164-5.d	5.00	0.266	0.280	36.7	138	0.056	1.09	0.175	138	0.024	0.018	n.r.	24.6	0.007	40.9	6.33	118	0.005	3.55	0.003	0.007	0.002	0.009	0.047	0.050	5.83	0.106
RX164-6.d	6.20	0.870	0.036	41.2	193	0.076	1.24	0.183	135	0.021	0.031	n.r.	24.7	0.007	43.7	6.34	206	0.100	4.17	0.003	0.007	0.002	0.004	0.013	0.045	6.86	0.190
RX164-7.d	5.90	0.214	0.207	44.5	156	0.011	0.830	0.202	145	0.024	0.018	n.r.	17.0	0.007	36.2	5.55	165	0.003	1.59	0.003	0.007	0.002	0.005	0.060	0.017	3.02	0.113
RX164-8.d	3.80	0.226	0.183	44.5	177	0.076	1.05	0.242	168	0.024	0.018	n.r.	19.5	0.009	41.9	6.12	201	0.003	1.39	0.005	0.008	0.002	0.009	0.102	0.005	6.60	0.224
RX164-9.d	4.10	0.229	0.053	39.0	172	0.106	1.21	0.241	172	0.024	0.018	n.r.	13.6	0.009	42.7	5.97	165	0.003	2.23	0.005	0.008	0.002	0.008	0.126	0.031	11.1	0.275
ST12CCP-01d	384	4.29	0.292	5.71	401	0.059	1.49	1.20	211	0.018	0.095	n.r.	1.25	0.013	0.740	0.014	0.180	0.003	0.035	0.007	0.130	0.548	0.014	7.E-04	0.040	1.86	0.003
ST12CCPr-01d	238	4.74	0.229	10.8	278	0.016	2.98	0.139	216	0.052	0.112	n.r.	1.23	0.011	0.800	0.007	0.036	0.008	0.036	0.027	0.042	0.015	0.033	0.001	6.E-04	2.04	0.005
ST12CCPr-02.d	235	2.50	0.410	10.9	430	0.100	1.80	0.300	177	0.136	0.144	n.r.	1.82	0.226	0.285	0.013	0.073	0.010	0.092	0.027	0.057	0.015	0.057	0.002	7.E-04	1.23	0.010
T10TCCP-01d	364	0.488	0.530	29.8	355	0.014	1.24	0.208	159	0.180	0.044	n.r.	8.30	0.034	1.85	0.329	0.271	0.012	0.101	0.016	0.031	0.015	0.014	2.30	0.020	16.1	0.037
T10TCCP-02.d	395	0.566	0.550	19.9	349	0.067	1.54	0.253	162	0.046	0.095	n.r.	21.6	0.013	2.20	0.689	0.053	0.086	0.062	0.033	0.031	0.012	0.014	0.002	0.091	25.9	0.300
T10TCCP-03.d	350	17.0	0.465	31.3	464	0.053	1.46	0.330	165	0.046	0.095	n.r.	8.77	0.013	2.98	0.343	0.049	0.039	0.087	0.007	0.031	0.012	0.014	0.002	0.034	10.7	0.005
T10TCCP-04.d	356	0.447	0.280	11.7	373	2.70	0.920	0.214	149	0.101	0.190	n.r.	21.9	0.013	1.66	0.292	0.058	0.043	0.054	0.012	0.031	0.180	0.014	0.001	0.172	9.96	0.010
T10TCCPr-01d	247	2.74	0.382	33.1	245	0.128	2.18	0.125	189	0.027	0.105	n.r.	8.30	0.011	1.42	0.269	0.029	0.010	0.052	0.027	0.057	0.005	0.033	0.001	0.147	10.2	0.005
T10TCCPr-02.d	252	0.601	0.350	25.7	297	0.030	2.18	0.223	152	0.041	0.270	n.r.	21.4	0.017	1.27	0.323	0.050	0.015	0.077	0.027	0.057	0.015	0.033	0.026	0.530	13.3	0.010
T10TCCPr-03.d	255	0.419	0.201	37.7	272	0.057	2.31	0.107	183	0.036	0.091	n.r.	9.56	0.017	1.82	0.331	0.076	0.006	0.047	0.027	0.057	0.015	0.033	0.001	0.009	13.7	0.005
T10TCCPr-04.d	260	2.01	0.260	29.0	337	0.029	2.41	0.218	166	0.054	0.120	n.r.	14.4	0.017	1.34	0.428	0.350	0.052	0.065	0.027	0.057	0.015	0.033	0.002	0.048	21.4	0.008
T1-1d	4.10	10.7	0.410	10.6	345	0.136	0.660	0.257	65.6	0.021	0.018	n.r.	1.80	0.007	2.61	0.938	0.500	0.003	3.03	0.003	0.007	0.002	0.010	3.E-04	0.007	0.550	0.030
T11-1d	4.60	45.0	0.124	6620	24.8	0.006	0.510	0.186	125	0.014	0.012	n.r.	0.770	0.007	2.84	4.12	1.90	0.044	27.9	0.005	0.011	0.003	0.008	5.E-04	1.36	9.36	0.021
T11-11d	3.50	15.9	0.101	4720	29.4	0.004	0.570	0.360	138	0.014	0.012	n.r.	1.37	0.007	4.60	3.07	0.400	0.003	31.4	0.005	0.011	0.003	0.004	7.E-04	0.800	48.6	0.085
T11-12.d	2.70	5.38	0.039	1816	42.4	0.006	0.610	0.410	139	0.014	0.012	n.r.	0.930	0.007	6.60	4.21	0.550	0.004	29.3	0.005	0.011	0.003	0.005	5.E-04	1.29	18.8	0.052
T11-2.d	3.90	2.55	0.082	5220	28.8	0.005	0.720	0.159	128	0.014	0.020	n.r.	1.05	0.007	4.81	5.87	1.53	0.043	30.5	0.005	0.011	0.001	0.008	5.E-04	1.26	12.0	0.017
T11-3.d	3.80	4.38	0.086	4720	32.5	0.005	0.690	0.241	124	0.014	0.012	n.r.	1.70	0.007	5.33	3.67	1.55	0.032	28.8	0.005	0.007	0.003	0.004	4.E-04	1.39	6.62	0.014

Grain ID (chalcopyrite)	Ti 49	Mn 55	Co 59	Ni 60	Zn 66	Ga 71	Ge 74	As 75	Se 82	Mo 95	Ru 101	Rh 103	Ag 107	Pd 108	Cd 111	In 115	Sn 118	Sb 121	Te 128	Re 185	Os 189	Ir 193	Pt 195	Au 197	Tl 205	Pb 208	Bi 209
55um	0.553	0.479	0.016	0.207	0.270	0.024	0.079	0.348	2.409	0.029	0.020	0.004	0.049	0.011	0.061	0.007	0.070	0.017	0.221	0.007	0.016	0.004	0.010	0.006	0.004	0.006	0.004
33um	0.661	1.030	0.028	0.410	0.526	0.051	0.149	0.582	5.311	0.030	0.020	0.007	0.100	0.026	0.118	0.012	0.147	0.027	0.501	0.012	0.028	0.007	0.018	0.014	0.007	0.011	0.007
T11-6.d	4.20	6.93	0.068	2910	30.9	0.005	0.690	0.310	119	0.014	0.026	n.r.	0.622	0.007	5.30	3.09	0.910	0.018	28.5	0.005	0.011	0.003	0.007	5.E-04	0.512	18.5	0.022
T11-7.d	3.20	3.26	0.056	3680	30.4	0.004	0.690	0.139	137	0.023	0.019	n.r.	0.440	0.007	4.94	5.33	0.950	0.019	30.9	0.005	0.011	0.003	0.005	3.E-04	0.937	15.3	0.013
T11-9.d	3.50	5.58	0.126	6160	23.9	0.006	0.710	0.228	118	0.014	0.012	n.r.	0.510	0.007	4.33	5.30	0.222	0.016	26.8	0.003	0.007	0.003	0.008	4.E-04	1.06	21.8	0.015
T11TCCP-01d	238	1.37	0.340	41.8	575	0.075	3.21	0.390	466	0.020	0.025	n.r.	0.630	0.004	32.6	1.09	0.055	0.002	0.040	0.003	0.008	0.160	0.097	0.080	2.E-04	0.740	0.015
T11TCCP-02.d	237	1.43	0.263	67.5	485	0.079	2.93	0.094	448	0.009	0.034	n.r.	0.349	0.004	29.5	1.39	0.048	0.006	0.350	0.013	0.008	0.002	0.016	0.048	5.E-04	1.72	1.80
T11TCCP-03.d	209	1.04	0.171	24.6	462	0.101	3.08	0.069	430	0.019	0.008	n.r.	3.20	0.004	31.7	1.75	0.030	0.003	0.213	0.005	0.008	0.005	0.100	1.E-03	0.002	10.5	0.086
T11TCCP-04.d	224	1.83	0.290	77.0	483	0.500	2.35	0.104	293	0.015	0.028	n.r.	1.00	0.010	24.7	2.20	0.313	0.004	0.043	0.003	0.008	0.002	0.058	0.021	9.E-04	6.40	0.003
T11TCCP-05.d	212	1.75	0.380	56.9	555	0.860	2.43	0.111	302	0.009	0.016	n.r.	2.50	0.004	31.0	2.53	0.060	0.006	0.074	0.035	0.090	0.600	0.090	0.042	0.140	7.86	2.50
T11TCCP-06.d	212	2.21	1.19	12.3	496	0.107	1.08	0.094	145	0.020	0.008	n.r.	40.6	0.004	8.17	0.485	0.163	0.003	0.029	0.032	0.600	0.003	0.081	0.006	0.005	2.58	0.006
T11TCCP-07.d	210	15.2	0.680	81.0	471	0.270	2.13	0.080	207	0.009	0.008	n.r.	25.9	0.004	10.5	1.66	0.223	0.006	0.054	0.520	0.008	0.005	0.113	0.001	0.021	11.3	0.012
T11TCCPr-01b.d	232	0.471	0.115	33.0	408	0.079	5.30	0.118	459	0.043	0.110	n.r.	0.490	0.007	25.1	0.890	0.032	0.004	0.062	0.007	0.018	0.006	0.007	0.002	4.E-04	3.10	0.005
T11TCCPr-02b.d	215	0.509	0.137	27.1	384	0.066	5.50	0.263	443	0.039	0.150	n.r.	0.190	0.017	25.5	1.29	0.047	0.006	0.085	0.007	0.018	0.004	0.018	0.001	7.E-04	5.45	0.006
T11TCCPr-03.d	230	0.378	0.151	24.2	352	0.123	5.35	0.122	437	0.023	0.106	n.r.	2.33	0.017	21.9	1.48	0.046	0.007	0.058	0.027	0.057	0.007	0.120	0.002	7.E-04	3.89	0.005
T11TCCPr-05.d	228	0.449	0.055	31.8	358	0.022	3.91	0.141	313	0.046	0.110	n.r.	0.375	0.017	20.1	1.85	0.035	0.007	0.062	0.027	0.057	0.005	0.063	0.002	9.E-04	10.4	0.007
T11TCCPr-06.d	242	0.548	0.177	39.6	530	0.156	4.00	0.204	328	0.047	0.190	n.r.	0.360	0.017	23.7	1.84	0.045	0.006	0.075	0.027	0.057	0.015	0.081	0.002	0.001	8.36	0.006
T1-3.d	2.70	7.62	0.350	9.10	311	0.081	0.280	0.237	69.0	0.021	0.018	n.r.	1.47	0.007	3.12	1.09	0.202	0.018	3.01	0.003	0.007	0.002	0.004	3.E-04	0.007	0.302	0.013
T1-4.d	4.50	10.9	2.41	195	305	0.380	0.350	0.370	60.0	0.021	0.018	n.r.	1.04	0.007	2.96	0.668	0.433	0.003	2.12	0.003	0.007	0.002	0.004	3.E-04	0.008	0.196	0.013
T1-8.d	3.00	8.78	0.760	17.3	263	0.051	0.330	0.258	62.8	0.038	0.018	n.r.	3.67	0.007	3.80	0.866	0.710	0.002	2.58	0.003	0.007	0.002	0.004	0.013	1.E-04	0.220	0.010
T1-9.d	3.90	8.82	0.660	43.1	242	0.066	0.370	0.270	67.3	0.044	0.038	n.r.	2.49	0.007	3.25	0.932	0.329	0.003	3.26	0.003	0.007	0.009	0.110	0.130	0.063	1.52	0.064
T2-1d	4.30	16.4	0.350	35.4	347	0.070	0.180	0.292	42.9	0.014	0.012	n.r.	0.520	0.007	3.63	0.405	0.500	0.029	0.390	0.005	0.011	0.003	0.029	3.E-04	3.E-04	1.22	0.023
T2-10.d	4.20	9.30	0.460	27.5	383	0.066	0.207	0.176	38.2	0.014	0.014	n.r.	0.890	0.007	4.94	0.987	0.690	0.029	0.460	0.003	0.011	0.003	0.040	2.E-04	0.005	2.43	0.011
T2-11d	3.60	8.80	2.12	142	387	0.031	0.150	0.157	43.3	0.014	0.012	n.r.	2.48	0.007	5.30	1.02	1.70	0.083	0.870	0.005	0.011	0.003	0.021	5.E-04	0.008	2.17	0.022
T2-2.d	3.40	17.5	0.710	39.0	328	0.053	0.320	0.156	38.4	0.030	0.012	n.r.	0.325	0.007	3.57	0.405	0.510	0.027	0.410	0.005	0.011	0.003	0.008	2.E-04	2.E-04	0.576	0.013
T2-3.d	3.80	20.6	0.259	32.7	384	0.052	0.380	0.226	38.5	0.014	0.026	n.r.	0.380	0.007	6.37	0.506	0.550	0.002	0.280	0.005	0.011	0.003	0.006	2.E-04	2.E-04	0.630	0.019
T2-7.d	3.03	14.5	0.330	26.8	544	0.052	0.240	0.410	41.6	1.10	0.012	n.r.	0.477	0.007	5.54	1.11	0.760	0.003	0.510	1.15	0.081	0.003	0.008	2.E-04	2.E-04	0.780	0.008
T2-8.d	3.10	11.6	0.600	33.4	408	0.082	0.210	0.253	43.2	0.022	0.020	n.r.	0.960	0.007	5.05	1.05	0.820	0.004	0.560	0.005	0.011	0.003	0.016	3.E-04	0.003	2.12	0.023
T2-9.d	3.50	29.1	0.454	34.8	518	0.077	0.271	0.126	46.1	0.014	0.012	n.r.	0.608	0.007	5.57	0.922	0.940	0.002	0.540	0.005	0.011	0.003	0.013	2.E-04	3.E-04	1.59	0.009
T3-1d	3.40	7.06	0.042	3510	28.4	0.005	0.550	0.217	126	0.018	0.012	n.r.	0.575	0.009	4.24	4.69	0.910	0.032	26.7	0.003	0.007	0.002	0.005	3.E-04	0.834	18.3	0.016
T3-10.d	4.50	4.84	0.270	7700	20.2	0.005	0.700	0.192	122	0.018	0.027	n.r.	0.354	0.009	2.73	3.46	1.44	0.061	24.9	0.003	0.007	0.002	0.005	3.E-04	0.511	10.4	0.010
T3-11d	2.20	4.55	0.115	6690	24.3	0.005	0.730	0.272	118	0.018	0.029	n.r.	0.730	0.009	3.11	3.82	1.81	0.046	27.6	0.003	0.007	0.002	0.005	4.E-04	0.381	7.54	0.023
T3-2.d	3.10	6.23	0.310	7900	23.1	0.006	0.680	0.233	125	0.018	0.021	n.r.	0.620	0.009	2.77	5.47	1.02	0.031	28.6	0.003	0.007	0.002	0.005	3.E-04	0.678	15.6	0.018
T3-5.d	3.60	5.92	0.123	7840	21.1	0.005	0.540	0.192	138	0.018	0.012	n.r.	0.530	0.009	2.51	4.47	1.35	0.025	27.5	0.003	0.007	0.002	0.005	0.011	0.809	22.6	0.035
T3-6.d	3.90	7.63	0.072	2540	28.3	0.006	0.650	0.285	120	0.018	0.012	n.r.	0.920	0.009	4.90	4.44	0.450	0.003	27.0	0.003	0.007	0.002	0.005	5.E-04	1.38	28.4	0.044
T3-8.d	4.30	4.92	0.005	2150	37.2	0.006	0.660	0.230	121	0.018	0.012	n.r.	0.252	0.010	4.64	3.11	0.640	0.041	24.6	0.003	0.007	0.002	0.005	3.E-04	1.10	24.0	0.014
T4-1d	2.20	1.20	0.220	51.0	104	0.006	1.35	10.9	163	0.029	0.012	n.r.	8.27	10.2	8.70	3.63	0.025	0.032	47.3	0.005	0.011	0.003	0.024	6.E-04	1.51	31.5	0.011
T4-10.d	3.00	0.175	0.061	48.5	109	0.006	0.920	11.2	158	0.014	0.012	n.r.	8.83	11.1	8.48	3.51	0.016	0.004	43.6	0.005	0.011	0.003	0.037	7.E-04	1.29	28.2	0.017
T4-12.d	3.50	0.870	0.124	49.0	114	0.006	0.780	11.6	153	0.041	0.035	n.r.	8.34	9.93	9.40	3.15	0.022	0.025	40.8	0.003	0.011	0.003	0.008	7.E-04	1.55	33.0	0.012

Grain ID (chalcopyrite)	Ti 49	Mn 55	Co 59	Ni 60	Zn 66	Ga 71	Ge 74	As 75	Se 82	Mo 95	Ru 101	Rh 103	Ag 107	Pd 108	Cd 111	In 115	Sn 118	Sb 121	Te 128	Re 185	Os 189	Ir 193	Pt 195	Au 197	Tl 205	Pb 208	Bi 209
55um	0.553	0.479	0.016	0.207	0.270	0.024	0.079	0.348	2.409	0.029	0.020	0.004	0.049	0.011	0.061	0.007	0.070	0.017	0.221	0.007	0.016	0.004	0.010	0.006	0.004	0.006	0.004
33um	0.661	1.030	0.028	0.410	0.526	0.051	0.149	0.582	5.311	0.030	0.020	0.007	0.100	0.026	0.118	0.012	0.147	0.027	0.501	0.012	0.028	0.007	0.018	0.014	0.007	0.011	0.007
T4-13.d	2.70	0.202	0.041	39.0	126	0.007	1.08	9.80	173	0.041	0.024	n.r.	8.74	8.35	12.1	3.21	0.023	0.029	41.6	0.005	0.011	0.003	0.008	6.E-04	0.790	33.1	0.009
T4-16.d	2.60	0.188	0.036	22.6	123	0.006	0.690	5.61	143	0.160	0.027	n.r.	6.94	4.45	8.30	3.12	0.036	0.004	29.3	0.005	0.011	0.003	0.008	5.E-04	1.22	20.2	0.025
T4-3.d	3.80	0.700	0.059	16.5	116	0.008	1.02	9.89	162	0.023	0.030	n.r.	7.89	9.92	7.50	3.01	0.022	0.004	42.8	0.003	0.011	0.003	0.032	0.009	1.20	25.3	0.010
T4-6.d	3.40	0.204	0.037	22.1	127	0.006	1.07	6.15	170	0.078	0.046	n.r.	7.67	5.48	11.0	3.78	0.018	0.005	47.3	0.003	0.011	0.003	0.022	6.E-04	1.17	32.9	0.008
T4-8.d	3.10	0.189	0.019	23.7	112	0.006	1.01	8.95	185	0.027	0.022	n.r.	7.82	8.67	9.80	3.04	0.018	0.033	52.8	0.003	0.011	0.003	0.016	4.E-04	1.07	33.1	0.005
TR15-1d	4.20	1.28	0.390	23.4	304	0.020	0.200	0.364	38.3	0.018	0.011	n.r.	15.8	0.017	9.70	2.22	2.55	0.019	1.52	0.008	0.018	0.005	0.010	0.034	0.013	4.79	0.157
TR15-2.d	2.30	2.50	0.860	160	318	0.022	0.340	0.375	40.8	0.018	0.011	n.r.	10.8	0.017	8.30	1.80	3.93	0.005	1.86	0.040	0.018	0.005	0.007	0.097	0.016	5.76	0.214
TR15-3.d	4.30	0.195	0.051	44.6	265	0.019	0.210	0.390	34.6	0.018	0.011	n.r.	2.80	0.017	5.17	3.21	5.22	0.004	0.061	0.104	0.018	0.080	0.008	5.E-04	3.E-04	1.61	0.076
TR15-4.d	3.20	0.830	0.380	24.8	363	0.025	0.200	0.411	40.1	0.018	0.040	n.r.	26.9	0.017	10.2	1.97	5.03	0.190	1.88	0.026	0.012	0.034	0.012	0.027	0.017	13.3	0.155
TR15-5.d	3.90	8.20	0.064	44.8	294	0.039	0.240	0.500	41.6	0.018	0.064	n.r.	6.22	0.017	5.25	2.01	3.44	0.039	1.18	0.110	0.034	0.330	0.090	0.023	6.E-04	4.03	0.183
TR15-6.d	3.20	0.640	0.268	37.1	369	0.036	0.290	0.362	37.6	0.018	0.011	n.r.	25.5	0.017	9.10	1.35	3.16	0.003	0.870	0.070	0.018	0.024	0.019	0.032	5.E-04	1.75	0.139
TR15-8.d	3.20	10.1	0.810	166	388	0.024	0.330	0.363	38.5	0.018	0.019	n.r.	17.8	0.017	10.7	1.54	3.24	0.029	1.97	0.137	0.018	0.095	0.012	0.029	9.E-04	4.54	0.142
TR20-10.d	5.30	0.259	0.199	28.3	325	0.025	0.380	0.606	55.9	0.018	0.090	n.r.	12.6	0.017	8.68	5.49	12.0	0.003	2.67	0.008	0.018	0.005	0.012	0.024	4.E-04	0.561	0.044
TR20-11.d	5.30	0.253	0.012	29.3	263	0.027	0.350	0.325	55.0	0.018	0.011	n.r.	18.8	0.017	3.96	5.91	11.0	0.102	1.59	0.008	0.015	0.005	0.012	0.131	7.E-04	0.800	0.030
TR20-3.d	3.30	0.309	0.199	14.7	270	0.017	0.170	0.585	57.3	0.018	0.021	n.r.	37.0	0.017	8.80	0.385	2.36	0.057	0.620	0.008	0.018	0.005	0.011	0.113	7.E-04	9.75	0.175
TR20-4.d	3.80	0.282	0.141	13.9	198	0.011	0.290	0.325	51.0	0.018	0.011	n.r.	29.7	0.017	4.59	0.120	2.22	0.051	0.630	0.008	0.018	0.005	0.012	0.078	6.E-04	4.19	0.151
TR20-5.d	23.0	0.288	0.059	34.0	302	0.180	0.370	0.501	58.2	0.018	0.011	n.r.	15.4	0.017	5.90	5.69	12.0	0.006	1.94	0.005	0.018	0.005	0.028	0.077	4.E-04	0.437	0.034
TR20-6.d	4.10	0.354	0.055	31.7	242	0.220	0.470	0.325	55.0	0.018	0.011	n.r.	13.4	0.017	4.20	5.71	10.2	0.007	1.58	0.008	0.018	0.005	0.019	0.001	9.E-04	1.90	0.050
TR20-7.d	4.60	0.238	0.012	31.4	349	0.106	0.480	0.446	56.9	0.018	0.021	n.r.	12.3	0.017	7.50	5.70	12.2	0.003	1.53	0.008	0.018	0.005	0.012	0.047	3.E-04	0.360	0.019
TR20-8.d	5.10	2.10	0.400	23.9	302	0.029	0.320	0.607	61.3	0.018	0.011	n.r.	19.9	0.017	8.30	4.86	11.2	0.075	1.40	0.008	0.018	0.005	0.012	0.076	0.015	10.4	0.059
VB21-1d	4.60	4.88	0.320	7.50	187	0.032	0.490	0.216	72.1	0.014	0.030	n.r.	1.82	0.007	2.78	14.6	7.68	0.005	8.41	0.005	0.011	0.003	0.004	5.E-04	6.E-04	4.33	0.070
VB21-3.d	5.00	1.98	0.085	4.60	181	0.030	0.470	0.285	76.6	0.014	0.017	n.r.	3.99	0.007	2.94	8.78	6.58	0.043	15.9	0.005	0.011	0.003	0.008	9.E-04	7.E-04	6.14	0.211
VB21-4.d	3.80	0.151	0.095	4.01	166	0.023	0.220	0.235	68.7	0.014	0.012	n.r.	0.660	0.007	2.82	8.86	7.38	0.031	1.41	0.005	0.011	0.003	0.008	2.E-04	3.E-04	4.62	0.009
VB21-5.d	4.10	0.138	0.124	4.72	193	0.008	0.330	0.208	67.8	0.014	0.033	n.r.	1.07	0.007	3.23	8.76	5.14	0.003	5.37	0.005	0.011	0.003	0.004	5.E-04	4.E-04	3.39	0.047
VB21-6.d	6.40	0.900	1.05	73.0	175	0.015	0.620	0.364	58.6	0.031	0.022	n.r.	1.87	0.007	3.90	11.8	4.34	0.004	6.78	0.005	0.011	0.003	0.008	6.E-04	6.E-04	6.25	0.081
VB21-9.d	4.80	0.900	0.250	9.20	168	0.019	0.560	0.397	67.0	0.038	0.060	n.r.	3.82	0.007	2.70	7.08	0.720	0.005	12.4	0.005	0.011	0.003	0.009	9.E-04	9.E-04	8.94	0.171
VB25-1d	3.90	0.600	0.063	4.67	183	0.033	0.360	0.243	61.2	0.014	0.043	n.r.	1.68	0.008	10.6	6.84	6.65	0.054	6.02	0.005	0.007	0.003	0.008	6.E-04	4.E-04	6.98	0.062
VB25-2.d	4.80	0.560	0.030	4.80	164	0.006	0.328	0.272	55.2	0.014	0.012	n.r.	2.63	0.007	11.2	5.70	5.35	0.032	6.79	0.002	0.006	0.003	0.006	7.E-04	0.002	7.22	0.144
VB25-5.d	5.00	0.580	0.090	3.08	222	0.063	0.390	0.268	60.0	0.079	0.012	n.r.	2.91	0.007	11.9	2.82	3.10	0.058	8.14	0.005	0.011	0.003	0.004	0.009	4.E-04	10.1	0.062
VB25-7.d	3.50	2.00	0.051	1.60	172	0.030	0.177	0.335	68.2	0.014	0.070	n.r.	2.87	0.007	11.0	6.55	8.36	0.039	8.08	0.005	0.011	0.003	0.004	7.E-04	7.E-04	10.7	0.058
VB25-8.d	3.50	0.670	0.030	2.93	190	0.053	0.290	0.223	58.5	0.014	0.012	n.r.	1.29	0.007	10.9	4.39	4.39	0.041	5.04	0.002	0.011	0.003	0.008	5.E-04	0.800	2.23	0.043
VB27-2.d	3.90	24.2	0.014	1.56	334	0.008	0.670	0.394	210	0.014	0.021	n.r.	14.1	0.007	58.9	15.8	29.0	0.009	31.0	0.005	0.011	0.003	0.008	1.E-03	0.717	10.7	0.339
VB27-3.d	3.20	25.7	1.92	610	169	0.034	1.09	0.234	175	0.028	0.024	n.r.	12.3	0.008	28.3	13.2	18.6	0.006	23.1	0.005	0.011	0.002	0.008	0.001	0.707	8.09	0.265
VB27-4.d	3.70	13.2	0.031	0.870	298	0.021	1.30	0.246	196	0.040	0.019	n.r.	26.8	0.007	48.0	20.5	21.0	0.008	31.2	0.003	0.011	0.003	0.005	0.008	0.921	11.8	1.90
VB27-5.d	5.10	7.98	0.007	3.70	143	0.014	0.910	0.230	178	0.014	0.012	n.r.	23.6	0.007	25.2	24.2	27.6	0.004	31.8	0.003	0.008	0.003	0.008	9.E-04	0.178	8.54	0.168

Grain ID (chalcopyrite)	Ti 49	Mn 55	Co 59	Ni 60	Zn 66	Ga 71	Ge 74	As 75	Se 82	Mo 95	Ru 101	Rh 103	Ag 107	Pd 108	Cd 111	In 115	Sn 118	Sb 121	Te 128	Re 185	Os 189	Ir 193	Pt 195	Au 197	Tl 205	Pb 208	Bi 209
55um	0.553	0.479	0.016	0.207	0.270	0.024	0.079	0.348	2.409	0.029	0.020	0.004	0.049	0.011	0.061	0.007	0.070	0.017	0.221	0.007	0.016	0.004	0.010	0.006	0.004	0.006	0.004
33um	0.661	1.030	0.028	0.410	0.526	0.051	0.149	0.582	5.311	0.030	0.020	0.007	0.100	0.026	0.118	0.012	0.147	0.027	0.501	0.012	0.028	0.007	0.018	0.014	0.007	0.011	0.007
VB29-1d	4.30	0.134	0.088	6.64	173	0.008	0.325	0.360	55.1	0.014	0.012	n.r.	1.83	0.007	10.7	0.895	5.33	0.040	7.74	0.005	0.006	0.003	0.008	7.E-04	0.010	3.87	0.135
VB29-3.d	4.20	0.133	0.065	4.70	242	0.006	0.280	0.210	59.0	0.016	0.012	n.r.	4.14	0.007	15.0	1.07	6.92	0.004	17.3	0.005	0.011	0.003	0.008	9.E-04	0.112	5.07	0.304
VB30-1d	4.90	2.46	0.290	26.3	139	0.010	0.310	0.257	49.4	0.250	0.012	n.r.	0.810	0.007	11.3	0.475	1.21	0.004	0.490	0.038	0.011	0.003	0.008	4.E-04	4.E-04	13.9	0.190
VB30-2.d	6.70	0.198	0.123	5.61	182	0.068	0.340	0.490	68.6	0.014	0.032	n.r.	3.83	0.007	14.8	1.18	4.24	0.020	13.7	0.005	0.011	0.003	0.008	9.E-04	5.E-04	19.4	0.166
VB30-3.d	5.90	0.660	1.25	28.8	221	0.014	0.350	0.259	56.3	0.014	0.012	n.r.	2.55	0.007	15.0	1.28	4.20	0.021	4.23	0.009	0.011	0.003	0.003	9.E-04	0.009	13.7	0.149
VB30-4.d	4.90	0.610	0.102	3.15	197	0.013	0.300	0.460	61.3	0.014	0.012	n.r.	3.33	0.007	11.2	1.35	4.37	0.020	6.09	0.005	0.011	0.003	0.042	0.012	6.E-04	8.98	0.344
VB30-5.d	7.00	1.50	0.125	4.30	252	0.013	0.440	0.232	69.1	0.014	0.012	n.r.	2.77	0.007	17.6	1.17	4.37	0.051	8.90	0.005	0.015	0.002	0.005	7.E-04	6.E-04	14.4	0.135
VB30-6.d	9.60	0.410	0.100	2.61	204	0.050	0.311	0.225	63.1	0.014	0.020	n.r.	2.57	0.007	15.2	1.89	6.57	0.018	6.79	0.005	0.011	0.003	0.003	0.010	6.E-04	9.54	0.110
VB31-1d	5.90	0.550	0.057	4.50	149	0.039	0.272	0.201	62.8	0.014	0.012	n.r.	2.73	0.007	11.5	5.24	7.45	0.025	7.57	0.005	0.011	0.003	0.004	0.049	0.123	27.5	0.454
VB31-10.d	3.80	0.610	0.107	7.30	137	0.011	0.330	0.233	60.7	0.022	0.012	n.r.	2.32	0.007	15.1	4.84	8.11	0.002	6.24	0.003	0.006	2.30	0.008	7.E-04	0.053	30.9	0.340
VB31-11d	4.90	0.590	1.59	67.0	192	0.013	0.340	0.229	61.4	0.014	0.020	n.r.	2.11	0.007	14.2	3.42	7.00	0.004	5.66	0.005	0.011	0.003	0.008	0.014	0.075	25.7	0.790
VB31-3.d	3.90	0.960	0.680	34.0	160	0.014	0.440	0.272	71.5	0.014	0.018	n.r.	2.73	0.007	12.7	4.22	7.08	0.006	8.44	0.005	0.008	0.003	0.008	1.E-03	0.146	28.0	0.276
VB31-5.d	4.00	0.980	18.4	646	355	0.015	0.310	0.219	56.7	0.022	0.012	n.r.	4.44	0.007	21.0	6.14	8.55	0.047	6.30	0.005	0.011	0.003	0.004	0.027	0.015	60.7	0.838
VB31-7.d	4.30	0.830	0.209	10.4	262	0.012	0.370	0.230	64.9	0.014	0.012	n.r.	3.33	0.007	13.7	6.61	9.80	0.032	8.32	0.006	0.006	0.003	0.004	0.017	0.168	19.9	0.291
VB31-9.d	2.20	1.12	0.500	23.7	182	0.008	0.540	0.283	57.8	0.014	0.027	n.r.	2.32	0.007	12.5	5.86	9.10	0.032	6.17	0.005	0.011	0.003	0.004	0.043	0.168	31.4	0.281
VB34-3.d	4.10	26.9	0.010	0.540	214	0.022	1.03	0.252	190	0.014	0.025	n.r.	23.0	0.007	33.8	19.2	31.3	0.012	28.4	0.005	0.011	0.002	0.008	1.E-03	0.513	11.9	0.216
VB34-4.d	4.20	17.8	0.014	1.33	233	0.014	0.970	0.210	169	0.014	0.024	n.r.	16.4	0.007	31.4	19.7	33.3	0.052	24.7	0.003	0.011	0.003	0.007	7.E-04	0.527	9.95	0.204
VB5-1d	3.70	28.4	0.020	0.900	165	0.030	1.16	0.236	185	0.014	0.032	n.r.	23.1	0.007	31.1	19.8	31.4	0.006	26.5	0.005	0.011	0.003	0.008	8.E-04	0.458	12.3	0.255
VB5-4.d	3.70	22.6	0.004	1.49	166	0.008	0.970	0.193	181	0.014	0.012	n.r.	27.8	0.007	30.4	15.1	24.6	0.015	24.6	0.005	0.011	0.001	0.008	9.E-04	0.561	7.91	0.223
VB5-7.d	3.90	24.0	0.370	11.0	261	0.030	0.990	0.393	178	0.014	0.050	n.r.	18.1	0.007	48.5	21.1	30.0	0.010	32.2	0.005	0.011	0.003	0.008	0.001	0.940	12.0	0.360
VB6-1d	3.30	1.23	0.320	18.6	240	0.011	0.620	0.400	92.7	0.014	0.029	n.r.	17.9	0.007	52.6	10.2	34.0	0.005	20.2	0.005	0.011	0.002	0.008	0.009	0.063	13.8	0.244
VB6-11d	4.00	0.660	0.700	36.0	148	0.006	0.420	0.230	75.2	0.021	0.012	n.r.	3.91	0.009	23.1	7.78	21.1	0.004	2.61	0.005	0.011	0.003	0.005	8.E-04	0.007	4.27	0.067
VB6-12.d	3.90	0.930	0.043	3.30	197	0.007	0.350	0.258	98.0	0.014	0.012	n.r.	9.80	0.007	36.8	6.16	18.7	0.037	19.0	0.019	0.011	0.003	0.004	0.034	0.027	12.2	0.233
VB6-13.d	3.70	0.750	0.013	2.94	181	0.015	0.450	0.203	94.0	0.028	0.012	n.r.	12.0	0.007	33.5	6.80	18.9	0.020	18.7	0.005	0.007	0.003	0.008	0.033	0.027	5.58	0.291
VB6-2.d	3.50	0.198	0.008	2.32	155	0.007	0.680	0.094	100	0.014	0.012	n.r.	13.7	0.007	32.6	8.74	19.4	0.005	20.9	0.005	0.011	0.003	0.008	0.011	0.084	7.13	0.305
VB6-3.d	2.40	0.690	0.029	5.16	215	0.011	0.500	0.264	100	0.014	0.012	n.r.	15.9	0.007	42.6	6.66	31.0	0.042	18.8	0.005	0.007	0.003	0.008	0.013	0.027	4.87	0.277
VB6-4.d	4.00	0.178	0.008	1.67	172	0.013	0.500	0.262	80.8	0.014	0.012	n.r.	11.1	0.007	33.2	7.99	28.8	0.003	15.7	0.006	0.011	0.003	0.008	0.014	0.049	3.67	0.221
VB6-5.d	3.90	0.690	0.004	2.65	186	0.010	0.445	0.239	90.4	0.014	0.012	n.r.	10.9	0.007	34.2	11.1	35.9	0.004	15.9	0.005	0.011	0.003	0.008	0.088	0.013	1.99	0.138
VB6-6.d	2.70	0.177	0.048	5.00	243	0.007	0.440	0.219	90.6	0.036	0.012	n.r.	7.34	0.007	35.2	9.64	31.9	0.031	10.6	0.005	0.008	0.002	0.008	0.040	0.023	11.6	0.073
VB6-7.d	4.30	0.410	0.068	2.40	186	0.007	0.400	0.215	82.5	0.014	0.023	n.r.	4.84	0.007	31.3	9.73	38.4	0.042	9.03	0.005	0.011	0.033	0.008	0.024	0.018	8.73	0.062
VB6-8.d	3.70	0.590	4.70	8.60	199	0.010	0.460	0.281	80.3	0.014	0.012	n.r.	3.29	0.008	28.2	9.13	28.1	0.005	6.19	0.005	0.011	0.003	0.008	0.015	5.E-04	8.80	0.111
VB7-11d	3.90	0.166	0.065	6.20	199	0.125	0.280	0.186	58.0	0.021	0.018	n.r.	3.71	0.007	23.0	1.50	5.75	0.023	16.6	0.003	0.007	0.002	0.004	6.E-04	4.E-04	4.73	0.189

Grain ID (chalcopyrite)	Ti 49	Mn 55	Co 59	Ni 60	Zn 66	Ga 71	Ge 74	As 75	Se 82	Mo 95	Ru 101	Rh 103	Ag 107	Pd 108	Cd 111	In 115	Sn 118	Sb 121	Te 128	Re 185	Os 189	Ir 193	Pt 195	Au 197	Tl 205	Pb 208	Bi 209
55um	0.553	0.479	0.016	0.207	0.270	0.024	0.079	0.348	2.409	0.029	0.020	0.004	0.049	0.011	0.061	0.007	0.070	0.017	0.221	0.007	0.016	0.004	0.010	0.006	0.004	0.006	0.004
33um	0.661	1.030	0.028	0.410	0.526	0.051	0.149	0.582	5.311	0.030	0.020	0.007	0.100	0.026	0.118	0.012	0.147	0.027	0.501	0.012	0.028	0.007	0.018	0.014	0.007	0.011	0.007
VB7-2.d	3.90	0.178	0.098	10.5	146	0.124	0.310	0.218	53.4	0.014	0.260	n.r.	6.67	0.007	27.2	1.73	5.93	0.014	17.1	0.005	0.011	0.003	0.008	7.E-04	5.E-04	7.16	0.190
VB7-3.d	5.10	0.207	0.151	7.14	147	0.119	0.330	0.253	54.6	0.014	0.017	n.r.	2.65	0.007	19.4	1.77	6.23	0.004	17.3	0.003	0.011	0.003	0.005	7.E-04	4.E-04	4.69	0.139
VB7-4.d	3.30	0.202	0.111	6.34	166	0.146	0.330	0.282	49.2	0.014	0.012	n.r.	2.71	0.007	23.3	2.48	7.20	0.004	15.4	0.005	0.011	0.003	0.008	8.E-04	5.E-04	3.68	0.188
VB7-5.d	4.10	0.199	0.300	11.0	147	0.063	0.270	0.170	53.4	0.014	0.041	n.r.	7.35	0.007	24.4	1.53	4.91	0.004	14.5	0.005	0.011	0.003	0.008	0.001	7.E-04	6.92	0.244
VB7-6.d	4.10	9.00	0.350	25.4	225	0.139	0.286	0.243	52.7	0.014	0.012	n.r.	6.78	0.007	30.0	2.09	7.29	0.017	18.1	0.005	0.007	0.003	0.008	7.E-04	7.E-04	4.86	0.254
VB7-7.d	3.10	1.45	0.139	10.9	185	0.102	0.320	0.315	61.8	0.014	0.012	n.r.	2.89	0.007	25.5	1.54	4.85	0.023	13.5	0.005	0.011	0.003	0.008	9.E-04	8.E-04	6.10	0.091

Grain ID (pentlandite)	Ti 49	Mn 55	Co 59	Ni 60	Zn 66	Ga 71	Ge 74	As 75	Se 82	Mo 95	Ru 101	Rh 103	Ag 107	Pd 108	Cd 111	In 115	Sn 118	Sb 121	Te 128	Re 185	Os 189	Ir 193	Pt 195	Au 197	Tl 205	Pb 208	Bi 209
DL	1.919	0.426	0.019	0.220	0.370	0.020	0.067	0.241	2.675	0.169	0.022	0.007	0.015	0.011	0.082	0.009	0.082	0.031	0.252	0.012	0.026	0.007	0.032	0.012	0.007	0.012	0.010
A2PN-01.d	347	1.26	3870	339000	1.60	0.012	1.19	0.167	208	0.102	0.013	0.004	4.65	1358	0.388	0.011	0.075	0.036	73.1	0.007	0.015	0.013	2.44	0.007	0.119	0.041	0.088
A2PN-02.d	326	1.66	3640	332000	0.570	0.047	1.58	0.134	213	0.200	0.013	0.093	26.0	0.007	0.049	0.015	4.40	0.030	65.8	0.007	0.015	0.162	0.420	0.007	0.018	0.013	0.165
A2PN-03.d	324	5.60	3510	330000	1.29	0.700	1.88	1.30	189	1.70	0.013	0.065	23.6	1552	0.120	0.051	0.060	0.074	74.5	0.026	0.037	0.244	1.20	0.007	0.810	0.160	0.830
B138405PN-01.d	313	3.40	6580	311000	140	0.012	1.32	104	145	0.102	8.00	0.007	0.145	0.160	0.049	0.021	0.051	3.84	11.5	1.19	1.16	0.222	0.031	0.018	0.004	0.130	0.850
B138405PN-02.d	333	1.57	7140	339000	4.80	0.048	1.12	200	138	0.102	11.8	0.006	0.640	2.54	0.049	0.120	0.098	5.40	9.36	1.85	1.63	0.312	0.026	0.068	0.004	0.095	0.940
B138405PN-03.d	317	7.15	11770	303000	22.0	0.065	1.05	259	112	0.250	9.69	0.002	0.680	0.832	0.032	0.189	0.111	2.28	7.70	3.23	1.21	0.067	2.60	0.070	0.064	3.82	2.70
CRTN12PN-01.d	561	1.18	17230	593000	5.10	0.046	0.880	1.60	87.2	0.145	0.384	0.004	0.930	0.897	0.020	0.012	0.034	0.330	0.360	0.026	0.203	0.004	0.007	0.200	0.008	0.281	0.130
CRTN12PN-02.d	562	0.710	16930	582000	7.00	0.130	0.990	0.310	83.5	0.247	0.256	0.003	0.172	1.81	0.110	0.003	0.496	0.110	0.151	0.019	0.185	0.094	0.023	0.006	0.012	0.019	0.035
CRTN12PN-03.d	548	0.209	16100	555000	0.800	0.062	0.930	0.250	74.9	0.030	0.210	0.009	0.183	0.007	0.110	0.003	0.038	0.019	0.931	0.013	0.234	0.094	0.023	0.009	0.012	0.045	6.00
CRTN14PN-01.d	562	0.143	16440	584000	20.0	0.055	0.930	0.300	92.9	0.715	1.95	0.087	0.183	1.59	0.443	0.003	0.050	0.118	0.270	0.301	0.071	0.080	0.007	0.011	0.006	0.180	0.455
CRTN14PN-02.d	571	0.750	17220	572000	0.990	0.049	0.870	0.490	90.1	0.715	0.013	0.002	0.320	1.70	0.037	0.006	0.320	0.460	5.20	0.301	0.011	0.003	0.007	0.017	0.005	3.21	0.880
CRTN14PN-03.d	559	0.590	16690	564000	3.50	0.045	0.790	0.194	101	0.180	0.013	0.004	0.206	1.37	0.071	0.011	0.062	0.034	0.207	0.007	0.011	0.009	0.094	0.039	0.004	0.146	0.438
CRTN18PN-01.d	529	33.0	8870	525000	0.790	0.093	0.950	2.06	67.4	0.035	0.022	0.007	0.160	1.93	0.110	0.002	0.052	0.246	3.51	0.008	0.122	0.094	0.012	0.020	0.012	0.005	0.021
CRTN18PN-02.d	544	0.378	8800	567000	1.60	0.120	1.07	0.870	90.0	0.058	0.006	0.007	2.12	1.52	0.600	0.004	0.080	0.250	2.76	0.034	0.045	0.094	0.053	0.023	0.012	0.024	0.085
CRTN18PN-03.d	522	0.510	8960	544000	0.720	0.018	0.870	50.8	101	0.246	0.006	0.007	1.70	1.68	0.035	0.004	0.077	0.420	29.7	0.013	0.160	0.032	0.022	0.016	0.004	0.043	0.086
CRTN19PN-01.d	505	13.5	8080	565000	17.1	0.430	0.820	1.20	79.3	0.102	0.013	0.002	39.0	1.15	0.700	0.339	0.114	0.108	0.540	0.007	0.015	0.003	0.018	0.007	0.360	9.50	2.72
CRTN19PN-02.d	519	0.540	8320	562000	1.19	0.038	0.960	0.540	86.2	0.102	0.013	0.039	2.22	1.94	0.045	0.004	0.104	0.044	0.136	0.130	0.039	0.002	0.018	0.004	2.16	2.80	0.174
CRTN19PN-03.d	579	17.0	8750	576000	80.0	0.054	1.07	12.6	136	0.102	0.388	0.004	1.05	1.56	0.400	0.012	0.100	0.006	23.5	0.023	0.190	0.018	0.180	0.054	1.96	3.11	0.440
CRTN6PN-06.d	204	7.50	10800	323600	80.0	0.150	0.796	0.477	95.7	0.607	0.013	0.004	1.87	0.476	0.646	0.076	0.330	0.150	0.740	0.066	0.057	0.032	0.054	0.021	0.980	17.7	1.62
CRTN6PN-07.d	216	14.2	10620	318000	1.39	0.240	1.04	3.60	94.9	0.150	0.013	0.004	2.22	0.523	0.237	0.056	0.048	0.319	0.930	0.027	0.086	0.030	0.025	0.017	0.253	16.8	3.45

Grain ID	Ti	Mn	Co	Ni	Zn	Ga	Ge	As	Se	Mo	Ru	Rh	Ag	Pd	Cd	In	Sn	Sb	Te	Re	Os	Ir	Pt	Au	Tl	Pb	Bi
(pentlandite)	49	55	59	60	66	71	74	75	82	95	101	103	107	108	111	115	118	121	128	185	189	193	195	197	205	208	209
DL	1.919	0.426	0.019	0.220	0.370	0.020	0.067	0.241	2.675	0.169	0.022	0.007	0.015	0.011	0.082	0.009	0.082	0.031	0.252	0.012	0.026	0.007	0.032	0.012	0.007	0.012	0.010
CRTN9BPN-01.d	544	0.350	14310	567000	0.510	0.073	0.880	0.300	84.0	0.013	0.013	0.005	1.89	4.71	0.107	0.004	0.070	0.207	3.64	0.008	0.025	0.036	0.023	0.016	0.136	0.021	0.029
CRTN9BPN-02.d	545	0.460	12890	570000	0.440	0.010	0.890	3.49	108	0.028	0.013	0.007	1.94	3.29	0.110	0.003	0.057	0.125	3.22	0.160	0.018	0.094	0.023	0.016	0.111	0.028	0.013
CRTN9BPN-03.d	556	0.580	14580	568000	0.272	0.127	1.07	0.206	94.5	0.013	0.174	0.007	1.95	0.017	0.110	0.014	0.090	0.100	30.0	0.129	0.090	0.094	0.023	0.014	0.350	0.241	0.019
E4PN-01.d	321	1.00	5540	355000	310	0.200	1.31	16.0	162	0.102	0.013	0.004	6.60	6.07	0.100	0.014	0.061	1.16	200	0.013	0.015	0.013	0.019	0.016	1.71	230	14.0
E4PN-02.d	343	1.15	5830	344000	90.0	0.031	0.890	4.13	104	0.170	0.013	0.004	9.00	7.69	0.900	0.011	0.079	1.54	7.60	0.040	0.096	0.026	0.018	0.380	1.67	0.940	0.700
MCR10BPN-01.d	492	10.7	3580	476000	1.10	0.039	1.34	0.620	167	0.130	0.013	0.004	47.0	1.58	0.570	0.014	1.82	0.130	70.0	1.40	0.021	0.004	0.014	0.058	3.52	68.4	4.88
MCR10BPN-03.d	509	49.0	4200	444000	1.10	0.120	0.920	0.710	171	0.102	0.013	0.004	27.3	1.21	0.650	0.075	2.50	0.250	25.4	0.007	0.021	0.004	0.044	0.137	7.16	75.0	2.22
MCR13PN-02.d	573	61.0	10500	497500	5.80	0.140	1.85	0.389	185	0.102	0.013	0.004	14.9	2.34	1.00	0.450	28.0	1.90	4.30	0.014	0.015	0.004	0.018	0.040	16.5	440	2.80
MCR13PN-03.d	537	0.760	10170	536000	0.267	0.023	2.56	20.2	335	0.102	0.013	0.004	1.96	0.436	0.048	0.004	0.065	0.174	105	0.006	0.015	0.004	0.018	0.006	0.380	2.80	0.169
MCR3PN-06.d	299	9.30	11180	302600	0.760	0.013	0.506	2.70	57.5	0.102	0.013	0.004	1.05	5.76	0.370	0.006	0.290	0.010	0.072	0.007	0.015	0.035	0.018	0.110	0.180	9.70	0.840
MCR4BPN-01.d	527	0.740	13200	530000	0.215	0.062	0.440	0.280	56.0	0.170	0.013	0.004	1.02	17.4	0.049	0.007	0.110	0.015	0.244	0.014	0.017	0.004	0.018	0.046	0.028	1.00	0.230
MCR4BPN-02.d	502	1280	10970	416000	3900	3.09	0.740	0.520	48.2	0.014	0.013	0.002	2.32	2.22	40.0	4.80	19.1	0.460	0.158	0.080	0.024	0.130	0.018	0.019	0.840	44.1	3.70
MCR4BPN-03.d	551	48.5	12690	524000	720	0.340	0.730	0.213	51.8	0.102	0.013	0.004	1.19	13.7	7.60	0.255	0.910	0.055	0.186	0.007	0.015	0.004	0.018	0.140	0.220	12.9	0.220
MCR5PN-01.d	497	1.14	12420	579000	400	0.054	0.830	0.400	83.3	0.102	0.013	0.004	0.390	4.52	4.10	0.205	0.130	0.038	0.160	0.007	0.015	0.004	0.010	0.007	0.024	3.57	0.253
MCR5PN-02.d	201	0.810	8040	313000	70.0	0.023	1.13	0.380	80.8	0.102	0.013	0.004	2.10	6.28	0.084	0.297	0.190	0.007	0.132	0.019	0.036	0.009	0.034	0.203	0.024	8.10	1.06
MCR5PN-03.d	195	1.45	8040	315000	0.710	0.042	0.780	0.072	88.8	0.180	0.013	0.003	0.060	5.64	0.087	0.069	0.214	0.013	0.081	0.046	0.040	0.010	0.689	0.007	0.064	1.58	0.870
MS8PN-01.d	363	29.2	9330	365000	0.890	0.060	0.580	11.4	36.5	5.60	0.013	0.004	0.550	1.26	0.150	0.009	0.179	0.560	0.950	0.580	0.240	0.100	0.900	0.025	6.50	7.60	0.344
MS8PN-02.d	366	6.20	8750	362000	12.0	0.049	0.740	20.8	54.2	3.39	0.013	0.004	0.900	0.006	0.049	0.014	0.064	0.486	33.2	0.269	0.062	0.030	0.022	0.007	0.080	0.810	0.070
VB25PN-01.d	496	4.20	20480	455300	3.50	0.056	0.649	0.360	56.0	0.102	0.013	0.137	3.76	0.608	0.046	0.005	0.064	0.016	2.70	0.007	0.015	0.004	0.018	0.008	0.043	27.8	0.573
VB25PN-02.d	443	12.1	14790	315000	2.70	0.075	0.510	0.530	50.2	0.280	0.013	0.002	13.2	0.589	0.044	0.060	0.046	0.033	1.10	0.096	0.090	0.094	0.007	0.005	0.094	27.8	0.300
VB25PN-03.d	487	80.0	16160	303200	20800	0.056	0.620	3.90	52.3	0.013	0.013	0.007	9.21	0.017	840	3.09	0.311	0.056	4.78	0.008	0.011	0.070	0.023	0.016	0.359	277	1.63
VB29PN-01.d	520	241	23130	448100	1.00	0.168	0.600	0.360	49.4	0.800	0.013	0.004	4.66	0.102	0.034	0.056	0.850	0.320	0.290	0.260	0.011	0.009	0.034	0.006	0.590	64.9	1.76
VB29PN-02.d	521	99.0	21540	489000	2.80	0.043	0.700	0.112	53.0	0.580	0.013	0.004	2.98	0.102	0.139	0.004	0.220	0.014	0.186	0.041	0.011	0.009	0.034	0.620	0.296	50.5	1.42
VB29PN-03.d	533	5.20	21900	452000	1.80	0.300	0.670	0.580	53.1	0.560	0.013	0.004	2.66	6.00	0.115	0.007	0.045	1.06	0.480	0.118	0.100	0.009	0.034	0.007	0.069	27.8	0.710

Grain ID (pyrrhotite)	Ti 49	Mn 55	Co 59	Ni 60	Zn 66	Ga 71	Ge 74	As 75	Se 82	Mo 95	Ru 101	Rh 103	Ag 107	Pd 108	Cd 111	In 115	Sn 118	Sb 121	Te 128	Re 185	Os 189	Ir 193	Pt 195	Au 197	Tl 205	Pb 208	Bi 209
DL	0.405	0.406	0.014	0.235	0.231	0.024	0.063	0.362	2.148	0.025	0.027	0.004	0.045	0.011	0.059	0.005	0.063	0.013	0.194	0.004	0.010	0.003	0.007	0.004	0.003	0.003	0.003
1533-10.d	4.20	0.254	32.8	3430	0.139	0.015	1.04	0.309	170	0.017	0.017	0.003	0.174	0.018	0.038	0.032	0.046	0.061	0.135	0.003	0.005	0.002	0.004	0.003	0.002	0.324	0.246
1533-12.d	3.54	0.215	25.7	2830	0.133	0.016	0.580	0.182	145	0.017	0.017	0.002	0.142	0.007	0.190	0.004	0.052	0.036	0.210	0.003	0.005	0.002	0.005	0.002	0.001	0.164	0.065
1533-15.d	3.70	0.286	22.8	2480	0.153	0.014	1.15	0.248	185	0.017	0.017	0.002	0.260	0.007	0.038	0.010	0.042	0.050	0.550	0.004	0.005	0.002	0.004	0.002	0.001	1.23	0.368
1533-2.d	2.44	0.235	27.8	4090	0.113	0.014	0.890	0.195	147	0.015	0.017	0.002	0.204	0.013	0.055	0.003	0.033	0.022	0.112	0.008	0.005	0.002	0.005	0.003	0.001	0.200	0.115
1533-4.d	2.90	4.00	28.8	4020	0.177	0.014	0.780	0.186	147	0.015	0.017	0.002	0.158	0.007	0.042	0.003	0.024	0.011	0.179	0.005	0.005	0.002	0.004	0.003	0.003	0.360	0.054
1533-5.d	1.91	7.90	32.6	4420	0.158	0.032	0.610	0.166	156	0.015	0.017	0.002	0.121	0.007	0.018	0.004	0.028	0.016	0.102	0.005	0.005	0.002	0.006	0.003	0.007	0.760	0.340
1533-9.d	3.90	0.227	24.9	4050	0.117	0.019	1.19	0.440	226	0.049	0.017	0.002	0.252	0.007	0.026	0.003	0.041	0.055	0.126	0.017	0.005	0.002	0.004	0.005	0.003	0.370	0.091
2523-11.d	4.60	7.00	57.3	5460	0.124	0.016	0.340	0.211	50.4	0.017	0.017	0.002	0.160	0.007	0.023	0.080	0.034	0.008	0.146	0.003	0.005	0.002	0.004	0.003	0.002	2.00	0.798
2523-5.d	3.90	2.70	54.0	2060	0.271	0.048	0.290	0.510	514	0.017	0.054	0.002	0.088	0.007	0.036	0.003	0.047	0.011	0.174	0.007	0.007	0.002	0.005	0.003	0.002	1.14	1.03
2523-6.d	4.40	0.264	87.0	2420	2.10	0.019	0.270	0.235	52.4	0.017	0.029	0.002	0.133	0.007	0.036	0.004	0.043	0.009	0.118	0.003	0.007	0.002	0.004	0.002	0.002	1.70	0.800
2523-8.d	3.80	0.310	82.9	2020	0.214	0.036	0.210	0.358	56.0	0.030	0.150	0.002	0.076	0.007	0.036	0.003	0.046	0.022	0.126	0.009	0.007	0.002	0.004	0.007	0.002	0.510	0.248
CRTN18-11.d	2.74	0.590	35.6	3790	1.49	0.014	0.338	0.157	619	0.059	0.830	0.002	0.124	0.007	0.120	0.008	0.153	0.034	0.173	0.010	0.069	0.002	0.005	0.002	0.002	0.416	1.12
CRTN18-9.d	2.70	0.660	64.1	5460	0.200	0.056	0.273	0.380	64.9	0.058	0.710	0.002	0.154	0.007	0.035	0.005	0.049	0.009	0.330	0.006	0.014	0.002	0.005	0.003	0.002	0.032	0.180
CRTN19-4.d	2.20	0.342	26.4	3050	0.702	0.021	0.200	0.325	75.0	0.027	0.470	0.002	0.204	0.007	0.066	0.003	0.066	0.011	0.222	0.006	0.056	0.002	0.006	0.008	0.002	0.332	1.82
CRTN19-5.d	2.30	0.166	41.7	3010	0.507	0.014	0.370	0.488	84.1	0.031	0.245	0.002	0.225	0.007	0.050	0.003	0.047	0.011	0.115	0.003	0.007	0.002	0.004	0.006	0.001	0.306	1.63
CRTN19-6.d	3.50	0.252	72.6	3340	0.536	0.030	0.370	0.325	88.0	0.025	0.295	0.002	0.092	0.007	0.054	0.003	0.052	0.020	0.147	0.003	0.044	0.002	0.005	0.010	0.002	0.152	1.28
CRTN19-7.d	3.21	0.490	66.8	3510	0.546	0.024	0.226	0.570	76.0	0.027	0.311	0.002	0.105	0.007	0.049	0.005	0.053	0.022	0.270	0.006	0.037	0.002	0.007	0.007	0.001	0.066	0.616
DC-18-05.d	2.00	1.52	51.8	1736	0.129	0.012	0.270	0.205	36.1	1.78	0.032	0.003	0.060	0.009	0.051	0.002	0.039	0.024	0.149	0.141	0.008	0.002	0.005	0.003	0.002	0.155	0.127
DC-18-06.d	2.60	0.346	48.5	1722	0.133	0.014	0.139	0.440	34.7	2.64	0.047	0.003	0.108	0.009	0.031	0.002	0.035	0.017	0.160	0.340	0.008	0.002	0.005	0.003	0.002	0.076	0.115
DC-18-14.d	2.90	0.780	35.6	1459	1.90	0.020	0.510	0.430	26.1	2.03	0.013	0.003	0.155	0.009	0.031	0.007	0.035	0.019	0.184	0.106	0.015	0.006	0.005	0.003	0.004	0.200	0.046
DC69-1d	3.10	0.310	118	4050	0.207	0.024	0.139	0.254	216	0.680	0.109	0.003	0.145	0.007	0.030	0.003	0.040	0.009	0.150	0.222	0.006	0.002	0.006	0.003	0.001	0.340	0.152
DC69-6.d	2.40	0.630	125	4380	0.140	0.014	0.143	0.278	316	0.620	0.114	0.003	0.091	0.007	0.050	0.003	0.050	0.015	0.201	0.026	0.014	0.002	0.005	0.006	0.002	0.250	0.047
DC69-7.d	3.40	0.310	114	3930	0.220	0.021	0.590	0.273	24.6	0.640	0.160	0.002	0.103	0.007	0.063	0.003	0.046	0.029	0.210	0.041	0.016	0.002	0.007	0.006	0.001	0.687	0.216
E1-10.d	3.10	1.02	27.5	2330	0.158	0.014	0.350	0.570	57.0	2.13	0.140	0.003	0.065	0.009	0.031	0.004	0.025	0.019	0.230	0.121	0.191	0.111	0.005	0.003	0.002	0.920	0.211
E1-2.d	2.90	5.40	36.3	2630	1.90	0.059	0.310	0.330	47.0	1.89	0.085	0.003	0.069	0.009	0.031	0.004	0.046	0.025	0.153	0.114	0.106	0.104	0.005	0.003	0.002	0.730	0.186
E1-6.d	3.50	6.30	1.26	1.97	0.197	0.039	0.300	0.315	510	0.670	0.033	0.003	0.800	0.007	0.051	0.003	0.060	0.031	0.150	0.125	0.131	0.146	0.202	0.004	0.002	0.840	0.360
E1-7.d	3.80	2.52	0.490	3.90	0.158	0.037	0.207	0.373	73.0	0.480	0.049	0.002	0.460	0.007	0.051	0.005	0.078	0.018	0.360	0.201	0.256	0.164	0.135	0.006	0.001	0.712	0.167
E13-1d	2.63	1.24	18.7	1550	0.220	0.014	0.241	0.290	49.8	1.80	0.059	0.003	0.130	0.009	0.031	0.002	0.020	0.044	0.116	0.125	0.098	0.104	0.011	0.003	0.002	0.886	0.226
E13-5.d	1.60	11.9	21.9	2390	4.50	0.410	0.211	0.255	514	2.17	0.186	0.003	0.223	0.009	0.073	0.002	0.080	0.024	0.155	0.138	0.224	0.118	0.026	0.003	0.004	1.21	0.383
E4-1d	6.50	0.540	16.9	1990	0.192	0.027	0.272	2.10	73.3	0.209	0.021	0.002	0.340	0.007	0.024	0.003	0.071	0.038	0.260	0.053	0.031	0.022	0.006	0.002	0.001	1.26	0.182
E4-8.d	4.37	0.201	17.7	2161	0.105	0.025	0.320	0.199	76.3	0.061	0.052	0.002	0.328	0.007	0.052	0.003	0.068	0.021	0.224	0.042	0.037	0.030	0.006	0.006	0.010	0.508	0.333
EDEEP-1d	3.40	0.770	52.2	3390	0.250	0.028	0.177	0.366	38.9	0.590	0.013	0.002	0.231	0.007	0.046	0.006	0.063	0.022	0.950	0.068	0.017	0.005	0.007	0.004	0.002	0.270	0.018
EDEEP-2.d	4.00	0.386	51.1	3470	0.208	0.028	0.088	0.313	37.3	0.850	0.013	0.002	0.205	0.007	0.049	0.005	0.073	0.014	1.26	0.150	0.019	0.005	0.007	0.004	0.002	0.151	0.042
EDEEP-6.d	2.80	0.517	49.3	3670	0.223	0.020	0.170	0.361	35.5	0.810	0.038	0.002	0.288	0.011	0.043	0.006	0.084	0.015	1.51	0.088	0.019	0.003	0.007	0.004	0.003	0.220	0.073
EDEEP-7.d	3.50	0.442	47.0	3750	0.400	0.035	0.320	0.361	36.8	0.460	0.013	0.002	0.460	0.007	0.046	0.017	0.069	0.011	1.28	0.175	0.007	0.008	0.007	0.004	0.002	0.285	0.084
EX0301-3.d	6.10	0.660	23.6	1829	0.144	0.028	0.147	0.316	29.3	0.019	0.090	0.002	0.071	0.007	0.046	0.004	0.062	0.017	0.141	0.003	0.007	0.002	0.004	0.003	0.003	0.193	0.022
EX0301-6.d	3.40	0.279	17.1	1820	0.151	0.110	0.203	0.269	29.6	0.019	0.059	0.002	0.167	0.007	0.036	0.006	0.049	0.008	0.151	0.003	0.007	0.004	0.007	0.004	0.002	0.910	0.043
EX0301-7.d	3.42	0.450	19.2	1727	0.096	0.027	0.113	0.243	27.6	0.019	0.033	0.003	0.063	0.007	0.023	0.004	0.047	0.017	0.106	0.003	0.007	0.002	0.004	0.003	0.001	0.790	0.053
EX0301-8.d	4.04	2.58	25.1	1670	0.700	0.017	0.147	0.460	29.6	0.019	0.095	0.002	0.091	0.007	0.036	0.003	0.033	0.008	0.098	0.004	0.032	0.048	0.034	0.002	0.002	0.487	0.036
K2-1d	3.87	0.600	37.4	2900	0.112	0.018	0.186	0.500	37.6	0.019	0.687	0.002	0.164	0.011	0.026	0.002	0.025	0.028	0.086	0.150	0.117	0.099	0.146	0.003	1.E-03	0.930	0.133
K2-3.d	4.60	0.530	22.1	4810	0.700	0.029	0.215	0.264	34.1	0.019	0.580	0.002	0.091	0.007	0.047	0.002	0.045	0.042	0.144	0.003	0.036	0.033	0.026	0.003	0.001	0.522	0.156
K2-8.d	2.25	1.08	23.3	4120	0.170	0.023	0.167	0.760	36.8	0.019	0.460	0.002	0.068	0.007	0.025	0.003	0.046	0.027	0.121	0.024	0.119	0.193	0.100	0.002	0.002	0.187	0.028
MCR4b-1d	3.44	0.330	63.7	3050	0.145	0.014	0.192	0.165	39.5	0.230	0.017	0.002	0.103	0.006	0.020	0.002	0.027	0.025	0.070	0.029	0.005	0.002	0.005	0.003	0.002	0.132	0.040
MCR4b-11.d	2.59	2.70	84.4	4070	1.59	0.008	0.265	0.183	43.3	0.150	0.017	0.002	0.048	0.007	0.021	0.010	0.055	0.045	0.094	0.029	0.005	0.022	0.005	0.003	0.002	0.313	0.072
MCR4b-5.d	2.53	0.289	63.5	2774	0.147	0.053	0.297	0.217	38.7	0.73	0.017	0.002	0.118	0.007	0.028	0.003	0.035	0.013	0.109	0.027	0.005	0.002	0.005	0.003	0.021	0.353	0.081
MCR4b-8.d	2.66	0.209	66.0	3160	0.137	0.012	0.178	0.175	42.0	0.015	0.047	0.002	0.058	0.007	0.021	0.002	0.028	0.021	0.099	0.005	0.018	0.036	0.005	0.003	0.002	0.249	0.048
MCR5-1d	3.10	1.37	116	6180	0.410	0.017	0.460	0.624	97.0	0.410	0.013	0.002	0.191	0.007	0.050	0.002	0.310	0.023	0.111	0.016	0.007	0.002	0.006	0.006	0.001	0.760	0.455
MCR5-7.d	3.25	0.610	84.9	5760	0.412	0.012	0.323	0.325	94.8	0.015	0.013	0.002	0.129	0.007	0.046	0.003	0.031	0.012	0.073	0.006	0.007	0.002	0.008	0.006	0.007	0.244	0.170
MCR5-9.d	2.48	0.860	90.9	5430	0.453	0.014	0.430	0.325	88.4	0.015	0.013	0.002	0.190	0.007	0.050	0.003	0.037	0.019	0.096	0.003	0.007	0.002	0.006	0.006	0.001	0.169	0.209
NR6-3.d	1.99	5.13	720	14800	0.135	0.018	0.199	0.192	26.9	0.100	0.030	0.002	1.62	1.72	0.038	0.004	0.028	0.050	0.131	0.063	0.024	0.018	0.180	0.004	0.002	1.48	0.186
NR6-4.d	2.93	4.55	279	7410	0.270	0.014	0.141	0.140	28.7	0.124	0.032	0.002	0.531	0.479	0.038	0.003	0.023	0.024	0.215	0.067	0.017	0.017	0.038	0.002	0.001	2.01	0.245

Grain ID (pyrrhotite)	Ti 49	Mn 55	Co 59	Ni 60	Zn 66	Ga 71	Ge 74	As 75	Se 82	Mo 95	Ru 101	Rh 103	Ag 107	Pd 108	Cd 111	In 115	Sn 118	Sb 121	Te 128	Re 185	Os 189	Ir 193	Pt 195	Au 197	Tl 205	Pb 208	Bi 209
DL	**0.405**	**0.406**	**0.014**	**0.235**	**0.231**	**0.024**	**0.063**	**0.362**	**2.148**	**0.025**	**0.027**	**0.004**	**0.045**	**0.011**	**0.059**	**0.005**	**0.063**	**0.013**	**0.194**	**0.004**	**0.010**	**0.003**	**0.007**	**0.004**	**0.003**	**0.003**	**0.003**
NR6-5.d	3.21	4.78	263	7530	0.118	0.013	0.155	0.139	28.7	0.221	0.049	0.002	0.564	0.081	0.026	0.002	0.020	0.017	0.107	0.079	0.007	0.016	0.149	0.002	0.002	3.65	0.292
NR6-9.d	1.65	2.21	159	5640	0.159	0.014	0.121	0.190	25.0	0.175	0.035	0.002	0.266	0.035	0.039	0.003	0.022	0.018	0.122	0.058	0.013	0.014	0.016	0.004	0.005	0.910	0.146
T1-10.d	2.19	5.20	23.1	1680	0.180	0.014	0.181	0.580	45.7	1.20	1.10	0.003	0.062	0.009	0.024	0.005	0.030	0.011	0.720	0.251	0.227	0.538	0.005	0.002	0.002	0.279	0.030
T1-11.d	1.93	7.60	19.6	1710	0.200	0.026	0.202	0.280	48.4	1.11	0.900	0.003	0.023	0.009	0.140	0.002	0.023	0.012	0.770	0.251	0.267	0.477	0.005	0.003	0.002	0.546	0.041
TR20-1.d	4.40	0.554	44.3	2370	0.289	0.022	0.250	0.463	32.4	0.033	0.017	0.003	0.260	0.009	0.055	0.006	0.086	0.014	0.305	0.005	0.008	0.003	0.010	0.006	0.003	0.510	0.093
TR20-2.d	3.20	0.880	41.2	2310	0.470	0.022	0.250	0.540	41.7	0.033	0.017	0.003	0.279	0.009	0.052	0.006	0.107	0.028	0.970	0.005	0.008	0.006	0.310	0.006	0.004	0.400	0.040
TR20-9.d	3.60	0.860	37.8	2070	0.233	0.022	0.260	0.501	47.4	0.033	0.042	0.003	0.176	0.009	0.054	0.004	0.116	0.013	0.325	0.023	0.008	0.003	0.010	0.006	0.003	0.180	0.022
VB21-2.d	2.60	24.1	21.3	1730	0.115	0.012	0.202	0.300	39.1	2.19	0.017	0.002	0.102	0.007	0.038	0.003	0.030	0.042	0.760	0.024	0.008	0.003	0.004	0.002	0.001	0.072	0.029
VB21-8.d	2.60	0.630	22.6	1815	1.10	0.029	0.193	0.780	39.1	2.66	0.017	0.002	0.290	0.007	0.034	0.002	0.047	0.024	0.480	0.080	0.008	0.003	0.003	0.002	0.001	0.090	0.082
VB25-3.d	3.55	0.780	14.5	1089	1.90	0.010	0.177	0.510	35.3	0.503	0.017	0.002	0.139	0.007	0.067	0.008	0.024	0.049	0.170	0.077	0.008	0.003	0.004	0.002	9.E-04	0.242	0.040
VB25-4.d	3.28	1.09	12.3	1048	0.117	0.013	0.196	0.650	34.8	0.566	0.017	0.002	0.349	0.007	0.100	0.005	0.038	0.042	0.292	0.076	0.008	0.003	0.004	0.002	0.001	0.374	0.045
VB25-6.d	3.70	0.750	19.9	1360	0.370	0.018	0.191	0.450	36.4	0.880	0.017	0.002	0.930	0.007	0.059	0.002	0.043	0.067	0.127	0.030	0.008	0.003	0.004	0.004	0.001	0.523	0.045
VB29-5.d	3.00	0.530	17.1	1500	0.123	0.026	0.190	0.276	34.2	0.400	0.017	0.002	0.237	0.011	0.051	0.005	0.056	0.037	0.540	0.133	0.008	0.003	0.005	0.002	0.009	0.069	0.070
VB29-6.d	2.41	0.540	19.9	1770	0.099	0.010	0.200	0.236	39.8	0.660	0.030	0.002	0.128	0.007	0.045	0.003	0.042	0.033	0.500	0.108	0.008	0.003	0.004	0.002	0.002	0.122	0.040
VB7-10.d	2.39	0.192	20.6	1419	0.090	0.025	0.170	0.168	29.5	0.185	0.017	0.003	0.245	0.009	0.031	0.002	0.030	0.019	0.174	0.076	0.028	0.008	0.003	0.003	0.003	0.314	0.063
VB7-9.d	2.70	0.870	20.1	1420	0.150	0.018	0.120	0.900	30.9	0.490	0.017	0.003	0.490	0.009	0.082	0.002	0.038	0.039	0.460	0.300	0.008	0.006	0.005	0.003	0.003	0.600	0.089

Grain ID (cubanite)	Ti 49	Mn 55	Co 59	Ni 60	Zn 66	Ga 71	Ge 74	As 75	Se 82	Mo 95	Ru 101	Rh 103	Ag 107	Pd 108	Cd 111	In 115	Sn 118	Sb 121	Te 128	Re 185	Os 189	Ir 193	Pt 195	Au 197	Tl 205	Pb 208	Bi 209
	0.49	**0.5**	**0.01**	**0.25**	**0.28**	**0.03**	**0.08**	**0.39**	**2.57**	**0.03**	**0.03**	**0.01**	**0.05**	**0.01**	**0.06**	**0.01**	**0.07**	**0.02**	**0.24**	**0**	**0.01**	**0**	**0.01**	**0**	**0**	**0**	**0**
MCR10a-10.d	3.50	0.520	0.680	110	258	0.022	1.34	0.246	219	0.018	0.034	0.004	87.6	0.008	54.0	0.558	4.40	0.030	3.01	0.003	0.007	0.002	0.009	0.028	0.051	470	0.880
MCR10a-11.d	4.80	0.342	0.066	15.8	39.7	0.180	1.14	0.324	210	0.019	0.017	0.004	88.8	0.008	40.5	3.29	106	0.029	3.08	0.003	0.007	0.002	0.006	0.047	0.169	26.4	0.310
MCR10a-16.d	4.00	9.50	0.130	9.00	95.0	0.036	1.18	0.403	260	0.019	0.017	0.004	108	0.008	18.2	0.933	215	0.290	5.10	0.003	0.007	0.002	0.006	0.004	0.118	274	0.206
MCR10a-1b.d	9.20	0.434	0.010	0.530	236	0.070	1.40	0.423	250	0.019	0.017	0.004	101	0.008	219	5.95	111	0.011	3.38	0.003	0.007	0.002	0.013	0.006	0.027	110	0.071
MCR10a-6.d	6.50	1.13	1.14	82.0	151	0.120	0.880	0.406	202	0.019	0.017	0.004	90.6	0.008	16.1	3.03	8.40	0.035	4.30	0.003	0.007	0.002	0.006	0.004	0.070	24.2	0.137
MCR10a-8.d	6.90	8.60	0.270	29.0	165	0.097	1.14	0.383	208	0.019	0.017	0.004	99.7	0.008	32.1	4.64	83.0	0.061	2.40	0.003	0.007	0.002	0.006	0.004	0.140	14.3	0.086
MCR10b-4.d	5.90	13.4	0.380	96.0	205	0.058	1.04	0.302	206	0.019	0.017	0.004	93.1	0.008	32.4	7.96	25.9	0.024	5.90	0.003	0.007	0.002	0.006	0.015	0.402	82.0	0.108
MCR13-10.d	4.40	0.249	0.870	53.4	284	0.012	0.740	0.222	157	0.019	0.017	0.004	46.3	0.008	13.4	1.08	1.82	0.121	8.90	0.003	0.007	0.002	0.005	0.016	0.026	146	0.475
MCR13-12.d	3.79	1.35	4.00	248	227	0.066	0.695	0.181	126	0.019	0.017	0.004	44.9	0.399	12.7	0.760	22.0	0.049	4.70	0.002	0.007	0.008	0.006	0.350	0.024	380	0.298
T11-10.d	4.80	16.7	0.022	1.80	6.60	0.014	0.460	0.312	134	0.022	0.017	0.003	1.27	1.75	1.35	0.015	1.07	0.029	26.1	0.003	0.008	0.002	0.005	0.003	0.472	68.5	0.090
T11-13.d	4.50	41.2	0.210	7.10	160	0.036	0.740	0.251	137	0.026	0.037	0.003	1.28	0.008	22.0	0.192	0.650	0.024	28.5	0.003	0.008	0.002	0.005	0.003	1.58	60.0	0.027
T11-4.d	3.90	41.6	0.018	1.04	1.32	0.019	0.620	0.203	126	0.022	0.017	0.003	1.60	0.308	0.730	0.311	0.250	0.037	29.5	0.003	0.008	0.002	0.005	0.013	0.812	86.8	0.027
T11-5.d	2.90	18.7	0.012	0.320	1.71	0.012	0.800	0.225	132	0.022	0.017	0.003	0.620	0.135	0.550	0.187	0.188	0.027	13.5	0.003	0.008	0.002	0.009	0.003	0.267	45.4	0.025
T11-8.d	4.90	13.4	0.017	3.30	256	0.012	0.610	0.201	142	0.019	0.017	0.003	1.81	0.008	23.3	0.175	0.520	0.020	30.7	0.003	0.008	0.002	0.004	0.003	1.10	75.0	0.040
T3-3.d	3.70	29.2	0.020	1.26	0.490	0.011	0.560	0.183	121	0.029	0.017	0.002	0.840	1.26	0.780	0.046	0.880	0.029	26.2	0.003	0.007	0.002	0.006	0.004	1.10	90.0	0.048
T3-4.d	4.80	26.0	0.040	5.40	0.770	0.013	0.560	0.243	129	0.032	0.017	0.004	0.371	0.764	0.450	0.052	0.630	0.053	28.3	0.004	0.160	0.002	0.006	0.003	1.41	86.3	0.076
T3-7.d	4.50	26.0	0.010	0.250	1.22	0.022	0.720	0.420	129	0.019	0.017	0.004	0.431	1.30	0.820	0.421	0.720	0.022	28.4	0.003	0.007	0.002	0.006	0.004	0.987	76.2	0.036
T3-9.d	4.50	18.8	0.140	2.60	6.10	0.022	0.600	0.245	125	0.020	0.017	0.004	1.70	0.654	1.04	0.021	0.460	0.023	27.4	0.003	0.007	0.002	0.010	0.004	1.00	63.3	0.049
T4-11.d	3.70	0.317	0.660	146	126	0.053	0.910	9.48	150	0.022	0.028	0.003	29.1	9.45	9.90	3.30	0.036	0.102	39.9	0.003	0.008	0.002	0.028	0.008	0.829	61.1	0.024
T4-14.d	2.60	0.370	0.290	14.2	152	0.017	0.890	12.1	155	0.022	0.017	0.003	30.2	10.2	12.1	3.28	0.027	0.027	42.0	0.003	0.008	0.002	0.047	0.084	1.44	49.9	0.011
T4-15.d	3.10	0.410	0.111	95.0	288	0.017	0.880	10.8	164	0.022	0.017	0.003	31.6	9.25	20.0	3.42	0.006	0.017	39.8	0.003	0.008	0.002	0.028	0.012	1.26	71.3	0.013
T4-2.d	3.43	0.560	0.127	40.0	120	0.017	0.860	11.3	168	0.022	0.017	0.003	25.0	10.9	13.4	2.74	0.034	0.028	47.4	0.003	0.008	0.002	0.040	0.006	1.56	55.6	0.013
T4-4.d	3.20	0.520	0.550	79.0	151	0.013	0.910	11.5	169	0.022	0.017	0.003	28.1	10.6	13.7	3.17	0.038	0.040	50.4	0.003	0.008	0.002	0.019	0.003	1.21	1.00	0.011
T4-5.d	3.40	0.780	0.900	14.2	3.20	0.021	1.16	6.94	187	0.114	0.017	0.003	4.64	10.5	0.850	0.015	0.039	0.040	42.8	0.003	0.008	0.002	0.010	0.005	0.146	107	0.012
T4-7.d	3.30	0.324	0.096	67.7	150	0.015	0.830	10.1	165	0.022	0.017	0.003	30.1	9.25	13.3	3.19	0.040	0.023	47.2	0.003	0.008	0.002	0.019	0.004	1.25	75.3	0.017
T4-9.d	3.20	0.313	0.245	66.1	164	0.023	0.760	10.6	152	0.022	0.017	0.003	26.1	9.82	15.0	3.11	0.034	0.038	40.3	0.003	0.008	0.002	0.008	0.003	1.18	61.2	0.012
VB27-6.d	2.50	2.00	0.680	20.0	46.0	0.015	0.950	0.315	179	0.022	0.017	0.003	68.0	0.008	15.5	19.4	1.20	0.047	35.4	0.003	0.008	0.002	0.008	0.003	0.670	24.2	0.248
VB27-7.d	3.80	10.1	0.040	1.23	32.6	0.017	0.890	0.240	177	0.022	0.160	0.003	26.2	0.008	13.5	13.5	43.0	0.015	30.4	0.003	0.008	0.002	0.005	0.016	0.228	16.3	0.178
VB27-8.d	4.00	15.8	0.190	1.80	437	0.017	1.17	0.286	194	0.022	0.017	0.003	49.9	0.008	17.5	13.8	12.7	0.036	39.7	0.003	0.008	0.002	0.007	0.005	0.693	36.0	0.479

Grain ID	Ti	Mn	Co	Ni	Zn	Ga	Ge	As	Se	Mo	Ru	Rh	Ag	Pd	Cd	In	Sn	Sb	Te	Re	Os	Ir	Pt	Au	Tl	Pb	Bi
(cubanite)	49	55	59	60	66	71	74	75	82	95	101	103	107	108	111	115	118	121	128	185	189	193	195	197	205	208	209
	0.49	**0.5**	**0.01**	**0.25**	**0.28**	**0.03**	**0.08**	**0.39**	**2.57**	**0.03**	**0.03**	**0.01**	**0.05**	**0.01**	**0.06**	**0.01**	**0.07**	**0.02**	**0.24**	**0**	**0.01**	**0**	**0.01**	**0**	**0**	**0**	**0**
VB27-9.d	4.40	16.9	0.141	169	201	0.017	0.850	0.253	185	0.022	0.017	0.003	38.3	0.008	126	9.58	16.9	0.032	32.0	0.003	0.008	0.002	0.004	0.003	0.818	23.7	0.375
VB31-12.d	3.40	6.50	107	50.8	231	0.037	0.310	0.319	59.6	0.022	0.017	0.003	3.17	0.008	114	4.30	14.0	0.460	6.33	0.005	0.009	0.002	0.005	0.014	0.019	38.6	170
VB31-2.d	3.70	0.337	0.170	6.60	200	0.031	0.330	0.480	60.2	0.022	0.042	0.003	3.79	0.008	7.00	116	0.140	0.011	6.19	0.005	0.009	0.002	0.004	0.003	0.004	10.8	0.073
VB31-6.d	3.90	138	19.0	474	447	0.059	0.256	0.363	60.4	0.022	0.017	0.003	2.93	0.008	12.5	2.64	3.20	0.128	138	0.005	0.009	0.002	0.005	0.003	0.075	33.1	0.150
VB34-2.d	4.00	9.70	15.9	213	302	0.020	0.850	0.339	174	0.022	0.017	0.003	36.7	0.008	75.7	6.02	7.20	0.030	26.6	0.005	0.009	0.002	0.005	0.005	0.690	17.6	0.140
VB34-5.d	5.70	23.9	3.60	56.0	1860	0.024	0.800	0.215	175	0.022	0.017	0.003	48.0	0.008	267	17.4	8.05	0.340	317	0.005	0.009	0.002	0.005	0.003	0.408	45.7	0.284
VB34-6.d	4.60	2.86	0.012	0.165	8.80	0.040	0.720	0.237	182	0.022	0.017	0.003	30.0	0.008	7.21	7.55	19.6	0.020	30.1	0.005	0.009	0.002	0.008	0.003	0.651	13.5	0.203
VB34-7.d	4.30	2.63	0.026	0.251	43.0	0.031	106	0.289	192	0.022	0.034	0.003	44.0	0.008	115	7.28	112	0.025	39.4	0.005	0.009	0.002	0.005	0.005	0.820	112	0.180
VB34-8.d	7.00	6.70	0.051	146	14.9	0.036	0.890	0.322	181	0.022	0.017	0.003	25.0	0.008	118	4.92	13.7	0.016	29.1	0.004	0.009	0.002	0.005	0.029	0.588	22.1	0.251
VB5-2.d	3.80	2.58	0.020	0.232	19.1	0.020	0.980	0.307	195	0.022	0.033	0.003	29.5	0.008	13.8	7.86	114	0.035	27.3	0.005	0.009	0.002	0.005	0.013	0.469	17.2	0.220
VB5-3.d	4.80	10.0	0.550	10.6	168	0.013	0.960	0.239	182	0.022	0.017	0.003	33.0	0.008	48.0	14.8	22.9	0.030	310	0.005	0.009	0.002	0.033	0.019	0.705	19.2	0.189
VB5-6.d	3.00	20.0	0.155	0.860	502	0.027	0.920	0.303	197	0.022	0.017	0.003	32.7	0.008	170	110	117	0.010	28.9	0.005	0.009	0.002	0.005	0.007	112	20.6	0.315
VB5-8.d	3.60	55.6	73.0	970	1390	0.018	108	0.195	193	0.022	0.017	0.003	100	0.008	269	16.5	7.81	0.026	34.8	0.005	0.009	0.002	0.005	0.006	186	55.7	0.619
VB6-1d	2.90	116	0.091	189	237	0.022	0.420	0.280	99.0	0.100	0.017	0.003	30.2	0.008	92.0	7.26	24.0	0.014	19.5	0.003	0.008	0.002	0.005	0.007	0.086	25.3	0.356
VB6-10.d	3.10	0.298	0.109	179	137	0.017	0.360	0.233	99.3	0.022	0.017	0.003	12.7	0.008	43.3	2.65	14.6	0.029	7.36	0.003	0.008	0.002	0.004	0.007	0.049	39.4	0.123
VB6-9.d	3.80	0.297	0.084	162	99.0	0.021	0.350	0.259	76.5	0.022	0.017	0.003	13.3	0.008	32.4	2.66	111	0.039	8.56	0.003	0.008	0.002	0.005	0.009	0.033	23.0	0.105

Annexe A6 Distribution of trace elements between chalcopyrite (ccp) and pentlandite (pn), pyrrhotite (po), and cubanite (cbn) calculated for each sample. in red: elements below detection limits, imputed values used.

Chalcopyrite and Pentlandite

Elements		Mn	Co	Ni	Zn	Ga	Se	Ag	In	Sn	Sb	Te	Au	Tl	Pb	Bi
		ppm	ppm	ppm	ppm	ppm	ppm	ppm	ppm	ppm	ppm	ppm	ppm	ppm	ppm	ppm
Median of detection limits (ccp)	55um	0.479	0.016	0.207	0.270	0.024	2.409	0.049	0.007	0.070	0.017	0.221	0.006	0.004	0.006	0.004
	33um	1.030	0.028	0.410	0.526	0.051	5.311	0.100	0.012	0.147	0.027	0.501	0.014	0.007	0.011	0.007
Median of detection limits (pn)		0.426	0.019	0.220	0.370	0.020	2.675	0.015	0.009	0.082	0.031	0.252	0.012	0.007	0.012	0.010
Sample																
Sample A2																
ccp median values - sample A2 (n=7)		0.165	0.043	37.1	79.7	0.030	230	9.35	0.550	0.042	0.034	76.8	6.8E-04	1.73	0.048	0.011
pn median values - sample A2 (n=3)		1.66	3640	332000	1.29	0.047	208	23.6	0.015	0.075	0.036	73.1	0.007	0.119	0.041	0.165
Dccp/pn		0.099	1.2E-05	1.1E-04	62.0	0.638	1.10	0.396	35.8	0.550	0.932	1.05	0.098	14.6	1.17	0.064
CRTN12																
ccp median values - sample CRTN12 (n=5)		1.34	0.330	50.3	544	0.131	74.1	8.42	0.911	5.36	0.026	0.315	0.002	4.8E-04	2.50	2.30
pn median values - sample CRTN12 (n=2)		0.945	17080	587500	6.05	0.088	85.4	0.551	0.008	0.287	0.220	0.262	0.103	0.011	0.150	0.083
Dccp/pn		1.41	1.9E-05	8.6E-05	89.9	1.49	0.868	15.3	121	18.7	0.118	1.20	0.023	0.046	16.6	27.8
CRTN13																
ccp median values - sample CRTN13 (n=5)		1.13	0.243	55.1	555	0.084	72.7	5.50	1.00	5.53	0.066	0.255	0.039	7.3E-04	3.86	2.97
pn median values - sample CRTN13 (n=1)		0.209	16100	555000	0.800	0.062	74.9	0.183	0.003	0.038	0.019	0.931	0.009	0.012	0.045	6.00
Dccp/pn		5.40	1.5E-05	9.9E-05	694	1.35	0.970	30.0	325	144	3.47	0.274	4.28	0.060	85.8	0.494
CRTN14																
ccp median values - sample CRTN14 (n=8)		0.855	0.920	74.0	464	0.057	77.0	3.28	1.35	11.4	0.120	0.370	0.123	3.8E-04	2.75	2.53
pn median values - sample CRTN14 (n=3)		0.590	16690	572000	3.50	0.049	92.9	0.206	0.006	0.062	0.118	0.270	0.017	0.005	0.180	0.455
Dccp/pn		1.45	5.5E-05	1.3E-04	133	1.15	0.828	15.9	212	183	1.02	1.37	7.21	0.079	15.3	5.56
CRTN18																
ccp median values - sample CRTN18 (n=5)		0.440	0.315	101	404	0.049	80.9	2.45	3.55	24.5	0.029	1.95	0.001	6.4E-04	2.19	1.25
pn median values - sample CRTN18 (n=3)		0.510	8870	544000	0.790	0.093	90.0	1.70	0.004	0.077	0.250	3.51	0.020	0.012	0.024	0.085
Dccp/pn		0.863	3.6E-05	1.8E-04	511	0.527	0.899	1.44	1010	318	0.116	0.556	0.055	0.052	91.3	14.7
CRTN19																
ccp median values - sample CRTN19 (n=19)		0.660	0.319	95.4	310	0.042	66.7	2.50	1.31	8.78	0.004	1.58	0.002	4.4E-04	1.97	2.53
pn median values - sample CRTN19 (n=3)		13.5	8320	565000	17.1	0.054	86.2	2.22	0.012	0.104	0.044	0.540	0.007	1.96	3.11	0.440
Dccp/pn		0.049	3.8E-05	1.7E-04	18.1	0.769	0.774	1.12	114	84.4	0.095	2.92	0.223	2.2E-04	0.632	5.75
CRTN6																
ccp median values - sample CRTN6 (n=5)		1.12	0.492	57.3	494	0.112	94.1	3.52	1.91	6.68	0.040	1.19	0.001	5.5E-04	3.14	0.479
pn median values - sample CRTN6 (n=2)		10.9	10710	320800	40.7	0.195	95.3	2.05	0.066	0.189	0.234	0.835	0.019	0.617	17.3	2.54
Dccp/pn		0.103	4.6E-05	1.8E-04	12.1	0.572	0.987	1.72	28.9	35.3	0.169	1.43	0.061	8.9E-04	0.182	0.189
CRTN9B																
ccp median values - sample CRTN9B (n=8)		1.43	0.602	85.9	478	0.085	86.1	1.64	3.25	53.0	0.060	1.49	0.019	4.3E-04	1.57	2.31
pn median values - sample CRTN9B (n=3)		0.460	14310	568000	0.440	0.073	94.5	1.94	0.004	0.070	0.125	3.64	0.016	0.136	0.028	0.019
Dccp/pn		3.10	4.2E-05	1.5E-04	1085	1.16	0.911	0.845	755	756	0.483	0.409	1.22	0.003	56.1	122
MCR10B																
ccp median values - sample MCR10B (n=10)		1.55	0.111	40.1	173	0.062	188	30.8	8.75	204	0.022	3.39	0.037	0.117	3.85	0.238
pn median values - sample MCRB10B (n=2)		29.9	3890	460000	1.10	0.080	169	37.2	0.045	2.16	0.190	47.7	0.098	5.34	71.7	3.55
Dccp/pn		0.052	2.8E-05	8.7E-05	157	0.780	1.11	0.828	196	94.3	0.113	0.071	0.382	0.022	0.054	0.067
MCR13																
ccp median values - sample MCR13 (n=12)		0.211	0.223	48.0	157	0.076	142	20.4	10.7	66.4	0.029	3.98	0.030	0.012	5.40	0.287
pn median values - sample MCR13 (n=2)		30.9	10335	516750	3.03	0.081	260	8.43	0.227	14.0	1.04	54.7	0.023	8.44	221	1.48
Dccp/pn		0.007	2.2E-05	9.3E-05	51.8	0.929	0.544	2.42	47.1	4.73	0.028	0.073	1.30	0.001	0.024	0.193
MCR3																
ccp median values - sample MCR3 (n=4)		1.89	0.291	48.7	446	0.067	55.6	0.825	4.54	12.1	0.005	0.035	0.002	4.4E-04	1.91	0.132
pn median values - sample MCR3 (n=1)		9.30	11180	302600	0.760	0.013	57.5	1.05	0.006	0.290	0.0096	0.072	0.110	0.180	9.70	0.840
Dccp/pn		0.203	2.6E-05	1.6E-04	586	5.00	0.966	0.786	794	41.9	0.471	0.490	0.018	0.002	0.196	0.157
MCR4B																
ccp median values - sample MCR4B (n=7)		0.680	0.142	46.0	337	0.048	54.2	0.840	4.32	5.49	0.029	0.089	4.9E-04	4.3E-04	1.22	0.087
pn median values - sample MCR4B (n=3)		48.5	12690	524000	720	0.340	51.8	1.19	0.255	0.910	0.055	0.186	0.046	0.220	12.9	0.230
Dccp/pn		0.014	1.1E-05	8.8E-05	0.468	0.141	1.05	0.706	16.9	6.03	0.527	0.479	0.011	0.002	0.095	0.378
MCR5																
ccp median values - sample MCR5 (n=5)		0.910	0.600	71.6	367	0.065	84.3	1.40	8.53	47.7	0.004	0.070	9.2E-04	5.2E-04	3.03	0.270
pn median values - sample MCR5 (n=3)		1.14	8040	315000	70.0	0.042	83.3	0.390	0.205	0.190	0.013	0.132	0.007	0.024	3.57	0.870
Dccp/pn		0.798	7.5E-05	2.3E-04	5.24	1.55	1.01	3.59	41.6	251	0.314	0.527	0.131	0.021	0.849	0.310
VB25																
ccp median values - sample VB25 (n=5)		0.600	0.051	3.08	183	0.035	60.0	2.63	5.70	5.35	0.041	6.79	6.9E-04	0.001	7.22	0.062
pn median values - sample VB25 (n=3)		12.1	16160	315000	3.50	0.056	52.3	9.21	0.060	0.064	0.033	2.70	0.008	0.094	27.8	0.573
Dccp/pn		0.050	3.2E-06	9.8E-06	52.3	0.625	1.15	0.286	95.1	83.6	1.24	2.51	0.086	0.011	0.260	0.108

Elements	Mn	Co	Ni	Zn	Ga	Se	Ag	In	Sn	Sb	Te	Au	Tl	Pb	Bi
VB29	ppm	ppm	ppm	ppm	ppm	ppm	ppm	ppm	ppm	ppm	ppm	ppm	ppm	ppm	ppm
ccp median values - sample VB29 (n=2)	0.143	0.077	5.67	207	0.008	57.1	2.99	0.980	6.13	0.022	12.5	8.8E-04	0.061	4.47	0.220
pn median values - sample VB29 (n=3)	99.0	21900	452000	1.80	0.168	53.0	2.98	0.007	0.220	0.320	0.290	0.007	0.296	50.5	1.42
Dccp/pn	0.001	3.5E-06	1.3E-05	115	0.047	1.08	1.00	139	27.8	0.069	43.1	0.128	0.206	0.089	0.155
Dccp/pn median values	0.103	2.6E-05	1.1E-04	89.9	0.780	0.970	1.12	121	83.6	0.314	0.556	0.128	0.021	0.632	0.310
Dccp/pn min	0.001	3.2E-06	9.8E-06	0.468	0.047	0.544	0.286	16.9	0.550	0.028	0.071	0.011	2.2E-04	0.024	0.064
Dccp/pn max	5.40	7.5E-05	2.3E-04	1085	5.00	1.15	30.0	1010	756	3.47	43.1	7.21	14.6	91.3	122

Chalcopyrite and Pyrrhotite

Elements		Mn	Co	Ni	Zn	Ga	Se	Ag	In	Sn	Sb	Te	Au	Tl	Pb	Bi
		ppm	ppm	ppm	ppm	ppm	ppm	ppm	ppm	ppm	ppm	ppm	ppm	ppm	ppm	ppm
Median of detection limits (ccp)	55um	0.479	0.016	0.207	0.270	0.024	2.409	0.049	0.007	0.070	0.017	0.221	0.006	0.004	0.006	0.004
	33um	1.030	0.028	0.410	0.526	0.051	5.311	0.100	0.012	0.147	0.027	0.501	0.014	0.007	0.011	0.007
Median of detection limits (po)		0.406	0.014	0.235	0.231	0.024	2.148	0.045	0.005	0.063	0.013	0.194	0.004	0.003	0.003	0.003
Sample																
1533																
ccp median values - sample 1533 (N=8)		6.85	0.133	38.6	348	0.176	185	6.12	10.0	52.5	0.071	3.12	0.001	0.154	42.7	0.925
po median values - sample 1533 (N=7)		0.254	27.8	4020	0.139	0.015	156	0.174	0.004	0.041	0.036	0.135	0.003	0.002	0.360	0.115
Dccp/po		26.9	0.005	0.0096	2493	11.9	1.18	35.2	2326	1266	1.97	23.1	0.489	66.8	119	8.04
2523																
ccp median values - sample 2523 (N=6)		0.585	0.236	48.1	423	0.164	67.5	1.51	3.03	7.55	0.077	1.88	0.017	4.0E-04	4.31	1.91
po median values - sample 2523 (N=4)		1.51	70.1	2240	0.242	0.028	51.9	0.111	0.003	0.045	0.0098	0.136	0.003	0.002	1.42	0.799
Dccp/po		0.389	0.003	0.021	1745	5.88	1.30	13.7	884	169	7.86	13.8	5.97	0.198	3.03	2.38
CRTN18																
ccp median values - sample CRTN18 (N=5)		0.440	0.315	101	404	0.049	80.9	2.45	3.55	24.5	0.029	1.95	0.001	6.4E-04	2.19	1.25
po median values - sample CRTN18 (N=2)		0.625	49.9	4625	0.845	0.035	63.4	0.139	0.007	0.101	0.021	0.252	0.002	0.002	0.224	0.650
Dccp/po		0.704	0.006	0.022	478	1.41	1.28	17.6	544	243	1.36	7.75	0.450	0.304	9.78	1.92
CRTN19																
ccp median values - sample CRTN19 (N=6)		0.660	0.319	95.4	310	0.042	66.7	2.50	1.31	8.78	0.004	1.58	0.002	4.4E-04	1.97	2.53
po median values - sample CRTN19 (N=4)		0.297	54.3	3195	0.541	0.023	80.1	0.155	0.003	0.053	0.015	0.184	0.008	0.001	0.229	1.46
Dccp/po		2.22	0.006	0.030	572	1.83	0.833	16.1	457	166	0.270	8.54	0.203	0.293	8.58	1.74
DC18																
ccp median values - sample DC18 (N=7)		0.470	0.159	12.5	211	0.448	57.1	3.27	1.35	2.19	0.015	2.37	5.2E-04	5.2E-04	8.43	0.085
po median values - sample DC18 (N=3)		0.780	48.5	1722	0.133	0.014	34.7	0.108	0.002	0.035	0.019	0.160	0.003	0.002	0.155	0.115
Dccp/po		0.603	0.003	0.007	1588	33.1	1.65	30.3	560	62.3	0.789	14.8	0.177	0.224	54.4	0.739
DC69																
ccp median values - sample DC69 (N=7)		1.08	0.730	31.8	274	0.520	44.3	0.460	1.37	4.66	0.043	4.02	8.1E-04	0.006	7.88	0.416
po median values - sample DC69 (N=3)		0.310	118	4050	0.207	0.021	24.6	0.103	0.003	0.046	0.015	0.201	0.006	0.001	0.340	0.152
Dccp/po		3.48	0.006	0.008	1326	24.6	1.80	4.47	486	101	2.87	20.0	0.141	3.98	23.2	2.74
E1																
ccp median values - sample E1 (N=4)		0.287	0.107	11.3	360	0.008	77.8	6.15	2.28	0.460	0.132	11.6	0.001	0.015	8.86	1.02
po median values - sample E1 (N=4)		3.32	24.7	2360	1.06	0.037	50.6	0.100	0.003	0.035	0.025	0.154	0.003	0.002	0.903	0.219
Dccp/po		0.086	0.004	0.005	339	0.232	1.54	61.8	771	13.1	5.37	74.8	0.367	6.31	9.81	4.67
E13																
ccp median values - sample E13 (N=3)		0.197	0.180	9.70	221	0.017	97.3	7.96	2.19	1.63	0.013	4.87	0.013	0.048	3.51	0.570
po median values - sample E13 (N=2)		4.41	0.875	2.94	0.178	0.038	62.0	0.630	0.004	0.069	0.025	0.255	0.005	0.002	0.776	0.264
Dccp/po		0.045	0.206	3.30	1245	0.436	1.57	12.6	570	23.6	0.531	19.1	2.54	29.7	4.52	2.16
E4																
ccp median values - sample E4 (N=6)		0.667	0.425	57.9	510	0.018	106	10.4	3.25	33.0	0.029	9.71	0.016	0.064	11.4	1.000
po median values - sample E4 (N=2)		0.370	17.3	2076	0.149	0.026	74.8	0.334	0.003	0.070	0.029	0.242	0.004	0.006	0.884	0.258
Dccp/po		1.80	0.025	0.028	3432	0.715	1.41	31.0	1198	473	0.973	40.1	3.77	10.8	12.9	3.88
EDEEP																
ccp median values - sample EDEEP (N=5)		0.353	0.132	13.2	229	0.260	56.0	2.07	2.68	2.61	0.004	10.0	0.001	6.5E-04	1.97	0.374
po median values - sample EDEEP (N=4)		0.479	50.2	3570	0.237	0.028	37.1	0.260	0.006	0.071	0.014	1.27	0.004	0.002	0.245	0.058
Dccp/po		0.736	0.003	0.004	967	9.23	1.51	7.98	474	36.8	0.273	7.87	0.271	0.298	8.04	6.50
EX0301																
ccp median values - sample EX0301 (N=9)		1.02	0.075	8.75	262	0.076	48.7	6.12	2.41	11.1	0.016	6.24	0.015	7.4E-04	3.38	0.097
po median values - sample EX0301 (N=4)		0.555	21.4	1774	0.148	0.027	29.5	0.081	0.004	0.048	0.012	0.123	0.003	0.002	0.639	0.040
Dccp/po		1.84	0.004	0.005	1773	2.77	1.65	75.5	615	233	1.30	50.5	5.86	0.432	5.29	2.46
K2																
ccp median values - sample K2 (N=8)		1.62	0.215	20.2	309	0.103	52.0	0.965	6.28	24.5	0.205	1.15	0.031	4.8E-04	2.26	0.149

Elements	Mn	Co	Ni	Zn	Ga	Se	Ag	In	Sn	Sb	Te	Au	Tl	Pb	Bi
	ppm	ppm	ppm	ppm	ppm	ppm	ppm	ppm	ppm	ppm	ppm	ppm	ppm	ppm	ppm
po median values - sample K2 (N=3)	0.600	23.3	4120	0.170	0.023	36.8	0.091	0.002	0.045	0.028	0.121	0.003	0.001	0.522	0.133
Dccp/po	2.69	0.0092	0.005	1820	4.56	1.41	10.6	2827	542	7.30	9.43	12.0	0.331	4.32	1.12
MCR4B															
ccp median values - sample MCR4B (N=7)	0.680	0.142	46.0	337	0.048	54.2	0.840	4.32	5.49	0.029	0.089	4.9E-04	4.3E-04	1.22	0.087
po median values - sample MCR4B (N=4)	0.309	64.9	3105	0.146	0.013	40.8	0.081	0.003	0.031	0.023	0.096	0.003	0.002	0.281	0.060
Dccp/po	2.20	0.002	0.015	2310	3.79	1.33	10.4	1572	175	1.26	0.924	0.175	0.176	4.34	1.45
MCR5															
ccp median values - sample MCR5 (N=5)	0.910	0.600	71.6	367	0.065	84.3	1.40	8.53	47.7	0.004	0.070	9.2E-04	5.2E-04	3.03	0.270
po median values - sample MCR5 (N=3)	0.860	90.9	5760	0.412	0.014	94.8	0.190	0.003	0.037	0.019	0.096	0.006	0.001	0.244	0.209
Dccp/po	1.06	0.007	0.012	891	4.78	0.889	7.37	3092	1305	0.218	0.723	0.160	0.357	12.4	1.29
NR6															
ccp median values - sample NR6 (N=5)	0.600	0.590	58.0	287	0.044	36.2	2.87	0.805	0.141	0.021	0.560	6.0E-04	0.033	13.7	0.156
po median values - sample NR6 (N=4)	4.67	271	7470	0.147	0.014	27.8	0.548	0.003	0.023	0.021	0.127	0.003	0.002	1.75	0.216
Dccp/po	0.129	0.002	0.008	1955	3.21	1.30	5.24	273	6.21	1.00	4.42	0.185	16.9	7.83	0.724
T1															
ccp median values - sample T1 (N=5)	8.82	0.660	17.3	305	0.085	65.6	1.80	0.932	0.433	0.003	3.01	3.8E-04	0.007	0.302	0.013
po median values - sample T1 (N=2)	6.40	21.4	1695	0.190	0.020	47.1	0.043	0.004	0.027	0.011	0.745	0.003	0.002	0.413	0.036
Dccp/po	1.38	0.031	0.010	1605	4.30	1.39	42.2	255	16.3	0.291	4.04	0.150	2.92	0.732	0.357
TR20															
ccp median values - sample TR20 (N=8)	0.309	0.100	28.8	286	0.109	56.4	17.1	5.59	11.1	0.029	1.56	0.077	8.7E-04	1.35	0.047
po median values - sample TR20 (N=3)	0.860	41.2	2310	0.289	0.022	41.7	0.260	0.006	0.107	0.014	0.325	0.006	0.003	0.400	0.040
Dccp/po	0.359	0.002	0.012	989	4.88	1.35	65.8	1010	104	2.07	4.78	12.5	0.281	3.38	1.18
VB21															
ccp median values - sample VB21 (N=6)	0.900	0.187	6.11	178	0.023	68.3	1.85	8.82	5.86	0.005	7.60	6.2E-04	8.7E-04	5.38	0.076
po median values - sample VB21 (N=2)	12.4	22.0	1773	0.607	0.021	39.1	0.196	0.003	0.038	0.033	0.620	0.002	0.001	0.081	0.055
Dccp/po	0.073	0.009	0.003	293	1.10	1.75	9.41	3481	153	0.147	12.3	0.254	0.755	66.4	1.36
VB25															
ccp median values - sample VB25 (N=5)	0.600	0.051	3.08	183	0.035	60.0	2.63	5.70	5.35	0.041	6.79	6.9E-04	0.001	7.22	0.062
po median values - sample VB25 (N=3)	0.780	14.5	1089	0.370	0.013	35.3	0.349	0.005	0.038	0.049	0.170	0.002	0.001	0.374	0.045
Dccp/po	0.769	0.004	0.003	495	2.76	1.70	7.54	1189	140	0.837	39.9	0.296	0.872	19.3	1.38
VB29															
ccp median values - sample VB29 (N=2)	0.143	0.077	5.67	207	0.008	57.1	2.99	0.980	6.13	0.022	12.5	8.8E-04	0.061	4.47	0.220
po median values - sample VB29 (N=2)	0.535	18.5	1635	0.111	0.018	37.0	0.183	0.004	0.049	0.035	0.520	0.002	0.006	0.096	0.055
Dccp/po	0.268	0.004	0.003	1868	0.435	1.54	16.4	251	125	0.628	24.0	0.363	10.4	46.8	3.99
VB7															
ccp median values - sample VB7 (N=7)	0.203	0.139	10.5	166	0.131	53.4	3.71	1.73	5.93	0.014	16.6	7.4E-04	6.4E-04	4.86	0.189
po median values - sample VB7 (N=2)	0.531	20.4	1420	0.120	0.022	30.2	0.368	0.002	0.034	0.029	0.317	0.003	0.003	0.457	0.076
Dccp/po	0.382	0.007	0.007	1382	6.09	1.77	10.1	915	176	0.483	52.4	0.270	0.236	10.6	2.49
Dccp/pn median values	0.736	0.005	0.008	1382	3.79	1.41	13.7	771	153	0.973	13.8	0.296	0.432	9.78	1.92
Dccp/po min	0.045	0.002	0.003	293	0.232	0.833	4.47	251	6.21	0.147	0.723	0.141	0.176	0.732	0.357
Dccp/po max	26.9	0.206	3.30	3432	33.1	1.80	75.5	3481	1305	7.86	74.8	12.5	66.8	119	8.04

Chalcopyrite and Cubanite

Elements		Mn	Co	Ni	Zn	Ga	Se	Ag	In	Sn	Sb	Te	Au	Tl	Pb	Bi
		ppm	ppm	ppm	ppm	ppm	ppm	ppm	ppm	ppm	ppm	ppm	ppm	ppm	ppm	ppm
Median of detection limits (ccp)	55um	0.479	0.016	0.207	0.270	0.024	2.409	0.049	0.007	0.070	0.017	0.221	0.006	0.004	0.006	0.004
	33um	1.030	0.028	0.410	0.526	0.051	5.311	0.100	0.012	0.147	0.027	0.501	0.014	0.007	0.011	0.007
Median of detection limits (cbn)		0.502	0.015	0.248	0.279	0.030	2.566	0.050	0.006	0.070	0.016	0.242	0.005	0.003	0.004	0.003
Sample																
MCR10A																
ccp median values - sample MCR10A (n=16)		1.94	0.094	52.0	171	0.062	212	35.6	7.04	204	0.030	2.90	0.036	0.103	4.62	0.184
cbn median values - sample MCR10A (n=7)		0.825	0.200	22.4	158	0.084	215	95.2	3.16	52.3	0.033	3.23	0.005	0.094	25.3	0.172
Dccp/cbn		2.35	0.468	2.32	1.08	0.740	0.986	0.374	2.23	3.91	0.908	0.899	7.09	1.10	0.183	1.07
MCR10B																
ccp median values - sample MCR10B (n=10)		2.08	0.111	41.3	172	0.062	204	34.6	8.10	200	0.021	3.80	0.037	0.121	3.91	0.260
cbn median values - sample MCR10B (n=1)		13.4	0.380	96.0	205	0.058	206	93.1	7.96	25.9	0.024	5.90	0.015	0.402	82.0	0.108
Dccp/cbn		0.155	0.292	0.430	0.840	1.07	0.990	0.372	1.02	7.72	0.875	0.644	2.48	0.301	0.048	2.40
MCR13																

Elements	Mn	Co	Ni	Zn	Ga	Se	Ag	In	Sn	Sb	Te	Au	Tl	Pb	Bi
	ppm	ppm	ppm	ppm	ppm	ppm	ppm	ppm	ppm	ppm	ppm	ppm	ppm	ppm	ppm
ccp median values - sample MCR13 (n=12)	0.197	0.223	48.0	157	0.076	142	20.4	10.7	66.4	0.029	3.98	0.030	0.012	5.40	0.287
cbn median values - sample MCR13 (n=2)	0.799	2.44	151	256	0.039	141	45.6	0.921	11.9	0.085	6.80	0.183	0.025	263	0.387
Dccp/cbn	0.247	0.092	0.319	0.615	1.93	1.00	0.447	11.6	5.58	0.341	0.585	0.164	0.499	0.021	0.743
T11															
ccp median values - sample T11 (n=8)	5.48	0.084	4720	29.9	0.005	127	0.850	4.16	0.930	0.019	29.1	5.4E-04	1.16	16.9	0.019
cbn median values - sample T11 (n=5)	18.7	0.018	1.80	6.60	0.014	134	1.28	0.187	0.520	0.027	28.5	0.003	0.812	68.5	0.027
Dccp/cbn	0.293	4.63	2622	4.53	0.363	0.944	0.664	22.3	1.79	0.685	1.02	0.166	1.43	0.247	0.686
T3															
ccp median values - sample T3 (n=7)	5.92	0.115	6690	24.3	0.005	122	0.575	4.44	1.02	0.032	27.0	4.7E-04	0.809	18.3	0.018
cbn median values - sample T3 (n=4)	26.0	0.030	1.93	0.995	0.017	127	0.636	0.049	0.675	0.026	27.9	0.004	1.05	81.3	0.049
Dccp/cbn	0.228	3.83	3466	24.4	0.298	0.965	0.905	91.1	1.51	1.23	0.969	0.131	0.771	0.225	0.371
T4															
ccp median values - sample T4 (n=8)	0.213	0.050	31.4	115	0.008	162	8.08	3.18	0.025	0.015	43.2	4.8E-04	1.21	32.2	0.010
cbn median values - sample T4 (n=8)	0.390	0.268	87.0	151	0.017	164	28.6	3.18	0.035	0.033	42.4	0.006	1.23	66.3	0.013
Dccp/cbn	0.546	0.187	0.360	0.764	0.494	0.988	0.283	1.000	0.713	0.458	1.02	0.085	0.983	0.486	0.802
VB27															
ccp median values - sample VB27 (n=4)	18.7	0.022	2.63	233	0.018	187	18.8	18.2	24.3	0.007	31.1	0.001	0.712	9.62	0.302
cbn median values - sample VB27 (n=4)	16.4	0.166	1.75	124	0.017	182	44.1	13.6	30.0	0.034	33.7	0.004	0.682	24.0	0.312
Dccp/cbn	1.14	0.133	1.51	1.89	1.08	1.03	0.427	1.33	0.811	0.214	0.923	0.288	1.04	0.401	0.970
VB31															
ccp median values - sample VB31 (n=7)	0.830	0.500	23.7	182	0.015	61.4	2.73	5.24	8.11	0.025	6.30	0.017	0.123	28.0	0.340
cbn median values - sample VB31 (n=3)	1.38	1.07	50.8	231	0.037	60.2	3.17	2.64	3.20	0.128	6.19	0.003	0.019	33.1	0.150
Dccp/cbn	0.601	0.467	0.467	0.788	0.394	1.02	0.861	1.98	2.53	0.195	1.02	4.86	6.47	0.846	2.27
VB34															
ccp median values - sample VB34 (n=2)	22.3	0.016	0.935	224	0.018	180	19.7	19.5	32.3	0.032	26.6	9.1E-04	0.520	10.9	0.210
cbn median values - sample VB34 (n=5)	6.70	0.051	1.46	43.0	0.031	181	36.7	7.28	11.2	0.025	30.1	0.005	0.651	17.6	0.203
Dccp/cbn	3.34	0.304	0.640	5.20	0.582	0.992	0.537	2.67	2.89	1.28	0.882	0.196	0.799	0.619	1.03
VB5															
ccp median values - sample VB5 (n=3)	24.0	0.020	1.49	166	0.030	181	23.1	19.8	30.0	0.011	26.5	0.001	0.561	12.0	0.255
cbn median values - sample VB5 (n=4)	15.0	0.353	5.73	335	0.019	194	32.9	12.9	11.6	0.028	30.0	0.0099	0.913	19.9	0.268
Dccp/cbn	1.60	0.057	0.260	0.496	1.59	0.932	0.703	1.54	2.59	0.378	0.885	0.103	0.615	0.602	0.953
VB6															
ccp median values - sample VB6 (n=11)	0.660	0.043	3.30	186	0.0095	90.6	10.9	8.74	28.8	0.006	15.9	0.019	0.027	7.13	0.221
cbn median values - sample VB6 (n=3)	0.298	0.091	1.79	137	0.021	99.0	13.3	2.66	14.6	0.029	8.56	0.007	0.049	25.3	0.123
Dccp/cbn	2.22	0.473	1.84	1.36	0.449	0.915	0.817	3.28	1.97	0.198	1.86	2.79	0.551	0.282	1.80
Dccp/cbn median values	0.601	0.304	0.640	1.08	0.582	0.988	0.537	2.23	2.53	0.458	0.923	0.196	0.799	0.282	0.970
Dccp/cbn min	0.155	0.057	0.260	0.496	0.298	0.915	0.283	1.000	0.713	0.195	0.585	0.085	0.301	0.021	0.371
Dccp/cbn max	3.34	4.63	3466	24.4	1.93	1.03	0.905	91.1	7.72	1.28	1.86	7.09	6.47	0.846	2.40

Annexe A7 Confusion matrices for the PLS-DA classification by deposit type (a) and ore type (b) of published data. Actual classes: classification from literature. Predicted classes: classification from model.

a. Deposit type

		Predicted		
		Ni-Cu sulfide	Reef-type PGE	Total
Actual	Ni-Cu sulfide	98	9	107
	Reef-type PGE	8	48	56
	Total	106	57	163
	Accuracy 90%			

b. Ore type

		Predicted		
		Cu-rich	Fe-rich/unzoned	Total
Actual	Cu-rich	13	37	50
	Fe-rich/unzoned	2	55	57
	Total	15	92	107
	Accuracy 64%			

Annexe A8 Confusion matrices for the binary discriminant diagrams by deposit type (a) and ore type (b) of literature data. Actual classes: classification from literature. Predicted classes: classification from model.

a. Deposit type

		Predicted			
		Ni-Cu sulfide	Reef-type PGE	Non-predicted	Total
Actual	Ni-Cu sulfide	244	12	16	272
	Reef-type PGE	12	30	34	76
	Total	256	42	50	348
	Accuracy 92%				

b. Ore type

		Predicted			
		Cu-rich	Fe-rich/unzoned	Non-predicted	Total
Actual	Cu-rich	33	32	6	71
	Fe-rich/unzoned	12	59	30	101
	Total	45	91	36	172
	Accuracy 68%				

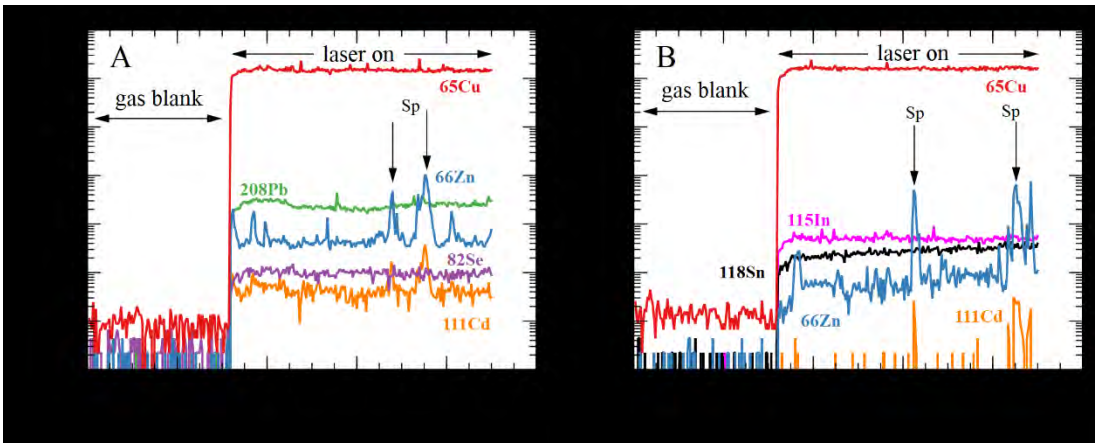

Annexe A9 Example of time-signal spectra for chalcopyrite showing inclusions of sphalerite (Sp)

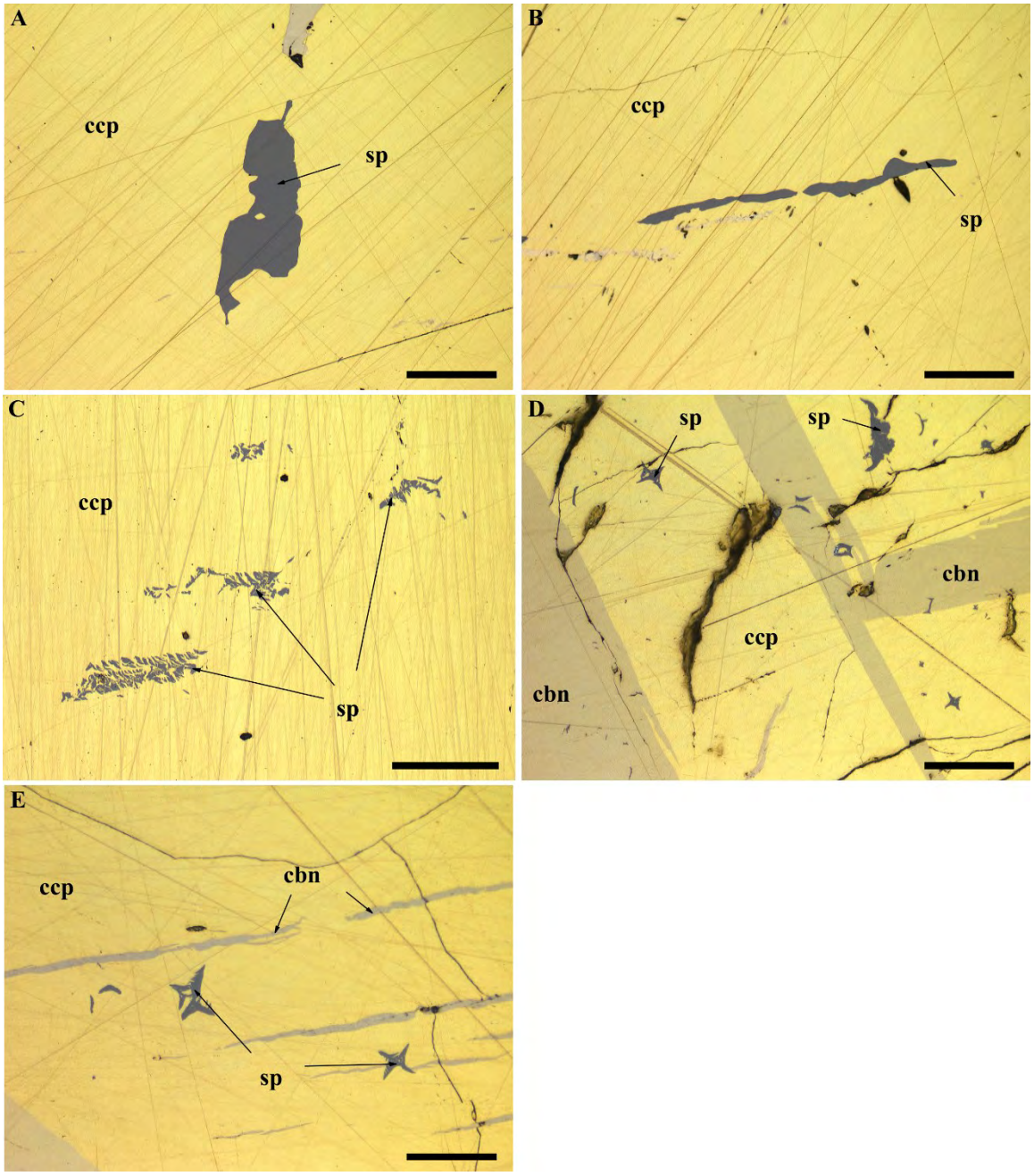

Annexe A10 Sphalerite (sp) exsolutions in chalcopyrite (ccp). Sphalerite in a and b are probably result of co-crystallization with chalcopyrite. Skeletal (c) and star-like forms(c-e) as result of exsolution in chalcopyrite. Presence of exsolution lamellae cubanite (cbn) in chalcopyrite are common. Scale bar: 100 µm

	Co	Ni	Zn	Ga	Se	Ag	In	Sn	Sb	Te	Au	Tl	Pb	Bi
Mn	-0.03	0.16	0.06	-0.02	-0.04	-0.19	-0.18	-0.28	-0.12	-0.12	-0.31	0.09	0.04	-0.31
Co		0.16	0.24	0.14	-0.28	-0.21	-0.12	0.04	0.03	-0.16	0.04	-0.33	-0.08	0.15
Ni			-0.04	-0.12	-0.07	-0.16	-0.15	-0.15	-0.03	0.03	-0.35	0.07	0.03	-0.21
Zn				0.37	0.11	-0.07	-0.27	-0.24	-0.09	-0.33	-0.13	-0.59	-0.12	-0.03
Ga					0.17	-0.13	-0.1	0	-0.21	-0.26	-0.08	-0.41	-0.12	-0.08
Se						0.11	0.03	-0.22	-0.34	0.12	-0.1	0.15	0.05	-0.29
Ag							0.06	0.11	-0.18	0.19	0.11	0.22	0.01	-0.11
In								0.53	0.01	0.26	0.08	0.09	0.04	0.06
Sn									0.02	0.18	0.27	-0.16	-0.12	0.42
Sb										-0.05	0	-0.04	-0.02	0.21
Te											-0.16	0.28	0.04	0.1
Au												-0.17	-0.2	0.27
Tl													0.21	-0.3
Pb														-0.09

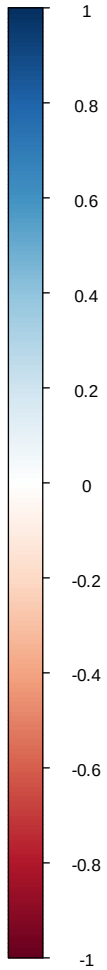

Annexe A11 Pearson correlation coefficient matrix of the trace elements of chalcopyrite from magmatic deposits (Ni-Cu sulfide and Reef-type PGE). In color, significant coefficients. Significance level α = 0.05

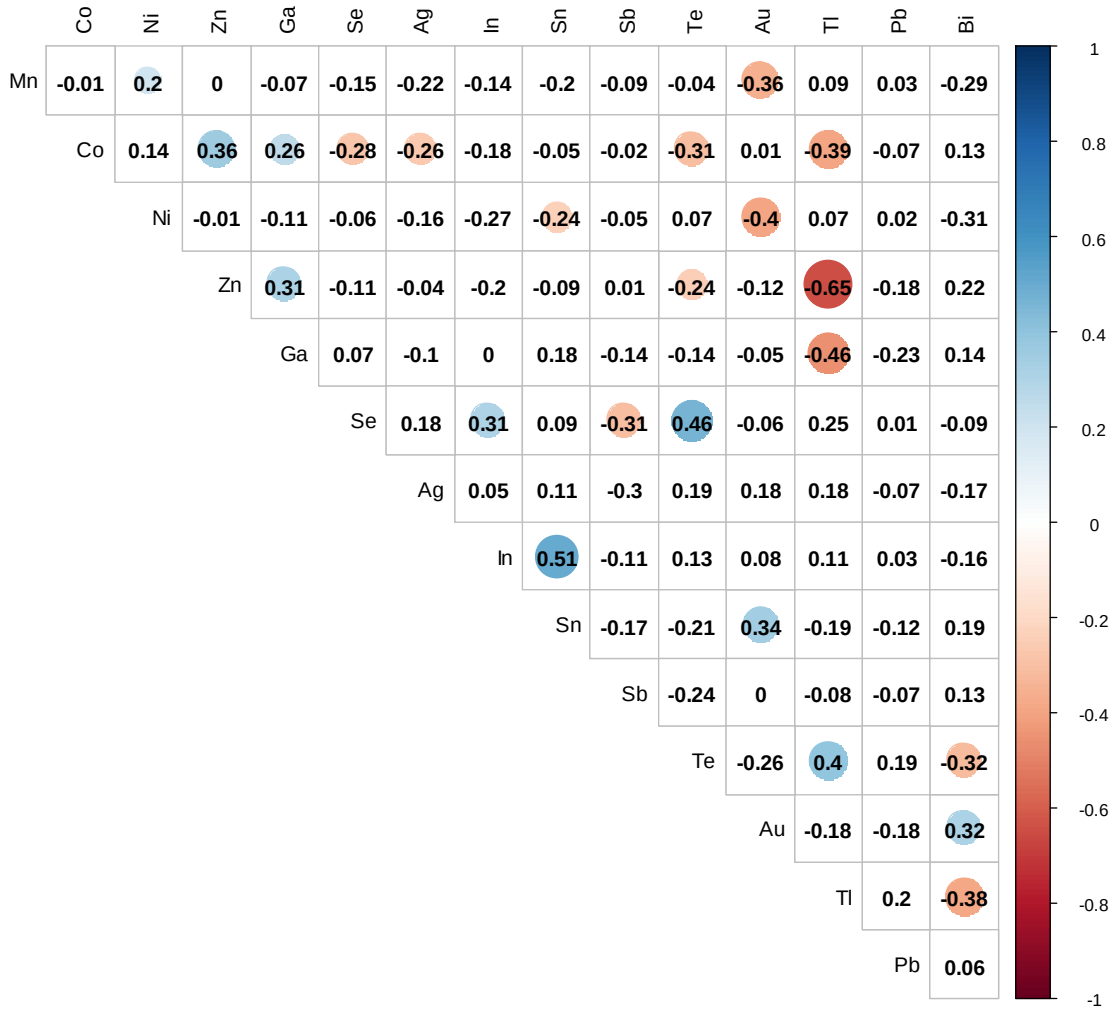

Annexe A12 Pearson correlation coefficient matrix of the trace elements of chalcopyrite from Ni-Cu sulfide deposits. In color, significant coefficients. In color, significant coefficients. Significance level α = 0.05

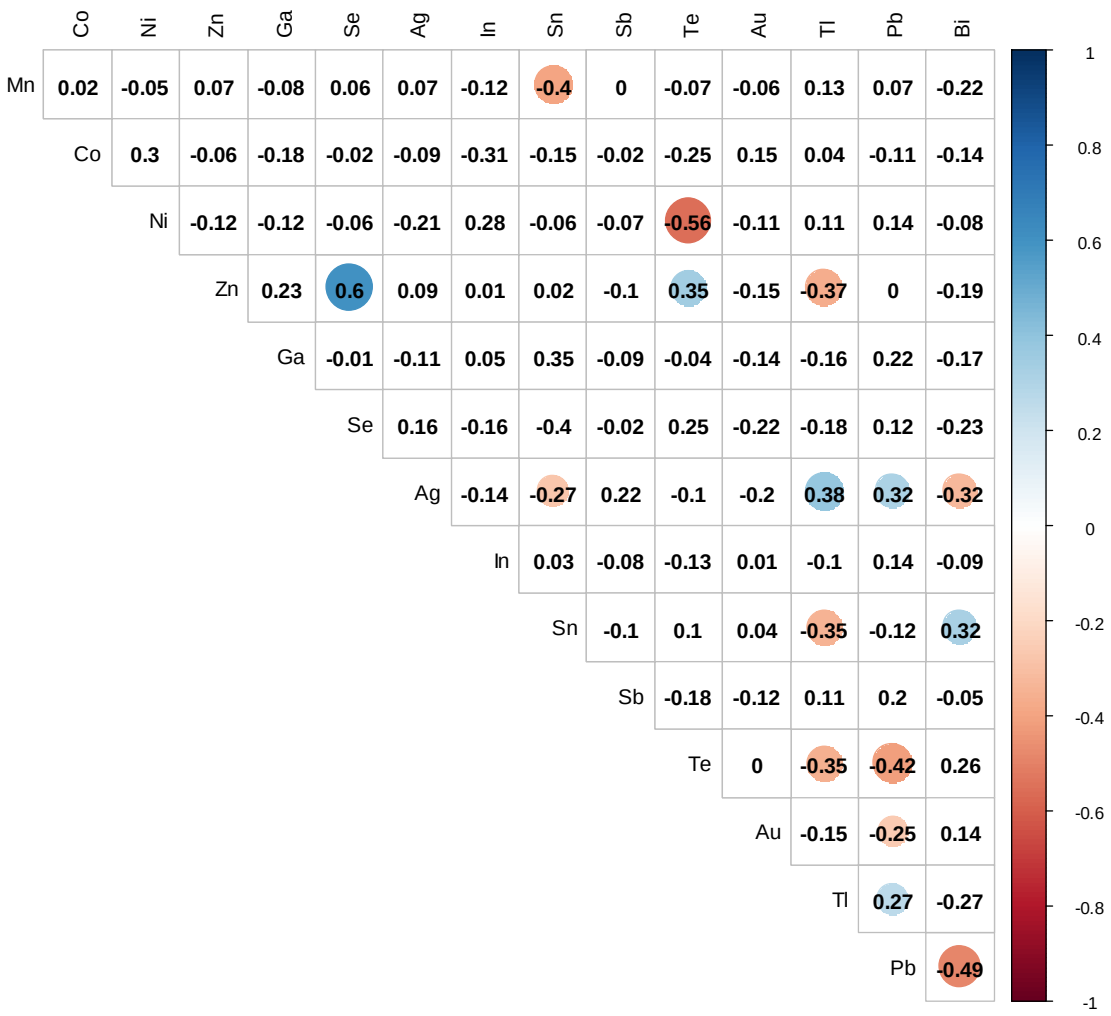

Annexe A13 Pearson correlation coefficient matrix of the trace elements of chalcopyrite from Reef-type PGE deposits. In color, significant coefficients. In color, significant coefficients. Significance level α = 0.05.

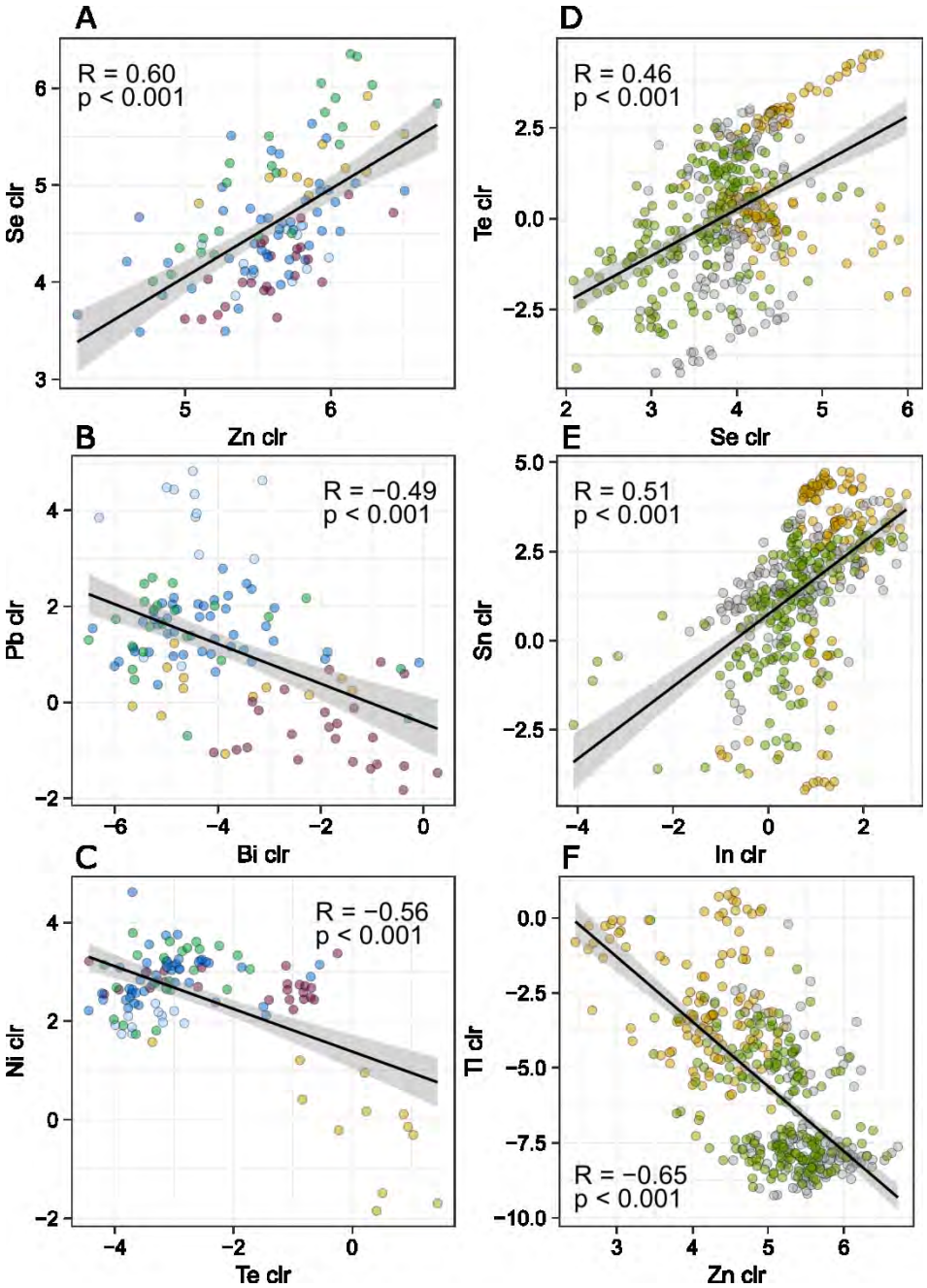

Annexe A14 Binary plots of centred log-ratio (clr) transformed trace elements data in chalcopyrite. a-c: binary diagrams for chalcopyrite from Reef-type PGE deposits. d-f: binary diagrams for chalcopyrite from Ni-Cu sulfide deposits. P-values indicate that the correlations are statistically significant (α=0.05)

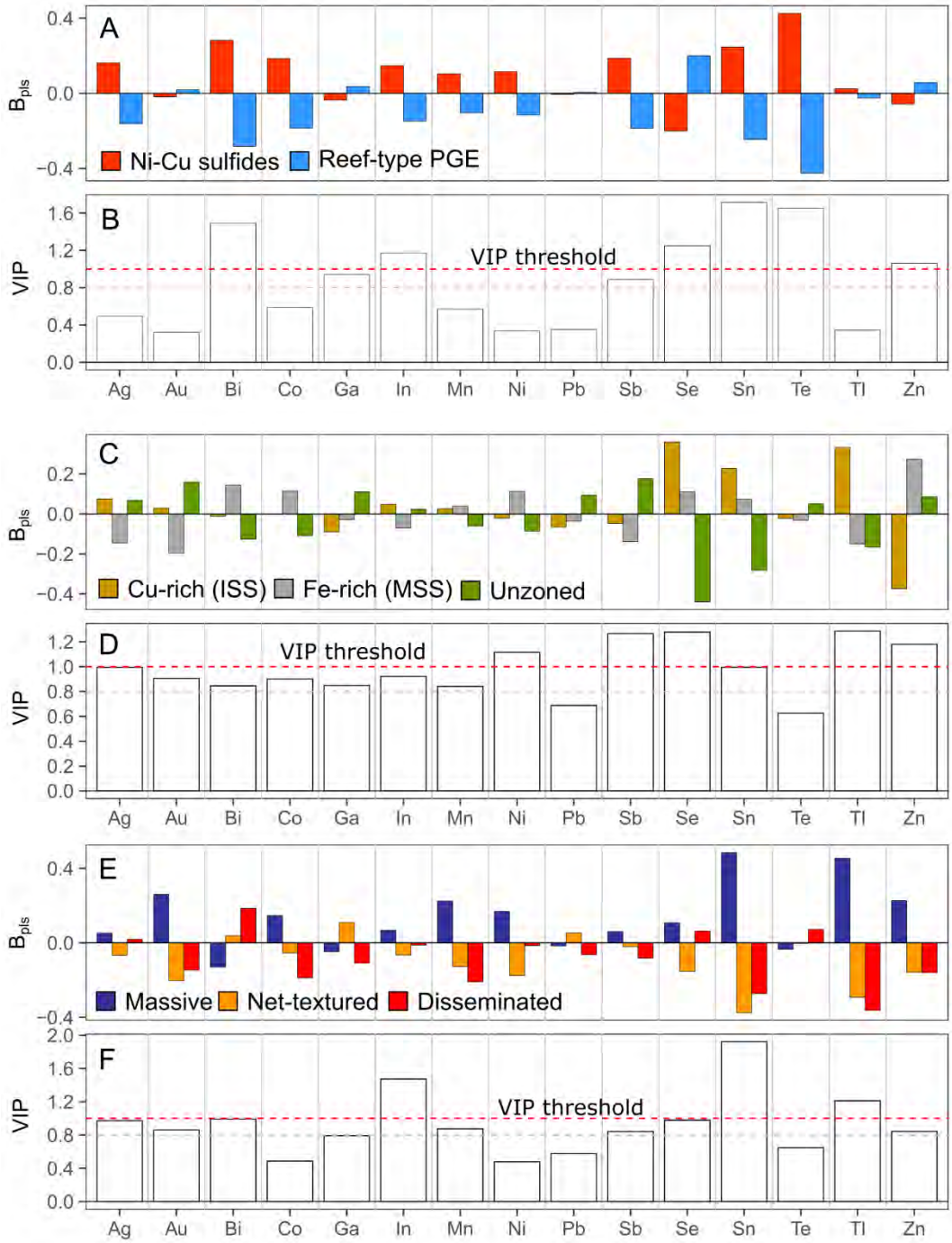

Annexe A15 VIP scores and regression coefficients (B_{pls}) from preliminary PLS-DA models for trace elements of chalcopyrite by deposit type (a-b), ore type (c-d) and texture (e-f).

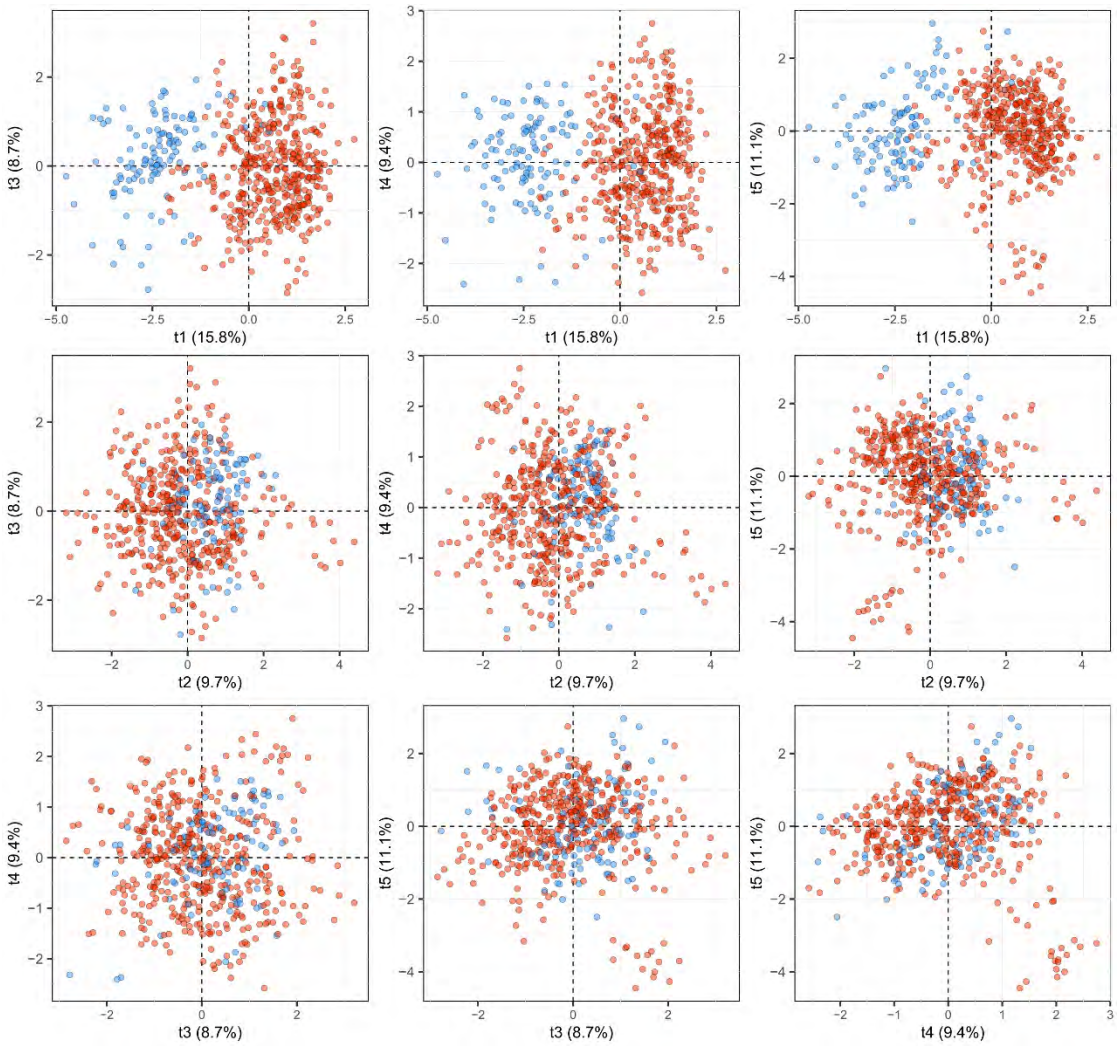

Annexe A16 Score plots for preliminary PLS-DA of trace elements in chalcopyrite by deposit type. Only combination between latent variables from t1 to t5 are shown. Red: Ni-Cu sulfide deposits, blue: Reef-type PGE deposits

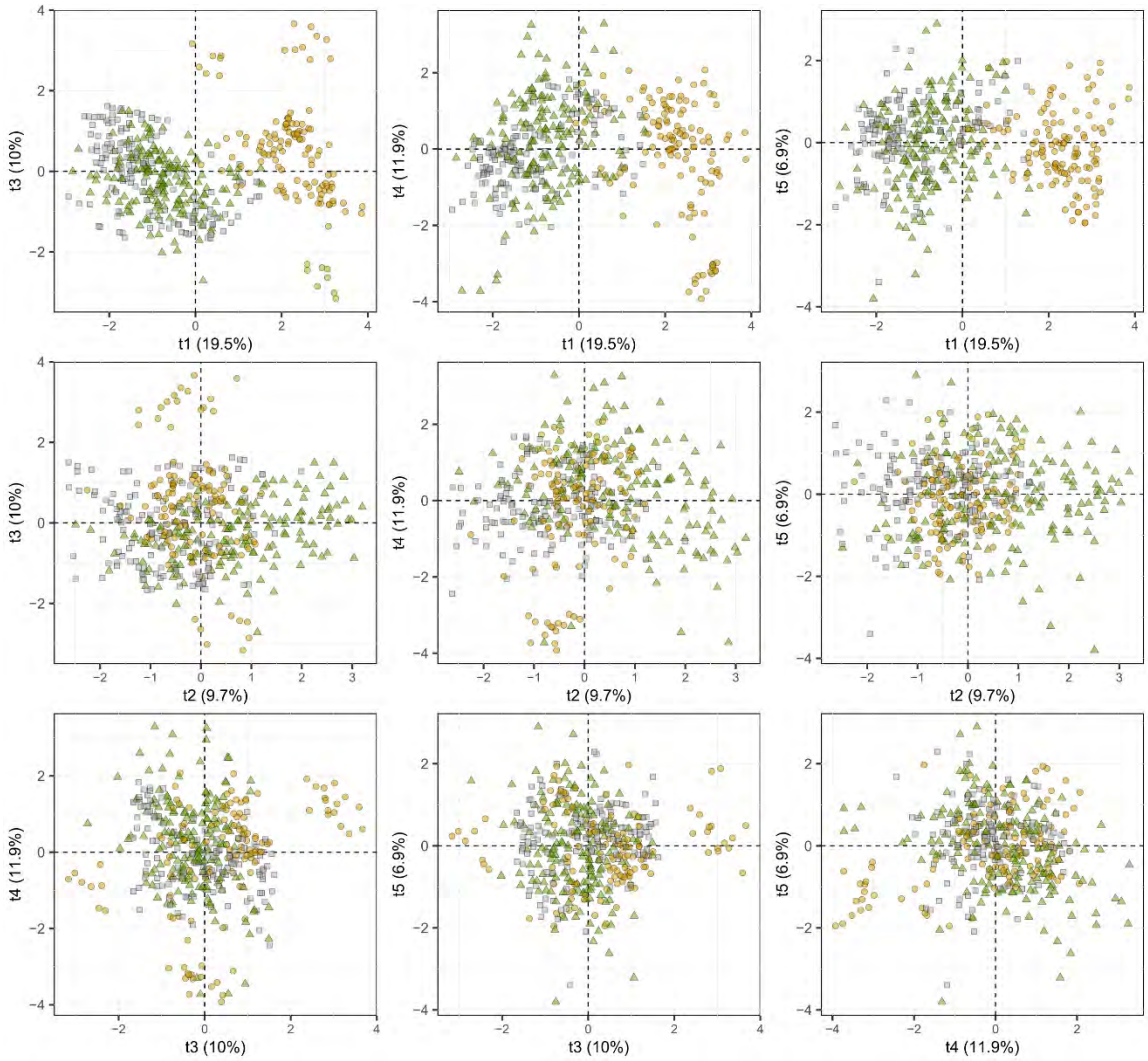

Annexe A17 Score plots for preliminary PLS-DA of trace elements in chalcopyrite by ore type (Ni-Cu sulfide deposits). Only combination between latent variables from t1 to t5 are shown. Yellow cercles: Cu-rich (ISS), grey squares: Fe-rich (MSS), green triangles: unzoned

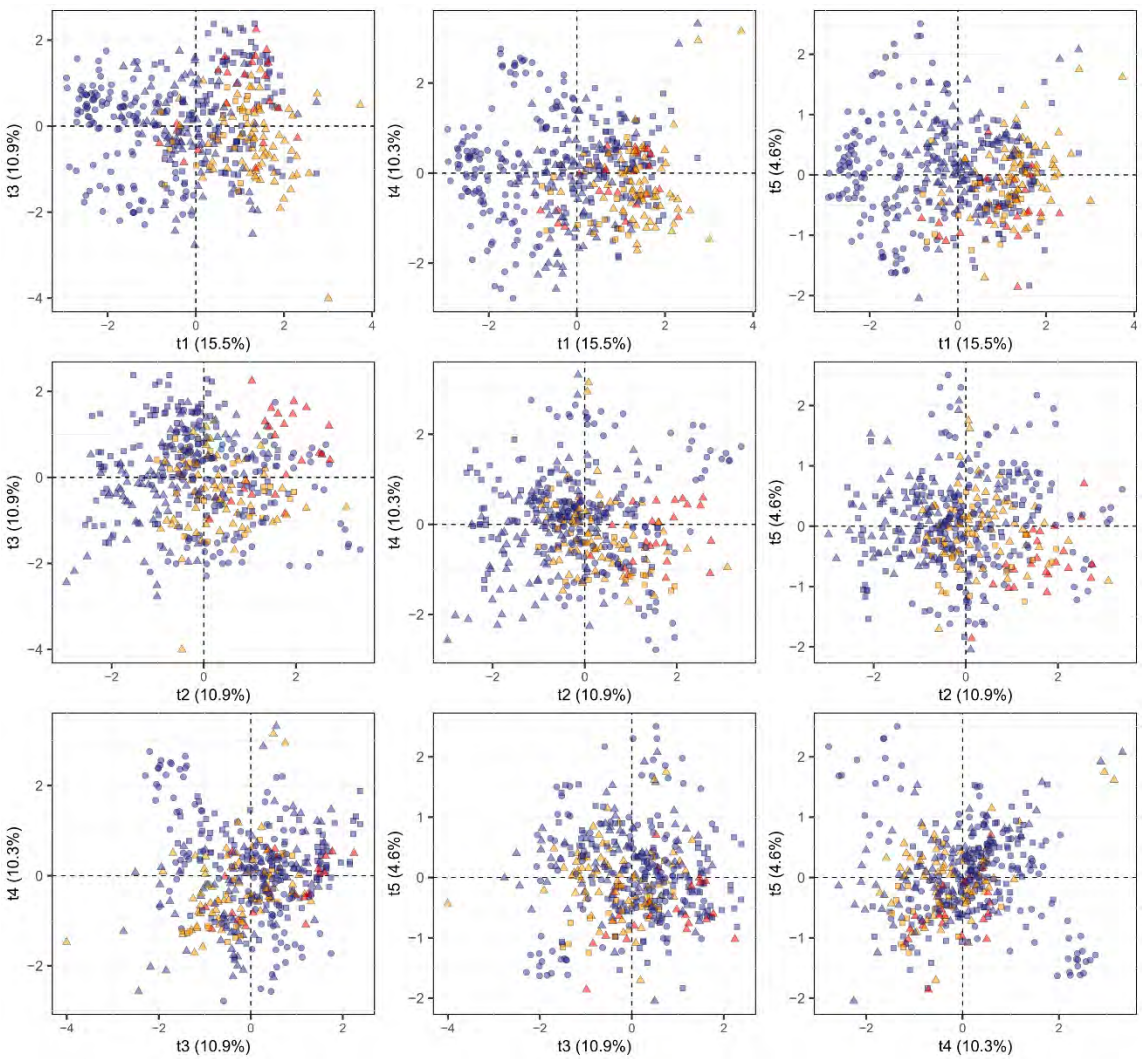

Annexe A18 Scores plots for preliminary PLS-DA on trace elements in chalcopyrite by sulfide texture (Ni-Cu sulfide deposits). Only combination between latent variables from t1 to t5 are shown. Blue: massive, yellow: net-textured/globular, red: disseminated. Cercles: Cu-rich (ISS), squares: Fe-rich (MSS), triangles: unzoned

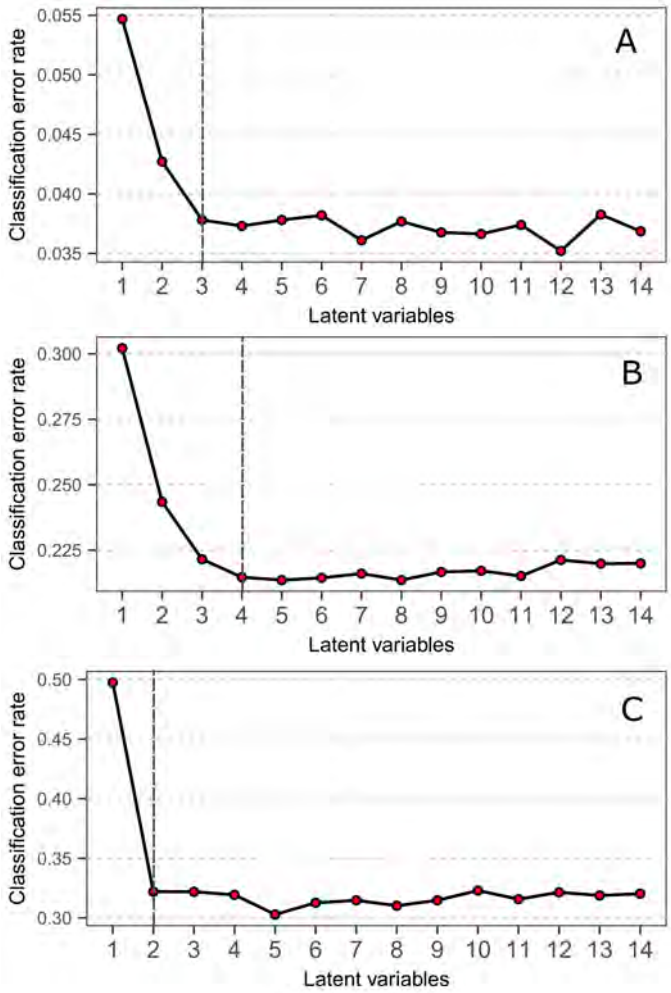

Annexe A19 Error rate in cross validation as a function of latent variables in the PLS-DA model by deposit type (a), ore type (b) and sulfide texture (c). Optimal number of latent variables by model are: 3 by deposit type, 4 by ore type and 2 by sulfide texture

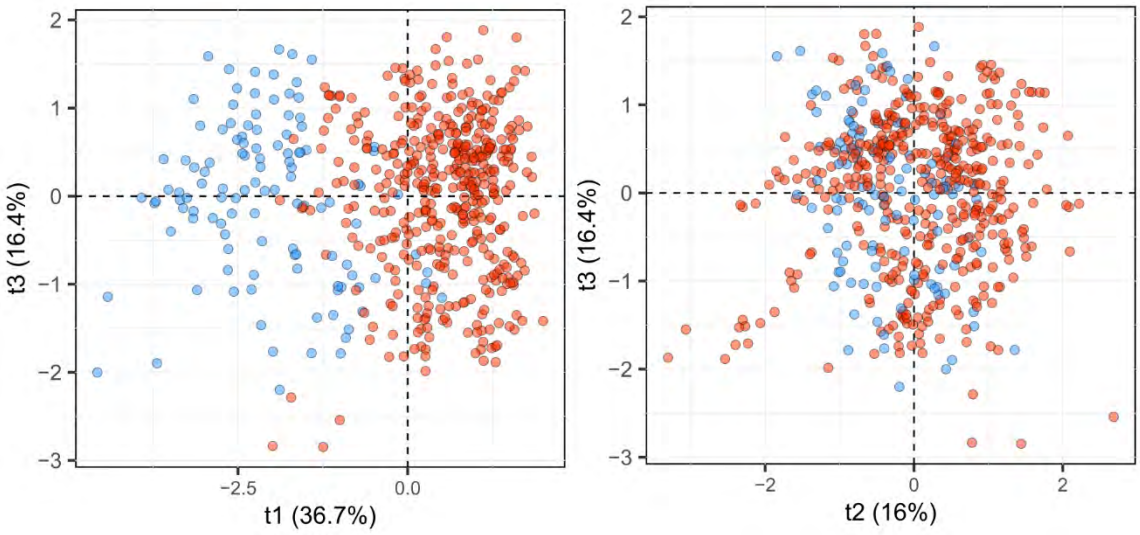

Annexe A20 Score plots for optimized PLS-DA of trace elements in chalcopyrite by deposit type. Total explained variance with 3 latent variables is 69.1%. Red: Ni-Cu sulfide deposits, blue: reef-type PGE deposits

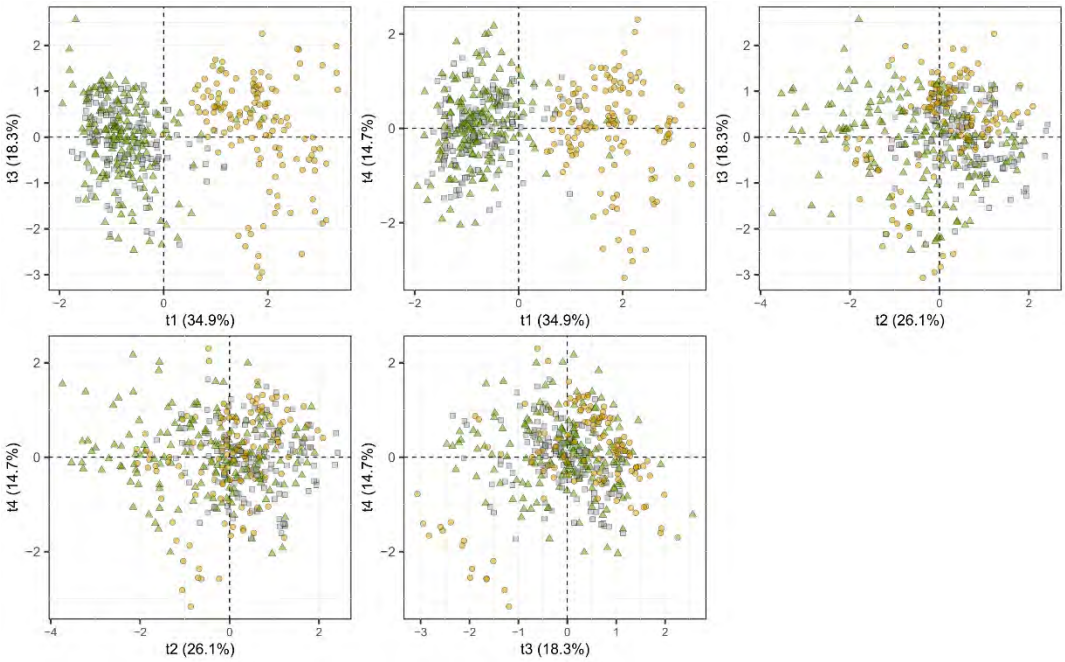

Annexe A21 Score plots for optimized PLS-DA on trace elements in chalcopyrite by ore type. Total explained variance with 4 latent variables is 94%. Yellow: Cu-rich (ISS), grey: Fe-rich (MSS), green: unzoned

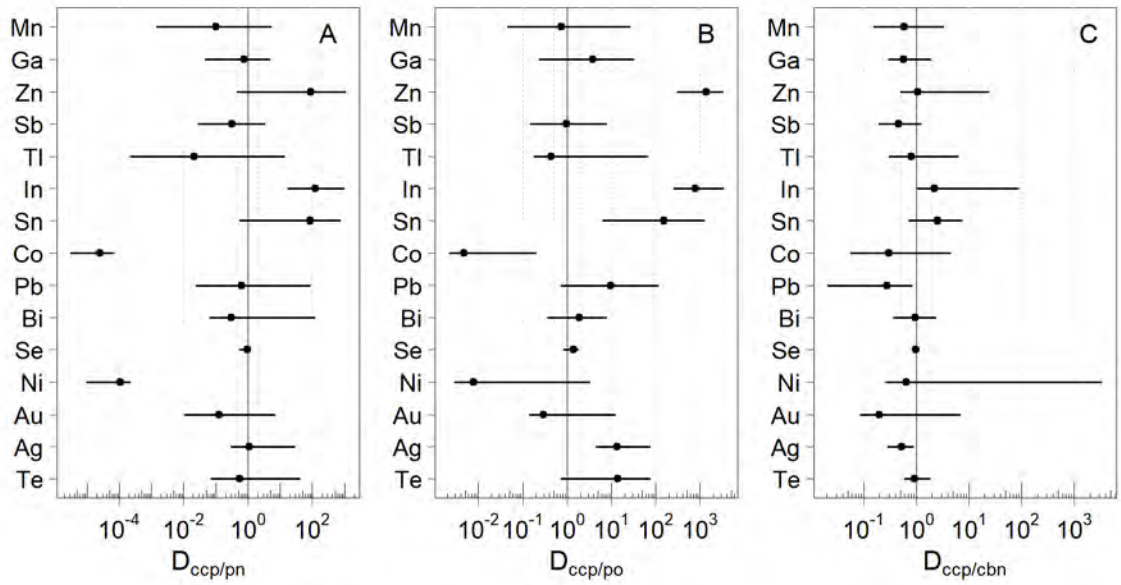

Annexe A22 Distribution of trace element calculated from LA-ICP-MS results between chalcopyrite and (a) pentlandite (pn), (b) pyrrhotite (po) and (c) cubanite (cbn). The range indicates the minimum and maximum of median values calculated from each sample. Order of elements according to Barnes and Ripley (2016) and Barnes (2016) from slightly chalcophile (Zn; top) to highly chalcophile (Te). Manganese and Ga are lithophile and slightly lithophile, respectively.

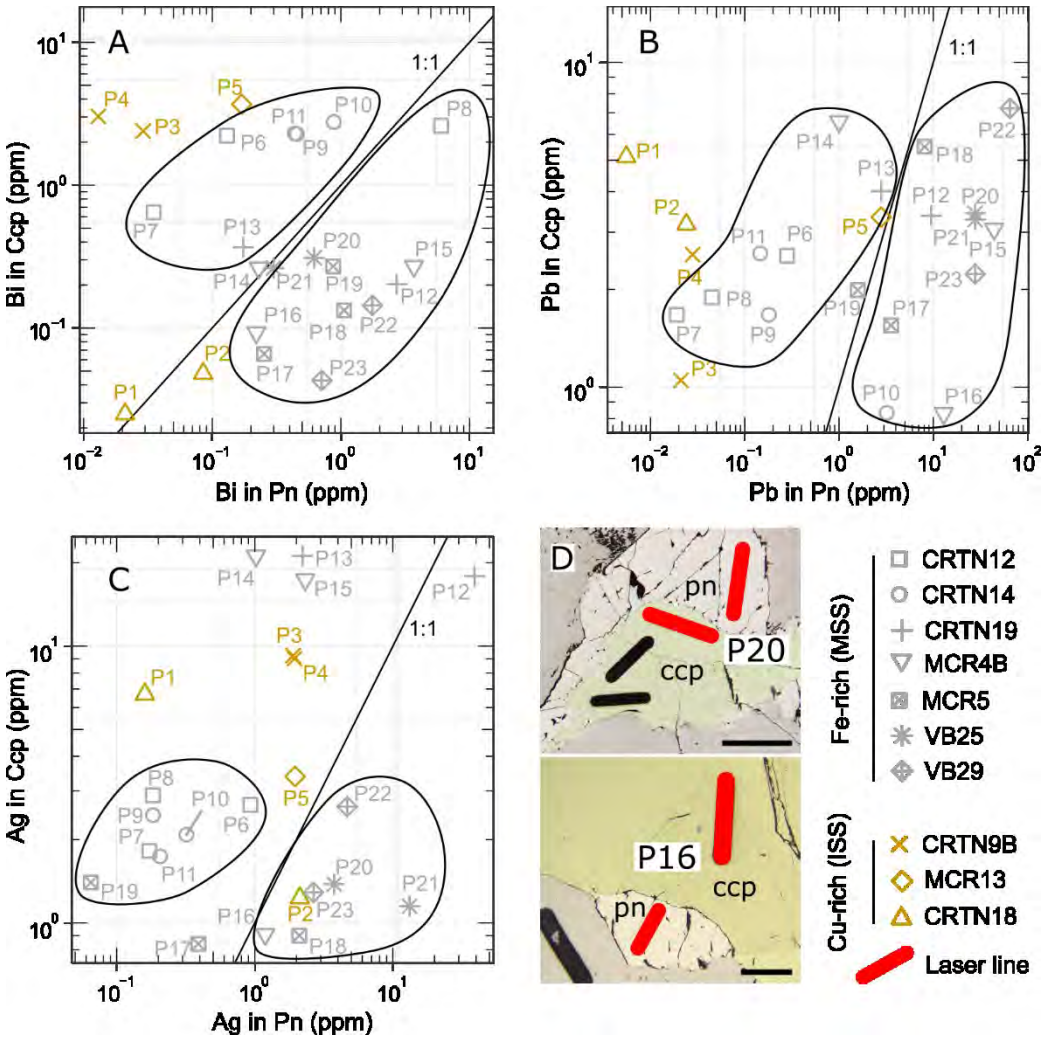

Annexe A23 Binary plots showing concentration of Bi, Pb and Ag (a, b, and c) between adjacent pairs of chalcopyrite and pentlandite (as indicated in d), according to sample and ore type (Cu-rich and Fe-rich). Solid black lines represent an elemental ratio of 1. Left regions show ccp from Fe-rich (MSS) ores without relation with contact-pn, whereas right regions draw ccp adjacent to contact-pn

Annexe B

Annexes correspondant à l'article: Trace element composition of chalcopyrite from volcanogenic massive sulfide deposits: variation and implications for provenance recognition

Annexe B1 Detailed information of the chalcopyrite-bearing samples from VMS and SMS deposits.

Setting	Sample	n	Deposit name	Host tectonostratigraphic complex (age)	Location	Host rocks composition	Sulfide texture	Ore type	Regional metamorphism	Sulfide content (%)	Ccp(%)	Cbn(%)	Bn(%)	Cv(%)	Dg(%)	Po(%)	Py(%)	Apy(%)	Sp(%)	Gn(%)	Mag(%)	Cst(%)	Brt(%)	ccp/(ccp+sp)	ccp/(ccp+po)	po/(po+sp+py)	References
Ultramafic	V553221	6	Irinovskoe	Mid-Atlantic Ridge (?)	Irinovskoe field, Atlantic Ocean	Peridotite-gabbronorite	Semi-massive	Massive	Unmet	37.5	816	np	np	np	2.0	np	11.7	np	4.7	np	np	np	np	0.95	100	0.00	Cherkashev et al. (2013); Petersen et al. (2009); Wohlgemuth-Ueberwasser et al. (2015)
	V557324A	8								61.5	98.0	np	np	<1	np	np	np	np	16	np	np	np	np	0.98	100	0.00	
	V557327A	6								36.1	94.6	np	np	np	2.1	np	np	np	3.3	np	np	np	np	0.97	100	0.00	
	V557327B	7								36.8	86.0	np	np	3.6	np	np	np	np	5.4	np	5.0	np	np	0.94	100	0.00	
	64ROV11	7	Candelabra	Mid-Atlantic Ridge (1-60 ka)	Logatchev-1 field, Atlantic Ocean		Massive			64.6	89.5	np	6.6	np	2.0	np	np	np	18	np	np	np	np	0.98	100	0.00	
	64ROV2	4					Semi-massive			26.0	98.9	np	np	np	<1	np	np	np	<1	np	np	np	np	0.99	100	0.00	
	53ROV13	6	Irina I				Massive			65.7	96.6	np	np	<1	1.4	np	np	np	<1	np	np	np	np	1.00	100	0.00	
	35GTV2B 2	6	Irina II							52.9	72.4	np	5.4	3.2	18.1	np	<1	np	<1	np	np	np	np	0.99	100	0.00	
Mafic	LS1	7	Lasail	Semail Ophiolite (95 Ma)	Al Batinah North, Oman	Basalts and basaltic andesites	Massive	Massive	Unmet	77.2	47.5	np	np	np	np	np	46.9	np	5.6	np	np	np	np	0.90	100	0.00	Gilgen et al. (2014); Stakes and Taylor (2003)
	LS10	7					Disseminat			5.1	46.3	np	np	np	np	np	10.1	np	43.6	np	np	np	np	0.51	100	0.00	
	LDR01	6	Little Deer	Dunnage Zone - Notre Dame Subzone (0.48 Ga)	Lushs Bight, Newfoundland, Canada	Pillow basalt	Massive	Stockwork	L- greensch	55.3	50.6	np	np	np	np	19.0	30.4	np	<1	np	np	np	np	1.00	0.73	0.38	Kean et al. (1995); Piercey (2007)

Mafic	WHB01	5	Whalesback	Dunnage Zone - Notre Dame Subzone (0.48 Ga)	Newfoundland, Canada	Pillow basalt	Semi-massive	Stockwork		46.0	36.8	np	np	np	np	52.8	10.0	np	<1	np	np	np	np	0.99	0.41	0.84	Cloutier et al. (2015); Piercey (2007)
	LB01	6	Little Bay							30.3	60.1	np	np	np	np	19.0	13.3	np	5.7	np	1.9	np	np	0.91	0.76	0.50	Kean et al. (1995); Piercey (2007)
	NAMA01	6	York Harbour	Humber Zone - Bay of Islands Ophiolite (0.48 Ga)						42.4	58.3	np	np	np	np	38.3	1.7	np	1.1	np	<1	np	np	0.98	0.60	0.93	Lode et al. (2015); Piercey (2007)
	ICEVMS01	5	Ice	Slide Mountain terrane (0.28 Ga)	Yukon, Canada	Basalt		Stockwork	L- greensch	65.3	15.4	np	24.9	np	np	np	55.8	np	3.8	np	np	np	np	0.80	1.00	0.00	Piercey et al. (2008)
Bimodal-mafic	2653	6	Poirier	Abitibi Greenstone Belt (2.7 Ga)	Joutel, Quebec, Canada	Rhyolite-dacite / andesite-basalt	Massive	Massive		63.4	85.2	np	np	np	np	<1	<1	np	np	np	13.8	np	np	1.00	1.00	0.02	Barrie et al. (1999); Dubé et al. (2007); Franklin et al. (2005); Gaboury and Pearson (2008); Lafrance et al. (2000); Mercier-Langevin et al. (2007); Shriver and MacLean (1993); Taylor et al. (2014); Genna et al. (2014a); Genna et al. (2014b); Ioannou et al. (2007)
	972146	4	Caber		Matagami, Quebec, Canada	Rhyolite				50.6	31.0	np	np	np	np	np	24.0	np	np	np	np	np	np	1.00	1.00	0.00	

Bimodal-mafic	972149	3	Caber	Abitibi Greenstone Belt (2.7 Ga)	Matagami, Quebec, Canada	Rhyolite	Massive	Massive	L- greensch	66.9	15.0	np	np	np	np	6.0	57.0	np	10.0	np	np	np	np	0.60	0.71	0.08	Barrie et al. (1999); Dubé et al. (2007); Franklin et al. (2005); Gaboury and Pearson (2008); Lafrance et al. (2000); Mercier-Langevin et al. (2007); Shriver and MacLean (1993); Taylor et al. (2014); Genna et al. (2014a); Genna et al. (2014b); Ioannou et al. (2007)
	972257	3					Semi-massive	Massive		26.3	1.0	np	np	np	np	np	55.0	np	np	np	44.0	np	np	1.00	1.00	0.00	
	3143	5	Ming	Dunnage Zone - Notre Dame Subzone (0.48 Ga)	Newfoundland, Canada	Boninite / basalt / rhyolite	Semi-massive	Stockwork	U- greensch	35.8	53.8	np	np	np	np	21.3	14.8	np	10.2	np	np	np	np	0.84	0.72	0.46	Brueckner et al. (2014); Brueckner et al. (2015); Pilote et al. (2020); Pilote and Piercey (2013)
	MN1	7					Massive	Massive		94.8	57.2	np	np	np	np	6.5	29.4	<1	6.4	np	np	np	np	0.90	0.90	0.15	
	MN2	6								95.6	49.0	np	np	np	np	8.0	35.8	<1	6.7	np	np	np	np	0.88	0.86	0.16	
	MN3	7					Semi-massive	Stockwork		29.9	53.3	np	np	np	np	21.7	16.3	np	8.7	<1	np	np	np	0.86	0.71	0.47	
	MN4	6					Massive	Massive		83.3	51.8	<1	np	np	np	2.4	41.4	<1	3.5	np	np	np	np	0.94	0.96	0.05	
	2722	6	Aldermac	Abitibi Greenstone Belt (2.7 Ga)	Noranda, Quebec, Canada	Rhyolite-andesite	Massive	Massive	L- greensch	76.3	82.0	np	np	np	np	18.0	np	np	<1	np	np	np	np	1.00	0.82	1.00	Barrie et al. (1999); Dubé et al. (2007); Franklin et al. (2005); Gaboury and Pearson (2008); Lafrance et al. (2000); Mercier-Langevin et al. (2007); Shriver and MacLean (1993); Taylor et al. (2014); Genna et al. (2014a); Genna et al. (2014b); Ioannou et al. (2007)
	2729	6					Semi-massive	Stockwork		31.8	90.3	np	np	np	np	5.8	3.8	np	<1	np	np	np	np	1.00	0.94	0.60	
	2730	6					Massive	Massive		93.1	79.3	np	np	np	np	11.4	<1	np	9.2	np	np	np	np	0.90	0.87	0.55	
	2643	6	Dufault			Rhyolite				81.3	42.3	np	np	np	np	7.7	28.3	np	21.4	np	<1	np	np	0.66	0.85	0.13	
	2647	7					Disseminated	Stockwork		13.8	67.1	np	np	np	np	31.2	1.6	np	<1	np	np	np	np	1.00	0.68	0.95	

Bimodal-mafic	2652	7	Dufault	Abitibi Greenstone Belt (2.7 Ga)	Noranda, Quebec, Canada	Rhyolite	Semi-massive	Stockwork	L- greensch	77.5	82.5	np	np	np	np	np	5.5	np	1.6	np	10.4	np	np	0.98	1.00	0.00	Barrie et al. (1999); Dubé et al. (2007); Franklin et al. (2005); Gaboury and Pearson (2008); Lafrance et al. (2000); Mercier-Langevin et al. (2007); Shriver and MacLean (1993); Taylor et al. (2014); Genna et al. (2014a); Genna et al. (2014b); Ioannou et al. (2007)
	56	6	Norbec				Disseminated			23.1	12.2	np	np	np	np	10.7	70.4	np	6.6	np	np	np	np	0.65	0.53	0.12	
	2704	6								11.6	80.6	np	np	np	np	13.2	6.0	np	<1	np	np	np	np	1.00	0.86	0.68	
	51	5	Normetal				Massive	Massive		71.9	80.6	np	np	np	np	11.6	<1	np	7.0	np	np	np	np	0.92	0.87	0.59	
	52	7	Waite-Amulet							79.7	24.9	np	np	np	np	<1	32.7	np	41.6	<1	np	np	np	0.37	0.97	0.01	
	601	6					Semi-massive			35.6	39.8	np	np	np	np	14.3	31.6	np	14.3	<1	np	np	np	0.74	0.74	0.24	
	2296	7					Massive			65.3	44.0	np	np	np	np	9.8	14.1	np	32.0	np	np	<1	np	0.58	0.82	0.18	
	2318	7								76.8	89.1	np	np	np	np	np	6.3	np	4.7	np	np	np	np	0.95	1.00	0.00	
	2325	6								91.5	69.8	np	np	np	np	14.0	5.8	np	10.4	np	np	np	np	0.87	0.83	0.46	
	62	7	Kidd Creek		Timmins, Ontario, Canada	Rhyolite-ultramafic	Semi-massive	Stockwork		78.0	90.8	np	np	np	np	np	6.8	np	2.3	<1	np	np	np	0.97	1.00	0.00	
	2369	7								39.4	85.1	np	np	np	np	np	9.0	np	5.9	np	np	np	np	0.94	1.00	0.00	
	2378	8					Massive			76.0	3.3	np	np	np	np	np	15.9	np	80.8	np	np	np	np	0.04	1.00	0.00	
	2383	6								82.7	83.3	np	np	np	np	4.6	11.1	np	<1	np	np	<1	np	0.99	0.95	0.28	
Bimodal-felsic	1872	6	Suffield Mine	Ascot-Weedon Complex (0.45 Ga)	Cantons de l'Est, Quebec, Canada	Felsic volcaniclastic rocks	Massive	Massive		5.0	5.0	np	np	np	np	np	37.4	np	57.4	<1	np	np	np	0.08	1.00	0.00	Gauthier et al. (1994)
	1869	7	Weedon							65.6	65.6	np	np	np	np	27.3	<1	np	7.0	np	np	np	np	0.90	0.71	0.79	

Bimodal-felsic	E612164	5	McLeod	Abitibi Greenstone Belt (2.7 Ga)	Matagami, Quebec, Canada	Rhyolite-rhyodacite	Semi-massive	Massive	L- greensch	45.9	28.0	np	np	np	np	32.0	15.0	np	7.0	np	np	np	np	0.80	0.47	0.59	Barrie et al. (1999); Dubé et al. (2007); Franklin et al. (2005); Gaboury and Pearson (2008); Lafrance et al. (2000); Mercier-Langevin et al. (2007); Shriver and MacLean (1993); Taylor et al. (2014); Genna et al. (2014a); Genna et al. (2014b); Ioannou et al. (2007)
	E612166-A	1					Disseminated	Stockwork		14.5	4.0	np	np	np	np	20.0	6.0	np	28.0	np	np	np	np	0.13	0.17	0.37	
	E612167	2								15.8	25.0	np	np	np	np	38.0	19.0	np	6.0	np	np	np	np	0.81	0.40	0.60	
	E612171-A	2					Semi-massive	Massive		37.8	5.0	np	np	np	np	12.0	34.0	np	11.0	np	np	np	np	0.31	0.29	0.21	
	972224	3	Perseverance				Massive			63.0	7.9	np	np	np	np	12.7	63.5	np	15.9	np	np	np	np	0.33	0.38	0.14	
	972228	3								80.0	6.3	np	np	np	np	np	43.8	np	50.0	np	np	np	np	0.11	1.00	0.00	
	E612152-A	2					Semi-massive			45.5	40.0	np	np	np	np	np	5.0	np	25.0	np	np	np	np	0.62	1.00	0.00	
	E612154-B	2								65.7	11.8	np	np	np	np	11.8	36.4	np	11.8	np	np	np	np	0.50	0.50	0.20	
	E612155-A	4								70.7	18.0	np	np	np	np	np	14.0	np	44.0	np	np	np	np	0.29	1.00	0.00	
	E612162-A	1					Massive			57.0	16.0	np	np	np	np	np	38.0	np	22.0	np	np	np	np	0.42	1.00	0.00	
	BVMS01	5	Boundary	Dunnage Zone - Exploits Subzone (0.51 Ga)	Newfoundland, Canada	Dacite-rhyolite / basalt				87.1	85.3	np	np	np	np	np	12.7	np	2.0	np	np	np	np	0.98	1.00	0.00	Buschette and Piercey (2016); Piercey (2007)
	3147	7	Duck Pond							92.3	33.6	np	np	np	np	np	62.6	<1	3.5	np	np	np	np	0.91	1.00	0.00	McNicoll et al. (2010); Piercey (2007)

Bimodal-felsic	2211	6	Horne	Abitibi Greenstone Belt (2.7 Ga)	Noranda, Quebec, Canada	Rhyolite-andesite	Massive	Stockwork	L- greensch	53.0	31.1	np	np	np	np	np	63.3	np	<1	np	np	np	np	1.00	1.00	0.00	Barrie et al. (1999); Dubé et al. (2007); Franklin et al. (2005); Gaboury and Pearson (2008); Lafrance et al. (2000); Mercier-Langevin et al. (2007); Shriver and MacLean (1993); Taylor et al. (2014); Genna et al. (2014a); Genna et al. (2014b); Ioannou et al. (2007)
	2215	5					Disseminated			18.2	90.4	np	np	np	np	np	5.3	np	4.4	np	np	np	np	0.95	1.00	0.00	
	2221	7					Massive	Massive		93.9	93.7	np	np	np	np	4.3	1.4	np	<1	np	np	np	np	0.99	0.96	0.69	
	2224	6					Semi-massive	Stockwork		64.2	52.2	np	np	np	np	np	41.4	np	6.4	np	np	<1	np	0.89	1.00	0.00	
	53	7					Semi-massive	Stockwork		51.1	94.4	np	np	np	np	np	5.0	np	<1	np	np	np	np	0.99	1.00	0.00	
	2359	6					Massive			58.8	96.9	np	np	np	np	np	<1	np	3.1	np	np	np	np	0.97	1.00	0.00	
	QT01	6	Quémont				Semi-massive	Stockwork		30.1	92.5	np	np	np	np	np	3.5	np	4.0	np	np	np	np	0.96	1.00	0.00	
	QT0MT	7								44.4	7.2	np	np	np	np	1.9	4.0	np	5.9	np	81.0	np	np	0.55	0.79	0.16	
	QT18	6								21.7	86.8	np	np	np	np	np	np	np	13.2	np	np	np	np	0.87	1.00	0.00	
Bimodal-felsic	53ROV6	8	Roman Ruins	Pual Ridge (20-50 ka)	Pacmanus field, Papua New Guinea	Dacite-rhyolite	Massive	Massive	Unmet	52.0	73.1	np	1.2	6.4	np	np	7.6	np	np	np	np	np	<1	1.00	1.00	0.00	Binns et al. (2007); Hannington et al. (2005); Reeves et al. (2011)

	31ROV13C	7	Satanic Mills	Pual Ridge (20-50 ka)	Pacmanus field, Papua New Guinea	Dacite-rhyolite	Massive	Massive	Unmet	61.9	87.7	np	1.9	np	9.7	np	<1	np	np	np	np	np	<1	100	100	0.00	Binns et al. (2007); Hannington et al. (2005); Reeves et al. (2011)
	27ROV8	6	Snowcap							85.9	92.7	np	1.3	np	3.0	np	3.0	np	np	np	np	np	<1	100	100	0.00	
Bimodal-felsic	2410	6	Adak	Bothnia-Skellefteå Unit (1.8 Ga)	Västerbotten, Sweden	Felsic volcanic rocks	Disseminated	Stockwork	L- greensch	16.2	90.6	<1	np	np	np	8.6	np	np	<1	np	np	np	np	100	0.91	0.99	Allen et al. (1996); Årebäck et al. (2005); Johansson (2017); Skyttä et al. (2020)
	2417	5					Massive			61.0	78.7	1.1	np	np	np	19.1	np	np	1.1	np	np	np	np	0.99	0.81	0.94	
	2414	6	Brannmyran				Semi-massive			41.1	92.8	<1	np	np	np	3.7	3.1	np	<1	np	np	np	np	100	0.96	0.54	
	2394	6	Lindsköld				Massive			53.2	76.9	<1	np	np	np	16.4	np	5.3	1.3	np	np	np	np	0.98	0.82	0.93	
	2398	6					Semi-massive			36.3	89.0	1.8	np	np	np	8.8	np	np	<1	np	np	np	np	100	0.91	0.96	
	2399	6								48.0	68.9	np	np	np	np	28.6	np	2.5	<1	np	np	np	np	100	0.71	1.00	
	2393	6	Rävliden			Felsic to mafic volcanic rock/argilites		Massive		46.8	83.1	np	np	np	np	16.9	np	np	<1	np	np	np	np	100	0.83	1.00	

	2575	6	Ely	Vermont Copper Belt (0.41 Ga)	Vermont, USA	Metabasaltic Amph/metasedimentary rocks and minor mafic metavolcanics	Massive	Massive	U- greensch	83.9	28.3	np	np	np	np	70.8	np	np	<1	np	np	np	np	0.97	0.29	0.99	McWilliams et al. (2010); Slack et al. (2001)
	2567	6	Pike Hill							86.4	90.7	<1	np	np	np	8.6	np	np	<1	np	np	np	np	0.99	0.91	0.92	
	2569	6								60.9	76.0	<1	np	np	np	219	<1	np	16	np	np	np	np	0.98	0.78	0.92	
Siliciclastic-mafic	AZN01	6	Aznalcollar	Iberian Pyrite Belt (0.34-0.38 Ga)	Andalucia, Spain	Rhyolite-dacite / phyllite-quartzite	Massive	Stockwork	Prehnite-pumpellyte	78.6	69.1	np	np	np	np	np	28.3	np	2.5	np	np	np	np	0.96	100	0.00	Almodóvar et al. (2019); Barrie et al. (2002); Inverno et al. (2015); Relvas et al. (2001); Relvas et al. (2006); Sáez et al. (1999); Tornos (2006)
	THA01	4	Tharsis				Semi-massive			34.4	92.1	np	np	np	np	np	3.5	np	3.7	<1	np	np	np	0.96	100	0.00	
	ALJ01	6	Aljustrel		Beja, Portugal		Massive	Massive		92.3	14.1	np	np	np	np	np	74.1	<1	118	np	np	<1	np	0.55	100	0.00	
	COR01	5	Corvo							62.2	95.8	np	np	np	np	np	2.0	np	<1	np	np	2.1	np	100	100	0.00	
	COR02	7								76.6	86.6	np	np	np	np	np	2.9	np	<1	2.0	np	np	np	100	100	0.00	
	COR03	10						Stockwork		61.8	94.8	np	np	np	np	np	5.2	np	<1	np	np	np	np	100	100	0.00	
	COR04	6					Disseminated			116	20.5	np	np	np	np	np	29.5	np	<1	np	np	49.3	np	100	100	0.00	

Siliciclastic-felsic	GRA01	6	Graça	Iberian Pyrite Belt (0.34-0.38 Ga)	Beja, Portugal	Rhyolite-dacite / phyllite-quartzite	Massive	Stockwork	Prehnite-pumpellyte	62.0	60.4	np	np	np	np	np	13.4	np	21.1	np	np	5.0	np	0.74	1.00	0.00	Almodóvar et al. (2019); Barrie et al. (2002); Inverno et al. (2015); Relvas et al. (2001); Relvas et al. (2006); Sáez et al. (1999); Tornos (2006)
	NEV01	3	Neves				Massive			58.3	17.0	np	np	np	np	np	80.7	np	2.3	np	np	<1	np	0.88	1.00	0.00	
	NEV02	4					Massive	Massive		81.8	88.7	np	np	np	np	np	6.8	3.2	1.2	np	np	np	np	0.99	1.00	0.00	
	ZAM01	7	Zambujal				Massive			74.1	54.3	np	np	np	np	np	7.7	np	21.4	<1	np	np	np	0.72	1.00	0.00	
	LS22	7	Lagoa Salgada		Setúbal, Portugal		Semi-massive	Stockwork		34.2	25.4	np	np	np	np	np	69.0	np	5.6	<1	np	<1	np	0.82	1.00	0.00	
	LOU01	7	Lousal							50.9	8.7	np	np	np	np	np	84.8	np	<1	<1	np	6.0	np	0.96	1.00	0.00	
	2925	6	Hajar	Guemassa Massif (0.34 Ga)	Marrakech-Safi, Morocco	Rhyolite-rhyodacite	Massive		L- greensch	91.6	7.0	np	np	np	np	41.8	<1	np	43.7	6.8	np	np	np	0.14	0.14	0.49	Admou et al. (2018); Marcoux et al. (2008); Moreno et al. (2008)
	2924	6	Draa Sfar	Jebilet Massif (0.34 Ga)				Massive		62.2	20.7	np	np	np	np	79.3	np	np	<1	np	np	np	np	1.00	0.21	1.00	
	3112	5	Tétrault	Greenville Province	Montauban, Quebec, Canada	Quartz-biotite and quartz-sillimanite gneiss			Amph	84.7	36.1	41.2	np	np	np	np	20.6	np	2.1	np	np	np	np	0.95	1.00	0.00	Tomkins (2007); Stamatelopoulou-Seymour and MacLean (1984)
	B5109	6	Bathurst	Bathurst Mining Camp (0.47 Ga)	New Brunswick, Canada	Rhyolite-rhyodacite	Semi-massive	Stockwork	U- greensch	49.0	83.5	np	np	np	np	14.6	np	np	1.9	np	np	np	np	0.98	0.85	0.88	Goodfellow (2007); Mireku and Stanley (2006)

Siliciclastic-felsic	B5110	5	Bathurst	Bathurst Mining Camp (0.47 Ga)	New Brunswick, Canada	Rhyolite-rhyodacite	Semi-massive	Stockwork	U- greensch	38.9	81.7	np	np	np	np	16.3	np	np	2.0	np	np	np	np	0.98	0.83	0.89	Goodfellow (2007); Mireku and Stanley (2006)
	B7157	5								36.7	81.0	np	np	np	np	17.3	np	np	1.7	np	np	np	np	0.98	0.82	0.91	
	B7158	5						Massive		47.5	80.3	np	np	np	np	17.8	np	np	1.9	np	np	np	np	0.98	0.82	0.90	
	07MPBR23	5	Halfmile Lake				Disseminated	Stockwork		19.6	15.9	np	np	np	np	57.1	2.4	np	np	<1	24.5	np	np	1.00	0.22	0.96	
	WV01	6	Wolverine	Yukon-Tanana Terrane (0.34 Ga)	Yukon, Canada	Mafic and felsic volcanic rocks / dark clastic rocks	Semi-massive	Stockwork	M- greensch	34.6	67.2	np	np	np	np	np	26.6	np	6.1	np	np	np	np	0.92	1.00	0.00	Piercey et al. (2008)

Setting: Classification scheme from Franklin et al. (2005) and Patten et al. (2022).
Sulfide texture: Classification based on modal percent of sulfides in thin section/hand specimen. Massive (>50%); Semi-massive (20-50%); Disseminated (0-20%).
Ore type: According to microscopic, hand sample observations and information provided by the source of sample.
Sulfide content: normalized to 100% opaques.
np: not present.
n: number of analyses.
Mineral abbreviations from Whitney & Evans (2010). Apy: arsenopyrite; Bn: bornite; Brt: barite; Ccp: chalcopyrite; Cbn: cubanite; Cst; cassiterite; Cv: covellite; Dg: digenite; Gn: galena; Mag: magnetite; Pn: pentlandite; Po: pyrrhotite; Py: pyrite; Sp: sphalerite.

Annexe B2 Electron Probe Micro Analysis results for chalcopyrite

	Weight percent			
Grain	S (wt%)	Cu (wt%)	Fe (wt%)	Total
Detection limit	0.367	0.503	0.836	
07MPBR23CCP-02.d	34.9	34.2	30.8	99.9
07MPBR23CCP-03.d	34.5	33.7	29.8	98.1
07MPBR23CCP-04.d	34.7	34.7	29.8	99.2
07MPBR23CCP-05.d	34.9	34.1	29.4	98.4
07MPBR23CCP-06.d	34.6	34.5	30.1	99.3
2211CCP-01.d	34.8	33.7	30.2	98.7
2211CCP-02.d	34.6	33.6	30.6	100.0
2211CCP-03.d	34.4	33.4	29.9	98.7
2211CCP-04.d	34.3	33.6	29.9	99.3
2211CCP-05.d	34.3	33.4	30.0	97.7
2211CCP-06.d	34.3	33.5	29.6	99.9
2215CCP-02.d	35.0	34.2	31.2	100.4
2215CCP-03.d	35.1	34.1	30.3	99.5
2215CCP-04.d	35.0	34.0	30.9	99.9
2215CCP-05.d	35.1	34.2	30.6	99.8
2215CCP-06.d	34.8	34.1	30.6	99.4
2221CCP-01.d	34.7	34.7	30.6	97.8
2221CCP-02.d	34.6	34.3	30.4	100.5
2221CCP-03.d	35.0	34.5	30.4	97.8
2221CCP-04.d	35.1	34.7	30.7	99.1
2221CCP-05.d	34.8	34.1	30.3	97.5
2221CCP-06.d	34.7	34.6	30.9	100.2
2221CCP-07.d	34.9	34.5	30.4	99.8
2224CCP-01.d	34.1	33.5	31.1	99.2
2224CCP-02.d	34.5	33.7	31.2	99.2
2224CCP-03.d	34.6	33.6	31.4	99.2
2224CCP-04.d	34.8	33.8	31.6	99.2
2224CCP-05.d	34.5	33.9	30.8	99.2
2296CCP-01.d	34.9	33.5	31.6	100.0
2296CCP-02.d	35.0	33.5	31.6	100.1
2296CCP-03.d	34.9	33.3	31.0	99.2
2296CCP-04.d	34.8	33.6	30.6	99.1
2296CCP-05.d	35.3	33.6	31.3	100.3
2318CCP-01.d	34.8	34.8	30.9	100.5
2318CCP-02.d	34.7	34.7	31.1	100.6
2318CCP-03.d	34.8	34.7	31.2	100.7
2318CCP-04.d	34.6	34.8	30.8	100.2
2318CCP-05.d	34.2	28.1	25.5	87.8
2318CCP-06.d	34.8	35.3	31.2	101.4
2318CCP-07.d	34.9	34.9	30.8	100.6
2325CCP-01.d	35.0	34.5	31.1	100.6
2325CCP-02.d	35.1	34.5	31.0	100.6
2325CCP-04.d	34.9	34.3	30.6	99.8
2325CCP-05.d	34.9	34.7	31.0	100.7
2325CCP-06.d	35.1	34.3	30.9	100.2
2369CCP-01.d	34.6	34.6	30.0	99.2
2369CCP-02.d	34.6	34.2	29.5	98.4
2369CCP-03.d	34.7	34.1	30.1	99.0
2369CCP-04.d	34.8	34.2	29.8	98.8

	Weight percent			
Grain	S (wt%)	Cu (wt%)	Fe (wt%)	Total
Detection limit	0.367	0.503	0.836	
2369CCP-05.d	34.5	33.8	30.4	98.7
2369CCP-06.d	34.9	34.3	29.8	99.0
2369CCP-07.d	34.4	34.1	29.7	98.2
2378CCP-01.d	35.0	34.4	30.2	99.6
2378CCP-02.d	34.7	34.5	30.9	100.2
2378CCP-03.d	34.8	34.4	30.8	100.0
2378CCP-04.d	34.9	34.6	30.3	99.8
2378CCP-05.d	34.8	34.3	30.6	99.8
2378CCP-06.d	35.0	34.8	30.5	100.3
2378CCP-07.d	34.9	34.5	30.5	99.9
2378CCP-08.d	34.9	34.6	30.6	100.0
2643CCP-01.d	34.6	34.6	30.3	99.5
2643CCP-02.d	34.6	34.4	30.4	99.4
2643CCP-03.d	34.6	34.4	30.4	99.4
2643CCP-04.d	34.7	34.5	30.7	99.9
2643CCP-05.d	34.8	34.6	30.0	99.4
2643CCP-06.d	34.6	34.3	30.3	99.3
2647CCP-01.d	34.6	34.5	30.0	99.1
2647CCP-02.d	35.0	34.3	30.6	99.9
2647CCP-03.d	34.8	34.3	30.6	99.8
2647CCP-04.d	34.1	33.1	29.5	96.6
2647CCP-05.d	34.8	34.5	30.3	99.5
2647CCP-06.d	34.5	34.5	30.3	99.3
2647CCP-07.d	34.7	34.6	30.9	100.2
2652CCP-01.d	34.9	34.5	30.0	99.5
2652CCP-02.d	34.8	34.4	30.4	99.5
2652CCP-03.d	34.9	34.7	30.8	100.4
2652CCP-04.d	34.7	34.5	30.4	99.6
2652CCP-05.d	34.9	34.7	30.2	99.7
2652CCP-06.d	34.9	34.9	30.9	100.7
2652CCP-07.d	34.8	34.7	30.4	99.9
27ROV8CCP-01.d	34.7	34.7	30.9	100.2
27ROV8CCP-02.d	34.6	34.8	30.3	99.7
27ROV8CCP-03.d	34.7	34.7	30.8	100.2
27ROV8CCP-04.d	34.8	34.7	31.2	100.8
27ROV8CCP-05.d	34.7	34.6	30.8	100.1
27ROV8CCP-07.d	34.7	35.1	30.5	100.3
2924CCP-01.d	34.6	34.8	30.6	99.9
2924CCP-03.d	34.6	34.8	31.2	100.6
2924CCP-04.d	34.5	34.6	30.4	99.5
2924CCP-05.d	34.8	34.8	30.6	100.2
2924CCP-06.d	34.5	34.5	30.8	99.8
2924CCP-08.d	34.6	34.8	30.7	100.1
2925CCP-01.d	34.9	34.0	30.4	99.2
2925CCP-02.d	34.8	34.3	30.4	99.5
2925CCP-03.d	34.8	34.0	30.8	99.5
2925CCP-04.d	34.7	34.0	29.9	98.6
2925CCP-05.d	34.8	34.0	30.2	99.1
2925CCP-06.d	34.8	34.2	30.3	99.3
3143CCP-01.d	34.5	33.5	29.9	98.0

	Weight percent			
Grain	S (wt%)	Cu (wt%)	Fe (wt%)	Total
Detection limit	0.367	0.503	0.836	
3143CCP-03.d	34.5	33.8	29.6	97.9
3143CCP-04.d	34.5	33.7	29.9	98.1
3143CCP-05.d	34.7	33.8	29.7	98.2
3143CCP-06.d	34.9	33.9	30.5	99.4
3147CCP-01.d	34.7	34.4	29.8	99.0
3147CCP-02.d	34.6	34.3	30.1	99.0
3147CCP-03.d	34.5	34.2	30.2	98.9
3147CCP-04.d	35.0	34.4	30.5	99.9
3147CCP-05.d	34.7	34.4	30.5	99.6
3147CCP-06.d	34.6	34.2	30.3	99.1
3147CCP-07.d	34.5	34.2	29.8	98.4
31ROV13CCCP-01.d	35.1	34.7	30.3	100.0
31ROV13CCCP-02.d	34.8	34.8	30.0	99.5
31ROV13CCCP-03.d	34.8	34.9	30.0	100.8
31ROV13CCCP-04.d	34.9	34.3	30.0	99.2
31ROV13CCCP-05.d	34.9	35.0	30.2	100.1
31ROV13CCCP-06.d	34.9	34.6	30.3	99.9
31ROV13CCCP-07.d	34.8	34.7	30.4	99.9
35GTV2B2CCP-001.d	34.7	34.5	30.1	99.2
35GTV2B2CCP-002.d	34.7	34.0	30.4	99.2
35GTV2B2CCP-003.d	34.6	33.9	30.6	99.1
35GTV2B2CCP-004.d	34.8	34.1	30.6	99.5
35GTV2B2CCP-005.d	34.8	34.5	30.5	99.9
35GTV2B2CCP-006.d	34.6	34.1	30.7	99.4
51CCP-01.d	34.7	34.3	30.2	99.3
51CCP-02.d	34.7	34.5	30.3	99.6
51CCP-03.d	34.9	34.5	30.3	99.7
51CCP-05.d	34.8	34.6	30.2	99.6
51CCP-06.d	34.6	34.5	30.1	99.2
52CCP-01.d	34.6	34.7	30.4	99.7
52CCP-02.d	34.6	34.7	30.4	99.7
52CCP-03.d	34.7	34.8	30.5	99.9
52CCP-04.d	34.5	34.7	30.7	100.0
52CCP-05.d	34.7	35.1	30.5	100.3
52CCP-06.d	34.6	35.0	30.6	100.2
52CCP-07.d	34.6	34.7	30.5	99.8
53CCP-01.d	34.8	34.3	29.7	98.8
53CCP-02.d	34.7	34.8	30.5	100.0
53CCP-03.d	35.1	34.3	30.6	100.0
53CCP-04.d	35.0	34.2	30.4	99.7
53CCP-05.d	34.8	34.6	30.0	99.4
53CCP-06.d	34.5	33.9	30.0	98.5
53CCP-07.d	34.8	34.7	29.9	99.4
53ROV13CCP-01.d	34.7	34.8	30.5	100.0
53ROV13CCP-02.d	35.2	34.9	30.9	101.0
53ROV13CCP-04.d	34.6	35.2	30.7	100.5
53ROV13CCP-05.d	34.8	34.8	30.9	100.4
53ROV13CCP-06.d	34.4	35.1	30.6	100.1
53ROV13CCP-07.d	34.5	34.8	30.6	100.6
53ROV6CCP-01.d	34.9	34.6	30.7	100.2

	Weight percent			
Grain	S (wt%)	Cu (wt%)	Fe (wt%)	Total
Detection limit	0.367	0.503	0.836	
53ROV6CCP-02.d	34.9	34.8	30.3	100.0
53ROV6CCP-04.d	34.8	34.5	30.2	99.5
53ROV6CCP-05.d	34.8	34.6	30.9	100.3
53ROV6CCP-06.d	34.9	34.9	30.6	100.4
53ROV6CCP-07.d	34.9	34.9	30.9	100.8
56CCP-01.d	34.9	34.6	30.8	100.3
56CCP-02.d	34.9	34.9	30.8	101.0
56CCP-03.d	35.0	34.7	30.8	100.5
56CCP-04.d	34.9	34.7	30.6	100.3
56CCP-05.d	35.2	35.1	30.9	101.3
56CCP-06.d	35.0	34.8	30.8	100.6
601CCP-01.d	34.6	34.6	30.1	99.3
601CCP-02.d	34.5	34.6	29.7	98.8
601CCP-03.d	34.8	34.3	29.9	99.0
601CCP-04.d	34.5	34.3	30.2	98.9
601CCP-05.d	34.9	34.3	30.0	99.2
62CCP-01.d	34.8	34.6	30.7	100.1
62CCP-02.d	34.8	34.7	30.3	99.7
62CCP-03.d	34.8	34.7	30.2	99.7
62CCP-04.d	34.8	34.7	30.7	100.2
62CCP-05.d	34.9	34.8	31.0	100.7
62CCP-06.d	34.9	34.7	30.2	99.8
62CCP-07.d	34.9	35.0	30.2	100.5
64ROV11CCP-01.d	34.6	33.7	31.0	99.4
64ROV11CCP-02.d	34.7	33.8	31.3	99.9
64ROV11CCP-03.d	34.6	33.9	30.9	99.4
64ROV11CCP-04.d	34.9	34.7	30.8	100.3
64ROV11CCP-05.d	34.8	34.7	30.9	100.4
64ROV11CCP-06.d	34.8	34.8	30.3	99.9
64ROV11CCP-07.d	34.7	34.8	30.9	100.4
ALJ01CCP-01.d	35.1	34.8	30.7	100.7
ALJ01CCP-02.d	35.2	34.6	31.0	100.7
ALJ01CCP-04.d	34.4	34.2	30.0	98.6
ALJ01CCP-05.d	34.9	34.5	30.3	99.7
ALJ01CCP-06.d	35.1	34.5	30.9	100.5
AZN01CCP-02.d	34.9	34.9	30.8	100.6
AZN01CCP-03.d	34.9	34.8	30.8	100.5
AZN01CCP-04.d	35.0	34.8	30.7	100.8
AZN01CCP-05.d	34.9	34.7	30.7	100.3
AZN01CCP-06.d	34.7	34.9	30.6	100.2
AZN01CCP-07.d	34.8	34.8	30.4	99.9
COR01CCP-01.d	34.8	34.8	30.7	100.3
COR01CCP-03.d	34.6	34.9	29.9	99.3
COR01CCP-04.d	35.0	34.9	30.4	100.3
COR01CCP-06.d	34.8	34.7	30.2	99.7
COR01CCP-08.d	34.8	34.9	30.9	100.5
COR02CCP-01.d	34.6	34.6	30.4	99.7
COR02CCP-02.d	34.8	34.5	30.4	100.3
COR02CCP-03.d	33.6	34.0	28.8	96.4
COR02CCP-04.d	34.6	34.9	30.5	100.0

	Weight percent			
Grain	S (wt%)	Cu (wt%)	Fe (wt%)	Total
Detection limit	0.367	0.503	0.836	
COR02CCP-05.d	34.9	35.0	30.7	100.6
COR02CCP-06.d	34.7	34.6	30.8	100.1
COR02CCP-07.d	34.7	34.8	30.7	100.2
COR03CCP-01.d	34.7	34.4	30.1	99.2
COR03CCP-02.d	34.7	34.8	30.4	99.9
COR03CCP-03.d	34.8	34.7	30.4	99.8
COR03CCP-04.d	34.9	34.1	30.3	99.3
COR03CCP-05.d	34.8	34.5	30.3	99.7
COR03CCP-07.d	34.6	34.7	30.2	99.6
COR03CCP-08.d	34.8	34.8	30.4	100.1
COR03CCP-09.d	34.9	34.5	30.8	100.2
COR03CCP-10.d	34.9	34.7	30.8	100.4
COR03CCP-11.d	34.5	34.4	30.4	99.4
COR04CCP-01.d	34.7	34.1	29.9	98.7
COR04CCP-02.d	34.9	34.3	30.0	99.2
COR04CCP-03.d	34.6	34.3	29.9	98.8
COR04CCP-04.d	34.6	34.3	29.8	98.6
COR04CCP-05.d	34.6	34.3	29.9	98.8
COR04CCP-06.d	35.0	34.6	30.6	100.2
GRA01CCP-01.d	34.8	34.8	30.4	100.1
GRA01CCP-02.d	34.9	34.5	30.5	99.8
GRA01CCP-03.d	34.8	34.5	30.7	100.0
GRA01CCP-04.d	35.0	34.7	31.0	100.7
GRA01CCP-05.d	34.8	35.1	30.7	100.5
GRA01CCP-06.d	34.7	35.0	30.6	100.4
LOU01CCP-01.d	35.0	34.6	30.6	100.2
LOU01CCP-02.d	35.0	34.6	30.3	99.9
LOU01CCP-03.d	34.8	34.1	29.5	98.4
LOU01CCP-04.d	35.0	34.7	30.7	100.4
LOU01CCP-05.d	35.0	34.8	30.8	100.7
LOU01CCP-06.d	35.0	34.8	30.6	100.4
LOU01CCP-07.d	34.8	34.8	30.6	100.2
LS10CCP-01.d	34.5	33.9	29.7	98.2
LS10CCP-02.d	34.9	34.6	30.0	99.5
LS10CCP-03.d	34.5	34.3	29.9	98.7
LS10CCP-04.d	34.5	34.7	30.0	99.1
LS10CCP-05.d	34.5	34.0	30.3	98.8
LS10CCP-06.d	34.7	34.6	30.3	99.6
LS10CCP-07.d	34.8	34.2	29.8	98.8
LS1CCP-01.d	34.9	35.0	30.2	100.1
LS1CCP-02.d	34.9	35.1	30.7	100.6
LS1CCP-03.d	34.9	35.2	30.5	100.6
LS1CCP-04.d	34.8	34.9	30.2	99.9
LS1CCP-05.d	35.0	34.8	30.6	100.4
LS1CCP-06.d	34.9	35.2	30.5	100.5
LS1CCP-07.d	34.9	35.5	30.6	101.1
LS22CCP-01.d	34.7	34.6	30.7	99.9
LS22CCP-02.d	34.6	34.6	30.6	99.9
LS22CCP-03.d	34.7	34.5	30.0	99.3
LS22CCP-04.d	34.7	34.4	30.3	99.4

	Weight percent			
Grain	S (wt%)	Cu (wt%)	Fe (wt%)	Total
Detection limit	0.367	0.503	0.836	
LS22CCP-05.d	34.8	34.7	30.2	99.7
LS22CCP-06.d	34.7	34.5	30.6	99.8
LS22CCP-07.d	34.8	34.4	30.3	99.5
MN1CCP-01.d	34.5	34.6	30.1	99.3
MN1CCP-02.d	34.5	34.7	30.1	100.4
MN1CCP-03.d	34.6	34.6	30.4	99.5
MN1CCP-04.d	35.1	34.9	30.8	100.8
MN1CCP-05.d	34.6	34.9	30.4	99.9
MN1CCP-06.d	34.7	34.9	30.7	100.3
MN1CCP-07.d	34.8	34.8	30.7	100.2
MN2CCP-01.d	34.4	34.9	30.5	99.7
MN2CCP-03.d	34.5	34.3	30.5	99.3
MN2CCP-04.d	34.6	34.5	31.3	100.4
MN2CCP-05.d	34.7	34.6	30.6	99.9
MN2CCP-06.d	34.5	34.8	30.3	99.5
MN2CCP-07.d	34.7	34.5	30.1	99.4
MN3CCP-01.d	34.3	34.9	30.6	99.8
MN3CCP-02.d	34.6	34.5	30.7	99.8
MN3CCP-03.d	34.7	34.5	30.9	100.1
MN3CCP-04.d	34.6	34.6	30.6	99.7
MN3CCP-05.d	34.7	34.6	30.5	99.8
MN3CCP-06.d	34.7	34.5	30.5	99.8
NEV01CCP-01.d	34.9	34.6	30.5	100.0
NEV01CCP-02.d	34.6	34.7	30.1	99.3
NEV01CCP-03.d	34.9	34.8	30.8	100.5
NEV02CCP-01.d	35.0	34.9	31.0	100.9
NEV02CCP-02.d	35.2	34.9	30.8	100.9
NEV02CCP-03.d	35.2	34.9	30.6	100.7
QT0MTCCP-01.d	34.6	34.6	30.6	99.8
QT0MTCCP-02.d	35.0	34.6	31.0	100.5
QT0MTCCP-03.d	34.8	34.6	30.7	100.1
QT0MTCCP-04.d	34.7	34.4	30.9	99.9
QT0MTCCP-05.d	34.6	34.3	30.6	99.5
QT0MTCCP-06.d	34.7	34.4	30.5	99.6
QT0MTCCP-07.d	34.7	34.4	30.8	99.8
V553221CCP-001.d	34.9	34.2	30.7	99.8
V553221CCP-002.d	34.6	34.1	30.8	99.5
V553221CCP-003.d	34.6	34.1	30.6	99.3
V553221CCP-004.d	34.8	34.4	30.6	100.2
V553221CCP-005.d	34.8	34.4	30.6	99.7
V553221CCP-006.d	34.8	34.2	30.2	99.2
V557327ACCP-001.d	34.6	33.7	30.5	98.7
V557327ACCP-002.d	34.6	33.5	30.2	98.3
V557327ACCP-003.d	34.6	34.0	30.5	99.1
V557327ACCP-004.d	34.9	33.9	31.0	99.8
V557327ACCP-005.d	34.7	33.6	30.1	98.4
V557327ACCP-006.d	35.0	33.9	30.6	99.4
ZAM01CCP-01.d	34.8	34.6	29.9	99.3
ZAM01CCP-02.d	34.8	34.4	30.3	99.5
ZAM01CCP-03.d	34.9	34.5	30.2	99.5

	Weight percent			
Grain	S (wt%)	Cu (wt%)	Fe (wt%)	Total
Detection limit	0.367	0.503	0.836	
ZAM01CCP-04.d	34.9	34.4	29.7	98.9
ZAM01CCP-05.d	34.7	34.5	30.2	99.5
ZAM01CCP-06.d	34.9	34.4	30.5	99.8
ZAM01CCP-07.d	34.9	34.4	30.0	99.2

Summarized data

	Weight percent			
	S (wt%)	Cu (wt%)	Fe (wt%)	Total
Detection limit	0.367	0.503	0.836	
Arithmetic mean	34.8	34.5	30.4	99.7
Standard deviation	0.201	0.540	0.496	

Annexe B3 Full LA-ICP-MS results for trace elements (in ppm) of chalcopyrite.

Grain ID	Mn	Co	Ni	Zn	Ga	As	Se	Mo	Ru	Rh	Ag	Pd	In	Sn	Sb	Te	Re	Os	Ir	Pt	Au	Tl	Pb	Bi
	55	59	60	66	71	75	82	95	101	103	107	108	115	118	121	128	185	189	193	195	197	205	208	209
33um	1.017	0.029	0.322	0.590	0.033	0.149	3.828	5.311	0.030	0.020	0.027	0.026	0.033	0.155	0.047	0.400	0.501	0.012	0.028	0.007	0.016	0.006	0.029	0.012
55um	0.449	0.024	0.211	0.357	0.028	0.079	2.455	2.409	0.029	0.020	0.019	0.011	0.015	0.071	0.025	0.277	0.221	0.007	0.016	0.004	0.012	0.004	0.015	0.008
07MPBR23CCP-06.d	1.15	1.03	0.940	383	0.221	0.290	57.1	<dl	0.021	n.r.	63.8	<dl	15.5	466	2.01	*0.024	<dl	<dl	<dl	0.004	0.029	0.050	5.88	12.7
07MPBR23CCP-03.d	1.00	1.10	1.05	422	0.322	0.051	54.2	0.008	0.007	n.r.	59.9	<dl	17.7	509	1.50	*0.027	<dl	0.006	<dl	0.004	0.074	0.018	6.54	8.66
07MPBR23CCP-04.d	1.27	1.02	1.31	419	0.286	0.160	53.8	0.015	0.013	n.r.	66.8	<dl	26.4	687	0.524	*0.027	0.003	<dl	<dl	<dl	0.239	0.009	4.12	5.29
07MPBR23CCP-05.d	1.18	1.09	1.39	555	0.340	0.029	57.8	<dl	0.005	n.r.	65.0	<dl	26.6	653	0.268	*0.032	0.002	0.004	<dl	0.003	0.381	0.004	1.88	1.91
07MPBR23CCP-02.d	1.19	0.970	1.10	405	0.304	0.130	58.4	0.005	0.021	n.r.	61.6	<dl	23.0	390	1.65	*0.028	<dl	<dl	0.001	0.003	0.019	0.045	5.75	7.32
1869CCP-01.d	1.06	5.66	*0.01	323	4.31	0.030	41.5	0.008	0.015	n.r.	12.4	<dl	9.68	4.46	0.437	1.19	<dl	<dl	0.003	<dl	*0.002	0.046	5.71	0.944
1869CCP-02.d	*0.318	2.98	*0.013	293	4.87	<dl	40.5	0.032	<dl	n.r.	12.3	<dl	9.02	3.99	0.295	1.91	<dl	<dl	<dl	<dl	*0.002	0.051	18.9	1.12
1869CCP-05.d	*0.314	2.37	12.4	285	4.34	0.062	40.9	<dl	0.030	n.r.	11.8	<dl	9.13	5.08	0.500	0.780	<dl	<dl	0.003	<dl	0.019	0.044	3.22	1.16
1869CCP-04.d	*0.353	5.52	0.890	368	2.95	<dl	47.0	<dl	0.016	n.r.	12.3	<dl	8.88	4.37	0.380	1.53	<dl	<dl	<dl	<dl	*0.002	0.037	3.40	1.16
1869CCP-03.d	0.700	5.93	0.540	308	3.65	0.038	41.6	0.024	0.028	n.r.	12.1	<dl	8.71	3.43	0.355	1.53	<dl	<dl	0.003	<dl	*0.001	0.035	2.04	0.750
1869CCP-06.d	*0.296	5.48	*0.014	322	5.45	0.040	39.5	<dl	0.015	n.r.	12.6	<dl	9.61	5.14	0.380	1.29	<dl	<dl	<dl	<dl	*0.002	0.057	12.1	1.31
1869CCP-07.d	1.03	4.02	0.770	275	4.56	0.055	49.6	0.001	0.010	n.r.	12.7	<dl	9.01	3.72	0.411	1.21	<dl	0.010	<dl	<dl	*0.002	0.084	12.9	1.62
1872CCP-03.d	*0.432	*0.014	*0.014	151	119	0.660	28.4	<dl	<dl	n.r.	15.4	<dl	5.79	147	25.1	*0.071	<dl	<dl	<dl	<dl	0.013	0.540	6.90	0.065
1872CCP-04.d	*0.34	*0.016	*0.009	137	127	0.470	32.3	0.027	<dl	n.r.	18.2	<dl	5.06	110	12.8	0.340	<dl	<dl	<dl	<dl	0.053	0.023	6.62	0.261
1872CCP-06.d	*0.303	*0.017	*0.01	141	133	0.060	34.7	0.020	<dl	n.r.	45.8	<dl	4.99	153	8.01	*0.07	0.006	<dl	<dl	<dl	0.072	0.030	4.96	0.107
1872CCP-02.d	1.45	*0.013	*0.01	194	137	0.670	33.9	0.021	<dl	n.r.	7.93	<dl	5.94	139	1.59	*0.056	<dl	<dl	<dl	<dl	*0.001	*0.001	1.38	0.022
1872CCP-05.d	*0.32	*0.015	*0.013	142	150	<dl	33.1	0.025	<dl	n.r.	23.2	<dl	6.27	104	2.24	*0.061	<dl	<dl	0.004	0.011	0.018	*0.003	5.17	0.163
1872CCP-01.d	*0.231	0.065	*0.008	148	10.2	0.180	21.9	0.330	<dl	n.r.	9.80	<dl	4.48	141	1.38	*0.044	<dl	0.016	<dl	0.008	0.016	0.004	2.76	0.106
2211CCP-04.d	*0.221	1.69	*0.015	153	0.870	0.030	3110	0.014	0.009	n.r.	56.9	<dl	110	92.6	0.437	2.94	<dl	0.004	<dl	<dl	0.392	0.006	5.46	4.90
2211CCP-03.d	3.89	1.61	*0.018	155	2.59	0.155	3062	<dl	<dl	n.r.	50.5	<dl	109	711	0.870	2.49	<dl	<dl	<dl	<dl	0.310	0.034	11.7	8.53
2211CCP-01.d	*0.268	1.69	*0.02	176	2.01	0.070	3037	<dl	<dl	n.r.	60.7	<dl	128	917	0.937	3.13	<dl	<dl	<dl	<dl	0.186	0.073	13.8	7.20
2211CCP-05.d	*0.304	1.74	*0.018	206	3.02	<dl	3300	<dl	0.029	n.r.	43.6	<dl	121	134	0.270	3.23	<dl	<dl	<dl	<dl	0.360	0.005	7.75	6.25
2211CCP-02.d	*0.344	1.63	*0.022	211	2.58	<dl	3360	<dl	<dl	n.r.	60.0	<dl	123	107	0.510	2.49	0.003	<dl	<dl	<dl	0.088	*0.001	5.65	4.53
2211CCP-06.d	*0.195	1.53	*0.019	160	0.400	0.020	2942	<dl	<dl	n.r.	74.4	<dl	124	153	0.204	6.90	<dl	<dl	<dl	<dl	0.088	*0.001	6.91	2.21
2215CCP-04.d	88.4	5.25	0.350	109	0.082	0.075	385	<dl	0.018	n.r.	56.1	<dl	5.43	46.5	0.950	2.31	<dl	<dl	<dl	<dl	0.900	0.046	7.12	4.43
2215CCP-05.d	2.90	6.66	0.440	121	0.041	<dl	408	<dl	<dl	n.r.	57.4	<dl	5.62	55.0	0.350	3.42	<dl	<dl	<dl	<dl	0.780	0.005	2.80	2.31
2215CCP-03.d	*0.151	5.78	0.410	114	0.052	<dl	378	<dl	0.032	n.r.	53.5	<dl	5.44	50.6	0.282	2.10	0.002	<dl	<dl	<dl	0.460	0.025	2.79	2.55
2215CCP-06.d	*0.285	5.52	*0.022	1070	0.096	<dl	410	<dl	<dl	n.r.	56.1	<dl	5.21	56.5	0.390	3.22	<dl	<dl	<dl	<dl	1.14	0.024	4.00	1.66
2215CCP-02.d	*0.184	5.46	0.300	127	0.043	<dl	406	<dl	<dl	n.r.	58.9	<dl	5.35	50.8	0.256	2.70	0.002	<dl	<dl	0.003	0.463	0.020	2.52	1.77
2221CCP-01.d	1.86	3.71	1.65	428	22.3	0.067	756	0.014	0.008	n.r.	86.8	<dl	18.5	75.4	0.170	20.6	<dl	<dl	<dl	<dl	0.274	0.056	3.72	26.4
2221CCP-05.d	3.98	7.00	12.4	327	29.5	0.085	630	0.009	0.009	n.r.	81.8	<dl	15.8	82.3	0.130	11.5	0.002	<dl	<dl	<dl	0.292	0.015	2.15	17.0
2221CCP-03.d	2.95	2.92	1.72	378	16.3	0.023	678	0.007	0.008	n.r.	77.3	<dl	19.6	58.0	0.112	41.0	<dl	<dl	7.E-4	0.020	0.678	0.025	2.21	60.0
2221CCP-02.d	2.05	12.7	22.6	338	28.9	0.100	659	0.012	0.012	n.r.	83.6	<dl	17.1	85.9	0.081	34.0	<dl	<dl	0.001	<dl	0.229	0.051	6.42	50.0

Grain ID	Mn	Co	Ni	Zn	Ga	As	Se	Mo	Ru	Rh	Ag	Pd	In	Sn	Sb	Te	Re	Os	Ir	Pt	Au	Tl	Pb	Bi
	55	59	60	66	71	75	82	95	101	103	107	108	115	118	121	128	185	189	193	195	197	205	208	209
33um	1.017	0.029	0.322	0.590	0.033	0.149	3.828	5.311	0.030	0.020	0.027	0.026	0.033	0.155	0.047	0.400	0.501	0.012	0.028	0.007	0.016	0.006	0.029	0.012
55um	0.449	0.024	0.211	0.357	0.028	0.079	2.455	2.409	0.029	0.020	0.019	0.011	0.015	0.071	0.025	0.277	0.221	0.007	0.016	0.004	0.012	0.004	0.015	0.008
2221CCP-07.d	1.72	4.58	2.09	368	15.2	0.002	665	0.004	0.020	n.r.	80.8	<dl	16.5	614	0.066	6.80	<dl	<dl	0.030	<dl	0.352	0.023	2.09	4.80
2221CCP-06.d	2.99	8.20	23.0	409	31.6	<dl	668	0.007	0.006	n.r.	83.9	<dl	16.9	93.0	0.054	31.0	<dl	<dl	<dl	<dl	0.113	0.004	1.47	41.0
2221CCP-04.d	1.53	2.70	12.5	430	30.4	0.052	629	0.011	0.010	n.r.	98.4	<dl	16.3	89.8	0.051	53.0	<dl	<dl	<dl	<dl	0.329	0.002	1.43	64.0
2224CCP-03.d	2.98	2.74	0.410	337	10.2	0.007	1720	0.017	0.014	n.r.	46.4	<dl	91.0	96.8	0.452	3.30	<dl	<dl	<dl	<dl	0.176	*0.002	4.40	2.15
2224CCP-04.d	1.32	4.35	0.400	271	1.96	0.061	1629	0.011	0.011	n.r.	54.6	<dl	97.0	127	0.460	5.48	<dl	0.017	<dl	0.005	0.178	*0.001	3.50	2.80
2224CCP-05.d	0.460	3.70	0.300	203	13.0	0.076	1892	<dl	<dl	n.r.	53.1	<dl	98.9	105	0.406	3.63	<dl	<dl	0.001	<dl	0.270	0.005	3.58	1.18
2224CCP-06.d	2.40	3.03	0.600	180	12.9	0.130	1743	0.011	0.010	n.r.	48.5	<dl	95.1	67.6	0.670	3.50	<dl	<dl	<dl	<dl	0.101	0.236	9.40	2.56
2224CCP-01.d	1.60	2.59	2.20	207	2.09	0.023	1733	0.006	0.022	n.r.	50.8	<dl	95.6	108	0.610	3.64	<dl	<dl	<dl	<dl	0.095	*0.001	3.45	2.45
2224CCP-02.d	*0.156	2.47	*0.014	213	13.8	0.026	1800	0.022	0.006	n.r.	51.7	<dl	95.9	82.1	0.850	2.82	<dl	<dl	<dl	<dl	0.183	0.024	8.60	2.82
2296CCP-07.d	1.99	0.748	*0.015	487	0.294	<dl	97.9	0.007	0.090	n.r.	127	<dl	24.1	97.0	0.537	0.199	<dl	<dl	<dl	<dl	0.043	0.355	1.46	1.60
2296CCP-06.d	0.660	0.733	*0.011	332	0.212	0.023	89.1	<dl	0.016	n.r.	76.0	<dl	21.6	67.5	1.52	*0.027	0.001	<dl	0.001	0.003	0.020	0.249	2.14	1.89
2296CCP-02.d	1.14	0.703	*0.01	395	0.240	0.017	90.9	0.011	0.008	n.r.	71.9	<dl	23.0	81.8	0.587	*0.024	<dl	<dl	1.E-4	<dl	*0.005	0.098	1.34	1.23
2296CCP-05.d	0.830	0.575	*0.01	380	0.263	0.050	83.1	0.002	0.013	n.r.	88.8	<dl	21.6	89.3	0.342	0.172	<dl	0.003	<dl	<dl	0.021	0.041	0.898	1.24
2296CCP-01.d	3.27	0.911	0.160	414	0.293	<dl	91.9	0.013	0.017	n.r.	243	<dl	24.4	85.0	0.339	*0.029	<dl	<dl	<dl	<dl	0.040	0.124	1.45	1.39
2296CCP-03.d	0.730	0.362	*0.011	380	0.353	0.026	85.0	0.026	0.017	n.r.	68.6	<dl	22.8	86.5	1.07	*0.032	<dl	<dl	<dl	0.100	0.088	0.141	1.97	2.18
2296CCP-04.d	2.13	0.860	*0.011	335	0.395	0.068	92.8	<dl	0.022	n.r.	63.7	<dl	23.3	78.8	0.725	*0.027	9.E-4	0.005	3.E-4	0.002	0.062	0.157	1.80	1.47
2318CCP-03.d	*0.16	0.920	3.43	428	*0.008	0.040	39.5	<dl	0.017	n.r.	30.3	<dl	27.6	5.55	*0.01	*0.046	<dl	<dl	<dl	<dl	*0.001	0.060	1.91	0.138
2318CCP-06.d	0.420	0.224	40.8	372	0.104	0.110	33.2	<dl	<dl	n.r.	22.8	<dl	38.4	5.13	0.029	*0.027	<dl	0.003	<dl	<dl	*0.001	0.003	6.08	0.239
2318CCP-04.d	1.10	0.353	56.1	308	0.285	0.070	40.1	0.010	0.013	n.r.	24.4	<dl	32.1	6.64	0.024	*0.041	<dl	<dl	<dl	0.003	*0.001	0.005	2.24	0.150
2318CCP-02.d	0.660	1.62	27.0	443	0.160	0.045	36.8	0.003	0.090	n.r.	30.3	<dl	33.1	8.77	*0.006	*0.031	<dl	<dl	<dl	0.002	*0.001	*0.002	1.60	0.098
2318CCP-01.d	*0.124	3.90	43.0	469	0.157	0.107	36.8	<dl	0.016	n.r.	31.3	<dl	30.8	7.03	*0.007	*0.035	0.001	0.005	3.E-4	<dl	*0.001	0.003	2.26	0.116
2318CCP-07.d	0.750	1.02	112	354	0.081	0.083	34.3	0.011	<dl	n.r.	33.0	<dl	37.0	4.59	*0.006	*0.036	<dl	<dl	<dl	0.003	*0.001	*0.002	1.09	0.029
2318CCP-05.d	0.800	0.332	29.3	401	0.219	0.027	41.6	0.009	0.036	n.r.	34.9	<dl	33.7	6.39	*0.006	*0.034	0.001	<dl	<dl	<dl	*0.001	*0.001	1.52	0.033
2325CCP-06.d	10.6	6.22	*0.026	337	0.590	<dl	35.3	0.036	0.011	n.r.	59.3	<dl	20.1	76.1	0.640	*0.05	<dl	<dl	<dl	<dl	0.339	0.004	5.85	8.18
2325CCP-04.d	11.1	1.07	*0.02	283	0.800	0.034	31.9	0.010	0.011	n.r.	54.8	<dl	19.7	48.2	0.890	*0.039	3.E-4	<dl	0.002	<dl	0.374	0.008	4.81	8.38
2325CCP-05.d	8.35	2.94	*0.025	303	0.650	<dl	33.7	<dl	0.019	n.r.	55.6	<dl	18.7	74.8	0.426	*0.044	<dl	<dl	<dl	<dl	0.401	0.008	2.71	6.66
2325CCP-02.d	4.03	2.81	*0.023	226	0.517	<dl	30.6	0.036	0.007	n.r.	59.8	<dl	19.1	46.4	1.31	*0.046	<dl	<dl	<dl	<dl	0.317	0.046	5.21	14.0
2325CCP-07.d	11.1	5.19	*0.018	312	0.590	0.070	36.5	<dl	0.022	n.r.	58.5	<dl	19.4	80.4	0.385	*0.053	<dl	<dl	<dl	<dl	0.320	0.002	4.42	6.13
2325CCP-01.d	12.4	4.65	*0.024	294	0.910	<dl	31.8	0.016	0.015	n.r.	62.5	<dl	18.3	82.1	0.342	*0.043	0.002	<dl	<dl	0.005	0.306	*0.001	2.88	5.18
2359-CCP-01.d	3.15	10.4	*0.046	174	*0.073	0.290	516	<dl	<dl	n.r.	170	<dl	60.7	104	1.28	0.560	<dl	<dl	<dl	0.006	0.580	0.059	7.40	5.87
2359-CCP-03.d	3.40	12.5	*0.083	173	0.215	0.050	503	0.001	0.013	n.r.	385	<dl	63.7	95.7	0.860	0.660	<dl	0.009	<dl	0.011	3.88	0.014	8.46	7.59
2359-CCP-02.d	2.45	10.0	2.10	174	*0.055	0.040	482	0.031	0.024	n.r.	118	<dl	58.7	92.9	0.139	0.540	<dl	<dl	<dl	<dl	0.410	*0.001	1.93	2.21
2359-CCP-04.d	2.35	9.37	3.13	191	0.241	0.036	503	0.008	0.002	n.r.	141	<dl	59.8	106	0.140	0.760	<dl	0.002	<dl	0.010	0.136	0.008	1.45	1.69
2359-CCP-06.d	3.21	9.45	*0.093	187	0.151	<dl	526	<dl	0.021	n.r.	169	<dl	62.9	98.8	0.211	0.520	<dl	<dl	<dl	<dl	0.391	0.011	1.76	2.09

Grain ID	Mn	Co	Ni	Zn	Ga	As	Se	Mo	Ru	Rh	Ag	Pd	In	Sn	Sb	Te	Re	Os	Ir	Pt	Au	Tl	Pb	Bi
	55	59	60	66	71	75	82	95	101	103	107	108	115	118	121	128	185	189	193	195	197	205	208	209
33um	1.017	0.029	0.322	0.590	0.033	0.149	3.828	5.311	0.030	0.020	0.027	0.026	0.033	0.155	0.047	0.400	0.501	0.012	0.028	0.007	0.016	0.006	0.029	0.012
55um	0.449	0.024	0.211	0.357	0.028	0.079	2.455	2.409	0.029	0.020	0.019	0.011	0.015	0.071	0.025	0.277	0.221	0.007	0.016	0.004	0.012	0.004	0.015	0.008
2359-CCP-05.d	2.49	9.45	3.30	223	0.430	<dl	579	<dl	0.015	n.r.	172	<dl	64.9	125	0.301	0.800	<dl	<dl	<dl	0.004	0.670	*0.002	4.56	4.31
2369CCP-06.d	*0.454	1.14	*0.021	234	0.840	0.110	119	<dl	<dl	n.r.	1010	<dl	279	102	0.910	*0.114	<dl	<dl	<dl	0.013	*0.005	0.129	9.57	5.84
2369CCP-04.d	*0.38	1.26	*0.027	305	1.28	0.280	122	<dl	0.014	n.r.	897	<dl	302	140	0.264	*0.09	<dl	<dl	<dl	0.004	*0.002	0.028	3.65	3.71
2369CCP-02.d	*0.377	1.38	*0.023	286	1.10	0.190	119	0.018	<dl	n.r.	944	<dl	299	123	0.245	*0.095	<dl	<dl	<dl	<dl	*0.003	0.012	3.20	3.78
2369CCP-05.d	*0.406	1.09	*0.023	287	0.830	0.100	117	<dl	<dl	n.r.	939	<dl	310	110	0.610	*0.086	<dl	<dl	<dl	9.E-4	*0.004	0.085	9.70	6.50
2369CCP-07.d	*0.321	1.33	*0.025	275	0.300	<dl	92.0	<dl	<dl	n.r.	1031	<dl	271	218	*0.018	*0.059	<dl	<dl	0.002	<dl	*0.002	0.005	0.546	0.440
2369CCP-03.d	*0.36	1.18	*0.024	328	1.98	<dl	141	0.021	0.026	n.r.	830	<dl	326	214	0.100	*0.069	<dl	<dl	<dl	0.010	0.009	0.011	2.10	1.58
2369CCP-01d	10.0	1.35	0.390	273	1.04	0.540	113	0.014	<dl	n.r.	932	<dl	307	207	*0.02	*0.091	<dl	<dl	<dl	0.003	*0.002	0.020	0.874	0.879
2378CCP-02.d	*0.213	0.098	*0.01	350	6.88	<dl	13.6	0.065	0.009	n.r.	5.56	<dl	81.0	51.0	0.213	*0.024	<dl	<dl	0.003	<dl	*0.001	0.012	2.02	0.031
2378CCP-05.d	*0.194	*0.004	*0.006	307	3.39	0.110	10.2	0.023	0.042	n.r.	4.56	<dl	79.4	36.4	0.138	*0.012	<dl	0.014	<dl	0.009	*0.001	0.016	1.62	0.076
2378CCP-07.d	*0.341	0.900	*0.02	292	1.79	0.700	13.0	0.026	0.021	n.r.	6.69	<dl	75.0	40.5	0.610	*0.036	<dl	<dl	<dl	<dl	*0.001	0.087	5.60	0.124
2378CCP-08.d	*0.234	0.110	*0.012	353	5.53	<dl	16.2	0.027	0.010	n.r.	4.91	<dl	76.6	49.2	0.257	*0.023	<dl	<dl	0.002	0.005	*0.001	0.016	2.64	0.133
2378CCP-01d	*0.281	0.089	*0.011	365	5.40	0.100	8.30	<dl	<dl	n.r.	3.55	<dl	104	47.3	0.107	*0.023	<dl	0.016	<dl	0.042	*0.001	0.011	1.58	0.015
2378CCP-03.d	*0.203	0.076	*0.009	314	5.90	<dl	8.70	0.022	<dl	n.r.	5.32	<dl	76.3	56.6	0.074	*0.019	<dl	0.029	<dl	<dl	*0.001	0.007	0.930	0.026
2378CCP-06.d	*0.17	0.075	*0.01	325	3.60	0.120	11.8	0.023	0.024	n.r.	4.39	<dl	76.2	46.1	0.135	*0.019	0.004	<dl	<dl	<dl	*0.001	0.010	1.16	0.030
2378CCP-04.d	*0.234	*0.011	0.380	280	1.53	0.020	*1.677	0.015	0.027	n.r.	4.37	<dl	82.7	28.7	0.217	*0.032	0.004	<dl	0.003	<dl	*0.001	0.010	1.70	0.190
2383-CCP-04.d	3.18	5.53	*0.053	358	3.95	<dl	673	0.003	0.011	n.r.	46.1	<dl	46.6	29.3	0.360	*0.115	0.001	<dl	<dl	0.007	*0.006	0.028	7.20	1.40
2383-CCP-01d	3.46	3.54	*0.045	324	2.29	0.040	559	0.007	<dl	n.r.	46.8	<dl	40.4	18.6	0.530	*0.108	0.003	<dl	<dl	4.E-4	*0.003	0.043	17.3	1.68
2383-CCP-02.d	4.04	2.02	*0.045	328	1.92	0.120	570	<dl	0.025	n.r.	41.9	<dl	43.4	21.0	0.530	*0.135	0.004	<dl	<dl	<dl	*0.002	0.068	17.1	1.42
2383-CCP-03.d	5.40	3.99	1.20	460	4.95	2.29	633	<dl	<dl	n.r.	51.1	<dl	49.3	23.3	0.350	*0.15	<dl	<dl	<dl	0.005	*0.006	*0.004	10.2	2.29
2383-CCP-05.d	3.12	1.48	*0.042	402	5.71	<dl	667	<dl	<dl	n.r.	46.8	<dl	45.1	40.7	0.191	*0.082	<dl	<dl	0.007	<dl	*0.005	0.018	4.91	1.07
2383-CCP-06.d	2.54	2.58	1.70	378	5.10	<dl	650	0.100	<dl	n.r.	46.2	<dl	47.2	35.6	0.260	*0.118	<dl	<dl	<dl	<dl	*0.003	*0.004	7.50	3.96
2393-CCP-02.d	3.63	2.43	*0.062	445	0.510	<dl	576	<dl	0.012	n.r.	79.5	<dl	82.5	71.6	0.351	0.610	<dl	0.029	8.E-4	<dl	0.088	*0.002	7.08	0.960
2393-CCP-01d	3.10	1.51	*0.043	488	0.460	0.040	608	<dl	<dl	n.r.	80.7	<dl	72.7	65.1	0.190	0.700	<dl	<dl	0.004	<dl	0.167	*0.002	8.28	0.680
2393-CCP-04.d	3.82	1.64	*0.049	515	0.563	0.050	605	0.056	0.027	n.r.	88.3	<dl	66.6	78.4	0.710	0.940	<dl	<dl	<dl	<dl	0.137	*0.003	10.9	1.51
2393-CCP-03.d	2.95	1.45	*0.062	376	0.414	<dl	567	<dl	0.003	n.r.	77.0	<dl	72.1	73.9	0.341	0.740	0.002	0.009	<dl	<dl	0.109	0.014	5.46	1.91
2393-CCP-06.d	3.78	2.62	2.40	520	0.680	0.033	613	0.018	0.021	n.r.	79.8	<dl	90.1	92.5	0.326	0.950	2.E-4	0.005	<dl	<dl	0.043	*0.002	8.72	0.794
2393-CCP-05.d	3.88	1.38	*0.046	557	0.560	<dl	605	<dl	<dl	n.r.	79.6	<dl	60.5	69.2	0.339	0.700	0.018	<dl	0.006	0.014	*0.013	*0.002	6.85	0.750
2394-CCP-04.d	3.44	18.0	*0.055	483	*0.098	0.168	269	<dl	0.018	n.r.	9.30	<dl	2.52	93.1	1.48	0.850	<dl	<dl	<dl	<dl	0.059	*0.001	1.57	0.530
2394-CCP-06.d	3.50	1.79	2.30	584	24.1	0.078	254	<dl	0.090	n.r.	22.1	<dl	364	130	1.58	1.24	<dl	<dl	<dl	<dl	*0.004	*0.002	1.85	0.038
2394-CCP-01d	1.28	22.2	1.70	408	*0.139	<dl	282	0.042	<dl	n.r.	14.0	<dl	1.99	105	5.93	1.31	<dl	<dl	<dl	<dl	*0.01	0.072	3.32	0.770
2394-CCP-05.d	2.54	1.21	2.10	581	18.6	0.124	253	<dl	0.094	n.r.	207	<dl	343	111	2.36	0.950	<dl	0.070	0.004	0.015	*0.005	*0.002	3.12	0.035
2394-CCP-02.d	2.37	21.5	3.20	560	*0.096	0.082	287	0.009	<dl	n.r.	9.54	<dl	2.97	126	3.34	0.780	<dl	<dl	<dl	<dl	*0.011	0.038	2.85	0.720
2394-CCP-03.d	2.26	29.6	1.80	482	*0.091	0.023	265	<dl	0.013	n.r.	12.8	<dl	3.16	107	3.54	0.580	<dl	0.014	<dl	<dl	*0.011	0.047	2.27	0.800

Grain ID	Mn	Co	Ni	Zn	Ga	As	Se	Mo	Ru	Rh	Ag	Pd	In	Sn	Sb	Te	Re	Os	Ir	Pt	Au	Tl	Pb	Bi
	55	59	60	66	71	75	82	95	101	103	107	108	115	118	121	128	185	189	193	195	197	205	208	209
33um	1.017	0.029	0.322	0.590	0.033	0.149	3.828	5.311	0.030	0.020	0.027	0.026	0.033	0.155	0.047	0.400	0.501	0.012	0.028	0.007	0.016	0.006	0.029	0.012
55um	0.449	0.024	0.211	0.357	0.028	0.079	2.455	2.409	0.029	0.020	0.019	0.011	0.015	0.071	0.025	0.277	0.221	0.007	0.016	0.004	0.012	0.004	0.015	0.008
2398-CCP-05.d	3.30	1.84	*0.047	400	0.515	0.007	560	0.014	<dl	n.r.	79.4	<dl	61.2	61.1	0.250	0.770	<dl	0.011	0.002	0.006	0.039	*0.002	42.8	0.630
2398-CCP-04.d	3.32	1.26	*0.048	541	0.266	<dl	540	0.018	0.008	n.r.	83.1	<dl	56.5	57.0	0.258	0.520	0.005	0.011	0.002	<dl	0.052	*0.004	49.1	0.750
2398-CCP-02.d	3.25	1.64	*0.064	710	0.480	0.025	609	<dl	<dl	n.r.	87.9	<dl	63.9	63.5	0.169	0.820	0.005	<dl	0.002	0.005	*0.003	*0.003	6.82	0.660
2398-CCP-01.d	3.65	1.96	1.55	554	0.442	0.050	573	0.020	0.006	n.r.	80.8	<dl	59.4	58.4	0.282	0.840	0.004	0.025	<dl	<dl	0.034	*0.002	17.3	0.700
2398-CCP-03.d	3.44	2.90	*0.064	342	0.450	<dl	525	0.025	<dl	n.r.	73.0	<dl	78.6	68.7	0.152	0.500	<dl	<dl	<dl	<dl	0.024	*0.003	15.4	0.610
2398-CCP-06.d	3.18	1.16	*0.056	422	0.420	0.026	508	0.036	<dl	n.r.	77.6	<dl	59.2	59.9	0.190	0.540	0.010	<dl	<dl	0.020	0.051	0.011	5.65	0.481
2399-CCP-06.d	6.40	0.183	*0.046	457	2.30	0.229	266	0.027	0.064	n.r.	140	<dl	41.6	136	2.35	0.890	<dl	<dl	0.003	<dl	*0.003	0.097	2.54	1.30
2399-CCP-04.d	5.09	0.307	*0.063	412	2.49	0.051	217	0.008	0.007	n.r.	118	<dl	40.6	114	2.30	0.740	0.010	<dl	0.003	0.015	*0.003	*0.003	2.52	0.969
2399-CCP-03.d	5.53	0.337	*0.073	529	2.81	0.037	245	0.020	0.010	n.r.	96.3	<dl	53.8	187	3.52	1.25	<dl	0.024	<dl	0.008	*0.003	0.016	4.57	1.64
2399-CCP-01.d	5.64	0.287	*0.075	501	1.66	0.133	233	0.022	<dl	n.r.	90.4	<dl	45.7	148	3.39	0.930	0.005	<dl	<dl	0.008	*0.005	*0.002	3.52	2.12
2399-CCP-05.d	5.81	0.206	2.14	437	2.42	0.101	258	0.009	0.080	n.r.	99.7	<dl	50.2	149	5.40	1.18	<dl	<dl	0.003	0.011	*0.002	0.015	5.30	1.78
2399-CCP-02.d	4.72	0.351	1.70	417	2.43	1.42	226	0.005	0.025	n.r.	124	<dl	39.7	133	1.84	0.530	0.006	0.008	0.004	0.004	0.186	*0.002	2.22	0.903
2410-CCP-04.d	2.92	1.09	*0.056	373	0.460	<dl	499	0.008	<dl	n.r.	77.1	<dl	106	71.2	0.108	0.370	0.005	<dl	<dl	0.007	0.095	*0.002	5.55	0.577
2410-CCP-06.d	3.03	0.863	*0.052	411	0.362	0.029	501	0.013	0.018	n.r.	73.9	<dl	93.3	74.7	0.168	0.380	0.010	<dl	<dl	<dl	0.056	0.009	6.15	0.695
2410-CCP-01.d	2.64	2.15	*0.039	373	0.482	<dl	540	<dl	<dl	n.r.	81.0	<dl	63.8	63.4	0.123	0.470	<dl	<dl	0.004	<dl	0.074	*0.002	8.78	0.550
2410-CCP-02.d	2.90	1.73	*0.041	425	0.480	0.046	522	0.043	0.013	n.r.	85.2	<dl	70.1	67.7	0.181	0.520	<dl	0.032	<dl	<dl	0.099	*0.002	9.71	0.900
2410-CCP-05.d	2.58	1.88	2.30	497	0.730	0.110	562	<dl	<dl	n.r.	82.5	<dl	65.3	63.4	0.340	1.19	<dl	0.120	<dl	<dl	0.180	*0.003	8.40	1.10
2410-CCP-03.d	2.52	1.58	2.20	541	0.370	<dl	609	0.017	<dl	n.r.	94.6	<dl	77.8	104	0.560	1.04	<dl	<dl	<dl	<dl	0.044	0.137	12.3	8.10
2414-CCP-03.d	3.93	1.55	1.25	617	1.57	<dl	433	0.022	0.003	n.r.	89.9	<dl	84.8	212	0.552	0.487	0.001	0.005	6.E-04	0.001	0.129	*0.002	4.16	1.90
2414-CCP-02.d	3.82	2.08	1.89	541	1.56	<dl	453	0.014	0.012	n.r.	86.4	<dl	69.6	185	1.18	0.590	<dl	0.006	<dl	<dl	0.081	*0.003	12.3	2.02
2414-CCP-06.d	3.78	2.70	*0.053	596	1.37	<dl	436	0.022	0.038	n.r.	85.5	<dl	63.6	170	0.700	0.480	<dl	0.024	<dl	0.007	0.035	*0.002	4.06	1.77
2414-CCP-01.d	3.87	1.74	*0.066	561	1.50	<dl	448	<dl	0.006	n.r.	88.7	<dl	76.8	198	0.456	0.440	<dl	<dl	0.002	0.006	0.113	0.012	4.18	1.41
2414-CCP-05.d	3.31	2.88	*0.054	604	1.24	0.056	396	<dl	0.013	n.r.	86.5	<dl	62.4	158	1.78	0.440	0.010	<dl	<dl	<dl	0.042	*0.002	5.60	3.44
2414-CCP-04.d	2.97	1.43	*0.067	474	1.42	<dl	393	0.021	<dl	n.r.	87.4	<dl	63.8	165	2.16	0.390	<dl	<dl	<dl	0.005	*0.004	*0.001	2.29	3.34
2417-CCP-02.d	3.19	1.04	*0.054	396	1.02	<dl	456	0.007	<dl	n.r.	83.4	<dl	94.9	90.4	0.263	0.530	<dl	<dl	0.005	0.004	*0.014	*0.002	4.47	1.15
2417-CCP-01.d	5.30	1.54	*0.065	800	1.10	0.048	495	0.007	0.007	n.r.	88.0	<dl	87.6	88.6	0.685	0.630	0.007	<dl	0.003	0.011	*0.004	*0.002	11.1	1.72
2417-CCP-03.d	3.83	0.990	1.54	481	1.08	0.028	448	0.005	0.002	n.r.	83.7	<dl	79.7	76.7	0.570	0.470	<dl	0.006	0.002	<dl	*0.004	*0.002	5.51	0.920
2417-CCP-05.d	4.06	1.11	*0.053	574	1.17	0.060	487	0.004	0.016	n.r.	88.8	<dl	98.0	102	0.800	0.380	<dl	<dl	<dl	<dl	*0.016	*0.003	27.5	1.59
2417-CCP-04.d	3.90	0.510	2.30	430	0.920	0.030	519	<dl	<dl	n.r.	90.4	<dl	97.5	104	0.570	0.300	<dl	<dl	0.007	<dl	*0.005	*0.002	6.72	1.22
2567-CCP-06.d	139	15.1	11.1	541	1.13	<dl	59.5	0.007	<dl	n.r.	74.6	<dl	5.57	6.26	0.118	0.960	0.008	<dl	<dl	0.006	*0.002	*0.001	0.116	0.381
2567-CCP-01.d	148	12.7	*0.121	552	0.939	<dl	613	0.002	<dl	n.r.	70.3	<dl	6.00	6.47	0.157	0.880	7.E-04	0.013	0.003	<dl	*0.002	*0.001	0.266	0.750
2567-CCP-05.d	115	14.3	2.90	511	1.43	0.120	60.2	0.014	0.008	n.r.	106	<dl	8.53	10.1	0.357	1.03	<dl	<dl	<dl	<dl	*0.003	*0.001	0.334	0.690
2567-CCP-02.d	138	18.1	2.10	638	1.26	<dl	67.5	0.004	0.003	n.r.	85.8	<dl	9.63	10.7	0.275	1.19	<dl	<dl	0.003	<dl	*0.003	*0.002	0.325	0.850
2567-CCP-04.d	98.3	8.08	8.10	464	1.19	0.009	60.3	<dl	0.012	n.r.	107	<dl	10.6	9.73	0.297	0.810	<dl	<dl	0.002	0.004	0.029	*0.001	0.315	0.740

Grain ID	Mn	Co	Ni	Zn	Ga	As	Se	Mo	Ru	Rh	Ag	Pd	In	Sn	Sb	Te	Re	Os	Ir	Pt	Au	Tl	Pb	Bi
	55	59	60	66	71	75	82	95	101	103	107	108	115	118	121	128	185	189	193	195	197	205	208	209
33um	1.017	0.029	0.322	0.590	0.033	0.149	3.828	5.311	0.030	0.020	0.027	0.026	0.033	0.155	0.047	0.400	0.501	0.012	0.028	0.007	0.016	0.006	0.029	0.012
55um	0.449	0.024	0.211	0.357	0.028	0.079	2.455	2.409	0.029	0.020	0.019	0.011	0.015	0.071	0.025	0.277	0.221	0.007	0.016	0.004	0.012	0.004	0.015	0.008
2567-CCP-03.d	186	14.1	3.70	551	1.37	0.015	58.3	<dl	0.004	n.r.	78.1	<dl	5.03	6.20	0.063	0.700	<dl	0.009	<dl	0.013	*0.002	*0.001	0.103	0.377
2569-CCP-03.d	280	0.833	*0.09	440	8.62	<dl	123	0.009	<dl	n.r.	87.5	<dl	5.05	80.9	0.210	0.440	0.006	0.014	<dl	<dl	*0.004	*0.002	1.61	0.670
2569-CCP-01d	99.1	2.44	2.45	522	6.95	<dl	114	0.024	0.034	n.r.	75.3	<dl	5.43	81.9	0.036	0.640	0.010	0.014	0.002	0.005	*0.003	0.006	0.650	0.648
2569-CCP-04.d	110	1.64	*0.072	450	7.96	<dl	115	0.016	0.004	n.r.	63.5	<dl	5.08	81.8	0.122	0.340	0.003	0.005	0.002	<dl	*0.002	*0.001	0.890	0.494
2569-CCP-02.d	100	0.603	2.90	562	7.40	0.033	110	0.006	0.005	n.r.	424	<dl	5.56	82.4	0.033	0.320	<dl	0.007	0.004	0.010	*0.003	*0.001	0.414	0.375
2569-CCP-05.d	102	2.53	*0.072	569	8.88	<dl	120	0.010	0.005	n.r.	89.6	<dl	5.97	86.7	0.045	0.740	<dl	0.022	0.004	0.013	*0.003	*0.001	1.00	1.19
2569-CCP-06.d	99.6	3.71	*0.091	386	5.81	0.021	93.4	0.013	<dl	n.r.	61.6	<dl	4.93	78.3	0.048	0.400	0.008	0.018	<dl	<dl	0.013	*0.001	1.00	0.568
2575-CCP-06.d	29.6	3.09	4.30	363	0.478	<dl	149	<dl	<dl	n.r.	11.4	<dl	4.68	6.74	0.106	1.23	0.009	<dl	<dl	0.003	*0.001	*0.001	0.550	0.225
2575-CCP-05.d	14.3	0.670	2.60	346	0.720	0.014	160	<dl	0.018	n.r.	15.0	<dl	3.62	5.21	0.067	1.58	<dl	0.015	<dl	<dl	*0.002	*0.001	0.700	0.361
2575-CCP-03.d	25.8	3.43	3.50	413	0.790	<dl	154	0.019	<dl	n.r.	11.8	<dl	3.30	5.25	0.103	1.71	0.004	0.007	<dl	0.003	*0.001	*0.001	0.670	0.201
2575-CCP-02.d	26.0	3.96	4.66	392	0.730	<dl	164	0.003	0.020	n.r.	12.6	<dl	3.59	5.00	0.220	1.29	<dl	0.015	<dl	0.009	0.015	0.008	2.23	2.18
2575-CCP-04.d	45.3	2.29	*0.081	371	1.35	<dl	170	<dl	<dl	n.r.	11.8	<dl	4.90	7.36	0.171	2.03	<dl	0.015	0.002	<dl	*0.007	*0.001	1.83	0.690
2575-CCP-01d	28.5	3.49	1.20	374	1.00	<dl	155	0.021	<dl	n.r.	12.0	<dl	4.31	6.36	0.117	1.63	<dl	<dl	0.004	<dl	*0.002	*0.002	1.07	0.265
2643CCP-06.d	14.9	1.49	*0.015	269	15.1	0.026	62.9	<dl	0.014	n.r.	96.8	<dl	46.7	76.9	0.472	*0.041	<dl	<dl	4.E-4	<dl	0.007	0.104	2.51	0.909
2643CCP-01d	3.59	4.92	*0.015	289	14.6	0.120	62.4	<dl	0.014	n.r.	90.6	<dl	50.9	78.9	0.357	*0.048	<dl	<dl	<dl	3.E-4	0.011	0.023	2.09	1.62
2643CCP-02.d	3.10	4.25	*0.011	286	16.3	0.070	59.0	<dl	0.025	n.r.	91.4	<dl	49.0	79.1	0.304	*0.048	<dl	<dl	<dl	3.E-4	*0.001	0.028	1.44	0.589
2643CCP-03.d	0.800	5.16	*0.011	281	10.9	0.100	56.7	<dl	<dl	n.r.	88.5	<dl	51.6	66.7	0.403	*0.045	<dl	<dl	<dl	<dl	*0.002	0.118	4.07	1.25
2643CCP-04.d	6.95	2.51	*0.022	271	14.7	<dl	76.5	<dl	<dl	n.r.	100	<dl	49.1	78.3	0.525	0.505	<dl	<dl	<dl	<dl	0.010	0.157	3.96	1.90
2643CCP-05.d	4.90	3.31	*0.013	289	13.6	0.060	57.2	<dl	0.013	n.r.	92.5	<dl	49.6	75.3	0.304	*0.053	<dl	<dl	<dl	1.E-4	0.010	0.052	2.20	1.15
2647CCP-03.d	0.420	0.910	*0.014	295	0.138	0.050	746	<dl	0.017	n.r.	35.0	<dl	156	73.1	0.281	*0.047	<dl	<dl	0.003	0.005	0.098	0.019	1.33	1.90
2647CCP-04.d	0.640	0.866	0.224	319	0.130	<dl	758	0.004	<dl	n.r.	39.1	<dl	155	85.1	0.053	0.180	0.002	<dl	<dl	<dl	0.121	*0.002	1.16	2.07
2647CCP-01d	*0.22	0.800	*0.015	343	0.135	0.080	793	0.028	0.021	n.r.	42.4	<dl	161	78.3	0.370	*0.047	<dl	<dl	<dl	<dl	0.099	0.024	2.39	4.00
2647CCP-02.d	*0.152	1.03	0.120	344	0.128	0.019	787	0.018	0.180	n.r.	40.2	<dl	161	74.2	0.430	*0.036	0.001	<dl	<dl	<dl	0.182	0.013	2.07	2.63
2647CCP-05.d	*0.155	1.28	*0.014	349	0.212	0.046	731	0.007	0.013	n.r.	40.0	<dl	162	83.4	0.196	*0.047	0.002	<dl	<dl	0.006	0.100	0.007	1.84	2.85
2647CCP-07.d	0.280	0.897	0.166	331	0.133	0.059	790	0.007	<dl	n.r.	39.2	<dl	198	62.5	0.594	*0.037	<dl	0.003	0.002	<dl	0.080	0.014	3.12	4.02
2647CCP-06.d	0.800	0.800	0.220	416	0.210	<dl	725	0.014	0.007	n.r.	37.9	<dl	203	90.2	0.660	*0.05	<dl	<dl	<dl	<dl	0.341	0.100	2.43	4.22
2652CCP-02.d	1.22	*0.007	*0.013	252	1.11	0.140	143	<dl	0.027	n.r.	121	<dl	283	131	0.620	*0.037	<dl	<dl	<dl	<dl	0.010	0.108	3.59	1.24
2652CCP-04.d	*0.281	*0.006	*0.016	253	1.27	0.141	139	<dl	<dl	n.r.	128	<dl	297	150	0.545	*0.049	<dl	<dl	<dl	<dl	*0.002	0.015	2.09	1.16
2652CCP-07.d	*0.228	0.026	*0.007	252	2.24	0.033	100	0.045	0.021	n.r.	163	<dl	544	178	0.083	*0.021	<dl	<dl	<dl	<dl	*0.001	0.018	1.76	0.256
2652CCP-05.d	3.19	*0.008	*0.019	250	1.22	0.038	150	<dl	<dl	n.r.	142	<dl	281	107	1.37	*0.061	<dl	<dl	<dl	<dl	0.084	0.423	8.76	4.29
2652CCP-03.d	12.1	*0.007	*0.029	254	1.30	0.152	150	<dl	<dl	n.r.	130	<dl	293	155	0.473	*0.057	<dl	<dl	2.E-4	<dl	0.019	0.073	2.39	1.50
2652CCP-06.d	1.02	0.024	*0.008	271	2.16	0.052	96.1	0.026	<dl	n.r.	172	<dl	554	197	0.051	*0.019	<dl	<dl	<dl	0.003	0.010	0.012	1.27	0.219
2652CCP-01d	2.73	*0.006	*0.021	264	1.13	<dl	126	<dl	<dl	n.r.	155	<dl	287	104	2.97	*0.067	<dl	<dl	<dl	<dl	0.131	0.358	9.92	6.68
2653-CCP-02.d	2.21	*0.026	6.00	168	*0.066	0.140	83.4	0.037	0.019	n.r.	34.7	<dl	6.88	20.6	0.119	0.780	<dl	<dl	<dl	0.016	0.094	*0.002	4.01	1.76

Grain ID	Mn	Co	Ni	Zn	Ga	As	Se	Mo	Ru	Rh	Ag	Pd	In	Sn	Sb	Te	Re	Os	Ir	Pt	Au	Tl	Pb	Bi
	55	59	60	66	71	75	82	95	101	103	107	108	115	118	121	128	185	189	193	195	197	205	208	209
33um	1.017	0.029	0.322	0.590	0.033	0.149	3.828	5.311	0.030	0.020	0.027	0.026	0.033	0.155	0.047	0.400	0.501	0.012	0.028	0.007	0.016	0.006	0.029	0.012
55um	0.449	0.024	0.211	0.357	0.028	0.079	2.455	2.409	0.029	0.020	0.019	0.011	0.015	0.071	0.025	0.277	0.221	0.007	0.016	0.004	0.012	0.004	0.015	0.008
2653-CCP-03.d	2.79	*0.02	6.40	154	*0.052	0.110	73.2	<dl	0.012	n.r.	29.9	<dl	6.54	19.5	*0.02	0.370	<dl	<dl	<dl	0.011	0.032	*0.002	3.49	1.02
2653-CCP-01d	2.54	*0.018	5.50	171	*0.048	0.061	79.7	0.006	0.005	n.r.	33.7	<dl	6.81	23.5	0.249	1.04	0.003	0.008	0.004	0.004	0.030	*0.001	3.99	1.96
2653-CCP-06.d	2.54	0.067	9.20	143	*0.052	0.046	75.4	0.310	0.016	n.r.	34.2	<dl	6.24	17.0	0.157	0.740	0.005	0.011	<dl	0.015	0.072	*0.002	6.20	2.13
2653-CCP-04.d	2.49	*0.013	4.52	163	*0.039	0.015	76.1	0.009	0.008	n.r.	30.2	<dl	6.63	22.0	0.158	0.722	0.003	0.008	0.002	0.003	0.078	*0.001	3.77	1.60
2653-CCP-05.d	2.49	0.218	13.2	158	0.134	<dl	75.2	0.011	0.008	n.r.	29.1	<dl	7.09	27.2	0.159	0.780	<dl	0.015	0.003	<dl	0.042	*0.001	2.92	1.29
2704CCP-02.d	0.520	0.681	2.89	306	0.630	0.023	480	0.009	<dl	n.r.	7.20	<dl	131	68.5	*0.009	*0.03	0.003	<dl	0.002	<dl	0.036	*0.002	1.19	1.82
2704CCP-06.d	*0.124	0.866	3.51	321	0.403	0.066	448	0.005	0.004	n.r.	6.94	<dl	120	52.7	0.016	*0.021	<dl	<dl	<dl	<dl	0.011	*0.002	1.28	1.85
2704CCP-05.d	0.370	0.664	2.86	347	0.445	<dl	463	0.006	<dl	n.r.	7.44	<dl	118	47.4	*0.006	*0.029	<dl	<dl	<dl	<dl	0.039	*0.002	1.37	2.77
2704CCP-03.d	0.340	1.56	2.73	292	0.498	0.013	454	0.004	0.010	n.r.	7.63	<dl	129	45.7	0.016	*0.02	0.001	<dl	<dl	<dl	0.021	*0.002	1.78	3.21
2704CCP-04.d	0.620	0.916	2.88	319	0.501	0.009	471	0.008	0.004	n.r.	6.91	<dl	124	74.0	0.018	*0.025	<dl	<dl	<dl	<dl	0.140	*0.002	0.840	1.33
2704CCP-01d	0.500	0.361	2.99	364	0.910	0.023	508	<dl	0.003	n.r.	7.56	<dl	118	91.2	*0.007	*0.027	<dl	<dl	<dl	0.002	0.008	*0.001	1.74	2.00
2722-CCP-05.d	6.36	6.44	2.77	624	0.289	0.009	195	0.062	0.006	n.r.	53.2	<dl	7.66	3.54	*0.006	1.55	0.003	0.004	4.E-4	0.002	0.039	*0.002	0.302	1.50
2722-CCP-06.d	7.04	5.34	*0.049	630	0.244	<dl	194	0.012	0.014	n.r.	52.7	<dl	7.37	3.23	*0.007	0.980	0.003	0.013	0.003	0.009	0.012	0.010	0.600	1.79
2722-CCP-01d	3.62	3.80	2.73	390	0.530	0.042	173	0.009	0.022	n.r.	51.0	<dl	8.18	3.68	*0.013	0.460	<dl	0.015	0.004	<dl	0.012	*0.001	1.29	2.02
2722-CCP-02.d	5.20	4.15	3.40	591	1.04	0.040	182	0.020	0.031	n.r.	50.3	<dl	8.34	4.46	0.066	0.610	<dl	<dl	0.002	0.015	0.050	0.038	2.09	3.11
2722-CCP-04.d	6.32	6.03	3.00	419	0.270	0.060	182	<dl	0.010	n.r.	52.7	<dl	7.18	3.75	*0.007	1.10	<dl	<dl	0.004	<dl	0.046	*0.001	0.330	1.21
2722-CCP-03.d	3.66	3.39	2.40	513	0.185	0.014	188	<dl	0.007	n.r.	52.3	<dl	6.75	2.55	*0.006	1.62	<dl	<dl	0.003	0.012	0.036	*0.002	0.213	1.51
2729-CCP-01d	3.28	1.15	4.50	355	0.760	<dl	149	<dl	<dl	n.r.	118	<dl	4.51	23.7	0.410	0.710	<dl	<dl	0.002	<dl	*0.003	*0.002	2.31	1.33
2729-CCP-03.d	3.00	1.16	2.50	439	1.03	0.200	142	0.003	0.019	n.r.	119	<dl	4.55	23.5	0.366	0.710	<dl	0.016	0.005	<dl	0.021	0.008	2.67	1.64
2729-CCP-05.d	3.04	1.28	*0.042	562	0.740	0.080	138	0.017	0.011	n.r.	123	<dl	4.47	23.6	0.159	1.15	<dl	<dl	0.001	0.006	*0.003	*0.001	1.52	1.05
2729-CCP-06.d	2.41	1.09	2.12	331	0.850	<dl	127	0.021	0.005	n.r.	113	<dl	4.55	20.0	0.456	0.370	<dl	0.005	<dl	0.005	*0.003	*0.001	3.53	1.59
2729-CCP-04.d	3.18	1.19	4.70	356	0.910	0.023	140	0.007	<dl	n.r.	114	<dl	4.43	21.0	0.264	0.420	0.009	0.011	<dl	<dl	*0.004	*0.001	2.25	1.41
2729-CCP-02.d	3.39	1.17	*0.038	366	0.780	0.066	153	<dl	0.012	n.r.	128	<dl	4.83	24.4	1.13	0.690	0.023	0.002	<dl	0.001	0.046	*0.002	5.82	4.89
2730-CCP-02.d	14.0	2.49	*0.07	433	15.1	<dl	129	0.006	0.012	n.r.	204	<dl	336	87.5	0.473	*0.048	<dl	<dl	<dl	0.006	0.014	0.010	1.61	0.045
2730-CCP-01d	260	2.11	*0.102	387	32.0	0.028	137	0.017	0.043	n.r.	206	<dl	332	85.7	0.791	*0.055	<dl	0.050	0.010	<dl	0.040	0.022	3.15	0.052
2730-CCP-06.d	2.45	*0.013	*0.047	330	0.590	<dl	123	<dl	<dl	n.r.	246	<dl	212	19.3	1.00	0.250	<dl	<dl	0.004	0.006	*0.001	0.045	2.38	0.018
2730-CCP-04.d	4.70	1.82	2.40	409	45.0	0.062	112	0.006	<dl	n.r.	201	<dl	341	19.9	0.360	*0.051	<dl	<dl	0.013	<dl	*0.008	0.015	1.58	*0.016
2730-CCP-05.d	2.30	*0.014	*0.05	375	0.570	<dl	112	<dl	0.007	n.r.	276	<dl	15.6	21.3	0.760	*0.041	0.004	<dl	<dl	0.002	0.016	0.067	2.38	0.017
2730-CCP-03.d	2.77	2.50	3.80	407	34.9	<dl	137	0.028	0.014	n.r.	205	<dl	348	21.0	0.910	*0.072	0.007	0.004	<dl	0.002	0.045	0.068	3.06	*0.02
27ROV8CCP-04.d	0.970	0.090	10.0	6.18	27.9	92.1	*1.014	126	0.023	n.r.	2.98	9.E-4	54.9	18.4	60.3	0.740	0.001	0.003	0.002	<dl	0.114	*0.001	0.386	5.81
27ROV8CCP-05.d	1.24	*0.007	1.50	6.62	30.2	367	*1.12	131	0.009	n.r.	5.20	<dl	68.2	120	374	4.26	0.006	8.E-4	0.035	<dl	3.29	*0.02	6.41	38.2
27ROV8CCP-02.d	2.00	0.033	15.0	6.55	31.9	381	*0.962	107	0.044	n.r.	4.92	0.128	76.2	112	412	4.76	0.004	0.011	0.004	0.003	4.79	0.008	8.08	40.3
27ROV8CCP-07.d	1.59	*0.007	9.10	3.93	11.9	5.09	*0.82	69.0	0.048	n.r.	4.96	0.695	19.2	38.2	2.70	*0.032	0.130	0.600	0.006	0.010	0.406	0.008	0.112	0.399
27ROV8CCP-03.d	1.00	0.520	98.0	6.68	27.8	332	*0.987	106	0.014	n.r.	6.30	<dl	75.6	120	360	5.20	0.320	0.004	9.E-4	<dl	3.21	0.007	6.32	34.5

Grain ID	Mn	Co	Ni	Zn	Ga	As	Se	Mo	Ru	Rh	Ag	Pd	In	Sn	Sb	Te	Re	Os	Ir	Pt	Au	Tl	Pb	Bi
	55	59	60	66	71	75	82	95	101	103	107	108	115	118	121	128	185	189	193	195	197	205	208	209
33um	1.017	0.029	0.322	0.590	0.033	0.149	3.828	5.311	0.030	0.020	0.027	0.026	0.033	0.155	0.047	0.400	0.501	0.012	0.028	0.007	0.016	0.006	0.029	0.012
55um	0.449	0.024	0.211	0.357	0.028	0.079	2.455	2.409	0.029	0.020	0.019	0.011	0.015	0.071	0.025	0.277	0.221	0.007	0.016	0.004	0.012	0.004	0.015	0.008
27ROV8CCP-01d	1.30	0.096	0.770	7.42	32.5	487	*1.623	120	0.018	n.r.	3.94	3.17	85.8	168	445	5.21	<dl	0.005	0.006	<dl	3.76	0.013	7.66	41.3
2924CCP-08.d	*0.325	0.150	*0.014	277	0.310	0.050	99.0	0.029	<dl	n.r.	2.16	<dl	5.97	25.4	4.57	*0.075	<dl	0.021	<dl	<dl	0.200	0.011	19.9	27.0
2924CCP-03.d	2.30	0.271	0.610	280	0.127	<dl	97.7	<dl	<dl	n.r.	3.59	<dl	8.91	46.9	1.31	*0.065	<dl	<dl	0.005	<dl	0.314	0.019	15.6	18.0
2924CCP-06.d	*0.367	0.111	*0.013	261	0.300	<dl	100	<dl	<dl	n.r.	3.36	<dl	7.54	30.6	4.92	*0.06	<dl	<dl	<dl	<dl	0.190	*0.001	27.1	32.9
2924CCP-01d	1.03	0.202	*0.014	320	0.270	<dl	98.2	<dl	<dl	n.r.	2.99	<dl	19.2	80.2	2.47	*0.043	<dl	<dl	<dl	0.017	0.580	0.017	20.5	36.2
2924CCP-05.d	*0.412	0.149	*0.015	273	0.320	<dl	101	<dl	<dl	n.r.	5.19	<dl	8.29	37.1	7.80	*0.078	<dl	<dl	<dl	<dl	0.290	0.030	41.4	43.8
2924CCP-04.d	1.95	0.305	*0.017	247	0.250	0.110	95.6	0.020	<dl	n.r.	3.08	<dl	5.99	24.2	4.77	*0.079	<dl	<dl	0.008	<dl	0.320	0.018	25.8	18.6
2925CCP-05.d	6.20	0.226	*0.011	446	16.8	0.070	6.70	<dl	0.015	n.r.	60.9	<dl	5.04	897	7.20	*0.034	<dl	<dl	<dl	<dl	0.061	0.093	5.11	0.061
2925CCP-01d	3.24	0.173	*0.008	537	16.2	0.060	5.40	0.080	0.014	n.r.	43.6	<dl	6.53	917	3.26	*0.025	<dl	<dl	<dl	0.001	0.012	*0.002	5.79	0.050
2925CCP-04.d	3.04	0.195	*0.008	509	10.8	0.130	9.00	<dl	<dl	n.r.	63.2	<dl	4.44	857	5.26	*0.026	<dl	<dl	0.001	<dl	0.027	0.003	11.1	0.155
2925CCP-03.d	5.75	0.183	*0.011	474	12.6	0.020	12.4	<dl	0.026	n.r.	64.4	<dl	5.64	850	14.6	*0.038	<dl	<dl	<dl	<dl	0.040	0.044	19.1	0.281
2925CCP-02.d	3.48	0.196	*0.01	436	10.7	<dl	13.9	<dl	<dl	n.r.	57.3	<dl	6.64	818	4.56	*0.032	<dl	<dl	<dl	<dl	0.023	0.016	13.2	0.184
2925CCP-06.d	1.37	0.184	*0.012	433	9.69	0.215	*3.132	<dl	<dl	n.r.	64.1	<dl	5.03	756	15.1	*0.051	<dl	<dl	<dl	<dl	0.032	0.046	14.2	0.279
3112-CCP-04.d	2.35	19.7	1.30	131	*0.085	0.021	42.3	<dl	0.023	n.r.	9.15	<dl	3.00	58.9	*0.01	0.334	<dl	<dl	<dl	<dl	*0.003	*0.001	3.22	0.570
3112-CCP-03.d	2.38	14.2	5.50	166	*0.07	0.088	43.7	0.012	<dl	n.r.	62.9	<dl	2.10	87.5	0.021	0.358	<dl	0.020	<dl	<dl	0.133	*0.001	1.39	1.65
3112-CCP-02.d	2.80	11.2	*0.05	193	*0.101	0.069	43.9	0.001	<dl	n.r.	45.7	<dl	*0.04	269	0.095	0.340	<dl	<dl	4.E-4	0.011	0.083	0.041	3.15	0.580
3112-CCP-05.d	2.56	18.4	2.30	172	*0.119	<dl	47.9	<dl	<dl	n.r.	20.1	<dl	2.93	187	*0.012	0.397	0.017	<dl	<dl	0.066	*0.007	*0.001	3.96	1.21
3112-CCP-01d	2.77	9.04	5.90	138	*0.088	0.004	41.5	<dl	0.020	n.r.	40.6	<dl	0.990	148	0.020	0.260	0.010	<dl	0.016	<dl	0.060	*0.001	2.95	0.500
3143CCP-03.d	*0.182	0.057	6.50	734	1.07	<dl	58.6	<dl	0.019	n.r.	626	<dl	28.8	161	0.459	3.69	<dl	<dl	<dl	<dl	*0.001	0.019	0.575	0.020
3143CCP-04.d	*0.224	0.031	6.85	541	1.57	0.040	53.2	<dl	<dl	n.r.	607	<dl	31.0	161	0.700	2.91	<dl	<dl	<dl	<dl	*0.001	0.014	0.820	0.024
3143CCP-06.d	*0.209	0.084	3.91	491	1.12	0.120	58.6	<dl	0.017	n.r.	846	<dl	56.2	205	1.25	2.84	0.001	<dl	<dl	<dl	0.031	0.410	1.69	0.043
3143CCP-05.d	*0.242	0.073	4.57	538	1.41	0.090	62.0	<dl	<dl	n.r.	639	<dl	37.5	163	1.31	2.53	<dl	<dl	<dl	<dl	0.009	0.580	1.16	0.044
3143CCP-01d	0.770	*0.005	5.25	559	1.22	0.010	74.4	0.021	<dl	n.r.	745	<dl	40.2	229	3.16	1.47	<dl	<dl	<dl	<dl	0.031	0.540	4.12	0.048
3147CCP-07.d	*0.244	*0.005	*0.006	114	56.9	2.89	28.6	<dl	<dl	n.r.	6.10	<dl	46.2	42.8	3.34	*0.053	<dl	<dl	<dl	<dl	0.022	0.009	12.6	5.50
3147CCP-06.d	0.380	*0.002	*0.003	162	53.0	1.16	32.2	<dl	0.018	n.r.	4.74	<dl	45.0	40.2	1.42	*0.031	<dl	<dl	4.E-4	<dl	*0.001	0.004	2.12	1.73
3147CCP-04.d	*0.192	*0.005	*0.008	122	41.3	4.55	56.7	0.010	0.007	n.r.	7.17	<dl	48.8	42.0	6.02	0.720	<dl	<dl	<dl	<dl	*0.001	0.034	8.43	7.89
3147CCP-01d	*0.212	*0.004	*0.007	126	44.8	11.9	20.6	0.130	0.022	n.r.	11.6	<dl	52.0	39.9	14.6	0.710	<dl	<dl	<dl	<dl	0.007	0.092	24.2	17.6
3147CCP-05.d	*0.185	*0.005	*0.007	151	28.0	1.17	45.4	0.170	<dl	n.r.	5.37	<dl	47.7	40.3	2.49	*0.049	<dl	<dl	<dl	<dl	*0.001	0.016	4.01	3.88
3147CCP-03.d	*0.165	*0.004	*0.006	167	46.8	1.99	38.2	<dl	0.022	n.r.	4.41	<dl	47.0	39.4	2.35	*0.046	<dl	<dl	9.E-4	<dl	*0.001	0.012	3.73	3.31
3147CCP-02.d	*0.225	0.018	*0.005	104	50.9	7.68	24.6	2.00	0.009	n.r.	8.30	<dl	56.0	43.0	8.36	0.490	<dl	<dl	<dl	<dl	*0.001	0.069	13.9	11.6
31ROV13CCCP-07.d	0.990	0.058	0.220	7.91	23.2	108	4.54	86.3	0.006	n.r.	2.39	0.003	72.6	298	144	4.43	<dl	<dl	0.004	<dl	0.366	*0.001	1.75	128
31ROV13CCCP-06.d	1.90	0.390	2.80	9.23	21.5	57.5	7.00	84.6	0.210	n.r.	2.86	<dl	54.3	941	45.6	1.53	<dl	<dl	<dl	<dl	0.280	*0.001	0.450	37.1
31ROV13CCCP-01d	0.880	0.300	0.500	6.91	25.4	39.8	1.52	87.3	0.014	n.r.	5.10	<dl	41.7	685	11.8	1.33	<dl	<dl	<dl	<dl	0.042	*0.001	0.091	7.46
31ROV13CCCP-05.d	1.24	0.034	0.260	7.98	23.3	19.8	6.60	109	0.015	n.r.	2.10	0.054	57.4	747	10.7	0.610	0.002	0.006	0.002	<dl	*0.022	*0.002	0.068	9.80

Grain ID	Mn	Co	Ni	Zn	Ga	As	Se	Mo	Ru	Rh	Ag	Pd	In	Sn	Sb	Te	Re	Os	Ir	Pt	Au	Tl	Pb	Bi
	55	59	60	66	71	75	82	95	101	103	107	108	115	118	121	128	185	189	193	195	197	205	208	209
33um	1.017	0.029	0.322	0.590	0.033	0.149	3.828	5.311	0.030	0.020	0.027	0.026	0.033	0.155	0.047	0.400	0.501	0.012	0.028	0.007	0.016	0.006	0.029	0.012
55um	0.449	0.024	0.211	0.357	0.028	0.079	2.455	2.409	0.029	0.020	0.019	0.011	0.015	0.071	0.025	0.277	0.221	0.007	0.016	0.004	0.012	0.004	0.015	0.008
31ROV13CCCP-04.d	1.08	0.050	0.290	7.40	12.5	24.8	5.30	1.01	0.013	n.r.	2.83	<dl	20.4	1300	13.3	1.68	0.005	<dl	<dl	0.006	*0.042	*0.002	0.285	13.6
31ROV13CCCP-02.d	1.30	0.052	7.00	8.18	22.9	90.5	2.30	76.8	0.012	n.r.	3.48	0.135	67.2	678	66.8	2.41	0.027	0.036	0.016	0.014	0.210	*0.002	0.511	40.5
31ROV13CCCP-03.d	2.10	0.220	1.30	6.82	15.1	27.4	5.60	73.9	<dl	n.r.	3.26	0.315	28.7	618	10.9	0.670	0.510	0.006	<dl	<dl	0.027	0.005	0.098	6.62
35GTV2B2CCP-004.d	3.81	895	0.700	1500	0.549	0.100	650	0.070	<dl	n.r.	2.57	<dl	4.84	224	*0.013	50.2	<dl	<dl	<dl	<dl	0.032	0.006	*0.16	0.107
35GTV2B2CCP-005.d	4.71	1140	*0.042	1261	*0.285	0.690	668	0.059	<dl	n.r.	1.44	<dl	3.31	171	1.20	42.0	0.330	0.015	0.002	0.004	0.036	*0.001	0.130	0.135
35GTV2B2CCP-006.d	2.95	733	5.00	545	1.37	0.940	93.5	0.016	0.010	n.r.	0.197	<dl	0.332	224	*0.007	2.82	<dl	<dl	0.003	0.003	0.032	*0.002	0.032	0.084
35GTV2B2CCP-001d	2.11	365	0.300	707	19.3	1.13	5.40	0.008	0.013	n.r.	0.226	<dl	*0.011	228	0.400	*0.069	0.002	0.007	0.007	<dl	*0.002	*0.001	0.840	0.250
35GTV2B2CCP-002.d	3.86	548	*0.028	2860	2.61	0.700	89.1	<dl	<dl	n.r.	1.79	<dl	0.395	282	*0.011	0.890	0.008	<dl	<dl	<dl	0.023	*0.001	0.231	0.209
35GTV2B2CCP-003.d	5.78	1262	1.50	1715	0.349	1.08	669	0.390	0.021	n.r.	2.98	<dl	2.96	189	*0.011	31.3	<dl	0.070	<dl	<dl	0.089	*0.002	*0.03	0.183
51CCP-06.d	*0.314	2.52	*0.019	248	4.19	0.010	130	<dl	<dl	n.r.	1384	<dl	19.5	36.4	3.67	*0.104	<dl	<dl	<dl	<dl	*0.002	0.041	4.07	5.61
51CCP-05.d	*0.255	2.11	*0.013	425	4.56	<dl	192	<dl	<dl	n.r.	1177	<dl	21.2	36.9	0.845	*0.074	<dl	<dl	<dl	<dl	*0.002	*0.001	*1.347	1.52
51CCP-01d	*0.22	2.21	*0.009	295	4.12	0.010	146	<dl	0.021	n.r.	1589	<dl	18.6	33.8	1.34	*0.07	<dl	<dl	<dl	0.002	*0.001	0.004	3.06	3.75
51CCP-02.d	*0.229	2.29	*0.016	242	0.425	0.075	96.3	<dl	<dl	n.r.	1500	<dl	19.2	34.3	1.72	0.320	<dl	<dl	<dl	<dl	*0.002	0.007	1.46	3.16
51CCP-03.d	*0.32	2.37	*0.013	322	3.79	0.280	140	<dl	<dl	n.r.	1640	<dl	20.2	35.0	2.82	*0.086	<dl	<dl	<dl	<dl	*0.003	0.010	8.10	4.78
52CCP-04.d	1.32	1.03	*0.011	311	6.66	0.075	217	0.027	<dl	n.r.	302	<dl	86.8	78.2	0.327	*0.055	0.003	<dl	<dl	<dl	0.033	0.194	3.31	2.59
52CCP-02.d	1.31	3.94	*0.013	285	30.6	<dl	175	0.008	0.005	n.r.	297	<dl	91.8	57.9	0.026	*0.065	0.002	0.009	<dl	<dl	0.184	0.040	1.16	1.63
52CCP-07.d	2.02	4.07	*0.015	319	12.9	0.160	207	<dl	<dl	n.r.	301	<dl	91.7	90.2	*0.014	*0.06	0.001	0.003	<dl	0.006	*0.002	0.031	1.25	1.14
52CCP-03.d	1.56	3.01	*0.015	322	34.8	0.046	163	0.008	0.010	n.r.	295	<dl	91.8	68.4	*0.015	*0.076	<dl	<dl	<dl	0.004	0.080	0.153	2.76	2.51
52CCP-01d	3.16	3.15	*0.015	313	41.2	<dl	192	<dl	0.027	n.r.	308	<dl	93.3	168	*0.012	*0.069	<dl	<dl	<dl	0.009	*0.002	0.059	2.77	1.42
52CCP-06.d	4.70	0.440	*0.011	293	24.2	0.104	192	0.010	0.003	n.r.	300	<dl	93.2	79.7	0.445	*0.045	<dl	0.003	7.E-4	<dl	0.066	0.220	1.55	1.96
52CCP-05.d	1.46	1.40	*0.009	273	16.5	0.085	202	0.015	0.008	n.r.	312	<dl	93.5	78.6	0.045	*0.044	<dl	<dl	<dl	<dl	0.184	0.023	1.18	1.73
53CCP-05.d	0.710	0.264	*0.01	103	0.118	0.132	382	<dl	<dl	n.r.	38.0	<dl	75.9	48.6	0.214	0.340	<dl	<dl	<dl	<dl	1.02	*0.002	3.08	1.27
53CCP-07.d	*0.159	0.427	0.180	119	0.110	0.069	416	0.005	0.024	n.r.	79.1	<dl	77.1	57.1	0.404	0.440	<dl	<dl	<dl	<dl	3.84	*0.001	4.70	2.29
53CCP-01d	*0.108	0.199	*0.009	95.0	0.104	0.034	461	<dl	0.015	n.r.	38.5	<dl	88.5	48.4	0.359	0.340	<dl	<dl	<dl	<dl	1.10	*0.001	1.80	0.990
53CCP-06.d	0.910	0.469	*0.013	133	0.109	0.100	439	0.006	0.016	n.r.	91.3	<dl	81.6	64.5	0.085	0.910	<dl	<dl	0.005	<dl	4.28	*0.001	1.04	0.687
53CCP-02.d	0.240	0.250	*0.007	134	0.141	<dl	436	<dl	0.011	n.r.	46.5	<dl	86.1	52.2	0.258	0.440	0.001	0.002	4.E-4	<dl	2.34	*0.001	2.04	0.866
53CCP-03.d	*0.138	0.344	*0.01	123	0.253	0.035	439	0.005	<dl	n.r.	46.6	<dl	80.7	47.6	0.149	0.480	<dl	<dl	<dl	<dl	0.449	*0.002	2.30	1.06
53CCP-04.d	0.570	0.370	*0.01	118	0.410	0.070	385	<dl	0.043	n.r.	62.4	<dl	79.1	37.4	0.177	0.590	<dl	<dl	<dl	<dl	0.280	*0.001	2.35	0.900
53ROV13CCP-07.d	2.95	201	1.40	108	0.077	0.030	1141	0.049	0.013	n.r.	0.347	<dl	5.64	86.2	*0.004	12.6	<dl	<dl	<dl	<dl	*0.002	*0.002	*0.044	0.018
53ROV13CCP-04.d	2.60	196	244	118	*0.011	0.059	1392	0.130	0.019	n.r.	4.78	<dl	5.03	42.1	0.013	25.9	0.003	0.009	0.005	<dl	0.190	*0.002	0.032	0.044
53ROV13CCP-05.d	5.20	223	315	133	0.043	0.190	1303	0.085	0.029	n.r.	5.25	<dl	5.12	39.6	0.500	22.4	<dl	<dl	0.007	0.007	0.019	0.014	0.390	0.027
53ROV13CCP-01d	3.75	287	63.5	135	0.063	0.055	1116	0.660	0.011	n.r.	6.64	<dl	7.91	37.3	0.600	31.6	<dl	5.E-4	0.001	<dl	*0.003	*0.002	0.065	0.068
53ROV13CCP-02.d	2.84	205	95.9	129	0.084	0.041	1116	0.094	0.017	n.r.	1.38	<dl	7.10	51.2	*0.005	38.9	<dl	<dl	<dl	<dl	*0.001	*0.002	0.043	0.022
53ROV13CCP-06.d	3.91	131	174	117	0.044	<dl	1221	0.095	0.012	n.r.	0.162	<dl	5.27	46.5	*0.008	19.8	<dl	<dl	0.002	0.053	*0.002	*0.002	0.039	0.280

Grain ID	Mn	Co	Ni	Zn	Ga	As	Se	Mo	Ru	Rh	Ag	Pd	In	Sn	Sb	Te	Re	Os	Ir	Pt	Au	Tl	Pb	Bi
	55	59	60	66	71	75	82	95	101	103	107	108	115	118	121	128	185	189	193	195	197	205	208	209
33um	1.017	0.029	0.322	0.590	0.033	0.149	3.828	5.311	0.030	0.020	0.027	0.026	0.033	0.155	0.047	0.400	0.501	0.012	0.028	0.007	0.016	0.006	0.029	0.012
55um	0.449	0.024	0.211	0.357	0.028	0.079	2.455	2.409	0.029	0.020	0.019	0.011	0.015	0.071	0.025	0.277	0.221	0.007	0.016	0.004	0.012	0.004	0.015	0.008
53ROV6CCP-08.d	1.82	0.327	0.800	52.9	2.12	0.038	303	1.60	0.007	n.r.	0.234	<dl	19.2	34.1	0.051	4.40	<dl	0.012	<dl	<dl	*0.002	*0.002	0.073	0.809
53ROV6CCP-03.d	2.30	0.810	*0.007	77.9	1.70	0.042	285	0.015	0.180	n.r.	8.65	<dl	9.24	10.9	*0.008	0.940	<dl	0.007	0.038	<dl	0.054	*0.002	*0.01	0.161
53ROV6CCP-05.d	1.19	0.304	0.190	56.5	2.58	0.031	383	0.140	0.016	n.r.	7.45	0.008	12.6	55.3	0.040	2.35	5.E-4	<dl	0.002	0.230	0.077	*0.002	0.054	0.341
53ROV6CCP-07.d	1.87	0.320	0.190	52.6	1.97	0.038	335	0.290	0.027	n.r.	0.612	<dl	11.7	53.3	0.100	2.46	<dl	<dl	<dl	0.003	*0.002	*0.002	0.062	0.385
53ROV6CCP-02.d	2.22	0.643	49.0	72.6	1.08	0.500	292	0.022	0.020	n.r.	7.97	<dl	9.00	9.54	*0.004	0.770	0.053	0.007	0.006	<dl	0.144	*0.002	0.022	0.067
53ROV6CCP-04.d	1.99	0.630	*0.008	63.2	1.87	0.190	286	0.045	0.047	n.r.	8.57	<dl	10.2	20.4	*0.006	0.790	<dl	0.007	0.016	0.010	0.039	*0.002	0.038	0.307
53ROV6CCP-06.d	1.69	0.356	1.70	58.5	0.930	<dl	329	0.108	0.070	n.r.	2.96	0.035	9.77	30.3	0.024	1.26	<dl	<dl	<dl	0.003	*0.001	*0.002	0.067	0.636
53ROV6CCP-01.d	2.25	0.540	0.160	61.0	0.980	<dl	260	0.110	0.009	n.r.	7.63	<dl	7.16	8.58	*0.004	0.530	0.024	<dl	<dl	<dl	0.131	*0.002	0.050	0.195
56CCP-04.d	2.44	0.112	0.750	304	0.250	0.080	55.2	<dl	0.013	n.r.	452	<dl	2.09	201	0.095	*0.02	<dl	<dl	<dl	<dl	*0.001	*0.002	0.441	*0.003
56CCP-02.d	2.97	0.141	1.59	394	0.244	0.027	55.8	<dl	0.008	n.r.	501	<dl	2.37	229	0.363	*0.025	<dl	<dl	<dl	<dl	*0.001	0.013	0.893	0.012
56CCP-01.d	4.84	0.125	1.63	345	0.257	0.013	53.6	0.003	<dl	n.r.	508	<dl	2.29	214	0.122	0.640	<dl	<dl	<dl	<dl	*0.002	*0.001	0.744	0.009
56CCP-03.d	1.07	0.116	0.890	343	0.185	<dl	60.9	<dl	<dl	n.r.	421	<dl	2.33	220	0.202	*0.018	<dl	<dl	<dl	<dl	*0.001	0.005	0.473	0.015
56CCP-06.d	0.420	0.108	0.800	341	0.190	0.038	55.4	<dl	<dl	n.r.	474	<dl	2.47	208	0.183	*0.017	0.001	0.003	0.001	<dl	*0.001	*0.001	0.534	0.008
56CCP-05.d	0.460	0.052	0.530	325	0.193	0.049	64.4	<dl	0.010	n.r.	403	<dl	2.71	215	0.290	*0.019	0.003	0.009	<dl	0.003	*0.001	0.010	0.550	0.012
601CCP-02.d	*0.281	0.950	*0.014	308	25.3	<dl	32.6	<dl	0.061	n.r.	78.8	<dl	24.6	84.7	0.439	*0.087	<dl	<dl	<dl	<dl	1.81	0.007	2.49	1.20
601CCP-04.d	1.08	1.17	*0.011	266	22.6	1.20	34.3	<dl	0.030	n.r.	67.5	<dl	24.6	60.5	1.48	*0.072	<dl	0.050	0.001	<dl	0.257	0.482	2.55	4.00
601CCP-03.d	0.740	0.892	*0.007	261	25.1	0.066	29.9	0.005	0.004	n.r.	87.6	<dl	24.8	87.1	2.38	*0.054	<dl	<dl	<dl	<dl	1.63	0.089	3.29	3.17
601CCP-01.d	0.820	1.06	0.260	272	24.6	0.050	25.6	<dl	0.011	n.r.	84.1	<dl	24.7	75.3	2.98	*0.074	<dl	<dl	<dl	<dl	1.64	0.158	5.17	3.81
601CCP-06.d	1.86	0.995	*0.012	280	15.7	<dl	38.6	0.002	<dl	n.r.	68.6	<dl	26.2	72.4	1.45	*0.095	<dl	<dl	<dl	<dl	0.634	0.070	2.39	1.95
601CCP-05.d	2.26	1.35	*0.009	290	28.0	0.039	38.4	<dl	0.007	n.r.	104	<dl	25.3	90.8	1.75	*0.071	<dl	<dl	<dl	<dl	0.213	0.070	2.63	1.31
62CCP-04.d	1.04	*0.006	*0.011	261	2.11	0.065	88.4	0.011	0.010	n.r.	142	<dl	544	171	0.147	*0.026	0.001	0.003	<dl	0.002	0.011	0.047	3.65	0.657
62CCP-07.d	0.855	*0.007	*0.015	267	2.08	0.094	85.2	0.013	0.008	n.r.	155	<dl	529	262	0.063	*0.032	<dl	<dl	<dl	0.005	0.016	0.010	0.785	0.156
62CCP-02.d	1.09	*0.007	*0.011	261	1.91	0.028	91.4	<dl	0.008	n.r.	139	<dl	536	152	0.074	*0.028	<dl	<dl	0.002	<dl	*0.002	0.011	1.37	0.290
62CCP-01.d	1.13	*0.007	*0.011	271	2.23	0.044	92.6	0.008	0.007	n.r.	141	<dl	525	199	0.056	*0.027	0.003	<dl	0.004	0.002	*0.001	0.010	1.04	0.224
62CCP-06.d	0.865	*0.006	*0.01	237	1.97	0.012	87.3	0.016	0.016	n.r.	167	<dl	495	159	0.105	*0.024	1.E-3	0.002	<dl	<dl	0.016	0.325	5.11	0.474
62CCP-05.d	0.925	*0.005	*0.01	250	1.90	0.045	88.3	0.014	0.016	n.r.	157	<dl	509	169	0.068	*0.024	<dl	<dl	0.002	0.002	*0.002	0.084	3.80	0.518
62CCP-03.d	1.00	*0.005	0.170	263	1.96	0.025	94.9	0.017	0.016	n.r.	140	<dl	543	149	0.086	*0.023	<dl	<dl	8.E-4	<dl	0.012	0.021	2.14	0.326
64ROV11CCP-05.d	2.50	516	332	1076	0.240	0.800	1396	0.099	0.038	n.r.	16.9	<dl	52.9	47.7	*0.009	93.4	0.019	<dl	0.006	0.004	0.311	*0.001	0.320	2.77
64ROV11CCP-04.d	1.49	495	164	1210	0.980	2.73	538	2.00	0.022	n.r.	14.8	<dl	18.4	101	0.490	26.1	<dl	<dl	<dl	<dl	0.171	0.440	1.48	2.60
64ROV11CCP-06.d	1.09	622	297	784	0.132	0.037	1496	0.230	0.024	n.r.	1.72	<dl	47.3	34.5	*0.005	113	0.008	<dl	<dl	0.003	*0.003	*0.002	0.110	0.072
64ROV11CCP-03.d	5.70	1243	327	1144	0.274	0.220	1321	0.116	0.026	n.r.	13.5	<dl	66.1	35.1	*0.073	91.9	<dl	<dl	0.002	<dl	0.049	*0.003	2.10	0.091
64ROV11CCP-01.d	3.13	1449	363	1285	1.04	0.270	862	0.091	0.031	n.r.	12.6	<dl	41.4	79.5	0.035	43.2	0.003	<dl	<dl	<dl	0.033	*0.002	0.017	0.120
64ROV11CCP-07.d	1.86	1800	453	956	0.570	0.040	1581	4.40	0.005	n.r.	8.43	<dl	73.9	24.3	*0.004	143	<dl	0.005	<dl	0.003	0.200	*0.002	0.031	0.243
64ROV11CCP-02.d	1.69	1390	352	1129	0.310	0.170	1460	0.200	0.017	n.r.	12.5	<dl	84.5	33.0	*0.005	135	0.033	<dl	<dl	<dl	0.041	*0.002	0.038	0.161

Grain ID	Mn	Co	Ni	Zn	Ga	As	Se	Mo	Ru	Rh	Ag	Pd	In	Sn	Sb	Te	Re	Os	Ir	Pt	Au	Tl	Pb	Bi
	55	59	60	66	71	75	82	95	101	103	107	108	115	118	121	128	185	189	193	195	197	205	208	209
33um	1.017	0.029	0.322	0.590	0.033	0.149	3.828	5.311	0.030	0.020	0.027	0.026	0.033	0.155	0.047	0.400	0.501	0.012	0.028	0.007	0.016	0.006	0.029	0.012
55um	0.449	0.024	0.211	0.357	0.028	0.079	2.455	2.409	0.029	0.020	0.019	0.011	0.015	0.071	0.025	0.277	0.221	0.007	0.016	0.004	0.012	0.004	0.015	0.008
64ROV2CCP-003.d	8.10	232	154	96.2	*0.011	0.890	1322	0.078	<dl	n.r.	6.55	<dl	4.04	48.9	*0.012	15.3	0.018	<dl	<dl	<dl	0.102	*0.002	*0.008	0.035
64ROV2CCP-004.d	3.20	202	140	87.8	0.048	1.39	1283	1.80	<dl	n.r.	5.11	<dl	3.98	80.4	*0.021	13.9	0.050	<dl	<dl	<dl	0.040	*0.002	0.320	1.25
64ROV2CCP-001d	7.10	241	202	100	0.056	2.31	1468	0.071	<dl	n.r.	5.78	<dl	4.17	62.0	*0.016	20.0	1.70	<dl	<dl	<dl	0.103	*0.002	0.157	0.113
64ROV2CCP-002.d	5.80	237	185	94.5	0.062	1.90	1345	0.048	0.015	n.r.	5.84	<dl	3.73	60.7	*0.01	12.5	0.051	<dl	<dl	<dl	0.092	*0.002	0.042	0.042
146-5-Ccp-1d	*0.186	*0.003	*0.01	105	0.266	0.150	926	0.310	<dl	n.r.	0.860	<dl	6.46	10.4	1.04	14.0	<dl	<dl	<dl	<dl	*0.001	0.028	2.05	0.157
146-3-Ccp-1d	2.95	0.033	*0.008	100	0.520	0.560	871	0.530	<dl	n.r.	0.660	<dl	6.60	9.92	0.738	13.9	<dl	<dl	<dl	<dl	*0.001	0.026	1.93	0.168
146-5-Ccp-2.d	*0.104	0.024	*0.006	112	0.228	<dl	937	4.20	<dl	n.r.	0.556	<dl	6.59	13.7	0.428	14.9	<dl	<dl	<dl	<dl	0.007	*0.002	1.29	0.075
146-2-Ccp-1d	*0.134	*0.003	*0.007	96.5	0.172	0.140	896	0.041	<dl	n.r.	1.60	<dl	6.84	8.58	3.67	17.0	<dl	<dl	<dl	<dl	*0.001	0.090	4.38	0.346
149-2-Ccp-1d	4.10	0.006	0.250	234	3.24	<dl	216	0.017	<dl	n.r.	1.50	<dl	14.2	9.71	1.29	26.0	<dl	<dl	<dl	<dl	0.010	0.067	4.14	0.063
149-1-Ccp-1d	*0.144	*0.003	*0.01	204	0.362	0.110	246	0.048	<dl	n.r.	1.37	<dl	15.6	11.3	1.56	22.2	<dl	<dl	<dl	<dl	0.015	0.013	4.18	0.075
149-6-Ccp-1d	*0.162	*0.003	*0.01	286	1.23	0.110	235	<dl	<dl	n.r.	0.830	<dl	17.0	16.3	0.323	28.4	<dl	<dl	<dl	<dl	0.009	0.006	1.03	0.022
24-4-ccp2.d	0.430	1.08	*0.026	252	0.950	<dl	403	0.005	<dl	n.r.	3.81	<dl	60.8	25.4	0.430	1.50	<dl	<dl	<dl	<dl	0.024	*0.001	3.40	0.440
24-4-ccp3.d	0.380	1.10	*0.027	248	0.980	0.070	363	0.015	<dl	n.r.	3.95	<dl	56.4	21.0	0.460	1.70	<dl	<dl	<dl	<dl	0.022	*0.001	2.85	0.370
24-4-ccp1d	0.330	0.900	*0.022	192	0.940	<dl	332	0.043	<dl	n.r.	2.89	<dl	47.7	18.4	0.460	1.08	<dl	<dl	<dl	<dl	0.014	0.009	1.86	0.170
28-2-ccp3.d	*0.12	*0.02	*0.018	190	42.4	<dl	940	0.015	<dl	n.r.	1.89	<dl	90.0	31.0	2.54	1.30	<dl	<dl	<dl	<dl	0.017	*0.002	4.75	0.140
28-2-ccp2.d	0.640	*0.014	*0.011	203	1.01	0.130	730	<dl	<dl	n.r.	1.47	<dl	67.1	20.6	1.82	1.38	<dl	<dl	<dl	<dl	*0.001	*0.002	3.59	0.085
28-2-ccp1d	4.70	*0.017	*0.021	303	1.01	0.110	781	<dl	<dl	n.r.	2.08	<dl	82.0	22.6	3.33	2.50	<dl	<dl	<dl	<dl	0.008	*0.003	5.40	0.080
57A-4-ccp1d	*0.114	2.00	*0.045	287	0.100	0.510	240	<dl	<dl	n.r.	76.1	<dl	45.5	25.8	0.660	0.950	<dl	<dl	<dl	<dl	0.036	*0.002	1.83	0.036
57A-3-ccp1d	0.180	*0.009	*0.011	224	0.134	<dl	262	0.020	<dl	n.r.	64.9	<dl	40.2	13.0	4.51	1.18	<dl	<dl	<dl	<dl	0.188	*0.002	13.3	0.108
57A-3-ccp2.d	*0.08	*0.018	*0.023	177	0.162	<dl	249	0.012	<dl	n.r.	47.9	<dl	38.1	20.4	0.680	1.50	<dl	<dl	<dl	<dl	0.077	*0.002	1.71	*0.009
ALJ01CCP-02.d	*0.327	*0.007	*0.011	364	5.69	<dl	67.8	0.015	<dl	n.r.	3.97	<dl	80.9	459	1.42	*0.044	<dl	<dl	<dl	0.015	0.026	0.053	0.720	0.333
ALJ01CCP-07.d	4.60	0.038	1.30	379	5.56	0.270	53.9	1.50	0.026	n.r.	4.16	<dl	75.4	276	5.90	*0.041	<dl	<dl	0.014	<dl	*0.004	0.530	3.65	1.45
ALJ01CCP-06.d	3.00	*0.008	*0.016	375	1.58	<dl	48.5	<dl	<dl	n.r.	3.99	0.267	75.4	449	1.71	*0.039	0.006	<dl	0.120	<dl	0.033	0.052	0.780	0.580
ALJ01CCP-05.d	9.00	0.700	*0.045	351	4.60	3.90	44.5	0.018	<dl	n.r.	6.34	<dl	66.4	144	9.20	*0.071	<dl	<dl	0.050	0.011	0.031	0.218	4.00	1.02
ALJ01CCP-04.d	17.0	0.480	11.0	392	6.59	1.30	58.0	0.080	<dl	n.r.	6.27	<dl	78.2	169	11.5	*0.087	0.028	0.019	0.180	<dl	0.120	0.514	4.81	2.74
ALJ01CCP-01d	*0.206	0.150	*0.03	306	1.40	<dl	46.2	<dl	<dl	n.r.	1.84	<dl	160	389	*0.014	*0.02	<dl	0.022	<dl	0.024	*0.001	*0.002	*0.011	0.099
AZN01CCP-06.d	0.760	*0.007	2.20	267	0.539	0.008	79.9	<dl	0.070	n.r.	0.122	<dl	240	382	1.98	*0.019	0.070	0.200	0.026	<dl	0.021	1.00	1.02	*0.069
AZN01CCP-05.d	7.00	0.130	43.0	210	0.636	0.100	76.0	0.700	0.023	n.r.	0.142	<dl	233	347	2.09	*0.023	0.025	<dl	0.430	<dl	*0.002	0.012	1.56	*0.068
AZN01CCP-02.d	0.590	*0.005	4.60	270	0.650	0.100	86.1	1.50	<dl	n.r.	0.571	<dl	234	368	5.25	*0.021	0.005	<dl	<dl	<dl	*0.002	0.064	5.41	0.354
AZN01CCP-04.d	0.690	0.210	45.0	262	0.660	0.120	87.0	0.009	0.080	n.r.	0.520	<dl	241	388	3.30	*0.033	0.290	<dl	<dl	<dl	*0.002	0.026	2.62	0.240
AZN01CCP-07.d	0.820	0.054	28.0	279	0.530	0.126	87.7	0.015	0.110	n.r.	0.500	<dl	236	417	4.73	0.210	<dl	<dl	<dl	0.005	*0.01	0.055	4.94	0.342
AZN01CCP-03.d	*0.246	0.051	0.135	223	0.630	0.120	82.9	<dl	0.013	n.r.	0.126	<dl	247	361	1.84	*0.027	<dl	<dl	<dl	<dl	*0.001	0.010	1.40	0.088
B5109CCP-003.d	2.73	0.251	*0.009	315	1.53	0.050	1016	<dl	0.096	n.r.	22.9	<dl	105	27.4	0.233	*0.062	0.004	<dl	<dl	0.007	0.288	*0.001	4.09	11.8
B5109CCP-002.d	8.50	0.258	0.160	310	1.12	<dl	1025	3.70	0.073	n.r.	38.1	<dl	100	42.6	0.139	*0.054	0.013	0.006	<dl	<dl	0.520	*0.001	2.48	13.3

Grain ID	Mn	Co	Ni	Zn	Ga	As	Se	Mo	Ru	Rh	Ag	Pd	In	Sn	Sb	Te	Re	Os	Ir	Pt	Au	Tl	Pb	Bi
	55	59	60	66	71	75	82	95	101	103	107	108	115	118	121	128	185	189	193	195	197	205	208	209
33um	1.017	0.029	0.322	0.590	0.033	0.149	3.828	5.311	0.030	0.020	0.027	0.026	0.033	0.155	0.047	0.400	0.501	0.012	0.028	0.007	0.016	0.006	0.029	0.012
55um	0.449	0.024	0.211	0.357	0.028	0.079	2.455	2.409	0.029	0.020	0.019	0.011	0.015	0.071	0.025	0.277	0.221	0.007	0.016	0.004	0.012	0.004	0.015	0.008
B5109CCP-001.d	1.82	0.390	0.260	292	0.835	0.050	1052	0.015	0.088	n.r.	25.7	<dl	95.5	47.2	0.390	*0.059	<dl	<dl	0.002	<dl	0.250	0.024	5.80	11.6
B5109CCP-006.d	1.94	0.195	*0.007	332	1.27	<dl	1126	0.022	0.057	n.r.	24.9	<dl	102	85.4	0.146	*0.046	<dl	<dl	<dl	<dl	0.401	*0.001	2.75	10.4
B5109CCP-004.d	3.50	0.294	*0.009	270	1.27	0.080	1043	0.005	0.082	n.r.	20.9	<dl	104	27.1	0.167	0.240	<dl	<dl	0.002	<dl	0.103	0.011	3.17	8.10
B5109CCP-005.d	2.18	0.231	*0.011	364	1.38	0.070	1130	0.010	0.041	n.r.	18.9	<dl	107	59.3	0.116	*0.054	<dl	<dl	<dl	<dl	0.140	0.013	2.12	10.3
B5110CCP-005.d	1.51	0.734	0.155	322	0.760	<dl	1008	<dl	0.027	n.r.	63.7	<dl	81.7	210	0.280	*0.042	<dl	<dl	<dl	<dl	0.144	*0.001	3.00	24.3
B5110CCP-003.d	2.07	0.310	*0.011	413	0.759	0.220	955	0.015	0.024	n.r.	50.5	<dl	83.8	220	0.101	*0.059	<dl	0.020	<dl	<dl	0.580	*0.001	1.45	12.5
B5110CCP-002.d	1.75	0.760	2.50	289	0.770	0.210	997	0.039	0.063	n.r.	58.4	<dl	90.4	181	0.266	*0.054	0.004	<dl	<dl	<dl	0.089	*0.001	5.60	15.0
B5110CCP-001.d	3.07	0.353	*0.017	300	0.417	0.020	1051	0.007	0.052	n.r.	36.6	<dl	87.3	161	0.317	*0.041	<dl	<dl	<dl	0.007	0.072	*0.001	3.18	12.4
B5110CCP-004.d	1.79	0.210	*0.01	356	0.840	<dl	998	0.014	0.009	n.r.	44.1	<dl	84.8	191	0.180	*0.041	<dl	<dl	<dl	<dl	0.063	*0.001	3.50	13.8
B7157CCP-001.d	1.82	0.131	0.770	338	6.92	0.200	869	0.015	0.074	n.r.	22.3	<dl	59.1	197	0.157	*0.071	<dl	<dl	<dl	<dl	0.323	*0.001	0.980	1.84
B7157CCP-003.d	1.13	0.299	*0.01	318	7.61	0.180	836	<dl	0.067	n.r.	17.3	<dl	57.5	179	0.135	*0.066	<dl	0.011	<dl	<dl	0.156	*0.001	0.480	2.77
B7157CCP-004.d	1.49	0.314	*0.01	370	7.38	<dl	914	0.011	0.068	n.r.	16.8	<dl	61.1	173	0.303	*0.057	<dl	<dl	0.047	<dl	0.045	*0.001	1.33	2.80
B7157CCP-002.d	1.40	0.291	*0.011	312	7.60	<dl	838	<dl	0.055	n.r.	23.4	<dl	60.9	202	0.074	*0.081	<dl	<dl	0.006	<dl	0.210	*0.001	0.227	1.15
B7157CCP-005.d	1.71	0.160	0.150	322	7.86	<dl	988	0.013	0.049	n.r.	21.1	<dl	61.2	197	0.278	*0.066	<dl	<dl	0.002	<dl	0.487	*0.001	0.710	2.75
B7158CCP-005.d	1.80	0.499	*0.012	338	2.82	0.020	571	0.020	0.063	n.r.	18.6	<dl	65.1	206	0.190	*0.058	<dl	<dl	<dl	<dl	0.490	*0.001	2.70	2.04
B7158CCP-002.d	2.09	0.523	0.150	331	5.10	0.210	598	0.007	0.011	n.r.	31.2	<dl	68.6	221	0.216	*0.056	<dl	<dl	<dl	<dl	0.545	*0.001	3.77	1.25
B7158CCP-001.d	1.69	0.280	*0.008	359	5.18	0.150	679	0.033	0.073	n.r.	18.1	<dl	69.8	168	0.401	*0.048	<dl	<dl	<dl	<dl	0.203	*0.001	1.70	1.38
B7158CCP-003.d	1.86	0.246	0.166	302	4.82	0.240	605	0.014	0.061	n.r.	20.0	<dl	70.1	143	0.560	*0.041	<dl	<dl	<dl	0.010	0.241	0.004	*2.5	2.27
B7158CCP-004.d	3.80	0.770	1.30	317	6.73	0.380	643	<dl	0.061	n.r.	21.6	<dl	68.0	209	0.451	*0.063	<dl	<dl	<dl	<dl	0.266	*0.001	3.30	1.40
BVMS01-CCP-05.d	9.20	*0.015	*0.064	450	1.79	0.120	256	2.32	<dl	n.r.	17.5	<dl	13.5	49.9	5.89	1.14	0.004	<dl	<dl	0.003	*0.002	0.025	11.3	1.59
BVMS01-CCP-02.d	2.17	14.8	*0.11	511	0.160	0.440	280	3.76	0.026	n.r.	0.531	<dl	6.27	42.5	15.1	1.83	0.010	<dl	<dl	<dl	0.025	0.040	28.9	0.512
BVMS01-CCP-01.d	2.41	11.5	*0.092	545	0.262	<dl	260	7.80	0.017	n.r.	0.611	<dl	6.42	42.6	6.70	0.720	0.003	<dl	<dl	0.006	0.036	0.120	6.70	0.607
BVMS01-CCP-03.d	1.90	14.2	*0.096	423	0.320	0.750	289	66.0	<dl	n.r.	1.28	<dl	7.55	45.9	12.4	1.73	<dl	<dl	0.009	<dl	0.034	*0.006	32.2	0.710
BVMS01-CCP-04.d	2.43	14.1	*0.067	497	0.190	0.070	274	<dl	0.029	n.r.	1.43	<dl	6.36	47.2	4.13	1.17	<dl	<dl	0.004	<dl	*0.004	*0.003	7.85	1.08
COR01CCP-08.d	*0.431	0.120	0.900	145	2.91	0.160	268	0.086	<dl	n.r.	15.0	<dl	194	823	9.30	*0.053	0.006	<dl	<dl	<dl	0.250	0.007	5.98	8.00
COR01CCP-06.d	*0.507	0.350	11.0	196	2.67	0.650	249	<dl	0.034	n.r.	14.4	0.172	99.2	963	3.19	*0.061	<dl	<dl	0.023	<dl	0.079	*0.001	2.76	3.41
COR01CCP-01.d	*0.417	*0.018	0.940	215	1.59	0.090	329	0.081	0.019	n.r.	10.1	<dl	296	1111	3.11	*0.041	<dl	<dl	<dl	<dl	*0.008	*0.001	1.61	2.25
COR01CCP-04.d	1.16	0.890	0.700	231	3.92	<dl	256	0.320	0.006	n.r.	13.4	<dl	158	989	7.60	*0.065	<dl	<dl	<dl	<dl	*0.003	*0.001	4.51	5.32
COR01CCP-03.d	2.04	0.500	3.20	225	5.79	0.900	320	<dl	<dl	n.r.	15.8	<dl	284	955	8.89	*0.047	<dl	<dl	0.006	0.014	0.026	0.009	6.23	8.30
COR02CCP-05.d	1.72	0.073	*0.012	13.7	5.77	6.34	36.1	0.024	0.051	n.r.	3.51	0.089	318	476	6.35	*0.033	0.600	<dl	<dl	0.011	*0.02	0.136	11.9	7.79
COR02CCP-02.d	4.90	0.022	*0.027	16.6	6.45	5.32	47.8	0.280	0.029	n.r.	3.14	0.245	284	437	2.70	*0.021	<dl	0.080	0.002	<dl	*0.003	0.078	16.1	3.44
COR02CCP-01.d	*0.47	*0.009	0.520	16.2	6.30	6.60	63.2	3.90	0.019	n.r.	3.04	0.169	266	458	3.23	*0.051	0.079	<dl	<dl	0.012	*0.004	0.200	11.4	3.80
COR02CCP-04.d	*0.398	0.130	*0.012	32.2	6.04	11.3	51.7	<dl	0.024	n.r.	6.15	<dl	307	514	3.79	*0.044	<dl	<dl	<dl	<dl	*0.002	0.700	20.1	1.65
COR02CCP-03.d	*0.554	0.410	0.400	311	7.15	4.35	65.4	3.30	0.021	n.r.	3.44	<dl	388	582	1.82	*0.055	0.058	0.090	<dl	<dl	*0.022	0.164	11.7	0.419

Grain ID	Mn	Co	Ni	Zn	Ga	As	Se	Mo	Ru	Rh	Ag	Pd	In	Sn	Sb	Te	Re	Os	Ir	Pt	Au	Tl	Pb	Bi
	55	59	60	66	71	75	82	95	101	103	107	108	115	118	121	128	185	189	193	195	197	205	208	209
33um	1.017	0.029	0.322	0.590	0.033	0.149	3.828	5.311	0.030	0.020	0.027	0.026	0.033	0.155	0.047	0.400	0.501	0.012	0.028	0.007	0.016	0.006	0.029	0.012
55um	0.449	0.024	0.211	0.357	0.028	0.079	2.455	2.409	0.029	0.020	0.019	0.011	0.015	0.071	0.025	0.277	0.221	0.007	0.016	0.004	0.012	0.004	0.015	0.008
COR02CCP-06.d	*0.408	*0.01	*0.019	11.8	5.85	4.51	34.4	<dl	<dl	n.r.	4.08	<dl	3.12	446	2.92	*0.034	0.220	<dl	<dl	<dl	*0.003	0.136	25.0	6.89
COR02CCP-07.d	*0.271	0.019	*0.006	17.3	5.92	2.75	35.1	<dl	0.021	n.r.	3.10	<dl	274	486	1.10	*0.023	0.420	<dl	<dl	<dl	*0.002	0.047	11.9	0.810
COR03CCP-10.d	3.96	*0.011	0.900	418	24.5	1.07	1083	0.035	<dl	n.r.	1.51	<dl	170	963	12.4	*0.105	<dl	<dl	<dl	0.002	*0.005	0.012	8.20	30.3
COR03CCP-04.d	*0.67	1.10	*0.02	350	11.7	1.12	1165	0.048	0.073	n.r.	2.08	<dl	174	926	9.18	*0.1	<dl	<dl	<dl	0.016	*0.005	0.015	6.11	19.0
COR03CCP-09.d	*0.445	0.036	1.00	403	23.6	1.13	1180	0.030	<dl	n.r.	2.10	<dl	177	976	5.64	*0.069	0.310	<dl	<dl	<dl	0.120	*0.002	2.43	14.4
COR03CCP-07.d	2.34	15.0	0.510	368	19.0	0.950	1205	<dl	0.064	n.r.	0.980	<dl	188	1034	4.49	*0.256	<dl	0.012	<dl	0.008	0.042	0.010	2.00	11.0
COR03CCP-08.d	2.39	1.30	*0.041	429	19.0	1.79	1237	0.068	0.015	n.r.	13.9	<dl	200	1058	10.9	*0.075	<dl	<dl	<dl	<dl	*0.006	0.075	65.0	228
COR03CCP-11.d	11.0	0.062	*0.054	563	21.9	1.15	1158	<dl	0.016	n.r.	1.16	<dl	168	1181	7.46	*0.065	<dl	<dl	0.024	<dl	*0.068	0.012	3.26	13.5
COR03CCP-05.d	*0.583	0.130	0.800	184	19.7	3.60	953	0.049	<dl	n.r.	2.07	<dl	190	596	9.90	*0.084	<dl	<dl	<dl	0.021	0.047	0.054	7.05	20.9
COR03CCP-02.d	2.80	4.20	170	183	10.3	8.10	756	0.700	0.280	n.r.	8.40	<dl	236	541	36.2	2.60	<dl	<dl	0.005	<dl	*0.006	0.335	34.5	85.8
COR03CCP-03.d	*0.512	*0.008	*0.02	128	13.2	5.10	923	0.043	<dl	n.r.	2.27	<dl	211	630	19.3	*0.09	<dl	<dl	<dl	0.060	*0.005	0.180	38.0	57.0
COR03CCP-01.d	1.30	*0.01	3.00	181	12.1	8.90	891	0.120	1.20	n.r.	7.06	<dl	232	621	25.4	*0.095	<dl	0.025	0.020	<dl	*0.005	0.114	20.5	50.3
COR04CCP-06.d	0.900	*0.02	*0.016	398	3.56	0.100	198	0.030	<dl	n.r.	1.57	<dl	874	1496	1.57	0.242	0.014	<dl	0.006	0.080	0.033	*0.001	1.27	3.30
COR04CCP-04.d	0.920	3.50	33.0	184	0.561	0.170	97.3	0.700	<dl	n.r.	0.890	<dl	941	358	0.660	*0.1	<dl	<dl	<dl	0.013	0.035	*0.001	0.810	1.64
COR04CCP-01.d	12.0	0.100	1.20	274	3.44	<dl	263	0.037	0.040	n.r.	2.32	6.67	1212	1193	1.30	0.500	<dl	0.012	<dl	0.033	*0.004	*0.001	2.81	5.71
COR04CCP-02.d	*0.299	0.200	11.0	207	1.80	0.370	219	2.20	0.016	n.r.	1.99	<dl	641	612	2.47	*0.049	0.003	<dl	0.100	<dl	0.290	*0.001	2.72	5.42
COR04CCP-05.d	*0.196	0.190	2.60	246	2.95	0.430	187	0.700	0.012	n.r.	1.85	<dl	1169	1194	0.760	*0.039	0.057	0.008	<dl	0.008	0.112	*0.001	1.15	2.71
COR04CCP-03.d	0.680	0.190	*0.014	171	2.70	0.390	209	1.40	<dl	n.r.	2.39	<dl	1549	605	4.21	0.800	<dl	<dl	6.E-4	<dl	0.261	*0.001	6.80	9.25
E52-A-6-Ccp-1d	2.21	4.92	0.300	241	0.294	<dl	983	0.008	<dl	n.r.	10.6	<dl	53.5	10.5	0.866	7.80	<dl	<dl	<dl	<dl	*0.001	0.006	4.80	0.392
E52-A-4-Ccp-1d	23.0	3.02	0.351	237	1.24	<dl	833	0.005	<dl	n.r.	11.1	<dl	56.7	14.2	1.72	9.24	<dl	<dl	<dl	<dl	0.014	0.023	8.75	0.610
E54-B-3-Ccp-1d	*0.128	*0.003	*0.009	288	1.09	<dl	567	<dl	<dl	n.r.	10.4	<dl	54.7	27.7	0.587	41.2	<dl	<dl	<dl	<dl	0.012	0.002	1.40	0.003
E54-B-2-Ccp-1d	*0.158	*0.003	0.190	332	1.18	0.050	570	<dl	<dl	n.r.	7.36	<dl	57.4	31.9	4.95	38.1	0.003	<dl	<dl	<dl	0.051	0.009	2.63	0.005
E55-A-1-CCP-1d	0.530	0.016	0.118	213	1.62	0.250	1275	<dl	<dl	n.r.	1.80	<dl	37.8	15.7	1.12	18.1	<dl	<dl	<dl	<dl	0.028	0.011	2.51	*0.002
E55-A-3-CCP-1d	*0.144	0.028	*0.005	193	6.11	0.150	1488	0.008	<dl	n.r.	1.67	<dl	49.2	26.3	1.79	13.6	<dl	<dl	<dl	<dl	0.019	0.004	2.09	0.007
E55-A-2-CCP-1d	0.280	0.015	*0.004	226	1.67	0.110	1235	0.038	<dl	n.r.	0.848	<dl	41.5	24.4	0.166	24.6	<dl	<dl	<dl	<dl	0.018	0.002	0.182	*0.001
E55-A-4-CCP-1d	*0.102	0.024	*0.004	223	1.84	0.140	1262	0.005	<dl	n.r.	1.35	<dl	43.2	20.8	0.578	20.1	0.001	<dl	<dl	<dl	0.031	*0.002	0.703	*0.002
E62-A-5-CCP-1d	0.350	0.011	*0.003	268	1.38	<dl	26.0	0.015	<dl	n.r.	50.0	<dl	32.8	30.7	0.193	0.720	<dl	<dl	<dl	<dl	0.028	*0.001	0.811	0.004
E64-5-CCP-1d	7.70	0.171	0.141	178	0.079	0.070	21.2	<dl	<dl	n.r.	29.8	<dl	9.77	20.2	0.270	0.620	<dl	<dl	<dl	<dl	*0.003	0.035	10.6	1.48
E64-2-CCP-1d	*0.131	0.142	0.102	210	0.099	0.040	13.9	0.011	<dl	n.r.	37.7	<dl	11.6	19.4	0.203	0.540	<dl	<dl	<dl	<dl	*0.001	0.035	2.49	0.325
E64-4-CCP-1d	5.00	0.180	*0.009	292	0.082	0.230	15.8	0.013	<dl	n.r.	36.3	<dl	12.0	37.2	0.084	0.650	<dl	<dl	<dl	<dl	0.012	0.008	1.12	0.223
E64-1-CCP-1d	0.470	0.072	*0.005	216	0.071	0.110	12.9	<dl	<dl	n.r.	37.4	<dl	11.9	18.0	0.113	0.420	<dl	<dl	<dl	<dl	*0.001	*0.002	2.03	0.247
E64-3-CCP-1d	16.2	0.197	0.124	238	0.190	0.240	12.2	0.011	<dl	n.r.	40.6	<dl	11.1	29.1	0.300	0.670	<dl	<dl	<dl	<dl	*0.002	0.005	1.47	0.387
E66-A-2-CCP-1d	0.530	3.77	*0.008	251	0.677	0.240	111	<dl	<dl	n.r.	76.0	<dl	113	38.1	0.051	0.680	<dl	<dl	<dl	<dl	*0.002	*0.002	0.463	0.754
E67-2-Ccp-2.d	56.0	0.524	*0.014	199	0.069	0.150	85.5	0.006	<dl	n.r.	12.5	<dl	41.1	20.8	0.160	0.250	<dl	<dl	<dl	<dl	0.044	0.025	3.87	0.120

Grain ID	Mn	Co	Ni	Zn	Ga	As	Se	Mo	Ru	Rh	Ag	Pd	In	Sn	Sb	Te	Re	Os	Ir	Pt	Au	Tl	Pb	Bi
	55	59	60	66	71	75	82	95	101	103	107	108	115	118	121	128	185	189	193	195	197	205	208	209
33um	1.017	0.029	0.322	0.590	0.033	0.149	3.828	5.311	0.030	0.020	0.027	0.026	0.033	0.155	0.047	0.400	0.501	0.012	0.028	0.007	0.016	0.006	0.029	0.012
55um	0.449	0.024	0.211	0.357	0.028	0.079	2.455	2.409	0.029	0.020	0.019	0.011	0.015	0.071	0.025	0.277	0.221	0.007	0.016	0.004	0.012	0.004	0.015	0.008
E67-5-Ccp-1d	3.50	0.511	0.106	224	0.079	<dl	96.0	<dl	<dl	n.r.	13.5	<dl	49.7	21.7	0.178	*0.027	<dl	<dl	<dl	<dl	0.037	0.008	2.07	0.075
E171-B-5-Ccp-2.d	*0.122	0.010	0.104	253	0.685	0.080	2464	2.60	<dl	n.r.	32.2	<dl	98.3	20.6	0.468	0.600	<dl	<dl	<dl	<dl	0.324	0.009	1.09	0.286
E171-B-5-Ccp-1d	*0.141	0.010	*0.004	310	0.560	<dl	2496	0.010	<dl	n.r.	36.3	<dl	96.0	15.5	0.840	0.320	<dl	<dl	<dl	<dl	0.500	0.003	1.88	0.392
GRA01CCP-02.d	*0.506	0.140	4.10	383	4.97	<dl	488	<dl	<dl	n.r.	10.5	<dl	439	1000	27.9	*0.068	<dl	<dl	0.024	<dl	*0.007	0.159	20.6	8.50
GRA01CCP-01d	1.92	*0.007	*0.038	304	2.71	0.060	138	<dl	0.015	n.r.	7.98	<dl	191	727	10.6	*0.028	<dl	0.900	<dl	<dl	*0.003	0.070	8.41	3.13
GRA01CCP-06.d	*0.325	0.117	2.30	299	3.10	0.370	216	<dl	<dl	n.r.	3.10	<dl	333	1172	1.32	*0.033	<dl	<dl	<dl	0.260	0.080	*0.001	2.70	1.03
GRA01CCP-05.d	*0.392	0.190	*0.022	477	4.37	2.17	356	<dl	<dl	n.r.	5.27	<dl	412	2480	6.40	*0.052	<dl	<dl	<dl	<dl	*0.005	0.058	3.20	1.44
GRA01CCP-03.d	1.25	0.029	*0.014	270	2.00	<dl	225	0.022	0.020	n.r.	4.10	<dl	241	599	4.05	*0.023	<dl	<dl	<dl	<dl	*0.003	0.010	2.24	1.03
GRA01CCP-04.d	*0.217	*0.012	*0.037	266	3.14	0.210	272	0.068	<dl	n.r.	4.10	<dl	294	1128	2.91	*0.031	0.008	<dl	<dl	<dl	*0.012	0.028	1.86	0.700
ICEVMS01CCP-01d	80.0	0.458	0.360	3.20	58.9	1.10	89.6	2.20	0.061	n.r.	7.81	<dl	20.6	0.360	0.700	*0.087	0.004	<dl	<dl	<dl	*0.001	0.052	34.4	0.270
ICEVMS01-CCP-05.d	5.94	2.12	1.82	*1.357	7.97	0.650	92.0	0.001	<dl	n.r.	32.8	<dl	5.41	0.650	0.390	*0.166	0.002	0.006	<dl	<dl	*0.002	*0.005	6.90	*0.004
ICEVMS01-CCP-02.d	2.59	*0.005	*0.009	*0.722	18.8	0.630	118	0.015	0.009	n.r.	1.93	0.009	28.6	0.280	0.182	*0.081	<dl	<dl	<dl	<dl	*0	*0.002	4.58	0.055
ICEVMS01-CCP-04.d	2.39	*0.004	*0.005	1.40	7.08	0.700	126	<dl	0.031	n.r.	4.54	<dl	45.7	0.490	0.630	*0.08	<dl	<dl	<dl	<dl	*0.001	0.072	22.7	0.160
ICEVMS01-CCP-03.d	2.66	*0.006	*0.006	0.970	26.8	0.130	135	0.350	0.010	n.r.	12.5	<dl	38.6	0.480	0.156	*0.073	0.002	<dl	<dl	0.002	*0.001	0.015	2.68	0.375
LB01-CCP-05.d	2.00	*0.027	*0.028	710	2.50	<dl	60.6	0.022	<dl	n.r.	1.45	<dl	13.0	2.31	0.073	6.65	<dl	0.023	<dl	0.011	*0.004	*0.002	6.46	8.60
LB01-CCP-06.d	2.39	0.416	1.40	510	47.5	<dl	610	13.0	0.010	n.r.	3.65	<dl	216	191	0.052	5.09	<dl	0.022	0.002	0.016	*0.001	0.029	9.50	0.028
LB01-CCP-01d	2.52	*0.038	4.20	790	2.50	<dl	106	0.014	<dl	n.r.	1.23	<dl	12.4	1.73	0.050	6.51	<dl	<dl	<dl	<dl	0.210	0.045	8.39	1.99
LB01-CCP-02.d	2.64	*0.031	*0.031	580	2.43	0.020	133	<dl	0.022	n.r.	2.93	<dl	12.5	2.62	0.061	5.30	<dl	<dl	0.008	<dl	*0.004	0.032	7.34	17.2
LB01-CCP-04.d	2.08	*0.036	1.60	640	2.56	<dl	141	0.028	<dl	n.r.	0.860	<dl	11.9	2.01	0.024	5.50	<dl	<dl	<dl	<dl	*0.004	0.012	4.19	4.05
LB01-CCP-03.d	2.52	*0.053	*0.031	653	2.35	0.006	155	4.60	0.017	n.r.	2.20	<dl	10.8	2.24	0.045	5.24	<dl	<dl	<dl	<dl	0.085	0.086	8.19	21.3
LDR01-CCP-06.d	5.76	0.298	2.30	310	2.34	0.410	400	<dl	0.016	n.r.	1.40	<dl	44.9	*0.145	3.40	2.39	<dl	0.011	<dl	<dl	*0.004	0.690	4.64	1.12
LDR01-CCP-05.d	6.75	0.211	*0.038	660	2.38	0.030	376	<dl	<dl	n.r.	83.1	<dl	36.6	0.246	3.06	5.35	<dl	<dl	<dl	<dl	*0.003	0.562	5.61	1.28
LDR01-CCP-01d	8.02	0.334	*0.03	464	1.69	0.100	432	<dl	<dl	n.r.	92.5	<dl	35.1	0.270	3.80	0.980	<dl	<dl	<dl	0.005	*0.001	0.910	5.79	1.55
LDR01-CCP-03.d	5.95	0.180	2.89	313	1.74	<dl	264	<dl	<dl	n.r.	93.4	<dl	35.1	*0.16	5.04	0.910	0.005	<dl	0.001	0.006	*0.002	0.670	9.37	0.910
LDR01-CCP-04.d	4.74	0.417	2.14	515	1.73	<dl	342	<dl	0.009	n.r.	94.9	<dl	32.6	*0.103	3.27	4.05	<dl	<dl	0.001	0.005	*0.003	0.760	7.80	0.728
LDR01-CCP-02.d	5.52	0.860	12.2	330	1.75	<dl	393	<dl	0.007	n.r.	98.2	<dl	38.2	*0.13	8.90	0.520	9.E-4	<dl	<dl	<dl	*0.002	3.68	15.5	1.16
LOU01CCP-04.d	1.02	*0.013	*0.015	226	0.390	<dl	86.9	0.028	<dl	n.r.	3.81	<dl	456	280	19.9	0.590	0.012	0.016	<dl	<dl	*0.003	0.053	22.7	20.0
LOU01CCP-07.d	4.00	0.140	3.90	197	0.350	0.040	82.9	0.180	0.014	n.r.	5.73	<dl	569	273	15.8	*0.037	<dl	<dl	<dl	0.060	0.100	0.024	15.6	10.8
LOU01CCP-03.d	*0.255	0.027	*0.011	227	0.101	0.370	50.9	0.095	0.015	n.r.	3.61	<dl	491	302	16.7	*0.012	0.016	<dl	<dl	<dl	*0.002	0.022	12.0	11.8
LOU01CCP-05.d	3.00	0.810	32.0	237	0.137	2.30	87.0	0.087	<dl	n.r.	7.38	<dl	282	308	41.0	*0.052	<dl	<dl	<dl	<dl	*0.004	*0.034	18.7	19.2
LOU01CCP-02.d	*0.448	8.00	*0.032	195	0.390	0.360	125	0.018	<dl	n.r.	10.1	<dl	1809	280	20.9	*0.051	<dl	<dl	<dl	0.090	0.100	0.009	20.7	19.2
LOU01CCP-06.d	5.60	1.30	0.800	286	0.220	1.03	105	0.930	0.015	n.r.	6.03	0.278	508	392	32.9	*0.076	0.006	<dl	<dl	0.008	2.40	0.042	35.3	22.4
LOU01CCP-01d	*0.217	0.034	*0.014	194	0.450	0.180	178	3.40	0.039	n.r.	1.37	<dl	720	441	0.324	*0.022	<dl	0.018	<dl	<dl	*0.001	*0.001	0.280	0.211
LS1CCP-05.d	0.300	*0.003	*0.002	1810	16.8	<dl	4.50	0.003	0.002	n.r.	5.24	<dl	13.9	8.64	*0.006	*0.015	<dl	<dl	0.001	0.005	0.026	0.001	0.875	0.059

Grain ID	Mn	Co	Ni	Zn	Ga	As	Se	Mo	Ru	Rh	Ag	Pd	In	Sn	Sb	Te	Re	Os	Ir	Pt	Au	Tl	Pb	Bi
	55	59	60	66	71	75	82	95	101	103	107	108	115	118	121	128	185	189	193	195	197	205	208	209
33um	1.017	0.029	0.322	0.590	0.033	0.149	3.828	5.311	0.030	0.020	0.027	0.026	0.033	0.155	0.047	0.400	0.501	0.012	0.028	0.007	0.016	0.006	0.029	0.012
55um	0.449	0.024	0.211	0.357	0.028	0.079	2.455	2.409	0.029	0.020	0.019	0.011	0.015	0.071	0.025	0.277	0.221	0.007	0.016	0.004	0.012	0.004	0.015	0.008
LS1CCP-03.d	0.420	*0.003	*0.003	1849	5.12	0.062	4.39	0.005	0.019	n.r.	9.17	<dl	14.2	9.22	*0.005	*0.014	<dl	0.003	<dl	0.001	0.063	*0.001	1.18	0.051
LS1CCP-04.d	0.270	*0.002	*0.002	2009	8.52	0.078	3.55	0.003	0.005	n.r.	5.25	<dl	14.4	8.89	*0.004	*0.013	<dl	<dl	<dl	<dl	0.057	*0.001	0.940	0.034
LS1CCP-02.d	1.06	0.022	*0.003	3430	27.0	0.085	6.10	0.042	0.014	n.r.	8.11	<dl	14.6	10.3	*0.005	*0.02	<dl	<dl	<dl	<dl	0.043	0.002	2.75	0.184
LS1CCP-01d	0.710	*0.003	*0.004	1859	7.75	0.023	5.20	0.006	0.016	n.r.	7.24	<dl	14.0	10.3	*0.006	*0.017	0.001	<dl	3.E-4	<dl	0.060	0.004	1.47	0.142
LS1CCP-06.d	0.320	*0.003	*0.002	1670	12.4	0.038	3.50	0.004	0.011	n.r.	6.60	<dl	14.5	8.84	0.012	*0.013	7.E-4	<dl	<dl	0.002	0.026	*0.002	1.08	0.090
LS1CCP-07.d	*0.117	*0.004	*0.005	3010	26.5	0.038	4.50	0.007	0.016	n.r.	6.85	<dl	14.5	9.06	*0.005	*0.023	<dl	<dl	0.002	<dl	0.103	0.003	1.18	0.078
LS10CCP-05.d	52.0	0.800	*0.021	7.00	0.620	0.070	77.5	0.035	0.015	n.r.	21.3	<dl	8.05	0.370	*0.036	2.85	<dl	0.026	<dl	<dl	0.006	0.022	43.2	0.402
LS10CCP-04.d	4.07	1.27	*0.012	12.1	0.710	0.200	91.5	<dl	0.029	n.r.	20.5	<dl	8.79	0.560	*0.036	3.96	<dl	<dl	0.003	<dl	*0.002	0.012	56.4	0.419
LS10CCP-06.d	2.76	0.490	*0.008	2.89	0.289	0.010	82.4	<dl	0.019	n.r.	28.6	<dl	4.18	0.580	*0.033	1.03	<dl	<dl	<dl	<dl	*0.001	0.013	14.8	0.444
LS10CCP-07.d	5.65	1.25	*0.008	12.6	0.990	0.190	66.8	<dl	0.038	n.r.	21.4	<dl	2.66	0.380	0.076	0.680	<dl	<dl	<dl	0.010	0.031	0.042	55.7	0.580
LS10CCP-03.d	*0.421	0.490	*0.009	4.60	0.580	<dl	95.0	<dl	0.025	n.r.	22.6	<dl	6.89	*0.087	*0.034	1.49	<dl	<dl	<dl	<dl	0.148	0.014	11.0	0.303
LS10CCP-01d	3.10	2.00	*0.013	22.6	0.790	0.800	66.0	0.029	<dl	n.r.	10.3	<dl	2.92	0.350	*0.029	2.40	<dl	0.024	<dl	0.063	*0.001	0.012	24.3	0.104
LS10CCP-02.d	2.60	0.900	*0.012	9.00	0.580	0.200	83.0	<dl	0.025	n.r.	20.4	<dl	2.61	*0.071	*0.043	1.43	<dl	<dl	<dl	<dl	*0.001	0.073	50.8	0.622
LS22CCP-03.d	*0.186	*0.004	*0.009	165	0.226	0.490	171	0.015	0.070	n.r.	11.0	<dl	17.5	331	37.7	*0.036	1.00	<dl	<dl	<dl	*0.003	0.168	36.6	7.89
LS22CCP-02.d	1.30	0.036	0.190	306	0.800	0.390	220	0.130	<dl	n.r.	1.90	<dl	90.7	1408	20.9	*0.032	<dl	<dl	<dl	<dl	0.025	0.039	10.7	3.56
LS22CCP-04.d	0.690	0.018	*0.014	180	0.372	0.200	193	<dl	<dl	n.r.	12.1	<dl	89.2	559	5.41	*0.027	0.070	<dl	<dl	<dl	0.900	0.005	3.08	1.64
LS22CCP-07.d	0.750	0.150	4.20	205	0.480	0.117	183	0.009	0.140	n.r.	17.1	<dl	27.1	678	5.91	*0.03	0.003	<dl	0.027	<dl	0.129	0.007	3.59	2.40
LS22CCP-05.d	5.30	*0.029	1.40	471	*0.199	4.60	227	0.021	<dl	n.r.	1.44	0.639	42.9	649	1.79	*0.048	<dl	<dl	<dl	0.002	0.270	0.195	3.79	1.00
LS22CCP-06.d	0.920	0.030	*0.006	195	0.347	0.310	167	<dl	0.008	n.r.	20.5	0.249	44.1	595	55.8	*0.024	<dl	<dl	0.080	0.010	*0.003	0.197	25.0	10.6
LS22CCP-01d	0.460	0.026	0.160	241	0.720	0.090	110	0.008	0.014	n.r.	1.58	<dl	66.6	1087	22.3	*0.025	<dl	<dl	<dl	0.008	*0.002	0.046	11.1	4.27
MN1CCP-02.d	1.15	1.23	*0.012	369	3.12	0.090	307	0.011	0.007	n.r.	18.2	<dl	4.54	612	0.600	1.74	<dl	<dl	<dl	<dl	0.087	0.005	2.87	0.461
MN1CCP-04.d	0.880	2.53	*0.013	480	3.47	<dl	313	<dl	0.026	n.r.	20.7	<dl	4.74	57.1	0.312	4.03	<dl	<dl	<dl	0.003	0.264	*0.001	2.61	0.464
MN1CCP-06.d	1.24	2.87	*0.015	440	2.60	0.005	310	0.018	<dl	n.r.	20.4	<dl	4.78	67.3	1.46	1.71	<dl	<dl	0.009	<dl	0.092	0.012	6.10	1.13
MN1CCP-01d	1.56	1.38	*0.015	466	4.58	0.110	321	0.010	0.012	n.r.	19.7	<dl	4.77	67.1	1.37	1.68	<dl	<dl	<dl	0.007	0.061	0.087	6.80	0.920
MN1CCP-07.d	0.850	3.50	*0.016	484	2.68	0.070	300	0.010	<dl	n.r.	24.0	<dl	5.81	76.3	1.57	2.42	<dl	0.014	<dl	<dl	0.082	0.006	6.85	1.17
MN1CCP-03.d	1.09	3.57	*0.017	510	3.32	0.110	298	0.017	0.019	n.r.	19.0	<dl	4.79	57.9	0.530	2.43	<dl	<dl	<dl	<dl	0.066	*0.001	3.14	0.496
MN1CCP-05.d	1.00	1.00	*0.014	460	3.19	<dl	310	0.026	0.010	n.r.	19.9	<dl	4.62	65.5	0.530	2.72	<dl	<dl	0.003	<dl	0.071	0.008	3.07	0.469
MN2CCP-05.d	1.49	0.800	*0.012	391	3.58	0.035	277	<dl	<dl	n.r.	20.7	<dl	4.29	62.2	0.451	1.83	0.002	<dl	<dl	<dl	0.055	0.005	3.24	0.549
MN2CCP-03.d	1.53	1.62	*0.014	453	4.37	0.040	279	<dl	<dl	n.r.	21.3	<dl	4.40	68.3	0.810	1.51	<dl	<dl	<dl	<dl	0.062	0.015	5.11	0.800
MN2CCP-04.d	0.740	0.730	3.70	403	3.94	<dl	292	0.039	<dl	n.r.	20.2	<dl	4.22	63.0	0.808	1.61	<dl	<dl	<dl	0.004	0.172	0.006	5.38	0.876
MN2CCP-06.d	1.20	0.439	*0.01	504	3.56	0.017	293	0.049	<dl	n.r.	21.1	<dl	4.02	60.5	0.561	1.62	<dl	<dl	<dl	<dl	0.045	*0.001	3.25	0.506
MN2CCP-01d	1.49	0.890	0.300	398	4.23	0.016	291	0.018	0.010	n.r.	20.6	<dl	4.33	65.3	0.670	1.92	<dl	<dl	<dl	<dl	0.056	0.006	3.47	0.510
MN2CCP-07.d	1.06	1.21	*0.011	415	3.42	0.040	284	<dl	0.014	n.r.	23.9	<dl	4.43	63.3	0.800	1.32	<dl	<dl	<dl	<dl	0.028	0.008	5.50	0.850
MN3CCP-04.d	0.770	0.045	3.85	521	1.50	0.022	110	0.008	0.023	n.r.	506	<dl	42.2	321	0.900	1.63	<dl	0.003	<dl	<dl	0.059	0.040	1.31	0.029

Grain ID	Mn	Co	Ni	Zn	Ga	As	Se	Mo	Ru	Rh	Ag	Pd	In	Sn	Sb	Te	Re	Os	Ir	Pt	Au	Tl	Pb	Bi
	55	59	60	66	71	75	82	95	101	103	107	108	115	118	121	128	185	189	193	195	197	205	208	209
33um	1.017	0.029	0.322	0.590	0.033	0.149	3.828	5.311	0.030	0.020	0.027	0.026	0.033	0.155	0.047	0.400	0.501	0.012	0.028	0.007	0.016	0.006	0.029	0.012
55um	0.449	0.024	0.211	0.357	0.028	0.079	2.455	2.409	0.029	0.020	0.019	0.011	0.015	0.071	0.025	0.277	0.221	0.007	0.016	0.004	0.012	0.004	0.015	0.008
MN3CCP-02.d	1.49	*0.01	5.86	533	1.26	0.011	74.8	0.023	0.013	n.r.	469	<dl	42.0	229	1.38	2.40	0.002	<dl	<dl	<dl	0.022	0.058	1.97	0.056
MN3CCP-01.d	0.800	0.038	14.7	524	1.00	0.063	59.0	0.022	0.011	n.r.	535	<dl	28.1	179	4.18	1.21	<dl	<dl	<dl	<dl	0.018	0.220	3.94	0.124
MN3CCP-03.d	1.48	0.040	7.20	639	1.32	0.300	62.2	0.041	<dl	n.r.	587	<dl	37.6	181	0.746	0.950	<dl	<dl	<dl	<dl	*0.002	0.007	3.21	0.031
MN3CCP-05.d	0.740	0.042	7.46	509	1.55	<dl	80.7	<dl	<dl	n.r.	563	<dl	37.5	214	2.49	2.66	<dl	<dl	<dl	<dl	0.030	0.057	3.43	0.048
MN3CCP-07.d	*0.222	0.059	5.71	450	1.38	<dl	84.1	0.008	0.012	n.r.	623	<dl	32.0	223	2.27	1.94	<dl	<dl	<dl	0.007	0.028	0.143	3.32	0.051
MN3CCP-06.d	0.510	0.081	9.39	545	1.60	0.130	73.1	0.004	0.010	n.r.	597	<dl	40.7	246	0.690	2.28	0.004	<dl	<dl	<dl	0.015	0.034	1.10	0.026
MN4CCP-06.d	1.76	*0.013	*0.015	575	0.364	<dl	887	0.160	<dl	n.r.	22.1	<dl	9.24	45.2	2.40	0.740	<dl	<dl	<dl	<dl	0.210	*0.002	2.19	0.587
MN4CCP-01.d	1.36	*0.009	*0.009	610	0.469	0.012	957	5.E-4	0.019	n.r.	24.5	<dl	8.53	38.0	2.93	0.650	<dl	<dl	1.E-4	<dl	0.018	0.010	1.46	0.320
MN4CCP-03.d	1.93	0.074	*0.01	620	0.339	0.026	800	<dl	0.010	n.r.	21.0	<dl	8.28	38.5	1.66	0.790	0.003	<dl	0.002	<dl	0.055	*0.001	0.910	0.211
MN4CCP-02.d	1.70	*0.012	*0.013	628	0.507	<dl	927	0.021	0.005	n.r.	27.7	<dl	8.86	39.7	2.28	0.810	0.002	<dl	0.003	<dl	0.346	0.004	1.06	0.441
MN4CCP-05.d	2.10	*0.012	*0.016	726	0.479	0.068	871	0.003	<dl	n.r.	21.7	<dl	9.25	44.1	0.208	2.12	<dl	0.002	<dl	<dl	0.150	*0.001	0.715	0.960
MN4CCP-04.d	2.09	0.029	*0.029	614	0.587	0.010	998	<dl	0.016	n.r.	27.2	<dl	9.21	44.1	4.56	0.890	<dl	<dl	<dl	<dl	0.070	0.012	2.16	0.382
NAMA-CCP-01.d	1.92	0.068	1.72	556	0.798	0.080	261	0.014	0.007	n.r.	146	<dl	24.7	2.14	*0.014	2.77	0.001	0.012	5.E-4	0.003	*0.001	*0.003	3.95	0.104
NAMA-CCP-05.d	2.46	13.5	1.90	534	0.200	0.140	289	<dl	0.007	n.r.	1.04	<dl	6.89	1.56	*0.019	2.75	0.003	0.024	0.004	<dl	0.064	*0.002	4.36	0.830
NAMA-CCP-04.d	3.11	*0.016	8.00	503	0.606	0.030	262	<dl	0.018	n.r.	163	<dl	27.2	2.05	0.044	2.30	0.005	0.003	<dl	0.008	0.014	*0.003	7.21	0.032
NAMA-CCP-03.d	2.70	*0.013	*0.025	474	0.593	0.020	256	<dl	<dl	n.r.	171	<dl	13.8	1.47	0.080	2.51	<dl	<dl	<dl	<dl	0.056	0.035	16.2	0.041
NAMA-CCP-06.d	2.25	15.6	*0.042	489	0.230	0.040	263	0.018	0.014	n.r.	0.890	<dl	6.59	0.990	*0.02	2.49	<dl	<dl	0.005	<dl	0.051	*0.002	6.18	0.900
NAMA-CCP-02.d	2.61	*0.011	*0.032	570	0.508	0.110	268	0.018	<dl	n.r.	238	<dl	26.0	2.19	*0.015	3.21	9.E-4	<dl	<dl	0.014	*0.001	*0.003	5.20	0.021
NEV01CCP-02.d	2.30	*0.004	0.160	73.3	0.770	0.590	914	<dl	<dl	n.r.	5.32	<dl	788	183	2.23	*0.023	0.015	<dl	<dl	<dl	*0.003	*0.002	2.72	1.13
NEV01CCP-03.d	2.93	0.180	20.0	817	0.800	1.85	86.0	0.037	0.034	n.r.	11.3	<dl	559	242	15.7	*0.043	1.10	<dl	0.041	<dl	*0.003	*0.003	10.8	3.68
NEV01CCP-01.d	2.50	*0.012	8.00	118	0.480	1.20	97.7	0.020	0.018	n.r.	5.12	2.E-4	703	176	1.10	*0.032	0.240	<dl	<dl	<dl	*0.003	0.110	1.22	0.521
NEV02CCP-02.d	2.07	0.063	0.670	356	1.85	0.430	*9.284	<dl	0.053	n.r.	4.15	<dl	246	1180	5.45	*0.025	0.140	0.005	0.004	0.020	*0.005	*0.002	3.22	*0.026
NEV02CCP-03.d	11.0	0.084	0.570	202	1.62	0.660	9.80	<dl	0.350	n.r.	3.25	<dl	298	1259	1.03	*0.009	<dl	0.020	0.004	0.012	*0.006	*0.001	0.710	*0.026
NEV02CCP-01.d	2.14	0.056	1.40	498	1.92	0.490	24.0	<dl	<dl	n.r.	4.40	<dl	250	1429	2.48	*0.016	0.006	0.076	0.008	<dl	*0.005	*0.006	1.92	*0.027
NEV02CCP-04.d	*0.315	0.036	3.00	201	2.24	0.930	315	0.180	0.085	n.r.	8.20	<dl	298	638	6.05	*0.021	0.140	0.020	0.080	0.063	*0.01	0.008	4.50	*0.034
QT01CCP-001.d	0.970	8.64	0.300	188	0.206	2.10	381	0.046	0.090	n.r.	257	<dl	48.4	116	0.197	0.520	0.003	0.003	0.013	0.017	1.88	0.008	3.91	4.14
QT01CCP-006.d	6.00	9.94	0.320	139	0.135	0.120	419	0.009	0.004	n.r.	274	<dl	50.1	108	0.303	0.630	0.001	0.003	0.002	<dl	3.72	*0.001	5.32	4.80
QT01CCP-005.d	0.580	10.0	4.60	115	0.132	0.160	396	0.020	<dl	n.r.	222	<dl	48.3	96.8	0.470	0.630	<dl	<dl	<dl	0.011	2.74	0.008	4.00	2.72
QT01CCP-004.d	1.90	11.6	23.0	139	0.169	1.90	363	0.100	0.008	n.r.	106	<dl	44.7	96.0	0.289	0.830	0.001	<dl	<dl	0.053	0.630	0.017	3.49	2.45
QT01CCP-003.d	0.570	8.88	13.0	182	0.200	1.40	404	0.036	0.006	n.r.	247	<dl	48.2	107	0.459	0.810	0.015	<dl	0.090	<dl	1.26	0.009	5.18	3.09
QT01CCP-002.d	0.830	8.47	15.0	157	0.138	2.40	401	0.012	0.005	n.r.	313	<dl	49.1	98.4	0.350	0.700	<dl	0.100	<dl	<dl	5.56	*0.001	5.55	4.67
QT0MTCCP-02.d	5.80	0.089	21.0	410	*0.041	0.240	169	0.012	0.044	n.r.	359	<dl	5.95	43.2	0.400	*0.051	0.006	0.074	0.016	<dl	0.080	*0.002	3.52	*0.052
QT0MTCCP-01.d	3.80	0.720	*0.005	469	*0.04	0.110	165	0.031	0.200	n.r.	398	0.616	6.16	36.2	*0.135	*0.037	<dl	<dl	<dl	0.038	*0.002	0.005	5.94	0.022
QT0MTCCP-07.d	12.0	0.180	34.0	308	0.161	0.028	151	0.024	0.054	n.r.	478	<dl	5.34	32.2	*0.006	*0.042	<dl	<dl	0.045	<dl	0.170	0.130	4.95	*0.127

Grain ID	Mn	Co	Ni	Zn	Ga	As	Se	Mo	Ru	Rh	Ag	Pd	In	Sn	Sb	Te	Re	Os	Ir	Pt	Au	Tl	Pb	Bi
	55	59	60	66	71	75	82	95	101	103	107	108	115	118	121	128	185	189	193	195	197	205	208	209
33um	1.017	0.029	0.322	0.590	0.033	0.149	3.828	5.311	0.030	0.020	0.027	0.026	0.033	0.155	0.047	0.400	0.501	0.012	0.028	0.007	0.016	0.006	0.029	0.012
55um	0.449	0.024	0.211	0.357	0.028	0.079	2.455	2.409	0.029	0.020	0.019	0.011	0.015	0.071	0.025	0.277	0.221	0.007	0.016	0.004	0.012	0.004	0.015	0.008
QT0MTCCP-05.d	4.30	0.067	29.0	311	0.810	<dl	166	0.030	<dl	n.r.	448	<dl	4.55	30.3	0.760	*0.07	<dl	<dl	0.210	0.011	*0.008	0.013	10.2	*0.005
QT0MTCCP-06.d	1.36	0.096	2.60	421	0.171	0.130	167	0.016	0.027	n.r.	393	0.275	4.96	66.2	0.191	*0.026	0.037	0.005	<dl	0.003	0.030	0.190	3.28	*0.086
QT0MTCCP-03.d	0.930	0.230	*0.016	289	0.180	0.011	167	0.008	0.019	n.r.	398	<dl	5.38	23.4	0.163	*0.031	1.50	0.006	<dl	0.004	0.070	0.016	4.27	0.260
QT0MTCCP-04.d	0.700	0.117	80.0	338	0.136	0.110	164	0.008	0.029	n.r.	399	<dl	4.66	39.6	0.492	*0.035	0.006	0.060	<dl	<dl	*0.003	0.008	4.27	*0.017
QT18CCP-003.d	3.10	10.7	0.610	125	0.197	0.280	406	0.027	<dl	n.r.	140	<dl	49.2	106	0.420	0.420	<dl	<dl	<dl	<dl	0.313	0.006	4.36	3.84
QT18CCP-001d	1.09	9.22	140	107	0.224	0.220	400	0.047	0.014	n.r.	140	<dl	47.6	105	0.710	0.700	0.004	0.018	0.002	<dl	0.495	0.028	5.60	2.82
QT18CCP-002.d	*0.196	9.61	*0.018	136	0.196	0.160	428	0.014	0.010	n.r.	205	<dl	49.2	111	0.440	0.620	<dl	<dl	<dl	<dl	1.66	0.140	6.13	4.56
QT18CCP-005.d	0.660	8.37	*0.023	135	0.149	<dl	366	0.055	0.080	n.r.	202	<dl	45.1	100	0.083	1.60	<dl	0.005	<dl	0.070	0.220	0.060	1.27	1.27
QT18CCP-004.d	*0.318	8.55	2.40	113	0.140	0.320	380	0.033	0.010	n.r.	111	<dl	46.6	90.7	0.310	0.410	0.045	<dl	<dl	<dl	*0.041	*0.001	2.28	1.88
QT18CCP-006.d	1.04	10.7	*0.014	101	0.154	0.800	373	0.039	<dl	n.r.	254	<dl	47.3	80.4	1.23	0.520	0.002	<dl	<dl	<dl	2.55	0.028	9.80	4.74
THA01-03.d	*0.151	*0.008	*0.005	394	4.66	0.100	3.20	<dl	0.012	n.r.	300	<dl	0.486	356	1.28	*0.012	<dl	<dl	<dl	<dl	0.010	0.118	2.11	*0.002
THA01-04.d	0.570	*0.01	*0.005	509	4.81	<dl	2.40	<dl	0.024	n.r.	326	<dl	0.377	414	0.297	*0.014	<dl	<dl	<dl	<dl	0.022	0.034	0.820	0.006
THA01-05.d	0.490	*0.008	*0.006	378	4.30	<dl	3.00	<dl	<dl	n.r.	324	<dl	0.709	267	0.188	*0.011	<dl	0.008	0.002	<dl	0.010	0.032	0.207	*0.002
THA01-02.d	*0.157	*0.01	*0.01	515	4.87	<dl	*1.013	0.011	0.027	n.r.	310	<dl	0.162	700	0.310	*0.026	<dl	<dl	<dl	<dl	0.026	0.026	0.261	0.010
V553221CCP-003.d	1.45	232	0.440	167	1.68	0.300	470	0.110	<dl	n.r.	46.5	<dl	5.66	59.2	*0.025	37.5	0.004	0.011	0.037	<dl	*0.004	*0.002	5.00	0.166
V553221CCP-002.d	2.22	258	1.60	175	24.0	0.680	306	0.013	<dl	n.r.	56.6	<dl	3.23	395	0.480	7.88	<dl	<dl	<dl	<dl	0.020	*0.001	0.047	0.314
V553221CCP-001d	4.70	246	0.630	137	8.69	0.710	420	0.150	0.006	n.r.	46.3	<dl	4.73	353	0.700	17.9	0.003	<dl	<dl	0.015	0.460	*0.001	0.029	0.607
V553221CCP-004.d	1.39	224	1.69	227	6.62	0.240	369	0.031	0.009	n.r.	30.9	<dl	4.71	195	*0.015	30.2	0.012	<dl	0.002	1.00	*0.004	*0.003	*0.016	0.178
V553221CCP-005.d	2.11	221	1.15	149	2.76	0.610	541	0.032	0.014	n.r.	65.3	<dl	5.24	73.1	*0.012	32.6	<dl	0.027	<dl	<dl	*0.004	*0.001	*0.011	0.037
V553221CCP-006.d	1.80	251	1.12	181	2.28	0.460	449	0.056	0.047	n.r.	116	0.016	6.45	77.3	*0.01	38.3	<dl	<dl	<dl	0.007	0.370	*0.002	0.051	0.069
V557324ACCP-008.d	1.49	318	6.00	1067	2.55	0.213	463	0.039	0.017	n.r.	8.32	<dl	1.50	162	*0.007	16.0	0.100	0.011	7.E-4	0.500	0.056	*0.002	0.076	0.240
V557324ACCP-003.d	1.46	106	3.90	351	0.670	0.460	986	0.500	0.005	n.r.	7.16	14.4	3.38	26.8	0.440	57.5	0.310	<dl	0.009	0.003	0.015	*0.001	1.20	0.111
V557324ACCP-004.d	5.60	144	3.80	753	10.0	0.480	184	0.045	0.022	n.r.	7.04	<dl	0.323	467	0.290	7.40	0.150	<dl	<dl	0.021	0.101	*0.002	0.084	1.22
V557324ACCP-001d	0.970	82.5	0.270	279	0.890	0.100	817	0.035	0.011	n.r.	6.58	<dl	2.10	50.2	*0.006	34.1	0.006	0.010	<dl	<dl	0.023	*0.002	0.073	0.279
V557324ACCP-002.d	1.15	95.2	18.0	331	0.850	0.097	619	0.025	0.029	n.r.	5.71	<dl	2.17	70.5	0.410	25.2	0.030	0.050	0.110	0.008	0.034	*0.002	0.076	0.324
V557324ACCP-007.d	1.31	349	30.0	955	2.96	0.480	417	5.00	0.018	n.r.	9.21	2.01	0.548	171	0.200	13.0	0.008	<dl	0.015	0.170	0.042	0.030	0.110	0.225
V557324ACCP-005.d	1.40	206	35.0	492	0.467	3.00	738	0.023	0.016	n.r.	7.61	<dl	2.16	33.3	0.130	27.8	0.460	0.007	0.200	0.054	2.40	0.070	0.016	0.126
V557324ACCP-006.d	1.42	220	10.0	1134	5.40	0.960	4.90	0.260	0.170	n.r.	7.59	<dl	0.029	7.70	*0.006	0.240	0.007	<dl	<dl	0.003	*0.001	0.110	3.50	0.028
V557327ACCP-002.d	2.10	239	80.0	140	4.28	1.17	503	0.240	0.010	n.r.	38.7	<dl	5.16	139	0.100	24.2	<dl	0.020	<dl	0.043	*0.004	*0.001	0.900	0.118
V557327ACCP-003.d	2.93	237	0.200	140	6.11	0.410	462	0.096	0.020	n.r.	45.6	<dl	6.06	202	*0.02	17.5	<dl	<dl	0.007	<dl	0.034	*0.002	0.082	0.283
V557327ACCP-004.d	5.50	263	4.90	151	2.24	0.900	822	0.049	<dl	n.r.	45.6	<dl	5.00	19.6	0.053	47.5	0.080	0.430	<dl	0.022	0.024	*0.002	0.066	0.277
V557327ACCP-001d	0.990	269	0.290	131	3.17	0.410	460	0.340	0.002	n.r.	24.2	<dl	1.62	172	0.076	18.6	0.007	<dl	0.004	<dl	0.019	*0.002	0.180	1.14
V557327ACCP-006.d	1.26	290	0.390	125	6.97	0.540	285	0.163	0.011	n.r.	36.3	<dl	0.993	192	0.084	8.22	<dl	<dl	0.010	0.014	0.044	*0.002	0.099	2.68
V557327ACCP-005.d	1.95	244	5.10	149	2.63	<dl	704	0.040	0.016	n.r.	50.3	<dl	5.64	319	*0.027	49.2	0.250	<dl	0.002	<dl	0.017	*0.001	*0.298	0.147

Grain ID	Mn	Co	Ni	Zn	Ga	As	Se	Mo	Ru	Rh	Ag	Pd	In	Sn	Sb	Te	Re	Os	Ir	Pt	Au	Tl	Pb	Bi
	55	59	60	66	71	75	82	95	101	103	107	108	115	118	121	128	185	189	193	195	197	205	208	209
33um	1.017	0.029	0.322	0.590	0.033	0.149	3.828	5.311	0.030	0.020	0.027	0.026	0.033	0.155	0.047	0.400	0.501	0.012	0.028	0.007	0.016	0.006	0.029	0.012
55um	0.449	0.024	0.211	0.357	0.028	0.079	2.455	2.409	0.029	0.020	0.019	0.011	0.015	0.071	0.025	0.277	0.221	0.007	0.016	0.004	0.012	0.004	0.015	0.008
V557327BCCP-03.d	2.60	242	0.580	165	4.57	0.600	420	0.023	0.040	n.r.	44.2	<dl	2.77	148	0.029	14.5	0.002	0.019	0.040	<dl	3.30	*0.002	0.132	0.870
V557327BCCP-07.d	1.97	225	0.520	187	3.17	<dl	676	0.052	0.009	n.r.	32.8	<dl	4.18	168	0.130	25.6	0.017	0.005	<dl	0.032	*0.004	*0.002	0.085	0.390
V557327BCCP-01d	1.67	136	1.60	230	9.87	0.400	322	0.080	0.160	n.r.	16.3	<dl	1.59	308	3.90	12.4	0.004	0.046	0.006	0.023	0.286	*0.001	0.507	1.53
V557327BCCP-06.d	2.80	306	0.430	173	19.8	0.520	210	0.370	0.044	n.r.	43.0	<dl	0.906	354	0.260	3.09	<dl	0.005	0.004	0.006	*0.02	0.021	0.412	0.749
V557327BCCP-04.d	1.87	326	0.350	166	1.72	0.170	728	0.070	0.001	n.r.	72.8	<dl	4.96	43.7	*0.006	31.4	<dl	<dl	0.001	0.003	*0.003	*0.002	*0.222	0.108
V557327BCCP-05.d	1.70	271	0.124	170	4.55	0.136	521	0.100	0.033	n.r.	95.4	1.05	3.66	137	3.20	18.1	<dl	<dl	0.190	0.013	0.500	2.20	0.480	0.243
V557327BCCP-02.d	2.06	233	1.70	160	2.07	0.150	1083	0.280	0.031	n.r.	23.9	<dl	4.18	34.3	*0.007	68.6	0.002	<dl	<dl	<dl	0.029	*0.002	0.114	0.126
WHB01-CCP-04.d	7.95	1.13	1.71	488	8.36	<dl	567	<dl	<dl	n.r.	97.3	<dl	3.58	3.53	49.3	2.14	<dl	<dl	<dl	0.007	*0.004	1.25	18.6	*0.003
WHB01-CCP-03.d	6.06	1.08	*0.037	462	8.78	<dl	692	<dl	0.003	n.r.	35.8	<dl	2.78	6.54	34.2	2.92	6.E-4	<dl	0.002	0.002	*0.002	0.570	15.6	*0.004
WHB01-CCP-01d	9.51	0.947	*0.041	710	8.92	<dl	387	1.90	0.013	n.r.	112	<dl	10.2	1.16	15.1	2.37	0.003	0.013	<dl	0.010	*0.002	0.670	15.5	*0.005
WHB01CCP-02.d	0.750	10.7	3.91	459	0.088	<dl	239	<dl	0.054	n.r.	37.4	<dl	13.1	0.850	19.1	2.28	<dl	<dl	<dl	<dl	0.050	0.470	17.9	3.37
WHB01-CCP-05.d	8.64	0.550	*0.034	529	8.80	<dl	761	<dl	0.007	n.r.	75.9	<dl	9.58	5.15	51.6	2.16	0.004	<dl	<dl	0.006	*0.002	1.92	51.4	*0.007
WV01-CCP-06.d	1.83	5.67	40.1	961	0.360	0.090	4580	0.026	<dl	n.r.	11.5	<dl	1.45	116	2.93	*0.091	0.007	<dl	0.001	<dl	*0.018	0.224	1.23	2.16
WV01-CCP-02.d	2.50	3.38	29.1	890	0.670	0.074	4240	0.098	0.024	n.r.	9.18	<dl	2.11	88.6	1.48	*0.086	0.010	0.011	<dl	0.007	0.050	*0.001	0.133	1.62
WV01-CCP-05.d	3.02	6.94	44.8	950	0.570	<dl	4390	0.034	0.008	n.r.	10.1	<dl	1.52	92.0	4.24	*0.094	<dl	<dl	<dl	<dl	*0.017	0.024	0.484	1.58
WV01-CCP-03.d	3.08	4.30	41.4	1086	0.590	0.061	4370	0.067	0.004	n.r.	13.8	<dl	1.62	101	8.50	*0.074	<dl	0.017	<dl	0.013	*0.02	0.048	0.558	4.68
WV01-CCP-04.d	2.54	5.23	47.4	1260	0.660	0.138	3980	0.030	<dl	n.r.	9.45	<dl	1.75	103	2.60	*0.077	0.007	<dl	<dl	<dl	*0.006	0.023	0.266	2.03
WV01-CCP-01d	2.64	6.48	50.4	1011	0.630	0.070	4240	0.043	0.027	n.r.	7.78	<dl	1.56	109	1.03	*0.082	<dl	<dl	<dl	0.008	*0.006	*0.001	0.120	1.17
ZAM01CCP-01d	1.37	0.069	17.0	174	7.76	0.560	1138	0.103	<dl	n.r.	0.850	0.006	238	1063	3.94	*0.037	<dl	0.059	0.029	0.029	0.018	*0.001	10.2	5.48
ZAM01CCP-06.d	0.650	0.037	22.0	133	6.11	0.830	988	0.073	0.009	n.r.	0.736	<dl	202	968	6.62	*0.048	<dl	<dl	<dl	0.050	*0.003	0.022	4.80	6.62
ZAM01CCP-03.d	1.90	3.70	60.0	196	8.09	0.800	1141	1.90	0.013	n.r.	0.590	<dl	244	1131	2.63	*0.051	0.009	0.007	0.110	<dl	0.080	0.006	1.44	3.17
ZAM01CCP-05.d	1.16	0.220	60.0	173	9.18	0.630	1144	<dl	0.047	n.r.	0.740	0.110	260	1120	5.75	*0.038	0.004	<dl	0.015	<dl	*0.003	0.011	2.31	4.16
ZAM01CCP-07.d	12.0	*0.031	0.410	189	7.01	2.00	1101	0.060	0.051	n.r.	1.01	<dl	209	1111	11.1	*0.112	<dl	<dl	0.004	0.012	*0.004	0.060	10.1	11.8
ZAM01CCP-04.d	19.0	0.800	0.300	160	9.01	0.540	1070	0.130	0.022	n.r.	0.390	<dl	249	929	5.01	*0.041	0.004	0.070	0.050	0.210	*0.003	0.022	2.94	4.62
ZAM01CCP-02.d	0.470	0.030	2.70	194	7.37	0.600	1036	0.074	0.190	n.r.	0.750	<dl	237	1029	3.69	*0.034	<dl	<dl	<dl	<dl	*0.003	0.012	2.10	3.63

(*) values calculated with IrEM imputation algorithm considering detection limit in each analysis. <dl: below detection limit. 1Informative values. n.r. not reported.

Annexe B4 Analyses reference materials used in the calibration of the LA-ICP-MS and in-house reference materials used to monitor the data quality. Concentrations in ppm. In bold-italic elements retained for further statistical analysis

	Element	Ti	*Mn*	*Co*	*Ni*	Cu	*Zn*	*Ga*	Ge	*As*	*Se*	*Mo*	*Ru*	*Rh*	*Ag*
	Isotope	49	*55*	*59*	*60*	65	*66*	*71*	74	*75*	*82*	*95*	*101*	*103*	*107*
Median of detection	55um	0.553	0.479	0.016	0.207	0.270	0.024	0.079	0.348	2.41	0.029	0.020	0.004	0.049	0.011
limits (ccp)	33um	0.661	1.03	0.028	0.410	0.526	0.051	0.149	0.582	5.31	0.030	0.020	0.007	0.100	0.026
Reference materials used for calibration		GSE-1g	GSE-1g	GSE-1g	GSE-1g	MASS1	MASS1	GSE-1g	GSE-1g	MASS1	MASS1	MASS1	Po-727	Po-727	GSE-1g
	Working value	450	590	380	440	134000	210000	490	320	65	51	59	36.5	41.6	200
	sd	42	20	20	30	500	5000	70	80	3	4	9	0.3	0.3	20
Values obtained for reference materials used as monitors															
UQAC-FeS1	Working value	298	56.3	643	25680	22542	260	*9.26*		1056	346	65.5	68.5	63.7	176
	Uncertainty	18.8	7.50	19.4	1769	902	31.9	1.00		116	42.0	3.70	5.00	3.50	19.6
This study	Average	465	46.6	637	24615	21643	287	9.03		1158	299	65.1	68.0	61.8	173
n = 83	sd	131	41.5	52.7	2814	1113	52.6	5.01		60.4	68.6	2.37	2.65	3.48	14.3
	RSD (%)	28.1	89.0	8.27	11.4	5.14	18.3	55.5		5.21	22.9	3.64	3.90	5.62	8.27
	rel. diff (%)	56.3	-17.2	-0.898	-4.15	-3.99	10.7	-2.48		9.74	-13.5	-0.541	-0.797	-2.97	-1.64
PTC-1b	Working value	696	193	3253	112900	79700	2083			222	120	*11.0*		*0.500*	53.1
	Uncertainty	4.10	1.80	38.0	1000	1000	38.0			17.0	11.0	1.00		1.00	1.00
This study	Average	759	179	3206	108956	82469	3093			307	127	6.54		0.798	66.1
n = 48	sd	130	11.7	239	12323	3092	469			81.5	14.2	2.19		0.435	38.8
	RSD (%)	17.1	6.53	7.46	11.3	3.75	15.1			26.6	11.2	33.5		54.4	58.7
	rel. diff (%)	9.08	-7.31	-1.46	-3.49	3.47	48.5			38.3	5.68	-40.6		59.7	24.6
CCu-1e	Working value	*54.9*	96.0	301	*7.27*	230700	30200	*3.00*	*1.00*	1010	*304*	*16.1*			205
	Uncertainty	1.90	4.00	6.00	0.430	2400	300	nd	nd	30.0	8.00	0.700			3.40
This study	Average	195	86.6	331	281	215859	42525	3.03	3.45	1302	292	18.5			227
n = 53	sd	116	14.3	23.0	669	6682	3895	0.315	0.541	146	21.1	33.1			36.7
	RSD (%)	59.6	16.5	6.94	238	3.10	9.16	10.4	15.7	11.2	7.22	179			16.2
	rel. diff (%)	256	-9.81	10.1	3772	-6.43	40.8	1.11	245	28.9	-3.85	14.9			10.6
	Others		MASS1	MASS1	MASS1		GSE-1g					GSE-1g			MASS1
	Working value		280	60.0	97.0		460					390			50.0
	Uncertainty		80.0	10.0	15.0		10.0					30.0			5.00
This study	Average		254	69.4	116		449					382			68.5
n = 49 (MASS1)	sd		21.1	1.44	24.1		90.9					8.58			3.54
n = 39 (GSE-1g)	RSD (%)		8.31	2.08	20.8		20.2					2.25			5.16
	rel. diff (%)		-9.41	15.7	19.8		-2.37					-2.16			37.0

	Element	*Pd*	Cd	*In*	*Sn*	*Sb*	*Te*	*Re*	*Os*	*Ir*	*Pt*	*Au*	*Tl*	*Pb*	*Bi*
	Isotope	*108*	111	*115*	*118*	*121*	*128*	*185*	*189*	*193*	*195*	*197*	*205*	*208*	*209*
Median of detection	55um	0.061	0.007	0.070	0.017	0.221	0.007	0.016	0.004	0.010	0.006	0.004	0.006	0.004	0.006
limits (ccp)	33um	0.118	0.012	0.147	0.027	0.501	0.012	0.028	0.007	0.018	0.014	0.007	0.011	0.007	0.004
Reference materials	used for calibration	Po-727	MASS1	GSE-1g	MASS1	MASS1	MASS1	GSE-1g	Po-727	Po-727	Po-727	Po-727	MASS1	MASS1	GSE-1g
	Working value	43.4	60	370	59	60	15	78.9	46.7	48	35.5	45.8	50	68	320
	sd	0.3	7	60	6	9	-	7.7	2.6	1.2	0.8	2.4	1.0	7.0	30
Values obtained for reference materials used as monitors															
UQAC-FeS1	Working value	52.4		9.50	183	92.6	151	65.2	86.6	62.8	60.1	66.2		91.1	120
	Uncertainty	8.70		1.10	18.3	15.3	24.7	11.6	11.8	10.1	13.6	9.70		7.70	16.6
This study	Average	43.6		10.5	180	86.5	145	54.9	89.1	57.0	49.0	64.4		79.6	125
n = 83	sd	3.89		1.04	11.5	16.5	60.4	3.81	3.61	2.83	5.33	4.50		7.71	11.7
	RSD (%)	8.93		9.95	6.39	19.1	41.7	6.94	4.05	4.97	10.9	6.98		9.69	9.36
	rel. diff (%)	-16.8		10.3	-2.04	-6.59	-4.26	-15.8	2.89	-9.26	-18.5	-2.73		12.6	4.43
PTC-1b	Working value	9.46	*38.0*		*120*	*6.00*	*30.0*							795	
	Uncertainty	0.200	1.00		1.00	1.00	1.00							1.50	
This study	Average	8.00	92.9		132	6.28	34.0							965	
n = 48	sd	4.25	12.0		9.07	0.655	9.92							90.5	
	RSD (%)	53.1	12.9		6.89	10.4	29.2							9.37	
	rel. diff (%)	-15.5	144		9.70	4.66	13.3							21.4	
CCu-1e	Working value		74.2	*6.00*	*13.7*	104	61.8					20.3	2.70	7030	*3.00*
	Uncertainty		1.90	nd	nd	3.00	2.60					0.520	0.090	90.0	nd
This study	Average		152	6.29	27.0	113	61.8					11.0	2.27	7807	2.88
n = 53	sd		20.7	0.512	83.3	34.1	21.2					7.51	0.213	720	0.490
	RSD (%)		13.6	8.14	309	30.2	34.3					68.5	9.36	9.22	17.0
	rel. diff (%)		105	4.77	97.1	8.57	0.017					-46.0	-15.9	11.0	-4.03
	Others			MASS1								MASS1	GSE-1g	GSE-1g	MASS1
	Working value			50.0								47.0	2.00	378	60.0
	Uncertainty			nd								nd	0.200	12.0	nd
This study	Average			62.5								49.3	1.31	319	65.7
n = 49 (MASS1)	sd			2.05								3.26	0.164	22.8	2.29
n = 39 (GSE-1g)	RSD (%)			3.28								6.61	12.5	7.12	3.49
	rel. diff (%)			25.0								4.95	-34.3	-15.5	9.43

italic: informational/provisional values. Interference of ^{115}Sn on ^{115}In on calibrant (GSE-1g) is negligible (0.27 %) and therefore correction not applied. Interference of $^{40}Ar^{63}Cu$ on ^{103}Rh on calibrant (Po-727) is negligible (4.63%) and therefore correction not applied. Interference of $^{40}Ar^{61}Ni$ on ^{101}Ru on calibrant (Po-727) is negligible (7.84%) and therefore correction not applied. Interference of ^{115}Sn on ^{115}In on UQAC-FeS1 is negligible (6.22%) and therefore correction not applied. Interference of $^{40}Ar^{63}Cu$ on ^{103}Rh on UQAC-FeS1 is negligible (3.55%) and therefore correction not applied.Interference of $^{40}Ar^{61}Ni$ on ^{101}Ru on UQAC-FeS1 is negligible (0.73%) and therefore correction not applied. RSD (%) : relative standard deviation. sd: standard deviation. rel. diff (%): relative difference. n: number of analyses

Annexe B5 Information of the deposits from literature data used to test RF models.

	Deposit name	n	Location	Setting	Host tectonostratigraphic complex	Sample type	Data source
Studies with all elements							
VMS	Vorta	8	Romania	Mafic		Massive sulfides	George et al. (2018)
VMS	Sulitjelma	111	Norway	Bimodal-mafic[1]	Upper Allochthon Caledonides		
SMS	Ashadze-2	7	Mid-Atlantic Ridge	Ultramafic		Hydrothermal chimneys - massive sulfides	Melekestseva et al. (2020a)
SMS	Kairei	16	Central Indian Ridge	Ultramafic		Massive sulfides	Wang et al. (2018)
Studies with missing elements							
VMS	Çayeli	58	Turkey	Bimodal-felsic	Pontide orogenic belt	Paleo-hydrothermal chimneys - massive sulfides	Revan et al. (2014)
VMS	Kutlular	9					
VMS	Apliki	55	Cyprus	Mafic	Troodos ophiolite	Massive sulfides, massive stockwork and disseminated	Martin et al. (2019)
VMS	Phoenix	21					
VMS	Phoucasa	20					
VMS	Three Hills	15					
VMS	Kokkinoyia	17					
VMS	Mala	3					
VMS	Mathiatis N	15					
VMS	Kalavsos	4					
VMS	Dergamysh	22	Russia	Ultramafic	Main Uralian Fault	Paleo-hydrothermal chimneys - massive sulfides	Melekestseva et al. (2020b)
VMS	Maria Teresa	27	Perú	Bimodal-felsic	West Peruvian Trough	Massive sulfides	Torró et al. (2022)
VMS	Cerro de Maimón	11	Dominican Republic	Mafic[1]	Ozama shear zone	Massive sulfides	Torró et al. (2022)
SMS	Roman Ruins	77	Papua New Guinea	Bimodal-felsic		Hydrothermal chimneys - massive sulfides	Wohlgemuth-Ueberwasser et al. (2015)
SMS	Satanic Mills	25	Papua New Guinea				
SMS	Logatchev	29	Mid-Atlantic Ridge	Ultramafic			

n: number of analyses. 1contested classification

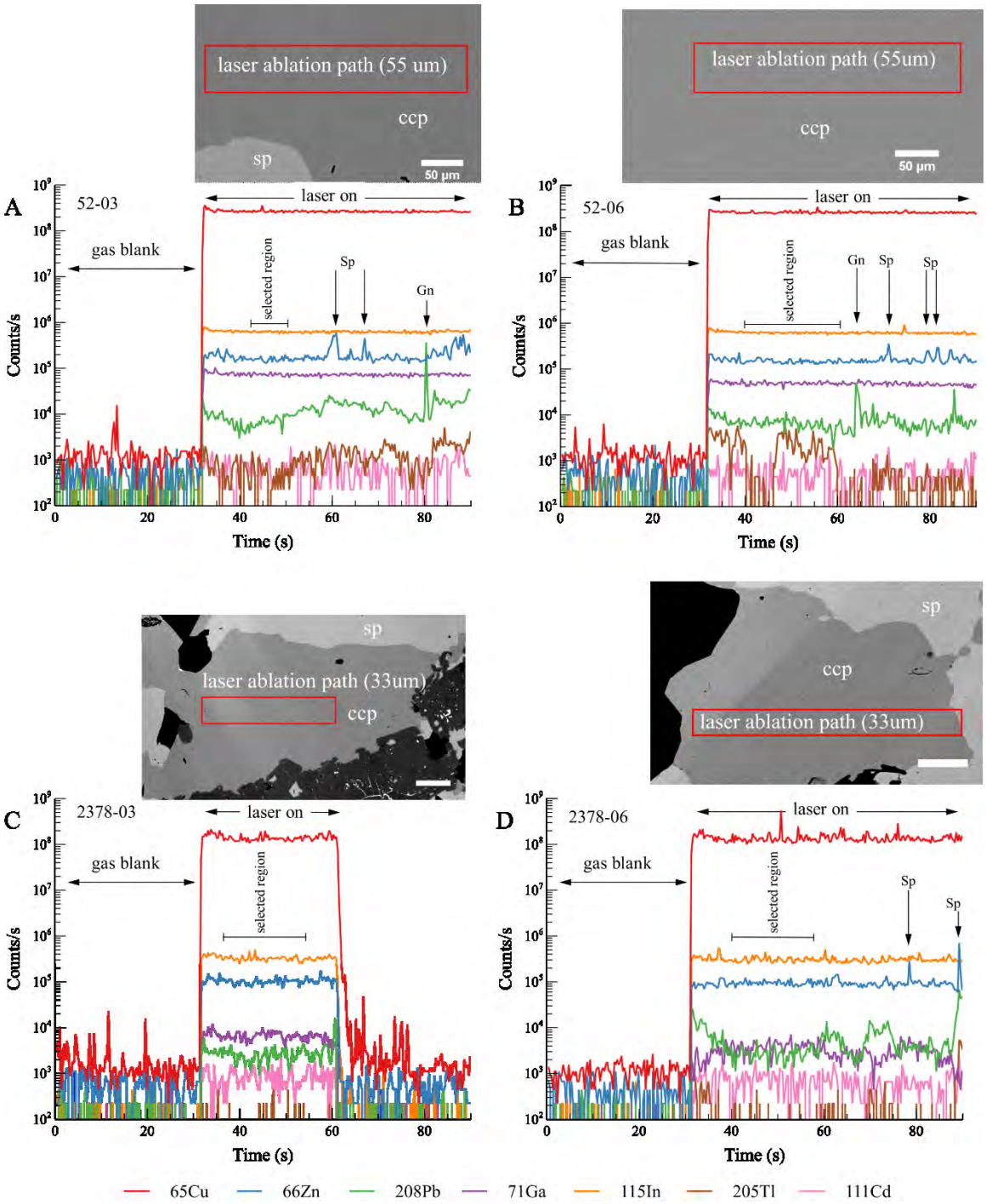

Annexe B6 Backscattered electron images and time-signal spectra for chalcopyrite in Zn-rich samples with inclusions of sphalerite (Sp). Inclusion-free regions were selected to obtain chalcopyrite trace element composition.

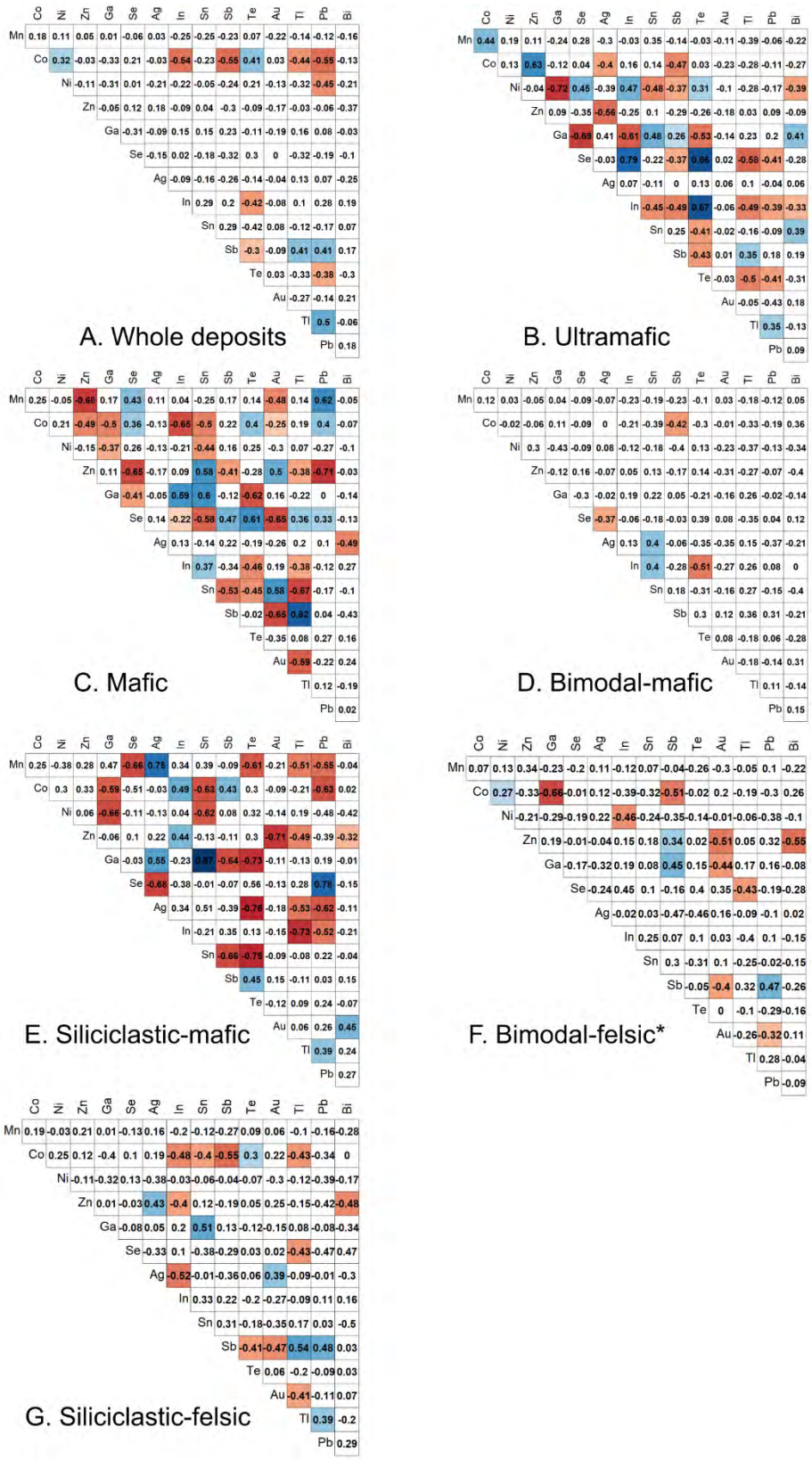

Annexe B7 Pearson correlation coefficient (r) of the trace elements in chalcopyrite from VMS and SMS deposits.

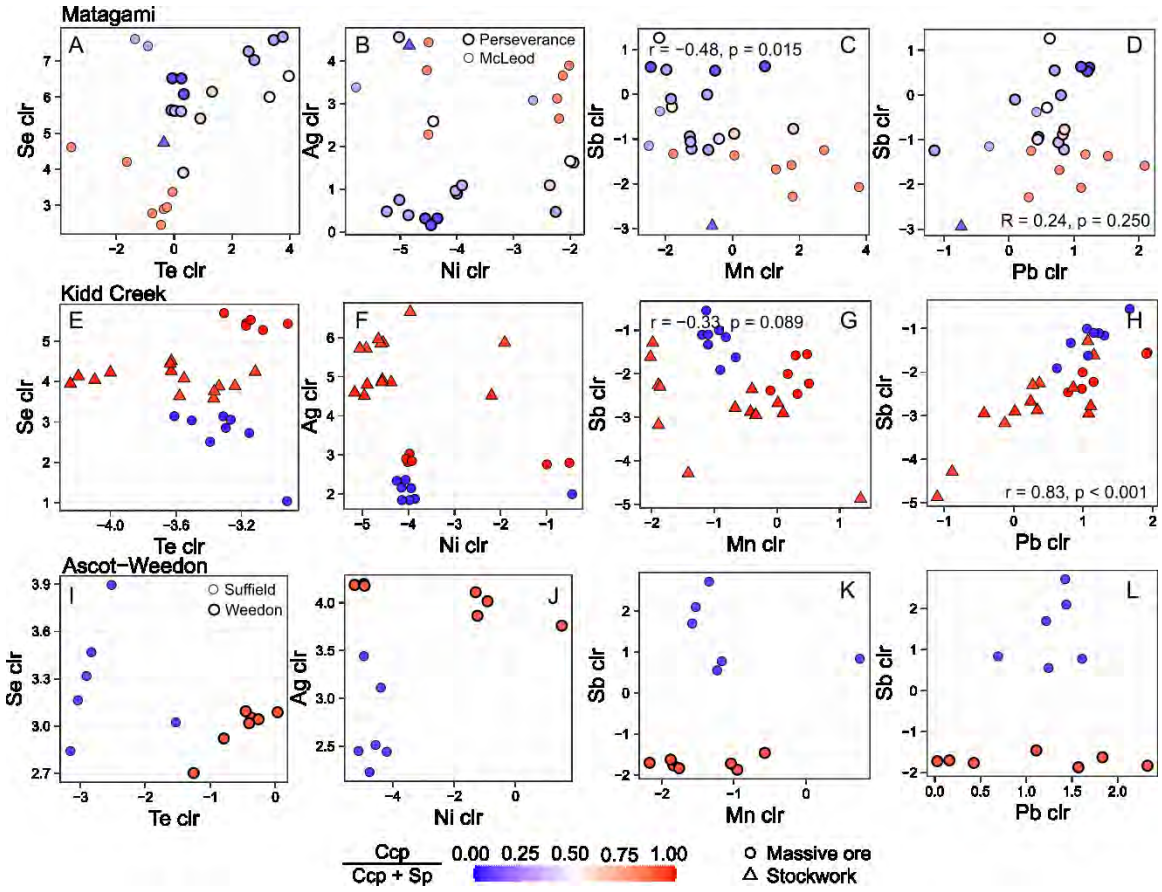

Annexe B8 Binary diagrams showing variation of trace elements in chalcopyrite from Matagami, Kidd Creek and Ascot-Weedon deposits, according to ccp/(ccp+sp) ratio.

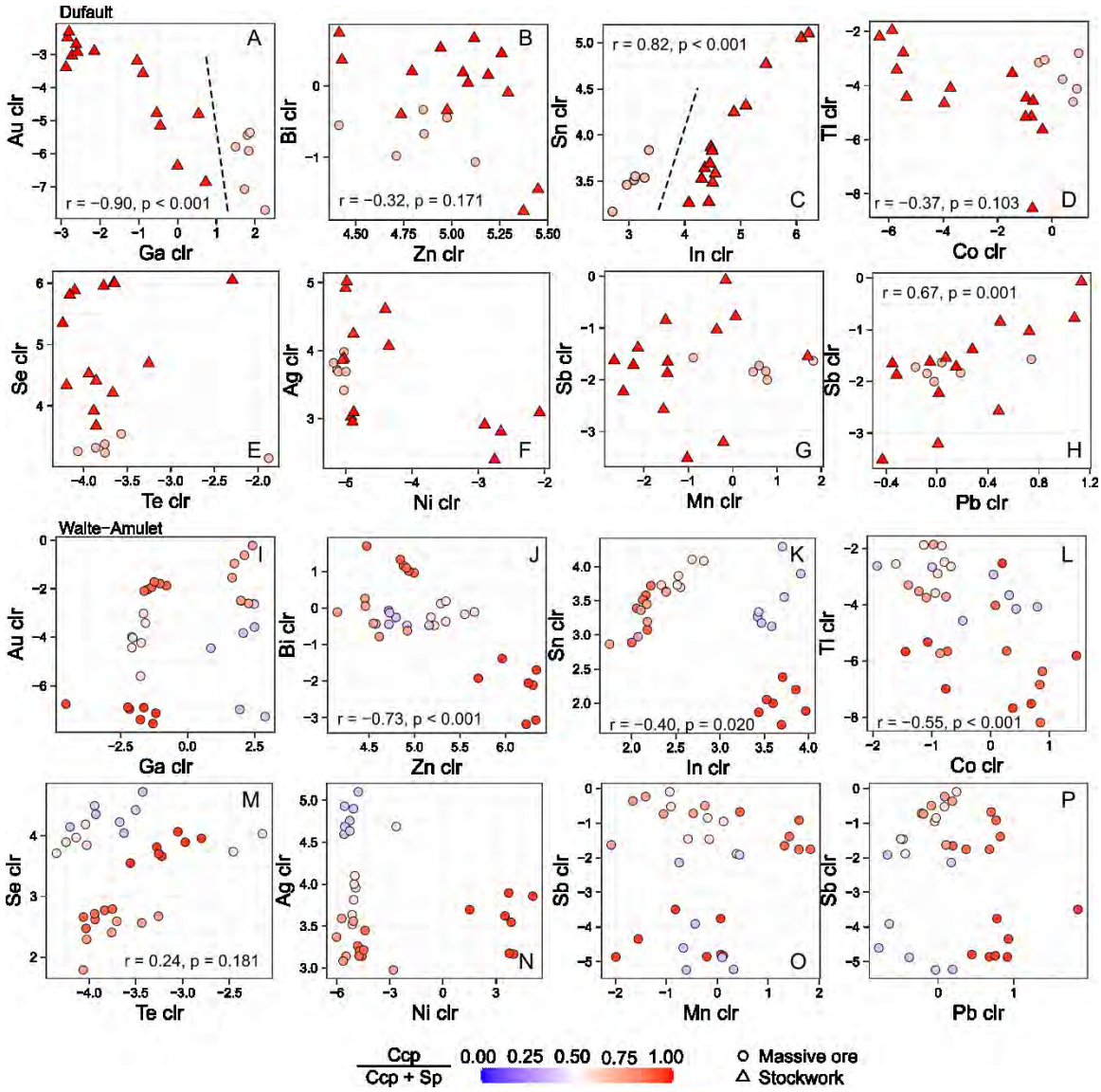

Annexe B9 Binary diagrams showing variation of trace elements in chalcopyrite from Dufault and Waite-Amulet deposits, according to ccp/(ccp+sp) ratio.

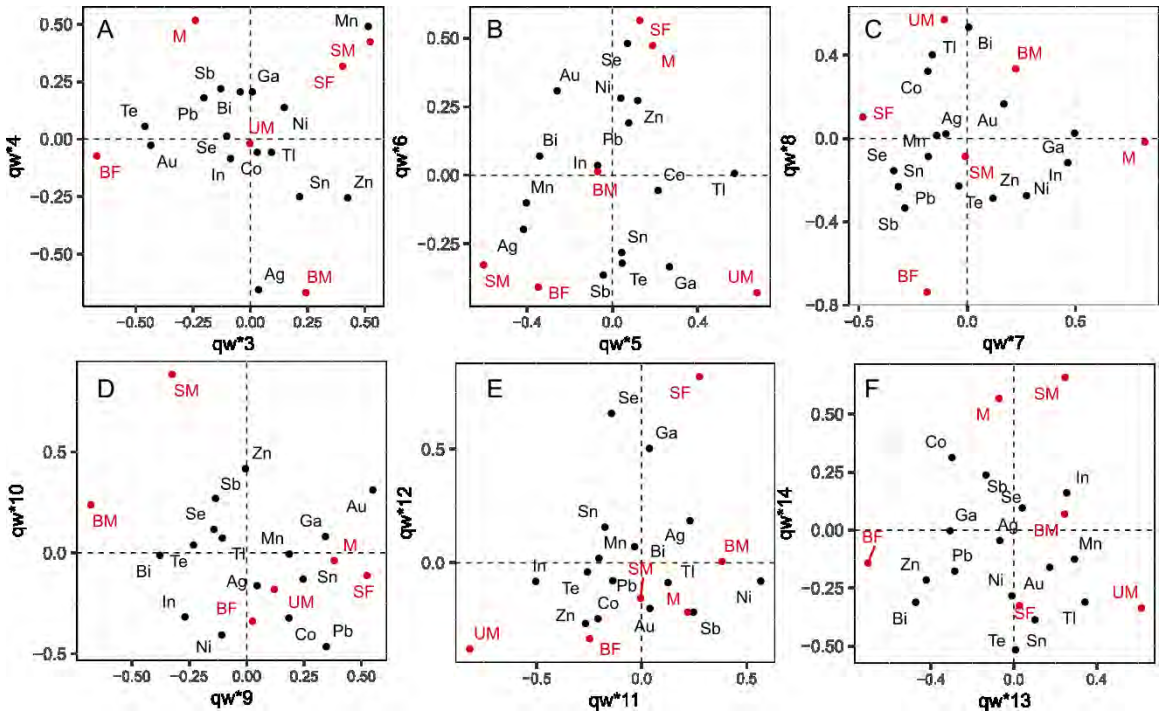

G

Latent variables	t1	t2	t3	t4	t5	t6	t7	t8	t9	t10	t11	t12	t13	t14
Explained variance	24.7	11.8	8.3	8.2	6.6	7.2	4.8	5.4	4.8	3.2	6.0	3.6	3.2	2.1
Cumulative explained variance	24.7	36.5	44.8	53.0	59.7	66.9	71.6	77.0	81.8	85.0	91.0	94.6	97.9	99.9
Perfomance	Accuracy=0.48		Kappa=0.29		Recall=0.38		F1-score=0.53							

Annexe B10 Biplots for PLS-DA results by subtype of VMS deposits showing correlations between elements and classes in other latent variables (A-F). (G) Explained variance by latent variable and cumulative explained variance. UM: ultramafic, M: mafic, BM: bimodal-mafic, SM: siliciclastic-mafic, BF: bimodal-felsic, SF: siliciclastic-felsic.

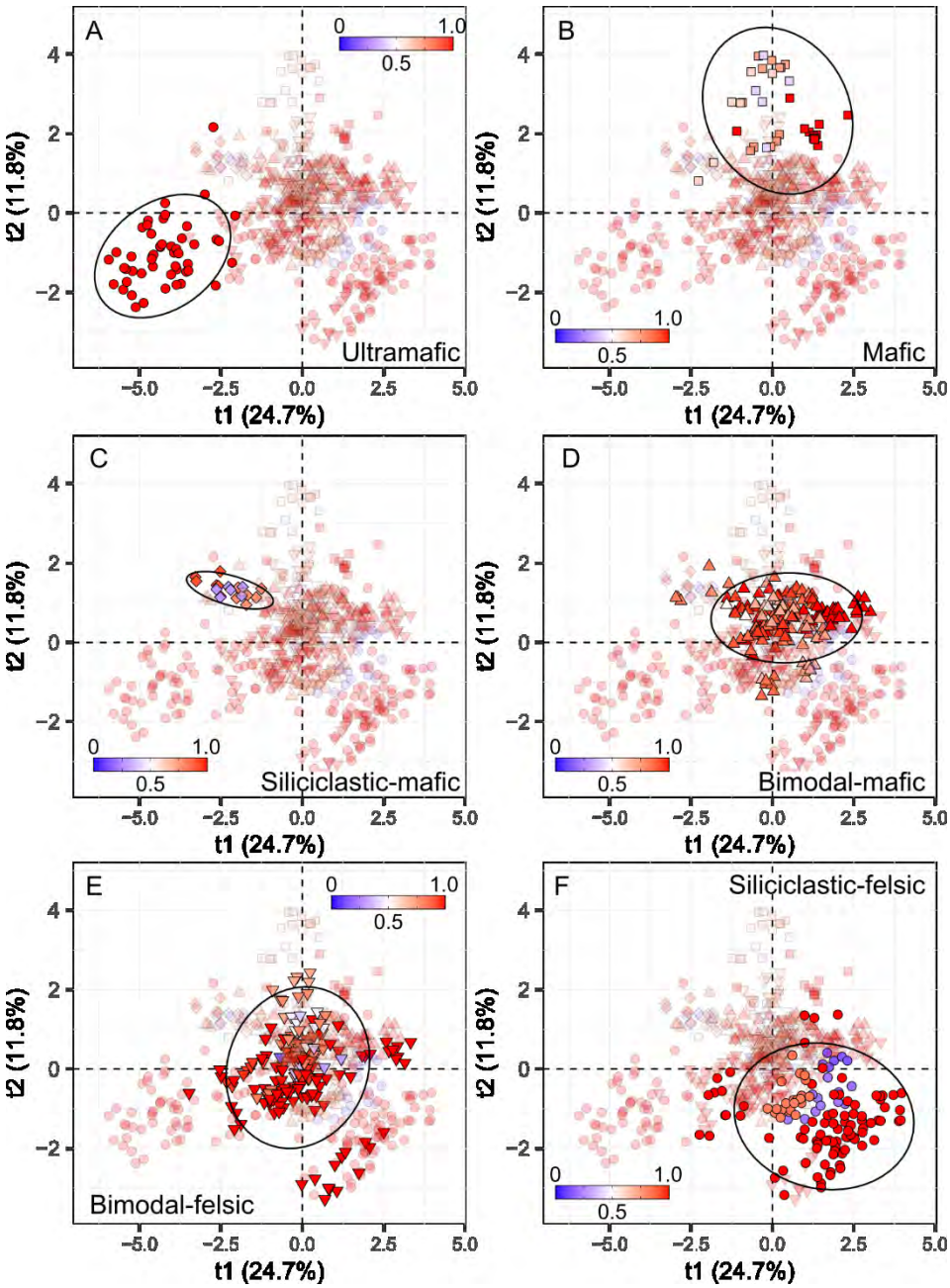

Annexe B11 Ccp/(ccp+po) ratio projected on score plot t1-t2 from PLS-DA results by VMS subtype.

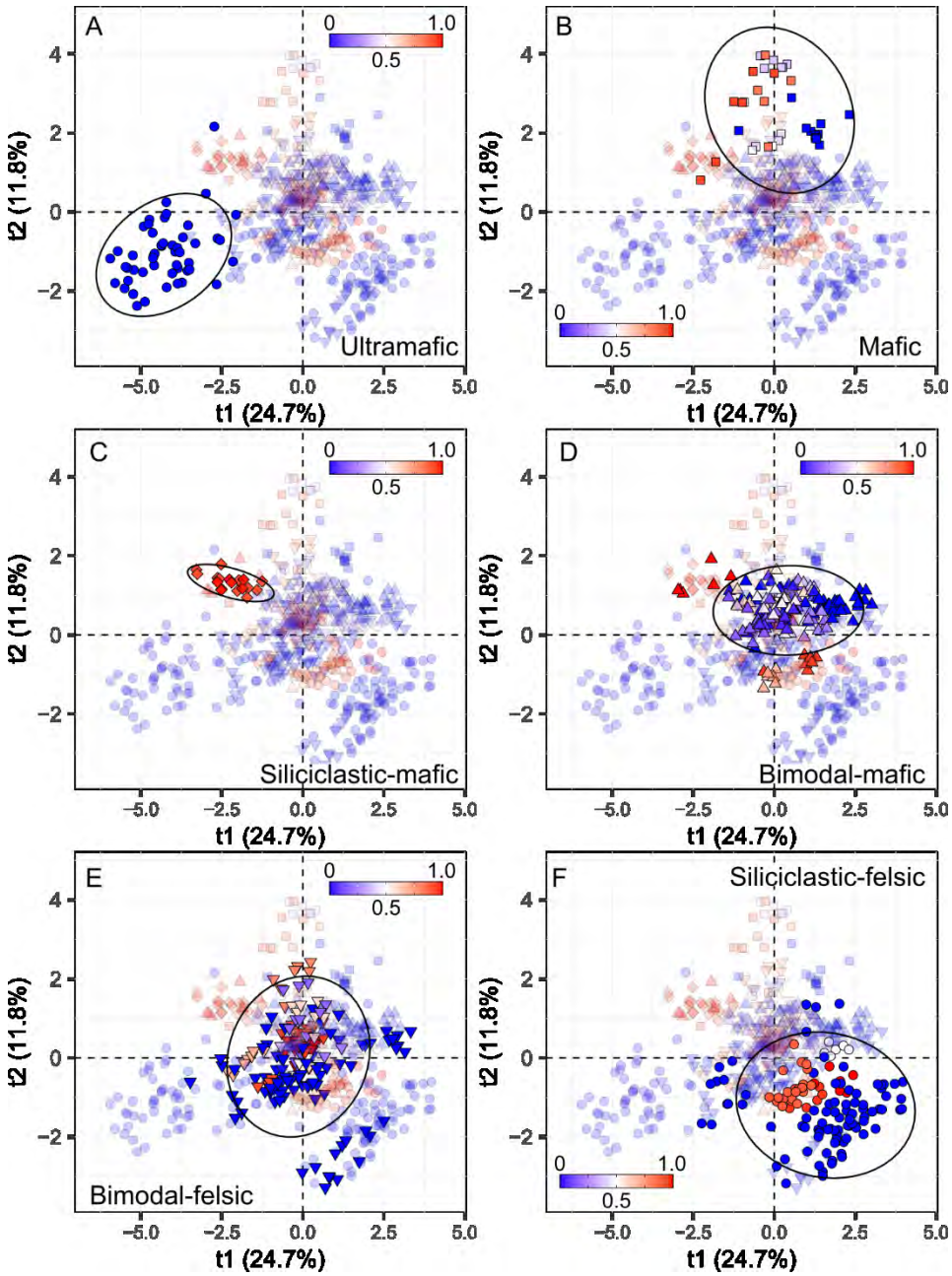

Annexe B12 Po/(po+py+sp) ratio projected on score plot t1-t2 from PLS-DA results by VMS subtype.

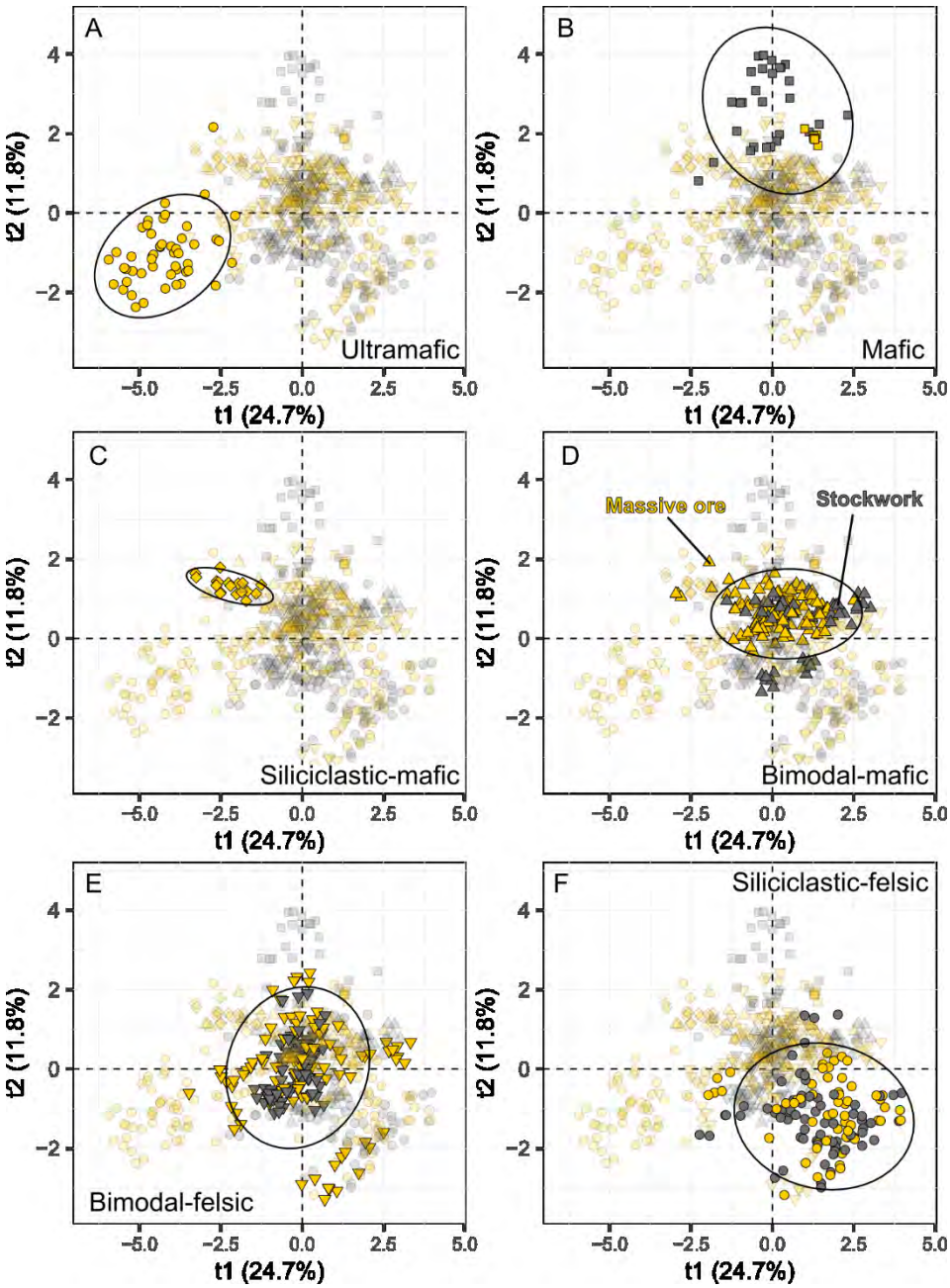

Annexe B13 Ore type projected on score plot t1-t2 from PLS-DA results by VMS subtype.

Performance metrics calculation

Performance metrics used in this study were calculated based on a confusion matrix for the classification model, whereas for the regression case, these were calculated from actual (y) and predicted values ($\hat{y}$). For the binary classification problem case we consider a positive and negative class, from which we can calculate: 1) the True positives (TP): the number of observations belonging to the positive class predicted as positive, 2) the True Negatives (TN): the number of observations belonging to the negative class predicted as negative, 3) the False Positives (FP): the number of observations belonging to negative class predicted as positive, and 4) the False Negatives (FN): the number of observations belonging to positive class predicted as negative. For multiclass problems the metrics are calculated with a "one-versus-all" approach (Annexe B14). From these values, performance metrics can be computed (Annexe B15). Recall, specificity, precision, and F1-score are calculated by class and then averaged.

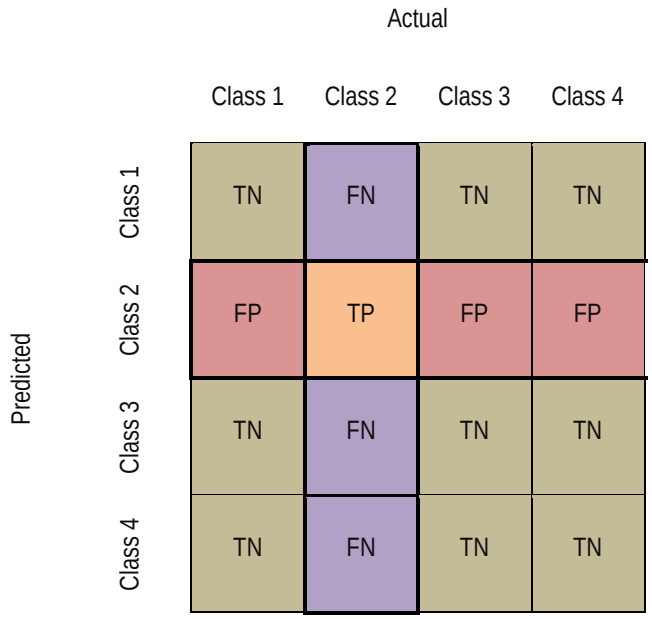

Annexe B14 Example of confusion matrix for multiclass problem (e.g., 4 classes).

Annexe B15 Performance metrics for multiclass classification and regression models. l: number of classes; n: total of observations. From Grandini et al. (2020); Kuhn (2008); Kvålseth (1985); Sokolova and Lapalme (2009).

Estimator	Formula	Description
Classification performance		
Accuracy (Acc)	$\frac{\sum_{i=1}^{l} TP_i}{n}$; $[0,1]$	Overall effectiveness
Kappa (K)	$\frac{Acc - P_e}{1 - P_e}$; $[0,1]$ where P_e is the hypothetical probability of chance agreement	Measure representing the dependence obtained by chance between the predicted and the true classification measure
Mean Recall ($Recall_M$)	$\frac{1}{l}\sum_{i=1}^{l}\frac{TP_i}{TP_i + FN_i}$; $[0,1]$	Effectiveness to identify positive labels

Estimator	Formula	Description
Mean Specificity (Spe_M)	$\frac{1}{l}\sum_{i=1}^{l}\frac{TN_i}{TN_i + FP_i};\ [0,1]$	Effectiveness to identify negative labels
Mean Precision (Pre_M)	$\frac{1}{l}\sum_{i=1}^{l}\frac{TP_i}{TP_i + FP_i};\ [0,1]$	Effectiveness to identify the truly positive labels
Mean F1 ($F1_M$)	$2 \times \frac{Recall_M \times Pre_M}{Recall_M + Pre_M};\ [0,1]$	Harmonic mean of recall and precision
Balanced accuracy (Bacc)	$\frac{\sum_{i=1}^{l} Recall_i}{l};\ [0,1]$	Accuracy when classes are unbalanced
Regression performance		
Root Mean Squared Error (RMSE)	$\sqrt{\frac{1}{n}\sum_{i=1}^{n}(y_i - \hat{y}_i)^2}$	Standard deviation of residuals
Mean Absolute Error (MAE)	$\frac{1}{n}\sum_{i=1}^{n}\lvert y_i - \hat{y}_i \rvert$	Variance of the residuals
Coefficient of determination (R^2)	$1 - \frac{\sum_{i=1}^{n}(y_i - \hat{y}_i)^2}{\sum_{i=1}^{n}(y_i - \bar{y})^2};\ [0,1]$	Proportion of the total variation of y (about its mean) that is explained (accounted for) by the fitted model

Annexe C

Annexes correspondant à l'article: Trace element composition of chalcopyrite as a tool for deposit type discrimination: a machine learning approach

Annexe C1. Detailed information of the studied deposits (dataset A). n: number of analyses.

Class	Type	Sample	n	Deposit name	Host tectonostratigraphic complex (age)	Location	Sulfide texture	Host rocks composition	Regional metamorphism	References
Hydrothermal	Epithermal gold	ROZ2	2	Rozalia	Central Slovakia Volcanic Field (15.0–11.4 Ma)	Banská Bystrica, Slovakia	Disseminated	Andesites	Unmet	Koděra et al. (2005); Kubač et al. (2018)
		2123	7	Palisades	Sonoma Volcanic Suite (2.8-3.2 Ma)	Calistoga, California, USA		Tuff, rhyolite and dacitic flows		Sherlock (2005)
		2125	8							
		PLS1	4							
		PLS2	2							
		2776	6	Federal	Connecticut Valley-Gaspé Synclinorium (0.39 Ga)	Gaspésie, Quebec, Canada		Mudstones	Greensch	D'Hulst (2007); Pilote (2005)
		2780	6							
		2807	6							
		2811	6				Massive			
		2819	6				Massive			
		2190	3	Cactus Queen	Middle Buttes Volcanic Dome Complex (16-21 Ma)	Mojave, California, USA	Disseminated	Quartz latite to rhyolite	Unmet	Albers (1981); Blaske et al. (1991); Burnett and Brady (1990)
		CM1	6	Comstock Lode	Walker Lane Structural Belt (25–50	Nevada, USA		Andesitic to dacitic rocks - lacustrine sedimentary rocks		Berger et al. (2003)
		CM2	6			Nevada, USA				
		1908	6	Camp Bird	Silverton Caldera (32 Ma)	San Juan, Colorado, USA	Semi-massive			Lipman et al. (1976); Rosemeyer (1990)
		1911	1	Sunnyside	San Juan-Uncompahgre Caldera (28 Ma)	Silverton, Colorado, USA	Disseminated	Latites - volcaniclastic rocks		Casadevall and Ohmoto (1977)
		1912	2							
		1914	7				Disseminated			
		1915	4				Semi-massive			

Class	Type	Sample	n	Deposit name	Host tectonostratigraphic complex (age)	Location	Sulfide texture	Host rocks composition	Regional metamorphism	References
Hydrothermal	IOCG	363	6	Candelaria	Candelaria Shear Zone (111 Ma)	Atacama, Copiapó, Chile	Disseminated	Andesites - volcanoclastic rocks	Unmet	Barra et al. (2017); Marschik and Fontboté (2001); Mathur et al. (2002)
		367	5							
		414	6							
		422	6							
		516	7							
		CND	7							
		PC1492	5							
		PC9174	6							
		PC98102	6				Semi-massive			
		PC99069	5							
		SF1	7	San Fernando	Cortés Terrain (111 Ma)	Baja California, Mexico	Disseminated	Gabbros - tonalites		Camprubí and González-Partida (2017)
		AF443	7	Alvo 118	Carajás Domain (1.88 Ga)	Carajás Mineral Province, Pará, Brazil	Semi-massive	Metavolcanic rocks - granitoid and gabbro rocks	Amph	Pollard et al. (2019); Torresi et al. 2012; Trunfull et al. (2020)
		AN01	6	Antas Norte			Massive	Volcanic rocks - gabbro dykes		Xavier et al. (2019); Pollard et al. (2019); Trunfull et al. (2020)
		AN02	6				Semi-massive			
		AN03	5							
		ALE	6	Igarapé Bahia/Alemao			Disseminated	Metavolcanic, metapyroclastic and metasedimentary rocks		Grainger et al. (2008); Melo et al. (2019); Pollard et al. (2019); Ronzê et al. (2000); Trunfull et al. (2020)
		ALEMAO	6				Semi-massive			
		F332B	4				Disseminated			
		F392	7							
		PI01	7	Pista			Massive	Felsic metavolcanic rocks - gneisses		Pollard et al. (2019); Trunfull et al. (2020)
		PI02	5				Semi-massive			
		SAL03	7	Salobo			Massive	Gneis and granitoids, amphibolite, and metasedimentary rocks		

Class	Type	Sample	n	Deposit name	Host tectonostratigraphic complex (age)	Location	Sulfide texture	Host rocks composition	Regional metamorphism	References
Hydrothermal	IOCG	F259	6	Sossego	Carajás Domain (1.88 Ga)	Carajás Mineral Province, Pará, Brazil	Massive	Granites	Amph	Moreto et al. (2015); Pollard et al. (2019); Trunfull et al. (2020)
		F263P	7				Disseminated			
		S080	6							
		S081	7				Massive			
		S084	7							
		SOS01	6							
		SOS02	7							
		194	5	Eloise	Eastern Fold Belt (1.76-1.78 Ga)	Cloncurry, Queensland, Australia	Semi-massive	Meta-arkoses, mica schists, amphibolites	Greensch - Amph	Chen (2013); Williams and Skirrow (2000)
		196	5				Massive			
		600	6							
		EH1	4	Ernest Henry			Disseminated	Metavolcanic rocks		Chen (2013); Kendrick et al. (2007); Mark et al. (2000); Mark et al. (2006); Williams and Skirrow (2000)
		EH3	8							
		EH4	6							
		CHA01	7	Chandman Uul	Gobi-Kherlen Belt (0.44 Ga)	Dornogobi, Mongolia	Semi-massive	Andesitic - pyroclastic rocks	Greensch	Gerel et al. (2021); Oyunjargal et al. (2020)
		EG113	5	Manxman	Eastern Gawler Craton (1.57 Ga)	Olympic Dam, South Australia, Australia	Massive	Quartz monzodiorite, quartz monzonite and granite	No evidence	Bastrakov et al. (2007); Direen and Lyons (2007); Macmillan (2016); Oreskes and Einaudi 1992; Verdugo-Ihl et al. (2017)
		EG198	5							
		EG204	6							
		EG216	5							
		EG2412	6				Semi-massive			
		2081017	5	Punt Hill			Disseminated	Volcanic - metasedimentary rocks		Reid et al. (2011)
		2129484	4				Semi-massive			
		LALA4	5	Lala	Yangtze block (1.7–1.5 Ga)	Sinchuan, China	Disseminated	Metasedimentary and metavolcanic rocks	Greensch - Amph	Zeng et al. (2018); Zhao and Zhou (2011); Zhimin and Yali (2013); Zhu et al. (2018)
		LALA5	6							

Class	Type	Sample	n	Deposit name	Host tectonostratigraphic complex (age)	Location	Sulfide texture	Host rocks composition	Regional metamorphism	References
Hydrothermal	Orogenic gold	C48121A	7	Beaufor	Abitibi Greenstone Belt (2.7 Ga)	Abitibi-Temiscamingue, Québec, Canada	Disseminated	Diorites	Greensch	Grzela et al. (2019); Roussy (2003); Tremblay (2001)
		MAL06	8	Malartic				Metasedimentary rocks - monzodiorites - granodiorites		De Souza et al. (2015); Sciuba and Beaudoin (2021)
		06A	6	Amaruq	Rumble Assemblage (2.7 Ga)	Amaruq, Nunavut, Canada		Ultramafic to felsic volcanic/intrusive and sedimentary rocks	Greensch - Amph	de Bronac de Vazelhes et al. (2021); Liu et al. (2021); Valette et al. (2020)
		18A	7						Greensch	
		25A	6							
		26A	5							
		49A	6				Semi-massive			
		HUGO02A	6	Hougou	Shuiquangou Complex (0.28 Ga)	Chincheng, Hebei, China	Disseminated	Syenites		Cook et al. (2009)
		HUGO02B	5							
		KOCH01	4	Kochkar	East Uralian Zone (0.35 Ga)	Kochkar, Urals, Russia	Disseminated	Gneiss - metavolcanic - metasedimentary rocks		Kolb et al. (2005)
		YOU01A	7	Young-Davidson	Abitibi Greenstone Belt (2.7 Ga)	Matachewan, Abitibi, Québec, Canada	Semi-massive	Syenites		Sciuba and Beaudoin (2020); Zhang et al. (2014a); Zhang et al. (2014b)
		YOU01B	7							
		LEGA05	6	Lega Dembi	Megado belt (0.54 Ga)	Megado, Sidamo-Borana, Ethiopia	Disseminated	Gneisses - volcanosedimentary rocks	Greensch - Amph	Billay et al. (1997); Liu et al. (2021); Tadesse (2004)
		LEGA06	6							
		BULY01	7	Bulyanhulu	Sukumaland Greenstone Belt (2.80-2.65 Ga)	Mwanza, Tanzania		Argillites - mafic volcanic rocks - rhyodacites	Greensch	Chamberlain (2003); Lawley et al. (2014)
		BULY02	7							

Class	Type	Sample	n	Deposit name	Host tectonostratigraphic complex (age)	Location	Sulfide texture	Host rocks composition	Regional metamorphism	References
Hydrothermal	Orogenic gold	BULY05	7	Bulyanhulu	Sukumaland Greenstone Belt (2.80-2.65 Ga)	Mwanza, Tanzania	Semi-massive	Argillites - mafic volcanic rocks - rhyodacites	Greensch	Chamberlain (2003); Lawley et al. (2014)
		3232	5	Linglong	North China Craton (0.12 Ga)	Shandong, China	Disseminated	Granites	Amph - Granul	Deng et al. (2020); Li et al. (2008); Wen et al. (2015)
		3195A	6	Cononish mine	Beinn Chuirn Anticline (0.40 Ga)	Stirling, Scotland	Massive	Metasedimentary rocks	Amph	Spence-Jones et al. (2018)
		3195B	6				Disseminated			
		3196A	6							
		3196B	3							
		RALE01	5	Raleigh	Zuleika Shear Zone (0.26 Ga)	Western Australia, Australia		Andesites - volcanogenic sediments	Greensch	Sciuba and Beaudoin (2021); Tripp (2013)
	Porphyry	501	6	Highland Valley	Mount Polley Intrusive Complex (0.20 Ga)	British Columbia, Canada		Volcaniclastics rock - basalts - sedimentary rocks	Unmet	Plouffe et al. (2016)
		651	8	Ajax-Afton	Quesnellia Terrane (0.21 Ga)			Sedimentary - volcanic rocks		McMillian et al. (1996); Ross et al. (1995)
		2086	3	Copper Mountain			Semi-massive			Celis et al. (2013)a; Celis et al. (2013)b; McMillian et al. (1996)
		90667	5	Mt. Milligan			Disseminated			Jago et al. (2014)
		NAF3	7	New Afton			Semi-massive			McMillian et al. (1996); Ross et al. (1995)
		NAF45	7	New Afton			Disseminated			
		GC06200	4	Galore Creek	Stikinia Terrane		Semi-massive	Volcanic and clastic sedimentary rocks		Byrne and Tosdal (2014); Micko et al. (2014)
		2045	6	Granisle	Wrangellia Terrane (0.16 Ga)		Disseminated	Volcanic rocks - clastic rocks		Dirom et al. (1995); Wilson et al. 1980; Zaluski et al. (1994)
		2047	6				Semi-massive			
		2048A	8				Disseminated			

Class	Type	Sample	n	Deposit name	Host tectonostratigraphic complex (age)	Location	Sulfide texture	Host rocks composition	Regional metamorphism	References
Hydrothermal	Porphyry	2048B	6	Granisle	Wrangellia Terrane (0.16 Ga)	British Columbia, Canada	Disseminated	Volcanic rocks - clastic rocks	Unmet	Dirom et al. (1995); Wilson et al. 1980; Zaluski et al. (1994)
		BU7101	4	Bolong	Gangdese Belt (0.12-0.11 Ga)	Duolong, Tibet, China		Sedimentary rocks	Unmet?	Li et al. 2012; Yang et al. (2020); Zhu et al. (2015)
		DB0004	6	Duobuza					Unmet?	
		JC7	8	Jinchang	Central Asian Orogenic Belt (0.20 Ga)	Jinchang, Hebei, China	Semi-massive	Granites	Unmet?	Zhang et al. (2014a); Zhao et al. (2019)
		OYU	6	Oyu Tolgoi	Tien Shan Mineral Belt (0.37 Ga)	Mongolia	Disseminated	Basalts - basaltic andesite - clastic sedimentary rocks	Greensch	Kirwin et al. (2005); Perello et al. (2001); Porter (2016)
		ALT08	5	Altar	Central Volcanic Zone (20-21 Ma)	San Juan, Argentina		Andesitic - dacitic lava flows	Unmet	Maydagán et al. (2013); Zwahlen et al. (2014)
		ALT4	5							
		3237	7	Xiongcun	Gangdese Belt (0.12-0.11 Ga)	Tibet, China		Diorites	Greensch	Tafti et al. (2014); Tang et al. (2015)
		2104A	6	Binghampton	Uinta–Cortez Axis (37-39 Ma)	Utah, USA	Disseminated	Quartzites - limestones	Unmet	Maughan et al. (2002); Redmond et al. (2004); Redmond and Einaudi (2010)
		2104B	7							
		2098	6	Utah Copper Mine						
		3241	7	Jiama	Gangdese Metallogenic Belt (15 Ma)	Xizang, Tibet, China		Volcaniclastic and clastic sedimentary rocks	Unmet?	Zheng et al. (2016)
	Skarn	450	6	Gaspé Copper	Connecticut Valley-Gaspé Synclinorium (0.39 Ga)	Gaspésie, Québec, Canada	Semi-massive	Carbonaceous silty limestones - calcareous siltstones - shales	Greensch	Allcock (1982); Shelton (1983); Wares and Berger (1995)
		457	5							
		654	7							
		2503	6				Disseminated			
		2506	7							

Class	Type	Sample	n	Deposit name	Host tectonostratigraphic complex (age)	Location	Sulfide texture	Host rocks composition	Regional metamorphism	References
Hydrothermal	Skarn	2513	8	Gaspé Copper	Connecticut Valley-Gaspé Synclinorium (0.39 Ga)	Gaspésie, Québec, Canada	Disseminated	Carbonaceous silty limestones - calcareous siltstones - shales	Greensch	Allcock (1982); Shelton (1983); Wares and Berger (1995)
		2515	5							
		2517	7							
		2518	6							
		M301	5	Mactung	Tombstone-Tungsten Belt (90–96 Ma)	Northwest Territory, Canada	Disseminated	Limestones	Unmet	Elongo et al. (2020)
		MTPo1	4							
		CEZGR	6	Cantung		Yukon, Canada				
		COPPoB	5							
		MARN	6	Marn						Brown and Nesbitt 1987; Burke et al. (2005); Hart et al. (2000)
	VMS	LS1	7	Lasail	Semail Ophiolite (95 Ma)	Al Batinah North, Oman	Massive	Basalts and basaltic andesites	Unmet	Gilgen et al. (2014); Stakes and Taylor (2003)
		LS10	7				Disseminated			
		AZN01	6	Aznalcollar	Iberian Pyrite Belt (0.34-0.38 Ga)	Andalucia, Spain	Massive	Rhyolite-dacite / phyllite-quartzite	Prehnite-pumpellyite	Almodóvar et al. (2019); Barrie et al. (2002); Inverno et al. (2015); Relvas et al. (2001); Relvas et al. (2006); Sáez et al. (1999); Tornos (2006)
		THA01	4	Tharsis			Semi-massive			
		ALJ01	6	Aljustrel		Beja, Portugal	Massive			
		COR01	5	Corvo						
		COR02	7							
		COR03	10							
		COR04	6				Disseminated			
		GRA01	6	Graça			Massive			
		NEV01	3	Neves			Massive			
		NEV02	4							
		ZAM01	7	Zambujal						
		1872	6	Suffield Mine	Ascot-Weedon Complex (0.45 Ga)	Cantons de l'Est, Quebec, Canada		Felsic volcaniclastic rocks	L Greensch	Gauthier et al. (1994)
		1869	7	Weedon						

Class	Type	Sample	n	Deposit name	Host tectonostratigraphic complex (age)	Location	Sulfide texture	Host rocks composition	Regional metamorphism	References
Hydrothermal	VMS	V553221	6	Irinovskoe	Mid-Atlantic Ridge (?)	Irinovskoe field, Atlantic Ocean	Semi-massive	Peridotite-gabbronorite	Unmet	Cherkashev et al. (2013); Petersen et al. 2009; Wohlgemuth-Ueberwasser et al. (2015)
		V557324A	8				Massive			
		V557327A	6				Semi-massive			
		V557327B	7							
		64ROV11	7	Candelabra	Mid-Atlantic Ridge (1-60 ka)	Logatchev-1 field, Atlantic Ocean	Massive			
		64ROV2	4				Semi-massive			
		53ROV13	6	Irina I			Massive			
		35GTV2B2	6	Irina II						
		LDR01	6	Little Deer	Dunnage Zone - Notre Dame Subzone (0.48 Ga)	Lushs Bight, Newfoundland, Canada	Massive	Pillow basalt	L Greensch	Kean et al. (1995); Piercey (2007)
		WHB01	5	Whalesback			Semi-massive			Cloutier et al. (2015); Piercey (2007)
		2925	6	Hajar	Guemassa Massif (0.34 Ga)	Marrakech-Safi, Morocco	Massive	Rhyolite-rhyodacite		Admou et al. (2018); Marcoux et al. (2008); Moreno et al. (2008)
		2924	6	Draa Sfar	Jebilet Massif (0.34 Ga)					
		2653	6	Poirier	Abitibi Greenstone Belt (2.7 Ga)	Joutel, Quebec, Canada		Rhyolite-dacite / andesite-basalt		Barrie et al. (1999); Dubé et al. (2007); Franklin et al. (2005); Gaboury and Pearson (2008); Lafrance et al. (2000); Mercier-Langevin et al. (2007); Shriver and MacLean (1993); Taylor et al. (2014); Genna et al. (2014a); Genna et al. (2014b); Ioannou et al. (2007)
		972146	4	Caber		Matagami, Quebec, Canada		Rhyolite		
		972149	3							
		972257	3				Semi-massive			
		E612164	5	McLeod				Rhyolite-rhyodacite		
		E612166-A	1				Disseminated			
		E612167	2							

Class	Type	Sample	n	Deposit name	Host tectonostratigraphic complex (age)	Location	Sulfide texture	Host rocks composition	Regional metamorphism	References
Hydrothermal	VMS	E612171-A	2	McLeod	Abitibi Greenstone Belt (2.7 Ga)	Matagami, Quebec, Canada	Semi-massive	Rhyolite-rhyodacite	L Greensch	Barrie et al. (1999); Dubé et al. (2007); Franklin et al. (2005); Gaboury and Pearson (2008); Lafrance et al. (2000); Mercier-Langevin et al. (2007); Shriver and MacLean (1993); Taylor et al. (2014); Genna et al. (2014a); Genna et al. (2014b); Ioannou et al. (2007)
		972224	3	Perseverance			Massive			
		972228	3							
		E612152-A	2				Semi-massive			
		E612154-B	2				Massive			
		E612155-A	4							
		E612162-A	1							
		3112	5	Tétrault	Greenville Province	Montauban, Quebec, Canada		Quartz-biotite and quartz-sillimanite gneiss	Amph	Tomkins (2007); Stamatelopoulou-Seymour and MacLean (1984)
		B5109	6	Bathurst	Bathurst Mining Camp (0.47 Ga)	New Brunswick, Canada	Semi-massive	Rhyolite-rhyodacite	U Greensch	Goodfellow (2007); Mireku and Stanley (2006)
		B5110	5							
		B7157	5							
		B7158	5							
		07MPBR23	5	Halfmile Lake			Disseminated			
		BVMS01	5	Boundary	Dunnage Zone - Exploits Subzone (0.51 Ga)	Newfoundland, Canada	Massive	Dacite-rhyolite / basalt	L Greensch	Buschette and Piercey (2016); Piercey (2007)
		3147	7	Duck Pond						McNicoll et al. (2010); Piercey (2007)
		LB01	6	Little Bay	Dunnage Zone - Notre Dame Subzone (0.48 Ga)		Semi-massive	Pillow basalt		Kean et al. (1995); Piercey (2007)
		3143	5	Ming				Boninite / basalt / rhyolite	U Greensch	Brueckner et al. (2014); Brueckner et al. (2015); Pilote et al. (2020); Pilote and Piercey (2013)

Class	Type	Sample	n	Deposit name	Host tectonostratigraphic complex (age)	Location	Sulfide texture	Host rocks composition	Regional metamorphism	References
Hydrothermal	VMS	MN1	7	Ming	Dunnage Zone - Notre Dame Subzone (0.48 Ga)	Newfoundland, Canada	Massive	Boninite / basalt / rhyolite	U Greensch	Brueckner et al. (2014); Brueckner et al. (2015); Pilote et al. (2020); Pilote and Piercey (2013)
		MN2	6							
		MN3	7				Semi-massive			
		MN4	6				Massive			
		NAMA01	6	York Harbour	Humber Zone - Bay of Islands Ophiolite (0.48 Ga)		Semi-massive	Pillow basalt		Lode et al. (2015); Piercey (2007)
		2722	6	Aldermac	Abitibi Greenstone Belt (2.7 Ga)	Noranda, Quebec, Canada	Massive	Rhyolite-andesite	L Greensch	Barrie et al. (1999); Dubé et al. (2007); Franklin et al. (2005); Gaboury and Pearson (2008); Lafrance et al. (2000); Mercier-Langevin et al. (2007); Shriver and MacLean (1993); Taylor et al. (2014); Genna et al. (2014a); Genna et al. (2014b); Ioannou et al. (2007)
		2729	6				Semi-massive			
		2730	6				Massive			
		2643	6	Dufault						
		2647	7				Disseminated			
		2652	7				Semi-massive			
		2211	6	Horne			Massive			
		2215	5				Disseminated			
		2221	7				Massive			
		2224	6				Semi-massive			
		56	6	Norbec			Disseminated			
		2704	6							
		51	5	Normetal			Massive			
		53	7	Quémont			Semi-massive			
		2359	6				Massive			
		QT01	6				Semi-massive			

Class	Type	Sample	n	Deposit name	Host tectonostratigraphic complex (age)	Location	Sulfide texture	Host rocks composition	Regional metamorphism	References
Hydrothermal	VMS	QT0MT	7	Quémont	Abitibi Greenstone Belt (2.7 Ga)	Noranda, Quebec, Canada	Semi-massive	Rhyolite-andesite	L Greensch	Barrie et al. (1999); Dubé et al. (2007); Franklin et al. (2005); Gaboury and Pearson (2008); Lafrance et al. (2000); Mercier-Langevin et al. (2007); Shriver and MacLean (1993); Taylor et al. (2014); Genna et al. (2014a); Genna et al. (2014b); Ioannou et al. (2007)
		QT18	6							
		52	7	Waite-Amulet			Massive	Rhyolite		
		601	6				Semi-massive			
		2296	7				Massive			
		2318	7							
		2325	6							
		53ROV6	8	Roman Ruins	Pual Ridge (20-50 ka)	Pacmanus field, Papua New Guinea		Dacite-rhyolite	Unmet	Binns et al. (2007); Hannington et al. (2005); Reeves et al. (2011)
		31ROV13C	7	Satanic Mills						
		27ROV8	6	Snowcap						
		LS22	7	Lagoa Salgada	Iberian Pyrite Belt (0.34-0.38 Ga)	Setúbal, Portugal	Semi-massive	Rhyolite-dacite / phyllite-quartzite	Prehnite-pumpellyite	Almodóvar et al. (2019); Barrie et al. (2002); Inverno et al. (2015); Relvas et al. (2001); Relvas et al. (2006); Sáez et al. (1999); Tornos (2006)
		LOU01	7	Lousal			Massive			
		62	7	Kidd Creek	Abitibi Greenstone Belt (2.7 Ga)	Timmins, Ontario, Canada	Semi-massive	Rhyolite-ultramafic	L Greensch	Barrie et al. (1999); Dubé et al. (2007); Franklin et al. (2005); Gaboury and Pearson (2008); Lafrance et al. (2000); Mercier-Langevin et al. (2007); Shriver and MacLean (1993); Taylor et al. (2014); Genna et al. (2014a); Genna et al. (2014b); Ioannou et al. (2007)
		2369	7							
		2378	8				Massive			
		2383	6							

Class	Type	Sample	n	Deposit name	Host tectonostratigraphic complex (age)	Location	Sulfide texture	Host rocks composition	Regional metamorphism	References
Hydrothermal	VMS	2410	6	Adak	Bothnia-Skelleftea Unit (1.8 Ga)	Västerbotten, Sweden	Disseminated	Felsic volcanic rocks	L Greensch	Allen et al. (1996); Årebäck et al. (2005); Johansson (2017); Skyttä et al. (2020)
		2417	5				Massive			
		2414	6	Brannmyran			Semi-massive			
		2394	6	Lindsköld			Massive			
		2398	6				Semi-massive			
		2399	6							
		2393	6	Rävliden				Felsic to mafic volcanic rock/argilites		
		2575	6	Ely	Vermont Copper Belt (0.41 Ga)	Vermont, USA	Massive	Metabasaltic amphibolite/metasedimentary rocks and minor mafic metavolcanics	U Greensch	McWilliams et al. (2010); Slack et al. (2001)
		2567	6	Pike Hill						
		2569	6	Pike Hill						
		ICEVMS01	5	Ice	Slide Mountain terrane (0.28 Ga)	Yukon, Canada	Massive	Basalt	L Greensch	Piercey et al. (2008)
		WV01	6	Wolverine	Yukon-Tanana Terrane (0.34 Ga)		Semi-massive	Mafic and felsic volcanic rocks / dark clastic rocks	M Greensch	
Magmatic	Ni-Cu sulfide	2523	6	Marbridge	Kidd-Munro assemblage (2.71 Ga)	Abitibi, Quebec, Canada	Net textured/globular	Peridotites	Amph	Barnes et al. (2007); Boutroy et al. (2014); Sproule et al. (2005)
		J12	7	Jinchuan	Jinchuan Complex (0.82 Ga)	Gansu, China			Greensch	Chen et al. (2015); Song et al. 2009, Ripley et al. (2005)
		J2	2				Massive			
		J3	6							
		J9B	6							
		MS2	7	Kotselvaara	Pechenga Complex (2.50 Ga)	Kola Peninsula, Russia	Net textured/globular	Ferropicrites	Prehnite-pumpellyite	Barnes et al. (2001); Brügmann et al. (2000); Hanski et al. (2011); Lagueux (1999)
		MS3	4							

Class	Type	Sample	n	Deposit name	Host tectonostratigraphic complex (age)	Location	Sulfide texture	Host rocks composition	Regional metamorphism	References
Magmatic	Ni-Cu sulfide	MS10	7	Semilekta	Pechenga Complex (2.50 Ga)	Kola Peninsula, Russia	Net textured/globular	Ferropicrites	Prehnite-pumpellyite	Barnes et al. (2001); Brügmann et al. (2000); Hanski et al. (2011); Lagueux (1999)
		MS12	5				Massive			
		MS8	7							
		IGCP4	5	Zhdanovskoe			Disseminated			
		A2	7	Medvezhy Creek	Noril'sk-Talnakh Intrusion (0.25 Ga)	Krasnoyarsk Krai, Russia	Massive	Basaltes - picritic rocks	Unmet	Barnes et al. (2006); Boutroy et al. (2014); Duran et al. (2017a); Krivolutskaya (2016); Naldrett (1997)
		NR6	5							
		T1	5	Talnakh						
		T11	8	Talnakh						
		T2	8	Talnakh						
		T3	7							
		T4	8							
		E1	4	Eagle	Eagle Intrusion (1.10 Ga)	Michigan,USA	Disseminated	Troctolites		Boutroy et al. (2014); Ding et al. 2010; Ripley (2014)
		E13	3							
		E4	6				Massive			
		DC18	7	Dunka Road	Duluth Complex (1.10 Ga)	Minnesota, USA	Net textured/globular	Norites - gabbronorite - troctolite - peridotites		Naldrett (2004); Thériault (1999); Samalens et al. (2017)
		DC69	7							
		B138405	4	Mesaba						
		B138439	6	Mesaba	Duluth Complex (1.10 Ga)					
		EDEEP	5	Eastern Deeps	Voisey's Bay Nain Plutonic Suite (1.33 Ga)	Newfoundland, Canada	Massive	Anorthosites - granites - troctolites		Boutroy et al. (2014); Naldrett (2004); Ripley and Li (2011); Salim Amaral (2017)
		OVOID	7	Ovoid						
		VB21	6				Net textured/globular			
		VB25	5				Massive			
		VB27	4							
		VB29	2							

Class	Type	Sample	n	Deposit name	Host tectonostratigraphic complex (age)	Location	Sulfide texture	Host rocks composition	Regional metamorphism	References
Magmatic	Ni-Cu sulfide	VB30	6	Ovoid	Voisey's Bay Nain Plutonic Suite (1.33 Ga)	Newfoundland, Canada	Massive	Anorthosites - granites - troctolites	Unmet	Boutroy et al. (2014); Naldrett (2004); Ripley and Li (2011); Salim Amaral (2017)
		VB31	7							
		VB34	2							
		VB5	3							
		VB6	11							
		VB7	7				Net textured/globular			
		TR15	7	Delta	Cape Smith Belt (1.88 Ga)	Northen Quebec, Canada	Massive	Komatiites	Greensch	Boutroy et al. (2014); Dionne-Foster (2007); Mungall (2007); Seabrook et al. (2004)
		TR20	8							
		EX0301	9							
		K2	8	Katinniq						
		MXNW	7	Mesamax						
		C0423	8	Zone Frontier						
		C0424	7							
		C0425	9							
		C0438	3				Net textured/globular			
		C0443	8							
		06MPBR15	9	Broken Hammer	Sudbury Igneous Complex (1.85 Ga)	Ontario, Canada	Massive	Granites - gneisses	Greensch	Boutroy et al. (2014); Dare et al. 2012; Dare et al. (2014); Dare et al. (2010a); Dare et al. (2010b); Dare et al. (2011); Naldrett (2004)
		06MPBR16	7							
		1533	8	Copper Cliff						
		CRTN12	10	Creighton						
		CRTN13	10							
		CRTN14	8							
		CRTN18	5							
		CRTN19	6							
		CRTN6	10	Creighton			Net textured/globular			
		CRTN9B	8	Creighton			Massive			
		MCR10A	16	McCreedy			Massive			

Class	Type	Sample	n	Deposit name	Host tectonostratigraphic complex (age)	Location	Sulfide texture	Host rocks composition	Regional metamorphism	References
Magmatic	Ni-Cu sulfide	MCR10B	10	McCreedy	Sudbury Igneous Complex (1.85 Ga)	Ontario, Canada	Massive	Granites - gneisses	Greensch	Boutroy et al. (2014); Dare et al. 2012; Dare et al. (2014); Dare et al. (2010a); Dare et al. (2010b); Dare et al. (2011); Naldrett (2004)
		MCR13	12							
		MCR3	8							
		MCR4B	7							
		MCR5	5							
		RX162	5							
		RX164	10							
	Reef-type PGE	F10304	12	PV Reef	Penikat (2.44Ga)	Finland	Disseminated	Anorthosites - gabbronorites	Greensch	Barnes et al. (2008)
		GD10	14	Mimosa	Great Dyke (2.57 Ga)	Mashonaland West, Zimbabwe		Orthopyroxenites	Unmet	
		GDN4	9							
		ST12	3	East Boulder	Stillwater Complex (2.70 Ga)	Montana, USA		Olivine gabbronorites	Greensch	Godel and Barnes (2008)
		T10T	8							
		T11T	12							
		2938	12	Merensky Reef	Bushveld Complex (2.05 Ga)	South Africa		Melanorites - chromitite	Unmet	Godel et al. (2007)
		CGMA	9	Rustenburg						
		CGMB	8							
		M1	9							
		M2	11							
		MR2	9							

Annexe C2. List of deposits compiled from literature (dataset B). n.r.: not reported; n: number of analyses; [1]censored values + missing values derived from non-analyzed elements

Source	Type	Deposit name	Location	n	Regional metamorphism	Reference materials	Internal standard	Beam size (µm)	Non-analyzed elements	% total missing values[1]
Duran et al. (2016)	Ni-Cu sulfide	Lac des Îles Complex	Canada	20		GSE-1g	n.r.	43-75	Ga, In, Mn	26%
George et al. (2018)	Epithermal gold	Herja	Romania	5	L greensch	MASS-1	Cu	26		21%
	Epithermal gold	Toroiaga	Romania	26	Amph-granu	MASS-1	Cu	26		
	Epithermal gold	Kochbulak	Uzbekistan	1	greensch	MASS-1	Cu	26		
	Porphyry	Assarel	Bulgaria	24	Unmet	MASS-1	Cu	26		
	Porphyry	Elatsite	Bulgaria	10	Unmet	MASS-1	Cu	26		
	Porphyry	Bor	Serbia	10	Unmet	MASS-1	Cu	26		
	Skarn	Baita Bihor	Romania	13	Unmet	MASS-1	Cu	26		
	Skarn	Oravita	Romania	34	Unmet	MASS-1	Cu	26		
	VMS	Sulitjelma	Norway	111	Unmet	MASS-1	Cu	26		
	VMS	Vorta	Romania	2	Unmet	MASS-1	Cu	26		
Li et al. (2018)	IOCG	Mina Justa	Perú	15	Unmet	STDGL2b2	n.r.	47	Ga, In	30%
Mansur & Barnes (2020)	Reef-type PGE	Bushveld Complex	South Africa	129	Unmet	Po727, MASS-1, GSE-1g	Fe	n.r.	Ga, Mn	29%
	Reef-type PGE	Stillwater Complex	Zimbabwe	57	greensch	Po727, MASS-1, GSE-1g	Fe	15-58	Ga, Mn	
Mansur et al. (2020)	Ni-Cu sulfide	Norilsk	Russia	97	Unmet	Po727, MASS-1, GSE-1g	Fe	n.r.	Ga, Mn	21%
Marfin et al. (2020)	Ni-Cu sulfide	Norilsk	Russia	87	Unmet	UAQ-FeS-1, GSD-1g, STD GL-	Fe	40-80	Au, Ga, In, Sb	29%
Melekestseva et al. (2020a)	VMS-SMS	Ashadze-2	Mid-Atlantic Ridge	7	Unmet	STDGL2b2, GSD-1g	Fe	40-60		2%
Melekestseva et al. (2020b)	VMS	Dergamysh	Russia	22	greensch	STDGL2b2, GSD-	Fe	40-60	Ga, In	14%
Torró et al. (2022)	VMS	Cerro de Maimón	Dominican Republic	11	greensch-bluesch	GSD-1g, NIST610, UQAC-FeS-1	n.r.	n.r.	Te	19%
Torró et al. (2022)	VMS	María Teresa	Perú	27	greensch-bluesch	GSD-1g, NIST610, UQAC-FeS-1	n.r.	n.r.	Te	
Tseluyko et al. (2022)	VMS	Yubileynoe	Russia	7	greensch	MASS-1, GSD-1g	Fe	25	Ga, In	14%
Yang et al. (2022)	Epithermal gold	Tiegelongnan	China	4	Unmet	Po727, MASS-1	Fe	33-75		7%
Yang et al. (2022)	Porphyry	Tiegelongnan	China	11	Unmet	Po727, MASS-2	Fe	33-76		

Annexe C3. List of deposits compiled from literature not included in dataset B (dataset D)

n.r.: not reported; n: number of analyses.

Source	Deposit name	Location	Regional metamorphism	n	Reference materials	Internal standard	Non-analyzed elements
Ni-Cu sulfide							
Barnes et al. (2006)	Noril'sk	Russia	Unmetamorphosed	7	Po52	S	Bi, Ga, In, Sb, Se, Sn, Te
Dare et al. (2010b)	Sudbury	Canada	Greenschist	18	Po727, JB-MSS5	Fe	Ga, In
Djon and Barnes (2012)	Lac des Iles	Canada	Greenschist	14	Po727, MASS-1	S	Ga, In, Sn
Piña et al. (2012)	Aguablanca	Spain	Greenschist	30	Po727, MASS-1	Fe	Ga, In, Se, Sb, Sb, Zn
Chen et al. (2015)	Jinchuan	China	Greenschist	3	NiS3 (PGE), STDGL2b2	Fe	Ga, In, Sb, Sn, Zn
Dare et al. (2014)	Sudbury	Canada	Greenschist	40	Po727, MASS-1, Fe-Zn-Cu-S	Fe	Ga, In
Piña et al. (2015)	El Gallego	Spain	Greenschist	6	Po727, MASS-1	Fe	Ga, In, Sb
Knight et al. (2017)	Santa Rita	Brazil	Greenschist	14	Ni-Fe-S	S	Ag, Ga, In, Sn
Salim Amaral (2017)	Voisey's Bay	Canada	Unmetamorphosed	20	Po727, MASS-1	Fe	Ga, In
Samalens et al. (2017)	Duluth	USA	Unmetamorphosed	8	Po727, MASS-1	Fe	Ga, In
Liang et al. (2019)	Yanpliuping	China	Greenschist	3	Po724-T, NiS3, STDGL2b2	n.r.	Ga, In, Zn
Reef-type PGE							
Barnes et al. (2008)	Penikat	Finland	Greenschist	11	Po727, Po62, MSS-1	S	Bi, Ga, In, Sb, Se, Sn, Te
Godel and Barnes (2008)	Stillwater	USA	Greenschist	14	Po727	S	Bi, Ga, In, Sb, Se, Sn, Te
Piña et al. (2016)	Great Dyke	Zimbabwe	Unmetamorphosed	20	Po727, MASS-1	Fe	Ga, In
Volcanogenic massive sulfides							
Revan et al. (2014)	Çayeli	Turkey	Unmetamorphosed	67	STDGL2b2	Fe	Ga, In
Wohlgemuth-Ueberwasser et al. (2015)	Roman Ruins (SMS)	Papua New Guinea	Unmetamorphosed	131	trans-1, NiS3	S	Ag, Bi, Co, Ga, In, Mn, Ni, Pb, Sn, Zn
Maslennikov et al. (2017)	Urals	Russia	Greenschist	21	STDGL2b2	Fe	Ga, In, Mn
Agangi et al. (2018)	Red Bore	Australia	Greenschist	128	NIST610, Po726	Fe	Ga, In
Martin et al. (2018)	Troodos	Cyprus	Unmetamorphosed	46	*n.r.*	S	Ga, In, Mn, Sn
Wang et al. (2018)	Kairei (SMS)	Central Indian Ridge	Unmetamorphosed	16	trans-1, NIST610	n.r.	

Annexe C3. continued

n.r.: not reported; n: number of analyses.

Source	Deposit name	Location	Regional metamorphism	n	Reference materials	Internal standard	Non-analyzed elements
Porphyry							
Lobo (2022)	Assarel	Bulgaria	Unmetamorphosed	6	MASS-1	Fe	
Yu et al. (2022)	Kuruer	China	Unmetamorphosed	71	NIST610, MASS-1	Cu	Ga, In, Ni, Pb, Sb
Stefanova et al .(2023)	Elatsite-Chelopech	Bulgaria	Unmetamorphosed	8	NIST610, MASS-1	n.r.	Ga
Skarn							
Xie et al. (2020)	Fenghuangshan	China	Unmetamorphosed	30	NIST610	Fe	In, Te
Chen et al. (2022)	Buziwannan	China	Greenschist	21	NIST610, NIST612	n.r.	Bi, Ga, Sb, Sn, Te
Iron Oxide-Copper Gold							
Liang et al. (2021)	Laoshankou	China	Unmetamorphosed	24	STDGL2b2	Fe	Ga, In
Mansur et al. (2023)	Jaguar	Brazil	Greenschist	34	Po727, MASS-1, GSE-1g	Fe	Mn
Epithermal gold							
Reich et al. (2020)	Cerro Pabellón	Chile	Unmetamorphosed	41	NIST610, MASS-1	Fe	Mn
Orogenic gold							
Vasilopoulos et al. (2023)	Naakenavaara-Hirvilavanmaa	Finland	Greenschist	46	MASS-1, UQAC	Fe	

Annexe C4. Electron Probe Micro Analysis results for chalcopyrite.Beam size was 10 µm with a voltage of 15 kV and a current of 20 nA.

	Weight percent			
Grain	S (wt%)	Cu (wt%)	Fe (wt%)	Total
Detection limit	0.367	0.503	0.836	
07MPBR23CCP-02.d	34.9	34.2	30.8	99.9
07MPBR23CCP-03.d	34.5	33.7	29.8	98.1
07MPBR23CCP-04.d	34.7	34.7	29.8	99.2
07MPBR23CCP-05.d	34.9	34.1	29.4	98.4
07MPBR23CCP-06.d	34.6	34.5	30.1	99.3
2211CCP-01.d	34.8	33.7	30.2	98.7
2211CCP-02.d	34.6	33.6	30.6	100.0
2211CCP-03.d	34.4	33.4	29.9	98.7
2211CCP-04.d	34.3	33.6	29.9	99.3
2211CCP-05.d	34.3	33.4	30.0	97.7
2211CCP-06.d	34.3	33.5	29.6	99.9
2215CCP-02.d	35.0	34.2	31.2	100.4
2215CCP-03.d	35.1	34.1	30.3	99.5
2215CCP-04.d	35.0	34.0	30.9	99.9
2215CCP-05.d	35.1	34.2	30.6	99.8
2215CCP-06.d	34.8	34.1	30.6	99.4
2221CCP-01.d	34.7	34.7	30.6	97.8
2221CCP-02.d	34.6	34.3	30.4	100.5
2221CCP-03.d	35.0	34.5	30.4	97.8
2221CCP-04.d	35.1	34.7	30.7	99.1
2221CCP-05.d	34.8	34.1	30.3	97.5
2221CCP-06.d	34.7	34.6	30.9	100.2
2221CCP-07.d	34.9	34.5	30.4	99.8
2224CCP-01.d	34.1	33.5	31.1	99.2
2224CCP-02.d	34.5	33.7	31.2	99.2
2224CCP-03.d	34.6	33.6	31.4	99.2
2224CCP-04.d	34.8	33.8	31.6	99.2
2224CCP-05.d	34.5	33.9	30.8	99.2
2296CCP-01.d	34.9	33.5	31.6	100.0
2296CCP-02.d	35.0	33.5	31.6	100.1
2296CCP-03.d	34.9	33.3	31.0	99.2
2296CCP-04.d	34.8	33.6	30.6	99.1
2296CCP-05.d	35.3	33.6	31.3	100.3
2318CCP-01.d	34.8	34.8	30.9	100.5
2318CCP-02.d	34.7	34.7	31.1	100.6
2318CCP-03.d	34.8	34.7	31.2	100.7
2318CCP-04.d	34.6	34.8	30.8	100.2
2318CCP-05.d	34.2	28.1	25.5	87.8
2318CCP-06.d	34.8	35.3	31.2	101.4
2318CCP-07.d	34.9	34.9	30.8	100.6
2325CCP-01.d	35.0	34.5	31.1	100.6
2325CCP-02.d	35.1	34.5	31.0	100.6

Grain	Weight percent			
	S (wt%)	Cu (wt%)	Fe (wt%)	Total
2325CCP-04.d	34.9	34.3	30.6	99.8
2325CCP-05.d	34.9	34.7	31.0	100.7
2325CCP-06.d	35.1	34.3	30.9	100.2
2369CCP-01.d	34.6	34.6	30.0	99.2
2369CCP-02.d	34.6	34.2	29.5	98.4
2369CCP-03.d	34.7	34.1	30.1	99.0
2369CCP-04.d	34.8	34.2	29.8	98.8
2369CCP-05.d	34.5	33.8	30.4	98.7
2369CCP-06.d	34.9	34.3	29.8	99.0
2369CCP-07.d	34.4	34.1	29.7	98.2
2378CCP-01.d	35.0	34.4	30.2	99.6
2378CCP-02.d	34.7	34.5	30.9	100.2
2378CCP-03.d	34.8	34.4	30.8	100.0
2378CCP-04.d	34.9	34.6	30.3	99.8
2378CCP-05.d	34.8	34.3	30.6	99.8
2378CCP-06.d	35.0	34.8	30.5	100.3
2378CCP-07.d	34.9	34.5	30.5	99.9
2378CCP-08.d	34.9	34.6	30.6	100.0
2643CCP-01.d	34.6	34.6	30.3	99.5
2643CCP-02.d	34.6	34.4	30.4	99.4
2643CCP-03.d	34.6	34.4	30.4	99.4
2643CCP-04.d	34.7	34.5	30.7	99.9
2643CCP-05.d	34.8	34.6	30.0	99.4
2643CCP-06.d	34.6	34.3	30.3	99.3
2647CCP-01.d	34.6	34.5	30.0	99.1
2647CCP-02.d	35.0	34.3	30.6	99.9
2647CCP-03.d	34.8	34.3	30.6	99.8
2647CCP-04.d	34.1	33.1	29.5	96.6
2647CCP-05.d	34.8	34.5	30.3	99.5
2647CCP-06.d	34.5	34.5	30.3	99.3
2647CCP-07.d	34.7	34.6	30.9	100.2
2652CCP-01.d	34.9	34.5	30.0	99.5
2652CCP-02.d	34.8	34.4	30.4	99.5
2652CCP-03.d	34.9	34.7	30.8	100.4
2652CCP-04.d	34.7	34.5	30.4	99.6
2652CCP-05.d	34.9	34.7	30.2	99.7
2652CCP-06.d	34.9	34.9	30.9	100.7
2652CCP-07.d	34.8	34.7	30.4	99.9
27ROV8CCP-01.d	34.7	34.7	30.9	100.2
27ROV8CCP-02.d	34.6	34.8	30.3	99.7
27ROV8CCP-03.d	34.7	34.7	30.8	100.2
27ROV8CCP-04.d	34.8	34.7	31.2	100.8
27ROV8CCP-05.d	34.7	34.6	30.8	100.1
27ROV8CCP-07.d	34.7	35.1	30.5	100.3
2924CCP-01.d	34.6	34.8	30.6	99.9
2924CCP-03.d	34.6	34.8	31.2	100.6
2924CCP-04.d	34.5	34.6	30.4	99.5

Grain	Weight percent			
	S (wt%)	Cu (wt%)	Fe (wt%)	Total
2924CCP-05.d	34.8	34.8	30.6	100.2
2924CCP-06.d	34.5	34.5	30.8	99.8
2924CCP-08.d	34.6	34.8	30.7	100.1
2925CCP-01.d	34.9	34.0	30.4	99.2
2925CCP-02.d	34.8	34.3	30.4	99.5
2925CCP-03.d	34.8	34.0	30.8	99.5
2925CCP-04.d	34.7	34.0	29.9	98.6
2925CCP-05.d	34.8	34.0	30.2	99.1
2925CCP-06.d	34.8	34.2	30.3	99.3
3143CCP-01.d	34.5	33.5	29.9	98.0
3143CCP-03.d	34.5	33.8	29.6	97.9
3143CCP-04.d	34.5	33.7	29.9	98.1
3143CCP-05.d	34.7	33.8	29.7	98.2
3143CCP-06.d	34.9	33.9	30.5	99.4
3147CCP-01.d	34.7	34.4	29.8	99.0
3147CCP-02.d	34.6	34.3	30.1	99.0
3147CCP-03.d	34.5	34.2	30.2	98.9
3147CCP-04.d	35.0	34.4	30.5	99.9
3147CCP-05.d	34.7	34.4	30.5	99.6
3147CCP-06.d	34.6	34.2	30.3	99.1
3147CCP-07.d	34.5	34.2	29.8	98.4
31ROV13CCCP-01.d	35.1	34.7	30.3	100.0
31ROV13CCCP-02.d	34.8	34.8	30.0	99.5
31ROV13CCCP-03.d	34.8	34.9	30.0	100.8
31ROV13CCCP-04.d	34.9	34.3	30.0	99.2
31ROV13CCCP-05.d	34.9	35.0	30.2	100.1
31ROV13CCCP-06.d	34.9	34.6	30.3	99.9
31ROV13CCCP-07.d	34.8	34.7	30.4	99.9
35GTV2B2CCP-001.d	34.7	34.5	30.1	99.2
35GTV2B2CCP-002.d	34.7	34.0	30.4	99.2
35GTV2B2CCP-003.d	34.6	33.9	30.6	99.1
35GTV2B2CCP-004.d	34.8	34.1	30.6	99.5
35GTV2B2CCP-005.d	34.8	34.5	30.5	99.9
35GTV2B2CCP-006.d	34.6	34.1	30.7	99.4
51CCP-01.d	34.7	34.3	30.2	99.3
51CCP-02.d	34.7	34.5	30.3	99.6
51CCP-03.d	34.9	34.5	30.3	99.7
51CCP-05.d	34.8	34.6	30.2	99.6
51CCP-06.d	34.6	34.5	30.1	99.2
52CCP-01.d	34.6	34.7	30.4	99.7
52CCP-02.d	34.6	34.7	30.4	99.7
52CCP-03.d	34.7	34.8	30.5	99.9

Grain	Weight percent			
	S (wt%)	Cu (wt%)	Fe (wt%)	Total
52CCP-04.d	34.5	34.7	30.7	100.0
52CCP-05.d	34.7	35.1	30.5	100.3
52CCP-06.d	34.6	35.0	30.6	100.2
52CCP-07.d	34.6	34.7	30.5	99.8
53CCP-01.d	34.8	34.3	29.7	98.8
53CCP-02.d	34.7	34.8	30.5	100.0
53CCP-03.d	35.1	34.3	30.6	100.0
53CCP-04.d	35.0	34.2	30.4	99.7
53CCP-05.d	34.8	34.6	30.0	99.4
53CCP-06.d	34.5	33.9	30.0	98.5
53CCP-07.d	34.8	34.7	29.9	99.4
53ROV13CCP-01.d	34.7	34.8	30.5	100.0
53ROV13CCP-02.d	35.2	34.9	30.9	101.0
53ROV13CCP-04.d	34.6	35.2	30.7	100.5
53ROV13CCP-05.d	34.8	34.8	30.9	100.4
53ROV13CCP-06.d	34.4	35.1	30.6	100.1
53ROV13CCP-07.d	34.5	34.8	30.6	100.6
53ROV6CCP-01.d	34.9	34.6	30.7	100.2
53ROV6CCP-02.d	34.9	34.8	30.3	100.0
53ROV6CCP-04.d	34.8	34.5	30.2	99.5
53ROV6CCP-05.d	34.8	34.6	30.9	100.3
53ROV6CCP-06.d	34.9	34.9	30.6	100.4
53ROV6CCP-07.d	34.9	34.9	30.9	100.8
56CCP-01.d	34.9	34.6	30.8	100.3
56CCP-02.d	34.9	34.9	30.8	101.0
56CCP-03.d	35.0	34.7	30.8	100.5
56CCP-04.d	34.9	34.7	30.6	100.3
56CCP-05.d	35.2	35.1	30.9	101.3
56CCP-06.d	35.0	34.8	30.8	100.6
601CCP-01.d	34.6	34.6	30.1	99.3
601CCP-02.d	34.5	34.6	29.7	98.8
601CCP-03.d	34.8	34.3	29.9	99.0
601CCP-04.d	34.5	34.3	30.2	98.9
601CCP-05.d	34.9	34.3	30.0	99.2
62CCP-01.d	34.8	34.6	30.7	100.1
62CCP-02.d	34.8	34.7	30.3	99.7
62CCP-03.d	34.8	34.7	30.2	99.7
62CCP-04.d	34.8	34.7	30.7	100.2
62CCP-05.d	34.9	34.8	31.0	100.7
62CCP-06.d	34.9	34.7	30.2	99.8
62CCP-07.d	34.9	35.0	30.2	100.5
64ROV11CCP-01.d	34.6	33.7	31.0	99.4
64ROV11CCP-02.d	34.7	33.8	31.3	99.9
64ROV11CCP-03.d	34.6	33.9	30.9	99.4
64ROV11CCP-04.d	34.9	34.7	30.8	100.3
64ROV11CCP-05.d	34.8	34.7	30.9	100.4
64ROV11CCP-06.d	34.8	34.8	30.3	99.9

Grain	Weight percent			
	S (wt%)	Cu (wt%)	Fe (wt%)	Total
64ROV11CCP-07.d	34.7	34.8	30.9	100.4
ALJ01CCP-01.d	35.1	34.8	30.7	100.7
ALJ01CCP-02.d	35.2	34.6	31.0	100.7
ALJ01CCP-04.d	34.4	34.2	30.0	98.6
ALJ01CCP-05.d	34.9	34.5	30.3	99.7
ALJ01CCP-06.d	35.1	34.5	30.9	100.5
AZN01CCP-02.d	34.9	34.9	30.8	100.6
AZN01CCP-03.d	34.9	34.8	30.8	100.5
AZN01CCP-04.d	35.0	34.8	30.7	100.8
AZN01CCP-05.d	34.9	34.7	30.7	100.3
AZN01CCP-06.d	34.7	34.9	30.6	100.2
AZN01CCP-07.d	34.8	34.8	30.4	99.9
COR01CCP-01.d	34.8	34.8	30.7	100.3
COR01CCP-03.d	34.6	34.9	29.9	99.3
COR01CCP-04.d	35.0	34.9	30.4	100.3
COR01CCP-06.d	34.8	34.7	30.2	99.7
COR01CCP-08.d	34.8	34.9	30.9	100.5
COR02CCP-01.d	34.6	34.6	30.4	99.7
COR02CCP-02.d	34.8	34.5	30.4	100.3
COR02CCP-03.d	33.6	34.0	28.8	96.4
COR02CCP-04.d	34.6	34.9	30.5	100.0
COR02CCP-05.d	34.9	35.0	30.7	100.6
COR02CCP-06.d	34.7	34.6	30.8	100.1
COR02CCP-07.d	34.7	34.8	30.7	100.2
COR03CCP-01.d	34.7	34.4	30.1	99.2
COR03CCP-02.d	34.7	34.8	30.4	99.9
COR03CCP-03.d	34.8	34.7	30.4	99.8
COR03CCP-04.d	34.9	34.1	30.3	99.3
COR03CCP-05.d	34.8	34.5	30.3	99.7
COR03CCP-07.d	34.6	34.7	30.2	99.6
COR03CCP-08.d	34.8	34.8	30.4	100.1
COR03CCP-09.d	34.9	34.5	30.8	100.2
COR03CCP-10.d	34.9	34.7	30.8	100.4
COR03CCP-11.d	34.5	34.4	30.4	99.4
COR04CCP-01.d	34.7	34.1	29.9	98.7
COR04CCP-02.d	34.9	34.3	30.0	99.2
COR04CCP-03.d	34.6	34.3	29.9	98.8
COR04CCP-04.d	34.6	34.3	29.8	98.6
COR04CCP-05.d	34.6	34.3	29.9	98.8
COR04CCP-06.d	35.0	34.6	30.6	100.2
GRA01CCP-01.d	34.8	34.8	30.4	100.1
GRA01CCP-02.d	34.9	34.5	30.5	99.8
GRA01CCP-03.d	34.8	34.5	30.7	100.0
GRA01CCP-04.d	35.0	34.7	31.0	100.7
GRA01CCP-05.d	34.8	35.1	30.7	100.5
GRA01CCP-06.d	34.7	35.0	30.6	100.4
LOU01CCP-01.d	35.0	34.6	30.6	100.2

Grain	Weight percent			
	S (wt%)	Cu (wt%)	Fe (wt%)	Total
LOU01CCP-02.d	35.0	34.6	30.3	99.9
LOU01CCP-03.d	34.8	34.1	29.5	98.4
LOU01CCP-04.d	35.0	34.7	30.7	100.4
LOU01CCP-05.d	35.0	34.8	30.8	100.7
LOU01CCP-06.d	35.0	34.8	30.6	100.4
LOU01CCP-07.d	34.8	34.8	30.6	100.2
LS10CCP-01.d	34.5	33.9	29.7	98.2
LS10CCP-02.d	34.9	34.6	30.0	99.5
LS10CCP-03.d	34.5	34.3	29.9	98.7
LS10CCP-04.d	34.5	34.7	30.0	99.1
LS10CCP-05.d	34.5	34.0	30.3	98.8
LS10CCP-06.d	34.7	34.6	30.3	99.6
LS10CCP-07.d	34.8	34.2	29.8	98.8
LS1CCP-01.d	34.9	35.0	30.2	100.1
LS1CCP-02.d	34.9	35.1	30.7	100.6
LS1CCP-03.d	34.9	35.2	30.5	100.6
LS1CCP-04.d	34.8	34.9	30.2	99.9
LS1CCP-05.d	35.0	34.8	30.6	100.4
LS1CCP-06.d	34.9	35.2	30.5	100.5
LS1CCP-07.d	34.9	35.5	30.6	101.1
LS22CCP-01.d	34.7	34.6	30.7	99.9
LS22CCP-02.d	34.6	34.6	30.6	99.9
LS22CCP-03.d	34.7	34.5	30.0	99.3
LS22CCP-04.d	34.7	34.4	30.3	99.4
LS22CCP-05.d	34.8	34.7	30.2	99.7
LS22CCP-06.d	34.7	34.5	30.6	99.8
LS22CCP-07.d	34.8	34.4	30.3	99.5
MN1CCP-01.d	34.5	34.6	30.1	99.3
MN1CCP-02.d	34.5	34.7	30.1	100.4
MN1CCP-03.d	34.6	34.6	30.4	99.5
MN1CCP-04.d	35.1	34.9	30.8	100.8
MN1CCP-05.d	34.6	34.9	30.4	99.9
MN1CCP-06.d	34.7	34.9	30.7	100.3
MN1CCP-07.d	34.8	34.8	30.7	100.2
MN2CCP-01.d	34.4	34.9	30.5	99.7
MN2CCP-03.d	34.5	34.3	30.5	99.3
MN2CCP-04.d	34.6	34.5	31.3	100.4
MN2CCP-05.d	34.7	34.6	30.6	99.9
MN2CCP-06.d	34.5	34.8	30.3	99.5
MN2CCP-07.d	34.7	34.5	30.1	99.4
MN3CCP-01.d	34.3	34.9	30.6	99.8
MN3CCP-02.d	34.6	34.5	30.7	99.8
MN3CCP-03.d	34.7	34.5	30.9	100.1
MN3CCP-04.d	34.6	34.6	30.6	99.7
MN3CCP-05.d	34.7	34.6	30.5	99.8
MN3CCP-06.d	34.7	34.5	30.5	99.8
NEV01CCP-01.d	34.9	34.6	30.5	100.0

Grain	Weight percent			
	S (wt%)	Cu (wt%)	Fe (wt%)	Total
NEV01CCP-02.d	34.6	34.7	30.1	99.3
NEV01CCP-03.d	34.9	34.8	30.8	100.5
NEV02CCP-01.d	35.0	34.9	31.0	100.9
NEV02CCP-02.d	35.2	34.9	30.8	100.9
NEV02CCP-03.d	35.2	34.9	30.6	100.7
QT0MTCCP-01.d	34.6	34.6	30.6	99.8
QT0MTCCP-02.d	35.0	34.6	31.0	100.5
QT0MTCCP-03.d	34.8	34.6	30.7	100.1
QT0MTCCP-04.d	34.7	34.4	30.9	99.9
QT0MTCCP-05.d	34.6	34.3	30.6	99.5
QT0MTCCP-06.d	34.7	34.4	30.5	99.6
QT0MTCCP-07.d	34.7	34.4	30.8	99.8
V553221CCP-001.d	34.9	34.2	30.7	99.8
V553221CCP-002.d	34.6	34.1	30.8	99.5
V553221CCP-003.d	34.6	34.1	30.6	99.3
V553221CCP-004.d	34.8	34.4	30.6	100.2
V553221CCP-005.d	34.8	34.4	30.6	99.7
V553221CCP-006.d	34.8	34.2	30.2	99.2
V557327ACCP-001.d	34.6	33.7	30.5	98.7
V557327ACCP-002.d	34.6	33.5	30.2	98.3
V557327ACCP-003.d	34.6	34.0	30.5	99.1
V557327ACCP-004.d	34.9	33.9	31.0	99.8
V557327ACCP-005.d	34.7	33.6	30.1	98.4
V557327ACCP-006.d	35.0	33.9	30.6	99.4
ZAM01CCP-01.d	34.8	34.6	29.9	99.3
ZAM01CCP-02.d	34.8	34.4	30.3	99.5
ZAM01CCP-03.d	34.9	34.5	30.2	99.5
ZAM01CCP-04.d	34.9	34.4	29.7	98.9
ZAM01CCP-05.d	34.7	34.5	30.2	99.5
ZAM01CCP-06.d	34.9	34.4	30.5	99.8
ZAM01CCP-07.d	34.9	34.4	30.0	99.2
E13 02 ccp	35.2	34.5	30.2	99.9
E13 03 ccp	35.2	34.4	30.2	99.8
E13 04 ccp	35.3	34.6	30.5	100.3
E13 06 ccp	35.2	34.9	30.2	100.4
E-DEEP 03 ccp	35.3	34.4	30.2	99.9
E-DEEP 04 ccp	35.2	34.6	30.1	99.9
E-DEEP 05 ccp	35.0	34.3	30.1	99.4
E-DEEP 08 ccp	35.1	34.5	30.8	100.4
E-DEEP 09 ccp	35.1	34.7	30.1	99.9
E-DEEP 10 ccp	35.3	34.6	30.3	100.2
DC69 02 ccp	35.1	34.4	30.1	99.5
DC69 03 ccp	35.2	34.5	29.7	99.4
DC69 04 ccp	35.2	34.5	31.1	100.7
DC69 05 ccp	35.3	34.3	30.3	99.8
DC69 08 ccp	35.0	34.5	30.1	99.6
DC69 09 ccp	35.2	34.5	29.6	99.3

Grain	Weight percent			
	S (wt%)	Cu (wt%)	Fe (wt%)	Total
DC69 10 ccp	35.1	34.3	29.9	99.4
DC69 11 ccp	35.0	34.1	30.3	99.4
T1 01 ccp	35.4	34.5	30.2	100.1
T1 02 ccp	34.0	32.9	29.5	96.4
T1 03 ccp	35.1	34.7	30.5	100.3
T1 04 ccp	35.3	34.6	30.3	100.2
T1 05 ccp	35.2	34.0	30.4	99.6
T1 06 ccp	35.3	34.5	30.7	100.5
T1 07 ccp	35.4	34.4	30.1	99.9
T1 08 ccp	35.2	34.3	30.1	99.7
T1 09 ccp	35.1	34.0	30.1	99.2
2523 01 ccp	35.3	34.0	30.6	99.8
2523 02 ccp	35.3	34.5	30.2	99.9
2523 03 ccp	35.5	34.4	30.2	100.1
2523 04 ccp	35.2	34.1	30.5	99.7
2523 07 ccp	35.3	34.0	30.4	99.8
2523 09 ccp	35.2	34.4	30.0	99.5
2523 10 ccp	35.3	34.6	30.7	100.7
NR6 01 ccp	35.1	34.2	30.7	100.0
NR6 02 ccp	35.1	34.2	30.7	100.0
NR6 06 ccp	35.2	34.3	30.2	99.8
NR6 07 ccp	35.1	34.6	30.4	100.2
NR6 08 ccp	35.4	34.6	30.2	100.2

Summarized data

	Weight percent			
	S (wt%)	Cu (wt%)	Fe (wt%)	Total
Detection limit	0.367	0.503	0.836	
Arithmetic mean	34.8	34.4	30.4	99.7
Standard deviation	0.24	0.52	0.48	

Annexe C5. Full LA-ICP-MS results for trace elements (in ppm) of chalcopyrite (dataset A).
<dl: below detection limit. *Informative values. n.r. not reported; in italic: elements used for statistical analyses

Grain ID	*Mn* 55	*Co* 59	*Ni* 60	*Zn* 66	*Ga* 71	As 75	*Se* 82	Mo 95	Ru 101	Rh 103	*Ag* 107	Pd 108	Cd 111	*In* 115	*Sn* 118	*Sb* 121	*Te* 128	Re 185	Os 189	Ir 193	Pt 195	*Au* 197	Tl 205	*Pb* 208	*Bi* 209
55um	0.470	0.023	0.241	0.353	0.028	0.223	2.53	0.030	0.023	0.005	0.023	0.014	0.046	0.012	0.073	0.022	0.256	0.009	0.021	0.007	0.013	0.010	0.004	0.012	0.007
33um	0.939	0.046	0.722	1.06	0.085	0.445	5.07	0.061	0.068	0.009	0.069	0.041	0.137	0.025	0.218	0.067	0.513	0.027	0.042	0.020	0.039	0.030	0.011	0.037	0.013
Epithermal gold																									
1908CCP-01d	1.01	10.1	0.800	4.23	0.031	<dl	0.930	<dl	<dl	n.r.	2.58	<dl	0.090	0.022	0.015	0.018	0.028	<dl	<dl	<dl	<dl	3.E-4	0.00	0.263	0.001
1908CCP-02.d	0.069	6.41	0.013	4.41	0.013	<dl	0.810	<dl	<dl	n.r.	2.62	<dl	0.008	0.030	0.014	0.001	0.017	<dl	<dl	<dl	<dl	2.E-4	0.00	0.340	0.001
1908CCP-03.d	0.085	6.33	0.014	2.54	0.031	<dl	0.697	<dl	<dl	n.r.	3.06	<dl	0.031	0.033	0.080	0.074	0.018	<dl	<dl	<dl	<dl	2.E-4	3.E-4	0.970	0.003
1908CCP-04.d	0.076	4.56	0.009	2.23	0.033	<dl	0.639	<dl	<dl	n.r.	2.89	<dl	0.007	0.027	0.046	0.096	0.014	<dl	<dl	<dl	<dl	2.E-4	2.E-4	0.680	0.003
1908CCP-05.d	0.065	3.50	0.008	1.87	0.029	<dl	0.575	<dl	<dl	n.r.	5.63	<dl	0.010	0.021	0.064	0.049	0.015	<dl	<dl	<dl	<dl	3.E-4	0.00	0.830	0.001
1908CCP-06.d	0.071	7.84	0.010	2.70	0.032	<dl	0.622	<dl	0.013	n.r.	2.69	<dl	0.010	0.031	0.013	0.026	0.015	<dl	<dl	<dl	<dl	3.E-4	0.00	0.394	0.001
1911CCP-01d	0.281	0.023	0.026	48.3	1.31	<dl	2.25	<dl	0.025	n.r.	9.90	<dl	0.230	4.64	9.87	0.630	1.10	<dl	<dl	<dl	<dl	0.001	4.E-4	1.21	0.005
1912CCP-01d	0.266	0.012	0.013	33.5	1.30	<dl	2.43	0.220	<dl	n.r.	11.4	<dl	0.043	1.81	4.15	1.89	0.031	<dl	<dl	<dl	<dl	0.001	9.E-4	2.97	0.006
1912CCP-03.d	1.29	0.014	0.034	37.3	0.950	<dl	2.90	<dl	<dl	n.r.	36.6	<dl	0.056	5.49	9.22	0.780	0.057	<dl	<dl	<dl	<dl	6.E-4	0.001	7.10	0.030
1914CCP-01d	12.0	0.012	0.043	51.0	0.600	<dl	6.24	0.110	0.100	n.r.	60.5	<dl	0.210	14.8	20.1	1.98	0.070	<dl	<dl	<dl	<dl	0.008	0.003	2.88	0.004
1914CCP-02.d	3.00	0.130	0.029	46.8	7.90	0.800	6.46	1.00	<dl	n.r.	29.1	<dl	0.840	12.6	2.75	5.40	0.079	<dl	<dl	<dl	<dl	0.041	0.018	5.42	0.008
1914CCP-03.d	0.276	0.006	0.024	67.9	0.920	<dl	4.69	<dl	<dl	n.r.	7.84	<dl	0.390	12.0	14.6	0.510	0.049	<dl	<dl	<dl	<dl	7.E-4	0.005	1.89	0.005
1914CCP-04.d	1.17	0.008	0.030	57.8	1.97	<dl	5.49	<dl	<dl	n.r.	48.8	<dl	0.450	12.4	14.9	1.66	0.089	<dl	<dl	<dl	<dl	0.021	0.066	19.0	0.004
1914CCP-05.d	0.364	0.019	0.030	66.7	3.19	<dl	4.76	<dl	<dl	n.r.	25.5	<dl	0.670	10.7	13.9	0.019	0.069	<dl	<dl	<dl	<dl	0.001	0.006	0.940	0.005
1914CCP-06.d	8.40	0.033	0.029	44.8	5.56	1.24	5.06	<dl	<dl	n.r.	30.0	<dl	0.360	11.2	17.0	4.30	0.063	<dl	<dl	<dl	<dl	0.094	0.127	9.90	0.004
1914CCP-07.d	9.00	0.103	0.040	63.5	7.70	<dl	5.30	<dl	<dl	n.r.	38.6	<dl	0.460	9.28	20.6	0.550	0.079	<dl	<dl	<dl	<dl	0.001	0.027	10.8	4.70
1915CCP-01d	1.59	0.010	0.033	55.4	0.770	<dl	5.54	<dl	<dl	n.r.	1.06	<dl	0.310	28.6	4.81	1.37	0.059	<dl	<dl	<dl	<dl	9.E-4	5.E-4	1.85	0.003
1915CCP-02.d	9.00	0.009	0.037	49.7	1.85	<dl	6.88	<dl	<dl	n.r.	3.78	<dl	0.210	33.6	3.23	1.20	0.062	<dl	<dl	<dl	<dl	0.002	3.E-4	0.690	0.005
1915CCP-03.d	0.252	0.007	0.027	66.7	0.710	<dl	6.75	<dl	<dl	n.r.	5.15	<dl	0.300	27.5	2.86	0.450	0.041	<dl	<dl	0.003	<dl	0.015	4.E-4	0.800	0.011
1915CCP-04.d	38.0	0.016	0.075	58.4	0.840	<dl	7.72	<dl	<dl	n.r.	51.3	<dl	0.980	52.0	18.9	1.52	0.147	<dl	<dl	<dl	<dl	0.002	0.021	2.37	0.005
2123CCP-01d	0.091	0.067	0.006	32.0	0.060	4.40	63.5	<dl	<dl	n.r.	1190	<dl	0.089	0.716	3.57	1.36	0.022	<dl	<dl	<dl	<dl	0.065	0.173	0.629	0.005
2123CCP-02.d	0.085	0.226	0.005	47.0	0.099	0.320	87.8	<dl	<dl	n.r.	1310	<dl	0.153	0.637	7.67	0.770	0.027	<dl	<dl	<dl	<dl	0.008	0.015	0.529	0.004
2123CCP-03.d	0.119	0.373	0.010	29.9	0.076	<dl	92.9	<dl	<dl	n.r.	1002	<dl	0.293	0.635	3.86	0.136	0.029	<dl	<dl	<dl	<dl	0.009	0.003	0.622	0.005
2123CCP-04.d	0.068	0.029	0.007	38.1	0.055	0.145	82.3	<dl	<dl	n.r.	910	<dl	0.173	0.632	11.4	0.077	0.019	<dl	<dl	<dl	<dl	0.008	2.E-4	0.392	0.008
2123CCP-05.d	0.470	0.120	0.009	34.5	0.027	<dl	13.0	<dl	<dl	n.r.	555	<dl	0.067	0.100	22.8	0.063	0.016	<dl	<dl	<dl	<dl	3.E-4	0.005	0.540	0.003
2123CCP-06.d	0.083	0.118	0.004	36.8	0.174	0.430	17.4	<dl	0.041	n.r.	1241	<dl	0.076	0.101	5.51	0.106	0.017	<dl	<dl	<dl	<dl	4.E-4	0.003	0.293	0.001
2123CCP-07.d	0.410	0.035	0.008	29.1	0.230	5.10	18.8	<dl	<dl	n.r.	587	0.058	0.135	0.098	5.59	0.248	0.025	<dl	<dl	<dl	<dl	0.006	0.410	0.850	0.009
2125CCP-01d	1.97	0.011	0.016	35.6	0.015	3.20	59.2	<dl	<dl	n.r.	1447	<dl	0.177	0.458	2.85	1.18	0.035	<dl	<dl	<dl	<dl	0.019	0.051	2.21	0.002
2125CCP-02.d	0.105	0.042	0.010	39.8	0.062	0.170	60.5	<dl	<dl	n.r.	1542	<dl	0.310	0.432	8.86	0.089	0.026	<dl	<dl	<dl	<dl	0.045	5.E-4	0.810	0.017
2125CCP-03.d	0.940	0.009	0.023	43.6	0.033	0.140	52.3	0.058	0.027	n.r.	1420	<dl	0.190	0.370	8.75	0.029	0.031	<dl	<dl	<dl	<dl	0.025	4.E-4	1.19	0.003
2125CCP-04.d	0.151	0.006	0.012	28.9	0.104	6.20	59.6	<dl	<dl	n.r.	1012	<dl	0.106	0.371	3.00	3.26	0.025	<dl	<dl	<dl	<dl	8.E-4	0.130	2.44	0.016
2125CCP-05.d	1.08	0.370	0.011	32.9	0.960	0.200	13.2	<dl	<dl	n.r.	2131	<dl	0.180	0.303	1.97	0.177	0.022	<dl	<dl	<dl	<dl	9.E-4	0.009	1.20	0.020
2125CCP-06.d	1.17	0.011	0.010	25.1	0.013	1.16	50.7	<dl	<dl	n.r.	764	<dl	0.057	0.313	1.70	0.224	0.024	0.005	<dl	<dl	<dl	8.E-4	0.009	2.13	0.012
2125CCP-07.d	0.880	0.008	0.017	36.1	0.087	31.5	60.7	0.036	0.032	n.r.	1120	<dl	0.111	0.303	3.06	21.1	0.034	<dl	<dl	<dl	0.008	0.021	0.198	4.37	0.012
2125CCP-08.d	0.960	0.007	0.010	31.9	0.118	0.180	64.1	0.037	<dl	n.r.	831	<dl	0.044	0.263	2.44	0.770	0.024	<dl	<dl	<dl	<dl	0.210	0.005	1.16	0.009
2190CCP-01d	0.267	0.054	0.048	203	0.170	14.6	6.06	<dl	<dl	n.r.	11.3	<dl	0.580	0.755	15.1	0.480	0.047	<dl	<dl	<dl	<dl	9.E-4	4.E-4	1.50	0.004
2190CCP-02.d	0.266	0.008	0.042	152	0.130	4.60	5.45	<dl	<dl	n.r.	12.2	<dl	0.140	0.287	15.4	1.76	0.053	<dl	<dl	<dl	<dl	0.027	0.010	4.90	0.004
2190CCP-03.d	0.255	0.012	0.058	403	0.185	7.50	19.0	<dl	<dl	n.r.	9.25	<dl	0.510	0.101	24.1	0.209	0.058	<dl	<dl	<dl	<dl	0.016	3.E-4	1.47	0.002
2776-CCP-01d	3.46	0.046	0.243	1600	0.031	0.230	204	<dl	<dl	n.r.	0.720	<dl	9.40	15.5	1.08	0.005	0.044	<dl	<dl	<dl	<dl	0.001	4.E-4	2.98	5.71
2776-CCP-02.d	2.55	0.046	1.95	1610	0.021	0.167	77.8	<dl	0.015	n.r.	1.27	<dl	10.2	8.43	0.173	0.004	0.030	<dl	<dl	<dl	<dl	9.E-4	3.E-4	2.95	5.36
2776-CCP-03.d	2.50	0.170	2.60	1320	0.024	0.400	73.3	<dl	<dl	n.r.	1.41	<dl	6.55	9.43	0.545	0.041	0.034	<dl	<dl	<dl	<dl	0.001	3.E-4	2.59	4.98
2776-CCP-04.d	5.50	0.092	2.10	1071	0.025	0.200	51.4	<dl	<dl	n.r.	0.803	<dl	8.20	12.0	0.181	0.005	0.033	<dl	<dl	<dl	<dl	9.E-4	3.E-4	1.58	2.08
2776-CCP-05.d	3.55	0.085	0.205	1630	0.017	0.204	59.2	<dl	<dl	n.r.	0.866	<dl	11.3	5.11	0.082	0.003	0.032	<dl	<dl	<dl	<dl	9.E-4	2.E-4	1.51	2.63
2776-CCP-06.d	3.08	0.096	0.199	1300	0.016	0.202	121	0.024	<dl	n.r.	0.709	<dl	8.03	7.79	0.109	0.004	0.028	<dl	<dl	<dl	<dl	6.E-4	3.E-4	2.57	3.01

Grain ID	*Mn* 55	Co 59	*Ni* 60	*Zn* 66	*Ga* 71	As 75	*Se* 82	Mo 95	Ru 101	Rh 103	*Ag* 107	Pd 108	Cd 111	*In* 115	*Sn* 118	*Sb* 121	*Te* 128	Re 185	Os 189	Ir 193	Pt 195	*Au* 197	Tl 205	*Pb* 208	*Bi* 209
55um	0.470	0.023	0.241	0.353	0.028	0.223	2.53	0.030	0.023	0.005	0.023	0.014	0.046	0.012	0.073	0.022	0.256	0.009	0.021	0.007	0.013	0.010	0.004	0.012	0.007
33um	0.939	0.046	0.722	1.06	0.085	0.445	5.07	0.061	0.068	0.009	0.069	0.041	0.137	0.025	0.218	0.067	0.513	0.027	0.042	0.020	0.039	0.030	0.011	0.037	0.013
2780-CCP-01d	2.62	0.010	2.50	110	0.154	<dl	9.40	<dl	<dl	n.r.	2.12	<dl	0.270	13.9	0.580	0.280	0.021	<dl	<dl	<dl	<dl	0.025	3.E-4	0.486	0.129
2780-CCP-02.d	3.17	0.009	0.034	107	0.588	<dl	6.80	<dl	<dl	n.r.	3.15	<dl	0.132	42.3	0.383	0.261	0.013	<dl	<dl	<dl	<dl	0.014	2.E-4	0.523	0.007
2780-CCP-03.d	2.83	0.006	0.041	93.9	0.395	0.840	4.50	<dl	0.016	n.r.	2.94	<dl	0.210	216	0.142	7.28	0.011	<dl	<dl	<dl	0.019	3.E-4	6.E-4	2.40	0.076
2780-CCP-04.d	2.93	0.008	2.10	75.0	1.69	1.23	2.30	<dl	<dl	n.r.	2.82	<dl	0.081	159	0.430	4.20	0.012	<dl	<dl	<dl	<dl	3.E-4	5.E-4	0.570	0.044
2780-CCP-05.d	3.27	0.011	0.040	76.2	1.11	<dl	8.60	<dl	<dl	n.r.	4.24	<dl	0.221	145	0.930	2.03	0.019	<dl	<dl	<dl	<dl	0.001	7.E-4	4.95	2.61
2780-CCP-06.d	2.61	0.012	0.015	77.0	22.1	0.530	9.20	<dl	<dl	n.r.	3.58	<dl	0.160	7.13	0.220	1.17	0.013	<dl	<dl	<dl	<dl	3.E-4	4.E-4	0.560	0.007
2807-CCP-01d	2.67	0.013	1.83	850	0.120	<dl	60.1	<dl	<dl	n.r.	0.340	<dl	2.17	2.30	0.029	0.003	0.030	<dl	<dl	<dl	<dl	6.E-4	0.00	0.207	0.343
2807-CCP-02.d	2.87	0.009	0.131	855	0.016	<dl	105	<dl	<dl	n.r.	0.398	<dl	2.76	104	0.065	0.001	0.020	<dl	<dl	<dl	<dl	1.E-4	0.00	0.015	0.018
2807-CCP-03.d	2.61	0.035	1.31	622	0.029	<dl	111	<dl	<dl	n.r.	0.361	<dl	2.07	112	0.029	0.003	0.018	<dl	<dl	<dl	<dl	6.E-4	0.00	0.043	0.164
2807-CCP-04.d	2.68	0.049	0.111	595	0.017	<dl	127	<dl	<dl	n.r.	0.252	<dl	2.15	127	0.117	0.002	0.019	<dl	<dl	<dl	<dl	2.E-4	0.00	0.028	0.077
2807-CCP-05.d	2.36	0.012	2.60	685	0.035	<dl	73.5	<dl	<dl	n.r.	0.411	<dl	3.02	306	0.030	0.005	0.030	<dl	<dl	<dl	<dl	6.E-4	0.00	0.121	0.260
2807-CCP-06.d	2.73	0.011	1.86	786	0.039	<dl	82.6	<dl	<dl	n.r.	0.283	<dl	2.76	223	0.037	0.003	0.027	<dl	<dl	<dl	<dl	5.E-4	0.00	0.039	0.049
2811-CCP-01d	2.47	0.093	110	6.74	0.372	36.1	0.743	1.27	<dl	n.r.	25.5	<dl	2.79	207	1.73	72.7	0.033	<dl	<dl	<dl	0.060	0.003	0.009	4.21	61.9
2811-CCP-02.d	3.14	0.007	0.015	4.02	0.178	0.400	0.525	0.156	<dl	n.r.	2.47	<dl	0.022	97.2	0.354	0.770	0.010	<dl	<dl	<dl	<dl	7.E-4	2.E-4	0.170	2.04
2811-CCP-03.d	3.01	0.008	0.038	5.39	0.237	<dl	0.550	0.120	<dl	n.r.	1.59	<dl	0.097	138	1.46	0.115	0.015	<dl	<dl	<dl	<dl	0.003	3.E-4	0.590	3.78
2811-CCP-04.d	2.87	0.010	0.028	5.62	0.535	0.296	0.603	<dl	<dl	n.r.	2.10	<dl	0.071	125	0.028	0.641	0.017	<dl	<dl	<dl	<dl	0.002	3.E-4	0.337	1.48
2811-CCP-05.d	3.53	0.045	0.035	12.2	0.601	8.16	0.756	1.17	0.019	n.r.	4.30	<dl	0.242	107	1.58	18.3	0.015	<dl	<dl	<dl	<dl	0.005	8.E-4	0.640	4.11
2811-CCP-06.d	3.04	0.179	0.065	4.38	0.764	127	0.647	6.85	<dl	n.r.	76.4	<dl	3.04	271	1.01	286	0.030	<dl	<dl	<dl	<dl	0.023	0.010	6.98	284
2819-CCP-01d	3.04	0.008	0.043	4.82	0.213	0.295	0.599	0.174	<dl	n.r.	0.803	<dl	0.213	101	0.328	0.386	0.016	<dl	<dl	<dl	<dl	7.E-4	2.E-4	0.187	2.68
2819-CCP-02.d	2.86	0.012	1.33	8.02	0.431	4.82	0.728	0.053	0.016	n.r.	1.34	<dl	0.360	170	1.33	8.19	0.021	<dl	<dl	<dl	<dl	0.002	3.E-4	0.086	13.7
2819-CCP-03.d	3.09	0.010	0.054	5.01	0.444	0.290	0.796	<dl	<dl	n.r.	1.09	<dl	0.340	124	0.317	0.509	0.020	<dl	<dl	<dl	<dl	8.E-4	3.E-4	0.167	2.19
2819-CCP-04.d	2.80	0.082	1.47	13.5	1.28	17.1	3.40	<dl	<dl	n.r.	3.66	<dl	0.910	964	14.0	26.6	0.019	<dl	<dl	<dl	<dl	0.007	5.E-4	0.590	22.9
2819-CCP-05.d	3.24	0.011	0.073	13.7	0.500	0.510	19.4	<dl	<dl	n.r.	1.26	<dl	0.520	268	9.80	3.51	0.023	<dl	<dl	<dl	<dl	0.002	5.E-4	0.770	3.91
2819-CCP-06.d	3.13	0.010	0.092	25.1	1.23	1.99	64.3	<dl	<dl	n.r.	1.85	<dl	1.15	512	231	7.99	0.028	<dl	<dl	<dl	<dl	0.003	0.006	4.15	10.0
CM1CCP-001d	1.82	0.113	0.057	180	1.30	<dl	3.70	<dl	<dl	n.r.	2.87	<dl	5.12	0.472	0.058	1.16	0.030	<dl	<dl	<dl	<dl	8.E-4	0.002	2.06	0.014
CM1CCP-002.d	2.51	0.380	0.068	202	0.018	<dl	2.04	0.060	0.190	n.r.	6.63	<dl	8.10	0.469	0.056	1.16	0.055	<dl	<dl	<dl	<dl	0.002	9.E-4	2.54	0.027
CM1CCP-003.d	1.60	0.280	0.100	186	0.092	<dl	5.00	<dl	<dl	n.r.	5.68	<dl	5.00	0.479	0.150	0.680	0.043	0.220	<dl	<dl	<dl	0.002	0.250	1.07	0.005
CM1CCP-004.d	0.304	0.280	0.086	178	0.059	<dl	3.70	<dl	<dl	n.r.	6.88	<dl	5.00	0.247	0.049	0.520	0.034	<dl	<dl	<dl	<dl	0.001	5.E-4	1.24	0.019
CM1CCP-005.d	0.292	0.610	13.0	187	0.410	<dl	1.73	<dl	0.140	n.r.	7.02	<dl	5.73	0.087	0.135	0.267	0.630	0.037	<dl	<dl	<dl	0.001	4.E-4	0.530	0.006
CM1CCP-006.d	1.72	0.390	0.062	164	0.090	<dl	2.85	<dl	<dl	n.r.	26.0	<dl	4.95	0.131	0.079	0.590	0.037	<dl	<dl	<dl	<dl	0.001	7.E-4	1.10	0.007
CM2CCP-001d	1.10	0.620	2.20	141	0.094	1.27	9.40	<dl	<dl	n.r.	3.99	<dl	4.03	0.238	0.055	4.90	0.036	<dl	<dl	<dl	<dl	9.E-4	0.006	1.07	0.022
CM2CCP-002.d	0.960	0.073	27.0	170	0.088	0.980	4.60	<dl	<dl	n.r.	9.33	<dl	4.25	0.043	0.040	0.250	0.035	<dl	<dl	<dl	<dl	5.E-4	7.E-4	3.10	0.011
CM2CCP-003.d	0.241	0.520	250	151	0.060	1.17	3.00	<dl	<dl	n.r.	8.22	<dl	3.75	0.057	0.170	0.001	0.037	0.050	<dl	<dl	<dl	5.E-4	2.E-4	0.670	0.032
CM2CCP-004.d	2.20	1.80	110	139	0.117	0.840	5.30	<dl	0.470	n.r.	4.36	<dl	3.78	0.055	0.049	0.820	0.041	<dl	<dl	0.011	<dl	7.E-4	8.E-4	2.30	0.024
CM2CCP-005.d	0.222	0.270	90.0	132	0.075	1.17	3.70	<dl	0.170	n.r.	3.99	<dl	3.39	0.077	0.115	0.750	0.043	0.020	<dl	<dl	<dl	0.028	6.E-4	1.49	0.007
CM2CCP-006.d	1.77	0.066	60.0	148	0.057	0.990	5.30	<dl	<dl	n.r.	5.47	<dl	4.22	0.147	0.180	0.098	0.042	<dl	<dl	<dl	<dl	6.E-4	7.E-4	15.0	0.004
PLS1CCP-001d	1.56	0.240	0.017	413	0.061	<dl	19.2	<dl	<dl	n.r.	1222	<dl	0.260	0.114	1.64	0.172	0.036	<dl	<dl	<dl	<dl	0.001	0.011	6.00	0.006
PLS1CCP-003.d	0.233	0.610	2.00	53.3	0.133	1.30	24.7	<dl	<dl	n.r.	1810	<dl	0.250	0.086	74.3	0.089	0.041	<dl	0.150	<dl	<dl	0.030	4.E-4	0.480	0.005
PLS1CCP-004.d	1.93	0.680	0.800	45.1	0.521	<dl	146	<dl	<dl	n.r.	1990	<dl	0.170	0.223	8.21	0.059	0.045	0.190	<dl	<dl	<dl	0.002	6.E-4	0.225	0.071
PLS1CCP-005.d	1.35	0.482	0.024	37.6	0.444	<dl	16.2	<dl	<dl	n.r.	1121	<dl	0.510	0.155	2.24	0.114	0.037	<dl	<dl	<dl	<dl	0.033	4.E-4	0.600	0.012
PLS2CCP-001d	2.30	0.380	0.022	49.1	0.500	8.50	415	<dl	<dl	n.r.	720	<dl	0.320	0.262	0.830	8.10	0.035	<dl	<dl	<dl	<dl	0.002	0.206	3.30	0.008
PLS2CCP-002.d	2.18	0.190	0.017	46.9	1.30	6.00	510	<dl	<dl	n.r.	554	<dl	0.130	0.232	4.36	1.66	0.036	<dl	<dl	<dl	<dl	0.002	0.035	8.00	0.007
ROZ2CCP-001d	2.40	0.470	1.40	112	0.250	<dl	20.3	<dl	<dl	n.r.	2.38	<dl	0.600	0.055	0.580	0.264	0.041	0.041	<dl	<dl	<dl	7.E-4	4.E-4	1.43	0.004
ROZ2CCP-002.d	17.0	0.100	0.046	25.5	0.570	<dl	28.8	<dl	<dl	n.r.	12.7	<dl	0.057	0.020	0.086	3.23	0.730	<dl	<dl	<dl	<dl	0.002	0.001	5.81	0.800
IOCG																									
080CCP-01d	0.570	0.081	10.6	145	0.309	<dl	37.4	<dl	0.021	n.r.	8.97	<dl	2.31	6.53	18.0	0.014	6.70	<dl	<dl	<dl	<dl	0.001	8.E-4	13.2	0.674
080CCP-02.d	0.178	0.039	10.1	143	0.350	<dl	37.4	<dl	<dl	n.r.	8.97	<dl	2.41	6.44	9.31	0.022	0.565	<dl	<dl	<dl	<dl	7.E-4	6.E-4	2.67	0.247

Grain ID	*Mn* 55	*Co* 59	*Ni* 60	*Zn* 66	*Ga* 71	As 75	*Se* 82	Mo 95	Ru 101	Rh 103	*Ag* 107	Pd 108	Cd 111	*In* 115	*Sn* 118	*Sb* 121	*Te* 128	Re 185	Os 189	Ir 193	Pt 195	*Au* 197	Tl 205	*Pb* 208	*Bi* 209
55um	0.470	0.023	0.241	0.353	0.028	0.223	2.53	0.030	0.023	0.005	0.023	0.014	0.046	0.012	0.073	0.022	0.256	0.009	0.021	0.007	0.013	0.010	0.004	0.012	0.007
33um	0.939	0.046	0.722	1.06	0.085	0.445	5.07	0.061	0.068	0.009	0.069	0.041	0.137	0.025	0.218	0.067	0.513	0.027	0.042	0.020	0.039	0.030	0.011	0.037	0.013
080CCP-03.d	0.590	0.023	8.62	143	0.336	<dl	35.9	<dl	<dl	n.r.	8.82	<dl	1.96	6.31	17.6	0.005	4.50	<dl	<dl	<dl	<dl	7.E-4	0.002	2.36	0.242
080CCP-04.d	0.620	0.030	8.26	153	0.350	<dl	35.9	<dl	<dl	n.r.	9.36	<dl	2.42	6.47	13.2	0.042	6.70	<dl	<dl	<dl	<dl	0.001	8.E-4	5.53	0.611
080CCP-05.d	0.148	0.070	9.50	146	0.271	<dl	36.5	<dl	<dl	n.r.	10.4	<dl	2.47	6.33	8.61	0.090	7.00	<dl	<dl	<dl	<dl	0.011	9.E-4	10.9	1.82
080CCP-06.d	0.130	0.028	5.31	118	0.047	<dl	36.4	<dl	<dl	n.r.	9.95	<dl	2.11	6.28	7.98	0.099	0.360	<dl	<dl	<dl	<dl	0.041	0.013	7.75	1.48
081CCP-01d	0.040	0.418	0.005	0.480	0.015	<dl	36.2	<dl	<dl	n.r.	0.108	<dl	0.003	2.85	5.71	0.002	0.016	<dl	<dl	<dl	<dl	2.E-4	0.00	0.302	0.099
081CCP-02.d	0.129	0.161	0.020	0.253	0.026	<dl	38.9	<dl	<dl	n.r.	0.720	<dl	0.057	2.48	1.80	0.006	0.042	<dl	<dl	<dl	<dl	0.001	0.036	6.72	1.21
081CCP-03.d	0.430	0.270	0.131	0.550	0.025	<dl	39.2	<dl	<dl	n.r.	0.319	<dl	0.014	2.75	5.73	0.005	0.029	<dl	<dl	<dl	<dl	0.001	5.E-4	3.82	0.588
081CCP-04.d	0.057	0.206	0.006	0.580	0.016	<dl	33.1	<dl	<dl	n.r.	0.113	<dl	0.008	2.79	5.13	0.003	0.022	<dl	<dl	<dl	<dl	5.E-4	0.002	0.522	0.151
081CCP-05.d	0.047	0.240	0.005	0.470	0.017	<dl	33.8	<dl	<dl	n.r.	0.212	<dl	0.007	2.91	5.15	0.010	0.019	<dl	<dl	<dl	<dl	4.E-4	1.E-4	0.823	0.304
081CCP-06.d	0.066	0.331	0.003	0.330	0.222	<dl	33.4	<dl	<dl	n.r.	0.325	<dl	0.005	2.90	6.21	0.003	0.018	<dl	<dl	<dl	<dl	8.E-4	0.00	1.15	0.381
081CCP-07.d	0.066	0.285	0.007	0.610	0.020	<dl	40.3	<dl	<dl	n.r.	0.208	<dl	0.007	2.88	4.56	0.003	0.025	<dl	<dl	<dl	<dl	3.E-4	3.E-4	2.35	0.467
084CCP-01d	0.149	0.035	2.14	132	0.550	<dl	34.2	<dl	<dl	n.r.	1.18	<dl	5.02	5.40	11.9	0.005	9.20	<dl	<dl	<dl	<dl	0.001	2.E-4	3.83	0.255
084CCP-02.d	0.168	0.028	3.10	182	0.685	<dl	30.9	<dl	<dl	n.r.	0.890	<dl	5.72	5.11	10.3	0.004	11.2	<dl	<dl	<dl	<dl	6.E-4	7.E-4	2.84	0.155
084CCP-03.d	0.156	0.058	4.00	159	0.770	<dl	32.9	<dl	<dl	n.r.	0.980	<dl	4.87	5.05	15.4	0.005	16.7	<dl	<dl	<dl	<dl	0.007	7.E-4	1.92	0.103
084CCP-04.d	0.145	0.035	3.02	146	0.724	<dl	30.2	<dl	<dl	n.r.	0.790	<dl	4.50	4.94	14.1	0.005	9.20	<dl	<dl	<dl	<dl	4.E-4	7.E-4	2.26	0.092
084CCP-05.d	0.162	0.046	3.67	129	0.710	<dl	32.4	<dl	<dl	n.r.	0.840	<dl	4.60	4.91	15.5	0.004	15.5	<dl	<dl	<dl	<dl	0.015	7.E-4	2.15	0.181
084CCP-06.d	0.161	0.107	3.08	178	0.520	<dl	32.9	<dl	<dl	n.r.	0.750	<dl	5.25	4.78	15.5	0.004	14.2	<dl	<dl	<dl	<dl	5.E-4	4.E-4	5.66	0.140
084CCP-07.d	0.164	0.062	3.60	151	0.630	<dl	30.6	<dl	<dl	n.r.	0.860	<dl	5.18	4.84	14.6	0.005	13.0	<dl	<dl	<dl	<dl	4.E-4	6.E-4	2.04	0.106
194-CCP-01d	2.62	6.30	0.116	132	0.463	<dl	145	<dl	<dl	n.r.	25.6	<dl	0.750	3.67	63.0	0.054	0.540	<dl	<dl	<dl	<dl	0.098	5.E-4	1.89	1.54
194-CCP-02.d	2.64	6.64	2.31	143	0.420	<dl	158	<dl	<dl	n.r.	28.1	<dl	0.800	4.53	79.1	0.091	1.10	<dl	<dl	<dl	<dl	0.094	4.E-4	0.920	2.27
194-CCP-03.d	2.61	5.79	1.62	134	0.455	<dl	139	<dl	0.012	n.r.	25.5	<dl	0.890	3.75	58.0	0.089	0.482	<dl	<dl	<dl	<dl	0.068	4.E-4	2.25	2.14
194-CCP-04.d	2.60	2.99	0.146	120	0.406	<dl	135	<dl	<dl	n.r.	24.9	<dl	0.950	3.20	58.4	0.120	0.420	<dl	<dl	<dl	<dl	0.200	0.013	1.93	1.62
194-CCP-05.d	2.85	3.41	0.137	135	0.458	<dl	149	<dl	<dl	n.r.	25.2	<dl	0.920	5.69	75.2	0.082	0.910	<dl	<dl	<dl	<dl	0.082	5.E-4	2.45	2.32
196-CCP-01d	3.67	9.65	110	562	0.600	<dl	28.6	<dl	<dl	n.r.	73.9	<dl	3.22	29.9	25.0	0.271	0.048	<dl	<dl	<dl	<dl	0.045	0.030	1.96	3.16
196-CCP-03.d	3.73	7.11	120	582	0.490	<dl	30.0	<dl	<dl	n.r.	71.1	<dl	3.22	29.2	24.6	0.346	0.056	<dl	<dl	<dl	<dl	0.002	0.042	3.90	5.37
196-CCP-04.d	3.96	9.99	111	592	0.473	<dl	24.7	<dl	0.027	n.r.	68.3	<dl	3.20	25.5	23.7	0.128	0.044	<dl	<dl	<dl	<dl	0.008	0.012	1.44	2.08
196-CCP-05.d	4.63	9.21	119	546	0.502	<dl	26.5	<dl	<dl	n.r.	62.1	<dl	3.14	23.5	22.2	0.097	0.310	<dl	<dl	<dl	<dl	0.030	0.032	1.39	1.73
196-CCP-06.d	4.15	2.06	123	571	0.420	<dl	29.1	<dl	<dl	n.r.	67.9	<dl	2.35	23.7	24.9	0.163	0.310	<dl	<dl	<dl	<dl	0.027	8.E-4	1.85	2.71
2081017CCP-01d	0.198	0.004	0.440	160	0.029	<dl	1.96	0.061	<dl	n.r.	4.23	<dl	0.280	28.2	2.26	0.007	0.027	<dl	<dl	<dl	<dl	0.001	0.017	3.60	0.383
2081017CCP-02.d	1.83	0.260	17.0	138	0.017	<dl	2.27	<dl	<dl	n.r.	3.73	<dl	0.360	43.4	17.2	1.00	0.050	2.50	<dl	<dl	<dl	0.007	0.069	1.33	0.012
2081017CCP-03.d	2.28	0.220	18.0	140	0.012	<dl	1.96	<dl	<dl	n.r.	3.56	<dl	1.10	29.4	2.64	0.007	0.069	0.029	0.130	<dl	<dl	0.001	6.E-4	1.32	0.172
2081017CCP-04.d	2.40	0.900	0.038	185	0.050	<dl	4.40	0.200	<dl	n.r.	5.18	<dl	0.200	42.1	5.60	0.014	0.032	<dl	<dl	<dl	0.080	0.001	0.014	0.880	1.60
2081017CCP-05.d	0.204	0.049	0.900	170	0.011	<dl	2.07	1.30	<dl	n.r.	4.71	<dl	0.150	25.2	2.64	0.007	0.024	<dl	<dl	<dl	<dl	0.002	3.E-4	0.920	0.178
2129484CCP-01d	2.65	6.10	5.40	493	0.061	<dl	28.0	<dl	<dl	n.r.	1.06	<dl	1.85	6.97	34.1	0.067	23.9	<dl	0.080	0.100	<dl	0.140	0.148	15.5	0.794
2129484CCP-02.c	2.48	10.4	0.058	508	0.015	24.0	31.9	<dl	<dl	n.r.	0.600	<dl	1.41	7.43	12.1	0.014	16.0	<dl	<dl	<dl	<dl	0.002	0.015	4.96	0.262
2129484CCP-03.c	1.64	4.13	1.00	386	0.066	<dl	40.0	<dl	<dl	n.r.	0.590	<dl	1.51	6.15	13.3	0.011	11.4	<dl	<dl	<dl	0.180	0.160	0.011	3.05	0.146
2129484CCP-04.c	1.92	2.05	1.10	441	0.015	<dl	38.8	0.210	0.060	n.r.	0.590	<dl	1.18	8.54	89.6	0.017	29.7	0.048	1.10	<dl	0.110	0.036	0.033	3.54	0.295
363CCP-02.d	1.22	23.3	3.91	584	0.172	<dl	16.4	<dl	<dl	n.r.	1.49	<dl	1.57	7.56	0.110	0.089	2.49	<dl	<dl	<dl	<dl	8.E-4	4.E-4	0.935	0.549
363CCP-03.d	1.12	27.2	4.50	390	0.207	<dl	17.7	<dl	<dl	n.r.	1.42	<dl	0.990	7.38	0.430	0.098	3.66	<dl	<dl	<dl	<dl	0.001	0.011	0.483	1.87
363CCP-04.d	0.950	9.07	0.032	418	0.227	<dl	14.3	<dl	<dl	n.r.	1.49	<dl	1.24	8.27	0.084	0.397	2.40	<dl	<dl	<dl	<dl	0.002	0.207	3.26	1.65
363CCP-05.d	1.00	25.8	0.480	730	0.188	<dl	22.4	<dl	<dl	n.r.	1.48	<dl	1.73	8.06	0.287	0.151	3.91	<dl	<dl	<dl	<dl	0.018	2.E-4	1.04	2.50
363CCP-06.d	0.870	32.0	0.850	366	0.212	<dl	20.1	<dl	<dl	n.r.	1.37	<dl	1.06	7.59	0.141	0.254	2.03	<dl	<dl	<dl	<dl	0.001	3.E-4	2.67	1.22
363-CCP-1d	0.930	35.4	5.46	506	0.145	<dl	22.9	<dl	0.049	n.r.	1.44	<dl	1.21	7.55	0.460	0.082	4.18	<dl	<dl	<dl	<dl	0.009	3.E-4	0.432	1.99
367CCP-01d	0.110	0.018	0.012	71.3	0.240	0.220	37.6	<dl	0.034	n.r.	62.5	<dl	0.290	2.83	0.026	0.170	0.970	<dl	<dl	<dl	<dl	0.038	3.E-4	2.22	0.651
367CCP-03.d	0.232	0.009	0.029	109	0.325	<dl	30.4	<dl	<dl	n.r.	60.1	<dl	0.355	2.84	0.128	0.243	1.50	<dl	<dl	<dl	<dl	0.088	5.E-4	2.59	0.784
367CCP-04.d	0.170	0.007	0.021	87.5	0.390	0.290	26.5	<dl	<dl	n.r.	61.9	<dl	0.320	3.11	0.195	0.448	1.28	<dl	<dl	<dl	<dl	0.046	0.003	5.51	1.46
367CCP-05.d	0.164	0.007	0.018	81.9	0.215	0.280	40.0	<dl	0.021	n.r.	61.5	<dl	0.415	3.30	0.062	0.400	0.870	<dl	<dl	<dl	<dl	0.025	0.023	5.87	2.15

Grain ID	*Mn* 55	*Co* 59	*Ni* 60	*Zn* 66	*Ga* 71	As 75	*Se* 82	Mo 95	Ru 101	Rh 103	*Ag* 107	Pd 108	Cd 111	*In* 115	*Sn* 118	*Sb* 121	*Te* 128	Re 185	Os 189	Ir 193	Pt 195	*Au* 197	Tl 205	*Pb* 208	*Bi* 209
55um	0.470	0.023	0.241	0.353	0.028	0.223	2.53	0.030	0.023	0.005	0.023	0.014	0.046	0.012	0.073	0.022	0.256	0.009	0.021	0.007	0.013	0.010	0.004	0.012	0.007
33um	0.939	0.046	0.722	1.06	0.085	0.445	5.07	0.061	0.068	0.009	0.069	0.041	0.137	0.025	0.218	0.067	0.513	0.027	0.042	0.020	0.039	0.030	0.011	0.037	0.013
367CCP-06.d	0.150	0.039	0.024	63.4	0.120	<dl	32.7	<dl	0.036	n.r.	59.1	<dl	0.480	2.65	0.033	0.166	1.39	<dl	<dl	<dl	<dl	0.053	0.002	2.92	0.743
414CCP-01d	1.67	8.99	3.65	940	0.388	<dl	18.6	<dl	0.035	n.r.	187	<dl	4.04	26.1	14.2	0.857	2.22	<dl	<dl	<dl	<dl	0.061	6.E-4	0.875	2.58
414CCP-02.d	2.65	6.17	2.98	401	0.420	<dl	16.4	<dl	<dl	n.r.	169	<dl	2.23	34.3	26.1	0.515	2.65	<dl	<dl	<dl	<dl	0.096	7.E-4	1.29	2.83
414CCP-03.d	1.45	6.80	3.11	399	0.275	<dl	16.0	<dl	<dl	n.r.	184	<dl	2.13	27.8	17.2	1.95	1.12	<dl	<dl	<dl	<dl	0.090	0.085	1.80	1.91
414CCP-04.d	6.98	8.59	3.89	457	0.320	<dl	15.3	<dl	<dl	n.r.	172	<dl	1.72	24.1	20.4	0.610	1.97	<dl	<dl	<dl	<dl	0.077	0.009	5.76	3.32
414CCP-05.d	1.33	8.39	3.78	444	0.278	<dl	16.4	<dl	0.020	n.r.	180	<dl	2.84	21.8	15.6	1.07	1.93	<dl	<dl	<dl	<dl	0.121	0.270	1.45	2.27
414CCP-06.d	1.07	8.41	3.09	571	0.340	<dl	19.8	<dl	<dl	n.r.	172	<dl	2.33	19.7	17.0	1.21	1.33	<dl	<dl	<dl	<dl	0.041	7.E-4	1.76	1.61
422CCP-01d	0.127	0.007	0.012	88.4	0.327	<dl	66.2	<dl	0.021	n.r.	190	<dl	0.300	3.28	0.222	0.024	0.560	<dl	<dl	<dl	<dl	6.E-4	0.001	0.948	0.364
422CCP-02.d	0.151	0.008	0.170	73.8	0.284	<dl	60.8	<dl	<dl	n.r.	208	<dl	0.206	3.14	0.089	0.080	0.450	<dl	<dl	<dl	<dl	0.001	0.009	2.83	1.55
422CCP-03.d	0.170	0.007	0.014	66.1	0.360	<dl	57.4	<dl	0.025	n.r.	211	<dl	0.200	3.35	0.080	0.039	0.420	<dl	<dl	<dl	<dl	8.E-4	0.004	1.68	0.732
422CCP-04.d	0.136	0.008	0.370	73.9	0.327	<dl	59.9	<dl	<dl	n.r.	218	<dl	0.246	3.34	0.176	0.045	0.520	<dl	<dl	<dl	<dl	7.E-4	0.001	2.39	1.02
422CCP-05.d	0.106	0.110	0.011	95.0	0.339	<dl	67.8	<dl	<dl	n.r.	195	<dl	0.215	1.52	0.032	0.004	0.590	<dl	<dl	<dl	<dl	9.E-4	1.E-4	0.253	0.142
422CCP-06.d	0.130	0.096	0.220	92.3	0.420	<dl	46.1	<dl	<dl	n.r.	202	<dl	0.129	1.36	0.032	0.052	0.740	<dl	<dl	<dl	<dl	0.001	5.E-4	1.85	1.28
516CCP-01d	0.900	0.365	0.027	243	0.231	<dl	26.1	<dl	<dl	n.r.	28.1	<dl	1.13	7.70	5.24	0.008	1.68	<dl	<dl	<dl	<dl	0.586	2.E-4	5.20	6.57
516CCP-02.d	0.520	0.500	0.030	171	0.280	<dl	20.6	<dl	<dl	n.r.	14.9	<dl	0.620	7.31	4.96	0.009	0.046	<dl	<dl	<dl	<dl	0.065	0.001	16.0	5.70
516CCP-03.d	0.660	0.555	0.026	179	0.314	<dl	20.9	<dl	0.036	n.r.	14.0	<dl	0.585	7.60	5.48	0.008	0.046	<dl	<dl	<dl	<dl	0.137	0.005	9.57	3.56
516CCP-04.d	0.610	0.396	0.024	228	0.344	<dl	22.4	<dl	<dl	n.r.	16.5	<dl	0.630	7.85	5.18	0.007	1.26	<dl	<dl	<dl	<dl	0.180	2.E-4	3.05	3.10
516CCP-05.d	7.07	0.910	0.037	244	0.308	<dl	23.7	<dl	<dl	n.r.	14.7	<dl	1.41	7.58	6.21	0.007	1.89	<dl	<dl	<dl	<dl	0.125	3.E-4	25.6	4.70
516CCP-06.d	0.770	0.384	0.033	242	0.320	<dl	23.0	<dl	<dl	n.r.	18.4	<dl	0.910	7.44	5.19	0.018	2.05	<dl	<dl	<dl	<dl	0.054	4.E-4	19.2	4.01
516CCP-07.d	1.52	0.521	0.034	234	0.272	<dl	19.2	<dl	<dl	n.r.	23.3	<dl	0.860	7.54	5.79	0.008	1.22	<dl	<dl	<dl	<dl	0.172	0.002	24.3	5.95
600-CCP-01d	2.33	1.31	1.82	329	28.8	<dl	555	<dl	<dl	n.r.	8.85	<dl	3.45	332	450	0.228	0.055	<dl	<dl	<dl	<dl	0.020	0.012	5.09	0.286
600-CCP-02.d	2.67	1.24	1.80	372	44.5	<dl	800	<dl	0.014	n.r.	74.9	<dl	3.58	366	631	0.231	0.056	<dl	<dl	<dl	<dl	0.002	0.008	3.90	0.240
600-CCP-03.d	3.03	1.24	0.086	430	40.8	<dl	819	<dl	<dl	n.r.	352	<dl	4.15	353	339	0.268	0.055	<dl	<dl	<dl	<dl	0.003	0.015	5.16	0.297
600-CCP-04.d	2.74	1.31	0.086	286	35.1	<dl	820	<dl	0.017	n.r.	67.1	<dl	3.41	323	569	0.275	0.062	<dl	<dl	<dl	<dl	0.016	0.012	4.03	0.290
600-CCP-05.d	190	1.83	0.199	249	32.0	<dl	886	0.035	<dl	n.r.	66.6	<dl	4.33	312	444	1.12	0.076	<dl	<dl	<dl	<dl	0.027	0.103	21.1	1.11
600-CCP-06.d	2.84	1.97	2.00	237	34.3	<dl	676	<dl	<dl	n.r.	61.0	<dl	2.80	310	440	0.175	0.079	<dl	<dl	<dl	<dl	0.018	0.015	3.35	0.210
AF443CCP-01d	0.068	1.43	0.009	0.730	0.072	<dl	22.3	<dl	<dl	n.r.	0.381	<dl	0.006	1.68	4.40	0.003	0.740	<dl	<dl	<dl	<dl	0.018	0.00	0.629	0.440
AF443CCP-02.d	0.072	1.25	0.007	0.365	0.155	<dl	23.8	<dl	0.020	n.r.	0.095	<dl	0.004	1.59	2.91	0.004	0.490	<dl	<dl	<dl	<dl	3.E-4	0.00	0.457	0.254
AF443CCP-03.d	0.070	1.47	0.011	1.80	0.056	<dl	22.0	<dl	0.029	n.r.	0.320	<dl	0.008	1.62	3.95	0.002	0.660	<dl	<dl	<dl	<dl	0.018	0.00	0.454	0.367
AF443CCP-04.d	0.063	1.48	0.010	0.590	0.022	<dl	25.7	<dl	<dl	n.r.	0.403	<dl	0.006	1.62	4.18	0.003	0.690	<dl	<dl	<dl	<dl	0.034	0.00	0.894	0.857
AF443CCP-05.d	0.103	1.31	0.025	0.159	0.084	<dl	23.1	<dl	<dl	n.r.	0.273	<dl	0.013	1.66	3.88	0.002	0.580	<dl	<dl	<dl	<dl	0.013	1.E-4	1.16	0.763
AF443CCP-06.d	0.390	1.40	0.009	0.190	0.090	<dl	19.5	<dl	0.017	n.r.	0.188	<dl	0.004	1.62	3.88	0.019	0.650	<dl	<dl	<dl	<dl	0.011	1.E-4	2.17	1.06
AF443CCP-07.d	0.055	1.09	0.006	0.270	0.004	<dl	23.1	<dl	0.020	n.r.	0.236	<dl	0.004	1.72	3.90	0.003	0.660	<dl	<dl	<dl	<dl	0.013	0.00	0.962	0.790
ALECCP-01d	0.131	0.298	20.6	20.1	0.010	<dl	35.4	<dl	0.021	n.r.	4.19	<dl	0.230	3.39	6.57	0.206	2.66	<dl	<dl	<dl	<dl	0.021	0.019	0.367	2.63
ALECCP-02.d	0.104	0.329	20.7	20.2	0.008	<dl	36.3	<dl	<dl	n.r.	2.21	<dl	0.131	3.43	7.09	0.118	1.24	<dl	<dl	<dl	<dl	0.038	0.004	0.245	3.19
ALECCP-03.d	0.142	0.139	22.0	19.4	0.009	<dl	40.0	<dl	<dl	n.r.	3.27	<dl	0.123	3.71	6.32	0.230	1.78	<dl	<dl	<dl	<dl	0.023	0.027	0.346	3.60
ALECCP-04.d	0.110	0.175	21.5	19.2	0.020	<dl	32.5	<dl	0.035	n.r.	3.17	<dl	0.202	3.52	6.48	0.172	2.70	<dl	<dl	<dl	<dl	0.020	0.019	0.274	4.80
ALECCP-05.d	0.129	0.248	21.9	19.6	0.011	<dl	30.3	<dl	<dl	n.r.	4.67	<dl	0.104	3.32	6.53	0.246	2.30	<dl	<dl	<dl	<dl	0.010	0.044	0.512	6.10
ALECCP-06.d	2.40	0.122	21.5	18.7	0.011	<dl	36.3	<dl	<dl	n.r.	2.04	<dl	0.052	3.49	6.24	0.080	1.09	<dl	<dl	<dl	<dl	7.E-4	0.006	0.249	1.46
ALEMAOCCP-01	0.131	1.40	21.2	18.8	0.011	<dl	37.4	<dl	0.018	n.r.	1.63	<dl	0.103	3.46	5.94	0.098	0.970	<dl	<dl	<dl	0.006	0.020	0.013	0.455	3.30
ALEMAOCCP-02	3.00	0.920	19.9	19.1	0.360	<dl	31.9	<dl	0.033	n.r.	1.87	<dl	0.025	3.37	6.05	0.083	1.03	<dl	<dl	<dl	<dl	0.012	0.005	0.419	1.91
ALEMAOCCP-03	0.168	0.895	21.6	19.1	0.011	<dl	36.8	<dl	<dl	n.r.	3.14	<dl	0.180	3.41	6.27	0.147	1.64	<dl	<dl	<dl	<dl	0.033	0.023	0.690	2.36
ALEMAOCCP-04	0.120	0.272	23.5	20.1	0.020	<dl	41.4	<dl	0.018	n.r.	5.45	<dl	0.131	3.62	6.90	0.222	18.9	<dl	<dl	<dl	<dl	0.060	0.011	1.06	6.63
ALEMAOCCP-05	0.113	0.133	21.5	19.3	0.019	<dl	39.2	<dl	<dl	n.r.	2.76	<dl	0.083	3.70	7.22	0.213	1.59	<dl	<dl	<dl	<dl	0.010	0.012	0.731	5.70
ALEMAOCCP-06	0.122	0.143	22.5	19.2	0.038	<dl	35.5	<dl	0.023	n.r.	2.57	<dl	0.138	3.56	7.01	0.111	1.62	<dl	<dl	<dl	<dl	0.013	0.004	0.759	4.20
AN01CCP-01d	10.7	0.300	30.0	550	0.700	0.250	102	<dl	<dl	n.r.	8.40	<dl	2.02	10.1	51.0	0.039	2.90	<dl	<dl	<dl	0.010	1.20	8.E-4	2.18	0.096
AN01CCP-02.d	12.1	0.243	34.9	533	0.590	0.110	95.1	<dl	<dl	n.r.	5.36	<dl	2.13	9.44	47.8	0.019	2.97	<dl	<dl	0.003	<dl	0.019	0.017	14.9	0.800

Grain ID	*Mn* 55	*Co* 59	*Ni* 60	*Zn* 66	*Ga* 71	As 75	*Se* 82	Mo 95	Ru 101	Rh 103	*Ag* 107	Pd 108	Cd 111	*In* 115	*Sn* 118	*Sb* 121	*Te* 128	Re 185	Os 189	Ir 193	Pt 195	*Au* 197	Tl 205	*Pb* 208	*Bi* 209
55um	0.470	0.023	0.241	0.353	0.028	0.223	2.53	0.030	0.023	0.005	0.023	0.014	0.046	0.012	0.073	0.022	0.256	0.009	0.021	0.007	0.013	0.010	0.004	0.012	0.007
33um	0.939	0.046	0.722	1.06	0.085	0.445	5.07	0.061	0.068	0.009	0.069	0.041	0.137	0.025	0.218	0.067	0.513	0.027	0.042	0.020	0.039	0.030	0.011	0.037	0.013
AN01CCP-04.d	5.97	0.820	38.7	563	4.70	<dl	108	<dl	<dl	n.r.	7.58	0.312	2.49	9.70	53.8	0.022	4.70	<dl	<dl	<dl	0.012	0.010	0.052	91.0	1.02
AN01CCP-05.d	13.6	0.620	40.2	596	0.480	<dl	106	<dl	<dl	n.r.	6.03	<dl	2.92	9.52	51.6	0.062	2.72	<dl	<dl	0.027	<dl	0.008	0.100	44.5	0.575
AN01CCP-06.d	2.50	1.41	44.7	476	0.170	0.260	72.3	<dl	<dl	n.r.	7.10	<dl	2.05	10.4	50.0	0.004	3.67	0.360	0.025	<dl	<dl	0.010	2.E-4	0.980	0.140
AN01CCP-07.d	4.90	0.480	34.4	567	0.520	0.270	107	<dl	1.30	n.r.	15.5	<dl	2.46	9.84	54.2	0.062	3.80	<dl	<dl	<dl	<dl	0.001	0.018	19.0	0.950
AN02CCP-01.d	3.20	5.04	8.70	473	0.216	<dl	84.8	<dl	<dl	n.r.	59.8	<dl	3.08	4.62	5.46	0.026	1.36	<dl	<dl	<dl	<dl	0.007	0.009	4.22	0.236
AN02CCP-02.d	0.228	4.66	14.3	580	0.236	1.10	94.0	<dl	<dl	n.r.	79.4	<dl	2.76	4.55	3.16	0.003	3.76	<dl	<dl	<dl	<dl	0.001	6.E-4	1.22	0.088
AN02CCP-03.d	0.930	4.22	90.0	567	0.274	<dl	83.0	<dl	0.540	n.r.	60.5	<dl	3.16	4.59	4.20	0.005	3.56	0.380	<dl	<dl	<dl	0.800	8.E-4	0.305	0.296
AN02CCP-05.d	0.208	4.12	150	499	0.273	<dl	83.6	0.044	0.035	n.r.	52.9	0.173	0.143	4.57	3.54	0.070	3.63	<dl	<dl	<dl	<dl	7.E-4	3.E-4	0.486	0.023
AN02CCP-06.d	0.910	4.63	15.0	403	0.178	<dl	74.0	<dl	<dl	n.r.	62.9	<dl	2.38	4.32	2.80	0.016	3.50	<dl	<dl	<dl	0.010	0.013	2.E-4	0.490	4.70
AN02CCP-07.d	13.0	4.68	15.3	523	0.650	<dl	82.3	<dl	<dl	n.r.	65.0	<dl	3.40	4.10	2.70	0.007	2.48	<dl	<dl	<dl	<dl	8.E-4	0.001	0.562	0.120
AN03CCP-02.d	0.630	2.09	130	631	0.860	0.310	111	<dl	<dl	n.r.	36.0	<dl	4.64	5.98	8.46	0.040	19.3	<dl	<dl	<dl	<dl	0.018	0.034	1.26	0.130
AN03CCP-03.d	0.920	1.84	0.550	406	0.413	<dl	88.9	<dl	0.100	n.r.	35.6	<dl	3.91	5.36	6.92	0.160	1.24	<dl	<dl	<dl	<dl	0.013	0.370	10.6	0.024
AN03CCP-05.d	1.14	0.760	110	434	0.220	<dl	101	<dl	<dl	n.r.	30.0	<dl	2.75	5.05	6.30	0.010	0.850	<dl	<dl	<dl	<dl	0.001	4.E-4	1.39	0.009
AN03CCP-06.d	0.830	0.284	0.112	760	0.150	<dl	78.5	<dl	<dl	n.r.	30.6	<dl	2.51	5.47	6.76	0.009	2.09	<dl	<dl	0.025	<dl	0.029	4.E-4	1.45	0.019
AN03CCP-07.d	1.07	0.910	2.70	604	0.013	<dl	67.1	<dl	<dl	n.r.	32.0	<dl	3.37	6.02	7.01	2.60	2.71	<dl	0.500	<dl	<dl	0.002	6.E-4	0.980	0.100
CHA01CCP-01d	1.30	0.186	0.048	8.14	0.072	<dl	83.8	0.110	<dl	n.r.	18.7	<dl	0.092	23.6	2.23	0.065	0.450	<dl	<dl	<dl	<dl	7.E-4	2.E-4	1.46	1.17
CHA01CCP-02.d	13.0	0.202	0.130	7.90	0.087	0.550	90.9	0.036	<dl	n.r.	19.2	<dl	0.025	23.0	2.23	0.260	0.710	<dl	0.049	0.034	<dl	0.018	0.004	2.60	4.00
CHA01CCP-03.d	0.990	0.313	120	7.00	0.013	<dl	90.0	0.130	<dl	n.r.	21.9	<dl	0.230	23.5	1.88	0.008	0.059	<dl	<dl	<dl	<dl	0.002	6.E-4	1.85	2.31
CHA01CCP-04.d	1.07	0.170	0.012	8.90	0.090	<dl	84.0	0.140	<dl	n.r.	13.5	<dl	0.050	22.3	1.62	0.128	0.040	<dl	<dl	<dl	<dl	0.002	5.E-4	2.25	2.32
CHA01CCP-05.d	1.11	0.320	0.042	13.1	0.110	0.330	93.3	<dl	0.320	n.r.	48.0	<dl	0.055	23.7	2.43	0.103	0.530	<dl	<dl	<dl	<dl	0.011	4.E-4	1.83	1.46
CHA01CCP-06.d	1.23	0.192	0.008	10.6	0.079	0.900	97.5	<dl	<dl	n.r.	38.9	<dl	0.047	24.6	2.12	0.169	1.27	<dl	<dl	0.050	<dl	0.002	0.009	1.81	2.64
CHA01CCP-07.d	0.650	0.136	0.700	8.30	0.053	0.170	97.3	<dl	<dl	n.r.	22.4	<dl	0.017	25.4	1.52	0.098	0.440	<dl	<dl	<dl	<dl	0.001	4.E-4	1.58	2.31
CNDCCP-01d	0.720	1.59	0.670	219	0.392	<dl	24.4	<dl	0.017	n.r.	68.3	<dl	0.690	4.89	13.8	0.040	4.49	<dl	<dl	<dl	<dl	0.048	2.E-4	1.23	0.820
CNDCCP-02.d	0.151	0.551	0.021	196	0.445	0.200	23.3	<dl	<dl	n.r.	65.8	<dl	0.640	4.34	4.11	0.337	0.930	<dl	<dl	<dl	<dl	0.014	0.009	5.69	1.43
CNDCCP-03.d	0.743	0.693	0.032	174	0.507	<dl	26.9	<dl	<dl	n.r.	69.1	<dl	0.720	5.27	8.10	0.011	2.98	<dl	<dl	<dl	<dl	0.040	3.E-4	1.21	2.70
CNDCCP-04.d	0.164	0.440	0.026	209	0.470	<dl	26.2	0.038	<dl	n.r.	69.3	<dl	0.850	5.18	5.96	0.089	3.92	<dl	<dl	<dl	<dl	0.038	3.E-4	1.21	3.37
CNDCCP-05.d	0.137	0.466	0.250	188	0.351	<dl	26.9	0.220	<dl	n.r.	72.1	<dl	0.790	5.25	8.13	0.007	5.28	<dl	<dl	<dl	<dl	0.120	1.E-4	0.425	3.36
CNDCCP-06.d	0.965	0.540	0.025	199	0.460	<dl	27.9	<dl	<dl	n.r.	67.0	<dl	0.630	5.02	5.59	0.040	3.54	<dl	<dl	<dl	<dl	0.001	3.E-4	1.46	2.14
CNDCCP-07.d	0.230	0.790	0.033	196	0.490	<dl	22.4	<dl	0.021	n.r.	68.8	<dl	0.890	5.18	9.93	0.033	3.12	<dl	<dl	<dl	<dl	0.017	0.003	1.30	2.60
EG113CCP-001d	2.04	0.740	1.30	151	0.234	1.36	742	<dl	0.300	n.r.	119	<dl	1.91	76.5	29.0	0.077	0.310	<dl	<dl	0.024	<dl	0.790	7.E-4	2.05	1.96
EG113CCP-002.d	1.68	1.60	1.00	110	0.430	<dl	646	0.210	<dl	n.r.	121	<dl	1.23	69.7	36.5	0.630	0.610	0.050	<dl	<dl	<dl	1.30	7.E-4	2.75	2.13
EG113CCP-003.d	0.298	0.260	8.00	127	0.188	<dl	631	<dl	<dl	n.r.	95.6	<dl	1.44	68.8	26.5	0.570	0.760	0.016	<dl	<dl	<dl	0.200	0.036	3.10	1.66
EG113CCP-004.d	0.320	0.490	2.10	184	0.139	1.30	719	0.045	<dl	n.r.	111	<dl	1.48	72.9	44.6	0.480	0.970	<dl	<dl	0.110	<dl	0.530	8.E-4	2.07	1.55
EG113CCP-005.d	4.10	2.50	110	144	0.205	1.63	687	1.20	<dl	n.r.	107	<dl	1.07	71.5	40.3	1.20	0.610	0.700	<dl	<dl	<dl	0.610	0.029	1.27	1.00
EG198CCP-3J-00	0.840	6.52	0.023	103	0.251	<dl	616	<dl	<dl	n.r.	210	<dl	3.85	138	14.5	0.057	0.058	<dl	<dl	<dl	<dl	2.27	8.E-4	2.18	3.92
EG198CCP-3J-00	1.26	6.60	53.0	98.5	0.390	<dl	670	0.200	<dl	n.r.	149	<dl	4.49	134	19.1	0.008	0.260	0.035	<dl	<dl	<dl	1.46	0.012	4.60	5.09
EG198CCP-3J-00	0.880	5.98	2.60	98.3	0.620	<dl	689	0.057	<dl	n.r.	190	<dl	4.19	131	21.2	0.048	0.410	<dl	<dl	<dl	<dl	1.37	7.E-4	2.88	4.60
EG198CCP-3J-00	0.740	5.88	12.0	106	0.710	<dl	619	<dl	<dl	n.r.	129	<dl	4.07	144	20.5	0.052	0.061	<dl	<dl	<dl	<dl	1.02	7.E-4	2.28	3.42
EG198CCP-3J-00	8.70	5.85	11.0	86.1	0.790	0.490	588	0.090	<dl	n.r.	226	<dl	3.70	133	15.1	0.390	0.283	<dl	<dl	<dl	<dl	0.780	1.E-3	3.69	4.29
EG204CCP-001d	0.880	2.38	0.400	379	0.079	<dl	279	<dl	<dl	n.r.	50.5	<dl	5.70	13.4	24.0	0.270	26.5	<dl	<dl	<dl	<dl	0.410	0.010	3.00	0.388
EG204CCP-002.c	1.41	3.74	1.00	345	0.077	1.33	294	<dl	<dl	n.r.	59.9	<dl	8.10	12.2	31.4	0.170	38.5	0.110	<dl	0.240	<dl	1.02	0.009	4.26	0.860
EG204CCP-003.c	1.00	1.40	20.0	304	0.080	1.80	281	<dl	<dl	n.r.	51.8	<dl	5.20	12.4	24.5	0.560	20.0	0.040	<dl	0.120	<dl	0.950	9.E-4	3.75	0.590
EG204CCP-004.c	1.52	3.00	0.910	280	0.400	<dl	265	<dl	<dl	n.r.	49.7	<dl	5.30	10.8	23.2	0.480	17.7	<dl	<dl	<dl	<dl	0.530	9.E-4	4.31	0.560
EG204CCP-005.c	0.810	2.55	0.073	293	0.084	0.560	277	<dl	<dl	n.r.	49.3	<dl	4.95	10.6	23.8	0.199	23.8	<dl	<dl	<dl	0.026	0.700	0.013	2.21	0.610
EG204CCP-006.c	1.48	0.410	0.062	297	0.130	<dl	261	<dl	<dl	n.r.	47.0	<dl	4.71	9.68	24.6	0.150	30.3	0.370	<dl	<dl	0.060	1.01	7.E-4	2.15	1.30
EG216CCP-001d	2.17	6.20	0.077	414	1.97	<dl	1152	<dl	<dl	n.r.	13.2	<dl	5.86	21.6	78.5	1.00	31.7	0.060	<dl	<dl	<dl	0.520	0.001	2.85	0.565
EG216CCP-002.d	1.58	4.29	0.850	348	1.47	1.39	1201	<dl	<dl	n.r.	11.7	<dl	5.20	21.7	73.4	1.69	23.7	<dl	<dl	<dl	<dl	0.300	0.001	5.07	0.590

Grain ID	*Mn* 55	*Co* 59	*Ni* 60	*Zn* 66	*Ga* 71	As 75	*Se* 82	Mo 95	Ru 101	Rh 103	*Ag* 107	Pd 108	Cd 111	*In* 115	*Sn* 118	*Sb* 121	*Te* 128	Re 185	Os 189	Ir 193	Pt 195	*Au* 197	Tl 205	*Pb* 208	*Bi* 209
55um	0.470	0.023	0.241	0.353	0.028	0.223	2.53	0.030	0.023	0.005	0.023	0.014	0.046	0.012	0.073	0.022	0.256	0.009	0.021	0.007	0.013	0.010	0.004	0.012	0.007
33um	0.939	0.046	0.722	1.06	0.085	0.445	5.07	0.061	0.068	0.009	0.069	0.041	0.137	0.025	0.218	0.067	0.513	0.027	0.042	0.020	0.039	0.030	0.011	0.037	0.013
EG216CCP-003.d	1.07	4.98	0.067	318	0.880	1.60	1210	0.056	<dl	n.r.	12.4	<dl	5.10	21.7	77.8	1.30	29.5	<dl	<dl	<dl	<dl	0.310	8.E-4	3.26	0.648
EG216CCP-004.d	2.01	2.77	0.920	372	0.290	0.900	1208	<dl	<dl	n.r.	10.5	<dl	5.30	22.3	69.0	1.72	25.6	<dl	<dl	<dl	<dl	0.158	9.E-4	4.38	0.770
EG216CCP-006.d	0.532	4.09	0.082	278	0.340	<dl	1168	0.090	<dl	n.r.	11.5	<dl	5.00	22.2	78.0	0.860	27.6	<dl	<dl	<dl	<dl	0.590	0.002	3.37	0.670
EG2412CCP-001(	2.50	0.410	0.041	115	6.75	0.810	10.3	<dl	0.300	n.r.	6.33	<dl	1.45	1.32	1.54	0.083	0.044	<dl	<dl	<dl	<dl	0.001	3.E-4	1.05	1.96
EG2412CCP-002.	1.92	0.030	0.041	125	5.70	4.30	12.8	<dl	<dl	n.r.	4.94	<dl	1.36	0.953	1.90	1.49	0.380	<dl	<dl	<dl	<dl	0.073	0.036	0.830	2.17
EG2412CCP-003.	1.18	0.380	0.034	123	2.99	0.690	13.7	<dl	<dl	n.r.	3.66	<dl	0.560	1.13	1.96	0.117	1.50	0.220	<dl	0.046	<dl	0.260	2.E-4	1.23	2.64
EG2412CCP-004.	1.32	0.130	12.0	125	3.52	<dl	13.1	<dl	<dl	n.r.	4.47	<dl	0.790	1.09	2.40	0.310	0.031	<dl	<dl	<dl	<dl	0.257	2.E-4	0.265	1.08
EG2412CCP-005.	2.46	0.360	44.0	140	6.10	<dl	15.1	<dl	0.220	n.r.	4.88	<dl	1.16	1.11	2.67	0.009	0.044	<dl	<dl	<dl	<dl	0.070	3.E-4	0.602	3.09
EG2412CCP-006.	1.09	0.025	35.0	120	3.76	<dl	13.4	<dl	<dl	n.r.	4.46	<dl	0.860	1.12	2.18	0.042	0.038	<dl	<dl	<dl	<dl	0.001	3.E-4	0.590	2.90
EH1CCP-001d	2.60	0.830	150	510	0.356	0.800	38.6	0.039	<dl	n.r.	14.5	0.244	0.151	3.95	64.8	1.10	0.426	<dl	<dl	0.320	0.012	0.250	0.008	1.09	14.5
EH1CCP-002.d	1.24	0.230	0.048	112	0.291	0.410	36.3	<dl	<dl	n.r.	17.2	<dl	0.155	4.16	158	0.596	0.029	0.041	<dl	<dl	<dl	0.090	0.170	0.628	6.69
EH1CCP-003.d	2.00	0.160	7.00	119	0.410	0.560	42.9	0.420	<dl	n.r.	10.7	<dl	0.088	4.27	109	4.15	0.038	<dl	<dl	0.046	<dl	0.009	0.027	0.470	4.41
EH1CCP-004.d	0.850	0.700	4.00	14.1	0.290	0.440	37.4	<dl	<dl	n.r.	5.91	<dl	0.139	3.98	72.9	1.27	0.093	<dl	<dl	<dl	<dl	0.035	0.012	0.720	9.80
EH3CCP-01d	0.105	0.018	0.141	14.0	0.251	<dl	28.9	<dl	<dl	n.r.	9.10	<dl	0.164	5.46	20.0	0.672	0.040	<dl	<dl	<dl	<dl	0.117	6.E-4	1.06	7.55
EH3CCP-02.d	0.144	0.193	7.00	13.9	0.325	0.250	314	<dl	<dl	n.r.	14.4	<dl	0.159	5.07	32.5	2.13	0.380	<dl	<dl	<dl	<dl	0.343	0.006	1.68	18.2
EH3CCP-03.d	0.108	0.025	0.210	10.9	0.282	<dl	319	<dl	<dl	n.r.	16.3	<dl	0.148	4.88	78.5	0.744	0.032	<dl	<dl	<dl	<dl	0.135	0.002	1.39	9.15
EH3CCP-04.d	0.500	0.004	0.009	14.0	0.224	<dl	34.5	<dl	<dl	n.r.	5.91	<dl	0.055	4.92	40.5	0.469	0.026	<dl	<dl	<dl	<dl	0.067	0.002	1.00	6.50
EH3CCP-05.d	0.095	0.005	0.010	9.88	0.266	<dl	315	<dl	<dl	n.r.	17.4	<dl	0.141	4.66	130	0.531	0.028	<dl	<dl	<dl	<dl	0.268	1.E-4	0.923	8.02
EH3CCP-06.d	0.108	0.017	0.135	14.9	0.224	0.135	30.7	<dl	<dl	n.r.	6.10	<dl	0.103	5.17	319	0.280	0.350	<dl	<dl	<dl	<dl	0.061	0.002	1.59	6.90
EH3CCP-07.d	0.145	0.005	0.600	12.3	0.280	<dl	29.1	<dl	<dl	n.r.	6.22	<dl	0.140	4.63	49.7	0.330	0.034	<dl	<dl	<dl	<dl	0.011	2.E-4	1.02	6.56
EH3CCP-08.d	0.092	0.005	0.007	111	0.254	<dl	34.7	<dl	<dl	n.r.	14.0	<dl	0.082	4.68	75.2	0.144	0.027	<dl	<dl	<dl	<dl	9.E-4	2.E-4	0.750	1.59
EH4CCP-01d	0.760	0.005	0.026	307	0.221	<dl	23.3	<dl	0.021	n.r.	30.9	<dl	0.440	16.8	26.5	0.395	0.031	<dl	<dl	<dl	<dl	0.228	5.E-4	23.1	1.42
EH4CCP-02.d	1.01	0.004	0.017	62.4	0.272	<dl	23.2	<dl	0.018	n.r.	33.3	<dl	0.176	17.3	28.8	0.444	0.460	<dl	<dl	<dl	<dl	0.071	0.011	38.1	1.03
EH4CCP-03.d	1.17	0.042	0.015	517	0.135	<dl	23.2	<dl	<dl	n.r.	29.2	<dl	0.184	12.9	218	0.293	0.028	<dl	<dl	<dl	<dl	0.025	0.021	9.42	2.44
EH4CCP-04.d	4.95	0.058	0.210	413	0.205	<dl	26.3	<dl	0.017	n.r.	28.9	<dl	0.476	13.0	22.6	0.525	0.520	<dl	<dl	<dl	<dl	0.062	5.E-4	9.80	7.80
EH4CCP-05.d	0.710	0.061	0.012	46.7	0.167	<dl	213	<dl	<dl	n.r.	28.7	<dl	0.100	13.0	20.9	0.169	0.022	<dl	<dl	<dl	<dl	0.016	0.023	7.21	2.51
EH4CCP-06.d	1.20	0.033	0.018	49.6	0.228	<dl	27.0	<dl	<dl	n.r.	44.4	<dl	0.230	12.8	22.4	0.920	0.033	<dl	<dl	<dl	<dl	0.185	0.022	9.70	6.58
F259CCP-01d	0.216	1.11	3.77	72.0	0.515	<dl	39.6	<dl	<dl	n.r.	6.52	<dl	0.320	2.56	4.33	0.011	0.054	<dl	<dl	<dl	<dl	0.001	0.012	6.95	0.117
F259CCP-02.d	0.116	0.004	0.016	135	0.710	<dl	49.2	<dl	<dl	n.r.	2.37	1.02	0.360	2.55	7.13	0.018	3.80	<dl	<dl	<dl	<dl	0.005	2.E-4	1.58	0.054
F259CCP-03.d	0.128	0.005	0.200	130	0.515	<dl	41.1	<dl	<dl	n.r.	3.37	0.861	0.460	2.52	5.47	0.004	2.31	<dl	<dl	<dl	<dl	5.E-4	6.E-4	2.69	0.032
F259CCP-04.d	0.135	0.057	0.360	145	0.360	<dl	44.7	<dl	<dl	n.r.	2.75	<dl	0.720	2.25	2.21	0.015	0.030	<dl	<dl	<dl	<dl	6.E-4	2.E-4	2.84	0.047
F259CCP-05.d	0.188	0.141	0.635	50.8	0.260	<dl	44.5	<dl	<dl	n.r.	4.40	<dl	0.285	2.29	4.03	0.007	0.045	<dl	<dl	<dl	<dl	1.E-3	7.E-4	4.29	0.073
F259CCP-06.d	0.206	0.170	0.041	120	0.260	0.590	120	<dl	<dl	n.r.	5.30	<dl	1.40	2.76	7.90	0.006	0.440	<dl	<dl	<dl	<dl	7.E-4	0.024	8.00	0.160
F263PCCP-01d	0.115	0.084	2.86	127	0.418	<dl	39.6	<dl	<dl	n.r.	27.5	0.060	0.182	2.74	3.29	0.005	1.80	<dl	<dl	<dl	<dl	4.E-4	1.E-4	0.618	0.090
F263PCCP-02.d	0.149	0.450	3.90	126	0.660	<dl	36.1	<dl	<dl	n.r.	25.9	0.289	0.089	2.60	9.89	0.006	2.85	<dl	<dl	<dl	<dl	9.E-4	2.E-4	0.821	0.128
F263PCCP-03.d	0.120	0.075	3.31	127	0.420	<dl	34.2	<dl	<dl	n.r.	25.6	0.035	0.220	2.68	8.79	0.005	0.810	<dl	<dl	<dl	<dl	0.004	2.E-4	0.930	0.161
F263PCCP-04.d	0.127	0.076	2.85	120	0.400	0.250	40.9	<dl	0.053	n.r.	25.1	0.034	0.130	2.66	6.93	0.005	0.650	<dl	<dl	<dl	<dl	5.E-4	2.E-4	0.980	0.097
F263PCCP-05.d	0.150	0.088	2.55	126	0.273	<dl	39.3	<dl	<dl	n.r.	27.5	<dl	0.187	2.64	5.32	0.037	0.034	<dl	<dl	<dl	<dl	7.E-4	0.005	3.83	0.554
F263PCCP-06.d	0.143	0.052	3.15	127	0.315	<dl	39.4	<dl	<dl	n.r.	28.8	<dl	0.220	2.79	6.15	0.032	0.500	<dl	<dl	<dl	<dl	0.005	3.E-4	3.81	0.670
F263PCCP-07.d	0.151	0.230	3.40	129	0.400	<dl	40.4	<dl	<dl	n.r.	27.4	<dl	0.199	2.71	6.84	0.029	0.380	<dl	<dl	<dl	<dl	0.004	0.002	2.56	0.293
F332BCCP-01d	0.139	0.930	0.360	6.70	0.010	<dl	30.2	<dl	0.037	n.r.	2.82	<dl	0.017	1.56	5.01	0.007	6.70	<dl	<dl	<dl	<dl	0.090	0.00	0.190	11.0
F332BCCP-02.d	0.195	0.960	260	4.90	0.006	<dl	55.2	0.050	<dl	n.r.	0.241	<dl	0.018	1.72	6.84	0.006	0.830	0.130	<dl	<dl	<dl	0.015	0.004	0.150	1.59
F332BCCP-03.d	0.173	0.900	0.030	4.60	0.018	<dl	33.9	<dl	<dl	n.r.	1.84	0.804	0.042	1.57	5.52	0.010	4.21	<dl	<dl	<dl	<dl	0.018	0.014	0.170	1.17
F332BCCP-04.d	0.196	1.01	150	2.30	0.047	<dl	419	<dl	<dl	n.r.	1.61	<dl	0.045	1.59	4.79	0.005	2.40	<dl	<dl	<dl	<dl	0.220	0.007	0.154	0.118
F392CCP-01d	8.60	0.842	0.049	0.171	0.027	<dl	316	<dl	<dl	n.r.	1.48	<dl	0.012	7.25	1.97	0.024	0.480	<dl	<dl	<dl	<dl	5.E-4	0.005	0.103	0.670
F392CCP-02.d	0.067	0.283	0.420	0.770	0.013	<dl	40.0	<dl	<dl	n.r.	0.580	<dl	0.007	7.29	1.82	0.002	1.41	<dl	<dl	<dl	<dl	6.E-4	0.00	0.130	1.08
F392CCP-03.d	0.050	0.433	0.006	0.260	0.003	<dl	33.1	<dl	<dl	n.r.	0.347	<dl	0.003	6.58	1.70	0.003	1.86	<dl	<dl	<dl	<dl	0.011	0.00	0.173	1.02

Grain ID	*Mn* 55	*Co* 59	*Ni* 60	*Zn* 66	*Ga* 71	As 75	*Se* 82	Mo 95	Ru 101	Rh 103	*Ag* 107	Pd 108	Cd 111	*In* 115	*Sn* 118	*Sb* 121	*Te* 128	Re 185	Os 189	Ir 193	Pt 195	*Au* 197	Tl 205	*Pb* 208	*Bi* 209
55um	0.470	0.023	0.241	0.353	0.028	0.223	2.53	0.030	0.023	0.005	0.023	0.014	0.046	0.012	0.073	0.022	0.256	0.009	0.021	0.007	0.013	0.010	0.004	0.012	0.007
33um	0.939	0.046	0.722	1.06	0.085	0.445	5.07	0.061	0.068	0.009	0.069	0.041	0.137	0.025	0.218	0.067	0.513	0.027	0.042	0.020	0.039	0.030	0.011	0.037	0.013
F392CCP-04.d	0.051	0.288	0.005	0.345	0.017	<dl	30.5	<dl	<dl	n.r.	0.348	<dl	0.004	7.27	1.49	0.030	1.01	<dl	<dl	<dl	<dl	3.E-4	0.00	0.168	1.38
F392CCP-05.d	0.041	0.293	0.250	0.460	0.004	<dl	35.7	<dl	<dl	n.r.	0.210	<dl	0.005	7.78	1.70	0.002	0.020	<dl	<dl	<dl	<dl	0.006	0.00	0.045	0.168
F392CCP-06.d	0.050	0.535	0.220	0.360	0.012	<dl	41.7	<dl	<dl	n.r.	0.410	<dl	0.005	7.51	1.67	0.002	1.50	<dl	<dl	<dl	<dl	3.E-4	0.00	0.091	0.250
F392CCP-07.d	0.660	0.520	0.030	0.192	0.008	1.50	28.0	<dl	<dl	n.r.	0.600	<dl	0.012	6.73	1.22	0.067	0.520	<dl	<dl	<dl	<dl	0.134	1.E-4	0.181	1.42
LALA4CCP-001d	1.03	4.41	1.00	26.4	0.458	<dl	28.6	<dl	0.210	n.r.	8.59	<dl	0.480	7.05	44.4	0.192	2.73	<dl	<dl	<dl	<dl	0.005	2.E-4	1.62	0.166
LALA4CCP-002.(	1.15	4.75	0.027	31.0	0.328	1.00	31.1	<dl	<dl	n.r.	9.86	<dl	0.790	7.22	30.0	0.244	1.24	<dl	<dl	<dl	<dl	0.080	0.017	2.53	0.398
LALA4CCP-003.(	1.08	4.81	0.030	30.3	0.370	<dl	33.1	<dl	<dl	n.r.	8.92	<dl	0.550	7.11	39.7	0.089	1.63	<dl	<dl	0.032	0.035	0.001	5.E-4	2.03	0.136
LALA4CCP-004.(	11.0	4.09	6.00	29.1	0.380	0.970	37.9	0.340	<dl	n.r.	10.1	<dl	0.430	7.29	25.6	0.400	0.850	<dl	<dl	0.064	<dl	0.032	5.E-4	3.25	0.453
LALA4CCP-005.(	0.930	4.34	0.037	27.2	0.840	<dl	37.4	<dl	<dl	n.r.	8.19	<dl	0.460	8.13	35.0	0.201	1.72	<dl	<dl	<dl	<dl	0.043	5.E-4	2.90	0.240
LALA5CCP-001d	0.850	2.57	3.30	29.3	0.354	0.690	47.1	<dl	<dl	n.r.	7.50	<dl	0.530	7.48	23.5	0.314	1.54	<dl	<dl	<dl	<dl	0.150	0.003	2.81	0.439
LALA5CCP-002.(	1.15	10.0	0.540	29.9	1.17	0.580	45.7	<dl	<dl	n.r.	8.39	<dl	0.710	7.38	20.2	0.275	1.13	0.150	<dl	<dl	<dl	0.012	5.E-4	2.22	0.228
LALA5CCP-003.(	0.890	4.17	14.0	27.2	0.330	<dl	39.7	0.062	<dl	n.r.	8.59	<dl	0.630	6.56	24.2	0.337	1.39	<dl	<dl	0.080	<dl	0.037	0.011	2.49	0.350
LALA5CCP-004.(	8.00	5.60	28.0	26.4	0.251	0.740	34.7	<dl	<dl	n.r.	10.3	<dl	0.400	6.74	26.3	0.176	1.12	<dl	<dl	<dl	<dl	0.016	5.E-4	1.50	0.208
LALA5CCP-005.(	2.05	4.83	4.80	26.6	0.306	0.420	34.0	<dl	<dl	n.r.	8.36	<dl	0.570	7.44	21.5	0.500	1.02	<dl	<dl	<dl	0.030	2.00	0.008	3.27	0.630
LALA5CCP-006.(	3.10	3.67	1.60	26.6	0.269	<dl	33.5	<dl	<dl	n.r.	8.09	<dl	0.730	6.70	24.9	0.182	1.07	<dl	<dl	<dl	<dl	0.001	4.E-4	1.59	0.255
PC1492CCP-001	1.75	0.500	0.066	29.3	0.282	<dl	13.8	<dl	<dl	n.r.	3.80	<dl	1.35	11.5	0.950	0.215	4.64	<dl	<dl	<dl	<dl	0.020	5.E-4	2.64	1.34
PC1492CCP-002.	1.81	0.083	1.80	21.3	0.370	<dl	15.0	<dl	<dl	n.r.	3.05	<dl	0.800	11.9	0.500	0.162	4.23	0.016	<dl	<dl	0.090	0.027	7.E-4	3.95	1.50
PC1492CCP-003.	1.54	0.140	0.044	34.7	0.340	0.600	14.7	<dl	<dl	n.r.	4.01	<dl	1.62	10.5	0.770	0.163	5.33	<dl	<dl	<dl	<dl	0.048	6.E-4	4.14	1.25
PC1492CCP-004.	0.335	0.650	28.0	32.8	0.333	<dl	15.5	<dl	<dl	n.r.	3.27	<dl	1.62	10.9	1.00	0.250	5.16	<dl	<dl	0.011	<dl	0.001	5.E-4	2.87	0.990
PC1492CCP-005.	2.23	2.80	10.0	27.1	0.240	<dl	13.3	0.500	<dl	n.r.	4.33	<dl	0.960	9.92	0.430	0.125	4.16	<dl	<dl	<dl	0.320	0.082	6.E-4	3.64	1.06
PC9174CCP-01d	0.262	2.01	0.042	28.1	0.440	<dl	16.4	<dl	0.034	n.r.	1.60	<dl	1.91	10.2	0.700	0.290	4.42	<dl	<dl	<dl	<dl	0.049	0.036	11.3	0.718
PC9174CCP-03.d	0.261	2.18	0.041	15.5	0.014	<dl	13.2	0.830	<dl	n.r.	1.17	<dl	1.46	3.58	0.109	0.700	0.710	<dl	<dl	<dl	<dl	0.171	0.312	24.1	1.37
PC9174CCP-04.d	0.139	2.72	0.220	23.3	0.013	<dl	11.0	0.352	<dl	n.r.	1.46	<dl	1.61	1.25	0.092	0.096	0.046	<dl	<dl	<dl	<dl	0.154	0.051	7.63	0.474
PC9174CCP-05.d	0.250	13.6	0.550	26.0	0.014	<dl	8.60	1.13	<dl	n.r.	1.78	<dl	1.03	4.21	0.075	0.080	2.08	<dl	<dl	<dl	<dl	0.036	0.367	8.32	0.580
PC9174CCP-06.d	0.174	1.65	0.370	33.8	0.208	<dl	13.6	<dl	0.039	n.r.	2.04	<dl	1.97	7.81	0.214	0.027	3.00	<dl	<dl	<dl	<dl	0.093	0.016	4.91	0.329
PC9174CCP-07.d	0.205	2.21	0.210	27.0	0.324	<dl	11.6	<dl	<dl	n.r.	2.01	<dl	1.63	7.30	0.225	0.024	2.72	<dl	<dl	<dl	<dl	0.056	0.016	5.63	0.356
PC98102CCP-01	0.233	0.005	0.020	77.1	0.460	0.365	15.5	<dl	<dl	n.r.	1.68	<dl	0.320	12.7	5.67	1.17	1.03	<dl	<dl	<dl	<dl	0.003	0.221	12.8	0.996
PC98102CCP-02.	1.02	0.009	0.024	51.7	0.550	<dl	14.5	<dl	<dl	n.r.	2.13	<dl	1.91	15.0	8.41	0.351	1.86	<dl	<dl	<dl	<dl	0.038	0.001	21.6	0.536
PC98102CCP-03.	0.470	0.017	0.016	65.8	0.519	<dl	17.3	<dl	<dl	n.r.	2.09	<dl	2.96	13.7	8.08	0.297	1.31	<dl	<dl	<dl	<dl	0.002	0.002	15.0	0.398
PC98102CCP-04.	0.141	0.003	0.018	63.5	0.513	<dl	15.7	<dl	<dl	n.r.	2.13	<dl	2.44	14.8	8.60	0.601	0.930	<dl	<dl	<dl	<dl	0.035	0.015	12.9	0.645
PC98102CCP-06.	0.860	0.006	0.024	40.7	0.460	<dl	17.1	<dl	<dl	n.r.	2.03	<dl	1.55	14.3	8.82	0.720	1.36	<dl	<dl	<dl	<dl	0.002	0.001	6.74	0.523
PC98102CCP-07.	0.206	0.005	0.019	87.8	0.550	<dl	15.6	<dl	<dl	n.r.	1.95	<dl	3.04	13.7	8.46	0.667	1.56	<dl	<dl	<dl	<dl	0.035	0.014	10.5	0.704
PC99069CCP-01	0.527	11.2	1.16	34.8	0.180	<dl	5.47	<dl	<dl	n.r.	2.62	<dl	2.04	6.96	1.23	0.570	0.124	<dl	<dl	<dl	<dl	0.003	4.E-4	3.38	1.66
PC99069CCP-02	0.469	20.6	1.32	35.9	0.055	<dl	6.13	<dl	<dl	n.r.	2.43	<dl	1.66	7.38	1.41	0.380	0.124	<dl	<dl	<dl	<dl	1.E-3	5.E-4	1.03	0.534
PC99069CCP-03	0.418	10.1	1.02	33.0	0.097	<dl	14.0	<dl	<dl	n.r.	2.44	<dl	1.73	6.66	1.27	0.430	1.15	<dl	<dl	<dl	<dl	0.019	6.E-4	2.58	2.18
PC99069CCP-04	16.1	13.8	1.25	30.0	0.200	<dl	15.0	<dl	<dl	n.r.	2.46	<dl	1.34	6.51	1.07	2.77	0.091	<dl	<dl	<dl	<dl	0.043	0.060	3.73	1.93
PC99069CCP-05	3.00	9.09	0.580	33.1	0.228	<dl	13.2	<dl	<dl	n.r.	2.67	<dl	1.54	6.54	1.48	0.175	1.59	<dl	<dl	<dl	<dl	0.002	2.E-4	0.634	2.20
PI01CCP-01d	0.230	1.94	2.90	28.4	1.45	<dl	9.00	<dl	0.041	n.r.	2.86	<dl	0.860	1.90	26.7	0.006	0.490	0.090	<dl	<dl	<dl	1.60	0.008	0.701	0.080
PI01CCP-02.d	4.70	1.13	0.100	33.8	1.48	0.420	4.00	0.160	<dl	n.r.	3.41	<dl	1.21	1.82	30.5	0.041	1.11	<dl	<dl	0.055	<dl	0.004	1.E-4	0.960	3.00
PI01CCP-03.d	2.00	1.59	0.480	30.0	1.50	0.250	2.54	<dl	<dl	n.r.	3.92	<dl	1.31	4.98	24.3	0.084	0.390	<dl	<dl	0.120	<dl	0.061	5.E-4	2.96	0.344
PI01CCP-04.d	1.39	2.11	6.10	34.4	1.48	<dl	3.30	<dl	<dl	n.r.	4.92	<dl	1.30	2.05	27.1	0.900	0.790	0.160	<dl	<dl	0.800	0.530	2.E-4	1.07	0.204
PI01CCP-05.d	3.60	1.40	90.0	33.1	9.00	<dl	4.10	0.050	0.220	n.r.	2.15	<dl	0.970	5.15	31.0	0.160	0.560	<dl	0.060	0.009	<dl	0.003	0.003	1.88	0.044
PI01CCP-06.d	1.61	1.06	0.109	28.9	1.58	<dl	3.30	0.049	<dl	n.r.	2.93	0.585	0.910	1.71	27.8	0.058	0.520	<dl	<dl	<dl	0.012	4.E-4	1.E-4	0.558	0.081
PI01CCP-07.d	1.39	1.28	0.111	33.9	1.84	<dl	7.29	<dl	<dl	n.r.	5.23	<dl	1.43	2.41	32.6	0.068	0.870	<dl	<dl	0.027	<dl	8.E-4	0.002	3.85	0.497
PI02CCP-01d	0.520	1.13	1.25	36.5	0.304	<dl	20.2	0.053	<dl	n.r.	7.72	<dl	3.79	4.50	22.8	0.004	0.650	<dl	<dl	0.022	0.038	5.E-4	0.002	0.368	0.043
PI02CCP-02.d	0.860	1.16	1.26	33.1	0.347	<dl	14.5	0.130	<dl	n.r.	7.26	<dl	3.91	4.81	36.6	0.004	1.12	<dl	<dl	<dl	0.009	6.E-4	1.E-4	0.490	0.068
PI02CCP-03.d	1.35	2.23	2.11	29.9	0.240	<dl	19.4	<dl	<dl	n.r.	7.41	<dl	3.53	4.14	37.5	0.004	1.06	<dl	<dl	<dl	0.037	7.E-4	4.E-4	0.343	0.250

Grain ID	*Mn* 55	*Co* 59	*Ni* 60	*Zn* 66	*Ga* 71	As 75	*Se* 82	Mo 95	Ru 101	Rh 103	*Ag* 107	Pd 108	Cd 111	*In* 115	*Sn* 118	*Sb* 121	*Te* 128	Re 185	Os 189	Ir 193	Pt 195	*Au* 197	Tl 205	*Pb* 208	*Bi* 209
55um	0.470	0.023	0.241	0.353	0.028	0.223	2.53	0.030	0.023	0.005	0.023	0.014	0.046	0.012	0.073	0.022	0.256	0.009	0.021	0.007	0.013	0.010	0.004	0.012	0.007
33um	0.939	0.046	0.722	1.06	0.085	0.445	5.07	0.061	0.068	0.009	0.069	0.041	0.137	0.025	0.218	0.067	0.513	0.027	0.042	0.020	0.039	0.030	0.011	0.037	0.013
PI02CCP-04.d	0.870	1.78	1.89	493	0.411	<dl	19.0	0.018	0.016	n.r.	7.42	<dl	4.31	4.45	27.1	0.002	0.079	<dl	<dl	<dl	<dl	0.002	1.E-4	0.428	0.080
PI02CCP-05.d	0.610	1.89	2.05	361	0.309	0.230	32.3	0.027	0.019	n.r.	7.97	<dl	4.24	4.69	44.3	0.400	1.19	0.027	<dl	<dl	<dl	7.E-4	0.020	0.445	0.084
SAL03CCP-01d	2.50	6.40	15.0	118	0.046	<dl	17.8	<dl	<dl	n.r.	0.850	2.51	0.096	1.71	19.7	3.70	1.26	<dl	<dl	0.140	<dl	0.007	2.E-4	0.702	0.483
SAL03CCP-02.d	1.32	7.66	16.0	20.2	0.105	<dl	20.1	<dl	<dl	n.r.	0.350	<dl	0.028	1.79	18.4	0.034	1.01	<dl	<dl	<dl	<dl	2.30	3.E-4	0.670	0.447
SAL03CCP-03.d	1.11	7.37	32.0	34.6	0.150	<dl	20.4	0.600	<dl	n.r.	0.272	<dl	0.052	1.69	21.9	0.400	1.26	0.070	<dl	0.110	<dl	6.E-4	1.E-4	0.192	0.111
SAL03CCP-04.d	4.00	4.49	0.950	6.00	0.105	<dl	14.7	0.140	<dl	n.r.	1.21	0.104	0.130	1.79	19.4	0.039	0.390	0.012	0.017	0.009	<dl	0.160	3.E-4	1.29	0.790
SAL03CCP-05.d	0.129	1.15	0.021	0.690	0.105	<dl	19.8	<dl	<dl	n.r.	0.930	<dl	1.00	1.58	12.6	0.003	0.057	<dl	<dl	<dl	<dl	0.008	0.004	0.740	0.116
SAL03CCP-06.d	0.820	1.80	15.0	0.500	0.027	<dl	20.5	<dl	0.036	n.r.	0.920	<dl	0.270	1.69	15.2	0.005	0.890	<dl	<dl	<dl	<dl	0.001	1.E-4	0.550	0.620
SAL03CCP-07.d	1.35	1.77	3.90	1.90	0.058	<dl	22.4	0.060	0.210	n.r.	1.37	<dl	0.016	1.71	15.6	0.027	1.42	0.700	<dl	0.036	0.014	0.800	2.E-4	0.405	0.870
SF1CCP-01d	8.05	0.172	0.133	125	0.310	0.360	29.4	<dl	<dl	n.r.	5.81	<dl	1.29	23.3	7.20	0.198	4.50	<dl	<dl	<dl	<dl	1.E-3	3.E-4	2.10	11.4
SF1CCP-02.d	7.12	0.236	10.0	179	0.460	0.310	27.0	<dl	<dl	n.r.	10.6	<dl	1.77	22.7	6.80	0.145	6.48	<dl	<dl	<dl	<dl	0.063	0.005	7.20	11.0
SF1CCP-03.d	4.40	0.350	0.037	84.1	0.500	<dl	23.4	0.360	0.034	n.r.	10.1	<dl	1.00	15.5	5.14	0.386	3.89	<dl	<dl	<dl	<dl	0.025	0.002	38.4	16.8
SF1CCP-04.d	4.00	0.380	0.023	153	0.036	<dl	28.4	<dl	0.037	n.r.	5.95	0.079	1.40	19.6	5.79	0.320	5.84	0.031	0.020	<dl	<dl	0.014	0.006	1.35	4.76
SF1CCP-05.d	2.14	0.244	50.0	143	0.028	<dl	25.3	<dl	0.029	n.r.	10.3	<dl	0.808	10.8	3.37	0.089	5.51	<dl	0.033	0.004	<dl	0.009	0.001	28.2	10.1
SF1CCP-06.d	2.24	0.320	0.035	76.0	0.430	<dl	29.9	<dl	<dl	n.r.	7.17	0.568	0.980	12.7	3.92	0.086	3.30	<dl	0.030	<dl	<dl	0.024	0.005	57.2	12.0
SF1CCP-07.d	1.32	0.046	0.021	121	0.320	<dl	28.5	0.033	0.270	n.r.	7.80	<dl	0.940	8.42	1.78	0.053	5.19	<dl	<dl	<dl	<dl	0.050	0.035	44.2	6.56
SOS01CCP-01d	3.40	3.77	0.790	9.50	1.10	0.132	33.4	<dl	<dl	n.r.	1.05	<dl	0.290	2.89	7.37	0.011	0.920	<dl	<dl	<dl	<dl	0.090	7.E-4	2.03	1.03
SOS01CCP-02.d	0.840	4.30	0.118	13.7	0.570	0.380	35.0	<dl	0.034	n.r.	1.33	<dl	0.340	2.95	19.2	0.009	2.20	0.070	<dl	<dl	0.021	0.007	2.E-4	2.06	1.66
SOS01CCP-03.d	29.0	3.82	1.80	29.8	0.340	<dl	36.6	0.250	<dl	n.r.	0.547	<dl	0.220	2.96	8.97	0.017	0.880	<dl	<dl	<dl	<dl	8.E-4	1.E-4	0.301	0.070
SOS01CCP-05.d	1.56	2.35	0.900	9.30	0.211	0.170	35.3	<dl	0.018	n.r.	1.95	<dl	0.220	3.33	6.42	0.008	1.19	0.700	<dl	<dl	<dl	0.007	2.E-4	2.73	2.48
SOS01CCP-06.d	1.19	3.10	0.460	19.1	0.400	<dl	35.0	<dl	0.022	n.r.	0.780	<dl	0.140	3.11	9.02	0.007	1.21	0.004	<dl	<dl	<dl	5.E-4	3.E-4	0.510	0.306
SOS01CCP-07.d	3.00	2.77	23.0	30.5	0.490	<dl	38.2	<dl	<dl	n.r.	0.640	<dl	0.190	3.25	10.0	0.280	1.20	<dl	<dl	<dl	<dl	7.E-4	3.E-4	0.188	1.50
SOS02CCP-01d	1.44	0.043	86.0	117	0.386	0.360	41.7	<dl	<dl	n.r.	8.27	<dl	0.700	5.82	15.3	0.021	0.512	<dl	<dl	<dl	<dl	0.500	0.010	2.94	0.895
SOS02CCP-02.d	0.440	0.046	13.5	119	0.496	<dl	40.5	<dl	<dl	n.r.	10.6	<dl	0.760	5.89	14.4	0.007	0.250	<dl	<dl	<dl	<dl	0.001	4.E-4	2.35	1.21
SOS02CCP-03.d	0.480	0.100	15.4	115	0.830	0.800	41.2	<dl	<dl	n.r.	8.56	<dl	0.850	5.84	27.8	0.009	0.043	<dl	<dl	<dl	<dl	0.017	0.004	2.34	0.266
SOS02CCP-04.d	1.20	0.011	18.6	116	0.386	0.220	39.8	<dl	<dl	n.r.	9.44	<dl	0.690	5.86	14.8	0.006	0.095	<dl	<dl	0.700	<dl	0.001	0.012	2.17	0.425
SOS02CCP-05.d	0.900	0.016	90.0	128	0.710	<dl	39.1	0.200	<dl	n.r.	9.00	<dl	0.880	8.35	29.7	0.008	1.80	<dl	<dl	<dl	<dl	0.001	0.005	1.01	0.121
SOS02CCP-06.d	2.50	0.120	17.0	111	0.190	<dl	39.8	<dl	<dl	n.r.	8.92	<dl	0.710	5.72	29.1	0.021	0.430	<dl	<dl	<dl	<dl	0.001	0.006	2.91	0.275
SOS02CCP-07.d	0.640	0.012	13.3	119	0.540	2.10	44.6	<dl	<dl	n.r.	8.67	<dl	0.740	6.15	17.5	0.009	0.480	0.510	<dl	0.060	<dl	0.170	0.007	2.75	0.345
Ni-Cu sulfides																									
06-MPB-R15-1d	0.169	0.145	0.015	15.5	0.160	<dl	211	<dl	<dl	n.r.	1.96	<dl	0.130	9.11	39.1	0.093	0.310	<dl	<dl	<dl	<dl	0.103	0.037	5.18	4.18
06-MPB-R15-2.d	0.118	0.086	0.017	30.1	0.124	<dl	218	0.032	<dl	n.r.	1.25	<dl	0.117	9.15	35.5	0.021	0.540	<dl	<dl	<dl	<dl	0.106	0.004	1.24	1.68
06-MPB-R15-3.d	0.121	0.029	0.017	14.3	0.097	<dl	215	<dl	<dl	n.r.	0.980	<dl	0.024	9.33	13.7	0.019	0.330	<dl	<dl	<dl	<dl	0.124	0.011	2.20	3.00
06-MPB-R15-4.d	0.125	0.029	0.360	18.0	0.045	<dl	218	<dl	<dl	n.r.	1.12	0.050	0.022	9.13	19.7	0.030	0.350	<dl	<dl	<dl	<dl	0.075	0.009	1.43	2.69
06-MPB-R15-5.d	0.169	0.009	0.570	24.0	0.200	<dl	200	<dl	<dl	n.r.	1.20	<dl	0.030	9.27	46.0	0.005	0.630	<dl	<dl	<dl	<dl	0.094	0.020	1.80	2.20
06-MPB-R15-6.d	0.163	0.006	0.020	27.0	0.008	<dl	188	<dl	<dl	n.r.	1.14	<dl	0.031	8.56	28.6	0.039	0.047	<dl	<dl	<dl	<dl	0.190	2.E-4	1.48	2.06
06-MPB-R15-7.d	0.142	0.080	0.026	26.8	0.023	<dl	208	<dl	<dl	n.r.	0.920	0.043	0.041	9.70	26.6	0.045	0.055	<dl	<dl	<dl	<dl	0.086	0.006	1.38	1.50
06-MPB-R15-8.d	0.093	0.055	0.014	25.7	0.058	0.220	210	<dl	0.020	n.r.	1.50	0.153	0.074	9.47	24.9	0.059	0.970	<dl	<dl	<dl	<dl	0.127	0.006	2.07	1.97
06-MPB-R15-9.d	0.112	0.049	0.180	31.7	0.118	<dl	212	<dl	<dl	n.r.	0.630	<dl	0.082	9.23	18.6	0.023	0.310	<dl	<dl	<dl	<dl	0.067	0.007	1.76	1.97
06-MPB-R16-11d	0.288	2.21	0.058	165	0.011	<dl	176	<dl	<dl	n.r.	1.07	<dl	11.1	9.45	97.9	0.004	0.570	<dl	<dl	<dl	<dl	0.857	5.E-4	6.31	3.66
06-MPB-R16-12.d	0.267	2.59	0.082	283	0.130	<dl	148	<dl	0.033	n.r.	0.460	<dl	22.0	9.94	115	0.005	1.03	<dl	<dl	<dl	<dl	0.078	0.023	4.00	1.59
06-MPB-R16-2.d	0.247	3.95	0.440	169	0.100	<dl	181	<dl	<dl	n.r.	0.680	<dl	12.5	8.92	133	0.040	0.580	<dl	<dl	<dl	<dl	0.282	0.003	4.74	2.87
06-MPB-R16-3.d	0.227	2.19	0.083	170	0.045	<dl	151	<dl	<dl	n.r.	0.800	<dl	6.95	9.07	123	0.008	0.810	<dl	<dl	<dl	0.007	0.550	2.E-4	3.39	1.69
06-MPB-R16-4.d	0.221	1.97	0.073	185	0.060	<dl	156	<dl	0.030	n.r.	0.950	<dl	7.44	8.79	137	0.041	0.640	<dl	<dl	<dl	<dl	0.345	0.008	4.90	2.18
06-MPB-R16-6.d	0.202	1.42	0.064	151	0.067	<dl	165	<dl	0.030	n.r.	1.00	<dl	4.67	9.32	110	0.031	0.630	<dl	<dl	<dl	<dl	0.462	0.004	5.48	2.29
06-MPB-R16-9.d	0.184	3.24	0.057	274	0.040	<dl	173	<dl	<dl	n.r.	1.85	<dl	13.1	9.85	169	0.004	1.30	<dl	<dl	<dl	<dl	1.52	0.002	5.50	1.56
1533-1d	12.1	0.136	33.0	337	0.080	<dl	188	<dl	<dl	n.r.	5.49	<dl	24.9	13.2	77.2	0.038	5.09	<dl	<dl	<dl	<dl	0.001	0.158	96.4	1.06

Grain ID	Mn 55	Co 59	Ni 60	Zn 66	Ga 71	As 75	Se 82	Mo 95	Ru 101	Rh 103	Ag 107	Pd 108	Cd 111	In 115	Sn 118	Sb 121	Te 128	Re 185	Os 189	Ir 193	Pt 195	Au 197	Tl 205	Pb 208	Bi 209
55um	0.470	0.023	0.241	0.353	0.028	0.223	2.53	0.030	0.023	0.005	0.023	0.014	0.046	0.012	0.073	0.022	0.256	0.009	0.021	0.007	0.013	0.010	0.004	0.012	0.007
33um	0.939	0.046	0.722	1.06	0.085	0.445	5.07	0.061	0.068	0.009	0.069	0.041	0.137	0.025	0.218	0.067	0.513	0.027	0.042	0.020	0.039	0.030	0.011	0.037	0.013
1533-11.d	3.52	0.129	47.0	393	0.157	<dl	181	<dl	0.021	n.r.	6.10	<dl	22.6	10.2	59.3	0.071	4.79	<dl	<dl	<dl	<dl	0.001	0.169	16.0	1.55
1533-13.d	1.25	0.230	39.9	307	0.175	0.470	191	<dl	<dl	n.r.	6.70	<dl	20.2	8.59	43.0	0.101	2.31	<dl	<dl	<dl	<dl	9.E-4	0.037	7.00	0.980
1533-14.d	11.9	0.065	31.9	344	0.190	<dl	194	<dl	<dl	n.r.	6.29	<dl	25.9	8.74	41.6	0.088	3.52	<dl	<dl	<dl	0.044	0.001	0.104	118	0.920
1533-16.d	7.20	0.074	26.9	351	0.202	<dl	208	<dl	0.027	n.r.	6.14	<dl	21.1	8.19	42.2	0.071	4.66	<dl	<dl	<dl	<dl	0.001	0.125	115	0.920
1533-3.d	0.950	0.105	46.9	378	0.008	<dl	174	<dl	0.037	n.r.	1.52	<dl	18.7	12.6	63.4	0.063	1.05	<dl	<dl	<dl	<dl	0.001	0.079	16.7	0.836
1533-6.d	6.50	0.169	47.7	364	0.085	<dl	170	<dl	<dl	n.r.	1.97	<dl	22.0	12.9	66.2	0.007	1.38	<dl	<dl	<dl	0.090	9.E-4	0.040	5.10	0.555
1533-8.d	11.6	0.215	37.2	339	0.260	<dl	160	<dl	<dl	n.r.	6.58	<dl	23.8	9.84	45.7	0.098	2.72	<dl	<dl	<dl	<dl	0.001	0.174	68.7	0.930
2523-10.d	0.520	0.161	48.3	410	0.158	<dl	59.8	<dl	0.034	n.r.	1.02	<dl	7.19	3.95	10.5	0.116	1.07	<dl	<dl	<dl	<dl	0.018	3.E-4	4.53	1.54
2523-2.d	0.680	0.155	45.8	380	0.153	<dl	58.0	0.050	<dl	n.r.	1.28	<dl	6.86	2.91	7.80	0.097	1.94	<dl	<dl	<dl	<dl	0.016	2.E-4	3.87	1.89
2523-3.d	0.780	0.361	47.8	436	0.190	<dl	69.7	<dl	<dl	n.r.	1.82	<dl	7.27	2.79	6.98	0.057	1.82	<dl	<dl	<dl	<dl	0.001	2.E-4	5.05	1.92
2523-4.d	0.650	0.279	47.1	437	0.154	<dl	68.8	<dl	<dl	n.r.	1.86	<dl	7.90	3.14	7.30	0.048	2.07	<dl	<dl	<dl	<dl	0.034	2.E-4	3.58	2.03
2523-7.d	0.480	0.580	62.0	382	0.127	0.470	67.3	<dl	<dl	n.r.	1.74	<dl	8.13	2.42	5.46	0.004	1.94	<dl	<dl	<dl	<dl	7.E-4	2.E-4	4.08	1.58
2523-9.d	0.196	0.193	48.6	510	0.213	<dl	67.6	<dl	<dl	n.r.	1.01	<dl	8.54	4.37	12.5	0.126	0.810	<dl	<dl	<dl	<dl	0.058	3.E-4	7.30	2.70
a2-1.d	0.151	0.054	36.9	79.7	0.028	<dl	240	0.047	0.024	n.r.	9.35	3.02	4.97	0.550	0.047	0.019	76.8	<dl	<dl	<dl	0.217	4.E-4	1.42	0.048	0.011
a2-10.d	0.114	0.046	41.4	105	0.003	<dl	227	0.084	<dl	n.r.	8.17	2.27	5.56	0.720	0.025	0.031	77.0	<dl	<dl	<dl	0.044	0.006	1.00	0.073	0.005
a2-2.d	0.137	0.036	36.7	89.0	0.034	0.540	228	0.170	0.045	n.r.	9.77	4.47	6.14	0.406	0.034	0.034	77.0	<dl	<dl	<dl	0.218	4.E-4	1.25	0.048	0.015
a2-4.d	0.154	0.031	37.1	75.5	0.008	<dl	230	<dl	0.030	n.r.	9.59	1.57	5.23	0.367	0.038	0.076	61.5	<dl	<dl	<dl	0.063	7.E-4	1.43	0.042	0.013
a2-5.d	0.130	0.043	36.5	72.4	0.033	<dl	208	0.072	<dl	n.r.	9.21	2.55	5.30	0.299	0.036	0.003	75.3	<dl	<dl	<dl	0.071	6.E-4	1.27	0.032	0.032
a2-7.d	0.163	0.045	46.5	76.5	0.029	<dl	236	0.081	<dl	n.r.	9.67	3.57	5.18	1.49	0.046	0.050	78.7	<dl	<dl	<dl	0.019	6.E-4	1.06	0.063	0.008
a2-9.d	0.143	0.018	45.4	83.6	0.038	<dl	232	0.087	0.028	n.r.	8.78	4.91	5.90	2.63	0.033	0.084	75.0	<dl	<dl	<dl	0.035	4.E-4	1.04	0.092	0.005
B1-384-05-2.d	0.149	0.033	83.3	37.1	0.370	2.80	102	<dl	<dl	n.r.	1.23	<dl	0.350	1.60	7.63	0.003	1.29	<dl	<dl	<dl	<dl	5.E-4	2.E-4	3.17	0.048
B1-384-05-5.d	0.176	0.028	92.6	34.9	0.318	<dl	110	<dl	<dl	n.r.	6.70	<dl	0.430	1.22	10.8	0.007	1.34	<dl	<dl	<dl	<dl	8.E-4	1.E-3	5.12	0.025
B1-384-05-6.d	0.117	0.004	66.8	42.4	0.315	<dl	163	<dl	<dl	n.r.	0.880	<dl	1.59	1.09	19.0	0.011	1.47	<dl	<dl	<dl	<dl	9.E-4	7.E-4	5.11	0.048
B1-384-05-7.d	0.183	0.007	71.5	39.5	0.340	<dl	158	<dl	0.032	n.r.	0.870	<dl	0.630	1.16	9.90	0.005	1.63	<dl	<dl	<dl	<dl	7.E-4	1.E-3	12.7	0.031
B1-384-39-3.d	1.26	0.795	10.9	191	0.270	<dl	53.6	<dl	<dl	n.r.	3.12	<dl	12.5	0.538	0.265	0.003	2.93	<dl	<dl	<dl	<dl	6.E-4	0.024	1.30	0.179
B1-384-39-4.d	1.60	0.520	11.4	385	0.134	<dl	50.0	<dl	<dl	n.r.	3.47	<dl	16.3	0.636	0.830	0.026	4.29	<dl	<dl	<dl	<dl	6.E-4	0.004	1.33	0.115
B1-384-39-5.d	0.690	0.630	7.80	323	0.290	0.450	53.6	<dl	<dl	n.r.	2.34	<dl	14.7	0.701	0.382	0.003	2.72	<dl	<dl	<dl	<dl	5.E-4	0.003	1.38	0.180
B1-384-39-6.d	0.850	0.410	7.25	232	0.169	<dl	58.6	<dl	<dl	n.r.	2.55	<dl	15.5	0.527	0.670	0.024	3.90	<dl	<dl	<dl	<dl	6.E-4	3.E-4	2.82	0.202
B1-384-39-7.d	1.21	0.740	5.24	244	0.170	<dl	57.3	<dl	<dl	n.r.	1.14	<dl	14.5	0.665	0.600	0.002	3.87	<dl	0.015	<dl	<dl	7.E-4	0.009	0.870	0.104
B1-384-39-9.d	1.15	0.920	7.30	228	0.117	<dl	48.4	<dl	<dl	n.r.	1.71	<dl	15.1	0.482	0.533	0.002	3.67	<dl	<dl	<dl	<dl	5.E-4	0.009	1.19	0.143
C-04-23-1.d	0.168	5.20	12.8	329	0.228	11.7	32.7	10.3	0.095	n.r.	9.29	<dl	4.99	21.9	28.1	0.029	1.13	0.224	<dl	0.022	0.071	0.021	6.E-4	2.27	0.187
C-04-23-2.d	0.237	5.20	24.7	314	0.320	9.60	31.7	9.90	0.110	n.r.	9.66	<dl	9.20	18.9	29.0	0.049	0.900	0.214	0.037	0.049	0.051	0.035	0.006	1.42	0.177
C-04-23-3.d	17.0	2.90	15.1	271	0.570	7.80	39.8	10.1	0.061	n.r.	11.2	<dl	3.38	21.2	29.1	0.083	0.050	0.203	<dl	0.033	0.102	0.064	0.013	4.55	0.187
C-04-23-4.d	0.203	7.10	22.3	308	0.176	18.3	34.5	10.1	0.112	n.r.	13.6	<dl	6.87	19.6	26.7	0.122	0.330	0.181	<dl	0.016	0.660	0.014	0.010	7.44	0.261
C-04-23-5.d	0.205	4.60	31.0	273	0.162	10.8	34.1	9.60	0.075	n.r.	11.5	<dl	7.00	19.8	27.3	0.066	0.440	0.215	<dl	0.017	0.124	0.001	0.012	3.19	0.185
C-04-23-6.d	0.250	4.80	17.4	308	0.300	10.4	30.4	9.60	0.068	n.r.	20.8	<dl	6.60	29.1	31.3	0.093	0.660	0.151	<dl	0.026	0.880	0.027	7.E-4	1.64	0.110
C-04-23-7.d	6.60	5.00	11.8	312	0.258	7.10	34.8	10.4	0.042	n.r.	11.1	<dl	5.28	21.9	24.8	0.037	0.820	0.093	0.019	0.019	0.033	0.042	0.011	2.08	0.143
C-04-23-8.d	0.224	16.9	16.9	276	0.137	32.0	34.6	15.2	0.099	n.r.	8.31	<dl	2.71	22.2	26.7	0.109	0.750	0.171	0.047	0.020	1.11	0.101	0.021	3.90	0.275
C-04-24-1.d	2.00	1.51	80.0	242	0.036	5.30	33.0	3.70	0.029	n.r.	11.3	<dl	2.69	4.33	11.2	0.114	0.400	0.044	<dl	0.049	0.023	0.016	0.011	12.4	0.230
C-04-24-2.d	0.336	0.160	10.8	228	0.031	<dl	38.0	2.10	0.050	n.r.	9.27	<dl	2.34	3.88	12.0	0.009	0.071	0.071	<dl	<dl	<dl	0.046	8.E-4	6.40	0.089
C-04-24-3.d	0.372	0.460	8.50	238	0.033	2.70	29.0	1.09	0.350	n.r.	11.0	<dl	1.68	4.65	11.2	0.038	0.080	0.023	<dl	0.027	<dl	0.001	6.E-4	8.49	0.113
C-04-24-4.d	3.90	0.870	38.0	250	0.039	2.80	45.0	1.40	0.100	n.r.	8.85	<dl	2.29	4.15	11.0	0.081	0.600	0.050	<dl	0.020	<dl	0.033	0.001	17.7	0.085
C-04-24-5.d	5.00	0.500	12.3	178	0.018	<dl	30.0	21.3	<dl	n.r.	15.4	<dl	1.48	4.61	9.90	0.117	0.079	0.124	<dl	<dl	0.110	0.002	0.137	22.8	0.270
C-04-24-6.d	2.30	0.890	51.0	226	0.034	0.470	28.0	2.00	<dl	n.r.	9.29	<dl	5.20	3.51	12.7	0.082	0.310	0.021	<dl	0.008	<dl	0.042	9.E-4	8.80	0.143
C-04-24-7.d	0.346	1.39	11.9	250	0.033	2.10	39.8	3.40	0.050	n.r.	9.27	<dl	5.25	4.09	10.5	0.008	0.090	0.059	0.034	0.019	0.032	0.058	4.E-4	5.39	0.096
C-04-25-1.d	0.383	0.900	20.0	247	0.013	2.90	46.0	1.50	0.070	n.r.	8.25	<dl	1.45	6.84	19.7	0.111	0.660	0.200	0.014	0.019	0.019	0.020	0.042	3.40	0.119
C-04-25-2.d	1.60	0.440	13.8	275	0.014	3.00	20.8	0.510	<dl	n.r.	7.16	<dl	1.89	12.3	27.4	0.380	0.062	0.097	0.023	0.029	2.30	0.079	5.E-4	3.70	0.133

Grain ID	*Mn* 55	*Co* 59	*Ni* 60	*Zn* 66	*Ga* 71	As 75	*Se* 82	Mo 95	Ru 101	Rh 103	*Ag* 107	Pd 108	Cd 111	*In* 115	*Sn* 118	*Sb* 121	*Te* 128	Re 185	Os 189	Ir 193	Pt 195	*Au* 197	Tl 205	*Pb* 208	*Bi* 209
55um	0.470	0.023	0.241	0.353	0.028	0.223	2.53	0.030	0.023	0.005	0.023	0.014	0.046	0.012	0.073	0.022	0.256	0.009	0.021	0.007	0.013	0.010	0.004	0.012	0.007
33um	0.939	0.046	0.722	1.06	0.085	0.445	5.07	0.061	0.068	0.009	0.069	0.041	0.137	0.025	0.218	0.067	0.513	0.027	0.042	0.020	0.039	0.030	0.011	0.037	0.013
C-04-25-3.d	0.325	0.690	25.4	254	0.016	2.50	42.3	2.30	<dl	n.r.	6.89	<dl	2.52	7.29	27.9	0.044	0.073	0.107	<dl	0.008	0.034	0.025	0.006	2.12	0.071
C-04-25-4.d	5.40	0.280	33.8	226	0.070	<dl	42.1	7.30	0.600	n.r.	8.73	<dl	1.37	6.98	25.0	0.250	0.770	0.230	<dl	0.033	0.090	0.027	0.019	28.1	0.470
C-04-25-5.d	22.0	0.240	19.9	205	0.075	<dl	36.5	<dl	<dl	n.r.	13.9	<dl	1.13	16.0	17.9	0.360	0.820	<dl	<dl	<dl	0.007	0.002	0.097	27.1	0.621
C-04-25-6.d	0.376	5.10	17.6	255	0.013	9.60	28.0	1.60	0.450	n.r.	11.3	<dl	1.85	10.5	24.6	0.046	0.078	0.029	0.029	0.052	0.160	0.001	4.E-4	1.33	0.107
C-04-25-7.d	0.540	0.390	12.7	291	0.145	0.430	43.7	1.70	0.048	n.r.	10.7	<dl	3.62	12.4	28.7	0.046	0.250	0.070	<dl	0.009	<dl	0.013	0.002	3.56	0.112
C-04-25-8.d	45.0	0.670	19.2	269	0.190	4.10	35.0	4.80	0.089	n.r.	10.4	<dl	1.62	15.5	31.6	0.097	0.069	0.060	0.044	0.025	<dl	0.020	6.E-4	5.60	0.093
C-04-25-9.d	0.334	1.28	22.2	280	0.210	5.80	34.2	4.00	0.070	n.r.	6.07	<dl	3.40	15.5	37.8	0.063	0.072	0.220	0.083	0.053	0.080	0.030	3.E-4	1.97	0.101
C-04-38-1d	104	1.52	37.0	190	1.06	0.620	51.6	<dl	<dl	n.r.	24.1	<dl	6.30	0.569	0.160	0.255	0.560	<dl	<dl	<dl	<dl	9.E-4	0.037	15.3	0.368
C-04-38-2.d	3.10	0.520	12.5	270	0.012	<dl	48.3	0.070	<dl	n.r.	7.26	<dl	12.5	1.47	0.075	0.246	1.06	<dl	<dl	<dl	0.008	0.011	0.063	25.6	0.369
C-04-38-3.d	8.40	1.20	37.0	212	0.054	<dl	48.2	<dl	0.067	n.r.	45.5	<dl	5.70	0.640	0.065	0.107	0.094	<dl	<dl	<dl	<dl	0.001	0.014	6.80	0.110
C-04-43-1d	0.344	0.380	12.4	240	0.014	1.25	55.0	4.80	0.480	n.r.	6.83	<dl	1.35	6.19	1.00	0.010	0.071	0.280	0.102	0.068	0.440	0.017	0.009	3.25	0.136
C-04-43-2.d	0.268	0.134	11.1	322	0.015	<dl	56.3	<dl	0.066	n.r.	8.99	<dl	2.30	2.77	1.85	0.055	0.064	<dl	<dl	<dl	<dl	0.078	4.E-4	4.15	0.110
C-04-43-3.d	0.254	0.093	11.7	322	0.012	<dl	46.8	<dl	<dl	n.r.	12.4	<dl	2.30	2.08	1.93	0.004	0.049	<dl	<dl	<dl	<dl	6.E-4	4.E-4	1.70	0.023
C-04-43-4.d	2.00	0.610	14.4	248	0.019	3.80	49.4	0.740	1.11	n.r.	13.1	<dl	1.35	1.86	1.53	0.059	0.076	0.312	0.112	0.104	0.370	7.E-4	0.046	7.81	0.304
C-04-43-5.d	1.74	0.330	18.1	334	0.012	0.750	50.8	1.08	0.200	n.r.	10.5	<dl	5.73	1.48	2.36	0.042	0.900	0.390	0.095	0.136	0.350	5.E-4	3.E-4	0.900	0.063
C-04-43-6.d	0.239	0.170	12.2	338	0.019	0.780	44.0	<dl	<dl	n.r.	9.42	<dl	2.48	1.77	2.18	0.062	0.950	<dl	<dl	<dl	<dl	0.006	3.E-4	1.68	0.071
C-04-43-7.d	8.10	0.110	12.3	259	0.018	<dl	50.7	<dl	<dl	n.r.	10.8	<dl	1.32	1.24	1.67	0.048	0.059	<dl	<dl	<dl	<dl	0.011	0.015	5.41	0.127
C-04-43-8.d	0.970	0.010	12.1	252	0.058	<dl	51.2	<dl	0.038	n.r.	12.4	<dl	0.920	1.69	1.93	0.054	0.740	<dl	<dl	<dl	<dl	7.E-4	0.013	4.36	0.077
CRTN12CCP-01c	1.80	0.530	61.5	619	0.114	<dl	82.3	<dl	<dl	n.r.	9.24	<dl	7.43	0.913	6.13	0.004	0.900	<dl	<dl	0.020	<dl	0.013	2.E-4	1.05	2.39
CRTN12CCP-02.c	2.40	0.422	52.1	678	0.173	<dl	73.5	0.047	0.036	n.r.	9.01	<dl	7.73	1.07	6.44	0.016	0.620	0.009	<dl	0.021	0.170	0.008	3.E-4	2.56	3.03
CRTN12CCP-03.c	1.67	0.305	44.1	494	0.185	<dl	72.4	0.070	<dl	n.r.	8.92	<dl	5.60	1.09	5.05	0.037	0.390	<dl	<dl	<dl	<dl	0.014	3.E-4	3.46	2.33
CRTN12CCP-04.c	0.213	0.310	48.0	476	0.021	<dl	69.2	0.180	0.028	n.r.	8.14	<dl	5.70	0.984	4.74	0.024	0.240	<dl	<dl	<dl	<dl	0.008	3.E-4	1.70	1.41
CRTN12CCP-05.c	1.49	0.382	49.7	489	0.155	<dl	66.5	<dl	<dl	n.r.	9.43	<dl	7.70	0.909	6.14	0.045	0.054	<dl	<dl	<dl	<dl	0.002	0.002	3.63	2.48
CRTN13CCP-01c	0.890	0.280	49.4	506	0.140	0.690	70.7	0.065	0.230	n.r.	5.85	<dl	5.46	2.15	12.4	0.167	0.250	0.033	0.270	<dl	<dl	0.008	0.003	6.19	3.34
CRTN13CCP-02.c	1.27	0.277	55.4	628	0.109	0.140	67.1	<dl	0.200	n.r.	6.24	<dl	6.85	1.37	6.02	0.050	0.250	<dl	<dl	0.027	0.060	0.019	4.E-4	3.03	3.80
CRTN13CCP-03.c	1.33	0.244	50.1	585	0.086	0.240	72.3	0.083	<dl	n.r.	6.06	<dl	6.76	0.786	5.29	0.111	0.323	<dl	<dl	<dl	<dl	0.160	0.110	3.32	2.57
CRTN13CCP-04.c	2.17	0.211	56.5	730	0.076	<dl	76.4	0.540	<dl	n.r.	5.41	<dl	7.59	0.973	5.46	0.082	0.052	5.00	<dl	<dl	0.037	0.009	0.019	4.99	3.38
CRTN13CCP-05.c	1.71	0.223	50.4	573	0.071	0.230	83.9	<dl	<dl	n.r.	5.58	<dl	6.41	2.17	5.60	0.100	0.052	<dl	<dl	0.060	<dl	0.120	6.E-4	4.60	2.96
CRTN13CCPr-01	0.840	0.242	54.8	564	0.109	<dl	71.1	<dl	<dl	n.r.	6.35	<dl	7.42	0.975	5.89	0.050	0.330	<dl	<dl	<dl	<dl	0.032	4.E-4	3.36	2.97
CRTN13CCPr-02	0.990	0.226	51.0	484	0.085	<dl	73.0	<dl	<dl	n.r.	5.39	<dl	6.40	0.859	5.17	0.046	0.280	<dl	<dl	<dl	<dl	0.132	4.E-4	3.69	3.26
CRTN13CCPr-03	0.850	0.291	63.5	532	0.081	<dl	77.7	<dl	<dl	n.r.	3.77	<dl	6.32	1.03	5.12	0.028	0.260	<dl	<dl	<dl	<dl	0.001	3.E-4	2.87	1.63
CRTN13CCPr-04	1.15	0.284	63.6	508	0.062	<dl	71.7	<dl	<dl	n.r.	4.13	<dl	6.26	0.775	4.80	0.084	0.044	<dl	<dl	<dl	<dl	0.113	5.E-4	4.77	2.85
CRTN13CCPr-05	1.11	0.234	58.8	546	0.082	<dl	78.1	<dl	<dl	n.r.	4.76	<dl	6.57	1.14	5.72	0.045	0.361	<dl	<dl	<dl	<dl	0.045	3.E-4	4.03	2.44
CRTN14-11CCP.d	0.870	0.613	65.2	465	0.036	<dl	84.0	<dl	<dl	n.r.	3.06	<dl	7.04	0.776	7.62	0.114	0.250	<dl	<dl	<dl	<dl	0.199	0.001	4.29	2.86
CRTN14-12CCP.c	0.680	0.450	64.0	458	0.023	0.560	77.8	<dl	0.190	n.r.	3.38	<dl	7.27	3.28	16.7	0.146	0.260	<dl	0.038	<dl	<dl	0.323	2.E-4	3.34	3.68
CRTN14-2CCP.d	0.640	1.90	87.0	423	0.071	<dl	76.1	<dl	0.023	n.r.	3.57	<dl	7.55	1.26	10.7	0.131	0.340	<dl	<dl	<dl	<dl	0.123	0.001	2.55	1.66
CRTN14-3CCP.d	0.700	0.499	72.0	478	0.036	<dl	77.9	<dl	0.076	n.r.	4.12	<dl	7.53	0.797	7.70	0.126	0.260	0.013	<dl	<dl	<dl	0.120	2.E-4	1.94	2.37
CRTN14-4CCP.d	0.910	2.13	74.3	463	0.120	<dl	82.2	<dl	0.021	n.r.	3.29	<dl	10.7	1.44	12.1	0.150	0.400	<dl	<dl	<dl	<dl	0.035	2.E-4	2.94	2.69
CRTN14-6CCP.d	0.840	0.790	73.7	475	0.030	<dl	75.4	<dl	0.022	n.r.	3.27	<dl	7.31	1.20	9.44	0.110	0.510	<dl	<dl	<dl	<dl	0.130	2.E-4	2.24	2.00
CRTN14-8CCP.d	1.18	1.43	94.3	469	0.135	0.470	73.8	<dl	<dl	n.r.	2.83	<dl	11.1	1.60	14.2	0.081	0.540	<dl	<dl	<dl	<dl	0.104	2.E-4	1.95	2.36
CRTN14-9CCP.d	0.880	1.05	86.2	434	0.160	<dl	69.0	<dl	0.030	n.r.	2.99	<dl	8.29	1.74	12.8	0.111	0.860	<dl	<dl	<dl	<dl	0.122	2.E-4	3.08	3.69
CRTN18-10.d	1.15	0.315	101	317	0.054	0.620	82.8	<dl	0.580	n.r.	1.70	<dl	15.4	3.17	19.9	0.019	0.680	0.011	0.058	<dl	<dl	8.E-4	0.006	1.80	0.895
CRTN18-2.d	0.440	0.900	106	515	0.045	<dl	79.7	<dl	0.029	n.r.	1.82	<dl	22.6	3.28	27.7	0.038	0.910	<dl	<dl	<dl	<dl	6.E-4	1.E-4	1.67	0.646
CRTN18-5.d	0.670	0.351	117	404	0.046	<dl	78.0	<dl	0.021	n.r.	2.67	<dl	18.0	3.55	24.7	0.029	2.03	<dl	<dl	<dl	<dl	1.E-3	2.E-4	2.54	2.22
CRTN18-6.d	0.221	0.257	96.4	550	0.014	<dl	80.9	<dl	0.034	n.r.	3.23	<dl	20.0	3.56	23.3	0.040	2.28	<dl	<dl	<dl	<dl	9.E-4	2.E-4	2.19	1.85
CRTN18-7.d	0.238	0.261	96.4	360	0.084	<dl	83.0	<dl	0.034	n.r.	2.45	<dl	17.5	3.78	24.5	0.025	1.95	<dl	<dl	<dl	<dl	8.E-4	3.E-4	2.20	1.25
CRTN19-1d	0.210	0.370	89.7	308	0.054	<dl	78.7	<dl	<dl	n.r.	2.54	<dl	18.2	1.99	11.9	0.037	1.22	<dl	<dl	<dl	<dl	0.002	2.E-4	2.37	2.46

Grain ID	Mn 55	Co 59	Ni 60	Zn 66	Ga 71	As 75	Se 82	Mo 95	Ru 101	Rh 103	Ag 107	Pd 108	Cd 111	In 115	Sn 118	Sb 121	Te 128	Re 185	Os 189	Ir 193	Pt 195	Au 197	Tl 205	Pb 208	Bi 209
55um	0.470	0.023	0.241	0.353	0.028	0.223	2.53	0.030	0.023	0.005	0.023	0.014	0.046	0.012	0.073	0.022	0.256	0.009	0.021	0.007	0.013	0.010	0.004	0.012	0.007
33um	0.939	0.046	0.722	1.06	0.085	0.445	5.07	0.061	0.068	0.009	0.069	0.041	0.137	0.025	0.218	0.067	0.513	0.027	0.042	0.020	0.039	0.030	0.011	0.037	0.013
CRTN19-10.d	1.24	0.920	99.0	311	0.008	<dl	77.0	<dl	0.140	n.r.	1.95	<dl	18.4	0.817	6.65	0.002	0.068	<dl	<dl	<dl	<dl	0.001	2.E-4	1.48	1.60
CRTN19-11.d	0.590	0.261	95.1	520	0.008	<dl	61.0	<dl	0.060	n.r.	2.89	<dl	23.9	0.893	7.35	0.003	1.90	<dl	<dl	<dl	<dl	0.001	2.E-4	1.89	2.60
CRTN19-2.d	0.203	0.268	100	296	0.130	<dl	53.2	<dl	<dl	n.r.	3.28	<dl	19.0	2.06	11.6	0.009	2.11	<dl	<dl	<dl	<dl	0.003	2.E-4	2.23	3.69
CRTN19-8.d	0.730	0.250	95.6	341	0.048	<dl	61.4	<dl	<dl	n.r.	2.45	<dl	18.8	1.24	7.75	0.003	1.70	<dl	<dl	<dl	<dl	0.001	3.E-4	1.67	2.28
CRTN19-9.d	0.990	0.800	94.8	280	0.031	2.00	72.0	0.190	<dl	n.r.	2.31	<dl	16.2	1.38	9.80	0.004	1.45	0.013	<dl	<dl	<dl	0.002	0.029	2.04	2.84
CRTN6CCP-01.d	1.41	0.670	57.3	575	0.023	0.083	110	0.077	0.031	n.r.	3.63	<dl	2.92	1.35	3.32	0.047	0.210	0.038	<dl	0.003	<dl	6.E-4	0.007	3.01	0.276
CRTN6CCP-02.d	1.19	6.00	67.4	495	0.133	<dl	87.9	0.033	0.056	n.r.	3.80	<dl	2.27	1.77	7.62	0.052	2.20	<dl	0.026	<dl	<dl	0.060	2.E-4	3.27	0.458
CRTN6CCP-03.d	1.42	0.570	62.0	533	0.111	0.200	90.2	0.019	0.043	n.r.	3.96	<dl	2.73	2.59	7.33	0.024	1.31	0.080	<dl	0.110	1.80	8.E-4	4.E-4	3.92	0.627
CRTN6CCP-04.d	1.36	0.310	52.4	495	0.127	<dl	94.1	<dl	<dl	n.r.	3.28	<dl	2.31	3.97	6.72	0.043	1.07	<dl	<dl	0.033	<dl	0.012	2.E-4	3.26	0.587
CRTN6CCP-05.d	1.17	0.680	57.2	541	0.095	0.150	95.3	<dl	0.021	n.r.	3.11	<dl	2.27	1.82	6.63	0.028	1.41	0.020	<dl	0.011	0.008	0.009	0.003	2.54	0.500
CRTN6CCPr-01.c	0.850	0.269	56.1	480	0.112	<dl	94.1	<dl	<dl	n.r.	3.33	<dl	2.33	2.05	7.68	0.036	2.34	<dl	<dl	<dl	<dl	0.001	4.E-4	3.85	0.541
CRTN6CCPr-02.c	0.640	0.433	59.2	492	0.105	<dl	98.9	<dl	<dl	n.r.	3.40	<dl	2.39	1.61	5.27	0.069	0.890	<dl	<dl	<dl	<dl	0.001	4.E-4	2.50	0.222
CRTN6CCPr-03.c	1.06	0.355	60.9	465	0.141	<dl	89.6	<dl	<dl	n.r.	3.55	<dl	2.54	2.00	6.83	0.018	1.31	<dl	<dl	<dl	<dl	0.001	4.E-4	2.49	0.346
CRTN6CCPr-04.c	0.600	0.293	56.0	404	0.135	0.270	91.6	<dl	0.037	n.r.	3.55	<dl	2.09	2.26	5.88	0.137	0.890	<dl	<dl	<dl	<dl	0.001	8.E-4	5.31	0.750
CRTN6CCPr-05.c	0.750	0.550	53.7	460	0.075	1.40	109	<dl	<dl	n.r.	3.48	<dl	1.90	1.78	5.49	0.031	0.920	<dl	<dl	1.00	0.070	9.E-4	4.E-4	0.960	0.160
CRTN9B-1.d	1.59	1.80	105	552	0.079	<dl	87.4	<dl	<dl	n.r.	1.44	<dl	22.3	3.12	48.6	0.077	1.32	<dl	<dl	<dl	<dl	0.020	2.E-4	2.38	2.11
CRTN9B-2.d	1.72	0.280	85.9	506	0.074	<dl	85.5	<dl	0.025	n.r.	2.08	<dl	19.8	3.38	51.3	0.062	1.86	<dl	<dl	<dl	<dl	0.139	2.E-4	0.833	2.77
CRTN9B-3.d	1.23	0.355	81.9	471	0.082	0.520	84.1	<dl	<dl	n.r.	1.74	<dl	20.2	3.36	53.4	0.081	1.50	<dl	<dl	<dl	<dl	0.064	3.E-4	2.58	2.30
CRTN9B-4.d	1.77	0.465	94.3	468	0.088	<dl	86.2	<dl	<dl	n.r.	2.47	<dl	19.2	3.29	54.4	0.059	2.59	<dl	<dl	<dl	<dl	0.018	2.E-4	1.25	2.33
CRTN9B-5.d	1.26	1.12	104	401	0.158	<dl	91.0	<dl	0.029	n.r.	1.33	<dl	18.4	3.30	51.4	0.038	1.25	<dl	<dl	<dl	<dl	0.010	2.E-4	1.40	1.08
CRTN9B-7.d	1.13	0.730	75.2	484	0.114	0.290	86.0	<dl	<dl	n.r.	3.04	<dl	21.0	3.14	54.5	0.005	4.10	<dl	<dl	<dl	<dl	0.001	2.E-4	1.30	5.70
CRTN9B-8-2.d	30.0	1.26	86.0	441	0.055	<dl	89.1	<dl	0.021	n.r.	1.48	<dl	19.8	3.02	52.5	0.042	1.48	<dl	<dl	<dl	<dl	0.010	3.E-4	1.74	1.59
CRTN9B-9.d	1.10	0.474	71.6	496	0.070	0.440	84.4	<dl	0.023	n.r.	1.54	<dl	20.2	3.21	55.4	0.064	1.37	<dl	<dl	<dl	<dl	0.030	0.001	1.76	2.32
CTRN12CCPr-01.	1.07	0.210	46.3	541	0.122	<dl	73.0	<dl	<dl	n.r.	8.23	<dl	6.56	0.743	3.60	0.028	0.400	<dl	<dl	<dl	<dl	0.001	4.E-4	3.39	2.81
CTRN12CCPr-02	1.01	0.329	54.9	582	0.162	<dl	77.1	<dl	<dl	n.r.	8.06	<dl	7.52	1.37	7.08	0.004	0.540	<dl	<dl	<dl	<dl	0.002	4.E-4	2.43	1.98
CTRN12CCPr-03	1.16	0.264	46.7	476	0.140	<dl	79.3	<dl	<dl	n.r.	8.54	<dl	5.69	0.700	4.15	0.042	0.056	<dl	<dl	<dl	<dl	0.004	0.012	3.63	2.19
CTRN12CCPr-04	1.18	0.330	50.9	547	0.110	<dl	74.6	<dl	0.043	n.r.	8.30	<dl	6.20	0.817	5.66	0.004	0.230	<dl	<dl	<dl	<dl	0.001	2.E-4	0.790	1.30
CTRN12CCPr-05	1.91	0.550	55.9	650	0.051	0.226	88.5	<dl	0.460	n.r.	8.01	<dl	8.64	0.775	3.48	0.035	0.220	0.021	0.199	<dl	<dl	0.001	3.E-4	1.67	2.26
DC-18-07.d	0.560	0.125	12.5	261	0.403	<dl	61.4	<dl	<dl	n.r.	3.46	<dl	5.40	1.32	2.81	0.025	2.64	<dl	<dl	<dl	<dl	6.E-4	2.E-4	8.43	0.232
DC-18-08.d	0.520	0.159	12.9	243	0.430	<dl	56.9	<dl	<dl	n.r.	3.27	<dl	4.82	1.61	2.71	0.004	1.94	<dl	<dl	<dl	<dl	6.E-4	3.E-4	15.7	0.130
DC-18-09.d	0.183	0.296	19.2	199	0.428	<dl	57.1	<dl	<dl	n.r.	3.06	<dl	3.69	1.07	2.15	0.004	1.84	<dl	<dl	<dl	<dl	5.E-4	3.E-4	3.67	0.084
DC-18-10.d	0.177	0.056	8.17	197	0.500	<dl	53.4	<dl	<dl	n.r.	3.57	<dl	4.26	1.36	2.19	0.015	2.37	<dl	<dl	<dl	<dl	4.E-4	3.E-4	11.1	0.053
DC-18-11.d	0.470	0.128	9.70	211	0.480	<dl	64.5	<dl	<dl	n.r.	3.55	<dl	4.62	1.35	2.37	0.014	2.54	<dl	<dl	<dl	<dl	5.E-4	3.E-4	6.51	0.059
DC-18-12.d	0.176	0.350	14.6	206	0.400	0.290	59.5	<dl	<dl	n.r.	2.53	<dl	3.86	1.64	2.18	0.018	2.46	<dl	<dl	<dl	<dl	5.E-4	0.002	8.06	0.085
DC-18-13.d	0.480	0.438	12.2	231	0.425	<dl	55.0	<dl	<dl	n.r.	2.37	<dl	3.98	1.26	2.12	0.019	2.18	<dl	<dl	<dl	<dl	0.007	3.E-4	8.49	0.178
DC69-10.d	1.46	0.454	26.2	273	0.540	<dl	45.4	<dl	<dl	n.r.	0.523	<dl	11.9	1.81	5.04	0.057	4.06	<dl	<dl	<dl	<dl	0.001	7.E-4	8.62	0.382
DC69-11.d	0.810	2.99	103	225	0.330	15.0	36.9	0.220	<dl	n.r.	0.750	<dl	10.2	1.37	4.65	0.029	2.58	0.105	<dl	<dl	<dl	0.001	7.E-4	14.3	0.655
DC69-3.d	1.22	1.53	37.8	348	0.500	<dl	46.1	<dl	<dl	n.r.	0.153	<dl	15.5	1.29	5.47	0.044	3.74	<dl	<dl	<dl	<dl	0.001	5.E-4	5.52	0.490
DC69-4.d	0.430	0.376	28.7	258	0.278	<dl	40.5	<dl	0.032	n.r.	0.336	<dl	11.4	1.15	3.31	0.005	5.21	<dl	<dl	<dl	<dl	0.001	5.E-4	7.88	0.377
DC69-5.d	0.720	0.870	31.8	277	0.375	<dl	44.3	<dl	<dl	n.r.	0.298	<dl	10.1	1.35	4.01	0.035	4.93	<dl	<dl	<dl	<dl	0.001	2.E-4	8.25	0.416
DC69-8.d	1.08	0.730	38.1	274	0.490	<dl	42.9	<dl	<dl	n.r.	0.460	<dl	13.0	1.56	5.82	0.043	2.42	0.007	<dl	<dl	0.016	0.001	6.E-4	7.34	0.478
DC69-9.d	1.09	0.338	24.1	275	0.620	<dl	44.6	<dl	0.021	n.r.	0.610	<dl	11.5	1.53	4.66	0.053	4.02	<dl	<dl	<dl	<dl	0.001	0.004	1.77	0.274
E13-2.d	0.800	0.180	25.0	221	0.015	<dl	51.0	0.340	<dl	n.r.	8.27	<dl	5.70	2.40	1.63	0.004	2.98	0.021	<dl	0.062	<dl	6.E-4	0.032	3.51	0.199
E13-3.d	0.179	0.400	9.70	192	0.047	<dl	97.3	<dl	<dl	n.r.	7.96	<dl	5.06	2.19	2.12	0.019	10.3	<dl	<dl	<dl	<dl	0.019	2.E-4	1.77	0.570
E13-6.d	0.183	0.041	4.30	309	0.014	<dl	100	<dl	0.034	n.r.	5.38	<dl	3.60	1.90	0.301	0.013	4.87	<dl	<dl	<dl	0.025	0.013	0.171	7.47	1.49
E1-4.d	0.217	0.042	9.60	305	0.008	<dl	73.0	1.91	<dl	n.r.	5.02	<dl	10.3	2.12	0.470	0.243	4.02	0.153	0.081	0.087	<dl	0.013	0.013	12.5	3.12
E1-5.d	0.155	0.035	9.12	353	0.024	0.390	76.1	2.18	<dl	n.r.	6.09	<dl	8.25	1.76	0.450	0.093	10.3	0.076	0.025	0.098	0.009	7.E-4	5.E-4	4.55	0.560

Grain ID	Mn 55	Co 59	Ni 60	Zn 66	Ga 71	As 75	Se 82	Mo 95	Ru 101	Rh 103	Ag 107	Pd 108	Cd 111	In 115	Sn 118	Sb 121	Te 128	Re 185	Os 189	Ir 193	Pt 195	Au 197	Tl 205	Pb 208	Bi 209
55um	0.470	0.023	0.241	0.353	0.028	0.223	2.53	0.030	0.023	0.005	0.023	0.014	0.046	0.012	0.073	0.022	0.256	0.009	0.021	0.007	0.013	0.010	0.004	0.012	0.007
33um	0.939	0.046	0.722	1.06	0.085	0.445	5.07	0.061	0.068	0.009	0.069	0.041	0.137	0.025	0.218	0.067	0.513	0.027	0.042	0.020	0.039	0.030	0.011	0.037	0.013
E1-8.d	1.15	0.490	16.5	366	0.009	0.270	79.4	1.40	0.035	n.r.	10.9	<dl	8.25	3.92	0.400	0.170	12.8	0.029	0.038	0.120	0.009	8.E-4	0.013	11.4	1.35
E1-9.d	0.220	0.172	13.0	399	0.007	<dl	96.0	2.48	<dl	n.r.	6.21	<dl	7.60	2.45	0.510	0.051	12.8	0.216	0.098	0.154	0.024	7.E-4	0.006	6.31	0.690
E4-10.d	0.258	0.760	118	364	0.020	<dl	129	<dl	<dl	n.r.	10.2	<dl	9.70	3.38	33.7	0.026	37.0	<dl	<dl	<dl	<dl	0.025	0.059	64.2	3.17
E4-11.d	1.06	0.390	33.8	570	0.016	<dl	116	<dl	<dl	n.r.	21.4	<dl	16.7	2.96	32.2	0.086	39.1	<dl	<dl	<dl	<dl	0.015	0.092	61.6	2.95
E4-3.d	1.15	0.113	26.5	578	0.013	<dl	93.3	0.064	<dl	n.r.	16.9	<dl	16.0	3.81	40.2	0.030	8.31	<dl	<dl	<dl	<dl	0.023	0.091	6.41	0.467
E4-5.d	1.85	0.460	82.0	580	0.017	<dl	92.3	<dl	<dl	n.r.	10.5	<dl	14.0	3.17	32.0	0.024	6.64	<dl	<dl	<dl	<dl	0.007	3.E-4	5.63	0.689
E4-6.d	0.250	0.710	190	450	0.017	<dl	100	<dl	<dl	n.r.	7.24	<dl	10.9	3.15	33.4	0.027	4.44	<dl	<dl	<dl	<dl	0.015	0.006	4.14	0.508
E4-9.d	0.225	0.072	24.6	412	0.017	<dl	111	<dl	0.023	n.r.	8.50	<dl	12.0	3.33	32.6	0.040	11.1	<dl	<dl	<dl	<dl	0.016	0.025	16.4	1.31
EDEEP-10.d	1.28	0.330	17.0	197	0.350	<dl	63.0	<dl	0.041	n.r.	0.960	<dl	16.9	2.23	2.49	0.014	10.0	<dl	<dl	<dl	<dl	0.001	4.E-4	1.21	0.301
EDEEP-4.d	0.328	0.067	9.20	255	0.250	<dl	57.3	<dl	0.040	n.r.	1.84	<dl	23.4	2.68	2.48	0.004	9.60	<dl	<dl	<dl	<dl	8.E-4	3.E-4	1.89	0.201
EDEEP-5.d	0.396	0.120	8.90	187	0.510	<dl	55.0	0.220	<dl	n.r.	2.07	<dl	17.4	2.39	3.21	0.004	8.20	0.370	0.015	<dl	<dl	0.001	4.E-4	1.97	0.374
EDEEP-8.d	0.391	0.166	13.2	229	0.170	<dl	50.0	<dl	<dl	n.r.	4.49	<dl	21.1	4.26	3.44	0.006	14.1	<dl	<dl	<dl	<dl	0.002	3.E-4	4.81	0.790
EDEEP-9.d	1.89	0.132	13.9	432	0.250	<dl	56.0	<dl	<dl	n.r.	3.74	<dl	27.3	3.29	2.61	0.007	13.4	<dl	<dl	<dl	<dl	0.002	5.E-4	2.94	0.781
EX0301-1d	15.8	0.460	10.6	257	0.234	<dl	48.7	<dl	0.091	n.r.	0.750	<dl	11.5	2.63	12.2	0.004	0.930	<dl	0.154	0.266	0.229	0.070	4.E-4	2.34	0.063
EX0301-10.d	2.36	0.128	7.49	259	0.064	<dl	46.4	<dl	<dl	n.r.	6.84	<dl	8.78	2.22	9.98	0.004	6.11	<dl	<dl	<dl	<dl	0.020	0.003	4.58	0.124
EX0301-11.d	0.182	0.098	11.3	255	0.012	<dl	54.3	<dl	<dl	n.r.	2.69	<dl	7.73	2.32	10.6	0.028	5.06	<dl	<dl	<dl	<dl	0.010	2.E-4	3.06	0.084
EX0301-12.d	0.174	0.034	6.21	265	0.094	<dl	57.8	<dl	<dl	n.r.	8.20	<dl	9.02	2.54	11.4	0.004	7.84	<dl	<dl	<dl	<dl	0.015	3.E-4	5.72	0.119
EX0301-13.d	1.66	0.049	6.60	247	0.054	<dl	41.8	<dl	<dl	n.r.	6.18	<dl	9.21	2.45	10.9	0.014	8.20	<dl	<dl	<dl	<dl	0.007	0.006	4.44	0.126
EX0301-2.d	1.02	0.068	8.75	264	0.097	<dl	47.8	<dl	0.050	n.r.	6.12	<dl	9.16	2.41	11.1	0.016	9.15	<dl	<dl	<dl	<dl	0.005	0.004	5.59	0.129
EX0301-4.d	0.510	0.075	8.80	300	0.012	<dl	50.7	<dl	<dl	n.r.	7.26	<dl	10.7	2.45	11.6	0.018	6.24	<dl	<dl	<dl	<dl	0.044	4.E-4	2.98	0.097
EX0301-5.d	0.184	0.053	4.98	262	0.102	<dl	52.0	<dl	<dl	n.r.	2.82	<dl	8.78	2.36	10.8	0.022	4.37	<dl	<dl	<dl	<dl	0.013	3.E-4	2.95	0.079
EX0301-9.d	2.06	0.233	10.3	343	0.073	8.00	47.6	<dl	<dl	n.r.	6.10	<dl	10.5	2.22	11.3	0.033	6.38	<dl	0.014	0.042	0.022	0.016	0.003	3.38	0.071
IGCP4-1d	0.310	0.053	5.40	351	0.019	<dl	87.0	<dl	<dl	n.r.	5.63	<dl	10.2	3.09	0.330	0.056	2.76	<dl	<dl	<dl	<dl	0.036	3.E-4	0.850	0.366
IGCP4-2.d	0.350	2.70	4.30	316	0.030	<dl	76.0	<dl	<dl	n.r.	2.71	<dl	10.2	2.86	0.078	0.060	1.48	<dl	<dl	<dl	<dl	0.002	3.E-4	2.26	0.519
IGCP4-3.d	33.6	0.204	7.20	320	0.012	<dl	75.8	<dl	<dl	n.r.	6.98	<dl	9.61	2.85	0.273	0.058	1.53	<dl	<dl	<dl	<dl	0.002	5.E-4	2.01	0.536
IGCP4-4.d	0.670	0.012	3.30	400	0.019	0.270	84.0	<dl	<dl	n.r.	4.46	<dl	10.6	2.90	0.340	0.023	1.17	<dl	<dl	0.025	<dl	0.019	3.E-4	1.10	0.578
IGCP4-5.d	0.139	0.013	2.90	391	0.024	<dl	91.0	<dl	<dl	n.r.	8.20	<dl	13.2	2.81	0.250	0.085	2.69	<dl	<dl	<dl	<dl	0.091	5.E-4	1.25	0.501
J12-10.d	0.182	0.062	21.7	532	0.013	<dl	96.7	<dl	0.035	n.r.	5.20	<dl	7.18	1.19	3.74	0.005	7.73	<dl	<dl	<dl	<dl	7.E-4	3.E-4	9.85	2.19
J12-2.d	0.195	0.155	26.4	395	0.046	<dl	90.0	<dl	0.056	n.r.	5.20	<dl	4.10	1.39	6.28	0.023	8.80	<dl	<dl	<dl	<dl	0.013	4.E-4	7.27	2.13
J12-3.d	0.207	0.123	34.7	430	0.092	<dl	86.2	<dl	<dl	n.r.	4.15	<dl	8.54	1.88	6.66	0.006	8.73	<dl	<dl	<dl	<dl	0.009	0.004	4.67	2.29
J12-6.d	0.203	0.730	73.0	389	0.012	<dl	83.8	<dl	0.034	n.r.	3.46	<dl	3.71	1.15	3.12	0.006	7.07	<dl	<dl	<dl	<dl	0.032	3.E-4	3.61	5.15
J12-7.d	0.188	0.101	23.4	374	0.039	<dl	84.0	<dl	<dl	n.r.	3.67	<dl	2.97	1.11	2.82	0.045	6.58	<dl	<dl	<dl	<dl	0.042	0.003	5.78	6.12
J12-8.d	0.160	0.151	33.8	473	0.014	0.740	111	0.044	<dl	n.r.	4.27	<dl	11.7	1.66	7.31	0.042	9.72	0.033	<dl	<dl	<dl	0.001	3.E-4	8.49	5.10
J12-9.d	0.222	0.290	34.0	362	0.061	<dl	102	0.700	<dl	n.r.	4.57	<dl	7.80	1.63	7.07	0.061	7.40	0.016	<dl	0.014	<dl	0.019	3.E-4	6.20	2.44
J2-3.d	3.22	0.412	18.2	346	0.012	<dl	77.0	<dl	0.520	n.r.	4.34	<dl	1.55	0.041	0.620	0.008	0.103	0.025	0.650	0.140	<dl	0.001	0.004	32.5	0.326
J2-4.d	4.51	0.460	29.0	275	0.014	<dl	95.1	0.220	0.076	n.r.	2.83	<dl	1.41	0.021	0.420	0.008	0.109	0.160	0.180	0.065	<dl	0.001	8.E-4	42.6	0.356
J3-1d	4.78	0.072	17.6	348	0.025	<dl	56.0	<dl	<dl	n.r.	1.41	<dl	1.89	1.47	0.700	0.008	3.30	<dl	<dl	<dl	<dl	9.E-4	4.E-4	4.18	0.383
J3-2.d	1.49	0.150	20.8	340	0.025	<dl	75.0	<dl	<dl	n.r.	2.37	<dl	2.32	1.32	0.750	0.007	1.03	<dl	<dl	<dl	<dl	0.018	6.E-4	16.1	0.820
J3-3.d	0.307	0.193	20.4	293	0.011	<dl	68.0	<dl	0.059	n.r.	3.23	<dl	2.52	1.83	0.550	0.006	1.67	<dl	<dl	<dl	<dl	0.016	0.006	11.3	1.25
J3-4.d	1.54	0.128	21.3	413	0.075	<dl	72.0	<dl	<dl	n.r.	4.24	<dl	3.00	2.30	0.850	0.008	3.60	<dl	<dl	<dl	<dl	0.039	9.E-4	13.9	1.14
J3-7.d	1.91	8.70	422	389	0.014	0.530	60.2	0.120	0.480	n.r.	11.1	<dl	3.93	0.062	0.350	0.440	1.29	0.640	0.440	0.083	<dl	0.122	0.024	117	5.78
J3-8.d	2.05	2.23	250	268	0.019	<dl	86.0	<dl	<dl	n.r.	16.7	<dl	5.55	0.067	0.860	0.120	0.190	<dl	<dl	<dl	<dl	0.081	0.019	128	4.59
J9B-1.d	2.23	0.008	7.60	276	0.028	<dl	60.0	0.050	<dl	n.r.	3.49	<dl	11.0	3.45	0.077	0.008	0.165	0.090	<dl	<dl	<dl	0.037	5.E-4	4.56	0.511
J9B-3.d	0.468	0.120	4.70	231	0.017	<dl	64.0	<dl	0.032	n.r.	7.10	<dl	10.4	1.34	0.067	0.006	0.181	<dl	<dl	<dl	<dl	0.003	0.009	15.5	1.01
J9B-4.d	8.90	0.100	7.30	201	0.029	<dl	82.0	<dl	<dl	n.r.	13.2	<dl	8.50	1.47	0.086	0.007	4.60	<dl	<dl	<dl	<dl	0.003	0.008	11.1	0.850
J9B-5.d	1.19	0.016	2.25	212	0.013	<dl	45.0	<dl	<dl	n.r.	13.1	<dl	10.1	1.55	0.070	0.005	7.60	<dl	<dl	<dl	<dl	0.002	6.E-4	16.6	0.562
J9B-6.d	2.20	0.055	5.20	270	0.027	<dl	62.0	<dl	0.023	n.r.	12.3	<dl	11.2	2.03	0.059	0.009	5.00	<dl	<dl	<dl	<dl	0.022	0.008	14.4	0.960

Grain ID	Mn 55	Co 59	Ni 60	Zn 66	Ga 71	As 75	Se 82	Mo 95	Ru 101	Rh 103	Ag 107	Pd 108	Cd 111	In 115	Sn 118	Sb 121	Te 128	Re 185	Os 189	Ir 193	Pt 195	Au 197	Tl 205	Pb 208	Bi 209
55um	0.470	0.023	0.241	0.353	0.028	0.223	2.53	0.030	0.023	0.005	0.023	0.014	0.046	0.012	0.073	0.022	0.256	0.009	0.021	0.007	0.013	0.010	0.004	0.012	0.007
33um	0.939	0.046	0.722	1.06	0.085	0.445	5.07	0.061	0.068	0.009	0.069	0.041	0.137	0.025	0.218	0.067	0.513	0.027	0.042	0.020	0.039	0.030	0.011	0.037	0.013
J9B-7.d	4.70	0.210	5.10	268	0.031	<dl	72.0	0.050	0.045	n.r.	15.0	<dl	12.2	2.35	0.081	0.008	9.90	<dl	<dl	<dl	<dl	0.002	0.001	9.84	0.753
K2-10.d	3.87	0.440	30.0	338	0.120	0.820	52.3	<dl	0.080	n.r.	1.13	<dl	21.5	6.71	26.3	0.189	1.58	0.066	0.133	0.150	0.045	0.045	2.E-4	1.61	0.135
K2-11.d	0.810	0.149	8.75	315	0.131	0.810	58.6	0.080	0.056	n.r.	0.601	<dl	16.4	8.86	28.9	0.039	0.620	0.390	0.121	0.137	0.095	0.004	2.E-4	2.69	0.100
K2-2.d	0.710	0.250	17.7	282	0.018	2.60	50.4	<dl	0.094	n.r.	2.24	0.194	17.8	6.68	25.4	3.20	6.00	<dl	0.250	0.330	1.60	0.066	3.E-4	1.45	0.710
K2-4.d	1.54	0.179	16.2	369	0.107	1.15	51.6	<dl	0.173	n.r.	2.12	<dl	21.1	6.12	24.8	2.10	7.50	0.052	0.168	0.171	0.078	0.037	4.E-4	2.53	0.640
K2-5.d	2.30	0.280	20.7	300	0.070	2.60	53.5	7.00	0.180	n.r.	1.42	<dl	21.9	5.85	24.1	0.480	3.44	0.210	0.500	0.270	0.226	0.042	0.007	2.07	0.161
K2-6.d	1.07	0.171	19.6	238	0.091	<dl	51.7	<dl	<dl	n.r.	0.620	<dl	15.7	6.18	21.7	0.220	0.670	<dl	<dl	0.022	0.040	0.011	5.E-4	7.86	0.469
K2-7.d	1.71	0.273	20.9	308	0.046	0.580	54.0	<dl	0.108	n.r.	0.473	<dl	19.6	5.99	24.0	0.069	0.390	<dl	0.097	0.192	0.080	0.024	2.E-4	1.62	0.114
K2-9.d	1.69	0.100	30.1	309	0.105	1.32	46.9	<dl	<dl	n.r.	0.800	<dl	21.0	6.38	24.0	0.096	0.710	0.023	0.163	0.320	0.173	0.008	2.E-4	2.44	0.137
MCR10a-10.d	1.55	0.078	43.9	177	0.049	<dl	22.3	<dl	0.043	n.r.	28.7	<dl	29.3	7.65	17.3	0.028	2.43	<dl	<dl	<dl	<dl	0.034	0.066	5.10	0.425
MCR10a-11.d	1.95	0.190	52.5	175	0.086	<dl	21.3	<dl	<dl	n.r.	30.5	<dl	28.1	7.60	18.9	0.018	4.03	<dl	<dl	<dl	<dl	0.035	0.087	4.64	0.167
MCR10a-12.d	1.90	0.104	48.9	185	0.029	<dl	17.5	<dl	<dl	n.r.	27.0	<dl	28.6	7.24	19.2	0.025	1.19	<dl	<dl	<dl	<dl	0.069	0.075	4.30	0.198
MCR10a-13.d	2.55	0.190	69.4	171	0.036	<dl	20.9	<dl	<dl	n.r.	32.6	<dl	29.0	7.28	20.5	0.044	3.66	<dl	<dl	<dl	<dl	0.027	0.052	3.58	0.140
MCR10a-14.d	1.54	0.071	51.5	158	0.049	<dl	19.9	<dl	<dl	n.r.	29.6	<dl	28.9	6.91	19.2	0.043	1.77	<dl	<dl	<dl	<dl	0.070	0.046	3.04	0.238
MCR10a-15.d	1.92	0.079	50.7	192	0.065	<dl	20.0	<dl	<dl	n.r.	30.4	<dl	30.7	6.85	21.1	0.031	2.95	<dl	<dl	<dl	0.009	0.070	0.080	4.80	0.141
MCR10a-16.d	2.13	0.043	48.2	170	0.056	<dl	25.5	<dl	<dl	n.r.	40.2	<dl	30.0	7.17	22.3	0.035	3.60	<dl	<dl	<dl	<dl	0.007	0.072	4.45	0.105
MCR10a-1b.d	1.71	0.051	45.8	167	0.084	<dl	20.1	<dl	<dl	n.r.	43.1	<dl	32.6	7.20	20.4	0.064	2.67	<dl	<dl	<dl	<dl	0.015	0.125	3.61	0.130
MCR10a-2.d	1.60	0.083	56.4	178	0.011	<dl	18.9	0.045	0.041	n.r.	37.1	<dl	30.7	7.05	19.5	0.004	1.83	<dl	<dl	<dl	<dl	0.014	0.072	4.60	0.298
MCR10a-3.d	2.13	0.112	54.0	162	0.094	<dl	21.9	<dl	<dl	n.r.	42.2	<dl	30.0	6.92	22.6	0.034	5.20	<dl	<dl	<dl	<dl	0.036	0.150	7.40	0.164
MCR10a-4.d	2.35	0.238	60.4	176	0.074	<dl	22.8	<dl	<dl	n.r.	43.7	<dl	33.1	7.03	21.8	0.008	5.10	<dl	<dl	<dl	<dl	0.030	0.087	9.60	0.271
MCR10a-5.d	2.30	0.211	57.3	171	0.105	<dl	23.5	<dl	<dl	n.r.	42.0	<dl	29.6	6.71	21.5	0.007	4.60	<dl	<dl	<dl	<dl	0.072	0.097	5.30	0.169
MCR10a-6.d	2.29	0.064	46.3	167	0.015	<dl	22.0	<dl	<dl	n.r.	35.4	<dl	28.6	6.98	17.4	0.066	2.72	<dl	<dl	<dl	<dl	0.054	0.053	3.74	0.203
MCR10a-7.d	2.62	0.239	61.4	339	0.043	<dl	22.3	<dl	0.051	n.r.	37.8	<dl	43.2	7.04	20.9	0.040	3.23	<dl	<dl	<dl	<dl	0.057	0.066	5.05	0.170
MCR10a-8.d	1.86	0.068	48.4	167	0.061	<dl	19.3	<dl	<dl	n.r.	32.7	<dl	29.8	7.39	19.6	0.008	2.86	<dl	<dl	<dl	<dl	0.027	0.288	5.73	0.332
MCR10a-9.d	1.66	0.106	55.5	162	0.078	<dl	21.0	<dl	<dl	n.r.	35.8	<dl	28.4	6.99	20.7	0.020	2.33	<dl	<dl	<dl	<dl	0.067	0.089	2.87	0.399
MCR10b-1.d	2.38	0.148	58.3	173	0.096	<dl	23.6	<dl	<dl	n.r.	38.4	<dl	30.4	7.31	21.8	0.026	3.90	<dl	<dl	<dl	<dl	0.007	0.161	4.55	0.208
MCR10b-10.d	0.990	0.064	34.9	178	0.134	0.580	14.0	<dl	<dl	n.r.	26.9	<dl	26.9	10.5	27.1	0.022	6.16	<dl	<dl	<dl	<dl	0.183	0.135	3.91	0.358
MCR10b-11.d	0.208	0.057	26.6	172	0.058	<dl	14.3	<dl	<dl	n.r.	21.2	<dl	26.6	10.9	24.0	0.016	4.68	<dl	<dl	<dl	<dl	0.027	0.090	4.01	0.367
MCR10b-2.d	2.17	0.111	51.7	165	0.054	<dl	20.7	<dl	<dl	n.r.	35.7	<dl	29.0	7.16	18.9	0.041	2.95	<dl	<dl	<dl	<dl	0.038	0.074	2.95	0.321
MCR10b-3.d	2.19	0.152	58.1	161	0.088	<dl	20.4	<dl	<dl	n.r.	34.6	<dl	26.3	7.61	20.0	0.021	2.76	<dl	<dl	<dl	<dl	0.008	0.085	2.27	0.175
MCR10b-4.d	2.08	0.044	41.3	189	0.054	<dl	22.4	<dl	0.025	n.r.	41.9	<dl	34.4	7.83	15.4	0.032	6.11	<dl	<dl	<dl	<dl	0.057	0.078	5.94	0.196
MCR10b-5.d	3.11	0.158	61.9	174	0.059	<dl	20.7	<dl	0.034	n.r.	38.2	<dl	30.0	8.10	18.2	0.006	3.80	<dl	<dl	<dl	<dl	0.020	0.207	4.44	0.217
MCR10b-6.d	0.765	0.160	38.8	162	0.040	<dl	17.3	0.043	<dl	n.r.	24.8	<dl	27.0	9.40	20.8	0.004	2.97	<dl	<dl	<dl	0.008	0.070	0.268	3.01	0.405
MCR10b-7.d	1.03	0.111	29.9	163	0.031	<dl	16.3	<dl	<dl	n.r.	21.3	<dl	26.4	13.3	15.1	0.017	1.84	<dl	<dl	<dl	<dl	0.037	0.069	3.79	0.260
MCR10b-9.d	0.210	0.070	25.2	211	0.103	<dl	14.1	<dl	<dl	n.r.	17.9	<dl	30.2	11.8	24.0	0.029	0.680	<dl	<dl	<dl	<dl	0.101	0.046	3.37	0.203
MCR13-1.d	0.190	0.413	52.6	160	0.056	<dl	15.5	<dl	<dl	n.r.	21.8	<dl	11.8	9.49	64.9	0.025	4.30	<dl	<dl	<dl	<dl	0.011	0.010	3.88	0.120
MCR13-11.d	0.177	0.199	45.5	157	0.050	<dl	13.9	<dl	<dl	n.r.	15.7	<dl	12.6	11.6	64.6	0.040	3.12	<dl	<dl	<dl	<dl	0.031	0.080	10.5	0.456
MCR13-11b.d	0.460	0.340	51.9	188	0.028	<dl	15.2	<dl	<dl	n.r.	19.6	<dl	14.0	10.9	62.1	0.005	4.55	<dl	<dl	<dl	<dl	0.036	0.009	3.69	0.291
MCR13-13.d	0.153	0.095	44.4	157	0.097	<dl	13.8	<dl	<dl	n.r.	17.2	<dl	13.0	10.4	68.9	0.005	2.73	<dl	<dl	<dl	<dl	0.019	0.041	11.4	0.586
MCR13-2.d	0.550	0.172	46.9	151	0.009	<dl	16.2	<dl	<dl	n.r.	24.1	<dl	13.0	9.72	67.8	0.066	5.10	<dl	<dl	<dl	<dl	0.007	0.007	5.40	0.291
MCR13-3.d	0.206	0.212	50.2	176	0.086	<dl	13.9	<dl	<dl	n.r.	21.2	<dl	12.9	10.0	69.8	0.046	3.67	<dl	<dl	<dl	<dl	0.011	0.017	8.29	0.184
MCR13-4.d	1.21	0.120	45.2	149	0.008	<dl	14.4	<dl	<dl	n.r.	22.4	<dl	11.8	9.40	64.2	0.004	2.15	<dl	<dl	<dl	0.022	0.015	5.E-4	5.40	0.313
MCR13-5.d	0.165	0.234	41.6	140	0.170	0.360	12.2	<dl	0.023	n.r.	17.4	<dl	11.4	10.9	65.0	0.029	3.45	<dl	<dl	<dl	<dl	0.092	0.002	3.07	0.271
MCR13-6.d	0.218	0.261	46.5	146	0.100	<dl	11.6	<dl	0.023	n.r.	16.8	<dl	11.6	10.6	64.6	0.110	3.21	<dl	<dl	<dl	<dl	0.055	0.010	3.72	0.323
MCR13-7.d	0.154	0.181	49.2	162	0.049	<dl	13.3	<dl	<dl	n.r.	19.3	<dl	13.3	11.1	71.6	0.019	4.29	<dl	<dl	<dl	<dl	0.029	0.009	6.58	0.259
MCR13-8.d	0.210	0.370	52.1	159	0.148	<dl	14.5	<dl	0.035	n.r.	21.2	<dl	12.7	11.8	69.7	0.029	5.65	<dl	<dl	<dl	<dl	0.050	0.013	6.58	0.264
MCR13-9.d	0.198	0.280	49.1	157	0.125	<dl	15.1	<dl	<dl	n.r.	22.4	<dl	12.2	12.4	73.7	0.039	5.50	<dl	<dl	<dl	0.270	0.069	0.008	4.63	0.283

Grain ID	*Mn* 55	*Co* 59	*Ni* 60	*Zn* 66	*Ga* 71	As 75	*Se* 82	Mo 95	Ru 101	Rh 103	*Ag* 107	Pd 108	Cd 111	*In* 115	*Sn* 118	*Sb* 121	*Te* 128	Re 185	Os 189	Ir 193	Pt 195	*Au* 197	Tl 205	*Pb* 208	*Bi* 209
55um	0.470	0.023	0.241	0.353	0.028	0.223	2.53	0.030	0.023	0.005	0.023	0.014	0.046	0.012	0.073	0.022	0.256	0.009	0.021	0.007	0.013	0.010	0.004	0.012	0.007
33um	0.939	0.046	0.722	1.06	0.085	0.445	5.07	0.061	0.068	0.009	0.069	0.041	0.137	0.025	0.218	0.067	0.513	0.027	0.042	0.020	0.039	0.030	0.011	0.037	0.013
MCR3CCP-01d	2.14	0.400	51.3	520	0.160	0.170	60.0	<dl	<dl	n.r.	0.670	<dl	6.80	4.60	13.4	0.060	0.035	<dl	<dl	<dl	<dl	0.003	3.E-4	1.52	0.130
MCR3CCP-03.d	1.86	0.290	46.4	427	0.110	<dl	50.3	<dl	0.440	n.r.	0.894	<dl	6.31	4.89	11.7	0.004	0.037	<dl	<dl	0.007	<dl	0.110	3.E-4	1.76	0.131
MCR3CCP-04.d	2.18	0.420	50.6	481	0.067	<dl	57.8	<dl	<dl	n.r.	0.710	<dl	6.37	4.76	13.6	0.004	0.039	0.460	<dl	<dl	<dl	8.E-4	3.E-4	1.95	0.129
MCR3CCP-05.d	1.91	0.022	41.5	491	0.028	<dl	59.7	<dl	<dl	n.r.	2.60	<dl	6.21	4.91	12.7	0.039	0.036	0.700	<dl	<dl	<dl	0.001	4.E-4	2.61	0.258
MCR3CCPr-01d	2.58	0.540	68.6	459	0.046	<dl	61.5	<dl	<dl	n.r.	2.07	<dl	5.87	3.71	11.4	0.003	0.035	<dl	<dl	<dl	<dl	0.002	4.E-4	2.35	0.133
MCR3CCPr-03.d	1.66	0.261	48.4	427	0.082	<dl	51.7	<dl	<dl	n.r.	0.590	<dl	6.12	3.97	11.7	0.002	0.051	<dl	<dl	<dl	<dl	0.002	3.E-4	1.86	0.220
MCR3CCPr-04.d	1.33	0.278	47.5	390	0.067	<dl	52.5	<dl	0.068	n.r.	0.810	<dl	4.78	4.40	11.7	0.005	0.036	<dl	<dl	<dl	<dl	0.001	4.E-4	2.41	0.236
MCR3CCPr-05.d	1.58	0.292	48.9	432	0.034	<dl	53.3	<dl	<dl	n.r.	0.840	<dl	5.84	4.47	12.6	0.004	0.046	<dl	<dl	<dl	<dl	0.001	0.004	1.40	0.086
MCR4b-10.d	0.800	0.270	48.3	350	0.044	<dl	48.0	<dl	0.030	n.r.	0.840	<dl	3.94	4.32	5.49	0.035	0.037	<dl	<dl	<dl	0.029	4.E-4	1.E-4	0.500	0.032
MCR4b-12.d	0.171	0.142	44.1	366	0.045	<dl	53.3	<dl	<dl	n.r.	0.700	<dl	4.03	4.32	5.67	0.029	0.220	<dl	<dl	<dl	0.038	4.E-4	2.E-4	1.22	0.087
MCR4b-2.d	0.580	0.131	47.3	284	0.034	0.400	51.5	<dl	0.029	n.r.	0.900	<dl	2.88	5.48	7.30	0.027	0.220	0.100	<dl	<dl	<dl	4.E-4	0.004	5.50	0.133
MCR4b-3.d	0.790	0.124	38.0	337	0.087	<dl	54.2	0.380	<dl	n.r.	0.840	<dl	3.38	3.83	5.29	0.026	0.031	0.018	<dl	<dl	<dl	3.E-4	2.E-4	1.55	0.066
MCR4b-4.d	0.680	0.155	46.0	363	0.073	0.800	63.5	<dl	<dl	n.r.	0.910	<dl	3.62	4.95	6.34	0.031	0.051	<dl	<dl	<dl	<dl	5.E-4	2.E-4	0.830	0.093
MCR4b-7.d	1.16	0.247	47.9	328	0.023	<dl	59.7	<dl	<dl	n.r.	0.880	<dl	4.33	3.16	3.68	0.028	0.330	<dl	<dl	<dl	<dl	4.E-4	2.E-4	0.730	0.077
MCR4b-9.d	0.450	0.089	42.4	331	0.072	<dl	55.0	<dl	<dl	n.r.	0.800	<dl	3.46	3.15	4.05	0.036	0.037	<dl	<dl	<dl	<dl	4.E-4	2.E-4	3.72	0.124
MCR5-10.d	0.940	0.600	71.6	341	0.010	<dl	84.3	<dl	<dl	n.r.	1.40	<dl	6.84	8.05	44.9	0.014	0.048	<dl	<dl	<dl	<dl	7.E-4	2.E-4	1.99	0.270
MCR5-2.d	0.780	0.300	59.7	382	0.068	<dl	67.7	<dl	<dl	n.r.	1.15	<dl	6.31	9.69	58.0	0.003	0.061	<dl	<dl	<dl	<dl	0.001	3.E-4	3.28	0.263
MCR5-4.d	0.166	0.362	59.4	367	0.053	<dl	77.4	<dl	<dl	n.r.	1.38	<dl	6.90	9.20	44.4	0.002	0.043	<dl	<dl	<dl	<dl	9.E-4	2.E-4	3.43	0.310
MCR5-5.d	0.910	1.29	80.0	417	0.062	<dl	88.8	<dl	<dl	n.r.	1.92	<dl	9.10	8.53	51.2	0.002	0.053	<dl	<dl	<dl	<dl	0.012	2.E-4	2.57	0.338
MCR5-8.d	1.02	1.00	75.2	356	0.085	<dl	87.2	<dl	<dl	n.r.	1.50	<dl	7.15	7.08	47.7	0.003	0.047	<dl	<dl	<dl	<dl	7.E-4	0.003	3.03	0.215
MS10-1d	6.30	0.180	10.6	425	0.018	<dl	66.3	2.20	<dl	n.r.	2.27	<dl	13.4	5.03	6.90	0.310	1.81	0.250	0.012	0.023	<dl	0.002	0.035	2.44	0.092
MS10-2.d	0.360	0.260	15.7	353	0.013	0.890	60.4	1.40	<dl	n.r.	1.81	<dl	14.3	3.43	2.55	0.700	1.04	0.018	0.021	0.034	0.015	0.001	0.039	5.30	0.370
MS10-3.d	2.50	0.058	11.5	346	0.011	<dl	66.7	<dl	<dl	n.r.	1.40	<dl	13.4	2.71	0.230	0.034	0.064	<dl	<dl	<dl	<dl	0.023	2.E-4	0.401	0.040
MS10-4.d	0.392	0.230	15.6	330	0.010	<dl	57.2	1.43	0.080	n.r.	0.690	<dl	14.3	2.85	0.820	0.390	1.60	0.037	0.031	0.028	0.009	0.001	0.014	4.68	0.187
MS10-5.d	0.344	0.160	18.2	378	0.014	<dl	63.0	0.700	<dl	n.r.	0.830	<dl	15.5	3.58	5.18	0.340	1.16	0.022	<dl	<dl	<dl	6.E-4	0.005	2.90	0.150
MS10-6.d	0.381	0.118	14.5	414	0.011	<dl	67.0	0.670	<dl	n.r.	1.28	<dl	17.6	2.89	1.25	0.510	1.41	<dl	<dl	<dl	<dl	0.001	0.016	2.87	0.187
MS10-7.d	1.46	0.031	14.7	353	0.010	<dl	63.9	<dl	0.062	n.r.	1.18	<dl	15.1	3.81	4.92	0.170	1.09	<dl	<dl	<dl	<dl	5.E-4	0.005	1.22	0.064
MS12-2.d	0.349	0.110	26.2	297	0.027	<dl	61.0	0.800	<dl	n.r.	0.170	<dl	12.9	4.45	9.80	0.220	1.28	0.031	<dl	<dl	0.044	0.015	4.E-4	2.69	0.139
MS12-4.d	6.90	0.100	22.8	241	0.035	0.810	41.0	0.740	<dl	n.r.	2.04	<dl	12.8	3.87	9.18	1.37	1.35	0.050	<dl	0.010	0.055	0.002	0.127	34.2	1.32
MS12-6.d	2.40	0.082	25.0	270	0.016	<dl	34.0	0.310	<dl	n.r.	0.290	<dl	11.3	3.53	10.5	0.390	0.113	0.030	<dl	<dl	<dl	0.001	0.038	10.6	0.750
MS12-7.d	13.9	0.116	20.0	279	0.016	<dl	45.0	0.170	<dl	n.r.	0.450	<dl	12.5	3.50	11.1	0.610	0.114	0.030	<dl	<dl	0.170	0.001	0.035	8.50	0.490
MS12-8.d	47.0	0.136	21.4	272	0.041	0.800	46.0	0.700	<dl	n.r.	0.820	<dl	13.8	4.35	7.19	0.810	1.20	0.026	<dl	<dl	0.078	0.002	0.064	22.0	0.860
MS2-1d	0.602	3.37	44.4	293	0.031	<dl	56.0	<dl	<dl	n.r.	2.35	<dl	38.3	1.61	1.67	0.750	0.660	<dl	<dl	<dl	<dl	0.104	0.049	20.7	4.90
MS2-2.d	2.30	0.150	30.0	301	0.020	<dl	66.0	<dl	<dl	n.r.	2.28	<dl	31.3	2.07	1.99	0.440	0.103	<dl	<dl	<dl	<dl	0.050	0.010	12.7	2.73
MS2-3.d	0.506	0.870	12.9	333	0.027	<dl	52.0	<dl	0.043	n.r.	1.79	<dl	42.4	2.21	1.85	0.470	0.124	<dl	<dl	<dl	0.500	0.068	0.027	3.64	1.05
MS2-4.d	1.66	0.012	9.30	315	0.027	<dl	55.0	<dl	0.080	n.r.	2.51	<dl	36.9	3.03	1.62	0.440	0.830	<dl	<dl	<dl	<dl	0.099	0.006	6.90	2.40
MS2-5.d	5.60	0.080	10.2	291	0.032	<dl	52.0	<dl	0.060	n.r.	3.30	<dl	29.8	3.16	1.88	0.880	0.730	<dl	<dl	<dl	<dl	0.030	0.034	21.9	4.77
MS2-6.d	2.30	0.200	25.0	311	0.028	<dl	49.0	<dl	<dl	n.r.	2.33	<dl	34.2	3.56	2.00	0.460	0.980	<dl	<dl	<dl	<dl	0.064	0.008	11.1	3.17
MS2-7.d	1.47	0.580	57.0	334	0.027	<dl	56.3	<dl	<dl	n.r.	2.52	<dl	45.4	3.46	2.05	0.470	1.08	<dl	<dl	<dl	<dl	0.114	0.018	5.10	1.56
MS3-2.d	0.480	0.580	84.0	318	0.027	<dl	51.7	<dl	0.027	n.r.	1.83	<dl	41.1	3.86	1.59	0.280	0.620	<dl	<dl	<dl	<dl	0.080	0.009	5.34	1.26
MS3-4.d	1.80	1.09	15.7	306	0.031	<dl	58.0	<dl	<dl	n.r.	2.56	<dl	29.1	3.84	1.98	1.23	0.670	<dl	<dl	<dl	<dl	0.075	0.023	22.3	6.00
MS3-5.d	0.610	0.230	20.0	305	0.020	<dl	55.6	<dl	0.160	n.r.	2.63	<dl	27.4	2.84	1.62	0.440	0.187	<dl	0.030	<dl	<dl	0.051	0.001	16.7	6.50
MS3-6.d	3.00	0.067	10.1	304	0.027	<dl	55.4	<dl	<dl	n.r.	2.13	<dl	34.1	3.72	2.40	0.380	0.700	<dl	<dl	<dl	<dl	0.102	9.E-4	3.40	1.02
MS8-2.d	3.01	0.430	14.0	366	0.080	0.790	47.4	2.62	<dl	n.r.	2.53	<dl	17.2	4.36	7.13	0.670	1.04	0.196	<dl	0.023	0.011	7.E-4	0.027	4.49	0.254
MS8-4.d	3.50	0.240	20.6	259	0.020	<dl	37.6	4.00	0.071	n.r.	4.61	<dl	13.4	5.45	5.72	1.97	1.37	0.140	<dl	<dl	<dl	0.002	0.068	16.5	1.15
MS8-5.d	4.29	0.340	8.16	323	0.039	0.650	41.8	5.80	0.032	n.r.	3.11	<dl	17.5	7.79	6.55	2.23	1.10	0.410	<dl	0.033	<dl	0.002	0.030	16.2	0.870
MS8-6.d	0.176	0.156	23.6	462	0.010	<dl	22.9	<dl	<dl	n.r.	1.20	<dl	18.9	2.02	4.36	0.537	0.043	<dl	<dl	<dl	<dl	5.E-4	0.007	2.96	0.119

Grain ID	Mn 55	Co 59	Ni 60	Zn 66	Ga 71	As 75	Se 82	Mo 95	Ru 101	Rh 103	Ag 107	Pd 108	Cd 111	In 115	Sn 118	Sb 121	Te 128	Re 185	Os 189	Ir 193	Pt 195	Au 197	Tl 205	Pb 208	Bi 209
55um	0.470	0.023	0.241	0.353	0.028	0.223	2.53	0.030	0.023	0.005	0.023	0.014	0.046	0.012	0.073	0.022	0.256	0.009	0.021	0.007	0.013	0.010	0.004	0.012	0.007
33um	0.939	0.046	0.722	1.06	0.085	0.445	5.07	0.061	0.068	0.009	0.069	0.041	0.137	0.025	0.218	0.067	0.513	0.027	0.042	0.020	0.039	0.030	0.011	0.037	0.013
MS8-7.d	0.48	0.056	30.5	415	0.010	<dl	68.4	<dl	<dl	n.r.	1.92	<dl	18.5	2.03	6.25	0.071	0.490	<dl	<dl	<dl	<dl	4.E-4	5.E-4	0.900	0.035
MS8-8.d	0.125	0.030	22.7	460	0.007	<dl	610	<dl	<dl	n.r.	2.22	<dl	18.5	2.49	4.38	0.050	0.300	<dl	<dl	<dl	<dl	6.E-4	2.E-4	0.394	0.024
MS8-9.d	0.660	0.118	25.5	471	0.012	<dl	36.8	<dl	<dl	n.r.	1.76	<dl	19.8	2.09	3.64	0.097	0.230	<dl	<dl	<dl	<dl	3.E-4	2.E-4	0.510	0.025
MXNW-01-51-10.d	4.42	0.520	10.6	302	0.074	<dl	69.7	<dl	<dl	n.r.	4.06	<dl	9.60	2.54	17.0	0.003	1.13	<dl	<dl	<dl	<dl	0.069	2.E-4	1.54	0.044
MXNW-01-51-11d	7.02	0.115	6.53	335	0.052	0.240	75.1	<dl	<dl	n.r.	17.3	<dl	8.87	2.62	19.0	0.014	7.39	<dl	<dl	<dl	0.077	0.046	0.010	1.58	0.068
MXNW-03-51-1d	27.0	0.306	12.6	355	0.067	0.230	75.2	<dl	<dl	n.r.	4.90	<dl	10.8	2.49	28.0	0.006	1.77	<dl	<dl	<dl	<dl	0.047	3.E-4	1.09	0.050
MXNW-03-51-2.d	2.04	0.240	8.00	330	0.010	<dl	72.6	<dl	<dl	n.r.	4.16	<dl	10.1	2.43	19.5	0.002	3.61	<dl	<dl	<dl	<dl	0.062	2.E-4	1.47	0.042
MXNW-03-51-4.d	3.98	0.182	9.30	278	0.036	<dl	73.3	<dl	0.034	n.r.	9.70	<dl	8.83	2.71	19.1	0.003	5.97	<dl	<dl	<dl	0.039	0.147	0.015	1.44	0.075
MXNW-03-51-5.d	21.1	0.089	8.03	338	0.058	0.240	74.5	<dl	<dl	n.r.	11.7	<dl	10.4	2.56	18.2	0.007	5.79	<dl	<dl	<dl	0.077	0.057	8.E-4	1.47	0.076
MXNW-03-51-6.d	3.59	0.530	8.04	306	0.027	<dl	73.0	0.080	0.079	n.r.	2.27	<dl	9.81	2.66	16.1	0.010	0.850	0.031	0.058	<dl	<dl	0.077	6.E-4	3.56	0.043
NR6-1d	0.247	0.590	85.0	383	0.060	<dl	37.8	<dl	<dl	n.r.	4.62	<dl	12.3	0.805	0.085	0.021	0.490	<dl	<dl	<dl	0.280	8.E-4	0.025	45.7	0.400
NR6-2.d	2.56	0.560	49.3	472	0.042	<dl	38.9	<dl	<dl	n.r.	2.87	<dl	11.3	0.558	0.141	0.025	0.610	<dl	<dl	<dl	0.052	4.E-4	0.023	11.8	0.076
NR6-6.d	3.16	0.640	58.0	287	0.048	<dl	36.2	<dl	<dl	n.r.	2.70	<dl	6.79	3.90	0.520	0.025	0.560	<dl	<dl	<dl	0.076	7.E-4	0.049	13.7	0.156
NR6-7.d	0.600	1.50	59.0	258	0.029	<dl	35.6	<dl	<dl	n.r.	2.61	<dl	5.95	1.67	0.347	0.004	0.450	<dl	<dl	<dl	0.096	0.011	0.034	20.7	0.159
NR6-8.d	0.550	0.478	46.4	283	0.038	<dl	34.2	<dl	<dl	n.r.	2.97	<dl	7.77	0.384	0.078	0.016	0.710	<dl	<dl	<dl	0.029	5.E-4	0.006	11.4	0.064
OVOID-1d	0.165	0.147	2.48	162	0.043	<dl	64.3	<dl	<dl	n.r.	2.57	<dl	7.30	2.25	3.06	0.003	9.52	<dl	<dl	<dl	<dl	6.E-4	3.E-4	10.2	0.057
OVOID-2.d	0.221	0.310	7.30	270	0.013	<dl	54.3	0.059	<dl	n.r.	1.24	<dl	10.3	1.25	2.49	0.005	1.13	0.037	<dl	<dl	<dl	5.E-4	3.E-4	24.4	0.044
OVOID-3.d	0.178	0.240	8.20	179	0.011	<dl	66.9	<dl	<dl	n.r.	2.53	<dl	5.63	1.84	2.60	0.003	11.3	<dl	<dl	<dl	<dl	4.E-4	4.E-4	7.32	0.027
OVOID-4.d	0.202	0.106	4.10	138	0.011	<dl	67.6	<dl	<dl	n.r.	3.92	<dl	7.60	1.50	3.23	0.004	15.1	<dl	<dl	<dl	<dl	0.013	4.E-4	13.7	0.086
OVOID-5.d	0.169	0.156	4.41	189	0.026	<dl	69.2	<dl	<dl	n.r.	2.57	<dl	8.05	2.17	3.77	0.002	9.07	<dl	<dl	<dl	<dl	0.010	3.E-4	14.3	0.075
OVOID-6.d	0.148	0.480	16.7	180	0.008	<dl	66.5	<dl	<dl	n.r.	1.65	<dl	7.24	2.18	3.78	0.018	5.88	<dl	<dl	<dl	<dl	5.E-4	3.E-4	9.76	0.038
OVOID-8.d	0.169	0.099	1.96	180	0.010	<dl	62.5	<dl	0.042	n.r.	2.56	<dl	7.56	1.55	2.26	0.004	10.5	<dl	<dl	<dl	0.012	0.006	3.E-4	9.19	0.114
RX162CCP-01d	2.30	0.110	15.0	267	0.049	0.220	196	<dl	<dl	n.r.	20.8	<dl	19.8	16.9	162	0.010	6.94	<dl	<dl	<dl	<dl	0.001	0.032	7.39	0.294
RX162CCP-02.d	3.36	0.069	16.8	255	0.021	0.151	186	<dl	0.020	n.r.	21.4	<dl	18.8	14.2	144	0.370	6.40	<dl	0.210	<dl	<dl	0.001	0.062	9.61	0.233
RX162CCP-03.d	4.36	0.117	17.9	268	0.039	<dl	211	<dl	0.150	n.r.	17.4	<dl	18.7	11.6	129	0.390	5.30	<dl	<dl	0.380	0.500	0.015	0.049	5.72	0.332
RX162CCP-04.d	10.2	0.032	19.4	262	0.068	4.20	199	<dl	<dl	n.r.	19.2	<dl	18.7	14.8	165	0.006	3.31	<dl	<dl	<dl	<dl	0.015	1.44	13.7	0.228
RX162CCP-05.d	13.6	0.064	17.5	272	0.082	<dl	215	<dl	0.025	n.r.	43.1	<dl	19.7	14.0	183	0.009	18.1	<dl	0.070	<dl	<dl	0.015	1.21	92.6	0.288
RX164-1d	0.380	0.100	37.5	100	0.012	<dl	99.0	<dl	<dl	n.r.	14.2	<dl	31.6	6.42	158	0.004	0.242	<dl	<dl	<dl	<dl	0.011	0.019	13.6	0.210
RX164-10.d	0.166	0.060	37.3	146	0.060	<dl	161	<dl	<dl	n.r.	14.8	<dl	36.9	5.81	145	0.003	2.50	0.007	<dl	<dl	<dl	0.091	0.053	10.5	0.386
RX164-2.d	0.790	0.123	39.6	123	0.128	<dl	134	<dl	0.034	n.r.	19.9	<dl	35.9	6.58	175	0.004	1.47	<dl	<dl	<dl	<dl	0.020	0.028	10.5	0.192
RX164-3.d	0.276	0.263	39.5	137	0.052	<dl	112	<dl	<dl	n.r.	24.1	<dl	33.5	6.77	142	0.003	3.70	<dl	<dl	<dl	<dl	0.033	0.012	2.91	0.092
RX164-4.d	0.730	0.290	40.8	153	0.041	<dl	131	<dl	<dl	n.r.	25.5	<dl	40.5	6.31	213	0.003	2.04	<dl	<dl	<dl	<dl	0.022	0.012	4.11	0.161
RX164-5.d	0.251	0.280	36.7	138	0.056	<dl	138	<dl	<dl	n.r.	24.6	<dl	39.9	6.33	118	0.004	3.55	<dl	<dl	<dl	<dl	0.047	0.037	5.83	0.106
RX164-6.d	0.870	0.036	41.2	193	0.076	<dl	135	<dl	0.031	n.r.	24.7	<dl	42.2	6.34	206	0.100	4.17	<dl	<dl	<dl	<dl	0.013	0.034	6.86	0.190
RX164-7.d	0.220	0.207	44.5	156	0.010	<dl	145	<dl	<dl	n.r.	17.0	<dl	34.6	5.55	165	0.004	1.59	<dl	<dl	<dl	<dl	0.060	0.012	3.02	0.113
RX164-8.d	0.230	0.183	44.5	177	0.076	<dl	168	<dl	<dl	n.r.	19.5	<dl	39.5	6.12	201	0.003	1.39	<dl	<dl	<dl	<dl	0.102	0.004	6.60	0.224
RX164-9.d	0.232	0.053	39.0	172	0.106	<dl	172	<dl	<dl	n.r.	13.6	<dl	40.1	5.97	165	0.003	2.23	<dl	<dl	<dl	<dl	0.126	0.023	11.1	0.275
T1-1d	10.7	0.410	10.6	345	0.136	<dl	65.6	<dl	<dl	n.r.	1.80	<dl	1.90	0.938	0.500	0.003	3.03	<dl	<dl	<dl	0.010	3.E-4	0.004	0.550	0.030
T11-1d	45.0	0.124	6620	24.8	0.008	<dl	125	<dl	<dl	n.r.	0.770	0.123	1.68	4.12	1.90	0.044	27.9	<dl	<dl	<dl	<dl	6.E-4	1.00	9.36	0.021
T11-11d	15.9	0.101	4720	29.4	0.006	0.360	138	<dl	<dl	n.r.	1.37	0.095	2.73	3.07	0.400	0.004	31.4	<dl	<dl	<dl	<dl	9.E-4	0.588	48.6	0.085
T11-12.d	5.38	0.039	1816	42.4	0.008	0.410	139	<dl	<dl	n.r.	0.930	<dl	3.90	4.21	0.550	0.005	29.3	<dl	<dl	<dl	<dl	7.E-4	0.945	18.8	0.052
T11-2.d	2.55	0.082	5220	28.8	0.006	<dl	128	<dl	0.020	n.r.	1.05	<dl	2.84	5.87	1.53	0.043	30.5	<dl	<dl	<dl	<dl	6.E-4	0.927	12.0	0.017
T11-3.d	4.38	0.086	4720	32.5	0.005	<dl	124	<dl	<dl	n.r.	1.70	<dl	3.14	3.67	1.55	0.032	28.8	<dl	<dl	<dl	<dl	4.E-4	1.02	6.62	0.014
T11-6.d	6.93	0.068	2910	30.9	0.005	0.310	119	<dl	0.026	n.r.	0.622	<dl	3.13	3.09	0.910	0.018	28.5	<dl	<dl	<dl	<dl	6.E-4	0.377	18.5	0.022
T11-7.d	3.26	0.056	3680	30.4	0.005	<dl	137	0.023	0.019	n.r.	0.440	<dl	2.92	5.33	0.950	0.019	30.9	<dl	<dl	<dl	<dl	4.E-4	0.689	15.3	0.013
T11-9.d	5.58	0.126	6160	23.9	0.008	<dl	118	<dl	<dl	n.r.	0.510	<dl	2.56	5.30	0.222	0.016	26.8	<dl	<dl	<dl	<dl	5.E-4	0.777	21.8	0.015
T1-3.d	7.62	0.350	9.10	311	0.081	<dl	69.0	<dl	<dl	n.r.	1.47	<dl	2.27	1.09	0.202	0.018	3.01	<dl	<dl	<dl	<dl	3.E-4	0.004	0.302	0.013

Grain ID	Mn 55	Co 59	Ni 60	Zn 66	Ga 71	As 75	Se 82	Mo 95	Ru 101	Rh 103	Ag 107	Pd 108	Cd 111	In 115	Sn 118	Sb 121	Te 128	Re 185	Os 189	Ir 193	Pt 195	Au 197	Tl 205	Pb 208	Bi 209
55um	0.470	0.023	0.241	0.353	0.028	0.223	2.53	0.030	0.023	0.005	0.023	0.014	0.046	0.012	0.073	0.022	0.256	0.009	0.021	0.007	0.013	0.010	0.004	0.012	0.007
33um	0.939	0.046	0.722	1.06	0.085	0.445	5.07	0.061	0.068	0.009	0.069	0.041	0.137	0.025	0.218	0.067	0.513	0.027	0.042	0.020	0.039	0.030	0.011	0.037	0.013
T1-4.d	10.9	2.41	195	305	0.380	0.370	60.0	<dl	<dl	n.r.	1.04	<dl	2.16	0.668	0.433	0.003	2.12	<dl	<dl	<dl	<dl	3.E-4	0.005	0.196	0.013
T1-8.d	8.78	0.760	17.3	263	0.051	<dl	62.8	0.038	<dl	n.r.	3.67	<dl	2.75	0.866	0.710	0.002	2.58	<dl	<dl	<dl	<dl	0.013	1.E-4	0.220	0.010
T1-9.d	8.82	0.660	43.1	242	0.066	0.270	67.3	0.044	0.038	n.r.	2.49	<dl	2.35	0.932	0.329	0.004	3.26	<dl	<dl	0.009	0.110	0.130	0.039	1.52	0.064
T2-1.d	16.4	0.350	35.4	347	0.070	<dl	42.9	<dl	<dl	n.r.	0.520	<dl	2.15	0.405	0.500	0.029	0.390	<dl	<dl	<dl	0.029	3.E-4	2.E-4	1.22	0.023
T2-10.d	9.30	0.460	27.5	383	0.066	<dl	38.2	<dl	<dl	n.r.	0.890	<dl	2.93	0.987	0.690	0.029	0.460	<dl	<dl	<dl	0.040	3.E-4	0.003	2.43	0.011
T2-11.d	8.80	2.12	142	387	0.031	<dl	43.3	<dl	<dl	n.r.	2.48	<dl	3.16	1.02	1.70	0.083	0.870	<dl	<dl	<dl	0.021	6.E-4	0.006	2.17	0.022
T2-2.d	17.5	0.710	39.0	328	0.053	<dl	38.4	0.030	<dl	n.r.	0.325	<dl	2.12	0.405	0.510	0.027	0.410	<dl	<dl	<dl	<dl	2.E-4	2.E-4	0.576	0.013
T2-3.d	20.6	0.259	32.7	384	0.052	<dl	38.5	<dl	0.026	n.r.	0.380	<dl	3.78	0.506	0.550	0.002	0.280	<dl	<dl	<dl	<dl	2.E-4	1.E-4	0.630	0.019
T2-7.d	14.5	0.330	26.8	544	0.052	0.410	41.6	1.10	<dl	n.r.	0.477	<dl	3.29	1.11	0.760	0.003	0.510	1.15	0.081	<dl	<dl	2.E-4	2.E-4	0.780	0.008
T2-8.d	11.6	0.600	33.4	408	0.082	<dl	43.2	<dl	0.020	n.r.	0.960	<dl	3.00	1.05	0.820	0.004	0.560	<dl	<dl	<dl	0.016	4.E-4	0.002	2.12	0.023
T2-9.d	29.1	0.454	34.8	518	0.077	<dl	46.1	<dl	<dl	n.r.	0.608	<dl	3.31	0.922	0.940	0.003	0.540	<dl	<dl	<dl	0.013	3.E-4	2.E-4	1.59	0.009
T3-1.d	7.06	0.042	3510	28.4	0.007	<dl	126	<dl	<dl	n.r.	0.575	<dl	2.82	4.69	0.910	0.032	26.7	<dl	<dl	<dl	<dl	4.E-4	0.624	18.3	0.016
T3-10.d	4.84	0.270	7700	20.2	0.006	<dl	122	<dl	0.027	n.r.	0.354	<dl	1.78	3.46	1.44	0.061	24.9	<dl	<dl	<dl	<dl	4.E-4	0.384	10.4	0.010
T3-11.d	4.55	0.115	6690	24.3	0.006	<dl	118	<dl	0.029	n.r.	0.730	<dl	2.03	3.82	1.81	0.046	27.6	<dl	<dl	<dl	<dl	5.E-4	0.286	7.54	0.023
T3-2.d	6.23	0.310	7900	23.1	0.008	<dl	125	<dl	0.021	n.r.	0.620	<dl	1.84	5.47	1.02	0.031	28.6	<dl	<dl	<dl	<dl	4.E-4	0.508	15.6	0.018
T3-5.d	5.92	0.123	7840	21.1	0.007	<dl	138	<dl	<dl	n.r.	0.530	0.168	1.66	4.47	1.35	0.025	27.5	<dl	<dl	<dl	<dl	0.011	0.606	22.6	0.035
T3-6.d	7.63	0.072	2540	28.3	0.007	<dl	120	<dl	<dl	n.r.	0.920	<dl	3.21	4.44	0.450	0.004	27.0	<dl	<dl	<dl	<dl	6.E-4	1.03	28.4	0.044
T3-8.d	4.92	0.006	2150	37.2	0.007	<dl	121	<dl	<dl	n.r.	0.252	<dl	3.04	3.11	0.640	0.041	24.6	<dl	<dl	<dl	<dl	4.E-4	0.821	24.0	0.014
T4-1.d	1.20	0.220	510	104	0.006	10.9	163	0.029	<dl	n.r.	8.27	11.0	5.29	3.63	0.023	0.032	47.3	<dl	<dl	<dl	0.024	8.E-4	1.10	31.5	0.011
T4-10.d	0.175	0.061	48.5	109	0.006	11.2	158	<dl	<dl	n.r.	8.83	11.9	5.40	3.51	0.016	0.005	43.6	<dl	<dl	<dl	0.037	8.E-4	0.920	28.2	0.017
T4-12.d	0.870	0.124	49.0	114	0.006	11.6	153	0.041	0.035	n.r.	8.34	10.7	6.06	3.15	0.022	0.025	40.8	<dl	<dl	<dl	<dl	7.E-4	1.09	33.0	0.012
T4-13.d	0.193	0.041	39.0	126	0.006	9.80	173	0.041	0.024	n.r.	8.74	9.35	7.81	3.21	0.022	0.029	41.6	<dl	<dl	<dl	<dl	7.E-4	0.554	33.1	0.009
T4-16.d	0.187	0.036	22.6	123	0.007	5.61	143	0.160	0.027	n.r.	6.94	5.12	5.44	3.12	0.036	0.005	29.3	<dl	<dl	<dl	<dl	6.E-4	0.850	20.2	0.025
T4-3.d	0.700	0.059	16.5	116	0.008	9.89	162	0.023	<dl	n.r.	7.89	10.6	4.59	3.01	0.022	0.004	42.8	<dl	<dl	<dl	0.032	0.009	0.866	25.3	0.010
T4-6.d	0.201	0.037	22.1	127	0.006	6.15	170	0.078	0.046	n.r.	7.67	6.46	6.84	3.78	0.018	0.005	47.3	<dl	<dl	<dl	0.022	7.E-4	0.840	32.9	0.008
T4-8.d	0.183	0.019	23.7	112	0.005	8.95	185	0.027	0.022	n.r.	7.82	9.54	6.14	3.04	0.017	0.033	52.8	<dl	<dl	<dl	0.016	4.E-4	0.761	33.1	0.005
TR15-1.d	1.28	0.390	23.4	304	0.025	<dl	38.3	<dl	<dl	n.r.	15.8	<dl	7.80	2.22	2.55	0.019	1.52	<dl	<dl	<dl	<dl	0.034	0.008	4.79	0.157
TR15-2.d	2.50	0.860	160	318	0.029	<dl	40.8	<dl	<dl	n.r.	10.8	<dl	6.70	1.80	3.93	0.005	1.86	0.040	<dl	<dl	<dl	0.097	0.010	5.76	0.214
TR15-3.d	0.202	0.051	44.6	265	0.019	<dl	34.6	<dl	<dl	n.r.	2.80	<dl	4.18	3.21	5.22	0.004	0.049	0.104	<dl	0.080	<dl	6.E-4	2.E-4	1.61	0.076
TR15-4.d	0.830	0.380	24.8	363	0.032	<dl	40.1	<dl	0.040	n.r.	26.9	<dl	8.29	1.97	5.03	0.190	1.88	0.026	<dl	0.034	<dl	0.027	0.010	13.3	0.155
TR15-5.d	8.20	0.064	44.8	294	0.039	0.500	41.6	<dl	0.064	n.r.	6.22	<dl	4.27	2.01	3.44	0.039	1.18	0.110	0.034	0.330	0.090	0.023	4.E-4	4.03	0.183
TR15-6.d	0.640	0.268	37.1	369	0.036	<dl	37.6	<dl	<dl	n.r.	25.5	<dl	7.44	1.35	3.16	0.003	0.870	0.070	<dl	0.024	0.019	0.032	3.E-4	1.75	0.139
TR15-8.d	10.1	0.810	166	388	0.031	<dl	38.5	<dl	0.019	n.r.	17.8	<dl	8.71	1.54	3.24	0.029	1.97	0.137	<dl	0.095	<dl	0.029	7.E-4	4.54	0.142
TR20-10.d	0.269	0.199	28.3	325	0.025	<dl	55.9	<dl	0.090	n.r.	12.6	<dl	6.26	5.49	12.0	0.003	2.67	<dl	<dl	<dl	<dl	0.024	3.E-4	0.561	0.044
TR20-11.d	0.285	0.013	29.3	263	0.032	<dl	55.0	<dl	<dl	n.r.	18.8	<dl	2.85	5.91	1.10	0.102	1.59	<dl	<dl	<dl	<dl	0.131	6.E-4	0.800	0.030
TR20-3.d	0.317	0.199	14.7	270	0.024	<dl	57.3	<dl	0.021	n.r.	37.0	<dl	6.30	0.385	2.36	0.057	0.620	<dl	<dl	<dl	<dl	0.113	5.E-4	9.75	0.175
TR20-4.d	0.274	0.141	13.9	198	0.011	<dl	51.0	<dl	<dl	n.r.	29.7	<dl	3.30	0.120	2.22	0.051	0.630	<dl	<dl	<dl	<dl	0.078	4.E-4	4.19	0.151
TR20-5.d	0.233	0.059	34.0	302	0.180	<dl	58.2	<dl	<dl	n.r.	15.4	<dl	4.22	5.69	12.0	0.005	1.94	<dl	<dl	<dl	<dl	0.077	2.E-4	0.437	0.034
TR20-6.d	0.313	0.055	31.7	242	0.220	<dl	55.0	<dl	<dl	n.r.	13.4	<dl	3.03	5.71	10.2	0.006	1.58	<dl	<dl	<dl	<dl	0.001	6.E-4	1.90	0.050
TR20-7.d	0.250	0.013	31.4	349	0.106	<dl	56.9	<dl	0.021	n.r.	12.3	<dl	5.40	5.70	12.2	0.003	1.53	<dl	<dl	<dl	<dl	0.047	2.E-4	0.360	0.019
TR20-8.d	2.10	0.400	23.9	302	0.036	<dl	61.3	<dl	<dl	n.r.	19.9	<dl	5.90	4.86	11.2	0.075	1.40	<dl	<dl	<dl	<dl	0.076	0.011	10.4	0.059
VB21-1.d	4.88	0.320	7.50	187	0.032	<dl	72.1	<dl	0.030	n.r.	1.82	<dl	1.78	14.6	7.68	0.004	8.41	<dl	<dl	<dl	<dl	5.E-4	4.E-4	4.33	0.070
VB21-3.d	1.98	0.085	4.60	181	0.030	<dl	76.6	<dl	<dl	n.r.	3.99	<dl	1.89	8.78	6.58	0.043	15.9	<dl	<dl	<dl	<dl	8.E-4	4.E-4	6.14	0.211
VB21-4.d	0.150	0.095	4.01	166	0.023	<dl	68.7	<dl	<dl	n.r.	0.660	<dl	1.81	8.86	7.38	0.031	1.41	<dl	<dl	<dl	<dl	3.E-4	3.E-4	4.62	0.009
VB21-5.d	0.134	0.124	4.72	193	0.008	<dl	67.8	<dl	0.033	n.r.	1.07	<dl	2.09	8.76	5.14	0.003	5.37	<dl	<dl	<dl	<dl	5.E-4	3.E-4	3.39	0.047
VB21-6.d	0.900	1.05	73.0	175	0.014	<dl	58.6	0.031	<dl	n.r.	1.87	<dl	2.51	11.8	4.34	0.005	6.78	<dl	<dl	<dl	<dl	7.E-4	4.E-4	6.25	0.081
VB21-9.d	0.900	0.250	9.20	168	0.020	<dl	67.0	0.038	0.060	n.r.	3.82	<dl	1.77	7.08	0.720	0.004	12.4	<dl	<dl	<dl	<dl	8.E-4	7.E-4	8.94	0.171

Grain ID	*Mn* 55	*Co* 59	*Ni* 60	*Zn* 66	*Ga* 71	As 75	*Se* 82	Mo 95	Ru 101	Rh 103	*Ag* 107	Pd 108	Cd 111	*In* 115	*Sn* 118	*Sb* 121	*Te* 128	Re 185	Os 189	Ir 193	Pt 195	*Au* 197	Tl 205	*Pb* 208	*Bi* 209
55um	0.470	0.023	0.241	0.353	0.028	0.223	2.53	0.030	0.023	0.005	0.023	0.014	0.046	0.012	0.073	0.022	0.256	0.009	0.021	0.007	0.013	0.010	0.004	0.012	0.007
33um	0.939	0.046	0.722	1.06	0.085	0.445	5.07	0.061	0.068	0.009	0.069	0.041	0.137	0.025	0.218	0.067	0.513	0.027	0.042	0.020	0.039	0.030	0.011	0.037	0.013
VB25-1d	0.600	0.063	4.67	183	0.033	<dl	61.2	<dl	0.043	n.r.	1.68	<dl	6.64	6.84	6.65	0.054	6.02	<dl	<dl	<dl	<dl	5.E-4	3.E-4	6.98	0.062
VB25-2.d	0.560	0.030	4.80	164	0.006	<dl	55.2	<dl	<dl	n.r.	2.63	<dl	7.02	5.70	5.35	0.032	6.79	<dl	<dl	<dl	<dl	7.E-4	0.002	7.22	0.144
VB25-5.d	0.580	0.090	3.08	222	0.063	<dl	60.0	0.079	<dl	n.r.	2.91	<dl	7.51	2.82	3.10	0.058	8.14	<dl	<dl	<dl	<dl	0.009	3.E-4	10.1	0.062
VB25-7.d	2.00	0.051	1.60	172	0.030	<dl	68.2	<dl	0.070	n.r.	2.87	<dl	6.96	6.55	8.36	0.039	8.08	<dl	<dl	<dl	<dl	7.E-4	6.E-4	10.7	0.058
VB25-8.d	0.670	0.030	2.93	190	0.053	<dl	58.5	<dl	<dl	n.r.	1.29	<dl	6.88	4.39	4.39	0.041	5.04	<dl	<dl	<dl	<dl	5.E-4	0.600	2.23	0.043
VB27-2.d	24.2	0.015	1.56	334	0.008	<dl	210	<dl	0.021	n.r.	14.1	<dl	37.8	15.8	29.0	0.010	31.0	<dl	<dl	<dl	<dl	0.001	0.529	10.7	0.339
VB27-3.d	25.7	1.92	610	169	0.034	<dl	175	0.028	0.024	n.r.	12.3	<dl	18.1	13.2	18.6	0.006	23.1	<dl	<dl	<dl	<dl	0.001	0.521	8.09	0.265
VB27-4.d	13.2	0.031	0.870	298	0.021	<dl	196	0.040	<dl	n.r.	26.8	<dl	30.3	20.5	21.0	0.009	31.2	<dl	<dl	<dl	<dl	0.008	0.679	11.8	1.90
VB27-5.d	7.98	0.008	3.70	143	0.014	<dl	178	<dl	<dl	n.r.	23.6	<dl	16.0	24.2	27.6	0.005	31.8	<dl	<dl	<dl	<dl	0.001	0.131	8.54	0.168
VB29-1d	0.132	0.088	6.64	173	0.008	0.360	55.1	<dl	<dl	n.r.	1.83	<dl	6.79	0.895	5.33	0.040	7.74	<dl	<dl	<dl	<dl	8.E-4	0.008	3.87	0.135
VB29-3.d	0.136	0.065	4.70	242	0.005	<dl	59.0	<dl	<dl	n.r.	4.14	<dl	9.55	1.07	6.92	0.004	17.3	<dl	<dl	<dl	<dl	1.E-3	0.083	5.07	0.304
VB30-1d	2.46	0.290	26.3	139	0.009	<dl	49.4	0.250	<dl	n.r.	0.810	<dl	9.20	0.475	1.21	0.003	0.490	0.038	<dl	<dl	<dl	5.E-4	3.E-4	13.9	0.190
VB30-2.d	0.195	0.123	5.61	182	0.068	0.490	68.6	<dl	0.032	n.r.	3.83	<dl	12.0	1.18	4.24	0.020	13.7	<dl	<dl	<dl	<dl	9.E-4	3.E-4	19.4	0.166
VB30-3.d	0.660	1.25	28.8	221	0.014	<dl	56.3	<dl	<dl	n.r.	2.55	<dl	12.1	1.28	4.20	0.021	4.23	0.009	<dl	<dl	<dl	9.E-4	0.005	13.7	0.149
VB30-4.d	0.610	0.102	3.15	197	0.012	0.460	61.3	<dl	<dl	n.r.	3.33	<dl	9.07	1.35	4.37	0.020	6.09	<dl	<dl	<dl	0.042	0.012	4.E-4	8.98	0.344
VB30-5.d	1.50	0.125	4.30	252	0.012	<dl	69.1	<dl	<dl	n.r.	2.77	<dl	14.2	1.17	4.37	0.051	8.90	<dl	<dl	<dl	<dl	8.E-4	4.E-4	14.4	0.135
VB30-6.d	0.410	0.100	2.61	204	0.050	<dl	63.1	<dl	0.020	n.r.	2.57	<dl	12.2	1.89	6.57	0.018	6.79	<dl	<dl	<dl	<dl	0.010	4.E-4	9.54	0.110
VB31-1d	0.550	0.057	4.50	149	0.039	<dl	62.8	<dl	<dl	n.r.	2.73	<dl	8.99	5.24	7.45	0.025	7.57	<dl	<dl	<dl	<dl	0.049	0.071	27.5	0.454
VB31-10.d	0.610	0.107	7.30	137	0.011	<dl	60.7	0.022	<dl	n.r.	2.32	<dl	11.6	4.84	8.11	0.002	6.24	<dl	<dl	2.30	<dl	7.E-4	0.031	30.9	0.340
VB31-11d	0.590	1.59	67.0	192	0.014	<dl	61.4	<dl	0.020	n.r.	2.11	<dl	10.8	3.42	7.00	0.004	5.66	<dl	<dl	<dl	<dl	0.014	0.044	25.7	0.790
VB31-3.d	0.960	0.680	34.0	160	0.014	<dl	71.5	<dl	<dl	n.r.	2.73	<dl	9.90	4.22	7.08	0.007	8.44	<dl	<dl	<dl	<dl	0.001	0.084	28.0	0.276
VB31-5.d	0.980	18.4	646	355	0.017	<dl	56.7	0.022	<dl	n.r.	4.44	<dl	16.3	6.14	8.55	0.047	6.30	<dl	<dl	<dl	<dl	0.027	0.009	60.7	0.838
VB31-7.d	0.830	0.209	10.4	262	0.012	<dl	64.9	<dl	<dl	n.r.	3.33	<dl	10.6	6.61	9.80	0.032	8.32	<dl	<dl	<dl	<dl	0.017	0.098	19.9	0.291
VB31-9.d	1.12	0.500	23.7	182	0.008	<dl	57.8	<dl	0.027	n.r.	2.32	<dl	9.60	5.86	9.10	0.032	6.17	<dl	<dl	<dl	<dl	0.043	0.099	31.4	0.281
VB34-3.d	26.9	0.011	0.540	214	0.023	<dl	190	<dl	0.025	n.r.	23.0	<dl	27.0	19.2	31.3	0.012	28.4	<dl	<dl	<dl	<dl	0.001	0.289	11.9	0.216
VB34-4.d	17.8	0.014	1.33	233	0.014	<dl	169	<dl	0.024	n.r.	16.4	<dl	24.9	19.7	33.3	0.052	24.7	<dl	<dl	<dl	<dl	8.E-4	0.298	9.95	0.204
VB5-1d	28.4	0.020	0.900	165	0.030	<dl	185	<dl	0.032	n.r.	23.1	<dl	23.5	19.8	31.4	0.006	26.5	<dl	<dl	<dl	<dl	9.E-4	0.274	12.3	0.255
VB5-4.d	22.6	0.004	1.49	166	0.008	<dl	181	<dl	<dl	n.r.	27.8	<dl	22.8	15.1	24.6	0.015	24.6	<dl	<dl	<dl	<dl	0.001	0.338	7.91	0.223
VB5-7.d	24.0	0.370	11.0	261	0.033	<dl	178	<dl	0.050	n.r.	18.1	<dl	36.1	21.1	30.0	0.012	32.2	<dl	<dl	<dl	<dl	0.002	0.574	12.0	0.360
VB6-1d	1.23	0.320	18.6	240	0.011	0.400	92.7	<dl	0.029	n.r.	17.9	<dl	32.8	10.2	34.0	0.005	20.2	<dl	<dl	<dl	<dl	0.009	0.046	13.8	0.244
VB6-11d	0.660	0.700	36.0	148	0.006	<dl	75.2	<dl	<dl	n.r.	3.91	<dl	13.9	7.78	21.1	0.004	2.61	<dl	<dl	<dl	<dl	9.E-4	0.005	4.27	0.067
VB6-12.d	0.930	0.043	3.30	197	0.007	<dl	98.0	<dl	<dl	n.r.	9.80	<dl	22.1	6.16	18.7	0.037	19.0	0.019	<dl	<dl	<dl	0.034	0.020	12.2	0.233
VB6-13.d	0.750	0.013	2.94	181	0.014	<dl	94.0	0.028	<dl	n.r.	12.0	<dl	20.0	6.80	18.9	0.020	18.7	<dl	<dl	<dl	<dl	0.033	0.020	5.58	0.291
VB6-2.d	0.207	0.009	2.32	155	0.007	<dl	100	<dl	<dl	n.r.	13.7	<dl	20.2	8.74	19.4	0.006	20.9	<dl	<dl	<dl	<dl	0.011	0.062	7.13	0.305
VB6-3.d	0.690	0.029	5.16	215	0.011	<dl	100	<dl	<dl	n.r.	15.9	<dl	26.4	6.66	31.0	0.042	18.8	<dl	<dl	<dl	<dl	0.013	0.020	4.87	0.277
VB6-4.d	0.186	0.009	1.67	172	0.012	<dl	80.8	<dl	<dl	n.r.	11.1	<dl	20.5	7.99	28.8	0.003	15.7	<dl	<dl	<dl	<dl	0.014	0.036	3.67	0.221
VB6-5.d	0.690	0.005	2.65	186	0.010	<dl	90.4	<dl	<dl	n.r.	10.9	<dl	21.0	11.1	35.9	0.005	15.9	<dl	<dl	<dl	<dl	0.088	0.010	1.99	0.138
VB6-6.d	0.183	0.048	5.00	243	0.007	<dl	90.6	0.036	<dl	n.r.	7.34	<dl	21.5	9.64	31.9	0.031	10.6	<dl	<dl	<dl	<dl	0.040	0.017	11.6	0.073
VB6-7.d	0.410	0.068	2.40	186	0.007	<dl	82.5	<dl	0.023	n.r.	4.84	<dl	19.1	9.73	38.4	0.042	9.03	<dl	<dl	0.033	<dl	0.024	0.013	8.73	0.062
VB6-8.d	0.590	4.70	8.60	199	0.010	<dl	80.3	<dl	<dl	n.r.	3.29	<dl	17.1	9.13	28.1	0.006	6.19	<dl	<dl	<dl	<dl	0.015	4.E-4	8.80	0.111
VB7-11d	0.157	0.065	6.20	199	0.125	<dl	58.0	<dl	<dl	n.r.	3.71	<dl	16.8	1.50	5.75	0.023	16.6	<dl	<dl	<dl	<dl	6.E-4	3.E-4	4.73	0.189
VB7-2.d	0.171	0.098	10.5	146	0.124	<dl	53.4	<dl	0.260	n.r.	6.67	<dl	20.0	1.73	5.93	0.014	17.1	<dl	<dl	<dl	<dl	7.E-4	3.E-4	7.16	0.190
VB7-3.d	0.210	0.151	7.14	147	0.119	<dl	54.6	<dl	<dl	n.r.	2.65	<dl	14.3	1.77	6.23	0.004	17.3	<dl	<dl	<dl	<dl	7.E-4	3.E-4	4.69	0.139
VB7-4.d	0.208	0.111	6.34	166	0.146	<dl	49.2	<dl	<dl	n.r.	2.71	<dl	17.2	2.48	7.20	0.004	15.4	<dl	<dl	<dl	<dl	9.E-4	3.E-4	3.68	0.188
VB7-5.d	0.195	0.300	11.0	147	0.063	0.170	53.4	<dl	0.041	n.r.	7.35	<dl	17.9	1.53	4.91	0.004	14.5	<dl	<dl	<dl	<dl	0.001	4.E-4	6.92	0.244
VB7-6.d	9.00	0.350	25.4	225	0.139	<dl	52.7	<dl	<dl	n.r.	6.78	<dl	22.0	2.09	7.29	0.017	18.1	<dl	<dl	<dl	<dl	6.E-4	5.E-4	4.86	0.254
VB7-7.d	1.45	0.139	10.9	185	0.102	<dl	61.8	<dl	<dl	n.r.	2.89	<dl	18.7	1.54	4.85	0.023	13.5	<dl	<dl	<dl	<dl	8.E-4	5.E-4	6.10	0.091

Grain ID	*Mn* 55	*Co* 59	*Ni* 60	*Zn* 66	*Ga* 71	As 75	*Se* 82	Mo 95	Ru 101	Rh 103	*Ag* 107	Pd 108	Cd 111	*In* 115	*Sn* 118	*Sb* 121	*Te* 128	Re 185	Os 189	Ir 193	Pt 195	*Au* 197	Tl 205	*Pb* 208	*Bi* 209
55um	0.470	0.023	0.241	0.353	0.028	0.223	2.53	0.030	0.023	0.005	0.023	0.014	0.046	0.012	0.073	0.022	0.256	0.009	0.021	0.007	0.013	0.010	0.004	0.012	0.007
33um	0.939	0.046	0.722	1.06	0.085	0.445	5.07	0.061	0.068	0.009	0.069	0.041	0.137	0.025	0.218	0.067	0.513	0.027	0.042	0.020	0.039	0.030	0.011	0.037	0.013
Orogenic gold																									
06ACCP-01d	2.08	0.600	6.60	364	0.135	<dl	36.3	1.00	<dl	n.r.	1.70	<dl	16.8	35.8	25.6	0.013	1.03	<dl	0.070	0.070	<dl	0.230	4.E-4	0.420	0.093
06ACCP-02.d	1.84	1.60	3.67	377	0.130	<dl	43.8	<dl	<dl	n.r.	2.40	<dl	15.6	38.6	26.7	0.017	2.20	<dl	<dl	0.027	<dl	0.440	0.001	0.920	0.200
06ACCP-03.d	1.05	0.056	6.50	343	16.0	0.600	51.2	<dl	<dl	n.r.	0.290	<dl	7.87	30.5	18.2	0.390	1.08	0.150	<dl	<dl	<dl	0.002	0.080	2.00	0.520
06ACCP-04.d	0.304	0.061	2.93	364	0.096	<dl	41.6	<dl	0.310	n.r.	0.078	<dl	6.60	34.9	14.4	0.300	1.31	<dl	<dl	0.120	<dl	0.002	0.270	1.77	0.019
06ACCP-05.d	0.491	0.057	40.0	347	0.037	<dl	41.4	0.800	<dl	n.r.	0.140	<dl	2.04	42.7	11.5	0.710	1.10	0.061	0.260	<dl	<dl	0.097	0.051	4.04	0.037
06ACCP-06.d	0.356	0.044	5.90	374	0.108	<dl	40.9	<dl	0.100	n.r.	2.30	<dl	5.77	58.7	7.52	0.003	0.058	0.130	<dl	<dl	<dl	0.005	9.E-4	2.95	1.00
18ACCP-01d	1.43	0.021	79.4	191	0.057	<dl	117	0.023	<dl	n.r.	1.11	<dl	5.17	5.43	25.9	0.200	0.036	0.005	<dl	<dl	<dl	0.024	4.E-4	0.540	0.032
18ACCP-02.d	1.05	0.054	74.8	194	0.064	<dl	104	0.480	0.090	n.r.	0.650	<dl	6.60	5.41	23.3	0.080	0.162	0.006	<dl	<dl	<dl	6.E-4	1.E-4	0.262	0.004
18ACCP-03.d	1.44	0.052	152	243	0.046	<dl	113	0.170	0.024	n.r.	0.400	<dl	5.91	4.94	23.4	0.002	0.038	0.019	<dl	<dl	<dl	0.230	2.E-4	0.680	0.004
18ACCP-04.d	1.41	0.136	82.4	178	0.077	<dl	106	0.020	0.017	n.r.	0.930	<dl	5.89	4.53	16.5	0.313	0.101	<dl	<dl	<dl	<dl	8.E-4	0.006	2.61	0.142
18ACCP-05.d	6.50	0.036	86.2	224	0.109	<dl	108	<dl	0.025	n.r.	2.00	<dl	4.71	4.81	19.2	0.270	0.042	0.100	0.038	<dl	<dl	0.007	0.001	1.64	0.220
18ACCP-06.d	0.760	0.202	102	198	0.044	<dl	106	0.043	<dl	n.r.	0.320	<dl	4.06	4.73	15.7	0.170	0.042	<dl	0.110	<dl	<dl	6.E-4	4.E-4	1.52	0.084
18ACCP-07.d	1.33	0.360	104	247	0.120	<dl	119	0.033	<dl	n.r.	1.52	<dl	8.90	5.66	24.3	0.260	0.037	<dl	<dl	<dl	0.010	0.027	2.E-4	0.610	0.018
25ACCP-01d	1.43	0.117	5.01	341	0.169	1.03	65.0	<dl	<dl	n.r.	3.73	<dl	28.2	13.7	110	0.127	0.036	<dl	<dl	<dl	<dl	0.063	3.E-4	0.780	0.286
25ACCP-03.d	1.16	0.207	6.20	345	0.221	1.17	44.5	<dl	<dl	n.r.	6.78	<dl	26.0	15.4	100	0.356	0.044	<dl	<dl	0.018	<dl	0.118	0.021	3.31	1.33
25ACCP-04.d	0.790	0.278	6.30	414	0.183	0.790	66.9	<dl	<dl	n.r.	5.06	<dl	27.5	14.9	115	0.110	0.074	<dl	<dl	<dl	0.220	0.180	0.007	0.782	0.316
25ACCP-05.d	1.50	0.285	25.0	349	0.113	0.890	60.3	<dl	<dl	n.r.	4.16	<dl	13.1	14.1	104	0.211	0.037	<dl	<dl	0.016	0.040	0.012	5.E-4	1.77	0.515
25ACCP-06.d	11.0	0.380	45.0	464	0.180	3.66	63.3	<dl	<dl	n.r.	4.45	<dl	38.2	15.8	126	0.395	0.050	<dl	<dl	<dl	<dl	0.009	6.E-4	2.70	0.820
25ACCP-07.d	0.258	0.371	37.0	384	0.380	0.990	61.9	<dl	<dl	n.r.	5.14	<dl	34.3	16.8	116	0.190	0.062	<dl	0.370	<dl	0.023	0.236	5.E-4	1.53	0.513
26ACCP-02.d	0.197	0.071	27.0	328	0.250	0.500	41.7	<dl	0.032	n.r.	1.68	<dl	20.5	22.4	94.4	0.163	0.379	<dl	<dl	<dl	<dl	0.021	0.003	1.13	0.900
26ACCP-03.d	1.33	0.167	13.0	366	0.340	<dl	50.7	<dl	<dl	n.r.	1.68	<dl	35.0	27.1	108	0.231	0.123	0.029	<dl	<dl	0.017	0.420	0.004	1.10	0.417
26ACCP-04.d	0.840	0.180	11.5	309	0.225	1.23	44.4	<dl	<dl	n.r.	3.78	<dl	14.4	25.0	94.3	0.900	0.062	<dl	<dl	<dl	<dl	0.055	0.004	2.68	1.36
26ACCP-05.d	0.650	0.026	150	340	1.50	1.68	52.4	<dl	<dl	n.r.	1.25	<dl	27.1	26.2	101	0.036	0.320	<dl	<dl	<dl	<dl	0.007	3.E-4	0.370	0.343
26ACCP-06.d	0.790	0.131	40.0	379	0.460	5.80	46.5	<dl	<dl	n.r.	1.70	<dl	30.7	27.8	93.2	0.037	0.057	<dl	<dl	<dl	0.013	0.006	0.004	1.81	0.810
3195ACCP-01d	0.208	0.186	0.050	551	0.246	<dl	7.90	<dl	<dl	n.r.	95.1	<dl	2.78	0.588	0.720	1.19	7.30	<dl	<dl	0.002	<dl	0.028	0.007	9.80	2.08
3195ACCP-02.d	0.610	0.188	0.068	662	0.190	<dl	6.17	<dl	<dl	n.r.	79.0	<dl	4.36	0.336	0.366	1.30	2.99	<dl	<dl	<dl	<dl	0.014	0.030	7.40	1.46
3195ACCP-03.d	0.232	0.110	0.049	423	0.196	<dl	4.40	<dl	0.039	n.r.	87.8	<dl	1.88	0.418	0.210	0.059	5.80	<dl	<dl	<dl	<dl	0.079	4.E-4	2.78	0.690
3195ACCP-04.d	0.189	0.035	0.034	99.6	0.113	<dl	2.12	<dl	<dl	n.r.	101	<dl	0.400	0.416	0.205	0.460	3.60	<dl	<dl	<dl	<dl	0.001	0.072	11.6	2.33
3195ACCP-05.d	0.109	0.027	0.019	114	0.179	<dl	2.90	<dl	<dl	n.r.	72.4	<dl	0.270	0.648	0.345	0.134	4.47	<dl	<dl	<dl	<dl	0.042	3.E-4	1.30	0.185
3195ACCP-06.d	0.820	0.012	0.032	99.4	0.132	<dl	4.60	<dl	<dl	n.r.	80.4	<dl	0.450	0.701	0.590	0.099	5.82	<dl	<dl	<dl	<dl	0.085	3.E-4	4.22	0.708
3195BCCP-02.d	0.469	2.45	0.116	6290	0.270	<dl	7.00	<dl	<dl	n.r.	77.4	<dl	33.8	0.247	0.720	0.730	6.43	<dl	<dl	0.003	<dl	0.003	0.231	19.2	2.57
3195BCCP-03.d	0.436	1.64	0.139	4150	0.253	<dl	13.5	0.400	<dl	n.r.	81.4	<dl	20.5	0.402	0.750	1.00	7.60	<dl	0.013	<dl	<dl	0.058	0.015	16.8	2.29
3195BCCP-04.d	1.81	0.780	0.090	1180	0.172	<dl	3.53	<dl	<dl	n.r.	73.5	<dl	7.20	0.574	0.430	2.14	4.40	<dl	<dl	<dl	<dl	0.610	0.039	16.7	1.82
3195BCCP-05.d	0.327	0.124	0.038	910	0.670	<dl	2.73	<dl	<dl	n.r.	76.6	<dl	0.340	0.143	8.63	3.05	0.063	<dl	<dl	<dl	<dl	0.016	0.154	11.7	3.17
3195BCCP-06.d	0.446	1.05	0.102	2190	0.357	<dl	2.50	0.110	<dl	n.r.	85.0	<dl	10.7	0.379	0.910	4.17	5.90	<dl	<dl	<dl	<dl	0.045	0.183	20.1	3.28
3195BCCP-07.d	0.327	0.198	0.059	243	0.133	<dl	3.59	0.220	<dl	n.r.	71.8	<dl	0.820	0.437	0.690	0.390	3.80	<dl	<dl	<dl	<dl	0.043	0.008	2.05	0.270
3196ACCP-01d	57.0	0.035	0.104	93.0	0.300	<dl	7.14	<dl	<dl	n.r.	1.66	<dl	3.10	6.14	1.39	3.30	0.092	<dl	<dl	<dl	<dl	8.E-4	0.010	4.67	0.031
3196ACCP-02.d	5.00	0.008	0.062	82.9	0.270	<dl	7.26	<dl	<dl	n.r.	1.12	<dl	2.31	6.51	1.37	4.77	0.091	<dl	<dl	<dl	<dl	5.E-4	0.027	4.51	0.022
3196ACCP-03.d	4.30	0.026	0.054	98.1	0.360	<dl	5.72	<dl	<dl	n.r.	0.990	<dl	3.93	6.89	1.53	2.68	0.070	<dl	<dl	<dl	<dl	9.E-4	0.010	2.70	0.024
3196ACCP-04.d	0.378	0.007	0.063	98.2	0.310	<dl	5.99	<dl	<dl	n.r.	2.32	<dl	2.31	6.85	1.42	3.49	0.081	<dl	<dl	<dl	<dl	9.E-4	0.022	3.40	0.052
3196ACCP-05.d	3.80	0.008	0.070	78.7	0.290	<dl	7.35	0.110	<dl	n.r.	3.68	<dl	2.00	7.12	1.35	7.30	0.122	<dl	<dl	<dl	<dl	7.E-4	0.036	8.80	0.137
3196ACCP-06.d	2.30	0.063	0.075	59.4	0.260	<dl	7.18	<dl	<dl	n.r.	4.78	<dl	2.49	7.22	0.760	8.29	0.117	<dl	<dl	<dl	<dl	0.002	0.058	18.4	0.152
3196BCCP-01d	5.40	0.023	0.036	78.0	0.277	0.250	1.90	<dl	<dl	n.r.	3.96	<dl	2.80	6.82	2.87	5.61	0.051	<dl	<dl	<dl	<dl	0.001	0.025	6.46	0.100
3196BCCP-02.d	2.10	0.040	0.047	86.0	0.320	0.640	2.16	0.074	<dl	n.r.	10.7	<dl	1.19	6.71	2.69	11.5	0.056	<dl	<dl	<dl	<dl	0.001	0.106	30.8	0.270
3196BCCP-03.d	1.45	0.006	0.028	75.2	0.388	0.310	2.31	<dl	<dl	n.r.	3.70	<dl	1.08	6.38	2.51	2.95	0.042	<dl	<dl	<dl	<dl	7.E-4	0.017	7.10	0.047
3232CCP-01d	1.60	0.024	0.013	214	0.162	0.940	4.78	0.150	<dl	n.r.	314	<dl	0.200	78.6	1.28	1.81	0.043	<dl	<dl	<dl	<dl	0.002	0.014	6.74	3.30

Grain ID	*Mn* 55	*Co* 59	*Ni* 60	*Zn* 66	*Ga* 71	As 75	*Se* 82	Mo 95	Ru 101	Rh 103	*Ag* 107	Pd 108	Cd 111	*In* 115	*Sn* 118	*Sb* 121	*Te* 128	Re 185	Os 189	Ir 193	Pt 195	*Au* 197	Tl 205	*Pb* 208	*Bi* 209
55um	0.470	0.023	0.241	0.353	0.028	0.223	2.53	0.030	0.023	0.005	0.023	0.014	0.046	0.012	0.073	0.022	0.256	0.009	0.021	0.007	0.013	0.010	0.004	0.012	0.007
33um	0.939	0.046	0.722	1.06	0.085	0.445	5.07	0.061	0.068	0.009	0.069	0.041	0.137	0.025	0.218	0.067	0.513	0.027	0.042	0.020	0.039	0.030	0.011	0.037	0.013
3232CCP-02.d	0.349	0.010	0.600	22.3	0.051	2.61	5.08	0.047	<dl	n.r.	384	0.021	0.290	78.4	1.50	5.40	0.086	<dl	<dl	<dl	<dl	0.001	0.031	17.2	10.1
3232CCP-03.d	1.41	0.008	0.022	20.3	0.071	2.10	4.85	0.050	<dl	n.r.	372	<dl	0.190	73.8	1.57	2.51	0.068	<dl	<dl	<dl	<dl	0.002	0.017	14.8	8.97
3232CCP-04.d	1.69	0.014	0.030	21.9	0.150	4.16	6.36	0.032	<dl	n.r.	454	<dl	0.260	80.7	1.26	2.71	0.095	<dl	0.012	<dl	<dl	0.002	0.015	20.4	9.50
3232CCP-05.d	2.90	0.014	0.023	20.1	0.170	1.97	6.88	<dl	<dl	n.r.	374	<dl	0.160	75.4	1.22	2.55	0.094	<dl	<dl	<dl	<dl	0.003	0.047	15.3	8.40
49ACCP-01d	1.13	0.004	60.0	340	0.034	1.00	8.10	<dl	<dl	n.r.	29.5	<dl	2.61	1.80	0.115	0.003	0.024	<dl	<dl	<dl	0.160	3.E-4	9.E-4	1.44	0.013
49ACCP-02.d	0.910	0.039	120	481	0.310	0.360	10.1	<dl	<dl	n.r.	33.5	<dl	6.80	1.13	0.150	0.006	0.053	0.017	<dl	0.240	0.110	0.050	0.013	1.51	0.006
49ACCP-03.d	4.90	0.021	29.0	438	0.177	0.570	8.80	0.090	0.029	n.r.	35.7	<dl	8.05	1.08	0.246	0.048	0.024	<dl	<dl	<dl	<dl	3.E-4	0.048	1.87	0.009
49ACCP-05.d	1.22	0.017	8.00	576	0.024	0.540	8.50	<dl	<dl	n.r.	34.2	<dl	7.14	1.24	0.195	0.079	0.030	0.250	0.060	<dl	<dl	0.001	0.163	1.30	0.100
49ACCP-06.d	0.950	0.110	18.0	362	0.017	0.300	8.30	<dl	<dl	n.r.	31.6	<dl	5.21	1.02	0.085	0.061	0.026	<dl	<dl	<dl	<dl	0.011	0.037	4.20	0.005
49ACCP-07.d	1.09	0.024	0.032	380	0.145	0.480	7.60	<dl	<dl	n.r.	32.5	<dl	5.50	1.12	0.400	0.044	0.027	<dl	<dl	<dl	<dl	6.E-4	0.158	5.30	0.005
BULY01CCP-01d	1.56	0.426	11.0	584	0.580	0.520	17.0	<dl	<dl	n.r.	699	<dl	6.70	12.5	50.2	0.203	0.032	<dl	<dl	<dl	<dl	0.003	7.E-4	1.46	1.90
BULY01CCP-02.d	3.20	0.189	11.3	551	0.750	<dl	16.5	<dl	0.040	n.r.	745	<dl	5.37	10.6	54.5	0.410	0.191	<dl	0.370	<dl	<dl	0.002	8.E-4	2.25	2.84
BULY01CCP-03.d	1.43	0.234	12.5	629	0.770	<dl	17.3	0.100	<dl	n.r.	431	<dl	6.25	10.1	54.4	0.195	0.030	0.019	0.061	<dl	<dl	1.90	6.E-4	1.00	1.51
BULY01CCP-04.d	1.19	0.140	13.8	507	0.750	0.900	16.4	0.021	0.040	n.r.	427	<dl	5.52	9.94	53.7	0.036	0.025	<dl	0.031	0.037	<dl	0.001	4.E-4	0.460	0.717
BULY01CCP-05.d	2.00	0.259	11.9	621	0.840	<dl	16.8	0.055	0.025	n.r.	553	<dl	6.50	11.1	58.9	0.720	0.180	<dl	0.070	<dl	0.100	0.002	0.005	4.91	7.66
BULY01CCP-06.d	1.48	0.492	10.0	625	0.720	<dl	27.0	<dl	0.034	n.r.	594	<dl	6.74	11.6	57.6	0.308	0.170	0.230	<dl	<dl	<dl	0.002	6.E-4	1.80	2.30
BULY01CCP-07.d	1.34	0.104	13.2	611	0.722	<dl	14.5	<dl	0.025	n.r.	677	0.370	6.05	10.3	52.9	0.460	0.340	<dl	0.180	0.009	<dl	0.002	7.E-4	2.17	3.54
BULY02CCP-01d	7.40	0.580	1.60	334	0.167	<dl	9.50	<dl	<dl	n.r.	154	<dl	4.23	9.41	15.5	2.29	0.047	<dl	<dl	<dl	0.048	0.002	0.056	18.0	10.3
BULY02CCP-02.(	1.30	0.025	0.062	353	0.240	<dl	11.8	0.240	0.120	n.r.	142	<dl	4.06	9.57	16.4	0.450	0.028	<dl	0.032	0.280	<dl	0.001	0.008	2.31	2.24
BULY02CCP-03.(	0.284	0.077	70.0	418	0.192	<dl	10.1	1.50	0.023	n.r.	147	<dl	3.67	9.98	16.7	0.338	0.036	0.070	<dl	<dl	<dl	0.001	0.021	1.83	1.17
BULY02CCP-04.(	4.80	0.079	1.10	419	0.260	<dl	12.1	0.038	<dl	n.r.	157	<dl	4.96	10.5	21.3	0.600	0.290	<dl	0.600	<dl	0.140	0.002	0.033	4.54	16.5
BULY02CCP-05.(	2.16	1.50	0.300	421	0.270	<dl	10.3	0.035	<dl	n.r.	152	<dl	4.37	9.62	18.1	1.03	0.036	0.011	<dl	<dl	<dl	0.004	0.009	4.29	4.68
BULY02CCP-06.(	2.00	0.800	120	457	0.280	11.0	7.50	<dl	0.120	n.r.	160	<dl	4.93	11.9	18.2	0.250	0.047	0.008	<dl	<dl	<dl	0.700	7.E-4	0.860	1.30
BULY02CCP-07.(	0.414	1.70	2.60	299	0.226	<dl	4.60	0.025	<dl	n.r.	142	<dl	3.25	11.1	14.3	0.406	0.041	0.015	<dl	<dl	<dl	0.002	0.006	1.50	1.69
BULY05CCP-01d	2.10	0.130	0.016	3.10	0.168	0.510	22.0	0.035	<dl	n.r.	33.2	<dl	0.017	18.0	17.9	4.51	0.035	<dl	<dl	<dl	<dl	0.027	0.024	16.3	9.41
BULY05CCP-02.(	0.990	0.032	1.80	74.4	0.192	0.250	47.0	0.140	<dl	n.r.	20.1	<dl	0.410	19.4	18.4	3.17	0.036	<dl	<dl	<dl	<dl	0.002	0.014	19.5	5.67
BULY05CCP-03.(	1.31	0.027	3.10	71.8	0.315	<dl	55.7	0.028	<dl	n.r.	20.6	<dl	0.074	16.2	15.3	1.94	0.370	<dl	<dl	0.022	<dl	0.002	0.007	11.1	6.01
BULY05CCP-04.(	1.20	0.023	60.0	37.5	0.100	<dl	40.9	0.034	<dl	n.r.	24.5	<dl	0.198	17.7	18.9	2.16	0.210	<dl	0.270	0.037	<dl	0.002	0.015	11.2	6.18
BULY05CCP-05.(	1.43	0.300	6.00	115	0.311	0.211	48.1	0.390	<dl	n.r.	111	<dl	0.129	16.6	15.2	0.940	0.103	0.021	<dl	0.008	<dl	0.001	0.009	4.56	2.67
BULY05CCP-06.(	1.10	0.020	0.260	13.4	0.310	0.570	61.1	<dl	<dl	n.r.	57.9	<dl	0.090	17.7	14.5	7.90	0.220	<dl	<dl	<dl	<dl	0.023	0.073	38.4	20.2
BULY05CCP-07.(	1.13	0.028	0.190	9.80	0.165	0.360	42.1	0.031	<dl	n.r.	28.1	<dl	0.040	16.8	16.6	2.62	0.020	<dl	<dl	<dl	<dl	0.016	0.014	15.9	9.73
C48121ACCP-01c	1.50	0.015	0.093	1.23	0.042	<dl	8.60	<dl	0.030	n.r.	0.204	<dl	3.77	6.64	0.550	0.008	0.015	1.80	<dl	<dl	<dl	0.001	1.E-4	0.390	0.073
C48121ACCP-02.(	0.540	0.058	0.120	20.7	0.092	0.102	9.50	0.290	<dl	n.r.	1.00	<dl	4.41	6.61	0.910	3.80	0.028	<dl	<dl	0.009	0.600	0.021	2.E-4	0.409	1.79
C48121ACCP-03.(	1.45	0.800	0.039	14.9	0.096	<dl	5.90	1.50	0.033	n.r.	0.006	<dl	3.98	6.91	0.800	0.004	0.039	<dl	0.045	<dl	0.310	0.600	0.006	0.180	0.520
C48121ACCP-04.(	20.0	0.270	0.028	19.5	0.102	0.139	8.80	0.100	<dl	n.r.	0.390	<dl	2.95	6.94	0.760	0.037	0.022	<dl	<dl	0.011	<dl	0.031	2.E-4	0.185	0.670
C48121ACCP-05.(	1.11	0.004	0.037	30.0	0.099	<dl	21.0	<dl	<dl	n.r.	0.070	<dl	4.33	6.62	0.850	0.004	0.031	<dl	<dl	<dl	0.027	0.008	0.004	0.200	0.458
C48121ACCP-06.(	1.03	0.009	0.340	26.7	0.800	0.500	4.90	0.019	0.016	n.r.	0.031	1.03	3.24	6.82	0.780	0.005	0.250	0.006	<dl	0.220	<dl	0.090	3.E-4	1.30	2.94
C48121ACCP-07.(	0.890	0.035	3.10	20.4	0.100	0.289	6.20	<dl	0.017	n.r.	0.056	<dl	3.59	6.85	0.725	0.006	0.170	<dl	<dl	<dl	<dl	0.025	2.E-4	2.28	15.8
HUGO02ACCP-0	1.66	1.10	70.0	216	0.062	<dl	1.34	0.160	<dl	n.r.	6.92	0.019	0.059	0.167	0.042	0.780	0.033	0.070	<dl	<dl	<dl	7.E-4	4.E-4	1.42	0.008
HUGO02ACCP-0	0.217	0.396	0.015	12.5	0.012	<dl	1.67	<dl	<dl	n.r.	11.1	<dl	0.054	0.222	0.036	1.69	0.024	0.013	<dl	<dl	<dl	7.E-4	4.E-4	2.84	0.014
HUGO02ACCP-0	1.80	0.390	1.60	15.6	0.043	0.310	1.78	0.043	<dl	n.r.	8.21	<dl	0.046	0.275	0.188	1.86	0.031	0.020	<dl	<dl	<dl	0.034	0.027	3.57	0.032
HUGO02ACCP-0	1.42	0.400	120	17.6	0.054	<dl	1.52	0.047	<dl	n.r.	8.80	<dl	0.078	0.184	0.033	0.570	0.034	<dl	<dl	<dl	<dl	0.016	0.002	1.70	0.044
HUGO02ACCP-0	0.208	0.350	0.019	9.00	0.039	0.240	1.42	<dl	<dl	n.r.	17.7	<dl	0.120	0.154	0.027	3.11	0.025	<dl	<dl	0.050	<dl	0.001	6.E-4	4.94	0.010
HUGO02ACCP-0	1.59	0.420	0.016	14.3	0.083	<dl	1.38	<dl	<dl	n.r.	12.9	<dl	0.034	0.146	1.40	1.56	0.021	0.008	<dl	<dl	<dl	7.E-4	5.E-4	3.68	0.009
HUGO02BCCP-0	0.218	0.404	0.700	15.5	0.085	<dl	1.59	0.270	0.170	n.r.	12.7	<dl	0.037	0.181	0.050	1.02	0.039	0.032	<dl	<dl	<dl	0.090	7.E-4	3.61	0.190
HUGO02BCCP-0	0.309	0.650	170	17.0	0.022	<dl	2.00	0.045	<dl	n.r.	10.9	0.567	0.140	0.242	0.040	2.77	0.045	<dl	0.034	<dl	<dl	1.E-3	8.E-4	5.34	0.013
HUGO02BCCP-0	1.66	0.510	23.0	15.4	0.040	0.320	1.99	<dl	0.031	n.r.	18.6	<dl	0.047	0.237	0.054	1.75	0.033	<dl	<dl	0.050	0.021	0.041	7.E-4	8.20	0.080

Grain ID	Mn 55	Co 59	Ni 60	Zn 66	Ga 71	As 75	Se 82	Mo 95	Ru 101	Rh 103	Ag 107	Pd 108	Cd 111	In 115	Sn 118	Sb 121	Te 128	Re 185	Os 189	Ir 193	Pt 195	Au 197	Tl 205	Pb 208	Bi 209
55um	0.470	0.023	0.241	0.353	0.028	0.223	2.53	0.030	0.023	0.005	0.023	0.014	0.046	0.012	0.073	0.022	0.256	0.009	0.021	0.007	0.013	0.010	0.004	0.012	0.007
33um	0.939	0.046	0.722	1.06	0.085	0.445	5.07	0.061	0.068	0.009	0.069	0.041	0.137	0.025	0.218	0.067	0.513	0.027	0.042	0.020	0.039	0.030	0.011	0.037	0.013
HUGO02BCCP-0	0.272	0.530	1.30	8.40	0.012	0.240	1.86	<dl	<dl	n.r.	11.1	0.018	0.028	0.199	0.056	0.610	0.099	<dl	<dl	<dl	<dl	0.002	0.002	2.46	0.010
HUGO02BCCP-0	0.284	0.860	4.60	14.0	0.081	<dl	1.74	0.150	0.024	n.r.	18.3	<dl	0.102	0.165	0.033	0.650	0.039	<dl	<dl	<dl	<dl	0.002	4.E-4	2.10	1.50
HUGO02BCCP-0	0.250	0.241	0.023	13.5	0.081	0.690	1.38	<dl	<dl	n.r.	17.6	<dl	0.220	0.220	0.033	2.64	0.260	<dl	<dl	<dl	<dl	9.E-4	0.017	5.80	0.011
KOCH01CCP-01c	0.320	0.800	5.00	293	0.230	<dl	140	<dl	<dl	n.r.	4.07	<dl	12.6	80.1	13.8	0.003	1.84	13.0	<dl	<dl	<dl	0.002	3.E-4	0.620	2.74
KOCH01CCP-02.	1.00	0.120	0.072	288	0.210	<dl	170	0.100	0.064	n.r.	4.17	<dl	11.7	74.7	14.7	0.042	0.057	<dl	<dl	0.024	<dl	0.070	3.E-4	0.240	0.440
KOCH01CCP-03.	1.32	0.660	4.10	352	0.288	0.620	403	<dl	<dl	n.r.	11.3	<dl	10.6	94.9	14.9	0.004	0.093	<dl	0.330	0.018	<dl	0.003	0.009	8.90	4.10
KOCH01CCP-06.	4.60	1.20	120	332	0.296	0.250	217	<dl	<dl	n.r.	4.74	<dl	13.7	88.6	8.93	0.096	0.102	0.050	<dl	<dl	<dl	0.003	6.E-4	1.04	1.67
LEGA05CCP-02.	1.99	7.00	8.80	830	0.490	<dl	69.0	0.189	<dl	n.r.	118	<dl	32.1	108	519	1.20	1.03	<dl	0.080	<dl	<dl	0.119	0.220	3.18	0.061
LEGA05CCP-03.	2.23	0.800	6.93	770	0.366	0.800	74.4	0.030	<dl	n.r.	137	<dl	37.5	108	540	1.22	0.270	0.009	<dl	<dl	0.150	0.083	0.470	1.17	0.036
LEGA05CCP-04.	0.750	1.30	6.60	535	0.355	<dl	69.5	0.028	0.024	n.r.	122	<dl	28.3	114	584	2.56	0.570	0.013	<dl	<dl	<dl	0.023	0.025	1.26	0.027
LEGA05CCP-05.	1.68	16.0	110	640	25.8	<dl	40.7	0.028	1.70	n.r.	241	<dl	22.6	27.9	636	0.490	3.10	<dl	<dl	0.028	<dl	0.025	0.300	0.458	2.10
LEGA05CCP-06.	1.69	0.438	60.0	721	37.7	<dl	35.8	0.049	<dl	n.r.	204	<dl	26.8	29.4	791	0.723	4.40	0.009	<dl	<dl	<dl	0.170	8.E-4	2.19	0.035
LEGA05CCP-07.	1.32	1.10	44.0	1180	31.3	0.250	46.0	<dl	<dl	n.r.	185	<dl	35.4	31.9	691	0.970	6.10	<dl	<dl	<dl	<dl	0.136	9.E-4	2.88	0.044
LEGA06CCP-01c	1.34	0.243	3.40	647	3.81	<dl	28.1	<dl	<dl	n.r.	184	<dl	30.7	4.66	40.1	0.560	1.18	<dl	0.090	0.019	<dl	0.011	0.180	2.20	0.370
LEGA06CCP-03.	1.49	0.194	0.680	517	3.26	<dl	43.0	<dl	<dl	n.r.	200	<dl	26.0	4.08	40.5	0.590	1.31	<dl	<dl	<dl	<dl	0.001	7.E-4	1.65	0.500
LEGA06CCP-04.	1.35	0.440	0.550	619	4.20	<dl	30.8	<dl	<dl	n.r.	167	<dl	32.6	4.28	45.7	1.08	1.75	<dl	<dl	<dl	<dl	0.002	0.008	3.37	0.195
LEGA06CCP-05.	2.16	0.565	0.870	526	3.10	<dl	42.8	<dl	0.027	n.r.	176	<dl	33.9	3.04	33.0	1.14	3.01	<dl	<dl	0.060	<dl	0.021	9.E-4	6.10	0.650
LEGA06CCP-06.	1.72	0.540	0.910	623	3.37	<dl	37.2	<dl	<dl	n.r.	246	<dl	26.7	3.53	29.3	1.04	8.00	0.023	<dl	<dl	0.048	0.002	0.005	3.21	1.00
LEGA06CCP-07.	0.910	4.70	1.89	584	14.1	<dl	41.6	<dl	<dl	n.r.	367	<dl	46.3	2.79	48.3	0.172	2.14	<dl	<dl	<dl	<dl	0.010	5.E-4	0.630	0.123
MAL06CCP-01d	1.28	0.120	34.0	198	0.753	<dl	21.8	0.062	<dl	n.r.	359	<dl	15.9	15.3	27.5	0.040	0.044	<dl	0.035	<dl	0.023	1.10	0.015	0.480	0.980
MAL06CCP-02.d	0.820	2.60	63.0	198	0.566	<dl	18.6	0.260	0.025	n.r.	350	<dl	13.6	15.3	25.9	0.006	0.200	<dl	0.027	0.017	<dl	0.140	3.E-4	0.440	0.167
MAL06CCP-03.d	1.18	2.00	16.0	215	0.530	<dl	19.4	0.042	0.018	n.r.	400	<dl	15.1	15.5	26.2	0.037	0.036	0.039	<dl	<dl	<dl	0.490	4.E-4	0.550	1.53
MAL06CCP-04.d	1.46	2.60	0.970	194	1.26	0.170	25.7	<dl	<dl	n.r.	497	<dl	15.8	16.5	27.5	0.240	0.040	0.140	<dl	<dl	<dl	0.142	5.E-4	0.770	1.05
MAL06CCP-05.d	1.70	0.260	25.0	228	0.032	<dl	9.50	<dl	<dl	n.r.	307	<dl	14.5	16.1	26.9	0.008	0.029	<dl	<dl	<dl	<dl	0.041	6.E-4	1.16	1.13
MAL06CCP-06.d	0.640	3.70	0.830	201	1.68	0.300	7.51	0.050	<dl	n.r.	140	<dl	14.9	16.0	27.5	0.022	0.199	<dl	<dl	<dl	<dl	0.170	6.E-4	2.32	1.40
MAL06CCP-07.d	0.700	0.031	1.90	227	1.06	<dl	13.5	0.053	<dl	n.r.	155	<dl	17.7	16.5	29.0	0.110	1.70	0.100	0.160	0.190	<dl	0.125	0.050	4.42	1.68
MAL06CCP-08.d	1.60	1.40	25.0	215	1.00	<dl	10.8	0.220	<dl	n.r.	139	<dl	17.5	16.0	27.7	0.180	0.240	<dl	<dl	<dl	0.039	0.103	0.008	7.90	1.52
RALE01CCP-01d	1.44	0.080	19.0	401	1.28	<dl	12.5	<dl	0.080	n.r.	1.54	<dl	3.26	74.3	68.4	17.0	1.50	<dl	<dl	<dl	0.600	0.051	0.170	61.0	1.78
RALE01CCP-02.c	1.60	0.570	0.430	236	1.72	0.530	14.7	<dl	0.029	n.r.	1.51	<dl	2.12	68.9	62.2	19.4	1.72	<dl	<dl	<dl	<dl	0.250	0.520	81.0	2.60
RALE01CCP-03.c	1.78	0.380	0.061	266	1.59	<dl	13.2	<dl	<dl	n.r.	1.64	<dl	3.25	67.1	52.6	23.8	2.39	0.023	0.120	<dl	<dl	0.250	0.449	79.4	1.91
RALE01CCP-04.c	0.399	0.510	18.0	246	3.36	<dl	6.58	<dl	<dl	n.r.	1.50	<dl	1.52	12.6	60.1	2.81	6.20	<dl	0.150	<dl	<dl	0.002	0.080	26.2	0.092
RALE01CCP-05.c	0.580	0.180	0.380	309	2.72	<dl	4.90	0.042	<dl	n.r.	0.980	<dl	2.12	15.0	49.3	9.70	0.760	<dl	0.042	<dl	<dl	0.120	0.261	38.3	0.185
YOU01ACCP-01d	0.710	0.039	5.74	148	0.077	<dl	10.9	0.110	<dl	n.r.	51.9	<dl	5.67	4.54	0.320	0.044	0.030	<dl	<dl	<dl	<dl	0.023	5.E-4	1.84	0.673
YOU01ACCP-02.c	0.970	0.720	5.80	147	0.072	0.180	14.4	<dl	<dl	n.r.	56.9	<dl	3.75	5.20	0.340	0.072	0.042	<dl	<dl	<dl	<dl	0.034	0.007	3.17	14.0
YOU01ACCP-03.c	1.11	0.260	4.62	110	0.032	<dl	18.4	<dl	<dl	n.r.	54.0	<dl	5.12	4.48	0.312	0.128	0.410	<dl	<dl	0.020	<dl	0.014	6.E-4	1.64	1.24
YOU01ACCP-04.c	0.910	0.033	4.86	84.8	0.043	0.210	14.7	<dl	<dl	n.r.	52.1	<dl	4.11	4.66	0.276	0.003	0.034	<dl	<dl	<dl	<dl	0.022	4.E-4	1.60	14.0
YOU01ACCP-05.c	1.15	0.026	4.92	86.3	0.085	<dl	16.6	<dl	<dl	n.r.	50.9	<dl	5.88	4.35	0.346	0.082	0.024	<dl	<dl	0.019	<dl	0.001	4.E-4	0.960	0.490
YOU01ACCP-06.c	0.820	0.700	5.62	68.2	0.068	<dl	14.9	<dl	<dl	n.r.	48.2	<dl	3.61	4.38	0.250	0.162	0.032	<dl	<dl	<dl	<dl	0.010	0.014	1.38	0.592
YOU01ACCP-07.c	0.560	0.007	5.38	112	0.048	<dl	18.0	<dl	<dl	n.r.	50.4	<dl	4.59	4.50	0.316	0.139	0.035	<dl	<dl	<dl	<dl	0.045	5.E-4	1.56	1.50
YOU01BCCP-01d	0.600	0.600	5.44	103	0.031	0.500	13.5	0.024	<dl	n.r.	51.7	<dl	3.60	4.44	0.300	0.206	0.031	<dl	<dl	<dl	<dl	0.070	5.E-4	2.20	0.950
YOU01BCCP-02.c	1.14	0.051	4.87	96.3	0.074	<dl	15.7	<dl	<dl	n.r.	53.9	<dl	6.66	4.66	0.304	0.241	0.037	<dl	<dl	<dl	<dl	0.068	0.006	2.73	1.38
YOU01BCCP-03.c	3.50	1.40	6.50	69.7	0.064	0.380	14.4	<dl	<dl	n.r.	54.6	<dl	5.62	4.48	0.339	0.580	0.263	<dl	<dl	<dl	0.014	0.040	0.800	9.10	3.45
YOU01BCCP-04.c	1.30	0.090	4.88	138	0.031	<dl	14.4	<dl	<dl	n.r.	53.1	<dl	7.57	4.74	0.310	0.400	0.360	0.120	<dl	<dl	<dl	0.147	6.E-4	3.53	5.40
YOU01BCCP-05.c	1.08	0.600	4.82	82.6	0.057	<dl	19.6	<dl	0.080	n.r.	56.5	<dl	7.90	4.79	0.270	0.690	0.860	<dl	<dl	<dl	<dl	0.051	9.E-4	5.54	2.95
YOU01BCCP-06.c	0.630	0.020	4.28	106	0.029	<dl	16.1	<dl	<dl	n.r.	53.6	<dl	6.60	4.66	0.148	0.124	0.037	<dl	<dl	<dl	<dl	0.140	5.E-4	1.68	1.67
YOU01BCCP-07.c	0.790	0.100	5.23	94.4	0.039	<dl	8.50	<dl	<dl	n.r.	53.0	<dl	5.80	4.41	0.315	0.261	0.190	<dl	<dl	<dl	<dl	0.049	4.E-4	2.27	0.965

Grain ID	*Mn* 55	Co 59	*Ni* 60	*Zn* 66	*Ga* 71	As 75	*Se* 82	Mo 95	Ru 101	Rh 103	*Ag* 107	Pd 108	Cd 111	*In* 115	*Sn* 118	*Sb* 121	*Te* 128	Re 185	Os 189	Ir 193	Pt 195	*Au* 197	Tl 205	*Pb* 208	*Bi* 209
55um	0.470	0.023	0.241	0.353	0.028	0.223	2.53	0.030	0.023	0.005	0.023	0.014	0.046	0.012	0.073	0.022	0.256	0.009	0.021	0.007	0.013	0.010	0.004	0.012	0.007
33um	0.939	0.046	0.722	1.06	0.085	0.445	5.07	0.061	0.068	0.009	0.069	0.041	0.137	0.025	0.218	0.067	0.513	0.027	0.042	0.020	0.039	0.030	0.011	0.037	0.013
Porphyry																									
2045CCP-01d	0.087	2.75	0.010	11.6	0.204	<dl	455	<dl	0.027	n.r.	3.64	<dl	0.040	5.54	21.9	0.020	0.860	<dl	<dl	<dl	<dl	6.E-4	0.00	0.403	0.030
2045CCP-02.d	0.104	3.71	0.013	16.4	0.455	<dl	413	<dl	<dl	n.r.	4.47	<dl	0.069	5.72	27.2	0.003	0.940	<dl	<dl	<dl	<dl	0.007	0.00	0.395	0.027
2045CCP-03.d	0.102	3.26	0.014	13.1	0.762	<dl	224	<dl	<dl	n.r.	5.24	<dl	0.083	5.43	27.9	0.005	1.17	<dl	<dl	<dl	<dl	0.003	1.E-4	0.871	0.021
2045CCP-04.d	0.088	2.63	0.010	3.13	0.245	<dl	623	<dl	<dl	n.r.	2.78	<dl	0.011	5.28	14.6	0.058	0.960	<dl	<dl	<dl	<dl	4.E-4	2.E-4	0.330	0.019
2045CCP-05.d	0.132	2.19	0.021	9.10	0.625	0.190	160	<dl	<dl	n.r.	0.385	<dl	0.081	5.62	18.9	0.003	1.01	<dl	<dl	<dl	<dl	4.E-4	1.E-4	0.475	0.013
2045CCP-06.d	0.101	2.04	0.014	4.90	0.461	<dl	129	<dl	<dl	n.r.	0.526	<dl	0.062	5.41	12.6	0.014	1.28	<dl	<dl	<dl	<dl	3.E-4	1.E-4	0.222	0.006
2047CCP-01d	17.7	0.768	0.025	411	3.78	0.370	2.64	<dl	0.016	n.r.	19.8	<dl	1.67	0.005	104	2.03	0.040	<dl	<dl	<dl	<dl	0.001	0.010	1.60	0.002
2047CCP-02.d	20.0	0.644	0.105	416	3.68	0.690	2.30	<dl	<dl	n.r.	14.4	<dl	1.91	0.003	119	0.653	0.037	<dl	<dl	<dl	<dl	6.E-4	0.010	2.83	0.002
2047CCP-03.d	15.7	0.617	0.029	405	3.91	0.530	2.69	<dl	<dl	n.r.	11.9	<dl	1.80	0.006	118	2.63	0.048	<dl	<dl	<dl	<dl	0.001	5.E-4	3.07	0.003
2047CCP-04.d	12.7	0.377	0.150	386	2.95	0.360	2.66	<dl	<dl	n.r.	12.9	<dl	1.74	0.006	110	1.73	0.039	<dl	<dl	<dl	<dl	9.E-4	0.053	3.74	0.002
2047CCP-05.d	18.0	0.633	0.030	305	1.19	0.360	2.25	0.039	<dl	n.r.	10.6	<dl	1.51	0.004	144	1.67	0.040	<dl	<dl	<dl	<dl	8.E-4	0.156	3.28	0.004
2047CCP-06.d	21.3	0.740	0.029	410	2.65	0.250	2.17	<dl	0.034	n.r.	10.8	<dl	1.92	0.006	108	0.920	0.036	<dl	<dl	<dl	<dl	7.E-4	0.048	3.06	0.005
2048ACCP-01d	0.910	1.60	0.047	18.7	0.492	0.310	205	<dl	<dl	n.r.	0.970	<dl	2.18	6.00	10.5	0.176	4.46	<dl	<dl	<dl	<dl	0.026	0.067	63.7	0.128
2048ACCP-02.d	0.730	1.70	0.037	27.8	0.541	<dl	196	<dl	<dl	n.r.	4.24	<dl	3.11	6.06	8.20	0.047	8.60	<dl	<dl	<dl	<dl	0.056	0.006	30.5	0.058
2048ACCP-03.d	1.31	1.97	0.044	41.4	0.596	<dl	211	<dl	<dl	n.r.	2.01	<dl	2.49	5.82	10.8	0.115	9.38	<dl	<dl	<dl	<dl	0.050	0.023	87.4	0.089
2048ACCP-04.d	0.720	0.871	0.031	7.50	0.483	<dl	193	<dl	<dl	n.r.	4.64	<dl	0.920	6.01	4.30	0.087	6.94	<dl	<dl	<dl	<dl	0.051	0.006	12.5	0.110
2048ACCP-05.d	0.304	1.31	0.060	10.5	0.610	<dl	188	<dl	<dl	n.r.	1.50	<dl	1.25	6.17	6.87	0.061	6.90	<dl	<dl	<dl	<dl	0.046	0.009	13.0	0.075
2048ACCP-06.d	1.15	1.24	0.045	14.8	0.480	0.210	208	<dl	<dl	n.r.	2.98	<dl	1.77	6.12	4.64	0.187	6.41	<dl	<dl	<dl	<dl	0.061	0.070	14.8	0.203
2048ACCP-07.d	0.540	1.43	0.029	17.3	0.600	<dl	200	<dl	<dl	n.r.	1.02	<dl	1.09	6.27	11.1	0.074	6.46	<dl	<dl	<dl	<dl	0.018	0.009	14.6	0.046
2048ACCP-08.d	1.42	0.720	0.028	3.89	0.530	<dl	185	<dl	<dl	n.r.	2.88	<dl	0.340	6.24	5.58	0.116	6.43	<dl	<dl	<dl	<dl	0.097	0.003	3.41	0.118
2048BCCP-01d	1.64	1.49	0.340	25.5	0.700	<dl	213	0.017	<dl	n.r.	0.994	<dl	1.02	5.88	14.0	0.043	8.83	<dl	<dl	<dl	<dl	0.035	5.E-4	23.9	0.081
2048BCCP-02.d	1.98	0.440	0.042	3.75	0.373	0.460	195	<dl	<dl	n.r.	0.770	<dl	0.440	5.91	4.28	0.173	4.30	<dl	<dl	<dl	<dl	0.014	0.003	3.59	0.104
2048BCCP-03.d	0.165	0.385	0.029	3.63	0.468	0.390	205	<dl	<dl	n.r.	0.840	<dl	0.360	6.13	5.28	0.246	4.00	<dl	<dl	<dl	<dl	0.036	5.E-4	3.07	0.142
2048BCCP-04.d	0.930	1.04	0.035	13.8	0.810	<dl	219	<dl	0.029	n.r.	1.68	<dl	0.780	5.91	11.4	0.043	6.26	<dl	<dl	<dl	<dl	0.022	0.002	6.13	0.129
2048BCCP-06.d	1.10	1.68	0.064	28.0	0.760	<dl	251	<dl	<dl	n.r.	0.950	<dl	1.33	6.50	18.4	0.133	8.20	<dl	<dl	<dl	<dl	0.027	0.005	34.1	0.088
2048BCCP-07.d	0.790	1.24	0.033	24.1	0.555	<dl	213	<dl	<dl	n.r.	1.34	<dl	0.740	6.21	11.1	0.005	10.8	<dl	<dl	<dl	<dl	0.023	5.E-4	6.28	0.056
2086CCP-01d	0.210	2.64	0.046	314	0.395	<dl	45.7	<dl	<dl	n.r.	4.55	<dl	6.74	11.9	6.34	0.006	4.31	<dl	<dl	<dl	<dl	1.E-3	3.E-4	2.14	0.145
2086CCP-02.d	1.09	0.970	0.053	453	0.500	<dl	45.2	<dl	<dl	n.r.	9.81	<dl	10.9	10.8	0.280	0.155	1.75	<dl	<dl	<dl	<dl	0.015	0.009	7.88	0.561
2086CCP-05.d	0.620	1.47	0.043	553	0.870	0.320	43.8	<dl	<dl	n.r.	5.76	<dl	7.90	10.6	1.34	0.130	1.48	<dl	<dl	<dl	<dl	0.001	0.004	3.88	0.220
2098CCP-01d	0.185	6.96	0.021	33.4	4.71	<dl	198	<dl	<dl	n.r.	0.242	<dl	0.059	4.08	112	0.005	0.840	<dl	<dl	<dl	<dl	0.001	0.00	0.093	0.005
2098CCP-02.d	0.178	10.8	0.027	37.7	5.47	<dl	138	<dl	0.027	n.r.	0.176	<dl	0.146	3.99	140	0.005	0.490	<dl	<dl	<dl	<dl	7.E-4	0.00	0.067	0.003
2098CCP-03.d	0.198	3.46	0.020	19.5	3.15	<dl	139	<dl	<dl	n.r.	0.350	<dl	0.061	4.45	57.9	0.006	0.046	<dl	0.060	0.040	<dl	5.E-4	0.00	0.307	0.024
2098CCP-04.d	0.173	5.63	0.022	28.0	4.18	<dl	154	<dl	<dl	n.r.	0.249	<dl	0.110	3.96	88.1	0.003	0.610	<dl	<dl	<dl	<dl	6.E-4	0.00	0.057	0.002
2098CCP-05.d	0.222	3.89	0.021	19.1	4.57	<dl	188	0.031	0.026	n.r.	0.280	<dl	0.029	6.72	57.1	0.005	0.046	<dl	<dl	<dl	<dl	4.E-4	1.E-4	0.300	0.010
2098CCP-07.d	0.610	8.44	0.029	32.6	4.50	<dl	152	<dl	<dl	n.r.	0.263	<dl	0.019	4.26	102	0.004	0.810	<dl	<dl	<dl	<dl	4.E-4	0.037	0.042	0.009
2104ACCP-01d	0.460	14.4	0.022	71.1	7.04	<dl	150	<dl	<dl	n.r.	0.273	<dl	0.099	4.58	189	0.007	0.042	<dl	<dl	<dl	<dl	8.E-4	0.003	6.24	0.042
2104ACCP-02.d	0.720	13.6	0.032	63.1	7.97	<dl	187	<dl	<dl	n.r.	0.780	<dl	0.220	4.40	166	0.017	0.049	<dl	<dl	<dl	<dl	0.001	3.E-4	7.59	0.058
2104ACCP-03.d	1.01	13.7	0.028	76.3	12.7	<dl	208	0.044	<dl	n.r.	0.390	<dl	0.123	4.47	193	0.020	0.270	<dl	<dl	<dl	<dl	7.E-4	4.E-4	8.25	0.058
2104ACCP-04.d	1.10	13.7	0.036	76.7	12.4	<dl	215	0.038	<dl	n.r.	0.250	0.013	0.021	4.11	198	0.007	0.063	<dl	<dl	<dl	<dl	9.E-4	4.E-4	4.84	0.053
2104ACCP-05.d	0.500	12.7	0.026	47.1	10.9	<dl	501	<dl	<dl	n.r.	1.00	<dl	0.330	4.24	153	0.017	0.055	<dl	<dl	<dl	<dl	0.002	0.003	1.56	0.119
2104ACCP-06.d	0.870	13.2	0.027	42.0	10.4	0.095	488	0.017	<dl	n.r.	0.533	<dl	0.310	4.10	145	0.035	0.053	<dl	<dl	<dl	<dl	7.E-4	2.E-4	1.02	0.071
2104BCCP-01d	0.250	11.0	0.050	56.8	4.80	<dl	793	<dl	<dl	n.r.	0.710	<dl	0.500	4.30	130	0.008	0.089	<dl	0.012	0.003	0.007	0.025	2.E-4	9.83	0.224
2104BCCP-02.d	0.228	10.1	0.043	33.1	5.61	<dl	754	<dl	<dl	n.r.	1.20	<dl	0.390	4.17	107	0.048	0.084	<dl	<dl	<dl	<dl	0.001	3.E-4	1.81	0.859
2104BCCP-03.d	0.810	11.8	0.036	78.2	10.7	1.46	223	<dl	<dl	n.r.	0.640	<dl	0.260	4.01	181	0.006	0.063	<dl	<dl	<dl	<dl	9.E-4	0.007	23.3	0.037
2104BCCP-04.d	0.195	11.6	0.220	59.9	11.1	<dl	232	<dl	<dl	n.r.	0.810	<dl	0.370	4.44	167	0.029	0.290	<dl	<dl	<dl	<dl	0.001	0.012	25.5	0.115
2104BCCP-05.d	0.930	13.8	0.028	60.9	10.5	<dl	223	<dl	<dl	n.r.	0.468	<dl	0.290	4.34	172	0.024	0.056	<dl	<dl	<dl	<dl	9.E-4	0.009	15.8	0.094

Grain ID	*Mn* 55	*Co* 59	*Ni* 60	*Zn* 66	*Ga* 71	As 75	*Se* 82	Mo 95	Ru 101	Rh 103	*Ag* 107	Pd 108	Cd 111	*In* 115	*Sn* 118	*Sb* 121	*Te* 128	Re 185	Os 189	Ir 193	Pt 195	*Au* 197	Tl 205	*Pb* 208	*Bi* 209
55um	0.470	0.023	0.241	0.353	0.028	0.223	2.53	0.030	0.023	0.005	0.023	0.014	0.046	0.012	0.073	0.022	0.256	0.009	0.021	0.007	0.013	0.010	0.004	0.012	0.007
33um	0.939	0.046	0.722	1.06	0.085	0.445	5.07	0.061	0.068	0.009	0.069	0.041	0.137	0.025	0.218	0.067	0.513	0.027	0.042	0.020	0.039	0.030	0.011	0.037	0.013
2104BCCP-06.d	0.720	13.1	0.030	43.1	10.6	<dl	221	<dl	<dl	n.r.	1.09	<dl	0.300	4.28	156	0.008	0.320	<dl	<dl	<dl	<dl	0.001	0.007	22.0	0.179
2104BCCP-07.d	0.770	10.9	0.035	77.2	5.56	<dl	744	<dl	<dl	n.r.	0.750	<dl	0.210	4.08	157	0.021	0.075	<dl	<dl	<dl	<dl	6.E-4	0.004	3.06	0.061
3237CCP-01d	10.0	0.010	0.130	318	0.220	<dl	239	<dl	<dl	n.r.	1.47	<dl	3.46	29.5	18.1	1.71	3.70	<dl	<dl	<dl	<dl	0.003	0.017	4.91	0.417
3237CCP-02.d	1.30	0.010	0.078	279	0.400	<dl	229	<dl	<dl	n.r.	3.02	<dl	3.29	29.1	10.7	0.760	7.40	<dl	<dl	<dl	<dl	0.002	0.008	0.990	0.111
3237CCP-03.d	0.417	0.006	0.081	345	0.320	<dl	297	<dl	<dl	n.r.	4.30	<dl	3.85	33.6	9.80	0.590	6.20	<dl	<dl	<dl	<dl	0.002	6.E-4	4.40	0.486
3237CCP-04.d	2.50	0.014	0.091	289	0.330	<dl	249	<dl	<dl	n.r.	2.20	<dl	4.50	43.9	5.50	2.08	2.20	<dl	<dl	<dl	<dl	0.003	0.009	5.40	0.770
3237CCP-05.d	1.18	0.007	0.071	400	0.360	<dl	226	<dl	<dl	n.r.	4.80	<dl	5.36	35.7	8.15	1.49	3.61	<dl	<dl	<dl	<dl	0.031	0.011	6.71	0.348
3237CCP-06.d	1.09	0.008	0.072	408	0.470	<dl	247	<dl	<dl	n.r.	7.37	<dl	4.78	34.7	12.8	1.59	5.70	<dl	<dl	<dl	<dl	0.002	0.019	14.1	1.00
3237CCP-07.d	0.551	0.500	0.103	587	0.880	<dl	250	<dl	<dl	n.r.	5.70	<dl	6.40	38.3	10.6	0.680	4.60	<dl	<dl	<dl	<dl	0.006	0.018	35.9	2.46
3241CCP-01d	0.132	0.847	0.019	7.67	0.149	<dl	57.0	<dl	<dl	n.r.	0.181	<dl	0.080	16.7	0.050	0.064	1.22	<dl	<dl	<dl	<dl	3.E-4	0.002	0.890	1.04
3241CCP-02.d	0.125	0.810	0.016	7.66	0.152	<dl	59.4	<dl	<dl	n.r.	0.096	<dl	0.052	17.4	0.083	0.079	0.860	<dl	<dl	<dl	<dl	3.E-4	0.009	0.497	0.318
3241CCP-03.d	0.124	1.07	0.017	9.15	0.123	<dl	71.0	<dl	0.030	n.r.	0.117	<dl	0.071	16.5	0.071	0.027	0.720	<dl	<dl	<dl	<dl	3.E-4	0.002	0.444	0.208
3241CCP-04.d	1.10	0.740	0.010	3.33	0.500	0.700	315	<dl	0.028	n.r.	0.403	<dl	0.017	7.69	0.030	0.124	0.400	<dl	<dl	<dl	<dl	0.006	1.E-4	0.864	1.19
3241CCP-05.d	0.178	0.690	0.041	180	0.130	<dl	87.0	<dl	<dl	n.r.	0.140	<dl	2.26	10.8	0.154	0.016	0.530	<dl	<dl	<dl	<dl	0.010	0.00	0.890	0.473
3241CCP-06.d	0.267	1.07	0.052	158	0.390	<dl	90.0	<dl	<dl	n.r.	0.123	<dl	2.88	12.5	0.330	0.003	0.078	<dl	<dl	<dl	<dl	7.E-4	1.E-4	1.19	0.650
3241CCP-07.d	0.232	1.37	0.029	164	0.300	<dl	52.2	<dl	<dl	n.r.	0.032	<dl	3.37	13.7	0.380	0.052	0.075	<dl	<dl	<dl	<dl	7.E-4	3.E-4	1.36	1.18
501CCP-01d	0.610	0.289	0.008	0.720	0.003	<dl	47.7	<dl	<dl	n.r.	1.08	<dl	0.009	7.36	0.088	0.003	0.280	<dl	<dl	<dl	<dl	4.E-4	0.001	1.25	0.322
501CCP-02.d	0.840	0.187	0.097	0.720	0.047	0.135	53.1	<dl	<dl	n.r.	5.11	<dl	0.029	2.40	0.052	0.286	0.500	<dl	<dl	<dl	<dl	4.E-4	0.008	24.3	1.20
501CCP-03.d	0.410	0.950	0.011	1.84	0.054	0.095	170	<dl	<dl	n.r.	1.58	<dl	0.033	2.25	0.209	0.031	0.416	<dl	<dl	<dl	<dl	4.E-4	3.E-4	1.84	0.052
501CCP-04.d	0.105	0.710	0.009	0.600	0.028	<dl	93.9	<dl	<dl	n.r.	1.53	0.038	0.007	4.28	0.165	0.059	0.320	<dl	<dl	<dl	<dl	7.E-4	2.E-4	3.53	0.217
501CCP-05.d	0.580	0.168	0.012	0.610	0.020	<dl	81.9	<dl	<dl	n.r.	1.49	<dl	0.036	5.00	0.211	0.059	0.400	<dl	<dl	<dl	<dl	6.E-4	3.E-4	2.29	0.219
501CCP-06.d	0.680	0.279	2.40	0.790	0.048	0.071	35.0	<dl	<dl	n.r.	2.23	<dl	0.019	3.33	0.095	0.060	0.491	<dl	<dl	<dl	<dl	5.E-4	2.E-4	3.60	0.164
651CCP-01d	0.540	1.28	0.024	6.93	0.189	<dl	23.8	<dl	<dl	n.r.	11.8	<dl	0.510	7.76	2.42	0.098	0.310	<dl	<dl	<dl	<dl	0.045	0.039	165	2.15
651CCP-02.d	0.120	1.19	0.012	2.70	0.209	<dl	29.9	<dl	<dl	n.r.	8.03	<dl	0.020	7.37	2.38	0.041	0.830	<dl	<dl	<dl	<dl	0.021	0.003	1.19	0.744
651CCP-03.d	1.46	1.52	0.040	8.75	0.126	<dl	26.5	<dl	<dl	n.r.	7.57	<dl	0.680	7.20	2.53	0.056	0.970	<dl	<dl	<dl	<dl	0.029	0.035	161	1.71
651CCP-04.d	0.151	1.09	0.025	5.90	0.249	<dl	30.0	<dl	<dl	n.r.	4.61	<dl	0.270	7.05	2.31	0.054	0.820	<dl	<dl	<dl	<dl	0.068	0.003	1.71	0.584
651CCP-05.d	0.141	1.14	0.020	5.23	0.284	<dl	32.6	<dl	0.033	n.r.	6.15	<dl	0.149	7.52	3.24	0.047	1.30	<dl	<dl	<dl	<dl	0.021	0.006	4.77	0.461
651CCP-06.d	0.186	1.18	0.028	5.15	0.275	<dl	26.8	<dl	0.041	n.r.	5.90	<dl	0.225	7.45	2.47	0.034	1.30	<dl	<dl	<dl	<dl	0.053	0.003	1.84	0.535
651CCP-06BIS.d	0.190	1.14	0.030	8.70	0.291	<dl	25.4	<dl	<dl	n.r.	4.95	<dl	0.230	7.81	2.46	0.008	0.880	<dl	<dl	<dl	<dl	0.067	0.016	11.4	0.668
651CCP-07.d	0.147	0.940	0.021	3.11	0.195	<dl	22.2	<dl	<dl	n.r.	11.2	<dl	0.190	7.68	2.36	0.130	1.75	<dl	<dl	<dl	<dl	1.E-3	0.013	26.7	0.855
90667CCP-01d	0.780	0.410	0.350	28.9	0.065	0.137	391	<dl	<dl	n.r.	115	0.423	2.02	7.67	0.340	1.90	0.075	0.023	0.032	<dl	<dl	0.075	0.005	12.4	0.187
90667CCP-04.d	0.189	0.139	0.017	46.0	0.110	0.130	386	<dl	<dl	n.r.	91.0	0.940	1.10	9.51	0.340	1.33	0.056	<dl	<dl	<dl	<dl	0.043	8.E-4	2.61	0.104
90667CCP-05.d	0.950	0.115	0.600	55.7	0.129	0.260	407	<dl	<dl	n.r.	107	<dl	2.32	10.6	0.335	1.48	0.300	<dl	<dl	<dl	<dl	0.038	0.001	9.62	0.112
90667CCP-06.d	0.950	0.125	0.028	186	0.111	0.320	443	<dl	0.490	n.r.	93.2	<dl	7.30	9.16	0.148	0.890	0.072	<dl	<dl	<dl	0.010	0.007	0.024	4.47	0.096
90667CCP-07.d	0.186	0.260	1.60	66.0	0.123	<dl	410	<dl	0.090	n.r.	97.3	<dl	3.56	11.5	0.367	1.44	0.390	<dl	<dl	<dl	0.800	0.016	0.003	6.74	0.097
ALT08CCP-003.c	13.5	2.76	56.0	81.0	4.79	0.670	167	<dl	<dl	n.r.	10.6	<dl	0.247	2.06	19.3	0.101	0.350	0.041	<dl	0.130	0.440	0.021	0.009	20.3	1.37
ALT08CCP-004.c	0.900	2.52	0.014	32.0	4.23	0.420	167	<dl	<dl	n.r.	8.75	<dl	0.080	1.80	19.7	0.058	0.330	0.025	<dl	<dl	<dl	0.130	2.E-4	0.840	0.900
ALT08CCP-005.c	1.67	3.60	45.0	56.0	4.06	0.500	181	0.058	<dl	n.r.	8.20	<dl	0.360	1.96	21.1	0.067	0.390	<dl	<dl	<dl	0.039	0.120	3.E-4	0.740	0.190
ALT08CCP-006.c	1.76	2.62	0.019	41.8	4.20	<dl	160	<dl	<dl	n.r.	8.31	<dl	0.082	1.91	18.3	0.069	0.400	<dl	0.250	<dl	<dl	0.002	0.140	2.60	0.910
ALT4CCP-01d	3.40	0.084	11.0	17.0	1.85	<dl	128	2.00	<dl	n.r.	3.64	<dl	0.039	1.52	5.79	0.490	0.050	<dl	<dl	<dl	<dl	0.002	7.E-4	1.59	0.332
ALT4CCP-02.d	0.138	0.090	0.009	12.9	1.52	0.510	161	<dl	<dl	n.r.	2.30	<dl	0.025	1.82	7.00	0.046	0.030	<dl	<dl	<dl	<dl	0.140	1.E-4	0.119	0.085
ALT4CCP-03.d	3.00	0.061	0.020	11.9	1.63	0.320	162	<dl	0.080	n.r.	3.81	<dl	0.031	1.74	4.54	0.090	0.042	<dl	<dl	<dl	<dl	0.037	3.E-4	0.430	0.440
ALT4CCP-04.d	1.70	0.145	0.019	6.10	1.30	1.12	156	0.140	<dl	n.r.	8.06	<dl	0.031	1.72	3.58	0.199	0.420	<dl	<dl	<dl	0.053	0.120	6.E-4	2.36	1.05
ALT4CCP-05.d	0.271	1.10	0.770	14.9	1.61	<dl	158	<dl	<dl	n.r.	2.97	<dl	0.035	5.77	5.38	0.046	0.052	0.220	<dl	0.040	<dl	0.002	3.E-4	0.740	0.320
BU7101CCP-01d	2.50	0.310	0.260	280	0.890	<dl	112	<dl	<dl	n.r.	26.6	<dl	2.92	5.59	33.2	0.010	1.98	<dl	<dl	<dl	<dl	0.001	4.E-4	2.28	1.18
BU7101CCP-03.d	2.04	0.243	0.047	293	0.530	<dl	95.0	<dl	0.023	n.r.	5.20	<dl	2.27	5.62	28.3	0.029	1.75	<dl	<dl	<dl	<dl	8.E-4	4.E-4	7.93	1.06
BU7101CCP-05.d	1.92	0.240	0.028	343	0.530	3.56	96.7	0.064	<dl	n.r.	11.2	<dl	1.88	5.74	17.3	7.50	2.20	<dl	<dl	<dl	<dl	0.001	0.024	16.0	1.33

Grain ID	*Mn* 55	*Co* 59	*Ni* 60	*Zn* 66	*Ga* 71	As 75	*Se* 82	Mo 95	Ru 101	Rh 103	*Ag* 107	Pd 108	Cd 111	*In* 115	*Sn* 118	*Sb* 121	*Te* 128	Re 185	Os 189	Ir 193	Pt 195	*Au* 197	Tl 205	*Pb* 208	*Bi* 209
55um	0.470	0.023	0.241	0.353	0.028	0.223	2.53	0.030	0.023	0.005	0.023	0.014	0.046	0.012	0.073	0.022	0.256	0.009	0.021	0.007	0.013	0.010	0.004	0.012	0.007
33um	0.939	0.046	0.722	1.06	0.085	0.445	5.07	0.061	0.068	0.009	0.069	0.041	0.137	0.025	0.218	0.067	0.513	0.027	0.042	0.020	0.039	0.030	0.011	0.037	0.013
BU7101CCP-06.d	1.79	0.120	0.035	132	0.590	0.240	92.4	0.032	<dl	n.r.	14.9	<dl	0.600	5.33	24.6	0.510	1.48	<dl	<dl	<dl	<dl	0.002	0.011	26.0	1.64
DB0004CCP-01d	0.700	0.101	0.015	0.620	0.064	<dl	145	<dl	<dl	n.r.	3.20	<dl	0.030	11.8	0.210	0.031	0.036	<dl	<dl	<dl	<dl	8.E-4	0.086	6.74	0.846
DB0004CCP-03.(	1.29	0.386	0.200	19.8	0.083	<dl	145	<dl	<dl	n.r.	13.3	1.28	0.173	9.03	0.123	0.059	6.60	<dl	<dl	0.004	0.290	9.E-4	0.149	42.2	1.01
DB0004CCP-04.(	0.460	0.177	0.014	0.880	0.043	<dl	78.6	<dl	<dl	n.r.	6.64	<dl	0.013	7.67	0.027	0.032	0.340	<dl	<dl	<dl	<dl	0.030	0.007	7.32	1.06
DB0004CCP-05.(	0.990	0.255	0.023	9.89	0.060	<dl	163	<dl	<dl	n.r.	9.43	<dl	0.042	9.69	0.070	0.075	0.360	<dl	<dl	<dl	<dl	0.001	0.258	41.6	1.84
DB0004CCP-06.(	1.57	1.36	0.025	21.3	0.084	<dl	98.5	<dl	<dl	n.r.	17.7	<dl	0.286	8.90	1.38	0.141	0.311	<dl	<dl	<dl	<dl	6.E-4	0.107	133	0.797
DB0004CCP-07.(	0.950	0.244	0.700	10.6	0.080	<dl	163	<dl	<dl	n.r.	7.12	<dl	0.100	11.6	0.167	0.066	0.200	<dl	<dl	<dl	0.012	6.E-4	0.166	30.7	0.520
GC06200CCP-02	0.660	2.89	120	214	0.132	0.370	217	<dl	<dl	n.r.	72.4	<dl	2.08	0.632	0.190	0.021	0.850	<dl	<dl	0.033	<dl	0.009	0.044	1.19	0.679
GC06200CCP-03	0.500	2.35	2.00	199	0.347	0.170	217	1.10	<dl	n.r.	25.1	<dl	2.09	2.38	3.90	0.187	0.660	<dl	<dl	<dl	<dl	0.009	0.021	1.81	1.29
GC06200CCP-05	4.00	2.03	0.560	223	0.287	0.140	178	1.50	<dl	n.r.	24.9	<dl	1.95	0.386	0.043	0.106	0.440	<dl	0.090	<dl	<dl	0.002	0.070	1.67	1.21
GC06200CCP-06	0.481	1.50	2.20	78.0	0.111	<dl	182	<dl	<dl	n.r.	18.7	<dl	0.467	0.530	0.120	0.190	0.600	0.019	0.430	<dl	<dl	0.001	0.017	1.25	0.067
JC7CCP-01d	2.00	7.00	48.0	746	1.16	4.90	154	<dl	<dl	n.r.	18.6	<dl	10.9	12.8	14.7	0.198	3.80	<dl	<dl	<dl	<dl	0.002	0.022	10.1	4.00
JC7CCP-02.d	2.17	1.01	70.0	836	0.480	0.280	25.2	<dl	<dl	n.r.	9.85	<dl	12.3	12.9	24.1	0.240	1.32	<dl	<dl	<dl	<dl	0.002	0.014	213	3.20
JC7CCP-03.d	3.69	3.80	44.0	624	0.540	<dl	37.5	<dl	0.108	n.r.	9.60	<dl	9.00	18.1	41.5	0.230	2.43	0.440	<dl	<dl	<dl	0.002	0.002	175	3.78
JC7CCP-04.d	0.358	0.147	0.071	481	0.029	<dl	42.6	<dl	<dl	n.r.	8.80	<dl	7.90	13.7	6.10	0.106	1.06	0.090	<dl	<dl	<dl	0.001	5.E-4	1.01	0.850
JC7CCP-05.d	2.00	13.0	0.490	553	2.51	<dl	20.6	<dl	<dl	n.r.	25.3	<dl	7.70	10.6	17.7	0.023	26.2	<dl	<dl	<dl	0.020	0.004	0.006	18.1	42.5
JC7CCP-06.d	1.73	0.640	41.0	421	0.050	0.600	71.0	<dl	<dl	n.r.	10.9	<dl	9.60	9.77	6.80	0.310	2.29	<dl	<dl	<dl	<dl	0.002	5.E-4	2.90	1.68
JC7CCP-07.d	3.90	0.680	0.077	710	0.035	<dl	56.0	<dl	<dl	n.r.	13.5	<dl	9.30	9.47	5.40	0.170	5.20	<dl	<dl	<dl	0.023	0.003	4.E-4	1.23	4.70
JC7CCP-08.d	1.31	4.50	0.065	543	0.610	0.490	64.2	<dl	<dl	n.r.	11.7	<dl	8.90	12.9	10.1	0.400	1.67	<dl	<dl	<dl	<dl	0.015	7.E-4	2.60	1.40
NAF3CCP-01d	1.63	0.147	0.101	1.19	0.350	<dl	98.8	0.250	0.013	n.r.	17.0	0.632	0.710	5.59	1.06	1.00	0.027	<dl	<dl	<dl	<dl	0.008	0.020	13.1	0.219
NAF3CCP-02.d	0.870	0.160	0.073	1.41	0.700	1.23	103	<dl	<dl	n.r.	21.8	<dl	0.910	4.83	0.242	0.624	0.038	<dl	<dl	0.038	<dl	0.013	0.006	25.3	1.35
NAF3CCP-03.d	1.12	0.310	0.112	1.36	0.180	0.980	86.2	<dl	0.012	n.r.	19.4	0.015	0.012	4.80	0.042	0.900	0.042	<dl	<dl	0.100	<dl	0.001	0.002	11.2	1.11
NAF3CCP-04.d	4.57	0.510	0.190	0.970	0.513	0.780	111	0.017	0.022	n.r.	23.7	0.374	0.320	5.05	4.44	0.890	1.19	0.027	<dl	<dl	<dl	0.028	0.028	433	1.32
NAF3CCP-05.d	1.61	0.293	0.270	0.790	0.390	0.520	95.4	<dl	<dl	n.r.	25.8	0.041	0.211	4.68	0.650	0.730	0.043	<dl	<dl	<dl	0.280	2.50	0.002	22.6	1.64
NAF3CCP-06.d	0.830	0.177	0.510	1.16	0.380	0.540	103	<dl	0.029	n.r.	16.5	0.187	0.350	5.31	0.480	0.550	0.043	<dl	<dl	<dl	<dl	0.260	0.007	13.0	0.980
NAF3CCP-07.d	1.43	0.186	0.052	0.730	0.364	0.260	99.1	0.041	0.030	n.r.	10.9	0.249	0.300	5.25	0.698	0.177	0.540	<dl	<dl	<dl	<dl	0.460	0.003	11.6	0.730
NAF45CCP-01d	2.80	0.323	0.740	1.53	0.480	1.08	46.0	<dl	<dl	n.r.	11.9	0.363	0.055	4.05	1.44	0.291	0.051	<dl	<dl	<dl	<dl	0.009	0.058	35.7	0.302
NAF45CCP-02.d	0.720	0.339	0.099	0.900	0.500	0.910	45.7	<dl	<dl	n.r.	21.1	<dl	5.20	3.12	2.19	0.454	0.081	<dl	<dl	0.036	<dl	0.001	0.032	23.9	0.447
NAF45CCP-03.d	1.33	0.359	60.0	3.14	0.475	0.510	49.6	<dl	<dl	n.r.	9.08	8.93	0.290	2.76	6.34	0.004	0.430	0.310	<dl	0.038	<dl	0.001	0.017	81.4	0.700
NAF45CCP-04.d	1.09	0.268	60.0	1.08	0.022	0.370	47.0	<dl	<dl	n.r.	14.2	0.539	0.113	3.60	0.790	0.003	0.052	<dl	<dl	<dl	<dl	1.E-3	0.008	19.8	0.260
NAF45CCP-05.d	1.40	0.330	11.0	1.05	0.113	0.350	40.2	<dl	<dl	n.r.	10.5	<dl	0.022	3.16	1.76	0.239	0.027	<dl	<dl	<dl	<dl	0.001	7.E-4	5.79	0.288
NAF45CCP-06.d	7.80	0.525	6.00	1.88	0.283	0.270	47.8	<dl	<dl	n.r.	6.01	0.215	0.700	3.39	3.91	0.300	0.250	<dl	<dl	<dl	<dl	8.E-4	0.035	92.4	0.157
NAF45CCP-07.d	1.54	0.438	8.00	4.93	0.318	0.280	46.6	<dl	<dl	n.r.	10.8	<dl	1.81	3.11	0.990	0.160	0.070	0.140	<dl	<dl	<dl	0.002	0.072	37.2	1.90
OYUCCP-001d	2.70	2.10	0.060	2.20	0.510	4.62	684	0.440	<dl	n.r.	20.6	<dl	0.980	1.34	0.071	3.24	0.450	<dl	<dl	0.030	<dl	0.055	1.20	21.6	2.41
OYUCCP-002.d	1.64	0.700	0.052	0.944	0.081	1.84	772	<dl	<dl	n.r.	7.38	<dl	0.340	1.67	0.170	0.410	0.780	<dl	<dl	<dl	<dl	0.002	9.E-4	2.13	0.474
OYUCCP-003.d	2.20	0.600	9.00	1.11	0.480	1.85	713	<dl	<dl	n.r.	9.80	<dl	0.350	1.89	0.070	1.14	0.087	0.016	<dl	<dl	<dl	0.006	0.029	15.9	2.20
OYUCCP-004.d	1.32	0.195	0.033	3.20	0.750	5.20	878	0.042	<dl	n.r.	30.5	<dl	0.430	2.70	1.17	2.20	1.14	<dl	<dl	<dl	<dl	0.150	0.025	19.1	1.98
OYUCCP-005.d	1.45	4.70	3.10	8.00	0.750	4.30	836	<dl	<dl	n.r.	18.2	<dl	0.280	2.76	0.289	2.52	0.440	0.500	<dl	<dl	<dl	0.046	0.043	12.3	1.50
OYUCCP-006.d	1.16	0.640	35.0	3.00	0.009	5.30	612	<dl	<dl	n.r.	21.4	0.136	1.20	1.10	0.074	4.19	0.570	<dl	<dl	<dl	<dl	0.052	0.011	26.1	2.50
Reef-type PGE																									
2938CCP-01d	2.46	0.120	14.9	622	0.540	<dl	114	<dl	0.022	n.r.	1.96	<dl	12.3	1.43	2.79	0.009	0.045	<dl	<dl	0.370	<dl	0.033	5.E-4	93.9	0.022
2938CCP-03.d	1.00	0.190	14.9	492	0.372	<dl	123	2.90	<dl	n.r.	2.61	<dl	11.3	1.99	2.63	0.009	0.139	<dl	<dl	<dl	<dl	5.E-4	1.10	4.48	0.019
2938CCP-04.d	1.80	0.360	13.3	715	0.690	<dl	127	0.200	0.500	n.r.	4.64	<dl	13.5	1.47	5.05	0.049	0.059	0.005	<dl	<dl	<dl	6.E-4	0.001	196	0.018
2938CCP-05.d	1.86	0.800	18.1	555	0.630	<dl	126	0.090	0.038	n.r.	4.97	<dl	12.8	1.52	4.67	0.068	0.050	0.007	<dl	<dl	<dl	0.012	0.045	125	0.005
2938CCP-06.d	1.43	0.210	10.5	731	0.370	<dl	129	<dl	0.025	n.r.	6.18	<dl	12.5	4.18	3.53	0.011	0.041	<dl	<dl	<dl	0.011	0.026	0.001	162	0.012
2938CCP-07.d	1.86	0.055	14.1	513	0.232	0.141	130	<dl	0.045	n.r.	8.16	<dl	9.89	1.39	2.93	0.013	0.057	<dl	<dl	0.012	<dl	0.005	8.E-4	43.0	0.080
2938CCPr-01d	0.627	0.039	22.7	356	0.740	<dl	106	<dl	<dl	n.r.	2.00	<dl	12.1	1.20	2.92	0.016	0.082	<dl	<dl	<dl	<dl	0.002	0.002	165	0.070

Grain ID	*Mn* 55	*Co* 59	*Ni* 60	*Zn* 66	*Ga* 71	As 75	*Se* 82	Mo 95	Ru 101	Rh 103	*Ag* 107	Pd 108	Cd 111	*In* 115	*Sn* 118	*Sb* 121	*Te* 128	Re 185	Os 189	Ir 193	Pt 195	*Au* 197	Tl 205	*Pb* 208	*Bi* 209
55um	0.470	0.023	0.241	0.353	0.028	0.223	2.53	0.030	0.023	0.005	0.023	0.014	0.046	0.012	0.073	0.022	0.256	0.009	0.021	0.007	0.013	0.010	0.004	0.012	0.007
33um	0.939	0.046	0.722	1.06	0.085	0.445	5.07	0.061	0.068	0.009	0.069	0.041	0.137	0.025	0.218	0.067	0.513	0.027	0.042	0.020	0.039	0.030	0.011	0.037	0.013
2938CCPr-02.d	0.526	0.071	16.7	470	0.400	0.640	149	<dl	<dl	n.r.	3.53	<dl	14.7	2.19	5.26	0.010	0.064	<dl	<dl	<dl	<dl	0.002	0.002	34.4	0.020
2938CCPr-03.d	1.66	0.066	12.1	449	0.410	<dl	133	<dl	<dl	n.r.	1.98	<dl	11.4	2.75	3.17	0.007	0.053	<dl	<dl	<dl	<dl	0.002	7.E-4	3.47	0.006
2938CCPr-04.d	0.279	0.035	14.1	325	0.590	<dl	157	<dl	<dl	n.r.	4.43	<dl	12.8	1.73	5.81	0.023	0.094	<dl	<dl	<dl	<dl	0.002	0.003	244	0.022
2938CCPr-05.d	0.458	0.054	13.3	515	0.510	0.240	143	<dl	0.145	n.r.	5.12	<dl	13.4	1.76	4.00	0.009	0.075	<dl	<dl	<dl	<dl	0.001	0.002	77.1	0.019
2938CCPr-06.d	1.75	0.006	14.8	543	0.460	<dl	160	<dl	<dl	n.r.	5.32	<dl	13.9	1.25	4.21	0.013	0.087	<dl	<dl	<dl	<dl	0.002	0.002	126	0.019
CGMACCPr-01d	1.80	0.047	14.5	373	0.096	<dl	112	<dl	0.149	n.r.	2.73	<dl	2.90	1.55	0.029	0.007	0.051	<dl	<dl	<dl	<dl	6.E-4	7.E-4	8.32	0.020
CGMACCPr-02.c	0.203	0.068	19.7	235	0.015	0.330	139	<dl	0.210	n.r.	2.61	<dl	3.25	1.12	0.210	0.007	0.085	<dl	<dl	0.060	0.079	0.001	0.001	9.46	0.009
CGMACCPr-03.c	10.8	0.190	37.6	203	0.160	<dl	112	<dl	0.110	n.r.	2.20	<dl	5.80	4.76	0.047	0.011	0.093	<dl	<dl	<dl	<dl	0.001	0.035	7.89	0.046
CGMBCCP-01d	1.67	0.060	15.3	284	0.026	<dl	90.1	<dl	<dl	n.r.	1.54	<dl	4.59	1.54	0.029	0.003	0.044	<dl	<dl	<dl	0.011	0.001	7.E-4	5.28	0.005
CGMBCCP-03.d	1.05	0.056	15.2	236	0.009	<dl	95.3	<dl	<dl	n.r.	1.80	<dl	3.85	1.87	0.035	0.004	0.049	<dl	<dl	<dl	<dl	0.001	6.E-4	2.66	0.004
CGMBCCP-05.d	1.74	0.046	16.7	246	0.051	<dl	103	<dl	<dl	n.r.	1.43	<dl	4.26	1.57	0.065	0.003	0.043	<dl	<dl	<dl	<dl	5.E-4	0.013	4.30	0.008
F10304CCP-01d	0.403	0.019	2.50	408	0.083	<dl	205	<dl	<dl	n.r.	5.13	<dl	8.51	0.309	0.069	0.002	0.310	<dl	<dl	0.007	<dl	6.E-4	0.003	2.14	0.039
F10304CCP-02.d	2.02	0.090	0.710	548	0.019	<dl	206	0.410	0.078	n.r.	3.70	<dl	14.6	0.378	0.037	0.003	2.10	<dl	<dl	<dl	<dl	0.004	3.E-4	1.33	0.020
F10304CCP-03.d	15.0	0.033	0.211	600	0.131	<dl	198	<dl	<dl	n.r.	2.17	<dl	12.9	0.235	0.064	0.008	4.90	<dl	<dl	<dl	<dl	0.008	4.E-4	1.49	0.290
F10304CCP-04.d	1.08	0.024	1.27	393	0.066	<dl	173	<dl	0.500	n.r.	1.76	<dl	11.6	0.472	0.160	0.002	2.70	<dl	<dl	<dl	<dl	9.E-4	2.E-4	1.86	0.230
F10304CCP-06.d	1.21	0.024	0.197	408	0.014	<dl	161	<dl	<dl	n.r.	3.81	<dl	13.2	0.411	0.187	0.001	1.52	<dl	<dl	<dl	<dl	0.002	3.E-4	1.23	0.049
F10304CCP-07.d	1.21	0.250	0.197	458	0.029	<dl	176	<dl	<dl	n.r.	3.98	<dl	13.3	0.328	0.294	0.029	1.99	<dl	<dl	<dl	<dl	0.003	4.E-4	1.49	0.029
FI0304CCP-01d	0.267	0.005	0.720	315	0.079	<dl	225	<dl	0.134	n.r.	4.15	<dl	9.26	0.260	0.028	0.003	0.770	<dl	<dl	<dl	<dl	8.E-4	3.E-4	1.26	0.004
FI0304CCP-02.d	2.20	0.024	0.730	288	0.092	<dl	145	<dl	<dl	n.r.	4.53	<dl	12.0	0.283	0.035	0.004	0.720	<dl	<dl	<dl	<dl	8.E-4	4.E-4	0.680	0.005
FI0304CCP-03.d	10.5	0.210	8.90	300	0.120	<dl	226	<dl	0.090	n.r.	3.06	<dl	8.20	0.277	0.032	0.007	0.077	<dl	<dl	<dl	<dl	0.001	0.022	1.70	0.006
FI0304CCP-04.d	0.252	0.005	0.580	300	0.007	<dl	178	<dl	0.170	n.r.	3.36	<dl	12.5	0.468	0.390	0.002	2.21	<dl	<dl	<dl	<dl	8.E-4	3.E-4	0.920	0.085
FI0304CCP-05.d	0.423	0.008	2.76	308	0.107	<dl	179	<dl	0.340	n.r.	3.44	<dl	11.5	0.343	0.300	0.003	1.31	<dl	<dl	<dl	<dl	9.E-4	4.E-4	1.45	0.050
FI0304CCP-06.d	0.900	0.008	1.82	318	0.200	<dl	193	<dl	<dl	n.r.	1.81	<dl	13.8	0.439	0.047	0.052	0.520	<dl	<dl	<dl	<dl	0.001	8.E-4	4.13	0.009
GCMACCP-01d	11.2	0.030	22.9	223	0.100	<dl	113	0.023	0.039	n.r.	1.37	<dl	3.08	2.53	0.069	0.009	0.052	<dl	<dl	<dl	<dl	1.70	0.009	4.19	0.250
GCMACCP-02.d	14.0	0.180	24.6	273	0.044	<dl	103	0.048	<dl	n.r.	1.70	<dl	3.72	2.62	0.074	0.006	0.034	<dl	<dl	<dl	0.071	0.600	0.008	6.23	0.029
GCMACCP-03.d	12.0	0.062	21.6	284	0.240	3.70	114	0.055	0.012	n.r.	1.61	<dl	3.58	2.62	0.040	0.007	0.037	<dl	<dl	<dl	0.008	0.011	0.003	6.25	0.008
GCMACCP-04.d	5.20	0.107	14.4	355	0.040	0.340	121	<dl	<dl	n.r.	2.67	<dl	3.86	2.01	0.023	0.200	0.036	0.049	<dl	<dl	<dl	5.E-4	0.004	4.43	0.045
GCMACCP-05.d	5.20	0.150	20.9	411	0.062	0.170	113	<dl	<dl	n.r.	2.71	<dl	3.74	2.61	0.072	0.006	0.045	<dl	<dl	0.018	<dl	0.039	0.018	8.62	0.003
GCMACCP-06.d	1.16	0.097	14.8	237	0.017	<dl	180	<dl	<dl	n.r.	3.15	<dl	1.75	1.20	0.140	0.028	0.031	0.190	0.018	<dl	0.060	5.E-4	0.022	20.2	0.025
GCMBCCP-01d	3.40	0.080	23.9	452	0.060	<dl	96.7	0.032	0.015	n.r.	1.94	<dl	4.81	2.11	0.030	0.006	0.055	<dl	<dl	<dl	0.009	5.E-4	0.014	11.2	0.038
GCMBCCP-02.d	11.0	0.079	20.7	307	0.012	0.340	93.7	1.10	<dl	n.r.	1.66	<dl	3.53	1.88	0.027	0.009	0.040	<dl	<dl	0.039	<dl	4.E-4	0.009	4.98	0.011
GCMBCCP-03.d	2.90	0.112	32.0	253	0.048	0.340	87.9	1.80	<dl	n.r.	3.10	<dl	3.08	1.74	0.033	0.060	0.098	<dl	<dl	<dl	0.031	0.001	3.E-4	2.38	0.022
GCMBCCP-04.d	1.09	0.109	25.2	389	0.013	<dl	79.1	<dl	<dl	n.r.	1.88	<dl	4.34	1.87	0.140	0.004	0.024	0.014	<dl	0.025	<dl	0.001	0.004	3.57	0.004
GCMBCCP-05.d	0.660	0.059	19.6	399	0.061	<dl	91.4	0.033	0.031	n.r.	1.93	<dl	4.10	2.67	0.037	0.019	0.033	<dl	<dl	<dl	0.046	0.170	6.E-4	1.66	0.007
GD10CCP-01d	1.19	0.071	29.3	621	0.055	<dl	148	<dl	<dl	n.r.	3.94	<dl	43.3	1.17	0.890	0.003	0.780	0.040	<dl	<dl	0.320	0.009	0.003	0.549	0.480
GD10CCP-02.d	1.42	0.123	27.5	622	0.140	0.092	140	<dl	<dl	n.r.	4.48	<dl	42.4	1.12	0.980	2.30	0.037	<dl	<dl	0.007	<dl	0.001	2.E-4	0.492	0.700
GD10CCP-03.d	2.10	0.290	38.5	588	0.335	<dl	128	0.018	0.017	n.r.	2.54	<dl	27.9	1.30	6.20	0.007	0.045	<dl	<dl	0.060	<dl	0.200	0.003	2.67	0.777
GD10CCP-04.d	1.61	0.146	37.8	651	0.230	0.170	128	0.019	0.049	n.r.	3.80	<dl	28.5	1.73	6.90	0.003	0.190	0.006	<dl	<dl	0.021	0.160	0.008	0.770	0.222
GD10CCP-05.d	0.990	0.242	66.0	703	0.327	0.180	132	<dl	0.016	n.r.	4.08	<dl	28.6	1.82	5.64	0.004	0.031	0.014	<dl	0.007	<dl	0.012	0.007	2.15	0.388
GD10CCP-06.d	1.08	0.450	39.2	637	0.050	<dl	134	0.021	0.016	n.r.	3.75	<dl	39.0	4.30	2.81	0.017	1.81	0.330	<dl	0.007	<dl	0.180	0.003	0.790	4.50
GD10CCP-07.d	1.54	1.00	44.5	571	0.082	<dl	144	<dl	<dl	n.r.	3.24	<dl	43.4	4.30	3.43	0.016	1.71	0.070	<dl	<dl	0.029	0.124	0.014	0.620	2.60
GD10CCPr-01d	0.493	0.062	28.3	589	0.140	<dl	174	<dl	<dl	n.r.	3.24	<dl	44.0	1.08	0.780	0.007	0.104	<dl	<dl	<dl	<dl	0.002	7.E-4	2.35	0.890
GD10CCPr-02.d	0.460	0.130	26.1	546	0.117	<dl	176	<dl	0.100	n.r.	4.46	<dl	49.1	1.22	1.21	0.004	0.560	<dl	<dl	<dl	0.310	0.002	4.E-4	0.800	0.620
GD10CCPr-03.d	0.223	0.030	36.2	554	0.330	<dl	180	<dl	<dl	n.r.	2.74	<dl	34.7	1.65	9.60	0.007	0.098	<dl	<dl	<dl	0.220	0.002	5.E-4	1.04	0.400
GD10CCPr-04.d	0.500	0.280	49.3	660	0.210	0.850	177	0.120	1.20	n.r.	2.29	<dl	32.9	1.28	7.10	0.076	0.078	0.470	0.130	0.900	0.350	0.002	0.025	1.59	0.460
GD10CCPr-05.d	0.459	0.184	31.1	740	0.145	<dl	148	<dl	0.120	n.r.	3.82	<dl	32.3	1.61	6.81	0.006	0.074	<dl	<dl	<dl	<dl	0.002	5.E-4	1.28	0.341
GD10CCPr-06.d	0.234	0.440	48.8	583	0.017	<dl	189	<dl	<dl	n.r.	3.04	<dl	43.9	4.56	4.55	0.006	1.69	<dl	<dl	<dl	<dl	0.048	5.E-4	0.890	2.30

Grain ID	*Mn* 55	*Co* 59	*Ni* 60	*Zn* 66	*Ga* 71	As 75	*Se* 82	Mo 95	Ru 101	Rh 103	*Ag* 107	Pd 108	Cd 111	*In* 115	*Sn* 118	*Sb* 121	*Te* 128	Re 185	Os 189	Ir 193	Pt 195	*Au* 197	Tl 205	*Pb* 208	*Bi* 209
55um	0.470	0.023	0.241	0.353	0.028	0.223	2.53	0.030	0.023	0.005	0.023	0.014	0.046	0.012	0.073	0.022	0.256	0.009	0.021	0.007	0.013	0.010	0.004	0.012	0.007
33um	0.939	0.046	0.722	1.06	0.085	0.445	5.07	0.061	0.068	0.009	0.069	0.041	0.137	0.025	0.218	0.067	0.513	0.027	0.042	0.020	0.039	0.030	0.011	0.037	0.013
GD10CCPr-07.d	1.20	0.187	31.2	780	0.022	<dl	18.1	<dl	0.090	n.r.	3.56	<dl	43.4	5.53	4.11	0.007	1.24	<dl	<dl	<dl	<dl	0.003	4.E-4	0.920	1.35
GDN4CCP-01.d	0.241	1.80	23.6	561	0.270	<dl	10.4	<dl	0.016	n.r.	0.160	<dl	12.7	1.32	2.82	0.003	0.780	<dl	0.100	0.021	0.010	0.051	1.E-4	1.51	0.072
GDN4CCP-02.d	1.26	0.053	30.4	429	0.140	<dl	10.3	<dl	<dl	n.r.	1.04	<dl	14.5	3.59	2.36	0.008	0.440	<dl	<dl	<dl	0.016	0.002	8.E-4	1.36	0.048
GDN4CCP-03.d	1.28	1.20	30.4	523	0.407	<dl	10.5	<dl	0.045	n.r.	0.571	<dl	10.8	0.732	9.62	0.003	0.910	<dl	<dl	<dl	0.380	5.E-4	1.E-4	0.750	0.053
GDN4CCP-04.d	14.8	0.330	32.3	472	0.250	<dl	10.6	0.120	<dl	n.r.	0.890	<dl	10.2	0.616	3.09	0.006	0.700	1.60	0.050	0.036	<dl	0.021	3.E-4	1.11	0.092
GDN4CCP-05.d	1.35	0.104	30.4	710	0.510	0.420	96.5	0.056	0.044	n.r.	0.576	<dl	20.7	0.958	23.3	0.007	1.27	<dl	<dl	<dl	<dl	0.016	0.003	0.896	0.043
GDN4CCP-06.d	1.23	0.038	21.3	710	0.370	<dl	10.2	0.014	0.012	n.r.	0.920	<dl	48.4	2.09	9.52	0.014	0.650	<dl	<dl	<dl	<dl	0.060	2.E-4	0.960	0.144
GDN4CCPr-01d	0.570	0.044	27.3	580	0.197	<dl	10.4	<dl	0.047	n.r.	0.454	<dl	11.5	0.532	2.78	0.002	0.730	<dl	<dl	<dl	<dl	7.E-4	3.E-4	1.85	0.149
GDN4CCPr-02.d	0.820	0.073	26.5	329	0.061	<dl	10.9	<dl	<dl	n.r.	0.530	<dl	11.8	0.627	0.950	0.003	0.056	<dl	<dl	<dl	0.020	9.E-4	3.E-4	1.69	0.086
GDN4CCPr-04.d	54.0	0.072	29.5	465	0.086	<dl	11.5	<dl	<dl	n.r.	0.500	<dl	9.60	0.490	0.600	0.005	0.710	<dl	<dl	<dl	<dl	0.001	0.001	4.90	0.920
M1CCP-01d	1.37	0.054	18.6	376	0.075	<dl	91.5	<dl	0.061	n.r.	3.17	<dl	6.05	2.93	0.029	0.005	0.039	0.016	<dl	<dl	<dl	0.001	0.020	8.37	0.017
M1CCP-02.d	1.66	0.111	24.3	401	0.073	0.270	77.9	0.020	0.037	n.r.	4.30	<dl	8.45	2.08	0.140	0.160	0.029	0.037	<dl	0.440	0.016	0.034	0.028	4.39	0.005
M1CCP-03.d	4.20	0.740	246	474	0.067	<dl	79.9	0.049	0.014	n.r.	4.77	<dl	11.2	1.03	0.213	0.005	0.062	<dl	<dl	<dl	0.057	0.013	0.017	9.10	0.044
M1CCP-04.d	2.87	0.041	22.5	291	0.051	<dl	87.5	<dl	0.075	n.r.	2.84	<dl	5.40	0.783	0.024	0.003	0.033	<dl	<dl	<dl	<dl	3.E-4	0.007	6.50	0.008
M1CCP-05.d	3.36	0.130	22.0	261	0.063	0.530	78.4	0.028	0.016	n.r.	2.71	<dl	3.76	0.923	1.30	0.250	0.028	<dl	<dl	0.011	0.010	0.013	0.016	5.51	2.20
M1CCP-06.d	1.03	0.310	38.8	365	0.016	0.180	13.0	0.150	0.410	n.r.	3.09	<dl	5.28	0.340	0.036	0.003	0.041	0.137	0.670	0.215	0.028	6.E-4	4.E-4	3.73	0.010
M1CCPr-02.d	4.60	0.087	25.0	313	0.026	<dl	87.8	<dl	<dl	n.r.	2.76	<dl	5.81	0.742	0.152	0.004	0.060	<dl	<dl	<dl	<dl	5.E-4	0.035	7.28	0.019
M1CCPr-04.d	0.375	0.037	20.1	320	0.047	<dl	19.7	<dl	<dl	n.r.	3.54	<dl	6.46	0.366	0.039	0.005	0.067	0.230	0.290	0.270	0.057	0.001	0.016	6.50	0.005
M1CCPr-07.d	1.37	0.029	17.6	255	0.010	<dl	20.1	<dl	<dl	n.r.	3.27	<dl	5.84	0.289	0.023	0.003	0.053	<dl	<dl	<dl	0.014	0.001	0.012	8.57	0.023
M2CCP-01d	7.50	0.035	15.7	370	0.143	<dl	11.2	<dl	0.023	n.r.	4.43	<dl	6.31	2.59	0.310	0.006	0.041	<dl	<dl	<dl	<dl	5.E-4	0.020	10.6	0.081
M2CCP-02.d	1.09	0.360	15.6	361	0.055	0.900	94.6	<dl	<dl	n.r.	4.42	<dl	6.15	2.53	0.225	0.030	0.046	<dl	<dl	<dl	<dl	0.150	0.005	4.36	0.007
M2CCP-03.d	1.34	0.035	18.1	337	0.099	3.40	11.1	0.042	<dl	n.r.	6.12	<dl	7.71	3.30	0.140	0.005	0.510	<dl	<dl	<dl	<dl	4.E-4	0.100	16.9	0.027
M2CCP-04.d	2.33	0.340	20.4	374	0.097	<dl	10.1	0.022	0.061	n.r.	3.67	<dl	6.58	2.89	0.154	0.004	0.035	<dl	<dl	<dl	0.070	0.036	0.009	3.74	0.011
M2CCP-05.d	2.53	0.086	20.9	450	0.090	<dl	87.6	0.015	0.015	n.r.	3.14	<dl	3.74	2.19	0.380	0.004	0.042	<dl	0.027	<dl	<dl	5.E-4	0.008	4.75	0.035
M2CCP-06.d	3.00	0.033	15.9	444	0.127	2.40	10.1	1.00	<dl	n.r.	4.09	<dl	7.37	2.73	0.262	0.017	0.182	0.020	<dl	<dl	<dl	0.009	0.003	4.23	0.005
M2CCP-07.d	1.34	0.061	16.8	486	0.130	<dl	90.3	<dl	<dl	n.r.	4.12	<dl	6.80	2.55	0.218	0.004	0.380	0.011	<dl	<dl	<dl	0.011	0.027	3.62	0.004
M2CCPr-01d	1.20	0.032	18.7	297	0.078	<dl	10.3	<dl	0.066	n.r.	4.03	<dl	7.51	2.33	0.220	0.004	0.510	<dl	<dl	<dl	<dl	1.E-3	0.028	5.54	0.004
M2CCPr-02.d	3.31	0.023	17.9	324	0.119	<dl	10.2	<dl	0.048	n.r.	3.99	<dl	7.06	2.34	0.288	0.005	0.040	<dl	<dl	<dl	<dl	0.012	0.025	8.62	0.016
M2CCPr-03.d	1.09	0.019	16.5	266	0.068	<dl	99.0	<dl	0.220	n.r.	3.75	<dl	7.04	2.14	0.033	0.005	0.410	<dl	<dl	<dl	0.014	1.E-3	9.E-4	4.69	0.004
M2CCPr-06.d	0.670	0.022	15.2	431	0.007	<dl	90.0	<dl	<dl	n.r.	3.28	<dl	3.28	1.52	0.018	0.003	0.033	<dl	<dl	<dl	0.060	7.E-4	0.006	3.46	0.004
MR2CCP-01d	0.980	0.057	21.5	274	0.030	<dl	19.8	<dl	0.070	n.r.	4.56	<dl	2.95	0.601	0.156	0.002	0.040	<dl	<dl	<dl	<dl	5.E-4	4.E-4	3.97	0.024
MR2CCP-02.d	3.30	0.120	27.3	224	0.046	<dl	22.1	0.780	0.620	n.r.	4.99	<dl	3.43	0.599	0.365	0.018	0.053	0.710	1.19	1.32	11.0	0.026	0.025	5.94	0.320
MR2CCP-05.d	1.55	0.350	52.7	237	0.014	<dl	16.1	<dl	<dl	n.r.	2.78	<dl	3.58	1.84	0.360	0.180	0.370	<dl	<dl	0.046	0.640	0.005	0.036	16.8	0.051
MR2CCP-06.d	0.690	0.580	57.0	309	0.012	0.200	15.5	<dl	1.92	n.r.	2.37	<dl	4.47	1.82	0.052	0.005	0.071	0.017	1.51	0.580	0.243	9.E-4	0.006	3.13	0.047
MR2CCPr-01d	0.710	0.037	21.9	276	0.008	<dl	21.8	<dl	<dl	n.r.	4.37	<dl	3.83	0.624	0.350	0.019	0.052	<dl	<dl	0.118	<dl	9.E-4	9.E-4	5.04	0.048
MR2CCPr-02.d	0.880	0.031	21.6	207	0.051	0.170	25.1	<dl	<dl	n.r.	3.96	<dl	3.21	0.586	0.380	0.004	0.053	0.137	0.280	0.250	0.053	9.E-4	8.E-4	3.66	0.055
MR2CCPr-03.d	4.10	0.067	32.6	264	0.097	<dl	87.8	<dl	<dl	n.r.	1.93	<dl	5.99	2.88	0.496	0.004	0.032	<dl	<dl	<dl	0.025	7.E-4	7.E-4	2.52	0.007
MR2CCPr-04.d	0.221	0.021	22.0	270	0.184	<dl	89.4	<dl	<dl	n.r.	1.38	<dl	3.96	9.13	0.171	0.005	0.042	<dl	<dl	<dl	<dl	6.E-4	8.E-4	5.00	0.005
MR2CCPr-05.d	1.27	0.045	20.2	264	0.158	<dl	98.5	<dl	<dl	n.r.	1.57	<dl	3.33	8.80	0.590	0.005	0.042	<dl	<dl	<dl	<dl	7.E-4	7.E-4	3.93	0.004
ST12CCP-01d	4.29	0.292	5.71	401	0.059	1.20	21.1	<dl	<dl	n.r.	1.25	<dl	0.460	0.014	0.180	0.003	0.038	<dl	0.130	<dl	<dl	5.E-4	0.020	1.86	0.003
ST12CCPr-01d	4.74	0.229	10.8	278	0.012	<dl	21.6	<dl	0.112	n.r.	1.23	<dl	0.550	0.007	0.035	0.007	0.044	<dl	<dl	<dl	<dl	0.001	6.E-4	2.04	0.005
ST12CCPr-02.d	2.50	0.410	10.9	430	0.100	<dl	17.7	<dl	<dl	n.r.	1.82	0.242	0.220	0.013	0.073	0.008	0.091	<dl	<dl	<dl	<dl	0.002	5.E-4	1.23	0.010
T10TCCP-01d	0.432	0.530	29.8	355	0.011	<dl	15.9	0.180	<dl	n.r.	8.30	<dl	1.07	0.329	0.271	0.011	0.105	<dl	<dl	<dl	<dl	2.30	0.011	16.1	0.038
T10TCCP-02.d	0.446	0.550	19.9	349	0.067	<dl	16.2	<dl	<dl	n.r.	21.6	<dl	1.29	0.689	0.058	0.086	0.072	0.033	<dl	<dl	<dl	0.002	0.051	25.9	0.300
T10TCCP-03.d	17.0	0.465	31.3	464	0.041	0.330	16.5	<dl	<dl	n.r.	8.77	<dl	1.75	0.343	0.050	0.036	0.094	<dl	<dl	<dl	<dl	0.001	0.019	10.7	0.005
T10TCCP-04.d	0.392	0.280	11.7	373	2.70	<dl	14.9	<dl	0.190	n.r.	21.9	<dl	0.980	0.292	0.058	0.044	0.067	<dl	<dl	0.180	<dl	0.001	0.094	9.96	0.010
T10TCCPr-01d	2.74	0.382	33.1	245	0.128	<dl	18.9	<dl	0.105	n.r.	8.30	<dl	0.960	0.269	0.029	0.010	0.058	<dl	<dl	<dl	<dl	1.E-3	0.106	10.2	0.006

Grain ID	*Mn* 55	*Co* 59	*Ni* 60	*Zn* 66	*Ga* 71	As 75	*Se* 82	Mo 95	Ru 101	Rh 103	*Ag* 107	Pd 108	Cd 111	*In* 115	*Sn* 118	*Sb* 121	*Te* 128	Re 185	Os 189	Ir 193	Pt 195	*Au* 197	Tl 205	*Pb* 208	*Bi* 209
55um	0.470	0.023	0.241	0.353	0.028	0.223	2.53	0.030	0.023	0.005	0.023	0.014	0.046	0.012	0.073	0.022	0.256	0.009	0.021	0.007	0.013	0.010	0.004	0.012	0.007
33um	0.939	0.046	0.722	1.06	0.085	0.445	5.07	0.061	0.068	0.009	0.069	0.041	0.137	0.025	0.218	0.067	0.513	0.027	0.042	0.020	0.039	0.030	0.011	0.037	0.013
T10TCCPr-02.d	0.523	0.350	25.7	297	0.021	<dl	152	<dl	0.270	n.r.	21.4	<dl	0.860	0.323	0.050	0.014	0.088	<dl	<dl	<dl	<dl	0.026	0.380	13.3	0.010
T10TCCPr-03.d	0.355	0.201	37.7	272	0.057	<dl	183	<dl	0.091	n.r.	9.56	<dl	1.21	0.331	0.076	0.005	0.049	<dl	<dl	<dl	<dl	8.E-4	0.006	13.7	0.005
T10TCCPr-04.d	2.01	0.260	29.0	337	0.020	<dl	166	<dl	0.120	n.r.	14.4	<dl	0.890	0.428	0.350	0.052	0.074	<dl	<dl	<dl	<dl	0.002	0.034	21.4	0.008
T11TCCP-01d	1.37	0.340	41.8	575	0.075	0.390	466	0.020	0.025	n.r.	0.630	<dl	17.3	1.09	0.057	0.002	0.038	<dl	<dl	0.160	<dl	0.080	1.E-4	0.740	0.015
T11TCCP-02.d	1.43	0.263	67.5	485	0.079	<dl	448	<dl	<dl	n.r.	0.349	<dl	15.7	1.39	0.049	0.004	0.350	<dl	<dl	<dl	0.016	0.048	3.E-4	1.72	1.80
T11TCCP-03.d	1.04	0.171	24.6	462	0.101	<dl	430	0.019	<dl	n.r.	3.20	<dl	16.8	1.75	0.030	0.002	0.228	<dl	<dl	0.005	0.100	7.E-4	0.001	10.5	0.080
T11TCCP-04.d	1.83	0.290	77.0	483	0.500	<dl	293	0.015	0.028	n.r.	1.00	<dl	13.2	2.20	0.318	0.004	0.042	<dl	<dl	<dl	0.058	0.021	6.E-4	6.40	0.003
T11TCCP-05.d	1.75	0.380	56.9	555	0.860	<dl	302	<dl	0.016	n.r.	2.50	<dl	16.6	2.53	0.060	0.006	0.074	0.035	0.090	0.600	0.090	0.042	0.080	7.86	2.50
T11TCCP-06.d	2.21	1.19	12.3	496	0.107	<dl	145	0.020	<dl	n.r.	40.6	<dl	4.38	0.485	0.163	0.003	0.029	0.032	0.600	0.003	0.081	0.006	0.003	2.58	0.006
T11TCCP-07.d	15.2	0.680	81.0	471	0.270	<dl	207	<dl	<dl	n.r.	25.9	<dl	5.64	1.66	0.236	0.006	0.062	<dl	<dl	<dl	<dl	0.001	0.013	11.3	0.012
T11TCCPr-01b.d	0.383	0.115	33.0	408	0.079	<dl	459	<dl	0.110	n.r.	0.490	<dl	15.7	0.890	0.033	0.003	0.074	<dl	<dl	<dl	<dl	0.001	6.E-4	3.10	0.005
T11TCCPr-02b.d	0.427	0.137	27.1	384	0.066	<dl	443	<dl	0.150	n.r.	0.190	<dl	15.8	1.29	0.049	0.004	0.088	<dl	<dl	<dl	<dl	9.E-4	5.E-4	5.45	0.006
T11TCCPr-03.d	0.314	0.151	24.2	352	0.123	<dl	437	<dl	0.106	n.r.	2.33	<dl	15.4	1.48	0.047	0.005	0.056	<dl	<dl	<dl	0.120	0.001	5.E-4	3.89	0.005
T11TCCPr-05.d	0.360	0.055	31.8	358	0.012	<dl	313	<dl	0.110	n.r.	0.375	<dl	14.0	1.85	0.034	0.005	0.067	<dl	<dl	<dl	0.063	0.001	7.E-4	10.4	0.007
T11TCCPr-06.d	0.476	0.177	39.6	530	0.156	<dl	328	<dl	0.190	n.r.	0.360	<dl	16.4	1.84	0.045	0.005	0.075	<dl	<dl	<dl	0.081	0.001	8.E-4	8.36	0.006
Skarn																									
2503CCP-01d	1.59	1.00	12.8	589	0.285	<dl	236	<dl	<dl	n.r.	9.19	<dl	3.96	16.2	28.9	0.009	23.3	<dl	<dl	<dl	<dl	0.001	4.E-4	9.45	9.40
2503CCP-02.d	1.40	1.35	14.1	530	0.275	0.200	225	<dl	<dl	n.r.	9.30	<dl	3.87	18.6	29.4	0.024	20.0	<dl	<dl	<dl	<dl	0.001	0.010	10.0	6.08
2503CCP-04.d	1.45	1.21	21.3	740	0.414	<dl	182	0.022	<dl	n.r.	10.1	<dl	5.55	17.7	28.9	0.008	32.7	<dl	<dl	<dl	<dl	0.002	0.006	5.41	41.9
2503CCP-05.d	1.56	0.660	18.5	417	0.209	<dl	230	<dl	<dl	n.r.	11.8	<dl	3.29	18.2	32.3	0.010	37.2	<dl	<dl	<dl	<dl	0.016	0.011	46.4	11.2
2503CCP-06.d	1.23	0.851	18.7	493	0.325	<dl	218	<dl	<dl	n.r.	2.26	<dl	3.58	17.3	33.0	0.014	9.41	<dl	<dl	<dl	<dl	4.E-4	0.00	0.085	0.007
2503CCP-07.d	1.14	1.14	18.8	539	0.300	<dl	207	<dl	<dl	n.r.	22.1	<dl	3.73	17.6	30.4	0.006	39.3	<dl	0.016	<dl	<dl	0.001	0.008	32.3	30.9
2506CCP-01d	1.45	9.62	5.84	432	0.473	<dl	140	<dl	<dl	n.r.	43.8	<dl	3.85	25.5	45.4	0.036	10.2	<dl	<dl	<dl	<dl	0.001	5.E-4	2.14	0.167
2506CCP-02.d	2.35	4.81	5.28	408	0.500	<dl	148	0.043	<dl	n.r.	44.1	<dl	2.69	37.0	44.6	0.028	10.3	<dl	<dl	<dl	<dl	0.002	0.015	3.72	0.206
2506CCP-03.d	1.89	8.60	6.12	389	0.520	<dl	149	<dl	<dl	n.r.	40.8	<dl	3.08	29.2	41.4	0.033	11.6	<dl	<dl	<dl	<dl	0.013	3.E-4	1.61	0.168
2506CCP-04.d	1.61	6.49	4.87	442	0.374	<dl	144	<dl	<dl	n.r.	41.6	<dl	3.20	42.7	58.5	0.026	10.7	<dl	<dl	<dl	<dl	0.009	0.004	2.53	0.149
2506CCP-05.d	1.55	7.17	5.33	408	0.354	<dl	135	<dl	<dl	n.r.	48.6	<dl	3.00	35.9	57.4	0.026	10.4	<dl	<dl	<dl	<dl	8.E-4	4.E-4	1.33	0.110
2506CCP-06.d	0.790	5.01	4.25	435	0.399	<dl	142	0.023	<dl	n.r.	46.7	<dl	2.54	26.7	62.3	0.090	9.46	<dl	<dl	<dl	<dl	0.008	0.011	1.20	0.089
2506CCP-07.d	1.50	7.64	5.14	486	0.400	<dl	134	0.096	<dl	n.r.	49.6	<dl	3.28	26.7	34.3	0.025	8.34	<dl	<dl	<dl	<dl	0.001	0.110	2.03	0.104
2513CCP-01d	3.13	8.96	5.83	582	0.510	2.07	915	<dl	<dl	n.r.	158	<dl	1.77	43.9	24.2	0.120	10.8	<dl	<dl	<dl	<dl	0.002	0.005	2.36	0.351
2513CCP-02.d	3.68	11.3	6.44	491	0.660	6.20	84.1	<dl	<dl	n.r.	142	<dl	2.40	36.9	22.8	0.063	5.62	<dl	<dl	<dl	<dl	0.002	6.E-4	3.51	0.454
2513CCP-03.d	2.04	9.91	5.68	629	0.570	1.50	83.9	<dl	<dl	n.r.	154	<dl	2.07	37.3	23.6	0.073	7.90	<dl	<dl	<dl	<dl	0.002	0.004	2.70	0.402
2513CCP-04.d	3.50	10.2	6.53	671	0.642	0.280	93.9	<dl	<dl	n.r.	157	<dl	2.83	21.5	21.9	0.050	13.2	<dl	<dl	<dl	<dl	0.006	5.E-4	1.92	0.218
2513CCP-05.d	2.43	11.5	6.45	628	0.714	0.720	82.8	<dl	<dl	n.r.	149	<dl	2.61	18.1	14.1	0.038	7.90	<dl	<dl	<dl	<dl	0.001	3.E-4	1.04	0.196
2513CCP-06.d	2.67	8.25	2.08	493	0.570	0.760	93.0	<dl	<dl	n.r.	124	<dl	1.62	28.1	31.7	0.009	16.7	<dl	<dl	<dl	<dl	0.036	0.007	5.14	0.114
2513CCP-08.d	2.51	5.61	2.83	667	0.543	0.670	86.6	<dl	<dl	n.r.	131	<dl	2.57	45.9	24.9	0.030	16.0	<dl	<dl	<dl	<dl	0.015	6.E-4	3.71	0.115
2513CCP-09.d	1.76	8.93	2.84	680	0.440	0.270	98.0	<dl	<dl	n.r.	119	<dl	2.54	31.9	20.2	0.094	7.83	<dl	<dl	<dl	<dl	0.002	3.E-4	1.67	0.229
2515CCP-01d	1.61	17.8	0.590	690	3.56	0.310	70.4	<dl	<dl	n.r.	60.1	<dl	6.35	28.9	41.9	0.178	1.81	<dl	<dl	<dl	<dl	0.002	4.E-4	0.710	0.801
2515CCP-02.d	0.680	18.3	0.053	594	3.28	<dl	76.3	<dl	<dl	n.r.	60.6	<dl	4.97	24.6	31.0	0.110	2.30	<dl	<dl	<dl	<dl	0.001	2.E-4	0.570	1.04
2515CCP-05.d	1.48	6.01	0.790	658	1.46	<dl	85.1	<dl	<dl	n.r.	61.8	<dl	5.00	45.2	25.8	0.272	0.850	<dl	<dl	<dl	<dl	0.002	5.E-4	0.840	0.841
2515CCP-06.d	1.35	4.82	0.850	673	3.97	<dl	73.7	<dl	<dl	n.r.	82.3	<dl	5.15	38.9	30.8	0.197	0.680	<dl	<dl	<dl	<dl	0.001	0.005	0.765	0.708
2515CCP-07.d	1.34	6.24	0.520	535	3.41	<dl	74.0	<dl	<dl	n.r.	54.7	<dl	5.66	27.6	29.9	0.370	0.960	<dl	<dl	<dl	<dl	0.002	0.006	1.09	1.02
2517CCP-01d	0.890	14.7	8.93	475	2.85	0.130	142	<dl	<dl	n.r.	30.1	<dl	3.48	14.1	29.2	0.004	12.8	<dl	<dl	<dl	<dl	0.001	5.E-4	2.15	0.390
2517CCP-02.d	1.58	17.1	9.15	355	3.17	<dl	163	0.035	<dl	n.r.	34.5	<dl	2.88	54.1	53.2	0.009	14.2	<dl	<dl	<dl	<dl	0.038	6.E-4	2.83	0.760
2517CCP-03.d	1.66	14.7	9.45	419	2.39	<dl	145	<dl	<dl	n.r.	34.4	<dl	3.10	24.4	33.1	0.006	13.5	<dl	<dl	<dl	<dl	0.002	6.E-4	3.41	0.770
2517CCP-04.d	1.35	17.2	8.87	482	2.24	<dl	168	<dl	<dl	n.r.	34.2	<dl	3.54	15.0	29.0	0.026	10.8	<dl	<dl	<dl	<dl	0.002	0.004	2.74	0.395
2517CCP-05.d	0.960	11.3	8.24	500	2.61	<dl	194	<dl	<dl	n.r.	34.1	<dl	3.43	17.3	31.0	0.007	16.1	<dl	<dl	<dl	<dl	0.003	6.E-4	4.09	3.82

Grain ID	*Mn* 55	*Co* 59	*Ni* 60	*Zn* 66	*Ga* 71	As 75	*Se* 82	Mo 95	Ru 101	Rh 103	*Ag* 107	Pd 108	Cd 111	*In* 115	*Sn* 118	*Sb* 121	*Te* 128	Re 185	Os 189	Ir 193	Pt 195	*Au* 197	Tl 205	*Pb* 208	*Bi* 209
55um	0.470	0.023	0.241	0.353	0.028	0.223	2.53	0.030	0.023	0.005	0.023	0.014	0.046	0.012	0.073	0.022	0.256	0.009	0.021	0.007	0.013	0.010	0.004	0.012	0.007
33um	0.939	0.046	0.722	1.06	0.085	0.445	5.07	0.061	0.068	0.009	0.069	0.041	0.137	0.025	0.218	0.067	0.513	0.027	0.042	0.020	0.039	0.030	0.011	0.037	0.013
2517CCP-06.d	1.01	11.1	8.93	452	2.51	<dl	164	<dl	<dl	n.r.	29.0	<dl	3.51	16.9	29.9	0.023	7.87	<dl	<dl	<dl	<dl	0.002	4.E-4	1.89	0.850
2517CCP-07.d	1.66	13.9	8.71	502	2.36	<dl	154	0.024	<dl	n.r.	33.5	<dl	3.41	14.8	28.4	0.006	10.6	<dl	<dl	<dl	<dl	0.002	5.E-4	2.38	0.670
2518CCP-01d	1.37	6.52	14.1	581	1.13	<dl	76.0	<dl	<dl	n.r.	19.5	<dl	5.35	34.0	56.2	0.058	5.74	<dl	<dl	<dl	<dl	0.046	0.006	1.10	2.91
2518CCP-02.d	2.43	7.67	11.2	715	0.953	<dl	67.2	<dl	<dl	n.r.	29.7	<dl	7.34	31.9	53.4	0.080	5.78	<dl	<dl	<dl	0.007	0.064	3.E-4	1.26	4.04
2518CCP-03.d	2.22	4.42	9.60	740	1.00	0.170	65.2	0.030	<dl	n.r.	36.6	<dl	7.20	26.3	63.4	0.062	4.89	<dl	<dl	<dl	<dl	0.033	0.005	1.50	1.50
2518CCP-04.d	2.16	6.03	9.30	633	0.790	<dl	77.4	0.036	<dl	n.r.	30.7	<dl	6.48	33.3	61.4	0.208	6.03	<dl	<dl	0.006	<dl	0.042	0.003	1.77	4.90
2518CCP-05.d	1.52	8.52	12.5	719	1.01	<dl	74.4	<dl	<dl	n.r.	22.8	<dl	7.84	36.2	54.7	0.063	6.27	<dl	<dl	<dl	<dl	0.073	2.E-4	1.05	3.75
2518CCP-06.d	1.95	7.87	15.0	675	1.27	<dl	72.6	<dl	0.031	n.r.	30.9	<dl	6.52	31.2	52.5	0.044	5.49	<dl	<dl	<dl	<dl	0.101	0.004	1.70	2.90
450CCP-01d	2.12	5.62	40.7	524	12.3	<dl	54.5	<dl	<dl	n.r.	12.4	<dl	3.80	21.4	68.8	0.031	10.1	<dl	<dl	<dl	<dl	0.138	3.E-4	6.40	11.8
450CCP-02.d	1.46	4.23	32.1	469	11.5	<dl	66.0	0.015	0.039	n.r.	9.48	<dl	3.40	22.0	72.1	0.150	5.33	<dl	<dl	<dl	<dl	0.157	0.014	3.11	0.729
450CCP-03.d	2.41	3.31	38.1	522	10.8	<dl	72.5	<dl	<dl	n.r.	7.52	<dl	3.19	22.1	74.2	0.036	2.10	<dl	<dl	<dl	<dl	0.216	5.E-4	3.68	0.740
450CCP-05.d	2.64	3.65	43.0	638	9.99	<dl	70.2	<dl	<dl	n.r.	5.71	<dl	4.67	24.0	80.2	0.031	1.63	<dl	<dl	<dl	<dl	0.105	2.E-4	2.58	0.559
450CCP-06.d	1.56	6.08	44.2	526	9.57	<dl	81.8	<dl	<dl	n.r.	10.9	<dl	3.94	24.6	80.8	0.023	2.95	<dl	<dl	<dl	<dl	0.111	2.E-4	2.70	0.478
450CCP-07.d	1.95	4.33	48.6	519	6.91	<dl	59.8	0.017	<dl	n.r.	15.8	<dl	4.07	19.7	61.1	0.010	8.60	<dl	<dl	<dl	<dl	0.114	0.003	2.84	6.90
457CCP-01d	0.215	5.55	2.70	350	1.57	<dl	139	<dl	<dl	n.r.	32.0	<dl	2.08	30.8	16.2	0.007	40.2	<dl	<dl	<dl	<dl	9.E-4	4.E-4	5.43	0.128
457CCP-02.d	1.78	6.10	3.28	377	1.44	<dl	138	<dl	<dl	n.r.	34.8	<dl	2.10	22.5	11.6	0.007	36.8	<dl	<dl	<dl	<dl	8.E-4	6.E-4	2.84	0.091
457CCP-03.d	1.02	9.88	3.51	384	2.20	<dl	134	<dl	<dl	n.r.	27.2	<dl	1.77	57.9	31.3	0.017	35.3	<dl	<dl	<dl	<dl	0.001	4.E-4	1.47	0.043
457CCP-05.d	0.800	3.44	2.37	328	1.65	<dl	139	0.030	<dl	n.r.	26.9	<dl	1.32	21.9	13.1	0.006	35.1	<dl	<dl	<dl	<dl	8.E-4	5.E-4	2.33	0.037
457CCP-06.d	1.20	12.0	2.71	426	2.03	<dl	131	<dl	<dl	n.r.	31.7	<dl	2.09	33.3	18.4	0.007	38.4	<dl	<dl	<dl	<dl	0.002	0.004	1.80	0.046
654CCP-01d	1.65	12.3	18.8	537	0.950	<dl	119	<dl	0.022	n.r.	27.1	<dl	3.65	17.0	19.9	0.004	5.01	<dl	<dl	<dl	<dl	0.019	2.E-4	0.300	0.034
654CCP-02.d	1.83	10.7	18.0	501	0.591	<dl	115	<dl	0.024	n.r.	24.3	<dl	3.97	16.2	21.0	0.004	4.52	<dl	<dl	<dl	<dl	0.019	3.E-4	0.336	0.049
654CCP-03.d	2.14	11.2	15.8	573	0.890	<dl	114	0.041	<dl	n.r.	24.5	<dl	4.23	14.8	18.9	0.004	4.64	<dl	<dl	<dl	<dl	0.001	4.E-4	0.620	0.070
654CCP-04.d	1.53	13.2	16.6	606	0.690	<dl	119	<dl	<dl	n.r.	23.9	<dl	4.70	19.9	19.7	0.002	5.57	<dl	<dl	<dl	<dl	0.007	1.E-4	0.150	0.010
654CCP-05.d	1.21	4.24	14.6	493	0.650	<dl	114	<dl	<dl	n.r.	24.6	<dl	4.26	13.5	16.1	0.026	4.61	<dl	<dl	<dl	<dl	0.031	4.E-4	1.47	0.180
654CCP-06.d	1.74	5.98	15.4	576	0.719	<dl	112	<dl	<dl	n.r.	23.5	<dl	5.70	14.0	16.2	0.005	4.17	<dl	<dl	<dl	<dl	0.026	0.002	2.31	0.107
654CCP-07.d	2.34	11.4	14.9	560	0.217	<dl	111	<dl	<dl	n.r.	29.6	<dl	3.89	17.4	19.4	0.004	4.19	0.019	<dl	<dl	<dl	9.E-4	3.E-4	0.530	0.055
CEZGRCCP-001	5.43	0.649	1.70	890	0.630	0.690	15.1	0.160	<dl	n.r.	111	<dl	27.2	12.0	268	0.016	0.044	<dl	<dl	<dl	0.031	0.010	0.001	0.890	0.444
CEZGRCCP-002	2450	0.640	4.60	743	2.08	<dl	17.8	0.031	0.070	n.r.	106	<dl	22.8	18.0	325	0.049	0.058	<dl	<dl	<dl	0.022	0.002	0.028	2.33	0.480
CEZGRCCP-003	3.70	0.570	1.80	864	0.620	<dl	13.8	0.037	<dl	n.r.	108	<dl	24.8	19.0	305	0.013	0.052	<dl	<dl	<dl	<dl	0.002	8.E-4	0.844	0.604
CEZGRCCP-004	3.60	1.30	50.0	705	0.730	0.870	16.9	<dl	<dl	n.r.	115	<dl	21.6	27.6	292	0.021	0.052	0.026	<dl	<dl	<dl	0.003	6.E-4	2.80	0.484
CEZGRCCP-005	3.68	0.720	27.0	779	0.580	<dl	13.0	<dl	<dl	n.r.	121	<dl	23.0	29.0	320	1.00	0.046	0.015	<dl	<dl	<dl	0.038	0.005	1.25	0.850
CEZGRCCP-006	6.50	1.11	2.30	819	0.533	<dl	15.4	0.082	<dl	n.r.	120	<dl	24.8	17.8	291	0.700	0.055	<dl	<dl	<dl	0.053	0.002	0.120	1.14	0.570
COPPOBCCP-0	2.48	1.20	2.46	919	0.920	<dl	12.7	<dl	0.041	n.r.	101	<dl	9.60	18.8	103	0.014	0.056	<dl	<dl	0.038	0.130	0.020	0.006	1.22	0.940
COPPOBCCP-0	2.88	5.57	8.00	974	1.06	<dl	10.8	0.450	<dl	n.r.	104	<dl	10.5	17.1	136	0.014	0.058	<dl	<dl	<dl	<dl	0.002	0.008	0.520	0.436
COPPOBCCP-0	2.10	1.62	1.56	939	1.40	0.630	8.20	<dl	<dl	n.r.	109	<dl	9.30	24.1	155	0.065	0.056	<dl	<dl	<dl	<dl	0.001	0.020	0.550	0.740
COPPOBCCP-0	3.67	2.01	34.0	901	1.34	<dl	10.6	<dl	<dl	n.r.	94.0	<dl	8.70	29.1	158	0.016	0.047	<dl	<dl	<dl	<dl	0.002	5.E-4	0.700	0.214
COPPOBCCP-0	0.385	1.11	100	839	3.40	<dl	10.0	0.134	<dl	n.r.	107	<dl	11.4	22.2	222	0.074	0.057	<dl	0.070	<dl	0.073	0.032	0.003	1.16	0.950
M301CCP-001d	3.20	5.35	0.770	653	0.540	<dl	61.5	0.044	<dl	n.r.	52.8	<dl	17.8	15.2	3.53	0.009	0.061	<dl	<dl	<dl	<dl	0.002	4.E-4	0.830	0.380
M301CCP-002.d	2.20	5.30	0.083	622	0.560	3.70	51.1	<dl	<dl	n.r.	28.4	<dl	18.6	11.9	2.25	0.013	0.088	<dl	<dl	<dl	<dl	0.450	6.E-4	5.10	0.320
M301CCP-003.d	4.67	4.80	1.20	656	0.580	<dl	55.9	<dl	<dl	n.r.	29.2	<dl	16.2	19.2	2.19	0.008	0.062	<dl	<dl	<dl	<dl	0.001	0.002	1.44	0.193
M301CCP-004.d	3.50	6.70	1.60	569	0.550	<dl	54.1	<dl	<dl	n.r.	28.5	<dl	15.7	22.8	1.59	0.018	0.081	<dl	<dl	<dl	<dl	0.001	0.003	3.28	0.950
M301CCP-005.d	3.60	5.75	0.720	639	0.570	<dl	60.1	<dl	<dl	n.r.	28.4	<dl	15.9	23.2	1.46	0.007	0.070	<dl	<dl	<dl	<dl	0.001	3.E-4	0.446	0.228
MARNCCP-001c	2.37	10.2	0.660	735	0.620	<dl	50.2	<dl	0.045	n.r.	105	<dl	6.90	4.18	9.26	0.157	1.96	<dl	0.260	<dl	<dl	0.045	0.034	1.64	0.029
MARNCCP-002.	0.420	9.99	23.0	590	0.780	<dl	55.4	<dl	<dl	n.r.	104	<dl	5.70	3.56	10.4	0.480	1.94	<dl	0.140	<dl	<dl	0.560	0.013	2.14	0.290
MARNCCP-003.	0.780	12.6	3.50	633	0.760	1.10	53.8	<dl	<dl	n.r.	100	<dl	6.02	3.73	11.9	0.042	2.22	<dl	<dl	0.060	<dl	0.003	8.E-4	4.35	0.171
MARNCCP-004.	2.64	9.77	90.0	553	0.820	<dl	50.9	<dl	<dl	n.r.	115	<dl	5.20	4.58	12.6	0.140	2.82	<dl	<dl	0.012	0.600	0.002	0.180	1.80	0.085
MARNCCP-005.	0.367	9.78	1.13	569	1.10	<dl	54.7	<dl	<dl	n.r.	105	<dl	6.29	6.94	14.3	0.004	2.35	<dl	<dl	<dl	<dl	0.003	0.009	4.24	0.123

Grain ID	*Mn* 55	*Co* 59	*Ni* 60	*Zn* 66	*Ga* 71	As 75	*Se* 82	Mo 95	Ru 101	Rh 103	*Ag* 107	Pd 108	Cd 111	*In* 115	*Sn* 118	*Sb* 121	*Te* 128	Re 185	Os 189	Ir 193	Pt 195	*Au* 197	Tl 205	*Pb* 208	*Bi* 209
55um	0.470	0.023	0.241	0.353	0.028	0.223	2.53	0.030	0.023	0.005	0.023	0.014	0.046	0.012	0.073	0.022	0.256	0.009	0.021	0.007	0.013	0.010	0.004	0.012	0.007
33um	0.939	0.046	0.722	1.06	0.085	0.445	5.07	0.061	0.068	0.009	0.069	0.041	0.137	0.025	0.218	0.067	0.513	0.027	0.042	0.020	0.039	0.030	0.011	0.037	0.013
MARNCCP-006.(	0.370	7.68	0.630	494	0.142	<dl	50.2	<dl	<dl	n.r.	110	<dl	6.64	6.07	14.9	0.192	1.94	<dl	0.360	0.027	<dl	0.003	7.E-4	3.55	0.227
MTP01CCP-001c	0.378	2.49	5.20	534	0.340	<dl	44.5	<dl	<dl	n.r.	20.8	<dl	21.7	9.46	6.30	0.360	0.091	0.016	<dl	<dl	0.150	0.028	0.119	8.00	2.50
MTP01CCP-002.(	3.30	2.37	0.156	641	0.960	0.660	45.9	0.039	<dl	n.r.	30.1	<dl	22.2	9.94	16.7	0.010	0.490	<dl	<dl	<dl	<dl	0.027	0.001	0.830	0.502
MTP01CCP-003.(	0.860	1.80	0.510	659	0.950	<dl	43.3	<dl	<dl	n.r.	31.0	<dl	27.9	8.06	13.3	0.066	0.360	0.150	<dl	<dl	<dl	0.001	0.005	0.920	0.056
MTP01CCP-004.(	1.54	1.94	0.710	619	1.01	<dl	39.0	<dl	<dl	n.r.	29.7	<dl	23.3	7.69	10.6	0.110	0.069	0.600	<dl	<dl	<dl	0.001	4.E-4	0.960	0.300
VMS																									
07MPBR23CCP-	1.19	0.970	1.10	405	0.304	<dl	58.4	<dl	<dl	n.r.	61.6	<dl	1.03	23.0	390	1.65	0.066	<dl	<dl	<dl	<dl	0.019	0.045	5.75	7.32
07MPBR23CCP-	1.00	1.10	1.05	422	0.322	<dl	54.2	<dl	<dl	n.r.	59.9	<dl	0.760	17.7	509	1.50	0.055	<dl	<dl	<dl	<dl	0.074	0.018	6.54	8.66
07MPBR23CCP-	1.27	1.02	1.31	419	0.286	<dl	53.8	<dl	<dl	n.r.	66.8	<dl	0.810	26.4	687	0.524	0.057	<dl	<dl	<dl	<dl	0.239	0.009	4.12	5.29
07MPBR23CCP-	1.18	1.09	1.39	555	0.340	<dl	57.8	<dl	<dl	n.r.	65.0	<dl	1.16	26.6	653	0.268	0.052	<dl	<dl	<dl	<dl	0.381	0.004	1.88	1.91
07MPBR23CCP-	1.15	1.03	0.940	383	0.221	0.290	57.1	<dl	<dl	n.r.	63.8	<dl	0.650	15.5	466	2.01	0.062	<dl	<dl	<dl	<dl	0.029	0.050	5.88	12.7
146-2-Ccp-1d	0.146	0.003	0.016	96.5	0.172	<dl	896	0.041	<dl	n.r.	1.60	<dl	0.410	6.84	8.58	3.67	17.0	<dl	<dl	<dl	<dl	0.001	0.090	4.38	0.346
146-3-Ccp-1d	2.95	0.033	0.021	100	0.520	0.560	871	0.530	<dl	n.r.	0.660	<dl	0.520	6.60	9.92	0.738	13.9	<dl	<dl	<dl	<dl	9.E-4	0.026	1.93	0.168
146-5-Ccp-1d	0.199	0.003	0.025	105	0.266	<dl	926	0.310	<dl	n.r.	0.860	<dl	0.750	6.46	10.4	1.04	14.0	<dl	<dl	<dl	<dl	0.001	0.028	2.05	0.157
146-5-Ccp-2.d	0.118	0.024	0.018	112	0.228	<dl	937	4.20	<dl	n.r.	0.556	<dl	0.393	6.59	13.7	0.428	14.9	<dl	<dl	<dl	<dl	0.007	4.E-4	1.29	0.075
149-1-Ccp-1d	0.163	0.003	0.024	204	0.362	<dl	246	0.048	<dl	n.r.	1.37	<dl	0.540	15.6	11.3	1.56	22.2	<dl	<dl	<dl	<dl	0.015	0.013	4.18	0.075
149-2-Ccp-1d	4.10	0.006	0.250	234	3.24	<dl	216	0.017	<dl	n.r.	1.50	<dl	0.590	14.2	9.71	1.29	26.0	<dl	<dl	<dl	<dl	0.010	0.067	4.14	0.063
149-6-Ccp-1d	0.179	0.004	0.023	286	1.23	<dl	235	<dl	<dl	n.r.	0.830	<dl	0.630	17.0	16.3	0.323	28.4	<dl	<dl	<dl	<dl	0.009	0.006	1.03	0.022
1869CCP-01d	1.06	5.66	0.031	323	4.31	<dl	415	<dl	<dl	n.r.	124	<dl	4.54	9.68	4.46	0.437	1.19	<dl	<dl	<dl	<dl	0.002	0.046	5.71	0.944
1869CCP-02.d	0.321	2.98	0.047	293	4.87	<dl	40.5	<dl	<dl	n.r.	123	<dl	3.84	9.02	3.99	0.295	1.91	<dl	<dl	<dl	<dl	0.002	0.051	18.9	1.12
1869CCP-03.d	0.700	5.93	0.540	308	3.65	<dl	416	<dl	<dl	n.r.	121	<dl	3.64	8.71	3.43	0.355	1.53	<dl	<dl	<dl	<dl	0.001	0.035	2.04	0.750
1869CCP-04.d	0.339	5.52	0.890	368	2.95	<dl	47.0	<dl	<dl	n.r.	123	<dl	4.07	8.88	4.37	0.380	1.53	<dl	<dl	<dl	<dl	0.002	0.037	3.40	1.16
1869CCP-05.d	0.304	2.37	12.4	285	4.34	<dl	40.9	<dl	<dl	n.r.	118	<dl	3.32	9.13	5.08	0.500	0.780	<dl	<dl	<dl	<dl	0.019	0.044	3.22	1.16
1869CCP-06.d	0.297	5.48	0.043	322	5.45	<dl	39.5	<dl	<dl	n.r.	126	<dl	4.19	9.61	5.14	0.380	1.29	<dl	<dl	<dl	<dl	0.002	0.057	12.1	1.31
1869CCP-07.d	1.03	4.02	0.770	275	4.56	<dl	49.6	<dl	<dl	n.r.	127	<dl	3.75	9.01	3.72	0.411	1.21	<dl	<dl	<dl	<dl	0.002	0.084	12.9	1.62
1872CCP-01d	0.237	0.065	0.027	148	10.2	<dl	219	0.330	<dl	n.r.	9.80	<dl	0.840	4.48	14.1	1.38	0.033	<dl	<dl	<dl	<dl	0.016	0.004	2.76	0.106
1872CCP-02.d	1.45	0.020	0.023	194	137	0.670	33.9	<dl	<dl	n.r.	7.93	<dl	0.820	5.94	139	1.59	0.035	<dl	<dl	<dl	<dl	1.E-3	5.E-4	1.38	0.022
1872CCP-03.d	0.497	0.025	0.039	151	119	0.660	28.4	<dl	<dl	n.r.	15.4	<dl	1.00	5.79	147	25.1	0.048	<dl	<dl	<dl	<dl	0.013	0.540	6.90	0.065
1872CCP-04.d	0.388	0.028	0.030	137	127	0.470	32.3	<dl	<dl	n.r.	18.2	<dl	0.530	5.06	110	12.8	0.340	<dl	<dl	<dl	<dl	0.053	0.023	6.62	0.261
1872CCP-05.d	0.364	0.028	0.035	142	150	<dl	33.1	<dl	<dl	n.r.	23.2	<dl	0.380	6.27	104	2.24	0.044	<dl	<dl	<dl	<dl	0.018	0.001	5.17	0.163
1872CCP-06.d	0.332	0.029	0.024	141	133	<dl	34.7	<dl	<dl	n.r.	45.8	<dl	0.570	4.99	153	8.01	0.045	<dl	<dl	<dl	<dl	0.072	0.030	4.96	0.107
2211CCP-01d	0.285	1.69	0.044	176	2.01	<dl	3037	<dl	<dl	n.r.	60.7	<dl	1.56	128	91.7	0.937	3.13	<dl	<dl	<dl	<dl	0.186	0.073	13.8	7.20
2211CCP-02.d	0.364	1.63	0.045	211	2.58	<dl	3360	<dl	<dl	n.r.	60.0	<dl	1.43	123	107	0.510	2.49	<dl	<dl	<dl	<dl	0.088	7.E-4	5.65	4.53
2211CCP-03.d	3.89	1.61	0.038	155	2.59	<dl	3062	<dl	<dl	n.r.	50.5	<dl	1.47	109	71.1	0.870	2.49	<dl	<dl	<dl	<dl	0.310	0.034	11.7	8.53
2211CCP-04.d	0.230	1.69	0.031	153	0.870	<dl	3110	<dl	<dl	n.r.	56.9	<dl	1.32	110	92.6	0.437	2.94	<dl	<dl	<dl	<dl	0.392	0.006	5.46	4.90
2211CCP-05.d	0.316	1.74	0.041	206	3.02	<dl	3300	<dl	0.029	n.r.	43.6	<dl	1.66	121	134	0.270	3.23	<dl	<dl	<dl	<dl	0.360	0.005	7.75	6.25
2211CCP-06.d	0.205	1.53	0.038	160	0.400	<dl	2942	<dl	<dl	n.r.	74.4	<dl	1.60	124	153	0.204	6.90	<dl	<dl	<dl	<dl	0.088	6.E-4	6.91	2.21
2215CCP-02.d	0.177	5.46	0.300	127	0.043	<dl	406	<dl	<dl	n.r.	58.9	<dl	0.970	5.35	50.8	0.256	2.70	<dl	<dl	<dl	<dl	0.463	0.020	2.52	1.77
2215CCP-03.d	0.145	5.78	0.410	114	0.052	<dl	378	<dl	<dl	n.r.	53.5	<dl	1.40	5.44	50.6	0.282	2.10	<dl	<dl	<dl	<dl	0.460	0.025	2.79	2.55
2215CCP-04.d	88.4	5.25	0.350	109	0.082	<dl	385	<dl	<dl	n.r.	56.1	<dl	0.970	5.43	46.5	0.950	2.31	<dl	<dl	<dl	<dl	0.900	0.046	7.12	4.43
2215CCP-05.d	2.90	6.66	0.440	121	0.041	<dl	408	<dl	<dl	n.r.	57.4	<dl	1.89	5.62	55.0	0.350	3.42	<dl	<dl	<dl	<dl	0.780	0.005	2.80	2.31
2215CCP-06.d	0.286	5.52	0.058	1070	0.096	<dl	410	<dl	<dl	n.r.	56.1	<dl	4.32	5.21	56.5	0.390	3.22	<dl	<dl	<dl	<dl	1.14	0.024	4.00	1.66
2221CCP-01d	1.86	3.71	1.65	428	22.3	<dl	756	0.014	<dl	n.r.	86.8	<dl	5.29	18.5	75.4	0.170	20.6	<dl	<dl	<dl	<dl	0.274	0.056	3.72	26.4
2221CCP-02.d	2.05	12.7	22.6	338	28.9	<dl	659	<dl	<dl	n.r.	83.6	<dl	4.85	17.1	85.9	0.081	34.0	<dl	<dl	<dl	<dl	0.229	0.051	6.42	50.0
2221CCP-03.d	2.95	2.92	1.72	378	16.3	<dl	678	<dl	<dl	n.r.	77.3	<dl	3.88	19.6	58.0	0.112	41.0	<dl	<dl	<dl	0.020	0.678	0.025	2.21	60.0
2221CCP-04.d	1.53	2.70	12.5	430	30.4	<dl	629	0.011	<dl	n.r.	98.4	<dl	5.04	16.3	89.8	0.051	53.0	<dl	<dl	<dl	<dl	0.329	0.002	1.43	64.0
2221CCP-05.d	3.98	7.00	12.4	327	29.5	<dl	630	<dl	<dl	n.r.	81.8	<dl	4.17	15.8	82.3	0.130	11.5	<dl	<dl	<dl	<dl	0.292	0.015	2.15	17.0

Grain ID	*Mn* 55	*Co* 59	*Ni* 60	*Zn* 66	*Ga* 71	As 75	*Se* 82	Mo 95	Ru 101	Rh 103	*Ag* 107	Pd 108	Cd 111	*In* 115	*Sn* 118	*Sb* 121	*Te* 128	Re 185	Os 189	Ir 193	Pt 195	*Au* 197	Tl 205	*Pb* 208	*Bi* 209
55um	0.470	0.023	0.241	0.353	0.028	0.223	2.53	0.030	0.023	0.005	0.023	0.014	0.046	0.012	0.073	0.022	0.256	0.009	0.021	0.007	0.013	0.010	0.004	0.012	0.007
33um	0.939	0.046	0.722	1.06	0.085	0.445	5.07	0.061	0.068	0.009	0.069	0.041	0.137	0.025	0.218	0.067	0.513	0.027	0.042	0.020	0.039	0.030	0.011	0.037	0.013
2221CCP-06.d	2.99	8.20	23.0	409	31.6	<dl	668	<dl	<dl	n.r.	83.9	<dl	4.54	16.9	93.0	0.054	31.0	<dl	<dl	<dl	<dl	0.113	0.004	1.47	41.0
2221CCP-07.d	1.72	4.58	2.09	368	15.2	<dl	665	<dl	<dl	n.r.	80.8	<dl	4.02	16.5	61.4	0.066	6.80	<dl	<dl	0.030	<dl	0.352	0.023	2.09	4.80
2224CCP-01d	1.60	2.59	2.20	207	2.09	<dl	1733	<dl	0.022	n.r.	50.8	<dl	1.25	95.6	108	0.610	3.64	<dl	<dl	<dl	<dl	0.095	4.E-4	3.45	2.45
2224CCP-02.d	0.161	2.47	0.029	213	13.8	<dl	1800	0.022	<dl	n.r.	51.7	<dl	1.53	95.9	82.1	0.850	2.82	<dl	<dl	<dl	<dl	0.183	0.024	8.60	2.82
2224CCP-03.d	2.98	2.74	0.410	337	10.2	<dl	1720	<dl	<dl	n.r.	46.4	<dl	1.83	91.0	96.8	0.452	3.30	<dl	<dl	<dl	<dl	0.176	0.001	4.40	2.15
2224CCP-04.d	1.32	4.35	0.400	271	1.96	<dl	1629	<dl	<dl	n.r.	54.6	<dl	1.63	97.0	127	0.460	5.48	<dl	0.017	<dl	<dl	0.178	5.E-4	3.50	2.80
2224CCP-05.d	0.460	3.70	0.300	203	13.0	<dl	1892	<dl	<dl	n.r.	53.1	<dl	1.63	98.9	105	0.406	3.63	<dl	<dl	<dl	<dl	0.270	0.005	3.58	1.18
2224CCP-06.d	2.40	3.03	0.600	180	12.9	0.130	1743	<dl	<dl	n.r.	48.5	<dl	1.15	95.1	67.6	0.670	3.50	<dl	<dl	<dl	<dl	0.101	0.236	9.40	2.56
2296CCP-01d	3.27	0.911	0.160	414	0.293	<dl	919	<dl	<dl	n.r.	243	<dl	1.53	24.4	85.0	0.339	0.037	<dl	<dl	<dl	<dl	0.040	0.124	1.45	1.39
2296CCP-02.d	1.14	0.703	0.021	395	0.240	<dl	90.9	0.011	<dl	n.r.	71.9	<dl	1.53	23.0	81.8	0.587	0.032	<dl	<dl	<dl	<dl	0.005	0.098	1.34	1.23
2296CCP-03.d	0.730	0.362	0.026	380	0.353	<dl	85.0	<dl	<dl	n.r.	68.6	<dl	1.68	22.8	86.5	1.07	0.041	<dl	<dl	<dl	0.100	0.088	0.141	1.97	2.18
2296CCP-04.d	2.13	0.860	0.023	335	0.395	<dl	92.8	<dl	0.022	n.r.	63.7	<dl	1.70	23.3	78.8	0.725	0.030	<dl	<dl	<dl	<dl	0.062	0.157	1.80	1.47
2296CCP-05.d	0.830	0.575	0.019	380	0.263	<dl	83.1	<dl	<dl	n.r.	88.8	<dl	1.24	21.6	89.3	0.342	0.172	<dl	<dl	<dl	<dl	0.021	0.041	0.898	1.24
2296CCP-06.d	0.660	0.733	0.024	332	0.212	<dl	89.1	<dl	<dl	n.r.	76.0	<dl	1.31	21.6	67.5	1.52	0.035	<dl	<dl	<dl	<dl	0.020	0.249	2.14	1.89
2296CCP-07.d	1.99	0.748	0.030	487	0.294	<dl	97.9	<dl	<dl	n.r.	127	<dl	2.01	24.1	97.0	0.537	0.199	<dl	<dl	<dl	<dl	0.043	0.355	1.46	1.60
2318CCP-01d	0.122	3.90	43.0	469	0.157	<dl	36.8	<dl	<dl	n.r.	31.3	<dl	5.45	30.8	7.03	0.005	0.036	<dl	<dl	<dl	<dl	5.E-4	0.003	2.26	0.116
2318CCP-02.d	0.660	1.62	27.0	443	0.160	<dl	36.8	<dl	0.090	n.r.	30.3	<dl	4.82	33.1	8.77	0.004	0.034	<dl	<dl	<dl	<dl	8.E-4	3.E-4	1.60	0.098
2318CCP-03.d	0.154	0.920	3.43	428	0.007	<dl	39.5	<dl	<dl	n.r.	30.3	<dl	5.35	27.6	5.55	0.007	0.043	<dl	<dl	<dl	<dl	9.E-4	0.060	1.91	0.138
2318CCP-04.d	1.10	0.353	56.1	308	0.285	<dl	40.1	<dl	<dl	n.r.	24.4	<dl	4.44	32.1	6.64	0.024	0.048	<dl	<dl	<dl	<dl	5.E-4	0.005	2.24	0.150
2318CCP-05.d	0.800	0.332	29.3	401	0.219	<dl	41.6	<dl	0.036	n.r.	34.9	<dl	5.55	33.7	6.39	0.004	0.035	<dl	<dl	<dl	<dl	6.E-4	4.E-4	1.52	0.033
2318CCP-06.d	0.420	0.224	40.8	372	0.104	<dl	33.2	<dl	<dl	n.r.	22.8	<dl	5.78	38.4	5.13	0.029	0.039	<dl	<dl	<dl	<dl	9.E-4	0.003	6.08	0.239
2318CCP-07.d	0.750	1.02	112	354	0.081	<dl	34.3	<dl	<dl	n.r.	33.0	<dl	4.78	37.0	4.59	0.004	0.039	<dl	<dl	<dl	<dl	7.E-4	2.E-4	1.09	0.029
2325CCP-01d	12.4	4.65	0.046	294	0.910	<dl	31.8	<dl	<dl	n.r.	62.5	<dl	1.44	18.3	82.1	0.342	0.044	<dl	<dl	<dl	<dl	0.306	3.E-4	2.88	5.18
2325CCP-02.d	4.03	2.81	0.049	226	0.517	<dl	30.6	0.036	<dl	n.r.	59.8	<dl	1.26	19.1	46.4	1.31	0.052	<dl	<dl	<dl	<dl	0.317	0.046	5.21	14.0
2325CCP-04.d	11.1	1.07	0.042	283	0.800	<dl	31.9	<dl	<dl	n.r.	54.8	<dl	1.03	19.7	48.2	0.890	0.039	<dl	<dl	<dl	<dl	0.374	0.008	4.81	8.38
2325CCP-05.d	8.35	2.94	0.049	303	0.650	<dl	33.7	<dl	<dl	n.r.	55.6	<dl	1.13	18.7	74.8	0.426	0.047	<dl	<dl	<dl	<dl	0.401	0.008	2.71	6.66
2325CCP-06.d	10.6	6.22	0.052	337	0.590	<dl	35.3	0.036	<dl	n.r.	59.3	<dl	1.42	20.1	76.1	0.640	0.056	<dl	<dl	<dl	<dl	0.339	0.004	5.85	8.18
2325CCP-07.d	11.1	5.19	0.036	312	0.590	<dl	36.5	<dl	<dl	n.r.	58.5	<dl	1.48	19.4	80.4	0.385	0.059	<dl	<dl	<dl	<dl	0.320	0.002	4.42	6.13
2359-CCP-01d	3.15	10.4	0.096	174	0.076	0.290	516	<dl	<dl	n.r.	170	<dl	3.17	60.7	104	1.28	0.560	<dl	<dl	<dl	<dl	0.580	0.059	7.40	5.87
2359-CCP-02.d	2.45	10.0	2.10	174	0.060	<dl	482	<dl	0.024	n.r.	118	<dl	2.56	58.7	92.9	0.139	0.540	<dl	<dl	<dl	<dl	0.410	1.E-3	1.93	2.21
2359-CCP-03.d	3.40	12.5	0.182	173	0.215	<dl	503	<dl	<dl	n.r.	385	<dl	3.13	63.7	95.7	0.860	0.660	<dl	<dl	<dl	<dl	3.88	0.014	8.46	7.59
2359-CCP-04.d	2.35	9.37	3.13	191	0.241	<dl	503	<dl	<dl	n.r.	141	<dl	2.74	59.8	106	0.140	0.760	<dl	<dl	<dl	<dl	0.136	0.008	1.45	1.69
2359-CCP-05.d	2.49	9.45	3.30	223	0.430	<dl	579	<dl	<dl	n.r.	172	<dl	3.46	64.9	125	0.301	0.800	<dl	<dl	<dl	<dl	0.670	0.001	4.56	4.31
2359-CCP-06.d	3.21	9.45	0.175	187	0.151	<dl	526	<dl	<dl	n.r.	169	<dl	2.49	62.9	98.8	0.211	0.520	<dl	<dl	<dl	<dl	0.391	0.011	1.76	2.09
2369CCP-01d	10.0	1.35	0.390	273	1.04	0.540	113	<dl	<dl	n.r.	932	<dl	8.08	307	207	0.018	0.116	<dl	<dl	<dl	<dl	0.002	0.020	0.874	0.879
2369CCP-02.d	0.371	1.38	0.047	286	1.10	<dl	119	<dl	<dl	n.r.	944	<dl	8.06	299	123	0.245	0.145	<dl	<dl	<dl	<dl	0.003	0.012	3.20	3.78
2369CCP-03.d	0.355	1.18	0.049	328	1.98	<dl	141	<dl	<dl	n.r.	830	<dl	9.06	326	214	0.100	0.126	<dl	<dl	<dl	0.010	0.009	0.011	2.10	1.58
2369CCP-04.d	0.378	1.26	0.055	305	1.28	<dl	122	<dl	<dl	n.r.	897	<dl	7.81	302	140	0.264	0.140	<dl	<dl	<dl	<dl	0.001	0.028	3.65	3.71
2369CCP-05.d	0.415	1.09	0.050	287	0.830	<dl	117	<dl	<dl	n.r.	939	<dl	6.77	310	110	0.610	0.149	<dl	<dl	<dl	<dl	0.003	0.085	9.70	6.50
2369CCP-06.d	0.462	1.14	0.045	234	0.840	<dl	119	<dl	<dl	n.r.	1010	<dl	7.26	279	102	0.910	0.187	<dl	<dl	<dl	<dl	0.005	0.129	9.57	5.84
2369CCP-07.d	0.317	1.33	0.042	275	0.300	<dl	92.0	<dl	<dl	n.r.	1031	<dl	6.75	271	218	0.017	0.097	<dl	<dl	<dl	<dl	0.002	0.005	0.546	0.440
2378CCP-01d	0.323	0.089	0.030	365	5.40	<dl	8.30	<dl	<dl	n.r.	3.55	<dl	1.88	104	47.3	0.107	0.025	<dl	<dl	<dl	0.042	5.E-4	0.011	1.58	0.015
2378CCP-02.d	0.234	0.098	0.026	350	6.88	<dl	13.6	0.065	<dl	n.r.	5.56	<dl	2.04	81.0	51.0	0.213	0.024	<dl	<dl	<dl	<dl	5.E-4	0.012	2.02	0.031
2378CCP-03.d	0.219	0.076	0.022	314	5.90	<dl	8.70	<dl	<dl	n.r.	5.32	<dl	2.18	76.3	56.6	0.074	0.020	<dl	0.029	<dl	<dl	5.E-4	0.007	0.930	0.026
2378CCP-04.d	0.264	0.015	0.380	280	1.53	<dl	1.58	<dl	0.027	n.r.	4.37	<dl	1.31	82.7	28.7	0.217	0.035	<dl	<dl	<dl	<dl	0.001	0.010	1.70	0.190
2378CCP-05.d	0.272	0.013	0.036	307	3.39	<dl	10.2	<dl	0.042	n.r.	4.56	<dl	1.54	79.4	36.4	0.138	0.026	<dl	<dl	<dl	<dl	6.E-4	0.016	1.62	0.076
2378CCP-06.d	0.186	0.075	0.026	325	3.60	<dl	11.8	<dl	0.024	n.r.	4.39	<dl	1.86	76.2	46.1	0.135	0.020	<dl	<dl	<dl	<dl	4.E-4	0.010	1.16	0.030

Grain ID	*Mn* 55	Co 59	*Ni* 60	*Zn* 66	*Ga* 71	As 75	*Se* 82	Mo 95	Ru 101	Rh 103	*Ag* 107	Pd 108	Cd 111	*In* 115	*Sn* 118	*Sb* 121	*Te* 128	Re 185	Os 189	Ir 193	Pt 195	*Au* 197	Tl 205	*Pb* 208	*Bi* 209
55um	0.470	0.023	0.241	0.353	0.028	0.223	2.53	0.030	0.023	0.005	0.023	0.014	0.046	0.012	0.073	0.022	0.256	0.009	0.021	0.007	0.013	0.010	0.004	0.012	0.007
33um	0.939	0.046	0.722	1.06	0.085	0.445	5.07	0.061	0.068	0.009	0.069	0.041	0.137	0.025	0.218	0.067	0.513	0.027	0.042	0.020	0.039	0.030	0.011	0.037	0.013
2378CCP-07.d	0.383	0.900	0.045	292	1.79	0.700	13.0	<dl	0.021	n.r.	6.69	<dl	1.51	75.0	40.5	0.610	0.041	<dl	<dl	<dl	<dl	0.001	0.087	5.60	0.124
2378CCP-08.d	0.256	0.110	0.036	353	5.53	<dl	16.2	<dl	<dl	n.r.	4.91	<dl	2.19	76.6	49.2	0.257	0.026	<dl	<dl	<dl	<dl	0.001	0.016	2.64	0.133
2383-CCP-01d	3.46	3.54	0.145	324	2.29	<dl	559	<dl	<dl	n.r.	46.8	<dl	2.16	40.4	18.6	0.530	0.111	<dl	<dl	<dl	<dl	0.003	0.043	17.3	1.68
2383-CCP-02.d	4.04	2.02	0.150	328	1.92	<dl	570	<dl	<dl	n.r.	41.9	<dl	2.16	43.4	21.0	0.530	0.147	<dl	<dl	<dl	<dl	0.002	0.068	17.1	1.42
2383-CCP-03.d	5.40	3.99	1.20	460	4.95	2.29	633	<dl	<dl	n.r.	51.1	<dl	2.09	49.3	23.3	0.350	0.138	<dl	<dl	<dl	<dl	0.005	0.003	10.2	2.29
2383-CCP-04.d	3.18	5.53	0.136	358	3.95	<dl	673	<dl	<dl	n.r.	46.1	<dl	1.87	46.6	29.3	0.360	0.111	<dl	<dl	<dl	<dl	0.005	0.028	7.20	1.40
2383-CCP-05.d	3.12	1.48	0.127	402	5.71	<dl	667	<dl	<dl	n.r.	46.8	<dl	2.09	45.1	40.7	0.191	0.082	<dl	<dl	<dl	<dl	0.005	0.018	4.91	1.07
2383-CCP-06.d	2.54	2.58	1.70	378	5.10	<dl	650	<dl	<dl	n.r.	46.2	<dl	1.72	47.2	35.6	0.260	0.117	<dl	<dl	<dl	<dl	0.002	0.002	7.50	3.96
2393-CCP-01d	3.10	1.51	0.144	488	0.460	<dl	608	<dl	<dl	n.r.	80.7	<dl	8.80	72.7	65.1	0.190	0.700	<dl	<dl	<dl	<dl	0.167	0.002	8.28	0.680
2393-CCP-02.d	3.63	2.43	0.190	445	0.510	<dl	576	<dl	<dl	n.r.	79.5	<dl	9.70	82.5	71.6	0.351	0.610	<dl	0.029	<dl	<dl	0.088	0.001	7.08	0.960
2393-CCP-03.d	2.95	1.45	0.197	376	0.414	<dl	567	<dl	<dl	n.r.	77.0	<dl	8.07	72.1	73.9	0.341	0.740	<dl	<dl	<dl	<dl	0.109	0.014	5.46	1.91
2393-CCP-04.d	3.82	1.64	0.158	515	0.563	<dl	605	<dl	0.027	n.r.	88.3	<dl	13.1	66.6	78.4	0.710	0.940	<dl	<dl	<dl	<dl	0.137	0.002	10.9	1.51
2393-CCP-05.d	3.88	1.38	0.153	557	0.560	<dl	605	<dl	<dl	n.r.	79.6	<dl	12.7	60.5	69.2	0.339	0.700	0.018	<dl	<dl	<dl	0.012	0.002	6.85	0.750
2393-CCP-06.d	3.78	2.62	2.40	520	0.680	<dl	613	<dl	<dl	n.r.	79.8	<dl	10.9	90.1	92.5	0.326	0.950	<dl	<dl	<dl	<dl	0.043	0.001	8.72	0.794
2394-CCP-01d	1.28	22.2	1.70	408	0.137	<dl	282	0.042	<dl	n.r.	14.0	<dl	6.60	1.99	105	5.93	1.31	<dl	<dl	<dl	<dl	0.011	0.072	3.32	0.770
2394-CCP-02.d	2.37	21.5	3.20	560	0.098	<dl	287	<dl	<dl	n.r.	9.54	<dl	5.24	2.97	126	3.34	0.780	<dl	<dl	<dl	<dl	0.012	0.038	2.85	0.720
2394-CCP-03.d	2.26	29.6	1.80	482	0.092	<dl	265	<dl	<dl	n.r.	12.8	<dl	6.26	3.16	107	3.54	0.580	<dl	<dl	<dl	<dl	0.013	0.047	2.27	0.800
2394-CCP-04.d	3.44	18.0	0.150	483	0.099	0.168	269	<dl	<dl	n.r.	9.30	<dl	3.73	2.52	93.1	1.48	0.850	<dl	<dl	<dl	<dl	0.059	7.E-4	1.57	0.530
2394-CCP-05.d	2.54	1.21	2.10	581	18.6	0.124	253	<dl	0.094	n.r.	207	<dl	3.25	343	111	2.36	0.950	<dl	<dl	<dl	<dl	0.005	0.001	3.12	0.035
2394-CCP-06.d	3.50	1.79	2.30	584	24.1	<dl	254	<dl	0.090	n.r.	221	<dl	3.50	364	130	1.58	1.24	<dl	<dl	<dl	<dl	0.004	0.001	1.85	0.038
2398-CCP-01d	3.65	1.96	1.55	554	0.442	<dl	573	<dl	<dl	n.r.	80.8	<dl	11.3	59.4	58.4	0.282	0.840	<dl	<dl	<dl	<dl	0.034	0.002	17.3	0.700
2398-CCP-02.d	3.25	1.64	0.238	710	0.480	<dl	609	<dl	<dl	n.r.	87.9	<dl	13.8	63.9	63.5	0.169	0.820	<dl	<dl	<dl	<dl	0.002	0.002	6.82	0.660
2398-CCP-03.d	3.44	2.90	0.230	342	0.450	<dl	525	<dl	<dl	n.r.	73.0	<dl	7.60	78.6	68.7	0.152	0.500	<dl	<dl	<dl	<dl	0.024	0.002	15.4	0.610
2398-CCP-04.d	3.32	1.26	0.237	541	0.266	<dl	540	<dl	<dl	n.r.	83.1	<dl	11.3	56.5	57.0	0.258	0.520	<dl	<dl	<dl	<dl	0.052	0.003	49.1	0.750
2398-CCP-05.d	3.30	1.84	0.205	400	0.515	<dl	560	<dl	<dl	n.r.	79.4	<dl	10.2	61.2	61.1	0.250	0.770	<dl	<dl	<dl	<dl	0.039	0.002	42.8	0.630
2398-CCP-06.d	3.18	1.16	0.200	422	0.420	<dl	508	0.036	<dl	n.r.	77.6	<dl	8.87	59.2	59.9	0.190	0.540	<dl	<dl	<dl	<dl	0.051	0.011	5.65	0.481
2399-CCP-01d	5.64	0.287	0.183	501	1.66	0.133	233	<dl	<dl	n.r.	90.4	<dl	6.23	45.7	148	3.39	0.930	<dl	<dl	<dl	<dl	0.004	0.001	3.52	2.12
2399-CCP-02.d	4.72	0.351	1.70	417	2.43	1.42	226	<dl	0.025	n.r.	124	<dl	4.65	39.7	133	1.84	0.530	<dl	<dl	<dl	<dl	0.186	0.001	2.22	0.903
2399-CCP-03.d	5.53	0.337	0.178	529	2.81	<dl	245	<dl	<dl	n.r.	96.3	<dl	6.89	53.8	187	3.52	1.25	<dl	<dl	<dl	<dl	0.002	0.016	4.57	1.64
2399-CCP-04.d	5.09	0.307	0.148	412	2.49	<dl	217	<dl	<dl	n.r.	118	<dl	5.09	40.6	114	2.30	0.740	<dl	<dl	<dl	0.015	0.003	0.002	2.52	0.969
2399-CCP-05.d	5.81	0.206	2.14	437	2.42	0.101	258	<dl	0.080	n.r.	99.7	<dl	6.45	50.2	149	5.40	1.18	<dl	<dl	<dl	<dl	0.002	0.015	5.30	1.78
2399-CCP-06.d	6.40	0.183	0.105	457	2.30	0.229	266	<dl	<dl	n.r.	140	<dl	5.08	41.6	136	2.35	0.890	<dl	<dl	<dl	<dl	0.003	0.097	2.54	1.30
2410-CCP-01d	2.64	2.15	0.142	373	0.482	<dl	540	<dl	<dl	n.r.	81.0	<dl	9.70	63.8	63.4	0.123	0.470	<dl	<dl	<dl	<dl	0.074	0.002	8.78	0.550
2410-CCP-02.d	2.90	1.73	0.146	425	0.480	<dl	522	0.043	<dl	n.r.	85.2	<dl	11.1	70.1	67.7	0.181	0.520	<dl	0.032	<dl	<dl	0.099	0.001	9.71	0.900
2410-CCP-03.d	2.52	1.58	2.20	541	0.370	<dl	609	<dl	<dl	n.r.	94.6	<dl	13.2	77.8	104	0.560	1.04	<dl	<dl	<dl	<dl	0.044	0.137	12.3	8.10
2410-CCP-04.d	2.92	1.09	0.197	373	0.460	<dl	499	<dl	<dl	n.r.	77.1	<dl	8.81	106	71.2	0.108	0.370	<dl	<dl	<dl	<dl	0.095	0.001	5.55	0.577
2410-CCP-05.d	2.58	1.88	2.30	497	0.730	<dl	562	<dl	<dl	n.r.	82.5	<dl	11.7	65.3	63.4	0.340	1.19	<dl	0.120	<dl	<dl	0.180	0.002	8.40	1.10
2410-CCP-06.d	3.03	0.863	0.176	411	0.362	<dl	501	<dl	<dl	n.r.	73.9	<dl	8.46	93.3	74.7	0.168	0.380	0.010	<dl	<dl	<dl	0.056	0.009	6.15	0.695
2414-CCP-01d	3.87	1.74	0.142	561	1.50	<dl	448	<dl	<dl	n.r.	88.7	<dl	3.00	76.8	198	0.456	0.440	<dl	<dl	<dl	<dl	0.113	0.012	4.18	1.41
2414-CCP-02.d	3.82	2.08	1.89	541	1.56	<dl	453	<dl	<dl	n.r.	86.4	<dl	2.92	69.6	185	1.18	0.590	<dl	<dl	<dl	<dl	0.081	0.002	12.3	2.02
2414-CCP-03.d	3.93	1.55	1.25	617	1.57	<dl	433	<dl	<dl	n.r.	89.9	<dl	3.21	84.8	212	0.552	0.487	<dl	<dl	<dl	<dl	0.129	0.001	4.16	1.90
2414-CCP-04.d	2.97	1.43	0.116	474	1.42	<dl	393	<dl	<dl	n.r.	87.4	<dl	2.22	63.8	165	2.16	0.390	<dl	<dl	<dl	<dl	0.003	8.E-4	2.29	3.34
2414-CCP-05.d	3.31	2.88	0.111	604	1.24	<dl	396	<dl	<dl	n.r.	86.5	<dl	3.55	62.4	158	1.78	0.440	<dl	<dl	<dl	<dl	0.042	0.001	5.60	3.44
2414-CCP-06.d	3.78	2.70	0.112	596	1.37	<dl	436	0.022	<dl	n.r.	85.5	<dl	3.75	63.6	170	0.700	0.480	<dl	<dl	<dl	<dl	0.035	1.E-3	4.06	1.77
2417-CCP-01d	5.30	1.54	0.207	800	1.10	<dl	495	<dl	<dl	n.r.	88.0	<dl	13.6	87.6	88.6	0.685	0.630	<dl	<dl	<dl	<dl	0.004	0.002	11.1	1.72
2417-CCP-02.d	3.19	1.04	0.165	396	1.02	<dl	456	<dl	<dl	n.r.	83.4	<dl	8.60	94.9	90.4	0.263	0.530	<dl	<dl	<dl	<dl	0.012	0.001	4.47	1.15
2417-CCP-03.d	3.83	0.990	1.54	481	1.08	<dl	448	<dl	<dl	n.r.	83.7	<dl	10.0	79.7	76.7	0.570	0.470	<dl	<dl	<dl	<dl	0.004	0.002	5.51	0.920

Grain ID	*Mn* 55	*Co* 59	*Ni* 60	*Zn* 66	*Ga* 71	As 75	*Se* 82	Mo 95	Ru 101	Rh 103	*Ag* 107	Pd 108	Cd 111	*In* 115	*Sn* 118	*Sb* 121	*Te* 128	Re 185	Os 189	Ir 193	Pt 195	*Au* 197	Tl 205	*Pb* 208	*Bi* 209
55um	0.470	0.023	0.241	0.353	0.028	0.223	2.53	0.030	0.023	0.005	0.023	0.014	0.046	0.012	0.073	0.022	0.256	0.009	0.021	0.007	0.013	0.010	0.004	0.012	0.007
33um	0.939	0.046	0.722	1.06	0.085	0.445	5.07	0.061	0.068	0.009	0.069	0.041	0.137	0.025	0.218	0.067	0.513	0.027	0.042	0.020	0.039	0.030	0.011	0.037	0.013
2417-CCP-04.d	3.90	0.510	2.30	430	0.920	<dl	519	<dl	<dl	n.r.	90.4	<dl	10.2	97.5	104	0.570	0.300	<dl	<dl	<dl	<dl	0.004	0.001	6.72	1.22
2417-CCP-05.d	4.06	1.11	0.196	574	1.17	<dl	487	<dl	<dl	n.r.	88.8	<dl	9.70	98.0	102	0.800	0.380	<dl	<dl	<dl	<dl	0.014	0.002	27.5	159
24-4-ccp1d	0.330	0.900	0.049	192	0.940	<dl	332	0.043	<dl	n.r.	2.89	<dl	0.730	47.7	18.4	0.460	1.08	<dl	<dl	<dl	<dl	0.014	0.009	1.86	0.170
24-4-ccp2.d	0.430	1.08	0.075	252	0.950	<dl	403	<dl	<dl	n.r.	3.81	<dl	1.90	60.8	25.4	0.430	1.50	<dl	<dl	<dl	<dl	0.024	9.E-4	3.40	0.440
24-4-ccp3.d	0.380	1.10	0.062	248	0.980	<dl	363	<dl	<dl	n.r.	3.95	<dl	0.780	56.4	21.0	0.460	1.70	<dl	<dl	<dl	<dl	0.022	8.E-4	2.85	0.370
2567-CCP-01d	148	12.7	0.234	552	0.939	<dl	613	<dl	<dl	n.r.	70.3	<dl	5.30	6.00	6.47	0.157	0.880	<dl	<dl	<dl	<dl	0.002	4.E-4	0.266	0.750
2567-CCP-02.d	138	18.1	2.10	638	1.26	<dl	67.5	<dl	<dl	n.r.	85.8	<dl	6.01	9.63	10.7	0.275	1.19	<dl	<dl	<dl	<dl	0.003	7.E-4	0.325	0.850
2567-CCP-03.d	186	14.1	3.70	551	1.37	<dl	58.3	<dl	<dl	n.r.	78.1	<dl	5.16	5.03	6.20	0.063	0.700	<dl	<dl	<dl	<dl	0.002	3.E-4	0.103	0.377
2567-CCP-04.d	98.3	8.08	8.10	464	1.19	<dl	60.3	<dl	<dl	n.r.	107	<dl	4.05	10.6	9.73	0.297	0.810	<dl	<dl	<dl	<dl	0.029	6.E-4	0.315	0.740
2567-CCP-05.d	115	14.3	2.90	511	1.43	<dl	60.2	<dl	<dl	n.r.	106	<dl	5.68	8.53	10.1	0.357	1.03	<dl	<dl	<dl	<dl	0.003	6.E-4	0.334	0.690
2567-CCP-06.d	139	15.1	11.1	541	1.13	<dl	59.5	<dl	<dl	n.r.	74.6	<dl	5.73	5.57	6.26	0.118	0.960	<dl	<dl	<dl	<dl	0.002	6.E-4	0.116	0.381
2569-CCP-01d	99.1	2.44	2.45	522	6.95	<dl	114	<dl	0.034	n.r.	75.3	<dl	8.66	5.43	81.9	0.036	0.640	0.010	<dl	<dl	<dl	0.002	0.006	0.650	0.648
2569-CCP-02.d	100	0.603	2.90	562	7.40	<dl	110	<dl	<dl	n.r.	424	<dl	8.08	5.56	82.4	0.033	0.320	<dl	<dl	<dl	<dl	0.002	7.E-4	0.414	0.375
2569-CCP-03.d	280	0.833	0.261	440	8.62	<dl	123	<dl	<dl	n.r.	87.5	<dl	8.17	5.05	80.9	0.210	0.440	<dl	<dl	<dl	<dl	0.004	0.001	1.61	0.670
2569-CCP-04.d	110	1.64	0.203	450	7.96	<dl	115	<dl	<dl	n.r.	63.5	<dl	8.31	5.08	81.8	0.122	0.340	<dl	<dl	<dl	<dl	0.002	9.E-4	0.890	0.494
2569-CCP-05.d	102	2.53	0.202	569	8.88	<dl	120	<dl	<dl	n.r.	89.6	<dl	8.88	5.97	86.7	0.045	0.740	<dl	0.022	<dl	<dl	0.002	7.E-4	1.00	1.19
2569-CCP-06.d	99.6	3.71	0.260	386	5.81	<dl	93.4	<dl	<dl	n.r.	61.6	<dl	7.04	4.93	78.3	0.048	0.400	<dl	<dl	<dl	<dl	0.013	8.E-4	1.00	0.568
2575-CCP-01d	28.5	3.49	1.20	374	1.00	<dl	155	<dl	<dl	n.r.	12.0	<dl	9.76	4.31	6.36	0.117	1.63	<dl	<dl	<dl	<dl	0.002	0.001	1.07	0.265
2575-CCP-02.d	26.0	3.96	4.66	392	0.730	<dl	164	<dl	<dl	n.r.	12.6	<dl	10.2	3.59	5.00	0.220	1.29	<dl	<dl	<dl	<dl	0.015	0.008	2.23	2.18
2575-CCP-03.d	25.8	3.43	3.50	413	0.790	<dl	154	<dl	<dl	n.r.	11.8	<dl	9.63	3.30	5.25	0.103	1.71	<dl	<dl	<dl	<dl	0.001	6.E-4	0.670	0.201
2575-CCP-04.d	45.3	2.29	0.310	371	1.35	<dl	170	<dl	<dl	n.r.	11.8	<dl	11.3	4.90	7.36	0.171	2.03	<dl	<dl	<dl	<dl	0.008	7.E-4	1.83	0.690
2575-CCP-05.d	14.3	0.670	2.60	346	0.720	<dl	160	<dl	0.018	n.r.	15.0	<dl	9.58	3.62	5.21	0.067	1.58	<dl	<dl	<dl	<dl	0.002	6.E-4	0.700	0.361
2575-CCP-06.d	29.6	3.09	4.30	363	0.478	<dl	149	<dl	<dl	n.r.	11.4	<dl	9.54	4.68	6.74	0.106	1.23	<dl	<dl	<dl	<dl	0.001	7.E-4	0.550	0.225
2643CCP-01d	3.59	4.92	0.023	289	14.6	<dl	62.4	<dl	<dl	n.r.	90.6	<dl	1.30	50.9	78.9	0.357	0.044	<dl	<dl	<dl	<dl	0.011	0.023	2.09	1.62
2643CCP-02.d	3.10	4.25	0.016	286	16.3	<dl	59.0	<dl	0.025	n.r.	91.4	<dl	1.37	49.0	79.1	0.304	0.041	<dl	<dl	<dl	<dl	7.E-4	0.028	1.44	0.589
2643CCP-03.d	0.800	5.16	0.019	281	10.9	<dl	56.7	<dl	<dl	n.r.	88.5	<dl	0.960	51.6	66.7	0.403	0.047	<dl	<dl	<dl	<dl	0.001	0.118	4.07	1.25
2643CCP-04.d	6.95	2.51	0.034	271	14.7	<dl	76.5	<dl	<dl	n.r.	100	<dl	1.36	49.1	78.3	0.525	0.505	<dl	<dl	<dl	<dl	0.010	0.157	3.96	1.90
2643CCP-05.d	4.90	3.31	0.021	289	13.6	<dl	57.2	<dl	<dl	n.r.	92.5	<dl	1.24	49.6	75.3	0.304	0.050	<dl	<dl	<dl	<dl	0.010	0.052	2.20	1.15
2643CCP-06.d	14.9	1.49	0.023	269	15.1	<dl	62.9	<dl	<dl	n.r.	96.8	<dl	1.57	46.7	76.9	0.472	0.037	<dl	<dl	<dl	<dl	0.007	0.104	2.51	0.909
2647CCP-01d	0.231	0.800	0.037	343	0.135	<dl	793	0.028	<dl	n.r.	42.4	<dl	4.99	161	78.3	0.370	0.060	<dl	<dl	<dl	<dl	0.099	0.024	2.39	4.00
2647CCP-02.d	0.153	1.03	0.120	344	0.128	<dl	787	0.018	<dl	n.r.	40.2	<dl	4.50	161	74.2	0.430	0.039	<dl	<dl	<dl	<dl	0.182	0.013	2.07	2.63
2647CCP-03.d	0.420	0.910	0.032	295	0.138	<dl	746	<dl	0.017	n.r.	35.0	<dl	3.90	156	73.1	0.281	0.057	<dl	<dl	0.003	<dl	0.098	0.019	1.33	1.90
2647CCP-04.d	0.640	0.866	0.224	319	0.130	<dl	758	<dl	<dl	n.r.	39.1	<dl	5.23	155	85.1	0.053	0.180	<dl	<dl	<dl	<dl	0.121	3.E-4	1.16	2.07
2647CCP-05.d	0.159	1.28	0.032	349	0.212	<dl	731	<dl	<dl	n.r.	40.0	<dl	5.48	162	83.4	0.196	0.056	<dl	<dl	<dl	<dl	0.100	0.007	1.84	2.85
2647CCP-06.d	0.800	0.800	0.220	416	0.210	<dl	725	0.014	<dl	n.r.	37.9	<dl	5.67	203	90.2	0.660	0.056	<dl	<dl	<dl	<dl	0.341	0.100	2.43	4.22
2647CCP-07.d	0.280	0.897	0.166	331	0.133	<dl	790	<dl	<dl	n.r.	39.2	<dl	4.53	198	62.5	0.594	0.044	<dl	<dl	<dl	<dl	0.080	0.014	3.12	4.02
2652CCP-01d	2.73	0.007	0.047	264	1.13	<dl	126	<dl	<dl	n.r.	155	<dl	3.35	287	104	2.97	0.104	<dl	<dl	<dl	<dl	0.131	0.358	9.92	6.68
2652CCP-02.d	1.22	0.010	0.031	252	1.11	<dl	143	<dl	<dl	n.r.	121	<dl	3.04	283	131	0.620	0.065	<dl	<dl	<dl	<dl	0.010	0.108	3.59	1.24
2652CCP-03.d	12.1	0.009	0.050	254	1.30	<dl	150	<dl	<dl	n.r.	130	<dl	3.64	293	155	0.473	0.076	<dl	<dl	<dl	<dl	0.019	0.073	2.39	1.50
2652CCP-04.d	0.314	0.008	0.036	253	1.27	<dl	139	<dl	<dl	n.r.	128	<dl	3.24	297	150	0.545	0.076	<dl	<dl	<dl	<dl	0.002	0.015	2.09	1.16
2652CCP-05.d	3.19	0.010	0.043	250	1.22	<dl	150	<dl	<dl	n.r.	142	<dl	3.47	281	107	1.37	0.095	<dl	<dl	<dl	<dl	0.084	0.423	8.76	4.29
2652CCP-06.d	1.02	0.024	0.020	271	2.16	<dl	96.1	0.026	<dl	n.r.	172	<dl	5.44	554	197	0.051	0.033	<dl	<dl	<dl	<dl	0.010	0.012	1.27	0.219
2652CCP-07.d	0.243	0.026	0.019	252	2.24	<dl	100	0.045	0.021	n.r.	163	<dl	5.74	544	178	0.083	0.035	<dl	<dl	<dl	<dl	1.E-3	0.018	1.76	0.256
2653-CCP-01d	2.54	0.017	5.50	171	0.041	<dl	79.7	<dl	<dl	n.r.	33.7	<dl	3.49	6.81	23.5	0.249	1.04	<dl	<dl	<dl	<dl	0.030	7.E-4	3.99	1.96
2653-CCP-02.d	2.21	0.024	6.00	168	0.056	<dl	83.4	<dl	<dl	n.r.	34.7	<dl	3.14	6.88	20.6	0.119	0.780	<dl	<dl	<dl	<dl	0.094	0.001	4.01	1.76
2653-CCP-03.d	2.79	0.020	6.40	154	0.044	<dl	73.2	<dl	<dl	n.r.	29.9	<dl	2.92	6.54	19.5	0.012	0.370	<dl	<dl	<dl	<dl	0.032	0.001	3.49	1.02
2653-CCP-04.d	2.49	0.012	4.52	163	0.034	<dl	76.1	<dl	<dl	n.r.	30.2	<dl	3.17	6.63	22.0	0.158	0.722	<dl	<dl	<dl	<dl	0.078	7.E-4	3.77	1.60

Grain ID	*Mn* 55	*Co* 59	*Ni* 60	*Zn* 66	*Ga* 71	As 75	*Se* 82	Mo 95	Ru 101	Rh 103	*Ag* 107	Pd 108	Cd 111	*In* 115	*Sn* 118	*Sb* 121	*Te* 128	Re 185	Os 189	Ir 193	Pt 195	*Au* 197	Tl 205	*Pb* 208	*Bi* 209
55um	0.470	0.023	0.241	0.353	0.028	0.223	2.53	0.030	0.023	0.005	0.023	0.014	0.046	0.012	0.073	0.022	0.256	0.009	0.021	0.007	0.013	0.010	0.004	0.012	0.007
33um	0.939	0.046	0.722	1.06	0.085	0.445	5.07	0.061	0.068	0.009	0.069	0.041	0.137	0.025	0.218	0.067	0.513	0.027	0.042	0.020	0.039	0.030	0.011	0.037	0.013
2653-CCP-05.d	2.49	0.218	13.2	158	0.134	<dl	75.2	<dl	<dl	n.r.	29.1	<dl	3.29	7.09	27.2	0.159	0.780	<dl	<dl	<dl	<dl	0.042	0.001	2.92	1.29
2653-CCP-06.d	2.54	0.067	9.20	143	0.041	<dl	75.4	0.310	<dl	n.r.	34.2	<dl	3.35	6.24	17.0	0.157	0.740	<dl	<dl	<dl	<dl	0.072	0.002	6.20	2.13
2704CCP-01d	0.500	0.361	2.99	364	0.910	<dl	508	<dl	<dl	n.r.	7.56	<dl	2.89	118	91.2	0.004	0.030	<dl	<dl	<dl	<dl	0.008	3.E-4	1.74	2.00
2704CCP-02.d	0.520	0.681	2.89	306	0.630	<dl	480	<dl	<dl	n.r.	7.20	<dl	2.57	131	68.5	0.005	0.031	<dl	<dl	<dl	<dl	0.036	3.E-4	1.19	1.82
2704CCP-03.d	0.340	1.56	2.73	292	0.498	<dl	454	<dl	<dl	n.r.	7.63	<dl	2.52	129	45.7	0.016	0.025	<dl	<dl	<dl	<dl	0.021	2.E-4	1.78	3.21
2704CCP-04.d	0.620	0.916	2.88	319	0.501	<dl	471	<dl	<dl	n.r.	6.91	<dl	2.58	124	74.0	0.018	0.027	<dl	<dl	<dl	<dl	0.140	2.E-4	0.840	1.33
2704CCP-05.d	0.370	0.664	2.86	347	0.445	<dl	463	<dl	<dl	n.r.	7.44	<dl	2.95	118	47.4	0.004	0.031	<dl	<dl	<dl	<dl	0.039	2.E-4	1.37	2.77
2704CCP-06.d	0.123	0.866	3.51	321	0.403	<dl	448	<dl	<dl	n.r.	6.94	<dl	2.65	120	52.7	0.016	0.026	<dl	<dl	<dl	<dl	0.011	2.E-4	1.28	1.85
2722-CCP-01d	3.62	3.80	2.73	390	0.530	<dl	173	<dl	0.022	n.r.	51.0	<dl	3.21	8.18	3.68	0.011	0.460	<dl	<dl	<dl	<dl	0.012	7.E-4	1.29	2.02
2722-CCP-02.d	5.20	4.15	3.40	591	1.04	<dl	182	<dl	0.031	n.r.	50.3	<dl	4.72	8.34	4.46	0.066	0.610	<dl	<dl	<dl	0.015	0.050	0.038	2.09	3.11
2722-CCP-03.d	3.66	3.39	2.40	513	0.185	<dl	188	<dl	<dl	n.r.	52.3	<dl	3.44	6.75	2.55	0.007	1.62	<dl	<dl	<dl	<dl	0.036	3.E-4	0.213	1.51
2722-CCP-04.d	6.32	6.03	3.00	419	0.270	<dl	182	<dl	<dl	n.r.	52.7	<dl	4.06	7.18	3.75	0.008	1.10	<dl	<dl	<dl	<dl	0.046	4.E-4	0.330	1.21
2722-CCP-05.d	6.36	6.44	2.77	624	0.289	<dl	195	0.062	<dl	n.r.	53.2	<dl	5.17	7.66	3.54	0.006	1.55	<dl	<dl	<dl	<dl	0.039	3.E-4	0.302	1.50
2722-CCP-06.d	7.04	5.34	0.159	630	0.244	<dl	194	<dl	<dl	n.r.	52.7	<dl	4.96	7.37	3.23	0.006	0.980	<dl	<dl	<dl	<dl	0.012	0.010	0.600	1.79
2729-CCP-01d	3.28	1.15	4.50	355	0.760	<dl	149	<dl	<dl	n.r.	118	<dl	14.5	4.51	23.7	0.410	0.710	<dl	<dl	<dl	<dl	0.002	0.001	2.31	1.33
2729-CCP-02.d	3.39	1.17	0.214	366	0.780	<dl	153	<dl	<dl	n.r.	128	<dl	14.5	4.83	24.4	1.13	0.690	0.023	<dl	<dl	<dl	0.046	1.E-3	5.82	4.89
2729-CCP-03.d	3.00	1.16	2.50	439	1.03	0.200	142	<dl	<dl	n.r.	119	<dl	18.9	4.55	23.5	0.366	0.710	<dl	<dl	<dl	<dl	0.021	0.008	2.67	1.64
2729-CCP-04.d	3.18	1.19	4.70	356	0.910	<dl	140	<dl	<dl	n.r.	114	<dl	16.4	4.43	21.0	0.264	0.420	<dl	<dl	<dl	<dl	0.004	7.E-4	2.25	1.41
2729-CCP-05.d	3.04	1.28	0.223	562	0.740	<dl	138	<dl	<dl	n.r.	123	<dl	21.1	4.47	23.6	0.159	1.15	<dl	<dl	<dl	<dl	0.003	6.E-4	1.52	1.05
2729-CCP-06.d	2.41	1.09	2.12	331	0.850	<dl	127	<dl	<dl	n.r.	113	<dl	13.0	4.55	20.0	0.456	0.370	<dl	<dl	<dl	<dl	0.003	9.E-4	3.53	1.59
2730-CCP-01d	260	2.11	0.104	387	32.0	<dl	137	0.017	0.043	n.r.	206	<dl	4.00	33.2	85.7	0.791	0.034	<dl	<dl	<dl	<dl	0.040	0.022	3.15	0.052
2730-CCP-02.d	14.0	2.49	0.074	433	15.1	<dl	129	<dl	<dl	n.r.	204	<dl	4.06	33.6	87.5	0.473	0.032	<dl	<dl	<dl	<dl	0.014	0.010	1.61	0.045
2730-CCP-03.d	2.77	2.50	3.80	407	34.9	<dl	137	0.028	<dl	n.r.	205	<dl	4.45	34.8	21.0	0.910	0.067	<dl	<dl	<dl	<dl	0.045	0.068	3.06	0.020
2730-CCP-04.d	4.70	1.82	2.40	409	45.0	<dl	112	<dl	<dl	n.r.	201	<dl	4.20	34.1	19.9	0.360	0.046	<dl	<dl	<dl	<dl	0.007	0.015	1.58	0.016
2730-CCP-05.d	2.30	0.015	0.157	375	0.570	<dl	112	<dl	<dl	n.r.	276	<dl	12.7	15.6	21.3	0.760	0.041	<dl	<dl	<dl	<dl	0.016	0.067	2.38	0.017
2730-CCP-06.d	2.45	0.013	0.145	330	0.590	<dl	123	<dl	<dl	n.r.	246	<dl	13.0	21.2	19.3	1.00	0.250	<dl	<dl	<dl	<dl	0.001	0.045	2.38	0.018
27ROV8CCP-01c	1.30	0.096	0.770	7.42	32.5	487	1.54	120	<dl	n.r.	3.94	3.17	0.140	85.8	168	44.5	5.21	<dl	<dl	<dl	<dl	3.76	0.013	7.66	41.3
27ROV8CCP-02.c	2.00	0.033	15.0	6.55	31.9	381	0.937	107	0.044	n.r.	4.92	0.128	0.023	76.2	112	41.2	4.76	<dl	<dl	<dl	<dl	4.79	0.008	8.08	40.3
27ROV8CCP-03.c	1.00	0.520	98.0	6.68	27.8	332	0.948	106	<dl	n.r.	6.30	<dl	0.036	75.6	120	36.0	5.20	0.320	<dl	<dl	<dl	3.21	0.007	6.32	34.5
27ROV8CCP-04.c	0.970	0.090	10.0	6.18	27.9	92.1	0.984	126	<dl	n.r.	2.98	<dl	0.011	54.9	184	60.3	0.740	<dl	<dl	<dl	<dl	0.114	5.E-4	0.386	5.81
27ROV8CCP-05.c	1.24	0.010	1.50	6.62	30.2	367	1.10	131	<dl	n.r.	5.20	<dl	0.100	68.2	120	37.4	4.26	<dl	<dl	0.035	<dl	3.29	0.014	6.41	38.2
27ROV8CCP-07.c	1.59	0.010	9.10	3.93	11.9	5.09	0.890	69.0	0.048	n.r.	4.96	0.695	0.017	19.2	38.2	2.70	0.026	0.130	0.600	<dl	<dl	0.406	0.008	0.112	0.399
28-2-ccp1d	4.70	0.026	0.048	303	10.1	<dl	781	<dl	<dl	n.r.	2.08	<dl	0.900	82.0	22.6	3.33	2.50	<dl	<dl	<dl	<dl	0.008	0.001	5.40	0.080
28-2-ccp2.d	0.640	0.025	0.032	203	10.1	<dl	730	<dl	<dl	n.r.	1.47	<dl	0.530	67.1	20.6	1.82	1.38	<dl	<dl	<dl	<dl	0.001	0.001	3.59	0.085
28-2-ccp3.d	0.137	0.034	0.061	190	42.4	<dl	940	<dl	<dl	n.r.	1.89	<dl	1.16	90.0	31.0	2.54	1.30	<dl	<dl	<dl	<dl	0.017	0.001	4.75	0.140
2924CCP-01d	1.03	0.202	0.053	320	0.270	<dl	98.2	<dl	<dl	n.r.	2.99	<dl	0.380	19.2	80.2	2.47	0.087	<dl	<dl	<dl	<dl	0.580	0.017	20.5	36.2
2924CCP-03.d	2.30	0.271	0.610	280	0.127	<dl	97.7	<dl	<dl	n.r.	3.59	<dl	0.950	8.91	46.9	1.31	0.106	<dl	<dl	<dl	<dl	0.314	0.019	15.6	18.0
2924CCP-04.d	1.95	0.305	0.079	247	0.250	<dl	95.6	<dl	<dl	n.r.	3.08	<dl	0.870	5.99	24.2	4.77	0.104	<dl	<dl	<dl	<dl	0.320	0.018	25.8	18.6
2924CCP-05.d	0.464	0.149	0.089	273	0.320	<dl	101	<dl	<dl	n.r.	5.19	<dl	1.17	8.29	37.1	7.80	0.136	<dl	<dl	<dl	<dl	0.290	0.030	41.4	43.8
2924CCP-06.d	0.435	0.111	0.075	261	0.300	<dl	100	<dl	<dl	n.r.	3.36	<dl	0.460	7.54	30.6	4.92	0.111	<dl	<dl	<dl	<dl	0.190	4.E-4	27.1	32.9
2924CCP-08.d	0.366	0.150	0.082	277	0.310	<dl	99.0	<dl	<dl	n.r.	2.16	<dl	0.820	5.97	25.4	4.57	0.114	<dl	0.021	<dl	<dl	0.200	0.011	19.9	27.0
2925CCP-01d	3.24	0.173	0.014	537	16.2	<dl	5.40	0.080	<dl	n.r.	43.6	<dl	1.12	6.53	91.7	3.26	0.023	<dl	<dl	<dl	<dl	0.012	9.E-4	5.79	0.050
2925CCP-02.d	3.48	0.196	0.022	436	10.7	<dl	13.9	<dl	<dl	n.r.	57.3	<dl	0.945	6.64	81.8	4.56	0.035	<dl	<dl	<dl	<dl	0.023	0.016	13.2	0.184
2925CCP-03.d	5.75	0.183	0.023	474	12.6	<dl	12.4	<dl	<dl	n.r.	64.4	<dl	1.02	5.64	850	14.6	0.038	<dl	<dl	<dl	<dl	0.040	0.044	19.1	0.281
2925CCP-04.d	3.04	0.195	0.018	509	10.8	<dl	9.00	<dl	<dl	n.r.	63.2	<dl	1.00	4.44	857	5.26	0.025	<dl	<dl	<dl	<dl	0.027	0.003	11.1	0.155
2925CCP-05.d	6.20	0.226	0.017	446	16.8	<dl	6.70	<dl	<dl	n.r.	60.9	<dl	0.800	5.04	897	7.20	0.025	<dl	<dl	<dl	<dl	0.061	0.093	5.11	0.061
2925CCP-06.d	1.37	0.184	0.027	433	9.69	<dl	3.15	<dl	<dl	n.r.	64.1	<dl	0.755	5.03	756	15.1	0.057	<dl	<dl	<dl	<dl	0.032	0.046	14.2	0.279

Grain ID	*Mn* 55	*Co* 59	*Ni* 60	*Zn* 66	*Ga* 71	As 75	*Se* 82	Mo 95	Ru 101	Rh 103	*Ag* 107	Pd 108	Cd 111	*In* 115	*Sn* 118	*Sb* 121	*Te* 128	Re 185	Os 189	Ir 193	Pt 195	*Au* 197	Tl 205	*Pb* 208	*Bi* 209
55um	0.470	0.023	0.241	0.353	0.028	0.223	2.53	0.030	0.023	0.005	0.023	0.014	0.046	0.012	0.073	0.022	0.256	0.009	0.021	0.007	0.013	0.010	0.004	0.012	0.007
33um	0.939	0.046	0.722	1.06	0.085	0.445	5.07	0.061	0.068	0.009	0.069	0.041	0.137	0.025	0.218	0.067	0.513	0.027	0.042	0.020	0.039	0.030	0.011	0.037	0.013
3112-CCP-01.d	2.77	9.04	5.90	138	0.083	<dl	41.5	<dl	<dl	n.r.	40.6	<dl	3.01	0.990	148	0.020	0.260	<dl	<dl	<dl	<dl	0.060	5.E-4	2.95	0.500
3112-CCP-02.d	2.80	11.2	0.108	193	0.090	<dl	43.9	<dl	<dl	n.r.	45.7	<dl	2.64	0.038	269	0.095	0.340	<dl	<dl	<dl	<dl	0.083	0.041	3.15	0.580
3112-CCP-03.d	2.38	14.2	5.50	166	0.063	<dl	43.7	<dl	<dl	n.r.	62.9	<dl	5.20	2.10	87.5	0.021	0.358	<dl	<dl	<dl	<dl	0.133	3.E-4	1.39	1.65
3112-CCP-04.d	2.35	19.7	1.30	131	0.072	<dl	42.3	<dl	<dl	n.r.	9.15	<dl	4.72	3.00	58.9	0.005	0.334	<dl	<dl	<dl	<dl	0.003	4.E-4	3.22	0.570
3112-CCP-05.d	2.56	18.4	2.30	172	0.101	<dl	47.9	<dl	<dl	n.r.	20.1	<dl	5.67	2.93	187	0.006	0.397	<dl	<dl	<dl	0.066	0.006	6.E-4	3.96	1.21
3143CCP-01.d	0.770	0.005	5.25	559	1.22	<dl	74.4	<dl	<dl	n.r.	745	<dl	3.02	40.2	229	3.16	1.47	<dl	<dl	<dl	<dl	0.031	0.540	4.12	0.048
3143CCP-03.d	0.176	0.057	6.50	734	1.07	<dl	58.6	<dl	<dl	n.r.	626	<dl	2.99	28.8	161	0.459	3.69	<dl	<dl	<dl	<dl	7.E-4	0.019	0.575	0.020
3143CCP-04.d	0.215	0.031	6.85	541	1.57	<dl	53.2	<dl	<dl	n.r.	607	<dl	3.90	31.0	161	0.700	2.91	<dl	<dl	<dl	<dl	0.001	0.014	0.820	0.024
3143CCP-05.d	0.242	0.073	4.57	538	1.41	<dl	62.0	<dl	<dl	n.r.	639	<dl	3.66	37.5	163	1.31	2.53	<dl	<dl	<dl	<dl	0.009	0.580	1.16	0.044
3143CCP-06.d	0.211	0.084	3.91	491	1.12	<dl	58.6	<dl	<dl	n.r.	846	<dl	3.37	56.2	205	1.25	2.84	<dl	<dl	<dl	<dl	0.031	0.410	1.69	0.043
3147CCP-01.d	0.235	0.006	0.020	126	44.8	11.9	20.6	0.130	0.022	n.r.	11.6	<dl	0.940	52.0	39.9	14.6	0.710	<dl	<dl	<dl	<dl	0.007	0.092	24.2	17.6
3147CCP-02.d	0.234	0.018	0.012	104	50.9	7.68	24.6	2.00	<dl	n.r.	8.30	<dl	1.35	56.0	43.0	8.36	0.490	<dl	<dl	<dl	<dl	1.E-3	0.069	13.9	11.6
3147CCP-03.d	0.185	0.006	0.018	167	46.8	1.99	38.2	<dl	0.022	n.r.	4.41	<dl	1.12	47.0	39.4	2.35	0.047	<dl	<dl	<dl	<dl	9.E-4	0.012	3.73	3.31
3147CCP-04.d	0.212	0.007	0.021	122	41.3	4.55	56.7	<dl	<dl	n.r.	7.17	<dl	0.950	48.8	42.0	6.02	0.720	<dl	<dl	<dl	<dl	0.001	0.034	8.43	7.89
3147CCP-05.d	0.212	0.008	0.023	151	28.0	1.17	45.4	0.170	<dl	n.r.	5.37	<dl	0.730	47.7	40.3	2.49	0.053	<dl	<dl	<dl	<dl	0.001	0.016	4.01	3.88
3147CCP-06.d	0.380	0.003	0.009	162	53.0	1.16	32.2	<dl	<dl	n.r.	4.74	<dl	0.710	45.0	40.2	1.42	0.032	<dl	<dl	<dl	<dl	6.E-4	0.004	2.12	1.73
3147CCP-07.d	0.285	0.009	0.025	114	56.9	2.89	28.6	<dl	<dl	n.r.	6.10	<dl	0.870	46.2	42.8	3.34	0.060	<dl	<dl	<dl	<dl	0.022	0.009	12.6	5.50
31ROV13CCCP-0	0.880	0.300	0.500	6.91	25.4	39.8	1.52	87.3	0.014	n.r.	5.10	<dl	0.020	41.7	685	11.8	1.33	<dl	<dl	<dl	<dl	0.042	2.E-4	0.091	7.46
31ROV13CCCP-0	1.30	0.052	7.00	8.18	22.9	90.5	2.30	76.8	<dl	n.r.	3.48	0.135	0.030	67.2	678	66.8	2.41	0.027	<dl	0.016	<dl	0.210	3.E-4	0.511	40.5
31ROV13CCCP-0	2.10	0.220	130	6.82	15.1	27.4	5.60	73.9	<dl	n.r.	3.26	0.315	0.027	28.7	618	10.9	0.670	0.510	<dl	<dl	<dl	0.027	0.005	0.098	6.62
31ROV13CCCP-0	1.08	0.050	0.290	7.40	12.5	24.8	5.30	101	<dl	n.r.	2.83	<dl	0.016	20.4	1300	13.3	1.68	<dl	<dl	<dl	<dl	0.021	2.E-4	0.285	13.6
31ROV13CCCP-0	1.24	0.034	0.260	7.98	23.3	19.8	6.60	109	<dl	n.r.	2.10	0.054	0.012	57.4	747	10.7	0.610	<dl	<dl	<dl	<dl	0.013	1.E-4	0.068	9.80
31ROV13CCCP-0	1.90	0.390	2.80	9.23	21.5	57.5	7.00	84.6	0.210	n.r.	2.86	<dl	0.014	54.3	941	45.6	1.53	<dl	<dl	<dl	<dl	0.280	5.E-4	0.450	37.1
31ROV13CCCP-0	0.990	0.058	0.220	7.91	23.2	108	4.54	86.3	<dl	n.r.	2.39	<dl	0.030	72.6	298	144	4.43	<dl	<dl	<dl	<dl	0.366	7.E-4	1.75	128
35GTV2B2CCP-(	2.11	365	0.300	707	19.3	1.13	5.40	<dl	<dl	n.r.	0.226	<dl	4.08	0.011	228	0.400	0.047	<dl	<dl	<dl	<dl	0.002	2.E-4	0.840	0.250
35GTV2B2CCP-(	3.86	548	0.065	2860	2.61	0.700	89.1	<dl	<dl	n.r.	1.79	<dl	11.4	0.395	282	0.004	0.890	<dl	<dl	<dl	<dl	0.023	1.E-4	0.231	0.209
35GTV2B2CCP-(	5.78	1262	1.50	1715	0.349	1.08	669	0.390	<dl	n.r.	2.98	<dl	7.32	2.96	189	0.006	31.3	<dl	0.070	<dl	<dl	0.089	3.E-4	0.035	0.183
35GTV2B2CCP-(	3.81	895	0.700	1500	0.549	<dl	650	<dl	<dl	n.r.	2.57	<dl	6.33	4.84	224	0.006	50.2	<dl	<dl	<dl	<dl	0.032	0.006	0.205	0.107
35GTV2B2CCP-(	4.71	1140	0.063	1261	0.293	0.690	668	<dl	<dl	n.r.	1.44	<dl	7.11	3.31	171	1.20	42.0	0.330	<dl	<dl	<dl	0.036	4.E-4	0.130	0.135
35GTV2B2CCP-(	2.95	733	5.00	545	1.37	0.940	93.5	<dl	<dl	n.r.	0.197	<dl	3.19	0.332	224	0.002	2.82	<dl	<dl	<dl	<dl	0.032	0.00	0.032	0.084
51CCP-01.d	0.212	2.21	0.016	295	4.12	<dl	146	<dl	0.021	n.r.	1589	<dl	1.87	18.6	33.8	1.34	0.058	<dl	<dl	<dl	<dl	0.001	0.004	3.06	3.75
51CCP-02.d	0.220	2.29	0.025	242	0.425	<dl	96.3	<dl	<dl	n.r.	1500	<dl	1.61	19.2	34.3	1.72	0.320	<dl	<dl	<dl	<dl	0.002	0.007	1.46	3.16
51CCP-03.d	0.316	2.37	0.023	322	3.79	<dl	140	<dl	<dl	n.r.	1640	<dl	1.30	20.2	35.0	2.82	0.075	<dl	<dl	<dl	<dl	0.002	0.010	8.10	4.78
51CCP-05.d	0.253	2.11	0.027	425	4.56	<dl	192	<dl	<dl	n.r.	1177	<dl	2.16	21.2	36.9	0.845	0.068	<dl	<dl	<dl	<dl	0.002	6.E-4	1.19	1.52
51CCP-06.d	0.308	2.52	0.033	248	4.19	<dl	130	<dl	<dl	n.r.	1384	<dl	1.59	19.5	36.4	3.67	0.087	<dl	<dl	<dl	<dl	0.002	0.041	4.07	5.61
52CCP-01.d	3.16	3.15	0.017	313	41.2	<dl	192	<dl	0.027	n.r.	308	<dl	1.06	93.3	168	0.010	0.056	<dl	<dl	<dl	0.009	0.001	0.059	2.77	1.42
52CCP-02.d	1.31	3.94	0.020	285	30.6	<dl	175	<dl	<dl	n.r.	297	<dl	0.830	91.8	57.9	0.026	0.060	<dl	<dl	<dl	<dl	0.184	0.040	1.16	1.63
52CCP-03.d	1.56	3.01	0.018	322	34.8	<dl	163	<dl	<dl	n.r.	295	<dl	0.865	91.8	68.4	0.012	0.061	<dl	<dl	<dl	<dl	0.080	0.153	2.76	2.51
52CCP-04.d	1.32	1.03	0.019	311	6.66	<dl	217	<dl	<dl	n.r.	302	<dl	0.995	86.8	78.2	0.327	0.064	<dl	<dl	<dl	<dl	0.033	0.194	3.31	2.59
52CCP-05.d	1.46	1.40	0.013	273	16.5	0.085	202	<dl	<dl	n.r.	312	<dl	0.680	93.5	78.6	0.045	0.041	<dl	<dl	<dl	<dl	0.184	0.023	1.18	1.73
52CCP-06.d	4.70	0.440	0.015	293	24.2	<dl	192	<dl	<dl	n.r.	300	<dl	0.800	93.2	79.7	0.445	0.038	<dl	<dl	<dl	<dl	0.066	0.220	1.55	1.96
52CCP-07.d	2.02	4.07	0.018	319	12.9	0.160	207	<dl	<dl	n.r.	301	<dl	0.965	91.7	90.2	0.011	0.051	<dl	<dl	<dl	<dl	0.002	0.031	1.25	1.14
53CCP-01.d	0.115	0.199	0.020	95.0	0.104	<dl	461	<dl	<dl	n.r.	38.5	<dl	0.910	88.5	48.4	0.359	0.340	<dl	<dl	<dl	<dl	1.10	9.E-4	1.80	0.990
53CCP-02.d	0.240	0.250	0.019	134	0.141	<dl	436	<dl	<dl	n.r.	46.5	<dl	1.65	86.1	52.2	0.258	0.440	<dl	<dl	<dl	<dl	2.34	9.E-4	2.04	0.866
53CCP-03.d	0.144	0.344	0.026	123	0.253	<dl	439	<dl	<dl	n.r.	46.6	<dl	2.03	80.7	47.6	0.149	0.480	<dl	<dl	<dl	<dl	0.449	3.E-4	2.30	1.06
53CCP-04.d	0.570	0.370	0.028	118	0.410	<dl	385	<dl	0.043	n.r.	62.4	<dl	2.37	79.1	37.4	0.177	0.590	<dl	<dl	<dl	<dl	0.280	6.E-4	2.35	0.900
53CCP-05.d	0.710	0.264	0.029	103	0.118	<dl	382	<dl	<dl	n.r.	38.0	<dl	1.87	75.9	48.6	0.214	0.340	<dl	<dl	<dl	<dl	1.02	3.E-4	3.08	1.27

Grain ID	*Mn* 55	*Co* 59	*Ni* 60	*Zn* 66	*Ga* 71	As 75	*Se* 82	Mo 95	Ru 101	Rh 103	*Ag* 107	Pd 108	Cd 111	*In* 115	*Sn* 118	*Sb* 121	*Te* 128	Re 185	Os 189	Ir 193	Pt 195	*Au* 197	Tl 205	*Pb* 208	*Bi* 209
55um	0.470	0.023	0.241	0.353	0.028	0.223	2.53	0.030	0.023	0.005	0.023	0.014	0.046	0.012	0.073	0.022	0.256	0.009	0.021	0.007	0.013	0.010	0.004	0.012	0.007
33um	0.939	0.046	0.722	1.06	0.085	0.445	5.07	0.061	0.068	0.009	0.069	0.041	0.137	0.025	0.218	0.067	0.513	0.027	0.042	0.020	0.039	0.030	0.011	0.037	0.013
53CCP-06.d	0.910	0.469	0.029	133	0.109	<dl	439	<dl	<dl	n.r.	913	<dl	2.45	816	64.5	0.085	0.910	<dl	<dl	<dl	<dl	4.28	8.E-4	1.04	0.687
53CCP-07.d	0.163	0.427	0.180	119	0.110	<dl	416	<dl	0.024	n.r.	79.1	<dl	1.09	77.1	57.1	0.404	0.440	<dl	<dl	<dl	<dl	3.84	6.E-4	4.70	2.29
53ROV13CCP-01	3.75	287	63.5	135	0.063	<dl	1116	0.660	<dl	n.r.	6.64	<dl	0.415	7.91	37.3	0.600	316	<dl	<dl	<dl	<dl	0.002	2.E-4	0.065	0.068
53ROV13CCP-02	2.84	205	95.9	129	0.084	<dl	1116	0.094	<dl	n.r.	1.38	<dl	0.377	7.10	51.2	0.001	38.9	<dl	<dl	<dl	<dl	9.E-4	0.00	0.043	0.022
53ROV13CCP-04	2.60	196	244	118	0.013	<dl	1392	0.130	<dl	n.r.	4.78	<dl	0.450	5.03	42.1	0.013	25.9	<dl	<dl	<dl	<dl	0.190	1.E-4	0.032	0.044
53ROV13CCP-05	5.20	223	315	133	0.043	0.190	1303	0.085	<dl	n.r.	5.25	<dl	0.490	5.12	39.6	0.500	22.4	<dl	<dl	<dl	<dl	0.019	0.014	0.390	0.027
53ROV13CCP-06	3.91	131	174	117	0.044	<dl	1221	0.095	<dl	n.r.	0.162	<dl	0.362	5.27	46.5	0.002	19.8	<dl	<dl	<dl	0.053	0.001	0.00	0.039	0.280
53ROV13CCP-07	2.95	201	140	108	0.077	<dl	1141	<dl	<dl	n.r.	0.347	<dl	0.440	5.64	86.2	0.002	12.6	<dl	<dl	<dl	<dl	0.001	1.E-4	0.121	0.018
53ROV6CCP-01c	2.25	0.540	0.160	610	0.980	<dl	260	0.110	<dl	n.r.	7.63	<dl	0.310	7.16	8.58	0.004	0.530	0.024	<dl	<dl	<dl	0.131	1.E-4	0.050	0.195
53ROV6CCP-02.	2.22	0.643	49.0	72.6	1.08	0.500	292	<dl	<dl	n.r.	7.97	<dl	0.590	9.00	9.54	0.004	0.770	0.053	<dl	<dl	<dl	0.144	1.E-4	0.022	0.067
53ROV6CCP-03.	2.30	0.810	0.015	77.9	1.70	<dl	285	<dl	0.180	n.r.	8.65	<dl	0.274	9.24	10.9	0.006	0.940	<dl	<dl	0.038	<dl	0.054	5.E-4	0.010	0.161
53ROV6CCP-04.	1.99	0.630	0.011	63.2	1.87	0.190	286	<dl	0.047	n.r.	8.57	<dl	0.210	10.2	20.4	0.005	0.790	<dl	<dl	0.016	<dl	0.039	1.E-4	0.038	0.307
53ROV6CCP-05.	1.19	0.304	0.190	56.5	2.58	<dl	383	0.140	<dl	n.r.	7.45	<dl	0.211	12.6	55.3	0.040	2.35	<dl	<dl	<dl	0.230	0.077	2.E-4	0.054	0.341
53ROV6CCP-06.	1.69	0.356	1.70	58.5	0.930	<dl	329	0.108	0.070	n.r.	2.96	0.035	0.232	9.77	30.3	0.024	1.26	<dl	<dl	<dl	<dl	0.001	1.E-4	0.067	0.636
53ROV6CCP-07.	1.87	0.320	0.190	52.6	1.97	<dl	335	0.290	<dl	n.r.	0.612	<dl	0.251	11.7	53.3	0.100	2.46	<dl	<dl	<dl	<dl	0.001	1.E-4	0.062	0.385
53ROV6CCP-08.	1.82	0.327	0.800	52.9	2.12	<dl	303	1.60	<dl	n.r.	0.234	<dl	0.230	19.2	34.1	0.051	4.40	<dl	<dl	<dl	<dl	0.001	0.00	0.073	0.809
56CCP-01d	4.84	0.125	1.63	345	0.257	<dl	53.6	<dl	<dl	n.r.	508	<dl	2.05	2.29	214	0.122	0.640	<dl	<dl	<dl	<dl	0.001	9.E-4	0.744	0.009
56CCP-02.d	2.97	0.141	1.59	394	0.244	<dl	55.8	<dl	<dl	n.r.	501	<dl	1.86	2.37	229	0.363	0.025	<dl	<dl	<dl	<dl	9.E-4	0.013	0.893	0.012
56CCP-03.d	1.07	0.116	0.890	343	0.185	<dl	60.9	<dl	<dl	n.r.	421	<dl	1.26	2.33	220	0.202	0.020	<dl	<dl	<dl	<dl	8.E-4	0.005	0.473	0.015
56CCP-04.d	2.44	0.112	0.750	304	0.250	<dl	55.2	<dl	<dl	n.r.	452	<dl	1.86	2.09	201	0.095	0.025	<dl	<dl	<dl	<dl	0.001	2.E-4	0.441	0.003
56CCP-05.d	0.460	0.052	0.530	325	0.193	<dl	64.4	<dl	<dl	n.r.	403	<dl	1.16	2.71	215	0.290	0.022	<dl	<dl	<dl	<dl	8.E-4	0.010	0.550	0.012
56CCP-06.d	0.420	0.108	0.800	341	0.190	<dl	55.4	<dl	<dl	n.r.	474	<dl	1.28	2.47	208	0.183	0.018	<dl	<dl	<dl	<dl	6.E-4	7.E-4	0.534	0.008
57A-3-ccp1d	0.180	0.013	0.038	224	0.134	<dl	262	<dl	<dl	n.r.	64.9	<dl	0.730	40.2	13.0	4.51	1.18	<dl	<dl	<dl	<dl	0.188	0.002	13.3	0.108
57A-3-ccp2.d	0.087	0.022	0.046	177	0.162	<dl	249	<dl	<dl	n.r.	47.9	<dl	0.450	38.1	20.4	0.680	1.50	<dl	<dl	<dl	<dl	0.077	0.001	1.71	0.010
57A-4-ccp1d	0.120	2.00	0.081	287	0.100	<dl	240	<dl	<dl	n.r.	76.1	<dl	1.19	45.5	25.8	0.660	0.950	<dl	<dl	<dl	<dl	0.036	0.002	1.83	0.036
601CCP-01d	0.820	1.06	0.260	272	24.6	<dl	25.6	<dl	<dl	n.r.	84.1	<dl	1.92	24.7	75.3	2.98	0.054	<dl	<dl	<dl	<dl	1.64	0.158	5.17	3.81
601CCP-02.d	0.275	0.950	0.028	308	25.3	<dl	32.6	<dl	0.061	n.r.	78.8	<dl	1.76	24.6	84.7	0.439	0.058	<dl	<dl	<dl	<dl	1.81	0.007	2.49	1.20
601CCP-03.d	0.740	0.892	0.014	261	25.1	<dl	29.9	<dl	<dl	n.r.	87.6	<dl	1.36	24.8	87.1	2.38	0.040	<dl	<dl	<dl	<dl	1.63	0.089	3.29	3.17
601CCP-04.d	1.08	1.17	0.022	266	22.6	1.20	34.3	<dl	<dl	n.r.	67.5	<dl	1.82	24.6	60.5	1.48	0.060	<dl	0.050	<dl	<dl	0.257	0.482	2.55	4.00
601CCP-05.d	2.26	1.35	0.016	290	28.0	<dl	38.4	<dl	<dl	n.r.	104	<dl	1.63	25.3	90.8	1.75	0.051	<dl	<dl	<dl	<dl	0.213	0.070	2.63	1.31
601CCP-06.d	1.86	0.995	0.025	280	15.7	<dl	38.6	<dl	<dl	n.r.	68.6	<dl	2.53	26.2	72.4	1.45	0.070	<dl	<dl	<dl	<dl	0.634	0.070	2.39	1.95
62CCP-01d	1.13	0.010	0.024	271	2.23	<dl	92.6	<dl	<dl	n.r.	141	<dl	5.40	525	199	0.056	0.045	<dl	<dl	0.004	<dl	9.E-4	0.010	1.04	0.224
62CCP-02.d	1.09	0.010	0.026	261	1.91	<dl	914	<dl	<dl	n.r.	139	<dl	5.03	536	152	0.074	0.049	<dl	<dl	0.002	<dl	0.001	0.011	1.37	0.290
62CCP-03.d	1.00	0.006	0.170	263	1.96	<dl	94.9	<dl	0.016	n.r.	140	<dl	5.57	543	149	0.086	0.036	<dl	<dl	<dl	<dl	0.012	0.021	2.14	0.326
62CCP-04.d	1.04	0.009	0.030	261	2.11	<dl	88.4	<dl	<dl	n.r.	142	<dl	5.55	544	171	0.147	0.054	<dl	<dl	<dl	<dl	0.011	0.047	3.65	0.657
62CCP-05.d	0.925	0.007	0.028	250	1.90	<dl	88.3	<dl	0.016	n.r.	157	<dl	5.39	509	169	0.068	0.053	<dl	<dl	<dl	<dl	0.001	0.084	3.80	0.518
62CCP-06.d	0.865	0.008	0.029	237	1.97	<dl	87.3	<dl	<dl	n.r.	167	<dl	5.20	495	159	0.105	0.053	<dl	<dl	<dl	<dl	0.016	0.325	5.11	0.474
62CCP-07.d	0.855	0.009	0.032	267	2.08	<dl	85.2	<dl	<dl	n.r.	155	<dl	5.42	529	262	0.063	0.053	<dl	<dl	<dl	<dl	0.016	0.010	0.785	0.156
64ROV11CCP-01c	3.13	1449	363	1285	1.04	0.270	862	0.091	<dl	n.r.	12.6	<dl	5.03	414	79.5	0.035	43.2	<dl	<dl	<dl	<dl	0.033	1.E-4	0.017	0.120
64ROV11CCP-02.	1.69	1390	352	1129	0.310	<dl	1460	0.200	<dl	n.r.	12.5	<dl	3.67	84.5	33.0	0.003	135	0.033	<dl	<dl	<dl	0.041	1.E-4	0.038	0.161
64ROV11CCP-03.	5.70	1243	327	1144	0.274	0.220	1321	0.116	<dl	n.r.	13.5	<dl	3.34	66.1	35.1	0.023	91.9	<dl	<dl	<dl	<dl	0.049	0.001	2.10	0.091
64ROV11CCP-04.	1.49	495	164	1210	0.980	2.73	538	2.00	<dl	n.r.	14.8	<dl	2.96	18.4	101	0.490	26.1	<dl	<dl	<dl	<dl	0.171	0.440	1.48	2.60
64ROV11CCP-05.	2.50	516	332	1076	0.240	0.800	1396	0.099	<dl	n.r.	16.9	<dl	3.23	52.9	47.7	0.005	93.4	0.019	<dl	<dl	<dl	0.311	3.E-4	0.320	2.77
64ROV11CCP-06.	1.09	622	297	784	0.132	<dl	1496	0.230	<dl	n.r.	1.72	<dl	1.14	47.3	34.5	0.002	113	<dl	<dl	<dl	<dl	0.002	1.E-4	0.110	0.072
64ROV11CCP-07.	1.86	1800	453	956	0.570	<dl	1581	4.40	<dl	n.r.	8.43	<dl	4.90	73.9	24.3	0.003	143	<dl	<dl	<dl	<dl	0.200	1.E-4	0.031	0.243
64ROV2CCP-001	7.10	241	202	100	0.056	2.31	1468	0.071	<dl	n.r.	5.78	<dl	0.380	4.17	62.0	0.005	20.0	1.70	<dl	<dl	<dl	0.103	5.E-4	0.157	0.113
64ROV2CCP-002	5.80	237	185	94.5	0.062	1.90	1345	0.048	<dl	n.r.	5.84	<dl	0.340	3.73	60.7	0.003	12.5	0.051	<dl	<dl	<dl	0.092	1.E-4	0.042	0.042

Grain ID	*Mn* 55	*Co* 59	*Ni* 60	*Zn* 66	*Ga* 71	As 75	*Se* 82	Mo 95	Ru 101	Rh 103	*Ag* 107	Pd 108	Cd 111	*In* 115	*Sn* 118	*Sb* 121	*Te* 128	Re 185	Os 189	Ir 193	Pt 195	*Au* 197	Tl 205	*Pb* 208	*Bi* 209
55um	0.470	0.023	0.241	0.353	0.028	0.223	2.53	0.030	0.023	0.005	0.023	0.014	0.046	0.012	0.073	0.022	0.256	0.009	0.021	0.007	0.013	0.010	0.004	0.012	0.007
33um	0.939	0.046	0.722	1.06	0.085	0.445	5.07	0.061	0.068	0.009	0.069	0.041	0.137	0.025	0.218	0.067	0.513	0.027	0.042	0.020	0.039	0.030	0.011	0.037	0.013
64ROV2CCP-003	8.10	2.32	1.54	96.2	0.012	0.890	13.22	0.078	<dl	n.r.	6.55	<dl	0.881	4.04	48.9	0.008	15.3	<dl	<dl	<dl	<dl	0.102	6.E-4	0.010	0.035
64ROV2CCP-004	3.20	2.02	1.40	87.8	0.048	1.39	12.83	1.80	<dl	n.r.	5.11	<dl	0.160	3.98	80.4	0.007	13.9	<dl	<dl	<dl	<dl	0.040	2.E-4	0.320	1.25
ALJ01CCP-01d	0.215	0.150	0.043	3.06	1.40	<dl	46.2	<dl	<dl	n.r.	1.84	<dl	0.600	1.60	3.89	0.009	0.024	<dl	<dl	<dl	0.024	8.E-4	2.E-4	0.010	0.099
ALJ01CCP-02.d	0.381	0.009	0.021	3.64	5.69	<dl	67.8	<dl	<dl	n.r.	3.97	<dl	1.37	80.9	4.59	1.42	0.048	<dl	<dl	<dl	<dl	0.026	0.053	0.720	0.333
ALJ01CCP-04.d	17.0	0.480	11.0	3.92	6.59	1.30	58.0	0.080	<dl	n.r.	6.27	<dl	0.990	78.2	1.69	11.5	0.071	0.028	<dl	0.180	<dl	0.120	0.514	4.81	2.74
ALJ01CCP-05.d	9.00	0.700	0.070	3.51	4.60	3.90	44.5	<dl	<dl	n.r.	6.34	<dl	1.59	66.4	1.44	9.20	0.058	<dl	<dl	0.050	<dl	0.031	0.218	4.00	1.02
ALJ01CCP-06.d	3.00	0.010	0.028	3.75	1.58	<dl	48.5	<dl	<dl	n.r.	3.99	0.267	1.41	75.4	4.49	1.71	0.045	<dl	<dl	0.120	<dl	0.033	0.052	0.780	0.580
ALJ01CCP-07.d	4.60	0.038	1.30	3.79	5.56	<dl	53.9	1.50	<dl	n.r.	4.16	<dl	1.01	75.4	2.76	5.90	0.047	<dl	<dl	0.014	<dl	0.003	0.530	3.65	1.45
AZN01CCP-02.d	0.590	0.008	4.60	2.70	0.650	<dl	86.1	1.50	<dl	n.r.	0.571	<dl	1.39	2.34	3.68	5.25	0.032	<dl	<dl	<dl	<dl	0.001	0.064	5.41	0.354
AZN01CCP-03.d	0.301	0.051	0.135	2.23	0.630	<dl	82.9	<dl	<dl	n.r.	0.126	<dl	2.00	2.47	3.61	1.84	0.032	<dl	<dl	<dl	<dl	9.E-4	0.010	1.40	0.088
AZN01CCP-04.d	0.690	0.210	45.0	2.62	0.660	<dl	87.0	<dl	0.080	n.r.	0.520	<dl	1.70	2.41	3.88	3.30	0.038	0.290	<dl	<dl	<dl	0.001	0.026	2.62	0.240
AZN01CCP-05.d	7.00	0.130	43.0	2.10	0.636	<dl	76.0	0.700	<dl	n.r.	0.142	<dl	3.00	2.33	3.47	2.09	0.026	0.025	<dl	0.430	<dl	0.002	0.012	1.56	0.062
AZN01CCP-06.d	0.760	0.008	2.20	2.67	0.539	<dl	79.9	<dl	0.070	n.r.	0.122	<dl	1.65	2.40	3.82	1.98	0.026	0.070	0.200	0.026	<dl	0.021	1.00	1.02	0.063
AZN01CCP-07.d	0.820	0.054	28.0	2.79	0.530	<dl	87.7	<dl	0.110	n.r.	0.500	<dl	1.74	2.36	4.17	4.73	0.210	<dl	<dl	<dl	<dl	0.008	0.055	4.94	0.342
B5109CCP-001d	1.82	0.390	0.260	2.92	0.835	<dl	10.52	0.015	0.088	n.r.	25.7	<dl	2.98	95.5	47.2	0.390	0.064	<dl	<dl	<dl	<dl	0.250	0.024	5.80	11.6
B5109CCP-002.d	8.50	0.258	0.160	3.10	1.12	<dl	10.25	3.70	0.073	n.r.	38.1	<dl	3.47	1.00	42.6	0.139	0.054	0.013	<dl	<dl	<dl	0.520	6.E-4	2.48	13.3
B5109CCP-003.d	2.73	0.251	0.029	3.15	1.53	<dl	10.16	<dl	0.096	n.r.	22.9	<dl	3.42	1.05	27.4	0.233	0.065	<dl	<dl	<dl	<dl	0.288	6.E-4	4.09	11.8
B5109CCP-004.d	3.50	0.294	0.025	2.70	1.27	<dl	10.43	<dl	0.082	n.r.	20.9	<dl	2.42	1.04	27.1	0.167	0.240	<dl	<dl	<dl	<dl	0.103	0.011	3.17	8.10
B5109CCP-005.d	2.18	0.231	0.032	3.64	1.38	<dl	11.30	<dl	<dl	n.r.	18.9	<dl	3.94	1.07	59.3	0.116	0.064	<dl	<dl	<dl	<dl	0.140	0.013	2.12	10.3
B5109CCP-006.d	1.94	0.195	0.022	3.32	1.27	<dl	11.26	<dl	0.057	n.r.	24.9	<dl	3.25	1.02	85.4	0.146	0.054	<dl	<dl	<dl	<dl	0.401	4.E-4	2.75	10.4
B5110CCP-001d	3.07	0.353	0.046	3.00	0.417	<dl	10.51	<dl	0.052	n.r.	36.6	<dl	2.72	87.3	16.1	0.317	0.058	<dl	<dl	<dl	<dl	0.072	5.E-4	3.18	12.4
B5110CCP-002.d	1.75	0.760	2.50	2.89	0.770	<dl	9.97	0.039	0.063	n.r.	58.4	<dl	3.48	90.4	18.1	0.266	0.072	<dl	<dl	<dl	<dl	0.089	0.001	5.60	15.0
B5110CCP-003.d	2.07	0.310	0.030	4.13	0.759	<dl	9.55	<dl	0.024	n.r.	50.5	<dl	3.60	83.8	22.0	0.101	0.080	<dl	0.020	<dl	<dl	0.580	4.E-4	1.45	12.5
B5110CCP-004.d	1.79	0.210	0.032	3.56	0.840	<dl	9.98	<dl	<dl	n.r.	44.1	<dl	3.12	84.8	19.1	0.180	0.065	<dl	<dl	<dl	<dl	0.063	9.E-4	3.50	13.8
B5110CCP-005.d	1.51	0.734	0.155	3.22	0.760	<dl	10.08	<dl	0.027	n.r.	63.7	<dl	3.07	81.7	21.0	0.280	0.056	<dl	<dl	<dl	<dl	0.144	8.E-4	3.00	24.3
B7157CCP-001d	1.82	0.131	0.770	3.38	6.92	<dl	8.69	<dl	0.074	n.r.	22.3	<dl	3.10	59.1	19.7	0.157	0.063	<dl	<dl	<dl	<dl	0.323	5.E-4	0.980	1.84
B7157CCP-002.d	1.40	0.291	0.024	3.12	7.60	<dl	8.38	<dl	0.055	n.r.	23.4	<dl	2.75	60.9	20.2	0.074	0.067	<dl	<dl	<dl	<dl	0.210	4.E-4	0.227	1.15
B7157CCP-003.d	1.13	0.299	0.024	3.18	7.61	<dl	8.36	<dl	0.067	n.r.	17.3	<dl	2.74	57.5	17.9	0.135	0.060	<dl	<dl	<dl	<dl	0.156	5.E-4	0.480	2.77
B7157CCP-004.d	1.49	0.314	0.024	3.70	7.38	<dl	9.14	<dl	0.068	n.r.	16.8	<dl	3.41	61.1	17.3	0.303	0.056	<dl	<dl	0.047	<dl	0.045	5.E-4	1.33	2.80
B7157CCP-005.d	1.71	0.160	0.150	3.22	7.86	<dl	9.88	<dl	0.049	n.r.	21.1	<dl	3.07	61.2	19.7	0.278	0.054	<dl	<dl	<dl	<dl	0.487	5.E-4	0.710	2.75
B7158CCP-001d	1.69	0.280	0.019	3.59	5.18	<dl	6.79	<dl	0.073	n.r.	18.1	<dl	3.32	69.8	16.8	0.401	0.043	<dl	<dl	<dl	<dl	0.203	5.E-4	1.70	1.38
B7158CCP-002.d	2.09	0.523	0.150	3.31	5.10	<dl	5.98	<dl	0.011	n.r.	31.2	<dl	3.49	68.6	22.1	0.216	0.052	<dl	<dl	<dl	<dl	0.545	5.E-4	3.77	1.25
B7158CCP-003.d	1.86	0.246	0.166	3.02	4.82	0.240	6.05	<dl	0.061	n.r.	20.0	<dl	3.11	70.1	14.3	0.560	0.037	<dl	<dl	<dl	<dl	0.241	0.004	2.95	2.27
B7158CCP-004.d	3.80	0.770	1.30	3.17	6.73	0.380	6.43	<dl	0.061	n.r.	21.6	<dl	3.17	68.0	20.9	0.451	0.055	<dl	<dl	<dl	<dl	0.266	6.E-4	3.30	1.40
B7158CCP-005.d	1.80	0.499	0.031	3.38	2.82	<dl	5.71	<dl	0.063	n.r.	18.6	<dl	2.86	65.1	20.6	0.190	0.060	<dl	<dl	<dl	<dl	0.490	9.E-4	2.70	2.04
BVMS01-CCP-01	2.41	11.5	0.267	5.45	0.262	<dl	2.60	7.80	<dl	n.r.	0.611	<dl	2.00	6.42	42.6	6.70	0.720	<dl	<dl	<dl	<dl	0.036	0.120	6.70	0.607
BVMS01-CCP-02	2.17	14.8	0.356	5.11	0.160	0.440	2.80	3.76	<dl	n.r.	0.531	<dl	2.46	6.27	42.5	15.1	1.83	<dl	<dl	<dl	<dl	0.025	0.040	28.9	0.512
BVMS01-CCP-03	1.90	14.2	0.320	4.23	0.320	0.750	2.89	66.0	<dl	n.r.	1.28	<dl	2.61	7.55	45.9	12.4	1.73	<dl	<dl	<dl	<dl	0.034	0.004	32.2	0.710
BVMS01-CCP-04	2.43	14.1	0.187	4.97	0.190	<dl	2.74	<dl	0.029	n.r.	1.43	<dl	2.37	6.36	47.2	4.13	1.17	<dl	<dl	<dl	<dl	0.003	0.002	7.85	1.08
BVMS01-CCP-05	9.20	0.017	0.156	4.50	1.79	<dl	2.56	2.32	<dl	n.r.	17.5	<dl	0.930	13.5	49.9	5.89	1.14	<dl	<dl	<dl	<dl	0.002	0.025	11.3	1.59
COR01CCP-01d	0.515	0.024	0.940	2.15	1.59	<dl	3.29	0.081	<dl	n.r.	10.1	<dl	0.167	2.96	111.1	3.11	0.058	<dl	<dl	<dl	<dl	0.007	6.E-4	1.61	2.25
COR01CCP-03.d	2.04	0.500	3.20	2.25	5.79	0.900	3.20	<dl	<dl	n.r.	15.8	<dl	0.150	2.84	9.55	8.89	0.061	<dl	<dl	<dl	<dl	0.026	0.009	6.23	8.30
COR01CCP-04.d	1.16	0.890	0.700	2.31	3.92	<dl	2.56	0.320	<dl	n.r.	13.4	<dl	0.133	1.58	9.89	7.60	0.076	<dl	<dl	<dl	<dl	0.003	7.E-4	4.51	5.32
COR01CCP-06.d	0.560	0.350	11.0	1.96	2.67	0.650	2.49	<dl	0.034	n.r.	14.4	0.172	0.083	99.2	96.3	3.19	0.074	<dl	<dl	0.023	<dl	0.079	7.E-4	2.76	3.41
COR01CCP-08.d	0.462	0.120	0.900	1.45	2.91	<dl	2.68	0.086	<dl	n.r.	15.0	<dl	0.900	1.94	82.3	9.30	0.058	<dl	<dl	<dl	<dl	0.250	0.007	5.98	8.00
COR02CCP-01d	0.564	0.015	0.520	16.2	6.30	6.60	63.2	3.90	<dl	n.r.	3.04	0.169	1.02	2.66	4.58	3.23	0.084	0.079	<dl	<dl	<dl	0.004	0.200	11.4	3.80
COR02CCP-02.d	4.90	0.022	0.046	16.6	6.45	5.32	47.8	0.280	<dl	n.r.	3.14	0.245	0.096	2.84	4.37	2.70	0.038	<dl	0.080	<dl	<dl	0.002	0.078	16.1	3.44

Grain ID	*Mn* 55	*Co* 59	*Ni* 60	*Zn* 66	*Ga* 71	As 75	*Se* 82	Mo 95	Ru 101	Rh 103	*Ag* 107	Pd 108	Cd 111	*In* 115	*Sn* 118	*Sb* 121	*Te* 128	Re 185	Os 189	Ir 193	Pt 195	*Au* 197	Tl 205	*Pb* 208	*Bi* 209
55um	0.470	0.023	0.241	0.353	0.028	0.223	2.53	0.030	0.023	0.005	0.023	0.014	0.046	0.012	0.073	0.022	0.256	0.009	0.021	0.007	0.013	0.010	0.004	0.012	0.007
33um	0.939	0.046	0.722	1.06	0.085	0.445	5.07	0.061	0.068	0.009	0.069	0.041	0.137	0.025	0.218	0.067	0.513	0.027	0.042	0.020	0.039	0.030	0.011	0.037	0.013
COR02CCP-03.d	0.587	0.410	0.400	31.1	7.15	4.35	65.4	3.30	<dl	n.r.	3.44	<dl	5.40	388	582	1.82	0.062	0.058	<dl	<dl	<dl	0.027	0.164	11.7	0.419
COR02CCP-04.d	0.443	0.130	0.028	32.2	6.04	11.3	51.7	<dl	<dl	n.r.	6.15	<dl	2.45	307	514	3.79	0.065	<dl	<dl	<dl	<dl	0.002	0.700	20.1	1.65
COR02CCP-05.d	1.72	0.073	0.023	13.7	5.77	6.34	36.1	<dl	<dl	n.r.	3.51	0.089	1.19	318	476	6.35	0.047	0.600	<dl	<dl	<dl	0.022	0.136	11.9	7.79
COR02CCP-06.d	0.514	0.024	0.085	11.8	5.85	4.51	34.4	<dl	<dl	n.r.	4.08	<dl	2.04	312	446	2.92	0.079	0.220	<dl	<dl	<dl	0.003	0.136	25.0	6.89
COR02CCP-07.d	0.314	0.019	0.016	17.3	5.92	2.75	35.1	<dl	<dl	n.r.	3.10	<dl	1.09	274	486	1.10	0.043	0.420	<dl	<dl	<dl	0.002	0.047	11.9	0.810
COR03CCP-01d	1.30	0.012	3.00	181	12.1	8.90	891	0.120	1.20	n.r.	7.06	<dl	1.80	232	621	25.4	0.107	<dl	<dl	<dl	<dl	0.005	0.114	20.5	50.3
COR03CCP-02.d	2.80	4.20	170	183	10.3	8.10	756	0.700	0.280	n.r.	8.40	<dl	1.00	236	541	36.2	2.60	<dl	<dl	<dl	<dl	0.005	0.335	34.5	85.8
COR03CCP-03.d	0.618	0.011	0.050	128	13.2	5.10	923	<dl	<dl	n.r.	2.27	<dl	0.630	211	630	19.3	0.124	<dl	<dl	<dl	0.060	0.005	0.180	38.0	57.0
COR03CCP-04.d	0.702	1.10	0.040	350	11.7	1.12	1165	<dl	<dl	n.r.	2.08	<dl	4.27	174	926	9.18	0.099	<dl	<dl	<dl	<dl	0.004	0.015	6.11	19.0
COR03CCP-05.d	0.629	0.130	0.800	184	19.7	3.60	953	<dl	<dl	n.r.	2.07	<dl	1.46	190	596	9.90	0.085	<dl	<dl	<dl	<dl	0.047	0.054	7.05	20.9
COR03CCP-07.d	2.34	15.0	0.510	368	19.0	0.950	1205	<dl	<dl	n.r.	0.980	<dl	1.64	188	1034	4.49	0.235	<dl	<dl	<dl	<dl	0.042	0.010	2.00	11.0
COR03CCP-08.d	2.39	1.30	0.101	429	19.0	1.79	1237	<dl	<dl	n.r.	13.9	<dl	1.38	200	1058	10.9	0.101	<dl	<dl	<dl	<dl	0.005	0.075	65.0	228
COR03CCP-09.d	0.452	0.036	1.00	403	23.6	1.13	1180	<dl	<dl	n.r.	2.10	<dl	3.87	177	976	5.64	0.064	0.310	<dl	<dl	<dl	0.120	0.001	2.43	14.4
COR03CCP-10.d	3.96	0.011	0.900	418	24.5	1.07	1083	<dl	<dl	n.r.	1.51	<dl	4.27	170	963	12.4	0.103	<dl	<dl	<dl	<dl	0.005	0.012	8.20	30.3
COR03CCP-11d	11.0	0.062	0.126	563	21.9	1.15	1158	<dl	<dl	n.r.	1.16	<dl	4.63	168	1181	7.46	0.064	<dl	<dl	0.024	<dl	0.052	0.012	3.26	13.5
COR04CCP-01d	12.0	0.100	1.20	274	3.44	<dl	263	<dl	<dl	n.r.	2.32	6.67	1.40	1212	1193	1.30	0.500	<dl	<dl	<dl	0.033	0.003	8.E-4	2.81	5.71
COR04CCP-02.d	0.321	0.200	11.0	207	1.80	0.370	219	2.20	<dl	n.r.	1.99	<dl	1.54	641	612	2.47	0.052	<dl	<dl	0.100	<dl	0.290	8.E-4	2.72	5.42
COR04CCP-03.d	0.680	0.190	0.018	171	2.70	0.390	209	1.40	<dl	n.r.	2.39	<dl	0.730	1549	605	4.21	0.800	<dl	<dl	<dl	<dl	0.261	9.E-4	6.80	9.25
COR04CCP-04.d	0.920	3.50	33.0	184	0.561	0.170	97.3	0.700	<dl	n.r.	0.890	<dl	0.329	941	358	0.660	0.154	<dl	<dl	<dl	<dl	0.035	3.E-4	0.810	1.64
COR04CCP-05.d	0.214	0.190	2.60	246	2.95	0.430	187	0.700	<dl	n.r.	1.85	<dl	0.930	1169	1194	0.760	0.049	0.057	<dl	<dl	<dl	0.112	5.E-4	1.15	2.71
COR04CCP-06.d	0.900	0.025	0.027	398	3.56	<dl	198	<dl	<dl	n.r.	1.57	<dl	5.83	874	1496	1.57	0.242	<dl	<dl	<dl	0.080	0.033	5.E-4	1.27	3.30
E171-B-5-Ccp-1d	0.166	0.010	0.011	310	0.560	<dl	2496	<dl	<dl	n.r.	36.3	<dl	0.710	96.0	15.5	0.840	0.320	<dl	<dl	<dl	<dl	0.500	0.003	1.88	0.392
E171-B-5-Ccp-2.d	0.135	0.010	0.104	253	0.685	<dl	2464	2.60	<dl	n.r.	32.2	<dl	0.610	98.3	20.6	0.468	0.600	<dl	<dl	<dl	<dl	0.324	0.009	1.09	0.286
E52-A-4-Ccp-1d	23.0	3.02	0.351	237	1.24	<dl	833	<dl	<dl	n.r.	11.1	<dl	0.930	56.7	14.2	1.72	9.24	<dl	<dl	<dl	<dl	0.014	0.023	8.75	0.610
E52-A-6-Ccp-1d	2.21	4.92	0.300	241	0.294	<dl	983	<dl	<dl	n.r.	10.6	<dl	1.24	53.5	10.5	0.866	7.80	<dl	<dl	<dl	<dl	1.E-3	0.006	4.80	0.392
E54-B-2-Ccp-1d	0.180	0.003	0.190	332	1.18	<dl	570	<dl	<dl	n.r.	7.36	<dl	0.780	57.4	31.9	4.95	38.1	<dl	<dl	<dl	<dl	0.051	0.009	2.63	0.005
E54-B-3-Ccp-1d	0.145	0.004	0.017	288	1.09	<dl	567	<dl	<dl	n.r.	10.4	<dl	0.670	54.7	27.7	0.587	41.2	<dl	<dl	<dl	<dl	0.012	0.002	1.40	0.003
E55-A-1-CCP-1d	0.530	0.016	0.118	213	1.62	<dl	1275	<dl	<dl	n.r.	1.80	<dl	0.450	37.8	15.7	1.12	18.1	<dl	<dl	<dl	<dl	0.028	0.011	2.51	0.002
E55-A-2-CCP-1d	0.280	0.015	0.009	226	1.67	<dl	1235	0.038	<dl	n.r.	0.848	<dl	0.561	415	24.4	0.166	24.6	<dl	<dl	<dl	<dl	0.018	0.002	0.182	0.001
E55-A-3-CCP-1d	0.164	0.028	0.012	193	6.11	<dl	1488	<dl	<dl	n.r.	1.67	<dl	0.670	49.2	26.3	1.79	13.6	<dl	<dl	<dl	<dl	0.019	0.004	2.09	0.007
E55-A-4-CCP-1d	0.109	0.024	0.009	223	1.84	<dl	1262	<dl	<dl	n.r.	1.35	<dl	0.629	43.2	20.8	0.578	20.1	<dl	<dl	<dl	<dl	0.031	3.E-4	0.703	0.002
E62-A-5-CCP-1d	0.350	0.011	0.006	268	1.38	<dl	26.0	0.015	<dl	n.r.	50.0	<dl	0.530	32.8	30.7	0.193	0.720	<dl	<dl	<dl	<dl	0.028	4.E-4	0.811	0.004
E64-1-CCP-1d	0.470	0.072	0.011	216	0.071	<dl	12.9	<dl	<dl	n.r.	37.4	<dl	0.540	11.9	18.0	0.113	0.420	<dl	<dl	<dl	<dl	9.E-4	3.E-4	2.03	0.247
E64-2-CCP-1d	0.131	0.142	0.102	210	0.099	<dl	13.9	0.011	<dl	n.r.	37.7	<dl	0.720	11.6	19.4	0.203	0.540	<dl	<dl	<dl	<dl	1.E-3	0.035	2.49	0.325
E64-3-CCP-1d	16.2	0.197	0.124	238	0.190	<dl	12.2	0.011	<dl	n.r.	40.6	<dl	0.760	11.1	29.1	0.300	0.670	<dl	<dl	<dl	<dl	0.001	0.005	1.47	0.387
E64-4-CCP-1d	5.00	0.180	0.016	292	0.082	<dl	15.8	0.013	<dl	n.r.	36.3	<dl	0.750	12.0	37.2	0.084	0.650	<dl	<dl	<dl	<dl	0.012	0.008	1.12	0.223
E64-5-CCP-1d	7.70	0.171	0.141	178	0.079	<dl	21.2	<dl	<dl	n.r.	29.8	<dl	0.830	9.77	20.2	0.270	0.620	<dl	<dl	<dl	<dl	0.002	0.035	10.6	1.48
E66-A-2-CCP-1d	0.530	3.77	0.010	251	0.677	<dl	111	<dl	<dl	n.r.	76.0	<dl	0.740	113	38.1	0.051	0.680	<dl	<dl	<dl	<dl	0.001	2.E-4	0.463	0.754
E67-2-Ccp-2.d	56.0	0.524	0.023	199	0.069	<dl	85.5	<dl	<dl	n.r.	12.5	<dl	0.460	411	20.8	0.160	0.250	<dl	<dl	<dl	<dl	0.044	0.025	3.87	0.120
E67-5-Ccp-1d	3.50	0.511	0.106	224	0.079	<dl	96.0	<dl	<dl	n.r.	13.5	<dl	0.430	49.7	21.7	0.178	0.026	<dl	<dl	<dl	<dl	0.037	0.008	2.07	0.075
GRA01CCP-01d	1.92	0.010	0.060	304	2.71	<dl	138	<dl	<dl	n.r.	7.98	<dl	0.380	191	727	10.6	0.044	<dl	0.900	<dl	<dl	0.003	0.070	8.41	3.13
GRA01CCP-02.d	0.592	0.140	4.10	383	4.97	<dl	488	<dl	<dl	n.r.	10.5	<dl	0.700	439	1000	27.9	0.087	<dl	<dl	0.024	<dl	0.006	0.159	20.6	8.50
GRA01CCP-03.d	1.25	0.029	0.018	270	2.00	<dl	225	<dl	<dl	n.r.	4.10	<dl	0.270	241	599	4.05	0.028	<dl	<dl	<dl	<dl	0.002	0.010	2.24	1.03
GRA01CCP-04.d	0.315	0.022	0.048	266	3.14	<dl	272	<dl	<dl	n.r.	4.10	<dl	0.150	294	1128	2.91	0.056	<dl	<dl	<dl	<dl	0.010	0.028	1.86	0.700
GRA01CCP-05.d	0.439	0.190	0.036	477	4.37	2.17	356	<dl	<dl	n.r.	5.27	<dl	2.08	412	2480	6.40	0.065	<dl	<dl	<dl	<dl	0.004	0.058	3.20	1.44
GRA01CCP-06.d	0.398	0.117	2.30	299	3.10	<dl	216	<dl	<dl	n.r.	3.10	<dl	0.310	333	1172	1.32	0.041	<dl	<dl	<dl	0.260	0.080	9.E-4	2.70	1.03
ICEVMS01CCP-0	80.0	0.458	0.360	3.20	58.9	1.10	89.6	2.20	<dl	n.r.	7.81	<dl	0.022	20.6	0.360	0.700	0.048	<dl	<dl	<dl	<dl	0.001	0.052	34.4	0.270

Grain ID	*Mn* 55	*Co* 59	*Ni* 60	*Zn* 66	*Ga* 71	As 75	*Se* 82	Mo 95	Ru 101	Rh 103	*Ag* 107	Pd 108	Cd 111	*In* 115	*Sn* 118	*Sb* 121	*Te* 128	Re 185	Os 189	Ir 193	Pt 195	*Au* 197	Tl 205	*Pb* 208	*Bi* 209
55um	0.470	0.023	0.241	0.353	0.028	0.223	2.53	0.030	0.023	0.005	0.023	0.014	0.046	0.012	0.073	0.022	0.256	0.009	0.021	0.007	0.013	0.010	0.004	0.012	0.007
33um	0.939	0.046	0.722	1.06	0.085	0.445	5.07	0.061	0.068	0.009	0.069	0.041	0.137	0.025	0.218	0.067	0.513	0.027	0.042	0.020	0.039	0.030	0.011	0.037	0.013
ICEVMS01-CCP-(	2.59	0.010	0.065	0.627	18.8	0.630	118	<dl	<dl	n.r.	1.93	<dl	0.047	28.6	0.280	0.182	0.056	<dl	<dl	<dl	<dl	7.E-4	0.001	4.58	0.055
ICEVMS01-CCP-(	2.66	0.011	0.007	0.970	26.8	<dl	135	0.350	<dl	n.r.	12.5	<dl	0.014	38.6	0.480	0.156	0.046	<dl	<dl	<dl	<dl	9.E-4	0.015	2.68	0.375
ICEVMS01-CCP-(	2.39	0.012	0.020	1.40	7.08	0.700	126	<dl	<dl	n.r.	4.54	<dl	0.029	45.7	0.490	0.630	0.070	<dl	<dl	<dl	<dl	0.001	0.072	22.7	0.160
ICEVMS01-CCP-(	5.94	2.12	1.82	1.27	7.97	0.650	92.0	<dl	<dl	n.r.	32.8	<dl	1.55	5.41	0.650	0.390	0.099	<dl	<dl	<dl	<dl	0.003	0.002	6.90	0.004
LB01-CCP-01d	2.52	0.038	4.20	790	2.50	<dl	106	<dl	<dl	n.r.	1.23	<dl	2.92	12.4	1.73	0.050	6.51	<dl	<dl	<dl	<dl	0.210	0.045	8.39	1.99
LB01-CCP-02.d	2.64	0.031	0.155	580	2.43	<dl	133	<dl	<dl	n.r.	2.93	<dl	2.58	12.5	2.62	0.061	5.30	<dl	<dl	<dl	<dl	0.003	0.032	7.34	17.2
LB01-CCP-03.d	2.52	0.052	0.162	653	2.35	<dl	155	4.60	<dl	n.r.	2.20	<dl	2.18	10.8	2.24	0.045	5.24	<dl	<dl	<dl	<dl	0.085	0.086	8.19	21.3
LB01-CCP-04.d	2.08	0.033	1.60	640	2.56	<dl	141	<dl	<dl	n.r.	0.860	<dl	2.56	11.9	2.01	0.024	5.50	<dl	<dl	<dl	<dl	0.003	0.012	4.19	4.05
LB01-CCP-05.d	2.00	0.030	0.143	710	2.50	<dl	60.6	<dl	<dl	n.r.	1.45	<dl	2.21	13.0	2.31	0.073	6.65	<dl	<dl	<dl	<dl	0.003	7.E-4	6.46	8.60
LB01-CCP-06.d	2.39	0.416	1.40	510	47.5	<dl	610	13.0	<dl	n.r.	3.65	<dl	0.140	21.6	1.91	0.052	5.09	<dl	<dl	<dl	<dl	0.001	0.029	9.50	0.028
LDR01-CCP-01d	8.02	0.334	0.119	464	1.69	<dl	432	<dl	<dl	n.r.	92.5	<dl	5.07	35.1	0.270	3.80	0.980	<dl	<dl	<dl	<dl	0.002	0.910	5.79	1.55
LDR01-CCP-02.d	5.52	0.860	12.2	330	1.75	<dl	393	<dl	<dl	n.r.	98.2	<dl	5.47	38.2	0.095	8.90	0.520	<dl	<dl	<dl	<dl	0.002	3.68	15.5	1.16
LDR01-CCP-03.d	5.95	0.180	2.89	313	1.74	<dl	264	<dl	<dl	n.r.	93.4	<dl	4.42	35.1	0.116	5.04	0.910	<dl	<dl	<dl	<dl	0.002	0.670	9.37	0.910
LDR01-CCP-04.d	4.74	0.417	2.14	515	1.73	<dl	342	<dl	<dl	n.r.	94.9	<dl	4.80	32.6	0.076	3.27	4.05	<dl	<dl	<dl	<dl	0.002	0.760	7.80	0.728
LDR01-CCP-05.d	6.75	0.211	0.158	660	2.38	<dl	376	<dl	<dl	n.r.	83.1	<dl	5.96	36.6	0.246	3.06	5.35	<dl	<dl	<dl	<dl	0.004	0.562	5.61	1.28
LDR01-CCP-06.d	5.76	0.298	2.30	310	2.34	0.410	400	<dl	<dl	n.r.	1.40	<dl	5.50	44.9	0.108	3.40	2.39	<dl	<dl	<dl	<dl	0.004	0.690	4.64	1.12
LOU01CCP-01d	0.276	0.034	0.020	194	0.450	<dl	178	3.40	0.039	n.r.	1.37	<dl	0.690	7.20	4.41	0.324	0.033	<dl	<dl	<dl	<dl	9.E-4	7.E-4	0.280	0.211
LOU01CCP-02.d	0.493	8.00	0.040	195	0.390	0.360	125	<dl	<dl	n.r.	10.1	<dl	1.14	18.09	2.80	20.9	0.061	<dl	<dl	<dl	0.090	0.100	0.009	20.7	19.2
LOU01CCP-03.d	0.325	0.027	0.024	227	0.101	<dl	50.9	0.095	<dl	n.r.	3.61	<dl	0.870	4.91	3.02	16.7	0.032	0.016	<dl	<dl	<dl	0.002	0.022	12.0	11.8
LOU01CCP-04.d	1.02	0.018	0.026	226	0.390	<dl	86.9	<dl	<dl	n.r.	3.81	<dl	0.880	4.56	2.80	19.9	0.590	0.012	<dl	<dl	<dl	0.002	0.053	22.7	20.0
LOU01CCP-05.d	3.00	0.810	32.0	237	0.137	2.30	87.0	0.087	<dl	n.r.	7.38	<dl	1.13	2.82	3.08	4.10	0.079	<dl	<dl	<dl	<dl	0.004	0.023	18.7	19.2
LOU01CCP-06.d	5.60	1.30	0.800	286	0.220	1.03	105	0.930	<dl	n.r.	6.03	0.278	0.940	5.08	3.92	32.9	0.101	<dl	<dl	<dl	<dl	2.40	0.042	35.3	22.4
LOU01CCP-07.d	4.00	0.140	3.90	197	0.350	<dl	82.9	0.180	<dl	n.r.	5.73	<dl	0.960	5.69	2.73	15.8	0.054	<dl	<dl	<dl	0.060	0.100	0.024	15.6	10.8
LS10CCP-01d	3.10	2.00	0.091	22.6	0.790	0.800	66.0	<dl	<dl	n.r.	10.3	<dl	2.05	2.92	0.350	0.017	2.40	<dl	<dl	<dl	0.063	7.E-4	0.012	24.3	0.104
LS10CCP-02.d	2.60	0.900	0.077	9.00	0.580	<dl	83.0	<dl	<dl	n.r.	20.4	<dl	1.10	2.61	0.055	0.027	1.43	<dl	<dl	<dl	<dl	0.001	0.073	50.8	0.622
LS10CCP-03.d	0.420	0.490	0.053	4.60	0.580	<dl	95.0	<dl	<dl	n.r.	22.6	<dl	1.48	6.89	0.070	0.022	1.49	<dl	<dl	<dl	<dl	0.148	0.014	11.0	0.303
LS10CCP-04.d	4.07	1.27	0.059	12.1	0.710	<dl	91.5	<dl	0.029	n.r.	20.5	<dl	1.42	8.79	0.560	0.022	3.96	<dl	<dl	0.003	<dl	0.002	0.012	56.4	0.419
LS10CCP-05.d	52.0	0.800	0.076	7.00	0.620	<dl	77.5	<dl	<dl	n.r.	21.3	<dl	0.850	8.05	0.370	0.024	2.85	<dl	0.026	<dl	<dl	0.006	0.022	43.2	0.402
LS10CCP-06.d	2.76	0.490	0.029	2.89	0.289	<dl	82.4	<dl	<dl	n.r.	28.6	<dl	0.125	4.18	0.580	0.020	1.03	<dl	<dl	<dl	<dl	0.002	0.013	14.8	0.444
LS10CCP-07.d	5.65	1.25	0.072	12.6	0.990	<dl	66.8	<dl	<dl	n.r.	21.4	<dl	1.03	2.66	0.380	0.076	0.680	<dl	<dl	<dl	0.010	0.031	0.042	55.7	0.580
LS1CCP-01d	0.710	0.005	0.020	1859	7.75	<dl	5.20	<dl	<dl	n.r.	7.24	<dl	7.18	14.0	10.3	0.005	0.017	<dl	<dl	<dl	<dl	0.060	0.004	1.47	0.142
LS1CCP-02.d	1.06	0.022	0.024	3430	27.0	<dl	6.10	0.042	<dl	n.r.	8.11	<dl	19.9	14.6	10.3	0.005	0.016	<dl	<dl	<dl	<dl	0.043	0.002	2.75	0.184
LS1CCP-03.d	0.420	0.005	0.017	1849	5.12	<dl	4.39	<dl	0.019	n.r.	9.17	<dl	8.97	14.2	9.22	0.004	0.013	<dl	<dl	<dl	<dl	0.063	4.E-4	1.18	0.051
LS1CCP-04.d	0.270	0.005	0.014	2009	8.52	0.078	3.55	<dl	<dl	n.r.	5.25	<dl	6.20	14.4	8.89	0.004	0.011	<dl	<dl	<dl	<dl	0.057	3.E-4	0.940	0.034
LS1CCP-05.d	0.300	0.006	0.017	1810	16.8	<dl	4.50	<dl	<dl	n.r.	5.24	<dl	5.21	13.9	8.64	0.005	0.014	<dl	<dl	<dl	<dl	0.026	0.001	0.875	0.059
LS1CCP-06.d	0.320	0.006	0.018	1670	12.4	<dl	3.50	<dl	<dl	n.r.	6.60	<dl	6.35	14.5	8.84	0.012	0.015	<dl	<dl	<dl	<dl	0.026	0.00	1.08	0.090
LS1CCP-07.d	0.128	0.006	0.024	3010	26.5	<dl	4.50	<dl	0.016	n.r.	6.85	<dl	13.8	14.5	9.06	0.004	0.018	<dl	<dl	<dl	<dl	0.103	0.003	1.18	0.078
LS22CCP-01d	0.460	0.026	0.160	241	0.720	<dl	110	<dl	<dl	n.r.	1.58	<dl	4.76	66.6	10.87	22.3	0.038	<dl	<dl	<dl	0.008	0.002	0.046	11.1	4.27
LS22CCP-02.d	1.30	0.036	0.190	306	0.800	0.390	220	<dl	<dl	n.r.	1.90	<dl	5.80	90.7	14.08	20.9	0.047	<dl	<dl	<dl	<dl	0.025	0.039	10.7	3.56
LS22CCP-03.d	0.214	0.005	0.027	165	0.226	0.490	171	<dl	0.070	n.r.	11.0	<dl	0.780	17.5	3.31	37.7	0.063	1.00	<dl	<dl	<dl	0.003	0.168	36.6	7.89
LS22CCP-04.d	0.690	0.018	0.027	180	0.372	0.200	193	<dl	<dl	n.r.	12.1	<dl	0.540	89.2	5.59	5.41	0.031	<dl	<dl	<dl	<dl	0.900	0.005	3.08	1.64
LS22CCP-05.d	5.30	0.030	1.40	471	0.197	4.60	227	<dl	<dl	n.r.	1.44	0.639	0.680	42.9	6.49	1.79	0.048	<dl	<dl	<dl	<dl	0.270	0.195	3.79	1.00
LS22CCP-06.d	0.920	0.030	0.017	195	0.347	0.310	167	<dl	<dl	n.r.	20.5	0.249	0.651	44.1	5.95	55.8	0.045	<dl	<dl	<dl	0.010	0.002	0.197	25.0	10.6
LS22CCP-07.d	0.750	0.150	4.20	205	0.480	<dl	183	<dl	0.140	n.r.	17.1	<dl	0.960	27.1	6.78	5.91	0.034	<dl	<dl	0.027	<dl	0.129	0.007	3.59	2.40
MN1CCP-01d	1.56	1.38	0.054	466	4.58	<dl	321	<dl	<dl	n.r.	19.7	<dl	5.95	4.77	67.1	1.37	1.68	<dl	<dl	<dl	0.007	0.061	0.087	6.80	0.920
MN1CCP-02.d	1.15	1.23	0.044	369	3.12	<dl	307	<dl	<dl	n.r.	18.2	<dl	5.96	4.54	61.2	0.600	1.74	<dl	<dl	<dl	<dl	0.087	0.005	2.87	0.461
MN1CCP-03.d	1.09	3.57	0.056	510	3.32	0.110	298	<dl	0.019	n.r.	19.0	<dl	5.50	4.79	57.9	0.530	2.43	<dl	<dl	<dl	<dl	0.066	7.E-4	3.14	0.496

Grain ID	*Mn* 55	*Co* 59	*Ni* 60	*Zn* 66	*Ga* 71	As 75	*Se* 82	Mo 95	Ru 101	Rh 103	*Ag* 107	Pd 108	Cd 111	*In* 115	*Sn* 118	*Sb* 121	*Te* 128	Re 185	Os 189	Ir 193	Pt 195	*Au* 197	Tl 205	*Pb* 208	*Bi* 209
55um	0.470	0.023	0.241	0.353	0.028	0.223	2.53	0.030	0.023	0.005	0.023	0.014	0.046	0.012	0.073	0.022	0.256	0.009	0.021	0.007	0.013	0.010	0.004	0.012	0.007
33um	0.939	0.046	0.722	1.06	0.085	0.445	5.07	0.061	0.068	0.009	0.069	0.041	0.137	0.025	0.218	0.067	0.513	0.027	0.042	0.020	0.039	0.030	0.011	0.037	0.013
MN1CCP-04.d	0.880	2.53	0.046	480	3.47	<dl	313	<dl	0.026	n.r.	20.7	<dl	8.02	4.74	57.1	0.312	4.03	<dl	<dl	<dl	<dl	0.264	4.E-4	2.61	0.464
MN1CCP-05.d	1.00	1.00	0.052	460	3.19	<dl	310	0.026	<dl	n.r.	19.9	<dl	6.90	4.62	65.5	0.530	2.72	<dl	<dl	0.003	<dl	0.071	0.008	3.07	0.469
MN1CCP-06.d	1.24	2.87	0.055	440	2.60	<dl	310	<dl	<dl	n.r.	20.4	<dl	6.76	4.78	67.3	1.46	1.71	<dl	<dl	0.009	<dl	0.092	0.012	6.10	1.13
MN1CCP-07.d	0.850	3.50	0.051	484	2.68	<dl	300	<dl	<dl	n.r.	24.0	<dl	4.17	5.81	76.3	1.57	2.42	<dl	0.014	<dl	<dl	0.082	0.006	6.85	1.17
MN2CCP-01d	1.49	0.890	0.300	398	4.23	<dl	291	<dl	<dl	n.r.	20.6	<dl	4.36	4.33	65.3	0.670	1.92	<dl	<dl	<dl	<dl	0.056	0.006	3.47	0.510
MN2CCP-03.d	1.53	1.62	0.051	453	4.37	<dl	279	<dl	<dl	n.r.	21.3	<dl	4.43	4.40	68.3	0.810	1.51	<dl	<dl	<dl	<dl	0.062	0.015	5.11	0.800
MN2CCP-04.d	0.740	0.730	3.70	403	3.94	<dl	292	0.039	<dl	n.r.	20.2	<dl	4.55	4.22	63.0	0.808	1.61	<dl	<dl	<dl	<dl	0.172	0.006	5.38	0.876
MN2CCP-05.d	1.49	0.800	0.048	391	3.58	<dl	277	<dl	<dl	n.r.	20.7	<dl	6.53	4.29	62.2	0.451	1.83	<dl	<dl	<dl	<dl	0.055	0.005	3.24	0.549
MN2CCP-06.d	1.20	0.439	0.043	504	3.56	<dl	293	0.049	<dl	n.r.	21.1	<dl	6.99	4.02	60.5	0.561	1.62	<dl	<dl	<dl	<dl	0.045	5.E-4	3.25	0.506
MN2CCP-07.d	1.06	1.21	0.042	415	3.42	<dl	284	<dl	<dl	n.r.	23.9	<dl	6.66	4.43	63.3	0.800	1.32	<dl	<dl	<dl	<dl	0.028	0.008	5.50	0.850
MN3CCP-01d	0.800	0.038	14.7	524	1.00	<dl	59.0	0.022	<dl	n.r.	535	<dl	3.71	28.1	179	4.18	1.21	<dl	<dl	<dl	<dl	0.018	0.220	3.94	0.124
MN3CCP-02.d	1.49	0.010	5.86	533	1.26	<dl	74.8	0.023	<dl	n.r.	469	<dl	3.40	42.0	229	1.38	2.40	<dl	<dl	<dl	<dl	0.022	0.058	1.97	0.056
MN3CCP-03.d	1.48	0.040	7.20	639	1.32	0.300	62.2	0.041	<dl	n.r.	587	<dl	3.73	37.6	181	0.746	0.950	<dl	<dl	<dl	<dl	0.001	0.007	3.21	0.031
MN3CCP-04.d	0.770	0.045	3.85	521	1.50	<dl	110	<dl	0.023	n.r.	506	<dl	2.19	42.2	321	0.900	1.63	<dl	<dl	<dl	<dl	0.059	0.040	1.31	0.029
MN3CCP-05.d	0.740	0.042	7.46	509	1.55	<dl	80.7	<dl	<dl	n.r.	563	<dl	3.13	37.5	214	2.49	2.66	<dl	<dl	<dl	<dl	0.030	0.057	3.43	0.048
MN3CCP-06.d	0.510	0.081	9.39	545	1.60	<dl	73.1	<dl	<dl	n.r.	597	<dl	3.30	40.7	246	0.690	2.28	0.004	<dl	<dl	<dl	0.015	0.034	1.10	0.026
MN3CCP-07.d	0.223	0.059	5.71	450	1.38	<dl	84.1	<dl	<dl	n.r.	623	<dl	2.99	32.0	223	2.27	1.94	<dl	<dl	<dl	0.007	0.028	0.143	3.32	0.051
MN4CCP-01d	1.36	0.009	0.027	610	0.469	<dl	957	<dl	0.019	n.r.	24.5	<dl	9.65	8.53	38.0	2.93	0.650	<dl	<dl	<dl	<dl	0.018	0.010	1.46	0.320
MN4CCP-02.d	1.70	0.011	0.037	628	0.507	<dl	927	<dl	<dl	n.r.	27.7	<dl	11.3	8.86	39.7	2.28	0.810	<dl	<dl	<dl	<dl	0.346	0.004	1.06	0.441
MN4CCP-03.d	1.93	0.074	0.034	620	0.339	<dl	800	<dl	<dl	n.r.	21.0	<dl	9.60	8.28	38.5	1.66	0.790	<dl	<dl	<dl	<dl	0.055	0.001	0.910	0.211
MN4CCP-04.d	2.09	0.029	0.176	614	0.587	<dl	998	<dl	<dl	n.r.	27.2	<dl	12.9	9.21	44.1	4.56	0.890	<dl	<dl	<dl	<dl	0.070	0.012	2.16	0.382
MN4CCP-05.d	2.10	0.011	0.040	726	0.479	<dl	871	<dl	<dl	n.r.	21.7	<dl	11.0	9.25	44.1	0.208	2.12	<dl	<dl	<dl	<dl	0.150	7.E-4	0.715	0.960
MN4CCP-06.d	1.76	0.012	0.046	575	0.364	<dl	887	0.160	<dl	n.r.	22.1	<dl	8.63	9.24	45.2	2.40	0.740	<dl	<dl	<dl	<dl	0.210	0.001	2.19	0.587
NAMA-CCP-01d	1.92	0.068	1.72	556	0.798	<dl	261	<dl	<dl	n.r.	146	<dl	16.3	24.7	2.14	0.011	2.77	<dl	<dl	<dl	<dl	0.001	0.002	3.95	0.104
NAMA-CCP-02.c	2.61	0.013	0.178	570	0.508	<dl	268	<dl	<dl	n.r.	238	<dl	13.8	26.0	2.19	0.012	3.21	<dl	<dl	<dl	<dl	0.001	0.002	5.20	0.021
NAMA-CCP-03.c	2.70	0.015	0.228	474	0.593	<dl	256	<dl	<dl	n.r.	171	<dl	13.8	13.8	1.47	0.080	2.51	<dl	<dl	<dl	<dl	0.056	0.035	16.2	0.041
NAMA-CCP-04.c	3.11	0.016	8.00	503	0.606	<dl	262	<dl	<dl	n.r.	163	<dl	13.8	27.2	2.05	0.044	2.30	<dl	<dl	<dl	<dl	0.014	0.002	7.21	0.032
NAMA-CCP-05.c	2.46	13.5	1.90	534	0.200	<dl	289	<dl	<dl	n.r.	1.04	<dl	2.76	6.89	1.56	0.010	2.75	<dl	<dl	<dl	<dl	0.064	7.E-4	4.36	0.830
NAMA-CCP-06.c	2.25	15.6	0.191	489	0.230	<dl	263	<dl	<dl	n.r.	0.890	<dl	2.32	6.59	0.990	0.011	2.49	<dl	<dl	<dl	<dl	0.051	9.E-4	6.18	0.900
NEV01CCP-01d	2.50	0.018	8.00	118	0.480	1.20	97.7	<dl	<dl	n.r.	5.12	<dl	0.380	703	176	1.10	0.055	0.240	<dl	<dl	<dl	0.003	0.110	1.22	0.521
NEV01CCP-02.d	2.30	0.007	0.160	73.3	0.770	0.590	914	<dl	<dl	n.r.	5.32	<dl	0.460	788	183	2.23	0.038	<dl	<dl	<dl	<dl	0.003	0.001	2.72	1.13
NEV01CCP-03.d	2.93	0.180	20.0	817	0.800	1.85	86.0	<dl	<dl	n.r.	11.3	<dl	0.540	559	242	15.7	0.053	1.10	<dl	0.041	<dl	0.003	0.002	10.8	3.68
NEV02CCP-01d	2.14	0.056	1.40	498	1.92	0.490	24.0	<dl	<dl	n.r.	4.40	<dl	0.570	250	1429	2.48	0.032	<dl	<dl	<dl	<dl	0.004	0.002	1.92	0.026
NEV02CCP-02.d	2.07	0.063	0.670	356	1.85	0.430	8.30	<dl	0.053	n.r.	4.15	<dl	0.540	246	1180	5.45	0.034	0.140	<dl	<dl	<dl	0.004	0.001	3.22	0.025
NEV02CCP-03.d	1.10	0.084	0.570	202	1.62	0.660	9.80	<dl	0.350	n.r.	3.25	<dl	0.190	298	1259	1.03	0.017	<dl	<dl	<dl	<dl	0.004	4.E-4	0.710	0.026
NEV02CCP-04.d	0.380	0.036	3.00	201	2.24	0.930	315	0.180	0.085	n.r.	8.20	<dl	0.300	298	638	6.05	0.036	0.140	<dl	0.080	0.063	0.008	0.008	4.50	0.033
QT01CCP-001d	0.970	8.64	0.300	188	0.206	2.10	381	0.046	<dl	n.r.	257	<dl	2.27	48.4	116	0.197	0.520	<dl	<dl	0.013	0.017	1.88	0.008	3.91	4.14
QT01CCP-002.d	0.830	8.47	15.0	157	0.138	2.40	401	<dl	<dl	n.r.	313	<dl	2.01	49.1	98.4	0.350	0.700	<dl	<dl	<dl	<dl	5.56	9.E-4	5.55	4.67
QT01CCP-003.d	0.570	8.88	13.0	182	0.200	1.40	404	0.036	<dl	n.r.	247	<dl	2.31	48.2	107	0.459	0.810	0.015	<dl	0.090	<dl	1.26	0.009	5.18	3.09
QT01CCP-004.d	1.90	11.6	23.0	139	0.169	1.90	363	0.100	<dl	n.r.	106	<dl	2.25	44.7	96.0	0.289	0.830	<dl	<dl	<dl	0.053	0.630	0.017	3.49	2.45
QT01CCP-005.d	0.580	10.0	4.60	115	0.132	<dl	396	<dl	<dl	n.r.	222	<dl	1.56	48.3	96.8	0.470	0.630	<dl	<dl	<dl	<dl	2.74	0.008	4.00	2.72
QT01CCP-006.d	6.00	9.94	0.320	139	0.135	<dl	419	<dl	<dl	n.r.	274	<dl	2.15	50.1	108	0.303	0.630	<dl	<dl	<dl	<dl	3.72	9.E-4	5.32	4.80
QT0MTCCP-01d	3.80	0.720	0.010	469	0.046	<dl	165	0.031	0.200	n.r.	398	0.616	0.780	6.16	36.2	0.080	0.035	<dl	<dl	<dl	0.038	0.001	0.005	5.94	0.022
QT0MTCCP-02.c	5.80	0.089	2.10	410	0.044	0.240	169	<dl	<dl	n.r.	359	<dl	0.650	5.95	43.2	0.400	0.048	<dl	0.074	0.016	<dl	0.080	0.001	3.52	0.054
QT0MTCCP-03.c	0.930	0.230	0.060	289	0.180	<dl	167	<dl	<dl	n.r.	398	<dl	0.400	5.38	23.4	0.163	0.039	1.50	<dl	<dl	<dl	0.070	0.016	4.27	0.260
QT0MTCCP-04.c	0.700	0.117	80.0	338	0.136	<dl	164	<dl	<dl	n.r.	399	<dl	0.510	4.66	39.6	0.492	0.043	<dl	0.060	<dl	<dl	0.004	0.008	4.27	0.018
QT0MTCCP-05.c	4.30	0.067	29.0	311	0.810	<dl	166	<dl	<dl	n.r.	448	<dl	0.510	4.55	30.3	0.760	0.073	<dl	<dl	0.210	<dl	0.009	0.013	10.2	0.005

Grain ID	*Mn* 55	*Co* 59	*Ni* 60	*Zn* 66	*Ga* 71	As 75	*Se* 82	Mo 95	Ru 101	Rh 103	*Ag* 107	Pd 108	Cd 111	*In* 115	*Sn* 118	*Sb* 121	*Te* 128	Re 185	Os 189	Ir 193	Pt 195	*Au* 197	Tl 205	*Pb* 208	*Bi* 209
55um	0.470	0.023	0.241	0.353	0.028	0.223	2.53	0.030	0.023	0.005	0.023	0.014	0.046	0.012	0.073	0.022	0.256	0.009	0.021	0.007	0.013	0.010	0.004	0.012	0.007
33um	0.939	0.046	0.722	1.06	0.085	0.445	5.07	0.061	0.068	0.009	0.069	0.041	0.137	0.025	0.218	0.067	0.513	0.027	0.042	0.020	0.039	0.030	0.011	0.037	0.013
QT0MTCCP-06.c	1.36	0.096	2.60	421	0.171	0.130	167	<dl	<dl	n.r.	393	0.275	0.910	4.96	66.2	0.191	0.035	0.037	<dl	<dl	<dl	0.030	0.190	3.28	0.097
QT0MTCCP-07.c	12.0	0.180	34.0	308	0.161	<dl	151	<dl	<dl	n.r.	478	<dl	0.630	5.34	32.2	0.005	0.040	<dl	<dl	0.045	<dl	0.170	0.130	4.95	0.136
QT18CCP-001.d	1.09	9.22	140	107	0.224	0.220	400	0.047	<dl	n.r.	140	<dl	2.15	47.6	105	0.710	0.700	<dl	0.018	<dl	<dl	0.495	0.028	5.60	2.82
QT18CCP-002.d	0.200	9.61	0.037	136	0.196	<dl	428	<dl	<dl	n.r.	205	<dl	2.25	49.2	111	0.440	0.620	<dl	<dl	<dl	<dl	1.66	0.140	6.13	4.56
QT18CCP-003.d	3.10	10.7	0.610	125	0.197	0.280	406	<dl	<dl	n.r.	140	<dl	2.40	49.2	106	0.420	0.420	<dl	<dl	<dl	<dl	0.313	0.006	4.36	3.84
QT18CCP-004.d	0.315	8.55	2.40	113	0.140	0.320	380	<dl	<dl	n.r.	111	<dl	2.04	46.6	90.7	0.310	0.410	0.045	<dl	<dl	<dl	0.044	5.E-4	2.28	1.88
QT18CCP-005.d	0.660	8.37	0.042	135	0.149	<dl	366	0.055	<dl	n.r.	202	<dl	1.92	45.1	100	0.083	1.60	<dl	<dl	<dl	0.070	0.220	0.060	1.27	1.27
QT18CCP-006.d	1.04	10.7	0.026	101	0.154	0.800	373	<dl	<dl	n.r.	254	<dl	1.33	47.3	80.4	1.23	0.520	<dl	<dl	<dl	<dl	2.55	0.028	9.80	4.74
THA01-02.d	0.142	0.010	0.020	515	4.87	<dl	108	<dl	0.027	n.r.	310	<dl	0.680	0.162	700	0.310	0.023	<dl	<dl	<dl	<dl	0.026	0.026	0.261	0.010
THA01-03.d	0.156	0.011	0.016	394	4.66	<dl	3.20	<dl	<dl	n.r.	300	<dl	0.400	0.486	356	1.28	0.016	<dl	<dl	<dl	<dl	0.010	0.118	2.11	0.002
THA01-04.d	0.570	0.012	0.016	509	4.81	<dl	2.40	<dl	0.024	n.r.	326	<dl	0.650	0.377	414	0.297	0.014	<dl	<dl	<dl	<dl	0.022	0.034	0.820	0.006
THA01-05.d	0.490	0.009	0.012	378	4.30	<dl	3.00	<dl	<dl	n.r.	324	<dl	0.480	0.709	267	0.188	0.011	<dl	<dl	<dl	<dl	0.010	0.032	0.207	0.002
V553221CCP-001	4.70	246	0.630	137	8.69	0.710	420	0.150	<dl	n.r.	46.3	<dl	0.820	4.73	353	0.700	17.9	<dl	<dl	<dl	<dl	0.460	5.E-4	0.029	0.607
V553221CCP-002	2.22	258	1.60	175	24.0	0.680	306	<dl	<dl	n.r.	56.6	<dl	1.17	3.23	395	0.480	7.88	<dl	<dl	<dl	<dl	0.020	2.E-4	0.047	0.314
V553221CCP-003	1.45	232	0.440	167	1.68	<dl	470	0.110	<dl	n.r.	46.5	<dl	1.47	5.66	59.2	0.012	37.5	<dl	<dl	0.037	<dl	0.003	0.001	5.00	0.166
V553221CCP-004	1.39	224	1.69	227	6.62	<dl	369	<dl	<dl	n.r.	30.9	<dl	1.37	4.71	195	0.010	30.2	<dl	<dl	<dl	1.00	0.003	0.003	0.018	0.178
V553221CCP-005	2.11	221	1.15	149	2.76	0.610	541	<dl	<dl	n.r.	65.3	<dl	0.790	5.24	73.1	0.009	32.6	<dl	<dl	<dl	<dl	0.004	8.E-4	0.013	0.037
V553221CCP-006	1.80	251	1.12	181	2.28	<dl	449	<dl	<dl	n.r.	116	<dl	0.950	6.45	77.3	0.007	38.3	<dl	<dl	<dl	<dl	0.370	2.E-4	0.051	0.069
V557324ACCP-0	0.970	82.5	0.270	279	0.890	<dl	817	0.035	<dl	n.r.	6.58	<dl	3.68	2.10	50.2	0.003	34.1	<dl	<dl	<dl	<dl	0.023	2.E-4	0.073	0.279
V557324ACCP-0	1.15	95.2	18.0	331	0.850	<dl	619	<dl	<dl	n.r.	5.71	<dl	3.24	2.17	70.5	0.410	25.2	0.030	0.050	0.110	<dl	0.034	2.E-4	0.076	0.324
V557324ACCP-0	1.46	106	3.90	351	0.670	0.460	986	0.500	<dl	n.r.	7.16	14.4	2.68	3.38	26.8	0.440	57.5	0.310	<dl	<dl	<dl	0.015	4.E-4	1.20	0.111
V557324ACCP-0	5.60	144	3.80	753	10.0	0.480	184	<dl	<dl	n.r.	7.04	<dl	4.94	0.323	467	0.290	7.40	0.150	<dl	<dl	<dl	0.101	1.E-4	0.084	1.22
V557324ACCP-0	1.40	206	35.0	492	0.467	3.00	738	<dl	<dl	n.r.	7.61	<dl	4.80	2.16	33.3	0.130	27.8	0.460	<dl	0.200	0.054	2.40	0.070	0.016	0.126
V557324ACCP-0	1.42	220	10.0	1134	5.40	0.960	4.90	0.260	0.170	n.r.	7.59	<dl	2.21	0.029	7.70	0.004	0.240	<dl	<dl	<dl	<dl	9.E-4	0.110	3.50	0.028
V557324ACCP-0	1.31	349	30.0	955	2.96	0.480	417	5.00	<dl	n.r.	9.21	2.01	3.36	0.548	171	0.200	13.0	<dl	<dl	0.015	0.170	0.042	0.030	0.110	0.225
V557324ACCP-0	1.49	318	6.00	1067	2.55	<dl	463	<dl	<dl	n.r.	8.32	<dl	3.45	1.50	162	0.003	16.0	0.100	<dl	<dl	0.500	0.056	0.00	0.076	0.240
V557327ACCP-0	0.990	269	0.290	131	3.17	<dl	460	0.340	<dl	n.r.	24.2	<dl	0.780	1.62	172	0.076	18.6	<dl	<dl	<dl	<dl	0.019	2.E-4	0.180	1.14
V557327ACCP-0	2.10	239	80.0	140	4.28	1.17	503	0.240	<dl	n.r.	38.7	<dl	0.880	5.16	139	0.100	24.2	<dl	<dl	<dl	0.043	0.004	8.E-4	0.900	0.118
V557327ACCP-0	2.93	237	0.200	140	6.11	<dl	462	0.096	<dl	n.r.	45.6	<dl	0.850	6.06	202	0.011	17.5	<dl	<dl	<dl	<dl	0.034	2.E-4	0.082	0.283
V557327ACCP-0	5.50	263	4.90	151	2.24	0.900	822	<dl	<dl	n.r.	45.6	<dl	0.670	5.00	19.6	0.053	47.5	0.080	0.430	<dl	<dl	0.024	2.E-4	0.066	0.277
V557327ACCP-0	1.95	244	5.10	149	2.63	<dl	704	<dl	<dl	n.r.	50.3	<dl	0.560	5.64	319	0.021	49.2	0.250	<dl	<dl	<dl	0.017	8.E-4	0.758	0.147
V557327ACCP-0	1.26	290	0.390	125	6.97	<dl	285	0.163	<dl	n.r.	36.3	<dl	0.690	0.993	192	0.084	8.22	<dl	<dl	<dl	<dl	0.044	2.E-4	0.099	2.68
V557327BCCP-0	1.67	136	1.60	230	9.87	0.400	322	0.080	0.160	n.r.	16.3	<dl	0.720	1.59	308	3.90	12.4	<dl	<dl	<dl	<dl	0.286	3.E-4	0.507	1.53
V557327BCCP-0	2.06	233	1.70	160	2.07	0.150	1083	0.280	<dl	n.r.	23.9	<dl	0.510	4.18	34.3	0.004	68.6	<dl	<dl	<dl	<dl	0.029	2.E-4	0.114	0.126
V557327BCCP-0	2.60	242	0.580	165	4.57	0.600	420	<dl	<dl	n.r.	44.2	<dl	0.730	2.77	148	0.029	14.5	<dl	0.019	0.040	<dl	3.30	2.E-4	0.132	0.870
V557327BCCP-0	1.87	326	0.350	166	1.72	<dl	728	0.070	<dl	n.r.	72.8	<dl	0.690	4.96	43.7	0.005	31.4	<dl	<dl	<dl	<dl	0.003	5.E-4	0.440	0.108
V557327BCCP-0	1.70	271	0.124	170	4.55	0.136	521	0.100	<dl	n.r.	95.4	1.05	0.640	3.66	137	3.20	18.1	<dl	<dl	0.190	<dl	0.500	2.20	0.480	0.243
V557327BCCP-0	2.80	306	0.430	173	19.8	0.520	210	<dl	0.044	n.r.	43.0	<dl	0.870	0.906	354	0.260	3.09	<dl	<dl	<dl	<dl	0.018	0.021	0.412	0.749
V557327BCCP-0	1.97	225	0.520	187	3.17	<dl	676	<dl	<dl	n.r.	32.8	<dl	0.760	4.18	168	0.130	25.6	0.017	<dl	<dl	0.032	0.003	2.E-4	0.085	0.390
WHB01-CCP-01.d	9.51	0.947	0.161	710	8.92	<dl	387	1.90	<dl	n.r.	112	<dl	3.36	10.2	1.16	15.1	2.37	<dl	<dl	<dl	<dl	0.003	0.670	15.5	0.005
WHB01CCP-02.d	0.750	10.7	3.91	459	0.088	<dl	239	<dl	<dl	n.r.	37.4	<dl	2.43	13.1	0.850	19.1	2.28	<dl	<dl	<dl	<dl	0.050	0.470	17.9	3.37
WHB01-CCP-03.c	6.06	1.08	0.159	462	8.78	<dl	692	<dl	<dl	n.r.	35.8	<dl	2.89	2.78	6.54	34.2	2.92	<dl	<dl	<dl	<dl	0.002	0.570	15.6	0.003
WHB01-CCP-04.c	7.95	1.13	1.71	488	8.36	<dl	567	<dl	<dl	n.r.	97.3	<dl	3.36	3.58	3.53	49.3	2.14	<dl	<dl	<dl	<dl	0.006	1.25	18.6	0.003
WHB01-CCP-05.c	8.64	0.550	0.151	529	8.80	<dl	761	<dl	<dl	n.r.	75.9	<dl	3.92	9.58	5.15	51.6	2.16	<dl	<dl	<dl	<dl	0.003	1.92	51.4	0.007
WV01-CCP-01.d	2.64	6.48	50.4	1011	0.630	<dl	4240	<dl	<dl	n.r.	7.78	<dl	5.01	1.56	109	1.03	0.065	<dl	<dl	<dl	<dl	0.005	4.E-4	0.120	1.17
WV01-CCP-02.d	2.50	3.38	29.1	890	0.670	<dl	4240	0.098	<dl	n.r.	9.18	<dl	4.84	2.11	88.6	1.48	0.065	<dl	<dl	<dl	<dl	0.050	5.E-4	0.133	1.62
WV01-CCP-03.d	3.08	4.30	41.4	1086	0.590	<dl	4370	0.067	<dl	n.r.	13.8	<dl	4.84	1.62	101	8.50	0.062	<dl	<dl	<dl	<dl	0.020	0.048	0.558	4.68

Grain ID	*Mn* 55	*Co* 59	*Ni* 60	*Zn* 66	*Ga* 71	As 75	*Se* 82	Mo 95	Ru 101	Rh 103	*Ag* 107	Pd 108	Cd 111	*In* 115	*Sn* 118	*Sb* 121	*Te* 128	Re 185	Os 189	Ir 193	Pt 195	*Au* 197	Tl 205	*Pb* 208	*Bi* 209
55um	0.470	0.023	0.241	0.353	0.028	0.223	2.53	0.030	0.023	0.005	0.023	0.014	0.046	0.012	0.073	0.022	0.256	0.009	0.021	0.007	0.013	0.010	0.004	0.012	0.007
33um	0.939	0.046	0.722	1.06	0.085	0.445	5.07	0.061	0.068	0.009	0.069	0.041	0.137	0.025	0.218	0.067	0.513	0.027	0.042	0.020	0.039	0.030	0.011	0.037	0.013
WV01-CCP-04.d	2.54	5.23	47.4	1260	0.660	0.138	3980	<dl	<dl	n.r.	9.45	<dl	5.50	1.75	103	2.60	0.064	<dl	<dl	<dl	<dl	0.005	0.023	0.266	2.03
WV01-CCP-05.d	3.02	6.94	44.8	950	0.570	<dl	4390	<dl	<dl	n.r.	10.1	<dl	4.10	1.52	92.0	4.24	0.077	<dl	<dl	<dl	<dl	0.017	0.024	0.484	1.58
WV01-CCP-06.d	1.83	5.67	40.1	961	0.360	<dl	4580	<dl	<dl	n.r.	11.5	<dl	4.58	1.45	116	2.93	0.084	<dl	<dl	<dl	<dl	0.018	0.224	1.23	2.16
ZAM01CCP-01d	1.37	0.069	17.0	174	7.76	0.560	1138	0.103	<dl	n.r.	0.850	<dl	0.029	238	1063	3.94	0.047	<dl	0.059	0.029	0.029	0.018	0.001	10.2	5.48
ZAM01CCP-02.d	0.470	0.030	2.70	194	7.37	0.600	1036	<dl	0.190	n.r.	0.750	<dl	0.169	237	1029	3.69	0.040	<dl	<dl	<dl	<dl	0.002	0.012	2.10	3.63
ZAM01CCP-03.d	1.90	3.70	60.0	196	8.09	0.800	1141	1.90	<dl	n.r.	0.590	<dl	0.068	244	1131	2.63	0.046	<dl	<dl	0.110	<dl	0.080	0.006	1.44	3.17
ZAM01CCP-04.d	19.0	0.800	0.300	160	9.01	0.540	1070	0.130	<dl	n.r.	0.390	<dl	0.112	249	929	5.01	0.039	<dl	0.070	0.050	0.210	0.002	0.022	2.94	4.62
ZAM01CCP-05.d	1.16	0.220	60.0	173	9.18	0.630	1144	<dl	<dl	n.r.	0.740	0.110	0.042	260	1120	5.75	0.039	<dl	<dl	0.015	<dl	0.002	0.011	2.31	4.16
ZAM01CCP-06.d	0.650	0.037	22.0	133	6.11	0.830	988	<dl	<dl	n.r.	0.736	<dl	0.131	202	968	6.62	0.060	<dl	<dl	<dl	0.050	0.003	0.022	4.80	6.62
ZAM01CCP-07.d	12.0	0.033	0.410	189	7.01	2.00	1101	<dl	<dl	n.r.	1.01	<dl	0.077	209	1111	11.1	0.130	<dl	<dl	<dl	<dl	0.003	0.060	10.1	11.8

Annexe C6. Analyses of reference materials used in the calibration of the LA-ICP-MS and in-house reference materials used to monitor the data quality.
Concentrations in ppm. In bold elements retained for further statistical analysis

Element		Ti	Mn	Co	Ni	Cu	Zn	Ga	Ge	As	Se	Mo	Ru	Rh	Ag	Pd
Isotope		49	55	59	60	65	66	71	74	75	82	95	101	103	107	108
Median of	55um	0.553	0.479	0.016	0.207	0.270	0.024	0.079	0.348	2.41	0.029	0.020	0.004	0.049	0.011	0.061
detection limits	33um	0.661	1.03	0.028	0.410	0.526	0.051	0.149	0.582	5.31	0.030	0.020	0.007	0.100	0.026	0.118
Reference materials used for calibration																
		GSE-1g	GSE-1g	GSE-1g	GSE-1g	MASS1	MASS1	GSE-1g	GSE-1g	MASS1	MASS1	MASS1	Po-727	Po-727	GSE-1g	Po-727
	Working value	450	590	380	440	134000	210000	490	320	65	51	59	36.5	41.6	200	43.4
	sd	42	20	20	30	500	5000	70	80	3	4	9	0.3	0.3	20	0.3
Values obtained for reference materials used as monitors																
UQAC-FeS1	Working value	298	56.3	643	25680	22542	260	*9.26*		1056	346	65.5	68.5	63.7	176	52.4
	Uncertainty	18.8	7.50	19.4	1769	902	31.9	1.00		116	42.0	3.70	5.00	3.50	19.6	8.70
This study	Average	455	50.5	644	25156	21761	283	9.26		1151	302	65.7	68.7	62.0	170	43.9
n=168	sd	165	30.7	41.3	2650	985	51.4	3.64		103	57.3	2.76	3.03	3.43	13.0	4.04
	%RSD	36.4	60.8	6.42	10.5	4.52	18.2	39.3		8.92	19.0	4.20	4.41	5.53	7.64	9.21
	rel.diff(%)	52.8	-10.4	0.159	-2.04	-3.46	9.05	-0.015		9.02	-12.8	0.238	0.265	-2.72	-3.14	-16.3
PTC1b	Working value	696	193	3253	112900	79700	2083			222	120	11.0		0.500	53.1	9.46
	Uncertainty	4.10	1.80	38.0	1000	330	38.0			17.0	11.0	1.00		1.00	1.00	1.00
This study	Average	732	178	3191	109791	82900	2841			299	122	7.78		0.871	61.3	8.16
n=129	sd	151	13.3	190	10308	3246	575			93.5	16.9	8.72		0.440	29.1	5.96
	%RSD	20.7	7.47	5.95	9.39	3.92	20.2			31.3	13.8	112		50.5	47.5	73.0
	rel.diff(%)	5.16	-7.87	-1.90	-2.75	4.02	36.4			34.6	2.04	-29.3		74.3	15.4	-13.7
CCu-1e	Working value	54.9	96.0	301	7.27	230700	30200	*3.00*	1.00	1010	304	16.1			205	
	Uncertainty	1.90	4.00	6.00	0.430	2400	300	nd	nd	30.0	8.00	0.700			3.40	
This study	Average	176	86.0	329	273	214881	40552	2.93	3.35	1243	283	15.2			213	
n=124	sd	153	11.8	23.2	628	6504	5090	0.359	0.602	172	27.7	24.3			43.6	
	%RSD	86.9	13.7	7.06	230	3.03	12.6	12.2	18.0	13.8	9.81	160			20.5	
	rel.diff(%)	220	-10.4	9.35	3657	-6.86	34.3	-2.18	235	23.1	-6.98	-5.86			3.75	
	Others		MASS1	MASS1	MASS1		GSE-1g					GSE-1g			MASS1	
	Working value		280	60.0	97.0		460					390			50.0	
	Uncertainty		80.0	10.0	15.0		10.0					30.0			5.00	
This study	Average		254	69.3	118		439					382			106	
n = 173 (MASS1)	sd		21.8	1.53	23.2		79.4					10.7			765	
n = 174 (GSE-1g)	RSD (%)		8.57	2.21	19.7		18.1					2.81			723	
	rel. diff (%)		-9.12	15.5	21.4		-4.59					-1.96			112	

Element		Cd	In	Sb	Te	Re	Os	Ir	Pt	Au	Tl	Pb	Bi
Isotope		111	115	121	128	185	189	193	195	197	205	208	209
Median of	55um	0.007	0.070	0.221	0.007	0.016	0.004	0.010	0.006	0.004	0.006	0.004	0.006
detection limits	33um	0.012	0.147	0.501	0.012	0.028	0.007	0.018	0.014	0.007	0.011	0.007	0.004
Reference materials used for calibration													
		MASS1	GSE-1g	MASS1	MASS1	GSE-1g	Po-727	Po-727	Po-727	Po-727	MASS1	MASS1	GSE-1g
	Working value	60	370	60	15	78.9	46.7	48	35.5	45.8	50	68	320
	sd	7	60	9	-	7.7	2.6	1.2	0.8	2.4	1.0	7.0	30
Values obtained for reference materials used as monitors													
UQAC-FeS1	Working value		9.50	92.6	151	65.2	86.6	62.8	60.1	66.2		91.1	120
	Uncertainty		1.10	15.3	24.7	11.6	11.8	10.1	13.6	9.70		7.70	16.6
This study	Average		10.4	83.5	140	55.0	89.3	56.3	47.7	63.2		81.0	124
n=168	sd		0.865	13.6	45.2	3.79	3.68	3.61	5.87	5.92		8.34	11.1
	%RSD		8.33	16.3	32.2	6.88	4.12	6.42	12.3	9.36		10.3	8.94
	rel.diff(%)		9.38	-9.80	-7.00	-15.6	3.17	-10.4	-20.7	-4.52		-11.1	3.64
PTC1b	Working value	38.0		6.00	30.0				6.47	1.99		795	
	Uncertainty	1.00		1.00	1.00				0.290	0.120		1.50	
This study	Average	82.3		6.40	31.8				3.35	1.03		959	
n=129	sd	18.5		3.46	9.36				1.73	1.41		108	
	%RSD	22.4		54.1	29.4				51.7	137		11.3	
	rel.diff(%)	117		6.69	6.07				-48.2	-48.5		20.6	
CCu-1e	Working value	74.2	6.00	104	61.8	0.004				20.3	2.70	7030	3.00
	Uncertainty	1.90	nd	3.00	2.60	nd				0.520	0.090	90.0	nd
This study	Average	135	6.01	108	58.9	0.037				4.21	2.15	7605	2.75
n=124	sd	28.7	0.631	30.2	19.9	0.082				70.4	0.278	887	0.494
	%RSD	21.3	10.5	28.0	33.8	224				1671	12.9	11.7	18.0
	rel.diff(%)	82.1	0.179	3.68	-4.62	815				-79.3	-20.2	8.18	-8.26
	Others		MASS1							MASS1	GSE-1g	GSE-1g	MASS1
	Working value		50.0							47.0	2.00	378	60.0
	Uncertainty		nd							nd	0.200	12.0	nd
This study	Average		62.0							49.1	1.32	323	65.3
n = 173 (MASS1)	sd		2.30							3.30	0.165	22.0	2.77
n = 174 (GSE-1g)	RSD (%)		3.71							6.72	12.5	6.80	4.25
	rel. diff (%)		24.0							4.49	-33.9	-14.5	8.80

italic: informational/provisional values. Interference of ^{115}Sn on ^{115}In on calibrant (GSE-1g) is negligible (0.27 %) and therefore correction not applied. Interference of $^{40}Ar^{63}Cu$ on ^{103}Rh on calibrant (Po-727) is negligible (4.63%) and therefore correction not applied. Interference of $^{40}Ar^{61}Ni$ on ^{101}Ru on calibrant (Po-727) is negligible (7.84%) and therefore correction not applied. Interference of ^{115}Sn on ^{115}In on UQAC-FeS1 is negligible (6.22%) and therefore correction not applied. Interference of $^{40}Ar^{63}Cu$ on ^{103}Rh on UQAC-FeS1 is negligible (3.55%) and therefore correction not applied.Interference of $^{40}Ar^{61}Ni$ on ^{101}Ru on UQAC-FeS1 is negligible (0.73%) and therefore correction not applied. RSD (%) : relative standard deviation. sd: standard deviation. rel. diff (%): relative difference. n: number of analyses

Annexe C7. Summary of selected trace element composition (ppm) of chalcopyrite (dataset C) used for multivariate statistical analysis and machine learning.

<dl: below detection limit; na: not applicable; *informative values; *med*: median; μ_t: trimmed mean (t=0.2); sd_t: trimmed standar deviation (t=0.2)

Class	Type	Deposit	n	Stat	Mn	Co	Ni	Zn	Ga	Se	Ag	In	Sn	Sb	Te	Au	Pb	Bi
				Isotope	55	59	60	66	71	82	107	115	118	121	128	197	208	209
		Median of detection limits*		55um	0.470	0.023	0.241	0.353	0.028	2.53	0.023	0.012	0.073	0.022	0.256	0.010	0.012	0.007
Magmatic	Ni-Cu sulfide	Broken Hammer	16	*med*	<dl	0.116	<dl	30.9	0.064	<dl	1.03	9.25	42.6	0.027	0.575	0.126	2.80	2.12
				μ_t	<dl	0.823	<dl	82.0	0.075	<dl	1.04	9.25	64.7	0.026	0.539	0.192	3.15	2.16
				sd_t	na	1.45	na	106	0.060	na	0.364	0.370	65.4	0.023	0.370	0.193	2.36	0.690
		Copper Cliff	8	*med*	6.85	0.133	38.6	348	0.166	<dl	6.12	10.0	52.5	0.071	3.12	<dl	42.7	0.925
				μ_t	7.00	0.138	39.3	352	0.148	<dl	5.43	10.5	53.3	0.072	3.23	<dl	53.3	0.942
				sd_t	5.95	0.070	9.57	23.3	0.077	na	1.40	2.70	15.4	0.028	1.96	na	62.7	0.110
		Creighton	57	*med*	1.10	0.355	63.6	489	0.084	78.7	3.40	1.60	7.35	0.042	0.680	<dl	2.54	2.30
				μ_t	1.06	0.418	68.7	493	0.088	79.7	3.75	1.71	9.04	0.046	0.773	0.016	2.59	2.15
				sd_t	0.454	0.223	22.6	71.5	0.050	9.42	1.95	1.07	5.72	0.037	0.742	0.025	1.10	1.13
		Delta	15	*med*	<dl	0.199	31.4	302	0.032	51.0	15.8	2.22	5.03	<dl	1.53	0.034	4.03	0.139
				μ_t	0.701	0.195	31.7	303	0.032	48.3	16.8	3.20	6.27	0.024	1.49	0.047	3.26	0.108
				sd_t	0.891	0.215	13.3	54.7	0.013	12.7	9.04	2.84	5.44	0.032	0.639	0.044	3.17	0.085
		Dunka Road	14	*med*	0.540	0.363	21.7	251	0.429	49.8	1.56	1.35	3.06	<dl	2.56	<dl	8.16	0.253
				μ_t	0.634	0.414	22.0	246	0.443	50.5	1.74	1.40	3.39	0.025	2.90	<dl	8.02	0.264
				sd_t	0.466	0.330	13.7	40.2	0.080	10.3	1.95	0.206	1.61	0.021	1.11	na	2.94	0.225
		Eagle	13	*med*	<dl	0.180	24.6	366	<dl	96.0	8.27	2.96	2.12	0.030	10.3	0.013	6.41	0.690
				μ_t	0.485	0.258	26.7	392	<dl	93.9	8.43	2.79	15.0	0.044	9.07	0.011	8.31	1.12
				sd_t	0.503	0.266	20.6	141	na	18.1	2.92	0.829	23.7	0.039	5.08	0.011	5.83	0.838
		Eastern Deeps	5	*med*	<dl	0.132	13.2	229	0.250	56.0	2.07	2.68	2.61	<dl	10.0	<dl	1.97	0.374
				μ_t	0.689	0.139	12.1	227	0.283	56.1	2.55	2.79	2.77	<dl	11.0	<dl	2.27	0.485
				sd_t	0.706	0.070	4.19	50.0	0.122	5.51	1.89	0.745	0.539	na	3.55	na	1.17	0.404
		Expo	9	*med*	1.02	0.075	8.75	262	0.073	48.7	6.12	2.41	11.1	<dl	6.24	0.015	3.38	0.097
				μ_t	1.14	0.101	8.39	266	0.071	49.6	5.43	2.39	11.1	<dl	6.31	0.018	3.85	0.100
				sd_t	1.26	0.066	2.53	15.3	0.047	4.16	2.79	0.155	0.519	na	2.04	0.012	1.44	0.034

Class	Type	Deposit	n	Stat	Mn	Co	Ni	Zn	Ga	Se	Ag	In	Sn	Sb	Te	Au	Pb	Bi
				Isotope	55	59	60	66	71	82	107	115	118	121	128	197	208	209
		Median of detection limits*		55um	0.470	0.023	0.241	0.353	0.028	2.53	0.023	0.012	0.073	0.022	0.256	0.010	0.012	0.007
		Jinchuan		*med*	1.49	0.150	21.3	346	<dl	77.0	4.34	1.47	0.700	<dl	4.60	0.013	11.1	1.14
			21	μ_t	1.33	0.170	21.7	333	<dl	77.1	5.63	1.46	1.15	<dl	4.39	0.014	11.3	1.61
				sd_t	1.56	0.160	16.2	93.1	na	18.1	4.52	0.805	1.81	na	4.85	0.018	7.29	1.73
		Katinniq		*med*	1.62	0.215	20.2	309	0.098	52.0	0.965	6.28	24.5	0.205	1.15	0.031	2.26	0.149
			8	μ_t	1.52	0.217	20.9	309	0.090	52.3	1.12	6.34	24.8	0.526	2.17	0.028	2.16	0.276
				sd_t	0.764	0.083	7.03	26.7	0.039	1.93	0.687	0.438	1.35	0.596	2.25	0.023	0.682	0.249
		Kharaelakh		*med*	6.94	0.353	43.2	438	0.067	58.4	3.68	2.49	2.18	0.143	6.91	0.040	44.0	0.091
			59	μ_t	7.39	0.459	43.2	447	0.069	60.2	4.02	2.61	2.27	0.136	6.09	0.042	46.9	0.128
				sd_t	3.79	0.454	37.0	199	0.024	21.7	3.18	1.31	1.63	0.077	5.91	0.023	42.4	0.135
		Kotselvaara		*med*	1.66	0.230	30.0	306	<dl	55.4	2.35	3.16	1.88	0.460	0.670	0.075	11.1	2.73
			11	μ_t	1.53	0.384	50.7	309	<dl	54.6	2.38	3.14	1.86	0.496	0.628	0.077	11.2	2.97
				sd_t	1.23	0.471	64.8	15.2	na	3.43	0.387	0.871	0.264	0.200	0.413	0.032	9.85	2.41
				med	40.6	5.53	2042	110	0.119	<dl	33.6	3.87	0.152	<dl	0.262	0.012	3.38	0.118
		Lac des Îles Complex	20	μ_t	41.4	155	2322	156	0.113	<dl	31.6	3.83	0.153	<dl	0.372	0.012	4.93	0.401
				sd_t	12.9	455	1020	234	0.051	na	31.9	1.01	0.090	na	0.430	0.005	4.36	0.696
		Marbridge		*med*	0.585	0.236	48.1	423	0.156	67.5	1.51	3.03	7.55	0.077	1.88	0.017	4.31	1.91
			6	μ_t	0.583	0.249	48.0	416	0.164	65.9	1.47	3.20	8.14	0.080	1.69	0.017	4.38	1.85
				sd_t	0.201	0.141	1.89	44.9	0.037	6.26	0.596	0.923	2.99	0.056	0.634	0.022	0.939	0.354
		McCreedy		*med*	1.03	0.155	47.3	176	0.059	<dl	21.2	7.17	145	<dl	2.72	0.020	4.01	0.217
			73	μ_t	1.20	0.165	47.0	208	0.061	<dl	19.7	7.60	127	<dl	2.40	0.024	4.27	0.219
				sd_t	1.12	0.118	9.54	91.1	0.033	na	18.1	2.88	103	na	2.39	0.028	2.36	0.103
		Medvezhy Creek		*med*	<dl	0.050	45.9	97.2	0.034	218	8.48	0.639	<dl	0.025	68.3	<dl	0.083	0.024
			12	μ_t	<dl	0.232	45.1	158	0.034	<dl	6.95	0.823	<dl	0.028	45.9	<dl	4.65	0.047
				sd_t	na	0.338	9.10	132	0.010	na	3.97	0.622	na	0.019	51.6	na	8.07	0.051
		Mesaba		*med*	0.770	0.465	11.2	210	0.280	58.0	2.03	0.683	0.750	<dl	2.83	<dl	2.10	0.110
			10	μ_t	0.710	0.394	29.3	163	0.255	72.6	2.01	0.798	3.36	<dl	2.72	<dl	2.52	0.106
				sd_t	0.731	0.497	43.7	160	0.120	38.5	1.36	0.408	5.96	na	1.65	na	2.28	0.090

Class	Type	Deposit	n	Stat	Mn	Co	Ni	Zn	Ga	Se	Ag	In	Sn	Sb	Te	Au	Pb	Bi
				Isotope	55	59	60	66	71	82	107	115	118	121	128	197	208	209
		Median of detection limits*		55um	0.470	0.023	0.241	0.353	0.028	2.53	0.023	0.012	0.073	0.022	0.256	0.010	0.012	0.007
		Mesamax		*med*	4.42	0.240	8.04	330	0.052	73.3	4.90	2.56	19.0	<dl	3.61	0.062	1.47	0.050
			7	μ_t	8.02	0.273	8.79	322	0.048	73.7	6.90	2.57	18.5	<dl	3.65	0.062	1.50	0.056
				sd_t	6.52	0.185	1.62	23.8	0.023	1.49	4.93	0.094	1.39	na	3.14	0.016	0.082	0.019
		Norilsk		*med*	4.12	2.21	98.1	685	0.077	<dl	5.03	2.58	2.22	0.119	9.48	0.051	10.0	0.660
			87	μ_t	5.31	17.7	540	709	0.074	<dl	6.41	2.63	3.21	0.118	9.59	0.065	11.7	0.711
				sd_t	6.75	34.2	910	371	0.027	na	6.31	0.535	3.44	0.064	8.18	0.057	10.5	0.711
		Noril'sk I		*med*	5.74	0.432	49.3	432	0.072	<dl	11.3	1.40	1.37	0.083	36.8	0.029	7.82	0.149
			33	μ_t	8.26	1.58	140	388	0.070	<dl	11.5	1.36	2.07	0.076	25.9	0.032	8.16	0.171
				sd_t	7.50	2.90	223	336	0.020	na	6.95	0.632	3.01	0.056	28.4	0.020	9.93	0.155
		Ovoid		*med*	0.635	0.104	4.90	183	<dl	67.3	3.33	6.00	7.14	<dl	10.5	<dl	8.96	0.180
			60	μ_t	0.723	0.133	5.92	186	<dl	69.6	4.47	5.52	9.79	<dl	11.7	<dl	9.16	0.175
				sd_t	0.743	0.146	4.77	35.6	na	18.0	4.20	4.91	10.0	na	7.72	na	4.98	0.125
		Semilekta		*med*	1.46	0.118	20.0	353	<dl	57.2	1.40	3.53	5.72	0.390	1.09	<dl	2.96	0.187
			19	μ_t	2.01	0.139	19.1	350	<dl	53.2	1.49	3.53	5.69	0.443	0.905	<dl	5.06	0.285
				sd_t	2.33	0.092	6.61	84.9	na	16.1	0.960	1.23	3.45	0.373	0.715	na	5.16	0.335
		Talnakh		*med*	6.58	0.124	50.0	113	<dl	<dl	0.945	3.11	0.550	<dl	27.3	<dl	13.7	0.015
			41	μ_t	6.68	0.189	1220	136	<dl	<dl	1.49	2.78	0.592	<dl	21.1	<dl	13.0	0.016
				sd_t	6.02	0.207	2411	168	na	na	2.08	2.07	0.560	na	22.0	na	15.1	0.008
		Zhdanovskoe		*med*	<dl	0.053	4.30	351	<dl	84.0	5.63	2.86	0.273	0.058	1.53	0.019	1.25	0.519
			5	μ_t	<dl	0.090	4.33	354	<dl	82.3	5.69	2.87	0.284	0.058	1.90	0.019	1.45	0.519
				sd_t	na	0.142	1.80	55.0	na	9.04	2.69	0.062	0.070	0.024	1.06	0.026	0.800	0.056
		Zone Frontier		*med*	0.540	0.690	16.9	259	0.036	39.8	10.5	6.19	12.7	0.063	0.310	0.017	4.36	0.127
			35	μ_t	1.52	1.06	16.9	265	0.066	39.7	10.3	7.83	15.9	0.072	0.342	0.018	4.89	0.142
				sd_t	2.32	1.50	7.21	47.5	0.086	10.4	2.67	8.49	16.1	0.050	0.414	0.021	3.75	0.084
		Summary Ni-Cu sulfide	*644*	med	1.60	0.287	43.2	316	0.060	76.1	4.48	2.85	4.98	0.043	2.76	0.018	5.50	0.239
				μ_t	2.41	0.353	41.8	323	0.061	80.8	5.74	3.08	6.66	0.051	3.92	0.021	7.01	0.334
				sd_t	3.16	0.379	36.8	192	0.049	40.8	5.79	2.21	8.73	0.054	4.91	0.027	6.97	0.414

Class	Type	Deposit	n	Stat	Mn	Co	Ni	Zn	Ga	Se	Ag	In	Sn	Sb	Te	Au	Pb	Bi
				Isotope	55	59	60	66	71	82	107	115	118	121	128	197	208	209
		Median of detection limits*		55um	0.470	0.023	0.241	0.353	0.028	2.53	0.023	0.012	0.073	0.022	0.256	0.010	0.012	0.007
	Reef-type	Bushveld Complex		*med*	5.04	0.234	43.8	285	0.157	80.6	1.30	1.40	0.475	0.066	0.358	0.024	8.19	0.101
			129	μ_t	5.47	0.607	44.7	286	0.158	81.4	1.33	1.42	0.665	0.069	0.456	0.025	8.35	0.161
				sd_t	2.59	0.938	19.3	65.0	0.054	12.4	0.516	0.639	0.740	0.033	0.430	0.011	5.24	0.226
		East Boulder		*med*	1.37	0.290	29.8	401	0.079	211	2.50	0.689	<dl	<dl	<dl	<dl	8.36	<dl
			23	μ_t	1.31	0.299	29.4	407	0.084	252	5.68	0.852	<dl	<dl	<dl	<dl	7.73	0.010
				sd_t	1.22	0.158	15.4	99.9	0.065	130	7.11	0.872	na	na	na	na	6.13	0.007
		Merensky reef		*med*	1.55	0.069	14.5	514	0.485	<dl	4.54	1.62	3.77	<dl	<dl	<dl	110	0.019
			12	μ_t	1.33	0.101	14.5	520	0.489	<dl	4.08	1.69	3.81	<dl	<dl	<dl	103	0.019
				sd_t	0.786	0.092	1.95	112	0.142	na	2.00	0.448	1.20	na	na	na	83.2	0.008
		Mimosa		*med*	1.19	0.146	30.4	588	0.145	<dl	2.74	1.30	3.43	<dl	0.650	<dl	1.04	0.400
			23	μ_t	1.03	0.182	32.0	599	0.182	<dl	2.40	1.51	4.05	<dl	0.536	0.016	1.16	0.445
				sd_t	0.644	0.158	6.85	98.6	0.145	na	2.01	0.864	3.42	na	0.547	0.025	0.587	0.446
		PV reef	12	*med*	1.15	0.024	0.725	356	0.081	<dl	3.57	0.335	<dl	<dl	1.42	<dl	1.47	0.034
				μ_t	1.18	0.029	1.07	364	0.074	<dl	3.46	0.346	0.112	<dl	1.39	<dl	1.48	0.036
				sd_t	0.988	0.024	0.959	83.3	0.056	na	1.02	0.092	0.104	na	1.07	na	0.412	0.034
		Rustenburg	46	*med*	1.67	0.062	20.8	302	0.058	<dl	2.97	1.94	0.140	<dl	<dl	<dl	5.02	0.014
				μ_t	2.08	0.071	20.6	310	0.058	<dl	2.97	1.95	0.124	<dl	<dl	<dl	5.50	0.017
				sd_t	1.75	0.050	5.10	83.9	0.047	na	1.33	1.05	0.128	na	na	na	2.83	0.019
		Stillwater Complex	7	*med*	5.34	0.383	19.2	347	0.183	<dl	5.26	0.620	0.256	0.037	0.455	0.035	5.96	0.103
				μ_t	5.82	0.582	22.1	364	0.187	<dl	5.95	0.566	0.290	0.045	0.613	0.034	5.78	0.251
				sd_t	2.42	0.775	19.3	156	0.085	na	6.87	0.340	0.256	0.030	0.786	0.024	4.96	0.443
		Summary Reef-type PGE	*302*	med	4.17	0.204	30.9	323	0.144	105	1.93	1.18	0.318	0.037	0.264	0.021	6.26	0.059
				μ_t	4.12	0.273	31.9	329	0.150	113	2.27	1.22	0.450	0.040	0.320	0.020	6.64	0.100
				sd_t	3.19	0.323	20.9	111	0.090	47.1	1.79	0.854	0.573	0.041	0.346	0.020	5.26	0.148

Class	Type	Deposit	n	Stat	Mn	Co	Ni	Zn	Ga	Se	Ag	In	Sn	Sb	Te	Au	Pb	Bi
				Isotope	55	59	60	66	71	82	107	115	118	121	128	197	208	209
		Median of detection limits*		55um	0.470	0.023	0.241	0.353	0.028	2.53	0.023	0.012	0.073	0.022	0.256	0.010	0.012	0.007
Hydrotherr	Epitherma	Cactus Queen	3	*med*	<dl	<dl	<dl	203	0.170	6.06	11.3	0.287	15.4	0.480	<dl	0.016	1.50	<dl
				μ_t	<dl	0.024	<dl	253	0.162	<dl	10.9	0.381	18.2	0.816	<dl	0.015	2.62	<dl
				sd_t	na	0.027	na	144	0.032	na	1.71	0.377	5.35	0.887	na	0.016	2.06	na
		Camp Bird	6	*med*	<dl	6.37	<dl	2.62	0.031	<dl	2.79	0.028	<dl	0.038	<dl	<dl	0.537	<dl
				μ_t	<dl	6.29	<dl	2.93	0.031	<dl	2.82	0.027	<dl	0.042	<dl	<dl	0.561	<dl
				sd_t	na	2.81	na	1.45	0.002	na	0.324	0.007	na	0.046	na	na	0.389	na
		Comstock Lode	12	*med*	1.35	0.330	7.60	167	0.089	3.70	6.16	0.139	<dl	0.635	<dl	<dl	1.37	0.012
				μ_t	1.20	0.355	24.1	165	0.084	3.98	6.03	0.182	0.087	0.630	<dl	<dl	1.61	0.014
				sd_t	0.998	0.253	35.6	25.3	0.030	1.40	2.21	0.148	0.054	0.490	na	na	0.953	0.011
		Federal	30	*med*	2.90	<dl	<dl	85.5	0.225	9.30	1.38	110	0.341	0.333	<dl	<dl	0.580	2.40
				μ_t	2.92	0.024	0.614	278	0.274	29.2	1.63	101	0.462	1.18	<dl	<dl	0.914	2.32
				sd_t	0.353	0.030	1.08	487	0.336	45.7	1.44	105	0.593	2.70	na	na	1.27	2.82
		Herja	5	*med*	49.0	4.47	1.23	1062	0.067	<dl	149	2.22	9.52	0.599	<dl	<dl	1.50	<dl
				μ_t	46.0	4.34	1.12	1133	0.057	<dl	145	2.24	10.3	0.509	<dl	<dl	1.65	<dl
				sd_t	17.3	1.30	0.781	202	0.029	na	63.4	0.837	6.51	0.323	na	na	0.588	na
		Kochbulak	1	*med*	2.88	0.404	1.12	1441	0.052	31.6	8.59	2.93	13.9	0.630	<dl	0.014	2.38	7.40
				μ_t	2.88	0.404	1.12	1441	0.052	31.6	8.59	2.93	13.9	0.630	<dl	0.014	2.38	7.40
				sd_t	na	na	na	na	na	na	na	na	na	na	na	na	na	na
		Palisades	21	*med*	0.880	0.118	<dl	36.8	0.099	52.3	1121	0.303	3.86	0.177	<dl	<dl	0.850	0.008
				μ_t	0.725	0.141	<dl	37.3	0.131	48.1	1122	0.292	4.70	0.418	<dl	0.010	1.15	0.008
				sd_t	0.823	0.198	na	8.49	0.163	33.4	464	0.199	3.84	0.649	na	0.015	1.09	0.006
		Rozalia	2	*med*	9.70	0.285	0.723	68.8	0.410	24.6	7.54	0.038	0.333	1.75	0.386	<dl	3.62	0.402
				μ_t	9.70	0.285	0.723	68.8	0.410	24.6	7.54	0.038	0.333	1.75	0.386	<dl	3.62	0.402
				sd_t	20.1	0.361	1.32	119	0.442	11.7	14.2	0.048	0.681	4.09	0.950	na	6.04	1.10
		Sunnyside	14	*med*	1.44	<dl	<dl	53.2	1.31	5.40	27.3	12.2	11.9	1.29	<dl	<dl	2.63	<dl
				μ_t	3.44	<dl	<dl	54.2	1.87	5.32	24.3	14.5	11.1	1.21	<dl	<dl	3.65	<dl
				sd_t	5.79	na	na	12.0	1.45	1.72	23.1	11.3	8.88	0.873	na	na	3.49	na

Class	Type	Deposit	n	Stat	Mn	Co	Ni	Zn	Ga	Se	Ag	In	Sn	Sb	Te	Au	Pb	Bi
				Isotope	55	59	60	66	71	82	107	115	118	121	128	197	208	209
		Median of detection limits*		55um	0.470	0.023	0.241	0.353	0.028	2.53	0.023	0.012	0.073	0.022	0.256	0.010	0.012	0.007
		Tiegelongnan	4	*med*	<dl	5.56	0.584	6.70	0.634	<dl	1.75	6.47	6.80	1.96	2.26	0.365	21.1	0.163
				μ_t	<dl	9.88	0.729	67.0	1.61	<dl	2.08	7.10	6.72	5.52	1.98	0.371	73.5	0.154
				sd_t	na	13.4	0.363	108	1.83	na	1.44	7.25	1.47	7.91	0.942	0.617	99.8	0.124
		Toroiaga	26	*med*	1.14	<dl	1.42	1563	0.277	<dl	83.3	17.8	13.5	0.687	0.297	0.018	1.27	0.021
				μ_t	1.31	<dl	1.32	1429	0.314	<dl	88.2	17.8	16.2	0.892	0.293	0.018	1.50	0.025
				sd_t	1.53	na	1.20	672	0.255	na	107	4.29	11.0	0.837	0.155	0.011	1.23	0.029
		Summary epithermal gold	*124*	*med*	*1.66*	*0.046*	*<dl*	*108*	*0.205*	*5.51*	*9.98*	*8.85*	*4.01*	*0.564*	*<dl*	*<dl*	*1.26*	*0.012*
				μ_t	*1.70*	*0.103*	*0.480*	*287*	*0.273*	*12.6*	*44.0*	*9.38*	*5.21*	*0.682*	*<dl*	*<dl*	*1.50*	*0.044*
				sd_t	*1.72*	*0.174*	*0.831*	*486*	*0.327*	*21.5*	*85.6*	*12.5*	*6.97*	*0.798*	*na*	*na*	*1.39*	*0.090*
	IOCG	Alvo 118	7	*med*	<dl	1.40	<dl	0.365	0.072	23.1	0.273	1.62	3.90	<dl	0.660	0.013	0.894	0.763
				μ_t	<dl	1.37	<dl	0.429	0.065	22.9	0.280	1.64	3.96	<dl	0.648	0.014	0.820	0.643
				sd_t	na	0.122	na	0.303	0.038	0.987	0.105	0.038	0.180	na	0.058	0.004	0.391	0.315
		Antas Norte	17	*med*	1.14	1.41	34.4	550	0.274	88.9	32.0	5.47	6.92	<dl	2.97	<dl	1.39	0.130
				μ_t	3.01	1.99	33.3	539	0.368	90.8	33.5	6.39	18.0	0.028	3.09	<dl	3.61	0.237
				sd_t	3.27	2.21	30.0	74.0	0.259	16.0	29.8	2.88	26.1	0.032	1.07	na	4.78	0.271
		Candelaria	59	*med*	0.527	0.555	<dl	260	0.320	<dl	148	7.44	1.23	0.163	1.59	0.038	2.92	1.46
				μ_t	0.612	2.17	0.328	272	0.310	<dl	133	7.36	2.85	0.200	1.80	0.036	3.64	1.52
				sd_t	0.592	4.04	0.563	171	0.132	na	99.7	4.47	4.21	0.233	1.50	0.041	3.31	1.12
		Chandman Uul	7	*med*	1.11	0.192	<dl	8.30	0.079	90.9	21.9	23.6	2.12	0.103	0.450	<dl	1.83	2.31
				μ_t	1.14	0.213	<dl	8.77	0.076	91.1	24.2	23.7	2.02	0.113	0.438	<dl	1.86	2.21
				sd_t	0.176	0.067	na	1.50	0.021	6.52	9.44	0.818	0.371	0.055	0.335	na	0.341	0.622
		Eloise	16	*med*	2.85	3.20	1.81	308	0.496	<dl	64.4	27.3	69.1	0.169	<dl	0.027	2.35	1.68
				μ_t	3.08	3.94	23.2	329	9.86	282	54.3	109	161	0.177	<dl	0.034	2.75	1.54
				sd_t	0.805	3.62	63.5	250	21.2	421	31.4	205	252	0.115	na	0.040	1.69	1.37
		Ernest Henry	18	*med*	0.735	0.029	<dl	14.0	0.260	31.1	15.4	4.99	36.5	0.528	<dl	0.069	1.24	6.64
				μ_t	0.662	0.052	0.453	25.4	0.257	30.5	17.2	6.87	45.5	0.585	<dl	0.091	3.07	6.26
				sd_t	0.697	0.070	0.590	24.6	0.051	6.64	12.4	4.77	31.8	0.376	na	0.091	4.31	3.76

Class	Type	Deposit	n	Stat	Mn	Co	Ni	Zn	Ga	Se	Ag	In	Sn	Sb	Te	Au	Pb	Bi
				Isotope	55	59	60	66	71	82	107	115	118	121	128	197	208	209
		Median of detection limits*		55um	0.470	0.023	0.241	0.353	0.028	2.53	0.023	0.012	0.073	0.022	0.256	0.010	0.012	0.007
		Igarapé Bahia/Alemao	23	*med*	<dl	0.329	20.7	18.7	<dl	35.7	1.87	3.52	6.05	0.080	1.59	0.015	0.245	1.91
				μ_t	<dl	0.482	14.2	11.5	<dl	35.7	1.92	4.17	5.20	0.077	1.61	0.017	0.270	2.34
				sd_t	na	0.418	15.5	12.5	na	5.03	1.54	2.41	2.53	0.092	0.948	0.016	0.190	2.04
		Lala	11	*med*	1.15	4.41	1.60	27.2	0.354	34.7	8.59	7.22	25.6	0.244	1.24	0.032	2.49	0.255
				μ_t	1.50	4.49	2.47	28.0	0.361	35.8	8.70	7.18	27.1	0.249	1.30	0.032	2.37	0.303
				sd_t	1.16	0.853	3.55	2.21	0.102	5.73	1.04	0.441	7.22	0.122	0.400	0.041	0.870	0.164
		Manxman	27	*med*	1.32	2.50	1.00	144	0.400	616	49.7	21.7	24.0	0.310	0.760	0.530	2.75	1.55
				μ_t	1.36	2.45	3.20	190	0.723	487	54.6	31.7	24.8	0.377	8.44	0.575	2.59	1.59
				sd_t	0.706	2.62	6.38	122	0.826	436	63.2	40.3	20.1	0.404	15.0	0.475	1.50	1.24
		Mina Justa	15	*med*	1.09	0.830	0.270	73.3	0.410	34.2	30.6	11.5	0.200	0.210	0.780	0.050	18.4	1.96
				μ_t	1.15	2.72	0.336	55.8	0.448	34.1	33.0	11.4	0.779	0.367	1.23	0.047	15.6	2.47
				sd_t	0.351	5.89	0.519	65.9	0.241	10.2	35.6	4.20	1.62	0.402	2.08	0.031	18.9	3.64
		Pista	12	*med*	1.37	1.50	1.58	335	1.47	8.14	5.08	4.30	29.2	0.050	0.720	<dl	0.630	0.083
				μ_t	1.26	1.52	1.51	330	1.07	<dl	5.31	3.62	29.9	0.053	0.756	<dl	0.816	0.149
				sd_t	0.728	0.488	1.44	34.0	0.900	na	2.82	1.81	5.53	0.060	0.379	na	0.511	0.127
		Punt Hill	9	*med*	1.92	0.900	1.00	185	<dl	4.40	3.56	25.2	13.3	<dl	<dl	<dl	3.05	0.262
				μ_t	1.82	1.96	3.70	282	0.028	<dl	2.64	21.1	23.6	<dl	7.35	0.027	2.67	0.319
				sd_t	0.793	2.66	4.78	205	0.024	na	2.69	18.3	26.5	na	11.5	0.037	2.08	0.252
		Salobo	7	*med*	1.32	4.49	15.0	6.00	0.105	20.1	0.920	1.71	18.4	0.034	1.01	<dl	0.670	0.483
				μ_t	1.42	4.37	10.2	8.12	0.084	<dl	0.852	1.72	17.7	0.101	0.962	0.195	0.613	0.491
				sd_t	0.902	3.63	10.1	9.19	0.041	na	0.441	0.056	2.98	0.127	0.443	0.270	0.192	0.352
		San Fernando	7	*med*	4.00	0.244	<dl	125	0.320	28.4	7.80	15.5	5.14	0.145	5.19	0.024	28.2	11.0
				μ_t	3.98	0.264	2.05	125	0.311	27.7	8.26	16.2	5.00	0.168	4.99	0.024	24.0	10.2
				sd_t	2.61	0.100	3.15	37.3	0.189	2.13	2.65	6.89	1.96	0.117	1.11	0.021	26.3	3.02
		Sossego	46	*med*	<dl	0.083	3.09	120	0.393	37.4	3.88	3.03	8.88	<dl	0.730	<dl	2.36	0.261
				μ_t	<dl	0.118	3.41	106	0.403	37.5	4.82	3.84	9.59	<dl	1.32	<dl	2.46	0.301
				sd_t	na	0.136	4.41	64.6	0.260	4.19	5.92	1.91	5.91	na	2.63	na	1.74	0.294

Class	Type	Deposit	n	Stat	Mn	Co	Ni	Zn	Ga	Se	Ag	In	Sn	Sb	Te	Au	Pb	Bi
				Isotope	55	59	60	66	71	82	107	115	118	121	128	197	208	209
		Median of detection limits*		55um	0.470	0.023	0.241	0.353	0.028	2.53	0.023	0.012	0.073	0.022	0.256	0.010	0.012	0.007
		Summary IOCG	*281*	*med*	*0.910*	*0.693*	*0.850*	*127*	*0.309*	*33.5*	*10.5*	*6.31*	*7.98*	*0.089*	*1.03*	*0.018*	*2.06*	*0.990*
				μ_t	*0.941*	*1.09*	*2.22*	*146*	*0.305*	*34.1*	*21.1*	*6.78*	*11.4*	*0.122*	*1.25*	*0.028*	*2.22*	*1.14*
				sd_t	*0.996*	*1.62*	*4.45*	*165*	*0.254*	*21.3*	*30.5*	*5.23*	*13.1*	*0.163*	*1.43*	*0.041*	*2.03*	*1.26*
	Orogenic	Amaruq	30	*med*	1.11	0.091	28.0	348	0.133	48.6	2.15	14.5	23.9	0.145	<dl	0.012	1.53	0.171
				μ_t	1.12	0.111	33.9	348	0.142	53.2	2.85	14.1	40.8	0.145	<dl	0.029	1.56	0.215
				sd_t	0.590	0.117	40.7	83.7	0.111	40.2	2.96	15.0	56.3	0.156	na	0.050	1.08	0.289
		Beaufor	7	*med*	1.11	0.035	<dl	20.4	0.099	8.60	0.070	6.82	0.780	<dl	<dl	0.025	0.390	0.670
				μ_t	1.20	0.077	<dl	20.4	0.098	7.80	0.150	6.76	0.783	<dl	<dl	0.035	0.497	1.28
				sd_t	0.377	0.089	na	5.93	0.005	2.31	0.162	0.183	0.066	na	na	0.033	0.389	1.28
		Bulyanhulu	21	*med*	1.43	0.140	6.00	418	0.280	<dl	152	11.1	18.2	0.600	<dl	<dl	4.29	3.54
				μ_t	1.50	0.192	6.65	354	0.355	20.4	199	12.3	25.8	0.927	<dl	<dl	5.25	4.37
				sd_t	0.694	0.231	8.30	305	0.295	16.7	256	3.90	21.7	1.11	na	na	6.84	4.05
		Cononish mine	21	*med*	0.610	0.040	<dl	99.4	0.270	4.60	72.4	0.648	0.760	2.68	2.99	<dl	7.40	0.270
				μ_t	1.34	0.082	<dl	211	0.259	4.88	49.2	2.83	0.972	2.40	2.42	0.015	8.71	0.786
				sd_t	1.99	0.109	na	285	0.099	3.00	57.4	4.45	0.728	2.49	3.60	0.026	7.71	1.23
		Hougou	12	*med*	<dl	0.412	1.45	14.9	0.049	<dl	11.9	0.191	<dl	1.63	<dl	<dl	3.59	0.013
				μ_t	0.750	0.463	12.7	14.7	0.053	<dl	12.9	0.197	<dl	1.49	<dl	<dl	3.57	0.027
				sd_t	0.879	0.140	17.9	2.44	0.032	na	5.00	0.043	na	0.940	na	na	1.82	0.024
		Kochkar	4	*med*	1.16	0.730	4.55	313	0.259	<dl	4.46	84.3	14.3	0.023	<dl	<dl	0.830	2.21
				μ_t	1.81	0.695	32.3	316	0.256	233	6.07	84.6	13.1	0.036	0.523	0.020	2.70	2.24
				sd_t	1.80	0.527	51.7	40.6	0.059	115	3.12	11.7	2.59	0.048	0.776	0.030	3.69	1.99
		Lega Dembi	12	*med*	1.59	0.683	5.00	632	3.59	42.2	185	16.3	284	1.01	1.95	0.022	2.20	0.159
				μ_t	1.57	1.24	9.18	642	7.27	44.5	187	26.7	307	0.913	2.24	0.037	2.22	0.247
				sd_t	0.444	1.09	10.1	117	8.28	12.8	51.3	29.1	401	0.379	1.76	0.045	1.26	0.288
		Linglong	5	*med*	1.60	<dl	<dl	21.4	0.150	5.08	374	78.4	1.28	2.55	<dl	<dl	15.3	8.97
				μ_t	1.57	<dl	<dl	21.2	0.128	5.43	377	77.5	1.35	2.59	<dl	<dl	15.8	8.96
				sd_t	1.08	na	na	1.39	0.071	1.16	55.3	3.59	0.198	0.693	na	na	4.34	1.21

Class	Type	Deposit	n	Stat	Mn	Co	Ni	Zn	Ga	Se	Ag	In	Sn	Sb	Te	Au	Pb	Bi
				Isotope	55	59	60	66	71	82	107	115	118	121	128	197	208	209
		Median of detection limits*		55um	0.470	0.023	0.241	0.353	0.028	2.53	0.023	0.012	0.073	0.022	0.256	0.010	0.012	0.007
		Malartic	8	*med*	1.23	1.70	20.5	208	0.877	<dl	329	16.0	27.5	0.039	<dl	0.141	0.965	1.27
				μ_t	1.17	1.50	17.1	209	0.862	<dl	285	15.9	27.2	0.066	<dl	0.195	1.62	1.27
				sd_t	0.514	1.61	19.4	15.9	0.425	na	161	0.608	0.805	0.073	na	0.136	1.49	0.356
		Raleigh	5	*med*	1.44	0.380	0.430	266	1.72	<dl	1.51	67.1	60.1	17.0	1.72	0.120	61.0	1.78
				μ_t	1.21	0.357	6.27	274	2.01	<dl	1.52	50.3	58.3	15.4	1.87	0.140	59.6	1.29
				sd_t	0.842	0.277	13.7	51.6	0.994	na	0.111	43.2	10.0	9.65	1.13	0.157	31.6	1.58
		Young-Davidson	14	*med*	0.940	0.095	5.08	99.4	0.053	<dl	53.1	4.52	0.311	0.151	<dl	0.043	2.02	1.44
				μ_t	0.931	0.250	5.18	101	0.053	<dl	52.9	4.56	0.306	0.182	<dl	0.042	2.22	2.02
				sd_t	0.310	0.363	0.562	26.9	0.025	na	2.06	0.182	0.033	0.143	na	0.031	1.07	1.69
		Summary orogenic gold	*139*	*med*	*1.20*	*0.186*	*4.62*	*227*	*0.192*	*14.4*	*33.2*	*6.91*	*14.3*	*0.406*	*<dl*	*0.014*	*2.46*	*0.717*
				μ_t	*1.19*	*0.234*	*5.92*	*233*	*0.226*	*18.4*	*47.9*	*9.39*	*13.4*	*0.659*	*<dl*	*0.023*	*3.10*	*0.956*
				sd_t	*0.757*	*0.291*	*9.39*	*230*	*0.221*	*20.3*	*69.5*	*9.54*	*19.8*	*0.922*	*na*	*0.037*	*2.97*	*1.20*
	Porphyry	Ajax-Afton	8	*med*	<dl	1.16	<dl	5.57	0.229	26.7	6.86	7.49	2.44	0.051	0.925	0.037	8.08	0.706
				μ_t	<dl	1.17	<dl	5.84	0.234	27.1	7.31	7.50	2.44	0.055	1.02	0.039	34.6	0.850
				sd_t	na	0.094	na	2.73	0.060	3.59	2.66	0.296	0.089	0.033	0.327	0.027	44.8	0.393
		Altar	9	*med*	1.70	1.10	<dl	17.0	1.85	161	8.06	1.82	7.00	0.069	0.330	0.037	0.840	0.440
				μ_t	1.81	1.33	8.12	26.6	2.73	162	6.25	1.86	11.4	0.090	<dl	0.062	1.33	0.592
				sd_t	1.63	1.85	12.0	22.0	1.98	6.21	3.89	0.185	10.6	0.047	na	0.086	1.26	0.519
		Asarel	24	*med*	<dl	<dl	11.5	9.89	0.269	45.7	1.91	2.61	0.710	0.043	0.710	0.023	4.97	3.19
				μ_t	<dl	<dl	9.67	10.5	0.301	84.1	1.95	2.91	0.720	0.059	0.829	0.025	6.16	5.48
				sd_t	na	na	7.46	5.60	0.224	119	0.951	2.35	0.648	0.065	0.651	0.017	4.72	7.59
		Binghampton	13	*med*	0.720	13.1	<dl	60.9	10.5	223	0.710	4.28	166	<dl	<dl	<dl	7.59	0.071
				μ_t	0.670	12.7	<dl	61.7	9.43	339	0.676	4.27	165	<dl	<dl	<dl	8.82	0.090
				sd_t	0.351	1.47	na	17.7	3.00	217	0.331	0.190	23.6	na	na	na	8.09	0.052
		Bolong	4	*med*	1.98	0.242	<dl	287	0.560	95.9	13.0	5.61	26.5	0.270	1.87	<dl	12.0	1.26
				μ_t	2.06	0.228	<dl	262	0.635	99.1	14.5	5.57	25.8	2.01	1.85	<dl	13.0	1.30
				sd_t	0.314	0.086	na	90.3	0.158	8.33	10.0	0.184	8.00	3.25	0.391	na	12.5	0.279

Class	Type	Deposit	n	Stat	Mn	Co	Ni	Zn	Ga	Se	Ag	In	Sn	Sb	Te	Au	Pb	Bi
				Isotope	55	59	60	66	71	82	107	115	118	121	128	197	208	209
		Median of detection limits*		55um	0.470	0.023	0.241	0.353	0.028	2.53	0.023	0.012	0.073	0.022	0.256	0.010	0.012	0.007
		Bor	10	*med*	2.35	0.027	21.4	76.3	0.098	<dl	8.43	0.673	14.0	0.115	1.17	0.064	11.6	6.06
				μ_t	2.37	0.037	21.8	75.9	0.112	<dl	10.1	0.686	13.6	0.118	1.16	0.066	11.1	6.01
				sd_t	1.64	0.063	4.65	14.1	0.146	na	8.07	0.235	7.50	0.140	0.171	0.060	11.4	3.26
		Copper Mountain	3	*med*	0.620	1.47	<dl	453	0.500	45.2	5.76	10.8	1.34	0.130	1.75	<dl	3.88	0.220
				μ_t	0.640	1.69	<dl	440	0.588	44.9	6.71	11.1	2.65	0.097	2.51	<dl	4.63	0.309
				sd_t	0.550	0.967	na	145	0.272	1.09	3.01	0.705	3.47	0.085	1.64	na	3.33	0.238
		Duobuza	6	*med*	0.970	0.250	<dl	10.2	0.072	<dl	8.28	9.36	0.145	0.063	0.326	<dl	36.2	0.928
				μ_t	0.983	0.266	<dl	10.3	0.072	<dl	9.12	9.80	0.143	0.058	0.303	<dl	30.5	0.928
				sd_t	0.519	0.173	na	12.8	0.018	na	6.15	2.28	0.121	0.033	0.228	na	28.6	0.359
		Elatsite	10	*med*	<dl	0.595	4.66	3.20	0.660	<dl	4.24	2.07	1.08	1.02	0.690	0.047	23.3	0.470
				μ_t	<dl	0.447	4.64	10.8	0.693	<dl	4.67	1.64	1.57	1.11	0.643	0.048	23.2	0.568
				sd_t	na	0.587	4.69	19.6	0.359	na	4.63	1.42	2.33	1.20	0.286	0.043	16.9	0.691
		Galore Creek	4	*med*	0.580	2.19	2.10	207	0.210	<dl	25.0	0.581	0.155	0.147	0.630	<dl	1.46	0.945
				μ_t	1.41	2.19	31.2	179	0.219	<dl	35.3	0.982	1.06	0.126	0.638	<dl	1.48	0.811
				sd_t	1.53	0.743	52.3	61.7	0.158	na	22.5	0.842	1.67	0.093	0.206	na	0.424	0.649
		Granisle	26	*med*	0.920	1.27	<dl	16.8	0.598	<dl	2.83	5.85	13.3	0.101	4.15	0.016	3.50	0.051
				μ_t	1.66	1.28	<dl	36.5	0.638	<dl	3.19	5.43	20.6	0.139	3.65	0.016	5.99	0.052
				sd_t	4.12	0.849	na	98.1	0.336	na	3.72	2.04	32.7	0.223	4.46	0.023	7.66	0.060
		Highland Valley	6	*med*	0.595	0.284	<dl	0.720	0.038	67.5	1.56	3.80	0.130	0.059	0.408	<dl	2.91	0.218
				μ_t	0.570	0.366	<dl	0.710	0.036	69.2	1.71	3.75	0.139	0.052	0.407	<dl	2.81	0.231
				sd_t	0.260	0.350	na	0.131	0.023	40.0	0.677	1.92	0.096	0.042	0.119	na	1.70	0.164
		Jiama	7	*med*	<dl	0.847	<dl	9.15	0.152	59.4	0.123	13.7	0.083	0.052	0.530	<dl	0.890	0.650
				μ_t	<dl	0.907	<dl	69.3	0.224	65.3	0.131	14.1	0.138	0.048	0.518	<dl	0.866	0.732
				sd_t	na	0.216	na	108	0.133	19.7	0.045	3.63	0.116	0.037	0.426	na	0.347	0.518
		Jinchang	8	*med*	2.00	2.41	20.7	589	0.510	49.3	11.3	12.9	12.4	0.214	2.36	<dl	6.50	3.49
				μ_t	2.15	2.94	22.3	610	0.479	49.4	12.4	12.1	13.3	0.209	2.79	<dl	35.0	3.13
				sd_t	1.18	3.26	34.3	150	0.506	25.2	3.59	2.25	8.88	0.100	1.81	na	47.3	1.92

Class	Type	Deposit	n	Stat	Mn	Co	Ni	Zn	Ga	Se	Ag	In	Sn	Sb	Te	Au	Pb	Bi
				Isotope	55	59	60	66	71	82	107	115	118	121	128	197	208	209
		Median of detection limits*		55um	0.470	0.023	0.241	0.353	0.028	2.53	0.023	0.012	0.073	0.022	0.256	0.010	0.012	0.007
		Mt. Milligan	5	*med*	0.780	0.139	0.350	55.7	0.111	407	97.3	9.51	0.340	1.44	<dl	0.038	6.74	0.104
				μ_t	0.640	0.175	0.326	55.9	0.115	403	99.1	9.76	0.338	1.42	<dl	0.032	6.94	0.104
				sd_t	0.563	0.105	0.445	26.6	0.015	19.2	11.1	1.81	0.025	0.433	na	0.028	4.95	0.012
		New Afton	14	*med*	1.42	0.317	0.390	1.18	0.372	67.9	15.3	4.36	1.03	0.377	<dl	<dl	23.3	0.715
				μ_t	1.48	0.302	2.70	1.25	0.372	71.9	15.4	4.19	1.40	0.442	<dl	0.032	28.4	0.749
				sd_t	0.624	0.130	4.59	0.447	0.155	39.2	6.91	1.28	1.20	0.408	na	0.043	20.2	0.650
		Oyu Tolgoi	6	*med*	1.55	0.670	1.58	2.60	0.495	743	19.4	1.78	0.122	2.36	0.510	0.049	17.5	2.09
				μ_t	1.65	1.01	3.05	2.38	0.455	751	17.5	1.90	0.151	2.28	0.560	0.040	17.2	2.02
				sd_t	0.646	1.16	6.13	1.69	0.437	134	10.6	0.997	0.151	1.86	0.424	0.043	8.75	0.642
		Tiegelongnan	11	*med*	1.65	0.145	0.400	13.5	3.84	67.9	45.0	1.49	2.18	4.10	5.10	7.40	505	0.949
				μ_t	3.45	0.162	0.821	21.8	4.03	<dl	29.7	1.86	5.20	22.3	4.60	5.22	335	0.940
				sd_t	6.86	0.221	1.91	25.5	2.21	na	40.7	1.10	11.9	38.9	5.09	7.52	390	0.571
		Utah Copper Mine	6	*med*	<dl	6.30	<dl	30.3	4.54	<dl	0.256	4.17	94.9	<dl	0.550	<dl	0.080	0.007
				μ_t	<dl	6.23	<dl	28.4	4.49	<dl	0.259	4.20	89.8	<dl	0.489	<dl	0.129	0.007
				sd_t	na	3.37	na	11.2	0.818	na	0.068	0.329	40.3	na	0.513	na	0.168	0.006
		Xiongcun	7	*med*	1.18	<dl	<dl	345	0.360	247	4.30	34.7	10.6	1.49	4.60	<dl	5.40	0.486
				μ_t	1.32	<dl	<dl	352	0.376	243	4.00	34.4	10.4	1.25	4.76	<dl	7.10	0.604
				sd_t	0.863	na	na	72.6	0.086	12.5	1.97	4.57	2.37	0.687	1.64	na	5.11	0.385
		Summary porphyry	*187*	*med*	*0.830*	*0.510*	*<dl*	*16.7*	*0.475*	*129*	*4.61*	*4.28*	*3.76*	*0.101*	*0.740*	*0.013*	*6.54*	*0.650*
				μ_t	*0.854*	*0.659*	*1.17*	*27.7*	*0.561*	*126*	*5.52*	*4.39*	*5.82*	*0.171*	*0.809*	*0.016*	*9.24*	*0.697*
				sd_t	*0.864*	*0.862*	*2.93*	*37.2*	*0.617*	*121*	*6.12*	*3.66*	*8.71*	*0.246*	*0.837*	*0.023*	*11.1*	*0.791*
	Skarn	Baita Bihor	13	*med*	2.12	11.5	0.400	769	0.600	113	28.0	154	158	0.034	1.53	0.041	3.26	4.16
				μ_t	2.54	11.9	0.767	833	0.471	75.4	24.4	150	155	0.040	1.47	0.056	2.87	3.75
				sd_t	2.78	4.02	0.911	266	0.618	91.4	17.6	61.7	48.9	0.039	1.33	0.063	2.89	4.70
		Cantung	11	*med*	3.67	1.11	4.60	864	0.920	<dl	108	19.0	268	<dl	<dl	<dl	1.14	0.570
				μ_t	3.63	1.10	11.5	859	0.957	<dl	108	21.1	242	0.036	<dl	<dl	1.03	0.596
				sd_t	2.14	0.584	19.2	101	0.527	na	8.64	6.89	105	0.038	na	na	0.474	0.286

Class	Type	Deposit	n	Stat	Mn	Co	Ni	Zn	Ga	Se	Ag	In	Sn	Sb	Te	Au	Pb	Bi
				Isotope	55	59	60	66	71	82	107	115	118	121	128	197	208	209
		Median of detection limits*		55um	0.470	0.023	0.241	0.353	0.028	2.53	0.023	0.012	0.073	0.022	0.256	0.010	0.012	0.007
		Gaspé Copper	57	*med*	1.59	7.64	8.93	524	0.950	<dl	31.7	24.6	30.8	0.026	8.60	<dl	2.14	0.402
				μ_t	1.66	7.71	9.45	530	1.20	<dl	33.8	25.0	33.7	0.028	8.96	<dl	2.14	0.613
				sd_t	0.574	4.39	7.83	119	1.12	na	21.2	9.94	18.1	0.029	6.36	na	1.44	0.826
		Mactung	9	*med*	3.20	4.80	0.720	639	0.570	51.1	29.2	11.9	3.53	<dl	<dl	<dl	0.960	0.320
				μ_t	2.60	4.00	0.809	628	0.673	50.7	29.3	13.8	5.67	0.033	<dl	<dl	1.91	0.410
				sd_t	1.60	2.46	0.669	31.5	0.287	9.47	1.48	7.15	5.66	0.039	na	na	1.76	0.295
		Marn	6	*med*	0.600	9.89	2.32	580	0.770	52.4	105	4.38	12.2	0.149	2.09	<dl	2.85	0.147
				μ_t	0.985	9.93	7.07	586	0.745	52.4	106	4.64	12.3	0.133	2.12	0.014	2.93	0.152
				sd_t	1.35	1.76	15.2	85.3	0.299	3.40	5.99	1.60	3.00	0.132	0.303	0.029	1.85	0.126
		Oravita	34	*med*	<dl	<dl	10.6	148	0.243	9.69	2.96	8.28	1.54	0.293	0.647	0.021	1.65	0.080
				μ_t	<dl	0.033	10.4	154	0.233	<dl	2.98	8.24	1.56	1.20	0.646	0.021	3.79	0.114
				sd_t	na	0.053	2.97	84.3	0.142	na	2.61	2.28	1.53	2.13	0.308	0.006	5.62	0.127
		Summary Skarn	*130*	*med*	*1.46*	*4.92*	*8.25*	*528*	*0.575*	*60.8*	*28.4*	*18.0*	*23.9*	*0.040*	*1.63*	*0.016*	*1.81*	*0.295*
				μ_t	*1.33*	*4.75*	*7.74*	*514*	*0.628*	*63.8*	*26.9*	*18.9*	*27.0*	*0.065*	*2.75*	*0.014*	*2.10*	*0.433*
				sd_t	*1.28*	*5.65*	*7.47*	*273*	*0.540*	*63.0*	*27.0*	*13.9*	*32.1*	*0.087*	*3.93*	*0.016*	*1.91*	*0.610*
	VMS	Adak	11	*med*	3.03	1.11	<dl	430	0.730	501	83.7	87.6	76.7	0.340	0.470	0.044	8.40	1.10
				μ_t	3.20	1.30	0.669	454	0.739	509	84.7	85.8	81.6	0.379	0.483	0.043	8.06	1.08
				sd_t	0.812	0.566	1.19	93.8	0.455	47.5	6.39	18.7	21.4	0.317	0.165	0.055	3.58	0.549
		Aldermac	18	*med*	3.51	1.97	2.40	408	0.770	141	118	7.52	23.6	0.363	0.535	0.015	2.17	1.37
				μ_t	4.04	2.18	1.84	421	1.93	149	124	35.7	42.9	0.344	0.534	0.021	1.98	1.10
				sd_t	1.89	1.81	2.00	84.4	2.06	32.7	86.1	43.6	51.5	0.389	0.525	0.023	1.23	1.08
		Aljustrel	6	*med*	3.80	0.094	<dl	370	5.08	51.2	4.08	76.8	333	3.81	<dl	0.029	2.22	0.800
				μ_t	4.25	0.170	0.360	367	4.36	51.7	4.60	77.5	321	4.56	<dl	0.023	2.29	0.846
				sd_t	5.78	0.315	0.882	25.5	3.10	9.05	2.02	9.30	198	6.11	na	0.025	2.97	0.880
		Ashadze-2	7	*med*	5.59	1859	121	571	0.910	685	18.2	0.800	21.5	1.33	29.0	7.41	1.76	0.670
				μ_t	6.73	2233	116	730	0.882	932	20.6	0.748	22.9	1.68	25.7	6.90	1.80	0.686
				sd_t	5.98	1110	49.6	476	0.402	485	8.99	0.378	8.05	0.819	17.3	4.40	0.271	0.283

Class	Type	Deposit	n	Stat	Mn	Co	Ni	Zn	Ga	Se	Ag	In	Sn	Sb	Te	Au	Pb	Bi
				Isotope	55	59	60	66	71	82	107	115	118	121	128	197	208	209
		Median of detection limits*		55um	0.470	0.023	0.241	0.353	0.028	2.53	0.023	0.012	0.073	0.022	0.256	0.010	0.012	0.007
		Aznalcollar	6	*med*	0.725	0.053	16.3	265	0.633	84.5	0.321	238	375	2.70	<dl	<dl	2.09	0.164
				μ_t	0.715	0.061	19.5	256	0.614	84.0	0.322	238	375	3.03	<dl	<dl	2.63	0.183
				sd_t	0.347	0.080	30.2	34.6	0.077	5.22	0.331	5.59	27.2	1.95	na	na	2.52	0.200
		Bathurst	21	*med*	1.82	0.294	<dl	322	1.53	988	22.9	81.7	179	0.216	<dl	0.241	2.75	8.10
				μ_t	1.94	0.309	<dl	324	3.06	936	25.2	78.9	165	0.221	<dl	0.247	2.59	7.04
				sd_t	0.576	0.142	na	30.9	3.57	184	10.0	22.1	70.6	0.121	na	0.199	1.52	7.48
		Boundary	5	*med*	2.41	14.1	0.267	497	0.262	274	1.28	6.42	45.9	6.70	1.17	0.025	11.3	0.710
				μ_t	2.34	13.3	0.258	486	0.257	271	1.11	6.78	45.2	8.33	1.35	0.021	16.0	0.799
				sd_t	0.421	2.31	0.119	64.9	0.117	18.4	0.736	0.939	3.78	5.71	0.588	0.024	16.1	0.396
		Brannmyran	6	*med*	3.80	1.91	<dl	579	1.46	434	87.0	66.7	178	0.940	0.460	0.062	4.17	1.96
				μ_t	3.70	2.02	0.405	576	1.46	428	87.3	68.4	179	1.05	0.462	0.068	4.50	2.26
				sd_t	0.393	0.817	0.790	51.2	0.140	35.8	1.97	9.60	26.1	0.876	0.065	0.068	1.98	1.18
		Caber	10	*med*	<dl	<dl	<dl	191	0.247	256	1.44	14.9	12.1	0.889	14.4	<dl	1.99	0.075
				μ_t	<dl	<dl	<dl	176	0.285	461	9.01	16.4	12.4	0.995	13.9	0.013	2.64	0.086
				sd_t	na	na	na	95.1	0.221	460	25.3	16.7	4.07	0.690	13.3	0.018	1.93	0.078
		Candelabra	11	*med*	3.13	516	297	956	0.240	<dl	8.43	41.4	48.9	<dl	43.2	0.092	0.110	0.120
				μ_t	3.41	678	266	755	0.235	<dl	9.30	33.5	52.6	<dl	57.5	0.085	0.145	0.293
				sd_t	2.78	706	132	723	0.285	na	5.88	39.8	28.2	na	63.6	0.082	0.197	0.597
		Cerro de Maimón	11	*med*	9.92	1.84	1.14	3.06	3.34	83.2	18.2	7.85	1.47	0.178	1.62	0.056	8.08	3.30
				μ_t	10.2	1.78	1.23	3.13	3.41	83.5	19.0	7.72	1.48	0.171	1.62	0.049	12.4	4.42
				sd_t	2.57	0.531	0.668	0.596	0.249	9.84	7.28	0.661	0.187	0.121	0.137	0.034	10.3	4.14
		Corvo	28	*med*	0.691	0.125	0.610	190	5.98	260	3.07	270	727	4.35	<dl	0.015	6.52	7.34
				μ_t	1.03	0.193	0.773	197	7.35	407	3.84	278	771	5.35	<dl	0.023	7.89	8.45
				sd_t	0.911	0.236	1.02	166	5.96	484	3.21	124	349	4.58	na	0.027	7.26	7.96
		Dergamysh	22	*med*	1.10	243	26.5	11904	7.19	239	3.82	50.6	16.0	1.02	0.535	0.030	13.0	0.165
				μ_t	2.12	305	223	9922	7.23	240	3.45	54.4	19.2	1.34	8.71	0.034	15.9	0.626
				sd_t	2.47	368	386	9721	2.62	89.4	3.78	16.4	24.2	1.31	18.3	0.022	21.4	1.20

Class	Type	Deposit	n	Stat	Mn	Co	Ni	Zn	Ga	Se	Ag	In	Sn	Sb	Te	Au	Pb	Bi
				Isotope	55	59	60	66	71	82	107	115	118	121	128	197	208	209
		Median of detection limits*		55um	0.470	0.023	0.241	0.353	0.028	2.53	0.023	0.012	0.073	0.022	0.256	0.010	0.012	0.007
		Draa Sfar	6	*med*	0.747	0.176	<dl	275	0.285	98.6	3.22	7.91	33.9	4.67	<dl	0.302	23.2	30.0
				μ_t	0.970	0.193	<dl	273	0.283	98.7	3.26	7.68	35.0	4.18	<dl	0.281	23.3	28.7
				sd_t	1.06	0.100	na	22.9	0.047	2.22	0.925	2.15	15.0	2.71	na	0.103	7.77	13.3
		Duck Pond	7	*med*	<dl	<dl	<dl	126	46.8	32.2	6.10	47.7	40.3	3.34	<dl	<dl	8.43	5.50
				μ_t	<dl	<dl	<dl	135	47.4	33.8	6.34	48.3	41.0	4.51	0.272	<dl	8.54	6.44
				sd_t	na	na	na	29.1	6.61	11.5	1.99	2.99	1.76	3.30	0.351	na	6.66	4.55
		Dufault	20	*med*	0.910	0.882	<dl	284	1.25	<dl	92.0	162	81.3	0.417	<dl	0.015	2.29	1.76
				μ_t	1.51	0.887	<dl	285	2.96	271	88.4	179	88.9	0.421	<dl	0.045	2.37	1.94
				sd_t	1.92	1.14	na	38.9	6.16	399	57.3	140	26.9	0.240	na	0.065	1.08	1.60
		Ely	6	*med*	27.3	3.26	3.05	373	0.760	<dl	11.9	3.97	5.81	0.112	1.61	<dl	0.885	0.313
				μ_t	27.5	3.08	2.90	375	0.810	<dl	12.1	4.05	5.89	0.124	1.55	<dl	1.07	0.385
				sd_t	10.5	1.01	2.25	28.2	0.311	na	0.682	0.921	1.25	0.062	0.351	na	0.829	0.317
		Graça	6	*med*	0.515	0.073	<dl	302	3.12	249	4.69	314	1064	5.23	<dl	<dl	2.95	1.24
				μ_t	0.670	0.077	0.611	314	3.33	267	5.36	320	1007	6.00	<dl	<dl	4.14	1.66
				sd_t	0.598	0.096	1.58	74.9	1.41	132	3.02	134	415	5.85	na	na	4.25	1.54
		Hajar	6	*med*	3.36	0.189	<dl	460	11.7	7.85	62.1	5.34	854	6.23	<dl	0.029	12.1	0.170
				μ_t	3.88	0.189	<dl	466	12.6	8.38	61.4	5.56	856	7.90	<dl	0.030	11.1	0.170
				sd_t	2.47	0.016	na	51.1	4.12	5.78	4.69	1.26	64.6	7.15	na	0.018	6.84	0.148
		Halfmile Lake		*med*	1.18	1.03	1.10	419	0.304	57.1	63.8	23.0	509	1.50	<dl	0.074	5.75	7.32
			5	μ_t	1.17	1.05	1.15	415	0.304	56.4	63.5	22.4	543	1.22	<dl	0.114	5.25	7.09
				sd_t	0.089	0.068	0.252	30.4	0.038	2.92	3.64	6.53	175	1.02	na	0.160	1.65	4.98
		Horne		*med*	1.57	3.37	0.405	209	2.80	<dl	57.2	55.3	84.1	0.370	3.46	0.283	3.86	4.48
			24	μ_t	1.45	3.64	0.691	243	7.46	<dl	61.5	57.4	82.2	0.357	5.43	0.285	4.52	6.36
				sd_t	1.59	2.23	1.01	133	9.83	na	16.3	67.5	27.8	0.287	4.09	0.198	2.92	6.35
		Ice		*med*	2.66	<dl	<dl	1.27	18.8	<dl	7.81	28.6	0.480	0.390	<dl	<dl	6.90	0.160
			5	μ_t	3.73	0.161	<dl	1.21	17.8	<dl	8.30	29.3	0.443	0.401	<dl	<dl	11.4	0.162
				sd_t	2.64	0.344	na	0.578	15.0	na	7.45	18.2	0.168	0.350	na	na	14.4	0.191

Class	Type	Deposit	n	Stat	Mn	Co	Ni	Zn	Ga	Se	Ag	In	Sn	Sb	Te	Au	Pb	Bi
				Isotope	55	59	60	66	71	82	107	115	118	121	128	197	208	209
		Median of detection limits*		55um	0.470	0.023	0.241	0.353	0.028	2.53	0.023	0.012	0.073	0.022	0.256	0.010	0.012	0.007
		Irina I		*med*	3.35	203	157	123	0.054	<dl	3.08	5.45	44.3	<dl	24.2	<dl	0.054	0.036
			6	μ_t	3.36	206	163	124	0.057	<dl	2.94	5.78	44.9	0.129	24.9	<dl	0.067	0.040
				sd_t	0.942	59.9	114	13.6	0.030	na	3.92	1.35	9.02	0.347	11.8	na	0.057	0.033
		Irina II		*med*	3.84	814	0.500	1381	0.960	372	1.62	1.68	224	<dl	17.1	0.032	0.167	0.159
			6	μ_t	3.83	829	0.641	1296	1.22	375	1.51	1.75	216	0.104	19.3	0.031	0.150	0.159
				sd_t	1.65	476	0.957	824	1.56	496	1.66	2.54	42.8	0.277	31.4	0.024	0.150	0.085
		Irinovskoe		*med*	1.80	239	1.60	173	3.17	463	36.3	3.38	139	0.076	24.2	0.024	0.099	0.243
			27	μ_t	1.80	240	2.09	201	3.77	503	32.3	3.36	123	0.108	23.3	0.045	0.180	0.282
				sd_t	0.631	53.3	2.54	83.4	2.90	222	25.7	2.30	101	0.144	14.8	0.048	0.222	0.229
		Kidd Creek		*med*	0.659	0.505	<dl	299	2.03	92.3	95.0	187	79.2	0.169	<dl	<dl	2.92	0.496
			28	μ_t	0.880	0.644	<dl	302	2.55	<dl	170	211	93.3	0.185	<dl	<dl	3.39	0.770
				sd_t	0.891	0.915	na	49.5	1.82	na	283	216	83.6	0.150	na	na	2.95	0.904
		Lagoa Salgada		*med*	0.750	0.030	<dl	205	0.372	<dl	11.0	44.1	649	20.9	<dl	0.025	10.7	3.56
			7	μ_t	0.824	0.028	0.361	225	0.429	<dl	8.75	54.0	714	18.5	<dl	0.086	10.8	3.95
				sd_t	0.441	0.009	0.452	60.2	0.231	na	9.14	34.1	301	17.6	na	0.115	8.98	2.88
		Lasail		*med*	0.885	0.256	<dl	846	3.06	36.1	9.76	11.4	4.61	<dl	0.349	0.029	6.88	0.163
			14	μ_t	1.58	0.398	<dl	926	5.43	40.0	13.2	10.2	4.69	<dl	0.711	0.032	15.2	0.223
				sd_t	1.86	0.579	na	1414	7.08	54.8	10.2	6.22	6.72	na	1.02	0.037	22.3	0.227
		Lindsköld		*med*	3.44	1.45	<dl	483	0.498	268	85.5	52.0	109	2.07	0.830	0.012	3.42	0.735
			18	μ_t	3.75	2.73	0.860	483	1.17	329	85.4	47.9	104	1.91	0.823	0.017	4.83	0.779
				sd_t	1.47	2.82	1.12	87.8	1.46	156	53.2	31.8	45.0	1.91	0.281	0.020	3.17	0.433
		Little Bay		*med*	2.46	0.036	0.781	647	2.50	<dl	1.83	12.5	2.13	0.051	5.40	<dl	7.77	6.33
			6	μ_t	2.38	0.039	0.829	646	2.50	<dl	1.95	12.4	2.12	0.052	5.64	0.023	7.60	7.96
				sd_t	0.345	0.014	1.17	127	0.135	na	1.34	1.40	0.393	0.019	0.902	0.058	1.89	11.0
		Little Deer		*med*	5.86	0.316	2.22	397	1.74	385	94.2	35.9	0.112	3.60	1.69	<dl	6.80	1.14
			6	μ_t	6.00	0.315	1.87	406	1.89	378	94.8	36.3	0.141	3.88	2.08	<dl	7.14	1.12
				sd_t	1.21	0.155	2.10	153	0.432	54.6	9.64	3.49	0.107	1.26	2.33	na	3.09	0.366

Class	Type	Deposit	n	Stat	Mn	Co	Ni	Zn	Ga	Se	Ag	In	Sn	Sb	Te	Au	Pb	Bi
				Isotope	55	59	60	66	71	82	107	115	118	121	128	197	208	209
		Median of detection limits*		55um	0.470	0.023	0.241	0.353	0.028	2.53	0.023	0.012	0.073	0.022	0.256	0.010	0.012	0.007
		Lousal		*med*	1.02	0.140	<dl	226	0.350	87.0	5.73	508	302	19.9	<dl	<dl	18.7	19.2
			7	μ_t	1.77	0.462	0.958	216	0.297	97.4	5.31	549	312	21.2	<dl	0.042	17.9	16.2
				sd_t	1.99	0.628	1.32	27.0	0.156	24.9	2.24	147	43.3	9.67	na	0.080	5.96	6.36
		Maria Teres		*med*	4.22	1.90	1.23	276	3.28	27.3	95.3	18.3	45.2	7.48	0.938	0.062	8.05	1.55
			27	μ_t	4.57	2.53	1.31	289	5.02	25.3	108	19.0	47.6	6.79	0.974	0.070	7.94	1.54
				sd_t	2.82	2.16	0.543	144	4.58	9.88	65.1	9.75	29.4	4.82	0.290	0.058	5.74	1.32
		McLeod		*med*	2.02	0.176	<dl	231	0.091	53.4	36.3	26.6	20.7	0.191	0.570	<dl	1.96	0.306
			10	μ_t	2.89	0.212	<dl	232	0.182	57.2	35.0	37.0	22.0	0.204	0.525	0.016	1.84	0.310
				sd_t	4.50	0.255	na	43.0	0.259	67.6	13.3	47.7	6.32	0.143	0.205	0.028	1.09	0.195
		Ming		*med*	1.09	0.074	<dl	510	1.55	291	24.0	8.86	67.1	0.900	1.74	0.055	3.07	0.441
			31	μ_t	1.11	0.366	1.78	513	1.99	230	187	14.9	99.2	1.15	1.86	0.050	2.72	0.346
				sd_t	0.645	0.649	3.36	95.7	1.67	188	352	18.4	83.2	0.898	0.880	0.042	1.83	0.385
		Neves		*med*	2.30	0.056	1.40	201	1.62	31.5	5.12	298	638	2.48	<dl	<dl	2.72	0.033
			7	μ_t	2.39	0.051	2.73	192	1.39	48.5	5.44	421	700	3.46	<dl	<dl	2.72	0.347
				sd_t	0.487	0.036	2.93	126	0.797	51.9	1.95	233	700	2.98	na	na	1.77	0.467
		Norbec		*med*	0.510	0.251	2.18	333	0.330	256	205	60.2	146	0.057	<dl	<dl	0.867	0.673
			12	μ_t	0.800	0.383	2.03	331	0.349	259	222	61.1	140	0.082	<dl	<dl	0.925	0.881
				sd_t	0.607	0.407	1.34	24.8	0.190	309	327	90.1	110	0.107	na	na	0.498	1.32
		Normetal		*med*	<dl	2.29	<dl	295	4.12	<dl	1500	19.5	35.0	1.72	<dl	<dl	3.06	3.75
			5	μ_t	<dl	2.29	<dl	288	4.03	<dl	1491	19.6	35.2	1.96	<dl	<dl	2.86	3.90
				sd_t	na	0.188	na	61.7	0.526	na	182	1.11	1.81	1.36	na	na	2.19	1.81
		Perseverance		*med*	<dl	0.026	<dl	237	1.38	781	2.89	54.7	22.6	0.866	7.80	0.018	2.63	0.080
			15	μ_t	<dl	0.239	<dl	235	1.90	782	3.98	53.3	23.0	1.04	8.43	0.019	2.79	0.096
				sd_t	na	0.582	na	42.9	2.28	482	4.44	13.0	7.24	0.981	11.2	0.011	2.07	0.172
		Pike Hill		*med*	112	5.90	2.28	532	3.62	80.5	82.0	5.56	44.5	0.120	0.720	<dl	0.374	0.659
			12	μ_t	119	7.44	1.85	519	4.17	85.2	83.3	5.90	45.0	0.130	0.696	<dl	0.524	0.618
				sd_t	26.7	8.31	2.04	62.7	4.41	36.5	18.3	0.970	55.6	0.108	0.320	na	0.429	0.212

Class	Type	Deposit	n	Stat	Mn	Co	Ni	Zn	Ga	Se	Ag	In	Sn	Sb	Te	Au	Pb	Bi
				Isotope	55	59	60	66	71	82	107	115	118	121	128	197	208	209
		Median of detection limits*		55um	0.470	0.023	0.241	0.353	0.028	2.53	0.023	0.012	0.073	0.022	0.256	0.010	0.012	0.007
		Poirier		*med*	2.52	<dl	6.20	160	0.043	75.8	31.9	6.72	21.3	0.158	0.760	0.057	3.88	1.68
			6	μ_t	2.52	0.032	6.78	161	0.046	76.6	32.0	6.72	21.4	0.148	0.756	0.056	3.82	1.65
				sd_t	0.217	0.035	2.83	11.1	0.013	3.86	3.71	0.360	4.12	0.082	0.224	0.036	0.767	0.532
		Quémont		*med*	1.01	8.51	0.310	148	0.153	401	187	49.1	91.8	0.302	0.520	0.538	4.14	1.99
			32	μ_t	1.48	5.65	2.41	162	0.160	392	204	51.3	79.6	0.303	0.507	0.832	3.95	2.04
				sd_t	1.50	6.79	4.45	58.4	0.062	104	150	26.0	37.0	0.192	0.294	1.03	2.08	2.04
		Rävliden		*med*	3.71	1.58	<dl	502	0.535	605	79.7	72.4	72.8	0.340	0.720	0.099	7.68	0.877
			6	μ_t	3.58	1.76	<dl	492	0.523	599	79.9	73.5	73.3	0.339	0.770	0.094	7.73	1.00
				sd_t	0.502	0.678	na	68.3	0.107	23.2	2.37	13.5	8.24	0.117	0.198	0.078	2.14	0.532
		Roman Ruins		*med*	1.93	0.448	<dl	59.8	1.79	298	7.54	9.97	25.4	<dl	1.10	0.047	0.052	0.324
			8	μ_t	1.97	0.469	0.509	60.8	1.62	305	5.87	10.4	26.4	<dl	1.43	0.051	0.049	0.338
				sd_t	0.327	0.219	0.618	8.19	0.695	31.9	3.77	2.06	20.1	na	1.08	0.059	0.023	0.233
		Satanic Mills		*med*	1.24	0.058	0.500	7.91	22.9	5.30	2.86	54.3	685	13.3	1.53	0.042	0.285	13.6
			7	μ_t	1.30	0.136	2.17	7.68	21.2	4.87	2.96	49.9	734	29.7	1.52	0.116	0.287	21.7
				sd_t	0.404	0.137	2.65	0.727	3.78	2.04	0.595	21.0	176	27.8	0.885	0.144	0.272	20.8
		Snowcap		*med*	1.27	0.062	9.55	6.59	29.1	<dl	4.94	71.9	144	367	4.51	3.25	6.37	36.4
			6	μ_t	1.28	0.057	8.90	6.51	29.5	<dl	4.76	68.7	148	302	3.74	2.67	5.19	29.7
				sd_t	0.406	0.068	9.79	0.769	3.55	na	1.41	18.8	52.1	245	2.96	2.63	4.92	23.4
		Suffield Mine		*med*	<dl	0.028	<dl	145	130	32.7	16.8	5.42	140	5.13	<dl	0.017	5.07	0.107
			6	μ_t	<dl	0.027	<dl	145	129	31.9	16.7	5.44	134	6.16	<dl	0.025	4.88	0.110
				sd_t	na	0.006	na	9.31	19.4	3.92	10.1	0.919	26.2	8.01	na	0.031	2.65	0.087
		Sulitjelma		*med*	<dl	0.863	1.41	414	0.239	<dl	110	1.33	0.860	0.037	1.17	0.091	0.900	0.318
			111	μ_t	0.571	1.01	2.46	439	0.424	<dl	110	2.71	8.89	0.214	1.25	0.106	0.962	0.392
				sd_t	1.12	1.26	3.33	218	0.805	na	120	3.68	19.9	0.449	0.906	0.093	0.910	0.418
		Tétrault		*med*	2.56	14.2	2.30	166	0.083	43.7	40.6	2.10	148	<dl	0.340	0.060	3.15	0.580
			5	μ_t	2.57	14.6	3.03	159	0.082	43.3	35.5	2.01	141	<dl	0.344	0.050	3.11	0.787
				sd_t	0.308	6.28	3.69	32.9	0.020	1.90	28.4	1.48	94.6	na	0.049	0.064	0.765	0.517

Class	Type	Deposit	n	Stat	Mn	Co	Ni	Zn	Ga	Se	Ag	In	Sn	Sb	Te	Au	Pb	Bi
				Isotope	55	59	60	66	71	82	107	115	118	121	128	197	208	209
		Median of detection limits*		55um	0.470	0.023	0.241	0.353	0.028	2.53	0.023	0.012	0.073	0.022	0.256	0.010	0.012	0.007
		Tharsis		*med*	<dl	<dl	<dl	452	4.74	2.70	317	0.431	385	0.304	<dl	0.016	0.541	<dl
			4	μ_t	<dl	<dl	<dl	449	4.66	<dl	315	0.433	434	0.519	<dl	0.017	0.850	<dl
				sd_t	na	na	na	107	0.263	na	15.4	0.288	189	0.458	na	0.011	0.889	na
		Vorta		*med*	<dl	<dl	46.6	325	0.665	<dl	40.7	<dl	0.373	2.93	22.8	0.027	30.4	0.008
			2	μ_t	<dl	<dl	46.6	325	0.665	<dl	40.7	<dl	0.373	2.93	22.8	0.027	30.4	0.008
				sd_t	na	na	4.21	246	0.869	na	30.2	na	0.985	0.585	41.8	0.014	61.2	0.004
		Waite-Amulet		*med*	1.32	1.03	<dl	313	0.590	39.5	68.6	24.8	76.1	0.385	<dl	0.066	2.26	1.63
			33	μ_t	1.64	1.40	<dl	325	6.16	60.6	91.0	30.0	70.1	0.426	<dl	0.123	2.27	1.89
				sd_t	1.38	1.22	na	58.2	11.7	41.5	73.8	11.1	28.1	0.508	na	0.176	1.06	1.68
		Weedon		*med*	<dl	5.48	0.540	308	4.34	41.5	123	9.02	4.37	0.380	1.29	<dl	5.71	1.16
			7	μ_t	0.539	4.73	0.458	306	4.35	42.3	123	9.13	4.32	0.393	1.35	<dl	7.45	1.14
				sd_t	0.336	1.41	0.558	24.0	0.633	2.65	2.61	0.364	0.729	0.045	0.238	na	6.61	0.184
		Whalesback		*med*	7.95	1.08	<dl	488	8.78	567	75.9	9.58	3.53	34.2	2.28	<dl	17.9	<dl
			5	μ_t	7.55	1.05	0.677	493	8.65	549	70.2	7.78	3.28	34.2	2.27	<dl	17.4	<dl
				sd_t	2.38	0.454	1.20	51.2	0.389	265	48.0	6.28	3.26	24.0	0.173	na	2.53	na
		Wolverine		*med*	2.59	5.45	43.1	986	0.610	4305	9.77	1.59	102	2.77	<dl	0.017	0.375	1.83
			6	μ_t	2.68	5.42	43.4	1002	0.613	4310	10.1	1.61	101	2.81	<dl	0.015	0.360	1.85
				sd_t	0.448	1.70	7.00	120	0.070	236	2.27	0.182	13.3	2.06	na	0.011	0.322	0.655
		York Harbour		*med*	2.54	0.042	0.974	519	0.551	263	155	19.2	1.81	<dl	2.63	0.033	5.69	0.073
			6	μ_t	2.51	3.40	1.01	521	0.484	264	120	17.8	1.81	<dl	2.63	0.031	5.74	0.252
				sd_t	0.525	9.43	1.40	54.3	0.322	7.15	141	14.2	0.544	na	0.326	0.043	2.16	0.550
		Yubileynoe		*med*	4.60	1.40	0.340	438	12.1	<dl	14.2	62.0	4.50	3.50	25.1	0.450	52.8	4.30
			7	μ_t	16.3	3.13	1.07	549	10.7	<dl	27.8	52.0	9.38	4.14	66.2	0.668	46.2	29.0
				sd_t	20.4	4.13	1.37	432	4.26	na	25.6	25.3	7.94	2.36	81.8	0.617	38.5	40.0
		Zambujal		*med*	1.37	0.069	17.0	174	7.76	<dl	0.740	238	1063	5.01	<dl	<dl	2.94	4.62
			7	μ_t	3.42	0.232	20.4	178	7.85	<dl	0.733	235	1058	5.00	<dl	<dl	4.45	4.90
				sd_t	3.72	0.268	23.7	19.2	1.08	na	0.131	21.0	79.7	1.73	na	na	3.27	1.66

Class	Type	Deposit	n	Stat	Mn	Co	Ni	Zn	Ga	Se	Ag	In	Sn	Sb	Te	Au	Pb	Bi
				Isotope	55	59	60	66	71	82	107	115	118	121	128	197	208	209
		Median of detection limits*		55um	0.470	0.023	0.241	0.353	0.028	2.53	0.023	0.012	0.073	0.022	0.256	0.010	0.012	0.007
		Summary VMS	*755*	*med*	1.69	0.990	0.500	331	1.28	171	37.0	20.1	58.0	0.440	0.700	0.038	2.61	0.850
				μ_t	1.84	1.37	1.10	335	2.07	219	45.8	29.5	64.0	0.769	0.835	0.052	3.06	1.11
				sd_t	1.93	2.02	1.81	202	2.92	250	56.1	37.5	72.3	1.17	1.07	0.071	3.18	1.42
		Summary hydrothermal	*1616*	*med*	1.23	0.602	0.749	267	0.490	67.4	20.6	9.47	20.2	0.250	0.630	0.021	2.45	0.670
				μ_t	1.39	1.04	1.78	262	0.785	94.2	30.6	14.2	28.0	0.393	0.790	0.030	2.95	0.894
				sd_t	1.44	1.64	3.28	256	1.12	114	42.0	18.1	38.8	0.600	1.05	0.042	3.08	1.18
				min	<dl	<dl	<dl	<dl	<dl	<dl	<dl	<dl	<dl	<dl	<dl	<dl	<dl	<dl
				max	2450	3931	1542	18591	150	4580	2131	1809	2480	445	1349	267	655	284
		Summary magmatic	*946*	*med*	2.37	0.263	37.7	318	0.078	86.3	3.29	2.18	2.16	0.042	1.31	0.019	5.72	0.170
				μ_t	2.99	0.327	37.7	328	0.085	91.9	4.32	2.32	3.30	0.046	2.06	0.021	6.74	0.251
				sd_t	3.34	0.367	30.7	164	0.071	46.6	4.48	1.79	4.74	0.047	2.99	0.024	6.12	0.338
				min	<dl	<dl	<dl	<dl	<dl	20.8	0.153	<dl	<dl	<dl	<dl	<dl	0.032	<dl
				max	824	5538	33008	9543	2.70	466	2866	29.1	271	3.20	78.7	2.30	411	15.9
		Summary all deposits	*2562*	*med*	1.82	0.678	11.1	294	0.311	91.2	14.6	6.75	14.8	0.160	1.13	0.025	4.24	0.600
				μ_t	1.99	1.05	18.3	234	0.412	83.0	21.3	8.20	23.8	0.245	1.59	0.033	4.50	0.851
				sd_t	1.47	0.360	5.65	293	0.217	80.9	8.74	4.90	7.38	0.091	0.779	0.020	3.47	0.369
				min	<dl	<dl	<dl	<dl	<dl	<dl	<dl	<dl	<dl	<dl	<dl	<dl	<dl	<dl
				max	2450	5538	33008	18591	150	4580	2866	1809	2480	445	1349	267	655	284

Annexe C8. Performances of the models using different data transformations. MCC: Matthews Correlation Coefficient.

RF: Random Forest; ANN: Artificial Neural Network; KNN: K-Nearest Neighbor; NB: Naive Bayes; PLS-DA Partial least square-discriminant analysis

A. Magmatic-hydrothermal Models (mag-hyd)

	Transformation															
	Raw				Standarized				Yeo-Jonhson (Fig. 6)				Centered-log ratio			
Training data	Model	MCC	Kappa	F1	Model	MCC	Kappa	F1	Model	MCC	Kappa	F1	Model	MCC	Kappa	F1
	RF	0.965	0.970	0.990	RF	0.974	0.969	0.991	*RF*	*0.976*	*0.976*	*0.991*	RF	0.954	0.954	0.983
	ANN	0.869	0.869	0.951	ANN	0.938	0.938	0.977	ANN	0.966	0.966	0.987	ANN	0.951	0.951	0.982
	KNN	0.853	0.849	0.941	KNN	0.902	0.901	0.962	KNN	0.946	0.946	0.979	KNN	0.944	0.943	0.978
	NB	0.716	0.698	0.869	NB	0.718	0.702	0.872	NB	0.902	0.902	0.963	NB	0.908	0.908	0.966
	PLS-DA	0.226	0.124	0.788	PLS-DA	0.231	0.131	0.789	PLS-DA	0.872	0.870	0.949	PLS-DA	0.871	0.869	0.949
Test data	Model	MCC	Kappa	F1	Model	MCC	Kappa	F1	Model	MCC	Kappa	F1	Model	MCC	Kappa	F1
	RF	0.961	0.971	0.990	RF	0.973	0.978	0.989	*RF*	*0.978*	*0.978*	*0.992*	RF	0.964	0.964	0.987
	ANN	0.849	0.848	0.942	ANN	0.942	0.942	0.978	ANN	0.964	0.964	0.987	KNN	0.954	0.953	0.982
	NB	0.717	0.700	0.872	NB	0.740	0.723	0.882	NB	0.907	0.906	0.964	ANN	0.925	0.925	0.972
	KNN	0.194	0.088	0.784	PLS-DA	0.157	0.048	0.780	KNN	0.124	0.000	0.774	NB	0.914	0.914	0.968
	PLS-DA	0.047	0.004	0.774	KNN	0.088	0.086	0.698	PLS-DA	0.091	0.000	0.774	PLS-DA	0.846	0.842	0.938

B. Magmatic deposits models (mag)

Training data	Model	MCC	Kappa	F1	Model	MCC	Kappa	F1	Model	MCC	Kappa	F1	Model	MCC	Kappa	F1
	RF	0.891	0.890	0.966	KNN	0.891	0.890	0.964	*RF*	*0.891*	*0.890*	*0.966*	ANN	0.869	0.869	0.957
	ANN	0.861	0.861	0.955	RF	0.891	0.889	0.966	ANN	0.872	0.871	0.959	KNN	0.827	0.826	0.942
	NB	0.724	0.717	0.898	ANN	0.858	0.858	0.954	KNN	0.845	0.844	0.950	NB	0.716	0.715	0.909
	KNN	0.722	0.721	0.912	NB	0.726	0.718	0.899	NB	0.777	0.776	0.930	PLS-DA	0.704	0.699	0.911
	PLS-DA	0.551	0.520	0.875	PLS-DA	0.664	0.639	0.903	PLS-DA	0.751	0.748	0.924	RF	0.851	0.851	0.953
Test data	Model	MCC	Kappa	F1	Model	MCC	Kappa	F1	Model	MCC	Kappa	F1	Model	MCC	Kappa	F1
	RF	0.920	0.920	0.974	ANN	0.911	0.910	0.972	*RF*	*0.935*	*0.935*	*0.979*	ANN	0.906	0.905	0.968
	ANN	0.868	0.866	0.955	RF	0.896	0.896	0.966	ANN	0.921	0.920	0.974	RF	0.897	0.896	0.966
	NB	0.759	0.744	0.906	NB	0.765	0.751	0.909	NB	0.822	0.822	0.943	KNN	0.844	0.842	0.947
	PLS-DA	0.290	0.280	0.651	KNN	0.080	0.079	0.610	PLS-DA	0.124	0.030	0.089	NB	0.766	0.766	0.925
	KNN	0.131	0.068	0.784	PLS-DA	0.035	0.034	0.697	KNN	0.083	0.000	0.809	PLS-DA	0.727	0.719	0.918

C. Hydrothermal deposits models (hyd)

Training data	Model	MCC	Kappa	F1	Model	MCC	Kappa	F1	Model	MCC	Kappa	F1	Model	MCC	Kappa	F1
	RF	0.887	0.885	0.998	RF	0.891	0.889	0.906	*RF*	*0.894*	*0.892*	*0.908*	ANN	0.606	0.603	0.651
	NB	0.434	0.430	0.897	KNN	0.698	0.697	0.714	KNN	0.847	0.846	0.863	KNN	0.787	0.785	0.813
	ANN	0.353	0.347	0.931	ANN	0.637	0.637	0.660	ANN	0.715	0.714	0.736	NB	0.641	0.640	0.692
	KNN	0.072	0.062	0.496	NB	0.482	0.479	0.538	NB	0.645	0.644	0.672	PLS-DA	0.329	0.299	0.371
	PLS-DA	0.024	0.008	1.000	PLS-DA	0.119	0.044	0.000	PLS-DA	0.424	0.405	0.454	RF	0.819	0.815	0.846
Test data	Model	MCC	Kappa	F1	Model	MCC	Kappa	F1	Model	MCC	Kappa	F1	Model	MCC	Kappa	F1
	RF	0.892	0.891	0.907	RF	0.890	0.888	0.998	*RF*	*0.902*	*0.900*	*0.998*	KNN	0.835	0.833	0.998
	KNN	0.678	0.677	0.703	ANN	0.661	0.660	0.987	ANN	0.674	0.671	0.984	RF	0.829	0.824	0.998
	NB	0.472	0.468	0.532	NB	0.447	0.444	0.904	NB	0.619	0.617	0.944	NB	0.620	0.619	0.987
	ANN	0.361	0.351	0.443	KNN	0.056	0.054	0.933	KNN	0.057	0.023	0.107	ANN	0.561	0.555	0.989
	PLS-DA	0.114	0.043	0.000	PLS-DA	0.035	0.012	0.991	PLS-DA	0.002	0.001	1.000	PLS-DA	0.318	0.289	0.982

Annexe C9. Confusion matrices by model on test data in discriminnation between magmatic and hydrothermal depos
Positive class (P): hydrothermal; negative class (N): magmatic; TP: true positive; TN= true negative; FP= false posi
RF: Random Forest; ANN: Artificial Neural Network; KNN: K-Nearest Neighbor; NB: Naive Bayes;
PLS-DA Partial least square-discriminant analysis.

A

RF		Actual: Hydrothermal	Actual: Magmatic	Total
Predicted	Hydrothermal	481	4	481
	Magmatic	4	280	288
	Total	485	284	769
Overall accuracy		99.0%		

B

ANN		Actual: Hydrothermal	Actual: Magmatic	Total
Predicted	Hydrothermal	477	5	478
	Magmatic	8	279	291
	Total	485	284	769
Overall accuracy		98.3%		

C

KNN		Actual: Hydrothermal	Actual: Magmatic	Total
Predicted	Hydrothermal	485	284	595
	Magmatic	0	0	174
	Total	485	284	769
Overall accuracy		63.1%		

D

NB		Actual: Hydrothermal	Actual: Magmatic	Total
Predicted	Hydrothermal	460	9	406
	Magmatic	25	275	363
	Total	485	284	769
Overall accuracy		95.6%		

E

PLSDA		Actual: Hydrothermal	Actual: Magmatic	Total
Predicted	Hydrothermal	485	284	182
	Magmatic	0	0	587
	Total	485	284	769
Overall accuracy		63.1%		

F

Model		Actual: Hydrothermal	Actual: Magmatic
Predicted	Hydrothermal	TP	FP
	Magmatic	FN	TN

Annexe C10. Confusion matrices by model on test data in discriminnation between magmatic deposit types (mag mode
Positive class (P): Ni-Cu sulfide; negative class (N): Reef-type PGE; TP: true positive; TN= true negative; FP= false positiv
RF: Random Forest; ANN: Artificial Neural Network; KNN: K-Nearest Neighbor; NB: Naive Bayes;
PLS-DA Partial least square-discriminant analysis

A

RF		Actual: Ni-Cu sulfide	Actual: Reef-type PGE	Total
Predicted	Ni-Cu sulfide	189	4	193
	Reef-type PGE	4	87	91
	Total	193	91	284
	Overall accuracy	97.2%		

B

ANN		Actual: Ni-Cu sulfide	Actual: Reef-type PGE	Total
Predicted	Ni-Cu sulfide	186	3	189
	Reef-type PGE	7	88	95
	Total	193	91	284
	Overall accuracy	96.5%		

C

KNN		Actual: Ni-Cu sulfide	Actual: Reef-type PGE	Total
Predicted	Ni-Cu sulfide	193	91	284
	Reef-type PGE	0	0	0
	Total	193	91	284
	Overall accuracy	68.0%		

D

NB		Actual: Ni-Cu sulfide	Actual: Reef-type PGE	Total
Predicted	Ni-Cu sulfide	182	11	193
	Reef-type PGE	11	80	91
	Total	193	91	284
	Overall accuracy	92.3%		

E

PLSDA		Actual: Ni-Cu sulfide	Actual: Reef-type PGE	Total
Predicted	Ni-Cu sulfide	9	0	9
	Reef-type PGE	184	91	275
	Total	193	91	284
	Overall accuracy	35.2%		

F

Model		Actual: Ni-Cu sulfide	Actual: Reef-type PGE
Predicted	Ni-Cu sulfide	TP	FP
	Reef-type PGE	FN	TN

Annexe C11. Confusion matrices by model on test data in discriminnation between hydrothermal deposit types (hyd models).

RF: Random Forest; ANN: Artificial Neural Network; KNN: K-Nearest Neighbor; NB: Naive Bayes; PLS-DA Partial least square-discriminant analysis

A

RF	Actual: Epithermal gold	IOCG	Orogenic gold	Porphyry	Skarn	VMS	Total
Predicted: Epithermal gold	34	0	1	0	0	0	35
IOCG	0	76	0	1	1	1	79
Orogenic gold	0	0	36	0	0	0	36
Porphyry	2	1	0	48	2	0	53
Skarn	0	0	0	0	31	0	31
VMS	1	7	5	7	5	226	251
Total	37	84	42	56	39	227	485
Accuracy by class	92%	90%	86%	86%	79%	100%	
Overall accuracy	93%						

B

KNN	Actual: Epithermal gold	IOCG	Orogenic gold	Porphyry	Skarn	VMS	Total
Predicted: Epithermal gold	36	79	41	53	39	187	435
IOCG	1	0	0	0	0	11	12
Orogenic gold	0	0	0	0	0	0	0
Porphyry	0	2	0	1	0	6	9
Skarn	0	0	0	0	0	0	0
VMS	0	3	1	2	0	23	29
Total	37	84	42	56	39	227	485
Accuracy by class	97%	0%	0%	2%	0%	10%	
Overall accuracy	12%						

C

ANN	Actual: Epithermal gold	IOCG	Orogenic gold	Porphyry	Skarn	VMS	Total
Predicted: Epithermal gold	25	2	2	1	0	2	32
IOCG	1	53	8	5	3	6	76
Orogenic gold	4	0	22	0	2	1	29
Porphyry	4	1	0	37	2	5	49
Skarn	1	5	5	1	27	3	42
VMS	2	23	5	12	5	210	257
Total	37	84	42	56	39	227	485
Accuracy by class	67.6%	63.1%	52.4%	66.1%	69.2%	92.5%	
Overall accuracy	77.1%						

D

NB	Actual: Epithermal gold	IOCG	Orogenic gold	Porphyry	Skarn	VMS	Total
Predicted: Epithermal gold	29	2	10	2	2	9	54
IOCG	0	54	4	6	1	5	70
Orogenic gold	4	1	19	1	5	1	31
Porphyry	3	2	0	33	1	10	49
Skarn	0	6	4	1	29	15	55
VMS	1	19	5	13	1	187	226
Total	37	84	42	56	39	227	485
Accuracy by class	78.4%	64.3%	45.2%	58.9%	74.4%	82.4%	
Overall accuracy	72.4%						

E

PLSDA (Predicted)	Actual: Epithermal gold	IOCG	Orogenic gold	Porphyry	Skarn	VMS	Total
Epithermal gold	0	0	0	0	0	0	0
IOCG	13	32	11	45	6	37	144
Orogenic gold	0	0	0	0	0	0	0
Porphyry	1	0	0	1	0	0	2
Skarn	16	32	14	5	28	169	264
VMS	7	20	17	5	5	21	75
Total	37	84	42	56	39	227	485
Accuracy by class	0.0%	38.1%	0.0%	1.8%	71.8%	9.3%	
Overall accuracy	16.9%						

F

Model (Predicted)	Actual: Epithermal gold	IOCG	Orogenic gold	Porphyry	Skarn	VMS
Epithermal gold	TN	FN	TN	TN	TN	TN
IOCG	FP	TP	FP	FP	FP	FP
Orogenic gold	TN	FN	TN	TN	TN	TN
Porphyry	TN	FN	TN	TN	TN	TN
Skarn	TN	FN	TN	TN	TN	TN
VMS	TN	FN	TN	TN	TN	TN

Annexe C12. Predictions and probabilities by sample of blind data (Dataset D) of chalcopyrite data using RF models

			RF mag-hyd model				RF hyd model							
			Actual	Predicted	Prob		Actual	Predicted	Prob					
ID	Author	Deposit			Hyd	Mag			Epithermal gold	IOCG	Orogenic gold	Porphyry	Skarn	VMS
TRBDD09 32m1	Agangi et al. (2018)	Red Bore	Hyd	Mag	0.50	0.50	VMS	VMS	0.01	0.08	0.03	0.06	0.18	0.64
TRBDD09 32m2			Hyd	Hyd	0.58	0.42	VMS	VMS	0.02	0.07	0.04	0.05	0.12	0.69
TRBDD09 32m3			Hyd	Hyd	1.00	0.00	VMS	VMS	0.01	0.09	0.03	0.02	0.09	0.76
TRBDD09 32m4			Hyd	Hyd	0.76	0.24	VMS	VMS	0.02	0.08	0.01	0.05	0.15	0.69
TRBDD09 32m5			Hyd	Hyd	0.99	0.01	VMS	VMS	0.00	0.03	0.04	0.02	0.11	0.79
TRBDD09 32m6			Hyd	Hyd	0.99	0.01	VMS	VMS	0.00	0.07	0.01	0.03	0.09	0.80
TRBDD09 32m7			Hyd	Hyd	1.00	0.00	VMS	VMS	0.00	0.07	0.01	0.02	0.11	0.79
TRBDD09 32m8			Hyd	Mag	0.41	0.59	VMS	VMS	0.01	0.10	0.05	0.07	0.21	0.56
TRBDD09_35_5m9			Hyd	Hyd	0.67	0.33	VMS	VMS	0.04	0.23	0.04	0.20	0.08	0.42
TRBDD09 32m10			Hyd	Hyd	0.71	0.29	VMS	VMS	0.01	0.05	0.06	0.04	0.09	0.75
TRBDD09 32m11			Hyd	Hyd	0.80	0.20	VMS	VMS	0.01	0.06	0.03	0.04	0.07	0.79
TRBDD09 32m12			Hyd	Hyd	1.00	0.00	VMS	VMS	0.00	0.02	0.01	0.01	0.06	0.90
TRBDD09 32m13			Hyd	Hyd	0.99	0.01	VMS	VMS	0.00	0.04	0.03	0.01	0.12	0.79
TRBDD09 32m14			Hyd	Hyd	1.00	0.00	VMS	VMS	0.00	0.08	0.01	0.02	0.10	0.78
TRBDD09_35_5m15			Hyd	Mag	0.23	0.77	VMS	VMS	0.05	0.13	0.06	0.17	0.29	0.29
TRBDD09 32m16			Hyd	Hyd	0.73	0.27	VMS	VMS	0.01	0.06	0.02	0.06	0.08	0.77
TRBDD09 32m17			Hyd	Hyd	0.75	0.25	VMS	VMS	0.01	0.07	0.03	0.07	0.11	0.71
TRBDD09 32m18			Hyd	Mag	0.48	0.52	VMS	VMS	0.02	0.07	0.03	0.05	0.16	0.67
TRBDD09 32m19			Hyd	Hyd	0.73	0.27	VMS	VMS	0.01	0.10	0.01	0.08	0.06	0.74
TRCDD04_31_5m20			Hyd	Hyd	0.97	0.03	VMS	VMS	0.01	0.12	0.06	0.22	0.11	0.47
TRBDD09_35_5m21			Hyd	Hyd	0.68	0.32	VMS	VMS	0.03	0.24	0.02	0.19	0.12	0.39
TRBDD09 32m22			Hyd	Hyd	0.73	0.27	VMS	VMS	0.01	0.10	0.02	0.05	0.17	0.66
TRBDD09 32m23			Hyd	Hyd	0.76	0.24	VMS	VMS	0.01	0.10	0.01	0.07	0.03	0.79
TRBDD09_35_5m24			Hyd	Mag	0.13	0.87	VMS	VMS	0.01	0.06	0.08	0.04	0.13	0.68
TRBDD09_35_5m25			Hyd	Mag	0.22	0.78	VMS	VMS	0.03	0.21	0.02	0.05	0.29	0.39

			RF mag-hyd model				RF hyd model							
			Actual	Predicted	Prob		Actual	Predicted	Prob					
ID	Author	Deposit			Hyd	Mag			Epithermal gold	IOCG	Orogenic gold	Porphyry	Skarn	VMS
TRBDD09_35_5m26	Agangi et al. (2018)	Red Bore	Hyd	Mag	0.30	0.70	VMS	Skarn	0.05	0.16	0.07	0.12	0.33	0.28
TRBDD09 32m27			Hyd	Hyd	0.52	0.48	VMS	VMS	0.01	0.10	0.05	0.05	0.22	0.58
TRBDD09 32m28			Hyd	Hyd	0.99	0.01	VMS	VMS	0.01	0.10	0.03	0.03	0.08	0.75
TRBDD09 32m29			Hyd	Hyd	0.75	0.25	VMS	VMS	0.00	0.07	0.04	0.02	0.04	0.82
TRBDD09_35_5m30			Hyd	Hyd	0.65	0.35	VMS	VMS	0.03	0.24	0.02	0.25	0.06	0.40
TRBDD09 32m31			Hyd	Hyd	0.72	0.28	VMS	VMS	0.01	0.13	0.01	0.07	0.04	0.74
TRBDD09 32m32			Hyd	Hyd	0.72	0.28	VMS	VMS	0.01	0.07	0.04	0.10	0.07	0.71
TRCDD04_31_5m33			Hyd	Hyd	0.95	0.05	VMS	VMS	0.02	0.07	0.04	0.04	0.12	0.70
TRBDD09_35_5m34			Hyd	Hyd	0.67	0.33	VMS	VMS	0.02	0.22	0.04	0.24	0.04	0.43
TRCDD04_31_5m35			Hyd	Hyd	0.96	0.04	VMS	VMS	0.05	0.10	0.05	0.08	0.11	0.60
TRBDD09_35_5m36			Hyd	Mag	0.19	0.81	VMS	VMS	0.03	0.21	0.03	0.09	0.24	0.41
TRBDD09 32m37			Hyd	Hyd	0.88	0.12	VMS	VMS	0.00	0.04	0.06	0.02	0.10	0.78
TRCDD04_31_5m38			Hyd	Hyd	0.68	0.32	VMS	VMS	0.01	0.11	0.04	0.14	0.02	0.68
TRCDD04_31_5m39			Hyd	Hyd	0.78	0.22	VMS	VMS	0.03	0.08	0.15	0.11	0.03	0.61
TRCDD04_31_5m40			Hyd	Hyd	0.98	0.02	VMS	VMS	0.01	0.08	0.04	0.25	0.02	0.60
TRBDD09 32m41			Hyd	Hyd	0.99	0.01	VMS	VMS	0.00	0.13	0.02	0.01	0.04	0.81
TRCDD04_31_5m42			Hyd	Hyd	0.99	0.01	VMS	VMS	0.05	0.09	0.04	0.18	0.05	0.60
TRBDD09_35_5m43			Hyd	Hyd	0.63	0.37	VMS	VMS	0.03	0.22	0.07	0.13	0.09	0.46
TRBDD09 32m44			Hyd	Hyd	0.66	0.34	VMS	VMS	0.00	0.06	0.04	0.03	0.12	0.74
TRBDD09_35_5m45			Hyd	Mag	0.19	0.81	VMS	VMS	0.04	0.16	0.07	0.13	0.15	0.45
TRBDD04 37m46			Hyd	Hyd	0.97	0.03	VMS	VMS	0.02	0.09	0.03	0.16	0.01	0.69
TRBDD09 32m47			Hyd	Hyd	0.59	0.41	VMS	VMS	0.01	0.05	0.06	0.03	0.08	0.78
TRBDD09 32m48			Hyd	Hyd	0.70	0.30	VMS	VMS	0.01	0.07	0.06	0.05	0.02	0.80
TRBDD09 32m49			Hyd	Hyd	0.70	0.30	VMS	VMS	0.01	0.07	0.06	0.05	0.02	0.80
TRBDD09_35_5m50			Hyd	Mag	0.10	0.90	VMS	VMS	0.04	0.12	0.25	0.13	0.12	0.34
TRCDD04_31_5m51			Hyd	Hyd	0.96	0.04	VMS	VMS	0.09	0.08	0.18	0.07	0.04	0.54

			RF mag-hyd model				RF hyd model							
			Actual	Predicted	Prob		Actual	Predicted	Prob					
ID	Author	Deposit			Hyd	Mag			Epithermal gold	IOCG	Orogenic gold	Porphyry	Skarn	VMS
TRBDD09 32m52	Agangi et al. (2018)	Red Bore	Hyd	Hyd	0.83	0.17	VMS	VMS	0.00	0.05	0.05	0.02	0.08	0.79
TRBDD09_35_5m53			Hyd	Mag	0.17	0.83	VMS	VMS	0.05	0.12	0.20	0.11	0.15	0.37
TRCDD04_31_5m54			Hyd	Hyd	1.00	0.00	VMS	VMS	0.01	0.08	0.02	0.02	0.12	0.76
TRBDD09 32m55			Hyd	Hyd	0.58	0.42	VMS	VMS	0.01	0.12	0.01	0.04	0.03	0.79
TRCDD04_31_5m56			Hyd	Hyd	0.97	0.03	VMS	VMS	0.03	0.10	0.04	0.07	0.04	0.72
TRBDD09_35_5m57			Hyd	Mag	0.08	0.92	VMS	VMS	0.04	0.12	0.27	0.12	0.14	0.31
TRBDD09_35_5m58			Hyd	Mag	0.31	0.69	VMS	Skarn	0.03	0.16	0.07	0.14	0.36	0.24
TRBDD09_35_5m59			Hyd	Hyd	0.61	0.39	VMS	Porphyry	0.02	0.26	0.04	0.31	0.07	0.30
TRBDD09_35_5m60			Hyd	Mag	0.25	0.75	VMS	VMS	0.04	0.20	0.07	0.19	0.09	0.40
TRBDD09_35_5m61			Hyd	Mag	0.22	0.78	VMS	Skarn	0.05	0.14	0.09	0.14	0.30	0.28
TRBDD09 32m62			Hyd	Hyd	0.65	0.35	VMS	VMS	0.00	0.05	0.06	0.03	0.08	0.77
TRBDD09_35_5m63			Hyd	Mag	0.11	0.89	VMS	VMS	0.06	0.11	0.31	0.07	0.11	0.35
TRBDD09_35_5m64			Hyd	Mag	0.15	0.85	VMS	VMS	0.05	0.10	0.23	0.12	0.12	0.38
TRBDD09_35_5m65			Hyd	Mag	0.41	0.59	VMS	VMS	0.03	0.24	0.07	0.16	0.16	0.35
TRBDD09_35_5m66			Hyd	Mag	0.08	0.92	VMS	VMS	0.04	0.11	0.29	0.11	0.12	0.33
TRBDD04 37m67			Hyd	Hyd	0.99	0.01	VMS	VMS	0.02	0.12	0.04	0.16	0.01	0.64
TRBDD09_35_5m68			Hyd	Mag	0.09	0.91	VMS	Skarn	0.04	0.13	0.12	0.15	0.32	0.24
TRCDD04_31_5m69			Hyd	Hyd	0.72	0.28	VMS	VMS	0.01	0.05	0.03	0.05	0.12	0.74
TRBDD09_35_5m70			Hyd	Mag	0.10	0.90	VMS	VMS	0.05	0.12	0.24	0.12	0.06	0.40
TRCDD04_31_5m71			Hyd	Hyd	0.78	0.22	VMS	VMS	0.01	0.09	0.04	0.10	0.02	0.74
TRBDD09_35_5m72			Hyd	Mag	0.10	0.90	VMS	VMS	0.02	0.12	0.27	0.13	0.18	0.28
TRBDD09 32m73			Hyd	Hyd	0.55	0.45	VMS	VMS	0.00	0.10	0.07	0.06	0.20	0.57
TRBDD09 32m74			Hyd	Hyd	0.89	0.11	VMS	VMS	0.00	0.05	0.04	0.02	0.09	0.80
TRBDD09_35_5m75			Hyd	Hyd	0.54	0.46	VMS	VMS	0.02	0.27	0.07	0.28	0.03	0.33
TRBDD09_35_5m76			Hyd	Mag	0.01	0.99	VMS	VMS	0.01	0.13	0.06	0.05	0.14	0.61
TRBDD09 32m77			Hyd	Hyd	0.81	0.19	VMS	VMS	0.00	0.05	0.03	0.03	0.14	0.74

			RF mag-hyd model				RF hyd model							
			Actual	Predicted	Prob		Actual	Predicted	Prob					
ID	Author	Deposit			Hyd	Mag			Epithermal gold	IOCG	Orogenic gold	Porphyry	Skarn	VMS
TRBDD09 32m78	Agangi et al. (2018)	Red Bore	Hyd	Hyd	1.00	0.00	VMS	VMS	0.00	0.06	0.01	0.00	0.03	0.90
TRBDD09_35_5m79			Hyd	Hyd	0.99	0.01	VMS	Skarn	0.02	0.11	0.04	0.04	0.48	0.30
TRBDD09 32m80			Hyd	Mag	0.48	0.52	VMS	VMS	0.00	0.07	0.04	0.04	0.12	0.74
TRBDD09_35_5m81			Hyd	Mag	0.46	0.54	VMS	VMS	0.05	0.13	0.05	0.12	0.31	0.34
TRBDD09_35_5m82			Hyd	Hyd	0.51	0.49	VMS	VMS	0.02	0.28	0.08	0.25	0.05	0.31
TRBDD09_35_5m83			Hyd	Mag	0.12	0.88	VMS	VMS	0.04	0.12	0.20	0.13	0.14	0.37
TRBDD09_35_5m84			Hyd	Mag	0.01	0.99	VMS	VMS	0.01	0.19	0.06	0.09	0.08	0.57
TRBDD08 51m85			Hyd	Hyd	1.00	0.00	VMS	VMS	0.02	0.03	0.01	0.04	0.06	0.83
TRBDD09 32m86			Hyd	Hyd	0.99	0.01	VMS	VMS	0.00	0.04	0.02	0.01	0.02	0.90
TRBDD09 32m87			Hyd	Hyd	1.00	0.00	VMS	VMS	0.01	0.07	0.01	0.01	0.05	0.85
TRBDD08 51m88			Hyd	Hyd	0.99	0.01	VMS	VMS	0.08	0.08	0.02	0.13	0.05	0.64
TRBDD09_35_5m89			Hyd	Hyd	0.63	0.37	VMS	VMS	0.02	0.21	0.04	0.17	0.09	0.47
TRBDD04 37m90			Hyd	Hyd	0.92	0.08	VMS	VMS	0.02	0.05	0.02	0.04	0.05	0.82
TRBDD09_35_5m91			Hyd	Mag	0.47	0.53	VMS	VMS	0.03	0.21	0.09	0.29	0.06	0.32
TRCDD04_31_5m92			Hyd	Hyd	0.77	0.23	VMS	VMS	0.02	0.14	0.06	0.11	0.02	0.65
TRBDD09 32m93			Hyd	Hyd	0.95	0.05	VMS	VMS	0.00	0.04	0.04	0.01	0.08	0.83
TRBDD09 32m94			Hyd	Hyd	0.71	0.29	VMS	VMS	0.00	0.05	0.03	0.02	0.09	0.81
TRBDD09 32m95			Hyd	Hyd	0.68	0.32	VMS	VMS	0.01	0.08	0.03	0.04	0.02	0.83
TRBDD09 32m96			Hyd	Hyd	0.62	0.38	VMS	VMS	0.00	0.06	0.02	0.03	0.04	0.85
TRBDD09 32m97			Hyd	Hyd	0.99	0.01	VMS	VMS	0.01	0.13	0.01	0.05	0.04	0.76
TRBDD09 32m98			Hyd	Hyd	0.79	0.21	VMS	VMS	0.00	0.06	0.05	0.02	0.10	0.76
TRBDD04 37m99			Hyd	Hyd	0.99	0.01	VMS	VMS	0.01	0.04	0.02	0.03	0.02	0.88
TRBDD09_35_5m100			Hyd	Hyd	0.99	0.01	VMS	VMS	0.05	0.04	0.10	0.02	0.07	0.72
TRCDD04_31_5m101			Hyd	Hyd	1.00	0.00	VMS	VMS	0.03	0.06	0.01	0.05	0.07	0.78
TRBDD09 32m102			Hyd	Hyd	0.94	0.06	VMS	VMS	0.00	0.04	0.02	0.01	0.11	0.81
TRBDD04 37m103			Hyd	Mag	0.35	0.65	VMS	VMS	0.09	0.07	0.02	0.10	0.04	0.67

			RF mag-hyd model				RF hyd model							
			Actual	Predicted	Prob		Actual	Predicted	Prob					
ID	Author	Deposit			Hyd	Mag			Epithermal gold	IOCG	Orogenic gold	Porphyry	Skarn	VMS
TRCDD04_31_5m104	Agangi et al. (2018)	Red Bore	Hyd	Hyd	0.56	0.44	VMS	VMS	0.04	0.14	0.05	0.04	0.08	0.64
TRBDD08 51m105			Hyd	Hyd	0.99	0.01	VMS	VMS	0.03	0.05	0.05	0.06	0.03	0.78
TRBDD04 37m106			Hyd	Hyd	0.62	0.38	VMS	VMS	0.13	0.08	0.02	0.14	0.05	0.58
TRBDD04 37m107			Hyd	Hyd	0.93	0.07	VMS	VMS	0.05	0.04	0.01	0.05	0.04	0.81
TRBDD04 37m108			Hyd	Hyd	0.97	0.03	VMS	VMS	0.04	0.11	0.04	0.16	0.02	0.63
TRBDD04 37m109			Hyd	Hyd	0.98	0.02	VMS	VMS	0.07	0.11	0.02	0.24	0.03	0.54
TRBDD04 37m110			Hyd	Hyd	0.98	0.02	VMS	VMS	0.04	0.11	0.02	0.14	0.01	0.67
TRBDD08 51m111			Hyd	Hyd	0.99	0.01	VMS	VMS	0.03	0.06	0.01	0.06	0.03	0.81
TRBDD04 37m112			Hyd	Hyd	0.99	0.01	VMS	VMS	0.01	0.22	0.01	0.09	0.02	0.65
TRBDD08 51m113			Hyd	Hyd	0.98	0.02	VMS	VMS	0.01	0.07	0.02	0.02	0.05	0.83
TRBDD08 51m114			Hyd	Hyd	0.65	0.35	VMS	VMS	0.05	0.11	0.01	0.10	0.02	0.71
TRBDD08 51m115			Hyd	Hyd	0.99	0.01	VMS	VMS	0.01	0.06	0.01	0.03	0.07	0.81
TRBDD08 51m116			Hyd	Hyd	0.99	0.01	VMS	VMS	0.02	0.07	0.04	0.07	0.03	0.77
TRBDD08 51m117			Hyd	Hyd	0.93	0.07	VMS	VMS	0.08	0.15	0.03	0.16	0.10	0.49
TRBDD08 51m118			Hyd	Hyd	0.74	0.26	VMS	VMS	0.03	0.29	0.03	0.08	0.06	0.51
TRBDD08 51m119			Hyd	Hyd	0.93	0.07	VMS	VMS	0.06	0.19	0.03	0.15	0.06	0.52
TRBDD08 51m120			Hyd	Hyd	0.99	0.01	VMS	VMS	0.07	0.14	0.02	0.16	0.03	0.57
TRBDD08 51m121			Hyd	Hyd	0.99	0.01	VMS	VMS	0.04	0.11	0.02	0.09	0.06	0.67
TRBDD08 51m122			Hyd	Hyd	0.98	0.02	VMS	VMS	0.09	0.15	0.02	0.17	0.05	0.52
TRBDD08 51m123			Hyd	Hyd	0.89	0.11	VMS	IOCG	0.07	0.41	0.04	0.14	0.03	0.30
TRBDD08 51m124			Hyd	Hyd	0.99	0.01	VMS	VMS	0.05	0.10	0.01	0.21	0.02	0.61
TRBDD08 51m125			Hyd	Hyd	0.99	0.01	VMS	Porphyry	0.06	0.23	0.02	0.36	0.02	0.31
TRBDD08 51m126			Hyd	Hyd	0.99	0.01	VMS	Porphyry	0.06	0.15	0.02	0.48	0.01	0.28
TRBDD08 51m127			Hyd	Hyd	0.96	0.04	VMS	IOCG	0.10	0.32	0.07	0.24	0.03	0.25
TRBDD08 51m128			Hyd	Hyd	0.94	0.06	VMS	Porphyry	0.13	0.23	0.09	0.35	0.04	0.17
TRBDD08 51m129			Hyd	Hyd	0.89	0.11	VMS	Porphyry	0.11	0.24	0.08	0.36	0.02	0.20

			RF mag-hyd model				RF hyd model							
			Actual	Predicted	Prob		Actual	Predicted	Prob					
ID	Author	Deposit			Hyd	Mag			Epithermal gold	IOCG	Orogenic gold	Porphyry	Skarn	VMS
TRBDD08 51m130	Agangi et al. (2018)	Red Bore	Hyd	Hyd	0.88	0.12	VMS	Porphyry	0.11	0.24	0.07	0.34	0.04	0.20
TRBDD08 51m131			Hyd	Hyd	0.90	0.10	VMS	Porphyry	0.11	0.20	0.14	0.37	0.02	0.15
TRBDD08 51m132			Hyd	Hyd	0.84	0.16	VMS	Porphyry	0.12	0.24	0.11	0.34	0.02	0.18
TRBDD08 51m133			Hyd	Hyd	0.84	0.16	VMS	IOCG	0.09	0.36	0.07	0.26	0.02	0.20
TRBDD08 51m134			Hyd	Hyd	0.76	0.24	VMS	Porphyry	0.04	0.21	0.02	0.45	0.02	0.26
BZ-11-Ccp1-01	Chen et al. (2022)	Buziwannan	Hyd	Hyd	0.97	0.03	Skarn	Orogenic gold	0.01	0.09	0.46	0.02	0.05	0.37
BZ-11-Ccp1-02			Hyd	Hyd	0.98	0.02	Skarn	VMS	0.02	0.05	0.42	0.02	0.02	0.48
BZ-11-Ccp1-03			Hyd	Hyd	1.00	0.00	Skarn	VMS	0.00	0.03	0.06	0.00	0.02	0.89
BZ-11-Ccp1-04			Hyd	Hyd	1.00	0.00	Skarn	VMS	0.00	0.01	0.02	0.01	0.01	0.96
BZ-11-Ccp1-05			Hyd	Hyd	1.00	0.00	Skarn	VMS	0.02	0.06	0.24	0.01	0.03	0.65
BZ-11-Ccp1-06			Hyd	Hyd	1.00	0.00	Skarn	VMS	0.01	0.02	0.16	0.00	0.03	0.77
BZ-11-Ccp1-07			Hyd	Hyd	1.00	0.00	Skarn	VMS	0.00	0.03	0.06	0.01	0.01	0.89
BZ-11-Ccp1-08			Hyd	Hyd	0.98	0.02	Skarn	VMS	0.00	0.03	0.03	0.01	0.01	0.92
BZ-11-Ccp1-09			Hyd	Hyd	1.00	0.00	Skarn	VMS	0.01	0.01	0.09	0.00	0.03	0.86
BZ-11-Ccp1-10			Hyd	Hyd	1.00	0.00	Skarn	VMS	0.01	0.02	0.22	0.00	0.10	0.65
BZ-16-Ccp2-01			Hyd	Hyd	0.99	0.01	Skarn	VMS	0.00	0.01	0.01	0.01	0.00	0.96
BZ-16-Ccp2-02			Hyd	Hyd	1.00	0.00	Skarn	VMS	0.00	0.03	0.03	0.02	0.02	0.91
BZ-16-Ccp2-03			Hyd	Hyd	0.99	0.01	Skarn	VMS	0.01	0.08	0.03	0.07	0.04	0.77
BZ-16-Ccp2-04			Hyd	Hyd	1.00	0.00	Skarn	VMS	0.00	0.00	0.00	0.00	0.02	0.98
BZ-16-Ccp2-05			Hyd	Hyd	1.00	0.00	Skarn	VMS	0.00	0.00	0.01	0.00	0.03	0.96
BZ-16-Ccp2-06			Hyd	Hyd	1.00	0.00	Skarn	VMS	0.03	0.33	0.03	0.14	0.13	0.35
BZ-16-Ccp2-07			Hyd	Hyd	0.93	0.07	Skarn	IOCG	0.03	0.37	0.01	0.13	0.09	0.37
BZ-16-Ccp2-08			Hyd	Hyd	0.99	0.01	Skarn	IOCG	0.02	0.46	0.01	0.04	0.13	0.35
BZ-16-Ccp2-09			Hyd	Hyd	0.99	0.01	Skarn	VMS	0.04	0.15	0.16	0.06	0.05	0.53
BZ-16-Ccp2-10			Hyd	Hyd	1.00	0.00	Skarn	VMS	0.00	0.00	0.01	0.00	0.02	0.97
BZ-16-Ccp2-11			Hyd	Hyd	1.00	0.00	Skarn	VMS	0.00	0.01	0.01	0.00	0.00	0.97

			RF mag-hyd model				RF hyd model							
			Actual	Predicted	Prob		Actual	Predicted	Prob					
ID	Author	Deposit			Hyd	Mag			Epithermal gold	IOCG	Orogenic gold	Porphyry	Skarn	VMS
LS-027-1-Ccp1	Liang et al. (2021)	Laoshankou	Hyd	Hyd	0.95	0.05	IOCG	VMS	0.01	0.10	0.03	0.09	0.07	0.70
LS-027-1-Ccp2			Hyd	Hyd	0.96	0.04	IOCG	VMS	0.02	0.06	0.04	0.09	0.04	0.75
LS-027-1-Ccp3			Hyd	Mag	0.40	0.60	IOCG	IOCG	0.03	0.45	0.09	0.10	0.16	0.17
LS-027-2-Ccp-1			Hyd	Mag	0.00	1.00	IOCG	Skarn	0.04	0.09	0.05	0.15	0.54	0.13
LS-027-2-Ccp-2			Hyd	Hyd	0.86	0.14	IOCG	VMS	0.04	0.07	0.02	0.16	0.03	0.67
LS-027-2-Ccp-3			Hyd	Mag	0.01	0.99	IOCG	Skarn	0.05	0.08	0.09	0.13	0.55	0.11
LS-027-2-Ccp-4			Hyd	Hyd	0.98	0.02	IOCG	VMS	0.01	0.08	0.04	0.07	0.04	0.77
LS-027-2-Ccp-5			Hyd	Hyd	0.91	0.09	IOCG	VMS	0.02	0.24	0.03	0.21	0.07	0.43
LS-027-6-Ccp1			Hyd	Hyd	0.98	0.02	IOCG	Porphyry	0.01	0.29	0.03	0.35	0.06	0.25
LS-027-6-Ccp2			Hyd	Hyd	0.82	0.18	IOCG	Porphyry	0.05	0.23	0.03	0.34	0.15	0.20
LS-027-6-Ccp3			Hyd	Mag	0.04	0.96	IOCG	VMS	0.02	0.21	0.03	0.27	0.04	0.43
LS14-012-1-Ccp-1			Hyd	Hyd	0.98	0.02	IOCG	IOCG	0.01	0.43	0.03	0.15	0.06	0.32
LS14-012-1-Ccp-2			Hyd	Mag	0.25	0.75	IOCG	VMS	0.04	0.21	0.05	0.29	0.06	0.35
LS14-012-1-Ccp-3			Hyd	Mag	0.24	0.76	IOCG	VMS	0.04	0.15	0.06	0.26	0.11	0.38
LS14-012-1-Ccp-4			Hyd	Mag	0.29	0.71	IOCG	IOCG	0.03	0.33	0.03	0.27	0.07	0.28
LS14-012-1-Ccp-5			Hyd	Mag	0.19	0.81	IOCG	VMS	0.01	0.06	0.01	0.24	0.01	0.67
LS14-012-3-Ccp-1			Hyd	Hyd	0.54	0.46	IOCG	VMS	0.03	0.23	0.02	0.20	0.04	0.48
LS14-012-3-Ccp-2			Hyd	Hyd	0.86	0.14	IOCG	Porphyry	0.03	0.22	0.05	0.46	0.02	0.22
LS14-012-4-Ccp-1			Hyd	Hyd	0.88	0.12	IOCG	Porphyry	0.03	0.19	0.04	0.36	0.03	0.34
LS14-012-4-Ccp-2			Hyd	Mag	0.34	0.66	IOCG	Porphyry	0.02	0.18	0.03	0.47	0.03	0.27
LS14-012-4-Ccp-3			Hyd	Hyd	0.97	0.03	IOCG	Porphyry	0.01	0.21	0.02	0.38	0.05	0.33
LS14-012-7-Ccp-1			Hyd	Hyd	0.58	0.42	IOCG	VMS	0.02	0.15	0.04	0.31	0.06	0.43
LS14-012-7-Ccp-2			Hyd	Mag	0.20	0.80	IOCG	VMS	0.04	0.25	0.05	0.26	0.05	0.35
LS14-012-7-Ccp-3			Hyd	Mag	0.24	0.76	IOCG	VMS	0.05	0.24	0.04	0.26	0.04	0.36

			RF mag-hyd model				RF hyd model							
			Actual	Predicted	Prob		Actual	Predicted	Prob					
ID	Author	Deposit			Hyd	Mag			Epithermal gold	IOCG	Orogenic gold	Porphyry	Skarn	VMS
ASLL09 (V2)	Lobo (2022)	Assarel	Hyd	Hyd	0.98	0.02	Porphyry	Porphyry	0.01	0.07	0.01	0.52	0.00	0.39
ASLL14 (V4)			Hyd	Hyd	0.94	0.06	Porphyry	Porphyry	0.00	0.04	0.01	0.84	0.01	0.10
ASLL04 (V6)			Hyd	Hyd	0.73	0.27	Porphyry	Porphyry	0.06	0.06	0.03	0.71	0.03	0.12
ASLL17 (V6)			Hyd	Hyd	0.94	0.06	Porphyry	Porphyry	0.02	0.04	0.01	0.62	0.01	0.30
ASLL07 (V6)			Hyd	Hyd	0.76	0.24	Porphyry	Porphyry	0.01	0.07	0.03	0.78	0.01	0.10
ASLL10 (V6)			Hyd	Hyd	0.62	0.38	Porphyry	VMS	0.06	0.05	0.04	0.14	0.07	0.66
DH-132-92	Mansur et al. (2023)	Jaguar	Hyd	Hyd	0.64	0.36	IOCG	IOCG	0.04	0.30	0.27	0.09	0.14	0.16
DH-132-99			Hyd	Mag	0.19	0.81	IOCG	IOCG	0.04	0.38	0.15	0.12	0.14	0.17
DH-132-92			Hyd	Hyd	0.62	0.38	IOCG	IOCG	0.08	0.34	0.30	0.07	0.13	0.09
DH-132-92			Hyd	Mag	0.35	0.65	IOCG	Orogenic gold	0.07	0.29	0.36	0.07	0.06	0.15
FD-04-173			Hyd	Hyd	0.56	0.44	IOCG	IOCG	0.08	0.28	0.13	0.23	0.17	0.12
DH-132-92			Hyd	Hyd	0.57	0.43	IOCG	Orogenic gold	0.03	0.32	0.40	0.07	0.08	0.10
FD-04-173			Hyd	Hyd	0.57	0.43	IOCG	IOCG	0.05	0.31	0.11	0.17	0.11	0.26
FD-04-173			Hyd	Hyd	0.51	0.49	IOCG	Porphyry	0.06	0.18	0.14	0.23	0.20	0.18
FD-04-173			Hyd	Mag	0.49	0.51	IOCG	IOCG	0.05	0.42	0.12	0.20	0.08	0.12
DH-01-124			Hyd	Hyd	0.72	0.28	IOCG	Skarn	0.08	0.19	0.19	0.20	0.23	0.11
DH-132-99			Hyd	Mag	0.18	0.82	IOCG	IOCG	0.06	0.32	0.21	0.14	0.06	0.22
FD-04-173			Hyd	Hyd	0.52	0.48	IOCG	IOCG	0.06	0.37	0.15	0.19	0.10	0.12
FD-04-173			Hyd	Hyd	0.59	0.41	IOCG	VMS	0.03	0.27	0.13	0.11	0.14	0.32
FD-04-173			Hyd	Hyd	0.50	0.50	IOCG	IOCG	0.05	0.45	0.13	0.20	0.06	0.12
DH-01-124			Hyd	Mag	0.16	0.84	IOCG	IOCG	0.09	0.26	0.18	0.21	0.16	0.10
DH-01-124			Hyd	Mag	0.27	0.73	IOCG	IOCG	0.05	0.34	0.15	0.13	0.22	0.11
DH-01-124			Hyd	Hyd	0.65	0.35	IOCG	Orogenic gold	0.20	0.17	0.29	0.17	0.11	0.07
DH-132-116			Hyd	Hyd	0.68	0.32	IOCG	Orogenic gold	0.04	0.34	0.36	0.08	0.13	0.05
DH-24-49			Hyd	Hyd	0.66	0.34	IOCG	IOCG	0.01	0.61	0.09	0.14	0.10	0.05
DH-132-116			Hyd	Hyd	0.63	0.37	IOCG	Orogenic gold	0.05	0.33	0.36	0.07	0.13	0.07

			RF mag-hyd model				RF hyd model							
			Actual	Predicted	Prob		Actual	Predicted	Prob					
ID	Author	Deposit			Hyd	Mag			Epithermal gold	IOCG	Orogenic gold	Porphyry	Skarn	VMS
DH-132-92	Mansur et al. (2023)	Jaguar	Hyd	Mag	0.31	0.69	IOCG	IOCG	0.02	0.49	0.11	0.13	0.15	0.09
DH-132-70			Hyd	Hyd	0.75	0.25	IOCG	IOCG	0.01	0.44	0.11	0.15	0.17	0.12
DH-24-49			Hyd	Hyd	0.77	0.23	IOCG	IOCG	0.09	0.44	0.14	0.17	0.09	0.07
DH-132-111			Hyd	Mag	0.16	0.84	IOCG	IOCG	0.06	0.33	0.18	0.09	0.13	0.21
DH-01-124			Hyd	Mag	0.07	0.93	IOCG	IOCG	0.06	0.28	0.14	0.16	0.20	0.16
DH-132-111			Hyd	Mag	0.19	0.81	IOCG	IOCG	0.02	0.40	0.18	0.09	0.08	0.23
DH-01-124			Hyd	Mag	0.20	0.80	IOCG	IOCG	0.04	0.33	0.11	0.17	0.13	0.21
DH-132-111			Hyd	Mag	0.33	0.67	IOCG	IOCG	0.00	0.37	0.09	0.12	0.12	0.30
DH-132-111			Hyd	Mag	0.29	0.71	IOCG	IOCG	0.02	0.45	0.14	0.09	0.07	0.24
DH-127-68			Hyd	Hyd	0.70	0.30	IOCG	IOCG	0.13	0.24	0.21	0.13	0.16	0.13
DH-127-68			Hyd	Hyd	0.68	0.32	IOCG	IOCG	0.12	0.34	0.16	0.13	0.11	0.13
DH-127-68			Hyd	Hyd	0.70	0.30	IOCG	IOCG	0.02	0.33	0.19	0.14	0.21	0.11
DH-132-111			Hyd	Hyd	0.50	0.50	IOCG	IOCG	0.01	0.39	0.22	0.08	0.07	0.22
DH-127-68			Hyd	Hyd	0.69	0.31	IOCG	IOCG	0.04	0.27	0.24	0.15	0.17	0.13
CY13-KV-E6-CCP-30	Martin et al. (2018)	Troodos	Hyd	Hyd	0.98	0.02	VMS	VMS	0.05	0.04	0.08	0.02	0.21	0.60
AM407 CCP1			Hyd	Hyd	0.99	0.01	VMS	VMS	0.04	0.05	0.20	0.02	0.06	0.63
AM448 CCP 1			Hyd	Hyd	0.73	0.27	VMS	VMS	0.03	0.04	0.04	0.06	0.06	0.76
AM CCP3			Hyd	Hyd	0.99	0.01	VMS	VMS	0.03	0.04	0.17	0.04	0.06	0.66
KWXCCP4			Hyd	Mag	0.10	0.90	VMS	Epithermal gold	0.29	0.16	0.03	0.04	0.22	0.27
KWXCCP1			Hyd	Mag	0.00	1.00	VMS	Skarn	0.28	0.12	0.02	0.04	0.36	0.18
KWXCCP2			Hyd	Mag	0.00	1.00	VMS	VMS	0.21	0.15	0.03	0.01	0.17	0.44
CY13-MT-E7-CCP-39			Hyd	Hyd	0.91	0.09	VMS	Epithermal gold	0.92	0.02	0.02	0.02	0.00	0.02
CY13-MT-E7-CCP-8			Hyd	Mag	0.03	0.97	VMS	IOCG	0.12	0.34	0.23	0.06	0.03	0.23
KY7574CP4			Hyd	Hyd	0.95	0.05	VMS	Epithermal gold	0.47	0.17	0.10	0.03	0.15	0.07
AM418CCP3			Hyd	Hyd	0.96	0.04	VMS	VMS	0.00	0.01	0.00	0.01	0.04	0.94
CY13-MT-E7-CCP-105			Hyd	Hyd	0.98	0.02	VMS	Skarn	0.25	0.14	0.07	0.02	0.38	0.14

			RF mag-hyd model				RF hyd model							
			Actual	Predicted	Prob		Actual	Predicted	Prob					
ID	Author	Deposit			Hyd	Mag			Epithermal gold	IOCG	Orogenic gold	Porphyry	Skarn	VMS
KW7574CP3	Martin et al. (2018)	Troodos	Hyd	Hyd	0.92	0.08	VMS	VMS	0.05	0.07	0.01	0.04	0.09	0.74
KWXCCP3			Hyd	Mag	0.00	1.00	VMS	VMS	0.03	0.09	0.01	0.01	0.30	0.56
AM408CCP4			Hyd	Hyd	0.95	0.05	VMS	VMS	0.06	0.26	0.06	0.08	0.17	0.37
AM408CCP8			Hyd	Mag	0.20	0.80	VMS	Orogenic gold	0.08	0.19	0.39	0.04	0.20	0.10
AM408CCP5			Hyd	Hyd	0.86	0.14	VMS	VMS	0.06	0.27	0.08	0.03	0.27	0.30
AM418 CCP5			Hyd	Hyd	1.00	0.00	VMS	VMS	0.00	0.01	0.01	0.00	0.00	0.98
CY13-MT-E7-CCP-82			Hyd	Hyd	0.83	0.17	VMS	VMS	0.04	0.13	0.12	0.03	0.09	0.59
AM418 CCP4			Hyd	Hyd	1.00	0.00	VMS	VMS	0.00	0.04	0.00	0.00	0.02	0.93
AM408CCP10			Hyd	Hyd	1.00	0.00	VMS	VMS	0.05	0.13	0.22	0.05	0.05	0.50
AM408CCP7			Hyd	Mag	0.06	0.94	VMS	Skarn	0.04	0.27	0.12	0.15	0.30	0.12
AM418 CCP6			Hyd	Hyd	0.89	0.11	VMS	VMS	0.01	0.03	0.00	0.02	0.02	0.93
AM418 CCP3			Hyd	Hyd	0.91	0.09	VMS	VMS	0.01	0.03	0.03	0.02	0.03	0.88
AM418 CCP1			Hyd	Hyd	0.98	0.02	VMS	VMS	0.00	0.02	0.02	0.02	0.03	0.91
AM408CCP3			Hyd	Mag	0.00	1.00	VMS	Orogenic gold	0.01	0.17	0.39	0.13	0.25	0.05
AM408CCP6			Hyd	Mag	0.02	0.98	VMS	IOCG	0.03	0.42	0.27	0.07	0.12	0.09
AM418CCP2			Hyd	Hyd	0.83	0.17	VMS	VMS	0.00	0.16	0.02	0.04	0.02	0.77
AM418CCP1			Hyd	Hyd	0.99	0.01	VMS	IOCG	0.00	0.52	0.00	0.00	0.00	0.48
AM408CCP2			Hyd	Hyd	0.56	0.44	VMS	Orogenic gold	0.02	0.05	0.59	0.02	0.02	0.31
AM408CCP2			Hyd	Mag	0.15	0.85	VMS	Orogenic gold	0.01	0.18	0.52	0.02	0.16	0.11
7751CCP3			Hyd	Hyd	1.00	0.00	VMS	VMS	0.00	0.03	0.01	0.01	0.01	0.94
AM408CCP9			Hyd	Mag	0.00	1.00	VMS	VMS	0.02	0.18	0.15	0.09	0.25	0.31
PHO2CCP6			Hyd	Hyd	1.00	0.00	VMS	VMS	0.01	0.05	0.03	0.03	0.04	0.85
7751CCP4			Hyd	Hyd	1.00	0.00	VMS	VMS	0.00	0.02	0.02	0.02	0.01	0.93
7751CCP6			Hyd	Hyd	0.99	0.01	VMS	VMS	0.01	0.01	0.00	0.01	0.01	0.96
7751CCP1			Hyd	Hyd	1.00	0.00	VMS	VMS	0.00	0.04	0.01	0.03	0.02	0.91
7751CCP5			Hyd	Hyd	0.99	0.01	VMS	VMS	0.00	0.03	0.00	0.01	0.00	0.96

			RF mag-hyd model				RF hyd model							
			Actual	Predicted	Prob		Actual	Predicted	Prob					
ID	Author	Deposit			Hyd	Mag			Epithermal gold	IOCG	Orogenic gold	Porphyry	Skarn	VMS
PHO2CCP5	Martin et al. (2018)	Troodos	Hyd	Hyd	1.00	0.00	VMS	VMS	0.01	0.03	0.00	0.02	0.01	0.94
PHO2CCP2			Hyd	Hyd	1.00	0.00	VMS	VMS	0.03	0.06	0.00	0.23	0.00	0.67
PHO2CCP3			Hyd	Hyd	0.99	0.01	VMS	VMS	0.02	0.14	0.01	0.16	0.00	0.67
PHO2CCP7			Hyd	Hyd	0.98	0.02	VMS	VMS	0.05	0.10	0.01	0.21	0.01	0.61
PHO2CCP4			Hyd	Hyd	1.00	0.00	VMS	VMS	0.05	0.17	0.01	0.30	0.01	0.47
CY13-SK-E1-CCP-39			Hyd	Hyd	0.99	0.01	VMS	VMS	0.08	0.08	0.02	0.34	0.02	0.47
CY13-SK-E1-CCP-34			Hyd	Hyd	0.98	0.02	VMS	Porphyry	0.05	0.06	0.00	0.51	0.00	0.38
CY13-SK-E1-CCP-28			Hyd	Hyd	0.99	0.01	VMS	Porphyry	0.03	0.06	0.00	0.73	0.00	0.17
CY13-SK-E1-CCP-65			Hyd	Hyd	0.98	0.02	VMS	Porphyry	0.07	0.11	0.01	0.55	0.02	0.24
CY13-SK-E1-CCP-38			Hyd	Hyd	0.99	0.01	VMS	Porphyry	0.13	0.07	0.01	0.41	0.02	0.36
CY13-SK-E1-CCP-64			Hyd	Hyd	0.97	0.03	VMS	Porphyry	0.06	0.11	0.01	0.54	0.02	0.26
PHO2CCP8			Hyd	Hyd	0.86	0.14	VMS	VMS	0.02	0.22	0.00	0.30	0.00	0.45
AM418CCP2			Hyd	Hyd	0.77	0.23	VMS	Porphyry	0.03	0.10	0.01	0.45	0.00	0.41
CY13-MT-E7-CCP-106			Hyd	Hyd	0.90	0.10	VMS	IOCG	0.15	0.59	0.14	0.08	0.02	0.03
CY13-MT-E7-CCP-18			Hyd	Mag	0.19	0.81	VMS	IOCG	0.05	0.67	0.02	0.24	0.01	0.01
PHO2CCP1			Hyd	Hyd	0.99	0.01	VMS	VMS	0.01	0.03	0.00	0.02	0.00	0.94
a01	Maslennikov et al. (2017)	Urals	Hyd	Hyd	0.99	0.01	VMS	VMS	0.05	0.06	0.09	0.05	0.05	0.70
a02			Hyd	Hyd	0.99	0.01	VMS	VMS	0.05	0.12	0.17	0.09	0.02	0.56
a03			Hyd	Hyd	0.98	0.02	VMS	VMS	0.09	0.12	0.07	0.03	0.13	0.56
a04			Hyd	Hyd	0.93	0.07	VMS	VMS	0.10	0.02	0.12	0.11	0.16	0.50
a05			Hyd	Hyd	0.98	0.02	VMS	VMS	0.06	0.02	0.32	0.04	0.13	0.44
a06			Hyd	Hyd	0.97	0.03	VMS	VMS	0.03	0.02	0.04	0.09	0.04	0.79
a07			Hyd	Hyd	0.98	0.02	VMS	VMS	0.07	0.11	0.09	0.08	0.17	0.46
a08			Hyd	Hyd	0.99	0.01	VMS	VMS	0.02	0.03	0.01	0.08	0.00	0.85
a09			Hyd	Hyd	0.96	0.04	VMS	VMS	0.05	0.13	0.18	0.14	0.03	0.47
a10			Hyd	Hyd	0.98	0.02	VMS	VMS	0.01	0.07	0.11	0.05	0.05	0.72

			RF mag-hyd model				RF hyd model							
			Actual	Predicted	Prob		Actual	Predicted	Prob					
ID	Author	Deposit			Hyd	Mag			Epithermal gold	IOCG	Orogenic gold	Porphyry	Skarn	VMS
a11	Maslennikov et al. (2017)	Urals	Hyd	Hyd	0.98	0.02	VMS	VMS	0.01	0.03	0.16	0.07	0.05	0.68
a12			Hyd	Hyd	0.95	0.05	VMS	Epithermal gold	0.30	0.09	0.10	0.20	0.04	0.27
a13			Hyd	Hyd	0.98	0.02	VMS	VMS	0.02	0.06	0.06	0.17	0.06	0.63
a14			Hyd	Hyd	0.99	0.01	VMS	VMS	0.05	0.12	0.02	0.16	0.03	0.63
a15			Hyd	Hyd	0.99	0.01	VMS	VMS	0.03	0.07	0.03	0.03	0.01	0.82
a16			Hyd	Hyd	0.98	0.02	VMS	VMS	0.01	0.03	0.12	0.04	0.05	0.75
a17			Hyd	Hyd	0.98	0.02	VMS	VMS	0.01	0.07	0.07	0.05	0.05	0.76
a18			Hyd	Hyd	0.98	0.02	VMS	VMS	0.02	0.06	0.09	0.04	0.05	0.75
a19			Hyd	Hyd	0.68	0.32	VMS	VMS	0.02	0.07	0.05	0.05	0.07	0.74
a20			Hyd	Hyd	0.93	0.07	VMS	VMS	0.01	0.02	0.09	0.05	0.04	0.79
a21			Hyd	Hyd	0.98	0.02	VMS	VMS	0.01	0.05	0.05	0.05	0.04	0.79
BA20_7_1	Reich et al. (2020)	Cerro Pabellon	Hyd	Hyd	0.96	0.04	Epithermal gold	VMS	0.04	0.03	0.04	0.05	0.00	0.84
BA20_7_2			Hyd	Hyd	0.97	0.03	Epithermal gold	VMS	0.05	0.02	0.04	0.05	0.00	0.84
BA20_7_3			Hyd	Hyd	0.96	0.04	Epithermal gold	VMS	0.16	0.03	0.03	0.03	0.00	0.75
BA20_7_4			Hyd	Hyd	0.96	0.04	Epithermal gold	VMS	0.16	0.03	0.03	0.03	0.00	0.75
BA20_7_5			Hyd	Hyd	0.96	0.04	Epithermal gold	VMS	0.16	0.03	0.03	0.03	0.00	0.75
BA20_9_1			Hyd	Hyd	0.97	0.03	Epithermal gold	Epithermal gold	0.58	0.09	0.14	0.03	0.02	0.13
BA20_9_2			Hyd	Hyd	0.96	0.04	Epithermal gold	VMS	0.17	0.03	0.03	0.03	0.00	0.73
BA20_9_3			Hyd	Hyd	0.96	0.04	Epithermal gold	VMS	0.17	0.03	0.03	0.03	0.00	0.73
BA20_9_4			Hyd	Hyd	0.96	0.04	Epithermal gold	VMS	0.27	0.04	0.06	0.05	0.00	0.58
BA20_9_5			Hyd	Hyd	0.96	0.04	Epithermal gold	VMS	0.16	0.02	0.03	0.04	0.00	0.75
BA20_9_6			Hyd	Hyd	1.00	0.00	Epithermal gold	VMS	0.02	0.01	0.01	0.00	0.01	0.96
BA20_13_1			Hyd	Hyd	0.96	0.04	Epithermal gold	VMS	0.16	0.02	0.03	0.04	0.00	0.75
BA20_13_2			Hyd	Hyd	0.96	0.04	Epithermal gold	VMS	0.16	0.02	0.03	0.04	0.00	0.75
BA20_13_3			Hyd	Hyd	0.98	0.02	Epithermal gold	Epithermal gold	0.56	0.09	0.18	0.03	0.02	0.11
BA20_13_4			Hyd	Hyd	0.97	0.03	Epithermal gold	Epithermal gold	0.58	0.09	0.09	0.03	0.02	0.19

			RF mag-hyd model				RF hyd model							
			Actual	Predicted	Prob		Actual	Predicted	Prob					
ID	Author	Deposit			Hyd	Mag			Epithermal gold	IOCG	Orogenic gold	Porphyry	Skarn	VMS
BA20_13_5	Reich et al. (2020)	Cerro Pabellon	Hyd	Hyd	0.96	0.04	Epithermal gold	Epithermal gold	0.56	0.10	0.17	0.03	0.02	0.11
BA20_15_2			Hyd	Hyd	1.00	0.00	Epithermal gold	VMS	0.01	0.01	0.01	0.01	0.01	0.96
BA20_15_3			Hyd	Hyd	0.99	0.01	Epithermal gold	Epithermal gold	0.67	0.10	0.15	0.01	0.01	0.06
BA20_15_4			Hyd	Hyd	1.00	0.00	Epithermal gold	VMS	0.02	0.01	0.01	0.00	0.01	0.96
BA20_15_5			Hyd	Hyd	1.00	0.00	Epithermal gold	VMS	0.02	0.01	0.01	0.00	0.01	0.96
BA20_16_1			Hyd	Hyd	0.95	0.05	Epithermal gold	Epithermal gold	0.70	0.06	0.11	0.01	0.01	0.10
BA20_16_2			Hyd	Hyd	0.98	0.02	Epithermal gold	Epithermal gold	0.70	0.08	0.12	0.01	0.01	0.08
BA20_16_3			Hyd	Hyd	0.98	0.02	Epithermal gold	Epithermal gold	0.60	0.08	0.08	0.04	0.01	0.18
BA20_16_5			Hyd	Hyd	0.94	0.06	Epithermal gold	Epithermal gold	0.58	0.10	0.10	0.04	0.01	0.17
BA20_17_1			Hyd	Hyd	0.91	0.09	Epithermal gold	VMS	0.17	0.03	0.03	0.05	0.00	0.72
BA20_17_2			Hyd	Hyd	0.99	0.01	Epithermal gold	VMS	0.08	0.03	0.05	0.06	0.02	0.76
BA30_8_1			Hyd	Hyd	0.83	0.17	Epithermal gold	VMS	0.01	0.13	0.02	0.13	0.02	0.69
BA30_9_1			Hyd	Hyd	0.99	0.01	Epithermal gold	VMS	0.02	0.05	0.14	0.04	0.01	0.74
BA34_1_5			Hyd	Hyd	0.96	0.04	Epithermal gold	IOCG	0.08	0.48	0.22	0.06	0.02	0.15
BA34_14_2			Hyd	Hyd	0.97	0.03	Epithermal gold	IOCG	0.06	0.62	0.16	0.04	0.02	0.10
BA34_14_3			Hyd	Hyd	0.96	0.04	Epithermal gold	IOCG	0.06	0.64	0.18	0.03	0.02	0.08
BA34_14_5			Hyd	Hyd	0.98	0.02	Epithermal gold	Epithermal gold	0.47	0.16	0.12	0.03	0.03	0.20
BA34_20_1			Hyd	Hyd	0.99	0.01	Epithermal gold	VMS	0.02	0.04	0.07	0.02	0.03	0.82
BA48_5_1			Hyd	Hyd	0.98	0.02	Epithermal gold	VMS	0.00	0.06	0.00	0.00	0.00	0.94
BA48_5_2			Hyd	Hyd	1.00	0.00	Epithermal gold	Orogenic gold	0.04	0.13	0.64	0.02	0.03	0.15
BA48_6_1			Hyd	Hyd	1.00	0.00	Epithermal gold	IOCG	0.12	0.75	0.06	0.01	0.02	0.04
BA48_6_2			Hyd	Hyd	0.99	0.01	Epithermal gold	VMS	0.03	0.07	0.04	0.04	0.02	0.79
BA48_14_1			Hyd	Hyd	0.84	0.16	Epithermal gold	VMS	0.02	0.05	0.02	0.03	0.01	0.87
BA48_14_2			Hyd	Hyd	0.92	0.08	Epithermal gold	Orogenic gold	0.02	0.04	0.70	0.01	0.04	0.19
BA48_15_3			Hyd	Hyd	0.98	0.02	Epithermal gold	VMS	0.03	0.07	0.08	0.02	0.02	0.79
BA48_17_3			Hyd	Hyd	0.81	0.19	Epithermal gold	VMS	0.02	0.05	0.02	0.00	0.01	0.89

			RF mag-hyd model				RF hyd model							
			Actual	Predicted	Prob		Actual	Predicted	Prob					
ID	Author	Deposit			Hyd	Mag			Epithermal gold	IOCG	Orogenic gold	Porphyry	Skarn	VMS
1	Revan et al. (2014)	Cayeli	Hyd	Hyd	0.69	0.31	VMS	Porphyry	0.03	0.07	0.01	0.75	0.00	0.14
2			Hyd	Hyd	0.98	0.02	VMS	Porphyry	0.12	0.16	0.04	0.45	0.01	0.23
3			Hyd	Hyd	0.99	0.01	VMS	VMS	0.09	0.26	0.12	0.11	0.06	0.36
4			Hyd	Hyd	0.97	0.03	VMS	VMS	0.04	0.04	0.05	0.14	0.08	0.66
5			Hyd	Hyd	0.96	0.04	VMS	VMS	0.04	0.03	0.05	0.09	0.12	0.67
6			Hyd	Hyd	0.99	0.01	VMS	VMS	0.13	0.18	0.19	0.10	0.06	0.34
7			Hyd	Hyd	0.97	0.03	VMS	VMS	0.05	0.10	0.10	0.18	0.01	0.56
8			Hyd	Hyd	0.97	0.03	VMS	VMS	0.03	0.03	0.04	0.17	0.02	0.71
9			Hyd	Hyd	0.98	0.02	VMS	VMS	0.02	0.09	0.04	0.07	0.03	0.75
10			Hyd	Hyd	0.97	0.03	VMS	VMS	0.03	0.08	0.03	0.26	0.04	0.57
11			Hyd	Hyd	0.99	0.01	VMS	VMS	0.07	0.18	0.08	0.10	0.02	0.55
12			Hyd	Hyd	0.99	0.01	VMS	VMS	0.04	0.10	0.04	0.11	0.02	0.68
13			Hyd	Hyd	0.99	0.01	VMS	Porphyry	0.06	0.07	0.02	0.71	0.01	0.12
14			Hyd	Hyd	0.99	0.01	VMS	VMS	0.09	0.15	0.23	0.19	0.05	0.30
15			Hyd	Hyd	0.97	0.03	VMS	VMS	0.05	0.02	0.11	0.05	0.17	0.60
16			Hyd	Hyd	0.98	0.02	VMS	VMS	0.03	0.02	0.05	0.11	0.04	0.75
17			Hyd	Hyd	0.96	0.04	VMS	Porphyry	0.04	0.20	0.05	0.38	0.05	0.29
18			Hyd	Hyd	0.86	0.14	VMS	VMS	0.07	0.08	0.18	0.08	0.07	0.52
19			Hyd	Hyd	0.98	0.02	VMS	VMS	0.10	0.07	0.20	0.05	0.09	0.48
20			Hyd	Hyd	0.98	0.02	VMS	VMS	0.13	0.08	0.06	0.20	0.06	0.46
21			Hyd	Mag	0.36	0.64	VMS	Porphyry	0.02	0.17	0.02	0.48	0.04	0.26
22			Hyd	Hyd	0.96	0.04	VMS	VMS	0.01	0.05	0.07	0.08	0.00	0.80
23			Hyd	Hyd	0.96	0.04	VMS	VMS	0.01	0.05	0.07	0.08	0.00	0.80
24			Hyd	Hyd	1.00	0.00	VMS	VMS	0.10	0.22	0.05	0.21	0.04	0.38
25			Hyd	Hyd	0.94	0.06	VMS	VMS	0.10	0.20	0.03	0.24	0.02	0.41
26			Hyd	Hyd	0.96	0.04	VMS	VMS	0.07	0.03	0.14	0.09	0.18	0.48

			RF mag-hyd model				RF hyd model							
			Actual	Predicted	Prob		Actual	Predicted	Prob					
ID	Author	Deposit			Hyd	Mag			Epithermal gold	IOCG	Orogenic gold	Porphyry	Skarn	VMS
27	Revan et al. (2014)	Cayeli	Hyd	Hyd	0.96	0.04	VMS	VMS	0.06	0.06	0.29	0.08	0.08	0.43
28			Hyd	Hyd	0.95	0.05	VMS	VMS	0.05	0.06	0.26	0.07	0.07	0.49
29			Hyd	Hyd	0.81	0.19	VMS	VMS	0.07	0.07	0.26	0.09	0.09	0.42
30			Hyd	Hyd	0.93	0.07	VMS	VMS	0.12	0.14	0.23	0.08	0.13	0.29
31			Hyd	Hyd	0.97	0.03	VMS	VMS	0.03	0.02	0.35	0.08	0.10	0.41
32			Hyd	Hyd	0.77	0.23	VMS	VMS	0.12	0.18	0.23	0.04	0.08	0.35
33			Hyd	Hyd	0.98	0.02	VMS	VMS	0.05	0.05	0.20	0.13	0.03	0.54
34			Hyd	Hyd	0.86	0.14	VMS	VMS	0.09	0.16	0.25	0.08	0.14	0.28
35			Hyd	Hyd	0.97	0.03	VMS	VMS	0.11	0.17	0.07	0.15	0.16	0.34
36			Hyd	Hyd	0.96	0.04	VMS	VMS	0.05	0.07	0.24	0.07	0.10	0.48
37			Hyd	Hyd	0.94	0.06	VMS	VMS	0.06	0.06	0.25	0.08	0.09	0.47
38			Hyd	Hyd	0.98	0.02	VMS	Porphyry	0.04	0.10	0.05	0.61	0.02	0.18
39			Hyd	Hyd	1.00	0.00	VMS	IOCG	0.07	0.38	0.18	0.10	0.05	0.22
40			Hyd	Hyd	0.92	0.08	VMS	VMS	0.05	0.05	0.23	0.08	0.06	0.52
41			Hyd	Hyd	0.93	0.07	VMS	VMS	0.06	0.04	0.13	0.09	0.08	0.59
42			Hyd	Hyd	0.97	0.03	VMS	VMS	0.03	0.06	0.06	0.15	0.02	0.69
43			Hyd	Hyd	0.98	0.02	VMS	VMS	0.06	0.02	0.13	0.15	0.11	0.53
44			Hyd	Hyd	0.99	0.01	VMS	VMS	0.11	0.06	0.28	0.05	0.06	0.44
45			Hyd	Mag	0.42	0.58	VMS	Porphyry	0.02	0.15	0.01	0.45	0.01	0.36
46			Hyd	Hyd	0.98	0.02	VMS	VMS	0.02	0.20	0.08	0.04	0.03	0.63
47			Hyd	Hyd	0.97	0.03	VMS	VMS	0.05	0.01	0.05	0.06	0.13	0.70
48			Hyd	Hyd	0.90	0.10	VMS	VMS	0.12	0.14	0.09	0.23	0.07	0.33
49			Hyd	Hyd	0.98	0.02	VMS	Orogenic gold	0.08	0.12	0.40	0.06	0.03	0.31
50			Hyd	Hyd	0.97	0.03	VMS	Porphyry	0.03	0.15	0.08	0.42	0.03	0.29
51			Hyd	Hyd	0.99	0.01	VMS	Porphyry	0.10	0.15	0.12	0.31	0.03	0.29
52			Hyd	Hyd	0.93	0.07	VMS	VMS	0.06	0.07	0.28	0.08	0.09	0.42

			RF mag-hyd model				RF hyd model							
			Actual	Predicted	Prob		Actual	Predicted	Prob					
ID	Author	Deposit			Hyd	Mag			Epithermal gold	IOCG	Orogenic gold	Porphyry	Skarn	VMS
53	Revan et al. (2014)	Cayeli	Hyd	Hyd	0.99	0.01	VMS	IOCG	0.06	0.34	0.12	0.25	0.05	0.18
54			Hyd	Hyd	0.99	0.01	VMS	VMS	0.05	0.04	0.22	0.13	0.09	0.47
55			Hyd	Hyd	0.99	0.01	VMS	VMS	0.07	0.05	0.27	0.06	0.05	0.50
56			Hyd	Hyd	0.98	0.02	VMS	Porphyry	0.02	0.24	0.01	0.36	0.03	0.34
57			Hyd	Hyd	0.99	0.01	VMS	VMS	0.06	0.08	0.01	0.10	0.01	0.75
58			Hyd	Hyd	0.97	0.03	VMS	VMS	0.06	0.02	0.09	0.11	0.19	0.53
59			Hyd	Hyd	0.98	0.02	VMS	VMS	0.06	0.03	0.16	0.12	0.10	0.54
60			Hyd	Hyd	1.00	0.00	VMS	VMS	0.01	0.06	0.02	0.08	0.02	0.81
61			Hyd	Hyd	0.98	0.02	VMS	VMS	0.01	0.04	0.13	0.09	0.03	0.70
62			Hyd	Hyd	0.96	0.04	VMS	VMS	0.05	0.03	0.15	0.11	0.10	0.57
63			Hyd	Hyd	0.98	0.02	VMS	VMS	0.07	0.17	0.08	0.17	0.02	0.49
64			Hyd	Hyd	0.99	0.01	VMS	VMS	0.07	0.05	0.30	0.10	0.04	0.43
65			Hyd	Hyd	0.98	0.02	VMS	VMS	0.08	0.12	0.02	0.16	0.01	0.61
66			Hyd	Hyd	0.99	0.01	VMS	Porphyry	0.09	0.05	0.22	0.52	0.07	0.04
67			Hyd	Hyd	0.97	0.03	VMS	VMS	0.06	0.02	0.31	0.07	0.16	0.38
68			Hyd	Hyd	0.98	0.02	VMS	VMS	0.13	0.09	0.05	0.24	0.06	0.43
69			Hyd	Hyd	0.80	0.20	VMS	Porphyry	0.03	0.23	0.02	0.40	0.05	0.27
70			Hyd	Mag	0.25	0.75	VMS	VMS	0.01	0.16	0.09	0.20	0.05	0.50
1360-2	Stefanova et al. (2023)	Elatsite-Chelopech	Hyd	Hyd	0.87	0.13	Porphyry	Porphyry	0.04	0.13	0.02	0.42	0.02	0.37
KS13-1-01			Hyd	Hyd	0.86	0.14	Porphyry	Porphyry	0.03	0.09	0.23	0.44	0.14	0.07
KS13-1-02			Hyd	Mag	0.05	0.95	Porphyry	IOCG	0.01	0.40	0.09	0.25	0.09	0.16
GK13-2b-01			Hyd	Hyd	0.53	0.47	Porphyry	VMS	0.02	0.19	0.13	0.10	0.22	0.34
GK13-2b-02			Hyd	Mag	0.21	0.79	Porphyry	Porphyry	0.06	0.30	0.08	0.39	0.04	0.13
GDK14-1			Hyd	Hyd	0.91	0.09	Porphyry	Porphyry	0.03	0.13	0.01	0.43	0.02	0.37
GDK14-9			Hyd	Hyd	0.71	0.29	Porphyry	Porphyry	0.02	0.13	0.03	0.70	0.03	0.09
C26-3			Hyd	Mag	0.47	0.53	Porphyry	Porphyry	0.01	0.15	0.01	0.63	0.02	0.17

			RF mag-hyd model				RF hyd model							
			Actual	Predicted	Prob		Actual	Predicted	Prob					
ID	Author	Deposit			Hyd	Mag			Epithermal gold	IOCG	Orogenic gold	Porphyry	Skarn	VMS
Naa-rim-023	Vasilopoulos et al. (2023)	Naakenavaara-Hirvilavanmaa	Hyd	Hyd	0.85	0.15	Orogenic gold	Orogenic gold	0.02	0.24	0.39	0.03	0.11	0.21
Naa-NA-028			Hyd	Mag	0.46	0.54	Orogenic gold	IOCG	0.01	0.65	0.09	0.04	0.13	0.08
Hir-Strong Au-010			Hyd	Hyd	0.89	0.11	Orogenic gold	IOCG	0.01	0.84	0.01	0.13	0.01	0.00
Hir-Strong Au-09			Hyd	Hyd	0.96	0.04	Orogenic gold	IOCG	0.04	0.81	0.05	0.09	0.01	0.01
Naa-rim-015			Hyd	Hyd	0.95	0.05	Orogenic gold	Skarn	0.01	0.14	0.28	0.10	0.28	0.18
Naa-rim-013			Hyd	Hyd	0.86	0.14	Orogenic gold	Skarn	0.01	0.23	0.22	0.08	0.28	0.18
Naa-rim-017			Hyd	Hyd	0.81	0.19	Orogenic gold	Skarn	0.04	0.16	0.14	0.13	0.35	0.19
Naa-core-09			Hyd	Hyd	0.83	0.17	Orogenic gold	IOCG	0.02	0.45	0.04	0.08	0.25	0.14
Naa-core-031			Hyd	Hyd	0.86	0.14	Orogenic gold	IOCG	0.01	0.31	0.23	0.11	0.17	0.16
Naa-rim-019			Hyd	Hyd	0.83	0.17	Orogenic gold	Skarn	0.02	0.22	0.15	0.15	0.33	0.12
Naa-rim-010			Hyd	Hyd	0.90	0.10	Orogenic gold	IOCG	0.01	0.57	0.07	0.04	0.21	0.09
Naa-core-012			Hyd	Hyd	0.89	0.11	Orogenic gold	Skarn	0.01	0.28	0.14	0.06	0.33	0.17
Naa-rim-021			Hyd	Hyd	0.71	0.29	Orogenic gold	Skarn	0.03	0.19	0.12	0.13	0.39	0.15
Naa-core-016			Hyd	Hyd	0.70	0.30	Orogenic gold	Skarn	0.03	0.20	0.13	0.15	0.30	0.20
Naa-rim-011			Hyd	Hyd	0.92	0.08	Orogenic gold	IOCG	0.01	0.45	0.16	0.05	0.20	0.13
Naa-core-014			Hyd	Hyd	0.94	0.06	Orogenic gold	Skarn	0.01	0.13	0.18	0.12	0.33	0.23
Naa-core-05			Hyd	Hyd	0.84	0.16	Orogenic gold	IOCG	0.01	0.40	0.07	0.13	0.26	0.12
Naa-core-02			Hyd	Hyd	0.82	0.18	Orogenic gold	IOCG	0.01	0.50	0.04	0.12	0.20	0.12
Naa-NA-036			Hyd	Mag	0.28	0.72	Orogenic gold	IOCG	0.02	0.39	0.10	0.13	0.17	0.19
Naa-rim-06			Hyd	Hyd	0.92	0.08	Orogenic gold	IOCG	0.01	0.58	0.04	0.06	0.16	0.14
Naa-rim-025			Hyd	Hyd	0.64	0.36	Orogenic gold	IOCG	0.02	0.49	0.08	0.15	0.14	0.12
Naa-rim-030			Hyd	Hyd	0.83	0.17	Orogenic gold	IOCG	0.01	0.39	0.25	0.15	0.09	0.10
Naa-rim-027			Hyd	Hyd	0.73	0.27	Orogenic gold	IOCG	0.02	0.57	0.06	0.11	0.12	0.13
Naa-core-04			Hyd	Hyd	0.83	0.17	Orogenic gold	IOCG	0.04	0.38	0.08	0.14	0.21	0.15
Hir-Strong Au-03			Hyd	Hyd	0.99	0.01	Orogenic gold	IOCG	0.01	0.48	0.03	0.46	0.01	0.01
Naa-core-08			Hyd	Hyd	0.88	0.12	Orogenic gold	IOCG	0.02	0.46	0.07	0.16	0.15	0.14

			RF mag-hyd model				RF hyd model							
			Actual	Predicted	Prob		Actual	Predicted	Prob					
ID	Author	Deposit			Hyd	Mag			Epithermal gold	IOCG	Orogenic gold	Porphyry	Skarn	VMS
Naa-rim-03	Vasilopoulos et al. (2023)	Naakenavaara-Hirvilavanmaa	Hyd	Hyd	0.93	0.07	Orogenic gold	IOCG	0.06	0.40	0.06	0.13	0.23	0.12
Naa-rim-033			Hyd	Hyd	0.81	0.19	Orogenic gold	IOCG	0.01	0.33	0.31	0.14	0.07	0.14
Hir-Strong Au-06			Hyd	Hyd	0.98	0.02	Orogenic gold	Porphyry	0.00	0.48	0.01	0.49	0.00	0.01
Naa-core-01			Hyd	Hyd	0.82	0.18	Orogenic gold	IOCG	0.03	0.49	0.03	0.10	0.21	0.14
Naa-c-026			Hyd	Hyd	0.73	0.27	Orogenic gold	IOCG	0.02	0.56	0.05	0.12	0.11	0.14
Hir-Strong Au-08			Hyd	Hyd	0.98	0.02	Orogenic gold	Porphyry	0.01	0.40	0.02	0.56	0.00	0.01
Hir-Strong Au-04			Hyd	Hyd	0.99	0.01	Orogenic gold	Porphyry	0.01	0.43	0.03	0.51	0.02	0.01
Hir-Strong Au-07			Hyd	Hyd	0.98	0.02	Orogenic gold	IOCG	0.00	0.51	0.03	0.44	0.01	0.01
Naa-rim-07			Hyd	Hyd	0.96	0.04	Orogenic gold	IOCG	0.02	0.49	0.18	0.06	0.12	0.13
Naa-rim-035			Hyd	Hyd	0.92	0.08	Orogenic gold	IOCG	0.02	0.25	0.21	0.21	0.18	0.13
Hir-Strong Au-01			Hyd	Hyd	1.00	0.00	Orogenic gold	Porphyry	0.02	0.39	0.05	0.51	0.02	0.01
Naa-core-029			Hyd	Hyd	0.89	0.11	Orogenic gold	IOCG	0.01	0.40	0.17	0.14	0.13	0.15
Hir-Strong Au-02			Hyd	Hyd	0.98	0.02	Orogenic gold	Porphyry	0.02	0.42	0.05	0.46	0.03	0.02
Naa-core-018			Hyd	Hyd	0.81	0.19	Orogenic gold	IOCG	0.03	0.27	0.10	0.11	0.24	0.25
Naa-core-034			Hyd	Hyd	0.85	0.15	Orogenic gold	IOCG	0.01	0.43	0.24	0.13	0.06	0.11
Naa-rim-032			Hyd	Hyd	0.88	0.12	Orogenic gold	IOCG	0.02	0.41	0.27	0.11	0.04	0.15
Naa-c-024			Hyd	Hyd	0.62	0.38	Orogenic gold	IOCG	0.05	0.30	0.10	0.10	0.16	0.29
Naa-core-020			Hyd	Hyd	0.67	0.33	Orogenic gold	Skarn	0.03	0.25	0.09	0.15	0.33	0.16
Hir-Strong Au-05			Hyd	Hyd	0.97	0.03	Orogenic gold	IOCG	0.02	0.36	0.14	0.33	0.07	0.08
Naa-core-022			Hyd	Hyd	0.87	0.13	Orogenic gold	Orogenic gold	0.01	0.26	0.33	0.05	0.14	0.21
19-7-1 spot7	Wang et al. (2018)	Kairei	Hyd	Hyd	0.53	0.47	VMS	VMS	0.05	0.08	0.03	0.06	0.02	0.76
19-6-1 spot1			Hyd	Hyd	0.78	0.22	VMS	VMS	0.02	0.06	0.03	0.06	0.18	0.66
19-7-1 spot6			Hyd	Hyd	0.88	0.12	VMS	VMS	0.02	0.04	0.01	0.06	0.06	0.80
19-7-1 spot1			Hyd	Hyd	0.76	0.24	VMS	VMS	0.03	0.05	0.02	0.08	0.04	0.78
19-6-1 spot2			Hyd	Hyd	0.99	0.01	VMS	VMS	0.02	0.04	0.01	0.03	0.05	0.85
17-7-3 spot6			Hyd	Hyd	0.84	0.16	VMS	Porphyry	0.12	0.16	0.03	0.39	0.02	0.29

			RF mag-hyd model				RF hyd model							
			Actual	Predicted	Prob		Actual	Predicted	Prob					
ID	Author	Deposit			Hyd	Mag			Epithermal gold	IOCG	Orogenic gold	Porphyry	Skarn	VMS
17-7-3 spot3	Wang et al. (2018)	Kairei	Hyd	Hyd	0.55	0.45	VMS	VMS	0.09	0.15	0.03	0.36	0.01	0.36
17-7-3 spot1			Hyd	Hyd	0.51	0.49	VMS	Porphyry	0.12	0.22	0.01	0.47	0.02	0.16
17-7-1D spot7			Hyd	Hyd	0.54	0.46	VMS	VMS	0.07	0.17	0.03	0.06	0.07	0.60
17-7-1D spot5			Hyd	Hyd	0.63	0.37	VMS	VMS	0.04	0.27	0.04	0.10	0.14	0.42
19-6-1 spot8			Hyd	Mag	0.41	0.59	VMS	VMS	0.02	0.07	0.01	0.08	0.06	0.75
19-6-1 spot4			Hyd	Hyd	0.84	0.16	VMS	VMS	0.01	0.12	0.04	0.11	0.14	0.59
17-7-1D spot4			Hyd	Hyd	0.98	0.02	VMS	VMS	0.06	0.11	0.01	0.06	0.05	0.71
17-7-1D spot8			Hyd	Hyd	0.74	0.26	VMS	VMS	0.02	0.33	0.07	0.08	0.13	0.36
17-7-1D spot1			Hyd	Hyd	0.65	0.35	VMS	VMS	0.07	0.08	0.02	0.05	0.06	0.72
19-6-1 spot3			Hyd	Mag	0.46	0.54	VMS	VMS	0.01	0.08	0.03	0.08	0.11	0.69
69RD(164-167)-11	Wohlgemuth-Ueberwasser et al. (2015)	Roman Ruins	Hyd	Hyd	0.99	0.01	VMS	Orogenic gold	0.01	0.37	0.38	0.03	0.07	0.15
69RD(164-167)-10			Hyd	Hyd	0.95	0.05	VMS	IOCG	0.11	0.60	0.10	0.05	0.04	0.11
69RD(38-42)-8			Hyd	Hyd	0.99	0.01	VMS	VMS	0.00	0.05	0.03	0.01	0.28	0.63
60RD(69-73)-5			Hyd	Hyd	0.99	0.01	VMS	VMS	0.00	0.41	0.01	0.06	0.05	0.48
69RD(164-167)-21			Hyd	Hyd	0.84	0.16	VMS	IOCG	0.04	0.46	0.33	0.05	0.03	0.09
66RD(26-30)-5			Hyd	Hyd	1.00	0.00	VMS	VMS	0.00	0.03	0.00	0.00	0.00	0.96
65RD(42-45)-4			Hyd	Hyd	0.98	0.02	VMS	VMS	0.01	0.20	0.08	0.04	0.07	0.61
65RD(42-45)-11			Hyd	Hyd	0.97	0.03	VMS	IOCG	0.02	0.46	0.10	0.06	0.14	0.22
58GTV6G-1			Hyd	Hyd	0.99	0.01	VMS	IOCG	0.18	0.36	0.15	0.03	0.17	0.11
65RD(42-45)-1			Hyd	Hyd	0.99	0.01	VMS	IOCG	0.01	0.54	0.04	0.04	0.04	0.34
66RD(74-77)-3			Hyd	Hyd	0.99	0.01	VMS	IOCG	0.04	0.46	0.28	0.01	0.02	0.19
66RD(74-77)-1			Hyd	Hyd	0.99	0.01	VMS	IOCG	0.04	0.46	0.28	0.01	0.02	0.19
69RD(164-167)-12			Hyd	Hyd	1.00	0.00	VMS	IOCG	0.05	0.59	0.12	0.04	0.06	0.15
69RD(75-79)-7			Hyd	Hyd	1.00	0.00	VMS	VMS	0.01	0.06	0.00	0.02	0.01	0.91
66RD(26-30)-6			Hyd	Hyd	1.00	0.00	VMS	IOCG	0.07	0.42	0.37	0.01	0.03	0.10
65RD(42-45)-10			Hyd	Hyd	0.99	0.01	VMS	VMS	0.00	0.02	0.00	0.00	0.01	0.97

			RF mag-hyd model				RF hyd model							
			Actual	Predicted	Prob		Actual	Predicted	Prob					
ID	Author	Deposit			Hyd	Mag			Epithermal gold	IOCG	Orogenic gold	Porphyry	Skarn	VMS
65RD(42-45)-6	Wohlgemuth-Ueberwasser et al. (2015)	Roman Ruins	Hyd	Hyd	1.00	0.00	VMS	Epithermal gold	0.72	0.05	0.14	0.02	0.01	0.05
65RD(42-45)-8			Hyd	Hyd	1.00	0.00	VMS	Epithermal gold	0.69	0.03	0.22	0.02	0.01	0.02
66RD(74-77)-5			Hyd	Hyd	0.99	0.01	VMS	Epithermal gold	0.69	0.07	0.17	0.02	0.04	0.01
66RD(26-30)-3			Hyd	Hyd	1.00	0.00	VMS	VMS	0.06	0.11	0.01	0.08	0.03	0.70
66RD(74-77)-8			Hyd	Hyd	1.00	0.00	VMS	VMS	0.05	0.11	0.14	0.11	0.05	0.55
66RD(26-30)-1			Hyd	Hyd	1.00	0.00	VMS	Epithermal gold	0.48	0.18	0.05	0.07	0.11	0.10
65RD(42-45)-3			Hyd	Hyd	1.00	0.00	VMS	VMS	0.01	0.02	0.02	0.03	0.01	0.92
66RD(26-30)-8			Hyd	Hyd	1.00	0.00	VMS	VMS	0.07	0.10	0.04	0.02	0.06	0.71
65RD(42-45)-7			Hyd	Hyd	1.00	0.00	VMS	VMS	0.01	0.02	0.02	0.03	0.01	0.92
66RD(26-30)-12			Hyd	Hyd	1.00	0.00	VMS	Epithermal gold	0.55	0.06	0.15	0.02	0.03	0.18
953GC(79)-3			Hyd	Hyd	1.00	0.00	VMS	VMS	0.01	0.03	0.02	0.03	0.01	0.92
65RD(42-45)-2			Hyd	Hyd	1.00	0.00	VMS	VMS	0.08	0.02	0.01	0.08	0.00	0.81
58GTV6G-5			Hyd	Hyd	1.00	0.00	VMS	VMS	0.17	0.15	0.12	0.03	0.10	0.42
66RD(26-30)-7			Hyd	Hyd	0.99	0.01	VMS	Orogenic gold	0.08	0.09	0.79	0.01	0.01	0.02
65RD(42-45)-9			Hyd	Hyd	0.97	0.03	VMS	VMS	0.03	0.10	0.02	0.05	0.04	0.77
60RD(30-33)-7			Hyd	Hyd	0.91	0.09	VMS	Epithermal gold	0.54	0.04	0.19	0.09	0.02	0.11
58GTV6G-4			Hyd	Hyd	1.00	0.00	VMS	Orogenic gold	0.04	0.03	0.89	0.01	0.02	0.01
60RD(30-33)-6			Hyd	Hyd	1.00	0.00	VMS	Orogenic gold	0.04	0.01	0.92	0.01	0.01	0.01
66RD(26-30)-2			Hyd	Hyd	0.97	0.03	VMS	IOCG	0.01	0.30	0.18	0.27	0.17	0.07
65RD(42-45)-12			Hyd	Hyd	0.98	0.02	VMS	Orogenic gold	0.22	0.13	0.27	0.11	0.09	0.17
65RD(42-45)-13			Hyd	Hyd	0.99	0.01	VMS	VMS	0.04	0.09	0.11	0.12	0.04	0.60
953GC(79)-2			Hyd	Hyd	1.00	0.00	VMS	VMS	0.03	0.21	0.10	0.04	0.06	0.57
66RD(26-30)-4			Hyd	Hyd	1.00	0.00	VMS	VMS	0.01	0.05	0.06	0.01	0.04	0.84
65RD(19-23)-4			Hyd	Hyd	1.00	0.00	VMS	VMS	0.00	0.00	0.00	0.00	0.00	1.00
66RD(26-30)-11			Hyd	Hyd	1.00	0.00	VMS	VMS	0.01	0.01	0.02	0.00	0.02	0.94
66RD(26-30)-9			Hyd	Hyd	1.00	0.00	VMS	Epithermal gold	0.34	0.08	0.26	0.05	0.01	0.26

			RF mag-hyd model				RF hyd model							
			Actual	Predicted	Prob		Actual	Predicted	Prob					
ID	Author	Deposit			Hyd	Mag			Epithermal gold	IOCG	Orogenic gold	Porphyry	Skarn	VMS
58GTV7H-5	Wohlgemuth-Ueberwasser et al. (2015)	Roman Ruins	Hyd	Hyd	0.99	0.01	VMS	VMS	0.02	0.05	0.08	0.04	0.02	0.79
60RD(30-33)-10			Hyd	Hyd	0.99	0.01	VMS	VMS	0.02	0.05	0.08	0.04	0.02	0.79
60RD(30-33)-9			Hyd	Hyd	1.00	0.00	VMS	VMS	0.01	0.19	0.13	0.02	0.03	0.62
69RD(38-42)-12			Hyd	Hyd	1.00	0.00	VMS	VMS	0.03	0.07	0.15	0.02	0.02	0.71
69RD(164-167)-13			Hyd	Hyd	1.00	0.00	VMS	VMS	0.01	0.05	0.15	0.01	0.02	0.76
58GTV7H-2			Hyd	Hyd	1.00	0.00	VMS	VMS	0.00	0.01	0.04	0.00	0.01	0.94
66RD(74-77)-9			Hyd	Hyd	1.00	0.00	VMS	VMS	0.00	0.01	0.04	0.00	0.01	0.94
60RD(30-33)-8			Hyd	Hyd	1.00	0.00	VMS	VMS	0.06	0.01	0.03	0.00	0.00	0.89
66RD(26-30)-10			Hyd	Hyd	1.00	0.00	VMS	VMS	0.03	0.06	0.06	0.01	0.02	0.82
66RD(74-77)-10			Hyd	Hyd	1.00	0.00	VMS	VMS	0.00	0.01	0.01	0.00	0.01	0.96
58GTV7H-1			Hyd	Hyd	1.00	0.00	VMS	VMS	0.00	0.01	0.05	0.02	0.02	0.90
953GC(79)-1			Hyd	Hyd	1.00	0.00	VMS	VMS	0.01	0.01	0.01	0.01	0.00	0.97
65RD(19-23)-1			Hyd	Hyd	0.96	0.04	VMS	VMS	0.07	0.21	0.07	0.07	0.07	0.52
69RD(38-42)-5			Hyd	Hyd	1.00	0.00	VMS	VMS	0.12	0.06	0.08	0.05	0.00	0.69
58GTV6G-14			Hyd	Hyd	1.00	0.00	VMS	VMS	0.01	0.02	0.07	0.04	0.01	0.85
953GC(79)-4			Hyd	Hyd	1.00	0.00	VMS	VMS	0.00	0.01	0.02	0.01	0.00	0.96
953GC(79)-5			Hyd	Hyd	1.00	0.00	VMS	VMS	0.10	0.01	0.01	0.05	0.06	0.76
58GTV6G-15			Hyd	Hyd	0.99	0.01	VMS	VMS	0.01	0.01	0.11	0.00	0.00	0.87
69RD(75-79)-8			Hyd	Hyd	0.99	0.01	VMS	VMS	0.01	0.01	0.10	0.00	0.01	0.87
58GTV7H-4			Hyd	Hyd	0.99	0.01	VMS	VMS	0.01	0.01	0.10	0.00	0.01	0.87
65RD(19-23)-5			Hyd	Hyd	0.99	0.01	VMS	VMS	0.01	0.01	0.10	0.00	0.01	0.87
58GTV7H-3			Hyd	Hyd	1.00	0.00	VMS	VMS	0.00	0.01	0.01	0.00	0.00	0.98
69RD(38-42)-11			Hyd	Hyd	1.00	0.00	VMS	VMS	0.13	0.06	0.08	0.05	0.00	0.68
69RD(75-79)-15			Hyd	Hyd	1.00	0.00	VMS	VMS	0.02	0.05	0.09	0.02	0.01	0.81
69RD(164-167)-15			Hyd	Hyd	1.00	0.00	VMS	VMS	0.12	0.06	0.08	0.05	0.00	0.69
65RD(19-23)-12			Hyd	Hyd	1.00	0.00	VMS	VMS	0.00	0.01	0.02	0.00	0.01	0.96

			RF mag-hyd model				RF hyd model							
			Actual	Predicted	Prob		Actual	Predicted	Prob					
ID	Author	Deposit			Hyd	Mag			Epithermal gold	IOCG	Orogenic gold	Porphyry	Skarn	VMS
65RD(19-23)-3	Wohlgemuth-Ueberwasser et al. (2015)	Roman Ruins	Hyd	Hyd	0.99	0.01	VMS	VMS	0.01	0.03	0.04	0.02	0.03	0.88
69RD(75-79)-10			Hyd	Hyd	0.99	0.01	VMS	VMS	0.04	0.04	0.01	0.09	0.01	0.82
69RD(164-167)-14			Hyd	Hyd	0.99	0.01	VMS	VMS	0.12	0.06	0.08	0.05	0.00	0.68
23ROV12C-2			Hyd	Hyd	1.00	0.00	VMS	VMS	0.00	0.01	0.01	0.02	0.00	0.96
65RD(19-23)-10			Hyd	Hyd	0.99	0.01	VMS	VMS	0.04	0.07	0.03	0.26	0.03	0.57
69RD(75-79)-14			Hyd	Hyd	1.00	0.00	VMS	VMS	0.02	0.03	0.30	0.01	0.01	0.63
23ROV12C-3			Hyd	Hyd	1.00	0.00	VMS	Porphyry	0.02	0.04	0.02	0.85	0.01	0.05
23ROV12C-1			Hyd	Hyd	1.00	0.00	VMS	VMS	0.01	0.01	0.02	0.01	0.00	0.95
58GTV5F-15			Hyd	Hyd	1.00	0.00	VMS	VMS	0.01	0.01	0.02	0.01	0.00	0.95
69RD(75-79)-9			Hyd	Hyd	1.00	0.00	VMS	VMS	0.02	0.01	0.02	0.01	0.00	0.95
58GTV5F-16			Hyd	Hyd	1.00	0.00	VMS	VMS	0.02	0.01	0.02	0.01	0.00	0.95
23ROV12C-4			Hyd	Hyd	1.00	0.00	VMS	VMS	0.00	0.02	0.01	0.01	0.00	0.96
58GTV5F-22			Hyd	Hyd	1.00	0.00	VMS	VMS	0.02	0.01	0.02	0.01	0.00	0.95
69RD(75-79)-21			Hyd	Hyd	1.00	0.00	VMS	VMS	0.02	0.01	0.02	0.01	0.00	0.95
69RD(75-79)-23			Hyd	Hyd	1.00	0.00	VMS	VMS	0.02	0.01	0.02	0.01	0.00	0.95
69RD(75-79)-24			Hyd	Hyd	1.00	0.00	VMS	VMS	0.02	0.01	0.02	0.01	0.00	0.95
69RD(75-79)-25			Hyd	Hyd	1.00	0.00	VMS	VMS	0.02	0.01	0.02	0.01	0.00	0.95
58GTV5F-23			Hyd	Hyd	1.00	0.00	VMS	VMS	0.02	0.01	0.02	0.01	0.00	0.95
65RD(19-23)-11			Hyd	Hyd	0.99	0.01	VMS	VMS	0.08	0.23	0.13	0.05	0.06	0.46
58GTV6G-3			Hyd	Hyd	1.00	0.00	VMS	VMS	0.04	0.07	0.14	0.01	0.04	0.69
69RD(38-42)-6			Hyd	Hyd	1.00	0.00	VMS	VMS	0.04	0.23	0.06	0.05	0.08	0.54
65RD(19-23)-2			Hyd	Hyd	0.99	0.01	VMS	Skarn	0.02	0.22	0.08	0.07	0.33	0.28
60RD(69-73)-4			Hyd	Hyd	1.00	0.00	VMS	VMS	0.00	0.01	0.00	0.00	0.00	0.98
60RD(69-73)-2			Hyd	Hyd	0.99	0.01	VMS	VMS	0.01	0.20	0.02	0.17	0.01	0.59
65RD(42-45)-5			Hyd	Hyd	1.00	0.00	VMS	VMS	0.08	0.20	0.22	0.06	0.06	0.38
58GTV5F-6			Hyd	Hyd	1.00	0.00	VMS	VMS	0.01	0.03	0.04	0.06	0.01	0.85

			RF mag-hyd model				RF hyd model							
			Actual	Predicted	Prob		Actual	Predicted	Prob					
ID	Author	Deposit			Hyd	Mag			Epithermal gold	IOCG	Orogenic gold	Porphyry	Skarn	VMS
139GTV2F3-16	Wohlgemuth-Ueberwasser et al. (2015)	Roman Ruins	Hyd	Hyd	0.99	0.01	VMS	VMS	0.02	0.02	0.01	0.03	0.23	0.69
23ROV12C-5			Hyd	Hyd	0.99	0.01	VMS	VMS	0.01	0.02	0.06	0.04	0.02	0.85
139GTV2F3-17			Hyd	Mag	0.02	0.98	VMS	VMS	0.01	0.05	0.01	0.08	0.01	0.84
58GTV5F-7			Hyd	Hyd	1.00	0.00	VMS	VMS	0.06	0.02	0.01	0.07	0.02	0.82
139GTV2F3-12			Hyd	Mag	0.26	0.74	VMS	VMS	0.00	0.03	0.01	0.02	0.02	0.93
60RD(69-73)-1			Hyd	Hyd	0.86	0.14	VMS	VMS	0.00	0.05	0.02	0.01	0.00	0.91
139GTV5E2-10			Hyd	Hyd	1.00	0.00	VMS	VMS	0.00	0.09	0.00	0.08	0.05	0.78
60RD(69-73)-17			Hyd	Hyd	0.99	0.01	VMS	VMS	0.00	0.01	0.00	0.00	0.00	0.98
139GTV2F3-13			Hyd	Hyd	1.00	0.00	VMS	VMS	0.00	0.04	0.03	0.03	0.02	0.88
139GTV5E2-8			Hyd	Hyd	0.56	0.44	VMS	Skarn	0.00	0.24	0.02	0.04	0.38	0.32
60RD(69-73)-3			Hyd	Hyd	1.00	0.00	VMS	VMS	0.09	0.04	0.04	0.26	0.04	0.54
58GTV5F-14			Hyd	Hyd	1.00	0.00	VMS	VMS	0.02	0.01	0.05	0.02	0.03	0.87
139GTV2F3-14			Hyd	Hyd	0.98	0.02	VMS	Porphyry	0.02	0.04	0.00	0.89	0.00	0.04
139GTV2F3-15			Hyd	Hyd	1.00	0.00	VMS	VMS	0.01	0.00	0.01	0.25	0.01	0.72
139GTV5E2-6			Hyd	Hyd	0.99	0.01	VMS	VMS	0.04	0.08	0.01	0.15	0.01	0.72
58GTV5F-13			Hyd	Hyd	1.00	0.00	VMS	VMS	0.02	0.02	0.03	0.01	0.00	0.93
139GTV2F3-20			Hyd	Hyd	0.99	0.01	VMS	VMS	0.01	0.14	0.03	0.18	0.11	0.53
58GTV5F-8			Hyd	Hyd	1.00	0.00	VMS	VMS	0.02	0.01	0.02	0.01	0.00	0.95
139GTV2F3-11			Hyd	Hyd	0.99	0.01	VMS	VMS	0.00	0.12	0.00	0.06	0.04	0.77
58GTV5F-11			Hyd	Hyd	1.00	0.00	VMS	VMS	0.02	0.01	0.02	0.01	0.00	0.95
58GTV5F-12			Hyd	Hyd	1.00	0.00	VMS	VMS	0.02	0.01	0.02	0.01	0.00	0.95
64ROV11D2-13			Hyd	Hyd	1.00	0.00	VMS	Porphyry	0.01	0.05	0.04	0.60	0.02	0.28
58GTV5F-9			Hyd	Hyd	1.00	0.00	VMS	VMS	0.01	0.01	0.04	0.01	0.00	0.93
58GTV5F-5			Hyd	Hyd	1.00	0.00	VMS	VMS	0.01	0.01	0.04	0.01	0.00	0.93
58GTV5F-10			Hyd	Hyd	1.00	0.00	VMS	Porphyry	0.03	0.04	0.01	0.83	0.00	0.07
139GTV5E2-7			Hyd	Mag	0.19	0.81	VMS	Porphyry	0.01	0.01	0.00	0.98	0.00	0.00

ID	Author	Deposit	Actual	Predicted	Prob		Actual	Predicted	Prob					
					Hyd	Mag			Epithermal gold	IOCG	Orogenic gold	Porphyry	Skarn	VMS
64ROV11D2-30	Wohlgemuth-Ueberwasser et al. (2015)	Roman Ruins	Hyd	Hyd	1.00	0.00	VMS	VMS	0.01	0.02	0.01	0.01	0.04	0.91
139GTV5E2-9			Hyd	Hyd	1.00	0.00	VMS	VMS	0.00	0.01	0.00	0.01	0.00	0.98
139GTV2F3-18			Hyd	Hyd	1.00	0.00	VMS	VMS	0.02	0.14	0.03	0.30	0.04	0.48
139GTV2F3-19			Hyd	Hyd	0.99	0.01	VMS	VMS	0.02	0.03	0.03	0.43	0.02	0.47
60RD(69-73)-16			Hyd	Hyd	1.00	0.00	VMS	VMS	0.02	0.08	0.07	0.18	0.04	0.62
64ROV11D2-31			Hyd	Hyd	1.00	0.00	VMS	VMS	0.05	0.21	0.02	0.15	0.05	0.52
64ROV11D2-29			Hyd	Hyd	1.00	0.00	VMS	VMS	0.01	0.07	0.00	0.01	0.05	0.84
962RD(3)-10			Hyd	Hyd	1.00	0.00	VMS	VMS	0.01	0.08	0.02	0.01	0.03	0.85
64ROV11D2-1			Hyd	Hyd	1.00	0.00	VMS	VMS	0.01	0.05	0.02	0.01	0.04	0.88
64ROV11D2-10			Hyd	Hyd	0.99	0.01	VMS	VMS	0.00	0.04	0.01	0.01	0.06	0.88
962RD(3)-6			Hyd	Hyd	1.00	0.00	VMS	VMS	0.00	0.01	0.00	0.00	0.01	0.98
64ROV11D2-9			Hyd	Hyd	1.00	0.00	VMS	VMS	0.02	0.06	0.00	0.01	0.10	0.80
64ROV11D2-2			Hyd	Hyd	0.95	0.05	VMS	VMS	0.00	0.03	0.01	0.01	0.03	0.92
64ROV11D2-8			Hyd	Hyd	1.00	0.00	VMS	VMS	0.01	0.17	0.02	0.01	0.10	0.69
962RD(3)-8			Hyd	Hyd	0.98	0.02	VMS	VMS	0.00	0.04	0.01	0.01	0.06	0.88
962RD(3)-7			Hyd	Hyd	1.00	0.00	VMS	IOCG	0.00	0.61	0.00	0.01	0.02	0.35
962RD(3)-9			Hyd	Hyd	1.00	0.00	VMS	VMS	0.02	0.04	0.02	0.01	0.03	0.88
64ROV11D2-4			Hyd	Hyd	1.00	0.00	VMS	VMS	0.00	0.37	0.01	0.02	0.07	0.52
64ROV11D2-7			Hyd	Hyd	1.00	0.00	VMS	VMS	0.02	0.09	0.01	0.05	0.02	0.80
64ROV11D2-3			Hyd	Hyd	1.00	0.00	VMS	VMS	0.01	0.12	0.01	0.01	0.12	0.72
64ROV11D2-6			Hyd	Hyd	0.99	0.01	VMS	VMS	0.00	0.13	0.02	0.01	0.11	0.73
64ROV11D2-5			Hyd	Hyd	0.99	0.01	VMS	VMS	0.00	0.13	0.02	0.01	0.11	0.73
ZK18-1<96>3-05	Xie et al. (2020)	Fenghuangshan	Hyd	Hyd	0.98	0.02	Skarn	IOCG	0.03	0.35	0.12	0.07	0.09	0.34
ZK18-1<96>3-06			Hyd	Hyd	1.00	0.00	Skarn	Skarn	0.23	0.19	0.10	0.02	0.27	0.19
ZK18-1<96>3-11			Hyd	Hyd	0.95	0.05	Skarn	IOCG	0.06	0.35	0.17	0.04	0.23	0.15
ZK18-1<96>3-12			Hyd	Hyd	0.97	0.03	Skarn	VMS	0.03	0.26	0.08	0.07	0.19	0.38

ID	Author	Deposit	Actual	Predicted	Prob		Actual	Predicted	Prob					
					Hyd	Mag			Epithermal gold	IOCG	Orogenic gold	Porphyry	Skarn	VMS
ZK18-1<96>3-15	Xie et al. (2020)	Fenghuang shan	Hyd	Hyd	0.99	0.01	Skarn	VMS	0.03	0.24	0.14	0.03	0.07	0.50
ZK18-1<96>3-16			Hyd	Hyd	1.00	0.00	Skarn	IOCG	0.07	0.43	0.15	0.13	0.03	0.19
ZK18-1<96>13-02			Hyd	Hyd	1.00	0.00	Skarn	Orogenic gold	0.10	0.34	0.36	0.05	0.03	0.12
ZK18-1<96>13-03			Hyd	Hyd	0.99	0.01	Skarn	IOCG	0.09	0.32	0.18	0.03	0.07	0.30
ZK18-1<96>13-04			Hyd	Hyd	0.83	0.17	Skarn	VMS	0.04	0.21	0.10	0.08	0.07	0.50
ZK18-1<96>13-06			Hyd	Hyd	0.97	0.03	Skarn	VMS	0.05	0.23	0.22	0.04	0.15	0.31
ZK18-2<96>11-03			Hyd	Hyd	0.99	0.01	Skarn	IOCG	0.05	0.37	0.07	0.35	0.08	0.08
ZK18-2<96>11-04			Hyd	Hyd	0.99	0.01	Skarn	VMS	0.04	0.25	0.07	0.11	0.14	0.39
ZK18-2<96>11-05			Hyd	Hyd	1.00	0.00	Skarn	VMS	0.15	0.11	0.08	0.07	0.27	0.31
ZK18-2<96>11-06			Hyd	Hyd	0.98	0.02	Skarn	IOCG	0.06	0.38	0.33	0.03	0.03	0.16
ZK18-3<96>8-01			Hyd	Hyd	1.00	0.00	Skarn	Skarn	0.22	0.23	0.12	0.02	0.24	0.17
ZK18-3<96>8-02			Hyd	Hyd	1.00	0.00	Skarn	IOCG	0.09	0.43	0.19	0.13	0.03	0.13
ZK18-3<96>8-03			Hyd	Hyd	0.96	0.04	Skarn	Skarn	0.07	0.19	0.12	0.11	0.29	0.21
ZK18-3<96>8-04			Hyd	Hyd	0.98	0.02	Skarn	IOCG	0.11	0.33	0.21	0.02	0.22	0.12
ZK18-3<96>8-06			Hyd	Hyd	1.00	0.00	Skarn	IOCG	0.11	0.33	0.15	0.10	0.12	0.20
ZK18-7<96>15-01			Hyd	Hyd	1.00	0.00	Skarn	Skarn	0.25	0.17	0.12	0.01	0.27	0.17
ZK18-7<96>15-02			Hyd	Hyd	0.98	0.02	Skarn	IOCG	0.07	0.42	0.12	0.24	0.04	0.12
ZK18-7<96>15-03			Hyd	Hyd	1.00	0.00	Skarn	IOCG	0.15	0.35	0.32	0.05	0.02	0.11
ZK18-7<96>15-04			Hyd	Hyd	1.00	0.00	Skarn	Skarn	0.14	0.20	0.07	0.07	0.26	0.26
ZK18-7<96>15-05			Hyd	Hyd	0.99	0.01	Skarn	Skarn	0.10	0.20	0.10	0.03	0.36	0.19
ZK18-7<96>15-06			Hyd	Hyd	0.99	0.01	Skarn	Skarn	0.14	0.13	0.06	0.05	0.39	0.23
LCK18-34<96>07			Hyd	Hyd	0.97	0.03	Skarn	VMS	0.17	0.24	0.16	0.04	0.15	0.25
LCK18-34<96>08			Hyd	Hyd	0.99	0.01	Skarn	Skarn	0.22	0.18	0.10	0.04	0.27	0.20
LCK18-34<96>09			Hyd	Hyd	0.98	0.02	Skarn	IOCG	0.03	0.37	0.12	0.11	0.07	0.30
ZYK-1<96>01			Hyd	Hyd	0.98	0.02	Skarn	Skarn	0.17	0.17	0.09	0.05	0.31	0.20
ZYK-1<96>02			Hyd	Hyd	1.00	0.00	Skarn	IOCG	0.07	0.39	0.19	0.13	0.05	0.17

ID	Author	Deposit	Actual	Predicted	Prob		Actual	Predicted	Prob					
					Hyd	Mag			Epithermal gold	IOCG	Orogenic gold	Porphyry	Skarn	VMS
304-121-1cpy - 4.d	Yu et al. (2022)	Tianshan	Hyd	Hyd	0.95	0.05	Porphyry	Porphyry	0.01	0.37	0.02	0.50	0.03	0.07
304-121-1cpy - 5.d			Hyd	Hyd	0.95	0.05	Porphyry	Porphyry	0.07	0.11	0.13	0.49	0.13	0.06
304-121-1cpy - 6.d			Hyd	Hyd	0.96	0.04	Porphyry	Porphyry	0.02	0.18	0.16	0.58	0.03	0.03
304-121-1cpy - 7.d			Hyd	Hyd	0.98	0.02	Porphyry	Porphyry	0.01	0.24	0.08	0.59	0.07	0.02
504-11-1cpy - 1.d			Hyd	Hyd	0.95	0.05	Porphyry	Porphyry	0.05	0.09	0.36	0.39	0.09	0.02
504-11-1cpy - 2.d			Hyd	Hyd	0.92	0.08	Porphyry	Porphyry	0.10	0.14	0.08	0.53	0.10	0.05
504-11-1cpy - 3.d			Hyd	Hyd	0.87	0.13	Porphyry	Porphyry	0.00	0.20	0.02	0.68	0.07	0.02
504-11-1cpy - 4.d			Hyd	Hyd	0.98	0.02	Porphyry	Porphyry	0.01	0.17	0.08	0.64	0.07	0.03
504-11-1cpy - 5.d			Hyd	Hyd	0.82	0.18	Porphyry	Porphyry	0.02	0.15	0.12	0.63	0.07	0.02
504-22-1cpy - 2.d			Hyd	Hyd	0.95	0.05	Porphyry	IOCG	0.01	0.79	0.03	0.15	0.01	0.01
504-22-1cpy - 3.d			Hyd	Hyd	0.98	0.02	Porphyry	Porphyry	0.03	0.22	0.20	0.35	0.17	0.03
504-22-1cpy - 4.d			Hyd	Hyd	0.91	0.09	Porphyry	Porphyry	0.05	0.16	0.07	0.59	0.06	0.07
504-22-1cpy - 5.d			Hyd	Hyd	0.89	0.11	Porphyry	Porphyry	0.05	0.18	0.19	0.45	0.08	0.04
302-83-1cpy - 1.d*			Hyd	Hyd	0.95	0.05	Porphyry	Porphyry	0.03	0.35	0.09	0.39	0.03	0.12
302-83-1cpy - 2.d*			Hyd	Hyd	0.96	0.04	Porphyry	Porphyry	0.03	0.06	0.13	0.64	0.07	0.06
302-83-1cpy - 3.d*			Hyd	Hyd	0.94	0.06	Porphyry	Orogenic gold	0.04	0.09	0.47	0.35	0.03	0.02
302-83-1cpy - 4.d*			Hyd	Hyd	0.94	0.06	Porphyry	Porphyry	0.01	0.33	0.13	0.43	0.06	0.04
302-83-1cpy - 5.d*			Hyd	Hyd	0.96	0.04	Porphyry	IOCG	0.02	0.57	0.06	0.23	0.08	0.05
302-83-1cpy - 6.d*			Hyd	Hyd	0.95	0.05	Porphyry	Orogenic gold	0.01	0.25	0.42	0.22	0.04	0.06
302-83-1cpy - 7.d*			Hyd	Hyd	0.95	0.05	Porphyry	Porphyry	0.02	0.07	0.15	0.56	0.18	0.02
302-83-4cpy - 1.d			Hyd	Hyd	0.94	0.06	Porphyry	Porphyry	0.02	0.12	0.11	0.61	0.10	0.03
302-83-4cpy - 2.d			Hyd	Hyd	0.89	0.11	Porphyry	Porphyry	0.08	0.13	0.21	0.49	0.04	0.05
504-26-1cpy - 2.d			Hyd	Hyd	0.91	0.09	Porphyry	Porphyry	0.01	0.17	0.12	0.59	0.05	0.06
504-26-1cpy - 3.d			Hyd	Mag	0.48	0.52	Porphyry	IOCG	0.03	0.67	0.02	0.22	0.02	0.04
504-26-1cpy - 4.d			Hyd	Hyd	0.94	0.06	Porphyry	Porphyry	0.03	0.10	0.13	0.50	0.23	0.01
504-26-1cpy - 5.d			Hyd	Hyd	0.84	0.16	Porphyry	Porphyry	0.04	0.11	0.08	0.58	0.18	0.01
504-26-1cpy - 6.d			Hyd	Hyd	0.96	0.04	Porphyry	Porphyry	0.02	0.06	0.21	0.53	0.18	0.01

ID	Author	Deposit	Actual	Predicted	Prob		Actual	Predicted	Prob					
					Hyd	Mag			Epithermal gold	IOCG	Orogenic gold	Porphyry	Skarn	VMS
504-26-1cpy - 7.d	Yu et al. (2022)	Tianshan	Hyd	Hyd	0.96	0.04	Porphyry	IOCG	0.02	0.36	0.17	0.35	0.05	0.06
504-26-1cpy - 8.d			Hyd	Hyd	0.96	0.04	Porphyry	IOCG	0.02	0.53	0.08	0.24	0.09	0.04
504-26-1cpy - 9.d			Hyd	Hyd	0.91	0.09	Porphyry	Porphyry	0.01	0.27	0.06	0.55	0.09	0.02
504-26-1cpy - 10.d			Hyd	Hyd	0.94	0.06	Porphyry	IOCG	0.02	0.69	0.05	0.14	0.05	0.04
302-83-2cpy - 3.d			Hyd	Hyd	0.96	0.04	Porphyry	Porphyry	0.03	0.06	0.14	0.69	0.05	0.03
302-83-2cpy - 4.d			Hyd	Hyd	0.97	0.03	Porphyry	Porphyry	0.04	0.04	0.11	0.76	0.03	0.02
302-83-2cpy - 5.d			Hyd	Hyd	0.97	0.03	Porphyry	Orogenic gold	0.03	0.04	0.49	0.35	0.09	0.01
302-83-2cpy - 6.d			Hyd	Hyd	0.97	0.03	Porphyry	Porphyry	0.11	0.04	0.26	0.55	0.02	0.02
302-83-2cpy - 7.d			Hyd	Hyd	0.92	0.08	Porphyry	Porphyry	0.01	0.15	0.04	0.71	0.06	0.02
302-83-3cpy - 1.d			Hyd	Hyd	0.98	0.02	Porphyry	Porphyry	0.12	0.10	0.16	0.43	0.04	0.15
302-83-3cpy - 2.d			Hyd	Hyd	0.97	0.03	Porphyry	Porphyry	0.05	0.04	0.17	0.63	0.08	0.03
302-83-3cpy - 3.d			Hyd	Hyd	0.97	0.03	Porphyry	Porphyry	0.03	0.05	0.15	0.69	0.06	0.03
302-83-3cpy - 4.d			Hyd	Hyd	0.95	0.05	Porphyry	Porphyry	0.01	0.02	0.06	0.83	0.07	0.00
103-18-1cpy - 1.d			Hyd	Hyd	0.96	0.04	Porphyry	Porphyry	0.02	0.08	0.31	0.51	0.05	0.03
103-18-1cpy - 2.d			Hyd	Hyd	0.98	0.02	Porphyry	Porphyry	0.02	0.09	0.27	0.52	0.04	0.06
103-18-1cpy - 3.d			Hyd	Hyd	0.95	0.05	Porphyry	Porphyry	0.04	0.35	0.16	0.35	0.01	0.09
103-18-1cpy - 4.d			Hyd	Hyd	0.98	0.02	Porphyry	Porphyry	0.04	0.06	0.15	0.64	0.08	0.03
103-18-1cpy - 5.d			Hyd	Hyd	0.96	0.04	Porphyry	Porphyry	0.01	0.10	0.17	0.65	0.05	0.03
103-23-2cpy - 1.d			Hyd	Hyd	0.96	0.04	Porphyry	Porphyry	0.03	0.10	0.19	0.55	0.10	0.03
103-23-2cpy - 2.d			Hyd	Hyd	0.99	0.01	Porphyry	Porphyry	0.04	0.04	0.15	0.66	0.07	0.04
103-23-2cpy - 3.d			Hyd	Hyd	0.94	0.06	Porphyry	IOCG	0.02	0.34	0.23	0.30	0.07	0.03
103-23-2cpy - 4.d			Hyd	Hyd	0.85	0.15	Porphyry	Porphyry	0.03	0.12	0.15	0.60	0.06	0.03
103-23-2cpy - 5.d			Hyd	Hyd	0.96	0.04	Porphyry	Porphyry	0.05	0.02	0.01	0.77	0.01	0.13
103-23-2cpy - 6.d			Hyd	Hyd	0.97	0.03	Porphyry	Porphyry	0.02	0.07	0.13	0.69	0.06	0.03
103-23-3cpy - 1.d			Hyd	Hyd	0.86	0.14	Porphyry	Orogenic gold	0.10	0.05	0.47	0.33	0.02	0.02
103-23-3cpy - 2.d			Hyd	Hyd	0.98	0.02	Porphyry	Porphyry	0.02	0.08	0.12	0.67	0.05	0.07
103-23-3cpy - 3.d			Hyd	Hyd	0.97	0.03	Porphyry	Porphyry	0.07	0.03	0.02	0.67	0.01	0.20

ID	Author	Deposit	Actual	Predicted	Prob		Actual	Predicted	Prob					
					Hyd	Mag			Epithermal gold	IOCG	Orogenic gold	Porphyry	Skarn	VMS
103-23-3cpy - 4.d	Yu et al. (2022)	Tianshan	Hyd	Hyd	0.96	0.04	Porphyry	Porphyry	0.05	0.22	0.09	0.34	0.07	0.24
103-23-4cpy - 2.d			Hyd	Mag	0.37	0.63	Porphyry	Porphyry	0.06	0.18	0.13	0.57	0.02	0.05
103-23-4cpy - 3.d			Hyd	Hyd	0.94	0.06	Porphyry	Porphyry	0.02	0.20	0.15	0.53	0.06	0.03
302-70-1cpy - 1.d			Hyd	Hyd	0.95	0.05	Porphyry	Orogenic gold	0.01	0.10	0.44	0.35	0.06	0.04
302-70-2cpy - 1.d			Hyd	Mag	0.05	0.95	Porphyry	IOCG	0.06	0.34	0.19	0.32	0.05	0.03
302-70-2cpy - 2.d			Hyd	Hyd	0.97	0.03	Porphyry	Orogenic gold	0.03	0.15	0.48	0.26	0.03	0.06
302-70-2cpy - 3.d			Hyd	Hyd	0.95	0.05	Porphyry	Porphyry	0.04	0.05	0.19	0.63	0.06	0.03
302-70-2cpy - 4.d			Hyd	Hyd	0.97	0.03	Porphyry	Orogenic gold	0.01	0.09	0.44	0.36	0.07	0.03
302-70-2cpy - 5.d			Hyd	Hyd	0.97	0.03	Porphyry	Porphyry	0.05	0.03	0.02	0.75	0.01	0.13
302-70-2cpy - 6.d			Hyd	Hyd	0.97	0.03	Porphyry	Porphyry	0.06	0.07	0.23	0.58	0.03	0.03
302-70-3cpy - 2.d			Hyd	Hyd	0.94	0.06	Porphyry	Porphyry	0.02	0.12	0.33	0.46	0.03	0.04
302-70-3cpy - 3.d			Hyd	Hyd	0.97	0.03	Porphyry	Porphyry	0.01	0.06	0.26	0.61	0.05	0.01
302-70-3cpy - 4.d			Hyd	Hyd	0.95	0.05	Porphyry	Porphyry	0.04	0.05	0.15	0.67	0.06	0.04
302-70-3cpy - 5.d			Hyd	Hyd	0.96	0.04	Porphyry	Porphyry	0.02	0.12	0.11	0.66	0.04	0.06
302-70-4cpy - 1.d			Hyd	Hyd	0.96	0.04	Porphyry	IOCG	0.12	0.30	0.18	0.29	0.02	0.09
302-70-4cpy - 2.d			Hyd	Hyd	0.99	0.01	Porphyry	Porphyry	0.06	0.11	0.09	0.49	0.04	0.20
302-70-4cpy - 3.d			Hyd	Hyd	0.99	0.01	Porphyry	Porphyry	0.04	0.15	0.24	0.25	0.17	0.15

ID	Author	Deposit	RF mag-hyd model				RF mag model			
			Actual	Predicted	Probabilites		Actual	Predicted	Probabilities	
					Hydrothermal	Magmatic			Ni-Cu sulfide	Reef-type PGE
E-1-01	Barnes et al. (2006)	Noril'sk	Magmatic	Magmatic	0.00	1.00	Ni-Cu sulfide	Ni-Cu sulfide	0.99	0.01
E-1-02			Magmatic	Magmatic	0.01	0.99	Ni-Cu sulfide	Ni-Cu sulfide	0.99	0.01
A-2-01			Magmatic	Magmatic	0.22	0.78	Ni-Cu sulfide	Ni-Cu sulfide	0.97	0.03
A-2-02			Magmatic	Hydrothermal	0.99	0.01	Ni-Cu sulfide	Ni-Cu sulfide	0.98	0.02
A-2-03			Magmatic	Hydrothermal	0.80	0.20	Ni-Cu sulfide	Ni-Cu sulfide	1.00	0.00
A-2-04			Magmatic	Magmatic	0.49	0.51	Ni-Cu sulfide	Ni-Cu sulfide	0.82	0.18
A-2-05			Magmatic	Hydrothermal	0.87	0.13	Ni-Cu sulfide	Ni-Cu sulfide	1.00	0.00
FI-02-06-01		Penikat	Magmatic	Hydrothermal	0.88	0.12	Reef-type PGE	Ni-Cu sulfide	1.00	0.00
FI-02-06-02			Magmatic	Magmatic	0.41	0.59	Reef-type PGE	Ni-Cu sulfide	0.94	0.06
FI-02-06-03			Magmatic	Magmatic	0.00	1.00	Reef-type PGE	Ni-Cu sulfide	1.00	0.00
FI-02-06-04			Magmatic	Magmatic	0.03	0.97	Reef-type PGE	Ni-Cu sulfide	0.99	0.01
FI-02-06-05			Magmatic	Magmatic	0.02	0.98	Reef-type PGE	Ni-Cu sulfide	0.64	0.36
FI-03-04-01			Magmatic	Magmatic	0.00	1.00	Reef-type PGE	Reef-type PGE	0.12	0.88
FI-03-04-02			Magmatic	Hydrothermal	0.81	0.19	Reef-type PGE	Ni-Cu sulfide	0.99	0.01
FI-03-04-03			Magmatic	Magmatic	0.02	0.98	Reef-type PGE	Ni-Cu sulfide	0.99	0.01
FI-03-04-04			Magmatic	Hydrothermal	0.99	0.01	Reef-type PGE	Ni-Cu sulfide	0.92	0.08
FI-03-04-05			Magmatic	Hydrothermal	0.82	0.18	Reef-type PGE	Ni-Cu sulfide	0.98	0.02
FI-03-04-06			Magmatic	Hydrothermal	0.96	0.04	Reef-type PGE	Ni-Cu sulfide	1.00	0.00
CRTN4	Dare et al. (2010)	Sudbury	Magmatic	Magmatic	0.02	0.98	Ni-Cu sulfide	Ni-Cu sulfide	0.99	0.01
CRTN1			Magmatic	Magmatic	0.24	0.76	Ni-Cu sulfide	Ni-Cu sulfide	0.96	0.04
CRTN6			Magmatic	Magmatic	0.01	0.99	Ni-Cu sulfide	Ni-Cu sulfide	0.98	0.02
CRTN7			Magmatic	Magmatic	0.19	0.81	Ni-Cu sulfide	Ni-Cu sulfide	1.00	0.00
CRTN11			Magmatic	Magmatic	0.04	0.96	Ni-Cu sulfide	Ni-Cu sulfide	0.87	0.13
CRTN18			Magmatic	Magmatic	0.04	0.96	Ni-Cu sulfide	Ni-Cu sulfide	1.00	0.00
CRTN12			Magmatic	Magmatic	0.02	0.98	Ni-Cu sulfide	Ni-Cu sulfide	0.85	0.15

ID	Author	Deposit	RF mag-hyd model Actual	Predicted	Probabilites Hydrothermal	Magmatic	RF mag model Actual	Predicted	Probabilities Ni-Cu sulfide	Reef-type PGE
CRTN10	Dare et al. (2010)	Sudbury	Magmatic	Magmatic	0.10	0.90	Ni-Cu sulfide	Ni-Cu sulfide	0.99	0.01
CRTN15			Magmatic	Magmatic	0.02	0.98	Ni-Cu sulfide	Ni-Cu sulfide	0.65	0.35
CRTN9			Magmatic	Magmatic	0.02	0.98	Ni-Cu sulfide	Ni-Cu sulfide	1.00	0.00
CRTN14			Magmatic	Magmatic	0.05	0.95	Ni-Cu sulfide	Ni-Cu sulfide	0.95	0.05
CRTN13			Magmatic	Magmatic	0.03	0.97	Ni-Cu sulfide	Ni-Cu sulfide	0.89	0.11
CRTN2			Magmatic	Magmatic	0.32	0.68	Ni-Cu sulfide	Ni-Cu sulfide	0.93	0.07
CRTN16			Magmatic	Magmatic	0.13	0.87	Ni-Cu sulfide	Ni-Cu sulfide	0.97	0.03
CRTN5			Magmatic	Magmatic	0.13	0.87	Ni-Cu sulfide	Ni-Cu sulfide	0.96	0.04
CRTN17			Magmatic	Magmatic	0.22	0.78	Ni-Cu sulfide	Ni-Cu sulfide	0.94	0.06
CRTN8			Magmatic	Magmatic	0.26	0.74	Ni-Cu sulfide	Ni-Cu sulfide	0.83	0.17
CRTN19			Magmatic	Magmatic	0.13	0.87	Ni-Cu sulfide	Ni-Cu sulfide	0.98	0.02
MCR7B-03	Dare et al. (2014)	Sudbury	Magmatic	Magmatic	0.27	0.73	Ni-Cu sulfide	Ni-Cu sulfide	0.99	0.01
MCR10-01			Magmatic	Magmatic	0.41	0.59	Ni-Cu sulfide	Ni-Cu sulfide	1.00	0.00
MCR3-01			Magmatic	Magmatic	0.23	0.77	Ni-Cu sulfide	Ni-Cu sulfide	0.89	0.11
MCR11-01			Magmatic	Magmatic	0.30	0.70	Ni-Cu sulfide	Ni-Cu sulfide	1.00	0.00
MCR5-01			Magmatic	Magmatic	0.44	0.56	Ni-Cu sulfide	Ni-Cu sulfide	0.50	0.50
MCR7B-01			Magmatic	Magmatic	0.18	0.82	Ni-Cu sulfide	Ni-Cu sulfide	1.00	0.00
MCR1-02			Magmatic	Magmatic	0.08	0.92	Ni-Cu sulfide	Reef-type PGE	0.04	0.96
MCR13-01			Magmatic	Magmatic	0.36	0.64	Ni-Cu sulfide	Ni-Cu sulfide	1.00	0.00
MCR14-01			Magmatic	Magmatic	0.30	0.70	Ni-Cu sulfide	Ni-Cu sulfide	1.00	0.00
MCR7B-02			Magmatic	Magmatic	0.07	0.93	Ni-Cu sulfide	Ni-Cu sulfide	1.00	0.00
MCR3-02			Magmatic	Magmatic	0.29	0.71	Ni-Cu sulfide	Ni-Cu sulfide	0.88	0.12
MCR4-02			Magmatic	Magmatic	0.11	0.89	Ni-Cu sulfide	Ni-Cu sulfide	0.88	0.12
MCR10-06			Magmatic	Magmatic	0.28	0.72	Ni-Cu sulfide	Ni-Cu sulfide	0.96	0.04
MCR11-02			Magmatic	Magmatic	0.16	0.84	Ni-Cu sulfide	Ni-Cu sulfide	0.97	0.03
MCR10-04			Magmatic	Magmatic	0.43	0.57	Ni-Cu sulfide	Ni-Cu sulfide	1.00	0.00

ID	Author	Deposit	RF mag-hyd model Actual	Predicted	Probabilites Hydrothermal	Magmatic	RF mag model Actual	Predicted	Probabilities Ni-Cu sulfide	Reef-type PGE
MCR4-03	Dare et al. (2014)	Sudbury	Magmatic	Magmatic	0.08	0.92	Ni-Cu sulfide	Ni-Cu sulfide	0.99	0.01
MCR4-01			Magmatic	Magmatic	0.23	0.77	Ni-Cu sulfide	Ni-Cu sulfide	0.96	0.04
MCR13-03			Magmatic	Magmatic	0.42	0.58	Ni-Cu sulfide	Ni-Cu sulfide	1.00	0.00
MCR10-03			Magmatic	Magmatic	0.35	0.65	Ni-Cu sulfide	Ni-Cu sulfide	0.95	0.05
MCR10-02			Magmatic	Magmatic	0.36	0.64	Ni-Cu sulfide	Ni-Cu sulfide	0.97	0.03
MCR11-03			Magmatic	Magmatic	0.14	0.86	Ni-Cu sulfide	Ni-Cu sulfide	1.00	0.00
MCR9-02			Magmatic	Magmatic	0.28	0.72	Ni-Cu sulfide	Ni-Cu sulfide	1.00	0.00
MCR14-03			Magmatic	Magmatic	0.37	0.63	Ni-Cu sulfide	Ni-Cu sulfide	0.99	0.01
MCR10-05			Magmatic	Magmatic	0.23	0.77	Ni-Cu sulfide	Ni-Cu sulfide	0.97	0.03
MCR9-03			Magmatic	Magmatic	0.05	0.95	Ni-Cu sulfide	Ni-Cu sulfide	1.00	0.00
MCR13-02			Magmatic	Magmatic	0.18	0.82	Ni-Cu sulfide	Ni-Cu sulfide	1.00	0.00
MCR13-05			Magmatic	Magmatic	0.34	0.66	Ni-Cu sulfide	Ni-Cu sulfide	1.00	0.00
MCR12-03			Magmatic	Magmatic	0.46	0.54	Ni-Cu sulfide	Ni-Cu sulfide	1.00	0.00
MCR12-01			Magmatic	Magmatic	0.37	0.63	Ni-Cu sulfide	Ni-Cu sulfide	0.97	0.03
MCR14-02			Magmatic	Magmatic	0.24	0.76	Ni-Cu sulfide	Ni-Cu sulfide	0.99	0.01
MCR5-03			Magmatic	Magmatic	0.42	0.58	Ni-Cu sulfide	Ni-Cu sulfide	0.84	0.16
MCR5-02			Magmatic	Magmatic	0.17	0.83	Ni-Cu sulfide	Ni-Cu sulfide	0.85	0.15
MCR13-04			Magmatic	Magmatic	0.35	0.65	Ni-Cu sulfide	Ni-Cu sulfide	1.00	0.00
MCR1-01			Magmatic	Magmatic	0.02	0.98	Ni-Cu sulfide	Reef-type PGE	0.05	0.95
MCR5-04			Magmatic	Magmatic	0.07	0.93	Ni-Cu sulfide	Ni-Cu sulfide	0.96	0.04
MCR12-02			Magmatic	Magmatic	0.42	0.58	Ni-Cu sulfide	Ni-Cu sulfide	0.99	0.01
MCR7A-02			Magmatic	Magmatic	0.19	0.81	Ni-Cu sulfide	Ni-Cu sulfide	0.99	0.01
MCR7A-01			Magmatic	Magmatic	0.17	0.83	Ni-Cu sulfide	Ni-Cu sulfide	0.99	0.01
MCR7A-03			Magmatic	Hydrothermal	0.52	0.48	Ni-Cu sulfide	Ni-Cu sulfide	0.99	0.01
MCR9-01			Magmatic	Magmatic	0.46	0.54	Ni-Cu sulfide	Ni-Cu sulfide	0.97	0.03

ID	Author	Deposit	RF mag-hyd model Actual	Predicted	Probabilites Hydrothermal	Magmatic	RF mag model Actual	Predicted	Probabilities Ni-Cu sulfide	Reef-type PGE
TZ-1-01	Djon and Barnes (2012)	Lac des Iles	Magmatic	Magmatic	0.00	1.00	Ni-Cu sulfide	Ni-Cu sulfide	1.00	0.00
TZ-1-02			Magmatic	Hydrothermal	0.95	0.05	Ni-Cu sulfide	Ni-Cu sulfide	0.99	0.01
TZ-1-03			Magmatic	Magmatic	0.01	0.99	Ni-Cu sulfide	Ni-Cu sulfide	0.95	0.05
TZ-1-04			Magmatic	Magmatic	0.31	0.69	Ni-Cu sulfide	Ni-Cu sulfide	0.97	0.03
TZ-1-05			Magmatic	Magmatic	0.00	1.00	Ni-Cu sulfide	Ni-Cu sulfide	0.99	0.01
TZ-1-06			Magmatic	Magmatic	0.00	1.00	Ni-Cu sulfide	Ni-Cu sulfide	0.99	0.01
TZ-7-01			Magmatic	Hydrothermal	0.68	0.32	Ni-Cu sulfide	Ni-Cu sulfide	0.99	0.01
TZ-7-02			Magmatic	Magmatic	0.01	0.99	Ni-Cu sulfide	Ni-Cu sulfide	0.98	0.02
TZ-7-03			Magmatic	Magmatic	0.02	0.98	Ni-Cu sulfide	Ni-Cu sulfide	1.00	0.00
TZ-7-04			Magmatic	Magmatic	0.02	0.98	Ni-Cu sulfide	Ni-Cu sulfide	0.98	0.02
TZ-10-01			Magmatic	Magmatic	0.00	1.00	Ni-Cu sulfide	Ni-Cu sulfide	0.99	0.01
TZ-10-02			Magmatic	Hydrothermal	0.99	0.01	Ni-Cu sulfide	Ni-Cu sulfide	0.95	0.05
TZ-10-03			Magmatic	Magmatic	0.00	1.00	Ni-Cu sulfide	Ni-Cu sulfide	1.00	0.00
TZ-10-04			Magmatic	Magmatic	0.00	1.00	Ni-Cu sulfide	Ni-Cu sulfide	0.99	0.01
TZ-19-01			Magmatic	Magmatic	0.00	1.00	Ni-Cu sulfide	Ni-Cu sulfide	0.87	0.13
TZ-19-02			Magmatic	Hydrothermal	0.80	0.20	Ni-Cu sulfide	Ni-Cu sulfide	0.97	0.03
TZ-19-03			Magmatic	Magmatic	0.00	1.00	Ni-Cu sulfide	Ni-Cu sulfide	0.97	0.03
TZ-19-04			Magmatic	Magmatic	0.00	1.00	Ni-Cu sulfide	Ni-Cu sulfide	0.54	0.46
RZ-30-01			Magmatic	Hydrothermal	0.72	0.28	Ni-Cu sulfide	Ni-Cu sulfide	0.99	0.01
RZ-30-02			Magmatic	Magmatic	0.04	0.96	Ni-Cu sulfide	Ni-Cu sulfide	0.99	0.01
RZ-30-03			Magmatic	Magmatic	0.03	0.97	Ni-Cu sulfide	Ni-Cu sulfide	0.97	0.03
RZ-30-04			Magmatic	Magmatic	0.00	1.00	Ni-Cu sulfide	Ni-Cu sulfide	0.99	0.01
RZ-45-01			Magmatic	Hydrothermal	0.92	0.08	Ni-Cu sulfide	Ni-Cu sulfide	0.57	0.43
RZ-45-02			Magmatic	Magmatic	0.00	1.00	Ni-Cu sulfide	Ni-Cu sulfide	0.99	0.01
RZ-45-03			Magmatic	Magmatic	0.00	1.00	Ni-Cu sulfide	Ni-Cu sulfide	0.58	0.42
RZ-45-04			Magmatic	Magmatic	0.00	1.00	Ni-Cu sulfide	Ni-Cu sulfide	1.00	0.00

ID	Author	Deposit	RF mag-hyd model Actual	Predicted	Probabilites Hydrothermal	Magmatic	RF mag model Actual	Predicted	Probabilities Ni-Cu sulfide	Reef-type PGE
TZ-15-01	Djon and Barnes (2012)	Lac des Iles	Magmatic	Hydrothermal	0.97	0.03	Ni-Cu sulfide	Ni-Cu sulfide	0.97	0.03
TZ-15-02			Magmatic	Hydrothermal	0.96	0.04	Ni-Cu sulfide	Ni-Cu sulfide	0.99	0.01
TZ-15-03			Magmatic	Hydrothermal	1.00	0.00	Ni-Cu sulfide	Ni-Cu sulfide	0.96	0.04
TZ-15-04			Magmatic	Hydrothermal	0.97	0.03	Ni-Cu sulfide	Ni-Cu sulfide	0.99	0.01
TZ-15-05			Magmatic	Magmatic	0.08	0.92	Ni-Cu sulfide	Ni-Cu sulfide	1.00	0.00
TZ-15-06			Magmatic	Hydrothermal	0.94	0.06	Ni-Cu sulfide	Ni-Cu sulfide	1.00	0.00
TZ-21-01			Magmatic	Hydrothermal	0.99	0.01	Ni-Cu sulfide	Ni-Cu sulfide	0.99	0.01
TZ-21-02			Magmatic	Magmatic	0.04	0.96	Ni-Cu sulfide	Reef-type PGE	0.48	0.52
TZ-21-03			Magmatic	Magmatic	0.05	0.95	Ni-Cu sulfide	Ni-Cu sulfide	0.52	0.48
TZ-28-01			Magmatic	Magmatic	0.01	0.99	Ni-Cu sulfide	Ni-Cu sulfide	0.95	0.05
TZ-28-02			Magmatic	Magmatic	0.33	0.67	Ni-Cu sulfide	Ni-Cu sulfide	1.00	0.00
TZ-28-03			Magmatic	Hydrothermal	0.90	0.10	Ni-Cu sulfide	Ni-Cu sulfide	1.00	0.00
TZ-28-04			Magmatic	Hydrothermal	0.93	0.07	Ni-Cu sulfide	Ni-Cu sulfide	0.94	0.06
TZ-28-05			Magmatic	Hydrothermal	0.99	0.01	Ni-Cu sulfide	Ni-Cu sulfide	0.99	0.01
TZ-28-06			Magmatic	Magmatic	0.17	0.83	Ni-Cu sulfide	Ni-Cu sulfide	0.98	0.02
TZ-28-07			Magmatic	Hydrothermal	0.69	0.31	Ni-Cu sulfide	Ni-Cu sulfide	0.99	0.01
RZ-17-01			Magmatic	Magmatic	0.02	0.98	Ni-Cu sulfide	Ni-Cu sulfide	0.81	0.19
RZ-17-02			Magmatic	Hydrothermal	1.00	0.00	Ni-Cu sulfide	Ni-Cu sulfide	0.98	0.02
RZ-17-03			Magmatic	Magmatic	0.20	0.80	Ni-Cu sulfide	Reef-type PGE	0.00	1.00
RZ-17-04			Magmatic	Hydrothermal	0.91	0.09	Ni-Cu sulfide	Ni-Cu sulfide	1.00	0.00
RZ-3-01			Magmatic	Magmatic	0.01	0.99	Ni-Cu sulfide	Ni-Cu sulfide	0.98	0.02
RZ-3-02			Magmatic	Magmatic	0.00	1.00	Ni-Cu sulfide	Ni-Cu sulfide	0.99	0.01
RZ-3-03			Magmatic	Hydrothermal	0.55	0.45	Ni-Cu sulfide	Ni-Cu sulfide	0.98	0.02
RZ-3-04			Magmatic	Magmatic	0.00	1.00	Ni-Cu sulfide	Ni-Cu sulfide	0.98	0.02
RZ-3-05			Magmatic	Hydrothermal	0.98	0.02	Ni-Cu sulfide	Ni-Cu sulfide	0.99	0.01
RZ-8-01			Magmatic	Hydrothermal	1.00	0.00	Ni-Cu sulfide	Ni-Cu sulfide	0.99	0.01

ID	Author	Deposit	RF mag-hyd model Actual	Predicted	Probabilites Hydrothermal	Magmatic	RF mag model Actual	Predicted	Probabilities Ni-Cu sulfide	Reef-type PGE
RZ-8-02	Djon and Barnes (2012)	Lac des Iles	Magmatic	Magmatic	0.31	0.69	Ni-Cu sulfide	Ni-Cu sulfide	0.94	0.06
RZ-8-03			Magmatic	Hydrothermal	0.99	0.01	Ni-Cu sulfide	Ni-Cu sulfide	0.87	0.13
RZ-50-01			Magmatic	Hydrothermal	0.98	0.02	Ni-Cu sulfide	Ni-Cu sulfide	0.83	0.17
RZ-50-02			Magmatic	Magmatic	0.39	0.61	Ni-Cu sulfide	Ni-Cu sulfide	0.97	0.03
RZ-50-03			Magmatic	Hydrothermal	0.68	0.32	Ni-Cu sulfide	Ni-Cu sulfide	0.54	0.46
RZ-50-04			Magmatic	Magmatic	0.45	0.55	Ni-Cu sulfide	Ni-Cu sulfide	0.90	0.10
RZ-54-01			Magmatic	Hydrothermal	0.99	0.01	Ni-Cu sulfide	Ni-Cu sulfide	1.00	0.00
RZ-54-02			Magmatic	Magmatic	0.35	0.65	Ni-Cu sulfide	Ni-Cu sulfide	1.00	0.00
RZ-54-03			Magmatic	Magmatic	0.32	0.68	Ni-Cu sulfide	Ni-Cu sulfide	0.91	0.09
RZ-54-04			Magmatic	Hydrothermal	0.62	0.38	Ni-Cu sulfide	Ni-Cu sulfide	1.00	0.00
RZ-54-05			Magmatic	Hydrothermal	1.00	0.00	Ni-Cu sulfide	Ni-Cu sulfide	0.97	0.03
RZ-54-06			Magmatic	Magmatic	0.00	1.00	Ni-Cu sulfide	Reef-type PGE	0.38	0.62
RZ-54-07			Magmatic	Magmatic	0.40	0.60	Ni-Cu sulfide	Ni-Cu sulfide	1.00	0.00
ST12a-01	Godel and Barnes (2008)	Stillwater	Magmatic	Magmatic	0.00	1.00	Reef-type PGE	Ni-Cu sulfide	1.00	0.00
ST12a-02			Magmatic	Hydrothermal	0.73	0.27	Reef-type PGE	Ni-Cu sulfide	0.86	0.14
ST12a-03			Magmatic	Magmatic	0.00	1.00	Reef-type PGE	Ni-Cu sulfide	0.91	0.09
ST14a-01			Magmatic	Magmatic	0.01	0.99	Reef-type PGE	Ni-Cu sulfide	0.98	0.02
ST14a-02			Magmatic	Magmatic	0.00	1.00	Reef-type PGE	Ni-Cu sulfide	0.54	0.46
ST14b-01			Magmatic	Magmatic	0.00	1.00	Reef-type PGE	Ni-Cu sulfide	0.98	0.02
ST14b-02			Magmatic	Magmatic	0.02	0.98	Reef-type PGE	Reef-type PGE	0.16	0.84
ST14b-03			Magmatic	Magmatic	0.00	1.00	Reef-type PGE	Reef-type PGE	0.48	0.52
ST14b-04			Magmatic	Magmatic	0.02	0.98	Reef-type PGE	Ni-Cu sulfide	0.61	0.39
ST16-01			Magmatic	Magmatic	0.13	0.87	Reef-type PGE	Ni-Cu sulfide	0.81	0.19
ST17-01			Magmatic	Magmatic	0.01	0.99	Reef-type PGE	Ni-Cu sulfide	0.76	0.24
ST17-02			Magmatic	Magmatic	0.00	1.00	Reef-type PGE	Ni-Cu sulfide	1.00	0.00
ST17-03			Magmatic	Magmatic	0.00	1.00	Reef-type PGE	Ni-Cu sulfide	1.00	0.00

ID	Author	Deposit	RF mag-hyd model Actual	Predicted	Probabilites Hydrothermal	Magmatic	RF mag model Actual	Predicted	Probabilities Ni-Cu sulfide	Reef-type PGE
ST17-04	Godel and Barnes (2008)	Stillwater	Magmatic	Magmatic	0.00	1.00	Reef-type PGE	Ni-Cu sulfide	1.00	0.00
PTR02-03	Knight et al. (2017)	Santa Rita	Magmatic	Magmatic	0.19	0.81	Ni-Cu sulfide	Ni-Cu sulfide	0.96	0.04
PTR04-01			Magmatic	Magmatic	0.07	0.93	Ni-Cu sulfide	Ni-Cu sulfide	0.97	0.03
PTR02-01			Magmatic	Magmatic	0.21	0.79	Ni-Cu sulfide	Ni-Cu sulfide	0.67	0.33
PTR03-01			Magmatic	Magmatic	0.17	0.83	Ni-Cu sulfide	Ni-Cu sulfide	0.58	0.42
PTR05-02			Magmatic	Magmatic	0.05	0.95	Ni-Cu sulfide	Ni-Cu sulfide	0.66	0.34
PTR05-03			Magmatic	Hydrothermal	0.99	0.01	Ni-Cu sulfide	Ni-Cu sulfide	0.57	0.43
PTR02-02			Magmatic	Magmatic	0.16	0.84	Ni-Cu sulfide	Ni-Cu sulfide	0.62	0.38
PTR06-02			Magmatic	Hydrothermal	1.00	0.00	Ni-Cu sulfide	Ni-Cu sulfide	0.55	0.45
PTR04-03			Magmatic	Magmatic	0.16	0.84	Ni-Cu sulfide	Reef-type PGE	0.48	0.52
PTR22-01			Magmatic	Magmatic	0.05	0.95	Ni-Cu sulfide	Ni-Cu sulfide	0.84	0.16
PTR05-01			Magmatic	Hydrothermal	0.99	0.01	Ni-Cu sulfide	Ni-Cu sulfide	1.00	0.00
PTR04-02			Magmatic	Magmatic	0.05	0.95	Ni-Cu sulfide	Reef-type PGE	0.47	0.53
PTR06-01			Magmatic	Magmatic	0.03	0.97	Ni-Cu sulfide	Ni-Cu sulfide	0.96	0.04
PTR04-04			Magmatic	Magmatic	0.10	0.90	Ni-Cu sulfide	Reef-type PGE	0.46	0.54
Leo-1	Pina et al. (2012)	Aguablanca	Magmatic	Magmatic	0.06	0.94	Ni-Cu sulfide	Ni-Cu sulfide	0.84	0.16
Leo-2			Magmatic	Magmatic	0.07	0.93	Ni-Cu sulfide	Ni-Cu sulfide	0.99	0.01
Leo-3			Magmatic	Magmatic	0.03	0.97	Ni-Cu sulfide	Ni-Cu sulfide	0.97	0.03
6580-281-1			Magmatic	Magmatic	0.13	0.87	Ni-Cu sulfide	Ni-Cu sulfide	0.98	0.02
6580-281-2			Magmatic	Magmatic	0.04	0.96	Ni-Cu sulfide	Ni-Cu sulfide	0.67	0.33
6580-281-3			Magmatic	Hydrothermal	0.89	0.11	Ni-Cu sulfide	Ni-Cu sulfide	0.99	0.01
6629-39-1			Magmatic	Magmatic	0.27	0.73	Ni-Cu sulfide	Reef-type PGE	0.32	0.68
6629-39-2			Magmatic	Hydrothermal	0.92	0.08	Ni-Cu sulfide	Ni-Cu sulfide	0.98	0.02
6749-390-1			Magmatic	Magmatic	0.03	0.97	Ni-Cu sulfide	Reef-type PGE	0.06	0.94
6749-390-2			Magmatic	Magmatic	0.11	0.89	Ni-Cu sulfide	Ni-Cu sulfide	0.57	0.43
6749-390-3			Magmatic	Magmatic	0.12	0.88	Ni-Cu sulfide	Reef-type PGE	0.43	0.57

ID	Author	Deposit	RF mag-hyd model				RF mag model			
			Actual	Predicted	Probabilites		Actual	Predicted	Probabilities	
					Hydrothermal	Magmatic			Ni-Cu sulfide	Reef-type PGE
6749-390-4	Pina et al. (2012)	Aguablanca	Magmatic	Magmatic	0.09	0.91	Ni-Cu sulfide	Ni-Cu sulfide	0.98	0.02
6749-390-5			Magmatic	Magmatic	0.16	0.84	Ni-Cu sulfide	Reef-type PGE	0.11	0.89
6749-390-6			Magmatic	Magmatic	0.13	0.87	Ni-Cu sulfide	Ni-Cu sulfide	0.98	0.02
AGU-5-29.70-1			Magmatic	Magmatic	0.05	0.95	Ni-Cu sulfide	Ni-Cu sulfide	0.96	0.04
AGU-5-29.70-2			Magmatic	Magmatic	0.02	0.98	Ni-Cu sulfide	Ni-Cu sulfide	0.96	0.04
AGU-5-29.70-3			Magmatic	Magmatic	0.03	0.97	Ni-Cu sulfide	Ni-Cu sulfide	0.92	0.08
AGU-5-29.70-4			Magmatic	Magmatic	0.43	0.57	Ni-Cu sulfide	Ni-Cu sulfide	0.90	0.10
6758-548.25-1			Magmatic	Magmatic	0.15	0.85	Ni-Cu sulfide	Ni-Cu sulfide	0.54	0.46
6758-548.25-2			Magmatic	Magmatic	0.09	0.91	Ni-Cu sulfide	Reef-type PGE	0.43	0.57
6758-548.25-3			Magmatic	Magmatic	0.14	0.86	Ni-Cu sulfide	Ni-Cu sulfide	0.96	0.04
6758-548.25-4			Magmatic	Magmatic	0.03	0.97	Ni-Cu sulfide	Reef-type PGE	0.35	0.65
6758-548.25-5			Magmatic	Magmatic	0.47	0.53	Ni-Cu sulfide	Ni-Cu sulfide	0.96	0.04
6479-45.60-1			Magmatic	Hydrothermal	0.60	0.40	Ni-Cu sulfide	Ni-Cu sulfide	0.98	0.02
6479-45.60-2			Magmatic	Magmatic	0.00	1.00	Ni-Cu sulfide	Ni-Cu sulfide	0.98	0.02
6479-45.60-3			Magmatic	Magmatic	0.04	0.96	Ni-Cu sulfide	Ni-Cu sulfide	0.98	0.02
6479-45.60-4			Magmatic	Magmatic	0.02	0.98	Ni-Cu sulfide	Ni-Cu sulfide	0.97	0.03
6479-45.60-5			Magmatic	Hydrothermal	0.68	0.32	Ni-Cu sulfide	Ni-Cu sulfide	1.00	0.00
6479-45.60-6			Magmatic	Hydrothermal	0.54	0.46	Ni-Cu sulfide	Ni-Cu sulfide	0.98	0.02
6479-45.60-7			Magmatic	Hydrothermal	0.63	0.37	Ni-Cu sulfide	Ni-Cu sulfide	0.99	0.01
EG5-C5A	Pina et al. (2015)	El Gallego	Magmatic	Magmatic	0.00	1.00	Ni-Cu sulfide	Ni-Cu sulfide	0.95	0.05
EG5-C5C			Magmatic	Magmatic	0.00	1.00	Ni-Cu sulfide	Ni-Cu sulfide	0.96	0.04
EG5-C7B			Magmatic	Magmatic	0.00	1.00	Ni-Cu sulfide	Ni-Cu sulfide	0.98	0.02
EG5-C8A			Magmatic	Magmatic	0.00	1.00	Ni-Cu sulfide	Ni-Cu sulfide	0.97	0.03
EG5-C8B			Magmatic	Magmatic	0.11	0.89	Ni-Cu sulfide	Ni-Cu sulfide	0.99	0.01
EG5-C9B			Magmatic	Magmatic	0.11	0.89	Ni-Cu sulfide	Ni-Cu sulfide	0.89	0.11

ID	Author	Deposit	RF mag-hyd model				RF mag model			
			Actual	Predicted	Probabilites		Actual	Predicted	Probabilities	
					Hydrothermal	Magmatic			Ni-Cu sulfide	Reef-type PGE
HAN-106-1-4.D	Pina et al. (2016)	Great Dyke	Magmatic	Magmatic	0.04	0.96	Reef-type PGE	Reef-type PGE	0.04	0.96
HAN-106-8-3.D			Magmatic	Magmatic	0.04	0.96	Reef-type PGE	Reef-type PGE	0.15	0.85
HAS-203-1-3.D			Magmatic	Magmatic	0.01	0.99	Reef-type PGE	Reef-type PGE	0.09	0.91
HAS-203-4-3.D			Magmatic	Magmatic	0.00	1.00	Reef-type PGE	Reef-type PGE	0.28	0.72
HAS-203-6-1.D			Magmatic	Magmatic	0.00	1.00	Reef-type PGE	Reef-type PGE	0.18	0.82
5863-2-3.D			Magmatic	Magmatic	0.01	0.99	Reef-type PGE	Reef-type PGE	0.14	0.86
5860-1-2.D			Magmatic	Hydrothermal	0.89	0.11	Reef-type PGE	Reef-type PGE	0.36	0.64
5535-4-1.D			Magmatic	Magmatic	0.02	0.98	Reef-type PGE	Ni-Cu sulfide	0.59	0.41
5535-6-1.D			Magmatic	Magmatic	0.00	1.00	Reef-type PGE	Reef-type PGE	0.08	0.92
5535-7-1.D			Magmatic	Magmatic	0.00	1.00	Reef-type PGE	Reef-type PGE	0.05	0.95
5221-2-2.D			Magmatic	Magmatic	0.16	0.84	Reef-type PGE	Ni-Cu sulfide	0.92	0.08
5221-4-2.D			Magmatic	Magmatic	0.01	0.99	Reef-type PGE	Ni-Cu sulfide	0.94	0.06
5221-6-1.D			Magmatic	Magmatic	0.00	1.00	Reef-type PGE	Ni-Cu sulfide	0.60	0.40
6041-1-1.D			Magmatic	Magmatic	0.03	0.97	Reef-type PGE	Reef-type PGE	0.39	0.61
6041-1-3.D			Magmatic	Magmatic	0.02	0.98	Reef-type PGE	Reef-type PGE	0.35	0.65
6041-8-1.D			Magmatic	Magmatic	0.00	1.00	Reef-type PGE	Reef-type PGE	0.48	0.52
5222-1-1.D			Magmatic	Magmatic	0.01	0.99	Reef-type PGE	Ni-Cu sulfide	0.93	0.07
5222-2-2.D			Magmatic	Magmatic	0.03	0.97	Reef-type PGE	Ni-Cu sulfide	0.97	0.03
5222-4-3.D			Magmatic	Magmatic	0.07	0.93	Reef-type PGE	Ni-Cu sulfide	1.00	0.00
5222-8-3.D			Magmatic	Magmatic	0.12	0.88	Reef-type PGE	Ni-Cu sulfide	0.67	0.33
VB21-2	Salim Amaral (2017)	Voisey's Bay	Magmatic	Magmatic	0.00	1.00	Ni-Cu sulfide	Ni-Cu sulfide	0.99	0.01
VB21-1			Magmatic	Magmatic	0.00	1.00	Ni-Cu sulfide	Ni-Cu sulfide	0.99	0.01
VB8-3			Magmatic	Magmatic	0.14	0.86	Ni-Cu sulfide	Ni-Cu sulfide	0.99	0.01
VB8-4			Magmatic	Magmatic	0.46	0.54	Ni-Cu sulfide	Ni-Cu sulfide	0.99	0.01
VB8-1			Magmatic	Magmatic	0.13	0.87	Ni-Cu sulfide	Ni-Cu sulfide	0.99	0.01
VB8-2			Magmatic	Magmatic	0.01	0.99	Ni-Cu sulfide	Ni-Cu sulfide	0.99	0.01

ID	Author	Deposit	RF mag-hyd model Actual	Predicted	Probabilites Hydrothermal	Magmatic	RF mag model Actual	Predicted	Probabilities Ni-Cu sulfide	Reef-type PGE
VB25-3	Salim Amaral (2017)	Voisey's Bay	Magmatic	Magmatic	0.00	1.00	Ni-Cu sulfide	Ni-Cu sulfide	0.99	0.01
VB25-2			Magmatic	Magmatic	0.00	1.00	Ni-Cu sulfide	Ni-Cu sulfide	0.97	0.03
VB25-1			Magmatic	Magmatic	0.00	1.00	Ni-Cu sulfide	Ni-Cu sulfide	1.00	0.00
VB26-2			Magmatic	Magmatic	0.01	0.99	Ni-Cu sulfide	Ni-Cu sulfide	0.88	0.12
VB26-1			Magmatic	Magmatic	0.01	0.99	Ni-Cu sulfide	Ni-Cu sulfide	0.92	0.08
VB29-1			Magmatic	Magmatic	0.00	1.00	Ni-Cu sulfide	Ni-Cu sulfide	1.00	0.00
VB29-2			Magmatic	Magmatic	0.00	1.00	Ni-Cu sulfide	Ni-Cu sulfide	1.00	0.00
VB29-3			Magmatic	Magmatic	0.00	1.00	Ni-Cu sulfide	Ni-Cu sulfide	0.99	0.01
VB29-4			Magmatic	Magmatic	0.01	0.99	Ni-Cu sulfide	Ni-Cu sulfide	0.97	0.03
VB31-4			Magmatic	Magmatic	0.01	0.99	Ni-Cu sulfide	Ni-Cu sulfide	1.00	0.00
VB36-3			Magmatic	Magmatic	0.01	0.99	Ni-Cu sulfide	Ni-Cu sulfide	0.89	0.11
VB31-3			Magmatic	Magmatic	0.00	1.00	Ni-Cu sulfide	Ni-Cu sulfide	1.00	0.00
VB36-1			Magmatic	Magmatic	0.00	1.00	Ni-Cu sulfide	Ni-Cu sulfide	0.92	0.08
VB36-2			Magmatic	Magmatic	0.00	1.00	Ni-Cu sulfide	Ni-Cu sulfide	0.99	0.01
VB31-2			Magmatic	Magmatic	0.00	1.00	Ni-Cu sulfide	Ni-Cu sulfide	1.00	0.00
VB31-1			Magmatic	Magmatic	0.10	0.90	Ni-Cu sulfide	Ni-Cu sulfide	1.00	0.00
B1-384-39	Samalens et al. (2017)	Duluth	Magmatic	Magmatic	0.31	0.69	Ni-Cu sulfide	Ni-Cu sulfide	0.89	0.11
DC-69-01			Magmatic	Magmatic	0.106	0.894	Ni-Cu sulfide	Ni-Cu sulfide	0.99	0.01
DC-69-02			Magmatic	Magmatic	0.174	0.826	Ni-Cu sulfide	Ni-Cu sulfide	0.85	0.15
DC-69-03			Magmatic	Magmatic	0.15	0.85	Ni-Cu sulfide	Ni-Cu sulfide	1.00	0.00
DC-69-04			Magmatic	Magmatic	0.134	0.866	Ni-Cu sulfide	Ni-Cu sulfide	1.00	0.00
DC-69-05			Magmatic	Magmatic	0.168	0.832	Ni-Cu sulfide	Ni-Cu sulfide	0.99	0.01
DC-69-06			Magmatic	Magmatic	0.176	0.824	Ni-Cu sulfide	Ni-Cu sulfide	1.00	0.00
DC-80-01			Magmatic	Magmatic	0.022	0.978	Ni-Cu sulfide	Ni-Cu sulfide	0.98	0.02
EC-07-01			Magmatic	Magmatic	0.36	0.64	Ni-Cu sulfide	Ni-Cu sulfide	0.94	0.06
EC-07-02			Magmatic	Magmatic	0.034	0.966	Ni-Cu sulfide	Ni-Cu sulfide	1.00	0.00

ID	Author	Deposit	RF mag-hyd model				RF mag model			
			Actual	Predicted	Probabilites		Actual	Predicted	Probabilities	
					Hydrothermal	Magmatic			Ni-Cu sulfide	Reef-type PGE
EC-07-03	Samalens et al. (2017)	Duluth	Magmatic	Magmatic	0.102	0.898	Ni-Cu sulfide	Ni-Cu sulfide	1.00	0.00
A4-15-01-01			Magmatic	Hydrothermal	0.89	0.11	Ni-Cu sulfide	Ni-Cu sulfide	0.99	0.01
A4-15-01-02			Magmatic	Hydrothermal	0.906	0.094	Ni-Cu sulfide	Ni-Cu sulfide	0.98	0.02
A4-15-01-03			Magmatic	Hydrothermal	0.918	0.082	Ni-Cu sulfide	Ni-Cu sulfide	0.99	0.01
A4-15-01-04			Magmatic	Hydrothermal	0.934	0.066	Ni-Cu sulfide	Ni-Cu sulfide	0.99	0.01
B1-384-04B-01			Magmatic	Magmatic	0.176	0.824	Ni-Cu sulfide	Ni-Cu sulfide	1.00	0.00
B1-384-04B-02			Magmatic	Magmatic	0.044	0.956	Ni-Cu sulfide	Ni-Cu sulfide	1.00	0.00
B1-384-05-01			Magmatic	Magmatic	0.008	0.992	Ni-Cu sulfide	Ni-Cu sulfide	0.75	0.25
B1-384-05-02			Magmatic	Magmatic	0.012	0.988	Ni-Cu sulfide	Ni-Cu sulfide	0.91	0.09
B1-384-08-01			Magmatic	Magmatic	0	1	Ni-Cu sulfide	Ni-Cu sulfide	0.91	0.09
B1-384-08-02			Magmatic	Magmatic	0.02	0.98	Ni-Cu sulfide	Ni-Cu sulfide	0.94	0.06
B1-384-12-01			Magmatic	Magmatic	0.016	0.984	Ni-Cu sulfide	Ni-Cu sulfide	1.00	0.00
B1-384-12-02			Magmatic	Magmatic	0.068	0.932	Ni-Cu sulfide	Ni-Cu sulfide	1.00	0.00
B1-384-12-03			Magmatic	Magmatic	0.308	0.692	Ni-Cu sulfide	Ni-Cu sulfide	0.96	0.04
DC-70			Magmatic	Hydrothermal	0.88	0.12	Ni-Cu sulfide	Ni-Cu sulfide	0.99	0.01
LTV-7555			Magmatic	Hydrothermal	0.828	0.172	Ni-Cu sulfide	Ni-Cu sulfide	0.54	0.46

Annexe C13. Confusion matrices from blind test for each model. Model to predict according to A) major geological system, B) magmatic deposit types, and C) hydrothermal deposit types. MCC: Matthew's Correlation Coefficient.

A

		Actual		
		Hydrothermal	Magmatic	Total
	Hydrothermal	637	55	692
Predicted	Magmatic	81	200	281
	Total	718	255	973
	Accuracy by class	89%	78%	
	Overall accuracy	86%		
	MCC	0.65		
	Kappa	0.65		
	F1-score	0.90		

B

		Actual		
		Ni-Cu sulfide	Reef-type PGE	Total
	Ni-Cu sulfide	195	30	225
Predicted	Reef-type PGE	15	15	30
	Total	210	45	255
	Accuracy by class	93%	33%	
	Overall accuracy	82%		
	MCC	0.31		
	Kappa	0.30		
	F1-score	0.89		

C

		Actual						
		Epithermal gold	IOCG	Orogenic gold	Porphyry	Skarn	VMS	Total
	Epithermal gold	10	0	0	0	0	11	21
	IOCG	4	29	30	10	15	21	109
	Orogenic gold	2	5	2	7	2	10	28
Predicted	Porphyry	0	7	5	66	0	34	112
	Skarn	0	3	9	0	9	10	31
	VMS	25	14	0	2	25	351	417
	Total	41	58	46	85	51	437	718
	Accuracy by class	24%	50%	4%	78%	18%	80%	
	Specificity by class	0.98	0.88	0.96	0.93	0.97	0.77	
	Precision by class	0.48	0.27	0.07	0.59	0.29	0.84	
	Recall by class	0.24	0.50	0.04	0.78	0.18	0.80	
	Overall accuracy	65%						
	MCC	0.43						
	Kappa	0.43						
	F1-score	0.42						

Annexe C14. Correlation coefficients (r) between accurcay in prediction and percentage of censored values by elements, number of analyses (n), percentage of missing elements (% miss) and percentage of elements without censored values (% compl); p-value with α=0.05.

A. Model by geological system

Magmatic deposits (11)

	% of censored values												
	Ni	Ga	In	Sb	Se	Ag	Zn	Pb	Sn	Bi	n	%miss	%compl
Accuracy	-0.30	NA	NA	-0.48	-0.70	-0.39	-0.04	-0.56	-0.47	-0.58	-0.16	-0.64	0.82
p-value	0.348	NA	NA	0.111	0.011	0.213	0.909	0.056	0.127	0.049	0.630	0.024	0.001

Hydrothermal deposits (15)

	% of censored values												
	Ni	Ga	In	Sb	Se	Ag	Zn	Pb	Sn	Bi	n	%miss	%compl
Accuracy	0.02	-0.18	-0.02	-0.76	0.04	0.14	0.09	0.19	0.09	0.29	0.13	0.21	0.20
p-value	0.950	0.539	0.947	0.002	0.905	0.629	0.757	0.516	0.753	0.321	0.649	0.465	0.489

All deposits (26)

	% of censored values												
	Ni	Ga	In	Sb	Se	Ag	Zn	Pb	Sn	Bi	n	%miss	%compl
Accuracy	-0.27	-0.16	-0.17	-0.55	-0.48	-0.35	-0.05	-0.33	-0.33	-0.31	-0.07	-0.29	0.47
p-value	0.213	0.489	0.429	0.007	0.015	0.104	0.805	0.127	0.127	0.154	0.746	0.162	0.017

B. Model by magmatic deposit type

Ni-Cu sulfide deposits (8)

	% of censored values								
	Te	Sn	Se	In	Bi	Zn	n	%miss	%compl
Accuracy	-0.10	-0.54	0.15	NA	0.15	-0.61	-0.06	-0.50	0.43
p-value	0.819	0.167	0.721	NA	0.721	0.110	0.880	0.204	0.290

All magmatic deposits (11)

	% of censored values								
	Te	Sn	Se	In	Bi	Zn	n	%miss	%compl
Accuracy	-0.60	-0.52	-0.68	NA	-0.62	0.07	0.28	-0.66	0.53
p-value	0.040	0.101	0.022	NA	0.031	0.843	0.400	0.019	0.044

C. Model by hydrothermal deposit type

VMS deposits (6)

	% of censored values														
	Se	Zn	Sn	In	Ga	Te	Ag	Sb	Bi	Co	Ni	Pb	n	%miss	%compl
Accuracy	-0.24	-0.16	-0.75	-0.25	-0.25	-0.36	-0.38	-0.82	-0.45	-0.54	-0.79	-0.62	-0.15	-0.28	0.84
p-value	0.645	0.763	0.083	0.629	0.629	0.482	0.462	0.047	0.376	0.271	0.063	0.192	0.773	0.595	0.036

All hydrothermal deposits (15)

	% of censored values														
	Se	Zn	Sn	In	Ga	Te	Ag	Sb	Bi	Co	Ni	Pb	n	%miss	%compl
Accuracy	-0.08	0.15	-0.31	0.12	0.001	-0.35	0.14	-0.28	-0.35	-0.10	0.04	0.15	0.25	0.04	0.16
p-value	0.773	0.597	0.268	0.674	0.997	0.195	0.607	0.305	0.200	0.730	0.897	0.600	0.361	0.885	0.565

Annexe C15. Predictions and probabilities by sample of chalcopyrite data from detrital grains in sediments from Churchill Province (Canada) using RF models. Data source: Duran et al. (2019).
Chalcopyrite analyses with Cu concentration >25% predicted as magmatic

	RFmodel model by geological system			RFmodel by magmatic deposit type		
		Probabilities			Probabilities	
Sample	Predicted	Hydrothermal	Magmatic	Predicted	Ni-Cu sulfide	Reef-type PGE
93724152	Magmatic	0.206	0.794	Ni-Cu sulfide	0.58	0.42
93724046	Magmatic	0.466	0.534	Ni-Cu sulfide	0.90	0.10
93724141	Magmatic	0.480	0.520	Ni-Cu sulfide	0.83	0.17
93724059	Magmatic	0.030	0.970	Reef-type PGE	0.49	0.51
93720066	Magmatic	0.240	0.760	Ni-Cu sulfide	0.67	0.33
93720042	Magmatic	0.026	0.974	Ni-Cu sulfide	0.95	0.05
93724062	Magmatic	0.470	0.530	Ni-Cu sulfide	0.91	0.09
93724036	Magmatic	0.090	0.910	Ni-Cu sulfide	0.95	0.05
93724123	Magmatic	0.388	0.612	Ni-Cu sulfide	0.98	0.02
93720066	Magmatic	0.288	0.712	Ni-Cu sulfide	0.86	0.14
93721013	Magmatic	0.308	0.692	Ni-Cu sulfide	0.88	0.12
93724272	Magmatic	0.006	0.994	Ni-Cu sulfide	0.54	0.46
93724025	Magmatic	0.324	0.676	Ni-Cu sulfide	0.81	0.19
93724058	Magmatic	0.450	0.550	Ni-Cu sulfide	0.75	0.25
93724099	Magmatic	0.158	0.842	Ni-Cu sulfide	0.89	0.11
93721044	Magmatic	0.138	0.862	Ni-Cu sulfide	0.98	0.02
93721013	Magmatic	0.486	0.514	Reef-type PGE	0.30	0.70
93724011	Magmatic	0.338	0.662	Ni-Cu sulfide	0.93	0.07
93724281	Magmatic	0.174	0.826	Reef-type PGE	0.14	0.86
93721128	Magmatic	0.048	0.952	Ni-Cu sulfide	0.91	0.09
93721128	Magmatic	0.072	0.928	Ni-Cu sulfide	0.95	0.05
93724062	Magmatic	0.078	0.922	Ni-Cu sulfide	0.71	0.29
93724099	Magmatic	0.294	0.706	Ni-Cu sulfide	0.89	0.11
93724059	Magmatic	0.176	0.824	Ni-Cu sulfide	1.00	0.00
93724099	Magmatic	0.274	0.726	Ni-Cu sulfide	0.90	0.10
93724046	Magmatic	0.396	0.604	Ni-Cu sulfide	0.83	0.17
93720062	Magmatic	0.262	0.738	Ni-Cu sulfide	0.95	0.05
93724099	Magmatic	0.306	0.694	Ni-Cu sulfide	0.89	0.11
93724112	Magmatic	0.340	0.660	Ni-Cu sulfide	0.88	0.12
93724284	Magmatic	0.036	0.964	Ni-Cu sulfide	0.88	0.12
93724086	Magmatic	0.054	0.946	Ni-Cu sulfide	0.99	0.01
93721044	Magmatic	0.224	0.776	Ni-Cu sulfide	0.93	0.07
93721013	Magmatic	0.290	0.710	Ni-Cu sulfide	0.80	0.20
93724099	Magmatic	0.382	0.618	Ni-Cu sulfide	0.90	0.10
93724099	Magmatic	0.260	0.740	Ni-Cu sulfide	0.89	0.11
93724099	Magmatic	0.366	0.634	Ni-Cu sulfide	0.88	0.12

	RFmodel model by geological system			RFmodel by magmatic deposit type		
		Probabilities			Probabilities	
Sample	Predicted	Hydrothermal	Magmatic	Predicted	Ni-Cu sulfide	Reef-type PGE
93724099	Magmatic	0.344	0.656	Ni-Cu sulfide	0.86	0.14
93720063	Magmatic	0.004	0.996	Ni-Cu sulfide	0.93	0.07
93724046	Magmatic	0.190	0.810	Ni-Cu sulfide	0.95	0.05
93724281	Magmatic	0.062	0.938	Reef-type PGE	0.15	0.85
93724156	Magmatic	0.430	0.570	Ni-Cu sulfide	0.97	0.03
93724048	Magmatic	0.064	0.936	Ni-Cu sulfide	0.87	0.13
93724099	Magmatic	0.332	0.668	Ni-Cu sulfide	0.87	0.13
93721044	Magmatic	0.206	0.794	Ni-Cu sulfide	0.69	0.31
93724112	Magmatic	0.460	0.540	Ni-Cu sulfide	0.86	0.14
93724040	Magmatic	0.068	0.932	Ni-Cu sulfide	0.95	0.05
93724059	Magmatic	0.310	0.690	Ni-Cu sulfide	0.89	0.11
93721084	Magmatic	0.092	0.908	Reef-type PGE	0.48	0.52
93724090	Magmatic	0.110	0.890	Ni-Cu sulfide	0.82	0.18
93721102	Magmatic	0.250	0.750	Ni-Cu sulfide	0.97	0.03
93724222	Magmatic	0.380	0.620	Ni-Cu sulfide	0.90	0.10
93724059	Magmatic	0.320	0.680	Ni-Cu sulfide	0.85	0.15
93724148	Magmatic	0.388	0.612	Ni-Cu sulfide	0.98	0.02
93720063	Magmatic	0.186	0.814	Ni-Cu sulfide	0.52	0.48
93720066	Magmatic	0.018	0.982	Ni-Cu sulfide	0.59	0.41
93720033	Magmatic	0.314	0.686	Reef-type PGE	0.37	0.63
93724085	Magmatic	0.282	0.718	Ni-Cu sulfide	0.64	0.36
93724085	Magmatic	0.226	0.774	Ni-Cu sulfide	0.68	0.32
93721199	Magmatic	0.476	0.524	Ni-Cu sulfide	0.64	0.36
93724086	Magmatic	0.328	0.672	Reef-type PGE	0.11	0.89
93724085	Magmatic	0.302	0.698	Ni-Cu sulfide	0.83	0.17
93721084	Magmatic	0.038	0.962	Ni-Cu sulfide	0.92	0.08
93724043	Magmatic	0.124	0.876	Reef-type PGE	0.29	0.71
93724085	Magmatic	0.380	0.620	Reef-type PGE	0.42	0.58
93720062	Magmatic	0.050	0.950	Ni-Cu sulfide	0.67	0.33
93724085	Magmatic	0.162	0.838	Ni-Cu sulfide	0.75	0.25
93721097	Magmatic	0.408	0.592	Ni-Cu sulfide	0.99	0.01
93724062	Magmatic	0.138	0.862	Ni-Cu sulfide	0.83	0.17
93724281	Magmatic	0.156	0.844	Reef-type PGE	0.01	0.99
93720063	Magmatic	0.230	0.770	Reef-type PGE	0.28	0.72
93724068	Magmatic	0.346	0.654	Ni-Cu sulfide	0.57	0.43
93724046	Magmatic	0.134	0.866	Ni-Cu sulfide	0.58	0.42
93724035	Magmatic	0.250	0.750	Ni-Cu sulfide	0.97	0.03
93724085	Magmatic	0.472	0.528	Reef-type PGE	0.50	0.50
93721102	Magmatic	0.124	0.876	Ni-Cu sulfide	0.87	0.13

	RFmodel model by geological system			RFmodel by magmatic deposit type		
		Probabilities			Probabilities	
Sample	Predicted	Hydrothermal	Magmatic	Predicted	Ni-Cu sulfide	Reef-type PGE
93724090	Magmatic	0.016	0.984	Reef-type PGE	0.34	0.66
93724151	Magmatic	0.354	0.646	Ni-Cu sulfide	0.55	0.45
93720042	Magmatic	0.438	0.562	Ni-Cu sulfide	0.97	0.03
93724159	Magmatic	0.298	0.702	Ni-Cu sulfide	0.74	0.26
93721044	Magmatic	0.276	0.724	Ni-Cu sulfide	0.55	0.45
93724148	Magmatic	0.344	0.656	Ni-Cu sulfide	0.91	0.09
93721097	Magmatic	0.416	0.584	Ni-Cu sulfide	0.98	0.02
93724141	Magmatic	0.362	0.638	Ni-Cu sulfide	0.88	0.12
93721097	Magmatic	0.378	0.622	Ni-Cu sulfide	0.92	0.08
93724285	Magmatic	0.176	0.824	Ni-Cu sulfide	0.53	0.47
93724136	Magmatic	0.208	0.792	Ni-Cu sulfide	0.70	0.30
93724095	Magmatic	0.164	0.836	Ni-Cu sulfide	0.60	0.40
93724060	Magmatic	0.420	0.580	Ni-Cu sulfide	0.56	0.44
93724009	Magmatic	0.246	0.754	Ni-Cu sulfide	0.99	0.01
93720063	Magmatic	0.360	0.640	Reef-type PGE	0.07	0.93
93724225	Magmatic	0.038	0.962	Reef-type PGE	0.42	0.58
93724085	Magmatic	0.360	0.640	Reef-type PGE	0.33	0.67
93724272	Magmatic	0.066	0.934	Reef-type PGE	0.32	0.68
93724085	Magmatic	0.300	0.700	Reef-type PGE	0.49	0.51
93724043	Magmatic	0.462	0.538	Ni-Cu sulfide	0.70	0.30
93721098	Magmatic	0.448	0.552	Ni-Cu sulfide	0.90	0.10
93721098	Magmatic	0.424	0.576	Ni-Cu sulfide	0.87	0.13
93724047	Magmatic	0.460	0.540	Ni-Cu sulfide	0.99	0.01
93724289	Magmatic	0.404	0.596	Ni-Cu sulfide	0.71	0.29
93724284	Magmatic	0.494	0.506	Reef-type PGE	0.34	0.66
93724062	Magmatic	0.256	0.744	Ni-Cu sulfide	0.69	0.31
93720063	Magmatic	0.450	0.550	Ni-Cu sulfide	0.93	0.07
93720031	Magmatic	0.296	0.704	Reef-type PGE	0.04	0.96
93724033	Magmatic	0.268	0.732	Ni-Cu sulfide	0.59	0.41
93721097	Magmatic	0.260	0.740	Reef-type PGE	0.26	0.74
93720066	Magmatic	0.080	0.920	Ni-Cu sulfide	0.58	0.42
93724222	Magmatic	0.452	0.548	Reef-type PGE	0.16	0.84
93724272	Magmatic	0.374	0.626	Ni-Cu sulfide	0.63	0.37
93724048	Magmatic	0.288	0.712	Ni-Cu sulfide	0.87	0.13
93724111	Magmatic	0.246	0.754	Reef-type PGE	0.24	0.76
93724048	Magmatic	0.474	0.526	Ni-Cu sulfide	0.89	0.11
93724055	Magmatic	0.392	0.608	Ni-Cu sulfide	0.56	0.44
93724006	Magmatic	0.446	0.554	Reef-type PGE	0.10	0.90
93724284	Magmatic	0.406	0.594	Ni-Cu sulfide	0.66	0.34

	RFmodel model by geological system			RFmodel by magmatic deposit type		
		Probabilities			Probabilities	
Sample	Predicted	Hydrothermal	Magmatic	Predicted	Ni-Cu sulfide	Reef-type PGE
93721013	Magmatic	0.454	0.546	Ni-Cu sulfide	0.61	0.39
93721093	Magmatic	0.344	0.656	Ni-Cu sulfide	0.86	0.14
93724048	Magmatic	0.496	0.504	Ni-Cu sulfide	0.93	0.07
93724059	Magmatic	0.432	0.568	Reef-type PGE	0.05	0.95
93721084	Magmatic	0.424	0.576	Reef-type PGE	0.48	0.52
93724059	Magmatic	0.410	0.590	Reef-type PGE	0.12	0.88
93720040	Magmatic	0.494	0.506	Ni-Cu sulfide	0.51	0.49
93721011	Magmatic	0.444	0.556	Ni-Cu sulfide	0.94	0.06
93724046	Magmatic	0.338	0.662	Reef-type PGE	0.07	0.93
93724046	Magmatic	0.344	0.656	Reef-type PGE	0.40	0.60
93724099	Magmatic	0.402	0.598	Reef-type PGE	0.44	0.56
93724178	Magmatic	0.422	0.578	Reef-type PGE	0.15	0.85
93720040	Magmatic	0.418	0.582	Ni-Cu sulfide	0.94	0.06
93724155	Magmatic	0.466	0.534	Ni-Cu sulfide	0.94	0.06
93721093	Magmatic	0.350	0.650	Ni-Cu sulfide	0.90	0.10
93720040	Magmatic	0.316	0.684	Ni-Cu sulfide	0.94	0.06
93721088	Magmatic	0.222	0.778	Ni-Cu sulfide	0.99	0.01
93720040	Magmatic	0.190	0.810	Ni-Cu sulfide	0.56	0.44
93720042	Magmatic	0.148	0.852	Ni-Cu sulfide	0.87	0.13
93720066	Magmatic	0.492	0.508	Ni-Cu sulfide	0.87	0.13
93724157	Magmatic	0.172	0.828	Ni-Cu sulfide	0.97	0.03
93724151	Magmatic	0.152	0.848	Ni-Cu sulfide	0.99	0.01
93724076	Magmatic	0.098	0.902	Ni-Cu sulfide	0.60	0.40
93721084	Magmatic	0.354	0.646	Ni-Cu sulfide	0.80	0.20
93721044	Magmatic	0.042	0.958	Ni-Cu sulfide	0.87	0.13
93724248	Magmatic	0.324	0.676	Ni-Cu sulfide	0.91	0.09
93724065	Magmatic	0.270	0.730	Ni-Cu sulfide	0.57	0.43
93721088	Magmatic	0.132	0.868	Ni-Cu sulfide	0.54	0.46
93721044	Magmatic	0.398	0.602	Ni-Cu sulfide	0.91	0.09
93724272	Magmatic	0.214	0.786	Ni-Cu sulfide	0.83	0.17
93720040	Magmatic	0.488	0.512	Ni-Cu sulfide	0.91	0.09
93720031	Magmatic	0.000	1.000	Ni-Cu sulfide	0.60	0.40
93721098	Magmatic	0.338	0.662	Ni-Cu sulfide	0.56	0.44
93724052	Magmatic	0.436	0.564	Ni-Cu sulfide	0.94	0.06
93721093	Magmatic	0.168	0.832	Ni-Cu sulfide	0.57	0.43
93724050	Magmatic	0.168	0.832	Ni-Cu sulfide	0.97	0.03
93724052	Magmatic	0.138	0.862	Ni-Cu sulfide	0.54	0.46
93724118	Magmatic	0.232	0.768	Ni-Cu sulfide	0.91	0.09
93724159	Magmatic	0.060	0.940	Ni-Cu sulfide	0.98	0.02

	RFmodel model by geological system			RFmodel by magmatic deposit type		
		Probabilities			Probabilities	
Sample	Predicted	Hydrothermal	Magmatic	Predicted	Ni-Cu sulfide	Reef-type PGE
93724049	Magmatic	0.374	0.626	Ni-Cu sulfide	0.96	0.04
93724254	Magmatic	0.248	0.752	Ni-Cu sulfide	0.97	0.03
93724033	Magmatic	0.204	0.796	Ni-Cu sulfide	0.95	0.05
93724068	Magmatic	0.010	0.990	Ni-Cu sulfide	1.00	0.00
93724051	Magmatic	0.448	0.552	Ni-Cu sulfide	0.50	0.50
93724049	Magmatic	0.164	0.836	Ni-Cu sulfide	0.51	0.49
93724177	Magmatic	0.098	0.902	Ni-Cu sulfide	0.82	0.18
93724047	Magmatic	0.014	0.986	Ni-Cu sulfide	0.84	0.16
93724051	Magmatic	0.144	0.856	Ni-Cu sulfide	0.58	0.42
93724049	Magmatic	0.118	0.882	Ni-Cu sulfide	0.51	0.49
93724275	Magmatic	0.352	0.648	Ni-Cu sulfide	0.60	0.40
93724011	Magmatic	0.146	0.854	Ni-Cu sulfide	0.57	0.43
93724032	Magmatic	0.176	0.824	Ni-Cu sulfide	0.90	0.10
93724284	Magmatic	0.472	0.528	Ni-Cu sulfide	0.98	0.02
93720057	Magmatic	0.150	0.850	Ni-Cu sulfide	0.53	0.47
93724049	Magmatic	0.304	0.696	Ni-Cu sulfide	0.97	0.03
93724086	Magmatic	0.386	0.614	Ni-Cu sulfide	0.99	0.01
93724004	Magmatic	0.336	0.664	Ni-Cu sulfide	0.56	0.44
93724274	Magmatic	0.212	0.788	Ni-Cu sulfide	0.80	0.20
93721099	Magmatic	0.386	0.614	Ni-Cu sulfide	0.91	0.09
93724281	Magmatic	0.192	0.808	Ni-Cu sulfide	0.85	0.15
93724009	Magmatic	0.256	0.744	Ni-Cu sulfide	0.61	0.39
93724031	Magmatic	0.458	0.542	Ni-Cu sulfide	0.91	0.09
93721099	Magmatic	0.246	0.754	Ni-Cu sulfide	0.90	0.10
93721011	Magmatic	0.236	0.764	Ni-Cu sulfide	0.53	0.47
93720057	Magmatic	0.290	0.710	Ni-Cu sulfide	0.92	0.08
93724033	Magmatic	0.354	0.646	Ni-Cu sulfide	0.68	0.32
93720062	Magmatic	0.290	0.710	Reef-type PGE	0.17	0.83
93724284	Magmatic	0.212	0.788	Reef-type PGE	0.05	0.95
93721098	Magmatic	0.244	0.756	Reef-type PGE	0.00	1.00
93721099	Magmatic	0.128	0.872	Reef-type PGE	0.09	0.91
93721014	Magmatic	0.014	0.986	Reef-type PGE	0.47	0.53
93721014	Magmatic	0.194	0.806	Reef-type PGE	0.32	0.68
93724159	Magmatic	0.110	0.890	Reef-type PGE	0.32	0.68
93721088	Magmatic	0.108	0.892	Reef-type PGE	0.06	0.94
93724284	Magmatic	0.328	0.672	Reef-type PGE	0.02	0.98
93724150	Magmatic	0.092	0.908	Reef-type PGE	0.11	0.89
93724284	Magmatic	0.090	0.910	Reef-type PGE	0.03	0.97
93724066	Magmatic	0.142	0.858	Reef-type PGE	0.19	0.81

	RFmodel model by geological system			RFmodel by magmatic deposit type		
		Probabilities			Probabilities	
Sample	Predicted	Hydrothermal	Magmatic	Predicted	Ni-Cu sulfide	Reef-type PGE
93724141	Magmatic	0.202	0.798	Reef-type PGE	0.38	0.62
93724141	Magmatic	0.116	0.884	Reef-type PGE	0.35	0.65
93724076	Magmatic	0.060	0.940	Reef-type PGE	0.10	0.90
93724049	Magmatic	0.070	0.930	Reef-type PGE	0.48	0.52
93724001	Magmatic	0.452	0.548	Reef-type PGE	0.06	0.94
93721044	Magmatic	0.338	0.662	Reef-type PGE	0.40	0.60
93724070	Magmatic	0.390	0.610	Reef-type PGE	0.12	0.88
93724117	Magmatic	0.438	0.562	Reef-type PGE	0.13	0.87
93724281	Magmatic	0.174	0.826	Reef-type PGE	0.05	0.95
93724159	Magmatic	0.130	0.870	Reef-type PGE	0.28	0.72
93724279	Magmatic	0.166	0.834	Reef-type PGE	0.10	0.90
93721277	Magmatic	0.056	0.944	Reef-type PGE	0.47	0.53
93724040	Magmatic	0.184	0.816	Reef-type PGE	0.47	0.53
93724010	Magmatic	0.490	0.510	Reef-type PGE	0.37	0.63
93724073	Magmatic	0.160	0.840	Reef-type PGE	0.04	0.96
93720062	Magmatic	0.436	0.564	Reef-type PGE	0.48	0.52
93721102	Magmatic	0.126	0.874	Reef-type PGE	0.47	0.53

Chalcopyrite analyses with Cu concentration <25% predicted as magmatic

	RFmodel model by geological system			RFmodel by magmatic deposit type		
		Probabilities			Probabilities	
Sample	Predicted	Hydrothermal	Magmatic	Predicted	Ni-Cu sulfide	Reef-type PGE
93720033	Magmatic	0.396	0.604	Ni-Cu sulfide	0.97	0.03
93721014	Magmatic	0.478	0.522	Ni-Cu sulfide	0.85	0.15
93721012	Magmatic	0.482	0.518	Ni-Cu sulfide	0.93	0.07
93721011	Magmatic	0.386	0.614	Ni-Cu sulfide	0.73	0.27
93720040	Magmatic	0.446	0.554	Ni-Cu sulfide	0.58	0.42
93721014	Magmatic	0.248	0.752	Ni-Cu sulfide	0.54	0.46
93721012	Magmatic	0.200	0.800	Ni-Cu sulfide	0.55	0.45
93721014	Magmatic	0.316	0.684	Ni-Cu sulfide	0.95	0.05
93720063	Magmatic	0.378	0.622	Ni-Cu sulfide	0.94	0.06
93720062	Magmatic	0.000	1.000	Ni-Cu sulfide	0.57	0.43
93721013	Magmatic	0.284	0.716	Ni-Cu sulfide	0.93	0.07
93721013	Magmatic	0.414	0.586	Ni-Cu sulfide	1.00	0.00
93720062	Magmatic	0.034	0.966	Ni-Cu sulfide	0.88	0.12
93720062	Magmatic	0.196	0.804	Ni-Cu sulfide	0.84	0.16
93721013	Magmatic	0.100	0.900	Ni-Cu sulfide	0.75	0.25
93721013	Magmatic	0.204	0.796	Ni-Cu sulfide	0.51	0.49

	RFmodel model by geological system			RFmodel by magmatic deposit type		
		Probabilities			Probabilities	
Sample	Predicted	Hydrothermal	Magmatic	Predicted	Ni-Cu sulfide	Reef-type PGE
93721011	Magmatic	0.352	0.648	Ni-Cu sulfide	0.88	0.12
93721012	Magmatic	0.416	0.584	Ni-Cu sulfide	0.82	0.18
93721011	Magmatic	0.398	0.602	Ni-Cu sulfide	0.76	0.24
93721013	Magmatic	0.374	0.626	Ni-Cu sulfide	0.73	0.27
93720066	Magmatic	0.314	0.686	Ni-Cu sulfide	0.67	0.33
93720066	Magmatic	0.404	0.596	Ni-Cu sulfide	0.68	0.32
93720040	Magmatic	0.262	0.738	Ni-Cu sulfide	0.83	0.17
93720066	Magmatic	0.284	0.716	Ni-Cu sulfide	0.58	0.42
93721014	Magmatic	0.420	0.580	Ni-Cu sulfide	0.99	0.01
93721011	Magmatic	0.450	0.550	Ni-Cu sulfide	0.82	0.18
93721011	Magmatic	0.418	0.582	Ni-Cu sulfide	1.00	0.00
93724154	Magmatic	0.126	0.874	Ni-Cu sulfide	0.98	0.02
93721013	Magmatic	0.316	0.684	Ni-Cu sulfide	0.75	0.25
93720042	Magmatic	0.498	0.502	Ni-Cu sulfide	0.93	0.07
93721011	Magmatic	0.428	0.572	Ni-Cu sulfide	0.67	0.33
93720042	Magmatic	0.146	0.854	Ni-Cu sulfide	0.84	0.16
93720033	Magmatic	0.472	0.528	Ni-Cu sulfide	0.51	0.49
93721014	Magmatic	0.322	0.678	Reef-type PGE	0.12	0.88
93721014	Magmatic	0.336	0.664	Reef-type PGE	0.39	0.61
93720062	Magmatic	0.264	0.736	Reef-type PGE	0.44	0.56
93721012	Magmatic	0.148	0.852	Reef-type PGE	0.40	0.60
93720063	Magmatic	0.362	0.638	Reef-type PGE	0.00	1.00
93721014	Magmatic	0.048	0.952	Reef-type PGE	0.00	1.00
93720063	Magmatic	0.324	0.676	Reef-type PGE	0.00	1.00
93721014	Magmatic	0.470	0.530	Reef-type PGE	0.17	0.83
93721011	Magmatic	0.240	0.760	Reef-type PGE	0.19	0.81
93721013	Magmatic	0.036	0.964	Reef-type PGE	0.01	0.99

Chalcopyrite analyses with Cu concentration >25% predicted as hydrothermal

	RFmodel model by geological system			hydrothermal deposit type						
		Probabilities			Probabilities					
Sample	Predicted	Hydrothermal	Magmatic	Predicted	Epithermal gold	IOCG	Orogenic gold	Porphyry	Skarn	VMS
93724285	Hydrothermal	0.586	0.414	Epithermal gold	0.44	0.08	0.13	0.10	0.08	0.18
93721098	Hydrothermal	0.606	0.394	Epithermal gold	0.38	0.13	0.18	0.01	0.12	0.17
93724049	Hydrothermal	0.984	0.016	Epithermal gold	0.31	0.15	0.11	0.13	0.03	0.26
93721044	Hydrothermal	0.784	0.216	Epithermal gold	0.35	0.16	0.16	0.25	0.05	0.03
93721266	Hydrothermal	0.520	0.480	Epithermal gold	0.23	0.13	0.19	0.20	0.08	0.18
93724058	Hydrothermal	0.724	0.276	Epithermal gold	0.29	0.19	0.24	0.01	0.09	0.17

	RFmodel model by geological system			hydrothermal deposit type						
		Probabilities			Probabilities					
					Epithermal		Orogenic			
Sample	Predicted	Hydrothermal	Magmatic	Predicted	gold	IOCG	gold	Porphyry	Skarn	VMS
93721266	Hydrothermal	0.590	0.410	Epithermal gold	0.24	0.13	0.17	0.20	0.08	0.18
93724113	Hydrothermal	0.914	0.086	Epithermal gold	0.21	0.21	0.20	0.04	0.14	0.20
93724049	Hydrothermal	0.828	0.172	Epithermal gold	0.58	0.10	0.08	0.08	0.05	0.12
93721093	Hydrothermal	0.984	0.016	Epithermal gold	0.50	0.18	0.15	0.02	0.07	0.08
93721266	Hydrothermal	0.560	0.440	Epithermal gold	0.23	0.16	0.17	0.18	0.07	0.19
93724253	Hydrothermal	0.846	0.154	Epithermal gold	0.48	0.20	0.06	0.06	0.11	0.09
93724253	Hydrothermal	0.732	0.268	Epithermal gold	0.25	0.22	0.11	0.09	0.18	0.14
93724053	Hydrothermal	0.928	0.072	IOCG	0.07	0.44	0.10	0.13	0.07	0.20
93724126	Hydrothermal	0.892	0.108	IOCG	0.20	0.42	0.15	0.17	0.02	0.03
93724270	Hydrothermal	0.806	0.194	IOCG	0.05	0.36	0.11	0.07	0.19	0.21
93721013	Hydrothermal	0.948	0.052	IOCG	0.05	0.40	0.02	0.38	0.02	0.12
93721014	Hydrothermal	0.602	0.398	IOCG	0.05	0.53	0.10	0.06	0.14	0.12
93724081	Hydrothermal	0.660	0.340	IOCG	0.13	0.34	0.10	0.04	0.08	0.31
93724270	Hydrothermal	0.944	0.056	IOCG	0.01	0.56	0.11	0.17	0.09	0.08
93721099	Hydrothermal	0.966	0.034	IOCG	0.00	0.69	0.09	0.12	0.02	0.07
93720040	Hydrothermal	0.574	0.426	IOCG	0.21	0.26	0.11	0.10	0.20	0.13
93721097	Hydrothermal	0.986	0.014	IOCG	0.05	0.38	0.11	0.05	0.03	0.37
93721093	Hydrothermal	0.858	0.142	IOCG	0.05	0.42	0.05	0.31	0.04	0.13
93724062	Hydrothermal	0.774	0.226	IOCG	0.03	0.42	0.04	0.08	0.08	0.35
93721099	Hydrothermal	0.952	0.048	IOCG	0.00	0.61	0.03	0.18	0.02	0.16
93724270	Hydrothermal	0.788	0.212	IOCG	0.08	0.32	0.13	0.08	0.20	0.19
93721098	Hydrothermal	0.976	0.024	IOCG	0.01	0.81	0.04	0.04	0.05	0.05
93721098	Hydrothermal	0.586	0.414	IOCG	0.13	0.33	0.10	0.19	0.08	0.17
93724061	Hydrothermal	0.818	0.182	IOCG	0.01	0.60	0.01	0.01	0.19	0.18
93724171	Hydrothermal	0.554	0.446	IOCG	0.05	0.65	0.05	0.07	0.05	0.13
93724151	Hydrothermal	0.896	0.104	IOCG	0.03	0.41	0.23	0.09	0.05	0.19
93724270	Hydrothermal	0.786	0.214	IOCG	0.03	0.48	0.12	0.05	0.11	0.22
93724051	Hydrothermal	0.968	0.032	IOCG	0.04	0.40	0.02	0.36	0.01	0.17
93721011	Hydrothermal	0.588	0.412	IOCG	0.08	0.43	0.10	0.17	0.05	0.17
93724162	Hydrothermal	0.650	0.350	IOCG	0.04	0.36	0.34	0.04	0.09	0.14
93724171	Hydrothermal	0.618	0.382	IOCG	0.05	0.50	0.11	0.03	0.13	0.19
93724032	Hydrothermal	0.890	0.110	IOCG	0.12	0.29	0.10	0.23	0.02	0.24
93724059	Hydrothermal	0.544	0.456	IOCG	0.09	0.32	0.07	0.05	0.31	0.15
93724264	Hydrothermal	0.938	0.062	IOCG	0.17	0.24	0.15	0.14	0.19	0.10
93724049	Hydrothermal	0.960	0.040	IOCG	0.09	0.40	0.28	0.17	0.03	0.03
93724150	Hydrothermal	0.872	0.128	IOCG	0.03	0.47	0.01	0.44	0.01	0.04
93724272	Hydrothermal	0.992	0.008	IOCG	0.00	0.72	0.02	0.04	0.05	0.16
93724086	Hydrothermal	0.946	0.054	IOCG	0.06	0.34	0.22	0.32	0.04	0.02
93724270	Hydrothermal	0.784	0.216	IOCG	0.03	0.45	0.09	0.04	0.12	0.26

	RFmodel model by geological system			hydrothermal deposit type						
		Probabilities			Probabilities					
					Epithermal		Orogenic			
Sample	Predicted	Hydrothermal	Magmatic	Predicted	gold	IOCG	gold	Porphyry	Skarn	VMS
93724058	Hydrothermal	0.744	0.256	IOCG	0.20	0.27	0.25	0.03	0.08	0.17
93721099	Hydrothermal	0.976	0.024	IOCG	0.03	0.46	0.16	0.21	0.06	0.08
93724147	Hydrothermal	0.646	0.354	IOCG	0.04	0.67	0.08	0.04	0.08	0.10
93724270	Hydrothermal	0.848	0.152	IOCG	0.02	0.55	0.09	0.04	0.11	0.21
93724062	Hydrothermal	0.698	0.302	IOCG	0.06	0.44	0.13	0.04	0.21	0.12
93724052	Hydrothermal	0.696	0.304	IOCG	0.06	0.49	0.10	0.12	0.11	0.12
93724132	Hydrothermal	0.912	0.088	IOCG	0.06	0.32	0.25	0.09	0.10	0.18
93724049	Hydrothermal	0.958	0.042	IOCG	0.12	0.52	0.07	0.17	0.09	0.03
93724146	Hydrothermal	0.716	0.284	IOCG	0.08	0.40	0.16	0.13	0.06	0.18
93720060	Hydrothermal	0.970	0.030	IOCG	0.24	0.42	0.04	0.09	0.16	0.06
93724052	Hydrothermal	0.636	0.364	IOCG	0.03	0.48	0.10	0.20	0.10	0.09
93724009	Hydrothermal	0.926	0.074	IOCG	0.10	0.30	0.28	0.25	0.04	0.03
93724270	Hydrothermal	0.780	0.220	IOCG	0.03	0.52	0.10	0.04	0.11	0.21
93721013	Hydrothermal	0.930	0.070	IOCG	0.02	0.49	0.03	0.34	0.04	0.07
93721099	Hydrothermal	0.918	0.082	IOCG	0.06	0.48	0.16	0.18	0.02	0.10
93724251	Hydrothermal	0.988	0.012	IOCG	0.02	0.74	0.04	0.07	0.03	0.11
93721099	Hydrothermal	0.978	0.022	IOCG	0.08	0.44	0.02	0.05	0.18	0.23
93724032	Hydrothermal	0.710	0.290	IOCG	0.13	0.28	0.03	0.23	0.10	0.23
93724151	Hydrothermal	0.724	0.276	IOCG	0.03	0.30	0.20	0.09	0.12	0.27
93724007	Hydrothermal	0.580	0.420	IOCG	0.06	0.33	0.08	0.15	0.10	0.28
93724126	Hydrothermal	0.882	0.118	IOCG	0.13	0.47	0.05	0.27	0.04	0.04
93724136	Hydrothermal	0.762	0.238	IOCG	0.15	0.36	0.13	0.16	0.13	0.07
93724243	Hydrothermal	0.836	0.164	IOCG	0.14	0.24	0.23	0.07	0.14	0.18
93724270	Hydrothermal	0.716	0.284	IOCG	0.01	0.58	0.06	0.03	0.08	0.23
93724217	Hydrothermal	0.948	0.052	IOCG	0.02	0.84	0.03	0.04	0.04	0.04
93720040	Hydrothermal	0.634	0.366	IOCG	0.17	0.32	0.13	0.12	0.12	0.14
93724002	Hydrothermal	0.682	0.318	IOCG	0.01	0.43	0.07	0.07	0.22	0.20
93721102	Hydrothermal	0.720	0.280	IOCG	0.05	0.40	0.12	0.16	0.10	0.17
93724025	Hydrothermal	0.988	0.012	IOCG	0.01	0.81	0.05	0.11	0.01	0.01
93724050	Hydrothermal	0.798	0.202	IOCG	0.01	0.51	0.03	0.04	0.12	0.30
93724243	Hydrothermal	0.886	0.114	IOCG	0.08	0.34	0.23	0.07	0.09	0.18
93724059	Hydrothermal	0.772	0.228	IOCG	0.08	0.41	0.08	0.03	0.29	0.10
93724289	Hydrothermal	0.630	0.370	IOCG	0.11	0.30	0.09	0.05	0.29	0.16
93724087	Hydrothermal	0.684	0.316	IOCG	0.04	0.72	0.06	0.06	0.07	0.05
93724053	Hydrothermal	0.984	0.016	IOCG	0.12	0.32	0.06	0.22	0.04	0.24
93724073	Hydrothermal	0.710	0.290	IOCG	0.02	0.59	0.07	0.10	0.18	0.03
93724059	Hydrothermal	0.732	0.268	IOCG	0.09	0.44	0.07	0.03	0.28	0.09
93720062	Hydrothermal	0.520	0.480	IOCG	0.01	0.41	0.02	0.04	0.25	0.27
93724167	Hydrothermal	0.626	0.374	IOCG	0.05	0.52	0.09	0.19	0.11	0.04

	RFmodel model by geological system			hydrothermal deposit type						
		Probabilities			Probabilities					
					Epithermal		Orogenic			
Sample	Predicted	Hydrothermal	Magmatic	Predicted	gold	IOCG	gold	Porphyry	Skarn	VMS
93724014	Hydrothermal	0.946	0.054	IOCG	0.14	0.33	0.19	0.28	0.04	0.03
93722387	Hydrothermal	0.988	0.012	IOCG	0.03	0.38	0.08	0.11	0.21	0.18
93724253	Hydrothermal	0.726	0.274	IOCG	0.18	0.25	0.05	0.15	0.16	0.21
93724086	Hydrothermal	0.710	0.290	IOCG	0.00	0.87	0.02	0.05	0.04	0.03
93724084	Hydrothermal	0.528	0.472	IOCG	0.06	0.31	0.13	0.22	0.13	0.14
93724178	Hydrothermal	0.958	0.042	IOCG	0.05	0.35	0.12	0.13	0.13	0.22
93724030	Hydrothermal	0.892	0.108	IOCG	0.11	0.28	0.04	0.23	0.11	0.23
93721099	Hydrothermal	0.934	0.066	IOCG	0.01	0.42	0.22	0.20	0.03	0.12
93724256	Hydrothermal	0.876	0.124	IOCG	0.02	0.62	0.04	0.16	0.10	0.05
93720116	Hydrothermal	0.918	0.082	IOCG	0.01	0.78	0.07	0.07	0.03	0.04
93724046	Hydrothermal	0.928	0.072	IOCG	0.20	0.42	0.17	0.18	0.01	0.02
93724046	Hydrothermal	0.936	0.064	IOCG	0.02	0.55	0.01	0.33	0.02	0.08
93720031	Hydrothermal	0.536	0.464	IOCG	0.00	0.46	0.03	0.13	0.12	0.27
93724086	Hydrothermal	0.518	0.482	IOCG	0.03	0.31	0.14	0.16	0.13	0.24
93724086	Hydrothermal	0.890	0.110	IOCG	0.07	0.44	0.06	0.36	0.03	0.03
93724079	Hydrothermal	0.978	0.022	IOCG	0.09	0.57	0.08	0.16	0.08	0.02
93720040	Hydrothermal	0.814	0.186	IOCG	0.07	0.38	0.16	0.28	0.05	0.07
93724038	Hydrothermal	0.830	0.170	IOCG	0.02	0.45	0.02	0.34	0.06	0.10
93724251	Hydrothermal	0.960	0.040	IOCG	0.29	0.30	0.27	0.08	0.04	0.02
93721099	Hydrothermal	0.984	0.016	IOCG	0.00	0.71	0.07	0.04	0.03	0.15
93724271	Hydrothermal	0.938	0.062	IOCG	0.07	0.35	0.12	0.34	0.03	0.09
93724031	Hydrothermal	0.960	0.040	IOCG	0.22	0.36	0.12	0.02	0.17	0.11
93724049	Hydrothermal	0.996	0.004	IOCG	0.04	0.40	0.12	0.31	0.06	0.06
93724038	Hydrothermal	0.868	0.132	IOCG	0.03	0.47	0.01	0.33	0.06	0.11
93720042	Hydrothermal	0.750	0.250	IOCG	0.02	0.40	0.10	0.03	0.09	0.35
93721088	Hydrothermal	0.874	0.126	IOCG	0.02	0.42	0.04	0.06	0.11	0.35
93721099	Hydrothermal	0.996	0.004	IOCG	0.01	0.56	0.05	0.19	0.06	0.13
93724086	Hydrothermal	0.982	0.018	IOCG	0.01	0.79	0.03	0.04	0.04	0.08
93724252	Hydrothermal	0.954	0.046	Orogenic gold	0.04	0.10	0.37	0.07	0.11	0.31
93721099	Hydrothermal	0.962	0.038	Orogenic gold	0.03	0.29	0.51	0.09	0.02	0.06
93721013	Hydrothermal	0.954	0.046	Orogenic gold	0.05	0.28	0.35	0.19	0.10	0.03
93721266	Hydrothermal	0.602	0.398	Orogenic gold	0.21	0.11	0.24	0.17	0.08	0.20
93720042	Hydrothermal	0.850	0.150	Orogenic gold	0.17	0.19	0.28	0.05	0.14	0.17
93724062	Hydrothermal	0.938	0.062	Orogenic gold	0.17	0.23	0.38	0.01	0.08	0.12
93721099	Hydrothermal	0.978	0.022	Orogenic gold	0.03	0.34	0.34	0.03	0.14	0.12
93720031	Hydrothermal	0.664	0.336	Porphyry	0.06	0.08	0.04	0.61	0.04	0.18
93721013	Hydrothermal	0.834	0.166	Porphyry	0.13	0.11	0.07	0.62	0.01	0.06
93724239	Hydrothermal	0.894	0.106	Porphyry	0.02	0.25	0.01	0.68	0.00	0.03
93724123	Hydrothermal	0.962	0.038	Porphyry	0.15	0.14	0.03	0.40	0.03	0.24

	RFmodel model by geological system			hydrothermal deposit type						
		Probabilities			Probabilities					
					Epithermal		Orogenic			
Sample	Predicted	Hydrothermal	Magmatic	Predicted	gold	IOCG	gold	Porphyry	Skarn	VMS
93724264	Hydrothermal	0.576	0.424	Porphyry	0.05	0.18	0.08	0.54	0.01	0.13
93720066	Hydrothermal	0.922	0.078	Porphyry	0.01	0.03	0.02	0.88	0.01	0.06
93721014	Hydrothermal	0.716	0.284	Porphyry	0.01	0.11	0.01	0.73	0.02	0.11
93724151	Hydrothermal	0.616	0.384	Porphyry	0.03	0.14	0.01	0.63	0.02	0.18
93724163	Hydrothermal	0.966	0.034	Porphyry	0.03	0.07	0.04	0.71	0.01	0.14
93724136	Hydrothermal	0.832	0.168	Porphyry	0.05	0.18	0.07	0.42	0.03	0.25
93721044	Hydrothermal	0.604	0.396	Porphyry	0.16	0.09	0.06	0.52	0.02	0.16
93720042	Hydrothermal	0.838	0.162	Porphyry	0.06	0.28	0.05	0.54	0.01	0.05
93724004	Hydrothermal	0.738	0.262	Porphyry	0.07	0.05	0.03	0.76	0.00	0.08
93721044	Hydrothermal	0.948	0.052	Porphyry	0.07	0.09	0.04	0.67	0.02	0.11
93721013	Hydrothermal	0.710	0.290	Porphyry	0.12	0.15	0.03	0.58	0.04	0.08
93721099	Hydrothermal	0.758	0.242	Porphyry	0.04	0.30	0.03	0.40	0.02	0.21
93724222	Hydrothermal	0.570	0.430	Porphyry	0.07	0.19	0.07	0.42	0.06	0.19
93724147	Hydrothermal	0.536	0.464	Porphyry	0.04	0.13	0.11	0.37	0.03	0.31
93721014	Hydrothermal	0.830	0.170	Porphyry	0.11	0.23	0.09	0.32	0.10	0.15
93724141	Hydrothermal	0.800	0.200	Porphyry	0.25	0.11	0.13	0.43	0.02	0.04
93720031	Hydrothermal	0.898	0.102	Porphyry	0.06	0.29	0.12	0.43	0.05	0.04
93721044	Hydrothermal	0.890	0.110	Porphyry	0.03	0.21	0.02	0.55	0.01	0.19
93721099	Hydrothermal	0.522	0.478	Porphyry	0.12	0.11	0.10	0.51	0.03	0.13
93724045	Hydrothermal	0.814	0.186	Porphyry	0.05	0.07	0.03	0.81	0.00	0.03
93724159	Hydrothermal	0.942	0.058	Porphyry	0.02	0.04	0.00	0.87	0.00	0.06
93724261	Hydrothermal	0.908	0.092	Porphyry	0.20	0.14	0.12	0.43	0.08	0.03
93724157	Hydrothermal	0.778	0.222	Porphyry	0.25	0.26	0.03	0.27	0.06	0.14
93724021	Hydrothermal	0.882	0.118	Porphyry	0.03	0.20	0.02	0.71	0.00	0.04
93724117	Hydrothermal	0.736	0.264	Porphyry	0.24	0.07	0.10	0.40	0.03	0.17
93724065	Hydrothermal	0.956	0.044	Porphyry	0.26	0.19	0.04	0.28	0.00	0.23
93720062	Hydrothermal	0.870	0.130	Porphyry	0.19	0.11	0.05	0.43	0.02	0.19
93724049	Hydrothermal	0.996	0.004	Porphyry	0.04	0.34	0.14	0.36	0.06	0.06
93724162	Hydrothermal	0.860	0.140	Porphyry	0.02	0.24	0.02	0.67	0.01	0.04
93724055	Hydrothermal	0.988	0.012	Porphyry	0.05	0.21	0.01	0.45	0.01	0.27
93724191	Hydrothermal	0.920	0.080	Porphyry	0.01	0.10	0.01	0.69	0.01	0.17
93724126	Hydrothermal	0.824	0.176	Porphyry	0.12	0.37	0.05	0.38	0.03	0.05
93721277	Hydrothermal	0.764	0.236	Porphyry	0.07	0.12	0.07	0.58	0.04	0.12
93721044	Hydrothermal	0.986	0.014	Porphyry	0.05	0.20	0.01	0.57	0.02	0.14
93724085	Hydrothermal	0.890	0.110	Porphyry	0.03	0.20	0.02	0.54	0.03	0.18
93724072	Hydrothermal	0.984	0.016	Porphyry	0.02	0.11	0.02	0.72	0.01	0.12
93724119	Hydrothermal	0.946	0.054	Porphyry	0.18	0.15	0.04	0.53	0.01	0.09
93724069	Hydrothermal	0.912	0.088	Porphyry	0.06	0.17	0.02	0.65	0.01	0.09
93721044	Hydrothermal	0.928	0.072	Porphyry	0.06	0.16	0.03	0.60	0.01	0.15

	RFmodel model by geological system			hydrothermal deposit type						
		Probabilities			Probabilities					
					Epithermal		Orogenic			
Sample	Predicted	Hydrothermal	Magmatic	Predicted	gold	IOCG	gold	Porphyry	Skarn	VMS
93720060	Hydrothermal	0.692	0.308	Porphyry	0.02	0.06	0.01	0.81	0.07	0.03
93724159	Hydrothermal	0.962	0.038	Porphyry	0.06	0.10	0.07	0.58	0.01	0.18
93721084	Hydrothermal	0.912	0.088	Porphyry	0.05	0.23	0.01	0.42	0.01	0.27
93724284	Hydrothermal	0.502	0.498	Porphyry	0.07	0.22	0.16	0.43	0.07	0.05
93724281	Hydrothermal	0.734	0.266	Porphyry	0.01	0.21	0.01	0.49	0.03	0.26
93724261	Hydrothermal	0.774	0.226	Porphyry	0.04	0.05	0.02	0.73	0.01	0.14
93724118	Hydrothermal	0.928	0.072	Porphyry	0.02	0.13	0.01	0.68	0.01	0.16
93721266	Hydrothermal	0.612	0.388	Porphyry	0.13	0.18	0.12	0.26	0.12	0.18
93724059	Hydrothermal	0.968	0.032	Porphyry	0.03	0.10	0.04	0.41	0.03	0.40
93721099	Hydrothermal	0.810	0.190	Porphyry	0.09	0.16	0.03	0.63	0.02	0.07
93724021	Hydrothermal	0.636	0.364	Porphyry	0.04	0.29	0.08	0.46	0.09	0.03
93724052	Hydrothermal	0.652	0.348	Porphyry	0.26	0.11	0.09	0.42	0.01	0.12
93721093	Hydrothermal	0.886	0.114	Porphyry	0.07	0.09	0.03	0.67	0.01	0.12
93724029	Hydrothermal	0.728	0.272	Porphyry	0.07	0.14	0.05	0.48	0.01	0.25
93721011	Hydrothermal	0.752	0.248	Porphyry	0.22	0.10	0.05	0.57	0.00	0.05
93724254	Hydrothermal	0.954	0.046	Porphyry	0.01	0.23	0.01	0.60	0.01	0.15
93724070	Hydrothermal	0.926	0.074	Porphyry	0.04	0.07	0.03	0.68	0.01	0.18
93724123	Hydrothermal	0.942	0.058	Porphyry	0.01	0.12	0.02	0.62	0.01	0.22
93724048	Hydrothermal	0.882	0.118	Porphyry	0.02	0.10	0.03	0.80	0.00	0.05
93724250	Hydrothermal	0.940	0.060	Porphyry	0.05	0.05	0.02	0.79	0.01	0.07
93724276	Hydrothermal	0.680	0.320	Porphyry	0.01	0.21	0.01	0.61	0.01	0.15
93720040	Hydrothermal	0.730	0.270	Porphyry	0.08	0.09	0.02	0.56	0.01	0.24
93724050	Hydrothermal	0.876	0.124	Porphyry	0.02	0.39	0.02	0.50	0.01	0.06
93724072	Hydrothermal	0.800	0.200	Porphyry	0.01	0.46	0.00	0.46	0.02	0.05
93720040	Hydrothermal	0.504	0.496	Porphyry	0.03	0.13	0.03	0.64	0.00	0.16
93724118	Hydrothermal	0.874	0.126	Porphyry	0.02	0.13	0.02	0.71	0.00	0.11
93721099	Hydrothermal	0.818	0.182	Porphyry	0.04	0.09	0.03	0.68	0.01	0.16
93724261	Hydrothermal	0.746	0.254	Porphyry	0.08	0.05	0.01	0.59	0.02	0.26
93724062	Hydrothermal	0.900	0.100	Porphyry	0.04	0.18	0.03	0.69	0.02	0.04
93724007	Hydrothermal	0.718	0.282	Porphyry	0.22	0.12	0.08	0.38	0.02	0.17
93724281	Hydrothermal	0.952	0.048	Porphyry	0.08	0.05	0.01	0.73	0.02	0.10
93724087	Hydrothermal	0.904	0.096	Porphyry	0.01	0.40	0.01	0.42	0.01	0.15
93721088	Hydrothermal	0.982	0.018	Porphyry	0.05	0.13	0.02	0.54	0.03	0.24
93724062	Hydrothermal	0.974	0.026	Porphyry	0.02	0.06	0.05	0.76	0.03	0.08
93720042	Hydrothermal	0.904	0.096	Porphyry	0.11	0.22	0.12	0.37	0.03	0.15
93724002	Hydrothermal	0.926	0.074	Porphyry	0.13	0.25	0.06	0.30	0.03	0.23
93724047	Hydrothermal	0.878	0.122	Porphyry	0.03	0.13	0.04	0.70	0.03	0.07
93722387	Hydrothermal	0.988	0.012	Porphyry	0.02	0.02	0.00	0.93	0.00	0.03
93724010	Hydrothermal	0.814	0.186	Porphyry	0.06	0.03	0.01	0.87	0.01	0.03

	RFmodel model by geological system			hydrothermal deposit type						
		Probabilities			Probabilities					
					Epithermal		Orogenic			
Sample	Predicted	Hydrothermal	Magmatic	Predicted	gold	IOCG	gold	Porphyry	Skarn	VMS
93721011	Hydrothermal	0.812	0.188	Porphyry	0.07	0.18	0.10	0.50	0.10	0.05
93721099	Hydrothermal	0.940	0.060	Porphyry	0.03	0.31	0.01	0.45	0.01	0.18
93724147	Hydrothermal	0.660	0.340	Porphyry	0.05	0.09	0.08	0.49	0.03	0.27
93724029	Hydrothermal	0.776	0.224	Porphyry	0.08	0.11	0.02	0.60	0.01	0.19
93721093	Hydrothermal	0.842	0.158	Porphyry	0.15	0.15	0.04	0.49	0.02	0.15
93724088	Hydrothermal	0.980	0.020	Porphyry	0.07	0.15	0.02	0.62	0.00	0.13
93721277	Hydrothermal	0.758	0.242	Porphyry	0.03	0.08	0.04	0.69	0.01	0.15
93724284	Hydrothermal	0.804	0.196	Porphyry	0.03	0.07	0.01	0.74	0.00	0.14
93721012	Hydrothermal	0.782	0.218	Porphyry	0.06	0.17	0.04	0.52	0.02	0.19
93721012	Hydrothermal	0.720	0.280	Porphyry	0.02	0.16	0.00	0.67	0.03	0.12
93721266	Hydrothermal	0.638	0.362	Porphyry	0.23	0.10	0.16	0.26	0.06	0.19
93724092	Hydrothermal	0.928	0.072	Porphyry	0.07	0.26	0.07	0.35	0.03	0.22
93724035	Hydrothermal	0.966	0.034	Porphyry	0.05	0.24	0.01	0.50	0.01	0.19
93724095	Hydrothermal	0.910	0.090	Porphyry	0.01	0.17	0.01	0.64	0.00	0.16
93724271	Hydrothermal	0.870	0.130	Porphyry	0.14	0.13	0.02	0.46	0.00	0.24
93724005	Hydrothermal	0.510	0.490	Porphyry	0.16	0.11	0.07	0.49	0.00	0.18
93720042	Hydrothermal	0.774	0.226	Porphyry	0.02	0.09	0.01	0.81	0.00	0.08
93721098	Hydrothermal	0.830	0.170	Porphyry	0.05	0.08	0.02	0.74	0.02	0.08
93724104	Hydrothermal	0.720	0.280	Porphyry	0.04	0.22	0.03	0.51	0.01	0.19
93724026	Hydrothermal	0.842	0.158	Porphyry	0.08	0.18	0.07	0.58	0.02	0.07
93724002	Hydrothermal	0.948	0.052	Skarn	0.01	0.20	0.04	0.05	0.40	0.30
93724073	Hydrothermal	0.738	0.262	Skarn	0.07	0.16	0.16	0.12	0.37	0.11
93721102	Hydrothermal	0.928	0.072	Skarn	0.01	0.18	0.09	0.14	0.30	0.27
93724113	Hydrothermal	0.656	0.344	Skarn	0.16	0.19	0.15	0.03	0.38	0.09
93724092	Hydrothermal	0.928	0.072	Skarn	0.01	0.13	0.08	0.09	0.43	0.27
93721011	Hydrothermal	0.962	0.038	VMS	0.05	0.14	0.17	0.14	0.06	0.44
93721084	Hydrothermal	0.558	0.442	VMS	0.09	0.28	0.06	0.02	0.21	0.35
93724046	Hydrothermal	0.658	0.342	VMS	0.21	0.11	0.05	0.09	0.14	0.42
93724055	Hydrothermal	0.510	0.490	VMS	0.04	0.04	0.03	0.06	0.02	0.81
93724272	Hydrothermal	0.948	0.052	VMS	0.06	0.06	0.03	0.18	0.03	0.65
93724071	Hydrothermal	0.500	0.500	VMS	0.02	0.14	0.02	0.08	0.05	0.69
93721277	Hydrothermal	0.700	0.300	VMS	0.01	0.08	0.08	0.08	0.10	0.64
93720033	Hydrothermal	0.958	0.042	VMS	0.08	0.10	0.02	0.26	0.03	0.50
93724148	Hydrothermal	0.982	0.018	VMS	0.00	0.02	0.02	0.02	0.06	0.88
93724059	Hydrothermal	0.964	0.036	VMS	0.03	0.29	0.01	0.02	0.14	0.51
93724141	Hydrothermal	0.862	0.138	VMS	0.06	0.25	0.03	0.09	0.09	0.48
93720064	Hydrothermal	0.862	0.138	VMS	0.07	0.14	0.02	0.36	0.04	0.36
93724151	Hydrothermal	0.826	0.174	VMS	0.15	0.22	0.07	0.07	0.18	0.31
93721084	Hydrothermal	0.748	0.252	VMS	0.01	0.10	0.03	0.03	0.02	0.81

	RFmodel model by geological system			hydrothermal deposit type						
		Probabilities			Probabilities					
					Epithermal		Orogenic			
Sample	Predicted	Hydrothermal	Magmatic	Predicted	gold	IOCG	gold	Porphyry	Skarn	VMS
93721088	Hydrothermal	0.966	0.034	VMS	0.01	0.09	0.07	0.03	0.19	0.62
93721098	Hydrothermal	0.886	0.114	VMS	0.08	0.28	0.03	0.19	0.14	0.29
93721014	Hydrothermal	0.628	0.372	VMS	0.01	0.18	0.11	0.14	0.22	0.33
93720066	Hydrothermal	0.528	0.472	VMS	0.03	0.32	0.09	0.10	0.07	0.38
93721014	Hydrothermal	0.978	0.022	VMS	0.09	0.11	0.07	0.23	0.11	0.39
93724062	Hydrothermal	0.664	0.336	VMS	0.04	0.26	0.21	0.10	0.11	0.28
93721014	Hydrothermal	0.778	0.222	VMS	0.06	0.33	0.04	0.07	0.12	0.39
93724081	Hydrothermal	0.976	0.024	VMS	0.06	0.30	0.02	0.27	0.02	0.33
93721044	Hydrothermal	0.746	0.254	VMS	0.03	0.09	0.04	0.14	0.03	0.67
93721097	Hydrothermal	0.852	0.148	VMS	0.12	0.30	0.02	0.13	0.10	0.34
93724048	Hydrothermal	0.532	0.468	VMS	0.02	0.10	0.03	0.10	0.04	0.71
93721013	Hydrothermal	0.976	0.024	VMS	0.01	0.06	0.20	0.02	0.08	0.62
93724048	Hydrothermal	0.572	0.428	VMS	0.03	0.10	0.03	0.11	0.03	0.69
93720033	Hydrothermal	0.536	0.464	VMS	0.13	0.16	0.08	0.20	0.09	0.34
93721013	Hydrothermal	0.886	0.114	VMS	0.05	0.11	0.04	0.35	0.01	0.44
93721128	Hydrothermal	0.970	0.030	VMS	0.08	0.18	0.05	0.29	0.03	0.36
93724272	Hydrothermal	0.884	0.116	VMS	0.04	0.09	0.04	0.05	0.06	0.72
93721084	Hydrothermal	0.906	0.094	VMS	0.02	0.28	0.04	0.13	0.02	0.51
93724141	Hydrothermal	0.658	0.342	VMS	0.16	0.14	0.18	0.16	0.10	0.26
93724156	Hydrothermal	0.912	0.088	VMS	0.02	0.05	0.16	0.19	0.03	0.55
93724141	Hydrothermal	0.618	0.382	VMS	0.08	0.31	0.08	0.07	0.09	0.38
93724141	Hydrothermal	0.884	0.116	VMS	0.07	0.28	0.06	0.11	0.09	0.40
93721011	Hydrothermal	0.678	0.322	VMS	0.00	0.28	0.03	0.08	0.22	0.40
93724068	Hydrothermal	0.690	0.310	VMS	0.03	0.22	0.02	0.11	0.07	0.56
93724044	Hydrothermal	0.966	0.034	VMS	0.05	0.24	0.09	0.20	0.08	0.34
93724140	Hydrothermal	0.990	0.010	VMS	0.04	0.15	0.02	0.05	0.15	0.59
93724029	Hydrothermal	0.508	0.492	VMS	0.01	0.06	0.02	0.02	0.02	0.87
93724071	Hydrothermal	0.980	0.020	VMS	0.01	0.16	0.09	0.07	0.16	0.51
93724123	Hydrothermal	0.824	0.176	VMS	0.16	0.24	0.07	0.06	0.12	0.35
93724048	Hydrothermal	0.544	0.456	VMS	0.02	0.14	0.04	0.13	0.06	0.61
93721098	Hydrothermal	0.996	0.004	VMS	0.01	0.07	0.04	0.02	0.03	0.82
93724146	Hydrothermal	0.738	0.262	VMS	0.05	0.18	0.21	0.08	0.10	0.38
93721014	Hydrothermal	0.926	0.074	VMS	0.02	0.14	0.16	0.15	0.08	0.45
93724117	Hydrothermal	0.600	0.400	VMS	0.06	0.14	0.05	0.09	0.23	0.44
93724284	Hydrothermal	0.832	0.168	VMS	0.10	0.25	0.07	0.12	0.14	0.32
93724072	Hydrothermal	0.944	0.056	VMS	0.01	0.13	0.04	0.04	0.02	0.77
93724048	Hydrothermal	0.548	0.452	VMS	0.04	0.09	0.03	0.13	0.06	0.65
93720057	Hydrothermal	0.760	0.240	VMS	0.04	0.26	0.09	0.06	0.04	0.51
93721013	Hydrothermal	0.940	0.060	VMS	0.02	0.06	0.08	0.11	0.04	0.70

	RFmodel model by geological system			hydrothermal deposit type						
		Probabilities			Probabilities					
					Epithermal		Orogenic			
Sample	Predicted	Hydrothermal	Magmatic	Predicted	gold	IOCG	gold	Porphyry	Skarn	VMS
93724081	Hydrothermal	0.996	0.004	VMS	0.01	0.10	0.01	0.04	0.04	0.81
93721266	Hydrothermal	0.588	0.412	VMS	0.28	0.18	0.11	0.09	0.06	0.28
93721099	Hydrothermal	0.928	0.072	VMS	0.03	0.27	0.02	0.31	0.03	0.34
93724048	Hydrothermal	0.554	0.446	VMS	0.02	0.11	0.02	0.12	0.05	0.68
93724086	Hydrothermal	0.998	0.002	VMS	0.00	0.04	0.03	0.01	0.05	0.87
93724064	Hydrothermal	0.954	0.046	VMS	0.00	0.08	0.01	0.04	0.01	0.86
93724021	Hydrothermal	0.970	0.030	VMS	0.03	0.05	0.08	0.09	0.05	0.71
93724159	Hydrothermal	0.994	0.006	VMS	0.07	0.22	0.06	0.17	0.05	0.43
93724281	Hydrothermal	0.924	0.076	VMS	0.08	0.20	0.15	0.06	0.11	0.39
93720062	Hydrothermal	0.656	0.344	VMS	0.00	0.14	0.01	0.03	0.04	0.77
93724004	Hydrothermal	0.958	0.042	VMS	0.18	0.05	0.07	0.21	0.03	0.46
93721266	Hydrothermal	0.620	0.380	VMS	0.22	0.09	0.22	0.15	0.08	0.23
93724281	Hydrothermal	0.704	0.296	VMS	0.02	0.07	0.02	0.06	0.06	0.78
93721277	Hydrothermal	0.778	0.222	VMS	0.15	0.05	0.06	0.11	0.04	0.59
93721093	Hydrothermal	0.858	0.142	VMS	0.01	0.11	0.07	0.08	0.03	0.70
93721014	Hydrothermal	0.656	0.344	VMS	0.02	0.16	0.16	0.19	0.10	0.37
93724271	Hydrothermal	0.826	0.174	VMS	0.09	0.25	0.06	0.02	0.21	0.36
93724030	Hydrothermal	0.998	0.002	VMS	0.00	0.05	0.02	0.01	0.18	0.74
93721044	Hydrothermal	0.686	0.314	VMS	0.04	0.13	0.07	0.16	0.04	0.56
93720042	Hydrothermal	0.554	0.446	VMS	0.08	0.12	0.31	0.06	0.10	0.33
93724179	Hydrothermal	0.848	0.152	VMS	0.17	0.24	0.02	0.22	0.02	0.32
93720066	Hydrothermal	0.620	0.380	VMS	0.02	0.33	0.08	0.08	0.08	0.41
93720033	Hydrothermal	0.864	0.136	VMS	0.06	0.08	0.02	0.29	0.06	0.48
93721099	Hydrothermal	0.984	0.016	VMS	0.06	0.10	0.07	0.09	0.05	0.64
93724005	Hydrothermal	0.786	0.214	VMS	0.13	0.18	0.10	0.17	0.11	0.31
93724086	Hydrothermal	0.942	0.058	VMS	0.00	0.13	0.11	0.03	0.08	0.65
93724002	Hydrothermal	0.952	0.048	VMS	0.01	0.10	0.08	0.05	0.06	0.70
93724171	Hydrothermal	0.796	0.204	VMS	0.01	0.39	0.01	0.10	0.09	0.40

Chalcopyrite analyses with Cu concentration <25% predicted as hydrothermal

	RFmodel model by geological system			hydrothermal deposit type						
		Probabilities			Probabilities					
					Epithermal		Orogenic			
Sample	Predicted	Hydrothermal	Magmatic	Predicted	gold	IOCG	gold	Porphyry	Skarn	VMS
93721014	Hydrothermal	0.718	0.282	Epithermal gold	0.33	0.14	0.16	0.29	0.03	0.04
93721013	Hydrothermal	0.946	0.054	Epithermal gold	0.40	0.10	0.19	0.21	0.00	0.09
93720062	Hydrothermal	0.842	0.158	Epithermal gold	0.35	0.20	0.14	0.08	0.11	0.12
93720040	Hydrothermal	0.578	0.422	IOCG	0.13	0.31	0.13	0.15	0.14	0.14
93721011	Hydrothermal	0.774	0.226	IOCG	0.07	0.38	0.08	0.05	0.06	0.37

	RFmodel model by geological system			hydrothermal deposit type						
		Probabilities			Probabilities					
					Epithermal		Orogenic			
Sample	Predicted	Hydrothermal	Magmatic	Predicted	gold	IOCG	gold	Porphyry	Skarn	VMS
93721011	Hydrothermal	0.800	0.200	IOCG	0.12	0.55	0.08	0.06	0.13	0.06
93720042	Hydrothermal	0.794	0.206	IOCG	0.13	0.29	0.26	0.08	0.11	0.13
93721014	Hydrothermal	0.742	0.258	IOCG	0.01	0.60	0.03	0.07	0.13	0.16
93721013	Hydrothermal	0.648	0.352	IOCG	0.02	0.56	0.07	0.07	0.13	0.15
93720062	Hydrothermal	0.974	0.026	IOCG	0.13	0.46	0.08	0.24	0.03	0.06
93721011	Hydrothermal	0.852	0.148	IOCG	0.11	0.32	0.18	0.08	0.10	0.21
93721013	Hydrothermal	0.986	0.014	IOCG	0.05	0.65	0.12	0.09	0.04	0.04
93720062	Hydrothermal	0.836	0.164	IOCG	0.01	0.42	0.08	0.37	0.08	0.03
93720040	Hydrothermal	0.724	0.276	IOCG	0.15	0.32	0.11	0.14	0.12	0.17
93720057	Hydrothermal	0.692	0.308	IOCG	0.14	0.43	0.06	0.15	0.09	0.13
93720063	Hydrothermal	0.520	0.480	IOCG	0.14	0.34	0.12	0.06	0.13	0.20
93721014	Hydrothermal	0.970	0.030	IOCG	0.01	0.37	0.03	0.36	0.03	0.20
93720066	Hydrothermal	0.594	0.406	IOCG	0.05	0.47	0.07	0.12	0.09	0.20
93721011	Hydrothermal	0.944	0.056	IOCG	0.18	0.38	0.18	0.20	0.03	0.02
93721014	Hydrothermal	0.842	0.158	IOCG	0.02	0.42	0.02	0.35	0.12	0.07
93721014	Hydrothermal	0.978	0.022	IOCG	0.01	0.49	0.02	0.04	0.19	0.25
93721011	Hydrothermal	0.618	0.382	IOCG	0.03	0.34	0.13	0.09	0.12	0.30
93720066	Hydrothermal	0.924	0.076	IOCG	0.09	0.57	0.05	0.05	0.11	0.13
93724158	Hydrothermal	0.582	0.418	IOCG	0.14	0.42	0.07	0.04	0.18	0.14
93721014	Hydrothermal	0.688	0.312	IOCG	0.04	0.44	0.04	0.16	0.16	0.15
93721011	Hydrothermal	0.616	0.384	IOCG	0.06	0.40	0.11	0.06	0.14	0.25
93721014	Hydrothermal	0.880	0.120	IOCG	0.13	0.47	0.08	0.08	0.12	0.13
93724151	Hydrothermal	0.666	0.334	IOCG	0.03	0.35	0.14	0.10	0.10	0.28
93721014	Hydrothermal	0.960	0.040	Orogenic gold	0.29	0.21	0.29	0.17	0.02	0.02
93720040	Hydrothermal	0.586	0.414	Orogenic gold	0.19	0.12	0.29	0.14	0.17	0.09
93721013	Hydrothermal	0.944	0.056	Orogenic gold	0.14	0.27	0.27	0.24	0.02	0.05
93721013	Hydrothermal	0.782	0.218	Porphyry	0.06	0.09	0.04	0.74	0.03	0.05
93721012	Hydrothermal	0.914	0.086	Porphyry	0.10	0.03	0.01	0.78	0.03	0.05
93721011	Hydrothermal	0.966	0.034	Porphyry	0.08	0.06	0.02	0.80	0.01	0.03
93720060	Hydrothermal	0.632	0.368	Porphyry	0.07	0.18	0.05	0.60	0.03	0.07
93721014	Hydrothermal	0.918	0.082	Porphyry	0.04	0.27	0.07	0.56	0.05	0.01
93720062	Hydrothermal	0.874	0.126	Porphyry	0.09	0.10	0.08	0.55	0.01	0.17
93720060	Hydrothermal	0.892	0.108	Porphyry	0.02	0.18	0.16	0.25	0.16	0.23
93721013	Hydrothermal	0.768	0.232	Porphyry	0.15	0.14	0.09	0.47	0.03	0.12
93720040	Hydrothermal	0.510	0.490	Porphyry	0.05	0.04	0.04	0.78	0.04	0.06
93721013	Hydrothermal	0.780	0.220	Porphyry	0.24	0.06	0.08	0.47	0.01	0.15
93721012	Hydrothermal	0.980	0.020	Porphyry	0.02	0.07	0.02	0.70	0.02	0.17
93721014	Hydrothermal	0.900	0.100	Porphyry	0.05	0.23	0.10	0.54	0.02	0.05
93721013	Hydrothermal	0.816	0.184	Porphyry	0.07	0.10	0.04	0.67	0.02	0.10

	RFmodel model by geological system			hydrothermal deposit type						
		Probabilities			Probabilities					
					Epithermal		Orogenic			
Sample	Predicted	Hydrothermal	Magmatic	Predicted	gold	IOCG	gold	Porphyry	Skarn	VMS
93721013	Hydrothermal	0.534	0.466	Porphyry	0.08	0.21	0.08	0.51	0.05	0.07
93721013	Hydrothermal	0.974	0.026	Porphyry	0.02	0.10	0.02	0.76	0.02	0.08
93721013	Hydrothermal	0.656	0.344	Porphyry	0.06	0.15	0.05	0.64	0.05	0.05
93721013	Hydrothermal	0.926	0.074	Skarn	0.16	0.19	0.05	0.02	0.51	0.07
93720062	Hydrothermal	0.600	0.400	Skarn	0.20	0.21	0.07	0.07	0.24	0.22
93721011	Hydrothermal	0.698	0.302	Skarn	0.00	0.08	0.15	0.04	0.47	0.26
93721014	Hydrothermal	0.900	0.100	VMS	0.04	0.12	0.02	0.36	0.01	0.45
93721014	Hydrothermal	0.830	0.170	VMS	0.10	0.05	0.03	0.05	0.04	0.74
93721014	Hydrothermal	0.956	0.044	VMS	0.13	0.17	0.08	0.19	0.15	0.27
93721013	Hydrothermal	0.640	0.360	VMS	0.04	0.09	0.01	0.06	0.05	0.75
93721012	Hydrothermal	0.610	0.390	VMS	0.02	0.18	0.15	0.08	0.17	0.39
93721012	Hydrothermal	0.566	0.434	VMS	0.07	0.09	0.11	0.24	0.08	0.41
93721013	Hydrothermal	0.618	0.382	VMS	0.04	0.08	0.03	0.08	0.04	0.73
93720062	Hydrothermal	0.840	0.160	VMS	0.15	0.22	0.09	0.04	0.05	0.45
93721011	Hydrothermal	0.718	0.282	VMS	0.02	0.10	0.09	0.19	0.03	0.58
93721011	Hydrothermal	0.520	0.480	VMS	0.06	0.06	0.02	0.10	0.03	0.73
93721014	Hydrothermal	0.510	0.490	VMS	0.09	0.09	0.09	0.18	0.05	0.50
93720033	Hydrothermal	0.598	0.402	VMS	0.03	0.28	0.05	0.09	0.10	0.45
93721014	Hydrothermal	0.612	0.388	VMS	0.04	0.21	0.19	0.16	0.12	0.29
93721013	Hydrothermal	0.592	0.408	VMS	0.11	0.20	0.12	0.06	0.11	0.41
93721013	Hydrothermal	0.914	0.086	VMS	0.04	0.28	0.04	0.03	0.07	0.54
93724150	Hydrothermal	0.680	0.320	VMS	0.21	0.21	0.09	0.06	0.18	0.24
93721014	Hydrothermal	0.522	0.478	VMS	0.12	0.22	0.06	0.13	0.11	0.36
93720042	Hydrothermal	0.964	0.036	VMS	0.04	0.15	0.14	0.07	0.29	0.31
93721013	Hydrothermal	0.554	0.446	VMS	0.06	0.29	0.03	0.22	0.08	0.32
93721014	Hydrothermal	0.984	0.016	VMS	0.01	0.04	0.01	0.01	0.25	0.68
93721014	Hydrothermal	0.710	0.290	VMS	0.04	0.16	0.23	0.21	0.11	0.24

Annexe C16. Predictions of detrital chalcopyrite grains from glacial sediment and eskers overlying the Churchill Province when analyses with inconclusive predictions are removed. Inconclusive prediction is defined according to the difference between the first and second highest class membership probability [1]. Three thresholds were tested, without removing ambiguous analyses (Case 1; Fig. 11), removing analyses with prob. diff <0.1 (Case 2), <0.2 (Case 3), and <0.3 (Case 4).

		Model mag-hyd			Model mag			Model hyd						
	Prob. diff[1]	Magmatic	Hydrothermal	Total	Ni-Cu sulfide	Reef-type PGE	Total	Porphyry	Skarn	IOCG	VMS	Epithermal gold	Orogenic gold	Total
Case 1	0	252	378	630	182	70	252	118	8	124	102	16	10	378
		40.0%	*60.0%*		*72.2%*	*27.8%*		*31.2%*	*2.1%*	*32.8%*	*27.0%*	*4.2%*	*2.6%*	
Case 2	<0.1	225	353	578	148	53	201	98	6	81	64	8	2	259
		38.9%	*61.1%*		*73.6%*	*26.4%*		*37.8%*	*2.3%*	*31.3%*	*24.7%*	*3.1%*	*0.8%*	
Case 3	<0.2	194	328	522	115	50	165	84	3	58	50	4	1	200
		37.2%	*62.8%*		*69.7%*	*30.3%*		*42.0%*	*1.5%*	*29.0%*	*25.0%*	*2.0%*	*0.5%*	
Case 4	<0.3	165	302	467	82	33	115	72	1	35	35	2	0	145
		35.3%	*64.7%*		*71.3%*	*28.7%*		*49.7%*	*0.7%*	*24.1%*	*24.1%*	*1.4%*	*0.0%*	

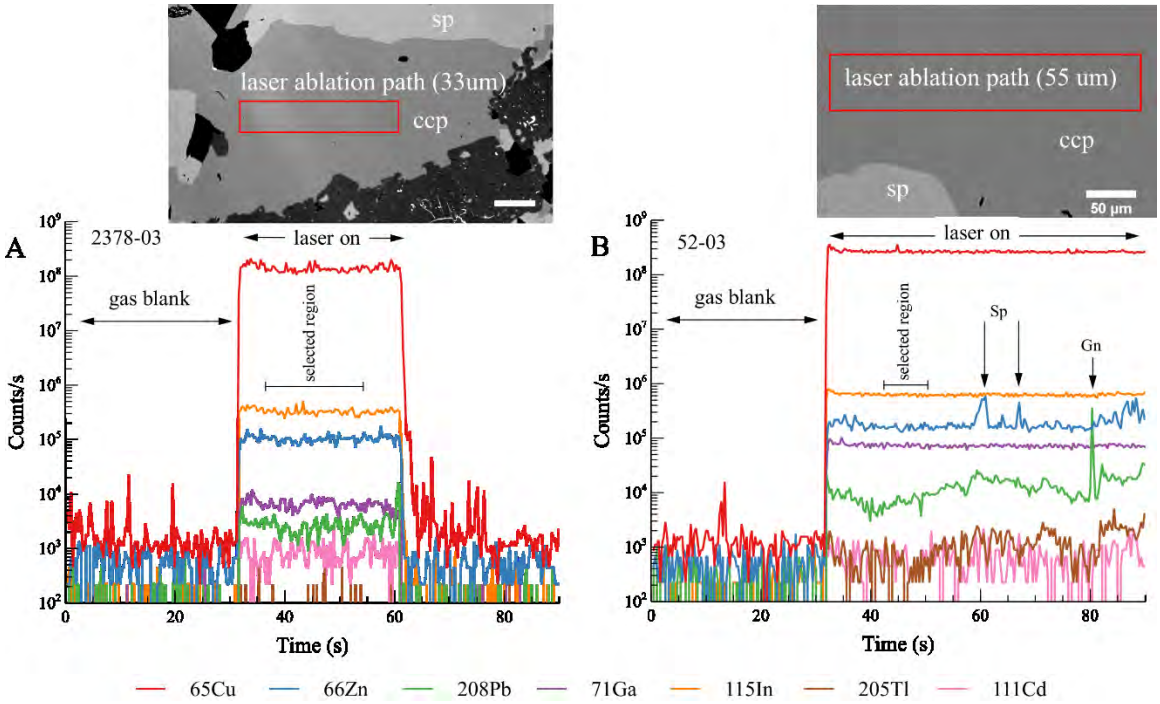

Annexe C17. Backscattered electron images and time-signal spectra for chalcopyrite with inclusion-free regions, which were selected to obtain the trace element composition (A), and chalcopyrite in Zn-rich sample with inclusions of sphalerite (Sp), where the selected region corresponds to the zone more stable in the spectre (B).

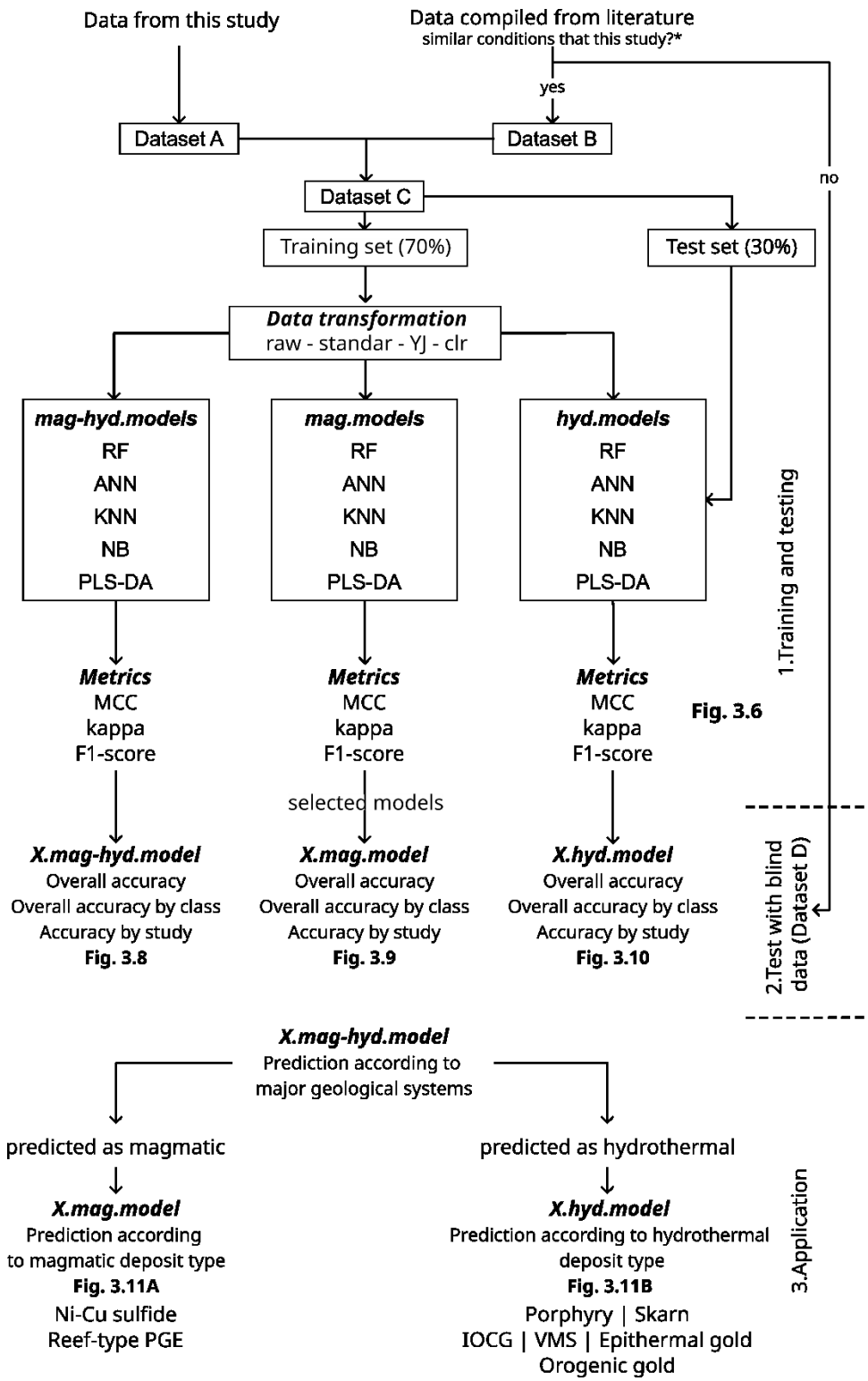

Annexe C18. Workflow with 1) steps to train, test and select the discrimination model; 2) validation with the blind data from known deposit types and 3) application of the model to detrital chalcopyrite grains of unknown origin from glacial sediments overlying Churchill Province, Canada.*analytical conditions and proportion of missing values (see text for details). Raw: untransformed data, standar: standardization, YJ: Yeo-Johnson, clr: centered-log ratio transformation.

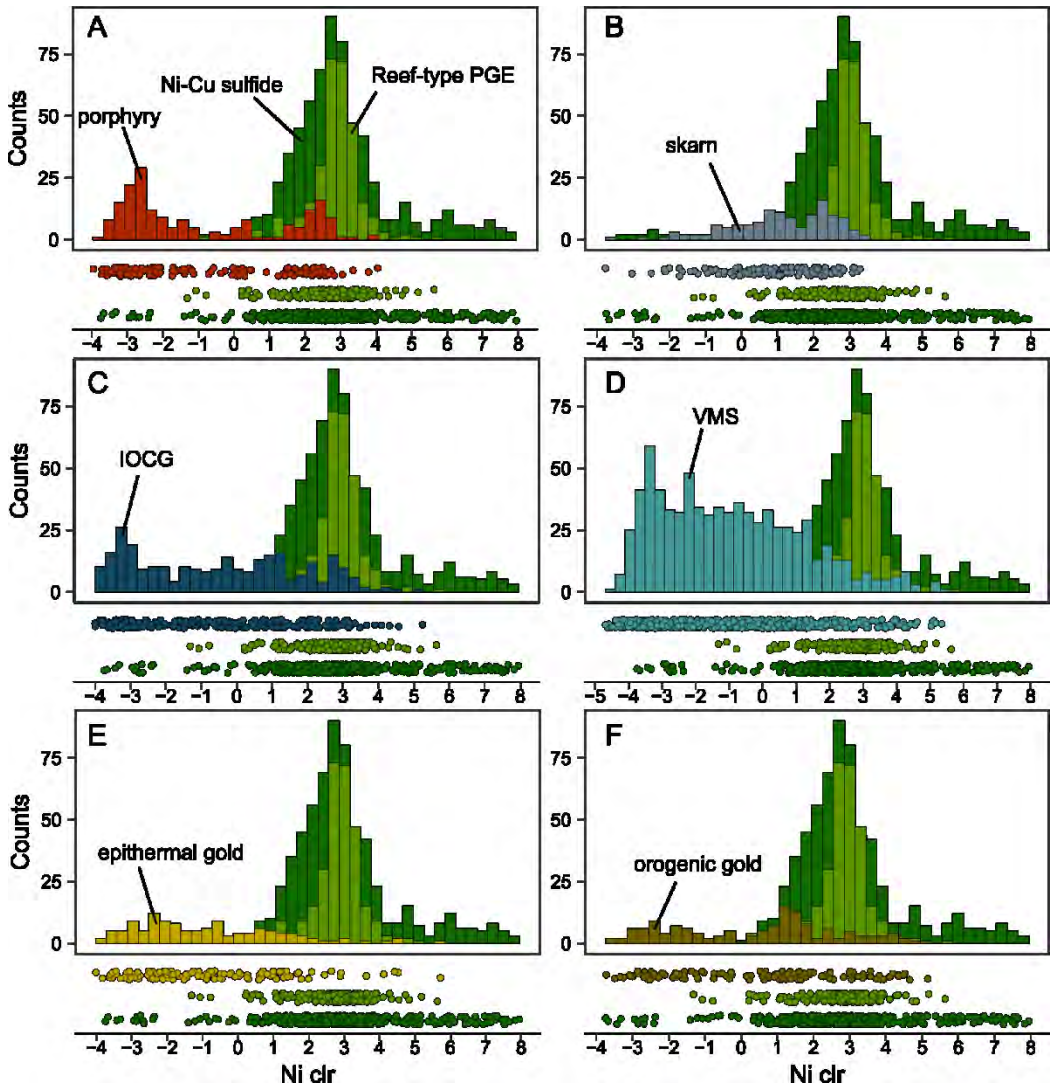

Annexe C19. Comparison of the distribution of Ni in chalcopyrite between different hydrothermal and magmatic deposits. Counts: number of analyses; clr: centered-log ratio transformation.